REMOVAL OF OIL FROM WASTEWATER BY ORGANOCLAY PREPARED FROM IRAQI BENTONITE

Prof.Dr. Abbas H. Sulaymon and Jassim M. Kshash
Department of Environmental Engineering
Baghdad University, 2008

ABSTRACT

The present study deals with the removal of oil from wastewater by organoclay. The organoclay was prepared by combination of Iraqi bentonite with quaternary amine (hexadecyltrimethyl ammonium chloride). The wastewater samples were obtained from the washing unit of fuel oil in the "*South Baghdad Gas Power Plant"*. The operating conditions of batch process for removal of oil from wastewater by using the prepared organoclays were studied in details (quantity of organoclay, mixer speed and time of adsorption). Initial concentration of wastewater used in this study was within a maximum range of 230-1512 mg/L. XRD and FTIR diagram of the prepared organoclay showed a considerable differences from those for natural bentonite which indicates the exchange of quaternary amine with Ca^{++} ions at the surface of bentonite. The concentration of oil in the wastewater samples decreased below 10 mg/L after treatment with organoclay. Batch kinetics studies were conducted by using kinetic equations (Lagergren and Ho et al) and batch isotherm studies was conducted by using isotherm models (Freundlich, Langmuir and BET).

الخلاصة

يتناول هذا البحث عملية إزالة الملوثات النفطية من المياه الصناعية باستخدام الطين العضوي. ان الطين العضوي المستخدم في هذا البحث تم تصنيعه عن طريق مزج خام البنتونايت العراقي (Iraqi bentonite) مع الامين الرباعي المسمى هكساديسايل تراي ميثايل امونيوم كلورايد (hexadecyltrimethyl ammonium chloride). إن مخلفات المياه (wastewater) المستخدمة في هذه الدراسة أخذت من وحده غسل زيت الوقود (fuel oil) الموجودة في محطة كهرباء جنوب بغداد الغازية. لقد تم دراسة الظروف التشغيلية لإزالة زيت الوقود (fuel oil) من نموذجين من المياه الصناعية بالتفصيل (كمية الطين العضوي و سرعة الخلاط وزمن الامدصاص). ان التراكيز الأولية للمياه الصناعية المستخدمة في التجارب كانت ضمن حدود 230 الى 1512 مل/لتر. النتائج التي تم الحصول عليها من مخططات الأشعة السينية (XRD) وكذلك مخططات الأشعة تحت الحمراء (FTIR) للطين العضوي المحضر اظهرت اختلاف واضح عن مثيلاتها العائدة للبنتونايت وهذا يشير الى استبدال ايونات الكالسيوم Ca^{++} الموجودة على سطح البنتونايت بايونات الأمين الرباعي الموجبة. النتائج المستخلصة من هذه الدراسة بينت إن تركيز الملوثات النفطية في المياه الصناعية انخفض دون 10 ملغم/لتر (الحدود المسموح بها لتصريف المياه الملوثة بالنفط) بعد معاملتها بالطين العضوي. كذلك تم دراسة حركية عملية الامتزاز (Kinetics)

(adsorption capacity) ودراسة سعة عملية الامتزاز (Lagergren and Ho. et al) باستخدام المعادلات الحركية
باستخدام النماذج الرياضية (Freundlich, Langmuir, and BET).

KEYWORDS: Oil removal; Wastewater treatment; Organoclays; Bentonite; Adsorption.

INTRODUCTION

Many natural and synthetic media have been used for treating oily waters. These media can be classified as filtering media (sand, coal, and diatomaceous earth), coalescing media (fiberglass, polyesterfelt, amberlite XAD-2, and polypropylene), and adsorption media (activated carbon, peat, attapulgite, bentonite, and organoclays) (Mathavan and Viraraghavan 1989, Zunan et al. 1995, Alther 1996a, Alther 1996b).

Adsorption is very efficient, cost effective and most importantly has the capability of meeting the environmental compliance as far as the discharge standard of the oil content of the wastewater is concerned.(Slejeiko 1981). Activated carbon is a common adsorbent used for the removal of hazardous pollutants from aqueous solutions. However, activated carbon adsorption is a nonselective process (Cadena 1989). Organoclay has emerged as a better substitute for activated carbon. In fact, studies show that if a comparison is made between the organoclay and activated carbon, organoclay has several advantages over the activated carbon as an adsorbent (Alther 2002).

Organoclays are manufactured by modifying bentonite (which is a kind of smectite group clay mineral, is almost made up of 80 wt.% of montmorillonite and contains a crystal lattice with three layers) or other clays with quaternary amines, thus changing the hydrophilic nature of clays to organophilic. Quaternary amine is a type of surfactant that contains a nitrogen ion. The nitrogen end of the quaternary amine (i.e., the hydrophilic end) is positively charged and ion exchanges onto the clay platelet for sodium or calcium (Lagaly1984, Alther 2002, Moazed and Viraraghavan 2005, Janes and Boyd 1991, Kowalska et al. 1994).

Moazed and Viraraghavan (2005) used powdered bentonite organoclay to remove oil from water. The concentrations of oil in oily waters varied from 26 to 381 mg/L. The results indicated that the organoclay can remove up to 100% oil from oil in water emulsions. Consequently, the organoclay could be considered an excellent media for treating oily waters. Carmody et al. (2007) investigated the synthesis of oranoclays by the ion exchange of sodium in Wyoming Na-Montmorillonite with three surfactants octadecyltrimethylammonium bromide (ODTMA), $C_{21}H_{46}NBr$, didecyldimethylammonium bromide (DDDMA),$C_{22}H_{48}BrN$, and di(hydrogenated tallow)dimethylammonium chloride (tallow).The organoclays were tested for hydrocarbon adsorption (diesel, hydraulic oil and engine oil), that are likely to be involved in land-based oil spills. Greater adsorption was obtained if the surfactant contained two or more hydrocarbon long chains.

The aim of the present research is to study the removal of oil from wastewater produced from washing unit of "South Baghdad Gas Power Plant" by using bentonitic organoclay. The organoclay was prepared by modifying Iraqi bentonite with quaternary amine (hexadecyltrimethyl ammonium chloride solution 25% wt./vol.). The operating conditions for oil removal were studied in details. Kinetics and adsorption isotherm were also predicted.

EXPERIMENTAL WORK

MATERIALS

Oily Water

The oily water samples were collected from the washing unit of fuel oil in the South Baghdad Gas Power Plant. Oil concentrations used in this study were within the maximum range of 230-1512 mg/L. The characteristics of oily water are shown in table 1.

Table 1. Characteristics of oily water

characteristics	Value
PH	10.13
Oil and grease, mg/L	549
Biological oxygen demand (BOD), mg/L	156
Chemical oxygen demand (COD), mg/L	120
Chlorides, mg/L	230
Nitrates, mg/L	16.1
Phosphates, mg/L	0.92
Sulphates, mg/L	14
Total dissolved solids, mg/L	775
Total suspended solids, mg/L	509
Electrical conductivity	1446

IRAQI BENTONITE

The bentonite used in this study was calcium bentonite powder from the State Company for Geological Survey and Mining (Iraq). The characteristics of the bentonite are presented in table 2.

HEXADECYLTRIMETHYL AMMONIUM CHLORIDE

This type of surfactant was used to modify the hydrophilic nature of bentonite to organophilic. It is produced by the Indian Company ,Unilab Chemicals and Pharmaceuticals PVT.LTD., as a solution in water with concentration of 24-26% (wt./vol.), pH value for 10% concentration of 2.8-3.2, and density of 0.97-0.98 g / cm^3 at 20 $^{\circ}$C.

Table 2. Characteristics of bentonite

Characteristics	Value
Partical size, mm	0.075
Cation exchange capacity (CEC), meq/100g	70-87
Chemical (wt% dry basis) Silica (SiO_2) Alumina (Al_2O_3) Ferric oxide (Fe_2O_3) Magnesium oxide (MgO) Calcium oxide (CaO) Sodium oxide (Na_2O) Potassium oxide (K_2O) Titanium oxide (TiO_2) Loss on ignition (L.O.I)	 54.26 14.87 4.94 3.8 5.53 0.98 0.38 0.75 12.8
Mineralogy	momntmorillonite, palygorskite, calcite, feldspar, quartz.

EXPERIMENTAL PROCEDURE

Synthesis of Organoclay

Organoclay was prepared by adding the required quantity of hexadecyltrimethy ammonium chloride solution (25% wt./vol.) to the desired quantity of bentonite (particle size of 0.075 mm) in a stainless steel container and mixed thoroughly by hand. The produced paste was then introduced into a meat grinder and the product was collected in a container. The reacted material (organoclay) is then dried in an electrical oven at 60 °C for 48 hours and then ground by agate mortar followed by screening to particle size of 0.075 mm. Organoclay with ratios of 10, 20, 30, 38 g amine/ 100 g bentonite was prepared in this study to find the best ratio of amine to bentonite that gives the highest oil removal efficiency.

Oil Removal From Wastewater

One liter of oily water was first placed into the glass beaker and a desired quantity of prepared organoclay was then added to the beaker. The materials were mixed using an electrical mixer at adjustable mixer speed for the required time. Then the slurry was filtered using vacuum filtration unit to separate organoclay from treated water. The filtrate was used for oil concentration measurement using partition graphmetric method 5520B (standard method, 1995).

RESULTS AND DISCUSSION

X-ray Diffraction Analysis of Bentonite and Organoclay

Figures 1 and 2 show the interlayer spacings of natural bentonite and organoclay. Tables 3 and 4 represent peak data list of these figures respectively. The organoclay and natural bentonite were previously dried at 60 °C.

The properties of organoclays were investigated by basal x-ray diffraction analysis. The basal spacings of the original clays were changed from 14.256 to 18.470 Å. The organoclay displayed a greater interlayer spacing than the corresponding natural bentonite. This behavior was confirmed by Diaz et al. (2005) and Diaz (1999, 2001).

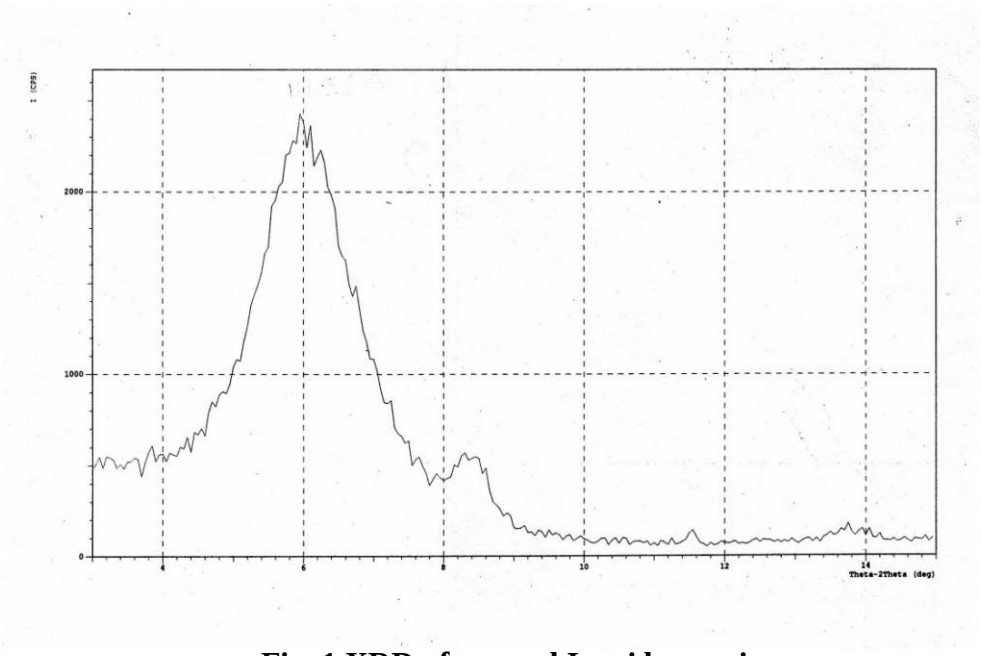

Fig. 1 XRD of natural Iraqi bentonite.

Table 3. Peak data list of natural Iraqi bentonite.

Peak №	2theta(deg)	d (Å)	I/I1	FWHM(deg)	Intensity (counts)	Integrated Int (counts)
1	3.8481	22.94287	4	0.63340	29	781
2	6.1949	14.25574	100	1.64190	782	28207
3	8.6621	10.20007	13	0.60000	98	2072

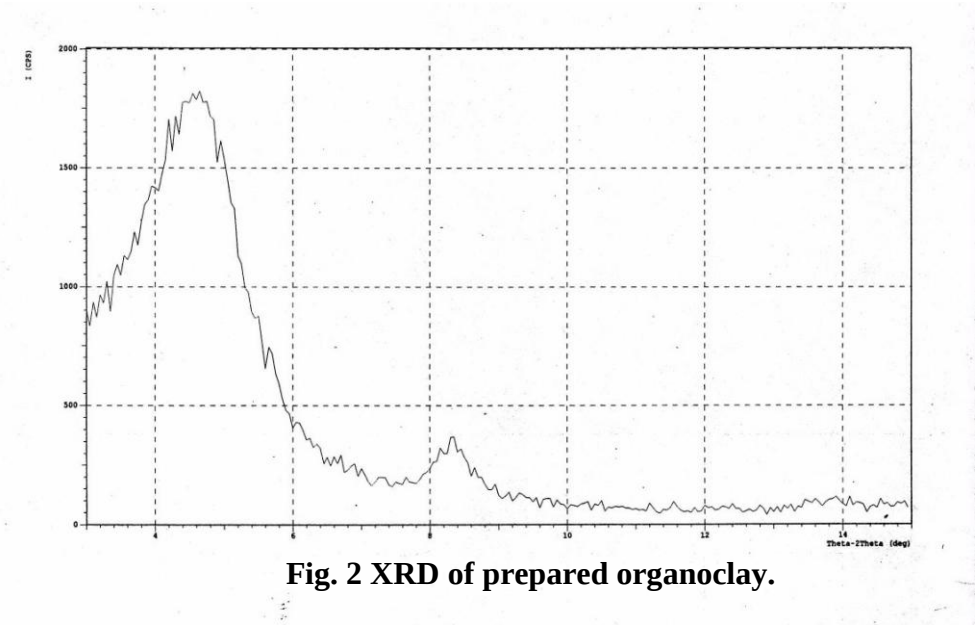

Fig. 2 XRD of prepared organoclay.

Table 4. Peak data list of prepared organoclay.

Peak №	2theta(deg)	d (Å)	I/I1	FWHM(deg)	Intensity (counts)	Integrated Int (counts)
1	4.7808	18.46877	100	1.40150	471	13955
2	8.4699	10.43109	10	0.64880	48	598
3	14.0156	6.31370	4	1.07500	17	506

INFRARED CURVES

The absorption of infrared radiation by clays was recorded over a range of 4000 to 400 cm^{-1} as shown in figures 3 and 4 for natural Iraqi bentonite and prepared organoclay respectively. The natural clay showed characteristics smectitic clay mineral peaks at 470.6, 524.6, 749.62, 918.05, 1033.77, 1635.52, 3417 and 3625.92 cm^{-1}. The natural clay showed no intense peaks corresponding to organic matter at 1464, 2827 and 2909 cm^{-1}. Bala et al. (2000) assigned the 1464 and 2827 cm^{-1} peaks to the CH_2 scissor vibration band and the symmetrical CH_3 stretching absorption band respectively. The 2909 cm^{-1} peak was assigned to *CH* stretching band.

The organophilic clay also showed the characteristic peaks of clay minerals, in spite of being of low density. This is an indication of the organophilic character of the clay. The organic

matter peaks at 1473.51, 2854.45 and 2923.88 cm^{-1} were sharper than those of the natural clay. The CH_3, CH_2 and CH bands confirmed the alkylammonium intercalation in the interlayer galleries of the clay mineral, and the lower intensity of the characteristic clay mineral peaks indicated the organophilic nature of the treated clay.

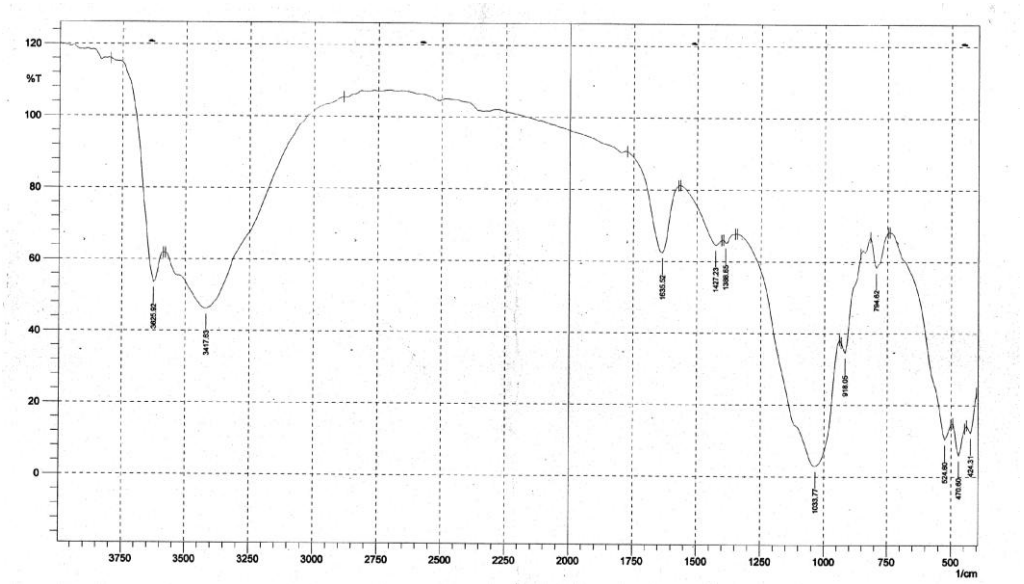

Fig. 3 Infrared curve of natural Iraqi bentonite.

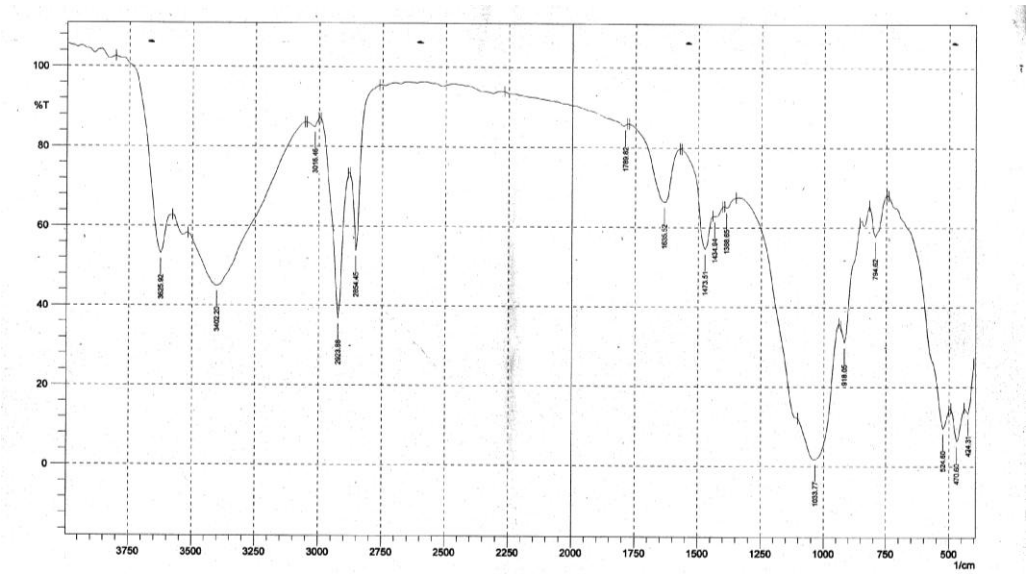

Fig. 4 Infrared curve of prepared organoclay.

EFFECT OF BENTONITE QUANTITY ON OIL REMOVAL

The ability of bentonite to remove oil from wastewater was studied by adding 5, 10, 15 and 20 g of Iraqi bentonite to 1 liter of wastewater with initial oil concentration 871.8 mg/L. Mixer speed used was 450 rpm, and time 1 hour. The results of these experiments is shown in figure 5.

Bentonite appears good capability for oil removal where the concentration of oil decreases rapidly from 871.8 to 298.4 mg/L when 5 g of bentonite is added. Using quantities of bentonite more than 5g, the concentration of oil decreases slowly until it reaches 183.4 mg/L for 15g of bentonite.

Oil concentration was not decreased below 10 mg/L (allowable limits of oil in the discharged effluents), as shown in, figure 5. This is because of the hydration of bentonite which causes that organic compounds with average molecular weights (amu) below 150 are weakly adsorbed or not adsorbed by pure montmorillonites (bentonite) due to their relatively large solubility in water (unless they carry a charge and can enter into an exchange reactions). The interaction forces under these conditions are the same in magnitude as hydration forces, so that competition with water molecules for the solid surface dominates. Soluble compounds with molecular weights above 150 amu, whether or not charged are often adsorbed by montmorillonites due to their reduced solubility in water (Cadena, 1989).

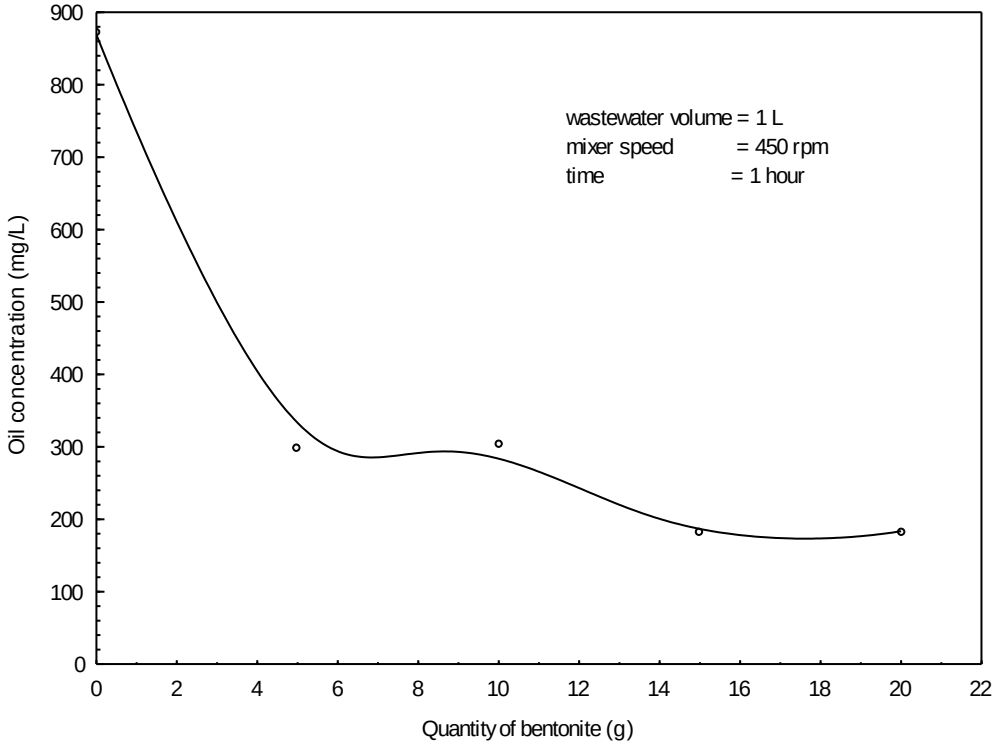

Fig. 5 Effect of bentonite quantity on oil concentration.

EFFECT OF QUANTITY OF ORGANOCLAY ON OIL REMOVAL

The prepared organoclays with quaternary amine weight ratios of 10, 20, 30 and 38 g/100g bentonite were investigated to find the quantity of organoclay required to remove the greatest amount of oil from wastewater. Figure 6 shows the effect of quantity of organoclay (2, 5, 10, 15 and 20g) on the concentration of oil in wastewater for the four organoclays prepared. One liter of wastewater with initial concentration of (1450 – 1512 mg/L), mixer speed 450 rpm, and time 1 hour were used.

As shown in figure 6, the concentration of oil in wastewater samples decreased rapidly as the quantity of organoclay increased until it reaches 10g for amine ratio of 10 and 2g for amine ratio of 20, 30 and 38 g amine/100g bentonite after which the concentration falls gently. The best quantity of organoclays were 20g for amine ratio of 10 g amine/100g bentonite and 15 g for amine ratios of 20, 30, and 38 g amine/100g bentonite respectively, where the lowest concentrations of oil obtained in treated water were 117, 13, 1 and 8.8 mg/L respectively Figure 6 also shows that the lowest oil concentrations of 1 and 8.6 mg/L are obtained for organoclay with amine ratios of 30 and 38 g amine/100g bentonite respectively, which represents oil removal efficiency of 99.93% and 99.4% respectively.

The reason for the rapid decrease of oil concentration especially for organoclays with high amine ratio is due to the organophillic nature of the organoclay. The concentration of oil decreases gently after this rapid decrease because the surface of the organoclay is filled with the oil and much more organoclay must be added to remove extra amount of oil, also the oil concentration difference between the bulk of the liquid and the surface of the organoclay, which represents a driving force for oil adsorption, decreased gradually causing a decrease in the adsorption rate, so another surface layer of organoclay must be added to overcome this problem (Patle 2004).

Mozed and Viraraghavan (2005), used organoclay to remove oil from produced water (a byproduct of oil and gas production) and they reach oil removal efficiency of 97%.

Same results were obtained for initial oil concentration of (255 – 264) mg/L, where best oil concentrations for treated water were 140, 20, 1 and 6 for organoclays with amine ratio of 10, 20, 30 and 38 g amine/100g bentonite respectively. In these experiments mixer speed was 450 rpm and time 1 hour. The results are shown in figure 7. The results from figures 6 and 7 prove that prepared organoclay can be used efficiently for removal of oil at wide range of concentration in wastewater.

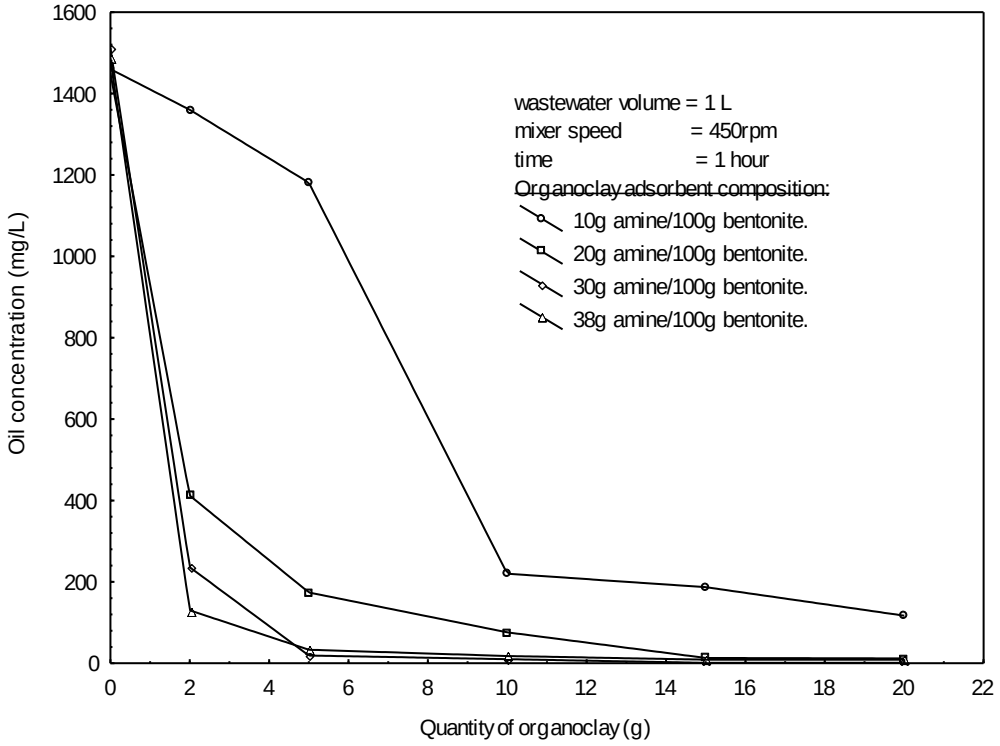

Fig. 6 Effect of organoclay quantity on oil concentration for different weight ratio of amine to bentonite ($C_\circ$ = 1450–1512mg/L).

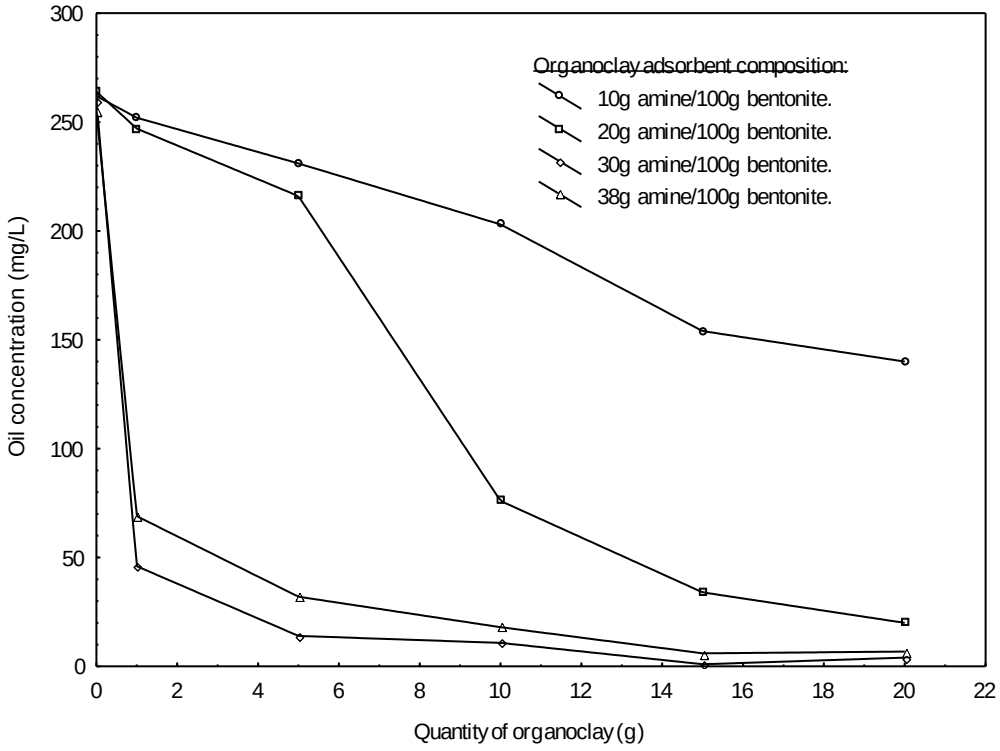

Fig. 7 Effect of organoclay quantity on oil concentration for different weight ratio of amine to bentonite ($C_\circ$ = 255–264 mg/L).

EFFECT OF AMINE TO BENTONITE WEIGHT RATIO ON ORGANOCLAY ADSORPTION OF OIL

In order to show the effect of weight ratio of amine to bentonite on oil removal, the equilibrium oil concentrations of treated water were plotted against amine to bentonite weight ratio figure 8. Mixer speed used for these experiments was 450 rpm, time 1 hour, quantity of prepared organoclays 20g for amine ratio 10 g amine/100g bentonite and 15g for amine ratios 20, 30 and 38 g amine/100g bentonite. One liter of wastewater was used with initial concentration of (1450 – 1512) mg/L. It can be seen clearly from figure 8 that the ratio of amine to bentonite has a significant effect on the oil removal efficiency where the concentration of oil decreases from 117 to 8.8mg/L as the amine ratio in organoclay increases from 10 to 38g amine/100g bentonite. The best amine ratio was 30g amine/100g bentonite, where oil concentration decreased to 1 mg/L.

Figure 9 shows the effect of amine ratio for initial concentration of oil of (255 – 264 mg/L). Similar effect is observed from this figure, where the best amine ratio was 30g amine/100g bentonite for which oil concentration decreased to 1 mg/L.

The weight ratio of amine to bentonite was also represented in term of cation exchange capacity (CEC). The cation exchange capacity for bentonite is 80 meq/100g bentonite. Weight ratio of amine to bentonite was calculated from its relation with cation exchange capacity percentage, where 80 meq/100g bentonite represnts 100% CEC. The results cited in table 5 and appropriate equation to satisfy these results is found to be:

$$\text{g amine/100g bentonite} = 0.256 \times \%\ \text{CEC} \quad (1)$$

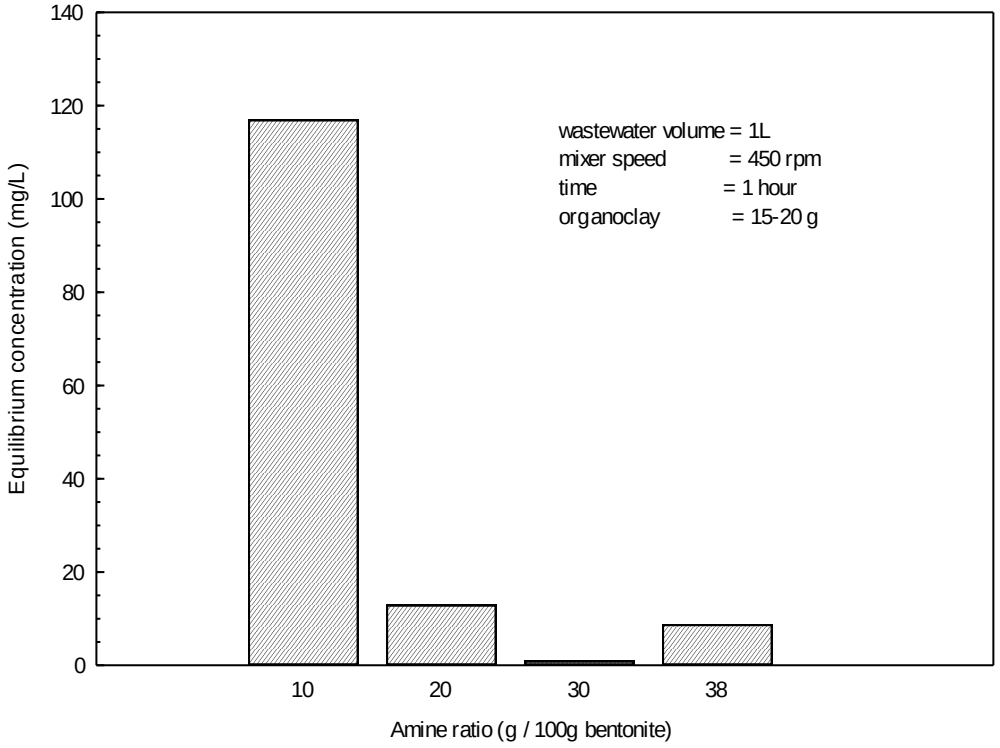

Fig. 8 Effect of amine to bentonite weight ratio on equilibrium concentration ($C_\circ$ = 1450–1512mg/L).

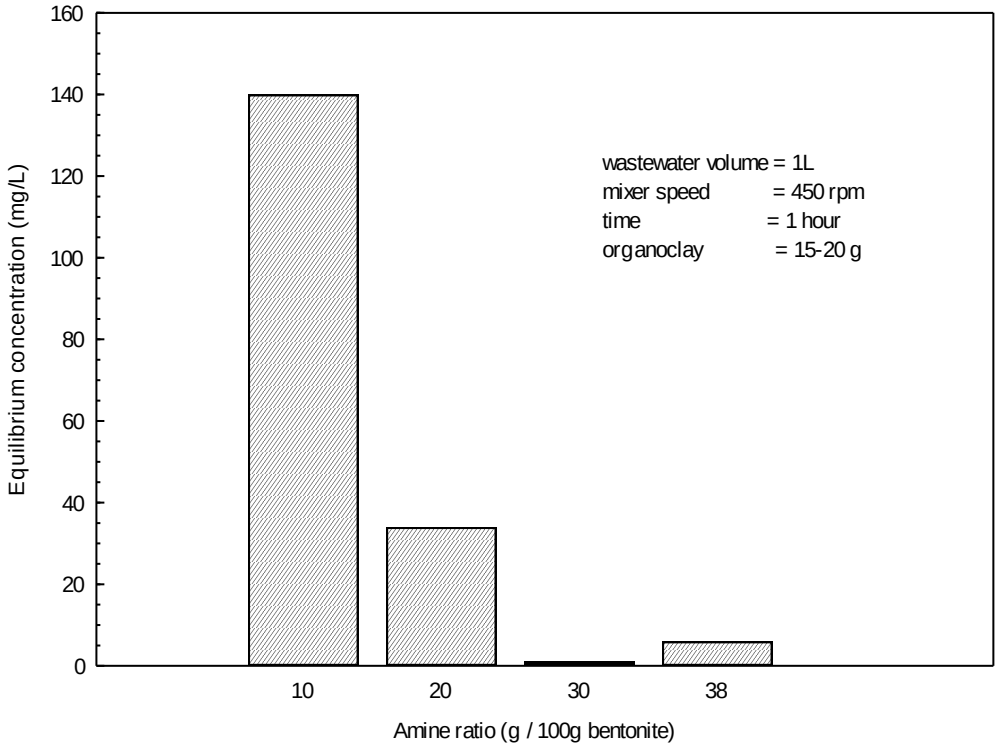

Fig. 9 Effect of amine to bentonite weight ratio on equilibrium concentration ($C_\circ$ = 255–264 mg/L).

Table 5. Amounts of amine used for preparation of bentonite organoclay (100% CEC equivalent to 25.6 g amine / 100g bentonite; CEC for bentonite = 80 meq/100g bentonite)

%CEC	0	39.1	78.12	117.18	148.4
g amine/100g bentonite	0	10	20	30	38

Figure 10 represents the effect of cation exchange capacity (%CEC) on the adsorption capacity.

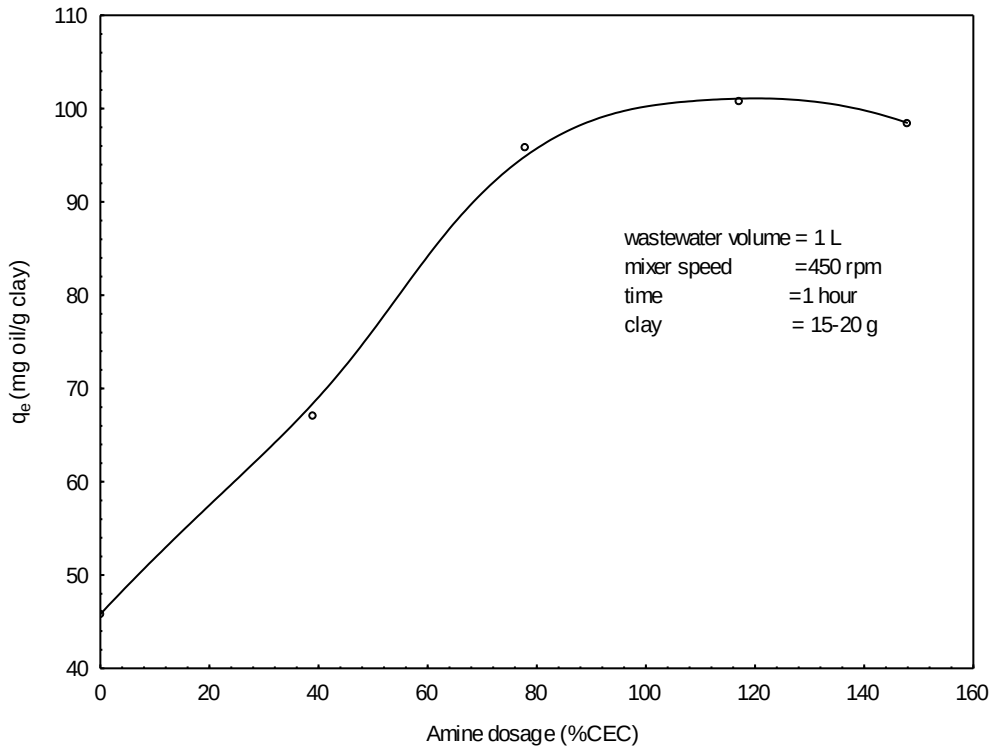

Fig. 10 Effect of amine dosage (%CEC) on adsorption capacity of organoclay ($C_\circ$ = 1450–1512mg/L).

Increasing amine dosage causes the increase of adsorption capacity of organoclay. 30g amine/100g bentonite (117% CEC) shows the maximum oil removal. Oil adsorption increased rapidly in the range from 0 to 78.12% CEC, above which the amine dosage had small effect on adsorption capacity.

EFFECT OF MIXER SPEED

To show the effect of mixer speed on the removal of oil from wastewater by organoclay, four experiments were conducted for the mixing speed 50, 150, 250, and 450 rpm. Initial oil concentration was 1221 mg/L, time 0.5 hour, and 15g organoclay of 30g amine/100g bentonite added to 1 litter of wastewater. The results is shown in figure 11.

Oil concentration decreases as mixer speed increases and the lowest oil concentration (below 8 mg/L) observed for mixer speed higher than 250 rpm. Oil concentration decreases to 3.2 mg/L for mixer speed 450 rpm.

The results of the effect of mixer speed is not surprising, where oil concentration decreases as mixer speed increases due to the decreasing in the resistance to mass transfer for oil from bulk of the wastewater to the surface of organoclay. The resistance to mass transfer is due to the diffusion layer surround each particle of organoclay. Patel (2004) stated that the mass transfer mechanism for oil adsorption by organoclay is a two phase process and can be described as diffusion of oil from the oil-water emulsion to the surface of the organoclay and the adsorption of oil within the pore structure of the organoclay.

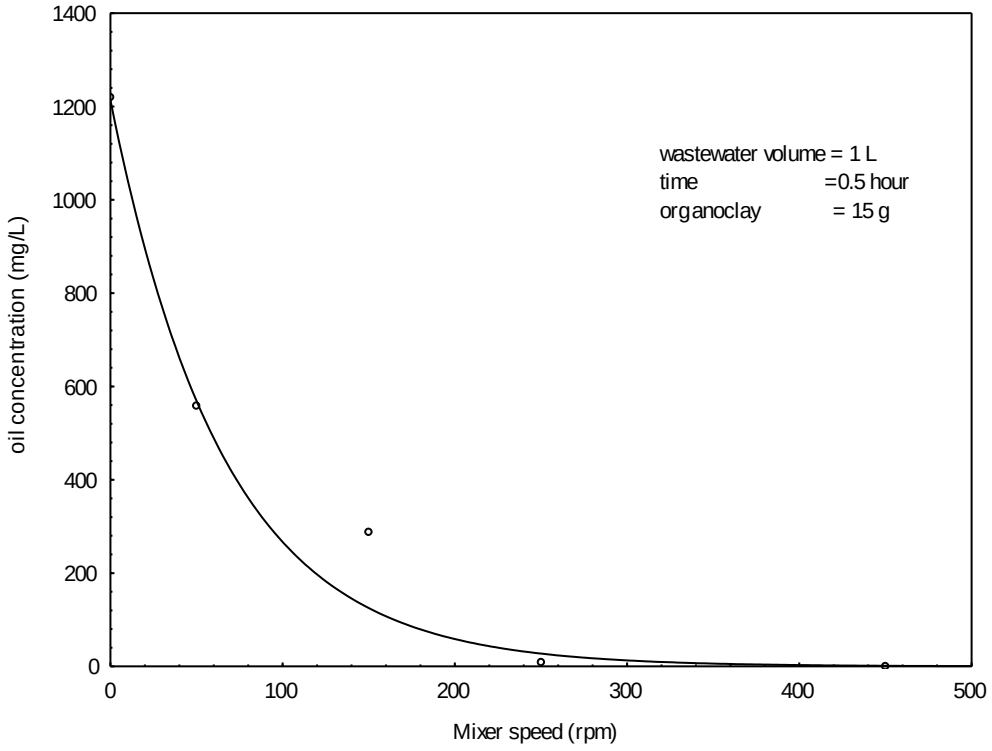

Fig. 11 Effect of mixer speed on oil removal using organoclay.

BATCH KINETICS STUDY

The plots of oil concentration versus time for initial oil concentration 1512 and 230 mg/L are shown in figures 12 and 13, respectively. In these experiments 15g organoclay of 30g amine/100g bentonite was added to 1 liter of wastewater and mixer speed fixed at 450 rpm.

From these plots, the equilibrium time was found to be 30 minutes for both concentrations. Also, it can be seen from these plots that adsorption of oil by organoclay included two phase adsorption fast followed by slow rate adsorption . The elapsed time for the rapid adsorption rate was 10 minutes. The residual oil concentrations of 1.6 and 1.2 mg/L were observed after the rapid adsorption phase for initial concentrations of 1512 and 230 mg/L respectively.

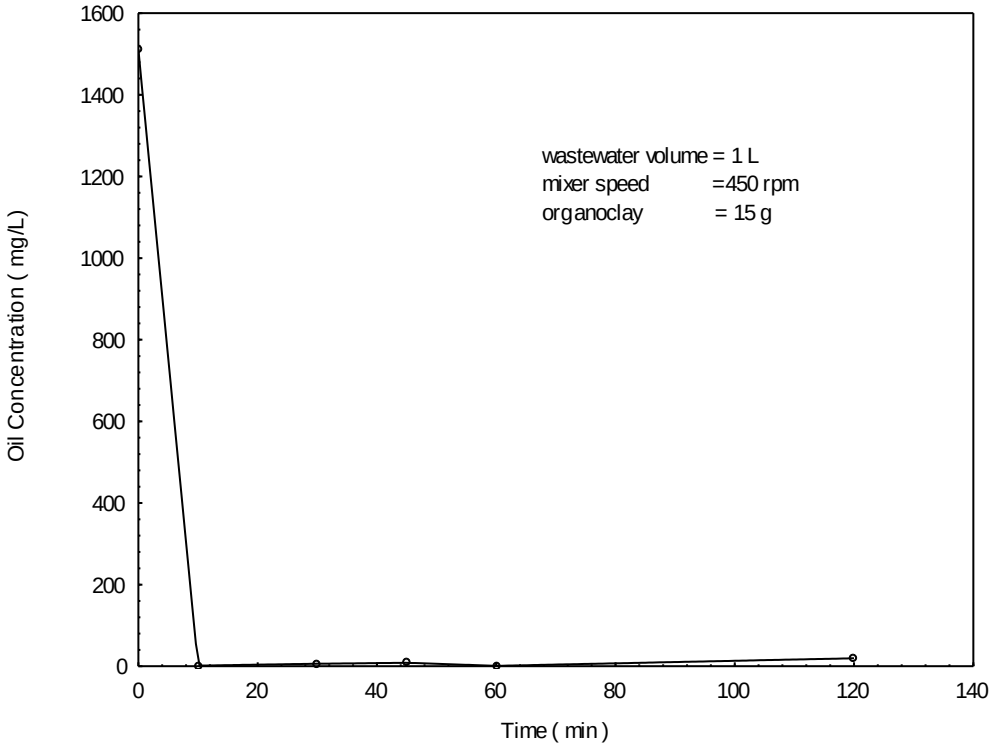

Fig. 12 Equilibrium time for the adsorption of oil by organoclay ($C_\circ$ = 1512mg/L).

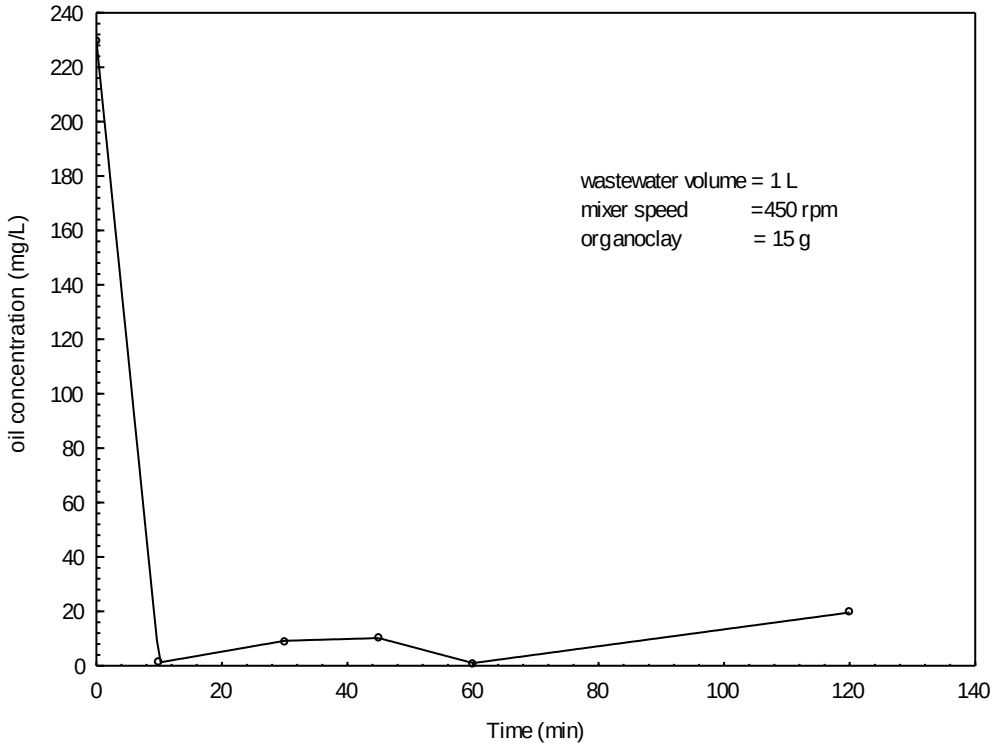

Fig. 13 Equilibrium time for the adsorption of oil by organoclay ($C_\circ$ = 230 mg/L).

Batch kinetic data was fitted to the Lagergren eq. (2) and Ho et al. eq. (3) models (Ho and McKay 1999; Ho et al. 1996) by non-linear regression analysis using software "STATISTICA".

$$q_t = q_e - q_e \exp(-kt) \quad (2)$$

$$\frac{t}{q_t} = \frac{1}{2k'q_e^2} + \frac{t}{q_e} \quad (3)$$

Where:

k = equilibrium rate constant of sorption (1/h);
k' = second-order reaction rate constant for adsorption (g/mg.h);
q_e = amount of metal ion adsorbed at equilibrium (mg/g); and
q_t = amount of metal ion adsorbed (mg/g) at any given time t (h)

Tables 6 and 7 show the Lagergren and Ho et al. models and parameters for the adsorption of oil by organoclay for initial oil concentrations 230 and 1512 mg/L. The Lagergren and Ho et al. models are plotted in figures 14 and 15 for both initial concentrations.

Table 6. Lagergren and Ho et al models for the adsorption of oil by organoclay.

Description	Equation	Correlation coefficient (r)
C_o = 230 mg/L		
Lagergren model	q_t =14.78436-14.78436 exp (-3.9986 t)	0.99713
Ho et al. model	t/q_t =1/[2×21.8776)(14.8126)2]+t/14.8126	0.99678
C_o = 1512 mg/L		
Lagergren model	q_t =100.307-100.307exp (-72.112 t)	0.999939
Ho et al. model	t/q_t =1/[2×17.51504)(100.3683)2]+t/100.3683	0.999930

Table 7. Parameters calculated using Lagergren and Ho et al. model for the adsorption of oil by organoclay

Description	Lagergren model		Ho et al. model	
	k (1/h)	q_e (mg/g)	k' (g/mg.h)	q_e (mg/g)
C_o = 230 mg/L	53.9986	14.78436	21.8776	14.8126
C_o = 1512 mg/L	72.112	100.307	17.51504	100.3683

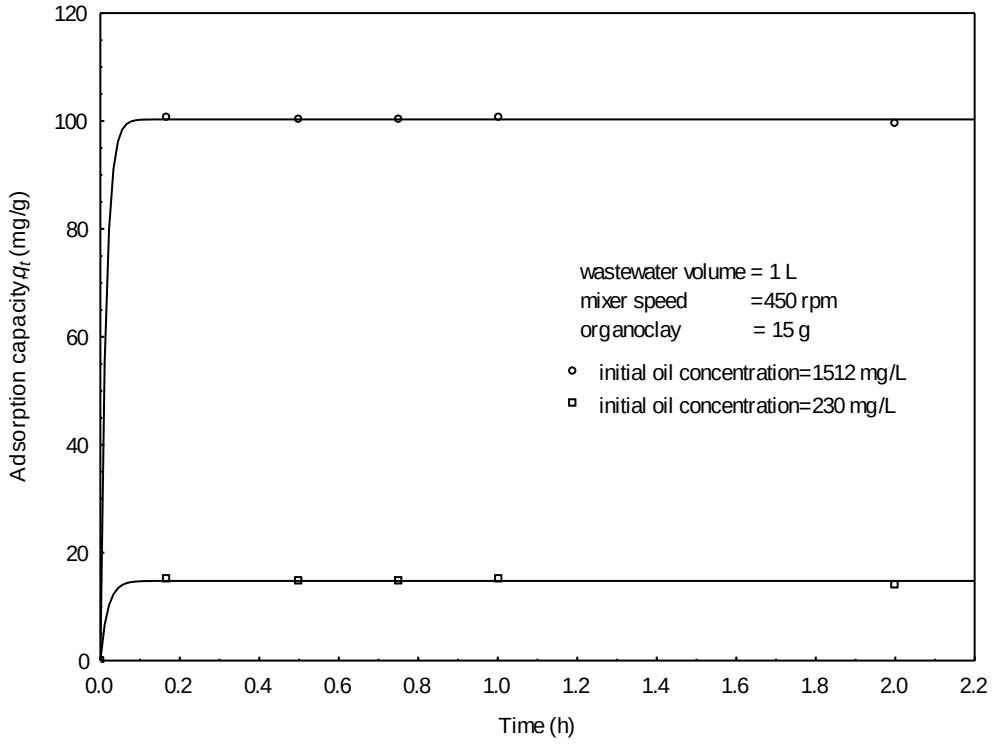

Fig. 14 Lagergren plot for the adsorption kinetics of oil by organoclay

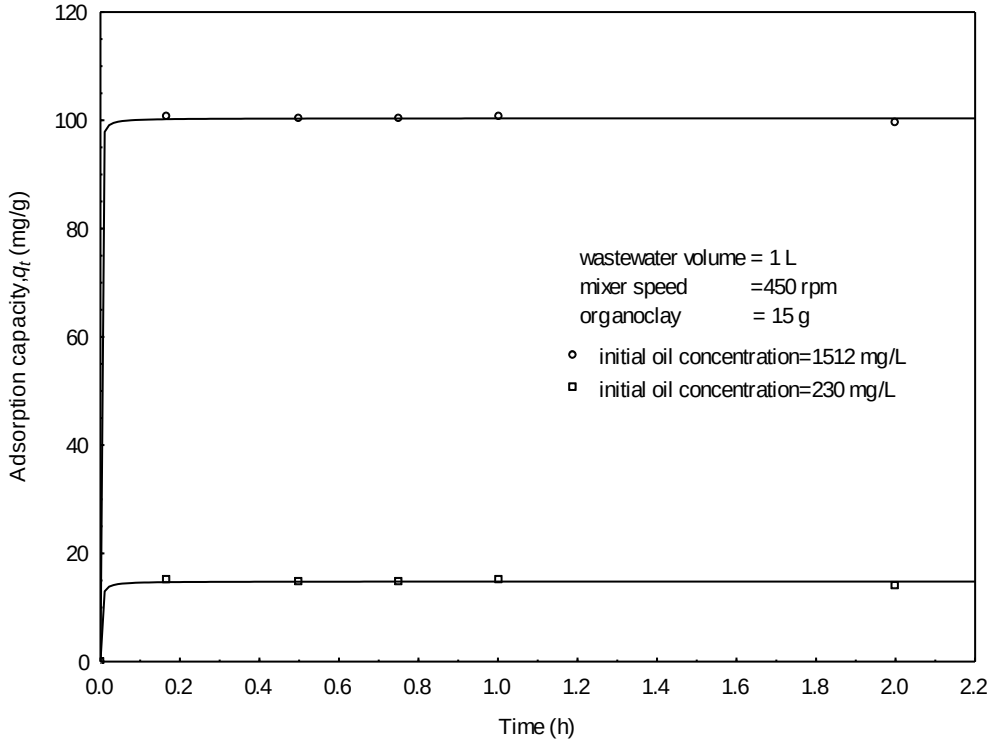

Fig. 15 Ho et al. plot for the adsorption kinetics of oil by organoclay

Based on the correlation coefficient values (r > 99%), it was found that the adsorption kinetics for oily wastewater concentrations of 230 and 1512 mg/L can be will described by lagergren and Ho et al. model as well.

BATCH ISOTHERM STUDIES

Several experiments were performed to study the isotherm of oil adsorption by organoclay. The quantity of organoclays were varied between 1 to 15 g and the concentration of oil in treated water was measured for each experiment. The organoclay used was 30 g amine/100 g bentonite and the mixer speed was 450 rpm, and time 0.5 hour. One liter of wastewater with oil concentrations of 245 and 1512 mg/L were used.

From these experiments the adsorption capacity of organoclay, mg oil adsorbed/ g organoclay (x/m), were calculated and plotted versus oil concentration by using a non – linear isotherm models Freundlich eq. (4), Langmuir eq. (5) and BET eq.(6) (Reynolds and Richards 1996).

$$\frac{x}{m} = kC_e^{\frac{1}{n}} \tag{4}$$

$$\frac{x}{m} = \frac{abC_e}{1+aC_e} \tag{5}$$

$$\frac{x}{m} = \frac{ACX_m}{(C_s - C)[1+(A-1)\frac{C}{C_s}]} \tag{6}$$

Where:

x = mass of solute adsorbed to the solid (mg);
m = mass of adsorbent used (g);
k = Freundlich equilibrium constant indicative of adsorptive capacity;
n = Freundlich constant indicative of adsorption intensity;
C_e = concentration of solute in solution in equilibrium (mg/L);
a = Langmuir constant; the amount of solute adsorbed per unit weight of an adsorbent in forming a complete monolayer (L/mg);
b = Langmuir constant (mg/g);
A = a constant describing energy interaction between the solute and the adsorbent surface;
X_m= amount of solute adsorbed in forming a complete monolayer (M/M);
C = concentration of solute in solution at equilibrium (M/L_n^3) in BET model; and
C_s = saturation concentration of solute in solution (M/L_n^3).

The non–linear estimation was performed using the "STATISTCA" and shown in figures 16, 17 and 18. The details of the regression equations obtained for the Langmuir, the Freundlich and the BET isotherms for the adsorption of oil from different oily waters by the organoclay are presented in tables 8 and 9.

From the statistical analysis (high values of the correlation coefficients) it was found that generally the adsorption of oil by organoclay could be well described by the all three isotherm models (Freundlich, Langmuir and BET isotherm). The correlation coefficients were in the range of 92-94% for initial oil concentration 245 mg/L, while it is in the range of 91- 92% for initial oil concentration 1512 mg/L.

Maximum adsorption capacity 641.8 mg oil/g organoclay was found for initial oil concentration 1512 mg/L which represents 64.18% of the weight organoclay. Alther (1995,

1996b, 2002) reaches oil adsorption capacity up to 70% of the organoclay weight, and he stated that organoclays are capable of removing emulsified oils from water by up to about 100 percent.

Table 8. Regression equations of various isotherm models for oil adsorption by organoclay.

Description	Equation of regression	r
C_o = 245 mg/L		
Freundlich	$x/m = 1.3842\ C_e(1/0.808)$	0.93981
Langmuir	$x/m = (0.00127\times2624.677\ C_e)/(1+0.00127C_e)$	0.92509
BET	$x/m=(0.7478\times856.3933C_e)/(C_s-C_e)\times[1+(0.7478-1)\ C_e/C_s]$	0.94310
C_o = 1512 mg/L		
Freundlich	$x/m = 68.23774\ C_e(1/2.41173)$	0.91648
Langmuir	$x/m = (0.03597\times658.377C_e)/(1+0.03597C_e)$	0.90869
BET	$x/m=(68.53088\times560.8312C_e)/(C_s-C_e)\times[1+(68.53088-1)C_e/C_s]$	0.91583

The values of parameters in the isotherm models applied to oily waters are presented in table 9.

Table 9. Values of isotherm constants for bentonite organoclay

Description	Freundlich		Langmuir		BET	
	k	*n*	*a*	*b*	*A*	X_m
C_o = 245 mg/L	1.3842	0.808	0.00127	2624.677	0.7478	856.3933
C_o = 1512 mg/L	68.2377	2.41173	0.03597	658.377	68.53668	560.8312

Depending on the isotherm figures, the strategy of choice of the adsorption capacity for the organoclay is that maximum adsorption capacity must be selected to get minimum oil concentration for the treated water. The weight of organoclay used for oil removal is calculated from the selected adsorption capacity at the desired final oil concentration of the treated water. Also isotherm equations are used with known initial and final oil concentration to calculate x/m from which the weight of oganoclay can be determined. These calculations can be used successfully in the scale up of adsorption unit (design of batch adsorption unat).

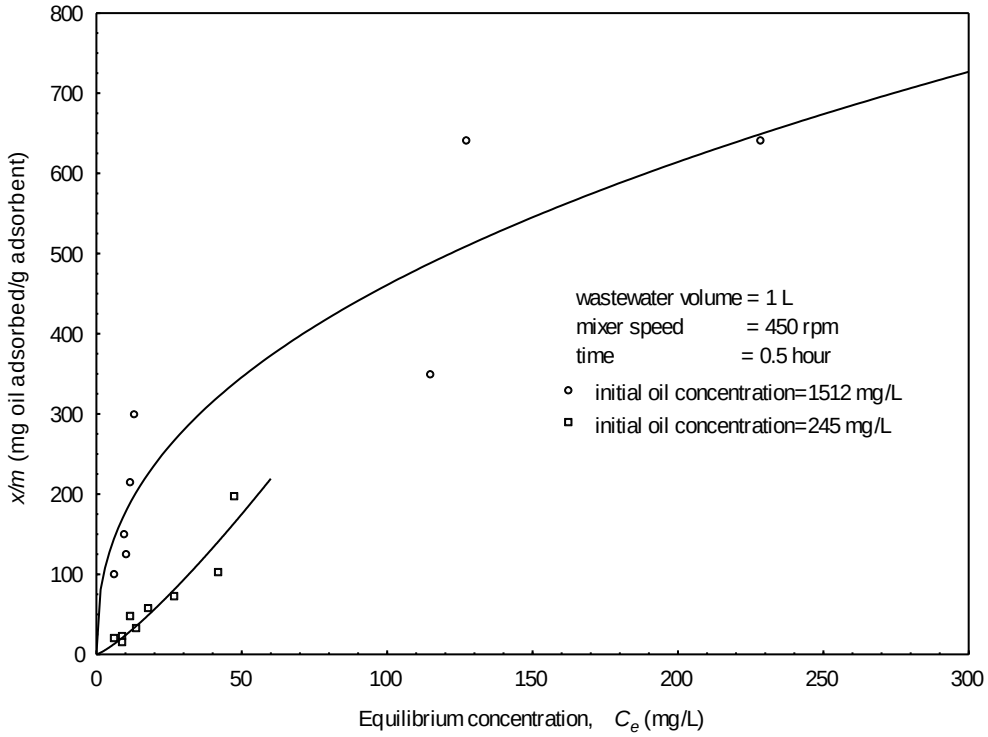

Fig. 16 Freundlich isotherm for the adsorption of oil by organoclay

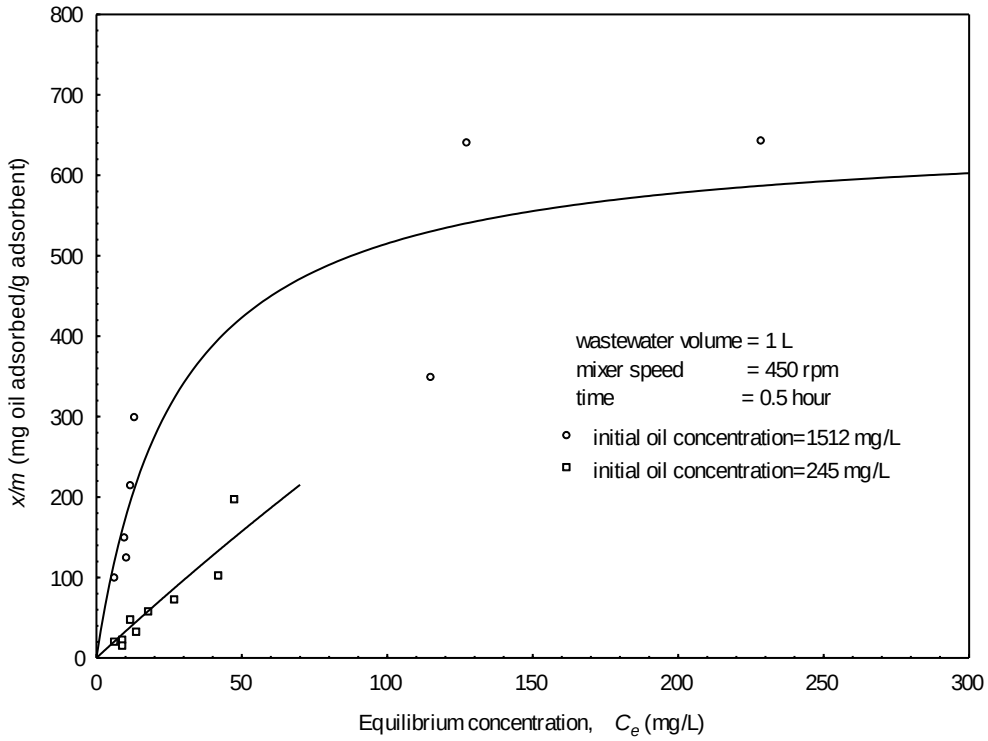

Fig. 17 Langmuir isotherm for the adsorption of oil by organoclay

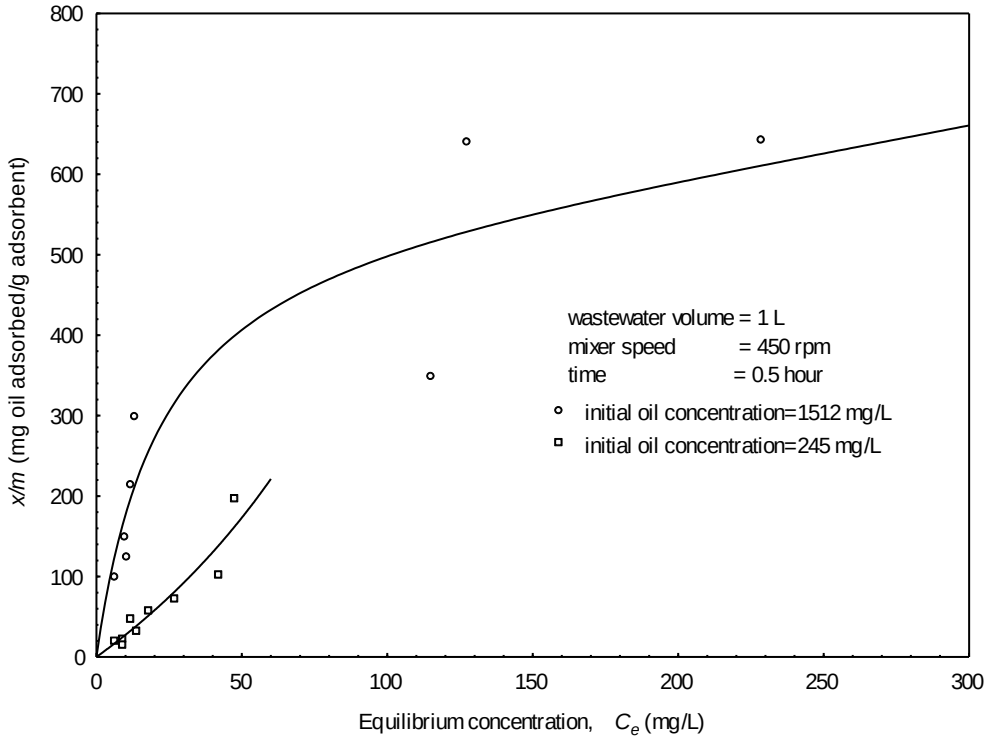

Fig. 18 BET isotherm for the adsorption of oil by organoclay

CONCLUSIONS

- Iraqi Bentonite has a good capability for oil removal where decreasing the oil concentration in waste water from 871 to 183.2 mg/L using maximum 20g/L of bentonite. But the oil concentration can not be achieved to decrease below the recommended limit for oily wastewater discharge (10 mg/L).
- Spectrophotometer measurements (XRD and FTIR) gave good approximation for the exchange of the quaternary amine (hexadecyltrimethyl ammonium HDTMA+ cation) in specify place of ca^{++} at the surface of bentonite to obtain organoclay.
- The quantity of quaternary amine that used in preparation of organoclay has very appreciable effect on the removal of oil from wastewater. As the weight ratio of quaternary amine in the organoclay increases then the oil removal increases. 15g/L of organoclay with amine ratio of 30g amine/ 100g bentonite is recommended to remove oil from wastewater
- Mixer speed has a considerable effect on the removal of oil from wastewater. Oil concentration falls from 1221 mg/L to 3.2mg/L when mixer speed increased from 0 to 450 rpm respectively for operating time of 0.5 hour.
- Batch kinetic studies showed that equilibrium time was reached within 0.5 hour of contact between the organoclay and wastewater.
- Results clearly followed that both pseudo first order (Lagergren) and pseudo second order (Ho et al.) models provided realistic descriptions of the kinetics of adsorption of fuel oil by organoclay. The correlation coefficients (r) obtained from "STATISICA PROGRAM" for the two models exceed 99%.

- The isotherm models (Freundlich, Langmuir and BET) gave excellent fitting for the adsorption capacity of organoclay versus equilibrium concentration of oil . The correlation coefficients (r) obtained from "SATISTICA PROGRAM" for these models were in the range of 90.87- 91.65% and 92.51- 94.31% for oil concentrations of 1512 and 245 mg /L respectively.
- Organoclay prepared from Iraqi bentonite is very effective in removing oil from wastewater. The best results obtained for the removal of oil from wastewater with concentration of 1512mg/L are 15g of prepared organoclay having 30g amine /100g bentonite added to 1 liter of wastewater for 0.5 hour and using mixing speed of 450 rpm to reduce the concentration of oil below 10mg/L which is the standard limit for discharge oily wastewater.

REFERENCES

- Alther, G. R. (1996a). *Hazardous Materials Management*, August /September, 45- 47.
- Alther, G. R. (1996b). *Environmental Solutions*, 9, 22-25.
- Alther, G. R. (2002). *American Water Works Association Journal*, 94, 115- 121.
- Bala, P., Samantary, B. K. and Sirvastava, S. K. (2000). *Materials Research Bulletin*, 35, 1717-1724.
- Cadena, F. (1989). *Journal of Environmental Engineering*, 115
- Slejeiko, L. (1981). Adsorption Technology: A step by step Approach to process Evaluation and Application, Marcel Dekker Inc., New York.

Carmody, O., Frost, R., Xi , Y. and Kokot, S. (2007). *Journal of Colloid and Interface Science*, 305,17-24

- Diaz, F. R. (1999). Processing of the 43th Brazilian congress of ceramics, Jun 2-5, Florianopolis, Brazil (cited in Diaz, F. R. (2005)).
- Diaz, F. R. (2001). *Key Engineering Materials*, 189, 203- 207.
- Diaz, F. R. (2005).*Materials Research*, 8, 77-80.
- Ho, Y. S. Wase, D. A. J. and Forster, C.F. (1996). *Environmental Technology*, 17, 71-77.
- Janes, W. F. and Boyd , S. A. (1991). *Clays and Clay Minerals*,39, 428-436
- Kowalska, M., Guler, H. and Cocke, D.L. (1994). *The Science of the Total Environment*, 4, 223- 240.
- Lagaly, G. (1984). Clay Organic Reactions, Interactions. Philosophical Transactions. Royal Soc., London, England.
- Mathavan, G. N. and Viraraghavan, T. (1989). *Water, Air, and Soil pollution*, 45, 17-26.

- Moazed, H. and Viraraghavan, T. (2005). *Practice Periodical of hazardous, toxic and radioactive waste management*, 9, 130-134.

- Patel, C. (2004). Management of produced water in oil and gas operations. M.S. dissertation. Texas A and M University, College Station, Texas.

- Reynolds, T.D. and Richards, P.A. (1996). Unit operations and processes in environmental engineering. PWS publishing Co. Boston, U.S.A.

- Standard Methods for Examination of water and wastewater, (1995). 19th Ed., American Public Health Assoc., Washington, D.C.

- Zunan, Q., Yi, Z. and Yuqiao, F. (1995). *Water Quality Research Journal of Canada*, 30, 89-99.

REGENERATION OF SPENT TRANSFORMER OIL

Abdul-Halim Adbul-Karim Mohammed, Mohammed Abbas Kadhum
Chemical Engineering Department-University of Baghdad

ABSTRACT

The regeneration of spent transformer oil taken from Al-Dora power station was studied. The regeneration process includes settling, filtration, thermo vacuum evaporation, and clay treatment. The settling was done by gravity to remove the mechanical particles. The filtration was done by filter paper [whatman quality1 and 18.5 cm diameter]. Thermo vacuum evaporation at 175˚C and 241 mm Hg was used for removing the dissolved water and light petroleum impurities. The clay treatment was used for final improvement of transformer oil properties. Iraqi clay, Algerian clay and zeolite (A) were used and the results were compared. It was studied the effect of clay to oil ratio and the mixing time on the water content, break down voltage and the acidity. It was considered that the best operation conditions are clay to oil ratio 2/100, and time 5 min. In these conditions the oil has water content 32 ppm, break down voltage 55 kV and acidity 0.028 mg KOH/g oil. It was found that Algerian clay gives better improvement than zeolite and Iraqi clay using the same operating conditions. Langmuir, Freundlich, and the combination of them adsorption isotherms were studied in this investigation and It was found that Freundlich adsorption isotherm well represented the adsorption of water on clay comparing with others isotherms.

الخلاصة

تم دراسة عملية إعادة استخدام زيت المحولات المستهلك والذي تم أخذه من محطة كهرباء الدورة. إن عملية إعادة الاستخدام تتضمن ترسيب, تصفية, تبخير بواسطة الحرارة والفراغ, ومعاملة بواسطة الأطيان. تم الترسيب بواسطة الجاذبية الأرضية لإزالة العوالق الميكانيكية. عملية التصفية بواسطة ورق تصفية (واتمان نوعية 1, قطر 18.5سم) استخدمت لإزالة الشوائب التي لا يمكن إزالتها بالترسيب. التبخير الحراري الفراغي في 175˚م و 241 مليمتر زئبق استخدمت لإزالة الماء الذائب و الملوثات النفطية الخفيفة المسببة زيادة الحامضية وقلة العزل للزيت. المعالجة الطينية إستعملتْ للتحسينِ النهائي لخواص زيت المحوّلاتِ.الطين العراقي, الطين الجزائري, والزيولايت نوع (أ) استخدموا للمعاملة النهائية وتم مقارنة النتائج. تم دراسة تاثير نسبة الطين الى الزيت ووقت المزج على خواص المحتوى المائي والعازلية والحامضية. قَدْ يَعتبرُ إن أفضل شروطِ العمليةِ إن نسبة الطين إلى الزيت هي 2\100، وبُوقّت 5 دقيقة. في هذه الشروط يكون للزيت محتوى مائي 32 جزء بالمليون ، والعازلية 55 ك ف, وحموضة 0.028 ملغم KOH \غم زيت. لقد وجد ان الطين الجزائري افضل من الزيولايت والطين العراقي باستخدام نفس الظروف التشغيلية. صيغ الامتزاز لونكماير, فريندلج, وصيغة اتحادهما قد دُرِسَت في هذا البحث وقد وجد ان صيغة فريندلج للامتزاز تصف عملية امتزاز الماء على الطين أفضل من الصيغ الأخرى.

KEY WORDS: Spent Lubricating Oil, Transformer Oil, Spent Mineral Oil, Regeneration, Insulating Oil, Clay Treatment,

INTRODUCTION

Transformer oil is one of the lubricating oils and it has several main functions in a transformer; like cooling and electrical insulation. Besides those there are several secondary functions and properties expected from transformer oil [1]. Impurities in transformer oil are unavoidable, the primary impurities are moisture and dissolved gases and usually accompanied by solids [2]. Used lubricating and industrial oils present a serious pollution problem and it was estimated that less than 45% of available waste oil was collected worldwide in 1995 and classified according to current world regulations as hazardous waste due to the effects that they can have both on health and the environment [3, 4]. A large range of used (waste) oils can be recycled and recovered [5]. The change in the composition of transformer oil in operation is related to the chemical processes that occur in the dielectric medium under the action of temperature and high voltage. This leads to the oxidation and decomposition of chemical compounds that enter into the composition of the oil and to the appearance in it of new gases (CO, CO_2, and volatile hydrocarbons), liquids (aldehydes, ketones, alcohols, acids, ethers, resins, and water), and solids (asphaltenes and carbenes) chemical products [6]. Water can be present in oil in a dissolved form, as tiny droplets mixed with the oil (emulsion), and in a free state at the bottom of the container holding the oil [7]. Regeneration is the procedure followed if oil purification is insufficient to return the oil to an acceptable condition and usually done by specialist companies [2, 8]. This work deals with decreasing the mechanical impurities, water content, and acidity and increasing the break down voltage of spent transformer oil, by settling, filtration, thermo vacuum evaporation, and clays treatment.

MATERIALS AND METHODS

A-Materials

-Spent Transformer Oil: The raw material was the spent oil of type (Diala-D), Germany origin. This oil was used in Al-Dora power station for about 15 years in transformer to change the voltage from 6600 V to 380 V. The spent transformer oil has the properties illustrated in table 1.

-Adsorbents: The Iraqi clay manufactured by the State Company for Geological Survey and Mining, Algerian clay (from Al- Dora refinery) and zeolite type (A) were used for final treatment of spent transformer oil. Table 2 shows the properties of these clays, while figure 1 shows the X-ray analysis for the zeolite.

Table 1 Properties of spent transformer oil

The property	The value
Water content, ppm	50
Break down voltage, kV	30
Acidity, mg KOH/g oil	0.1122
Specific gravity at 60/60˚F	0.87167

Table 2 Properties of clays

The property	The value (Iraqi clay)	The value (Algerian clay)
Particle size, micro meter	Greater than 85	Greater than 85
Ignition loss at 100˚C, wt %	8	6
SiO_2, wt %	48	78
Al_2O_3, wt %	34	12
Fe_2O_3, wt %	4	2
MgO, wt %	2	1
CaO, wt %	4	1

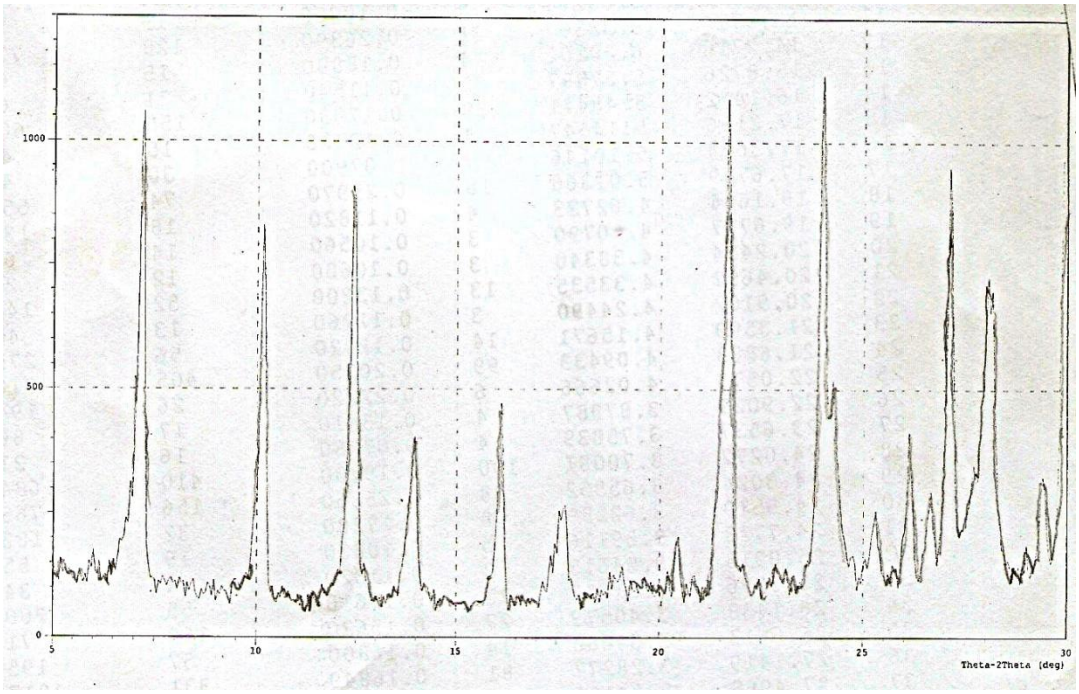

Figure 1 X-ray analysis for the zeolite

B-Methods

- Settling: The mechanical particles would be found as impurities, the spent oil was settled for a week in a reservoir. Settling was done by gravity because the mechanical particles are heavier than oil.

- Filtration: The fine particles could not be settled by gravity so the filtration is very important step because it removes any remaining particles. The filter papers (WHATMAN type and quality 1, 18.5 cm diameter) were used for filtration. Figure 2 shows a photo for batch filtration unit. To calculate the quantity of the remaining particles on the filter paper, the paper washed by gasoline. The gasoline dissolved the oil from the filtration paper and then the filtration paper put in oven at 100 ˚C for 3 hours.

Figure 2 Photo of Batch Filtration Unit

- Thermo Vacuum Evaporation: This step took place at a temperature of 175˚C and a pressure of 241 mm Hg in a laboratory evaporation unit shown in figure 3. During the thermo vacuum evaporation light petroleum impurities was separated. The percentage of light petroleum impurities on the settled and filtered oil was 10.37 %.

Figure 3 Photo of Thermo Vacuum Evaporation Unit

-Adsorbents treatment: This is the final step of the treatment and used for final decreasing of water content in the oil. In this study the Algerian clay to oil ratio range

was 1/100 to 10/100 while contact time varied from 5 to 30 min. All tests were taken place at 80˚C. Iraqi clay was tested at ratio 2/100 at different contact times, while zeolite was tested at ratio 1/100 and different contact times (5 – 30 min.). 523 g of the oil produced from thermo vacuum evaporation was injected into flask and heated up to 80 ˚C. Then, the specified quantity of clay or zeolite was added during mixing for specific contact time. Figure 4 shows the unit of clay and zeolite treatment. After specific contact time the mixture of the oil and adsorbent filtered by filtration paper [WHATMAN quality 1, having a diameter 18.5 cm] using the filtration unit shown in figure 2.

Figure 4 Photo of Adsorbent Treatment Unit

The clay that produced from the adsorption process was washed by a gasoline to dissolve the oil deposited on the clay and on filter paper for the adsorbate estimation. The washed clay and filtration paper were put in the oven at 100˚C to evaporate the gasoline from them.

RESULTS AND DISCUSSION

-The Settling and Filtration Steps: The settling of spent transformer oil for one week resulted in 0.01% of mechanical impurities removal, while the filtration of the oil after settling removed 0.23 % of impurities. This means that the total percentage of mechanical impurities removed by settling and filtration is 0.24 %.

-The Thermo Vacuum Evaporation Step: The total light petroleum impurities removed during the thermo vacuum evaporation step was 10.37 % based on settled and filtered oil. This means that the percentage of oil produced from thermo vacuum evaporation was 89.61 % based on the original raw material. Table 3 shows the properties of the oil before and after thermo vacuum evaporation.

Table 3 The Basic Properties of Spent Transformer Oil Before and After Thermo Vacuum Evaporation

Property	Before thermo vacuum evaporation	After thermo vacuum evaporation
Water content, ppm	50	42
Break down voltage, kV	30	57
Acidity, mg KOH/g oil	0.112	0.028

-The Results of Clays and Zeolite Treatments: For reducing the water content down to acceptable value, clay treatment was used. The Iraqi clay was used in 2/100 clay to oil ratio and duration time (5 - 30 min) at 80˚C. The water content of oil decreased from 41 ppm to 39 ppm, this value is not acceptable by standard properties. So, the Algerian clay was used in this step. The operating conditions are clay to oil ratio (1/100 -10/100) and duration time (5 - 30 minutes) and temperature 80˚C. Zeolite was also used using 1/100 zeolite to oil ratio, duration time (5 -30 minutes) and temperature 80˚C. The basic properties of the transformer oil after Iraqi clay, zeolite and Algerian clay treatments were presented in tables 4, 5 and 6, respectively.

Table 4 Water content of transformer oil after Iraqi clay treatment for 2/100 clay to oil ratio

No.	Time, min	Water content, ppm
1	5	41
2	15	39
3	30	39

Table 5 Water Content of transformer oil after zeolite treatment for 1/100 zeolite to oil ratio

No.	Time, min	Water content, ppm
1	5	40
2	15	39
3	30	38

Table 6 Basic properties of transformer oil after Algiers clay treatment

No.	Clay to Oil Ratio	Time, min	Water content, ppm	B.D.V., kV
1	1/100	5	36	-
2		10	-	-
3		15	35.4	-
4		20	-	-
5		30	34	-
6	2/100	5	32	55
7		10	-	54
8		15	31	46
9		20	-	44.5
10		30	30	36.5
11	5/100	5	26	52.5
12		10	-	47
13		15	23	45
14		20	-	42
15		30	22	35
16	7/100	5	25	51.5
17		10	-	46
18		15	23	40
19		20	-	35
20		30	21	34
21	10/100	5	25	51
22		10	-	45
23		15	22	38
24		20	-	34
25		30	20	32

- Effect of Algerian Clay to Oil Ratio on Water Content: Figure 5 shows the effect of Algerian clay to oil ratio on the water content at different duration time. The increase of clay to oil ratio decreased the water content in the oil for the same contacting time because of the increasing of contact surface between the oil and the clay.

- Effect of Mixing Time on Water Content: Figures 4-6 – 4-8 show the effect of mixing time on the water content at different adsorbent to oil ratio. Whenever the contact time increases, the water content decreases for the same adsorbent quantity. Figure 6 shows a comparison between Algerian clay and zeolite treatments at different duration time. This figure shows that the Algerian clay is better than the zeolite in removing dissolved water. Figure 7 shows a comparison between the Iraqi clay and the Algerian clay. This figure illustrates that Algerian clay is better than the Iraqi clay. This may be because of the low percentage of silica in the Iraqi clay than the Algerian clay and the high percentage of Fe_2O_3, MgO, and CaO in the Iraqi clay as shown in table 2. The silica had a large adsorption area and it was a good adsorbent for the water

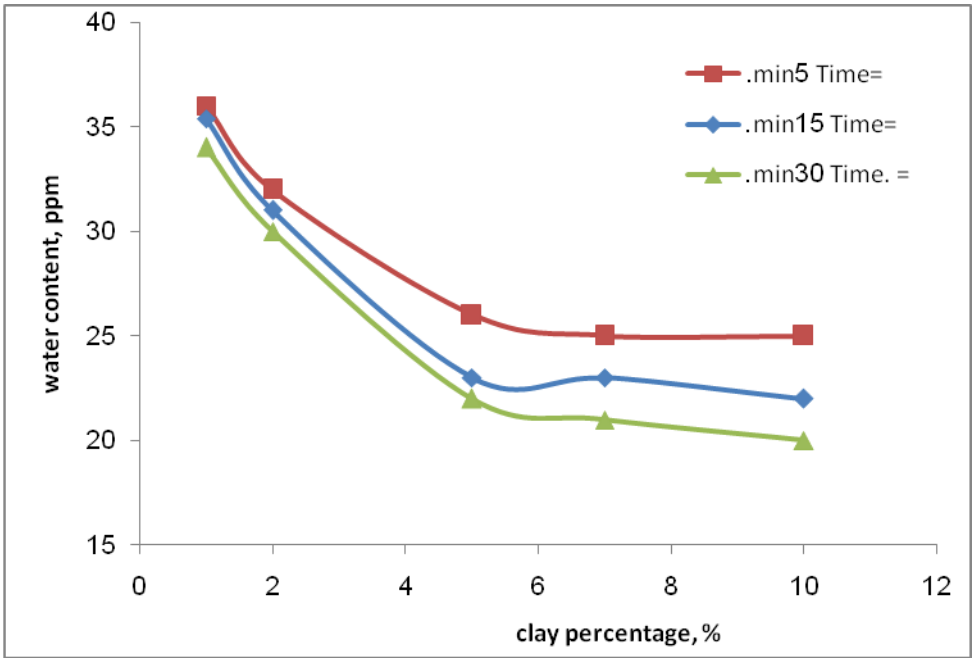

Figure 5 Effect of Algerian clay to oil ratio on the water content at different mixing times

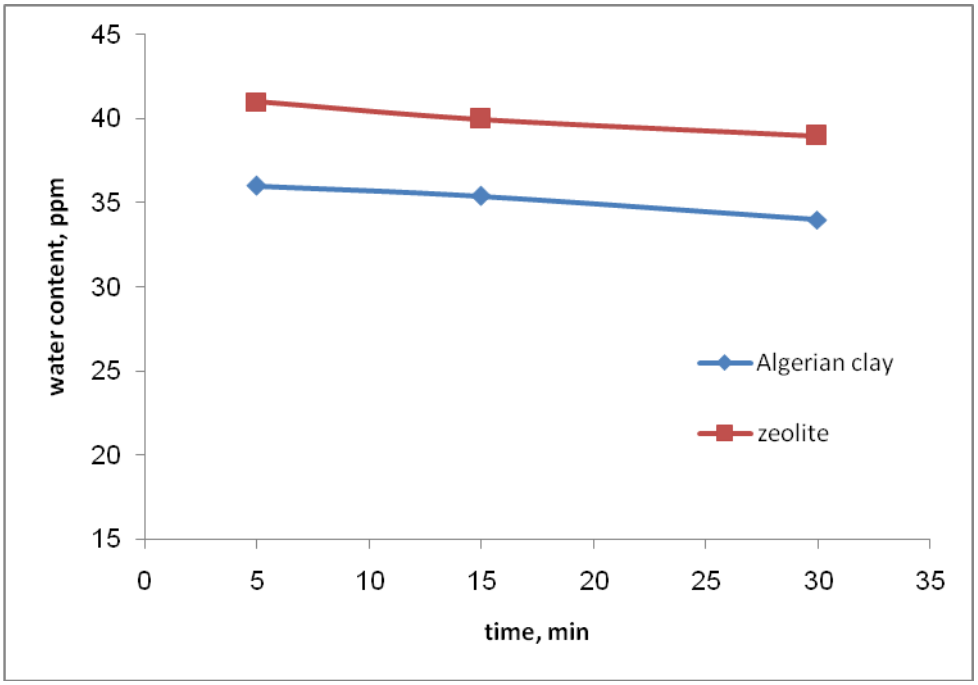

Figure 6 Effect of mixing time on the water content at 1/100 Algerian clay and zeolite to oil ratio

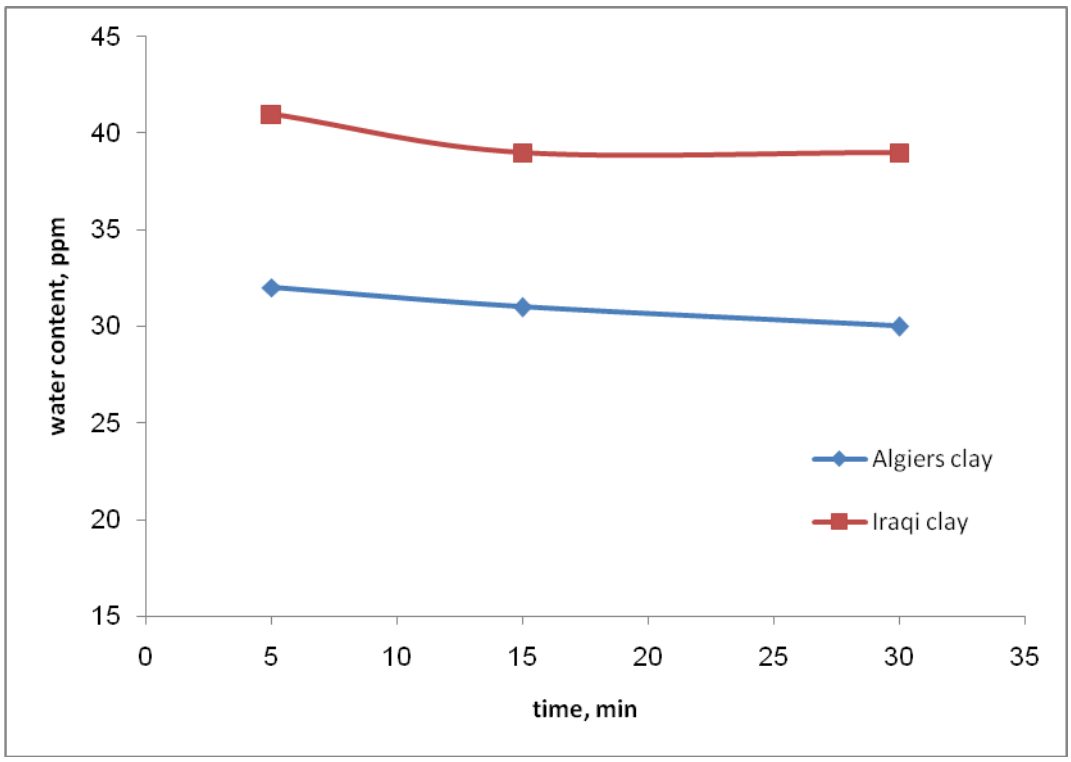

Figure 7 Effect of mixing time on the water content at 2/100 clays to oil ratio

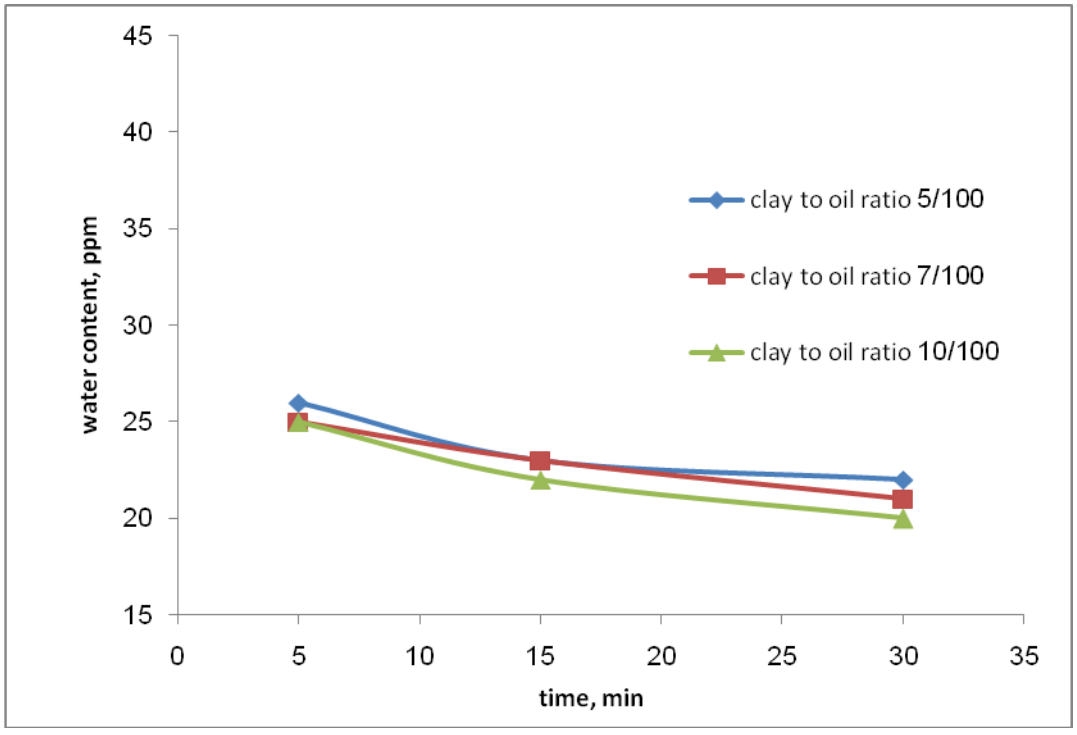

Figure 8 Effect of mixing time on the water content at 5/100, 7/100, 10/100 Algerian clay to oil ratios

- Effect of Algerian Clay to Oil Ratio on Break Down Voltage: Figure 9 shows the effect of clay to oil ratio on break down voltage at different contacting time. The more important conclusion from this figure that the increases in clay to oil ratio give decreases in break down voltage for the same duration time. This may be because the clay adsorbed the anti-oxidation additives presented in the oil.

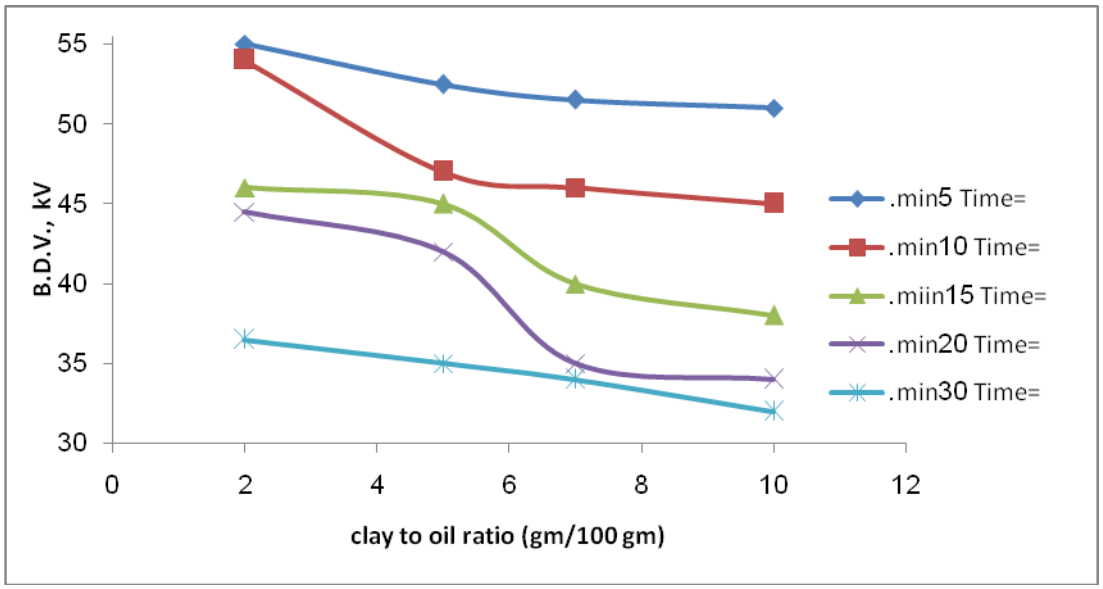

Figure 9 Effect of Algerian clay to oil ratio on the break down voltage at different mixing times

- Effect of Mixing Time on Break Down Voltage: Figure 10 shows the effect of mixing time on break down voltage. Whenever the mixing time increases, the break down voltage decreases at the same Algerian clay to oil ratio.

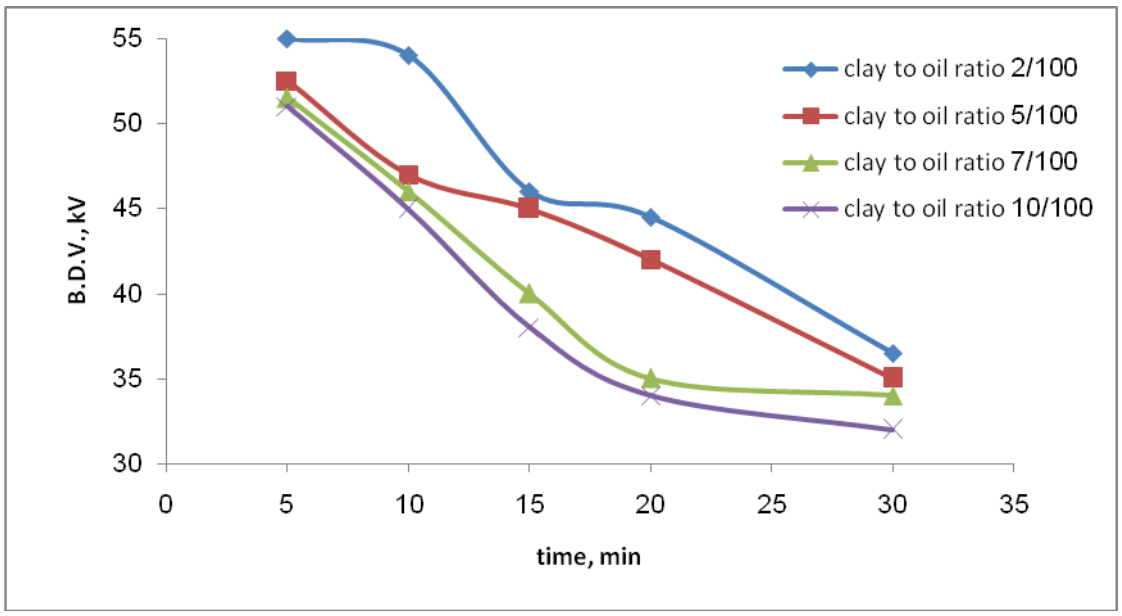

Figure 10 Effect of mixing time on break down voltage at different Algerian clay to oil ratios

- Acidity Values: Table 7 shows the acidity values for oil produced uses Algerian clay and zeolite treatments. The increasing of clay to oil ratio at constant duration time or increasing duration time for the same clay to oil ratio resulted a decrease in acid value of the oil. This is because the clay is a good adsorbent for the acidic impurities that found in the oil.

Table 7 Acidity values

No.	Clay to oil ratio	Time, min.	Acidity mg KOH/ gm oil
1	1/100	5	-
2		10	0.028
3		15	-
4		20	0.014
5		30	-
6	2/100	5	0.028
7		10	0.028
8		15	0
9		20	0.028
10		30	0.014
11	5/100	5	0.028
12		10	0.028
13		15	0.028
14		20	0.014
15		30	0.014
16	7/100	5	0.028
17		10	0.014
18		15	0.014
19		20	0
20		30	0
21	10/100	5	0.014
22		10	0.014
23		15	0
24		20	0
25		30	0
26	1/100 (zeolite)		-
27			0.028
28			-
29			0.014
30			-

- Color Improvement: The color of Algerian clay treated transformer oil with 10/100 clay to oil ratio was further improved by repeating clay treatment. The Algerian clay was used in this treatment using 35/100 clay to oil ratio and 80 ˚C for one hour. The color values for the spent oil, the oil treated in thermo vacuum evaporation and the improved color oil are 3.5, 6.3, and 0.4, respectively.

- **Conclusion**: The possibility of spent transformer oil regeneration was studied in four stages, these are settling, filtration, thermo vacuum evaporation, and clay treatment. Iraqi clay was used in 2/100 clay to oil ratio for 5 – 30 minutes duration time using a temperature 80 ˚C but it decreased the water content from 41 ppm to 39 ppm only. The study of Algerian clay treatment at 80 ˚C, duration time range 5 – 30 minutes and clay to oil ratio 1/100 – 10 /100 considerably decreases the water content. It could be considered that the best operating conditions for Algerian clay treatment are 2/100 clay to oil ratio and 5 minutes duration time. The values of water content, acidity and break down voltage in the above mentioned conditions were 32 ppm, 0.028 mg KOH/ g oil and 55 kV, respectively. Zeolite treatment at 1/100 zeolite to oil ratio and 5 – 30 minutes duration time using the same temperature (80 ˚C) gave worse improvement comparing with Algerian clay treatment. Freundlich and Langmuir isotherms and the combination of them were applied to calculate the adsorption rates and it was found that Freundlich adsorption isotherm well represented the adsorption of water on clay comparing with others isotherms.

REFERENCES

- Eklund, M., Sweden 2006, "Mineral Insulating Oils; Functional Requirements Specifications and Production", Nynas Naphthenics ABSE-149 82 Nynashamn, IEEE International Symposium on Electrical Insulation, 68-72.

- Hodgson, P., "Transformer Oil Processing", Redragon Oil & Gas Systems International Inc., Cambridge, Ontario, Canada www.redragon.com**.**

- Luki´c, J., Orlovi´c, A., Spiteller, M., Jovanovi´c, J., Skala, D., 2006, "Re-refining of waste mineral insulating oil by extraction with *N*-methyl-2-pyrrolidone", Separation and Purification Technology, 51, 150–156.

- Regional Activity Centre for Cleaner Production (RAC/CP), 2000, "Recycling Possibilities and potential uses of used oils".

- Basel convention technical guidelines on used oil re-refining or other re-uses of previously used oil no. 5, prepared by the technical working group of the basel convention and adopted by the third meeting of the conference of the parties to the basel convention in September 1995, Geneva.

- Zakharich, M., Zaitsev, I., Komar, V., Nikonovich, F., Ryzhkov, M. and Skornyakov, I., 2001, "Analysis of transformer oil using IR analyzers", Journal of Applied Spectroscopy, Vol. 68, No. 1, p 61.

- Groves, M. , 1990, " Maintenance Of Liquid insulation", power system maintenance manual, western.

- Lansdown, A.,1982, "Lubrication" first editon, Programon Press.

REMOVAL OF LEAD FROM SIMULATED WASTEWATER BY ELECTROCOAGULATION METHOD

Dr. Ahmed A.Mohammed and Muhanned Dhia Fadhil Al-Mureeb
Environmental Engineering Department, College of Engineering, University of Baghdad

ABSTRACT

The separation of lead ions from wastewater was carried out in an electrocoagulation cell which has a set of electrodes, aluminum anode and stainless steel cathode. The effect of several working parameters such as pH, current density, initial lead concentration, electrodes surface area, gap between electrodes and sodium chloride concentration on the performance of electrocoagulation cell were examined.

From the experiments found that the higher removal efficiency achieved at pH 9, with increasing current density and decreasing gap between electrodes the removal efficiency enhanced and the treatment time decreased. Using a flowrate of 0.025 l/min after (7min) electrolysis, the Pb(II) concentration decay from (250mg/l) to only (2.5mg/l) corresponding to a 99% removal efficiency.

Key words: heavy metals, wastewater, electrocoagulation.

الخلاصة

آيونات ألرصاص في المياه الصناعية الملوثة فصلت داخل خلية التختير الكهروكيمياوي التي تحتوي على قطب انود من الألمنيوم وقطب كاثود من الحديد المقاوم للصدأ. عدة متغيرات والتي لها تأثير على كفاءة ألإزالة مثل الدالة الحامضية, كثافة التيار, تركيز الرصاص ألأولي, درجة الحرارة, تركيز كلوريد الصوديوم, المسافة بين ألأقطاب, المساحة السطحية للأقطاب ونوعيتها تم دراستها.

من التجارب وجد ان أعلى كفاءة ازالة تتحقق عندما تكون الدالة الحامضية 9 , وبزيادة كثافة التيار التيار وتقليل المسافة بين ألأقطاب تتحسن كفاءة ألأزالة ويقل وقت المعالجة. كذلك وجد ان كفاءة ألأزالة تتحسن عند تقليل معدل الجريان.

INTRODUCTION

One of the main causes of industrial pollution is the discharge of effluents containing heavy metals. Disposal of industrial wastewater has always been a major environmental issue. Pollutants in industrial wastewater are almost invariably so toxic that wastewater has to be treated before its reuse or disposal in water bodies [1].

Lead ion is one of the most toxic species, it's a natural constituent of the earth's crust, and it is present in many wastes as a result of its wide spread use. Because of its chemical properties, resistance to corrosion, ability to form desirable alloys and acceptable electrical conductivity, lead is used in a variety of application in the construction, communications,

energy production and distribution, pigments, dying and transport industries. An important use of lead is in lead-acid batteries [2].

Lead ions not biodegradable and tend to accumulate in living organisms, causing various health problems. According to the world health organization, the acceptable range of Pb^{2+} in water is 0.01ppm [3].

Various techniques have been employed for the treatment of heavy metals including precipitation, adsorption, ion-exchange, and reverse osmosis.

For many years the conventional treatment method for polluted water still used all-over the world without significant change. It includes dosing the chemical coagulant, such as aluminum sulfate and ferric chloride, the metal ions agglomerate the pollutants causing them either to sink to bottom or become sufficiently large that they can be filtered out or floated out using dissolved air flotation.

This method of treatment has certain drawbacks like handling large quantities of chemicals and production large volume of sludge causing disposal problem. Therefore there is an urgent need to develop innovative and more effective techniques for treatment of wastewaters. Electrochemical techniques have attracted, in this case, a great deal of attention because of their versatility, safety, selectively, amenability to automation and environmental compatibility [4].

Electrocoaculation appears to be one of the most effective approaches. An electro coagulation reactor is an electrochemical cell wherein a sacrificial metal anode usually aluminum but occasionally iron is used to dose polluted water with a coagulating agent [5]. In this process, the treatment is done without adding any chemical coagulant or flocculent, thus reducing the amount of sludge which must be disposed [6]. The electrocoagulation has been successfully used to treat heavy metal containing solutions [4,7,8], dye-containing solutions with a removal efficiency as high as 99% [9], potable water[10], urban and restaurant wastewater[11], oil-water emulsions [12] and phenolic compounds [13]. Electrocoagulation compared with other techniques has many advantages, such as fast rate of removal pollutant particles, simple equipment and easy operation, reduction or absence of equipment for adding chemicals, and a decreased amount of precipitated or sludge. However the most disadvantages of EC is the sacrificial electrodes are dissolved into wastewater streams as a result of oxidation and need to be regularly replaced.

The objective of the present work were (1) to examine the applicability of electrocoagulation process for removal of lead from simulated wastewater and (2) to determine the effects of various parameters such as pH, current density, initial lead ion concentration, sodium chloride concentration, electrolysis time, electrode surface area, gap between electrodes and solution flowrate on the removal efficiency.

- EQUIPMENT AND MATERIALS

Materials

Synthetic polluted water samples with various concentrations of lead were prepared by dissolving lead nitrate $Pb(NO_3)_2$ (fluka products)without any further purification in deionized water. The required mass of $Pb(NO_3)_2$ were calculated as follows:

$$W = V \times C_i \times \frac{M.wt}{At.wt} \qquad \ldots\ldots\ldots(1)$$

Where:

W: Weight of $Pb(NO_3)_2$ (g)

V: Volume of solution (3L)

Ci: Initial concentration of lead ions in solution (g/L)

M.wt: Molecular weight of $Pb(NO_3)_2$ (331.21g/mole)

At.wt: Atomic weight of lead (207.21g/mole)

In order to increase the conductivity of the solution, sodium chloride was added to the solution before injecting it into the cell. The chloride salt added to the solution can also prevent the formation of oxide layer on the anode and therefore reduce the passivation problem of the electrode.

The initial pH of the solutions was adjusted by adding either (1M) hydrochloric acid or (1M) sodium hydroxide.

The standard solutions used in the atomic absorption analysis were prepared using a Titrisol standard solution from merck.

Reactor design and procedure for Pb(II) removal

The experimental work was performed in two parts (batch and continuous modes). The effect of pH, current density, lead ions concentration, NaCl concentration, electrolysis time, surface area and gap between electrodes were studied.

A schematic diagram of the experimental set-up is shown in fig.(1).

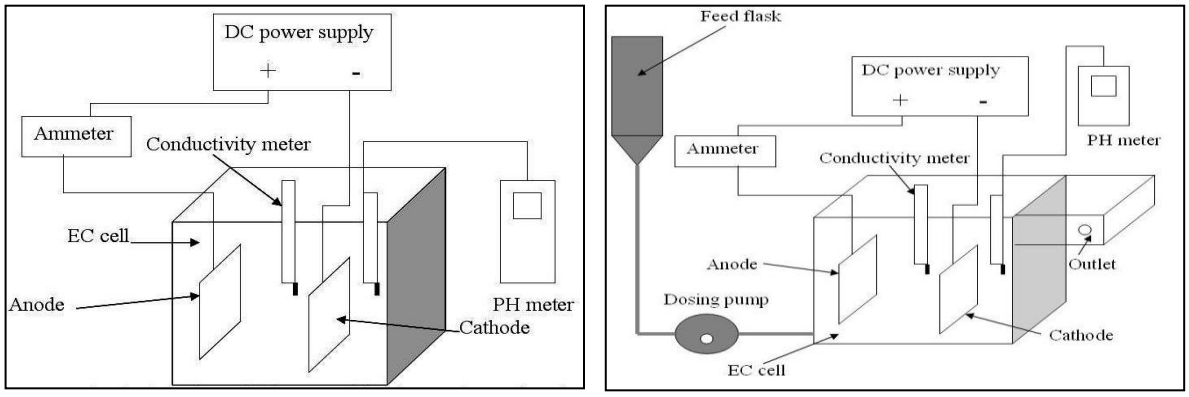

(a) (b)

Fig.(1): Schematic diagram of batch and continuous experimental. (a): Batch mode, (b): continuous mode

The batch electrocoagulation cell (fig 1-a) was constructed from 6mm thickness of glassy material with a square cross section and effective volume of (4L). 3L of polluted water was introduced into EC cell for each experiment. The cell comprised of two parallel plate electrodes, Al as anode and St.St. as cathode of 99% purity.

The two electrodes dipped in wastewater with a variable distance (1-4)cm between them. The electrodes were connected to the terminals of a DC power supply and the electrical circuit switched on as soon as the electrodes were covered by the wastewater. The desired current was achieved by altering the voltage of the electrical circuit.

Samples of 5ml withdrawn from the cell each (3min) and then these samples were filtrated and taken to be analyzed. At the end of each run, the system was washed several times with water and once with HCl to remove any solids tended to cling at the inside walls of the cell

and to avoid passivity of the electrodes. The same procedure was applied in continuous mode (fig.1-b) where the EC cell of (3.5L) effective volume and divided into two compartments with dimensions of (9*12*30cm)and (9*12*9cm). The first compartment is provided with two electrodes Al as anode and St.St. as cathode. This compartment receives the polluted water from a conical flask by using the regulator of dosing pump. While, the effluent undergoes settling the suspended solids at the second compartment, where the samples were collected.

BRIEF DESCRIPTION OF ELECTROCOAGULATION MECHANISM

The main reaction occurring during the electrolysis in the electrochemical cell produced aluminum ion at anode and hydroxide as well as hydrogen ions at cathode as shown below:

$$Al \rightarrow Al^{3+} + 3e^{-} \quad \text{Anode reaction} \qquad \text{.....(2)}$$

Cathode reaction

$$2H_2O + 2e^{-} \rightarrow 2OH^{-} + H_2 \qquad \text{.....(3)}$$

In addition the active metal cation (Al^{3+}) react with hydroxide ions (OH^{-}) to form a metal hydroxide $Al(OH)_3$ which then acts as a coagulant with the pollutant particles and metal hydroxide forming layer aggregates which may settle out or be carried to the surface by hydrogen bubbles produced at the cathode [14]. The equilibrium for the aluminum water system occurs as a result of passivation (i.e. formation of an oxide layer) and corrosion is identified. The presence of the chloride ion in solution has been reported to decrease passivation and thereby increase electrocoagulation treatment efficiency. The mechanism for chloride ion reducing passivation of the oxide layer formed on aluminum as shown in equations below:

$$Al + 3HCl \rightarrow AlCl_3 + H_2 \qquad \text{.....(4)}$$

$$AlCl_3 + 3H_2O \rightarrow Al(OH)_3 + 3HCl \qquad \text{.....(5)}$$

RESULTS AND DISCUSSION

In order to examine the efficiency of electrocoagulation process for removing lead ions. Several operating parameters such as pH, current density, initial lead concentration, electrodes surface area, gap between electrodes and sodium chloride concentration have been explored.

Effect of initial pH

pH has a considerable effect on the performance of electrocoagulation process [11], also the pH of the medium change during the process. This change depends on the type of electrode material and initial pH. In this study a series of experiments were performed, using solutions containing Pb^{2+} of (250 mg/l) each, with an initial pH varying in the range (3-10). The effect of initial pH on the removal efficiency is shown in figure (2), it can be seen that the removal efficiency (Re) after (20 min) electrolysis time at (5.49 mA/cm^2) current density reached values as high as 99% when pH equal 9. At pH of 10, the removal rate was slower by about (60 min), however it showed a good removal rate later. In contrast, when the initial pH

is decreased, a dramatic decrease of the removal efficiency is observed (40%) after (120 min) at pH equal to 3. The decrease of removal efficiency at a pH less than 5 was attributed to an amphoteric behavior of $Al(OH)_3$ which lead to soluble Al^{3+} cations when the initial pH is low and to monomeric anions $Al(OH)_4^-$ when the initial pH is high [15]. These soluble species are useless for water treatment. When the initial pH was kept in the range (5-9), all aluminum cations produced at the anode formed polymeric species $Al_{13}O_4(OH)_{24}^{7+}$ [16], and precipitated $Al(OH)_3$ leading to a more effective treatment.

The treatment induced an increase in pH by about (1-2) unit at the first (2-3 minutes) and then decreased. This might be explained by the excess of hydroxyl ions produced at the cathode in sufficiently acidic conditions and by liberation of OH^- due to occurrence of a partial exchange of Cl^- with OH^- in $Al(OH)_3$ [7].

As a result of the previous discussion of the effect of pH on the removal efficiency, the initial pH was adjusted to 9 for all subsequent studies.

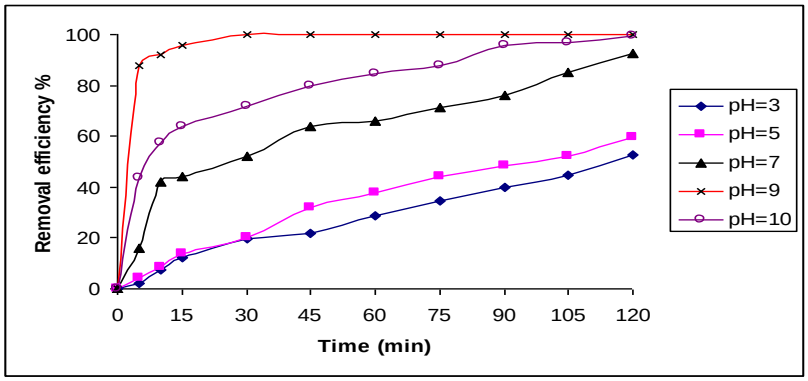

Fig. (2): Variation of lead removal efficiency with different pH. (Vertical Al/St.St electrodes, i=5.49mA/cm^2, [lead] =250ppm, [NaCl] =200ppm, gap=2cm, T=20°C).

Effect of current density

Current can be directly controlled in batch electrocoagulation runs. It is significant because it directly determines both coagulant dosage and bubble generation rate, also influences both mixing and mass transfer at the electrodes [5].

In this study, the current intensity was varied in the range (0.25-1.5)Ampere which linearly corresponds to (0.915-5.49 mA/cm^2) current density defined as current divided by electrode active area in an attempt to investigate the influence of this parameter on the removal efficiency of lead.

The variation of removal efficiency with different current density (0.915-5.49 mA/cm^2) is shown in figure (3). From this figure it can be noticed that the removal efficiency increased upon increasing current density. The highest current density (5.49 mA/cm^2) produced the quickest removal rate with a 99% concentration reduction occurring just after (20min).

This behavior is explained by the excess amount of aluminum and hydroxide ions generated at a given time within the electrocoagulation cell which are related to the current flow using Faraday's law [7].

$$w = \frac{ItM}{zF} \qquad \text{.....(6)}$$

Where: W is the amount of aluminum dissolving (g/cm^2), I is the current density, t is the time, M is the molecular weight of aluminum (g/mol), z is the number of electrons transferred in the reaction and F is the Faraday's constant (96486 C/mol) which leads to increase the floc production, also bubbles density increase and their sizes decrease resulting in a more efficient and faster removal. The relationship between current density and amount of aluminum released is shown in figure (4).

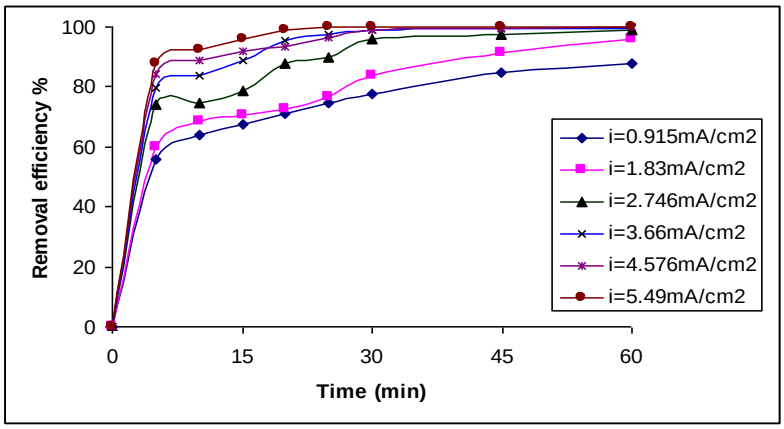

Fig.(3):Variation of lead removal efficiency with different current density. (Vertical Al/St.St electrodes, pH=9, [lead] =250ppm, [NaCl] =200ppm, gap=2cm, T=20ºC).

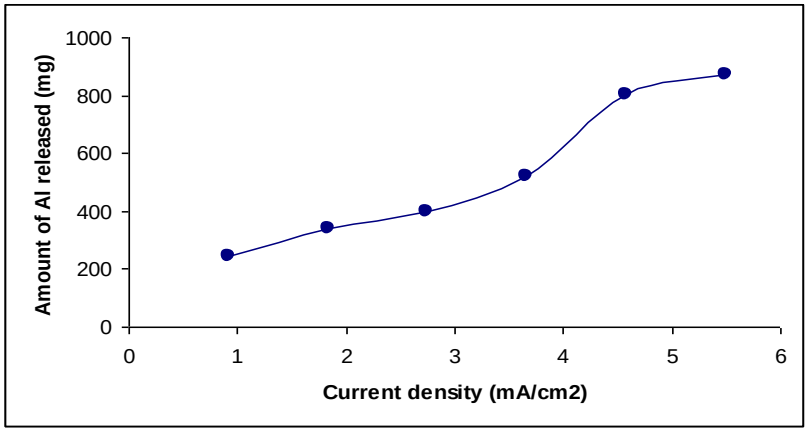

Fig.(4):Relation between current density and Al released. (Vertical Al/St.St electrodes, pH=9, [lead] =250ppm, [NaCl]=200ppm, gap=2cm, T=20ºC).

Effect of initial lead concentration

The effect of various lead concentrations (50-250ppm) on the removal efficiency in the electrocoagulation cell is investigated and plotted in figure (5). As expected, it appears that the removal efficiency decreased upon increasing initial concentration. It is clear from figure (4) that in higher concentrations, longer time is needed for removal of lead, but higher initial

concentration of lead were reduced significantly in relatively less time compared to lower concentrations.

The time taken for reduction thus increase with the increase in concentration. This decreased is explained by the theory of dilute solution. In dilute solution, formation of the diffusion layer at the vicinity of the electrode causes a slower reaction rate, but in concentrated solution the diffusion layer has no effect on the rate of diffusion or migration of metal ions to the electrode surface [17], however 20 min was necessary to achieve 99% removal efficiency.

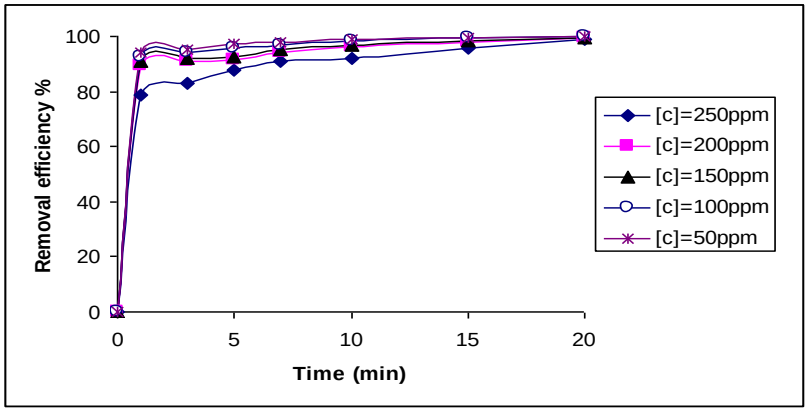

Fig.(5):Variation of lead removal efficiency with different initial lead concentration.(Vertical Al/St.St electrodes, pH=9, i=5.49 mA/cm^2, [NaCl] =200ppm, gap=2cm, T=20ºC).

Effect of sodium chloride concentration

Sodium chloride concentration was varied in the range (100-400 ppm) to evaluate the impact of solution conductivity on the electrocoagulation efficiency. As shown in figure (6), the highest NaCl concentration produced the quickest removal rate with (99%) removal efficiency occurring just after 15min; however 20min was necessary to achieve the efficient removal of lead.

This behavior is attributed to the change in the ionic strength effects on the solution which leads to destabilization between charged species and lead ions during the treatment [4].

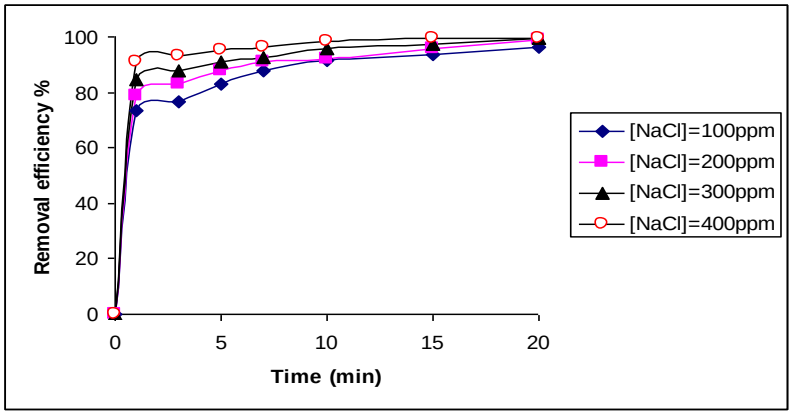

Fig. (6): Variation of lead removal efficiency with different NaCl concentration (Vertical Al/St.St electrodes, pH=9, [lead] =250ppm, gap=2cm, i=5.49mA/cm^2, T=20ºC).

Effect of electrodes spacing

The effects of electrodes spacing on the removal efficiency is shown in figure (7). It seems from this figure that faster removal happened with decreasing electrodes gap, and this is due to increase the current passage through the cell which lead to increase the amount of Al^{3+} released in the solution (The resistance of the solution decrease with decreasing the gap).

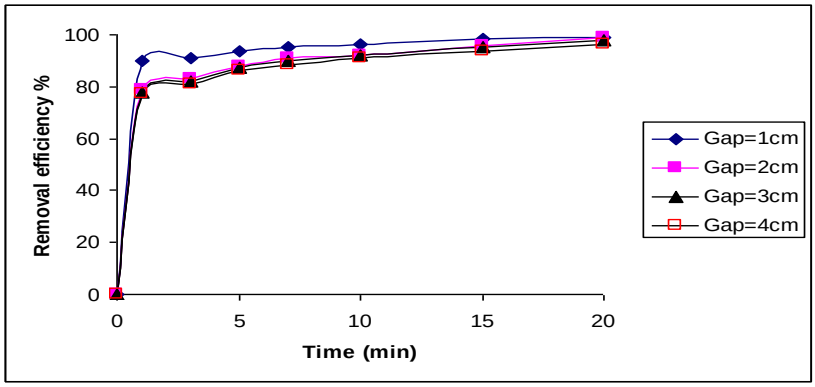

Fig. (7): Variation of lead removal efficiency with different gap.
(Vertical Al/St.St electrodes, pH=9, [lead] =250ppm,
[NaCl] =200ppm, i=5.49mA/cm^2, T=20ºC).

Effect of electrodes surface area

Two electrodes sizes with different types (Al/St.St and Al/Al) are used to investigate their effect on the electrocoagulation efficiency. The results are shown in figures (8) and (9) respectively.

Figure (8) indicate that increasing the active area from (101.95 to 273.12 cm^2) enhanced the removal efficiency and reducing the treatment time required, the explanation of this phenomena as follows: larger electrode surface area resulted in a great dispersion of bubbles throughout the reactor, whereas a smaller electrode surface area resulted in a concentrated source of bubbles within the reactor, and with increasing the dispersion of bubbles in the reactor, probability of collision between the bubbles and coagulant increased leading to increase the removal efficiency.

Figure (9) shows that the removal efficiency influences with different electrodes type. From this figure, it can be seen that Al/Al electrodes produced the quickest removal rate with a 99% concentration reduction occurring just after 5min. However 20min was necessary for Al/St.St to achieve nearly the same removal efficiency for Al/Al electrodes. This is due to that with using Al/Al electrodes both anode and cathode release Al^{3+}, thus increased the amount of aluminum hydroxide which lead to enhanced the removal efficiency.

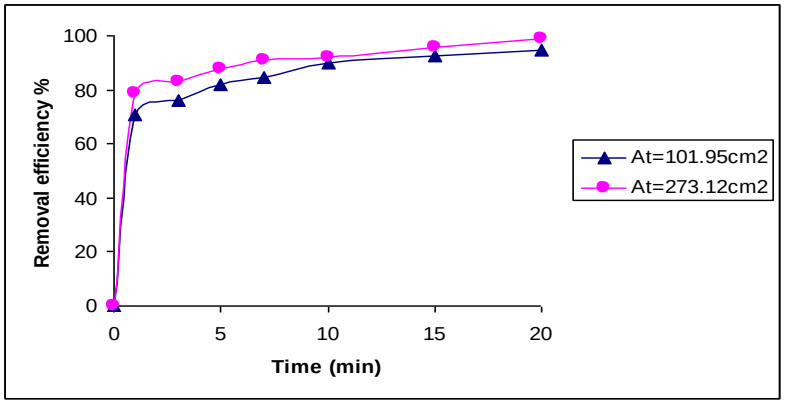

Fig.(8):Variation of lead removal efficiency with different electrodes surface area (Vertical Al/St.St electrodes, pH=9, [lead] =250ppm, [NaCl]=200ppm, gap=2cm, I=1.5A/,T=20ºC).

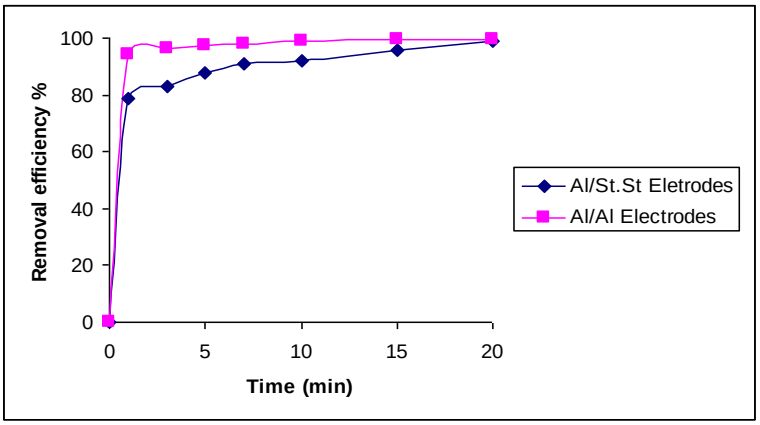

Fig.(9):Variation of removal efficiency with different electrodes. (pH=9, [lead] = 250ppm, [NaCl] =200ppm, gap=2cm, i=5.49mA/cm^2,T=20ºC).

Continuous mode

Effect of wastewater flowrate

To investigate the effect of liquid flowrate containing lead ions on the electrocoagulation efficiency, a series of experiments carried out on solutions containing a constant lead concentration (250mg/l) where the initial pH was fixed at 9, flowrate being varied from 0.025-0.15 l/min at 5.49 mA/cm^2 current density by using (Al/St.St) electrodes.

Figure (10) represent the relationship between removal efficiency and treatment time for different flowrate. It is noted from this figure that the removal efficiency decreased upon increasing solution flowrate. This reduction in efficiency is explained by the decrease of residence time in the electrocoagulation cell with increasing solution flowrate. Indeed the amounts of aluminum and hydroxide ions generated at a given time is constant since the current density is constant.

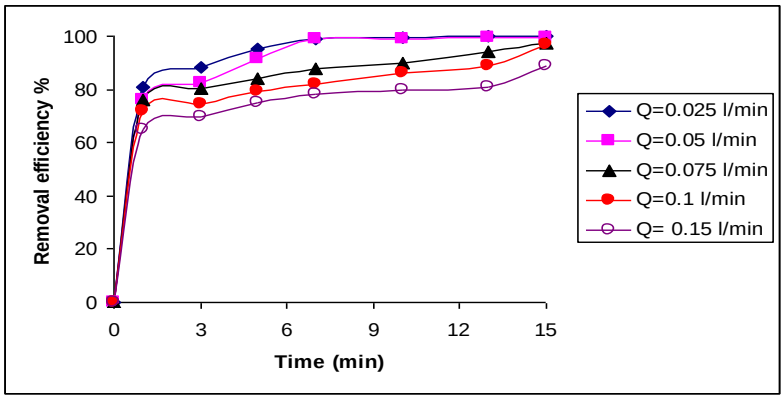

Fig.(10): Variation of lead removal efficiency with different flowrate.
(Vertical Al/St.St electrodes, pH=9, [lead] =250ppm, [NaCl] =200ppm, gap=2cm, i=5.49mA/cm^2, T=20ºC).

CONCLUSIONS

In the present study the applicability of electrocoagulation process in the treatment of polluted water containing lead ions has been investigated. The effect of different operating parameters (pH, current density, initial lead concentration, electrodes surface area, gap between electrodes and sodium chloride concentration) on the electrocoagulation efficiency have been studied and the results can be summarized as follows:

- With regard to pH, the highest removal efficiency with shorter time achieved at pH 9.
- The removal rate was shown to increase upon increasing the current density. While the removal rate decrease with increasing initial lead concentration.
- The removal efficiency increased and the treatment time decreased with increasing sodium chloride concentration.
- An aluminum electrodes where preferable for electrocoagulation treatment of lead due to higher removal efficiency (99.08%) in 10min compared with 99% in 20min for St.St cathode.
- With respect to electrode size the best removal obtained at the higher electrode surface area and lower spacing between the electrodes due to the grater dispersion of bubbles throughout the reactor.
- With increasing the initial lead concentration the time required to achieve the highest efficiency increased but that higher initial concentration of lead was reduced in relatively less time than the lower concentrations.
- With respect to solution flowrate the removal efficiency decreased with increasing flowrate.

REFERENCES

- Badmus, M.A.O., Audu, T.O.K. and Anyata, B.U., "**Removal of heavy metal from industrial wastewater using hydrogen peroxide**", African Journal of Biotechnology, 6 (3), 238-242, (2007).
- United Nations Environment program (UNEP), TECHNICAL Working Group of the Basel Connection, (2000).
- Omar, W., and Al-Itawi, H., "**Removal of Pb^{2+} Ions from aqueous solutions by adsorption on kaolinite clay**", American journal of applied sciences, 4, 7,502-507, (2007).
- Mouedhen, G., Feki, M., Wery, M.D. and Ayedi, H.F., "**Behavior of aluminum electrodes in electrocoagulation process**", J. of Hazardous Materials, 150, 124-135, (2008).
- Holt, P.K.,**Electrocoagulation unraveling and synthesizing the mechanisms behind awater treatment process**", Ph.D thesis, Faculty of Engineering, the university of Sydney, (2003).
- Cenkin,V.E.,Belevstev,A.N., "**Electrochemical treatment of industrial wastewate**r", Eff.water treat.J. 25, (7), 243-249, (1985).
- Adhoum, N., Monser, L., Bellakhal, N., Belgaied, J., "**Treatment of electroplating wastewater containing Cu^{+2}, Zn^{+2} and Cr(VI) by electrocoagulation**" , J. Hazardous Materials, B12, (3), 207-213, (2004).
- Farkas, J. and Michell, G.D., "**An electrochemical treatment process for heavy metal recovery from wastewater**", AICHE Symposium Series, 81, (243), 57-65, (1985).
- Line, S.H., Peng, C.F., "**Treatment of textile wastewater by electrocoagulation methode**", Water Res. 28. 277-282, (1994).
- Vik, E.A., Carlson, D.A., Eikun, A.S. and Gjessing, E.T., "**electrocoagulation of potable water**", Water Research, 18, (11), 1355-1360, (1984).
- Chen, G.H., Chen, X.M., Yue, P.L., "**Separation of pollutants from restaurant wastewatere by electrogoagulation"**, Sep.Purif.Technol.19, 65-76, (2000).
- Nahui, F.N.B., Nascimento, M.R., Cavakanti, E.B., And Vilar, E.O., "**Electroflotation of emulsified oil in industrial wastes evaluated with a full factorial design**", Brazilian J.chem.Eng. 25, 3, 435-442, (2008).
- Weerachai, P., Sombat, C., and Duang, B., "**Electrocoagulation and subsequent recovery of phenolic compounds**", Japan society of Analytical chemistry., October, vol.6, 1083-1084, (2000).
- Jiaqian, J., "**An anodic passivation of electrocoagulation in the process of water treatment**", water treatment, 3, 344-352, (1988).
- Do, J.S., Chen, M.L., "**Decolourization of dye-containing solutions by electrocoagulation**", J.Appl.Electrochem., 24, 785-790, (1994).
- Kobya, M., Can, O.T., Bayramolgu, M.,". **Treatment of textile wastewater by electrocoagulation using iron and aluminum electrodes",** J. Hazard. Mater. B100, 163- 178, (2003).
- Ghaudhany, A.J., Goswami, N.C., Grimes, S.M., "**Electrolytic removal of hexavalent chromium from aqueous solutions**", J.Chem.Technol.Biotechnol. 78, 877-883, (2003).

Number 4 Volume 16 December 2010 Journal of Engineering

CONSTRUCTION WATER SUITABILITY MAPS OF TIGRIS RIVER FOR IRRIGATION AND DRINKING USE

Khalid Adel Abdulrazzaq, Ph.D Wardah Sabah Kamil, M.Sc.
Department of Water Resources, University of Baghdad

ABSTRACT

The Tigris River is one of two major sources of surface water in Iraq, with 1900 km length, 1415 km of which are in Iraq. Increasing demands of the river water for beneficial uses lead to increase the concern about its quality.

World Health Organization (WHO, 2004) and Iraqi Quality Standards (IQS, 2001) have been adopted along the river to compare and examine the degree of permissibility of polluted parameters T.H, SO_4^{-2}, Cl^{-1}, and T.D.S for drinking use, whereas American Salt Laboratory Standards has been adopted basing on SAR and EC for irrigation use. Different international methods have been applied to classify the water quality index for the Tigris River at north of Baghdad station which are Brown (1970), Mecllelend (1974), and Bhargava (1983).

A general program was constructed to estimate the surface water quality variation with time and location for drinking and irrigation adopting Bahrgava,1983 method, since it is more effective in dealing with many sensitive functions related to the pollutant parameters through the analysis of T.H, SO_4^{-2}, Cl^{-1}, T.D.S, EC, Ca^{+2}, SAR, pH, and BOD which are the relative parameters to the previous mentioned beneficial uses.

The program use Visual Basic Studio, 2008 language as a tool because it is easy to operate automatically by engineers or the decision makers for the water quality assessment. Thirteen stations along Tigris River were taken in the analysis, starting at Feeshkabour and ending at Al-Qurna. The historical recorded data which were used had been selected through 2007/2008 as a monthly base.

In general, the results showed that the Tigris River is class I to II for irrigation use, while its class ranges from II –V for drinking use. According to these classes, the Tigris River is divided into two reaches as follows:

- From Feeshkhabour to Tarmiyah, the water quality index (WQI) is classified as class I for irrigation, and class II for drinking use.
- From North of Baghdad till Qurna, WQI is classified as class II for irrigation, and class IV for drinking use.

The results also indicate that there is an increase in T.H values leading to deterioration in water quality for drinking use; also, an increase in SO_4^{-2} parameter after Tarmiyah, and Cl^{-1} parameter after Kut that affects the suitability of water for irrigation use.

Finally, different suitability maps are constructed to classify water of 2007/2008 for irrigation and drinking use, which will be a base to trace the type of pollutants and their weight that cause the deterioration of the previously mentioned uses.

الخلاصة:

أن نهر دجلة احد المصادر الرئيسية للمياه في العراق حيث يبلغ طوله 1900 كم منها 1415 كم داخل العراق وبسبب الازدياد الحاصل في عدد السكان ونشاطاتهم ادى الى ازدياد الطلب على الموارد المائية للاستخدامات الحياتية المختلفة وبالتالي زيادة الاهتمام بنوعية المياه والسيطرة على مقدار التلوث فيها.

في هذا البحث تمت مقارنة نوعيه مياه نهر دجلة للسنة المائية 2007/2008 للعناصر المقاسة(T.H, SO_4^{-2}, Cl^{-1}, T.D.S) مع مواصفات منظمة الصحة العلميه(WHO, 2004) و المواصفات العراقية(IQS, 2001) لاغراض الشرب واعتماد مواصفات مختبر الملوحة الامريكي الذي يعتمد في تصنيفه على قيم (SAR, EC) لمقارنة نوعية المياه لاغراض الري.

تم مقارنة ثلاث طرق عالمية مختلفة معتمدة في تصنيف المياه السطحية في محطة شمال بغداد لحساب مؤشر نوعية المياه (WQI) وهي (Brown/1970, Mccllend/1974, and Bhargava/1983) ومن ثم تم بناء برنامج بلغة Visual Basic Studio/2008 كوسيلة كفوءة وسهلة للمتابعة والاستفادة من قبل المهندسين لحساب (WQI) بالاعتماد على طريقة Bhargava/1983 لتصنيف صلاحية مياه نهر دجلة لإغراض الري والشرب.

تم تحليل العناصر الملحية(T.H, SO_4^{-2}, Cl^{-1}, T.D.S, EC, Ca^{+2}, SAR, pH, BOD) كمعدلات شهرية للسنة المائية 2007/2008 واستخراج القيم المقابلة لوزن كل عنصر ومن ثم استخراج النسبة المئوية لمساهمة كل عنصر في صلاحية المياه لاستخدامات الري والشرب من خلال المنحنيات الخاصة المعتمدة لهذا الغرض.

تم تحليل ثلاثة عشر محطة على نهر دجلة وهي (فيشخابور, مقدم سد الموصل, الموصل, الشرقاط, تكريت, سدة سامراء, الطارمية, شمال بغداد, جنوب بغداد, العزيزية, الكوت, العمارة والقرنة).

وقد أوضحت النتائج المستحصلة من البرنامج إن تصنيف المياه لنهر دجلة بصورة عامة لاستخدامات الري تتراوح من رتبة (I) إلى رتبة (II) وللاستخدامات الشرب من رتبة (II) إلى رتبة (V) وقد تم تقسيم النهر على أساس المعدل السنوي للتحاليل إلى مقطعين بالاستناد إلى النتائج المستخرجة :

- من فيشخابور إلى الطارمية حيث يكون مؤشر نوعية المياه (WQI) للري رتبة (I) وللشرب رتبة (II) .
- من شمال بغداد إلى القرنة حيث يكون للري رتبة (II) وللشرب رتبة (IV).

بينت النتائج ان هنالك دورا لارتفاع تراكيز T.H على طول النهر أدى الى تردي نوعية المياه للاستخدامات الشرب إضافة لارتفاع تراكيز SO_4^{-2} بعد محطة الطارمية وتراكيز Cl^{-1} بعد محطة الكوت وأخيرا تم بناء خرائط تبين صلاحية مياه نهر دجلة للسنة المائية 2007/2008 لاستخدامات الري والشرب ؛ وهذه الخرائط ستكون قاعدة لاستتباع الملوثات ومعرفة وزن تأثيرها في التردي.

KEY WORD:
WQI, Drinking Water, Irrigation

INTRIODUCTION

Surface waters are facing an increasing problem through the disposal of pollutants due to the rapid growth of industrial and municipal activities because of the increasing of population growth as well as the increase of land drainage due to agricultural activities. Thus, there have been increasing concerns about the management of water quality all over the world.

A river can be classified into various grades indicating the beneficial use(s) to which it can be put to. The grades are based on the permissible limits of relevant pollution parameters (water quality variables) or standards, set by the various authorities. Depending on the quality of water in various stretches of a river, the river can be zoned according to stretch suitability for the beneficial use(s). It would be appropriate to base river classification on the ranges of an index representing the integrating effect of the concentrations and importance values of the relevant variables for a use.

The Tigris River is one of the major sources of surface water in Iraq; so, studying its quality and quantity and its management has become one of the major concerns. Thirteen stations on the River are taken in the analysis (Feeshkhabour, U/S Mosul Dam, Mosul, Shirkat, Tikrit, Samara Barrage, Tarmiyah, North of Baghdad, South of Baghdad, Al-Azeezia, Kut, Al-Amara, Qurna). The monthly historical recorded data includes nine pollutant parameters (T.H, SO_4^{-2}, Cl^{-1}, T.D.S, EC, Ca^{+2}, SAR, pH, and BOD) to evaluate the water quality for irrigation and drinking uses.

Objectives of the Research

- To study the variation of the water quality parameters for the Tigris River according to the beneficial uses.
- To construct a general program to classify surface water quality using Visual Basic language.
- To evaluate the importance of each pollutant parameters on the beneficial uses.
- To trace the cause of deterioration in water quality locally.
- To build suitability maps for irrigation and drinking use for Tigris River.

Literature Review

Water Quality Index(WQI) was first mentioned by **Horton (1965)**, which was considered as an effective tool for collecting various sorts of water quality data to enhance representing them by a principal parameter. He used the WQI to classify water and to identify eight physical and chemical determinants to estimate the degradation of water quality. Also, Horton proposed the rating scales and the weightings for the determinants to give the relative importance for each determinant in the water quality. The formula which he used is eq. (1):

$$WQI = \left[\frac{\sum_{i=1}^{n} C_i . W_i}{\sum_{i=1}^{n} W_i} \right] . M_1 . M_2 \qquad (1)$$

Where:
WQI: water quality index
C_i : the rating of the i th determinant
n: number of determinants
M_1, M_2: additional determinant parameters
W_i: the weighting of the i th determinant.

Brown et al., (1970) developed the theoretical idea of choosing the determinants of WQI in addition to determine the relative weights and the rating scales depending on the questionnaires which are distributed among water experts in the United States. They used the arithmetic weighted mean to determine the WQI as eq.2:

$$WQI = \sum_{i=1}^{n} q_i . w_i \qquad (2)$$

Where:
q_i: rating of the i th determinant, this value varies from (0-100);

W_i: weighting of the i th determinant and this value varies from (0-1) and $\sum w_i = 1$;
n: number of determinants.

Mccllelland et al., (1974) studied the WQI of Kansas River adopting Browen's study (1970). They concluded that the multiplicative weights were the most appropriate for this purpose, because of their sensitivity to the changes which occurred in the water quality. This method was later known as the Geometric Weighted Mean eq. (3):

$$WQI = \pi_{i=1}^{n} q_i^{wi} \quad (3)$$

Bhargava (1983) studied the WQI to evaluate the water quality for several activities in Ganga River in India and Saigon River in Vietnam using the sensitivity function method. He transferred the values of variables according to the standard specifications on (0 – 1) scale. This index was used to classify rivers into five groups and to determine WQI for each activity of different water activities depending on the variables which affected that activity.

Al-Ansari and Al-Sinawi (1985) studied the water quality of the Tigris River in Baghdad City using multi-variate analysis. They had selected (9) variables (TDS, Ca^{+2}, Mg^{+2}, Na^{+1}, K^{+1}, Cl^{-1}, SO_4^{-2}, $HCO3^{-1}$, and CO_3^{-2}) with the discharge (Q) for the period 1967-1985 to evaluate the water quality of the river in Baghdad. Their results showed that, the continuous decrease of flow and the simultaneous increase in agricultural and industrial development with time, showed general deterioration in water quality of the Tigris River in Baghdad over the period of study.

Al-Ani (1988) studied the WQI of the Tigris River in Baghdad reach. He used the sensitivity function to convert the variables on scale (0 – 1) depending on a standard specification of water activities. He collected the results using the geometric mean according to Bhargava formula. He concluded that the Tigris River is classified as class I for irrigation and as class III for potable and industrial uses.

Al-Rawi and Shihab (1994) studied the WQI for the Tigris River in Mosul. They used the geometric mean previously used in Baghdad, India and Vietnam, depending on the sensitivity function on the range(0 – 1). The results of this study clearly showed that the water quality of excellent class was for irrigation and for the domestic and industrial uses; it was classified as class II.

Mohammad (1998) evaluated the Tigris River in Mosul City using WQI. Seventeen sections were selected along a stretch of the river from north of Mosul City to Hamam Al-Alil. Samples were collected and analyzed during a period of six months. The study showed that the Tigris River water quality for irrigation use falls within classes I and II; for industrial use it fell within class II; and for drinking water, it was classified in class III.

Al-Saffar (2001) has developed an expert system for the WQI for multi-uses for one year (2000) along the Tigris River using nine samples site (Mosul Dam, Mosul, Shirkat, Bejee, Samara, Baghdad, Al-Azeezia, Al-Kut, and Al-Amara). She concluded that Tigris water quality is classified as class II to class III for general uses at all sites except Al-Kut site which represents class II and III for general purposes and shifts to class IV for potable use and class V for industrial uses.

AREA OF STUDY (THE TIGRIS RIVER)

The Tigris is the second longest river in the Southwest of Asia at 1,900 km length of which 1415 km is in Iraq, it also has its springs in the highlands of Eastern Turkey, but the main contribution to the river comes from the tributaries in Iraq. The Tigris River follows a southeastern route in Turkey to the city of Cizre, forming a border between Turkey and Syria for 32 km before entering Iraq at upstream of Feeshkhabour City, where the Khabour tributary 160 km in length joins the main river

course. In Iraq, it meets its tributaries: the Greater Zap, the Lesser Zap, the Adhaim, and Diyala. It joins the Euphrates in Qurna and continues its journey to Shatt Al-Arab after the extensive irrigation and diversification canals remove around 70-80 percent of its waters before forming Shatt al-Arab then falls to the Arabian Gulf. **(El-Fadel, et al., 2002)**

BENEFICIAL USES:

Drinking water (DR): Iraqi Quality Standard, 2001 (IQS) and World Health Organization, 2004 (WHO) as shown in **Table 1** are adopted along the river to compare it with the recorded data for (T.H, SO_4^{-2}, Cl^{-1}, and T.D.S) parameters through the year 2007/2008.

Table (1) Guideline for Drinking water after IQS and WHO

Characteristics	Units	IQS,2001	WHO,2004
- Calcium (Ca)	ppm	200	200
- Chloride (Cl)	ppm	600	250
- Total Hardness (T.H)	ppm as $CaCO_3$	500	500
- pH (Range)	---	6.5-8.5	---
- Sulfate (SO_4)	ppm	400	250
- T.D.S	ppm	1500	1000

Irrigation use (IRR): The Tigris River water quality is classified according Richard Classification, 1954**(Richard, 1954)** with respect to the value of SAR and EC in water (**Table 2 and 3)** for the year 2007/2008.

T**able (2)** Richard Classification, 1954 for irrigation use **(Richard, 1954)**

Water Class	SAR	Index	EC(ds/m)	Index
Excellent	≤ 10	S1	0.1-0.25	C1
Good	10-18	S2	0.25-0.75	C2
Fair	18-26	S3	0.75-2.25	C3
Poor	≥ 26	S4	≥ 2.25	C4

Table (3) Water classification acording to Richard Classification, 1954 for irrigation use **(Richard, 1954)**

Index	Water class	Index	Water class
C1S1	Excellent	C3S1	Approprate
C1S2	Good	C3S2	Acceptable
C1S3	Approprate	C3S3	Acceptable
C1S4	Poor	C3S3	Poor
C2S1	Good	C4S1	Poor
C2S2	Good	C4S2	Poor
C2S3	Acceptable	C4S3	Very Poor
C2S4	Poor	C4S4	Very Poor

VARIATION OF WATER QUALITY PARAMETERS:

Limitations of Water Quality for Drinking Use

The Tigris River water quality behaviour is classified into three different trends which divide the river into three reaches as compared with WHO/2004 and IQS/2001 standards as shown in **Figs. 1, 2, 3 and4**. The first reach starts from Feeshkhabour to Tarmiyah City (reach I) has low concentrations for each parameter so, it is within the acceptable limit. Reach II from Tarmiyah to Kut, where the concentrations of all parameters rapidly increases due to Tigris–Tharthar arm carrying salts from the stratification of the Tharthar Lake, which is same conclusion mentioned by **Nader, et.al, 1986 (Arabic Ref.)** this makes water unacceptable in some sites for drinking purposes. The last reach from Kut to Qurna, reach III with very high concentrations of the relative parameters, and this reach is also unacceptable for drinking.

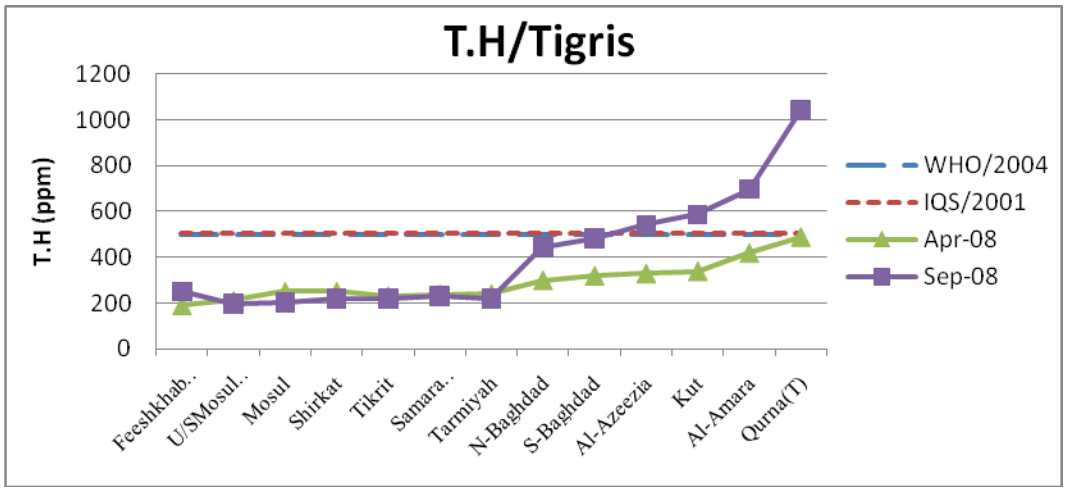

Figure (1) Comparison of T.H concentration according to WHO and IQS standards

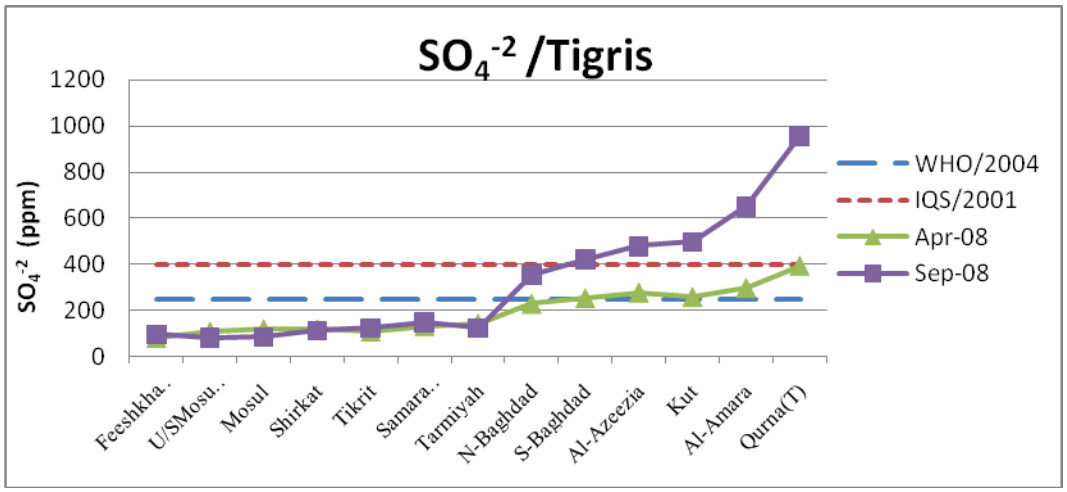

Figure (2) Comparison of SO_4^{-2} concentration according to WHO and IQS standards

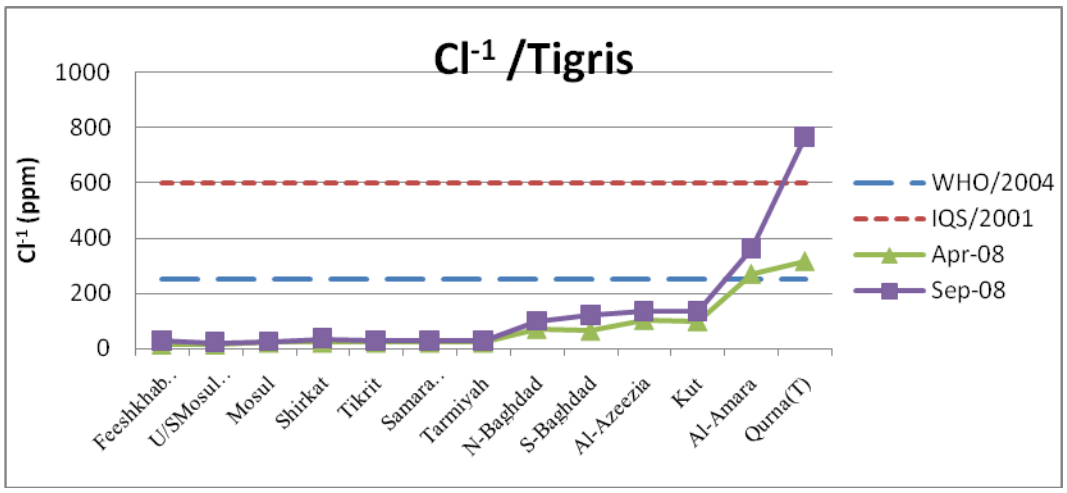

Figure (3) Comparison of Cl^{-1} concentrations according to WHO and IQS standards

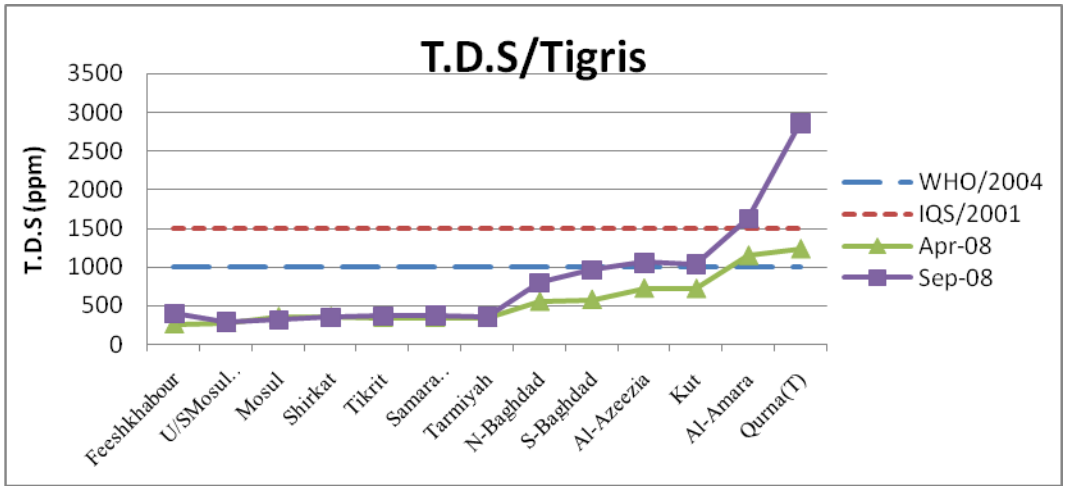

Figure (4) Comparison of T.D.S concentrations according to WHO and IQS standards

Limitations of Water Quality for Irrigation Use

In general, Tigris River is classified as (C2S1) from Feeshkhabour to Tarmiyah, so water is good for irrigation .From Tarmiyah to Qurna it is classified (C3S1) therefore; water is approprate for irrigation. In the three last months at Amara to Qurna the water quality is classified as (C4S2) as shown in Table 3. It is obvious that the value of SAR and EC increase after Tarmiyah because of the mixing with Tigris–Tharthar arm which contains high concantrations of salts **(Nader, et.al, 1986) (Arabic Ref.).**

Table (3) Classification of the Tigris water quality for irrigation use according To Richard Classification, 1954 for irrigation use

Station	Oct. 2007	Nov. 2007	Dec. 2007	Jan. 2008	Feb. 2008	Mar. 2008	Apr. 2008	May. 2008	Jun. 2008	Jul. 2008	Aug. 2008	Sep. 2008
Feeshkhabour	C2S1	C2S1	C2S1	-	C2S1	C2S1	C2S1	C2S1	C2S1	C2S1	C2S1	C2S1
U/S Mosul Dam	C2S1	C2S1	C2S1	-	C2S1	C2S1	C2S1	C2S1	C2S1	C2S1	C2S1	C2S1
Mosul	C3S1	C2S1	C2S1	-	C2S1	C2S1	C2S1	C2S1	C2S1	C2S1	C2S1	C2S1
Shikat	C2S1	C2S1	C2S1	-	C2S1	C2S1	C2S1	C2S1	C2S1	C2S1	C2S1	C2S1
Tikrit	C2S1	C2S1	C2S1	C2S1	C2S1	C2S1	C2S1	C2S1	C2S1	C2S1	C2S1	C2S1
Samara Barrage	C2S1	-	C2S1	C2S1	-	C2S1	C2S1	C2S1	C2S1	C2S1	C2S1	C2S1
Tarmiyah	C2S1	-	C2S1	C2S1	C2S1	C2S1	C2S1	C2S1	C2S1	C2S1	C2S1	C2S1
N-Baghdad	C3S1	C3S1	C3S1	C3S1	C3S1	C3S1	C3S1	C3S1	C3S1	C3S1	C3S1	C3S1
S-Baghdad	C3S1	C3S1	C3S1	C3S1	C3S1	C3S1	C3S1	C3S1	C3S1	C3S1	C3S1	C3S1
Al-Azeezia	C3S1	C3S1	C3S1	C3S1	C3S1	C3S1	C3S1	C3S1	C3S1	C3S1	C3S1	C3S1
Kut	C3S1	C3S1	C3S1	C3S1	C3S1	C3S1	C3S1	C3S1	C3S1	C3S1	C3S1	C3S1
Amara	C3S1	C3S1	C3S1	C3S1	C3S1	C4S1	C3S1	C3S1	-	C4S2	C4S2	C4S2
Qurna(T)	C3S1	C3S1	C3S1	C3S1	C3S1	C4S1	C3S1	C3S1	-	C4S2	C4S3	C4S3

NATIONAL METHODS SELECTION:

A comparison of three different national methods is applied to a selected station on Tigris River in the north of Baghdad to classify the water quality as shown in **Fig. 5**. It can be seen from the figure that the previous mentioned methods can be used for WQI analysis. Bhargava method is selected since it is more effective in dealing with many sensitive functions; and it gives a detailed description to analyze the WQI for irrigation and drinking uses.

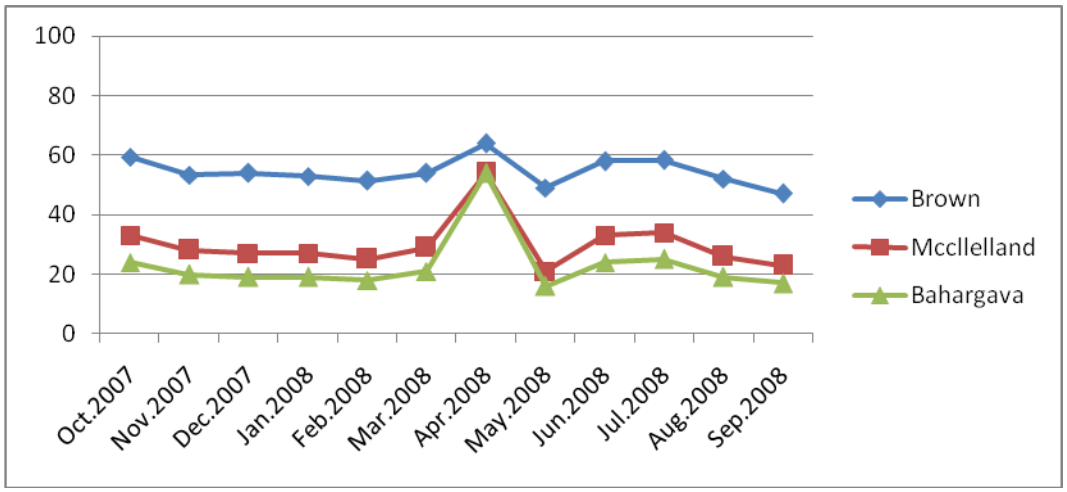

Figure (5) WQI at N-Baghdad for drinking use using different methods

BHARGEAVA METHOD:

Bhargava Method is one of the important methods which is used in many countries. It is easy to deal with relative parameters for different uses by using sensitivity functions curves which take the value between 0 and 1. The results are accumulated by using the geometric mean **eq. 4** to determine the WQI for each activity of water depending on the variables affecting that activity. This index classify rivers into five groups as shown in **Table 5**, that was formulated by the following equation***(*Abdul-Razzaq et al., (2001) (Arabic Ref.))***:

$$WQI = \left[\pi_{i=1}^{n} fi(P_i)\right]^{1/n} \quad *100 \qquad (4)$$

Where:

f_i (P_i) is the sensitivity function for each variable including the effect of variable weight concentration which is related to a certain activity and varies from 0 – 1.

The relative parameters for irrigation are TDS, pH, $SO4^{-2}$, SAR, EC, and Cl^{-1}, while the relative parameters of drinking are TDS, T.H, Cl^{-1}, SO_4^{-2}, BOD, pH, and Ca^{+2}***(*Abdul-Razzaq et al., (2001) (Arabic Ref.))***.

Table (5) Water quality classification according to Bhargava

Class	WQI Value	Water Quality
I	100 - 90	Excellent
II	89 - 65	Good
III	64 - 35	Acceptable
V	34 - 11	Polluted
IV	Less than 10	Severe Polluted

DESCRIPTION OF THE CONSTRUCTED MODEL:

A general program has been constructed to classify surface water using Visual Basic Studio 2008 software adopting Bhargava method for irrigation and drinking use. The constructed program

uses nine figures which were adopted by Bhargava to compute the sensitivity functions for irrigation and drinking use. The program works automatically and operates easily. It offers an easy base for the people who are dealing with water quality and need no high knowledge to run the program. Also it could be used as a management tool in water quality assessments. The program operating mechanism is listed below:

The main window will appear which contains six options, each performs when clicked on as shown in **Fig 6**, and these options are:

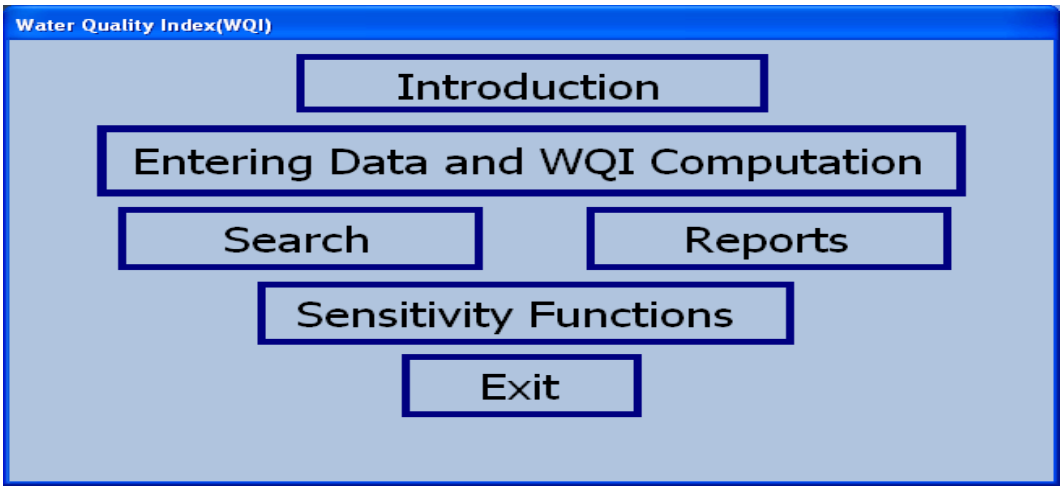

Figure (6) The main window

Fig. 7 shows the **Introduction,** a short definition of WQI and its classification.

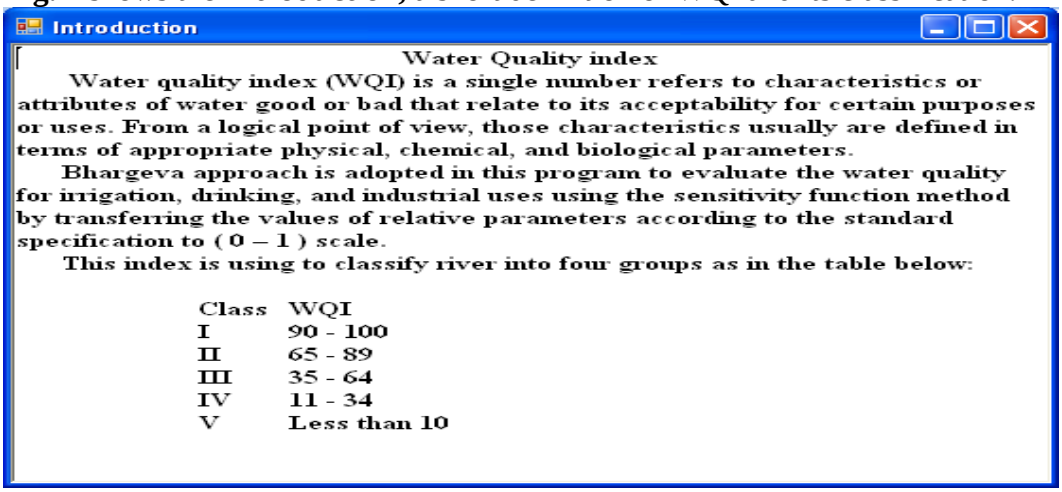

Figure (7) Introduction window

Entering Data and WQI Computation: The main purpose of this window is to enter any new data for any station along the river and calculating WQI then save it.

A detailed description of the operation of the option in the task bar is explained below:

A. Add new **(✚):** When clicking on this option, a new window will appear which is ready to receive any new data of any station as shown in **Fig. 8**.

B. Delete **(✕):** When clicking on this option, the data that are already entered before to the shown window will be deleted.

C. Save data **(🖫):** Clicking this option, the data that has been entered will be saved into data base figure.

D. Next **(▶):** The program will move forward to the next saved data.

E. Back **(◀):** The program will move back to the pervious saved data.

The main options of this window which work by clicking on it are as following:

1. WQI%**:** When clicking on this option, the program will calculate WQI for the entered data (station, river, date, and relative parameters) as shown in **Fig. 9**.

2. Back**:** The main window will appear as soon as clicking on it.

Note: The decimal for the number that represents WQI and sensitivity functions can be chosen by two options that can be seen in the bottom of this window.

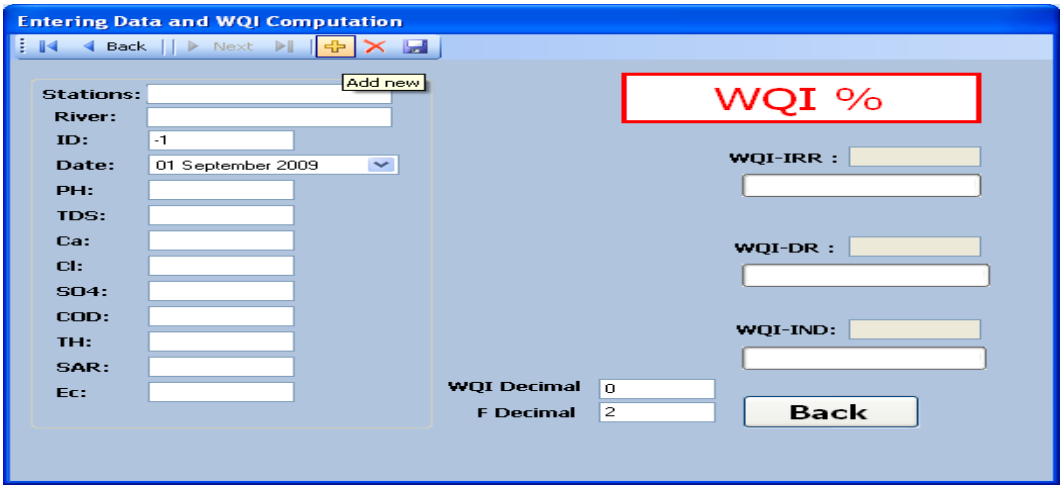

Figure (8) Entering new data window

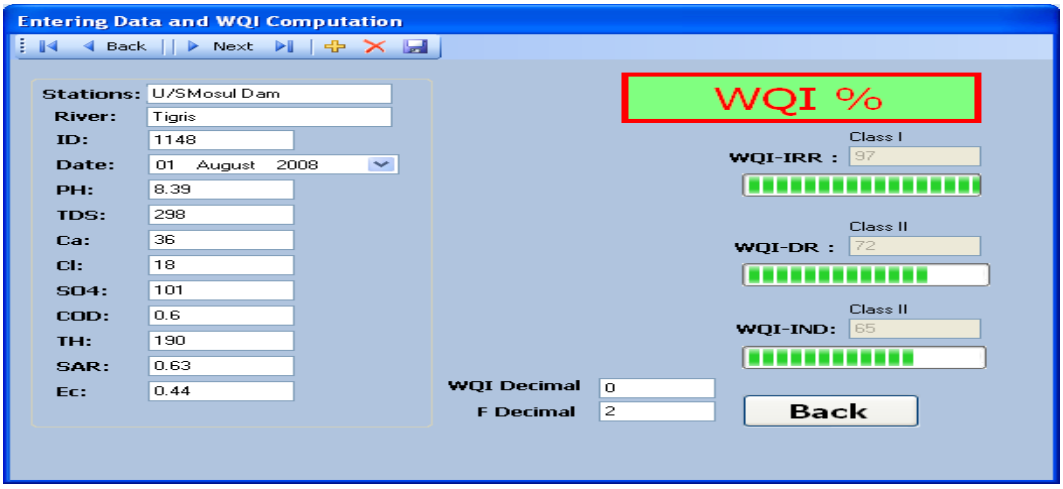

Figure (9) Entering data calculating WQI window

Search: This window prepares the model to search for any data which have been saved **(Figs. 10 and 11)**.

There are two ways to make search:

A. By date and station**:** in this option, the station can be selected by another option and the period of time from-to for a specific date can be chosen.

B. By date and river**:** in this option the river Tigris can be selected by another option and the period of time from-to for specific date can be chosen.

Those two options can be more specific by selecting particular use (irrigation, drinking, industrial, or all uses).

By clicking on:

1. Search: The search for all data for relative parameters, WQI, and sensitivity functions for the selected period will start.

2. Back: By clicking on this option the search window will close and go back to the main window.

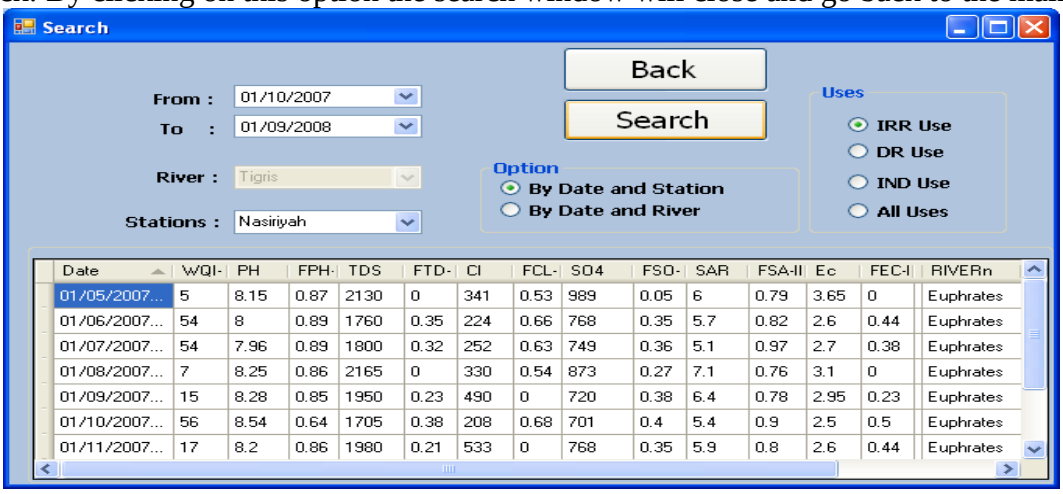

Figure (10) Search by date and station for irrigation use window

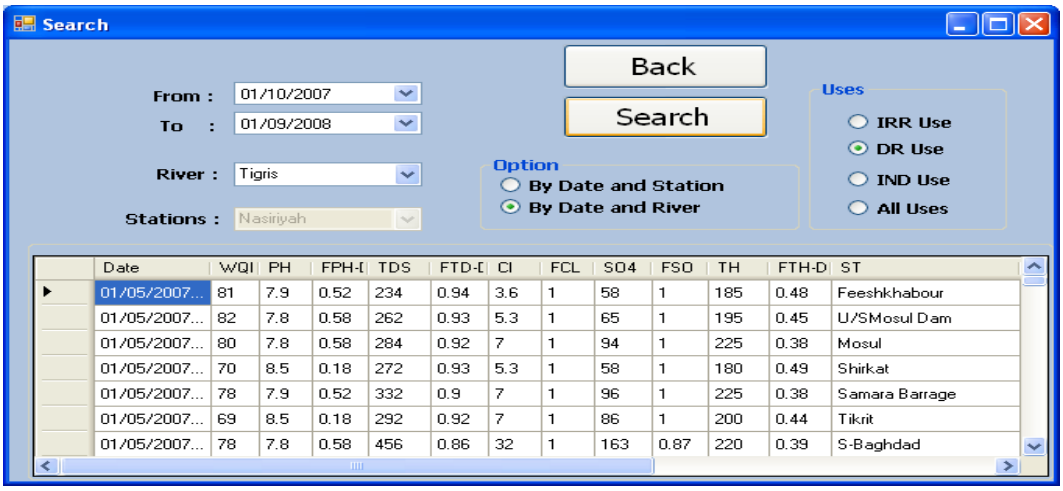

Figure (11) Search by date and river for drinking use window

Reports: When clicking on this option another window will appear which contains three kinds of reports, each one performs when clicking on it:

A. Total review.
B. WQI review by station.
C. WQI review by date.

Back: To go back to the main window.

All reports have the same task bar which contains several icons as followes:

●Next **(▶):** To move forward to a different page.

- Back **(◀):** To move back to a pervious page.
- Print **(🖶):** To print the selected report.
- Print layout **(📄):** To show the final shape of the report that will be printed.
- Page set up **(🕮):** When clicking on this icon, a sub window will appear to choose the size of the report paper that will be printed.
- Save **(💾):** To save the report either as an Excel document or as an Acrobat (pdf) file.
- Zoom**:** To zoom the report.
- Search text: To make sub-search for any text inside the report by clicking on Find and move inside the sub-search by clicking on Next. **(Figs. 12, 13, 14, and15)**.

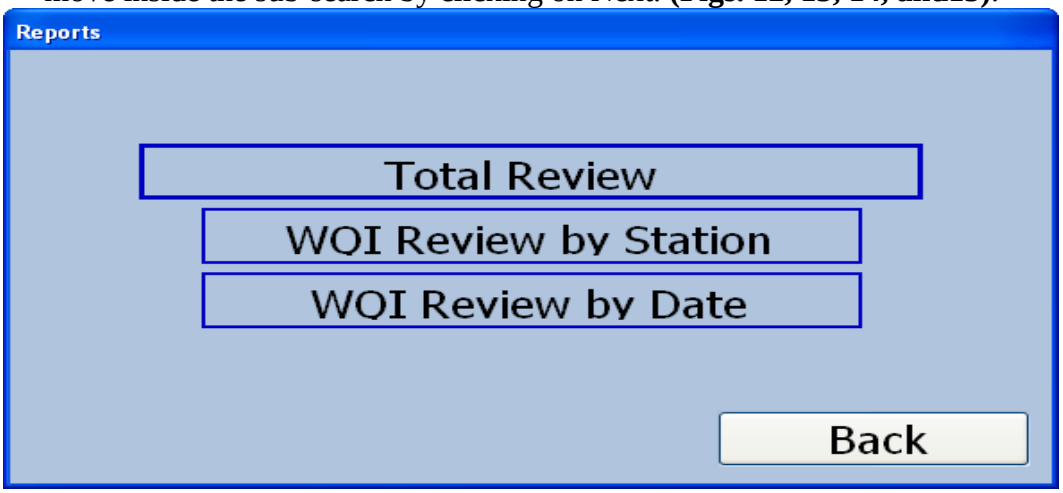

Figure (12) Reports window

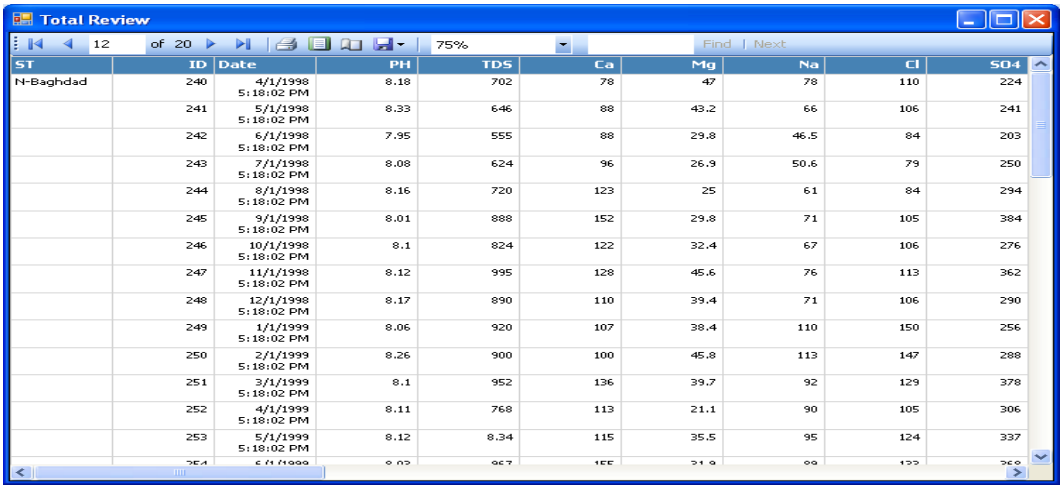

ST	ID	Date	PH	TDS	Ca	Mg	Na	Cl	SO4
N-Baghdad	240	4/1/1998 5:18:02 PM	8.18	702	78	47	78	110	224
	241	5/1/1998 5:18:02 PM	8.33	646	88	43.2	66	106	241
	242	6/1/1998 5:18:02 PM	7.95	555	88	29.8	46.5	84	203
	243	7/1/1998 5:18:02 PM	8.08	624	96	26.9	50.6	79	250
	244	8/1/1998 5:18:02 PM	8.16	720	123	25	61	84	294
	245	9/1/1998 5:18:02 PM	8.01	888	152	29.8	71	105	384
	246	10/1/1998 5:18:02 PM	8.1	824	122	32.4	67	106	276
	247	11/1/1998 5:18:02 PM	8.12	995	128	45.6	76	113	362
	248	12/1/1998 5:18:02 PM	8.17	890	110	39.4	71	106	290
	249	1/1/1999 5:18:02 PM	8.06	920	107	38.4	110	150	256
	250	2/1/1999 5:18:02 PM	8.26	900	100	45.8	113	147	288
	251	3/1/1999 5:18:02 PM	8.1	952	136	39.7	92	129	378
	252	4/1/1999 5:18:02 PM	8.11	768	113	21.1	90	105	306
	253	5/1/1999 5:18:02 PM	8.12	8.34	115	35.5	95	124	337

Figure (13) Reports total review window

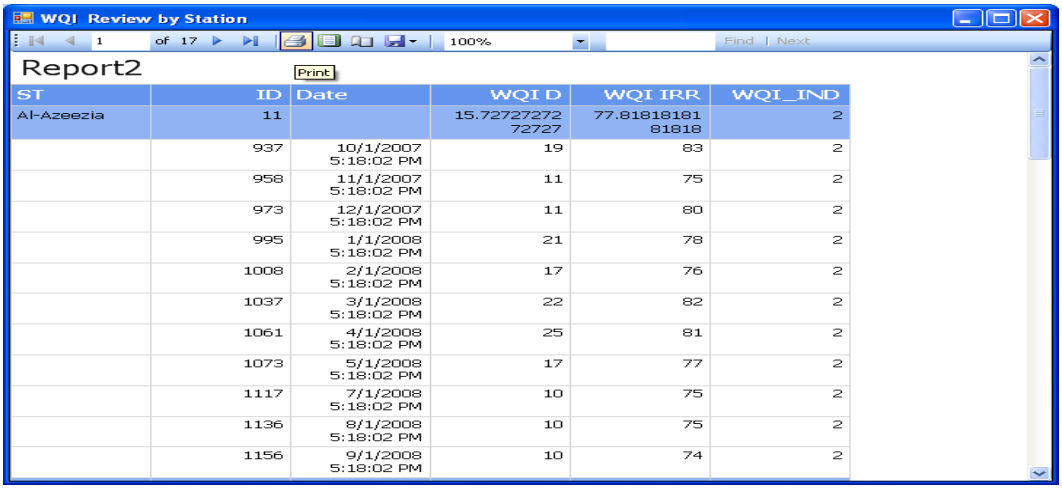

ST	ID	Date	WQI D	WQI IRR	WQI_IND
Al-Azeezia	11		15.72727272 72727	77.81818181 81818	2
	937	10/1/2007 5:18:02 PM	19	83	2
	958	11/1/2007 5:18:02 PM	11	75	2
	973	12/1/2007 5:18:02 PM	11	80	2
	995	1/1/2008 5:18:02 PM	21	78	2
	1008	2/1/2008 5:18:02 PM	17	76	2
	1037	3/1/2008 5:18:02 PM	22	82	2
	1061	4/1/2008 5:18:02 PM	25	81	2
	1073	5/1/2008 5:18:02 PM	17	77	2
	1117	7/1/2008 5:18:02 PM	10	75	2
	1136	8/1/2008 5:18:02 PM	10	75	2
	1156	9/1/2008 5:18:02 PM	10	74	2

Figure (14) Reports WQI review by station window

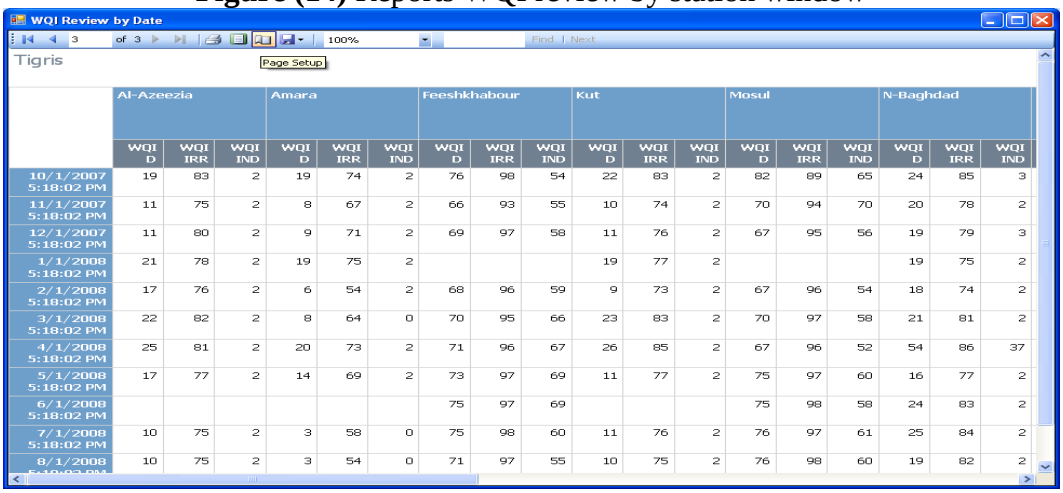

	Al-Azeezia			Amara			Feeshkhabour			Kut			Mosul			N-Baghdad		
	WQI D	WQI IRR	WQI IND	WQI D	WQI IRR	WQI IND	WQI D	WQI IRR	WQI IND	WQI D	WQI IRR	WQI IND	WQI D	WQI IRR	WQI IND	WQI D	WQI IRR	WQI IND
10/1/2007 5:18:02 PM	19	83	2	19	74	2	76	98	54	22	83	2	82	89	65	24	85	3
11/1/2007 5:18:02 PM	11	75	2	8	67	2	66	93	55	10	74	2	70	94	70	20	78	2
12/1/2007 5:18:02 PM	11	80	2	9	71	2	69	97	58	11	76	2	67	95	56	19	79	3
1/1/2008 5:18:02 PM	21	78	2	19	75	2				19	77	2				19	75	2
2/1/2008 5:18:02 PM	17	76	2	6	54	2	68	96	59	9	73	2	67	96	54	18	74	2
3/1/2008 5:18:02 PM	22	82	2	8	64	0	70	95	66	23	83	2	70	97	58	21	81	2
4/1/2008 5:18:02 PM	25	81	2	20	73	2	71	96	67	26	85	2	67	96	52	54	86	37
5/1/2008 5:18:02 PM	17	77	2	14	69	2	73	97	69	11	77	2	75	97	60	16	77	2
6/1/2008 5:18:02 PM							75	97	69				75	98	58	24	83	2
7/1/2008 5:18:02 PM	10	75	2	3	58	0	75	98	60	11	76	2	76	97	61	25	84	2
8/1/2008	10	75	2	3	54	0	71	97	55	10	75	2	76	98	60	19	82	2

Figure (15) Reports WQI review by date window

Sensitivity Functions: The main purpose of this window is to view the sensitivity functions for all uses to show the relative parameters that have affect on WQI. **(Fig. 16)**

The task bar contains the following icons:

A. Back **(◀):** When clicking on this option, the program will move back to the pervious saved sensitivity functions.

B. Next **(▶):** When clicking on this option the program will move forward to the next saved sensitivity functions.

Back: To go back to the main window**.**

Exit: To close the main window and shut down the program.

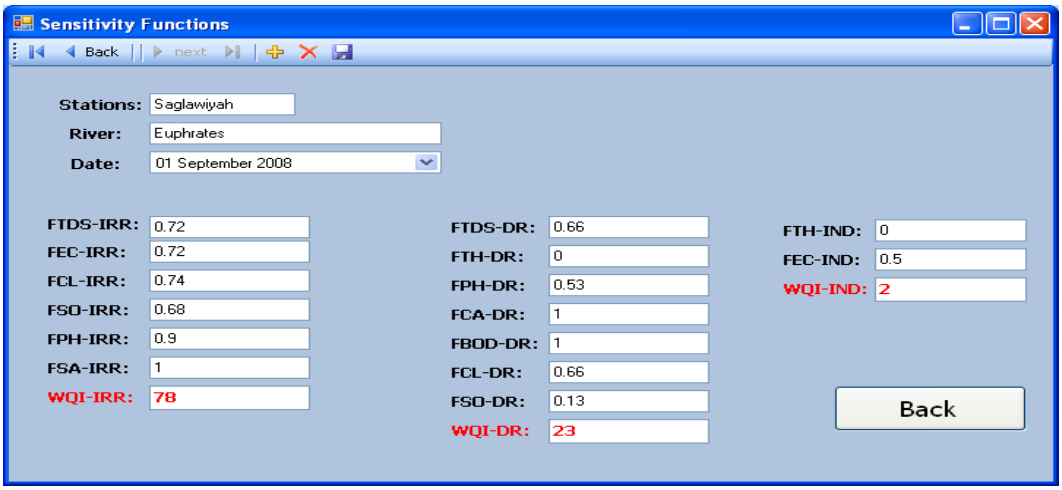

Figure (16) Sensitivity functions window

RESULTS AND DISCUSSION:

Different historical data for thirteen stations along Tigris River were adopted in the program for calculating the WQI to evaluate the water quality through one year 2007/2008 and the data are recorded on monthly base.

WQI for Tigris River (2007/2008):

Tigris River is classified for irrigation use as class I from Feeshkhabour to Tarmiyah reach, after Tarmiyah till Qurna, WOI shifts from class I to class II. In the last three months in addition to March WQI is classified as class III – V in Kut-Qurna reach due to high concentrations of T.D.S, Cl^{-1}, SO_4^{-2}, and EC. **Fig. 17** represents the average suitability maps for the Tigris River for irrigation use and shows the parameter(s) which are the most dominant (i.e. responsible for water quality deterioration that has sensitivity function less than 0.5).

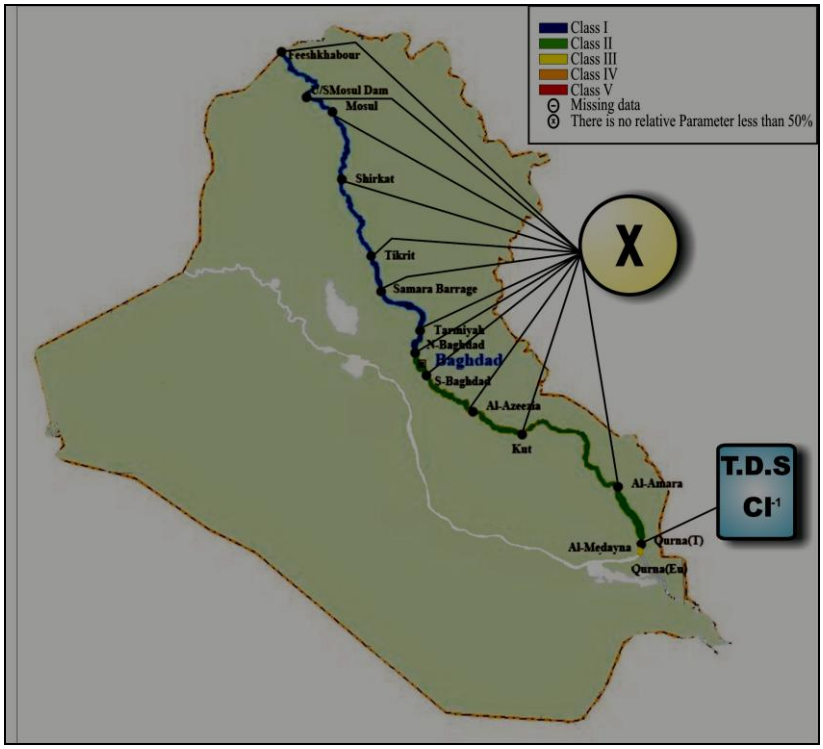

Figure (17) Average suitability map of Tigris River for irrigation use (2007/2008)

Fig. 18 represents the percentage of the deterioration of SO_4^{-2} parameter (100 - f (SO_4^{-2}) %) along the Tigris River for irrigation in 2007/2008 as one parameter from seven that affect the WQI.

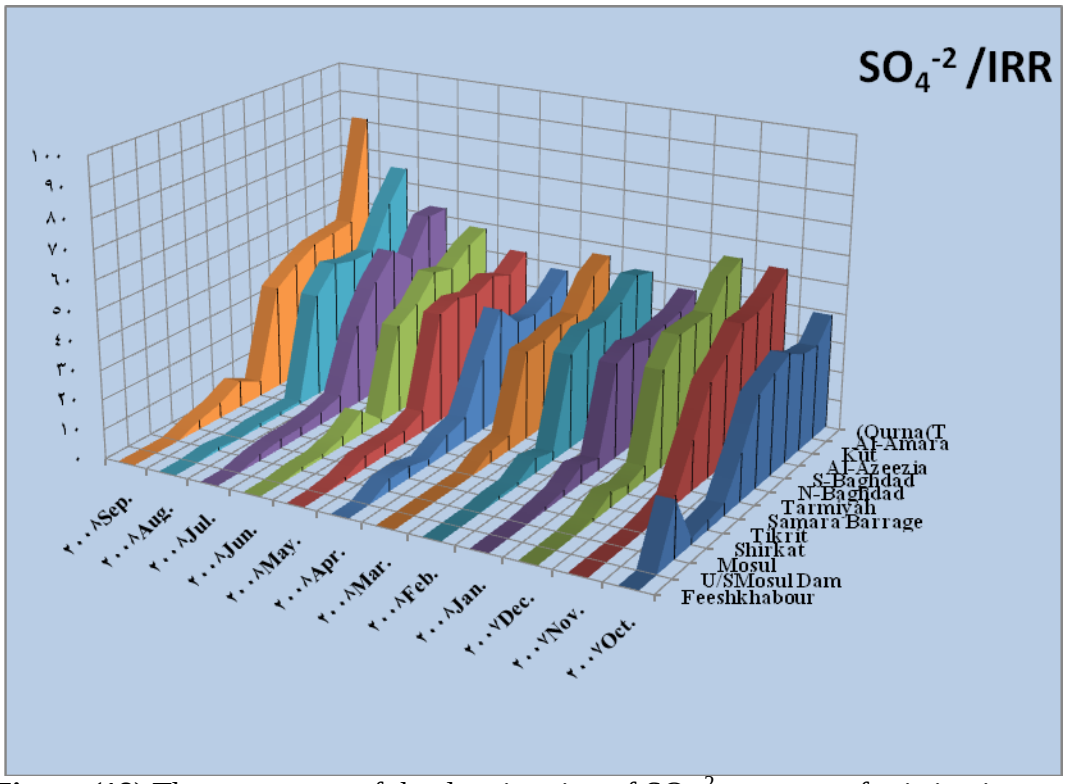

Figure (18) The percentage of the deterioration of SO_4^{-2} parameter for irrigation use

Tigris River within Feeshkhabour –Tarmiyah reach**,** in general is classified for drinking use as class II except at Tarmiyah in November, 2007 which is classified as class IV, due to T.H and pH. From Tarmiyah to Al-Azeezia, the reach is classified as class IV due to high concentration of SO_4^{-2} in addition to T.H and pH. After Al-Azeezia till Qurna, water quality is classified as class IV–V and this is mainly because of the higher increase in the relative parameters as mentioned to the sequence, T.H, SO_4^{-2}, T.D.S, pH, and, Cl^{-1}.

Fig. 19 represents the average suitability maps for the Tigris River for drinking water and shows the parameter(s) with sensitivity function less than 0.5.

Figs 20 and 21 show the percentage of the deterioration of the SO_4^{-2} (100 - f (SO_4^{-2}) %) and T.H (100 - f (T.H) %) parameters along Tigris River for drinking use in 2007/2008 as two polluted parameters from six that affect the WQI.

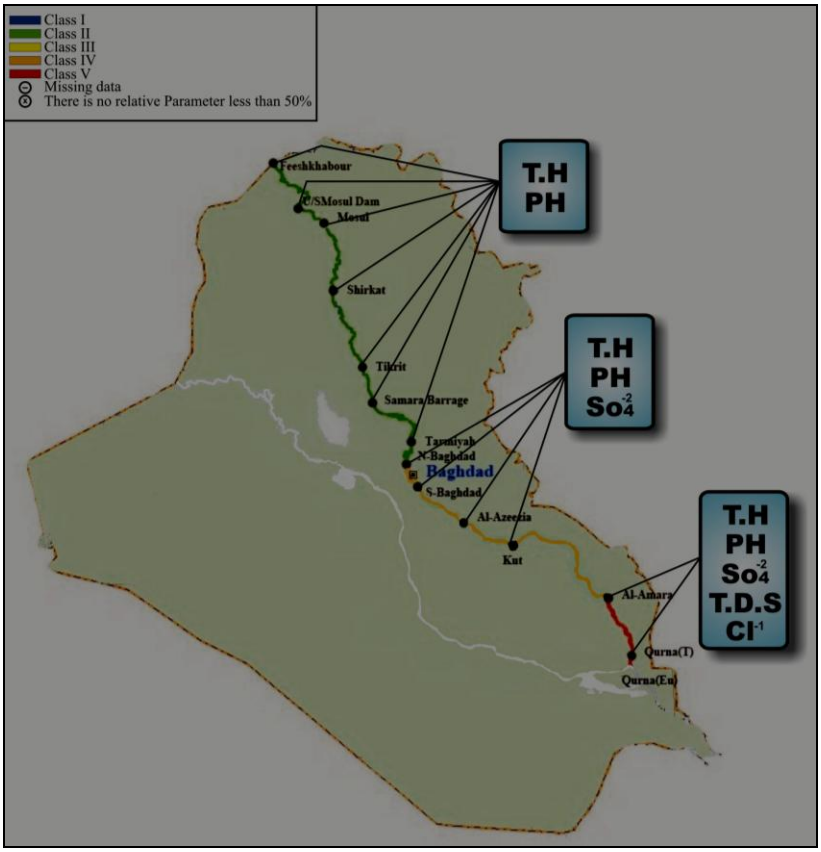

Figure (19) Average suitability map of Tigris River for drinking use (2007/2008)

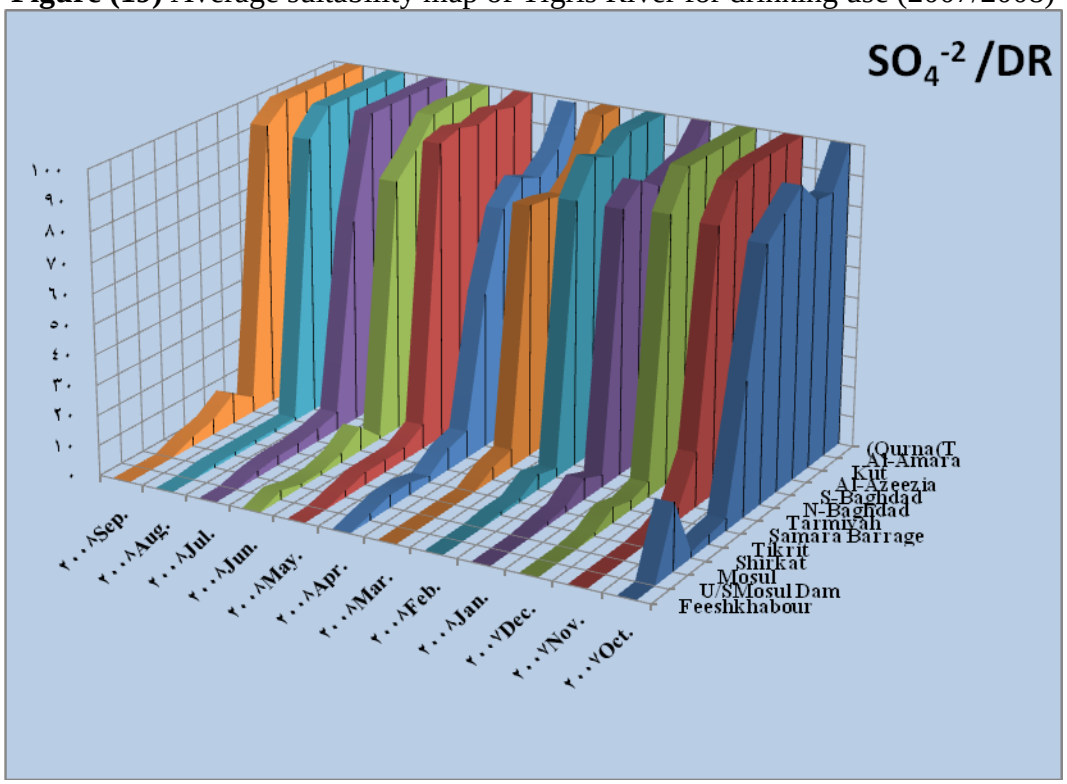

Figure (20) The percentage of the deterioration of the SO_4^{-2}parameter along Tigris for drinking use

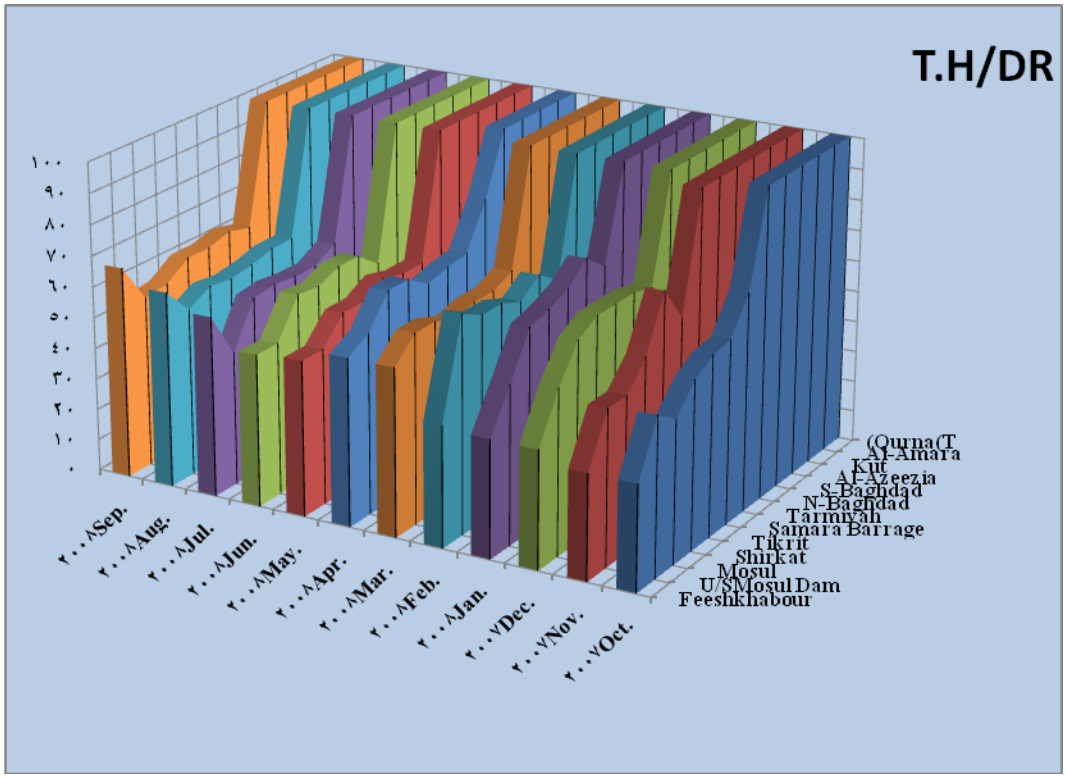

Figure (21) The percentage of the deterioration of the T.H parameter along Tigris River for drinking use

CONCLUSIONS:

- In general, WQI in the Tigris River grades for irrigation use from class I to class II, while for drinking use it is classified as class II to class V.
- In general, the deterioration in water quality along the Tigris River starts after Tarmiyah for beneficial uses due to the effect of Tigris-Tharthar arm.
- The river suitability for irrigation use is better in its classification as compared with drinking use.
- The Effect of the Total Hardness (T.H): very high concentrations which badly affects the drinking use along the Tigris and becomes worse after Tarmiyah station.
- The effect of sulfate (SO_4^{-2}) for drinking use, it can be noticed after Tarmiyah to shift WQI from class II to class IV, while for irrigation use, it can be considered an acceptable.
- The chloride ($Cl^{-1)}$ effect on drinking use is noticed after Kut while for irrigation use it is the main cause in the deterioration in water quality in the last three months in Qurna(T) .
- In general, Calcium (Ca^{+2}) values are accepted for drinking use except in the last three months in (2007/2008) after Kut in Tigris River.
- Sodium Adsorption Ratio (SAR) and the electrical conductivity (EC) values are acceptable for irrigation use.

REFERENCES

- Al-Ani, M.A., 1988, "Water Quality Index for Tigris River Classification", J. Biol. Sci. Res. Vol. 19, No.3, PP.(715–733) .
- Al-Ansari and Al-Sinawi, 1985, "Water Quality of Tigris River Water at Baghdad Using Multi Variant Analysis" , Proceeding of Iraq, Conference on Engineering, ICE.
- Al-Saffar, A.E.A, 2001, "Proposed Water Quality Management System for Tigris River", Ph.D, thesis, Civil Engineering, University of Baghdad.
- Al-Rawi and Shihab A.S., 1994, "Application of Water Quality Index to Tigris River within Mosul City ", J. Al-Rafidain Engineering. Vol. 4, No. 4, PP. (80 – 91).
- Bhargava, D.S., 1983, "Use of Water Quality Index for River Classification and Zoning of Ganga River", Environmental Pollutants, Series B, England, PP. 52-67.
- Brown, R.M., Mcclelland, N.I, Deininger R.A., and Tozer, R.G., 1970, "A Water Quality Index – Do we dare?" Water and Sewage works, 117, 10. PP. 339-343.
- El-Fadel, M., El-Sayegh, Y., Abou Ibrahim, A., Jamali, D. and El-Fadi, K., 2002, "The Euphrates-Tigris basin: a case study in surface water conflict resolution" Journal of Natural Resources and Life Sciences Education, at

  http://www.jnrlse.org/pdf/2002...E01-13.pdf
- Horton , R.K., 1965, "An Index Number System for Rating water quality", J. Water Pollut. Control Fed. 37, 3, PP. 300-305.
- Iraqi Quality Standard (IQS), 2001, " guideline for Drinking water".
- Mcclelland , N.I. ;Brown , R.M. ;Dieningar , R.A. and Landwehr, J.M., 1974, "Water Quality Index Application in the Kansas River Basin", EPA publication No. EPA- 907/9 – 74 – 001, February.
- Mohammad, M.H., 1998, "Establishment of Water Quality Index for Tigris River within Mosul City", M.Sc. thesis, Civil Engineering Department/ Environment, University of Mosul .
- Richard, L.A. 1954 "Diagnosis and Improvement of Saline and Alkali Soils" Agric, Handbook 60, U.S. Dept. Agric. Washington D.C., P16

  World Health Organization(WHO) , 2004, " guideline for Drinking water".


``````````````````````````````````````````````

**المصادر العربية**


- عبد الرزاق، خالد عادل والدباغ، عبد الستار وعلي، مقداد حسين(2001)، **"**البرنامج الوطني للاستخدام الأمثل للموارد المائية في حوض الفرات/ النماذج التنبؤية لنوعية مياه نهر الفرات وصلاحيتها لأغراض الشرب**"**، تقرير مقدم الى وزارة الزراعة،تقرير رقم 7.
- نادر وآخرون, (1986), **"**نوعية مياه نهر الفرات**"** الجزء الثاني, وزارة الري.
``````````````````````````````````````````````

MULTI-BASIS WAVENET-BASED SPEED ESTIMATION IN DIRECT TORQUE CONTROLLED ASYNCHRONOUS MOTOR

Adel A. OBED
Electrical Department, College of Engineering, Basrah University.

ABSTRACT:

This paper presents a proposed method for speed estimation of asynchronous motor in Direct Torque Control (DTC) system, based on a new architecture of multi-basis wavenet model. Such multi-basis model utilizes multi-set daughter wavelets. Firstly, the structure and training algorithm of the proposed method is discussed. The descent gradient method is used to fulfill both system structure and parameters initialization. Secondly, the proposed speed estimator and the DTC asynchronous motor are combined based on stator current signal and the motor speed is then estimated online with the operation of the system. Finally, the effectiveness of this method is proved by simulation carried out using Matlab/Simulink library and compared with the actual results obtained from the dynamic equations of the motor. The simulation results are obtained over the entire speed of starting, load conditions and motor braking. These results show that the proposed method is effective for speed estimation in DTC drives.

KEYWORDS: Wavenet, Multi-basis wavenet, Direct torque control, Speed estimation, Asynchronous motor.

تقدير السرعة في نظام التحكم المباشر لعزم المحرك الغير متزامن باعتماد الشبكات العصبية المويجية متعددة الأساسات

الخلاصة :

في هذا البحث تم اقتراح طريقة لتقدير سرعة المحرك الغير متزامن في نظام التحكم المباشر للعزم باعتماد الشبكات العصبية المويجية المتعددة الأساسات بتوظيف عدة مجاميع من بنات المويجات. تمت في البداية مناقشة تركيب وخطوات تدريب النظام المقترح باستخدام خوارزمية الانحدار الهابط لتحقيق بنية النظام وحساب المعاملات. وتم ثانيا تركيب وربط نظام تقدير السرعة المقترح مع نظام التحكم المباشر للعزم عبر تيار الجزء الثابت للمحرك حيث تم تقدير السرعة بشكل مباشر أثناء عمل النظام. وأخيرا تم التحقق من كفاءة الطريقة المقترحة لتقدير السرعة من خلال نتائج المحاكاة التي انجزت باستخدام مكتبة Simulink في Matlab وقورنت نتائج السرعة المقدرة مع السرعة الحقيقية المحسوبة من معادلات الحركة للمحرك. أستحصلت نتائج المحاكاة لعدة مديات للسرعة عند البدء وحالات التحميل وعند حالة إيقاف المحرك. وقد أظهرت النتائج فعالية الطريقة المقترحة قي تقدير السرعة في أنظمة التحكم المباشر للعزم.

INTRODUCTION

The speed estimation in DTC asynchronous motor systems have developed during the last few years and become the main development direction of the AC speed adjustment [C. J. Chen, et al., 2007]. Generally to establish the speed loop feedback in DTC system, information of rotor speed is essential. Installation sensor for detecting rotor speed will increase hardware cost and add some volume of system as well as the installation and maintenance bring many difficulties beside the mechanical error which affect the detection precision and performance of DTC control.

Several methods that eliminate the speed sensor have been developed. The observer-based [J. Maes, et al., 2000, H. Kubota, et al., 1993, G. Yang, et al., 1993, C. Lascu, et al., 2004, and Y. R. Kim, et al.,, 1992] and the Model Reference Adaptive System (MRAS) [C. Schauder, 1992, C. Lascu, et al., 2000. and T. BANA, et al., 2002] seem the most used methods for sensorless speed DTC system. However, the estimated speed is affected by machine parameters. Moreover, these methods need to detect all the terminal voltages and currents of the motor. A good technique for speed sensorless operation based on Neural Network (NN) has been presented over the last years [M. P. Kazmiorkowski, et al., 1997, and L. Brahim, et al., 1993]. This method is based only on signals detected from motor terminals which eliminate the effect of motor parameters sensitivity on the estimated speed. However, the estimated speed could not be perfectible due to some problems such as trapping in to local minima and slow convergence.

The combination of NN with wavelet transform (wavenet), behaves good localization property in both time and frequency space and multi-scale property. It is used for the analysis of non-stationary signals and learning of the nonlinear functions [S. Mallat, 1999]. This technique is also proposed to estimate the speed in DTC system [C. Zhi, et al., 2003 and M. A Alwan, et al., 2008].

In this paper, the theory of wavenet is presented and a method of speed estimation based on multi-basis wavenet is proposed. The proposed method includes multi-set daughter wavelets from different mother functions in the hidden layer which is believed useful to represent functions containing different signal cutting, ripples and rapid signal changes. The simulink model of DTC asynchronous motor system is implemented and a speed estimator based on the above proposed method is combined with the system based on one line of stator current signal. Simulation results include developed torque, stator current beside the rotor speed which is compared with the actual motor speed. Note that the theory of DTC control has not been discussed here, however it can be found in details in [G. S. Buja, et al., 2004].

WAVENET

Wavenet can be considered a particular case of the feed forward basis function neural network model. In ordinary network, several types of basis functions, such as radial basis functions, splines and polynomial functions of synapse neurons are used instead of sigmodial function. The connection weights are taken to represent the corresponding coefficients. The output layer performs the sum of the output of all synapse neurons. Since wavelets have been shown their excellent performance in non stationary signal analysis and nonlinear function modeling, the neural network using wavelet basis function, wavenet, provides higher availability of rate of convergence for the approximation than an ordinary feed forward neural network [S. Mallat, 1999].

The wavenet can be constructed by means of replacing the nonlinear sigmodial function with nonlinear wavelet basis function. Figure 1 illustrates the wavenet structure and Fig. 2 shows some typical wavelet functions.

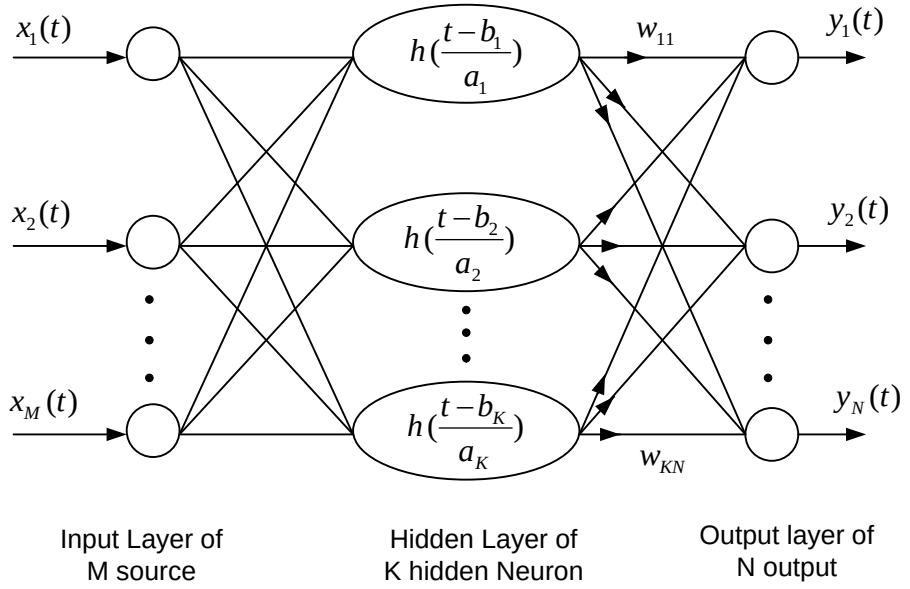

Fig.(1) The structure of wavenet

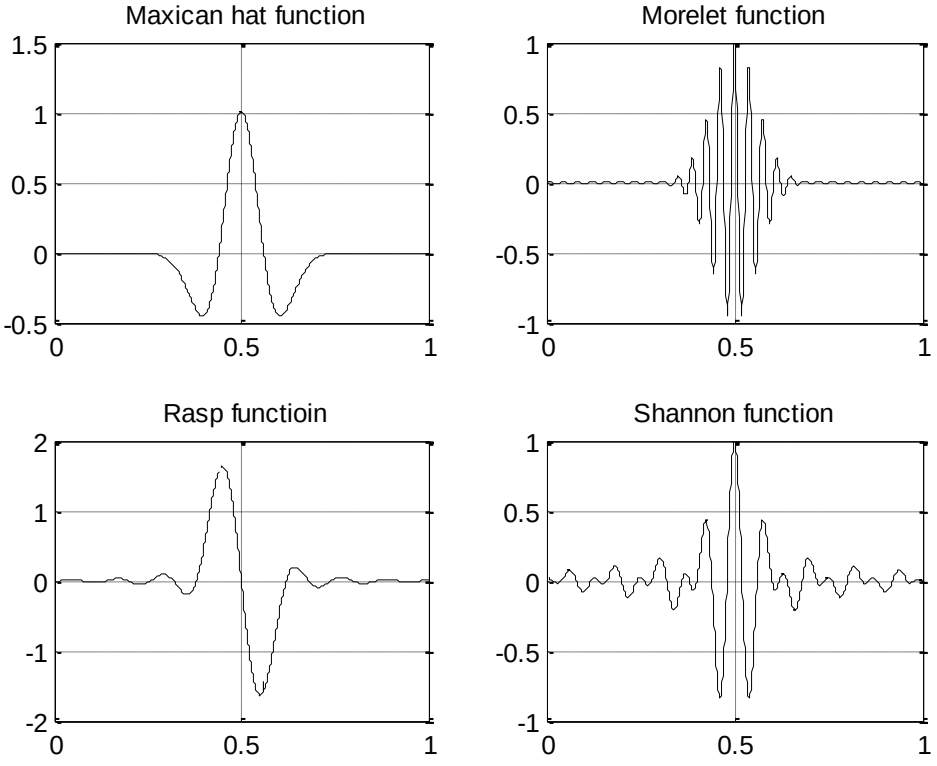

Fig. 2 Some typical wavelet functions

The network exhibits a multi-input to multi-output nonlinear system, realizing mapping from $R^m \Rightarrow R^n$. The approximated output signal of the network can be expressed as follows

$$y_i = f\left[\sum_{k=1}^{K} w_{ki} \sum_{m=1}^{M} x_m(t)\ h_m((t-b_k)/a_k)\right] \quad (1)$$

where $x_m(m=1,2,...,M)$ is the input for the m-th training vector $X(t)$, $y_i(i=1,2,...,N)$ is the output for the i-th training vector $Y(t)$, M is the node numbers of the input layer, K is the node numbers of hidden layer, w_{ki} is the weight between the k-th node of the hidden layer and the i-th node of the output layer, $h(t)$ is the mother wavelet, a,b are the dilation and translation and f is the linear function.

PROPOSED WAVENET SPEED ESTIMATOR

The structure of the proposed P-based wavenet speed estimator is shown in Fig. 3 and the set up of its training and estimation for online speed changes in DTC asynchronous motor system is shown in Fig. 4.

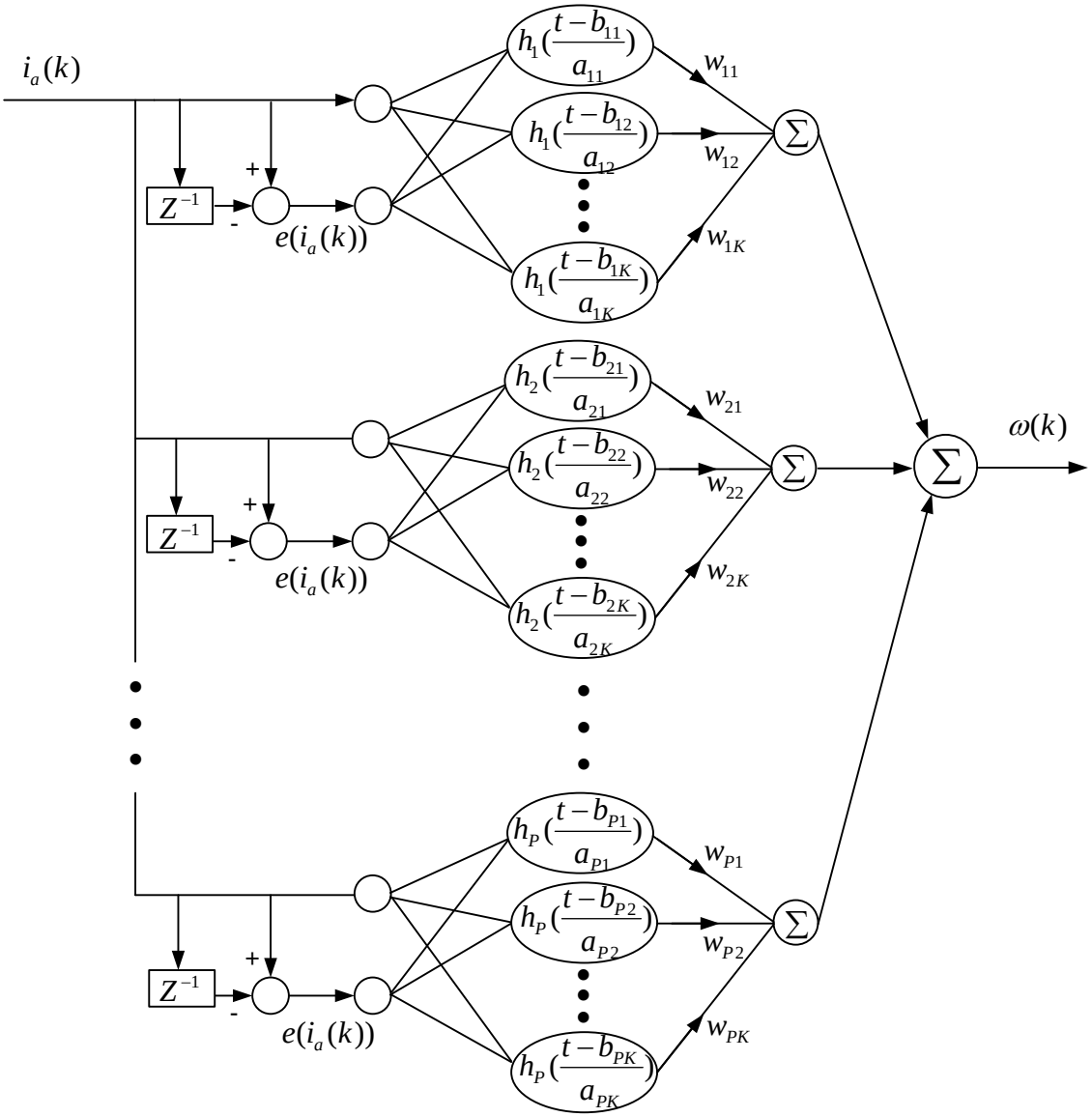

Fig.3 The proposed 2-input/ single output P-based (each of K daughters) wavenet speed estimator.

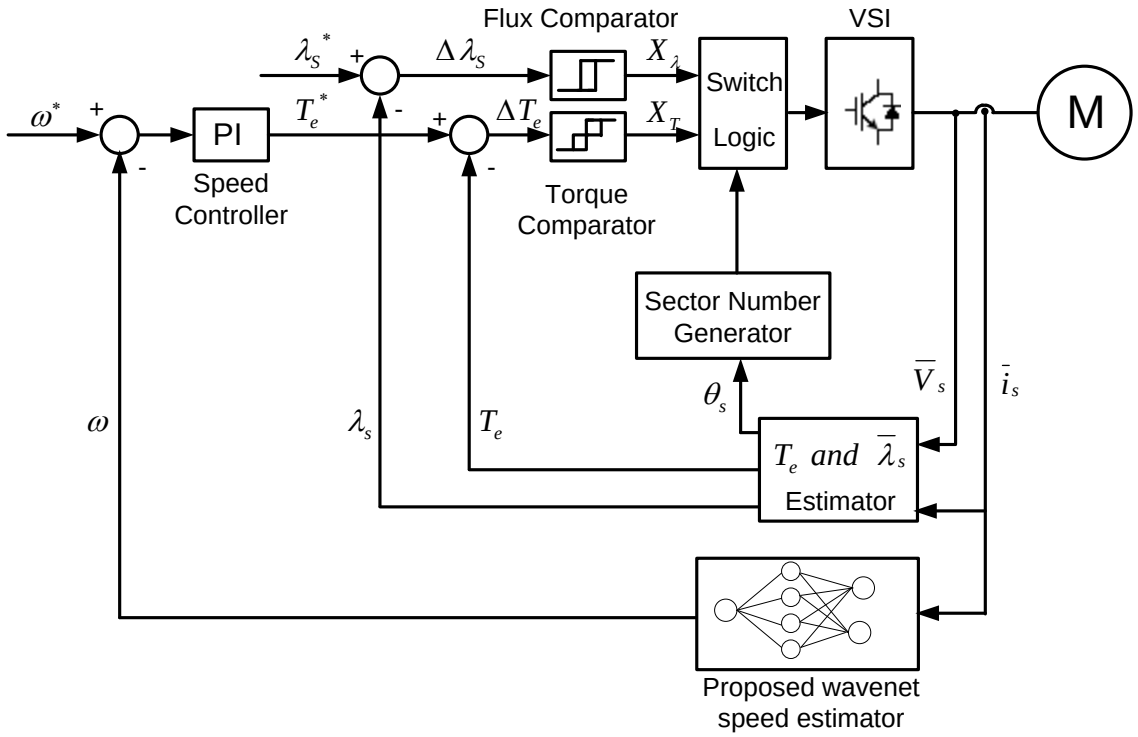

Fig.4 The set up for online training and estimation for speed in DTC asynchronous motor system.

The wavenet speed estimator exhibits two inputs and single output. The input nodes are the stator current $i_a(k)$ and the error in the stator current $e(i_a(k))$. They are defined as follows

$i_a(k)$ = instantaneous value of stator current.

$$e(i_a(k)) = i_a(k) - i_a(k-1) \tag{2}$$

A single signal from one line current is used here which uses a single current sensor. This is useful for simplicity and economy [M. A. Alwan, et al., 2008]. The hidden layer is of P different sets of daughter wavelets. The output of the wavenet is the motor speed which can be given as follows [C. Zhi, et al., 2003]

$$y = \omega(k) = f\left[\sum_{p=1}^{P}\sum_{k=1}^{K} w_{pk}\sum_{m=1}^{M} X_m\, h_p((t-b_{pk})/a_{pk})\right] \tag{3}$$

In order to determine the adjustable weights $w_{kp}(k=1,2,...K,\ p=1,2,...P)$ and the adjustable parameters a_{pk} and b_{pk}, a least mean square (LMS) energy minimizing function can be applied:

$$E = \frac{1}{2}\sum_{l=1}^{q}\sum_{i=1}^{n}(e^l)^2 \tag{4}$$

where $e^l = F^l - y^l$, q and F^l are the number of training samples and the desired value of y^l. To minimize the energy error E, a method of steepest descent which requires the gradients $\frac{\partial E}{\partial w_{pk}}, \frac{\partial E}{\partial a_{pk}}$ *and* $\frac{\partial E}{\partial b_{pk}}$ is used for updating the incremental changes to each parameter w_{pk}, a_{pk}, *and* b_{pk}. The gradients of E are:

$$\frac{\partial E}{\partial w_{pk}} = -\sum_{l=1}^{q}\sum_{i=1}^{N}\sum_{m=1}^{M} e^l \; X_m{}^l \; h(\tau) \tag{5}$$

$$\frac{\partial E}{\partial b_{pk}} = -\sum_{l=1}^{q}\sum_{i=1}^{N}\sum_{m=1}^{M} e^l \; X_m{}^l * \; w_{pk}\frac{\partial h(\tau)}{\partial b_{pk}} \tag{6}$$

$$\frac{\partial E}{\partial a_{pk}} = -\sum_{l=1}^{q}\sum_{i=1}^{N}\sum_{m=1}^{M} e^l \; X_m{}^l * w_{pk}\,\tau\frac{\partial h(\tau)}{\partial b_{pk}} = \tau\frac{\partial E}{\partial b_{pk}} \tag{7}$$

where $\tau = \frac{t - b_{pk}}{a_{pk}}$. The updated weight w_{pk} and the parameters a_{pk} and b_{pk} are:

$$w_{pk}(n+1) = w_{pk}(n) - b_w\frac{\partial E}{\partial w_{pk}} + c_w\,\Delta w_{pk}(n) \tag{8}$$

$$a_k(n+1) = a_k(n) - b_a\frac{\partial E}{\partial a_k} + c_a\,\Delta a_k(n) \tag{9}$$

$$b_k(n+1) = b_k(n) - b_b\frac{\partial E}{\partial b_k} + c_b\,\Delta b_k(n) \tag{10}$$

where b_w, b_a, and b_b are steps size, c_w, c_a, and c_b are the forgetting factors which are variable factors and can greatly reduce the number of iterations for convergence.

SIMULATION RESULTS

Two sets of daughter wavelet functions $(P = 2)$ with seven neurons $(K = 7)$ in each set are used to represent the hidden layer of a 2-basis wavenet speed estimator. The two mother wavelets used in these sets are Mexican hat and Shannon functions. These functions with their derivative with respect to the translation b are given as follows

Mexican hat function

$$h(\tau) = \frac{2}{\sqrt{3}}\,\pi^{\frac{1}{4}}\,(1-\tau^2)\,e^{-\frac{\tau^2}{2}} \tag{11}$$

$$\frac{\partial h(\tau)}{\partial b} = \frac{1}{a}(3\tau - \tau^3)\exp(-\frac{\tau^2}{2}) \tag{12}$$

and for Shannon function

$$h(\tau) = \frac{\sin 2\pi\tau - \sin \pi\tau}{\pi\tau} \tag{13}$$

$$\frac{\partial h(\tau)}{\partial b} = \frac{\pi}{a} \frac{(-\pi\tau \cos \pi\tau - 2\pi \cos 2\pi\tau + \sin \pi\tau + \sin 2\pi\tau)}{(\pi\tau)^2} \tag{14}$$

where $\tau = \frac{t - b_{pk}}{a_{pk}}$. The wavenet speed estimator was trained off line before combining it with the DTC system based on data obtained from the conventional operation of the DTC system. The training is based on eq. 2 to 10 which can programmed in M-file in Matlab library as given in the Appendix. The simulation was carried out to verify the function of the speed estimator where the motor used in this system is a 3-ph, 1250 hp, 4160V, 150A, 6 poles, and 60 Hz induction motor (asynchronous motor). The simulation parameters of the motor are described as follows: N_s=1200r.p.m., R_s=0.21Ω, R_r=0.146Ω, $L_s = L_r = 2mH$, $L_m = 0.155H$ and $J = 22kg.m^2$.

The rotor speed of the motor which is used to complete the torque loop in the DTC system (Fig. 4) is taken either from the actual value calculated from the dynamic motor equations or from the proposed wavenet speed estimator.

Figure 5 shows the actual rotor speed for starting the DTC system with no load from standstill to a speed of 100 rad./sec. through 2 seconds, then the speed is increased suddenly to 200 rad./sec. through the next 2 seconds. Figure 6 shows the estimated rotor speed identified by the proposed wavenet speed estimator for the case above. It shows higher dynamical following performance. The starting current and the starting torque for the same previous case are show in Fig. 7 and 8 respectively.

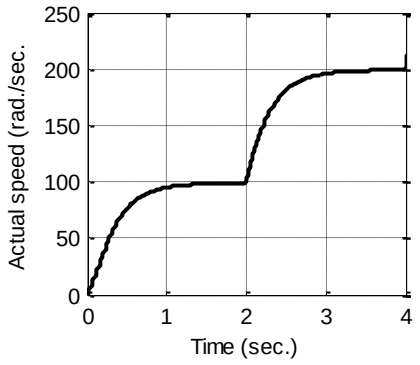

Fig. 5 Actual speed (electrical) during starting

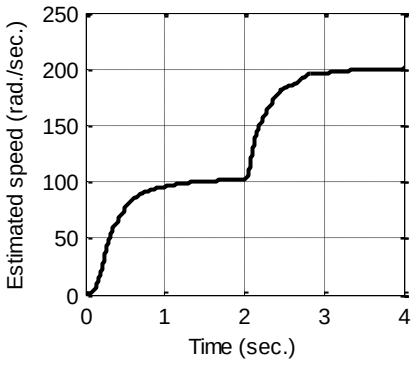

Fig. 6 Estimated speed (electrical) during starting

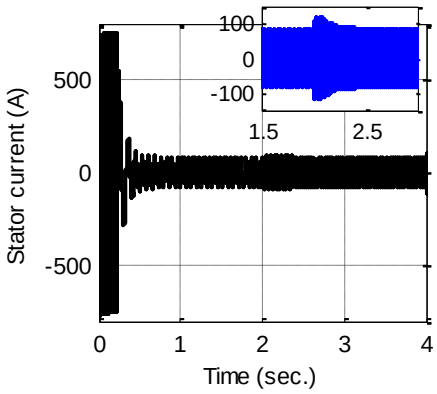

Fig. 7 Stator current during starting with magnified portion at speed step change instant.

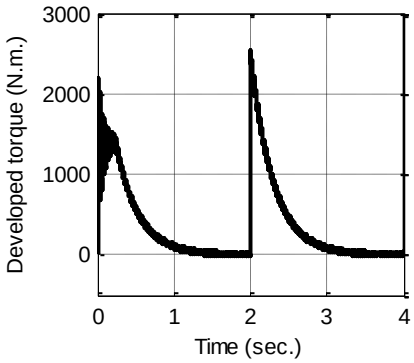

Fig. 8 Developed torque during starting.

ROBUSTNESS

In order to test the robustness of the proposed method, the effect of system braking and sudden change for full load torque have studied on the performance of the torque control and speed changes.

To illustrate the performance of braking control, the operating mode have simulated without load and the motor runs at rated speed of 377.8 rad./sec., the braking starts at the instant of 3 sec. and the system is kept at standstill after the braking. Figure 9 and 10 show the actual and estimated speed during braking while Fig. 11 and 12 show the stator current and developed torque for the same mentioned case. The estimated speed follows the actual with an error less than 1% which reflect the ability of the proposed speed estimator.

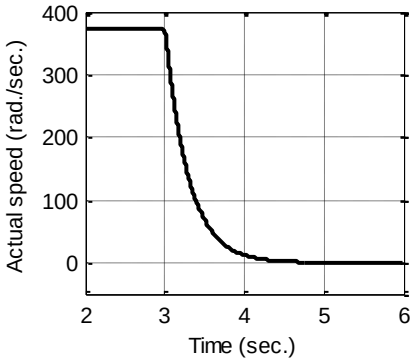

Fig. 9 Actual speed (electrical) during braking

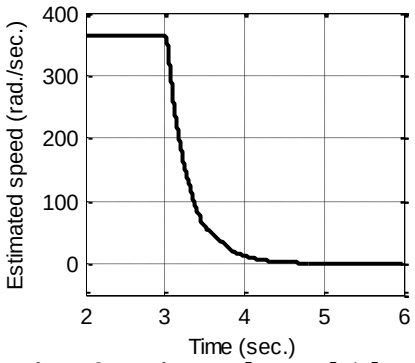

Fig. 10 Estimated speed (electrical) during braking

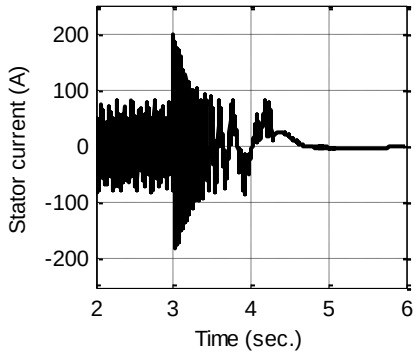

Fig. 11 Stator current during braking.

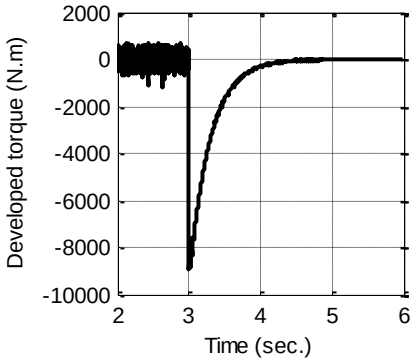

Fig. 12 Developed torque during braking.

Figures 13-15 show the tests of robustness realized with sudden change in load torque from no load to full load of the motor used, 7490 N.m, at the instant t=4sec. and its elimination at t=6 sec. This process is repeated two times. In this case, the estimated speed is used as a feed back signal to complete the torque loop of the DTC system. The developed torque curve in Fig. 15 reflects the direct control of torque. The developed torque follows its demand quickly with a time less than 0.05 sec.

For the robustness of control, a braking case, the estimated speed follows its actual and for system loading when the speed is used as feed back signal, the DTC system gives an adequate accuracy of system performance.

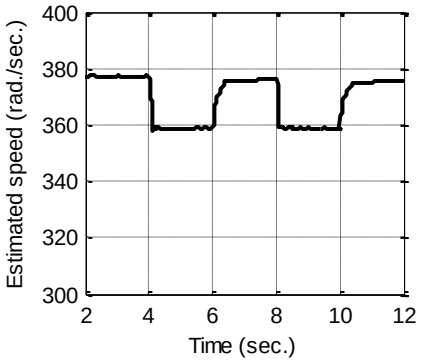

Fig. 13 Estimated speed (electrical) during load change.

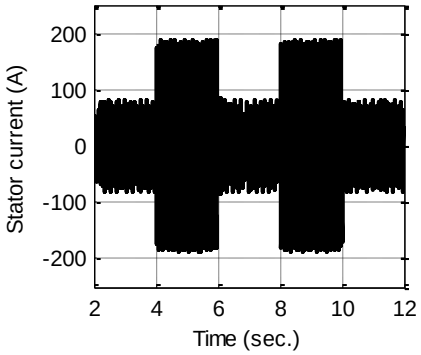

Fig. 14 Stator current during load change

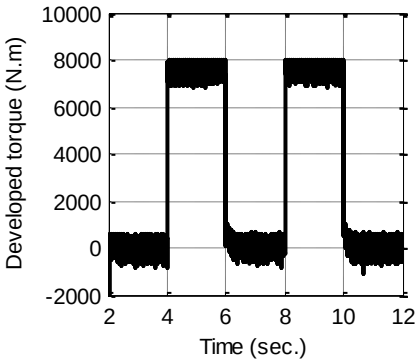

Fig. 15 Developed torque during load change

CONCLUSIONS

The paper presents a new multi-basis wavenet speed estimator based on multi-set daughter wavelet functions in DTC asynchronous motor system. The multi-basis wavenet is useful because of high nonlinearity in the stator current waveform. The wavenet speed estimator is trained offline based on stator current information obtained from the conventional operation of the DTC system. The advantage of using multi-basis wavenet is the adequate speed estimated for different operating conditions. The simulation results reveals a good system performance.

REFERENCES

- C. J. Chen and T. C. Chen, "Speed Sensorless of an Induction Motor Using Self-Tuning Fuzzy Identification", 2nd International Conference on Information and Control ICICIC, 5-7 Sep. 2007.

- C. Lascu and A. M. Trzynadlowski, "A Sensorless Hybrid DTC Drive for High Volume Low-Cost Application", IEEE Trans. Ind. Electron., Vol. 51, No. 5, pp. 1048-1055, Oct. 2004.

- C. Lascu, and F. Blaabjerg, "A Modified Direct Torque Control for Induction Motor Sensorless Drive", IEEE Trans. Ind. Applicat., Vol.36, No. 1, Jan./Feb., 2000.

- C. Schauder, "Adaptive Speed Identification for Vector Control of Induction Motors without rotational transducers", IEEE Trans. Ind. Applicat., Vol. 28, No. 5, pp. 1054-1061, Sept./Oct. 1992.

-C. Zhi Cao, Mu_ping Lu, and Xin Wang, "Speed Estimation and Stimulation of DTC System Based on Wavelet Neural Network", Proc. On 2nd International on Machine Learning and Cybernetics, Xi'an, 2-5 Nov. 2003.

- G. S. Buja and M. P. Kazmierkowski, "Direct Torque Control of PWM Inverter-Fed AC Motors-A Survey", IEEE Trans. Ind. Electron., Vol. 51, No. 4, pp. 744-757, Aug. 2004.

- G. Yang and T.-H. Chin, "Adaptive-Speed Identification Scheme for a Vector-Controlled speed Sensorless Inverter Induction Drive." IEEE, Trans. Ind. Applicat, Vol. 29, No. 4, pp 820-825, July/Aug. 1993.

- H. Kubota, K. Matsuse, and T. Nakano, "DSP-Based Speed Adaptive Flux Observer of Induction Motor", IEEE Trans. Ind. Applicat., Vol. 29, No. 2, pp. 344-348, Mar./Apr. 1993.

- J. Maes and A. Melkebeek, "Speed Sensorless Direct Torque Control of Induction Motors Using Adaptive Flux Observer", IEEE Trans. Ind. Applicat., Vol., 36, No. 3, pp. 778-785, May/June 2000.

- L. Brahim and R. Kurosawa, "Identification of Induction Motor Speed Using Neural Networks", in PCC-Yokohama, pp. 689-694, 1993.

- M. A. Alwan, J. M. Abdul-Jabbar and A. A. Obed, " Speed Estimation of DTC Induction Motor Using Single Current Sensor Based on Wavenet Theory", Basrah Journal of Engineering Sciences, Vol. 8, No. 1, pp 27-38, 2008.

- M. P. Kazmiorkowski, D. L. Sobczuk and Filipek, "Sensorless Control of Induction Motor Using a Neural Network for Speed Estimation", Industrial Electronics, Vol. 3, PP. 1242-1246, July, 1997.

- S. Mallat, "A Wavelet Tour of Signal Processing", Academic Press, 1999.

- T. PANA, C. RUSU, "Speed and Rotor Flux Estimation in Speed Sensorless Control of Induction Motor", Ion BIVOL Fascicle III, 2002.

- Y. R. Kim, S.-K. Sul, and M.-H. Park, " Speed Sensorless Vector Control of an Induction Motor Using an Extended Kalman Filter", in conf. Rec. IEEE-IAS Annu. Meeting, pp. 594-599 1992.

LIST OF SYMBOLES AND ABBREVIATIONS

A.C: Alternating Current.
DTC: Direct Torque Control.
LMS: Least Mean Square.
MRAS: Model Reference Adaptive System.
a : Dilation
b : Translation.
c : Forgetting factor.
$e(i_a)$: error in stator current (A).
E : Energy error.
f : Linear function.
F : Desired vector of the output vector.
h : Mother wavelet.
i_a : Stator current (A).
J : Moment of inertia ($kg.m^2$).
K : Node numbers of hidden layer.
L : Inductance (H).
M : Node numbers of the input layer.
N : Node numbers of the output layer, Motor speed (rad./sec.).
P : Number of daughter wavelets.
q : Number of training samples.
R : Resistance Ω.
w : Weight.
x : Input vector.
y : Output vector.

APPENDIX

```
%Matlab program for learning the proposed wavenet speed estimator based on eq.2 to10.
%Mexican Hat and Shannon mother wavelet functions are used in learning
w1=[.1,.1,.1,.1,.1,.1,.1];a1=[.1,.1,.1,.1,.1,.1,.1];b1=[-.1,0,.1,.2,.5,.8,1.2];
w2=[.1,.1,.1,.1,.1,.1,.1];a2=[.1,.1,.1,.1,.1,.1,.1];b2=[-.1,.1,.3,.5,.9,1,1.3];
DW1=[0,0,0,0,0,0,0]; DB1=[0,0,0,0,0,0,0]; DA1=[0,0,0,0,0,0,0];
DW2=[0,0,0,0,0,0,0]; DB2=[0,0,0,0,0,0,0]; DA2=[0,0,0,0,0,0,0];
t=[0:1700];% time sample 1701samples
x11=[];% input current, can be loaded from file,1701 samples
F1=[];% target speed, can be loaded from file, 1701 samples
x=(x11-min(x11))/(max(x11)-min(min(x11));%  normalized input current
F=(F1-min(F1))/(max(F1)-min(F1));%normalized target
aw1=.993;aa1=.993;ab1=.993;bw1=.0001;ba1=.0001;bb1=.0001;
aw2=.1;aa2=.1;ab2=.1;bw2=.01;ba2=.01;bb2=.01;
for I=[1:1000]%iteration counter
    E=0;
    for n=[1:1701];%sampled number
       y(n)=0;
       for k=[1:7];%weighs counter
          y1=w1(k)*(x(n))*(2/sqrt(3))*(pi^(-1/4))*(1-(((x(n)-b1(k))/a1(k))^2))*(exp(-(((x(n)-
b1(k))/a1(k))^2)/2));
          y2=w2(k)*(x(n))*(sin(2*pi*((x(n)-b2(k))/a2(k)))-sin((x(n)-b2(k))/a2(k)))/(pi*(x(n)-
b2(k))/a2(k));
          y(n)=y(n)+y1+y2;
       end; %end k
       E1=0.5*((F(n)-y(n))^2); E=E+E1;
    end %end n
     if E< abs(.01)
       disp('end of work')
       break;
     else
        for k=[1:7
         PEPW1(k)=0;PEPB1(k)=0;PEPA1(k)=0;PEPW2(k)=0;PEPB2(k)=0;PEPA2(k)=0;
          for n=[1:1701];
            t1=(x(n)-b1(k))/a1(k);
            PEPW11(k)=-(F(n)-y(n))*(x(n))*(2/sqrt(3))*(pi^(-1/4))*(1-(((x(n)-
b1(k))/a1(k))^2))*(exp(-(((x(n)-b1(k))/a1(k))^2)/2));
            PEPB11(k)=-(F(n)-y(n))*x(n)*w1(k)*(2/sqrt(3))*(pi^(-1/4))*(1/a1(k))*(3*t1-
t1^3)*exp(-(t1^2)/2);
            PEPA11(k)=PEPB1(k)*t1; PEPW1(k)=PEPW1(k)+PEPW11(k);
            PEPB1(k)=PEPB1(k)+PEPB11(k); PEPA1(k)=PEPA1(k)+PEPA11(k);
            t2=(x(n)-b2(k))/a2(k);
            PEPW22(k)=-(F(n)-y(n))*((x(n)-b2(k))/a2(k))/((((x(n)-b2(k))/a2(k))^2+1)^2);
            PEPB22(k)=-(F(n)-y(n))*x(n)*w2(k)*(1/a2(k))*((pi*t2*cos(pi*t2)-
2*pi*cos(2*pi*t2)+sin(pi*t2)+sin(2*pi*t2))/((pi*t2^2)));
            PEPA22(k)=PEPB2(k)*t2; PEPW2(k)=PEPW2(k)+PEPW22(k);
            PEPB2(k)=PEPB2(k)+PEPB22(k); PEPA2(k)=PEPA2(k)+PEPA22(k);
          end % end n
          storew1(k)=w1(k);
          w1(k)=w1(k)-bw1*PEPW1(k)+aw1*DW1(k);
```

```
        DW1(k)=w1(k)-storew1(k);
        storeb1(k)=b1(k);
        b1(k)=b1(k)-bb1*PEPB1(k)+ab1*DB1(k);
        DB1(k)=b1(k)-storeb1(k);
        storea1(k)=a1(k);
        a1(k)=a1(k)-ba1*PEPA1(k)+aa1*DA1(k);
        DA1(k)=a1(k)-storea1(k);
        storew2(k)=w2(k);
        w2(k)=w2(k)-bw2*PEPW2(k)+aw2*DW2(k);
        DW2(k)=w2(k)-storew2(k);
        storeb2(k)=b2(k);
        b2(k)=b2(k)-bb2*PEPB2(k)+ab2*DB2(k);
        DB2(k)=b2(k)-storeb2(k);
        storea2(k)=a2(k);
        a2(k)=a2(k)-ba2*PEPA2(k)+aa2*DA2(k);
        DA2(k)=a2(k)-storea2(k);
      end %end k
    end;%end if
end %end I
%Plot the training results
subplot(2,2,1)
plot(t,y,'k'); grid on
xlabel('time(sec)')
ylabel('output speed')
title('Fig.1.identified speed')
subplot(2,2,2)
plot(t,F,t,y); grid on
xlabel('time(sec)')
ylabel('target identified speed')
title('Fig.2.target and identified speed')
subplot(2,2,3)
plot(t,x11,'r'); grid on
xlabel('time(sec)')
ylabel('input1')
title('Fig.3.input')
subplot(2,2,4)
plot(t,E,'g')
grid on
xlabel('time(sec)')
ylabel('Error')
title('Fig.4.Error')
```

Number 4 Volume 16 December 2010 Journal of Engineering

HAND WRITTEN RECOGNITION USING NEURAL NETWORK ALGORITHM

Ammar O. Hoori
University of Baghdad, College of Engineering, Computer Engineering Department , Baghdad, Iraq.

ABSTRACT

Hand written recognition problem can be done in two major steps, first by separating each character alone and second by detecting the separated shape to its corresponding like alphabetic letter. A backpropagation neural network found to be a good artificial intelligence algorithm in facing character recognition problem.

In this work, backpropagation neural network is used with 3-layers to detect and separate 26 English letter from (A to Z). In addition, a previous steps should be taken to detect the boundaries of each single written letter. Detecting a complete text can be done by separating each character through finding its boundaries, resizing the separated character to be suitable for pre-trained neural network, detecting the hand-written letter and finally saving the guessed letter to a text file. This work is developed using Matlab 2008 version 7.6. The obtained results show good representations of letter contaminated by noise and non-trained letters.

KEYWORDS: Character Recognition, Neural Network, Artificial Intelligence, Backpropogation, Hand written recognition

الخلاصة

مشكلة تمييز خط اليد المكتوب تتم على خطوتين رئيسيتين ، أولاً من خلال فصل كل شكل على حدة وثانياً بتمييز الشكل المفصول للحرف الأبجدي المشابه له. الخلية العصبية ذات الانتشار الخلفي وجدت كلوغارتمية ذكاء اصطناعي جيدة في مواجهة مشكلة تمييز الأشكال.

في هذا العمل، . الخلية العصبية ذات الانتشار الخلفي استخدمت بثلاث طبقات لإيجاد وفصل 26 حرف انكليزي من (A إلى Z). بالإضافة لذلك ، هنالك خطوات مسبقة يجب أن تتخذ ، وذلك لإيجاد حدود كل حرف مكتوب بخط اليد. إيجاد نص كامل ممكن أن يتم بعزل كل شكل من خلال إيجاد حدوده ، ثم تعديل حجم الشكل المعزول ليكون ملائماً للخلية العصبية المُعلمة مسبقاً، ثم بإيجاد الحرف المكتوب بخط اليد ، وأخيراً حفظ الحرف المحزور في ملف كتابة. هذا العمل أنجز باستخدام برنامج Matlabالإصدار 7.6 لعام 2008. النتائج المكتسبة أظهرت تمثيل جيد للأحرف الملوثة بالشوائب والأحرف الغير معلمة مسبقاً.

INTRODUCTION:

One of the most important applications in Artificial Neural Network field is the character recognition. It is the base for many different types of applications in various fields, many of which we use in our daily lives. Cost effective and less time consuming, businesses, post offices, banks and security systems. Whether you are processing a check, performing an eye/face scan at the airport entrance, or teaching a robot to pick up and object, you are employing the system of character recognition. One field that has developed from character recognition is optical character recognition (OCR) which is used in scanner devices to recognize a complete scanned page (graphical images form of written text) and convert them to computer typed editable text documents. Newer applications have even expanded outside the limitations of just characters. Eye, face, and fingerprint scans used in high-security areas employ a newer kind of recognition [1,2].

A system which employ connectionist network to solve pattern recognition problem are currently of greet interest. Previous work [1,3] applied a neural network to a hand writing single character. This paper discusses the recognition of hand written letter, by applying it into backpropagation neural network to solve this problem.

SYSTEM OVERVIEW

The system is organized in two stages (illustrated in Fig. 1). The first stage converts the input character into highly compressed format available for recognition. The second stage is character recognition neural network which is previously learned [4].

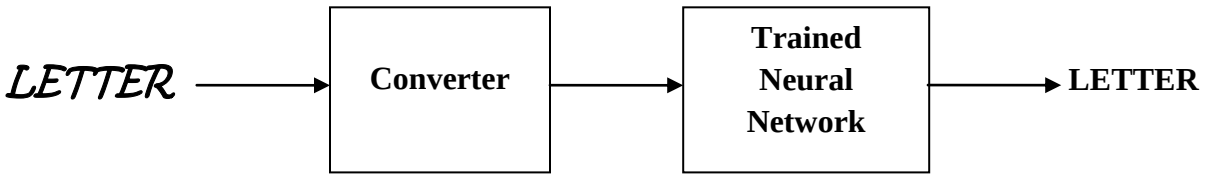

Fig. 1. Block diagram of letter recognition system

CHARACTER RECOGNITION:

Character is entered to the system as an image which produces a 9×9 matrix with a continuous stream of 1's and -1's, the 1's referred to the black part (character bits) while the -1's referred to the empty part as shown in the Fig. (2.a). The cause of selection the (1 and -1) representation in order to meet the requirements of the activation function which will be discussed later.

To provide suitable input pattern, the 9×9 two dimensional matrix converted to a vector (one dimensional array). Since each element in the vector will be represented as an input neuron to the neural network, as shown in Figs. (2.a), (2.b) and (2.c).

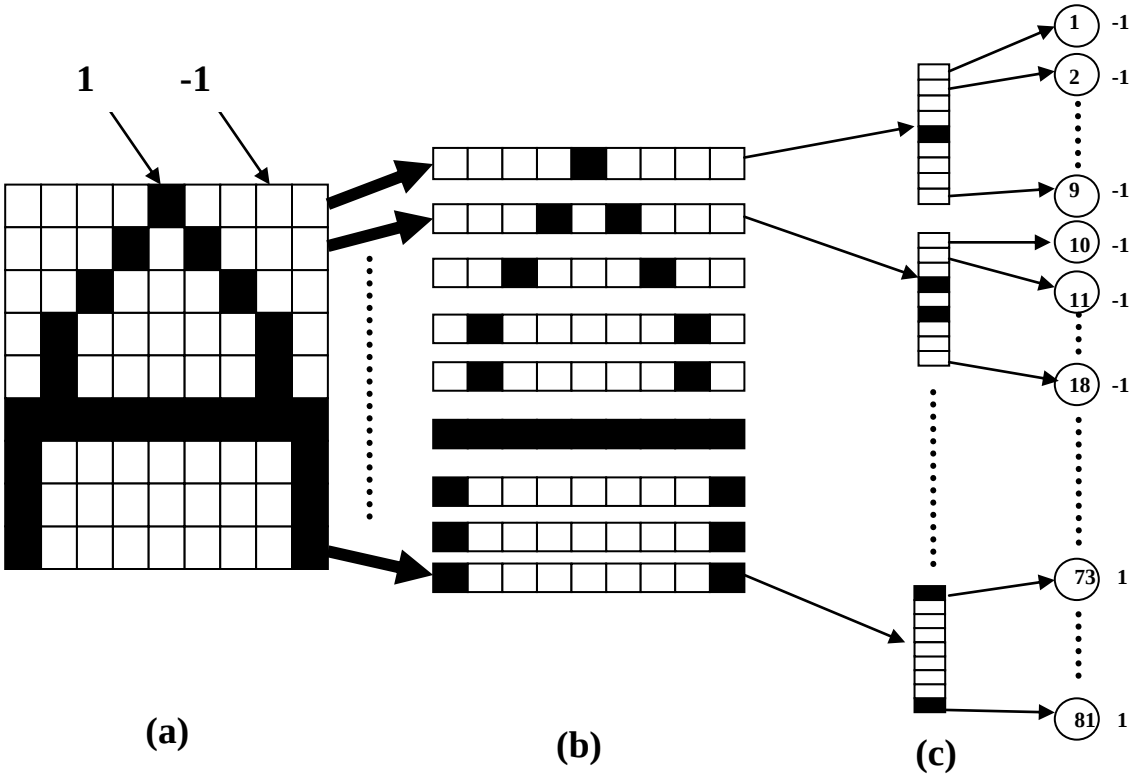

Fig. 2. Providing character to the neural network throw converting the 9×9 matrix into 81 elements vector.

NEURAL NETWORK ARCHITECTURE:

Fig. (3) describes the architecture of the neural network used in this paper. It consists of three layers (input , hidden and output layer) fully interconnected with each other by weight matrices [4,5,6].

The first layer (the input layer) consist of 81 neuron (from 9×9 = 81), each input neuron assigned to each bit of the pattern vector. The output layer with which the neural network needs to be learned is 26 neurons. The 26 output neurons refer to the number of 26 different English letters.

There are two sets of weights; input-hidden layer weights and hidden-output layer weights. These weights represent the memory of the neural network, where final training weights can be used when running the network [1].

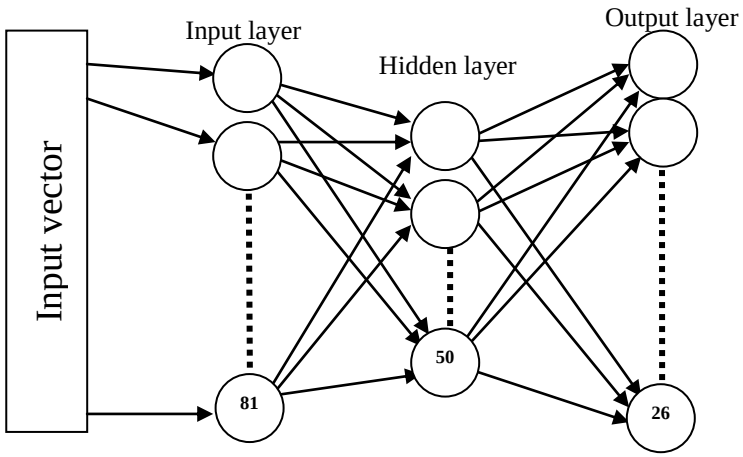

Fig. 3 . Architecture of the used neural [4,5,7].

TRAINING THE NEURAL NETWORK:

In the training phase, the neural network needs a set of input and desired output pairs for each single pattern, these set are entered by the supervisor of the network. The input vector is supplied as previously discussed while the desired output vector is set by putting a one in the output neuron location (where the character suppose to be represented) and a minus one everywhere else (the other 25 remaining output neuron) [2,6,7].

For example, to represent a pattern of A letter shape, the output vector is set as a 1 in the first output neuron (because A is the first letter in the alphabet) and -1 in output neurons from 2 through 26 neurons [2,8,9].

Many parameters should be chosen carefully before starting of the training phase. Such as the range of input values (here from -1 to 1), the range of output values (also from -1 to 1), the activation function (here it is tangent sigmoid at each hidden and output neurons illustrated in Fig. (4.b)), number of neurons at the input layer (here it is 81 and it is fixed), number of output neurons (here it is 26 and it also fixed) [5].

The training was implemented in MATLAB 2008 software package. Using a backpropagation neural network training algorithm with learning rate = 0.5, error goal = 0.001 and the number of hidden neurons were 50 neurons. Each hidden and output neurons have tangent sigmoid activation function Fig. (4) [2].

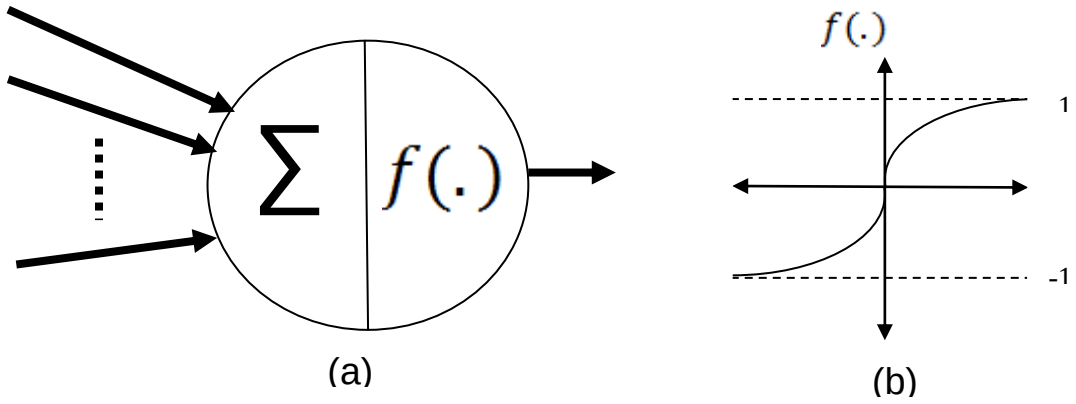

Fig. 4. Hidden or output neuron with tangent sigmoid activation function [2].

Some parameters used in the neural network have a great effects on the updating of the weights, such as (number of the hidden layers, number of the hidden neurons and the value of the learning rate), which can be tuned until a critical limit where there is no interesting of changing it . These parameters can be changed only in the starting of learning phase. Changing these parameters needs to restart the whole learning process [5,7,9].

This network was trained to recognize 26 alphabetic English letters from A to Z. Each letter with three different shapes. Therefore ; the total number of learned shaped was (26× 3=78) different patterns. one additional shape for each letter was used for testing the trained neural network.

Testing of the Neural Network:

The neural network succeeded in recognizing the letter which previously learned. It also succeeds in the same letter with some noise added into it. But changing the shape of the entered letters gives less ratio of detection than its original learned letters sets.

For example the neural network succeeded to recognize letter A Fig. (5.a) which was trained previously, but when testing the neural network with letter A in different shape shown in Fig. (5.b) the network gave a guess that the character is mostly A.

(a) (b)

Fig. 5. Two representations of letter A.

DETECTING CHARACTER BOUNDARIES:

The hand written system accepts a complete image file with written text in different rows and with shapes of letters in different sizes.

A process of detecting the boundaries of each letter shape is done by searching and detecting for each row of text alone from up of the image file to down. And for each row, from left to right Fig. (6.a).

For each detected letter shape boundaries, the size may not meet the fixed 9×9 size of the trained neural network. Therefore; resizing process (minimizing or maximizing)is done to each shape in order to be prepared for the network Figs. (6.b) and (6.c).

The input shape is ready to be enter to the neural network. The neural network then makes its decision on the current single pattern and gives the guessed letter as an output layer vector describes the letter Fig. (6.d). The recognition system translate the output vector to its corresponding letter and saves the letter in an output text file Fig. (6.e) . And the whole process is repeated again till the completion on the entire image file as shown in the flow chart in Fig.(7).

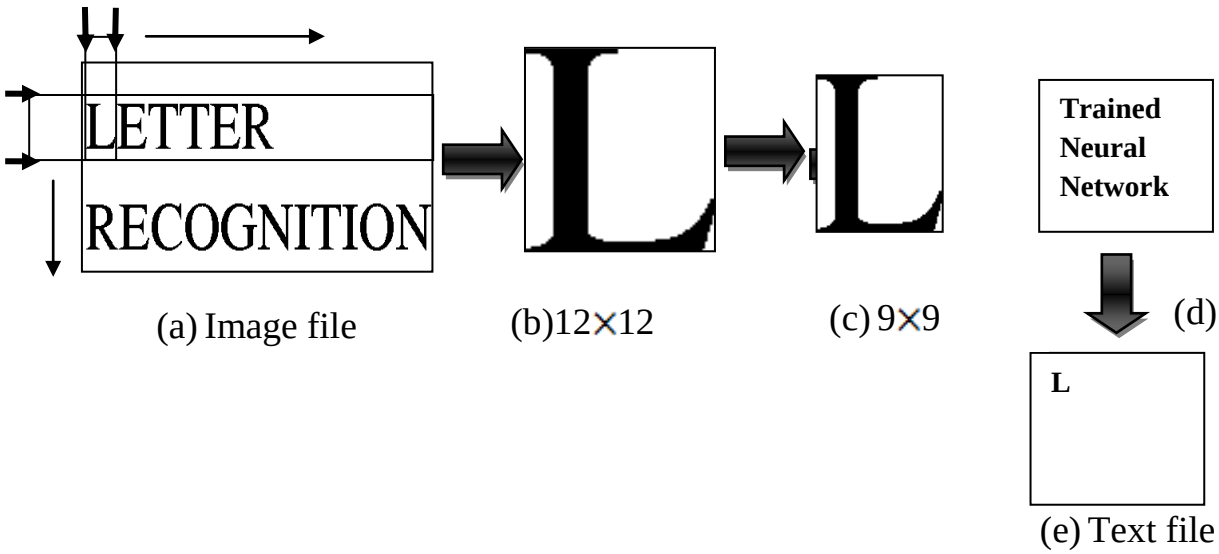

Fig. 6. The process of letter recognition step by step.

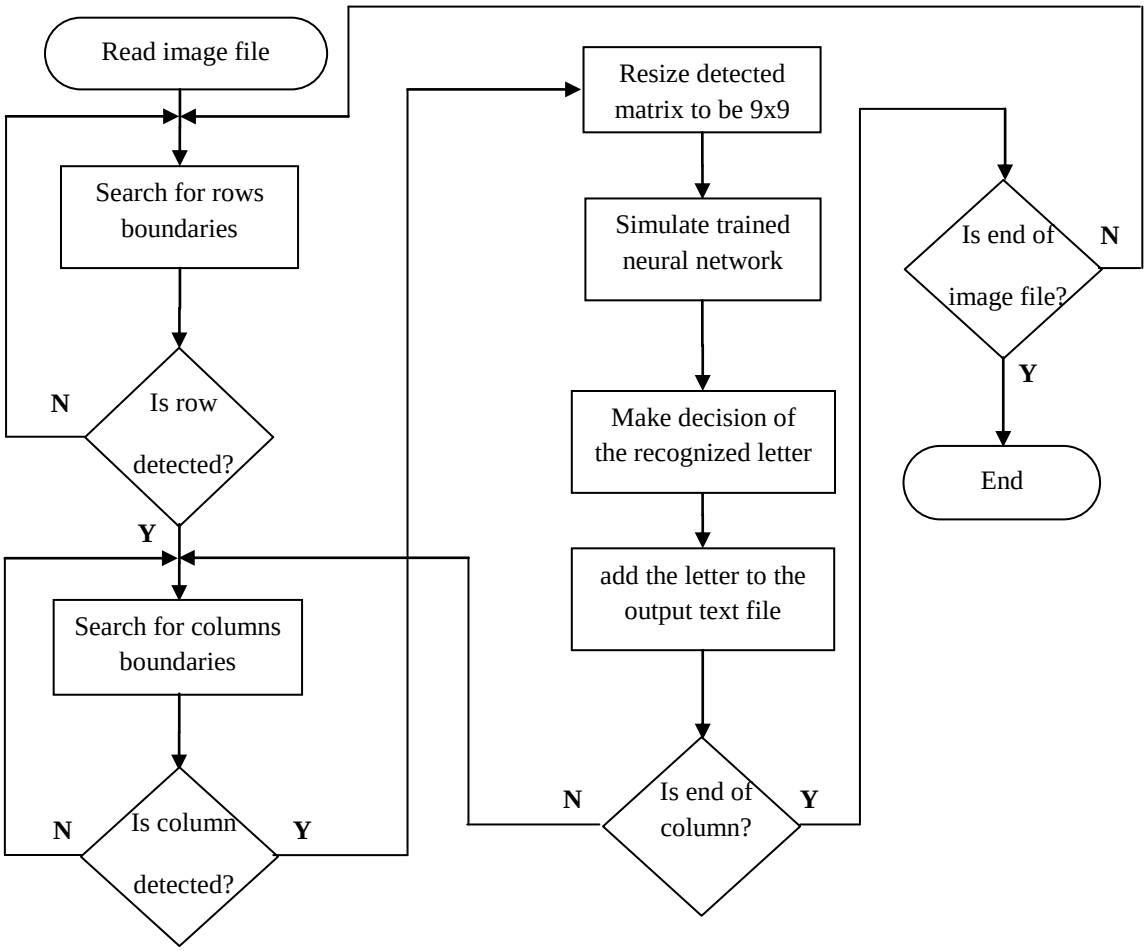

Fig. 7. Flow chart of hand written recognition system.

RESULTS AND CONCLUSIONS:

- A neural network is a powerful artificial intelligent system. It can be tuned to give better results by changing learning rate, number of hidden layers and number of hidden neurons, etc. The decision of putting the number of neurons in input and output layer are forced by the system.
- Selecting the ranges of input and output to be from one to minus one gives neural network wider range and better convergences in searching for optimal error cost function.
- Many training algorithms was tested in character recognition problem and the backpropagatoin algorithm gave encouraging results.
- Neural network can fully detect its learned letters and most of that shapes that is near to its trained letters. To improve the neural network detection, more patterns should be supplied into it.
- Neural network has fixed number of input layer neurons, therefore; action should be made in the input pattern to resize it to the 9×9 input matrix.

REFERENCES

- F. Mamedov, J. F. Abu Hasna, "Character Recognition Using Neural Networks". Near East University, North Cyprus, Turkey via Mersin-10, KKTC 2004.

- Howard Demuth and Mark Beale, Neural Network Toolbox User's Guide, Math works Inc., 2008.

- D.J. Burr, "A Neural Network Digit Recognizer", Proceedings of IEEE Conference on Systems, Man, and Cybernetics, Atlanta, GA, October, 1986, pp.1621-1625.

- D.J. Burr, "Experiments with a Connectionist Text Reader", Bell Communications Research, Morristown, N.J.07960.

- L. Fausett, "Fundamentals Of Neural Network", Prentice Hall ,1994.

- J. T. Heaton, "Introduction to Neural Network with Java", Heaton Research, Inc., November 25,2005.

- K. Gurney, "An Introduction to Neural Networks", CRC; 1st edition, August 5, 1997.

- Christopher M. Bishop, "Neural Networks for Pattern Recognition", Oxford University Press, USA; 1st edition, January 18,1996.

- S. Kumar, "Neural Network, A Classroom Approach", 1st edition, 2004.

STATISTICAL ESTIMATION OF THE COMPRESSIBITY OF BAGHDAD COHESIVE SOIL

Dr. Bushra S. Al-Busoda
Instructor
Department of Civil Engineering
University of Baghdad

Abbas Jawad Al-Taie
Assistant Instructor
Ministry of Higher Education
and Scientific Research

ABSTRACT

Because of the time and expense involved in performing consolidation tests, it is often desirable to obtain approximate values of (C_c and C_r) by using other soil properties which are more easily determined. The literature contains numerous equations linking soil compressibility to its physical and index properties. As these equations are often used to obtain preliminary evaluations of (C_c) and (C_r), it is important to know the reliability of these equations.

In this paper an attempt was made to estimate (C_c and C_r) of Baghdad cohesive soil from other soil properties. A number of commonly used empirical correlation equations that have been developed during the last six decades to estimate (C_c and C_r) were compiled and evaluated. The results of routine laboratory tests of a large number of databases of Baghdad soil were correlated with more sophisticated laboratory consolidation results by conducting simple and multiple regression analyses. It was concluded that the compression index of Baghdad cohesive soil cannot be estimated from Atterberg limits and the better values of compression and recompression indices of Baghdad soil can be obtained when more than one index property is used in the regression analysis.

تقييم احصائي لانضغاطية تربة بغداد المتماسكة

الخلاصة

نظرا للوقت والكلفة المتضمنة عند اجراء فحوص الانضمام, فانه من المفضل الحصول على قيم تقريبية لـ (C_c) و (C_r) باستخدام خصائص اخرى للتربة تحدد بطرق اسهل. تضمنت المصادر العديد من المعادلات التي تربط بين انضغاطية التربة والخصائص الفيزياوية والدليلية لها. على الرغم من استخدام هذه المعادلات للحصول على تقييم اولي لـ (C_c) و(C_r) الا ان معرفة مدى ملائمتها المعدلات يعد امرا مهما.

في هذا البحث تم اجراء محاولة لتخمين قيم (C_c) و(C_r) الخاصة بتربة بغداد باستخدام الخائص الاخرى لها. تم جمع وتقييم عدد من المعدلات الوضعية الشائعة الاستخدام عتد تخمين قيم (C_c) و(C_r) والتي تم تطويرها خلال العقود الستة الماضية. تم تكوين قاعدة بيانات تتضمن نتائج الفحوص التقليدية لتربة بغداد المتماسكة وتم اجراء ترابط احصائي لهذه النتائج مع فحص الانضمام الاكثر تعقيدا وذلك باستخدام التحليل الاحصائي البسيط والمتعدد. اظهرت نتائج الدراسة عدم امكانية الاعتماد على حدود اتربيرك لتخمين قيم معامل الانضغاط لتربة بغداد, كما بينت النتائج ان استخدام اكثر من صفة دليلية ضمن التحليل الاحصائي يعطي نتائج افضل لقيم (C_c) و(C_r) الخاصة بتربة بغداد.

KEYWORDS: compression index, recompression index, correlation, initial void ratio, natural moisture content, total unit weight, dry unit weights.

INTRODUCTION

The analysis of all geotechnical problems requires the adoption of a soil behavioral model complete with all relevant soil properties. These soil properties are not known beforehand, and therefore the design engineer must either measure the properties under controlled conditions in the laboratory or field or estimate the properties from other test data. These estimates are made most often from laboratory index tests and in-situ test results, which are correlated to soil properties either by calibration studies or by back calculation from full scale load test data obtained in the field.

Comprehensive characterization of the soil at a particular site would require an elaborate and costly testing program, well beyond the scope of most projects budgets. Instead, the design engineer must rely upon more limited soil information, and that is when correlations become most useful, (Kulhawy and Mayne 1990).

There is large number of empirical equations presented in the geotechnical literature for the estimation of compression and/or recompression indices (Skempton, 1944; Helenelund, 1951; Cozzolino, 1961; Sowers, 1970; Wroth and Wood, 1978; Nagaraj and Murthy, 1986; Nakase et al., 1988; Bowles, 1996; Gunduz and Arman, 2007: Ahadiyan et. al., 2008: Isik, 2009).

Bowles 1996, suggested that to identify the published equations, one should start compiling a local database with minor adjustments to the numerical constants, as defining the local soil..

Kulhawy and Mayne 1990 mentioned that caution must always be exercised when using broad, generalized correlation of index parameters with soil properties. The source, extent, and limitation of each correlation should be examined carefully before use to ensure that extrapolation is not being done beyond the original boundary conditions. Local calibrations where available, are to be preferred over the board, generalized correlations.

In addition, many of the common correlations in the literature have been developed from test data on relatively insensitive clays of law to moderate plasticity. Extrapolation of these correlations to special soils should be done with particular care because the correlations do not apply strictly to these soils.

THE OBJECTIVES OF THIS STUDY

It is very important in geotechnical engineering to know the compressibility properties of a soil. Usually compression and/or recompression indices are used for the calculation of consolidation settlement of fine grained soils. They are conventionally determined by laboratory oedometer tests. However, the duration of consolidation tests is very long compared to standard index tests. For this reason, it is important to estimate compression and recompression indices with reasonable accuracy for preliminary calculations and to control the validity of consolidation tests.

Numerous attempts have been made to correlate compressibility with some simple index properties. Giasi, et. al., 2003, stated that the multitude of equations present in the literature indicates that none of them can be assumed to have general validity, but that each of them can be valid within defined ranges.

It is known that the compressibility characteristics of a soil can be correlated to different characteristic properties, such as the liquid limit, the plasticity index, the natural water content, the void ratio, etc. The use of one property rather than another is linked to the kind of soil being considered and to the conditions in which it is analyzed, Giasi, et.. al., 2003.

As such this study will include the following

- Investigation of the soil data generated by soil investigation for different projects in Baghdad city to explore the range of values and variations of (C_c) and (C_r).
- Compiling a local database to identify the local soil.
- Comparing the results of (C_c) and (C_r) obtained from existing proposed relations to those of laboratory measurements.

- Correlating routine laboratory tests results with more sophisticated laboratory results used to determine geotechnical design parameters by conducting simple and multiple regression analysis.

DATABASE COMPILATION AND DESECRIPTION

In order to build the database, a large number of consolidation and physical test results was compiled. These results were generated by soil investigation for different projects in Baghdad city during the last three decades.

Soil parameters used in the database were natural water content (wn), initial void ratio (e_o), total unit weight (γ_t), dry unit weight (γ_d), liquid limit (LL), plastic limit (PL), plasticity index (I_p), effective overburden pressure (Po), compression index (C_c), and recompression index (C_r). In order to assess the adequacy of the database, descriptive statistics of each data set present in the database were determined. **Table 1** presents the descriptive statistics of each variable and **Fig. 1** presents the histogram of the variables.

It should be mentioned that (50.9%) of the values of (C_c) used in the present work are less than (0.2), while (46.6%) of the values ranged from (0.2 to 0.4). Thus, the degree of compressibility of Baghdad cohesive soil, according to Kulhawy and Mayne 1990, can be classified as low to intermediate. The ratio of (C_s/C_c) for Baghdad soil was calculated from the data and found to vary from (0.047 to 0.533). On the other hand, more than (59%) of the (LL) of the samples is less than (50%) which indicated that the predominated consistency of Baghdad clay is Low. Also, the values of the natural water content, in general, are closer to the plastic limit than to liquid limit. This trend suggests that the soil is somewhat heavily overconsolidated. (Bowles, 1996).

According to **Table 1**, it can be concluded that the database consists of a wide range of data. Therefore, this database can be used for the comparison of the performance of existing empirical equations and for the development of new equations. On the other hand, as can be observed from the frequency histograms and from the statistical parameters given in **Table 1**, for most of the soil parameters it appears realistic to assume a normal distribution.

Table 1 summary of statistical parameters

	w_n	LL	PL	PI	γ_t	γ_d	eo	Po	Cc	Cs
No.of values	596	820	817	818	390	386	350	425	328	330
Minimum	2	21	4	3	16.2	11.33	0.411	9.3	0.1	0.01
Maximum	43	83	38	58	21.7	19.71	1.14	430	0.71	0.099
Range	41	62	34	55	5.5	8.377	0.729	420.7	0.61	0.089
Mean	24.5	47.2	23.39	23.8	19.6	15.8	0.708	121.24	0.213	0.045
Median	24	47	23	24	19.6	15.84	0.7	95.6	0.2	0.042
Std. deviation	4.694	10.83	4.726	9.087	0.835	1.107	0.118	83.85	0.069	0.0156
Units	%	%	%	%	kN/m^3	kN/m^3	--	kN/m^2	--	--

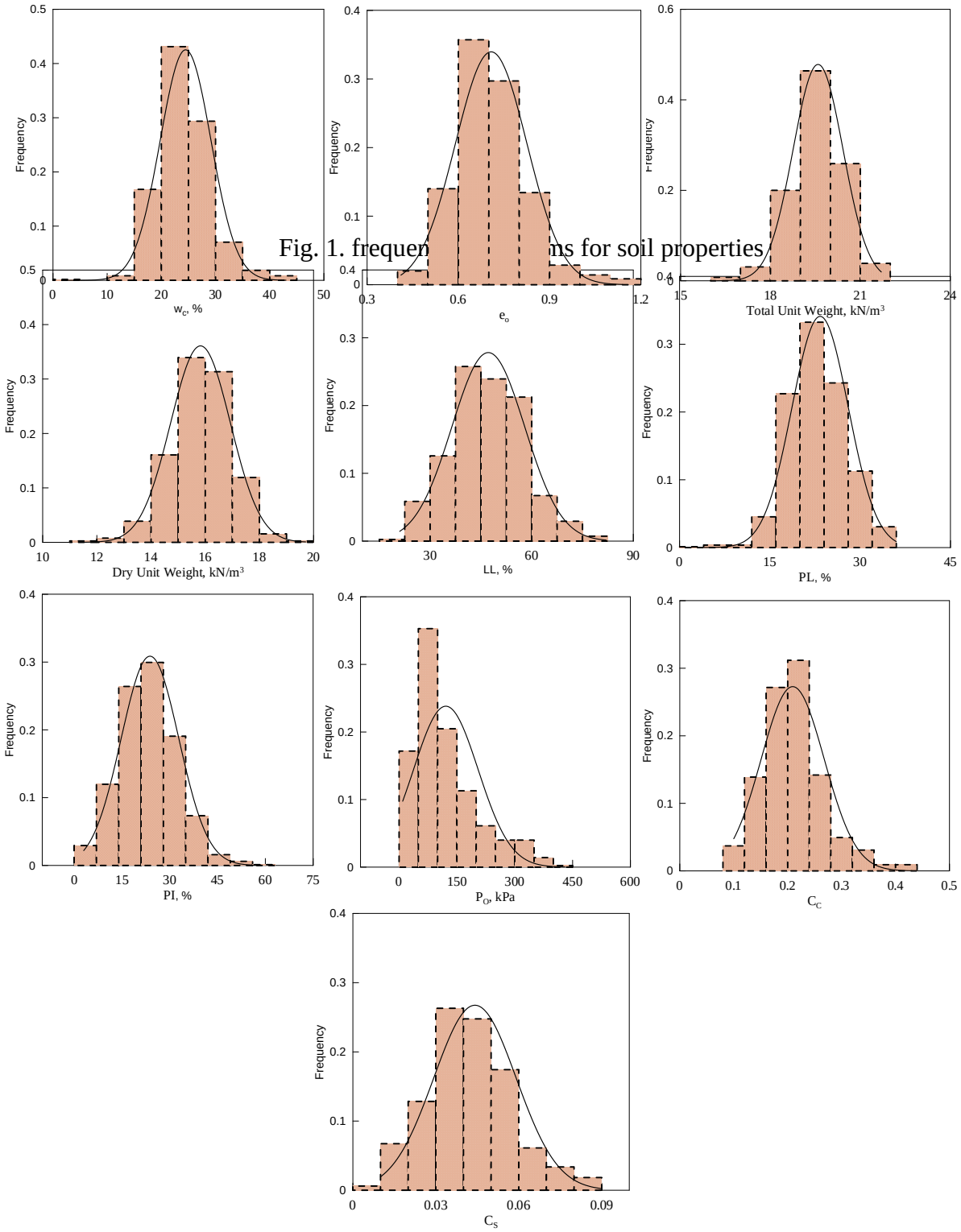

Fig. 1. frequen ms for soil properties

Fig. 1. continued

A COMPENDIUM OF THE EXISTING CORRELATIONS

Over the past six decades, a number of empirical equations have been developed for relating compression and recompression indices to deferent soil properties. Al-Khafaji 2005, stated that the lack of uniformity in data collection and data interpretation makes it difficult to verify the accuracy of derived empirical equations. However, a large number of published equations are now available to warrant a closer look at the validity, accuracy, and usefulness of many available empirical formulas for compression index estimation.

Table 2 and **Fig. 2** summarize the equations correlated between (C_c) and (C_r) with other index properties of soils consisting of (LL), (PI), (w_n), (e_o), (γ_t), and (γ_d). These equations were proposed or established by many different authors from various places, between the years 1944 and 2009.

It should be noted that there have been continuous attempts, right from the early stages (1944), to develop simple methods to predict (C_c) of soils from simple soil index parameters. In contrast to (Cc), only few empirical equations were developed for the estimation of (C_r), were such attempts started latterly after (1980).

Nevertheless, one may observe that the correlation equations vary one with another, with some indicating great differences and some being non linear. Also, some of these correlations are supposed to reflect compression index of all soils while others are limited to specific soil types and/or geographic location.

Djoenaidi, 1985, and Lav, and Ansal 2001, mentioned that the differences in the correlation equations may be attributed to the use of different data sources from which those equations were established. Using linear correlation, as stated by Djoenaidi 1985, indicated that the (C_c) can be forecast as a linear function of the index properties. However, in practice, care should be taken in selecting or using the existing correlations for a given soil, because most of these correlations are applicable only to certain regions.

To examine the applicability of the correlation equations summarized in **Table 2** to Baghdad cohesive soils, these relationships are plotted in **Fig. 2** in which (C_c) and (C_r) of Baghdad Soil are plotted against (LL), (PI), (w_n), (e_o), (γ_t), and (γ_d) successively. The following statements can be made based on **Table 2** and **Fig. 2**:

- These relationships indicated the same trend, i.e, the greater (LL), (PI), (w_n), and (e_o) or the lesser (γ_t), and (γ_d), gives the higher the (C_c) and (C_r).
- Although there is considerable scatter, most of the lines agree fairly well.
- Because the compression settlement depends on the initial in situ void ratio (e_o), it is probably better to use these equations that include (e_o) either directly or indirectly, (Bowels, 1996).
- It can clearly be observed that the correlation equations using one independent variable might not satisfy the compressibility of Baghdad cohesive soil for the given range of data.
- Correlation equations using more than one independent index property, like equations (F7 or F9) in **Table 2**, seem to be better to provide the best reliability.

However, attention should be given to the conditions in which the correlation had been made and the statistical accuracy of the equations, before choosing a single empirical equation for a particular type of soil.

Table 2 summary of empirical equations developed for relating C_r or C_c

	Equation	Notes	Reference
	C_r or C_c = f(LL)		
A1	$C_c = 0.007\ (LL - 10)$	Remolded clays	Skempton (1944)
A2	$C_c = 0.0046\ (LL - 9)$	Brazilian clays	Cozzolino (1961)
A3	$C_c = 0.009(LL - 10)$	N.C. Clays of moderate sensitivity	Terzaghi and Peck (1967)
A4	$C_c = 0.006\ (LL - 9)$	Clay from Greece and some parts of USA	Azzouz et al. (1976)
A5	$C_c = (LL - 9)/109$	All clays	Mayne (1980)
A6	$C_c = 0.00234\ LL\ G_s$	All inorganic clays	Nagaraj and Srinivasa Murthy(1985, 1986)
A7	C_c=0.009 LL + 0.035	$R^2 = 0.705$	Ferreira and Ladeira (1995)
A8	$C_c = 0.006\ (LL + 1)$	All soil ($R^2 = 0.259$)	Lav and Ansal (2001)
A9	C_c= 0.009 (LL - 16)	For (16< LL < 200)	Al-Khafaji (2005)
A10	$C_r = 0.000463\ LL\ G_s$	-	Nagaraj and Srinivasa Murthy(1985)
A11	$C_r = 0.0007\ LL + 0.0062$	42 test data, Turkey	Isik (2009)

C_r or C_c = f(I_p)			
B1	$C_c = 0.005\ I_p\ G_s$	All remolded normally consolidated clays	Wroth and Wood (1978)
B2	$C_c = 0.046 + 0.0140\ I_p$	For $I_p < 50$	Nakase et al. (1988)
B3	$C_c = I_p/74$	Data from different soils	Kulhawy and Mayne (1990)
B4	$C_c = 0.011\ (I_p - 5.7)$	For cohesive soil (R^2=0.79)	Heng (2006)
B5	$C_r = 0.00194\ (I_p - 4.6)$	Best for $I_p < 50\%$	Nakase et al. (1988)
B6	$C_r = I_p/370$	Data from different soils	Kulhawy and Mayne (1990)
C_r or C_c = f(w_n)			
C1	$C_c = 0.85\ (w_n/100)^{1.5}$	Finnish mud and clay	Helenelund (1951)
C2	$C_c = 0.01(w_n - 5)$	Clay from Greece and some parts of USA	Azzous et al., (1976)
C3	$C_c = 0.01\ w_n$	Canada	Koppula (1981)
C4	$C_c = 0.01(w_n - 7.549)$	Soil from 9 sites in USA	Rendon-Herrero (1983)
C5	$C_c = 0.0115\ w_n$	Organic silts and clays	Bowles (1984)
C6	C_c=0.015 (w_n - 8)	Cohesive soil in Taiwan	Moh et. al. (1989)
C7	C_c=0.01 w_n - 0.042	R^2 = 0.856	Ferreira and Ladeira (1995)
C8	$\ln C_c = 1.235 \ln w_n - 5.65$	All soil (R^2=0.54)	Lav and Ansal (2001)
C9	$C_c = 0.00454\ (w_n - 10)$	soft soils in southern Germany	Kempfert Gebreselassie (2006)
C10	$C_r = 0.0133\ e^{0.036.wn}$	42 test data, Turkey	Isik (2009)
C_r or C_c = f(e_o)			
D1	$C_c = 1.15(e_o - 0.35)$	All clays	Nishida (1956)
D2	$C_c = 0.29\ (e_o - 0.27)$	Inorganic silty clays	Hough (1957)
D3	C_c=0.43 (e_o - 0.25)	Brazilian clays	Cozzolino (1961)
D4	$C_c = 0.75\ (e_o - 0.50)$	Soil with low plasticity	Sowers, (1970)
D5	$C_c = 0.40\ (e_o - 0.25)$	Clay from Greece and some parts of USA	Azzous et al., (1976)
D6	$C_c = 0.141\ G_s^{1.2}\ [(1+e_o)/G_s]^{2.38}$	Soil from 9 sites in USA	Herrero (1980)
D7	$C_c = 0.5\ ((1+e_o)/G_s)^{2.4}$	-	Oswald (1980)
D8	C_c= 0.54 (e_o - 0.23)	Taiwan clay	Moh et. al. (1989)
D9	$C_c = 0.379\ e_n - 0.046$	R^2 = 0.855	Ferreira and Ladeira (1995)
D10	$C_c = 0.61\ e_o - 0.17$	-	Tan and Gue (2000)
D11	$\ln C_c = 1.272 \ln e_0 - 1.282$	All soil (R=0.817)	Lav and Ansal (2001)
D12	$C_c = 1.02 - 0.95\ e_o$	For overconsolidated low plasticity clay	Gunduz and Arman (2007)
D13	C_c=0.287 e_o - 0.015	Ahwaz Soil (R2 = 0.47)	Ahadiyan et. al. (2008)
D14	C_c= 0.3 (e_o - 0.27)	Soils in Southeastern Wisconsin.	Edilm and Benson (2009)
D15	$C_r = 0.0121\ e^{1.3131\ eo}$	R^2 = 0.6501	Isik (2009)
C_r or C_c = f(γ_d or γ_n)			
E1	$C_c = 0.5\ (\gamma_w / \gamma_d)^{2.4}$	Soil of all types	Cited in Kempfert Gebreselassie (2006)
E2	$C_r = 9.3158\ e^{-2.8048\ \gamma n}$	42 test data, Turkey, (γ_d is t/m^3)	Isik (2009)
E3	$C_r = 0.1257\ \gamma_d^{-2.8826}$	42 test data, Turkey, (γ_d is t/m^3)	Isik (2009)
C_r or C_c = f(Different Variables)			
F1	C_c=0.37(e_o+0.003LL+0.0004w_n-0.34)	Clay from Greece and some parts of USA	Azzouz et al. (1976)
F2	$C_c = 0.141\ G_s\ (\gamma_{sat} / \gamma_d)^{2.4}$	Clay from Greece and some parts of USA	Rendon-Herrero (1983)

F3	C_c=0.37(e_o + 0.003 LL - 0.34)	R^2 = 0.86	Bowles (1984)
F4	C_c = 0.009 w_n + 0.005 LL	All clays	Koppula (1986)
F5	C_c = -0.156 + 0.41I e_o + 0.00058 LL	72 data points	Al-Khafaji and Andersland (1992)
F6	C_c= -0.048+ 0.005w_n+0.179 e_n	Soil from Aveiro in Portugal	Ferreira and Ladeira (1995)
F7	C_c = (0.001 w_n + 0.114) (1+e_o)	For alluvial soils	Crumley, et. al. (2003)
F8	C_c= -0.023 + 0.001 LL + 0.271e_o	R^2 = 0.48	Ahadiyan et. al. (2008)
F9	C_r = 0.037-0.00032 w_n -0.0273 γ_d +0.064 e_o	42 test data, Turkey (γ_d is t/m^3)	Isik (2009)

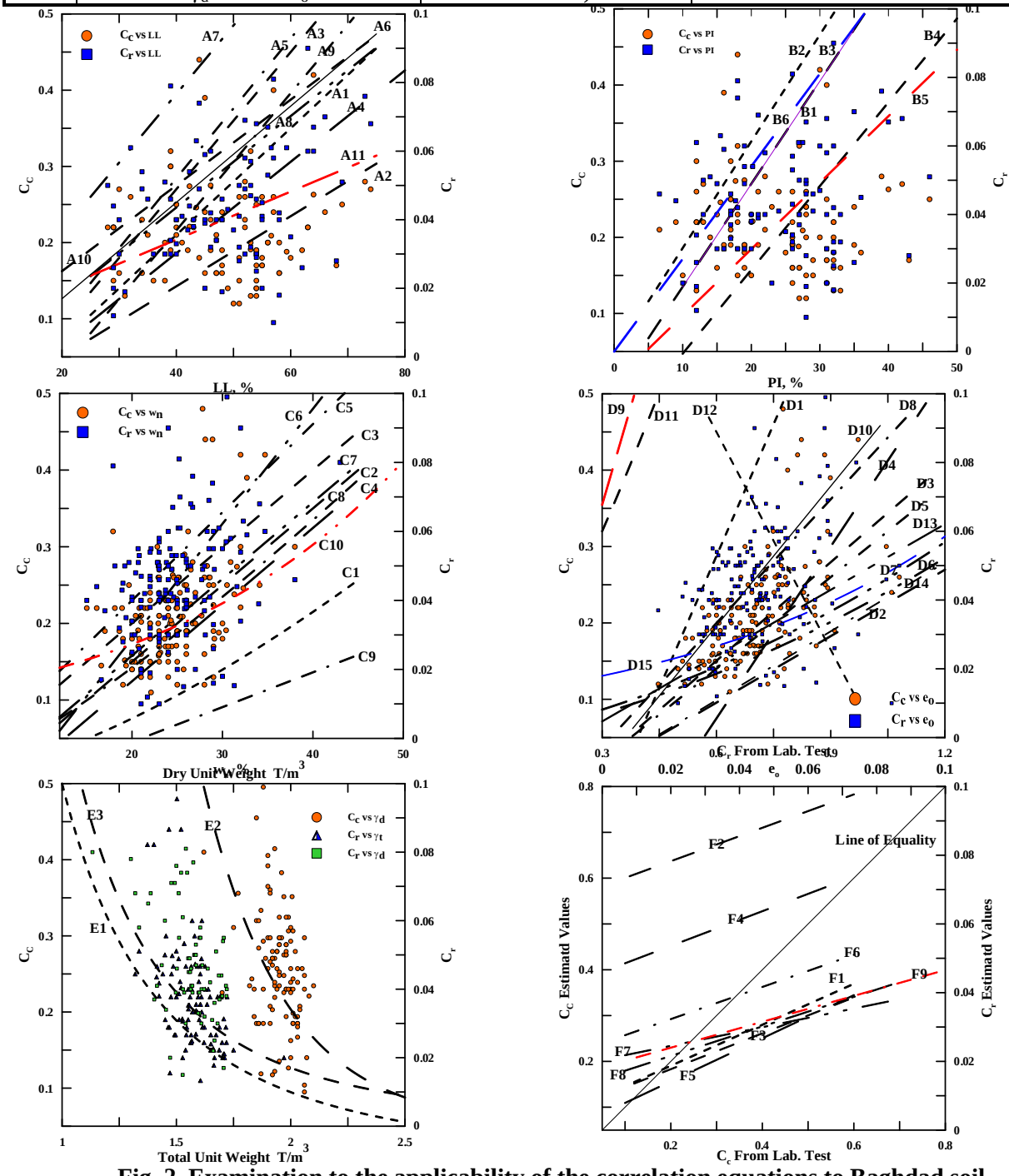

Fig. 2. Examination to the applicability of the correlation equations to Baghdad soil

SIMPLE AND MULTIPLE REGRESSION ANALYSIS OF (C_c) and (C_r)

To examine whenever the (C_c) and (C_r) of Baghdad cohesive soil can be predicted from the knowledge of other soil properties, regression analysis was performed using the database compiled in this paper. Simple and multiple regression analysis were carried out using a computer program (SPSS).
In order to observe the improvement in the correlations developed due to the adopted parameters, the correlation coefficient (R) matrices for the whole data should be establish. Lav and Ansal 2001, stated that a lower limit of ($R \geq \pm 0.5$) can adopted for developing various regression models. Accordingly, a correlation coefficient (R) with values greater than or equal to (± 0.5) was adopted in the present regression models.

Simple regression analysis was performed between the (C_c) and (C_r) and the selected soil properties. The (C_c) and (C_r) are dependent variables and are treated as functions of natural water content (w_n), initial void ratio (e_o), total unit weight (γ_t), dry unit weight (γ_d), liquid limit (LL), plastic limit (PL), plasticity index (I_p), and effective overburden pressure (P_o) which are termed as independent variables. The resulting (R) values for all cases adopted in the simple analysis are shown in **Table 3.**

Table 3 Simple regression analysis performed to estimate (C_c) and (C_r).

Independent Variables	Correlation Coefficient (R)					
	Linear Regression		Curve Estimation			
	C_c	C_r	C_c	Model	C_r	Model
w_o	0.460	0.402	0.475	Cubic	0.399	Cubic
e_o	0.570	0.420	0.591	Cubic	0.448	Cubic
γ_t	0.452	0.374	0.454	Exponential	0.373	Logarithmic
γ_d	0.528	0.451	0.530	Logarithmic	0.452	Logarithmic
LL	0.114	0.356	0.189	Cubic	0.389	Cubic
PL	0.260	0.355	0.266	Power	0.355	Cubic
PI	0.000	0.441	0.084	Cubic	0.442	Power
P_o	0.621	0.336	0.621	Cubic	0.374	Cubic

Values of the coefficient of correlation ($R<0.5$) shown in **Table 3** indicate that direct correlation between (C_r) and other soil properties are rather poor when applied to a large number of data from Baghdad cohesive soil. Unlike what has been observed for (C_r), the statistical significance of the direct correlations between (C_c) and (e_o),(γ_d), and (P_o) , where ($R \geq \pm 0.5$), are moderate. As can be observed in this table, the Atterberg limits and the natural water content have a low correlation coefficient value for all cases considered in evaluating the (C_c) and (C_r).
Giasi et. el. 2003, mentioned that the compressibility characteristics of a soil can be correlated to different characteristic properties, and the use of one property rather than another is linked to the kind of soil being considered and to the conditions in which it is analyzed. Finally he stated that the Atterberg limits can be used to evaluate the compression index of remoulded soils samples. It can be concluded that the correlation equations using Atterberg limits in a simple regression correlation might not satisfy the compressibility of Baghdad cohesive soil for the given range of data**.**
Curve estimation using models shown in **Table 3** were performed and the related correlation coefficients were calculated to investigate the effect of these models on the value of (R). It was observed that, in most cases, no significant increase in the value of the correlation coefficient was obtained when the curve estimation is used in the regression analysis**.**
On the other hand, multiple linear regression studies were conducted to express (C_c) and (C_r) in terms of the aforementioned database for Baghdad soil. In this analysis, the emphasis is on the soil properties which have a reasonable value of (R) obtained in the simple analysis, i.e. (e_o), (γ_d), and

(P_o). The results of the multiple analyses between (C_c) and (C_r) and other soil properties are shown in **Table 4**. An examination to this table reveals that introducing Atterberg limits conjugated with other parameters reduced the coefficient of correlation in many cases. Nevertheless, in comparison with the results from simple linear regression analysis, the inclusion of more than one independent variable statistically improves the relationships. The best improvement in the value of (R) can be reached when (w_o) or (γ_t) or (γ_d) are included in addition to (e_o) and (P_o) in multiple regression analysis.

Table 4 Multiple regression analysis performed to estimate (C_c) and (C_r)

Independent Variables			Correlation Coefficient (R) Dependent Variables	
1	2	3	C_c	C_r
e_o	LL	-	0.551	0.452
e_o	PL	-	0.560	0.422
e_o	PI	-	0.549	0.398
e_o	w_o	-	0.595	0.460
e_o	w_o	γ_t	0.649	0.552
e_o	w_o	γ_d	0.649	0.552
e_o	w_o	P_o	0.752	0.571
e_o	γ_t	-	0.642	0.532
e_o	γ_t	γ_d	0.648	0.552
e_o	γ_t	P_o	0.782	0.567
e_o	γ_d	-	0.648	0.551
e_o	γ_d	P_o	0.782	0.577
e_o	P_o	-	0.757	0.557
γ_d	LL	-	0.447	0.531
γ_d	PL	-	0.492	0.543
γ_d	PI	-	0.444	0.455
γ_d	w_o	-	0.533	0.457
γ_d	w_o	γ_t	0.541	0.461
γ_d	w_o	P_o	0.692	0.486
γ_d	γ_t	-	0.530	0.455
γ_d	γ_t	P_o	0.692	0.485
P_o	LL	-	0.652	0.495
P_o	PL	-	0.670	0.487
P_o	PI	-	0.644	0.403
P_o	w_o	-	0.658	0.460
P_o	w_o	γ_t	0.692	0.486
P_o	γ_t	-	0.679	0.445

A list of possible relationships for estimating the (C_c) and (C_r) using various index parameters developed in this study is summarized in **Tables 5 and 6**. During this study, all possible relationships were tried; however, naturally in some of these relationships, the correlation coefficients were low. The equations given in these tables are the ones which had the highest correlation coefficient ($R \geq \pm 0.5$).

Table 5 Summary of relationships developed to evaluate (C_r).

Relationships Developed to Evaluate (C_r)		
Independent Variables	(R)	Regression Equation
e_o, w_o, γ_t	0.552	$C_r= 0.017 + 0.061\ e_o + 0.0004\ w_o – 0.001\ \gamma_t$
e_o, w_o, γ_d	0.552	$C_r= 0.02 + 0.061\ e_o + 0.00023\ w_o – 0.001\ \gamma_d$
e_o, w_o , P_o	0.571	$C_c= -0.009 + 0.061\ e_o + 0.0004\ w_o + 0.00003\ P_o$
e_o, γ_t , P_o	0.567	$C_r= 0.0178 + 0.0622\ e_o - 0.0011\ \gamma_t + 0.00004\ P_o$
e_o, γ_d	0.551	$C_r= 0.038 + 0.068\ e_o - 0.002\ \gamma_d$
e_o, γ_d , P_o	0.577	$C_r= 0.0196 + 0.0614\ e_o - 0.00134\ \gamma_d + 0.00003\ P_o$
e_o, P_o	0.557	$C_r= -0.005 + 0.067\ e_o + 0.00004\ P_o$

Table 6 Summary of relationships developed to evaluate (C_c).

Relationships Developed to Evaluate (C_c)		
Independent Variables	(R)	Regression Equation
e_o	0.570	$C_c=0.31\ e_o - 0.006$
e_o	0.591	$C_c=0.620 - 2.42\ e_o + 3.84\ (e_o)^2 – 1.74\ (e_o)^3$
P_o	0.621	$C_c= 0.159 + 0.0005\ P_o$
e_o, w_o	0.590	$C_c= -0.034 + 0.25\ e_o + 0.003\ w_o$
e_o, w_o, γ_d	0.649	$C_c= 0.113+ 0.31\ e_o + 0.001\ w_o – 0.009\ \gamma_d$
e_o, w_o, γ_t	0.649	$C_c= 0.103+ 0.308\ e_o + 0.002\ w_o – 0.008\ \gamma_t$
e_o, w_o , P_o	0.752	$C_c= -0.02 + 0.274\ e_o + 0.00008\ w_o + 0.0004\ P_o$
e_o, γ_t	0.642	$C_c= 0.2 + 0.345\ e_o - 0.012\ \gamma_t$
e_o, γ_t , P_o	0.782	$C_c= -0.003 + 0.298\ e_o + 0.0018\ \gamma_t + 0.0004\ P_o$
e_o, γ_d	0.648	$C_c= 0.19 + 0.313\ e_o - 0.012\ \gamma_d$
e_o, γ_d , P_o	0.782	$C_c= -0.0405 + 0.3018\ e_o + 0.0001\ \gamma_d + 0.00044\ P_o$
γ_d, γ_t , P_o	0.692	$C_c= 0.463 - 0.019\ \gamma_d + 0.0001\ \gamma_t + 0.0005\ P_o$
e_o, P_o	0.757	$C_c= -0.021 + 0.278\ e_o + 0.00042\ P_o$

A comparison between the relationships proposed by various authors that are shown in **Table 2** and the ones developed in this study is conducted. It is very interesting that the relationship proposed to calculate the compression index in terms of void ratio of Baghdad soil from the simple linear analysis is exactly the same as the relationship developed by Ahadiyan et. al. 2008 for Ahwaz Soil (D13 in **Table 2**). Also, one can notice that the relationship proposed to predict the (C_c) of Baghdad soil as a function to void ratio and water content (multiple analysis) is similar to equation (F6) shown in Table 2 and suggested by Ferreira and Ladeira 1995 for Soil from Aveiro Portugal. Moreover, equation (F9) shown in Table 2 proposed by Isik 2009 to estimate the recompression index of the Turkish soils is like that developed in this study from multiple analysis to void ratio, water content, and dry unit weight.

Finally, it appears from the study conducted that initial void ratio, dry unit weight, and effective overburden pressure yielded sufficiently reliable correlation to estimate recompression index of Baghdad cohesive soil. Also, a good estimation was obtained for compression index of Baghdad cohesive soil from multiple analyses of initial void ratio, dry unit weight, and effective overburden pressure.

CONCLUSIONS:

A database consisting of large numbers of data sets containing consolidation and physical properties test results obtained during the last years from different parts of Baghdad city was compiled, identified, and used to conduct a statistical study to determine suitable correlations for estimating compression and recompression indices. A number of commonly used empirical correlation equations that have been developed during the last six decades to estimate (C_c and C_r) were summarized and evaluated. A simple and multiple regression analysis were adopted and a parametric study was carried out in order to obtain the most suitable and practically applicable relationships.

The main conclusions of the present study are as follow:

- The evaluation of the database indicates that the degree of compressibility of Baghdad cohesive soil can be classified as low to intermediate. While the ratio of (C_s/C_c) for Baghdad soil varies from (0.047 to 0.533).
- The examination of the commonly used empirical correlation equations shows that no one of existing simple empirical correlation equations given by different researchers is valid to estimate the recompression indices of Baghdad cohesive soil.
- The results of regression analysis conducted in this study reveal that the compression index of Baghdad cohesive soil cannot be estimated from Atterberg limits and the better values of compression and recompression indices of Baghdad soil can be obtained when more than one index property is used in the regression analysis.
- Finally, in practice, care should be taken in selecting or using the existing correlations for a given soil, because most of these correlations are applicable only to certain regions.

REFRENECES:

- Ahadiyan, J., Jalal, R. E., and Bajestan, M., S., (2008) "Determination of Soil Compression Index, Cc, in Ahwaz Region", Journal of Faculty of Eng., Vol. 35, No.3 (Civil Eng.).

- Al-Khafaji A., (2005). "Empirical Compression Index Equations", Intentional Workshop on Innovations in Materials and Design of Civil Infrastructure, Cairo, Egypt, pp 252- 271.

- Al-Khafaji A., W., and Andersland O.,B., (1992), "Equations for Compression Index Approximation", J. Geotech. Eng. ASCE 118(1): 148-153.

- Azzous, A.S., Krizek, R.J., and Corotis, R.B., (1976), "Regression Analysis of Soil Compressibility", Soils and Foundations, 16(2), 19-29.

- Bowles, J., W., (1984). "Physical and Geotechnical Properties of Soil", New York: McGraw Hill.

- Bowles, J. E. (1996), "Foundation Analysis and Design", 5th edition Mc Graw-Hill Book Company Inc. New York.

- Burland, J., B., (1990), "On the Compressibility and Shear Strength of Natural Clays". Geotechnique 40-3, pp 329 – 378.

- Cozzolino, V., M., (1961), "Statistical Forecasting of Compression Index", Proc. of the 5th Int. Conf. on Soil Mechanics and Foundation Engineering, Paris, 1, 51-53.

- Crumley, A., R., Fernández, A., L., Regalado, C., A., (2003), "Compressibility Relationships for Soils in Puerto Rico", 12th Panamerican Conference on Soil Mech. And Geotechnical. Eng. , Cambridge, Massachusetts.

- Djoenaidi, W., J., (1985) " A Compendium of Soil Properties and Correlation" M.Sc. Thesis, University of Sydney.

- Edilm T. B., and Benson, C., H., (2009), "Comparison of Basic Laboratory Test Results with More Sophisticated Laboratory and In-Situ Tests Methods on Soils in Southeastern Wisconsin", Wisconsin Highway Research Program No.0092-06-05

- Ferreira Gomes, L. M., and Ladeira, F. L, (1995), "Equacoes Para Determinear o Indeice De Compressao", Engenharia Civil, UM, Numero 2. pp 17-28.

- Giasi, C., I, Cherubini, C., Paccapelo, F., (2003), "Evaluation of Compression Index of Remoulded Clays by Means of Atterberg Limits", Bull Eng Geol Env , 62, pp:333–340

- Gunduz Z., and Arman, H., (2007), "Possible Relationships Between Compression. and Recompression Indices of a Low–Plasticity Clayey Soil", The Arabian Journal for Science and Engineering, Volume 32, Number 2Bm pp 179-190.

- Helenelund, K., V., (1951)."On Consolidation and Settlement of Loaded Soil Layers". Dissertation, Finland Technical Institute, Helsinki, Finland.

- Heng, C., S., (2006), "Correlation Between Compression Index And Plasticity Index Of Cohesive Soil", BSc. Thesis , Universiti Teknologi Malaysia .

- Herrero O., R., (1980). "Universal compression index equation"; Discussion. J. Geotech. Eng. Div. ASCE 106, pp 1178-1200.

- Hough, B.K., , (1957), "Basic Soils Engineering", The Ronald Press Company, New York, 114-115.

- Isik, N., S., (2009), "Estimation of Swell Index of Fine Grained Soils Using Regression Equations and Artificial Neural Networks", Scientific Research and Essay, Vol.4 (10), pp. 1047-1056.

- Kempfert, H., and Gebreselassie, B., (2006), "Excavations and Foundations in Soft Soils", Springer-Verlag Berlin Heidelberg.

- Koppula, S., D., (1981), "Statistical Estimation of Compression Index,", GTJ, ASTM, vol. 4, no. 2, June, pp. 68-73.

- Koppula, S., D., (1986), “Discussion: Consolidation Parameters Derived from Index Tests” Geotechnique, Vol. 36, No. 2, pp. 291-292.

- Kulhawy, F., H., and Mayne, P., H., (1990), "Manuel on Estimating Soil Properties for Foundation Design",. Electric Power Research Institute, EPRI.

- Lav, M. A. , Ansal, A., M., (2001), "Regression Analysis of Soil Compressibility ", Turk J Engin Environ Sci, 25, pp. 101 – 109
- .
- Mayne, P. W, (1980), "Cam-Clay Predictions of Undrained Strength," JGED, ASCE, vol. 106, GT 11, Nov, pp.1219-1242
- Moh, Z. C., Chin, C.T., Lin, C.J., and Woo. S.M., (1989), "Engineering Correlations for Soil Deposits in Taipei", Journal of Chinese Inst, of Engineering, Vol. 12, No. 3, pp 273-283.
- Nagaraj T.S., Murthy B.R.S. (1986). "A Critical Reappraisal of Compression Index Equations", Geotechnique 36(1): 27-32.
- Nagaraj, T. S., and B. R. Srinivasa Murthy (1985), " Prediction of the Preconsolidation Pressure and Recompression Index of Soils," GTJ, ASTM, vol. 8, no. 4, pp. 199-202.
- Nakase, A., Kamei, T., and Kusakabe, O.,(1988), "Constituted Parameters Estimated by Plasticity Index", Journal of Geotechnical Engineering Division, American Society of Civil Engineers, Vol. 114, No. 7, pp. 844-858.
- Nishida, Y. (1956), "A Brief Note on Compression Index of Soils," JSMFD, ASCE, vol. 82, SM 3, pp 1027-1-1027-14.
- Oswald, R., H. (1980). "Universal Compression Index Equation," Journal Geotechnical.Engineering Div. Am. Soc. Civil Engineering, 106, 1179-1199.
- Rendon-Herrero, O. (1983), "Closure: Universal Compression Index Equation," JGED, ASCE, vol. 109, GT 5, May, pp. 755-761.
- Skempton, A.W., (1944), "Notes on the Compressibility of Clays", Quarterly Journal of Geological Society of London, 100, 119-135.
- Sowers, G.B., (1970), "Introductory Soil Mechanics and Foundations", The Macm illan Company, Collier-Macmillan Limited, London, 3rd Edition, 102.
- Tan, Y. C., and Gue, S, .S., (2000), "Subsurface Investigation and Interpretation of Test Result for Foundation Design in Soft Clay", Seminar on Ground Improvement - Soft Clay (SOGIS2000), 23rd & 24th, UTM, Kuala Lumpur.
- Terzaghi, K. and Peck, R.B., (1967), "Soil Mechanics in Engineering Practice", John Wiley & Sons Inc. New York.
- Wroth, C., P., and Wood, D., M., (1978), "The Correlation of Index Properties with some Basic Engineering Properties of Soils", Canadian Geotechnical Journal 15,pp 137 – 145.

NOMENCLATURE:

e : void ratio

e_o: natural void ratio

LL: liquid limit

I_p : plasticity index

P : consolidation pressure

PL: plastic limit

P_o : effective overburden pressure

R : Correlation Coefficient

w_o: natural moisture content

γ_d :dry unit weight

γ_t: total unit weight

ECG SLANTLET TRANSFORM WITH FPGA DESIGN

Zainab N. Ghanim
University of Baghdad

ABSTRACT

The ECG is used for the clinical analysis of physiological data has occurred in the field of cardiology. Certain abnormalities of the ECG are quite well defined and can be readily identified. The digital signal processing Slantlet Transform is used in the feature extraction of ECG monitoring and Diagnosis system to convert the continuous ECG signal to a form can be classified by a classifier of the ECG monitoring and Diagnosis system to detect the cardiac abnormalities.

In this paper, FPGA is used to build the slantlet Transform of the ECG feature extraction .VHDL program of FPGA is used in the work, the obtained output results are similar to the past work results, which is built by using Mat Lab program, in accuracy and closing to the original ECG signal. Using FPGA decreases the cost and time for building hardware system of ECG Monitoring and Diagnosis system. It also gives more flexibility than the alternate approaches. Mat-Lab program is used only for displaying the input and output discrete signals of slantlet transform.

الخلاصة:

يستعمل تخطيط القلب الكهربائي لغرض التحليل الطبي للبيانات الفسلجية التي تحدث للقلب. الحالات غير الطبيعية المؤكدة للتخطيط الكهربائي للقلب هي معرفة بشكل واضح ويمكن تحديدها. إن التحويل (Slantlet) في معالج الإشارة الرقمية يستعمل في نظام المعاينة والتشخيص لتخطيط القلب الكهربائي لاستخراج خاصية إشارة تخطيط القلب الكهربائية المستمرة حتى يمكن تصنيفها بواسطة نظام تصنيف في نظام المعاينة والتشخيص لتخطيط القلب الكهربائي لاكتشاف الحالات غير الطبيعية للقلب.

تم استعمال المبرمج الحقلي لمصفوفات البوابة (FPGAs) في هذا البحث لبناء التحويل (Slantlet) لاستخراج خاصية تخطيط القلب الكهربائي. تم استعمال برنامج (VHDL) التابع ل (FPGAs) في هذا العمل كانت النتائج مقاربة لنتائج عمل سابق تم بناءه باستخدام برنامج (Mat-Lab) من ناحية الدقة والمقاربة مع

الإشارة الأصلية، لكن استعمال (FPGAs) قلل الوقت والكلفة اللازمين لبناء الدائرة الالكترونية لنظام المعاينة والتشخيص لتخطيط القلب الكهربائي كما انه يعطي مرونة أكثر من أي نظام بديل آخر. وقد تم استخدام برنامج Mat-Lab فقط لعرض الإشارات الداخلة إلى التحويل Slantlet والخارجة منه.

INTRODUCTION:

The human heart is a complex muscular pump. Owing to the importance of the heart, a great interest has been given to monitor the heart operation, to detect its abnormalities. ECG measurements are used to monitor the contraction of the cardiac muscles by measuring the propagation of electrical depolarization and repolarization in the atria and ventricles. The ECG interpretation is important for cardiologists to decide diagnostic categories of cardiac problems.

The ECG pattern recognition as shown in fig. 1 is studied and programmed by Mrs. Rasha Thabit in her thesis . The first block is the sampler, where is necessary to convert the continuous ECG electrical signal (x(t)) to a discrete one. The recognition of cardiac abnormalities is done in the third block by using neural network, depending on the features representing the ECG signal. Different types of digital signal processing transformation are tested in feature extraction block of ECG pattern such as FFT, Discrete Wavelet Transform and SLT, etc. In the thesis of Rasha, SLT gave better results than the other systems because it is the more accurate system, where the results of classification in the third block (neural network) has minimum percentage error rate, when SLT is used with respect to other types. Mat Lab program is used to implement the thesis work.

In this paper, FPGAs is used to build the SLT of ECG feature extraction instead of using Mat Lab program, to design a hardware circuit for this part..

FPGA is on the verge of revolutionizing digital signal processing. Many front-end digital signal processing algorithms are now most often replaced by FPGAs. This allows users to by pass the hardware design engineer leading to a significant reduction in development time and cost. VHDL program is used to build FPGA SLT design, where it is widely used in this field to offer software implementation. Different types of ECG signals are used to test the new system, by applying the samples of these signals to the ECG feature extraction block, which is built by FPGA. The input and output signals of the feature extraction block are plotted using Mat Lab program.

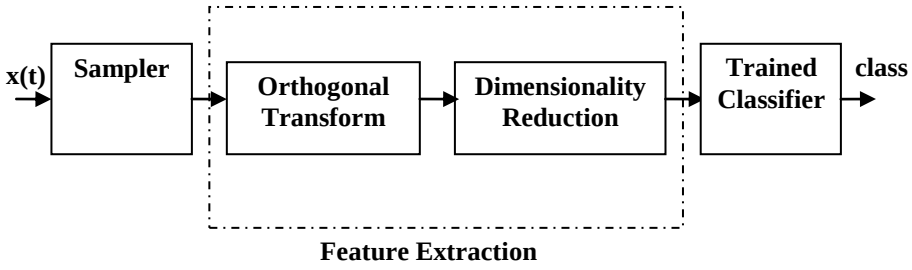

Fig. 1: Pattern recognition system

DESCRIPTION OF THE ECG WAVEFORM:

Atypical ECG waveform is shown in fig. 2. The initial wave is the P-wave, it is small and rounded. Next a sharp combination wave known as QRS complex which is comprised of the sharp downward Q-wave, followed by the upward R-wave and subsequently the downward S-wave. The final wave, T-wave is rounded. The R-R interval represents the period from the R-peak of one beat of the ECG signal to the next R-peak. The P-R interval represents the period from the start of the P-wave to the beginning of the QRS complex, Q-T interval represents the period from the beginning of the QRS complex to the end of T-wave.

There are 12-lead ECG system, which includes three limb leads (I, II or (MLII), III), three augmented leads (aVR, aVL, aVF) and six precordial leads (V1, V2, V3, V4, V5, V6). It is the commonly used ECG system in clinic or health care centers.

Abnormalities of cardiac rhythm are easy to work out, by looking at the shape and width of the ECG waveforms such as P-wave, Q-wave, ST segment and T-wave. Then, the heart disease is diagnosed depending on the ECG waveform shape, such as Right Bundle Branch Block, Left Bundle Branch Block, Myocardial Infarction, Ventricular Tachycardia and Fibrillation.

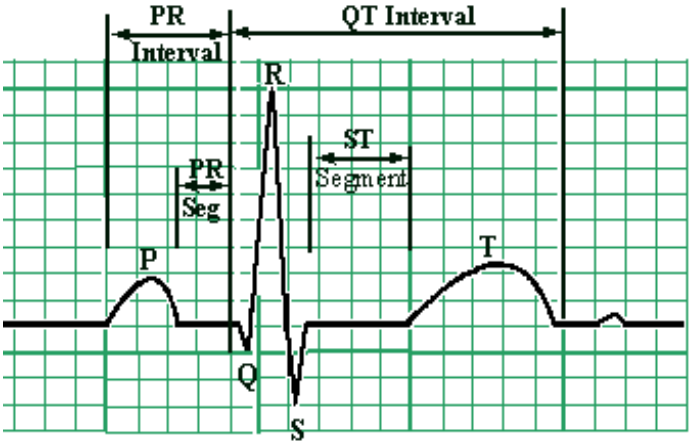

Fig. 2: Typical ECG waveform

Feature Extraction Using Slantlet Transform:

The slantlet filter bank used in feature extraction is based on three-scale filter bank as shown in fig. 3. The L-scale filter bank has 2L channel . The low pass filter is to be called $h_L(n)$. The filter adjacent to the low pass channel is to be called $f_L(n)$. Both $h_L(n)$ and $f_L(n)$are being followed by downsampling by 2^L. The remaining 2L-2 channels are filtered by $g_i(n)$ and its shifted time reverses for ***i*** = 1,……..,L-1. Each is to be followed by downsampling by 2^{i+1} . Note that in the slantlet filter bank, each filter $g_i(n)$ appears together with its reverse, while $h_i(n)$ does not appear with its time reverse. It always appears paired with the filter $f_i(n)$. The filters $g_i(n)$, $h_i(n)$ and $f_i(n)$ have two zero moments that is, their inner products with linear polynomial sequences are zero.

The sought-after filter $g_i(n)$ is to be linear over the interval $n \in \{0,\ldots, 2^i\text{-}1\}$ and over the interval $n \in \{2^i,\ldots, 2^{i+1}\text{-}1\}$, therefore, it is described by four parameters and can be written as:

$$g_i(n)=\begin{cases} a_{00}+a_{01}n & for \quad n=0,...,2^i-1 \\ a_{10}+a_{11}(n-2^i) & for \quad n=2^i,...,2^{i+1}-1 \end{cases} \qquad (1)$$

Where

$m = 2^i$

$s_1 = 6\sqrt{m/((m^2-1)(4m^2-1))}$

$t_1 = 2\sqrt{3/(m\cdot(m^2-1))}$

$s_0 = -s_1 \cdot (m\text{-}1)/2$

$t_0 = ((m+1)\cdot s_1/3 - m\, t_1)(m\text{-}1)/(2m)$

$a_{00} = (s_0 + t_0)/2$

$a_{10} = (s_0 - t_0)/2$

$a_{01} = (s_1 + t_1)/2$

$a_{11} = (s_1 - t_1)/2$

The same approach works for $h_i(n)$ and $f_i(n)$, they can be written in terms of eight unknown parameters b_{00}, b_{01}, b_{10}, b_{11}, c_{00}, c_{01}, c_{10} and c_{11}.

$$h_i(n)=\begin{cases} b_{00}+b_{01}n & for \quad n=0,...,2^i-1 \\ b_{10}+b_{11}(n-2^i) & for \quad n=2^i,...,2^{i+1}-1 \end{cases} \qquad (2)$$

$$f_i(n)=\begin{cases} c_{00}+c_{01}n & for \quad n=0,...,2^i-1 \\ c_{10}+c_{11}(n-2^i) & for \quad n=2^i,...,2^{i+1}-1 \end{cases} \qquad (3)$$

Where

$m = 2^i$

$u = 1/\sqrt{m}$

$v = \sqrt{(2m^2+1)/3}$

$b_{00} = u \cdot (v+1) / (2m)$

$b_{10} = u - b_{00}$

$b_{01} = u/m$

$b_{11} = - b_{01}$

$q = \sqrt{3/(m \cdot (m^2-1))} /m$

$c_{01} = q \cdot (v - m)$

$c_{11} = - q \cdot (v + m)$

$c_{10} = c_{11} \cdot (v +1-2m)/2$

$c_{00} = c_{01} \cdot (v+1)/2$

The filters are implemented by a sequence of convolutions and down sampling, only four terms are needed to compute $y_i(n)$. The output sample of channel ***i*** is written as an inner product.

$$y_i(n) = \sum_{k=0}^{2^{i+1}-1} x(2^{i+1}n+k) \cdot g_i(k) \qquad (4)$$

$$y_i(n)=a_{00} \sum_{k=0}^{2^i-1} x(2^{i+1}n+k) + a_{01} \sum_{k=0}^{2^i-1} kx(2^{i+1}n+k) + a_{10} \sum_{k=0}^{2^i-1} x(2^{i+1}n+(k+2^i)) + a_{11} \sum_{k=0}^{2^i-1} kx(2^{i+1}n+(k+2^i)) \qquad (5)$$

The same equation will be used for $h_i(n)$ and $f_i(n)$, the number of x input data sampling for this work is 256 samples and the number of y output data sampling is dependent on the value of downsampling, which is limited by the value of **L** and ***i*** .

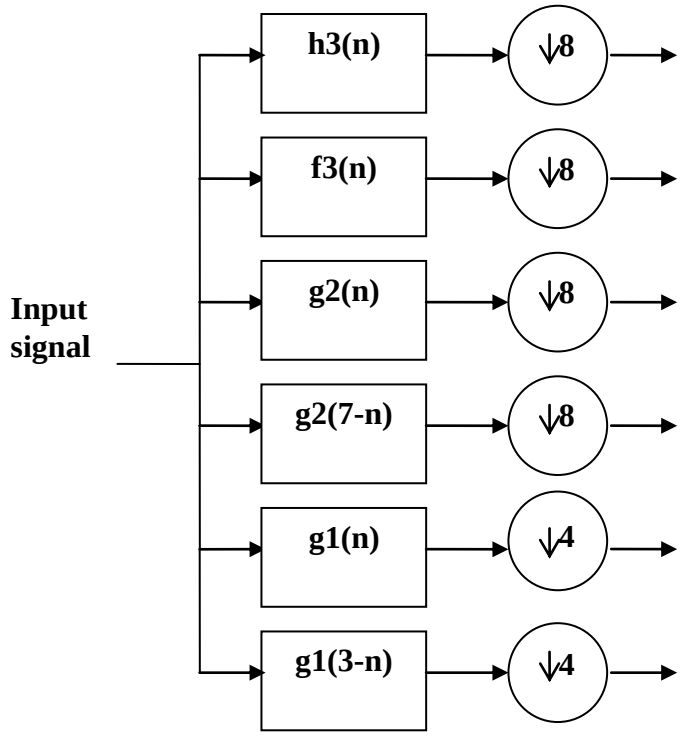

Fig. 3: 3-scale slantlet filter bank

FPGA DESIGN OF SLANTLET TRANSFORM:

VHDL program provides language constructs for parametrizing and customizing designs, and for definition and usage of design libraries. These constructs enable a designer to generate a functional design independent of the specific technology and customize this generic design at a later stage. Specifically, library, use clause, package, and configuration declarations of VHDL are used for grouping or categorizing various components into design libraries and for customizing designs to use components in these libraries.

Several levels of components are nesting in the design of SLT. Fig. 4 shows the composition aspect for a configuration declaration of wiring and testing the SLT components architecture (architecture is a statement in VHDL program), where Slantlet Transform level (top level) and SLT filters level (second level) are shown in the figure. The Slantlet Transform level is the block of the whole SLT architecture. Inside this top level, SLT filters blocks are used as another level (filters level), each filter has a specified architecture.

Algorithm for the Slantlet Transform level (SLT block) is:

Step 1: Read a Text file of sampling data of ECG waveform (input data file),which is taken from MIT-BIH ECG database. A specified procedure (procedure is a

VHDL statement) is used to read only 256 sampling values (real values) ,where the ECG waveform is repeated after that .

Step 2: Convert these real values to binary values, with eighteen bits. A specified procedure is used for this operation. The binary values are stored in XX matrix.

Step 3: Give the XX matrix to the second block (filter block), the six filter blocks receives the XX matrix in parallel.

Step 4: SLT block receives the output of filters by a matrix Y with 32 cells for h3, f3 and g2 filters output and 64 cells for g1 filter output, depending on the downsampling of each filter. Each cell with thirty six bits length.

Step 5: The binary values of Y matrix are converted to real values by a specified procedure.

Step 6: write the real values in a text file (output data file) by a procedure.

Algorithm for the filters level (filter block) is:

Step 1: Take the XX matrix from the SLT block.

Step 2: Apply eq. (5) by replacing XX in x matrix and replacing filters functions g, h and f with their equations (1,2 and 3) respectively in eq. (4). Y output is obtained as a result. Specified circuit design is used to apply eq. (5), as shown in fig. 5.

Step 3: Return Y matrix to the SLT block.

Fig. 5 shows the block diagram of the filters architectures design in the second level. This design is applied for the filters with downsampling by eight such as h3,f3 and g2.

In the design eight values of inputs data x are taken at each time. The first four inputs data from the eight values are added by adder component, the component has four inputs each input eighteen bits and one output acts the result of addition. The first four inputs data are also multiplied by k as in eq. (5). Multiplier component is used to multiply the four inputs data with four k values to obtain four results of multiplication (parallel multiplication), each input and output of this multiplier are eighteen bits. Another adder component is used to add the four results of multiplier component. The same operation is done for the second four inputs data, also two adders and one multiplier are used for the second four inputs data.

Four multipliers are used to multiply the outputs of four adders with filter constants (a, b or c as in eq. (5)). Each multiplier has two inputs, each one is eighteen bits. One output result of multiplication thirty six bits. At last the four outputs of multipliers are added by adder component with four inputs ,each input thirty six bits and one output result of addition thirty six bits.

The output is loaded in the matrix of output data Y. This operation is repeated for another eight values of input data. The same design is used for the g1 filter but four inputs data are taken at each time.

IMPLEMENTATION AND RESULTS:

The whole FPGA design of SLT is implemented by VHDL program. The output of the low pass filter h3 (Y5) is the approximation of the signal and the other outputs are the details, therefore the output of the h3 filter is only displayed to obtain a close signal to the input one.

The input ECG signals are taken from MIT-BIH ECG database; the records 202,102 and 111 are used for Normal, Paced and Left Bundle Branch ECG signals respectively. 256 samples are enough to take from the sampling data file as input to the SLT filters, where the same data are repeated after that. The output of the h3 filter is 32 samples of data.

The input and output ECG samples real data, which is written in input data text file and output data text file are plotted using MAT-LAB program. The results are shown in fig. 6, fig. 7 and fig. 8 for normal, paced and left bundle branch ECG signals respectively. The continuous ECG signal for a patient is shown in (a), the ECG signal after the sampler (input to SLT) is shown in (b) and the signal after SLT is shown in (c), a single beat of MLII signal for normal and left bundle branch is taken and a single beat of V5 for paced beat is taken.

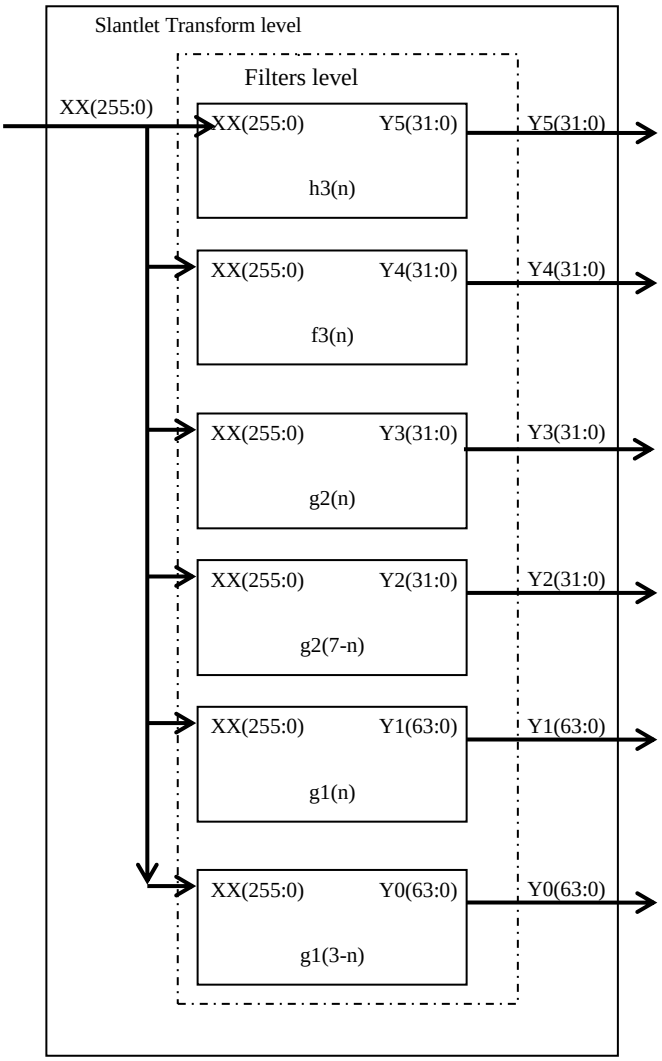

Fig. 4 : Composition aspect of the Slantlet Transform for testing ECG feature extraction

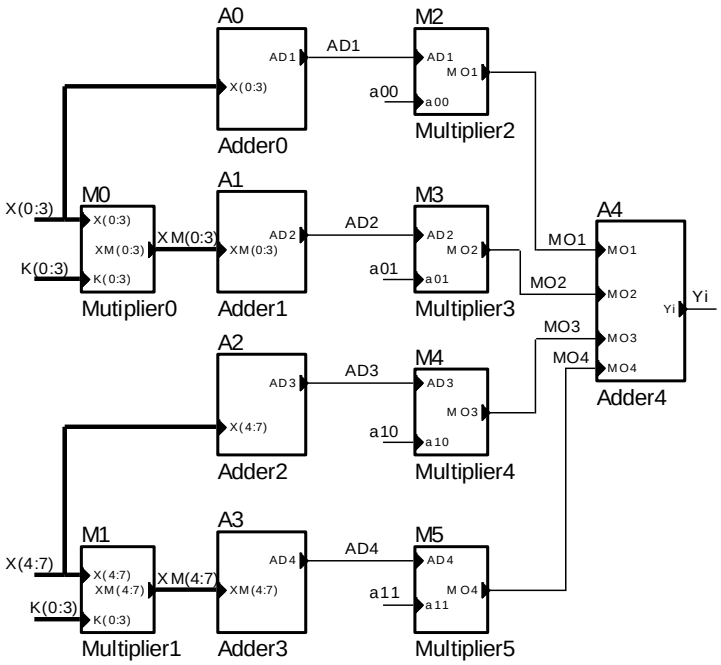

Fig. 5 : Block diagram of filter architecture design.

CONCLUSIONS:

The work with VHDL program gives output waveform of SLT very close to input one. It is clear from the output signal figures, that is the output waveform has the features of the original ECG signal to accurately classify the heart arrhythmias.

As in any high level language, VHDL allows the definition and usage of functions and procedures. In addition to the important hardware implications of subprograms, these language constructs greatly improve readability and organization of a hardware description.

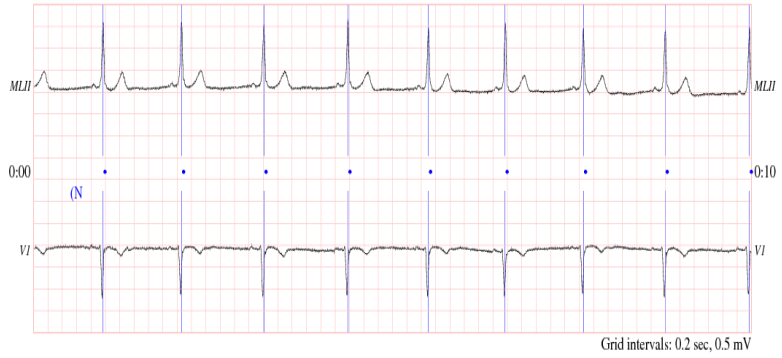

(a)

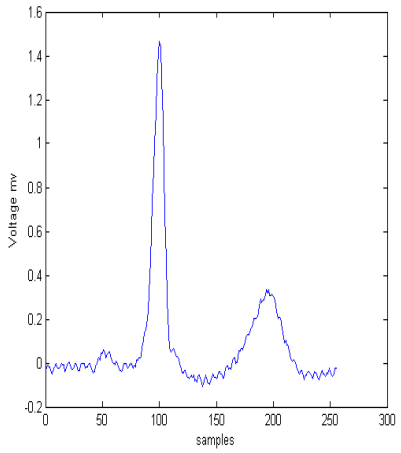

(b)

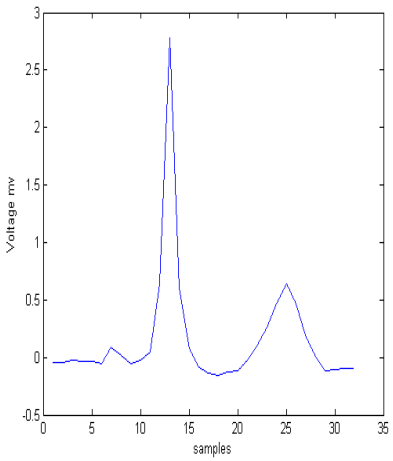

(c)

Fig. 6:
(a) The ECG record (Normal Sinus Rhythm).
(b) The Extracted single beat.
(c) 32 samples of the SLT (h3 output).

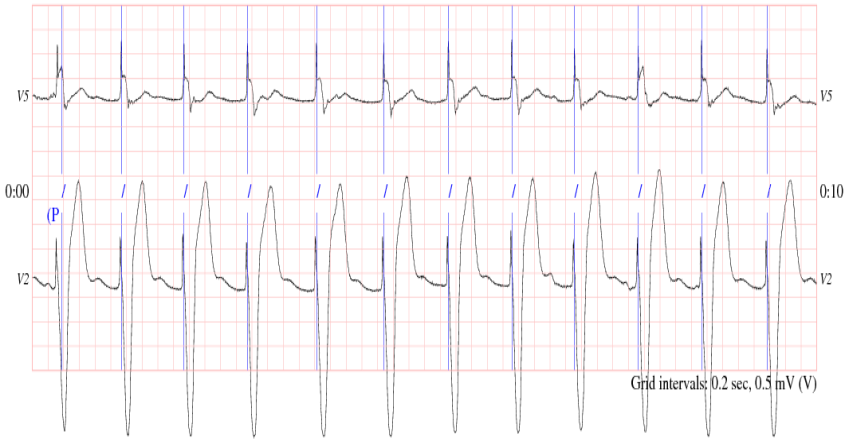

(a)

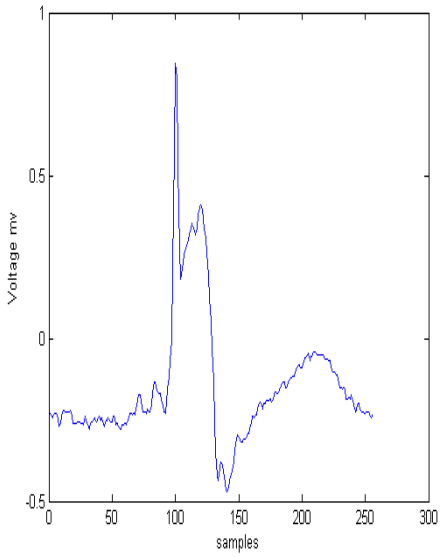

(b)

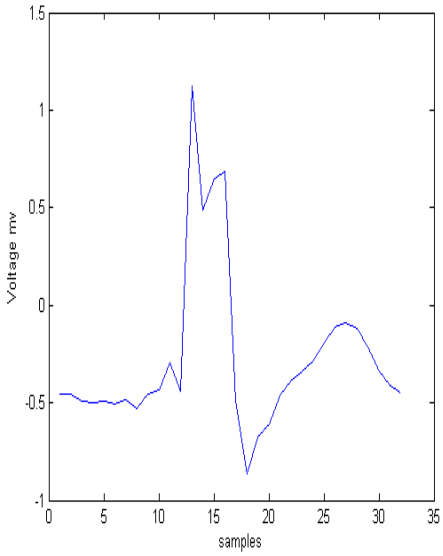

(c)

Fig. 7:
(a) The ECG record (Myocardial Infarction (Paced beats)).
(b) The Extracted single beat.
(c) 32 samples of the SLT (h3 output).

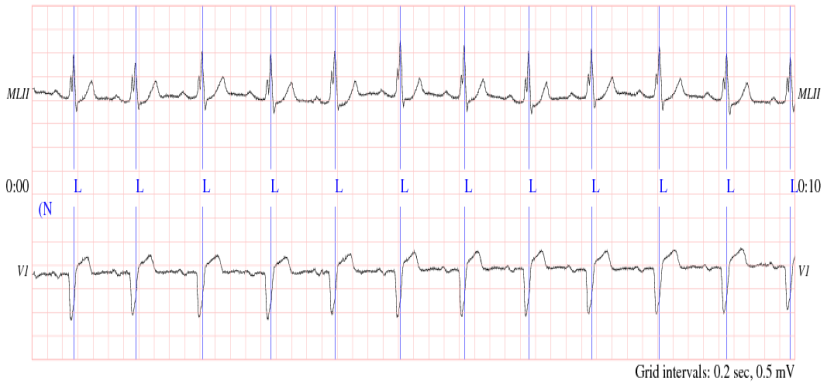

(a)

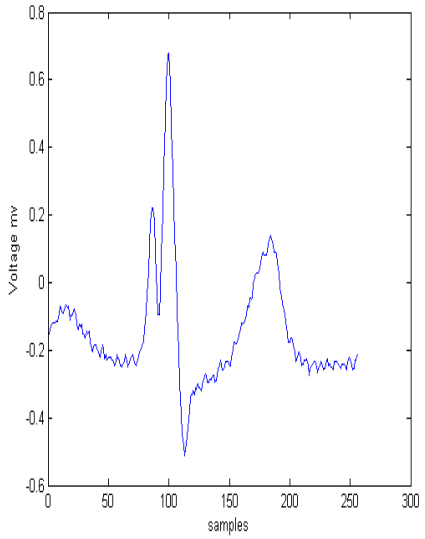

(b)

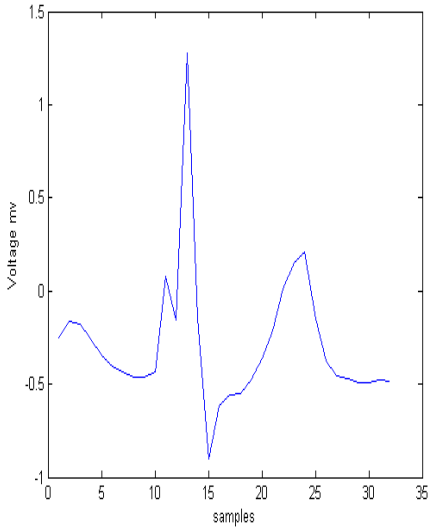

(c)

Fig. 8:
(a) The ECG record (Left Bundle Branch).
(b) The Extracted single beat.
(c) 32 samples of the SLT (h3 output).

REFERENCES:

- D. A. Demarre and D. Michaels, "Bio electronic measurements", Prentice Hall, Inc., Englewood cliffs, New Jersey, USA, 1983.
- http://www.physionet.org/, Explore Physio Bank from a web browser, ECG MIT-BIH database.
- Ivan W. Selesnick, "The Slantlet Transform", IEEE transactions on signal processing, vol. 47, no. 5, May 1999.
- J. D. Enderle, S. M. Blanchardend, and J. D. Branzino, "Introduction to Biomedical Engineering", Academic Press, 2000.
- J. R. Hampton, "The ECG made Easy", Elsevier Science limited, sixth edition, 2003.
- Mc Sharry PE, Clifford GD, Tarassenko L., Smith L., "A Dynamic Model For Generating Synthetic Electrocardiogram Signals", IEEE transactions on biomedical engineering 50 (3), 289-294, March 2003.
- N. Ahmed and K.R. Rao, "Orthogonal Transforms For Digital Signal Processing", Springer-Verlag, 1975.
- N. M. Saad, A. R. Abdullah, and Y. F. Low, "Detection of Heart Blocks in ECG signals by Spectrum and Time-Frequency analysis", IEEE 4th student conference on research and development, pp. 61-65, 2006.
- R. Thabit, "ECG Monitoring And Diagnosis Using Hybrid Transform Method", M.Sc. Thesis, Department of Electrical Engineering, University of Baghdad, 2008.
- Uwe Meyer-Baese[a], A. Vera[b], A. Meyer-Baese[a], M. Pattichis[b], R. Perry[a], [a]FAMU-FSU, "Discrete Wavelet Transform FPGA Design using Matlab/simulink", ECE Dept., 2525 Pottsdamer Street, Tallahassee, FL USA-32310; [b]University of New Mexico, ECE Dept., Albuquerque, NM 87131, 2006.
- Zainalabedin Navabi, "VHDL Analysis and Modeling of Digital Systems", McGraw-Hill Series in Electrical and Computer Engineering, 1993 .

LIST OF ABBREVIATIONS:

ECG : Electrocardiogram.
FFT : Fast Fourier Transform.
FPGAs : Field Programmable gate arrays.
SLT : Slantlet Transform.
VHSIC : Very High Speed Integrated Circuit.
VHDL : VHSIC Hardware Description Language.

THE INFLUENCE OF TENSION STIFFNENING MODELS ON THE DYNAMIC ANALYSIS OF REINFORCED CONCRETE SLABS

Dr.K.S. Mahmood
Professor
Baghdad University

Dr.A.A. Abdul-Razzak
Assistant Professor
Mosul University

M.K. Kasim
Assistant Professor
Tikrit University

ABSTRACT

In the present work, the finite element method has been used to investigate the behavior of reinforced concrete slabs subjected to dynamic loads. Eight-node Serendipity degenerated elements have been employed. This element is based on isoperimetric principles with modifications, which relax excessive constraints. The modifications include reduced order integration to overcome the shear locking.

A layered approach is adopted to discretize the concrete through the thickness. Both an elastic-perfectly plastic and strain hardening plasticity approaches have been employed to model the compressive behavior of the concrete. A tensile strength criterion is used to initiation of crack and a smeared fixed crack approach is used to model the behavior of the cracked concrete. Five models are used to consider the effect of tension stiffening in the cracked concrete.

Implicit Newmark with corrector-predictor algorithm is employed for time integration of the equation of motion.

Several examples are analyzed using the proposed model. The numerical results showed good agreement with other sources.

ألخلاصة

استخدمت طريقة العناصر المحددة لدراسة التصرف اللاخطي الديناميكي للبلاطات الخرسانية المسلحة. استخدمت العناصر ثمانية العقد في هذا البحث. هذه العناصر تعتمد على مبدأ توحيد المتغيرات مع اعتماد مجموعة من التعديلات التي تخفف القيود الإضافية. هذه التعديلات تتضمن قواعد التكامل المخفض وذلك لتفادي حالة القفل بالقص

استخدم مبدأ الطبقات لتمثيل الكونكريت وحديد التسليح على امتداد ارتفاع مقطع البلاطة. و مثل سلوك الخرسانة في حالة الانضغاط كمادة مرنة- تامة اللدونة أو كمادة مرنة مع انفعالات لدنة متصلدة. تم استخدام سلوك مقاومة الخرسانة للشد للتنبؤ بحدوث تشقق واستخدم اسلوب الشق الثابت لتمثيل الخرسانة المتشققة مع تثبيت حدود مقاومة تصلد الشد للتنبؤ بحدوث الشق. أخذت في الاعتبار خمسة نماذج لتمثيل تأثير صلابة الشد في الخرسانة المتشققة.

تم أعتماد طريقة نيومارك الضمنية مع طريقة التنبؤ-التصحيح لحل معادلة الحركة التفاضلية.

تم حل عدة أمثلة أظهرت النتائج توافقا" جيدا" مع النتائج المستحصلة بالطرق الأخرى

KEY WWORDS

Dynamics, Finite elements, Nonlinear analysis, Reduced integration, Reinforced concrete slabs, Tension stiffening models.

NOTATION

B	Strain-nodal displacement matrix.
B_b	Bending strain- nodal displacement matrix.
B_s	Transverse shear strain- nodal displacement matrix.
D	Flexural (or Shear) Rigidities.
D_b	Flexural rigidities.
D_s	Shear rigidities.
d	Displacements.
$\dot{d}$	Velocities.
$\ddot{d}$	Accelerations
E_c	Initial modulus of elasticity of concrete.
E_s	Modulus of elasticity of steel.
E_s'	Second modulus of elasticity of steel (hardening coefficient).

f_c'	Uniaxial compressive strength of concrete.
f_t'	Uniaxial tensile strength of concrete.
Gc	Fracture energy of concrete.
K	Elastic stiffness matrix.
K^*	Effective stiffness matrix.
K_T	Tangential stiffness matrix.
M_x , M_y , M_{xy}	Generalized stress components(moments).
N	Shape function.
ρ	Mass density.
Q_x , Q_y	Generalized stress components (shear forces).
R.C.	Reinforced concrete.
β , γ	Newmark's integration parameters.
ε_x , ε_y	Strains in x and y-direction.
ε_b	Bending strain tensor.
ε_s	Transverse shear strain tensor.
ε_u	Crushing strain.
ν	Poisson's ratio.
σ_x , σ_y	Normal stress components.

INTRODUCTION

The finite element method was introduced for structural analysis many years ago. It has been recognized as a powerful and widely used approach for analysis of R.C. structures [1,5,10,11,20].

Farag and Leach [9] analyzed reinforced concrete structures under transient dynamic loading. The three dimensional isoparametric element with 20 nodes is used to simulate the concrete. The smeared approach is used to represent the reinforcement in the elements. A viscoplastic model is used to simulate the concrete in compression with two surfaces, the failure surface expressed as a function of the first and the second deviatoric stress invariant.

Shirai et al. [21] investigated and proposed a method to improve impact resistance of reinforced concrete plates against projectile impact, and the damage of

double-layered reinforced concrete plates was examined experimentally and simulated analytically.

Sziveri et al. [22] analyzed reinforced concrete plates under transient dynamic loading. A layered triangular element was considered for determining the dynamic transient nonlinear response of reinforced concrete plates.

Manjuprasad et al. [18] analyzed reinforced concrete rectangular slabs and containment shell subjected to seismic load. A 20-noded three-dimensional, solid isoparametric finite element is used for spatial discretisation.

Agbossou and Mougin [3] used a layered approach to the non – linear static and dynamic analysis of rectangular reinforced concrete slabs. The proposed model considers the slab as a layered structure and leads to explicit relations, which account for the macroscopic linear and non-linear behavior of slabs on lines of simple supports.

Xu and Lu [24] analyzed reinforced concrete plates subjected to blast loading using three-dimensional nonlinear finite element. Pseudo-tensor concrete/geological model is employed to model the concrete, taking into account the strain rate effect. A strain rate multiplier is used to modify the dynamic yield strength of the concrete material.

BASIC THEORY

By Mindlin thick plate element, the variation of displacements and rotations are given by the expression as[12]:

$$\left[w,\ \theta_x,\ \theta_y\ \right]^T = \sum_{i=1}^{n} N_i d_i \qquad \text{……..(1)}$$

The plate curvature-displacement and shear strain-displacement relations are then written as:

$$\varepsilon_b = \sum_{i=1}^{n} B_{bi} d_i \quad , \quad \varepsilon_s = \sum_{i=1}^{n} B_{si} d_i \qquad \text{…….....(2)}$$

The moment-curvature and shear force–shear strain relations can be written as:

$$[M_x,\ M_y,\ M_{xy}\ ]^T = D_b\varepsilon_b \quad , \quad [Q_x,\ Q_y\ ]^T = D_s\varepsilon_s \qquad \text{…….(3)}$$

Based on the energy minimization, the elastic stiffness and the mass matrices can be determined from the relations:

$$[K] = \int_v [B]^T [D][B]dv \qquad \text{……..(4)}$$

$$[M] = \rho\int_v [N]^T [N]dv \qquad \text{…….(5)}$$

REDUCED INTEGRATION

Based on the work of Dohestry et al. [8] to eliminate the parasitic shear on plane quadrilateral elements, the implementation of the reduced integration for the degenerated shell element was firstly introduced by Zeinkiewics et al. [25]. Then many papers about the reduced integration technique have been published[13,19].

Using the full integration rule a shear-locking problem will appear. Therefore reduced integration rule (2x2) for 8-node Serendibity element is applied in this study to overcome this problem.

MATERIAL MODELING

Based on the flow theory of plasticity, the nonlinear compressive behavior of concrete is modeled. Adopting Kupfer's results[16], the yield condition for the slab can be written in term of the stress components as[10]:

$$f(\sigma) = \left\{1.355\left[(\sigma_x^2+\sigma_y^2-\sigma_x\sigma_y)+3(\tau_{xy}^2+\tau_{xz}^2+\tau_{yz}^2)\right]+0.355\sigma_o(\sigma_x+\sigma_y)\right\}^{0.5} = \sigma_o \qquad \text{…...(6)}$$

where (σ_o) is the equivalent effective stress taken as the compressive strength ($f_c^{'}$) which is obtained from uniaxial test.

The crushing of concrete is a strain control phenomenon. A simple way of incorporation in the model is to convert the yield criterion of stresses directly into the strains, and the crushing condition can be expressed in terms of the total strain components as:

$$1.355\left\{(\varepsilon_x^2+\varepsilon_y^2-\varepsilon_x\varepsilon_y)+0.75\,(\gamma_{xy}^2+\gamma_{xz}^2+\gamma_{yz}^2)\right\}+0.355\varepsilon_u(\varepsilon_x+\varepsilon_y)=\varepsilon_u^2 \quad ....(7)$$

The concrete is assumed to lose all its characteristics of strength and rigidity when (ε_u) reaches the specified ultimate strain.

Tension stiffening, illustrates that the cracked reinforced concrete as a result of bond mechanisms carries, between cracks, a certain amount of tensile stress normal to the cracked plane. The concrete between cracks adheres to the reinforcing bars and contributes to the overall stiffening of the structure. The strain softening or descending branch of the stress strain curve of concrete in tension, in one form or another, may be used to simulate this "tension stiffening" effect. In the present study five types of tension stiffening models are used.

(i) Model (1) linear model. In this model a linear gradual release of the concrete stress component normal to the cracked plane is assumed. as shows in Fig (1).

(ii) Model (2) tension stiffening (parabolic model). The relationship between stress and strain after cracking is given in Fig(2) as cited in reference [1,4,5] :

$$\sigma = f_t' \left(\frac{\varepsilon_1-\varepsilon_m}{\varepsilon_t-\varepsilon_m}\right)^2 \quad \text{.....(8)}$$

The maximum tensile strain (ε_m) can be evaluated from equation (9) as:

$$\varepsilon_m = \frac{3G_c}{h_c\ f_t'}+\varepsilon_t \quad \text{.....(9)}$$

The typical values for (G_c) lie in the range $(200 f_t'^2/E_c)$ to $(400 f_t'^2/E_c)$. In the present study (G_c) is taken equal to 100 N/m.

(iii) Model (3) is used in the present study, and is given by Collins and Vecchio [23] and by Collins and Mitichell [7], see Figure(3)

$$\sigma = \frac{\alpha_1\alpha_2\ f_t'}{1+\sqrt{500\varepsilon_1}} \quad \text{.....(10)}$$

where

α_1= factor accounting for bond characteristics of reinforcement equal (1.0) for deformed reinforcing bars and (0.7) for plain bars, wires, or bonded strands and (0) for unbounded reinforcement.

α_2= factor accounting for sustained or repeated loading equal to (1.0) for short-term monotonic loading and (0.7) for sustained and or repeated loading.

It must be noted that the stress in the reinforcement at a crack location cannot exceed the yield stress of reinforcement.

(iv) Model (4) This model is developed by Abrishami [2] tack the splitting effect into account. After cracking the maximum tension is limited to the yield force of the reinforcement. To account for the detrimental effects of the influence of splitting cracks on the tension stiffening, the factors $(\alpha_1, \alpha_2, \alpha_3)$ [2] are including, see Fig (4).

$$\sigma = \frac{\alpha_1 \alpha_2 \alpha_3 \ f_t^{'}}{1+\sqrt{500\varepsilon_1}} \quad \text{.....(11)}$$

where

α_1 and α_2 are defined as in equation (10)

$\alpha_3 = 1.0$ for $c/d_b > 2.5$

$\alpha_3 = 0.8c/d_b - 1$ for $1.25 \le c/d_b \le 2.5$

$\alpha_3 = 0$ for $c/d_b < 1.25$

where (c) is the concrete cover to the centroid of steel and (d_b) is the diameter of the bar, $(f_t^{'})$ is the tensile strength of concrete and (ε_1) is the strain in concrete in direction (1). Both models (3 & 4) have a limited value of $\varepsilon_m = \varepsilon_y$

(v) Model (5) is a linear model. This model is developed by Johanson [5] and adopted in the present analysis where by assuming unloading and reloading of cracked concrete, the behavior is linear which is shown in Fig. (5)

CRACKED SHEAR MODULUS

In the present study, the cracked shear modulus is assumed to be a function of the current tensile strain. In this approach a value of $(G^{'})$ linearly decreasing with the current tensile strain is adopted by Cedolin and Deipoli [6] and used by many investigators [1,5,10] .

For concrete cracked in direction 1.

$$\begin{aligned} G_{12}^{'} &= 0.25G(1-\varepsilon_1/0.004) && \text{for} \quad \varepsilon_1 < 0.004 \\ G_{12}^{'} &= 0 && \text{for} \quad \varepsilon_1 > 0.004 \\ G_{13}^{'} &= G_{12}^{'} \\ G_{23}^{'} &= \frac{5}{6}G \end{aligned} \qquad \text{.....(12)}$$

where (G) is the uncracked shear modulus and (ε_1) is the tensile strain in direction (1). For concrete cracked in both directions:

$$\begin{aligned} G_{13}^{'} &= 0.25G(1-\varepsilon_1/0.004) && \text{for} \quad \varepsilon_1 < 0.004 \\ G_{13}^{'} &= 0 && \text{for} \quad \varepsilon_1 > 0.004 \\ G_{23}^{'} &= 0.25G(1-\varepsilon_2/0.004) && \text{for} \quad \varepsilon_2 < 0.004 \\ G_{23} &= 0 && \text{for} \quad \varepsilon_2 > 0.004 \\ G_{12}^{'} &= 0.5G_{23}^{'} && \text{for} \quad G_{23}^{'} < G_{13}^{'} \end{aligned} \qquad \text{.....(13)}$$

NEWMARK METHOD

The Newmark method as cited in reference[11], and adopted in this work, is an extension of the linear acceleration method. The dynamic equilibrium equation is linearized and written at time t_{n+1} as:

$$M\ddot{d}_{n+1} + C\dot{d}_{n+1} + Kd_{n+1} = f_{n+1} \qquad \text{.....(14)}$$

and $$[C] = c\int_v [N]^T [N] dv \qquad \text{.....(15)}$$

where c is a damping coefficient (per unit volume).

The following assumptions on the variation of displacements and velocities are made within a typical time step:

$$d_{n+1} = d_n + \Delta t \dot{d}_n + \frac{\Delta t^2}{2}[(1-2\beta)\ddot{d}_n + 2\ \beta\ \ddot{d}_{n+1}] \quad \ldots\ldots\ldots\ldots\ldots\ldots(16)$$

$$\dot{d}_{n+1} = \dot{d}_n + \Delta t[(1-\gamma)\ddot{d}_n + \gamma\ \ddot{d}_{n+1}] \quad \ldots\ldots\ldots\ldots\ldots\ldots\ldots...(17)$$

The Newmark family of direct integration includes, as particular cases, many well known integration schemes.

In the present work an unconditionally stable time stepping scheme is adopted with $\gamma = 0.5$ and $\beta = 0.25$

Huang[12] and Hughes et al[14] have developed a predictor-corrector form of the Newmark method which is most suitable for nonlinear transient analysis.

The Newmark formulas can be written in terms of predictor and corrector values as

$$d_{n+1} = d^{p}_{n+1} + \Delta t^2 \beta\ \ddot{d}_{n+1} \quad \ldots\ldots\ldots\ldots\ldots\ldots\ldots\ldots\ldots\ldots(18)$$

$$\dot{d}_{n+1} = \dot{d}^{p}_{n+1} + \Delta t\ \gamma\ \ddot{d}_{n+1} \quad \ldots\ldots\ldots\ldots\ldots\ldots\ldots\ldots\ldots\ldots(19)$$

with predictor values given as

$$d^{p}{}_{n+1} = d_n + \Delta t \dot{d}_n + \frac{\Delta t^2}{2}(1-2\beta)\ddot{d}_n \quad \ldots\ldots\ldots\ldots\ldots\ldots\ldots\ldots(20)$$

$$\dot{d}^{p}{}_{n+1} = \dot{d}_n + \Delta t(1-\gamma)\ddot{d}_n \quad \ldots\ldots\ldots\ldots\ldots\ldots\ldots\ldots(21)$$

The terms d_{n+1} , $\dot{d}_{n+1}$ are corrector values and $d^{p}{}_{n+1}$, $\dot{d}^{p}{}_{n+1}$ are the predictor values. The corrector values for the acceleration values can be obtained from equations (18) and (19) as:

$$\ddot{d}_{n+1} = (d_{n+1} - d^{p}_{n+1})/(\beta \Delta t^2) \quad \ldots\ldots\ldots\ldots\ldots\ldots\ldots\ldots\ldots(22)$$

Substituting equations(18), (19) and (22) into equation(14) an effective static problem is formed in terms of unknown Δd where:

$$K^{*}\Delta d = \psi \quad \ldots\ldots\ldots\ldots\ldots\ldots\ldots\ldots\ldots\ldots\ldots\ldots\ldots\ldots(23)$$

and where the effective stiffness matrix is

$$K^{*} = M/(\beta\ \Delta t^2) + \gamma\ C_T/(\beta\ \Delta t) + K_T \quad \ldots\ldots\ldots\ldots\ldots\ldots\ldots\ldots(24)$$

and the residual forces are

$$\psi = f_{n+1} - M\ddot{d}^{p}_{n+1} - C_T \dot{d}^{p}_{n+1} - p(d^{p}_{n+1}) \quad \ldots\ldots\ldots\ldots\ldots\ldots\ldots\ldots\ldots\ldots(25)$$

where $p(d) = Kd$ ……..……...(26)

When solving nonlinear problems, the linearization makes it necessary to perform iterative correction to Δd to achieve equilibrium at time $t + \Delta t$. A Newton-Raphson type scheme is used in this work.

NUMERICAL EXAMPLES

Example(1): Clamped rectangular R.C. slab subjected to a jet force

The clamped reinforced concrete slab shown in Fig.(6) is subjected to a jet force at the center. The percentage of reinforcement placed near the upper and lower surfaces in each direction is 1.5% .

From symmetry only one quarter of the slab is considered. The finite element mesh is shown in Fig.(7). Nine elements with six concrete layers and four steel layers are used in the thickness direction.

The selected time step is approximately 1/25 of the elastic fundamental period. Thus the time step is nearly 0.001 second. The material properties of the concrete and steel are given in Table(1).

The dynamic response for different tension stiffening models (for cracking strains 0.00015 and 0.0002) are shown in Figs.(8-9).(assume deformed bar of diameter 25mm is used). Numerical results are in good agreement with reference[5,18].

Example(2): Clamped circular R.C. slab

The clamped reinforced concrete slab shown in Fig.(10) is subjected to a uniformly distributed load of intensity 0.14 N/mm^2. The slab has a radius of 10m and a thickness of 1m. The load is applied with a rise time equal to half of the elastic fundamental period (T=0.06 second). The materials properties are given in Table(2).

The percentage of reinforcement placed near the upper and lower surfaces in the radial and tangential directions is 1% .

From symmetry only one quarter of the slab is considered. The finite element mesh is shown in Fig.(11). Eight elements with six concrete layers and four steel layers are used in the thickness direction.

The selected time step is approximately 1/100 of the elastic fundamental period this is nearly 0.0005 second.

The dynamic response for different tension stiffening models (for cracking strains 0,00015 and 0.0002) are shown in Figs.(12-13). Numerical results are in good agreement with reference[5,11,17].

CONCLUSIONS

A finite element technique has been used successfully for the nonlinear dynamic analysis of reinforced concrete slabs. No locking was observed in the results due to adopting the 8-node Serendipity element with reduced integration.

An good agreement is found between the present results and other source results throughout the entire structural response. This demonstrates the effectiveness of the proposed element and the solution procedure.

Model(2) gives lower deflection and less amplitude compared to other models. The difference in the central displacement for different tension stiffening models is due to difference post-cracking energy from the different models.

REFERENCES

- Abdul-Razzak,A.A.," Nonlinear finite element analysis of fibrous reinforced concrete structure members" Ph.D Thesis , Mosul University , Mosul ,Iraq,240pps (1996).
- Abrishami, H.H. and Michell, D., " Influnce of splitting cracks on tension stiffening", ACI Structure Journal, Vol 93, No 6, pp 703-710, Nov.-Dec.(1996).
- Agbossou,A., and Mougin ,J.P.," A Layerd Approach to the non- linear static and dynamic analysis of reinforced concrete slabs", International Journal of Mechanical Science, Vol.48,pp.294-306.(2006).
- Al-Samarrai, A.T.A.H.," Nonlinear finite element analysis of reinforced concrete slabs ", M.Sc. Thesis, University of Tikrit, Tikrit, Iraq, (2005)

- Ayyad, H.I.A.," Nonlinear dynamic analysis of reinforced concrete stiffened shells using the finite element method ", Ph.D. Thesis, University of Mosul, Iraq, 271pps.,(2003).
- Cedolin, L. and Deipoli, S., "Finite element studies of shear-critical reinforced concrete beams", ASCE Journal of the Engineering Mechanics Division, Vol. 103, No. EM3, pp. 395-410 June.(1977).
- Collins,M.P. and Mitchell, D.," Prestressed Concrete Structures", Prentice Hall Inc., Englewood Cliffs , NJ, 766 pps.(1991).
- Dohestry, W.P., Wilson, E.L., and Taylor, R.L., "Stress analysis of axi-symmetric solids using higher order quadrilateral finite elements", Structural Engineering Laboratory Report, No.SESM69-3, University of California, Berkeley, (1969).
- Farag, H.M. and Leach, P., "Material modeling for transient dynamic analysis of reinforced concrete structures", International Journal for Numerical Methods in Engineering, Vol.39, No.12, pp.2111-2129, (1996).
- Hinton, E. and Owen, D.R.J., "Finite element Software for plates and shells" Pineridge Press, Swansea, U.K., (1984).
- Hinton, E., "Numerical methods and software for dynamic analysis of plates and shells", Pineridge Press, Swansea U.K.,(1988) .
- Huang, H.C., "Static and dynamic analysis of plates and shells Theory, Software and Applications", Springer Verlag, Berlin, Heidelberg (1989).
- Hughes, T.J.R., Cohen, M. and Haroun, M., "Reduced and selective integration techniques in the finite element analysis of plates", Nuclear Eng. and Design, Vol. 46, pp. 203-222.(1978).
- Hughes, T.J.R. , Pister, K.S. and Taylor, R.L.," Implicit – explicit finite element in transient analysis ", Computer Method Journal in Applied Mechanics and Engineering , Vol 17/18, pp 159-182.(1979).
- Johanson, M.," Nonlinear finite element analysis of concrete frame corners" ASCE Journal of the structure engineering Vol.126, No.2, pp. 190-199, Feb.(2000).

- Kupfer, H., Hilsdorf, K.H. and Rush, H., "Behavior of concrete under biaxial stresses", Proceedings, American Concrete Institute, Vol. 66, No. 8, , pp. 656-666. August.(1969)
- Liu, G.O. and Owen, D.R.J., "Ultimate load behavior of reinforced concrete plates and shells under dynamic transient loading", International Journal For Numerical Methods in Engineering, Vol.22, pp.189-208, (1986).
- Manjuprasad, M., Gopalakrishan, S. and Appa Rao, T.V.S.R.," Non-linear dynamic response of reinforced concrete secondary containment shell subjected to seismic load", Engineering Structures, Vol.23, pp.397-406, (2001).
- Parisch, H., "A critical survey of the 9- node degenerated shell element with special emphasis on thin shell applications and reduced integration", in Comp. Meths. Appl. Mech. Eng., Vol. 20, (1979).
- Riera, J.D. and Iturrioz, I., "Discrete elements model for evaluating impact and impulsive response of reinforced concrete plates and shells subjected to impulsive loading", Nuclear Engineering and Design 179, , pp.135-144. (1998).
- Shirai, T., Kambayashi, A., Ohno, T., Taniguchi, H., Ueda, M. and Ishikawa, N., "Experimental and numerical simulation of double-layered RC plates under impact loadings", Nuclear Engineering and Design 176, pp.195-205. (1998).
- Sziveri, J., Topping, B.H.V. and Ivanyi, P., "Parallel transient dynamic nonlinear analysis of reinforced concrete plates", Advances in Engineering Software 30, pp.867-882. (1999).
- Vechion, F.J. and Collins, M.P.," The modified compression field theory for reinforced concrete elements subjected to shear" , ACI journal, Proccedings, Vol.83, No.2,pp.219-231, March-April (1986).
- Xu, K. and Lu,Y. ," Numerical simulation study of spallation in reinforced concrete plates subjected to blast loading", Computers and structures , Vol.84, pp.431-438,(2006).

• Zienkiewicz, O.C., Taylor, R.L., and Too, J.M., "Reduced integration technique in general analysis of plates and shells", International Journal for Numerical Methods In Engineering, Vol.3, 275-290. (1971).

Table(1) Material properties for simply supported R.C. beam of example(1)

E_c MPa	ν	f_c' MPa	ε_u	cracking strain	ρ N.sec^2/mm^4	E_s MPa	f_y MPa
28000	0.2	35.0	0.0035	0.00015 & 0.0002	0.245E-8	200000	460

Table(2) Material properties for clamped R.C. circular slab of example(2)

E_c MPa	ν	f_c' MPa	ε_u	cracking strain	ρ N.sec^2/mm^4	E_s MPa	f_y MPa
280000	0.2	35.0	0.0035	0.00015 & 0.0002	0.245E-8	210000	460

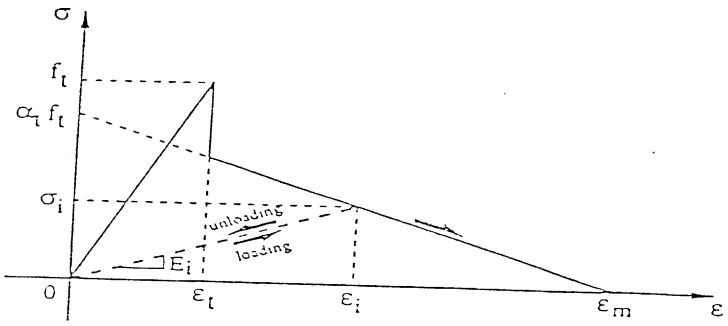

Fig. (1) Loading and unloading behavior of cracked concrete illustrating tension stiffening behavior[14].

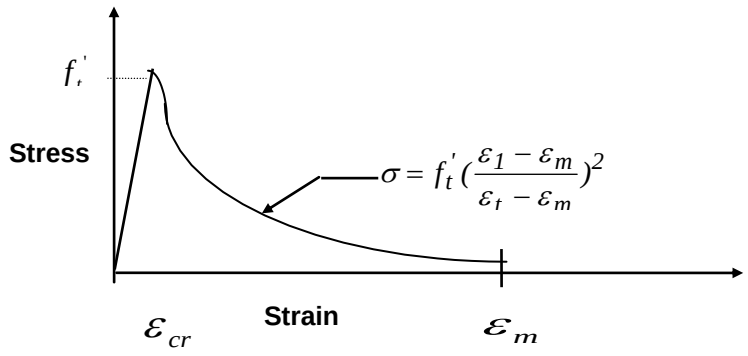

Figure(2) Tension softening (parabolic model), model 2.

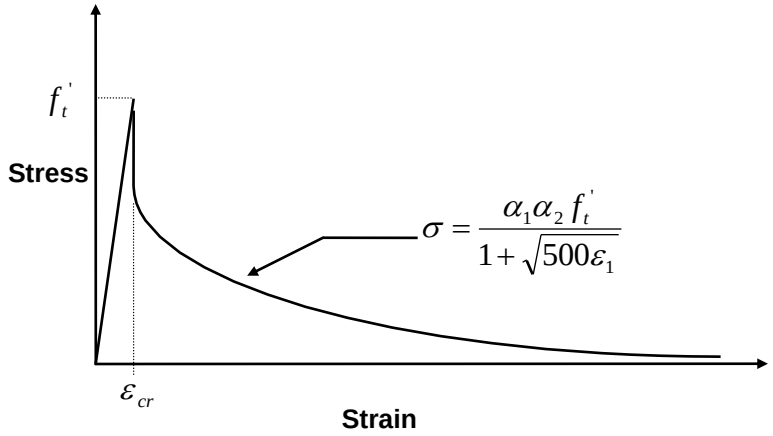

Figure(3) Tension stiffening for model (3)

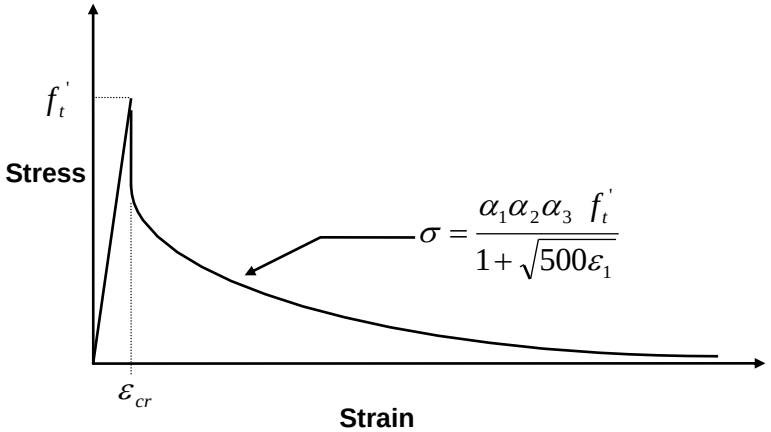

Figure(4) Splitting crack effect on tension stiffening model (4)

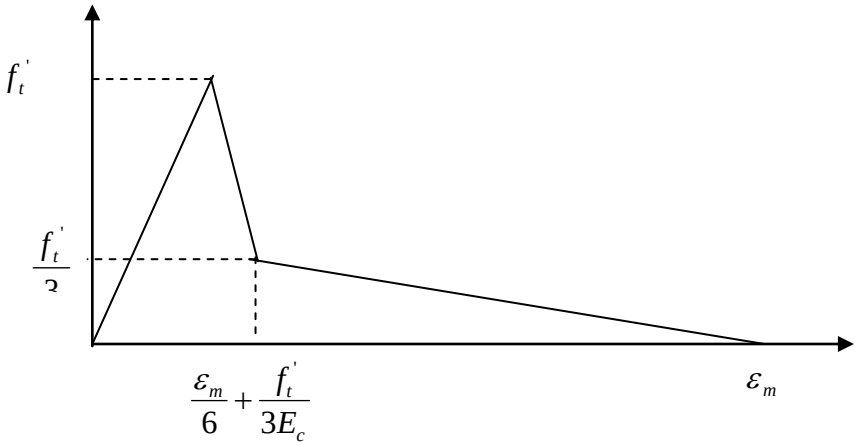

Figure (5) Tension stiffening for model (5).

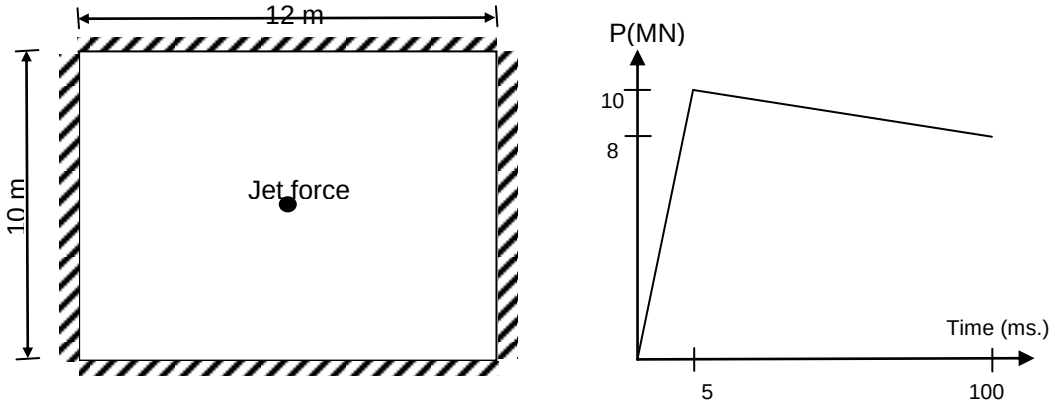

Figure(6) Loading and geometry of clamped reinforced concrete slab.

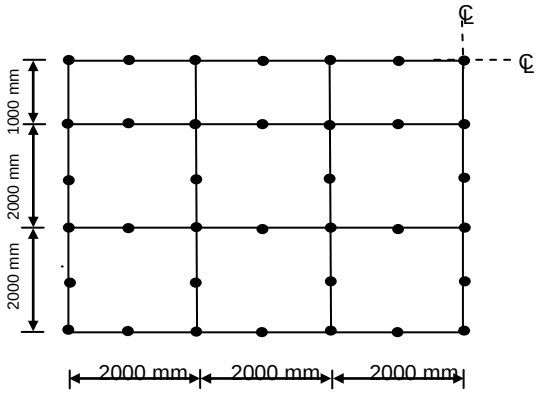

Figure(7) Finite element mesh for example (1).

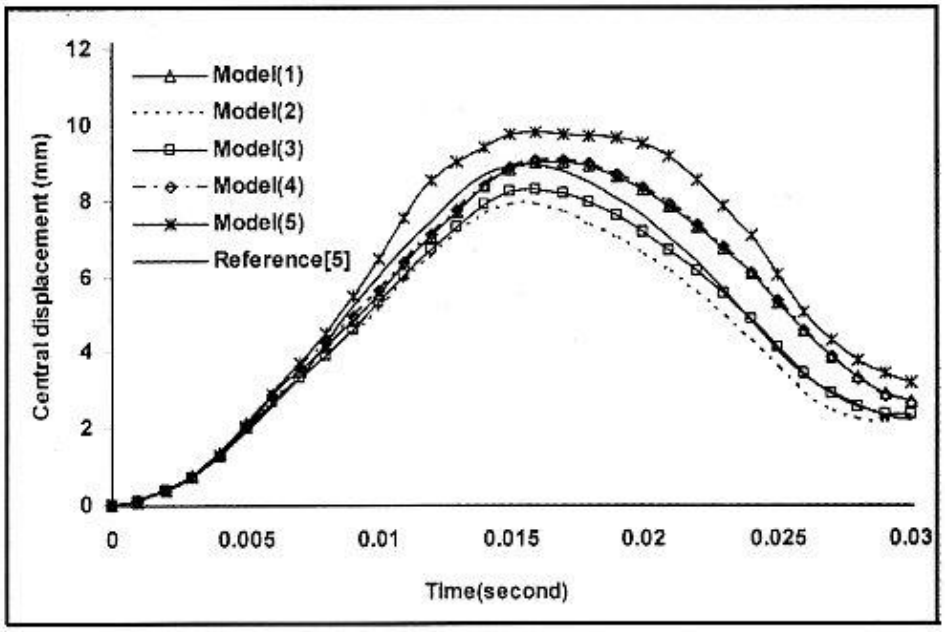

Fig.(8) Nonlinear dynamic response of example(1) (cracking strain 0.00015) for different tension stiffening models.

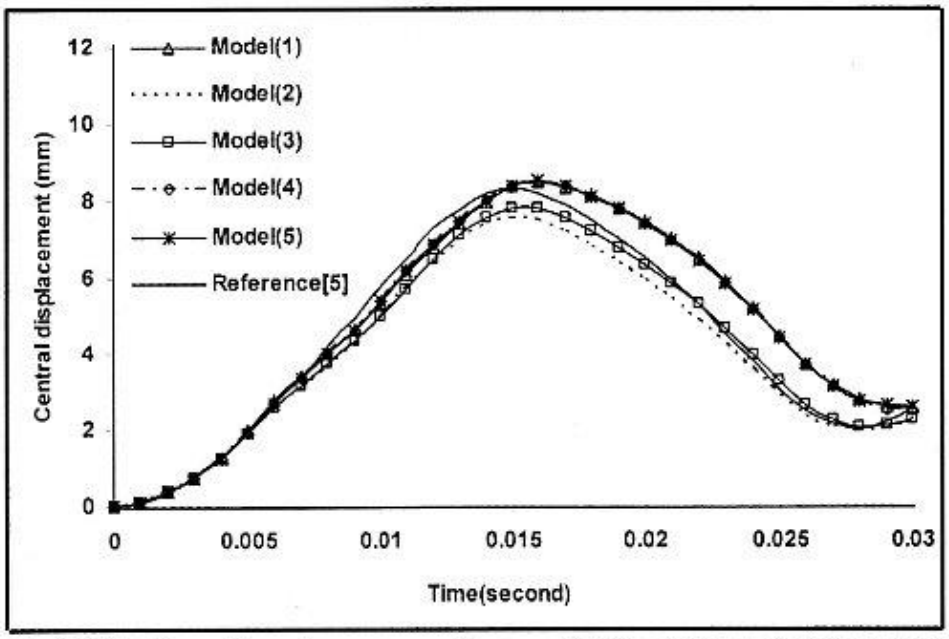

Fig.(9) Nonlinear dynamic response of example(1) (cracking strain 0.0002) for different tension stiffening models.

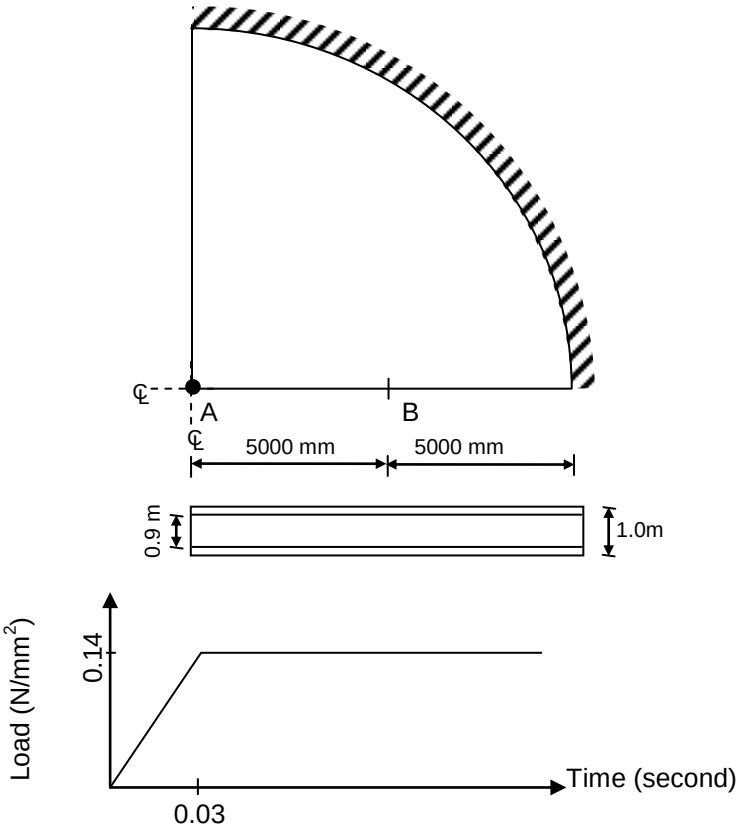

Figure (10) Geometry and Load-time history for example (2)

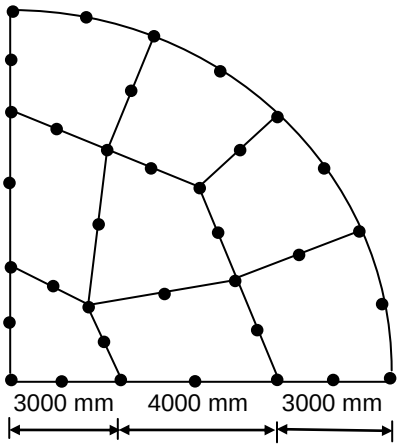

Figure (11) Finite element mesh for example(2).

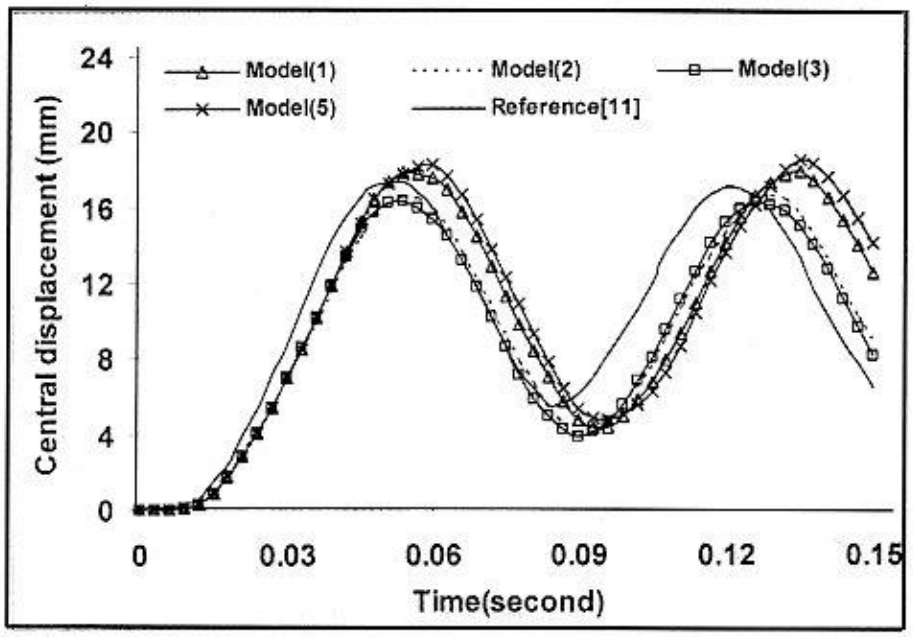

Fig.(12) Nonlinear dynamic response of example(2) (cracking strain 0.00015) for different tension stiffening models

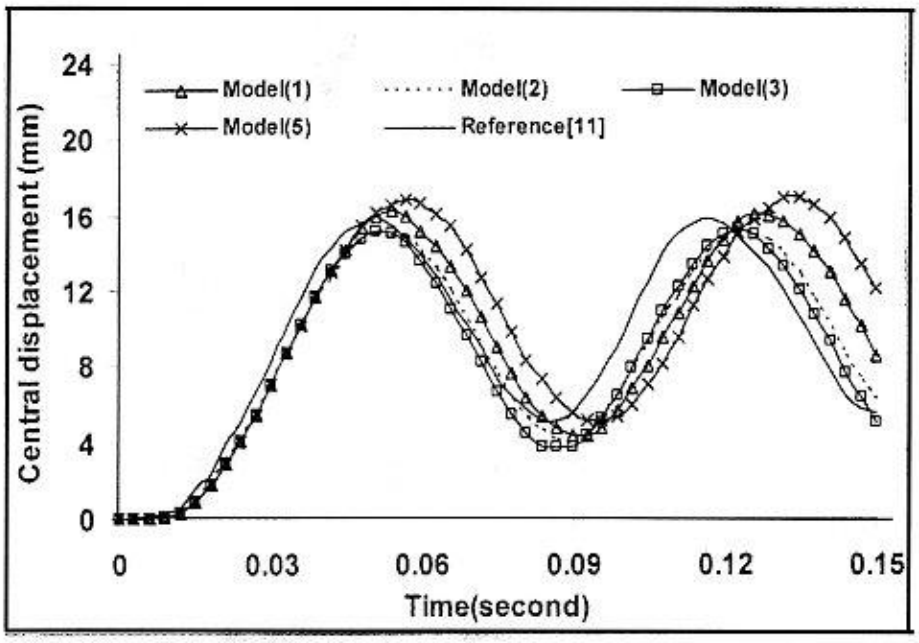

Fig.(13) Nonlinear dynamic response of example(2) (cracking strain 0.0002) for different tension stiffening models

THE TRANSITION TO A PG GRADING SYSTEM FOR ASPHALT CEMENT IN IRAQ

Prof. Hamed M. H. Alani, (Civil Eng. Dept.) / Baghdad Univ.
Dr. Amjad H. Albayati, (Civil Eng. Dept.) / Baghdad Univ.
Alaa S. Abbas, (Highway and Transportation Eng. Dept.) / Al-Mustansiriya Univ.

ABSTRACT

In Iraq, as well as many other developing countries the performance graded (PG) based System is not yet implemented to evaluate the currently used asphalt cements for paving works. It appears that not only the unavailability of test equipments is resulting in this delay but also the lack of clear understanding of what steps could be taken to incorporate this system. This research is an attempt to highlight the important aspects of a (PG) system that can be readily implemented without the need for expensive equipments. It includes the development of a Performance based System employing the conventional test methods and available nomographs from literature. It also, shows how climatic data, traffic data, and asphalt binder properties can be combined to propose a possible major improvement for the specifications of asphalts in Iraq.

To achieve the objective of this research, an extensive air temperature data for a period of 18 years was reviewed for five cities (Mosul, Kirkuk, Rutba, Baghdad, and Basrah) to establish the required PG asphalt binder for each city. Also, the currently used asphalt cements with penetration grades (40-50) and (60-70) were tested by both of conventional test methods and Superpave methods to determine the equivalent performance grade for each type of the penetration graded asphalt and to evaluate the capability for these two types of asphalt cement to satisfy the required performance of pavement for each city.

The results indicate that both the new proposed method and Superpave method give the same final performance grade, The asphalt with penetration grade 40-50 is equivalent to PG70-16 while that with penetration grade 60-70 is equivalent to PG64-16.

KEY WORDS: Asphalt cement, Superpave, Performance grade.

الخلاصه

في العراق وفي كثير من الدول النامية لم يطبق نظام تدرج الاداء (PG) لتقييم الاسفلت المستخدم في اعمال التبليط لغاية الان. لقد تبين ان الكلفة لم تكن وحدها سببا" في هذا التاخير بل النقص في فهم الخطوات التي يجب ان توخذ لتطبيق الفقرات الخاصة بهذا النظام . في هذا البحث تم القاء الضوء على الاقسام المهمة الخاصة بنظام تدرج الاداء والتي يمكن تطبيقها دون الحاجة الى المعدات المكلفة الثمن وذلك عن طريق استخدام الطرق التقليدية لفحص الاسفلت في العراق. لقد بين البحث كيفية استخدام نتائج هذه الفحوصات بطريقة غير مباشرة لتخمين الخصائص المتعلقة بالاداء بناءا" على مخططات بيانية (nomograph) وبين كيف يمكن للبيانات الخاصة بالطقس والبيانات المروية والخصائص الريولوجية او خصائص الفشل التي اشتقت من المخططات البيانية ان تشترك فيما بينها

لاقتراح تطوير لمواصفة الاسفلت في العراق.لتحقيق الهدف من البحث تم مراجعة بيانات الانواء الجوية العراقية وجمع المعلومات المتعلقة بدرجة حرارة الجو خلال فترة 18 سنة ولخمسة مدن عراقية (موصل، كركوك، رطبة، بغداد، والبصرة) وبناءا" على نظام تصنيف الخرسانة الاسفلتية العالية الجودة (Superpave) تم استنباط تدرج الاداء الخاص بكل منطقة. كذلك تم فحص الاسفلت السمنتي ذو درجة اختراق (40-50) و (60-70) باستخدام الطرق التقليدية و طريقة (Superpave) لحساب تدرج الاداء لكل نوع وتقييم مدى ملائمة هذين النوعين لكل منطقة.لقد بينت النتائج بان كلا الطريقتين (الطريقة المقترحة وطريقة Superpave) قد اعطت اقيام متماثلة لتدرج الاداء، الاسفلت السمنتي ذو اختراق (40-50) يكافي تدرج اداء PG70-16 والاسفلت السمنتي ذو اختراق (70-60) يكافي تدرج اداء PG64-16.

INTRODUCTION

Currently, the local specification for asphalt concrete paving works states two methods for asphalt cements grading, either based on viscosity or penetration of original asphalt. The two methods describe the physical properties of asphalt cements at standard test temperatures employing empirical means of testing which can not be related to field performance during service life. Another drawback of the above grading system is that long-term asphalt aging is not taken into consideration. The tests are performed on unaged or "tank" asphalt and on artificially short-term aged asphalt to simulate construction aging. No tests are performed to simulate in-service aging, which occurs when the asphalt reacts with the oxygen in the atmosphere by oxidation. Also, the current grading systems do not cover the temperature extremes that a pavement endures, binders that produce similar results at the temperatures used for penetration and viscosity testing may have very different results at other temperatures experienced by the pavement.

Since 1993, a new system for specifying asphalt materials and mix design have been developed in USA and widely used in the world, this system called Superpave (Superior Performing Asphalt Pavements). The Superpave performance grading (PG) for binder was developed to address the shortcomings of the previous asphalt grading systems. PG is reported using two numbers – the first being the average seven-day maximum pavement temperature (in °C) and the second being the minimum pavement design temperature likely to be experienced (in °C). Thus, a PG 64-16 is intended for use where the average seven-day maximum pavement temperature is 64°C and the expected minimum pavement temperature is -16°C.

The direct implementation of the Superpave approach required a direct measurement of the performance-related properties such as complex shear modules (G*) and phase angle (δ). In this approach, expensive and complex equipment are required, which is apparently out of reach of many pavement researchers and road laboratories at this time in Iraq as well as many other developing and developed countries. The best alternative to address the lack of reliable specification dose not keep the traditional testing specifications, but rather implementing components of performance grading that is attainable and less expensive. The concept of indirectly estimated performance-related properties based on available nomographs from literature could be used. That is to say, establishing a performance-grading framework in which grades are truly selected based on application conditions including pavement temperature and traffic. The criteria for accepting bitumen in such PG framework could be based on engineering properties which are performance related but derived from simple index properties such as penetration, softening point, or viscosity.

Although, the PG system has been adopted by the ASTM as well as AASHTO since 1999, it's not yet implemented in Iraq to evaluate the currently used asphalt cements for paving works.

REVIEW OF LITERATURE

At present, there is no attempt existed or presented in the local literature dealing with implementation of Superpave performance grading requirements for local asphalt cements, therefore the review presented herein is limited to the foreign literatures.

According to Superpave requirements, Al-Abdul Wahhab et al. (1997) have evaluated different types of asphalt cements produced from the oil refineries in the Arabian Gulf countries. They found that the maximum pavement temperatures which can these types of asphalt cements sustain is 64°C while the temperature zoning indicated that more than 50 percent of the Gulf countries areas experience a maximum pavement temperature of 76°C. Therefore, The researchers suggest to modifiers for the asphalt binders in order to meet Gulf countries performance requirements in arid areas.

Asi (2007) tested the locally produced asphalt in Jordan with penetration grade 60-70. He found that the asphalt with this penetration grade is equivalent a performance grade PG64-16. He also developed a temperature zoning map for Jordan as shown in **Figure (1)**. It consists of three grade zones, PG64-10, PG64-16 and PG70-10. He conducted that the locally produced asphalt can be used without the need for modification in all parts of Jordan except Aqaba, Ruwaishied and Ghorsafi.

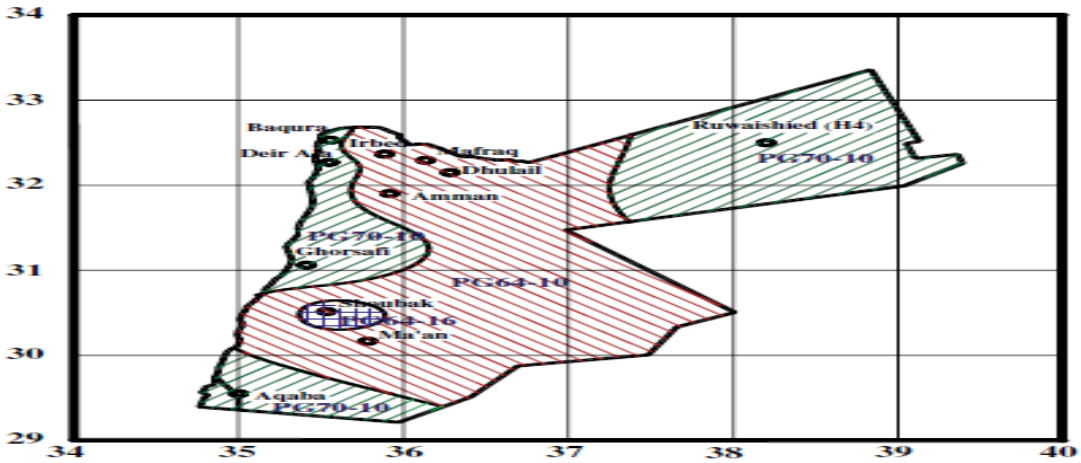

Figure (1) Jordan Temperature Zoning for Asphalt Binder (Asi ,2007)

The best alternative to address the lack of reliable specification dose not keep the traditional testing specifications, but rather implement components of performance grading that is attainable and less expensive. The concept of indirectly estimated performance- related properties based on available nonmograph from literature could be used. The first attempt for using this concept was made by van de Ven et al. (2004) in South Africa. They establishing a performance-grading framework in which grades are truly selected based on "application conditions" including pavement temperature and traffic. While the criteria for accepting bitumen in such PG framework could be based on engineering properties which are performance related but derived from simple index properties such as penetration, softening point or viscosity. Finally, the second attempt was made by Bahia and Vivanco (2005). They applied this concept to formulate PG specification in Chile.

THE BASIC PRINCIPLES OF PERFORMANCE GRADING SYSTEM

Performance grading could be defined as "a system in which fundamental mechanical properties that are related to pavement performance are used to select binders to minimize critical failures at critical conditions of pavement temperatures and traffic characteristics." The fundamental properties could be measured directly, but if not possible, could be derived numerically. The three basic elements for a performance grading system could therefore be listed as follows:

- It should be based on bitumen specific constitutive models. In others words, models describing stress-strain relationship under loading conditions experience in the field and that leads to failures.

- It should include the pavements` conditions as defined by temperature, traffic speed and traffic volume. It should also consider pavement structure in the sense that stresses and strains used in testing are within realistic ranges seen in pavements.
- It should include acceptance limits derived from experience and documented field performance to reduce, if not eliminate, initiating and progression of damage due to thermal or mechanical loading.

To achieve the first element, without direct measurements, it is necessary to define the model that can be used for getting the bitumen constitutive relationships based on Penetration and Softening Point. One of the well known alternatives is the Van der Poel nomograph (1954), (**Figure 2**), in which the creep stiffness can be estimated for a wide temperature range and loading times using Penetration Index (PI) which can be calculated by using the following equation:

$$PI=20-500A/ (1+50A) \qquad \text{equ. (1)}$$

Where:
PI = Penetration Index
A = Slop of the straight line plot between the logarithm of penetration and temperature, or

$$A=\log (\text{pen at } 25^0C) – \log 800 / (25- T_{R\&B}) \qquad \text{equ. (2)}$$

Where:
$T_{R\&B}$ = Ring and Ball softening point in ^0C

Although the nomograph is empirically derived, it is based on measuring the fundamental properties of a very large number of asphalts. In addition to the creep stiffness, failure properties are required. To estimate fatigue properties, a nomograph published by Shell (1978), (**Figure 3)**, for estimating the fatigue life of mixtures from PI of bitumen and mixture stiffness, can be used. To control brittleness of asphalt binders at minimum pavement temperature, the elongation at break estimated from chart developed by Heukelom (1973), (**Figure 4**), can be used. These three nomographs are numerical tools that can be used as initial substitutes to the dynamic shear rheometer, the bending beam rheometer, and the direct tension test, which are the main devices in the Superpave system and that are out of reach of many pavement technologists around the world.

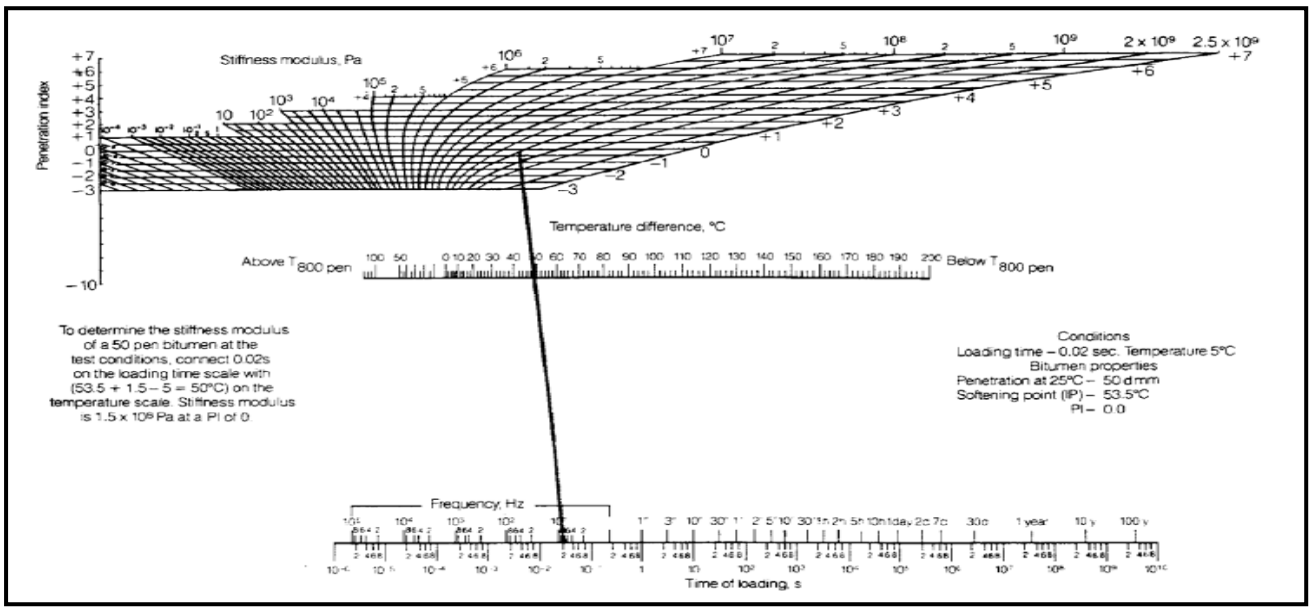

Figure (2) Creep Stiffness Nomograph (Van der Poel, 1954)

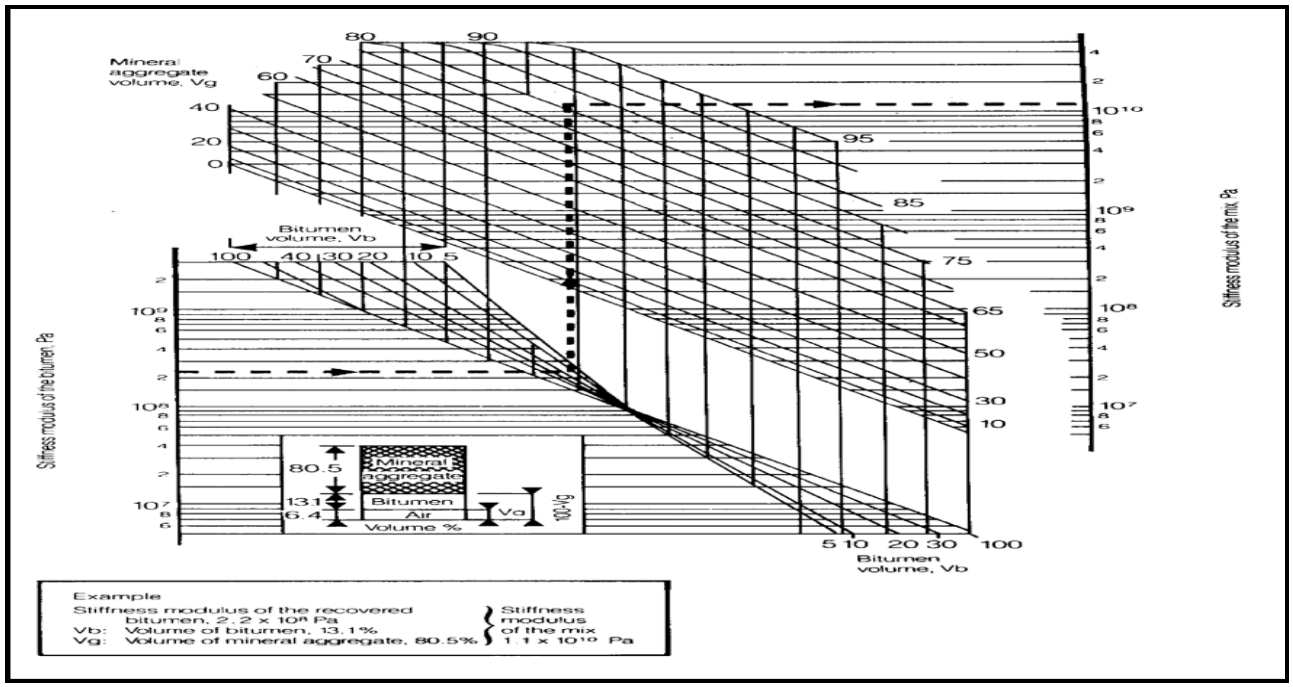

Figure (3) Nomograph for Stiffness Modulus of Mixes (Shell, 1978)

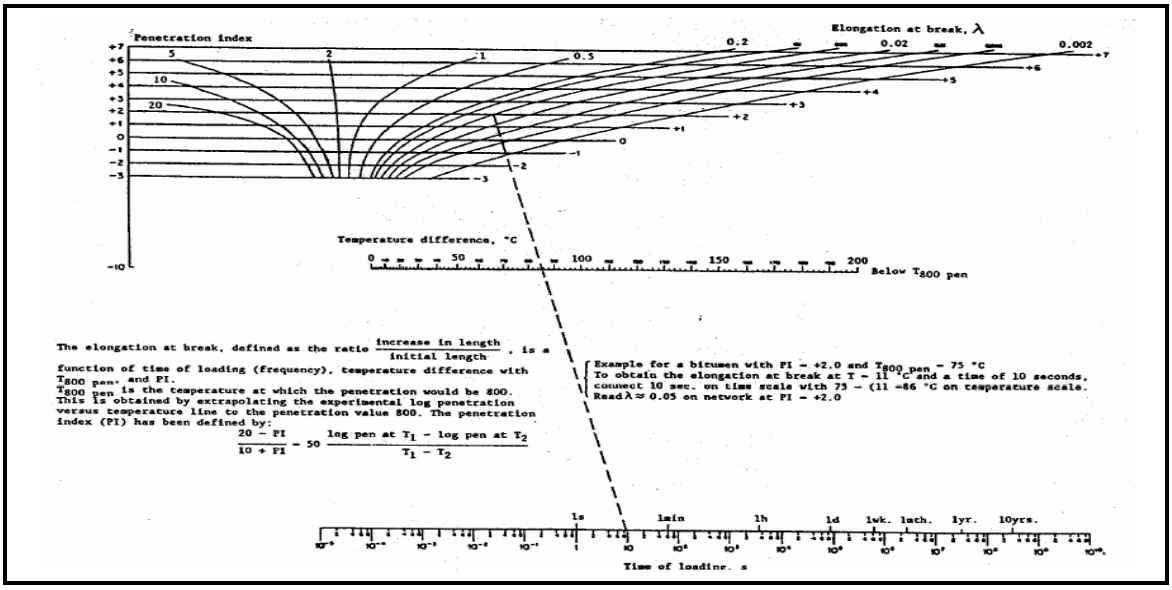

Figure (4) Estimating Elongation at Break (Heukelom, 1973)

To achieve the second element of performance grading system, the distribution of pavement temperature in various climatic conditions is necessary. These include the maximum and the minimum pavement design temperature, which can be based on weather data available from Iraqi Metrological Organization. These temperatures can be used to define the Performance Grades required for various regions in the country.

The air temperature data from the Iraqi Metrological Organization used in this research cover 18 years time period (1985-2002) for five Iraqi cities (Mosul, Kirkuk, Rutba, Baghdad and Basrah). Which represent climatically unique regions in Iraq. At each year, the hottest seven-day period is identified and the average maximum air temperature for this seven-day period was calculated and then based on 18 years a mean and standard deviation are determined. Similarly, the one-day minimum air temperature of each year was identified and the mean and standard deviation are calculated. The calculated mean and standard deviation for the five regions of Iraq are presented in **Table (1)** below**.** The latitude value for Mosul, Kirkuk, Rutba, Baghdad, Basrah, is 36.32, 35.47, 33.03, 33.23, 30.57 respectively (Iraq Metrological Organization, 1989)

Table (1) Mean and Standard Deviation for Maximum and Minimum Air Temperature

Region	Maximum Air Temperature ˚C		Minimum Air Temperature ˚C	
	Mean	Standard Deviation	Mean	Standard Deviation
Mosule	45.149	1.982	-2.5	3.8
Kirkuk	45.663	1.969	-0.5	5.4
Rutba	41.6	0.962	-2.6	3.7
Baghdad	47.5	1.077	-2.8	1.8
Basrah	48.594	1.103	1.8	1.8

Based on 98 percent reliability, temperatures can be determined based on the standard deviations for the high and low air temperature data. From statistics, 98 percent reliability is approximately two standard deviations from the mean value. The data presented in **Table (2)** shows the high and low air temperatures for 98 percent reliability level for the five regions of Iraq.

Table (2) High and Low Air Temperature for 98% Reliability level

Region	High Air Temperature ^{0}C	Low Air Temperature ^{0}C
Mosul	49	- 11
Kirkuk	50	- 12
Rutba	43	- 11
Baghdad	50	- 6
Basrah	51	- 2

These temperatures converted to pavement temperatures based on 98% reliability level. In Superpave, the high pavement design temperature at a depth of 20mm is computed by the following equation (SHRP, 1994)

$$T_{20mm} = 0.9545\,[T_{air} - 0.00618\,lat^2 + 0.2289\,lat + 42.2] - 17.78 \quad \text{equ.(3)}$$

Where:

T_{20mm} = high pavement design temperature at a depth of 20 mm in ˚C.

T_{air} = seven- day average high air temperature in ˚C.

lat. = the geographical latitude of the project in degrees.

The low pavement design temperature simply can be assumed to be the same as the low air temperature. This method was originally recommended by SHRP researchers. **Table (3)** shows the maximum and minimum pavement temperature for the regions under consideration.

Table (3) Maximum and Minimum Pavement Temperature

Region	Maximum Pavement Temperature ^{0}C	Minimum Pavement Temperature ^{0}C
Mosul	70	-11
Kirkuk	70	-12
Rutba	64	-11
Baghdad	70	-6
Basrah	73	-2

The required PG for each city was established based on 6 ^{0}C increments. **Table (4**) shows the standard grades presented in the SHRP binder specification (Asphalt Institute, 2003). Therefore, based on this table and the results obtained from the analysis of pavement temperature, the suggested PG grade of asphalt cements for paving works within the five regions of Iraq is as that presented in **Figure (5)**.

Table (4) Superpave Binder Performance Grades (Asphalt Institute 2003)

	High Temperature Grade	Low Temperature Grade
PG	46	-34, -40, -46
PG	52	-10, -16, -22, -28, -34, -40, -46
PG	58	-16, -22, -28, -34, -40
PG	64	-10, -16, -22, -28, -34, -40
PG	70	-10, -16, -22, -28, -34, -40
PG	76	-10, -16, -22, -28, -34
PG	82	-10, -16, -22, -28,-34

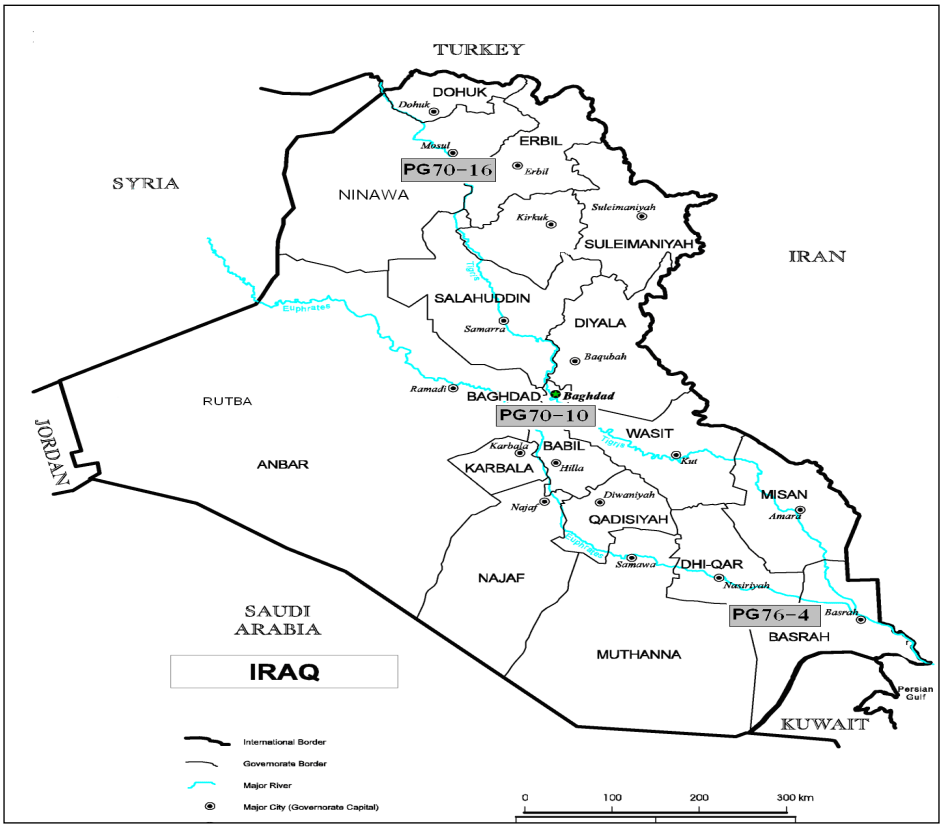

Figure (5) Temperature Zoning Map for PG Requirement in Iraq

To achieve the third element of a performance grading system, the performance related properties should be selected and the acceptable limits of asphalt cement should be defined. To estimate these limits, the conventional testing results (penetration and softening point) from previous studies for different asphalt types in Iraq can be used, these data are shown in **Table (5)**. The following sections explain how the properties and their limits were selected.

Table (5) Penetration and Softening Point Data

	Penetration 25 C^0	Softening point C^0	Source of Data
Pen 40/50			
A1	42	51	Albayati, A.H. (2006)
A2	47	49	Namir,G.A. (2002)
A3	45	52	Zaid,I. (2006)
A4	49	48	Abbas, F. (2005)
A5	47	49	Nahla, Y.A. (2005)
A6	42	49	Ahlam, K.R. (2007)
A7	43	54	Hanaa, K. (2004)
A8	42	51	Alazawy, A.M. (2006)
A9	43	48.5	Alekaby,K.H. (2005)
A10	45	52	Alaredi,H.A. (2006)
Pen 60/70			
B1	66	46.5	Alani, H.M.(1986)
B2	67	45	Albayati, A.H. (2006)
B3	67	47	Hanaa, K. (2004)
B4	69	45	Safar, M.M.(1992)
B5	62	46	Shakir, S. (1999)
B6	67	49.5	Taher, M. (1999)
B7	65	46	Asal, F.N. (2007)
B8	67	49.5	Magd Aldeen,A. (2003)
B9	63	45.5	Almudhadi, T.H.(2007)
B10	67	48.5	Aljumily, M.A. (2007)

- **For Workability**, The viscosity at 135ºC can be used. In performance specifications, the limits should remain the same for all grades since the contractors are expected to use the same heating and storage temperatures regardless of the binder source or grade, and regardless of pavement conditions. A range of 0.12 – 0.65 Pa.s, can be used which is based on the current specifications used in Chile (Bahia and Vivanco ,2005). The range is a better property than the maximum used in the current Superpave specifications. The minimum limit will control drain down and the maximum will ensure proper workability.

- **For Rutting Resistance**, It is proposed to use penetration and softening point to calculate the Penetration Index (PI) for the grades used currently in Iraq. The PI values are used for calculating the creep Stiffness at speed of traffic normally seen in the field by using the Van der Poel nomograph **(Figure 2)**. For a typical speed of 80 km/hr, and a pavement surface layer thickness of 20 mm, the loading time is estimated at 0.012 seconds based on **Figure (6).** To estimate an acceptable specification limit for rutting, the data in **Table (5)** can be used. The values of the PI's for such asphalts were calculated by using the equation (1), and used to estimate creep stiffness values from the Van der Poel nomograph. A loading time of 0.012 seconds, and the temperature of 64, 70 and 76ºC, which represent local performance grade, were used for all these asphalt cements. The results are shown in **Table (6).** Experience had to be used to derive acceptable limits for a PG framework. According to road engineers in Iraq it seems that the penetration grade of (40-50) has worked well for moderate traffic volume roads in moderate climate. The average results in **Table (6)** indicate that if the PG76 grade is a reasonable performance grade within which these binders should fit, then the estimated average stiffness value S(0.012) is >= 9 kPa for the unaged condition.It can therefore be assumed that for an asphalt to provide sufficient contribution to rutting resistance, the value of S(0.012), at maximum pavement design temperature, should be equal to or greater than 9 kPa. In other words, for other grades (PG64 and PG70) this stiffness minimum value should be met at 64 ºC and 70ºC respectively. Based on experience with RTFO aging the increase in G* values ranges

between 1.8 and 2.5 times the unaged value (Bahia and Vivanco 2005). As a compromise between the high and low range mentioned, aged requirement after RTFO that is 2.5 times the unaged condition, which results in a limit for S(0.012) of greater than or equal to 22.5 kPa, should be used. This limit is based on the average estimated values that are shown in **Table (7)**.

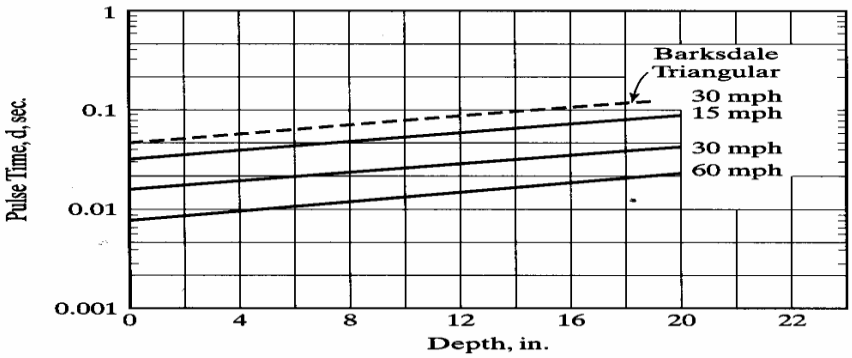

Figure (6) Speed-Loading Time Relationship (McLean, 1974)

Table (6) Asphalt Binder Stiffness at High Pavement Temperatures (Original Binders)

T=64 ^{0}C				T=70 ^{0}C				T=76 ^{0}C			
	T_{DIFF} ^{0}C	PI	S (N/M^2)		T_{DIFF} ^{0}C	PI	S (N/M^2)		T_{DIFF} ^{0}C	PI	S (N/M^2)
Pen 40/50				**Pen 40/50**				**Pen 40/50**			
A1	**-13**	**-1.25**	**3.5*10^4**	**A1**	**-19**	**-1.25**	**2*10^4**	**A1**	**-25**	**-1.25**	**6*10^3**
A2	**-15**	**-1.477**	**2*10^4**	**A2**	**-21**	**-1.477**	**1.5*10^4**	**A2**	**-27**	**-1.477**	**1*10^4**
A3	**-14**	**-1.411**	**3.5*10^4**	**A3**	**-20**	**-1.411**	**1*10^4**	**A3**	**-26**	**-1.411**	**9*10^3**
A4	**-14**	**-1.253**	**3*10^4**	**A4**	**-20**	**-1.253**	**1.5*10^4**	**A4**	**-26**	**-1.253**	**7*10^3**
A5	**-15**	**-1.563**	**2*10^4**	**A5**	**-21**	**-1.563**	**2*10^4**	**A5**	**-27**	**-1.563**	**2*10^4**
A6	**-15**	**-1.689**	**1.9*10^4**	**A6**	**-21**	**-1.689**	**1.5*10^4**	**A6**	**-27**	**-0.689**	**1*10^4**
A7	**-10**	**-0.58**	**4*10^4**	**A7**	**-16**	**-0.58**	**2.5*10^4**	**A7**	**-22**	**-0.58**	**1.2*10^4**
A8	**-13**	**-1.321**	**2.5*10^4**	**A8**	**-19**	**-1.321**	**2*10^4**	**A8**	**-25**	**-1.321**	**1.3*10^4**
A9	**-15.5**	**-1.891**	**2*10^4**	**A9**	**-21.5**	**-1.891**	**1*10^4**	**A9**	**-27.5**	**-1.891**	**7*10^3**
A10	**-12**	**-0.94**	**2*10^4**	**A10**	**-18**	**-0.94**	**2*10^4**	**A10**	**-24**	**-0.94**	**1.1*10^4**
Average Binder Stiffness			**2.64*10^4**	**Average Binder Stiffness**			**1.67*10^4**	**Average Binder Stiffness**			**9*10^3**
Pen 60/70				**Pen 60/70**				**Pen 60/70**			
B1	**-17.5**	**-1.477**	**3*10^4**	**B1**	**-23.5**	**-1.477**	**2*10^4**	**B1**	**-29.5**	**-1.477**	**5*10^3**
B2	**-19**	**-1.89**	**2*10^4**	**B2**	**-25**	**-1.89**	**8*10^3**	**B2**	**-31**	**-1.89**	**4*10^3**
B3	**-17**	**-1.253**	**2.5*10^4**	**B3**	**-23**	**-1.253**	**1*10^4**	**B3**	**-29**	**-1.253**	**8*10^3**
B4	**-19**	**-1.792**	**2.5*10^4**	**B4**	**-25**	**-1.792**	**5*10^3**	**B4**	**-31**	**-1.792**	**4*10^3**
B5	**-18**	**-1.751**	**3*10^4**	**B5**	**-24**	**-1.751**	**1*10^4**	**B5**	**-30**	**-1.751**	**4.5*10^3**
B6	**-14.5**	**-0.613**	**5*10^4**	**B6**	**-20.5**	**-0.613**	**1.5*10^4**	**B6**	**-26.5**	**-0.613**	**5*10^3**
B7	**-18**	**-1.648**	**2.8*10^4**	**B7**	**-24**	**-1.648**	**8*10^3**	**B7**	**-30**	**-1.648**	**4*10^3**
B8	**-14.5**	**-0.613**	**5*10^4**	**B8**	**-20.5**	**-0.613**	**1.5*10^4**	**B8**	**-26.5**	**-0.613**	**5*10^3**
B9	**-18.5**	**-1.87**	**3*10^4**	**B9**	**-24.5**	**-1.87**	**5*10^3**	**B9**	**-30.5**	**-1.87**	**4*10^3**
B10	**-15.5**	**-0.87**	**5.5*10^4**	**B10**	**-21.5**	**-0.87**	**1*10^4**	**B10**	**-27.5**	**-0.87**	**6*10^3**
Average Binder Stiffness			**3.4*10^4**	Average Binder Stiffness			1*10^4	**Average Binder Stiffness**			**4.95*10^3**

Table (7) Average Results for Asphalt Binder Stiffness at High Pavement Temperatures

	S(kpa) (Time of loading =0.012 sec)					
	64(^{0}C)		70(^{0}C)		76(^{0}C)	
	Original	Aged	Original	Aged	Original	Aged
Pen 40/50						
A1	35	87.5	20	50	6	15
A2	20	50	15	37.5	10	25
A3	35	87.5	10	25	9	22.5
A4	30	75	15	37.5	7	17.5
A5	20	50	20	50	10	25
A6	19	47.5	12	30	12	30
A7	40	100	25	62.5	13	32.5
A8	25	62.5	20	50	7	17.5
A9	20	50	10	25	5	12.5
A10	20	50	20	50	11	27.5
Average	26.5	66	16.7	41.75	9	22.5
Pen 60/70						
B1	20	50	20	50	5	12.5
B2	10	25	8	20	4	10
B3	20	50	10	25	8	20
B4	15	37.5	5	12.5	4	10
B5	20	50	10	25	4.5	11.25
B6	40	100	15	37.5	5	12.5
B7	18	45	8	20	4	10
B8	40	100	15	37.5	5	12.5
B9	20	50	5	12.5	4	10
B10	45	112.5	10	25	6	15
Average	24.8	62	10.6	26.5	4.95	12.37

- **For Fatigue Resistance**, To derive binder stiffness limits for fatigue, the nomograph published by Shell that shown in **Figure(3),** for estimating the fatigue life of mixtures from PI of binder and mixture stiffness can be used in a back calculation method. It is assumed that in a typical pavement structure strain levels of $1.0 * 10^{-4}$ mm/mm for stress controlled conditions and $5.0 * 10^{-4}$ mm/mm for strain controlled conditions are acceptable values that could be used. Specifying a minimum fatigue life of $1.0 * 10^{6}$ cycles, the mixture stiffness required to achieve this fatigue life is estimated at $7 * 10^{8}$ Pa. Using PI values and assuming a volume concentration of 13% binder in a typical asphalt mixture, the maximum allowable bitumen stiffness at 0.012 seconds loading time should be 50000 kPa. In this approximation it was assumed that PAV aging results in increasing the softening point by 20ºC for grades tested and to insure proper application of this change, the PI value for each binder was increased by 0.75 points. By using Van der Poel nomograph the values shown in **Table (8)** could be obtained. based on penetration 40-50 and PG76-4 with intermediate grade temperature 40^0C, a maximum limit of 50000 kpa could be also derived for fatigue resistance.

Table (8) Asphalt Binder Stiffness at Intermediate Pavement Temperatures

T=28 ^{0}C			
	T_{DIFF} ^{0}C	PI	S (N/M^2)
Pen 40/50			
A1	43	-0.5	$9*10^7$
A2	41	-0.727	$9*10^7$
A3	42	-0.661	$1*10^8$
A4	42	-0.503	$7*10^7$
A5	41	-0.813	$1*10^8$
A6	41	-0.939	$1.2*10^8$
A7	46	0.17	$8*10^7$
A8	43	-0.517	$9*10^7$
A9	40.5	-1.14	$1*10^8$
A10	44	-0.19	$6*10^7$
Average Binder Stiffness			$9*10^7$
Pen 60/70			
B1	35.5	-0.727	$7*10^7$
B2	34	-1.14	$6*10^7$
B3	36	-0.503	$5*10^7$
B4	34	-1.042	$5*10^7$
B5	35	-1.00	$5.5*10^7$
B6	38.5	0.137	$4.8*10^7$
B7	35	-0.898	$3*10^7$
B8	38.5	0.137	$4.8*10^7$
B9	34.5	-1.12	$8*10^7$
B10	37.5	-0.12	$5*10^7$
Average Binder Stiffness			$5.4*10^7$

T=31 ^{0}C			
	T_{DIFF} ^{0}C	PI	S (N/M^2)
Pen 40/50			
A1	40	-0.5	$1.3*10^8$
A2	38	-0.727	$1*10^8$
A3	39	-0.661	$9*10^7$
A4	39	-0.503	$7*10^7$
A5	38	-0.813	$1*10^8$
A6	38	-0.939	$1.2*10^8$
A7	43	0.17	$2*10^7$
A8	40	-0.517	$5*10^7$
A9	37.5	-1.14	$5*10^7$
A10	41	-0.19	$4*10^7$
Average Binder Stiffness			$7.7*10^7$
Pen 60/70			
B1	35.5	-0.727	$4*10^7$
B2	34	-1.14	$4*10^7$
B3	36	-0.503	$4.5*10^7$
B4	34	-1.042	$5*10^7$
B5	35	-1.00	$5.8*10^7$
B6	38.5	0.137	$4.5*10^7$
B7	35	-0.898	$5.5*10^7$
B8	38.5	0.137	$4.5*10^7$
B9	34.5	-1.12	$6*10^7$
B10	37.5	-0.12	$3*10^7$
Average Binder Stiffness			$4.68*10^7$

T=34 ^{0}C			
	T_{DIFF} ^{0}C	PI	S (N/M^2)
Pen 40/50			
A1	37	-0.5	$7*10^7$
A2	35	-0.727	$6*10^7$
A3	36	-0.661	$12*10^7$
A4	36	-0.503	$6*10^7$
A5	35	-0.813	$7.5*10^7$
A6	35	-0.939	$7.5*10^7$
A7	40	0.17	$7*10^7$
A8	37	-0.517	$5*10^7$
A9	34,5	-1.14	$1*10^8$
A10	38	-0.19	$5*10^7$
Average Binder Stiffness			$6.4*10^7$
Pen 60/70			
B1	32.5	-0.727	$4*10^7$
B2	31	-1.14	$5*10^7$
B3	33	-0.503	$5*10^7$
B4	31	-1.042	$5*10^7$
B5	32	-1.00	$4.5*10^7$
B6	35.5	0.137	$3*10^7$
B7	32	-0.898	$4*10^7$
B8	35.5	0.137	$3*10^7$
B9	31.5	-1.12	$2.5*10^7$
B10	34.5	-0.12	$2.3*10^7$
Average Binder Stiffness			$3.8*10^7$

T=40 ^{0}C			
	T_{DIFF} ^{0}C	PI	S (N/M^2)
Pen 40/50			
A1	31	-0.5	$5*10^7$
A2	29	-0.727	$4*10^7$
A3	30	-0.661	$5.5*10^7$
A4	30	-0.503	$4*10^7$
A5	29	-0.813	$5*10^7$
A6	29	-0.939	$6*10^7$
A7	34	0.17	$5*10^7$
A8	31	-0.517	$5.5*10^7$
A9	28.5	-1.14	$6*10^7$
A10	32	-0.19	$4*10^7$
Average Binder Stiffness			$5*10^7$
Pen 60/70			
B1	26.5	-0.727	$1*10^7$
B2	25	-1.14	$1.5*10^7$
B3	27	-0.503	$1*10^7$
B4	25	-1.042	$2*10^7$
B5	26	-1.00	$1.8*10^7$
B6	29.5	0.137	$1*10^7$
B7	26	-0.898	$1.9*10^7$
B8	29.5	0.137	$1*10^7$
B9	25.5	-1.12	$1.8*10^7$
B10	28.5	-0.12	$1*10^7$
Average Binder Stiffness			$1.4*10^7$

- **or Thermal Resistance,** The main approach used in Superpave specification is followed for this type of pavement failure. The stiffness at 60 seconds loading time, at temperatures 10ºC higher than the minimum grade temperature, was estimated for both penetration grades (40-50) and (60-70). The shift in temperature is used to offset the effect of short loading time of 60 seconds compared to the loading time of a cooling cycle in the field, as used in the Superpave specifications. Also, the logarithmic creep rate (m (60)) should also be controlled. **Table (9)** shows the creep stiffness (S (60)) and creep rate (m (60)) at 6 ºC, 0 ºC and -6 ºC respectively. Using the properties of the penetration (60-70) and assuming that the bitumens of this grade performed well in cold climates in Iraq, the limits of S(60)=347000 kpa and m(60)=0.349 could be derived. Similar to the fatigue requirement the effect of long-term aging was considered by increasing the softening point by 20 ºC and PI increased by 0.75. To control brittleness of bitumen at minimum pavement temperature, the elongation at break (λ) from nomograph developed by Heukelom (shown in **Figure (4)**) could be used. The minimum strain at break should be more than 0.02 estimated by using a 60 second loading time and softening point of the PAV aged material (increasing softening point by 20 ºC and PI increased by 0.75).

Table (9) Asphalt Binder Stiffness at Low Pavement Temperatures

T= 6 ^{0}C						
	T_{DIFF} (^{0}C)	PI	S(N/M^2) (t=30sec)	S(N/M^2) (t=60sec)	m (60sec)	λ (60sec)
Pen 40/50						
A1	65	-0.5	$8*10^7$	$6*10^7$	0.415	0.059
A2	63	0.727	$9*10^7$	$7*10^7$	0.362	0.4
A3	64	-0.661	$1*10^8$	$7*10^7$	0.514	0.1
A4	64	-0.503	$9*10^7$	$6*10^7$	0.584	0.1
A5	63	-0.813	$1.5*10^8$	$1*10^8$	0.584	0.42
A6	63	-0.939	$1.5*10^8$	$1.2*10^8$	0.323	0.43
A7	68	0.17	$9*10^8$	$6*10^7$	0.584	0.1
A8	65	-0.517	$9*10^7$	$7*10^7$	0.584	0.05
A9	62.5	-1.141	$1*10^8$	$7*10^7$	0.514	0.02
A10	66	-0.19	$7*10^7$	$5*10^7$	0.485	0.1
Average				$7.3*10^7$	0.494	0.177
Pen 60/70						
B1	60.5	-0.727	$6*10^7$	$4*10^7$	0.585	0.1
B2	59	-1.14	$6*10^7$	$5*10^7$	0.678	0.15
B3	61	-0.503	$5*10^7$	$3.5*10^9$	0.514	0.18
B4	59	-1.042	$6*10^7$	$4.5*10^7$	0.415	0.2
B5	60	-1.00	$8*10^7$	$6*10^7$	0.415	0.2
B6	63.5	0.137	$5*10^7$	$3.5*10^7$	0.514	0.15
B7	60	-0.898	$6*10^7$	$4*10^7$	0.585	0.1
B8	63.5	0.137	$5*10^7$	$3.5*10^7$	0.514	0.15
B9	59.5	-1.12	$6*10^7$	$5*10^7$	0.687	0.21
B10	62.5	-0.12	$2.7*10^7$	$2*10^7$	0.432	0.1
Average				$4.1*10^7$	0.533	0.154

Table (9) Continued

T= 0 ^{0}C						
	T_{DIFF}(^{0}C)	PI	S(N/M^2) (t=30sec)	S(N/M^2) (t=60sec)	m (60sec)	λ (60sec)
Pen 40/50						
A1	71	-0.5	$2*10^8$	$1.5*10^8$	0.415	0.04
A2	69	0.727	$3*10^8$	$2*10^8$	0.321	0.22

A3	70	-0.661	$3*10^8$	$2*10^8$	0.321	0.1
A4	70	-0.503	$2*10^8$	$1.5*10^8$	0.415	0.1
A5	69	-0.813	$3*10^8$	$2*10^8$	0.585	0.2
A6	69	-0.939	$4.2*10^8$	$3*10^8$	0.585	0.2
A7	74	0.17	$1.5*10^8$	$1.3*10^8$	0.206	0.05
A8	71	-0.517	$2*10^8$	$1.5*10^8$	0.415	0.04
A9	68.5	-1.141	$3*10^8$	$2*10^8$	0.585	0.03
A10	72	-0.19	$1.5*10^8$	$1*10^8$	0.585	0.05
Average				$1.78*10^8$	0.443	0.103
Pen 60/70						
B1	66.5	-0.727	$1.5*10^8$	$1*10^8$	0.585	0.05
B2	65	-1.14	$2*10^8$	$1.5*10^8$	0.415	0.01
B3	67	-0.503	$1*10^9$	$8*10^7$	0.321	0.05
B4	65	-1.042	$1.6*10^8$	$1*10^8$	0.678	0.05
B5	66	-1.00	$1.5*10^8$	$1*10^8$	0.585	0.049
B6	69.5	0.137	$9*10^7$	$7*10^7$	0.362	0.075
B7	66	-0.898	$1.4*10^8$	$1*10^8$	0.485	0.048
B8	69.5	0.137	$1.5*10^8$	$1*10^8$	0.585	0.075
B9	65.5	-1.12	$2.5*10^8$	$1.8*10^8$	0.437	0.05
B10	68.5	-0.12	$8.5*10^8$	$6*10^7$	0.502	0.1
Average				$1.04*10^8$	0.495	0.0557

T= - 6 ^{0}C

	T_{DIFF} (^{0}C)	PI	S(N/M^2) (t=30sec)	S(N/M^2) (t=60sec)	m (60sec)	λ (60sec)
Pen 40/50						
A1	77	-0.5	$3.5*10^8$	$3*10^8$	0.222	0.01
A2	75	0.727	$6*10^8$	$5*10^8$	0.263	0.048
A3	76	-0.661	$7.5*10^8$	$5*10^8$	0.585	0.015
A4	76	-0.503	$4*10^8$	$3*10^8$	0.415	0.015
A5	75	-0.813	$8*10^8$	$6*10^8$	0.415	0.049
A6	75	-0.939	$8*10^8$	$6*10^8$	0.415	0.01
A7	80	0.17	$4*10^8$	$2.9*10^8$	0.463	0.02
A8	77	-0.517	$3.8*10^8$	$3*10^8$	0.341	0.055
A9	74.5	-1.141	$6*10^8$	$5*10^8$	0.263	0.023
A10	78	-0.19	$2.5*10^8$	$2*10^8$	0.321	0.059
Average				$4.0*10^8$	0.3703	0.0304
Pen 60/70						
B1	72.5	-0.727	$4.5*10^8$	$3.5*10^8$	0.362	0.02
B2	71	-1.14	$3.5*10^8$	$3*10^8$	0.285	0.01
B3	73	-0.503	$4*10^8$	$3*10^8$	0.533	0.02
B4	71	-1.042	$5.2*10^8$	$4*10^8$	0.486	0.012
B5	72	-1.00	$5*10^8$	$4*10^8$	0.413	0.05
B6	75.5	0.137	$3*10^8$	$2.4*10^8$	0.413	0.023
B7	72	-0.898	$5*10^8$	$4.2*10^8$	0.323	0.015
B8	75.5	0.137	$3.5*10^8$	$2.8*10^8$	0.413	0.021
B9	71.5	-1.12	$5.5*10^8$	$4.4*10^8$	0.413	0.01
B10	74.5	-0.12	$4*10^8$	$3.4*10^8$	0.301	0.02
Average				$3.47*10^8$	0.394	0.020

The results of the previous analyses are shown in **Table (10)**. The table shows proposed system of performance grades based on the concept of using the index properties to derive engineering criteria that are performance related.

Table (10) Proposed Performance Grading for Iraq

High Temperature Grade (HT)		PG64	PG70		PG76
Low Temperature Grade (LT)		-16	-16	-10	-4
Performance Related Property	**Performance Criteria**				
For Workability					
Viscosity (pa-s)	0.12- 0.65	135 ºC			
For Rutting Resistance					
Estimated Creep Stiffness (Unaged)@ HT (kpa)	S(0.012)>=9	64	70		76
Estimated Creep Stiffness (RTFO-Aged) (kpa)	S(0.012)>=22.5	64	70		76
For Fatigue Resistance					
Estimated Creep Stiffness (PAV-Aged) ,(kpa)	S(0.012)<=50000	28	31	34	40
For Thermal Cracking Resistance					
Estimated creep stiffness (PAV-Aged), (kpa)	S(60)<=347000	-6	-6	0	6
Estimated Creep Rate (PAV-Aged)	m(60) >= 0.349	-6	-6	0	6
Elongation at break (PAV-Aged)	λ(60) >=0.02	-6	-6	0	6

TESTING LOCAL ASPHALT CEMENT BY CONVENTIONAL METHODS AND VERIFICATION OF CONCEPT

Two asphalt types with penetration grade (40-50) and (60-70) are tested using the conventional test methods (penetration and softening point). Both asphalt types are obtained from Daurah refinery, south-west of Baghdad. The tests are conducted on asphalt before aging and after aging with the RTFO and PAV, the results are shown in **Table (11)**. From this table it appeared that, the change in the softening point is less than the 20 ºC that is assumed previously in the analysis used to develop a PG framework. Since PAV represents only moderate long term aging (5-10 years), it is considered acceptable to continue the increasing of the softening point by 20 ºC to represent long term aging. As for the change in PI, an increase by 0.75 points is assumed. This table also shows that the change in PI value for both asphalt does not appear possible. Although sample size is small, it appears that it is necessary to conduct a laboratory aging procedure that would simulate long term aging. A test such as the PAV could be used.

Penetration and softening point values before and after aging are used in the nomographs mentioned previously to calculate the stiffness values in order to estimate rutting resistance, fatigue resistance, and thermal resistance. **Table (12)** includes the values of the selected parameters used in the proposed specification including S(0.012) of the unaged, RTFO-aged asphalts and PAV aged binders. The S(60), m(60) and λ(60) of the PAV-aged asphalts. The parameters are shown for both asphalt types at various temperatures representing the temperature grades selected for Iraq. In the last column of **Table (12)**, the estimated grades of the binders are listed, which indicate that the asphalt with penetration grade 40-50 is equivalent to PG70-16 while that penetration grade 60-70 is equivalent to PG64-16.

In the **Table (12)** the PAV properties are also estimated using a standard shift of 20 ºC increase in softening point of the unaged binders, and a standard increase of 0.75 in the PI values calculated for the unaged binders. This was done to compare the effect of using standard shift versus the measured values after PAV aging. The results shown in the table under (Estimated PAV) significant discrepancy compared to the values of the measured (Tested PAV). The results confirm that it is required that a

long term aging procedure be used in a PG grading system with and without expensive rheology equipment.

Table (11) Conventional Testing Results for Different Performance Stages

	Original Asphalt	Short Term Aging (RTFO)	Long Term Aging (PAV)	Difference Between PAV and Original Asphalt
Pen 40-50				
penetration	45	27.45	15	-30
Softening Point	50.5	55	67	16.5
Penetration Index(PI)	- 1.3	- 1.27	- 0.180	1.12
Pen 60-70				
penetration	63	40	22	-41
Softening Point	45.3	49	57	11.5
Penetration Index(PI)	- 1.89	- 1.913	- 1.275	0.615

Table (12) Asphalt Grades According to Proposed Performance Classification System

Rutting Resistance								
	Original				RTFO			
pen	S(kpa) (Time of loading =0.012sec)				S(kpa) (Time of loading =0.012 sec)			
	>=9 kpa				>=22.5 kpa			
	58 ºC	64 ºC	70 ºC	76 ºC	58 ºC	64 ºC	70 ºC	76 ºC
40-50	90	40	20	8	22.5	100	50	20
60-70	40	10	6	3.8	100	25	15	9.5

Fatigue Resistance					
Tested in PAV					
pen	S (kpa)(t=0.012sec)				
	<=50000 kpa				
	25ºC	28ºC	31ºC	34ºC	40ºC
40-50	71200	58452	40840	24220	20760
60-70	57900	42000	30450	20722	15530

	Thermal Resistance									Grade
	Tested in PAV									
Pen	S (MPa)(t =60 sec)			m (60)			λ (60)			
	<=347000			>= 0.349			>=0.02			
	6 ºC	0 ºC	-6 ºC	6 ºC	0 ºC	-6 ºC	6 ºC	0 ºC	-6 ºC	
40-50	65	101	295	0.591	0.534	0.552	0.19	0.12	0.04	PG 70-16
60-70	45	98	290	0.432	0.423	0.452	0.21	0.94	0.085	PG 64-16

Table (12) Continued

Fatigue Resistance					
Estimated PAV					
pen	S (kpa)(t=0.012sec)				
	<=50000 kpa				
	25ºC	28ºC	31ºC	34ºC	40ºC
40-50	80800	60100	43760	31630	25500
60-70	67400	49900	36500	26600	18000

	Thermal Resistance									Grade
	Estimated PAV									
Pen	S (MPa)(t =60 sec)			m (60)			λ (60)			
	<=347000			>= 0.349			>=0.02			
	6 ºC	0 ºC	-6 ºC	6 ºC	0 ºC	-6 ºC	6 ºC	0 ºC	-6 ºC	
40-50	70	120	305	0.585	0.514	0.450	0.1	0.05	0.035	PG 70-16
60-70	50	110	300	0.447	0.415	0.384	0.15	0.081	0.054	PG 64-16

SUPERPAVE PERFORMANCE GRADE (PG) TESTS

The same two types of asphalt cement with penetration grade (40-50) and (60-70) that have been tested conventional methods are also tested using Superpave approach. All Superpave tests have been performed in the Ministry of Transportation lab. of Saudi Arabia except the Rotational Viscometer test was performed in the University of Baghdad lab. to determine the performance grade for each one. These tests are performed according to AASHTO R29-02 "Standard Practice for Grading or Verifying the Performance Grade of an Asphalt Binder" on original (unaged binder), Rolling Film Oven aged residue (i.e. Rolling Film Oven Test RTFOT) and Pressure Aging Vessel (PAV) residue. While, The PG grades of asphalt binder was determined according to AASHTO M320-05 "Standard Specification for Performance -Graded Asphalt Binder". The results of Superpave binder tests for asphalt cement with penetration grade (40-50) are shown in **Table (13)** whereas, for asphalt cement with (60-70) penetration grade are shown in **Table (14)**. It is obvious from these tables that the asphalt with penetration (40-50) is equivalent to PG70-16 while asphalt with penetration (60-70) is equivalent to PG64-16.

Table (13) Summary of Superpave Binder Test Results for Penetration (40-50)

Asphalt	Parameters	Specification M320 (AASHTO,2007)	Temperature Measured		Measured Parameters	Pass/ Fail
Original	Flash Point Temperature	230 °C, min.	-		320 °C	Pass
	Viscosity at 135 °C	3 pa.s, max.	-		0.516 pa.s	Pass
	DSR, G*/sinδ at 10 rad/s	1.00 Kpa, min.	**58**		4.2361 Kpa	Pass
			G*=4.2320	δ=87.5		
			64		2.0113 Kpa	Pass
			G*=2.0108	δ=88.8		
			70		1.0619 Kpa	Pass
			G*=1.0617	δ=89.2		
			76		0.5604 Kpa	Fail
			G*=0.5603	δ=89.7		
RTFO Aged	Mass Loss	1%, max.	-		0.446	Pass
	DSR, G*/sinδ at 10 rad/s	2.2 Kpa, min.	**58**		9.6342 Kpa	Pass
			G*=9.6118	δ=86.1		
			64		4.9117 Kpa	Pass
			G*=4.9062	δ=87.3		
			70		2.2655 Kpa	Pass
			G*=2.2646	δ=88.4		
			76		1.4025 Kpa	Fail
			G*=1.4023	δ=89.3		
PAV Aged	DSR, G*sinδ at 10 rad/s	5000 Kpa, max.	**31**		4270 Kpa	Pass
			G*=3548.3	δ=56.2		
	BBR, Creep Stiffness	300 Mpa, max.	**-6**		211.0Mpa	Pass
	BBR, m- value	0.3, min.	**-6**		0.334	Pass

Table (14) Summary of Superpave Binder Test Results for Penetration (60-70)

Asphalt	Parameters	Specification M320 (AASHTO,2007)	Temperature Measured		Measured Parameters	Pass/ Fail
Original	Flash Point Temperature	230 °C, min.	-		310 °C	Pass
	Viscosity at 135 °C	3 pa.s, max.	-		0.400 pa.s	Pass
	DSR, G*/sinδ at 10 rad/s	1.00 Kpa, min.	**58**		2.1516 Kpa	Pass
			G*=2.1506	δ=88.3		
			64		1.0603 Kpa	Pass
			G*=1.0601	δ=89.0		
			70		0.5286 Kpa	Fail
			G*=0.5285	δ=89.5		
			76		0.2566 Kpa	Fail
			G*=0.2565	δ=89.9		
RTFO Aged	Mass Loss	1%, max.	-		0.540	Pass
	DSR, G*/sinδ at 10 rad/s	2.2 Kpa, min.	**58**		5.3793 Kpa	Pass
			G*=5.3741	δ=87.5		
			64		2.2066 Kpa	Pass
			G*=2.2056	δ=88.3		
			70		1.3479 Kpa	Fail
			G*=1.3474	δ=88.5		
			76		0.6535 Kpa	Fail
			G*=0.6534	δ=89.2		
PAV Aged	DSR, G*sinδ at 10 rad/s	5000 Kpa, max.	**28**		3100 Kpa	Pass
			G*=2560.9	δ=55.7		
	BBR, Creep Stiffness	300 Mpa, max.	**-6**		103 Mpa	Pass
	BBR, m- value	0.3, min.	**-6**		0.373	Pass

COMPARISON OF MEASURED AND ESTIMATED PROPERTIES

One of the objectives of this study is to compare the estimated performance related properties with the measured Superpave properties in different performance stages, under the same temperature and loading time conditions. The summary of the results are shown in **Table (15)**. It is important to

note that the G* values were measured at 10 rad/sec frequency, as required by the Superpave system. This corresponds to a loading time of approximately 0.10 second, which is much higher than the 0.012 second that was chosen for the estimated stiffness values. Therefore the comparison should not be about equivalency but about the obtained final grade for each asphalt cement. The results indicated that a low G* value obtained from Superpave tests corresponds to low stiffness value S(0.012) obtained from the proposed method. It appears that both methods (proposed and Superpave system) give the same performance grade. PG70-16 for asphalt cement with penetration grade (40-50) and PG64-16 for asphalt cement with penetration grade (60-70).

Table (15) Modules of Different Performance Stages

Pen	Original		RTFO		PAV			
	G* (KPa)	S(0.012) (KPa)	G* (KPa)	S(0.012) KPa	G* (KPa)	S(0.012) (KPa)	S (MPa)	S(0.012) (MPa)
40-50	**T=70°C**	**T=70°C**	**T=70°C**	**T=70°C**	**T=31°C**	**T=31°C**	**T=-6°C**	**T=-6°C**
	1.0617	20	2.2646	50	3548.3	40840	211	295
60-70	**T=64°C**	**T=64°C**	**T=64°C**	**T=64°C**	**T=28°C**	**T=28°C**	**T=-6°C**	**T=-6°C**
	1.0601	10	2.2056	25	2560.9	42000	103	209

CONCLUSIONS

- A temperature zoning map was developed for Iraq based on Superpave criteria. The required PG for asphalt binders are:
- PG70-16 for Mosul and Kirkuk
- PG64-16 for Rutba
- PG70-10 for Baghdad
- PG76-4 for Basrah
- Both of proposed and Superpave method give the same final performance grade. The Daurah asphalt with penetration grade 40-50 is equivalent to PG70-16 while that with penetration grade 60-70 is equivalent to PG64-16.
- Asphalt modifier is needed in the south parts of Iraq to modify asphalt stiffness.

REFERENCES

- AASHTO, (2007), "Standard Specifications for Transportation Materials and Methods of Sampling and Testing", 5th edition, American Association of State Highway and Transportation Officials, Washington, D.C., USA.
- Abbas, F., (2006), "Evaluation of Contributory Factors Influencing Permanent Deformation of Asphalt Paving Materials", M.Sc. Thesis, Al-Mustansiriya University.
- Al-Abdul Wahhab, H.I., Al-Dubabe, I.A., Asi, I.M., and Ali, M.F.,(1998), "Performance Based Characterization of Arab Asphalt", journal of building and environment, Kingdom of Saudi Arabia, Vol.33, PP375-383.
- Alani, H.M., (1986), "Temperature Susceptibility of Paving Grade Asphalt Cements" Engineering and Technology, Scientific Journal Published by University of Technology, Baghdad, Vol.4, No.2.
- Alaredi, H.A., (2006), "Reduction of Reflection Cracks in Overlay of Rigid Pavements" M.Sc. Thesis, Al-Mustansiriya University.
- Alazawy, N.M., (2006),"Comparative Evaluation for the Performance of Paving Materials by Using Marshall and Superpave Compaction Methods" M.Sc. Thesis, Al-Mustansiriya University.
- Albayati, A.H., (2006),"Permanent Deformation Prediction of Asphalt Concrete Under Repeated Loading" Ph.D. Thesis, Baghdad University.
- Alekaby, K.H.., (2005)," The Frictional Properties as a Design Control of Pavement Surface Mixtures" M.Sc. Thesis, Baghdad University.
- Aljumily, M.A., (2007), "Influence of Aging on Performance of Asphalt Paving Materials" Ph.D. Thesis, Baghdad University.
- Almudhadi, T.H., (2007), "Some Requirements to Control Reflective Cracking of Overlay Asphalt Pavement" Ph.D. Thesis, Baghdad University.
- Asal, F.N., (2007), "Fatigue Behavior of Flexible and Rigid Pavements under Cyclic Loads", Ph.D. Thesis, Baghdad University.
- Asi, I.M., (2007), "Performance Evaluation of SUPERPAVE and Marshall Asphalt Mix Designs to Suite Jordan Climatic and Traffic Conditions", journal of construction and building materials, Vol.21, PP.1732-1740.
- Asphalt Institute, (2003), "Performance Graded Asphalt Binder Specification and Testing", Manual Series No.1, (SP-1),Asphalt Institute, Lexington, Kentucky.
- Bahia H.I. and Vivanco J., (2005), "The Transition to a PG Grading System for Asphalt Binders in Developing Countries", University of Wisconsin, Madison.
- Hanaa, K., (2004), "Minimizing Reflective Cracking Potential of Asphalt Concrete Overlay", M.Sc. Thesis, AL-Mustansiriya University.
- Heukelom, W., (1973), "An Improved Method of Characterizing Asphaltic Bitumens with the Aid of Their Mechanical Properties", Proceedings of the Association of Asphalt Paving Technologists, USA, Vol.42, pp 67-98.
- Iraq Metrological Organization, (1989), "Climatic Atlas of Iraq 1951-1980", Baghdad, Republic of Iraq.
- Magd Aldeen, A. (2003), "Evaluation of The Factors Influencing The Tensile Properties of Asphalt Paving Materials", M.Sc. Thesis, Baghdad University.
- McLean, D.B., (1974), "Permanent Deformation Characteristics of Asphalt Concrete", Ph.D. Dissertation, University of California, Berkeley.
- Nahla, Y.A., (2005), "Prediction Model of Rutting Potential in Flexible Pavements.", Ph.D. Thesis, Baghdad University.

- Namir, G.A., (2002), "The Development of Models for the Prediction of Thermal Cracking in Flexible Pavements." Ph.D. Thesis, Baghdad University.
- Safar, M.M., (1992), "Influence of Temperature on Performance of Paving Materials.", M.Sc. Thesis, Baghdad University.
- Shakir, S., (1999), "Contributory Factors Related to Rutting of Local Asphalt Pavements." M.Sc. Thesis, Baghdad University.
- Shell, (1978), "Shell Pavement Design Manual –Asphalt Pavement and Overlays for Road Traffic", Shell International Petroleum, London.
- SHRP, (1994), "The Superpave Mix Design Manual for New Construction and Overlays", Strategic Highway Research Program Report No.SHRP-A-407, National Research Council, Washington, D.C..USA.
- Taher, M.H., (1999), "Influence of Accelerated Weathering of Asphalt Cement on Performance of Paving Materials." M.Sc. Thesis, Baghdad University.
- Van der Poel, (1954), "A General System Describing the Viscoelastic Properties of Bitumens and Its Relation to Routine Test Data", Journal of Applied Chemistry, Vol.4.
- Van de Van, M.F.C., Jenkines, K.J, and Bahia, H.U., (2004),"concepts used for development of bitumen specifications" Proceedings of the 8th Conference on Asphalt Pavements for Southern Africa.
- Zaid, I., (2006), "Superpave Mineral Aggregate Properties as Related to Moisture Sensitivity of Paving Mixtures" M.Sc. Thesis, Baghdad University.

COLORING OF GRAY-SCALE IMAGE USING FPGA

Ammar A. Hassan
University of Baghdad \ College of Engineering \ Department of Computer Engineering

ABSTRACT

The image processing is one from the most powerful fields in the modern DSP techniques; also it has wide range of applications this day such as image compression, filtering and coloring. However, these processes required to a huge data processing so it has a problem under real time or movie.

The huge data processing under real time requires spatial processing tools such as super parallel processing computers or spatial hardware systems. This paper introduces a mechanism of coloring gray scale image algorithm through dedicated hardware devices.

The FPGA devices are used as a more suitable platform for image processing applications, special methods of parallelism and pipelining technique can be reconfigured and synthesized on FPGA categories. Xilinx series are selected as a platform of coloring algorithm by transferring the color property between pair image, source (colored) and target (gray) images.

The algorithm colorizes each gray scaled pixel by matching chromatic value of it with each pixel of colored image and synthesis it on the Xilinx FPGA devices using VHDL synthesizer tool. Many computational and process manners of this scheme are presented of 8-bit precision for each pixel of pair image.

Finally, testing and performance of this technique obtained on ISE 4.1i software implementation and comparing results with other simulator results.

المستخلص

أن معالجة الصور هي واحدة من أغلب المجالات الرائعة في تقنيات معالجة الإشارة الرقمية الحديثة والتي لها مدى واسع من التطبيقات في الوقت الحاضر, مثالاً على ذلك ضغط الصور; الترشيح والتلوين. مع ذلك هذه العمليات تتطلب معالجة بيانات واسعة جداً لذلك تعتبر مشكلة ضمن تطبيقات الزمن الحقيقي والأفلام السينمائية

أن معالجة البيانات الواسعة ضمن تطبيقات الزمن الحقيقي تتطلب أدوات معالجة خاصة مثل حاسبات معالجة متوازية عالي أو منظومات كيان مادي خاصة. هذا البحث يقدم خوارزمية لتلوين الصور الرمادية من خلال أجهزة كيان مادي مخصصة.

أن أجهزة الكيان المادي المسماة حيز البوابات المرتب بهيئة صفوف قابلة للبرمجة (FPGAs) والتي تستخدم أرضية جداً مناسبة لتطبيقات معالجة الصور بطرق خاصة من التقنيات المتوازية ومجموعة التقنيات شبه الموازية التي يمكن

إعادة تشكلها وتراكيبها على أصناف (FPGAs).أن سلسلة Xilinx التي تم اختيارها كأرضية لخوارزمية التلوين بواسطة نقل اللون المناسب بين الصورتين [المصدر (ملونة) والهدف (الرمادية)].

الخوارزمية المقترحة تقوم بتلوين كل نقطة رمادية بمطابقة قيمة اللون الخاص بها مع كل نقطة بالصورة الملونة وتراكيبها على أجهزة ال (FPGAs) باستخدام أدوات تراكيب بلغة الكيان المادي المسماة بـ (VHDL). عدد من الحسابات وطرق المعالجة لهذه الهيكلية يتم طرحها بدقة "8" بت لكل نقطة لكلا الصورتين.

أخيراً اختبار ألأداء لهذه التقنية تم الحصول عليها من خلال برنامج البناء والتنفيذ المسمى بـ (ISE 4.1i) ومقارنة النتائج مع نتائج محاكاة أخرى.

KEYWORDS: coloring, Gray-scale, DSP, VHDL, Xilinx, FPGA.

INTRODUCTION

Any form of digital image based on main elements called (pixels) and pixels characteristic lead to construct the characteristic of image. The acceptable appearance of image exceeds with respect to pixels characteristic are difference from image to other according to features. Image features selection and representation are largest problem in research of machine learning and vision science.

The color images have two main features: Luminance (brightness) and chromatic (color) channels which are represented in the RGB color space system (Red, Green and Blue). By assignment certain value of it leads to have pixel characteristics.

In gray scale image each pixel carry up three channels (RGB) equally values which are produced one feature (luminance) of image. To produce this feature there are many colors adding together in coloring image. Since, color images and gray scale image have important properly which is called "*luminance*".

The mechanism of color transfer technique (colorization) has been studies in the movie industry since 1975's. Various analogue techniques have been used to accomplish this challenging [1].

The fundamental process of transferring color from one image to another is introduced by Welsh et. al. [2]. they attempted to provide a method to minimize the amount of human labor required for this task by matching luminance and texture information among images (color image (Source) and gray scale image (Target)). While, Karthilceyani [3] used Welsh idea to enhance his procedure by allowing the user to match areas of the two images using rectangular swatches.

Other works such as YaoLi [1] introduce the fast colorization using edge and gradient constrains to reduce the color confusion near the boundary and applying it on movie. Also, Bara'a A. Attea [4] applied the technique of evolutionary algorithms (EAs) adding to previous ideas, probabilistic search algorithms based on the model of natural evolution, for colorization problem.

This paper interested in digital colorization and related work of digital image processing on Field Programmable Gate Array (FPGAs). On FPGAs, there are several researches of image processing which can be classified according to hardware topologies and image processing algorithm implemented. As in Daggu Ven. [5] that implemented and evaluated of image processing algorithm on reconfigurable architecture using C-based HDLs. This algorithm applied on Xilinx Virtex-E FPGA platform to speed up of processing approximately '15' times faster than the software implementation.

Finally, Muthukumar [6] used image processing algorithms (such as edge detection) on reconfigurable architecture using handel-C on Xilinx FPGA board.

COLORIZATION ALGORITHMS

This section discusses main topologies of colorization algorithms such as color space conversion and pixel selection. Furthermore, it finds a suitable solution to accomplish this task on Virtex FPGA board with minimum cost and high performance.

Color Space Conversions

To extract specific properties from an image (such as Luminance and colorimetric information) this leading to understand color space and color space conversions.

A digital color image is a digital image that includes color information for each pixel. The RGB color space system is commonly used in computer displays, but it does not have enough data to match between pair of image [7]. It is necessary to change RGB space to another space system which has more benefit of matching process and this called color space conversion.

This paper applied YIQ space model because it used in commercial color TV broadcasting by mapping function, it can convert RGB to YIQ color space as defined in [7,8].

$$\begin{bmatrix} Y \\ I \\ Q \end{bmatrix} = \begin{bmatrix} 0.299 & 0.587 & 0.114 \\ 0.596 & -0.275 & -0.321 \\ 0.212 & -0.528 & 0.311 \end{bmatrix} * \begin{bmatrix} R \\ G \\ B \end{bmatrix} \quad (1)$$

In YIQ color space; the Y coordinate represents the luminance Y while I and Q coordinates represent the chrominance components I and Q respectively.

YIQ space is converted to RGB space by inverse matrix transformation [7].

$$\begin{bmatrix} R \\ G \\ B \end{bmatrix} = \begin{bmatrix} 1.000 & 0.956 & 0.620 \\ 1.000 & -0.272 & -0.647 \\ 1.000 & -1.108 & 1.705 \end{bmatrix} * \begin{bmatrix} Y \\ I \\ Q \end{bmatrix} \quad (2)$$

Pixel Selection

The use of local memory to store pixels already loaded from the picture memory provides saving in the number of memory accesses to the picture memory [9]. Therefore; search pixels process must be fetched from two different data sources.

The algorithm of color transferring form source image (color image) to target image (gray scale image) is presented by Welsh et al [2]. This mechanism can be achieved by following steps: First; converting source and target images from RGB color space in to the YIQ space. This color space has been chosen because it promptly provides the luminance value (Y channel) which is a crucial datum for our procedure [10]. According to this, compression process based on comparison of each pixel of target image with all pixels of source image upon luminance value and selects the best value (closer) from source image. Then, color values (represent in I & Q channels) of the selected source pixel are transferred to the gray scale pixel with remains luminance (Y of target) value. This process will continuous for all target pixels until forming new image similar to gray scale image with color information. Finally, retain a new image into RGB space to discover the new color appearance of gray scale image.

This algorithm required a very high complexity and a very large of multiplication numbers or in result it will required to high speed or to parallel processing for real time. According this scheme, Virtex FPGAs series are typically suitable to use with intensive

computations; especially complex operations because of it provides fasting hardware resources comparing with software resources.

HARDWARE

This section will discuss the principles of hardware resources, architecture, the implementation and the cost calculation.

Hardware Resources

The selection is focused on the selected mechanism of the hardware devices as more suitable in digital image processing field and properly applied on color transferring task. Virtex FPGA is the more suitable for this task because it is based on basic element called logic cell (LC) which can be programmed and reprogrammed for any logic function (as a function generator for any operation) has four inputs and one output.

Architecture

Block diagram of color transfer architecture (coloring of gray scale image) is constructed by most efficient method and suitable configuration on FPGA platform as shown in figure (1). Main stages of architecture are:-

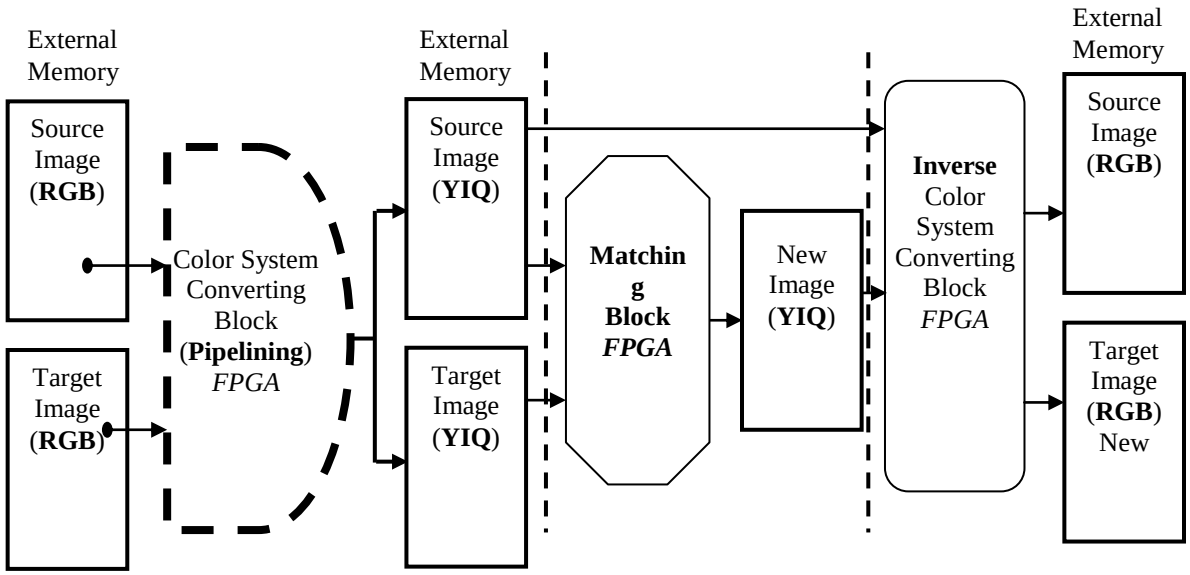

Figure 1: coloring gray scale image Architecture

- External Memory: The function of this block is to store source and target images points (pixels) during processing (in "RGB" or "YIQ"). The same unit can be used in a stage because the process is sequenced; each stage is distinct from other stage.

- Color System Converting Block: The function of this block is to convert each point of images (source and target) from RGB into YIQ system. This block constructs on Virtex FPGA platform in pipelining technique (configuration is per each column).

- Matching Block: The function of this block is to match each point of target image with source points according to luminance (Y dimension) of target image with luminance (Y dimension) of source image and selects chromatic information (I &Q dimensions) from source point to target point. This block constructed on the Virtex FPGA platform.

- Inverse Color System Converting Block: The function of this block is to back convert each point of images (source and new target) from YIQ into RGB system. This block not needed to

construct on Virtex FPGA platform because it can used the same block in the previous stage with new coefficient values as shown in figure (1).

FPGA Implementation

FPGAs have traditionally been configured by hardware engineers using Hardware Design Language (HDL) [6]. Adding to this, several attempts have been introduced to use other resources of languages and simulation software to implement algorithms on FPGAs.

This section describes the methodology of color transfer algorithm on Xilinx FPGA device, in other words; number of hardware resources and arithmetic operations of algorithm implementation are discussed.

As an example, a pair of image (gray and color images) with size of (256 × 256) pixels (8-bit / pixel) is demonstrated in details and compared with other sizes.

The same component of color space conversion will be used in the 1st and 3rd stages, then in 1st stage each point of image (source and target) converting from RGB to YIQ system as shown in figure (2)

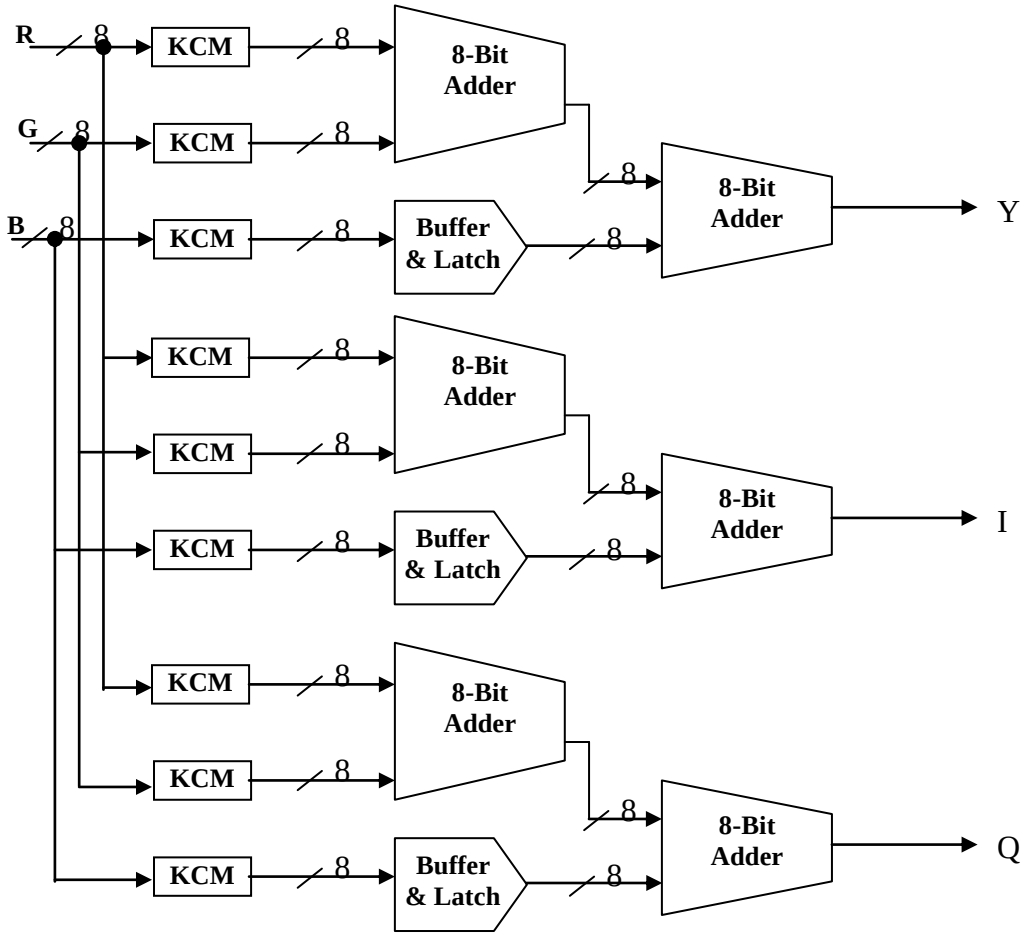

Figure (2): Block Diagram of each point in RGB-To-YIQ Converting on FPGA

Components Cost

The cost of the system and its parts measured on Virtex FPGA platform arithmetic operations are based on basic logic storage called logic cell (LC) formed as a Look-Up-Table (LUT) of four inputs one output.

Color System Converting Block

To implemented color system conversion block diagram on Virtex series. For (8 x 1) Constant Coefficient Multiplier (KCM) is required to "16" LCs, while (8 x 8) KCM needed to "128" LCs as shown in figure (3), while adder block has been implemented as adder technique in [11]. This scheme is suitable in both of size and propagation delay. For 8-bit adder, it required to "16" LCs at mostly. The total number of LCs for converting RGB-to-YIQ space system on Virtex FPGA is:

$$Po\,\mathrm{int}_{(YIQ)} = \{\ [N*\alpha]+[M*\beta]+\delta\ \}*(3)_{YIQ} \qquad (3)$$

Where,
N = Number of KCMs; α = cost of each KCM in Virtex FPGA
M = Number of Adder; β = cost of each Adder in Virtex FPGA, and δ = cost of 8-bit Buffer in Virtex FPGA.

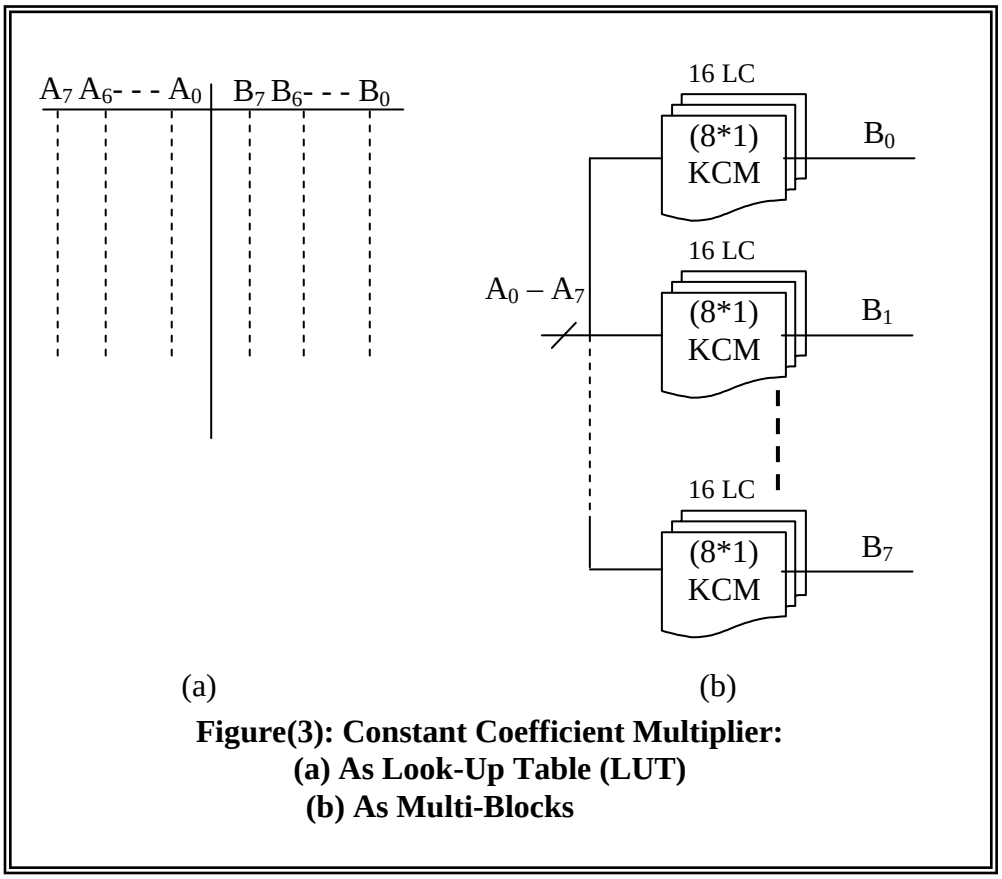

Figure(3): Constant Coefficient Multiplier:
(a) As Look-Up Table (LUT)
(b) As Multi-Blocks

For (8 x 8) KCM, 8-bit Adder and 8-bit buffer the cost of each point for one channel in (YIQ) is about "425" LCs for maximum, for three channels is "1275" LCs.
Using pipeline technique cost of one column is:

$$C_C = N_P * CPo\,\mathrm{int}_{YIQ} \qquad (4)$$

Where, C_C is cost of one column; N_P is Number of points per each column and $CPo\,\mathrm{int}_{YIQ}$ is Cost for one point (for 3-channels) which it's "1275" LCs. According to this representation, C_p is equally to "326400" LCs; at mostly for each column contains "256" points.

Other columns are not required to compute cost but only propagation delay because they have been passed sequentially for both source and target images on the same component on platform.

Matching Block

The matching process based on subtraction and comparing operations (all this process based on Y-channel value of each point for source and target images) as shown in figure (4). This can be accomplished by subtracted Y-channel value of target point (Y_t) from Y-channel of all source points in one column (Y_S).

In other words, comparing subtracted values of each subtractor to select smallest subtraction value by using comparator in a tree of comparators. This mechanism provides the closer source point to target point (with respect to luminance matching). According to this, other properties such as chromatic values (I & Q channels) of the selected point of sources image resultant from matching process are transferred to the target point of gray-scale image to form final image (i.e. replaced I & Q of target point by I & Q of the selected (winner) point resultant from tree comparators of source image). In pipeline technique, searching process continues for all points in source image with each point of target image.

Finally, using same component of color system converting block to retain new image which resultant from gray image to the color vision image by reversed color space transferring from YIQ-to-RGB dimensions and forming final image, this can be achieved without needed to present cost of computation on Virtex platform; it's one of most benefits of FPGA properties.

To implement matching architecture on Virtex series, it is required to find a mechanism to represent it as digital arithmetic operations technique to accomplish in simplification form, since a suitable architecture of 8-bit word length shown in figure (4).

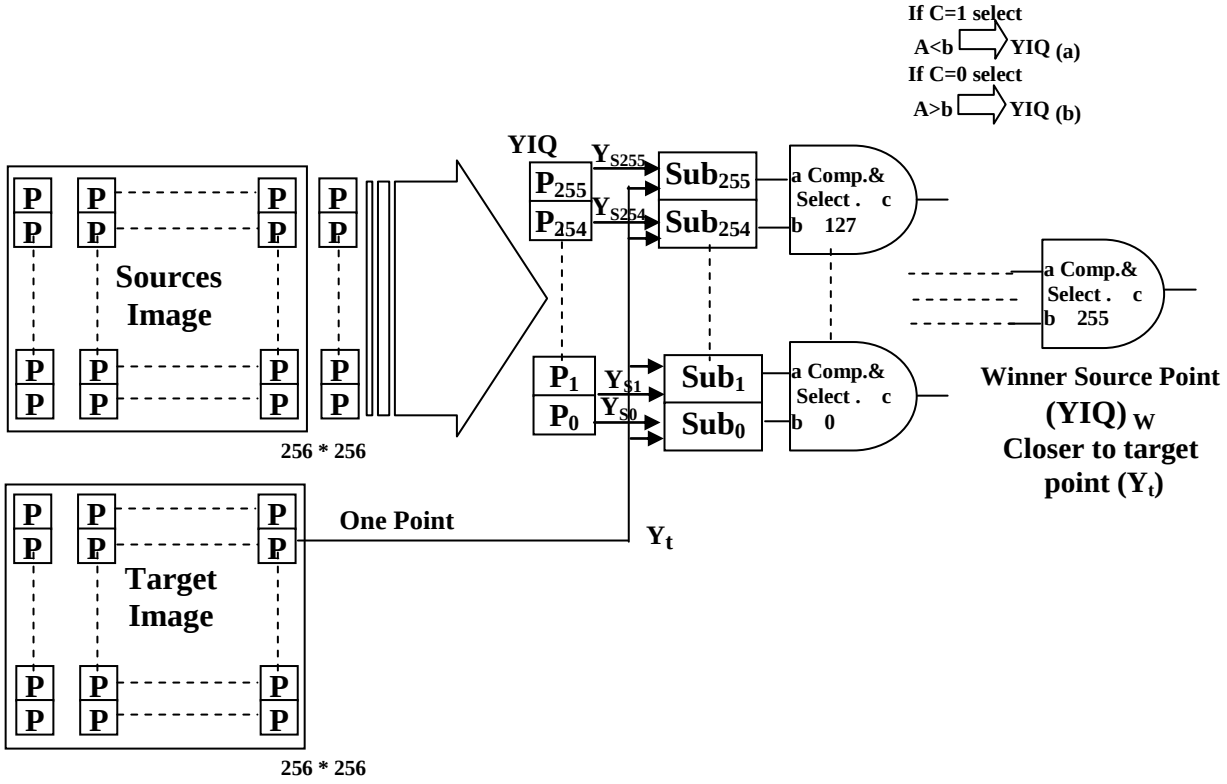

Figure (4): Matching Block Diagram

The main function of matching block is to find the closer point of source image to target point and selected the chromatic information from it. This scheme applied by obtaining minimum error value of point in target image with each points of source image. From figure (4) each point value (Y-channel) of target subtracts from each points of source image which arranged in one column using subtractor component (sub.) and finds minimum subtraction

value (winner point) from these subtractors by passing in a tree of comparator & selector component (comp & select).

Cost of matching block based on cost of (subtractors) and (comparators & selectors) components. Cost of 8-bit subtractor is similar to cost of 8-bit adder in previous section as demonstrated in [11], while; 8-bit of comparator & selector component based on technical idea shown in figure (5).

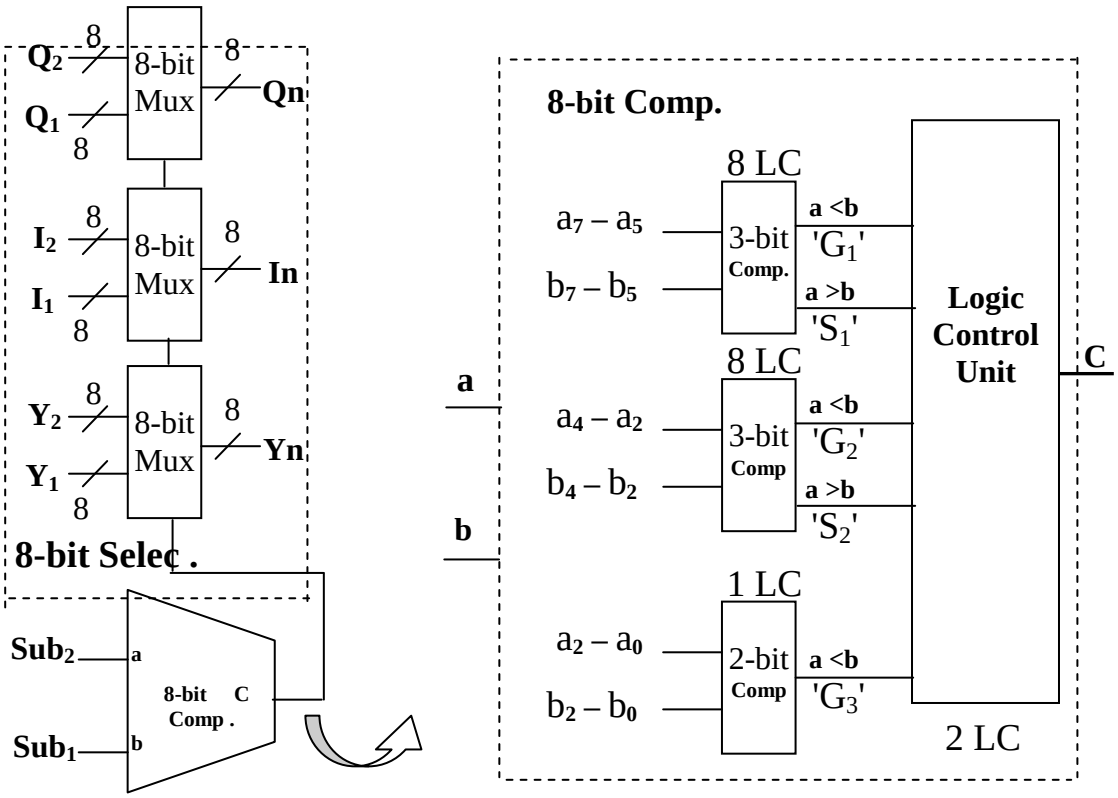

Figure (5): Comp. & Select. Block Diagram

Where, $C = G_1 + \overline{G}_1 \overline{S}_1 G_2 + \overline{G}_1 \overline{S}_1 \overline{G}_2 \overline{S}_2 G_3 \approx 19 \ \ LCs$. While 8-bit selector represented as a multiplexer (Mux.) which occupied "8" LCs for each Mux in virtex platform, then "24" LCs for three selector (8-bit Mux) of 3-channels. Since, cost of 8-bit **comp. & select.** component is equal to approximately "43" LCs and this lead to cost of matching block is:

Cost of Matching Block = [No. of subtractors * cost of subtractor] + [No. of (Comp. & Select.) components * cost of component] (5)

Total cost of (8-bit) matching block is approximately equal to "15061" LCs. Finally, system cost produced by combining cost of color system converting block with matching block which approximated equally to "341461 " LCs.

Propagation Delay (PD)

Propagation delay is the time consuming to achieve a specific task. To compute propagation delay of image colorization technique, it is divided into three stages. First stage is to convert both color and gray scale images from "RGB" to "YIQ" space system using color converting block. Each point in this stage based in idea on KCM and buffer as main

components which are required to one clock pulse, while 8-bit adder needed to maximum four clock pulses (if dividing to 2-bit adder) [11]. By using Xilinx FPGAs, maximum clock pulse 330 MHz [data sheet], then maximum propagation delay $\mathbf{(PD)}_{Max.}$ required to convert each point from "RGB" to "YIQ" space system is about vibrating between (5 - 10) ns without needed to storage state and applied pipeline technique. Then, propagation delay of an image is depended on the number of columns in the image. As a result, time delay one image to convert it from "RGB" to "YIQ" space systems is:

$$\mathbf{(PD)}_{Image} = \mathbf{(PD)}_{Max.} * \text{Number of Columns in image} \quad (6)$$

Since, our example there are "256" columns for each of source and target images. Then, $\mathbf{(PD)}_{Image} \approx$ "2.56" μs of each image and for pair image ≈ "5" μs.

The same delay required in the third stage when used inverse converting from "YIQ" to "RGB" space because of it used same components in stage one with other KCMs value according to inverse matrix transformation.

Time delay interval of the second stage is based on maximum Propagation Delay $\mathbf{(PD)}_{Max.}$ of matching block components (Subtractor component and comparator & selector component). Since, PD of (8-bit) subtractor is also reach to about four clock pulses (because of it constructed by the same technique of (8-bit) adder in the previous stage), While (8-bit) comparator & selector component is required maximum three clock pulses in virtex FPGAs platform (because of it divided to three parts as shown in figure (5). Then, $\mathbf{(PD)}_{Max.}$ is about to (10 ns) as demonstrated in later . It become clear, time delay of matching block is:

$$\mathbf{(PD)}_{Matching} = \mathbf{(PD)}_{Max.} * \mathbf{[1 + \gamma]} * N_C * N_T \quad (7)$$

Where: $\mathbf{(PD)}_{Max.}$ is maximum Propagation Delay;

$\mathbf{[1 + \gamma]}$ is number of subtractor block & Comp. & Select. Blocks in propagation tree;

N_C is number of columns in source image; N_T is number of points in target image

Since, our example there are "256 *256" points each of source and target images. Then, $\mathbf{(PD)}_{Matching}$ equal to "1497.6" μs or ≈ "1.5" s as propagation delay of second stage.

Finally, propagation delay of the system $\mathbf{(PD)}_{System}$ is the total delay of three stages which approximately to "1502.6 " μs.

RESULTS

The colorization algorithm of Gray image using color transferred architecture is presented and synthesized simulation using software implementation of ModelSim Xilinx edition and Integrated Software Environment ISE 4.1i Xilinx. All results are demonstrated in reports (such as Routing, Mapping, Number of LCs, propagation Delay (PD) and warring notes and compared with software results introduced from Pentium machine using Visual Basic (Visual Studio 7.0) program by simply way without any optimization. table (1) includes some of importance results that dealing with special hardware resources (time consuming (PD) and number of LCs), where it considered in order to present two major parameters in the implementation of gray-scaled image colorization on FPGAs. Since; VHDL tool is used in software implementation to achieve high performance (minimum area and high speed processing; less Propagation Delay) result rather than schematic tool.

The hardware results of coloring algorithm are compared with it results on simulation tool according to Welsh et al [2] without optimization. In presented solution and by exhaustion from FPGA resources it can speed up performance and achieved agreeable good image outfacing of color transfer algorithm.

Table 1: results of Gray scale coloring Images

Colored image	Required Time according to [4] (sec.)	*System Cost_ Logic Cells (LCs)*	Propagation Delay $(PD)_{System}$ on Virtex FPGAs (sec.)
(A)	448	144029	0.284
(B)	235	154973	0.154
(C)	645	216065	0.251
(D)	718	212063	0.286
(E)	715	312893	0.291
(F)	500	189221	0.314
(G)	496	224069	0.186
(H)	312	143489	0.202
(I)	2726	295682	1.203
(J)	668	206468	0.342
(K)	790	208061	0.320

3rd column consider in table (1) demonstrate number of Logic cells of the system according to ISE 4.1i software results. ISE 4.1i offers integration with Synopsys Inc.'s Formality™ and Verplex Systems Inc.'s Conformal™-LEC equivalency checkers, leveraging the same technology that was adopted in past years to check highdensity ASICs. In the equivalence method of testing, design passes can be checked in "blocks of logic" against a previous knowngood version. This can occur at any point in the design cycle, particularly in post-synthesis and place-and-route passes. This strategy offers a rapid checking method that is proving invaluable to high-density design work For Virtex-II designers moving to 1-million gate designs and above [12].

Source Image **Target Image** **Colored Image**

171 x 108 171 x 108 171 x 108

(A)

135 x 99 108 x 117 108 x 117

(B)

135 x 162

135 x 153

(C)

135 x 153

144 x 159

144 x 153

(D)

144 x 153

Source Image **Target Image** **Colored Image**

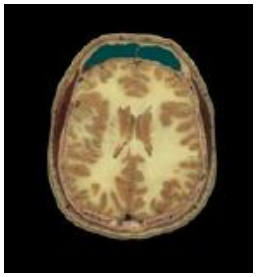

144 x 156

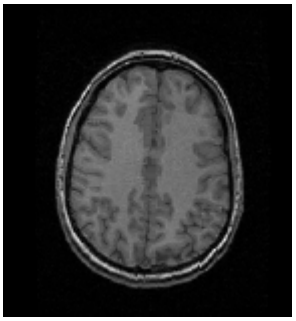

144 x 156

(E)

144 x 156

126 x 96

192 x 144

(F)

192 x 144

111 x 168

111 x 168

111 x 168

(G)

144 x 108

144 x 108

144 x 108

(H)

Source Image **Target Image** **Colored Image**

198 x 150

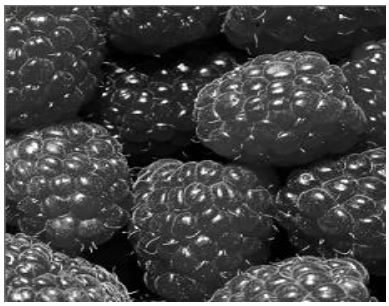
300 x 225

144 x 108

(I)

153 x 129

159 x 156

159 x 156

(J)

Figure 6: Examples of Color images for some of Gray-Scale Images acquired by color transferred approach. First column is the source image, second column is the target image and third column is colored image.

CONCLUSIONS

A fast and low hardware componets (number of logic cells) wae presented in this paper to solve hardware resources problem of of color transferring technique using FPGA devices.

Various different ideas have been combined together to produce low hardware cost and high performance scheme by using the flexibility of Virtex FPGA technologies. Pipelining technique applied as a main idea to obtain a suitable number of LCs with acceptable PDs. Table (1) shows the influence of different sizes of source & target images on hardware cost and time consuming in system processing. All images in figure (6) colorized within one second or less and the system cost can be implemented on one chip with all blocks of algorithm process. Where, maximum number of logic cells presents in image (I) of table (1) because the target image size (300 x 225) points is relatively large size for image to be colored although time required to do this is about one second and this is fast than it result in [4].

Finally, this chip can be used in more critical and complex applications such as colorization of images which have lost some data of information, also in wireless image applications and aerial photos according to relationship to chromaticity information (I&Q channels) with the luminance value (Y channel) between source & target images.

REFERENCES

- Yao Li, Ma Lizhuang & Wu Di, " Fast Colorization Using Edge and Gradient Constrains ", Copyright UNION Agency – Science Press, Plzen, Czech Republic. 2006.
- Welsh T., Ashikhmin M. & Mueller K., " Transferring color to grayscale images " ACM Transactions on Graphics 21, 277-280, 2002.
- Karthikeyani.V., Duraiswamy.K. & Kamalakkannan.P., "Conversion of Gray-scale image to Color Image with and without Texture Synthesis ", IJCSNS International Journal of Computer Science and Network Security, VOL.7 No.4, April 2007.
- Bara'a A. Attea & Amina D. Aboud, " Evolutionary Colorization of Grayscale Images", Int. J. Advanced Media and Communication, Vol. 1, No. 3, 2007.
- Daggu Venkateshwar Rao, Shruti Patil, Naveen Anne Babu and V Muthukumar, "Implementation and Evaluation of Image Processing Algorithms on Reconfigurable

Architecture using C-based Hardware Descriptive Languages", International Journal of Theoretical and Applied Computer Sciences Volume 1 Number 1 pp. 9–34, 2006.

- Muthukurnar K. & Daggu V., "Image Processing Algorithms on Reconfigurable Architecture Using Handel-C", Journal of Engineering and Applied Sciences Volume 1 Number 2 pp. 103-111, 2006.
- Laylan M. Rashid, "A Genetic Algorithm for Texture Synthesis and transfer", A M.Sc. Thesis submitted to Department of Computer Science, University of Baghdad, Baghdad-Iraq, 2005.
- GONZALE, R.C., & WINTZ, P., "Digital Image Processing", Addison-Wesley Publishing, Reading, MA, 1987.
- Tiago M. B. S. Dias, "High-Performance VLSI Motion Estimation Processors: Data Reuse and Sub-Pixel Accuracy", A M.Sc. Dissertation submitted to Department of Electrical & Computer Engineering, Pires, September 2004.
- G. Di Blasi, and R. D. Reforgiato, "Fast colorization of gray images", In proceedings of Eurographics Italian Chapter, D.M.I., University of Catania, 2003.
- Dafer R. Z., "Design and Implementation of A general Digital Down Converter using FPGA",A PhD thesis submitted to Department of Electrical Engineering, University of Baghdad, Baghdad-Iraq, 2002
- "Xilinx ISE Delivers the Speed You need", *www.xilinx.com/ise/xcell*, winter 2001.

CORRELATIONS BETWEEN PHYSICAL AND MECHANICAL PROPERTIES OF AL-AMMARAH SOIL IN MESSAN GOVERNORATE

Rana Mohammed Al-Kahdaar/ Assistant Lecturer

Abbas Fadhil Ibrahim Al-Ameri /Assistant Lecturer

ABSTRACT:

This paper describes the geotechnical properties of Al-Ammarah soil of Ammarah city in Messan Governorate-southern parts of Iraq. Data and other information taken from numbers of geotechnical reports that performed under the supervision of Consulting Engineering Bureau of Baghdad University. This research is devoted to study the correlation between different physical properties such as (LL, PI, LI, ω_n,γ_t, e_o) with different mechanical properties such as (q_u, c_c, c_s, SPT). The correlation is verified using simple regression analysis. From the regression results it was found that there is direct correlation between different parameters. By using the correlation-with some information- preliminary investigation stages and studies of any structure can be performed to find indicative design parameters.

الخلاصة:

تم في هذا البحث وصف الخصائص الهندسية لتربة مدينة العمارة في محافظة ميسان. في هذا البحث تم الاستفادة من المعلومات والبيانات المتوفرة من التقارير الصادرة من مكتب الأستشارات الهندسية التابع لجامعة بغداد والأستفادة منها في تخمين بعض العلاقات بين الخصائص الفيزيائية (LL, PI, LI, ω_n ,γ_t, e_o) والخصائص الميكانيكية (q_u, c_c, c_s, SPT) باستخدام التحليل الأحصائي. أن هذه العلاقات مهمة في مرحلة الدراسة والتخطيط والتصميم الاولي لاي منشأ وبأستخدام هذه العلاقات يمكن اعطاء مجموعة من المعاملات الخاصة بالتصميم دون الحاجة لاجراء تحريات تربة تفصيلية.

KEY WORDS: Ammarah city, Liquidity index, Plasticity index, Unconfined compressive

strength, Natural water content, simple regression.

NTRODUCTION:

Ammarah city is a land which subjected periodically to erosion and accumulated fluctuation of the sea. The thickness of sediments that consists of clayey silt to silty clay is about (150-200)m. The bearing capacity at shallow depth is ranging from (6-8) ton/m^2, the area imposes high water table

between (1-3)m below nature ground level. In general the area consist of an erratic distribution of the layers at shallow depth. This is may be attributed to the nature of the area which can be described as a recent sediments (Buringh, 1960).

This study use geotechnical properties of Ammarah soil from about 40 boreholes taken at different locations within Ammarah city as shown in Figure (1). All data was taken from geotechnical reports performed by the CEB. Some of these reports and investigations were made by or under the supervision of the researchers. Any unusual data and test results have been excluded from the analysis. The statistical analysis was made using simple regression analysis using Microsoft office software.

GEOLOGY OF MISSAN

Millions of years ago, Iraq was laying in a large hollow part of the surface called the Tethgs geosyncline. It was submerged by the sea and bordered by plateaus and tablelands.

The youngest geological process is the sedimentation of fines material of loamy sand, silt and clay in the extensive lower Mesopotamia plain, a process which still continuous at present time.

The surface of the area covered with recent of flood plain deposit by Tigris with some sediments came by air as dust during the end of spring and the beginning of summer. The recent sediment is of silt clay, and some fine sand. The light minerals consists of carbonate (20% - 30%) quarts, Albite, clay minerals as montmorllionite and some gypsum and halite because of arid climate of Al-Ammarah.

Because of an advantages geographic position and morphological situation the basin of the Mesopotamia plain was most probably subjected to periodically repeating phases of accumulation and erosion in accordance with the periodical fluctuations of the sea level caused by the cyclic changes during Pleistocene. The thickness of the sediments is about (150-200)m.

Marine in layers were described at Hammar formations. The formation is composed of sand and silts in its lower part and clay in the upper part. The formation is up to 20m thick and is distributed south wards from Ammarah as far as Zubair and Nahr Omar (Buringh, 1960) as shown in figure (2).

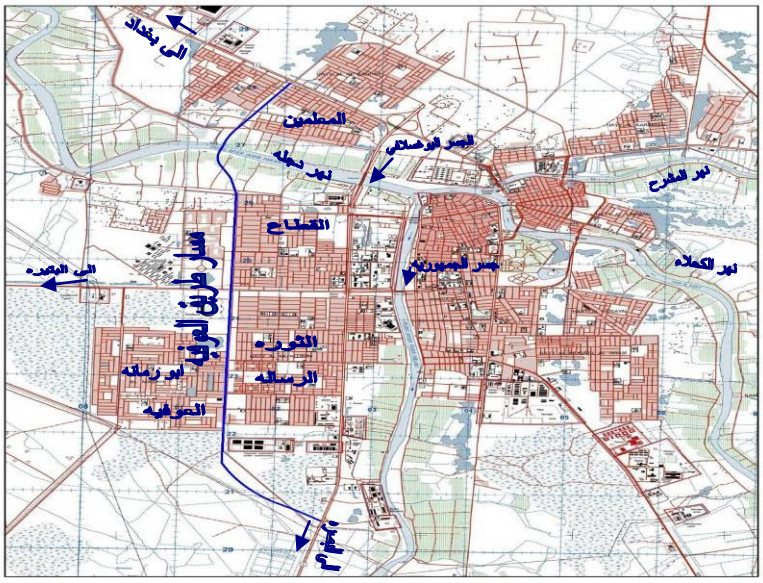

Figure (1) Administrative Map of Al-Ammarah city.

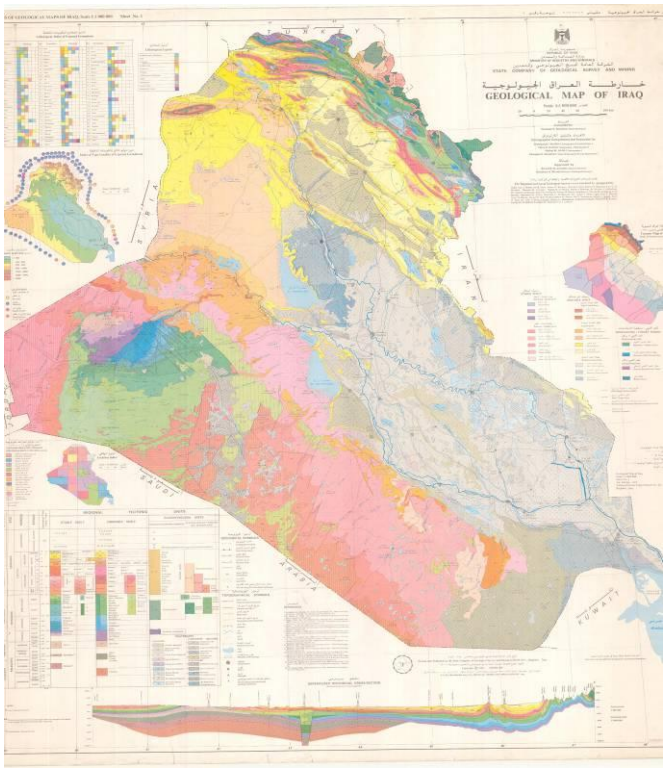

Figure (2) Geological Map of Iraq

PREVIOUS WORK

In the last decay, many research was performed to correlate the physical properties with the mechanical properties. This approach was adopted for the purpose of time saving and reduce cost of investigations. This approach was adopted from the earlier researcher in the filed of soil mechanics and foundation engineering. Some of these correlations are listed in Bowles (1996). However, the following are some of the present works.

In (1982) Abdel-Rahman has made correlation between index tests and the engineering properties of Egyption clay from different locations along the Nile valley and Delta.

In (1994) Khamehchiyan and Iwao studied the properties of Ariak soft clay (the most problematic soil in Japan). They made intensive study on its geotechnical properties and make a correlations between physical and mechanical properties with simple regression and multiple regression analysis in spite of the simple regression were enough for estimating.

Isik Yilmaz (2000) perform another study to evaluate the shear strength of clayey soil by using the liquidity index from various locations in Turkey.

On the other hand; USDA published a data and make a correlation between soil plasticity as well as plasticity index and strength parameter (residual strength) (USDA, 2004).

Al-Busoda (2009) evaluate and correlate between physical and engineering properties of Baghdad cohesive soil based on Atterberg limits and unit weight tests.

GEOTECHNICAL PROPERTIES OF Al-AMMARAH SOIL.

Physical Properties

The collected physical and mechanicsl properties of Al-Ammarah silty clay soil is presented in Table (1). The plasticity chart is shown in Figure (3); the relation between plasticity index PI, and liquid limit LL, is shown in Figure (4).

Table (1) The soil properties of Al-Ammarah soil

Soil properties	Range
Physical properties:	
Gs	**2.62-2.82**
Void ratio e	**0.687-0.998**
Liquid limit	**22-62**
Plasticity Index	**5-34**
Liquidity Index	**0.43-2.78**
Natural water content	**10.27-39.2**
Total unit weight (kN/m^3)	**18.29-20.17**
Mechanical properties:	
SPT	**3-50**
Unconfined compressive strength (kN/m^2)	**44.0-296.6**
Compression index	**0.125-0.458**
Swelling index	**0.016-0.043**

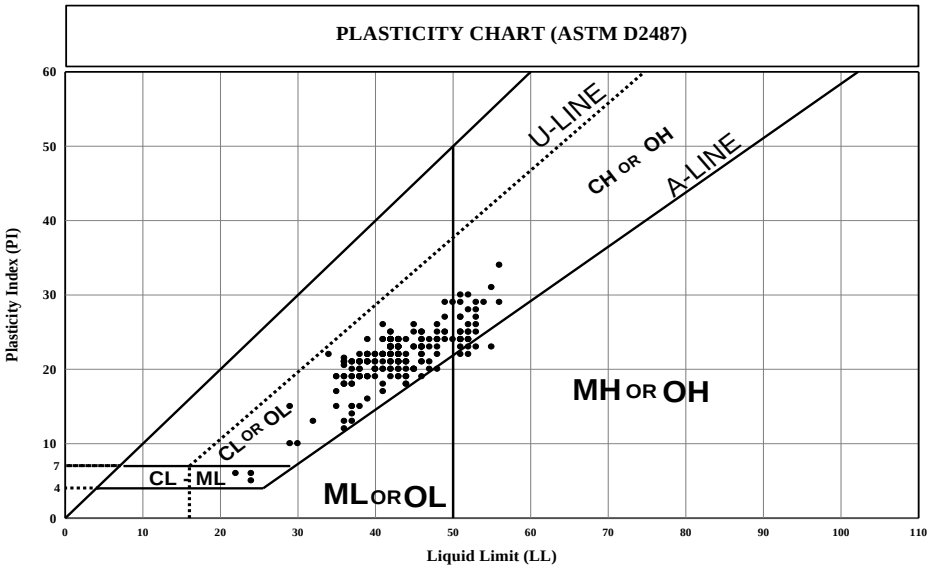

Figure (3) The Unified Soil Classification chart for Ammarah soil.

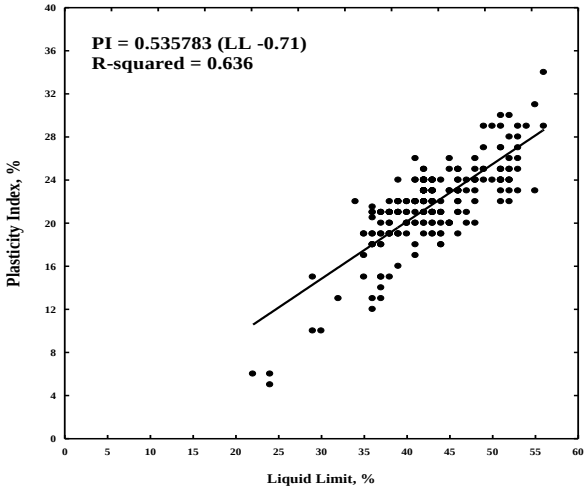

Figure (4) Relation between plasticity index and liquid limit.

From these figures it can be seen that all the cohesive soil-according to USCS-at the investigated area are clayey soil with low to high plasticity (CH to CL). To compare these results with the plasticity chart; Figure (4) was drawn. From this figure it can be seen that the fitting line can be described by the following equation:

$$PI = 0.536\ (LL-0.71) \quad (1)$$

While the equation of the A-Line is **[PI = 0.73 (LL-10)]**

The relation between total density and initial void ration is presented in Figure (5). The correlation for this figure can be given by the nonlinear equation with correlation coefficient of 0.811:

$$\gamma_t = 30.28 - 21.46\, e_o + 10.17\, e_o^2 \quad (2)$$

The relation between initial void ratio e_o and natural water content ω_n is given in Figure (6) and can be represented by the following equation with correlation coefficient equals 0.945.

$$e_o = 0.025\, \omega_n + 0.078 \quad (3)$$

4.2 MECHANICAL PROPERTIES

The summary of the ranges for mechanical properties of Ammarah city are presented in Table (1). Single regression analysis was adopted to obtain the relations between mechanical properties and physical properties of Ammarah city**.**

- ***COMPRESSIBILITY***

The variation of swelling index c_s with compression index c_c is presented in Figure (7) and this variation can be represented by the following equation with a correlation coefficient of 0.97.

$$c_s = 0.091\, c_c \quad (4)$$

Equation (4) satisfies the variation of c_s with c_c for most clayey soils. Bowles (1996) stated that c_s=0.05 to 0.10 c_c.

The relation between compression index c_c and liquidity index LI, is shown in Figure (8). This variation can be described by the following equation with correlation coefficient of 0.61 as.

$$c_c = 0.24\, LI + 0.21 \quad (5)$$

In Figure (9) the relation between compression index and natural water content. This relation can be written by the following equation with correlation coefficient of 0.946.

$$c_c = 0.0092\, \omega_n \quad (6)$$

The relation between swelling index and natural water content is shown in Figure (10) with a correlation coefficient of 0.975.

$$c_s = 0.00087\, \omega_n \quad (7)$$

The relation between compression index and liquid limit as shown in figure (14) with coefficient of 0.868, when compared this equation with correlation equation of Terzaghi and Peck its found that the curve run above Terzaghi line.

$$c_c = 0.00556\, LL \quad (8)$$

$$c_c = 0.009\, (LL-10) \text{ (Terzaghi and Peck)} \quad (9)$$

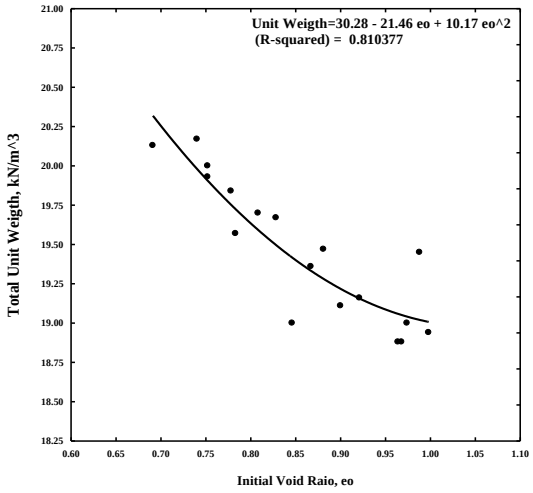

Figure (5) Relation between total unit weight and initial void ratio.

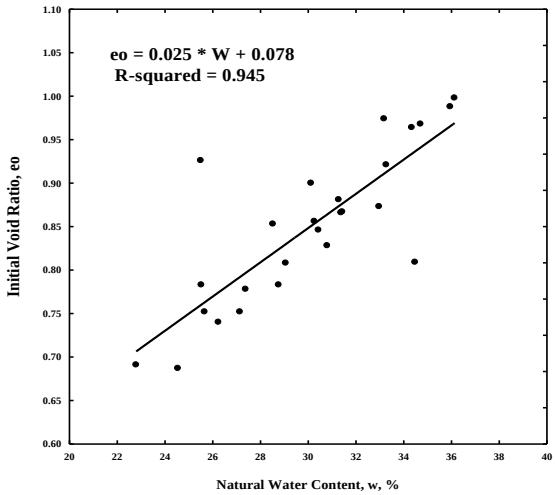

Figure (6) Relation between initial void ratio and natural water content.

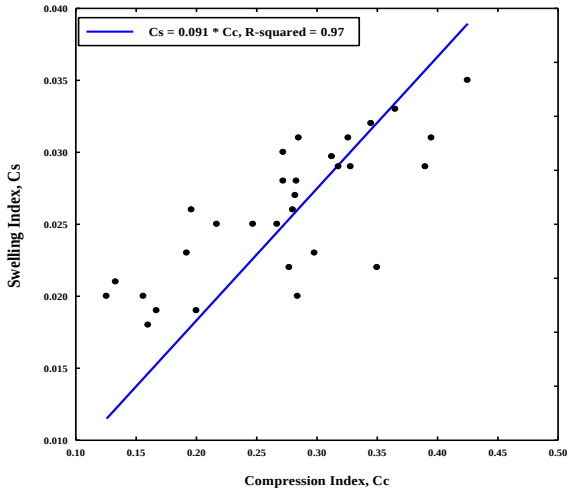

Figure (7) Relation between swelling index and compression index.

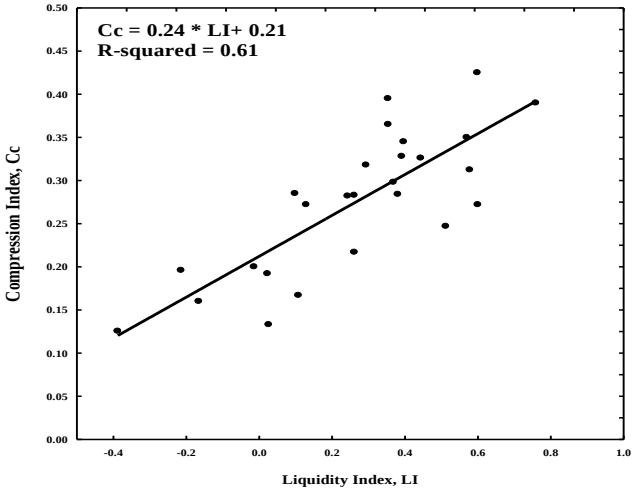

Figure (8) Relation between Compression index and Liquidity index.

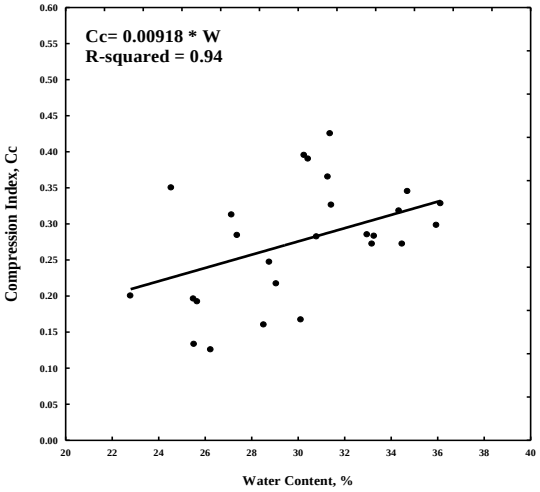

Figure (9) Relation between compression index and natural water content.

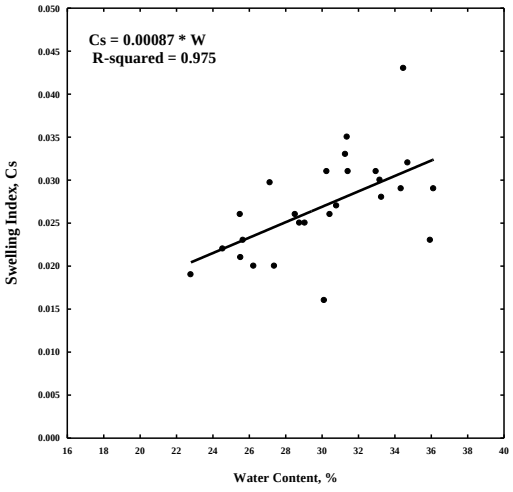

Figure (10) Relation between swelling index and natural water content.

Unconfined Compressive Strength

The shear strength of a soil is the internal resistance per unit area that the soil mass can offer to resist failure and sliding along any plane inside it. Therefore, the engineer should understand the nature of shearing resistance in order to analyze soil stability problems such as bearing capacity, slope stability and lateral pressure on earth retaining structures (Das, 2002).

The shear strength parameters dependent on type of laboratory test, previous stress history, particle packing, grain shape and water table, one of the tests that obtained from it the shear strength helping for obtained the bearing capacity that used in design is unconfined compression test. With these considerations, from figure (11) the relation between unconfined compressive strength qu and liquidity index LI, with correlation coefficient 0.53.

$$qu = 186.3-172.5\ LI + 24.2\ LI^2 \quad (10)$$

The relation between unconfined compressive strength to standard penetration test qu /SPT to plasticity index PI, with coefficient of 0.872 as shown in figure (12).

$$qu/SPT = 0.186\ PI \quad (11)$$

From figure (13) the relation of qu to standard penetration test SPT with coefficient of 0.898.

$$qu = 4.24\ SPT \quad (12)$$

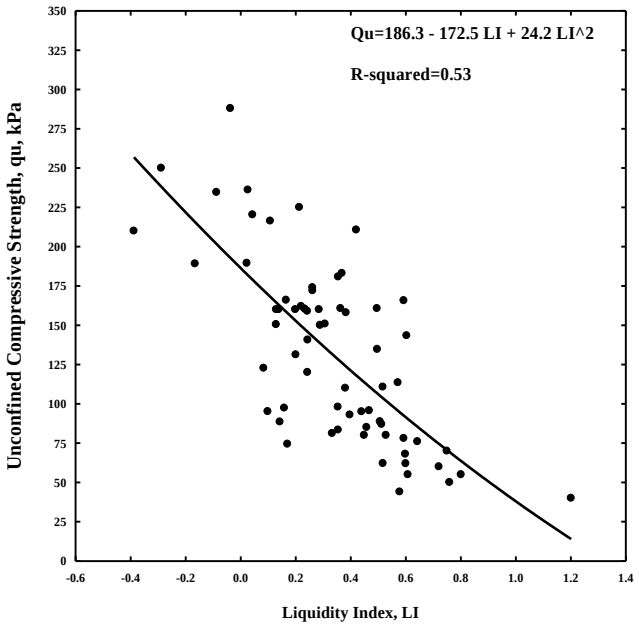

Figure (11) Relation between unconfined compressive strength and liquidity index.

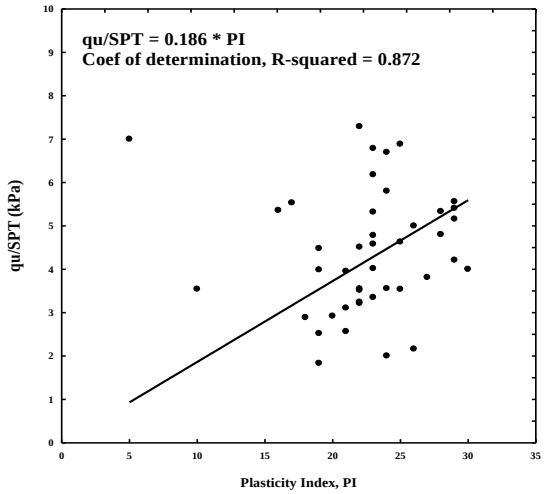

Figure (12) Relation between unconfined compressive strength to standard penetration test and plasticity index.

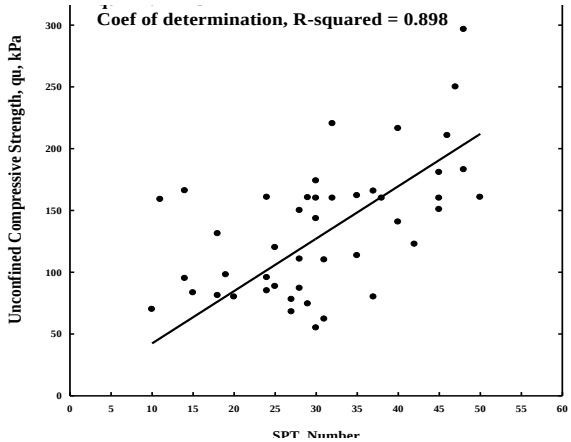

Figure (13) Relation between unconfined compressive strength and standard penetration test.

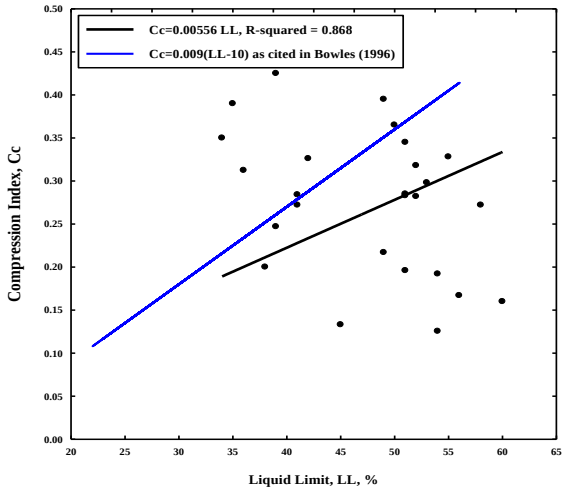

Figure (14) Relation between Compression index and liquid limit.

SUMMARY OF THE RESULT

From all the correlation that connect between physical and mechanical propreties of Ammarah soil, it can be summarized in table (2):

Table (2) Summary of the correlations between physical and mechanical properties of Ammarah soil.

Parameter	Equation	R^2	Equation number	Figure number
|PI	$PI = 0.536 (LL-0.71)$	0.636	1	4
γ_t	$\gamma_t = 30.28 – 21.46\ e_o + 10.17\ e_o^2$	0.811	2	5
e_o	$e_o = 0.025\ \omega_n + 0.078$	0.945	3	6
c_s	$c_s = 0.091\ c_c$	0.97	4	7
c_c	$c_c = 0.24\ LI + 0.21$	0.61	5	8
c_c	$c_c = 0.0092\ \omega_n$	0.946	6	9
c_s	$c_s = 0.00087\ \omega_n$	0.975	7	10
c_c	$c_c = 0.00556\ LL$	0.868	8	14
qu	$qu = 186.3-172.5\ LI + 24.2\ LI^2$	0.53	10	11
qu/SPT	$qu/SPT = 0.186\ PI$	0.872	11	12
qu	$qu = 4.24\ SPT$	0.898	12	13

CONCLISION

The soil of Al-Ammarah city is found to be clayey silt to silty clay with low to high plasticity with:

- For physical properties the equation of (1-3) can be useful and easy to find plasticity index, total unit weight and initial void ratio without using and preliminary test from liquid limit, initial void ratio or natural water content.
- The cost of consolidation test is high in comparison with other tests. So, the equation (4-8)
- it's easy way and power full for estimating the compression index and swelling index.
- Also, the unconfined compressive test is not always available. So, equation (10-12) consider convenient and simple for estimating the compressive strength by knowing plasticity index , liquidity index or number of drops.
- The correlation equation of 4 and equation 8 is considered more convenient, simple and easy for estimating swell index and compressibility index.

LIST OF SYMBOLS

c_c = compressibility index.

c_s = swelling index.

e_o= initial void ratio.

LI= Liquit index.

LL= Liquid limit.

Qu = Unconfined compressive strength.

R^2 = Coefficient of determination

SPT = Standard compressive strength.

γ_t = Total unit weigth.

ω_n = natural water content.

REFERENCES

- Abdel-Rahman, G. E. (1982) " Correlations Between index tests and the properties of Egyption Clay". Ms.C. Thesis, college of engineering, university of Cairo.

- Al-Busoda, b. S. Z. (2009) "Evaluation and correlations Associated with liquid Limit and Plasticity index of Baghdad Cohesive Soil", The 6th Engineering Conference, Proceedings of the Conference, Civil Engineering, Volume 1.

- Bowels, J.E. (1996) " Foundation Analysis and Design". McGraw-Hill Companies.

- Buringh, P. (1960) " Soil and condition in Iraq" Ministry of Agriculture, Baghdad.

- Das, B.M. (2002) " Principles of Geotechnical Engineering". Fifth edition, Wadsworth Group.

- Khamehchiyan, M. and Iwao, Y. (1994) "Geotechnical properties of Ariake clay in Saga Plain- Japan". Journal of Geotechnical Engineering, No.505, V.29, PP. 11-18, December.

- Rahardjo, P.P. (2007) " In situ testing and soil properties correlations". In conjunction with International Conference on In Situ Measurement of Soil Properties and Case Histories, Parahyangan Catholic University.

- USDA, (2004) " Correlations between soil plasticity and strength Parameters". Advanced Engineering Geology & Geotechnics.

- Yilmaz., Isik (2000) "Evaluation of shear strength of of clayey soils by using their liquidity index". Bull Eng. Geo. Env., V. 59, P. 227-229.

DEVELOPING A METHODOLOGY TO PREPARE DESIGN ACCORDING TO PRODUCTION REQUIREMENT

Asst. Prof. Dr. Ghassan A. AL – Kindi
Mechanical Engineering Department
University of Technology

Kawakib A. K. AL – Mendwi
Mechanical Engineering Department
University of Baghdad

ABSTRACT:

This paper aims to develop a program based on a methodology to enable the preparation of design according to production requirement. Thus, the appropriate algorithms were developed to evaluate the product design according to assembly requirements and also to assess the product design according to manufacturing requirements.

The programs were applied to four case studies, two of them for Design for Assembly (DFA) and other two were for Design for Manufacturing (DFM). The study concluded that the method gives very good results for (DFA) and results of the studied two cases showed to lower the total assembly time, as well as increases the quality of the operation by lowering the probability of error expectation. However, results of (DFM) studies cases showed that the proposed program needs more development to cover all factors affecting the manufacturing processes.

The paper concluded that the suggested and developed DFA and DFM programs are a valid and beneficial approach; however, more research work is required to establish a complete and comprehensive database to match the experience of human experts in the field. Adding such database to the developed programs will increase its reliability and applicability.

KEYWORDS:
Concurrent Engineering, Design for Assembly, Design for Manufacturing.

الخلاصة :

يهدف هذا البحث إلى تطوير خوارزميات مناسبة لكي تمكن من إعداد التصاميم على ضوء متطلبات الإنتاج. لذلك طورت الخوارزميات الملائمة لكي تقيم تصميم المنتج على ضوء متطلبات التجميع وكذلك لكي تساند تصميم المنتج على ضوء متطلبات التصنيع.

طبقت البرامج على أربع حالات دراسية, اثنان منها للتصميم لغرض التجميع والاثنان الآخران للتصميم لغرض التصنيع. استنتجت الدراسة آن الطريقة أعطت نتائج جيدة جدا للتصميم لغرض التجميع ونتائج الحالتين الدراسيتين أظهرت تقليل زمن التجميع الكلي وكذلك زيادة النوعية للعملية عن طريق تقليل احتمالية الخطأ المتوقع. مع ذلك, أظهرت نتائج الحالتين الدراسيتين للتصميم لغرض التصنيع إن البرنامج المقترح يحتاج إلى تطوير اكثر لكي يغطي كل المتغيرات المؤثرة في العمليات التصنيعية.

لقد استنتج البحث على أن الطريقة المقترحة في تقييم التصميم لغرض التجميع والتصميم لغرض التصنيع باستخدام البرامج المقترحة والمطورة هو توجه فعال ومفيد, ومع ذلك يتطلب عمل بحوث اكثر لكي يرسخ قاعدة بيانات واسعة وشاملة تجاري الخبرة البشرية في هذا المجال. إضافة مثل قاعدة البيانات هذه إلى البرامج المطورة سوف يرفع من معوليتها وقابليتها على التطبيق.

INTRODUCTION:

Major changes in product design practices are occurring in all phases of the "new product development process". These changes, therefore, will have a significant impact on cost. Hence, addressing all product aspects including cost during the design stage will reduce costs [Bedworth, D. 91]. This approach is usually referred to as Concurrent Engineering (CE) [Singh, N. 96], which is a systematic approach to the integrated, concurrent design of products and their related processes, including manufacture and assembly.

In this paper a methodology is developed as a computer program to enable the preparation of product design according to production requirements. Two phase of production tasks were selected to be the main objectives in the developed methodology. These are manufacturing and assembly

DESIGN FOR ASSEMBLY (DFA): Very often, the most significant benefits with design for assembly come by simplifying the product so that it has fewer parts which conclude on easier and faster assembly process [Bralla, J. 99].

DESIGN FOR MANUFACTURING (DFM): It is important for the manufacturing engineer to act as an advisor to the design engineer in matters of manufacturability because manufacturability matters, not only to the production departments but to the design engineer. A product design that is functionally superior and at the same time can be produced at minimum cost holds the greatest promise of success in the marketplace. Successful careers in design engineering are built on successful products. [Groover, M. 02]:

It is important to make the right manufacturing decisions early in the design process, before the cost penalty of making changes becomes too high [Esawi, A. and Ashby, M. 98]. The selection of appropriate processes for a particular part is based upon a matching of the required attributes of the part and the various process capabilities [Boothroyd, G., Dewhurst, P., Winston, K., 02].

Manufacturing process can be analyzed to determine the range of its capabilities in terms of attributes of the parts that can be produced. Included in these capabilities are shape features that can be produced, natural tolerance ranges, surface roughness capabilities, and so on. These capabilities determine whether a process can be used to produce the corresponding part attributes [Boothroyd, G., Dewhurst, P., and Winston, K., 02].

The materials selected for a design often will determine the fabrication processes that can be used to manufacture the product, its performance characteristics, and its recyclability and environmental impact. As result, engineers should acquire a robust understanding of material characteristics and criteria that one should use in making material selection.

Engineers must select the most appropriate materials for their designs, that is, materials that match both the performance requirements of the product and processing requirements for its manufacture [Voland, G., 99].

Unnecessarily tight tolerances result in high production costs, yet the tolerances should ensure that the functional performance requirements of the products stay within a satisfactory range. Tolerances which are too loose can affect the product quality, and increase the scrap rate and production costs [Ji, S., and others, 00].

In a machining operation, the machined parts may appear to be identical, but close inspection reveals dimensional differences form one part to the next. Manufacturing variations can be divided into two types: random and assignable. One important measure usually used in the evaluation of manufacturing is the process capability [Groover, M., 02] which can be defined as follows:

$$\text{Process Capability} = \mu \pm 3\sigma \quad (3)$$

Where μ = process mean, which is set at the nominal value of the product characteristic when bilateral tolerancing is used; and σ = standard deviation of the process.

THE PROPOSED SYSTEM ARCHITECTURE: The developed system architecture which is programmed in C^{++} language is shown in figure (1) as a block diagram. It describes the process of analyzing product designs in order to identify design changes that improve assembly and manufacturing efficiency. The process consists of the main steps: (1) DFA, (2) DFM which consist of (a) selection of materials and processes, (b) selection of tolerance and secondary operation (3) design guidelines and recommendation. References [Bralla, J. 99, Boothroyd, G., Dewhurst, P., and Winston, K., 02, Whitney, D., 04, Zendin, K., 01 and Anderson, D., 04] are used as the sources of the standard data implemented in the developed system program.

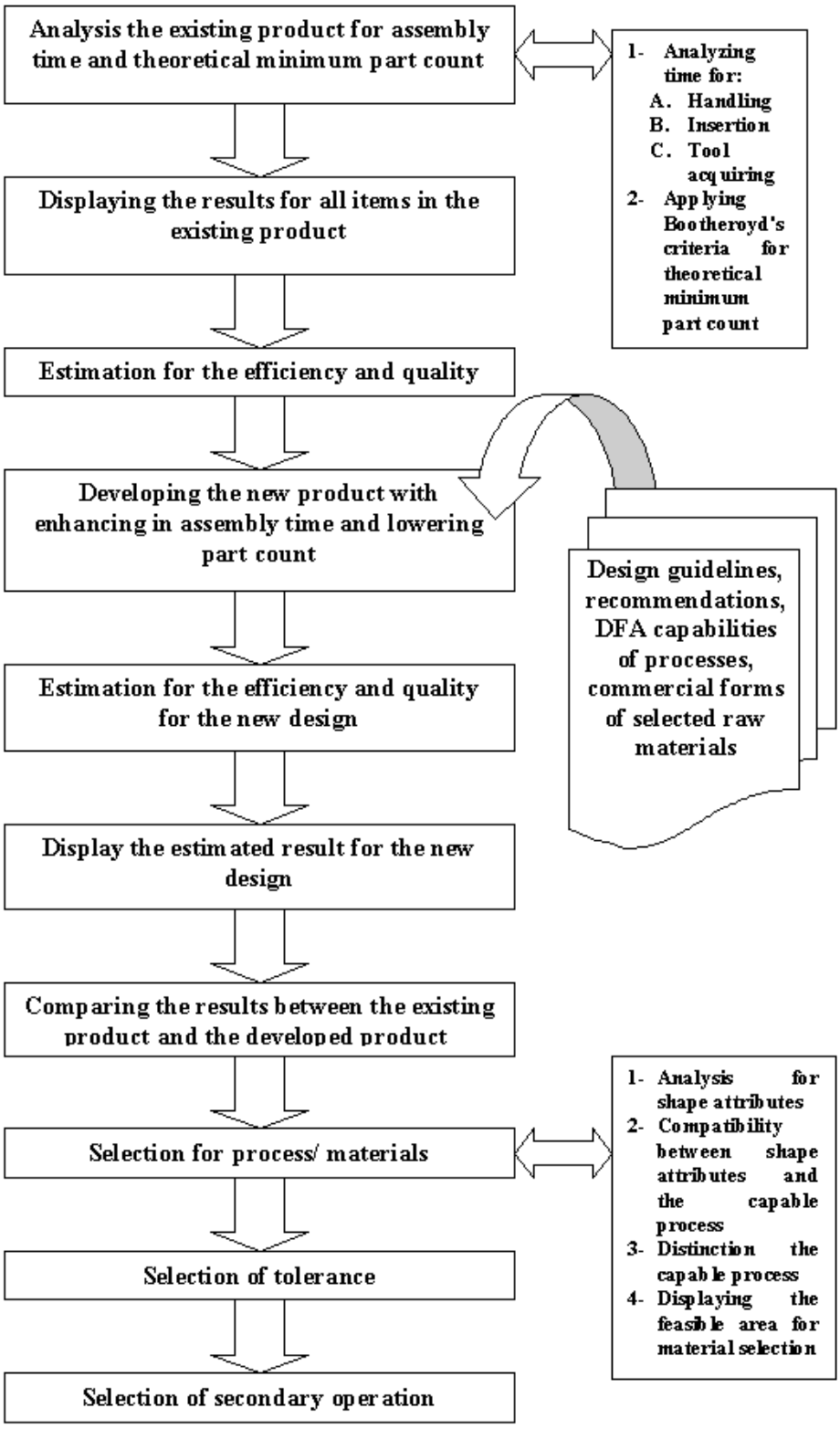

Figure (1) Block diagram of the proposed system

A. Design for Assembly: The part of the developed program that deals with the DFA is illustrated as a flow chart in figure (2), and starts with a main menu to acquire the followings:

a. Input:

- Product's name.
- Item's name.
- Item's number.

b. Select symmetry angle degree for both Alpha[1] and Beta[2].

- Type of item as part or operation.
- Part weight as less then 9 Kg. or equal or more then 9 Kg (see figure (3)).

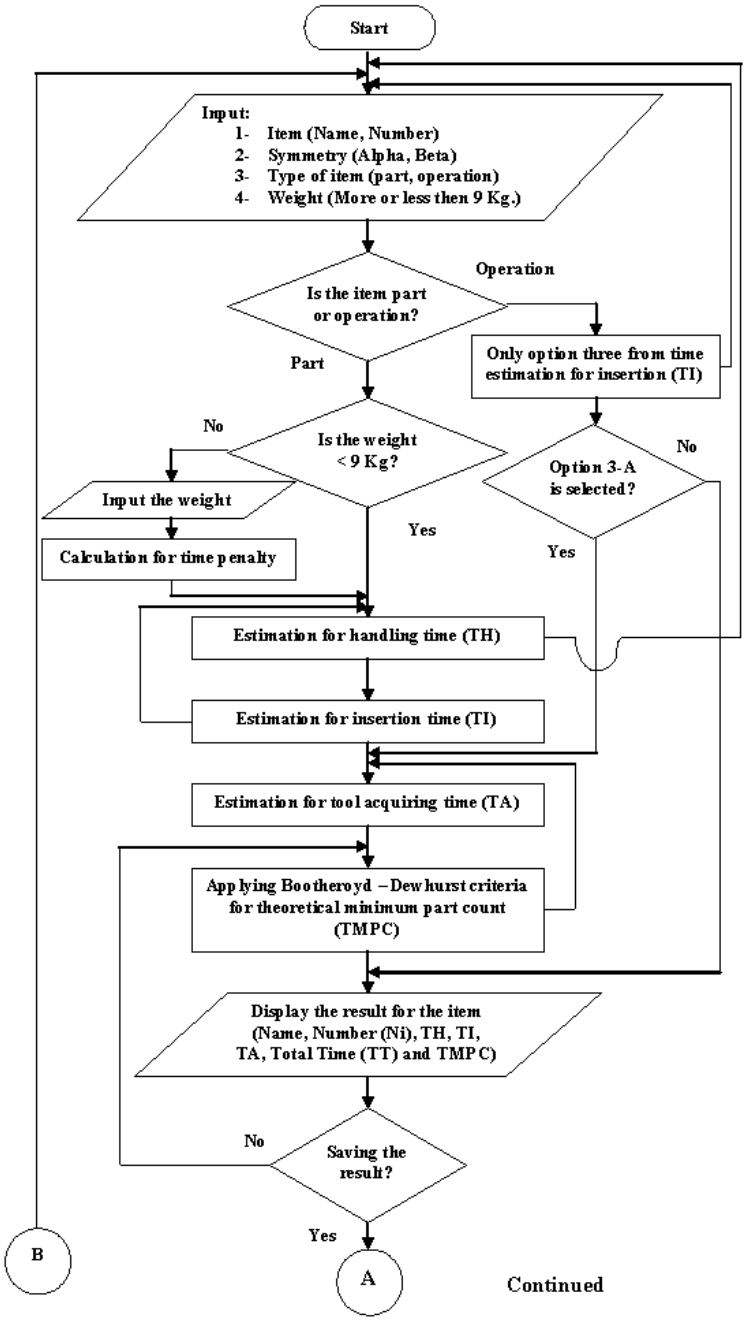

[1] **Alpha symmetry:** it is the rotational symmetry of a part about an axis perpendicular to its axis of insertion. For parts with one axis of insertion, end-to-end orientation is necessary when alpha equals 360 degrees, otherwise equals 180 degrees.

[2] **Beta symmetry:** It is the rotational symmetry of a part about its axis of insertion. The magnitude of rotational symmetry is the smallest angle through which the part can be rotated and repeat its orientation. For cylinder inserted into a circular hole, beta equals zero.

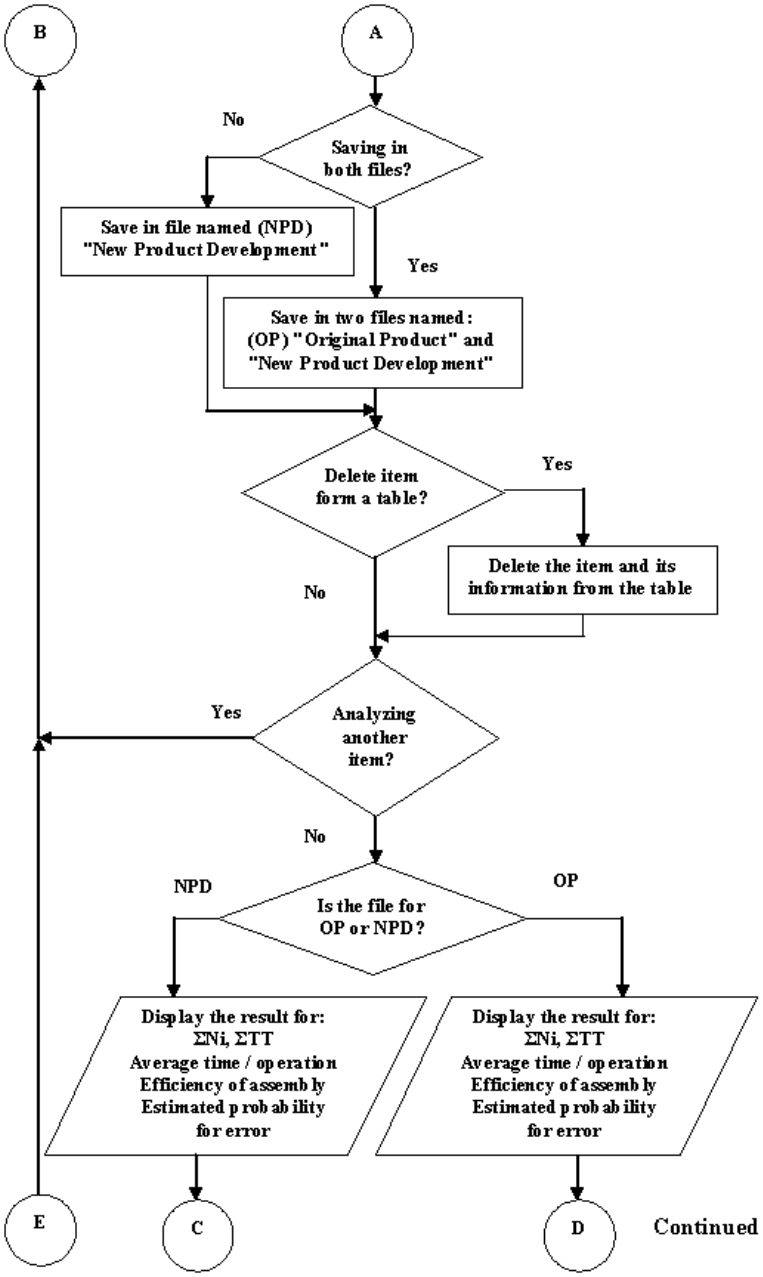
B
A
No
Saving in both files?
Save in file named (NPD) "New Product Development"
Yes
Save in two files named: (OP) "Original Product" and "New Product Development"
Delete item form a table?
Yes
Delete the item and its information from the table
No
Yes
Analyzing another item?
No
NPD
Is the file for OP or NPD?
OP
Display the result for: ΣNi, ΣTT Average time / operation Efficiency of assembly Estimated probability for error
Display the result for: ΣNi, ΣTT Average time / operation Efficiency of assembly Estimated probability for error
E
C
D
Continued

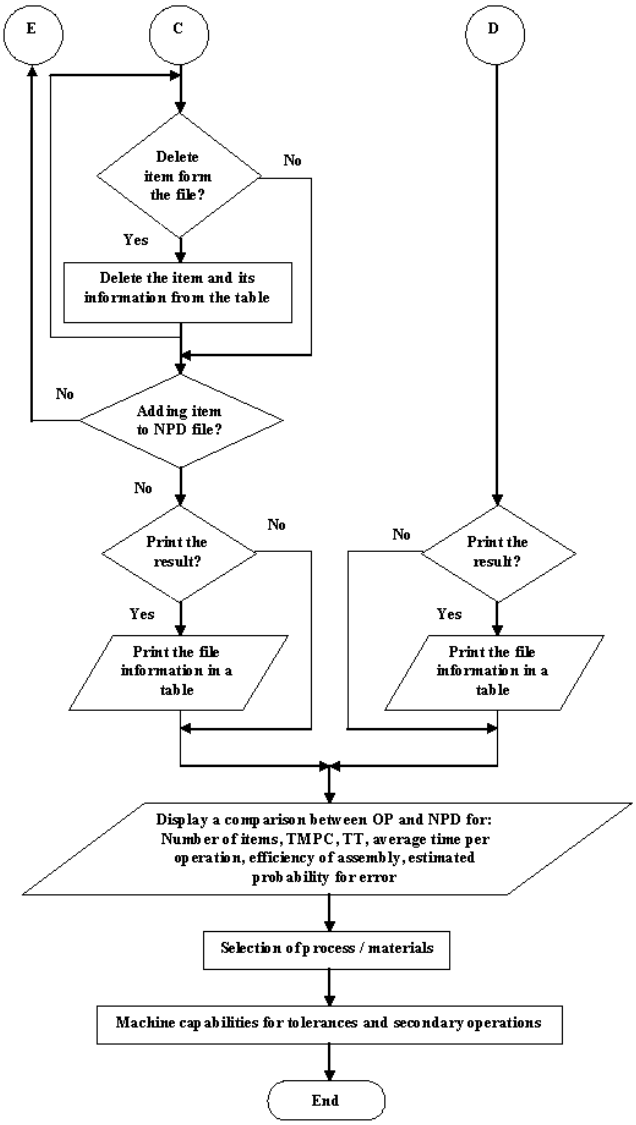

Figure (2) Main flow chart of the proposed program

(A – 1) Time Estimation for Handling: The flow chart of the handling time estimation module is shown in figure (4). However, the flow chart for options one, two, three and four from the handling time estimation module is shown in figures (4 – a), (4 – b), (4 – c) and (4 – d) respectively.

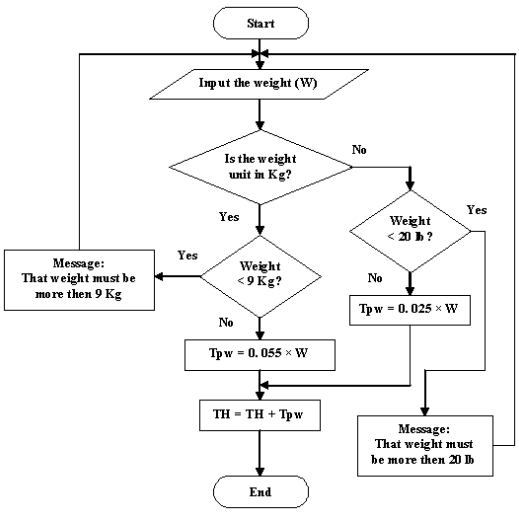

Figure (3) Flow chart of the effect of weight on handling time estimation module

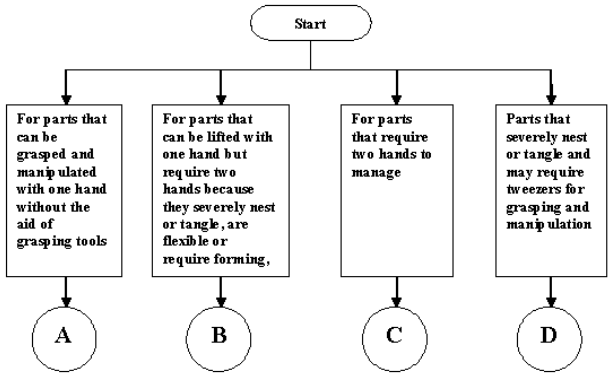

Figure (4) Flow chart of the handling time estimation module

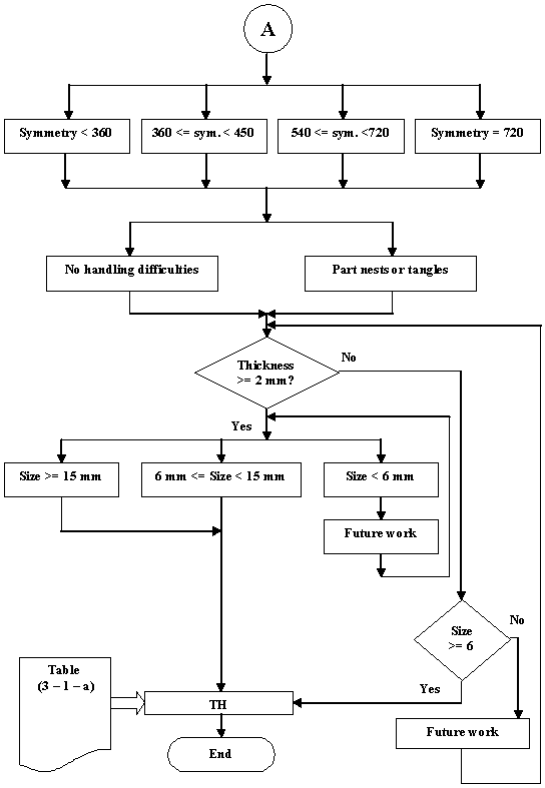

Figure (4 – a) Flow chart of the handling time estimation module for the parts that can be grasped and manipulated with one hand without the aid of grasping tools

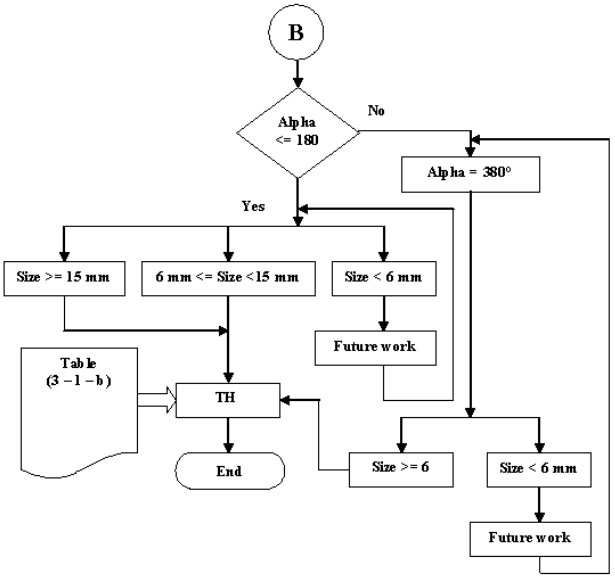

Figure (4 – b) Flow chart of the handling time estimation module for parts that can be lifted with one hand and require two hands

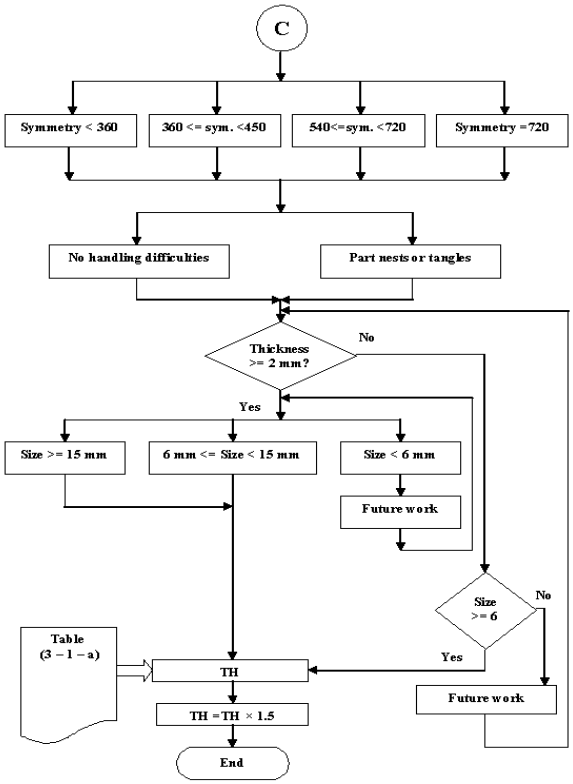

Figure (4 – c) Flow chart of the handling time estimation module for parts that require two hands for manipulation

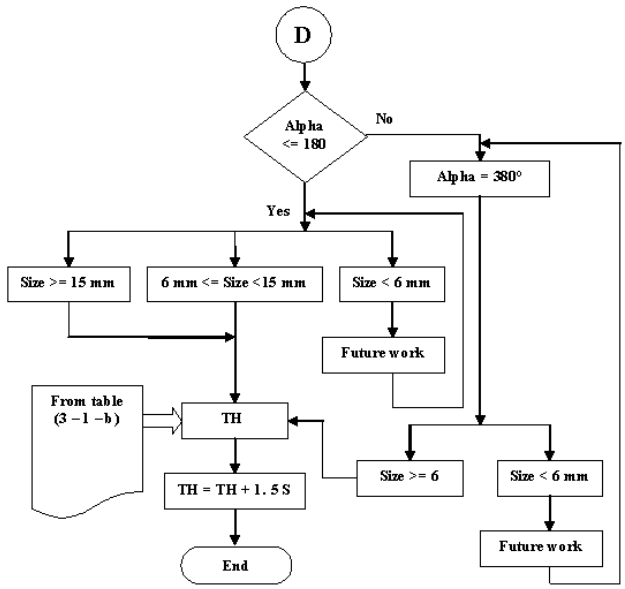

Figure (4– d) Flow chart of the handling time estimation module for parts that severely nest or tangle and may require tweezers for grasping and manipulation

(A – 2) Time Estimation for Insertion: The flow chart that carries insertion time estimation is shown in figure (5). The flow chart for options one, two and three from the insertion time estimation module is shown in figure (5 – a), (5 – b) and (5 – c) respectively

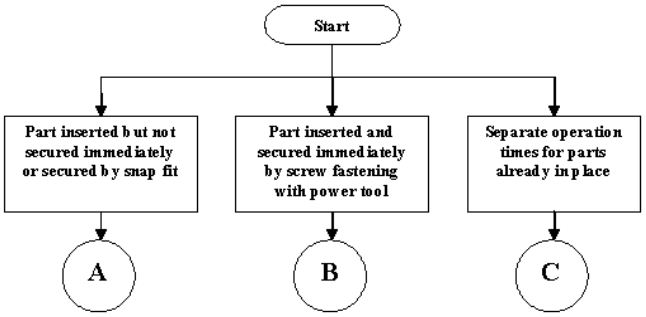

Figure (5) Flow chart of the insertion time estimation module

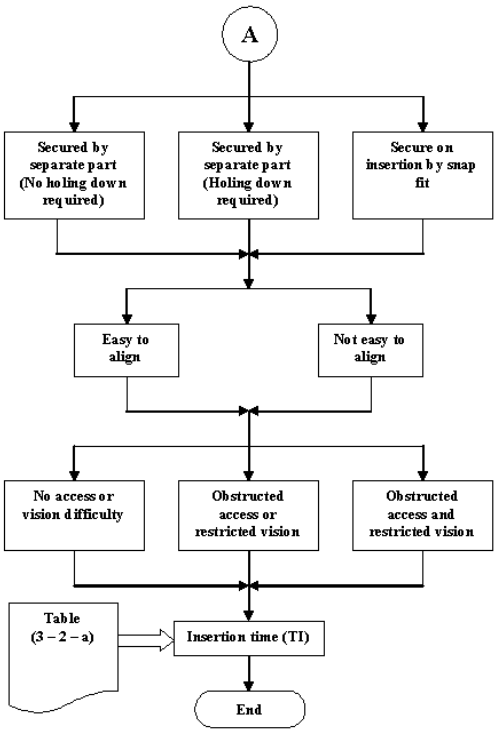

Figure (5 – a) Flow chart of the insertion time estimation module for parts inserted but not secured immediately, or secured by snap fit

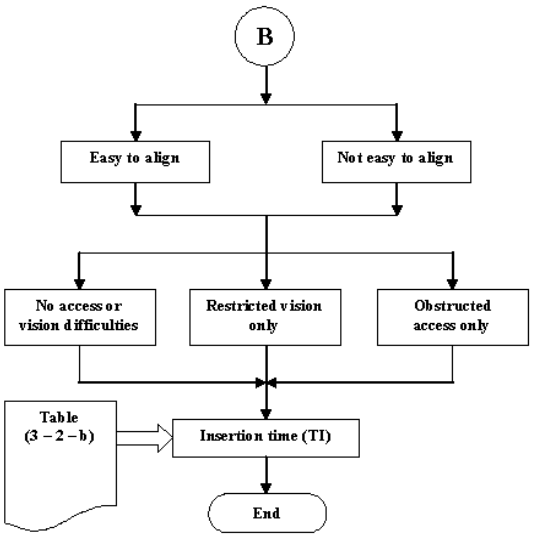

Figure (5 – b) Flow chart of the insertion time estimation module for parts inserted and secured immediately by screw fastening with power tool

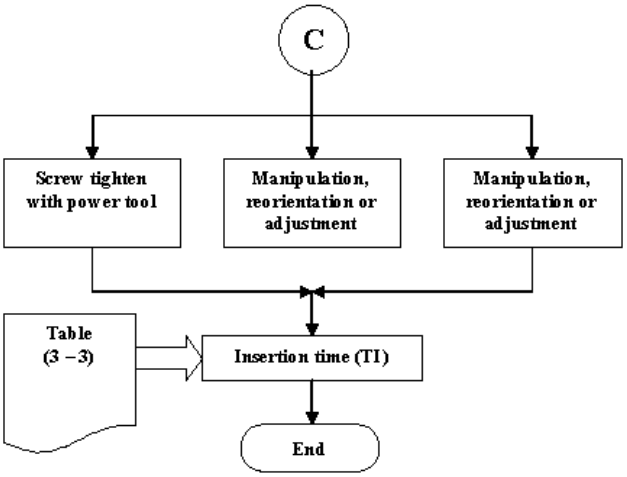

Figure (5 – c) flow chart of the insertion time estimation module for parts inserted separate operation times for solid parts already in place

(A – 3) Time Estimation for Tool Acquiring: The flow chart that represents this part is shown in figure (6).

(A – 4) Theoretical Minimum Part Count Module: The flow chart that represents this module is shown in figure (7).

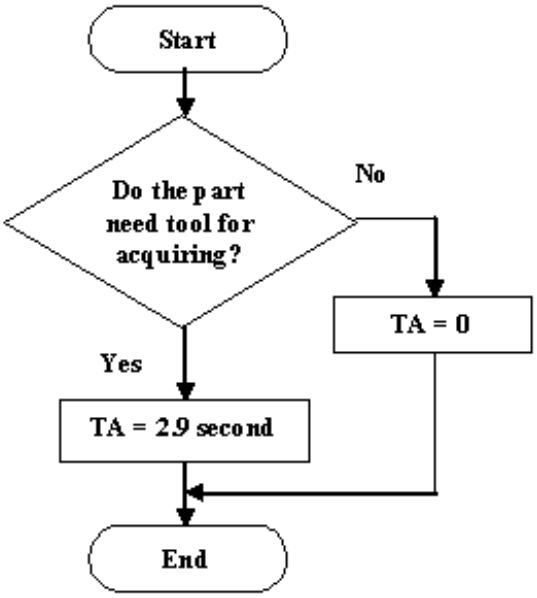

Figure (6) Flow chart for acquiring time estimation module

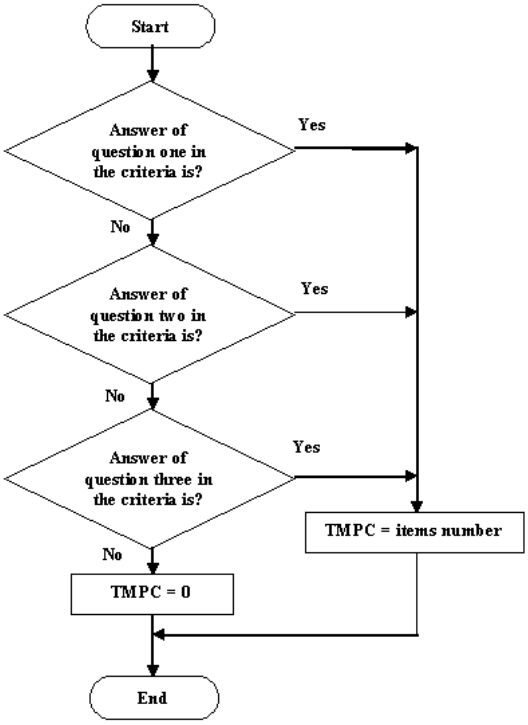

Figure (7) Flow chart of the Theoretical Minimum Part Count (TMPC) module

(A – 5) Creation of the Table "Original Product": This table contains columns for: name of the item, number of items, handling time, insertion time, acquiring time, total time and theoretical minimum part count.

In the end of these columns the user can see a row with the summation of:

a) Number of items.
b) Total time.
c) Theoretical minimum part count.

Results of these columns gives the user quick estimation about the design quality and error expectation in the production process, where the high number of items, total time, and TMPC means low quality and more error expectation in the production process. Lowering of any of these results may raise the quality. TMPC gives the user the minimum number of parts which required not to be exceeded when changing the design in the new product development and give a target for raising the quality and lowering error expectation in the production process whereas trying to be closer to that number, and away to identify possible simplifications in the product structure.

In the end of that table the user can see the results of the followings:

- Average time per operation.
- Percentage efficiency of the assembly (DFA index).
- Percentage estimated error probability.

(A – 6) Creation of the Table "New Product Development": The "New Product Development" table is designed to help in the evaluation of the new design, hence it contains the related information to the "Original Product" table through it belongs to the new design to ease comparisons.

(A – 7) The Comparison between Two Designs: The last menu in DFA analysis program makes a comparison between the two preceding files, this comparison includes:

A. Item Number.
B. Total time.
C. Results of TMPC.
D. Average time per operation.
E. Efficiency of the assembly.
F. Estimated probability.

The program then gives a weight to the part count and time consuming in the assembly operation which can be converted to a cost affecting the product design.

The program is aimed to work with parts that are within easy reach, are not smaller than 6 mm in size, do not stick together, and are not fragile or sharp.

B. Design for Manufacturing: The developed DFM program is aimed to:

1. Appropriate process / material selection based on realistic cost estimates.
2. Establishing or highlighting the relationships between part features and manufacturing costs for a given process.

(B – 1) Selection of Materials and Processes: This part of program is systematic procedure for selection of primary process/ material combinations. Such procedure operates by eliminating processes and materials as more detailed specification of the required part's attributes occurs. The flow chart that represents the selection of material and process is shown in figure (8).

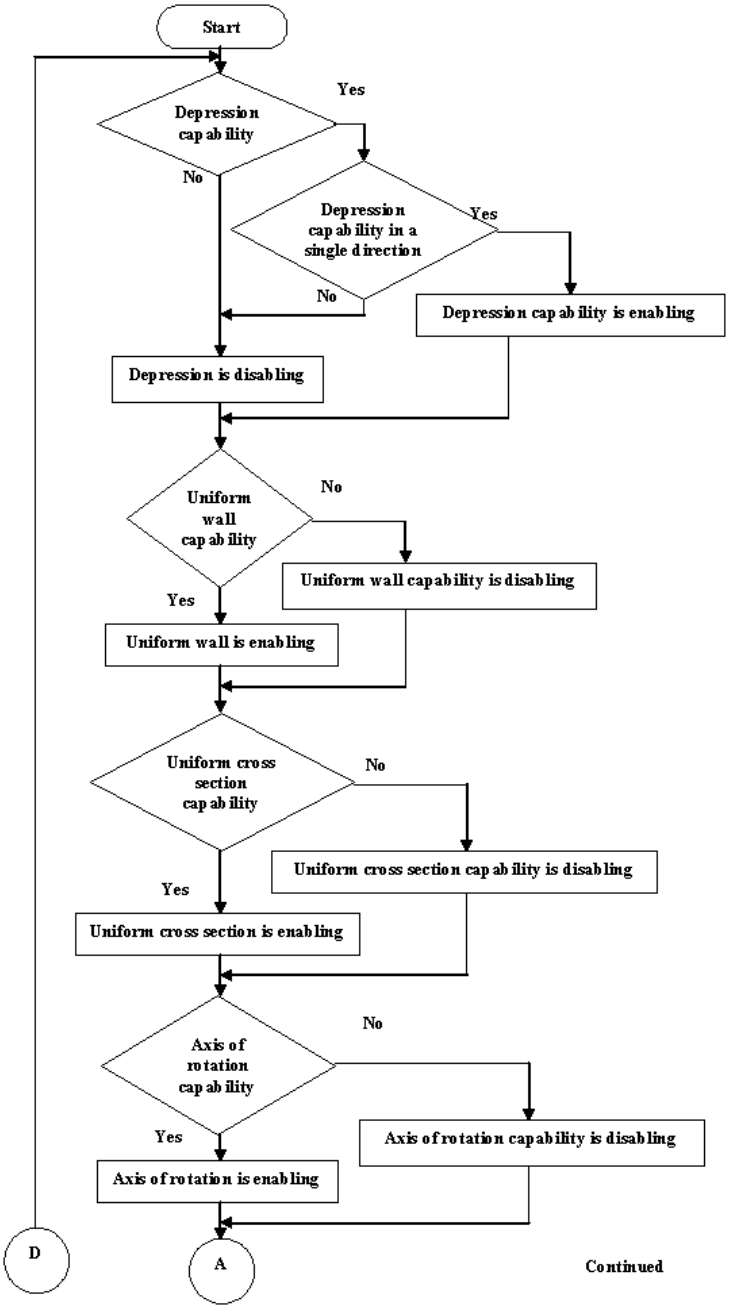
Start
Depression capability
Yes
No
Depression capability in a single direction
Yes
No
Depression capability is enabling
Depression is disabling
Uniform wall capability
No
Uniform wall capability is disabling
Yes
Uniform wall is enabling
Uniform cross section capability
No
Uniform cross section capability is disabling
Yes
Uniform cross section is enabling
Axis of rotation capability
No
Axis of rotation capability is disabling
Yes
Axis of rotation is enabling
D
A
Continued

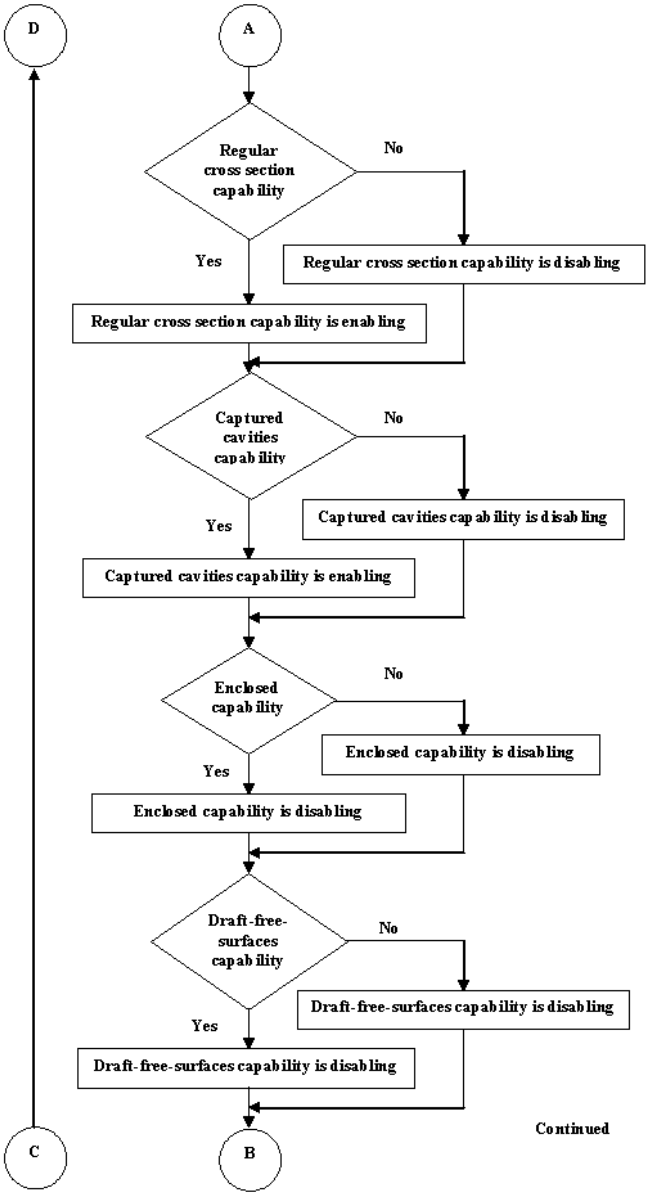
D
A
Regular cross section capability
No
Yes
Regular cross section capability is disabling
Regular cross section capability is enabling
Captured cavities capability
No
Yes
Captured cavities capability is disabling
Captured cavities capability is enabling
Enclosed capability
No
Yes
Enclosed capability is disabling
Enclosed capability is disabling
Draft-free-surfaces capability
No
Yes
Draft-free-surfaces capability is disabling
Draft-free-surfaces capability is disabling
Continued
C
B

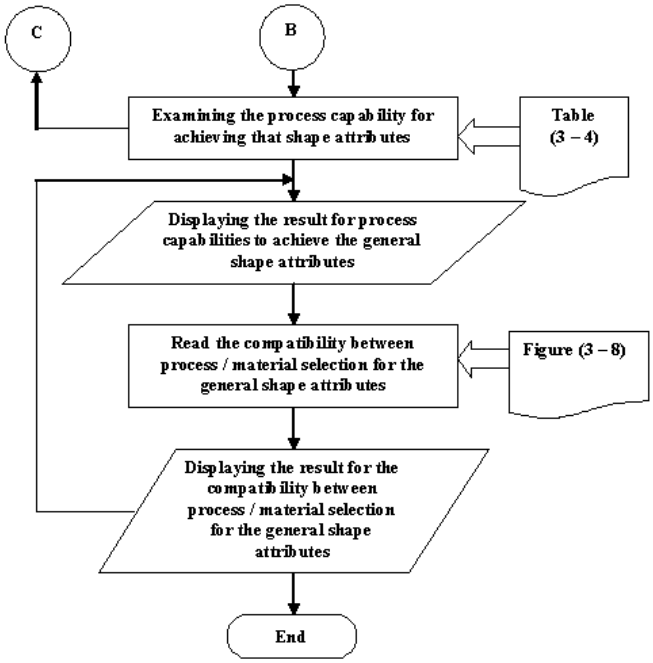

Figure (8) Flow chart of selection of materials and processes module

The program gives the compatibility of the selected shape attribute with the following manufacturing process: Sand casting, Investment casting, Die casting, Injection molding, Structural foam molding, Blow molding (extrusion), Blow molding (injection), Rotational molding, Impact extrusion, Cold heading, Closed die forging, Powder metal parts, Hot extrusion, Rotary swaging, Machining (from stock), ECM, EDM, Wire – EDM, Sheetmetal stamp /bend, Thermoforming and Metal spinning

The program displays the compatibility between all the capable manufacturing processes for doing the shape attributes with the following materials: Cast iron, Carbon steel, Alloy steel, Stainless steel, Aluminum and its alloys, Copper and its alloys, Zinc and its alloys, Magnesium and its alloys, Titanium and its alloys, Nickel and its alloys, Refractory metals, Thermoplastics and Thermosets.

All manufacturing processes that are incapable of achieving the shape attribute are displayed by the program with shaded colour for all available materials.

All manufacturing processes that are capable of achieving the shape attribute are displayed by the program with white, gray and black cells for normal practice, less common and not applicable for practice with each particular material.

The obtained combinations can then be ranked by other criteria, such as estimates of manufacturing costs.

(B – 2) Machine Capabilities for the Selected Tolerances and Secondary Operation: The developed program flow chart that represents this part is shown in figure (9).

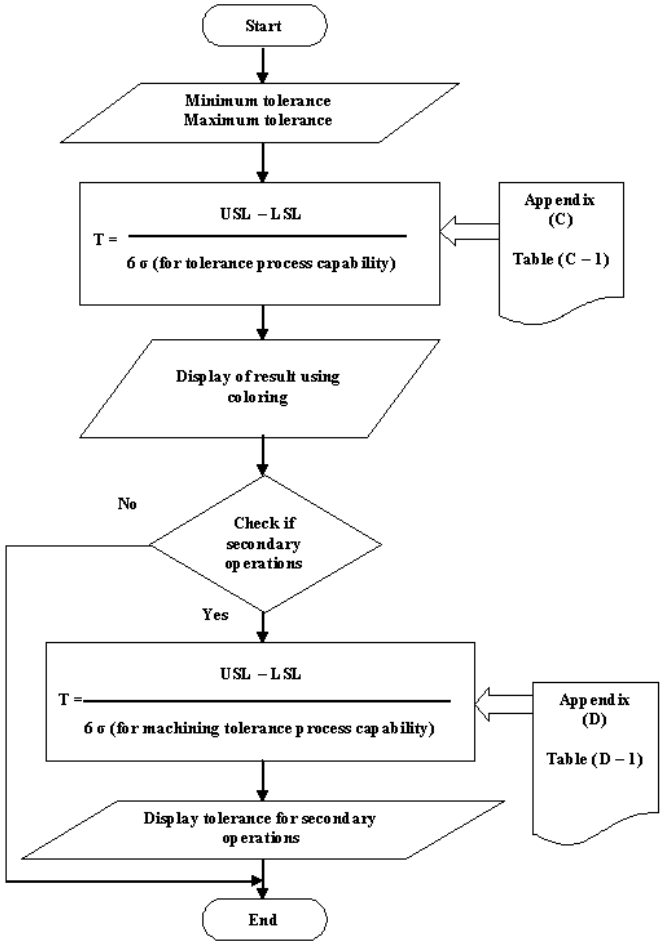

Figure (9) Flow chart of machine capabilities for tolerances and secondary operations module

The program displays the process capability index C_p for tolerance and to all manufacturing process that are examined in the previous section.

C_p index is displayed with five colors; every color refers to different area of C_p.

From the C_p area, the user can distinguish if the specified tolerance is inadequate, sufficient or tighter than necessary for a particular manufacturing process, and if it needs a secondary operation.

If the tolerance is inadequate, and needs a secondary operation, the program displays the machine capability of following machining processes operation: Rough machining, Standard machining, Fine machining, Grinding and Honing.

C. Design Principles and Guidelines

The proposed and developed system gives design principles and guidelines as a help in the program to enable the designer to develop the new design to be easer in manufacturing and assembly. These help include:

C – 1 Capabilities of the Manufacturing Processes: The proposed program displays the main capabilities of the twenty- one manufacturing processes that deals with many properties, comments and guidelines such us: Part size, Tolerances, Surface finish, Shapes produced competitively, Process limitations, Typical application, Comments, Typical characteristics of that manufacturing process, Economic production quantities and General design considerations.

C – 2 Design for Manufacturing and Assembly Guidelines: The proposed program displays about forty guidelines for manufacturing and assembly to help the designer changing the existing design to a better developed one.

C – 3 DFA Compatibility Attributes: The program also displays the main compatibility of attributes of the twenty- one manufacturing processes together with the related DFA guidelines. The attributes are: Part consolidation, Alignment features and Integral fasteners.

C – 4 The Common Commercial Forms of Selected Raw Materials: The program displays a table with thirteen cells containing thirteen materials with their commercial form availability in the market: Ingots for casting, Molding compounds, Round bars, Rectangular bars, Tubing, Sheets, Foils or films, Wires and Powder for sintering.

The displayed table also include whether these material forms are usually available, have limited availability or they are rarely or never available. Hence the designer can make the decisions with initial information about the availability of selected raw material.

IMPLEMENTATION RESULTS AND DISCUSSION

A. Design for Assembly: Two case studies are given these includes: Electrical shaver cover (figure 10) and Ball pen (figure 11).

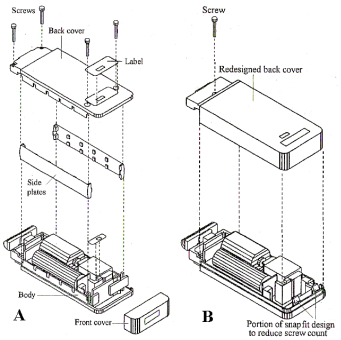

Figure (10) The electrical shaver cover. (a) The original design. (b) The suggested redesign.

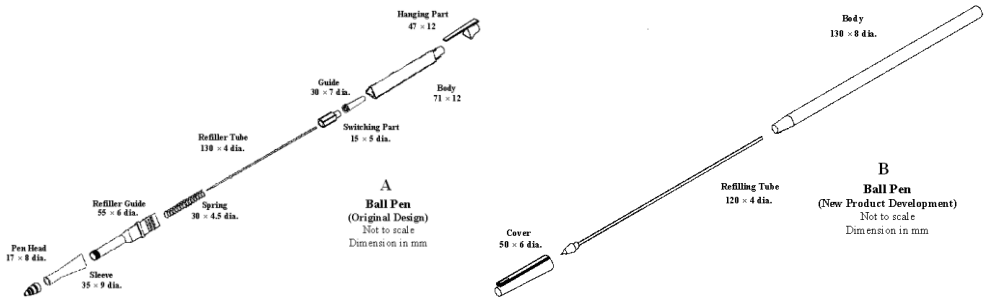

Figure (11) The ball pen. (a) **The original design.** (b) **The new developed design.**

(A – 1) Electrical Shaver Cover Case Study: The original subassembly consists of nine parts: the back cover, the front cover, two side plates that slide into place on the body and are then held in place by the back cover, four screws to secure the back cover to the body, and a label. The redesigned back cover subassembly consists of two parts, a redesigned back cover, and a screw in addition to the body.

The design data of the electrical shaver cover is analyzed step by step and input into the developed program. Results of the program are gained in the form of two tables namely "The original product table" and "The new product development table" which are shown in figures (12) and (13) respectively. However, program results shown in figure (14) presents comparison between the original and the modified design.

According to the acquired results the following enhancements to the design are gained when using the modified design:

a. The number of items decreased by 70 %
b. The total time decreased by 77 %
c. The average time per operation decreased by 23.6 %

d. The efficiency of the assembly increased by 4 times
e. The error expectation probability decreased by 84 %

It is worth to know that the modified design is made to follow the guidelines implemented in the developed program.

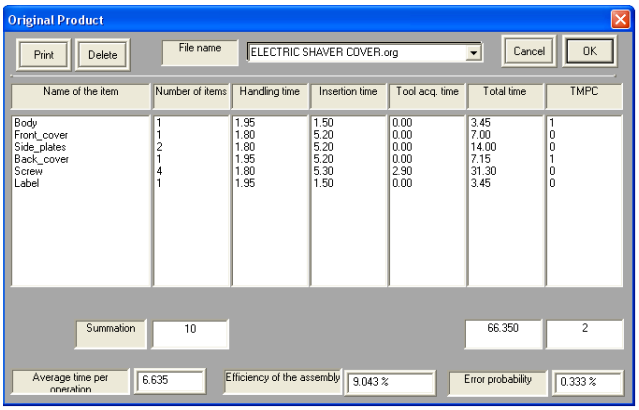

Figure (12) Results of the original design of the electric shaver cover

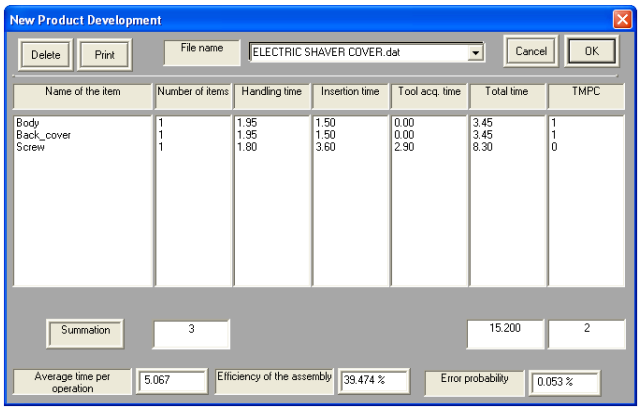

Figure (13) Results of the new product development of the electric shaver cover

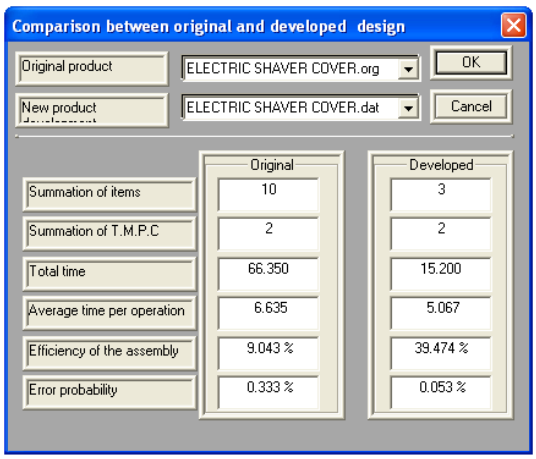

Figure (14) Comparison results of the original and the modified design for the electric shaver cover as acquired from the developed DFA program

(A – 2) The Ball Pen Case Study: A proposed pen design consists of nine parts, namely: body, hanging part, guide, switching part, refilling tube, spring, refiller guide, sleeve, and pen head. The redesigned pen consists of only three parts: Body, refilling tube and the cover.

Two ball pens that match the two designs were taken from the market by the researcher. Tests were conducted to disassemble and reassemble these two ball pens repeatingly for 30 times each to estimate the actual assembly time.

The two ball pens data were analyzed step by step and input to the DFA program which is shown in figures (15) and (16) respectively. However, figure (17) presents the acquired comparisons of results between the two cases of the pen assembly as given by the developed program. It can be seen from these results that the new design of the ball pen which follows the recommendations and guidelines stated in the developed DFA program has enhanced the assembly operation as follows:

a. The number of items decreased by 70 %
b. The total time decreased by 76.7 %
c. The average time per operation decreased by 22.45 %
d. The efficiency of the assembly increased by 4.3 times

e. The error expectation probability decreased by 91.4 %

It is obvious from these results that the enhancement of the assembly operation when implemented in the new design reduced the time required for the assembly operation by about 4.3 times as acquired by the developed DFA program. This reduction of time approximately matches the reduction of time acquired from the actual assembly operations that were conducted by the authors of this paper where about 4.2 times reduction was achieved.

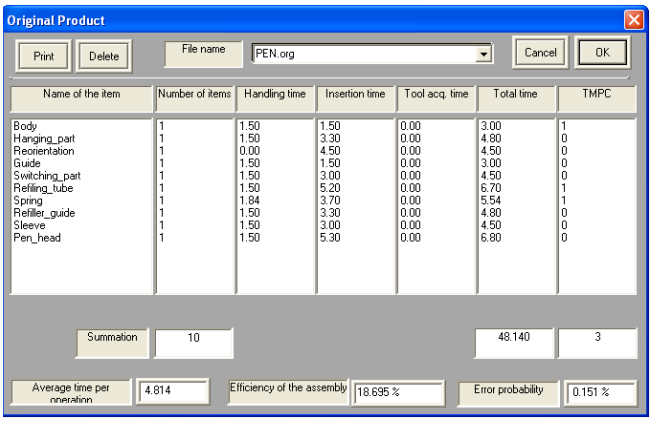

Figure (15) The original product of the ball pen assembly

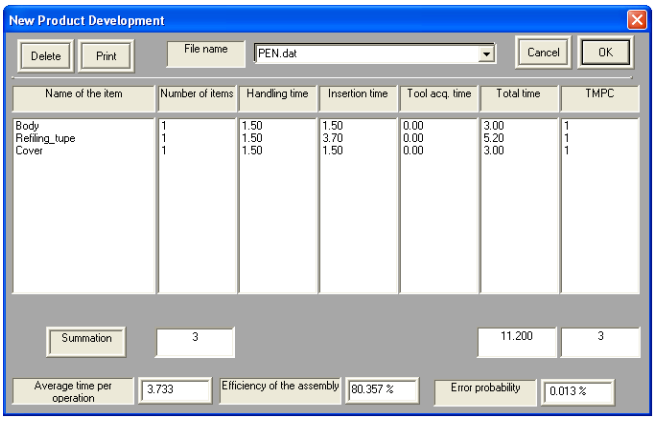

Figure (16) Program results of new design of the ball pen

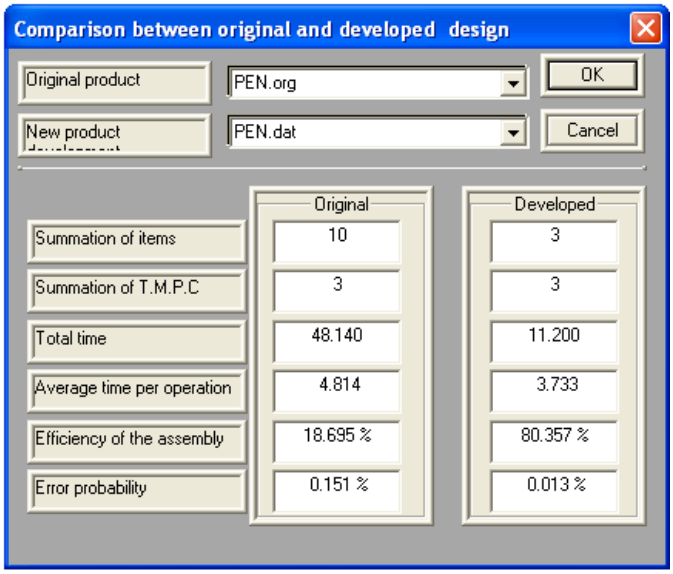

Figure (17) Results of comparisons between the original and modified design for the ball pen assembly as acquired from the developed DFA program

B. Design for Manufacturing

Two case studies are given in this section to demonstrate the capability and limitations of the developed DFM program, these case studies include: (a) The Bracket part, (figure 18) and an air conditioner fan part (figure 19).

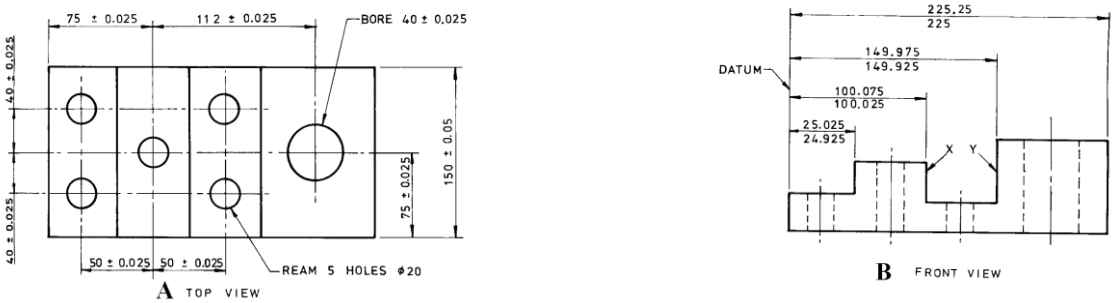

Figure (18) The bracket part. (a) Top view. (b) Front view.

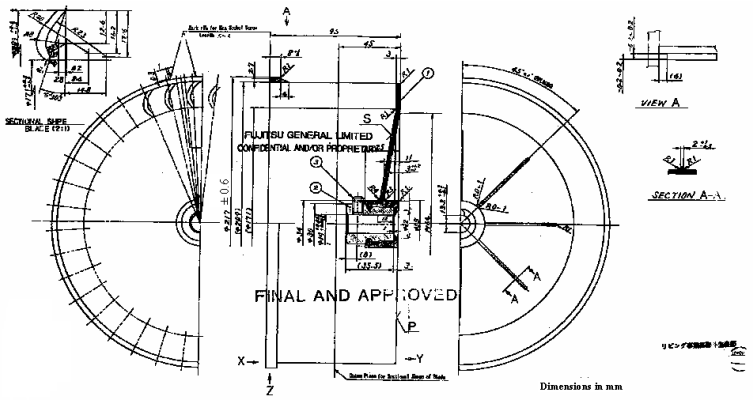

Figure (19) Air conditioner centrifugal fan design obtained from the State Company for Electrical Appliances – AL – Waszeria, Baghdad, Iraq

(B – 1) The Bracket Part: The bracket part that is used as a case study is taken from an engineering drawing, analyzed by its terms of shape attributes producing capabilities and applying it to the developed DFM program which gives the results presented in figure (20).

The DFM program displays the processes that are capable of achieving the shape attributes of the bracket part, figure (21). In this case the only option is by the machining process.

The DFM program then displays the capable processes of achieving the shape attributes using available materials, figure (22).

However by examining figure (20) carefully, it seems to be that the "no draft angle attribute" is the most likely obstacle that prevented the program to allocate other manufacturing process alternatives to this part. Hence if the designer adds a drafting angle to his design which may not affect the part functionality other manufacturing process alternatives will result, see figure (23).

Results of the re-design of the bracket widen the options for process selection that include (see figure (24)): sand casting, investment casting, die casting, injection molding, structure foam, closed die forging, machining, ECM, EDM sheet metal (stamping / bending) and thermoforming. Hence, the user may select a more economical operation from these.

The effective tolerance of the bracket was selected to be ± 0.025 mm. Using this tolerance as an input to the developed DFM program as shown in figure (25), showed that "machining" is the only capable process to produce the required design, whereas all other processes were excluded.

It is clear from the program results that the tolerance specified for the bracket is very strict, and imposing the fourth step in the tolerance step function [4], the grinding. This will impose 6 times the original cost compared with parts that has no strict tolerances. Therefore this will remind the designer to study the possibility of less strict tolerances to be used for this part.

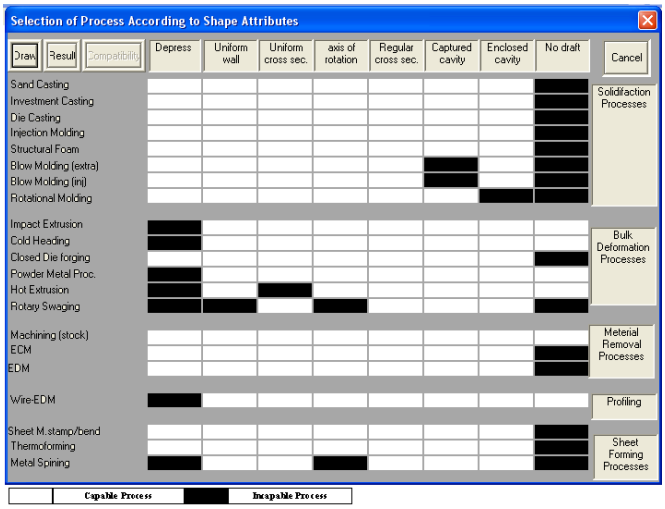

Figure (20) The capable and incapable processes for the shape attributes of the bracket part

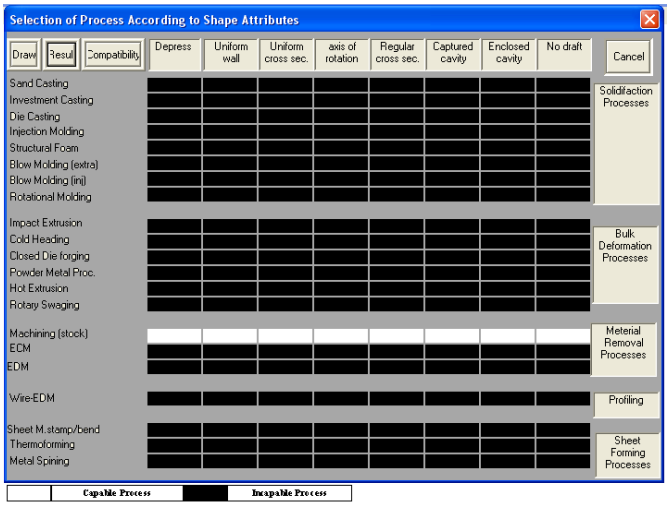

Figure (21) The capable processes for the shape attributes of the bracket part manufacturing

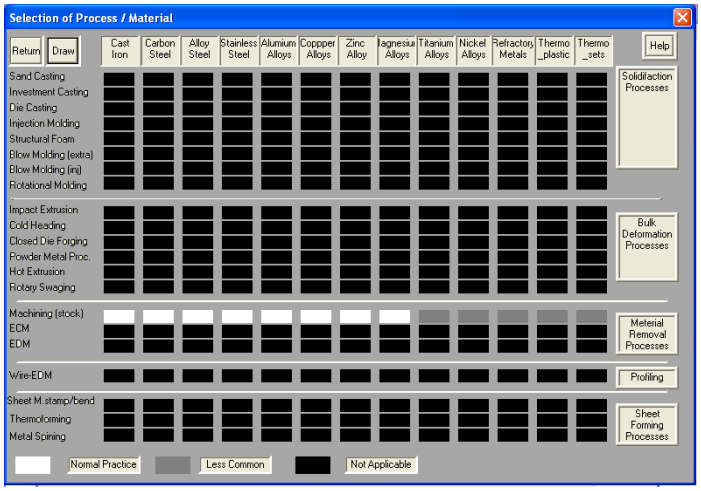

Figure (22) Results of compatibility between process and materials of the bracket part

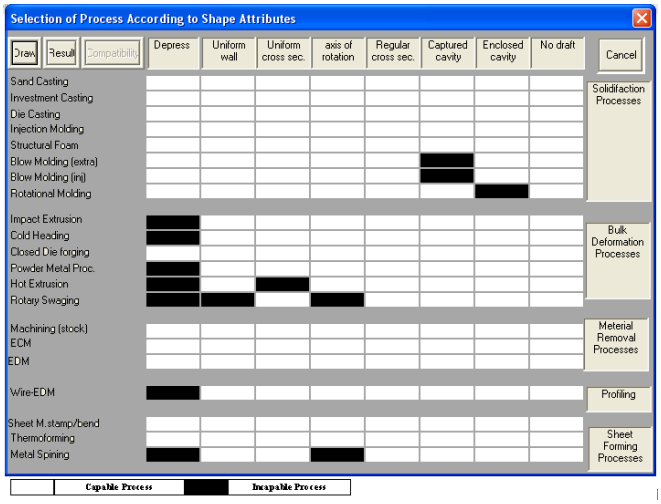

Figure (23) The capable and incapable processes for the shape attributes of the bracket part manufacturing applying "no draft angle attribute"

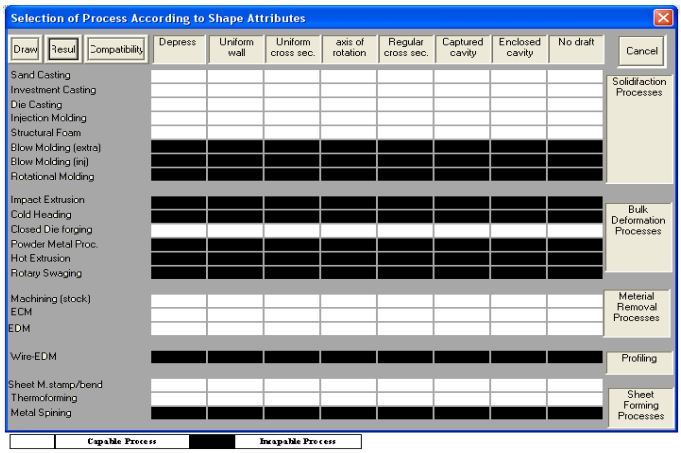

Figure (24) The capable processes for the shape attributes of the bracket part manufacturing applying "no draft angle attribute"

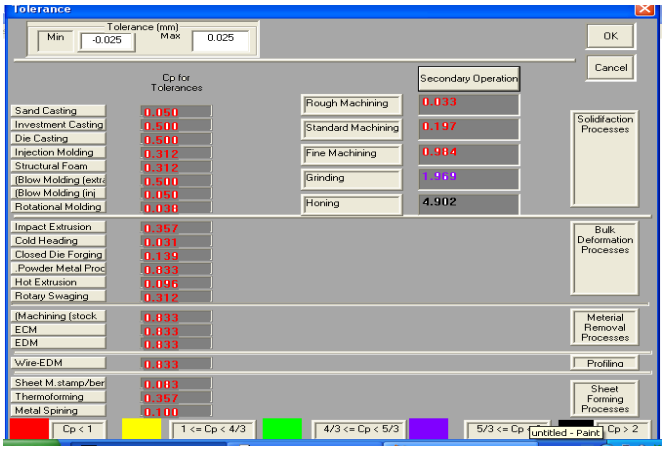

Figure (25) The tolerance process capability to the bracket

(B – 2) Air Conditioner Centrifugal Fan Case Study:

This part is selected from the production range of the State Company for Electrical Industries. One of the products produced in that company is air conditioner, and one of its parts is the centrifugal fan. The centrifugal fan is a plastic part made in injection molding; functionally, the fan must rotate and withstand the forces of the air wind speed, must rotate without vibration and must not hit the surrounding insulator.

The blade must keep its designed shape because it is responsible for air distribution equally in all directions, and that will not be happened exactly if there is any distortion in the blades shape. If the selected manufacturing process is incapable to produce the part to be within the design limits then, unbalanced forces will occur while the part functions, thus will introduce vibration and noise.

The outside diameter of the fan must be kept within its tolerances which is ± 0.6 mm. If the tolerance is over the limits the fan will hit the insulator surroundings and make damage or destroy it. If it is less than the limits the fan will not work properly.

The blade thickness is not uniform; it is less than 3 mm in one area and its bend have more than one arc.

The air conditioner manufactured in the company by patch quantity, the quantity may be about 300 product / patch. That leads to a quantity about 300 fan / patch.

Applying the shape attributes for the air conditioner centrifugal fan to the program gives the results presented in figure (26). The program identified the processes that are capable of achieving the shape attributes namely: sand casting, investment casting, die casting, injection molding, structural foam, closed die forging, machining form stock, ECM and EDM as shown in figure (27).

The program then displays the capable processes of achieving the shape attributes with its possible available materials as shown in figure (28).

The effective tolerance of the centrifugal fan is the tolerance added to the outside diameter which is 217 ± 0.6 mm. Implementing this range of values in the program gives the result shown in figure (29). This range of tolerance is liberal.

In this case study the processes that are identified to be capable of manufacturing the centrifugal fan, were examined one by one. It could be concluded that limitations of some of the stated processes make them infeasible to be adopted to manufacture the fan, hence they may be discarded, and these processes are: Sand Casting, Investment Casting, Structural Foam, Machining (from stock), ECM and EDM.

. The reason that the program identified these processes as valid alternatives is due to the incomplete database and product information available to the program, hence, future work to establish a more comprehensive database and further development of the program are suggested for future development.

According to the employed operation capability database, the three processes that can be used successfully to produce the fan regardless of its given material are: Die Casting, Closed Die Forging and Injection Molding. Both die casting and close die forging requires secondary operations.

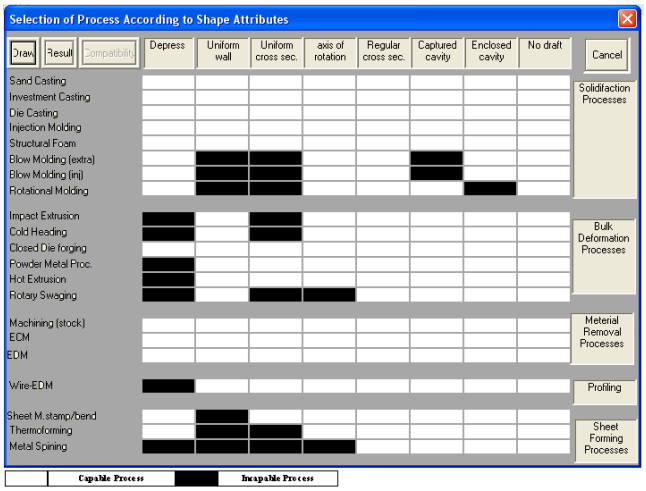

Figure (26) The capable and incapable processes for the shape attributes of the centrifugal fan

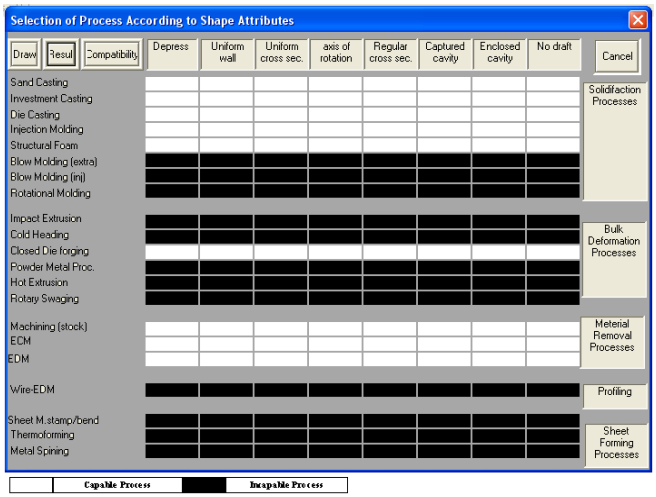

Figure (27) The capable processes for the shape attributes of air conditioner fan production as identified by the DFM program

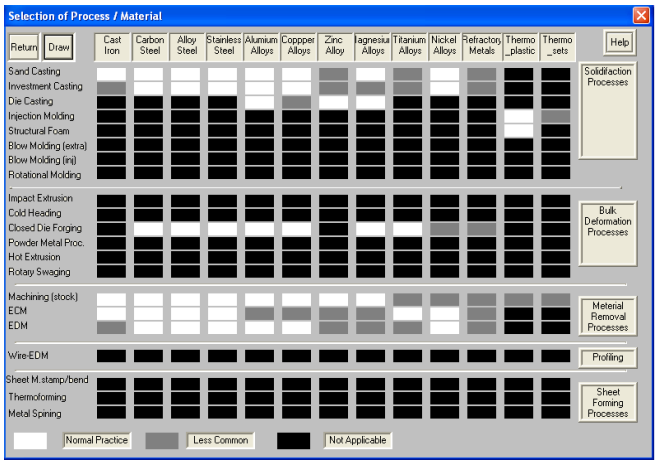

Figure (28) Compatibility between process and materials of the centrifugal fan

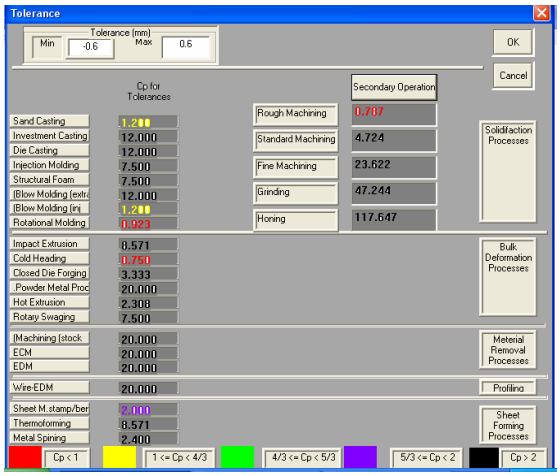

Figure (29) Tolerance process capability to the centrifugal fan

CONCLUSIONS

- The method adopted in the DFA gave very good enhancement in the efficiency of the assembly, which increased by 4 times, and error expectation probability increased by 84%.
- Verification of DFA program results and actual assembly of a conducted tests showed that the obtained results are close to each other when comparing the percentage of the design improvements, however, the actual resulting time values differs due to human and environment factors.
- The developed DFA method did not overlap with the usual work of the designer. It only gives support to the work to achieve the goal, therefore the DFA system can be implemented beneficially.
- In spite of good estimation that comes from DFA, the developed program still requires more developments and verification of its database to enable its commercial implementation in the industry.
- The adopted method of DFM succeeded to give valuable aid to the designer by reducing the many available alternatives to those which are capable to produce the part hence it will save time by reducing the possible rework time.

- The developed DFM program succeeded to give aid to the designer to select the appropriate material that is available in the required shape and form. In addition the program verifies whether the selected manufacturing process is capable to achieve the required tolerances, else it notifies the user that a secondary operation is required.
- Results of the case studies showed the importance of designing a draft angle where possible. This draft angle will help to extend the list of possible manufacturing process alternatives so that the user can select the best of these.
- Results of this paper showed that the way to automate the process of DFMA is still require more attention and further research specially to develop a full comprehensive database that covers all the variables affecting the process and integration the intelligence of the experts in the field. Therefore, to develop a comprehensive commercial and industrial system employing the DFMA more research work is needed. However, the step taken to reach the develop level of the DFMA program has contributed to this important field.

REFERENCES:

- Anderson, D.M., Design for manufacturability and concurrent engineering- How to: design for low cost-design for high quality-design for lean manufacture-design quickly for fast production, California: CIM Press, 2004.
- Bedworth, D.D., Henderson, M.R., Wolfe, P.M., Computer-integrated design and manufacturing, New York: McGraw-Hill, 1991.
- Boothroyd, G., Dewhurst, P., Winston, K., Product design for manufacture and assembly, second edition, York: Marcel dakker, 2002.
- Bralla, J.G., Design for manufacturability handbook, second edition, Boston: McGraw-Hall, 1999.
- Esawi, A.K., Ashby, M.F., computer-based selection of manufacturing processes: methods. Software and case studies, Journal of engineering manufacture, proceedings of the institution of mechanical engineers, Volume 212, B8, pp 595-610, 1998.
- Groover, M.P., Fundamentals of modern manufacturing: Materials, processes, and systems, second edition New Jersey: Prentice Hall, 2002.
- Ji, S. and others, Optimal tolerance allocation based on fuzzy comprehensive evaluation and genetic algorithm, International journal of advance manufacturing technology, No. 16, PP. 461-468, 2000.
- Singh, N., Systems approach to computer-integrated design and manufacturing, New York: John Wiley & Sons, Inc., 1996.
- Voland, G., Engineering by design, London: Addison-Wesley, 1999.
- Whitney, D.E., Mechanical assembles: Their design, manufacture, and role in product development, New York-Oxford: Oxford University press, Inc. 2004.
- Zendin, K.B., Maynard's industrial engineering handbook, fifth edition, New York: McGraw-Hill, 2001.

ABBREVIATION

CE	Concurrent Engineering.
DFA	Design for Assembly.
DFM	Design for Manufacturing.
TMPC	Theoretical Minimum Part Count.
ECM	Electrochemical Machining.
EDM	Electrical Discharge Machining.

`

ON THE DYNAMICS OF DUAL-SPIN SPACECRAFT CONTAINING A NUTATION DAMPER

By
Dr. Ahmed A. Al-Ragihy / Kerbala University, College of Engineering
Dr. Alaa M. Hussein Al-jussani, Ali Mohammed Hussein, Babylon University, College of Engineering

ABSTRACT

The dynamics of dual-spin spacecraft which containing a proposed nutation damper which consisting of a ring totally filled with a viscous liquid with offset center, to improve damping, is investigated. The equations of motion were developed using Newton-Lagrange approach resulting equations in terms of spacecraft's and damper's parameters , which are given in dimensionless form. The expression of the nutation angle and time constant in both modes are developed using zero-order approximation technique. The equilibria states and stability condition, and the analytical expression for residual nutation angle were derived. The analytical results were compared with those found numerically using computer simulation program named MATLAB, ver. 7.
Also the effect of various spacecraft's and damper's parameters on the dynamic and damping characteristics are discussed. The three dimensional graphical representation of the first and the second relative equilibria states are introduced. The numerical results are compared with the analytical for both modes of motion, where the percentage error of the time constant for nutation mode is less than ($\approx$3.6%), and for spin mode is less than ($\approx$8%). As an important result its concluded that the proposed damper works better than that used by Alfriend[2].

الخلاصة

تم تحليل ديناميكية الأقمار الصناعية ذات البرم المزدوج والتي تحوي على مخمد ترنحي مقترح يتألف من حلقة مملوءة كليا بسائل وبمركز مزاح عن محور الدوران للحصول على أحسن تخميد للحركة الترنحية للأقمار الصناعية. استخدمت طريقة نيوتن-لاگرانج لاشتقاق معادلات الحركة وتم الحصول على معادلات بدلالة متغيرات القمر الصناعي ومتغيرات المخمد الترنحي, حيث تم جعل هذه المتغيرات بحيث تكون لا بعدية. وجدت التعابير الخاصة بزاوية الترنح (Nutation angle) وثابت الزمن في كلا الطورين باستخدام طريقة تقريب المرتبة الصفرية (zero-order approximation) وكذلك نوقشت حالات الاتزان وشروط الاستقرارية الخاصة بهذه الأقمار؛ وكذلك تم الحصول على التعبير الرياضي لزاوية الترنح المتبقية. تم مقارنة النتائج التحليلية المستحصلة

في هدا البحث مع النتائج العددية المستحصل عليها باستخدام المحاكاة بواسطة برنامج MATLAB 7 نوقشت أيضا تأثير المتغيرات المختلفة الخاصة بالقمر الصناعي ومنظومة التخميد على الخواص الديناميكية والتخميدية للمنضومة. وأخيرا وضَحت حالة الاستقرارية النسبية الأولى والثانية من خلال رسوم ثلاثية الأبعاد. (Three Dimensional Representation). تم مقارنة النتائج العددية مع التحليلية لكلا الطورين, حيث وجدت نسبة الخطأ لثابت الزمن لطور التزامن الترنحي اقل من (3.6%) ولطور التزامن التدويمي اقل من (8%)

NOMENCLATURE

Symbol	Description	Unit
A	Principal transverse moment of inertia of the spacecraft	$kg.m^2$
b	Ratio of the ring height to the ring mean radius	-
C, C_p	Moment of inertia of the rotor and the platform along z-axis	$kg.m^2$
d	Distance of the offset.	M
F_d	Drag force	N
h_t	Transverse angular momentum	
h_{tt}	Total angular momentum	
$[I_{s/c}]$	Spacecraft inertia matrix	$kg.m^2$
I_u, I_v, I_z	Moments of inertia of the damping viscous liquid measured along u, v, and z axes	$kg.m^2$
I_{uz}	Product moment of inertia of the fluid	$kg.m^2$
m	Mass of the fluid	kg
p, q, r	Dimensionless angular velocity components of the spacecraft about x,y and z, respectively.	
Q_α	Generalized moment associated with the generalized coordinate α	N.m
{Q}	Column matrix of the moment component of the non conservative forces	N.m
R	Ring mean radius of the nutation damper	m
T	Total kinetic energy of the spacecraft equipped with nutation damper	N.m
t	Time	sec
x, y, z	Body fixed frame.	

Greek Symbol

α	Relative angular displacement between the fluid and the spacecraf	rad
α_o	Initial value of α in the spin-synchronous mode	rad
$\tilde{\alpha}$	Small variation in α in the spin-synchronous mode	rad
$\dot{\alpha}$	Relative angular velocity of the fluid	rad/s
ε	Inertia ratio of the fluid to the transverse inertia of the spacecraft	-
η	Damping constant of the damping fluid	-
θ	Nutation angle of the spacecraft	rad
θ_n	Nutation angle in the nutation-synchronous mode	rad

θ_r	Residual nutation angle of the spacecraft	rad
θ_s	Nutation angle in the spin-synchronous mode	rad
σ	Inertia ratio of the spacecraft (σ=C/A)	-
τ	Dimensionless time	-

INTRODUCTION

The attitude control system of the spacecraft is to control the attitude and position of the spacecraft as it performs its mission. The techniques that provide attitude stabilization and control of spacecraft are; passive control system, semi-passive and active control system[15]. The type of the system adopted in the present study is the passive type system. Passive system does not require any external power source, once they are in place, they use gravity or momentum to create the necessary control forces and moments[19].

Dual-spin stabilization type is the method of attitude stabilization adopted in the present study. A spin and Dual-spin stabilized spacecraft, or spinners, utilizes its own spinning motion to keep it's self aligned in a certain inertial direction. The spinning motion creates stiff angular momentum vector, which tend to resist external disturbance torques. A spinner is stable if it is spun about the axis of largest principal moment of inertia, if it is spun about a different axis, any disturbance could cause the spin axis to shift to the major axis.

In single spin stabilization the whole body rotates about the axis of maximum principal moment of inertia. Early communication satellites, such Syncom I, ATS I, II and Inelsat I, II were single spin stabilized. Its advantages are simple, reliable, and long life time but the main limitations of these satellites are that they could not use earth oriented antennas. These limitations are overcome in a dual spin spacecraft. Whereas dual spin spacecraft consisting of spinning rotor producing gyroscopic stiffness and a platform rotating at a much slower rate in accordance with the desired attitude of the spacecraft. There are two types which are commonly known as the external rotor and body stabilized spacecraft, each type employs a different method of attitude stabilization. The external rotor type or "Gyrostat" uses spin stabilization where the rotor of relatively large moment of inertia rotates to provide gyroscopic stiffness, while the platform usually containing communication equipment and antennas are despun.

Chang, and Liu [4], studied the dynamic and stability of an inertially symmetric, spinning, rigid body with a partial filled viscous-ring damper mounted normal to the spin axis. They used the nonlinear equations directly by using center manifold theory; they generated the stability criteria and the decay time constant. Then Alfriend[2], studied the attitude stability of

Dual-spin spacecraft with a partial filled viscous-ring damper utilizing zero order approximation technique. Hamed [31], studied the ball in ring nutation damper, he utilized neon gas and many percentage of glycerin water mixture as damping fluid in his study.

The present work represents an attempt to study the full filled viscous ring damper mounted normally to the spin axis with offset centre (d) from the spin axis.

-EQUATION OF MOTION

The total angular momentum can be written in terms of angular velocity component:

$$\vec{h} = [(A+I_u)\omega_u - I_{uz}(\omega_z+\dot{\alpha})]e_u + [(A+I_v)\omega v]e_v + [C\omega_z + I_z(\omega_z+\dot{\alpha}) - I_{uz}\omega_u + C_p\omega_{pz}]e_z \qquad 1$$

When the external torque components are zero, the system referred to as a freely precessing system, then the principle of conservation of angular momentum can be applied, such that[21]:

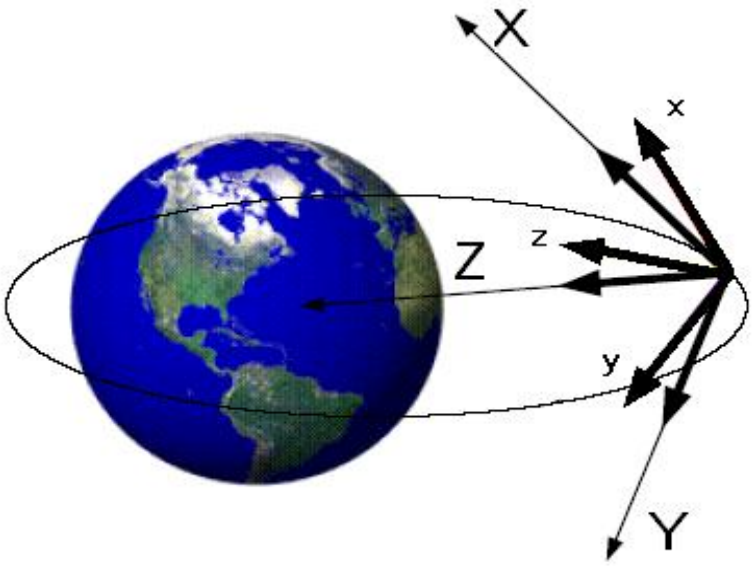

Fig. A: Body fixed coordinate system.

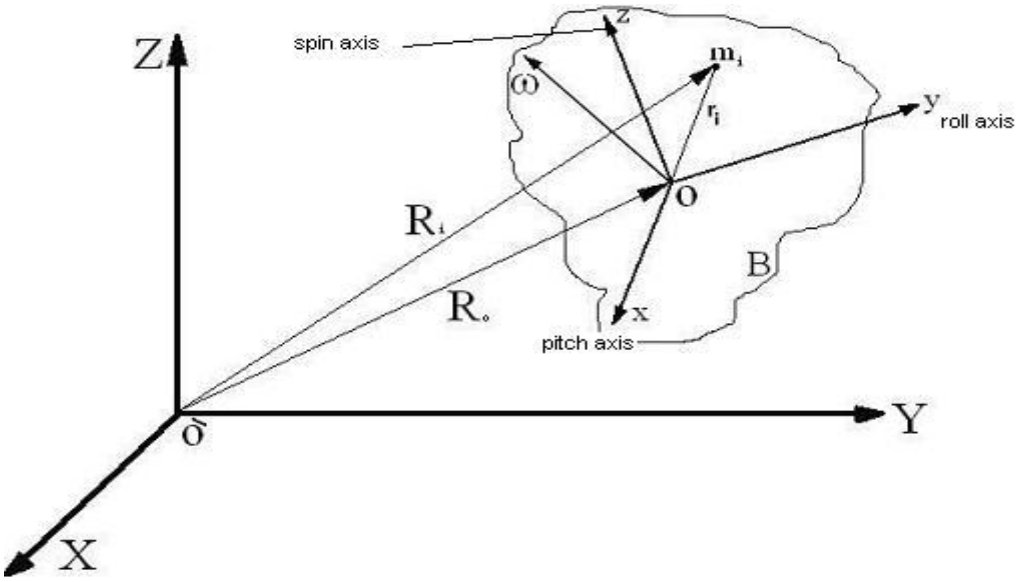

Fig. B: Rigid body angular momentum.

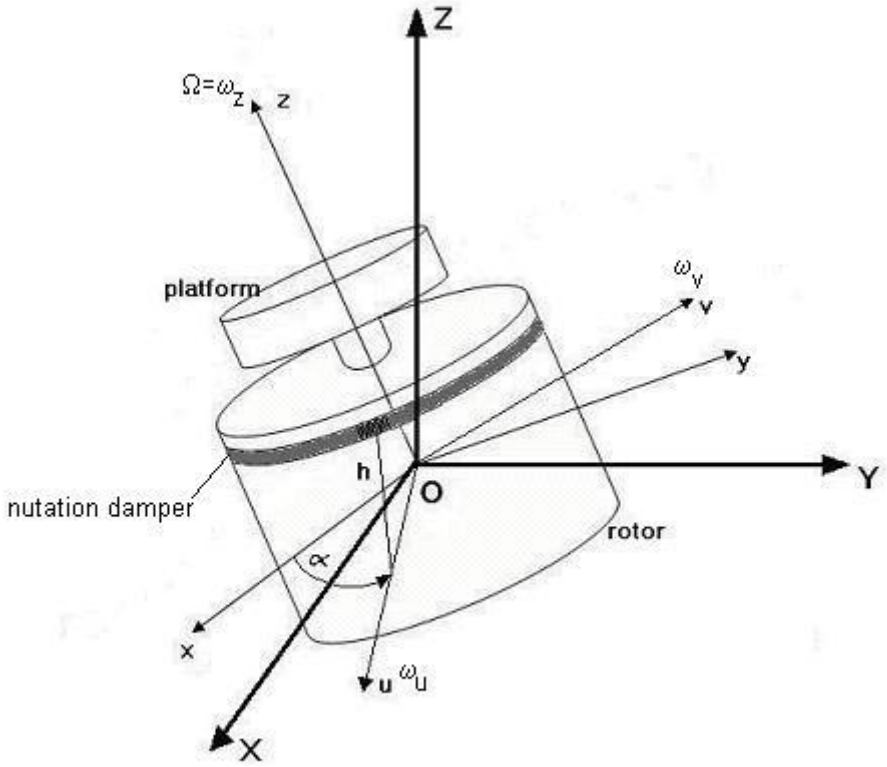

Fig.C: Spacecraft model with viscous ring damper.

$$\vec{M} = \left(\frac{d\vec{h}}{dt}\right)_{oxyz} = \left(\frac{d\vec{h}}{dt}\right)_{ouvz} + \vec{\omega}\times\vec{h} = 0 \qquad 2$$

the equation which describes the motion of the fluid inside the ring, can be obtained by using Lagrange's equation expressed in terms of quasi-coordinate.

$$\frac{d}{dt}\frac{\partial T}{\partial \dot{\alpha}} - \omega_v \frac{\partial T}{\partial \omega_u} + \omega_u \frac{\partial T}{\partial \omega_v} = Q_\alpha \qquad 3$$

where Q_α is the generalized moment associated with the generalized coordinate α, and it is given by:

$$Q_\alpha = C_f R^2 \dot{\alpha} \qquad 4$$

C_f : coefficient of viscous friction between fluid and ring wall.(N s/m)

The kinetic energy (T) of the system is in the form:

$$T = \frac{1}{2}\left[A\left(\omega_u{}^2 + \omega_v{}^2\right) + C\omega_z{}^2 + C_p\Omega_p{}^2 + I_u\omega_u{}^2 + I_v\omega_v{}^2 + I_z\left(\omega_z + \dot{\alpha}\right)^2 - 2I_{uz}\left(\omega_z + \dot{\alpha}\right)\omega_u \right] \qquad 5$$

Using Eqs.1, 4 and 5, then Eqs. 2 and 3 yields:

$$p' + \frac{\left(\lambda\, r - \alpha' + \lambda_s\right)}{D_1} q + \frac{\left(A_1 r + A_2\alpha' - A_3 p\right)}{D_1} q - \frac{A_4}{D_1} r' + \frac{A_5}{D_1}\alpha' = 0 \qquad 6$$

$$q' - \frac{\left(\lambda\, r - \alpha' + \lambda_s\right)}{D_2} p + \frac{\left(B_1 r + B_2\alpha' + B_3 p\right)}{D_2} p - \frac{B_4}{D_2}(r + \alpha')^2 = 0 \qquad 7$$

$$\alpha'' + C_1\alpha' + C_2 pq + C_3[(r + \alpha')q - p'] = 0 \qquad 8$$

$$r' - C_4\alpha' = 0 \qquad 9$$

where, ( )′ = (d/dt), D_1 & D_2 are given in the appendix

-SOLUTION OF THE PROBLEM

Before developing the solution for the attitude equations of the spacecraft, the equation which is describing the nutation angle in terms of dimensionless parameters and variables, will be developed.

$$\cos\theta = \frac{h_z}{h_{tt}}, \quad \sin\theta = \frac{h_t}{h_{tt}}, \quad h_{tt}{}^2 = h_t{}^2 + h_z{}^2 = \text{constant}, \quad h_t{}^2 = h_u{}^2 + h_v{}^2 \qquad 10a, b, c, d$$

differentiate Eq. 10a and substitute in Eq. 10b gives:

$$\therefore \quad \theta' = -\frac{h_z{}'}{h_t} \qquad 11$$

from Eq. 2, the time derivative of the spin axis angular momentum vector h_z, may be given by (in dimensionless angular velocity variables (p, q)):

$$h_z' = qh_u - ph_v \quad (12)$$

Substitute Eq. 11 into Eq. 12, yields the following equation:

$$\theta' = \frac{ph_v - qh_u}{h_t} \quad (13)$$

Substitute h_u, h_v, h_t and h_{uz} into Eq. 13 yields (details in appendix):

$$\theta' = \frac{\left(-pG^2 + bG(r+\alpha')\right)q\varepsilon}{\sqrt{p^2+q^2}} \quad (14)$$

apply zero-order approximation procedure to Eqs. 6, 7, 8, and 9 to get:

$$p' + (\lambda\, r + \lambda_s - \alpha')q = 0 \quad (15)$$

$$q' - (\lambda\, r + \lambda_s - \alpha')p = 0 \quad (16)$$

$$r' = 0 \quad (17)$$

$$\alpha'' + \frac{\eta\lambda_n}{\sigma^2\varsigma}\alpha' - \frac{bG}{\varsigma}p' + \left[-\frac{G^2}{\varsigma}p + \frac{bG}{\varsigma}(r+\alpha')\right]q = 0 \quad (18)$$

The solution of the angular velocity component r is obtained from Eq. 17, with the fact that the initial value of the r-components equal to 1, then the solution of Eq. 17 is:

$$r=1 \quad (19)$$

substitute the solution of the r-component Eq. 19 in Eqs. 15 and 16, then one get:

$$p' + (\lambda_n - \alpha')q = 0, \quad q' - (\lambda_n - \alpha')p = 0 \quad (20, 21)$$

where,

$$\lambda_n = \lambda + \lambda_s$$

the solution of p and q are given by:

$$p = \omega_t \cos(\lambda_n\tau - \alpha), \; q = \omega_t \sin(\lambda_n\tau - \alpha) \quad (22, 23)$$

substitute Eqs. 22 and 23 into Eq. 14, then Eq. 14 becomes:

$$\theta' = \left[-G^2\omega_t \cos(\lambda_n\tau - \alpha) + bG(1+\alpha')\right]\varepsilon \sin(\lambda_n\tau - \alpha) \quad (24)$$

Now, it is required to express for ω_t in terms of the nutation angle θ.

Divide Eq. 10b by Eq. 10a and substitute h_t and h_z then apply zero-order approximation to get:

$$\tan\theta = \frac{\omega_t}{\sigma_n} \qquad 25$$

where, $\sigma_n = \sigma + \lambda_s$

sub. p' given by Eq. 15 into Eq. 18 results:

$$\alpha'' + \frac{\eta\lambda_n}{\sigma^2\varsigma}\alpha' - \left[\frac{bG}{\varsigma}(\alpha' - \lambda_n) + \frac{G^2}{\varsigma}p - \frac{bG}{\varsigma}(1+\alpha')\right]q = 0 \qquad 26$$

DAMPER MOTION

The symmetric rigid body, which is spinning about its axis of symmetry, has a constant nutation angle when no damping is present. The transverse angular velocity ω_t rotates at a rate of $(\sigma\Omega + \sigma_p\Omega_p)\cos\theta$ and the body rotates relative to ω_t at a rate of $((1-\sigma)\Omega + \sigma_p\Omega_p)$, when no damping is present, a plane containing the angular momentum vector $\vec{h}$ or ω_t and the z-axis, called the nutation plane, is formed. the fluid is then moving at a constant rate of $((1-\sigma)\Omega + \sigma_p\Omega_p)$ (relative spin), with respect to the body. At the same time, the fluid subjected to centrifugal force due to the relative rotation (spin) about the z-axis. This type of motion is called "nutation-synchronous" motion. In this mode the fluid is moving at a constant rate with respect to the spacecraft (damper ring); hence the energy dissipation rate is constant. If σ >1the nutation angle decreases which cause a decrease in the centrifugal force. Eventually the component of the centrifugal force is not large enough to balance the damping and friction forces, and the fluid begins to decelerate and oscillate until becomes at rest. This type of motion is called "spin-synchronous" motion.

<u>Nutation-Synchronous Mode</u>

Let β measure the position of the center of a portion of the fluid with respect to the nutation plane. Assuming that at $\tau = 0$, $\alpha = 0$, then

$$\beta = \alpha - \lambda_n\tau \qquad 27$$

Substituting for β in Eq. 26 and using Eqs. 22, 23 then Eq. 26 becomes:

$$\beta'' + \frac{\eta_n\lambda_n}{\sigma^2\varsigma}\beta' + \left[\left(\frac{bG}{\varsigma} - \frac{bG}{\varsigma}\right)\beta' + \frac{G^2}{\varsigma}p - \frac{bG}{\varsigma}(1+\lambda_n)\right]\omega_t\sin(\beta) = -\frac{\eta_n\lambda^2{}_n}{\sigma^2\varsigma} \qquad 28$$

where, η_n refer to the damping constant in the nutation-synchronous mode.

Since that, the motion of the fluid in this mode is constant, then the solution of Eq.28 is, $\beta = \beta_s = con.$, so, $\beta'' = \beta' = 0$, substituting in Eq.28 and take into account that $\lambda_n = \lambda + \lambda_s$ and $\sigma = 1 + \lambda$, then

$$-\left[-G^2 p + bG(1+\lambda_n)\right]\omega_t \sin\beta = -\frac{\lambda^2{}_n \eta_n}{\sigma^2} \quad 29$$

substitute for $\beta = \beta_s$ and $\beta_s' = 0$ into Eq. 24, then 24 becomes:

$$\theta_n' = -\left[-G^2 \omega_t \cos\beta + bG(1+\lambda_n)\right]\varepsilon \sin\beta_s \quad 30$$

where, θ_n refer to the nutation angle in the nutation-synchronous mode.

Substituting for the left hand side of Eq.29 in Eq.30, and using Eq.25 then,

$$\theta' \tan\theta_n = -\frac{\eta_n \lambda^2{}_n}{\sigma^2 \sigma_n}\varepsilon \quad 31$$

Carrying out the integration, then the nutation angle θ_n is given by:

$$\cos\theta_n = \cos\theta_{n0}\ e^{\frac{\tau}{\tau_n}} \quad 32$$

where, θ_{n0} is the initial value of θ_n, τ_n is the time constant of the system which it is given by:

$$\tau_n = \frac{\sigma_n \sigma^2}{\eta_n \lambda^2{}_n \varepsilon} \quad 33$$

At the end of the nutation-synchronous mode, the system goes into the spin-synchronous mode and the nutation angle θ_n gain its minimum value. Referring to Eq.29, to satisfy the condition of minimum value of the nutation angle in this mode, the angle β_s should be equal to $\pm\frac{\pi}{2}$ substituting for this value and for ω_t from Eq.25, then;

$$\tan\theta = \frac{\eta \lambda_n^2}{\sigma^3 bG\sigma_n\left(1+\frac{\lambda_s}{\sigma}\right)} \quad 34$$

Spin-Synchronous Mode

In the Spin-Synchronous mode, the spacecraft becomes more closely to the state of pure spin about the spin axis (z-axis). Accordingly, the relative speed of the fluid, about the spin axis with respect to the spinning rotor, will be decreased. Eventually the relative speed between the fluid and the spinning rotor becomes zero, then the spacecraft spin axis is aligned with the initial direction of the total angular momentum vector. In the spin-synchronous

mode, it can be shown that the fluid is moving with a small variation in its speed with respect to the damper ring therefore it is necessary to find the solution for the motion of the fluid (α) as a function of dimensionless time (τ), substituting for p and q from Eqs.22 and 23 into Eq.26, yields:

$$\alpha'' + \frac{\eta\lambda_n}{\varsigma\sigma^2}\alpha' - \left[\frac{bG}{\varsigma}(1+\lambda_n)\right]\omega_t \sin(\alpha - \lambda_n\tau) = 0 \qquad 35$$

As mentioned above that the fluid moving with a small variation in its speed, then the following equation can be assumed:

$$\alpha = \alpha_0 + \tilde{\alpha} \qquad 36$$

where, α_0 is the initial value of α and $\tilde{\alpha}$ represent the small variation of the speed of the fluid such that $\alpha_0 >> \tilde{\alpha}$, which gives the following expressions:

$$\sin(\alpha - \alpha_0) = \sin\tilde{\alpha} = \tilde{\alpha},\ \ \cos(\alpha - \alpha_0) = \cos\tilde{\alpha} = 1,\ \ \sin(\alpha - \lambda_n\tau) \approx \sin(\alpha_0 - \lambda_n\tau),$$
$$\cos(\alpha - \lambda_n\tau) \approx \cos(\alpha_0 - \lambda_n\tau) \qquad 37$$

The basis of the above assumptions is that the change in α is small compared with $\lambda_n\tau$.
Using the above assumption, then Eq.35 becomes:

$$\alpha'' + \frac{\eta\lambda_n}{\varsigma\sigma^2}\alpha' - \left[\frac{bG}{\varsigma}(1+\lambda_n)\right]\omega_t \sin(\alpha_0 - \lambda_n\tau) = 0 \qquad 38$$

assume the forced oscillating solution of Eq.38 is given by

$$\tilde{\alpha} = \alpha - \alpha_0 = A\sin(\alpha_0 - \lambda_n\tau) + B\cos(\alpha_0 - \lambda_n\tau) \qquad 39$$

to find the constants A and B, substituting Eq.39 in Eq.38, and after some mathematical manipulations we get:

$$A = -\left[\frac{bG\sigma^2(1+\lambda_n)}{\varsigma\lambda_n^2\left(\sigma^2 + \frac{\eta^2}{\varsigma^2\sigma^2}\right)}\right]\omega_t, \quad B = \left[\frac{bG\eta(1+\lambda_n)}{\varsigma^2\lambda_n^2\left(\sigma^2 + \frac{\eta^2}{\varsigma^2\sigma^2}\right)}\right]\omega_t$$

substitute A and B in Eq. 39, and substitute for ω_t, then the expression of $\tilde{\alpha}$ becomes:

$$\tilde{\alpha} = F\tan\theta_s\left[-\varsigma\sin(\alpha_0 - \lambda_n\tau) + \frac{\eta}{\sigma^2}\cos(\alpha_0 - \lambda_n\tau)\right] \qquad 40$$

where θ_s referred to the nutation angle in the spin-synchronous mode and the constant F is given by:

$$F = \frac{\sigma_n}{\lambda_n^2}\left[\frac{bG\sigma^2(1+\lambda_n)}{\varsigma^2\left(\sigma^2 + \frac{\eta^2}{\varsigma^2\sigma^2}\right)}\right]$$

The differential equation of the nutation angle rate Eq.24 is given by:

$$\theta_s' = -\left[-G^2\sigma_n \tan\theta_s \cos(\alpha-\lambda_n\tau)+bG(1+\alpha')\right]\varepsilon\sin(\alpha-\lambda_n\tau) \quad 41$$

it was mentioned that $\tilde{\alpha}$ represents small variation in α such that

$\alpha = \alpha_0 + \tilde{\alpha}$, where $\alpha_0 >> \tilde{\alpha}$ .using the approximation of small angle, then

$$\sin(\alpha-\alpha_0)=\sin\tilde{\alpha}\approx\tilde{\alpha},\ \cos(\alpha-\alpha_0)=\cos\tilde{\alpha}\approx 1,\ \sin(\alpha+\alpha_0)\approx\sin\alpha_0,$$
$$\sin(\alpha+\alpha_0)=\sin(2\alpha_0+\tilde{\alpha})\approx\sin 2\alpha_0, \quad 42$$

using the above mentioned relations, then the expression of $\sin(\alpha-\lambda_n\tau)$ may be given by

$$\sin(\alpha-\lambda_n\tau)=\sin(\alpha_0+\tilde{\alpha}-\lambda_n\tau)=(\sin\alpha_0+\tilde{\alpha}\cos\alpha_0)\cos\lambda_n\tau-(\cos\alpha_0-\tilde{\alpha}\sin\alpha_0)\sin\lambda_n\tau \quad 43$$

Substituting $\tilde{\alpha}$ from Eq.40 in Eq.43 (θ_s is small in the spin-synchronous mode $\tan\theta_s=\theta_s$), then (by expanding the trigonometric terms) Eq.41 becomes:

$$\theta_s' = -\varepsilon\left\{\begin{array}{l} -\sigma_n\theta_s G^2\left[\sin\alpha_0\cos\alpha\cos^2\lambda_n\tau+\sin\lambda_n\tau\cos\lambda_n\tau(\sin\alpha_0\sin\alpha-\cos\alpha_0\cos\alpha)-\cos\alpha_0\sin\alpha\sin^2\lambda_n\tau\right] \\ +bG\left[\sin(\alpha_0-\lambda_n\tau)+F\theta_s\left[\begin{array}{l} -\varsigma\left(\begin{array}{l}\sin\alpha_0\cos\alpha_0\cos^2\lambda_n\tau-\cos\alpha_0^2\sin\lambda_n\tau\cos\lambda_n\tau \\ +\sin\alpha_0^2\sin\lambda_n\tau\cos\lambda_n\tau-\sin\alpha_0\cos\alpha_0\sin^2\lambda_n\tau\end{array}\right) \\ +\frac{\eta}{\sigma^2}\left(\begin{array}{l}\cos\alpha_0^2\cos^2\lambda_n\tau+2\sin\alpha_0\cos\alpha_0\sin\lambda_n\tau\cos\lambda_n\tau \\ +\sin\alpha_0^2\sin^2\lambda_n\tau\end{array}\right) \\ +\varsigma\lambda_n\left(\begin{array}{l}\sin\alpha_0\cos\alpha_0\cos^2\lambda_n\tau-\cos\alpha_0^2\sin\lambda_n\tau\cos\lambda_n\tau \\ +\sin\alpha_0^2\sin\lambda_n\tau\cos\lambda_n\tau-\sin\alpha_0\cos\alpha_0\sin^2\lambda_n\tau\end{array}\right) \\ +\frac{\eta\lambda_n}{\sigma^2}\left(\begin{array}{l}\sin\alpha_0^2\cos^2\lambda_n\tau-2\sin\alpha_0\cos\alpha_0\sin\lambda_n\tau\cos\lambda_n\tau \\ +\cos\alpha_0^2\sin^2\lambda_n\tau\end{array}\right)\end{array}\right]\right]\end{array}\right\} \quad 44$$

then Eq.44 is written as:

$$\theta_s' = -\theta_s\left[E_1\cos 2\lambda_n\tau+E_2\sin 2\lambda_n\tau+\frac{FbG\eta(1+\lambda_n)}{2\sigma^2}\varepsilon\right]+bG\varepsilon\sin(\alpha_0-\lambda_n\tau) \quad 45$$

where,

$$E_1=\left[-\frac{\varsigma}{2}\sin 2\alpha_0+\frac{\eta}{2\sigma^2}\cos 2\alpha_0+\frac{\varsigma\lambda_n}{2}\sin 2\alpha_0-\frac{\eta\lambda_n}{2\sigma^2}\cos 2\alpha_0\right]FbG\varepsilon+\frac{G^2\sigma_n}{2}\sin 2\alpha_0$$

$$E_2=\left[\frac{\varsigma}{2}\cos 2\alpha_0+\frac{\eta}{2\sigma^2}\sin 2\alpha_0-\frac{\varsigma\lambda_n}{2}\cos 2\alpha_0-\frac{\eta\lambda_n}{2\sigma^2}\sin 2\alpha_0\right]FbG\varepsilon-\frac{G^2\sigma_n}{2}\cos 2\alpha_0$$

Eq.45 can be written in terms of spin-synchronous time constant as:

$$\theta_s' = -\theta_s\left[E_1\cos 2\lambda_n\tau+E_2\sin 2\lambda_n\tau+\frac{1}{\tau_{cs}}\right]+bG\varepsilon\sin(\alpha_0-\lambda_n\tau) \quad 46$$

where,

$$\tau_{cs} = \frac{2\sigma^2}{FbG\eta(1+\lambda_n)\varepsilon} = \frac{2\lambda_n^2\varsigma^2\left(\sigma^2 + \frac{\eta^2}{\varsigma^2\sigma^2}\right)}{\sigma_n b^2 G^2 \eta(1+\lambda_n)^2 \varepsilon} \quad 47$$

one can see that the nutation angle time history consists of dominant exponential decay super imposed on it an oscillation of small amplitude represents the effect of the trigonometric terms. So that, the general solution of Eq.46 is given by:

$$\theta_s = \theta_{sc} + \theta_{sP.I.} \quad 48$$

where, θ_{sc} : is the complementary part of the, $\theta_{sP.I.}$: is the particular part of the solution. These solutions may be given by:

$$\theta_{sc} = ce^{-\frac{\tau}{\tau_{cs}}} \quad 49$$

$$\theta_{sP.I.} = A'\sin(\alpha_0 - \lambda_n\tau) + B'\cos(\alpha_0 - \lambda_n\tau) \quad 50$$

substitute Eq.50 in Eq.46 to get:

$$A' = \frac{bG\varepsilon}{\tau_{cs}\left(\lambda_n^2 + \frac{1}{\tau_{cs}^2}\right)}, \qquad B' = \frac{\lambda_n bG\varepsilon}{\left(\lambda_n^2 + \frac{1}{\tau_{cs}^2}\right)}$$

substituting the solution of Eq.50 in Eq.48 and using the initial condition ($\theta_s = \theta_{s0}$ at time $\tau = \tau_0$) then the constant c is given by:

$$c = \theta_{s0} - \frac{\left(\left(\frac{\sin(\alpha_0 - \lambda_n\tau_0)}{\tau_{cs}}\right) + \lambda_n\cos(\alpha_0 - \lambda_n\tau_0)\right)}{\left(\lambda_n^2 + \frac{1}{\tau_{cs}^2}\right)} bG\varepsilon$$

and from Eq.48 the complete solution of the nutation angle θ_s is given by:

$$\theta_s = \left[\theta_{s0} - \frac{\left(\left(\frac{\sin(\alpha_0 - \lambda_n\tau_0)}{\tau_{cs}}\right) + \lambda_n\cos(\alpha_0 - \lambda_n\tau_0)\right)}{\left(\lambda_n^2 + \frac{1}{\tau_{cs}^2}\right)} bG\varepsilon\right] e^{\frac{-(\tau-\tau_0)}{\tau_{cs}}} + \frac{\left(\left(\frac{\sin(\alpha_0 - \lambda_n\tau_0)}{\tau_{cs}}\right) + \lambda_n\cos(\alpha_0 - \lambda_n\tau_0)\right)}{\left(\lambda_n^2 + \frac{1}{\tau_{cs}^2}\right)} bG\varepsilon \quad 51$$

RESULTS AND DISCUSSION

Figures (1) and (2) shows the nutation angle time history prepared in this work and that presented by Alfriend[2] respectively, where figure (2) represent the experimental work of Alfriend[2]. One can see that the trend of results of the present work is acceptable in comparison with Alfriend[2]. Figure (3) shows the comparison of the nutation angle time history of this work compared with that predicted by Alfriend [2], for nutation-synchronous mode. This figure shows that the time constant in this work is decreased compared with the time constant Alfriend[2]. In figure (4), the comparison of the nutation angle time history for both nutation-synchronous mode and spin-synchronous mode is shown. It is seen that the analytical solution very well agrees with the numerical solution. The time constant for nutation-synchronous mode obtained analytically is (99981) and numerically is (96428.5) which means that the percentage error is less than ($\approx 3.6\%$), and this means that the analytical solution predicts the time constant very well, and for spin-synchronous mode, it could be seen the numerical is (866.66) and the analytical is (802.17), i.e. the percentage error is ($\approx 8\%$). Figures (5, 6, 7, 8, 9 and 10) show the variation of the time constant with the inertia ratio σ, ring mean radius (R), and damping constant, respectively. The variation of the time constant with the ratio of the ring height to the ring mean radius (b) for spin-synchronous mode is shown in Fig. (11). In Fig. (12), the variation of the time constant with the distance of offset center (d) is shown. Figure (13) shows the degradation of p component while, the time history of the r component of the spacecraft angular velocity for the first relative equilibrium state is shown in Fig. (14). A three dimensional visualization of the first relative equilibrium state is shown in Fig. (15). It is shown that even the system being at a point in neighborhood of the second relative equilibrium state, it will converge to the first relative equilibrium state. This is because that the system parameters satisfy the stability condition of the first relative equilibrium state.

CONCLUSIONS

From the results shown, it is concluded that a good agreement was obtained between the analytical and numerical solutions. The proposed damper overcomes the problems of the spreading and sloshing which occur in the partially filled nutation dampers. Utilizing fluids with high damping coefficient will decrease the time constant in both modes of motion.

REFERENCES

- Adam, G. J., "Dual-spin spacecraft dynamics during platform spinup", AIAA Journal, Vol. 3, No.1, Feb. 1980.
- Alfriend, K. T.," Partially filled viscous ring nutation damper", AIAA Journal, Vol. 11, No. 7, 1974.
- Bhuta, P. G., and Koval, L. R., "A viscous ring damper for a freely precessing satellite", Int. J. Mech. Sci. Vol. 8, Jan. 1966, P.P. 283-295.
- Chang, C. O. and Liu, L. Z., "Dynamic and stability of a freely precessing spacecraft containing a nutation damper", AIAA Journal, Vol. 19, No. 2, April 1996.
- Clark, J.P.C., Debra, D.B., Dobroton, B.M., Fischell, R.E., Flleig, A.J., Fosth, D.C., Gatlin, J.A., Perkel, H., Roberson, R.E., Sabroff, A.E., Scott, E.D., Tinling, B.E, and Wheeler, P.C.," Spacecraft aerodynamic torques", NASA Space vehicle, Design criteria, Guidance and Control, SP-8085, Jan. 1971.
- Cloutier, G. J., "Nutation damper instability on Spin-stabilized spacecraft", AIAA Journal, Vol. 7, No. 11, Nov. 1969.
- Cochran, J. E., and Shu, P.H., "Effects of energy addition and dissipation on Dual-spin spacecraft attitude motion", AIAA Journal, Vol. 6, No. 5, Oct. 1983.
- Hall, C. D.," Attitude kinematics", Virginia university, Aerospace and ocean engineering, 2003.
- Hall, D. Christopher," Escape from gyrostat trap state", AIAA Journal, Vol. 21, No. 3, June 1998.
- Hall, D. Christopher, "Gravity Gradient Stabilization", AOE Aerospace and Ocean Engineering, Virginia Tech. 2003.
- Hall, C. D.,"Satellite attitude control and power tracking with momentum wheels", AIAA Astrodynamics specialist conference, 19 August 1999.
- Hall, C. D., and Rand, R. H., " Spin up dynamics of axial Dual-spin spacecraft", Journal of Guidance, Control, and Dynamics, Vol. 17, No. 1, Feb. 1994.
- Hamed, D.L., "Analysis and design of passive nutation damping for dual-spin spacecraft" PhD. Thesis, Baghdad University, College of engineering, Mechanical eng. Dep., July 2003.
- Ibanez, L.," Tutorial on Quaternions", Part I, 13 August, 2001.

- Likins, P.," Spacecraft attitude dynamics and control-a personal perspective", AIAA Journal, Vol. 9, No. 2, April 1986.
- 16- Makovec, K. L.,"A nonlinear magnetic controller for three-Axis stability of nanosatellites", Msc. Thesis, Virginia university, Aerospace engineering, 23 July 2001.
- 17- Meehan, P. A. and Asokanthan, S. F.,"control of chaotic instability in a Dual-spin spacecraft with dissipation using energy methods", Multibody system dynamics 7, 2002, p.p.171-188.
- 18-Sandfry, R.A.," Equilibrium of a gyrostat with a discrete damper", PhD. Thesis, Virginia University, Aerospace engineering dep., 9 July 2001.
- 19- Ali H. H., "Dynamic of Dual-spin Spacecraft Containing a Nutation Damper", M.Sc. Thesis, Babylon University, College of Engineering, 2007.
- 20- Shibly A. H.,"Sliding mode controller for a three-axis gas get satellite Attitude control system", Msc. Thesis, Al-Nahrain university, college of engineering, Dec. 1995.
- 21- Yang, W. Y., Cao, W., Chung, T., and Morris, J.," Applied numerical methods using MATLAB", John Wiley and sons, 2005.
- 22- "البرمجة باستخدام ماتلاب", عبد الكريم البيكو, 2006.

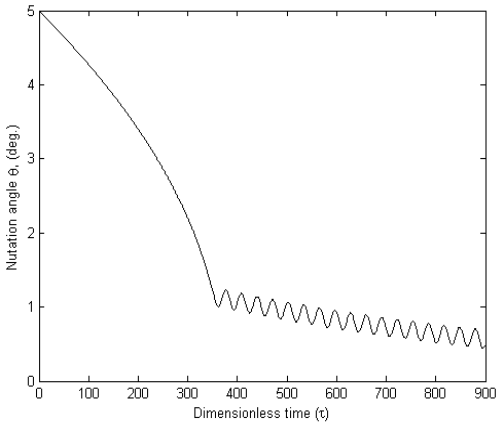

Fig. (1). Nutation angle time history of present work.

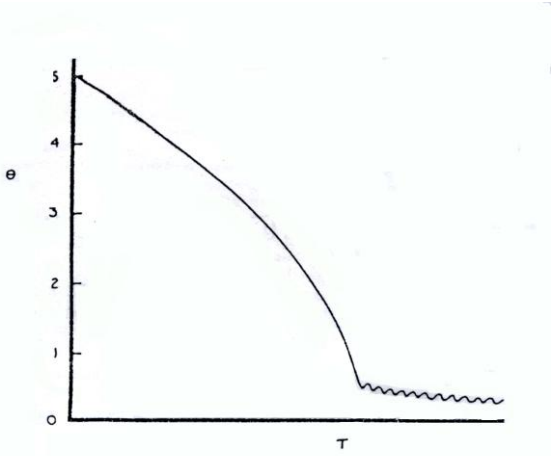

Fig. (2).Nutation angle time history of the ref.(2).

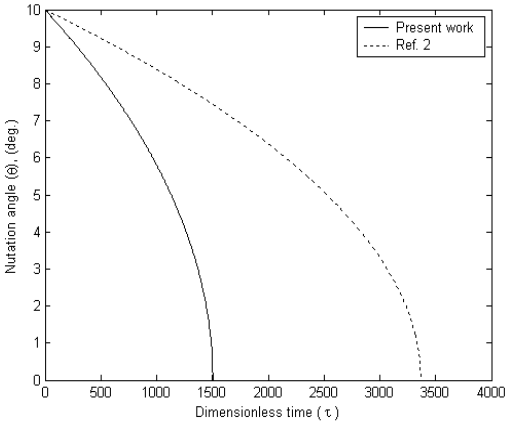

Fig. (3). Comparison of the nutation angle time history of present work with ref.(2) for the nutation-synchronous mode.

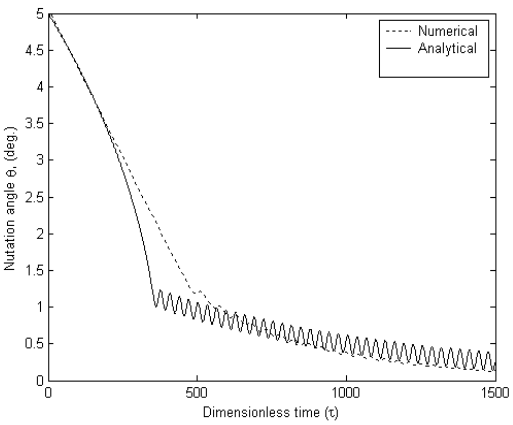

Fig. (4). Comparison between numerical and analytical solution of the nutation angle time history.

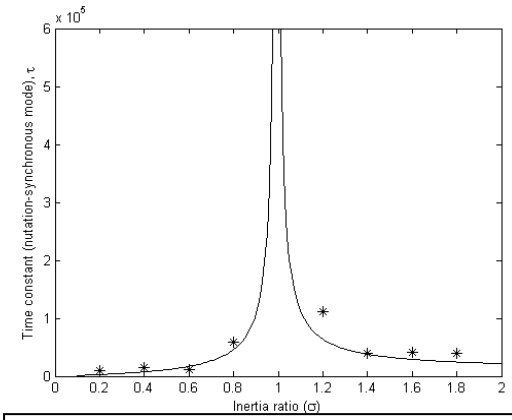

Fig. (5). Influence of the inertia ratio (σ) on the time constant for the nutation-synchronous mode.

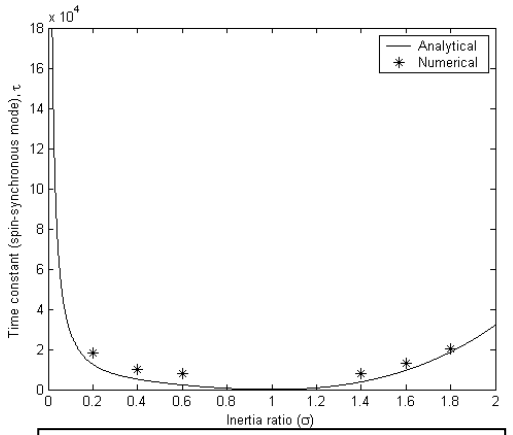

Fig. (6). Influence of the inertia ratio (σ) on the time constant for the spin-synchronous mode.

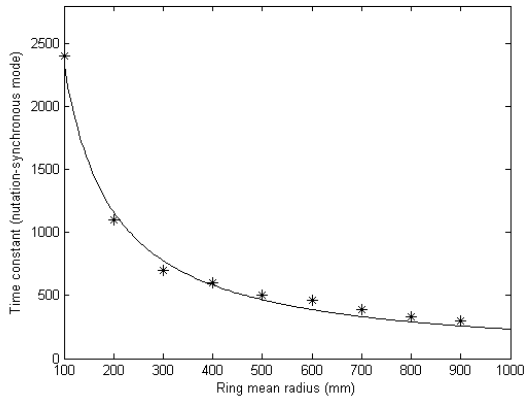

Fig. (7) Influence of the ring mean radius on the time constant for nutation-synchronous mode.

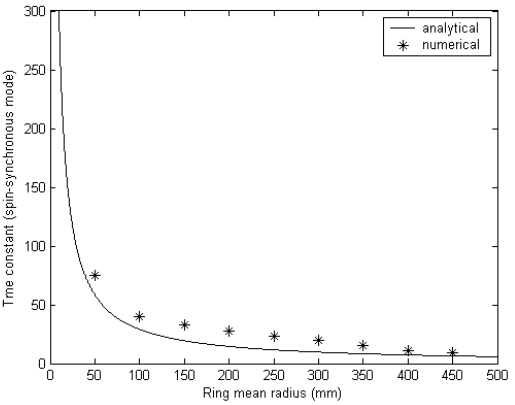

Fig. (8) Influence of the ring mean radius on the time constant for spin-synchronous mode.

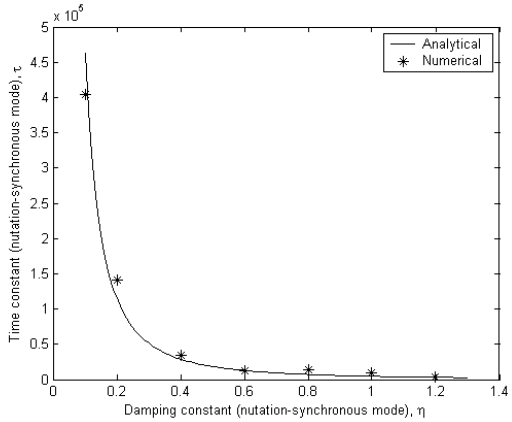

Fig. (9) Influence of the damping constant on the time constant for nutation-synchronous mode.

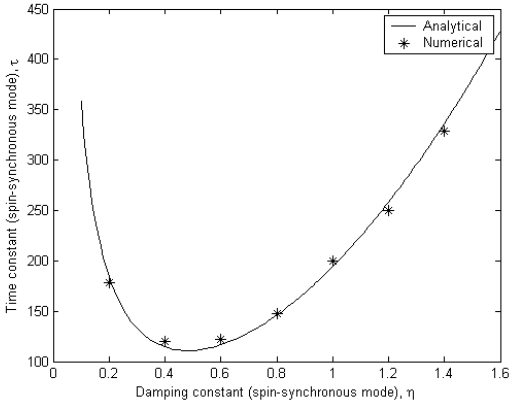

Fig. (10) Influence of the damping constant on the time constant for spin-synchronous mode.

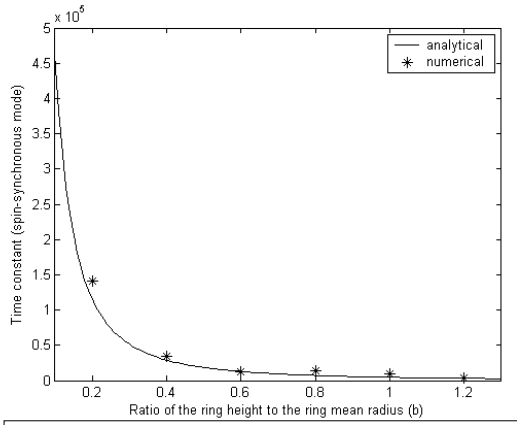

Fig. (11) Influence of the ratio of the ring height to the ring mean radius, b on the time constant for spin-synchronous. mode.

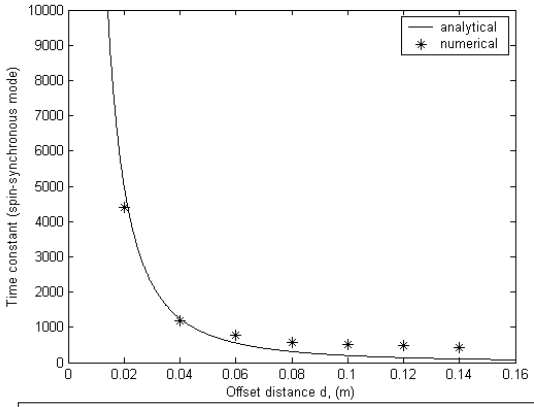

Fig. (12) Influence of the offset distance, d on the time constant for spin-synchronous mode.

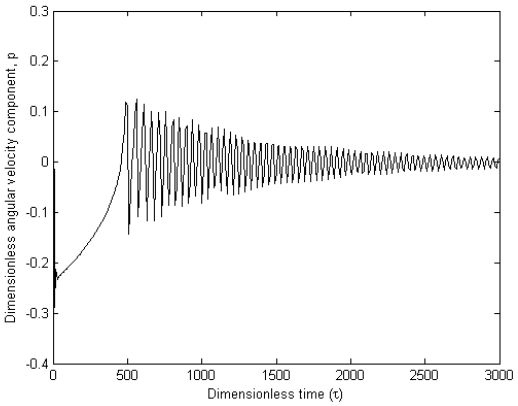

Fig. (13) Time history of dimensionless angular velocity component (p) for condition $(p_0, q_0, r_0)^T=(0.15, 0.3, 0.9)^T$. First relative equilibrium state.

.

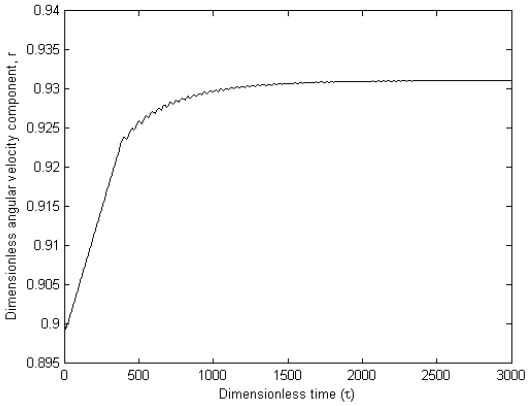

Fig. (14) Time history of dimensionless angular velocity component (r) for condition $(p_0, q_0, r_0)^T=(0.15, 0.3, 0.9)^T$. For the first relative equilibrium state.

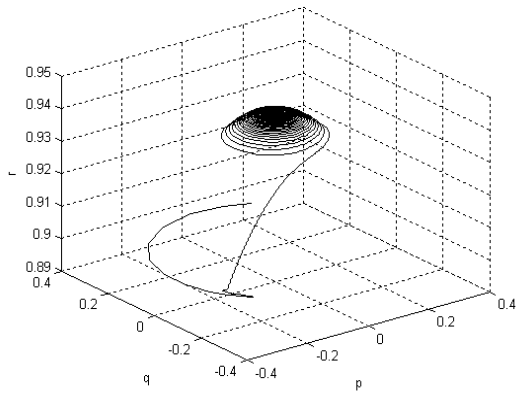

Fig. (15) Three dimensional visualization shows that the spacecraft diverge from second relative stability and reaches to the first relative stability, σ =1.2, $(p_o, q_o, r_o)^T$=(0.15, 0.3, 0.9)^T.

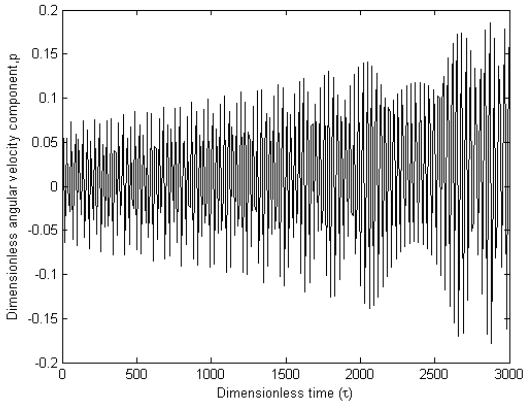

Fig. (16) Time history of dimensionless angular velocity component (p) for condition $(p_0, q_0, r_0)^T$=(0.01, 0.07, 0.95)^T.
Second relative equilibrium state.

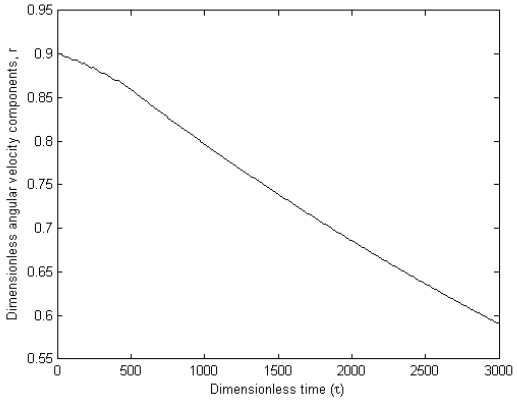

Fig. (17) Time history of dimensionless angular velocity component (r) for condition $(p_0, q_0, r_0)^T$=(0.01, 0.07, 0.95)^T
For the second relative equilibrium state.

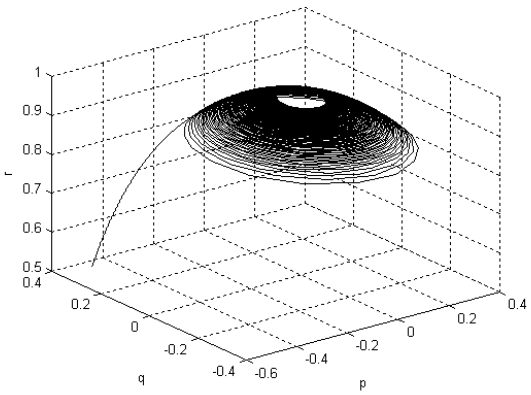

Fig. (18) Three dimensional visualization shows that the spacecraft diverge from first relative stability and reaches to the second relative stability, σ =0.75, $(p_o, q_o, r_o)^T$=(0.01,

Appendix

$$p=\frac{\omega_u}{\Omega},\ q=\frac{\omega_v}{\Omega},\ r=\frac{\omega_z}{\Omega},\ b=\frac{h}{R},\ \varepsilon=\frac{mR^2}{A},\lambda=\sigma-1,\lambda_s=\frac{C_p\Omega_p}{A\Omega},\lambda_n=\lambda+\lambda_s$$

$$D_1=1+\varepsilon\left(\frac{1}{2}+\frac{h^2}{R^2}+\frac{d^2}{R^2}-\frac{b^2G^2}{\varsigma}\right),A_1=\varepsilon\left(\frac{1}{2}+b^2G^2+G^2-b^2\right),$$

$$A_2=\varepsilon\left(\frac{1}{2}+b^2G^2+G^2-b^2\right)=A_1,\ A_3=-\varepsilon\left(bG\left(1+\frac{G^2}{\varsigma}\right)\right),\ A_4=\varepsilon bG,\ A_5=\varepsilon C_1bG$$

$$D_2=1+\varepsilon\left(\frac{1}{2}+\frac{h^2}{R^2}\right),B_1=\varepsilon\left(\frac{h^2}{R^2}-\frac{1}{2}\right),B_2=\varepsilon\left(\frac{h^2}{R^2}-\frac{1}{2}\right)=B_1,B_3=\varepsilon bG,B_4=\varepsilon bG=B_3$$

$$C_1=\frac{\eta\lambda_n}{\varsigma\sigma^2}\left(1+\frac{\varepsilon\varsigma}{\sigma}\right),\ C_2=-\frac{G^2}{\varsigma},\ C_3=\frac{bG}{\varsigma},\ \ C_4=\frac{\eta}{\sigma}\varepsilon$$

$$h_u=(A+I_u)\omega_u-I_{uz}\left(\omega_z+\dot{\alpha}\right),\ h_v=(A+I_v)\omega_v,\text{ and }\ h_t=\sqrt{h_u{}^2+h_v{}^2}$$

BEHAVIOUR OF CROSS - PLY LAMINATED HYBRID COMPOSITE PLATES WITH AN INCLINED CRACK SUBJECTED TO A UNIFORM TEMPERATURE RISE

Dr. Majid H. Faidh-Allah,
Dept. of Mech. Eng./ Baghdad University

ABSTRACT

Thermal buckling analysis of symmetric and antisymmetric cross-ply laminated hybrid composite plates with an inclined crack subjected to a uniform temperature rise are presented in this paper. The first-order shear deformation theory in conjunction with variational energy method is employed in the mathematical formulation. The eight-node Lagrangian finite element technique is used for obtaining the thermal buckling temperatures of hybrid composite laminates. The effects of crack size and lay-up sequences on the thermal buckling temperatures for symmetric and a antisymmetric plates are investigated. The results are shown in graphical form for various boundary conditions. Finally , from this paper, the following main results have been found from which the buckling temperature is affected the larger crack length more than the small crack length, together with other result that the buckling temperature of the plate for every perforation angle is to increase while crack length is increasing .

KEYWORDS: hybrid composite plates, thermal buckling, finite element method.

الخلاصة

ان تحليل الانبعاج الحراري للصفائح الرقيقة الهجينة المصنعة من مواد مركبة ذات الطبقات المتماثلة وغير المتماثلة ذات الشق المائل والتي تخضع لإرتفاع منتظم لدرجات الحرارة تمت دراستها في هذا البحث . وقد تم استخدام نظرية تشوه القص ذات الرتبة الاولى المرتبطة بنظرية الطاقة المتغيرة في الصياغة الرياضية لهذا البحث، كذلك تم استخدام تقنية العناصر المحددة بثمانية عقد للحصول على درجات حرارة الانبعاج الحراري للصفائح المركبة الهجينة. كما تم دراسة تأثيرات حجم الشق ومواضع تسلسل درجات حرارة الانبعاج الحراري للصفائح المتماثلة وغير المتماثلة. ان النتائج موضحة على شكل مخطط وبشروط حدية مختلفة.وأخيراً ومن خلال البحث تم الحصول على اهم النتائج ومنها تأثير الانبعاج الحراري على طول الشق الكبير اكثر من الشق الصغير بالاضافة الى ان الأنبعاج الحراري للصفيحة لكل زاوية ناتجة يزداد مع زيادة طول الشق .

INTRODUCTION

Fiber reinforced structures are widely used in so many engineering applications. because of their low weight and high strength. Stability of these structures is important especially at elevated temperatures.

The thermal buckling analyses or orthotropic plates including a crack, were investigated by **Avci , A. and Sahin , O.S.,2005** Thermal buckling analysis of symmetric and antisymmetric cross-ply laminated hybrid composite plates with a hole subjected to a uniform temperature rise for different boundary conditions was studied by using finite elements method by **Avci ,**

A. and Sahin , O.S.,2005. In that paper the effects of hole size, lay-up sequences and boundary conditions on the thermal buckling temperatures were investigated. **Akbulut, H. and Sayman,O.,2001** were studied the buckling behavior of laminated composite plates with central square openings for various boundary conditions and stacking sequences by using finite element method.

The thermal buckling of isotropic and composite plates with a hole by using both closed form solution and finite elements method was investigated by **Chang, J.S.and Shiao,F.J.,1990**. Thermal buckling of antisymmetric cross-ply composite laminates was investigated by **Mathew, T.C. and Rao, G.V.,1992**. Abramovich investigated the thermal buckling behavior of cross-ply symmetric and nonsymmetrical laminated beams employing the first-order deformation theory. **Murphy, K.D. and Ferreira, D.,2000**. Studied theoretical and experimental approaches to obtain the buckling temperature and buckling mode for flat rectangular plates. **Huang, N.N. and Tauchert, T.R., 1992.** Studied the thermal buckling of clamped symmetric angle-ply laminated plates employing a Fourier series approach and the finite element method. **Prabhu, M.R. and Dhanaraj, R., 1994 Thangaratnam, K.R. and Ramaohandran,J.,1989** , also studied the thermal buckling of the laminates subjected to uniform temperature rise or non uniform temperature fields using the finite element approach.

An extensive overview of the general buckling problems of laminated composite plate was made by **Liessa,A.W.,1987.**

In that study, some complicated effects were investigated such as shear deformation, hydrothermal factors and post buckling behavior. The influence of temperature distribution on buckling modes has investigated by **Bednarczyk,H. and Rihter,M.,1985**. The thermally induced buckling of antisymmetic angle-ply laminated plates with Levy-type boundary conditions was investigated by **Chen,L.W. and Liu, W.H., 1993** . Thermal buckling behavior of composite laminated plates with transverse shear deformation was studied by **Sun,L.X. and Hsu,T.R.,1990. Chockalingam, S. ,1992.** investigated the thermal buckling of antisymmetric cross-ply hybrid laminates by using finite element technique based on first-order shear deformation theory. **Chen ,W. and Liu, W.H., 1993**. also studied thermal buckling of laminates subjected to uniform temperature rise or non uniform temperature fields using finite element approach. Local buckling of composite laminar plates was considered and the critical strains of laminated plates with various shaped local delamination and different stacking patterns are obtained by making use of the energy principle. by **Wang, X.and Lu,G.,2003**. Also non-linear thermal buckling for local delamination near the surface of laminated cylindrical shell problem was studied by **Wang, X.and Lu,G.,2003**.

The present paper aims to determine the buckling temperature and buckling mode shapes for hybrid composite laminates with different inclined crack by using the finite element method. The thermal buckling of symmetric and antisymmetric cross-ply laminates with cracks is investigated, based on the first-order deformation theory in conjunction with the variational energy method. The finite clement approach is used for obtaining the thermal buckling temperatures for boron/epoxy-glass/epoxy hybrid laminates. The effects of crack length, crack inclination angle and lay-up sequences on the thermal buckling temperatures have been studied numerically . The buckling behavior of boron/epoxy-glass/epoxy hybrid composite plates was compared with E-glass/epoxy plates.

MATHEMATICAL FORMULATION

The laminated orthotropic construction of the plate is consisted of N layers. Each layer is of thickness t_k, so that $h = \sum_{k=1}^{N} t_k$ is the total thickness of the laminate.

The longitudinal and lateral dimensions of the laminate are a and b and subjected to uniform

temperature difference ΔT between ambient and laminated plate as shown in **Fig. 1**. The linear stress-strain relation for each layer is expressed with x, y-axes and has the form**(Whitney,J.M.,1973)** .

$$\begin{Bmatrix}\sigma_x\\ \sigma_y\\ \tau_{xy}\end{Bmatrix}_k = \begin{bmatrix}\bar{Q}_{11} & \bar{Q}_{12} & \bar{Q}_{16}\\ \bar{Q}_{12} & \bar{Q}_{22} & \bar{Q}_{26}\\ \bar{Q}_{16} & \bar{Q}_{26} & \bar{Q}_{66}\end{bmatrix}_k \begin{Bmatrix}\varepsilon_x & -\alpha_x\Delta T\\ \varepsilon_y & -\alpha_y\Delta T\\ \varepsilon_{xy} & -\alpha_{xy}\Delta T\end{Bmatrix}_k$$

$$\begin{Bmatrix}\tau_{yz}\\ \tau_{xz}\end{Bmatrix} = \begin{bmatrix}\bar{Q}_{44} & \bar{Q}_{45}\\ \bar{Q}_{45} & \bar{Q}_{55}\end{bmatrix}\begin{Bmatrix}\gamma_{yz}\\ \gamma_{xz}\end{Bmatrix} \qquad (1)$$

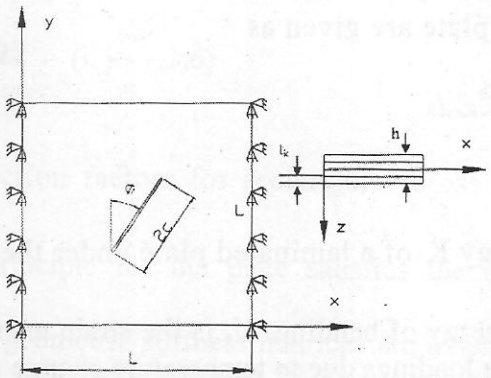

Fig. 1. Geometry of the problem and coordinates

where $\sigma_x, \sigma_y, \tau_{xy}, \tau_{yz}$ and τ_{xz} are the stress components, $\bar{Q}_{ij}$ are transformed reduced stiffnesses, which can be expressed in terms of the orientation angle and the engineering constant of the material. ΔT is temperature difference, α_x, and α_y, are the coefficients of thermal expansion in directions of x and .y-axes, respectively. α_{xy} is the apparent coefficient of thermal shear, such as**(Jones, R.M.,1975)**

$$\alpha_x = \alpha_1\cos^2\theta + \alpha_2\sin^2\theta$$
$$\alpha_y = \alpha_2\cos^2\theta + \alpha_1\sin^2\theta \qquad (2)$$
$$\alpha_{xy} = 2(\alpha_1 - \alpha_2)\sin\theta.\cos\theta$$

α_1 and α_2 are the thermal expansion coefficients of the lamina along the longitudinal and transverse directions of fibers, respectively.

In this study first-order shear deformation theory is used. The displacements u, v and w can be written as follows:

$$u(x, y, z) = u_0(x, y) + z\,\psi_x(x, y)$$
$$v(x, y, z) = v_0(x, y) + z\,\psi_y(x, y) \qquad (3)$$
$$w(x, y, z) = w(x, y)$$

where. u_0, v_0 , w are the displacements along to x, y, and z-axes. respectively, at any point of the middle surface, and, ψ_x , ψ_y are the bending rotations of normal to the mid plane about the x and y axes, respectively. The bending strains ε_x , ε_y and transverse shear strains γ_{xy}, γ_{yz} , γ_{xz} at any point of the laminate are **(Jones, R.M.,1975)**

$$\begin{Bmatrix}\varepsilon_x\\ \varepsilon_y\\ \gamma_{xy}\end{Bmatrix}=\begin{vmatrix}\frac{\partial u_0}{\partial x}\\ \frac{\partial v_0}{\partial y}\\ \frac{\partial u_0}{\partial y}+\frac{\partial v_0}{\partial x}\end{vmatrix}+z\begin{vmatrix}\frac{\partial \psi_x}{\partial x}\\ \frac{\partial \psi_y}{\partial y}\\ \frac{\partial \psi_x}{\partial y}+\frac{\partial \psi_y}{\partial x}\end{vmatrix}$$

$$\begin{vmatrix}\gamma_{yz}\\ \gamma_{xz}\end{vmatrix}=\begin{vmatrix}\frac{\partial w}{\partial y}-\psi_y\\ \frac{\partial w}{\partial x}+\psi_x\end{vmatrix} \quad (4)$$

The resultant forces N_x, $N_y$and N_{xy}, moments M_x , $M_y$and M_{xy} and shearing forces Q_x ,Q_y per unit length of the plate are given as

$$\begin{bmatrix}N_x & M_x\\ N_y & M_y\\ N_{xy} & M_{xy}\end{bmatrix}=\int_{-h/2}^{h/2}\begin{Bmatrix}\sigma_x\\ \sigma_y\\ \tau_{xy}\end{Bmatrix}(1.z)dz$$

$$\begin{Bmatrix}Q_x\\ Q_y\end{Bmatrix}=\int_{-h/2}^{h/2}\begin{Bmatrix}\tau_{xz}\\ \tau_{yz}\end{Bmatrix}dz \quad (5)$$

The total potential energy K of a laminated plate under thermal loading is equal to

$$K=U_b+U_s+V \quad (6)$$

where U_b is the strain energy of bending, U_s is the strain energy of shear and V represents the potential energy of in-plane loadings due to temperature change

$$U_b=1/2\int_{-h/2}^{h/2}\left[\int\int_R(\sigma_X\varepsilon_X+\sigma_Y\varepsilon_Y+\tau_{XY}\gamma_{xy})dA\right]dz$$

$$U_S=1/2\int_{-h/2}^{h/2}\left[\int\int_R(\tau_{xz}\gamma_{xz}+\tau_{yz}\gamma_{yz})dA\right]dz$$

$$V=1/2\int\int_R[\bar{N}_1(\partial w/\partial x)^2+\bar{N}_2(\partial w/\partial y)^2+2\bar{N}_{12}(\partial w/\partial x)(\partial w/\partial y)dA-\int_{\partial R}(\bar{N}_n^b u_n^o+\bar{N}_n^b u_z^o)ds \quad (7)$$

Here $dA=d_x d_y$, R is the region of a plate excluding the crack. $\bar{N}_n^b$ and $\bar{N}_s^b$ are in-plane loads applied on the boundary ∂R. For the equilibrium, the potential energy K must be stationary. The equilibrium equations of the cross-ply laminated plate subjected to temperature change can be derived from the variational principle through use of stress-strain and swain-displacement relations. One may obtain these equations by using $\delta K = 0$.

Finite Element Formulation

In general, a closed form solution is difficult to obtain for buckling problems Therefore numerical methods are usually used for obtaining an approximate solution. In order to study the buckling of the plate, an eight-node Lagrangian finite element analysis is applied in this study. The stiffness matrix of the plate is obtained by using the minimum potential energy principle. Bending stiffness [K_b], shear stiffness [K_s] and geometric stiffness [K_g] matrices can be expressed as

$$[K_b]=\int_A[B_b]^T[D_b][B_b]dA \quad (8)$$

$$[K_s]=\int_A[B_s]^T[D_s][B_s]dA \quad (9)$$

and

$$[K_g] = \int_A [B_g]^T [D_g][B_g]\, dA \qquad (10)$$

Where

$$[D_b] = \begin{bmatrix} A_{ij} & B_{ij} \\ B_{ij} & D_{ij} \end{bmatrix} \qquad [D_b] = \begin{bmatrix} K_1^2 A_{44} & 0 \\ 0 & K_2^2 A_{55} \end{bmatrix}$$

and $$[D_g] = \begin{bmatrix} \bar{N}_1 & \bar{N}_{12} \\ \bar{N}_{12} & \bar{N}_2 \end{bmatrix} \qquad (11)$$

$$(A_{ij}, B_{ij}, D_{ij}) = \int_{-h/2}^{h/2} \bar{Q}_{ij}(1, z, z^2)\, dz \quad (i, j = 1,2,6) \qquad (12)$$

$$(A_{44}, A_{55}) = \int_{-h/2}^{h/2} (\bar{Q}_{44}, \bar{Q}_{55})\, dz \qquad (13)$$

A_{44} and A_{55} are the shear correction factors for rectangular cross section are given by $K_1^2 = K_2^2 = 5/6$ (Whitney)

The total potential energy principle for the plate satisfies the assembly of the element equations.

The element stiffness and the geometric stiffness matrices are assembled. The corresponding eigenvalue problem can be solved using any standard Eigen value extraction procedures **(Bathe, K.J.,1982)**

$$\left[[K_\theta] - \lambda_b [K_{\theta g}]\right] \begin{Bmatrix} u_j \\ u_i \\ w_i \end{Bmatrix} = 0 \qquad (14)$$

where

$[K_\theta] = [K_b] + [K_s]$, and $-\lambda_b [K_{\theta g}] = [K_g]$ **(15)**

The product of λ_b and the initial guess value ΔT is the critical buckling temperature T_{cr}. that is

$T_{cr} = \lambda_b \Delta T$ **(16)**

NUMERICAL RESULTS AND DISCUSSION

There are many techniques to solve Eigen value problems. In this study the Newton Raphson method is applied to obtain numerical solutions of the problem. For thermal buckling due to a ΔT temperature change in the plate, the uniaxial or biaxial in-plane loads are developed along the rectangular edges, while the crack edges are free.

The E-glass/epoxy, and boron/epoxy are considered as components of hybrid plate and their thermo-elastic properties are given in **Table 1.** Here, E_1 and E_2 are elastic moduli in 1 and 2 directions, respectively. υ_{12} is Poisson's ratio and α_1 and α_2, are thermal expansion coefficients of the materials used in the solution. The effect of α_{12}, is neglected.

Stacking sequence of hybrid composite plates have been taken both symmetric and antisymmetric. Stacking sequences have been represented below. Boron/epoxy and glass/epoxy layers are named B and G, respectively.

Table 1 Material properties

Material	E_1 (Gp_a)	E_2 (Gp_a)	E_{12} (Gp_a)	υ_{12}	$\alpha_1(1/°C)$	$\alpha_2(1/°C)$
E-glass / epoxy	15	6	3	0.3	7.0×10^{-6}	2.30×10^{-5}
Boron/ epoxy	101	19	4.8	0.12	4.17×10^{-6}	1.91×10^{-5}

The sequence of 4 Layers symmetric lay up of glass/ epoxy-boron / epoxy is 0°G / 90°B /90°B /0°G The sequence of 4 Layers ant symmetric lay up of glass / epoxy-boron/epoxy is 0°G /90°B /0°G/90°B

Each layer has 0.25 mm thickness and the length of one edge of square plate is 100 mm. 2c/L. ratio. represents the crack size to length of one side of composite plate and ϕ represents the crack inclination angle as shown in **Fig. 1**.

A wide range of boundary conditions can be accommodated, but only one kind of boundary conditions is chosen as defined below:

Two edges clamped and two edges are free

$$At\ x = -\frac{L}{2}\ and\ \frac{L}{2}\quad u = w = \psi_y = \psi_x = 0$$

Fig. 2 shows the meshed plate. Four edges of plate have divided into ten parts disregarding the crack size.

Buckling in this paper , ANSYS program version 9 has been used .Behavior of anti symmetrically stacked hybrid composite plate is shown in **Fig.3**. In this figure. T/T_0 ratio is used instead of buckling temperature and 2C/L ratio is used instead of crack length C. Here T_0 represents the buckling temperature of hybrid plate without crack. Thus graph is plotted by using dimensionless axes. It can be seen that when the crack inclination angle $\phi = 90°$' and $\phi = 60°$ T/T_0 ratio decreases while crack length increases. The case of $\phi = 30°$ and $\phi = 0°$ T/T_0 ratio increases while crack length increases. If inclination angle decreases, the buckling temperature or T/T_0 ratio decreases. For larger values of crack length, the difference between temperatures for different inclination angles increase. These results show that buckling temperature is effected by both crack length and inclination angle.

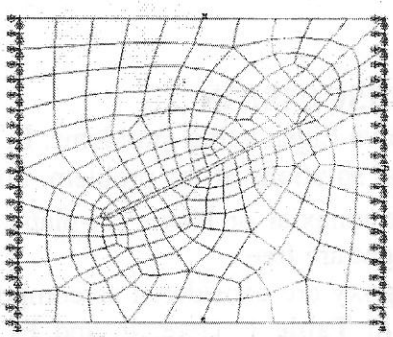

Fig.2.Typical mesh

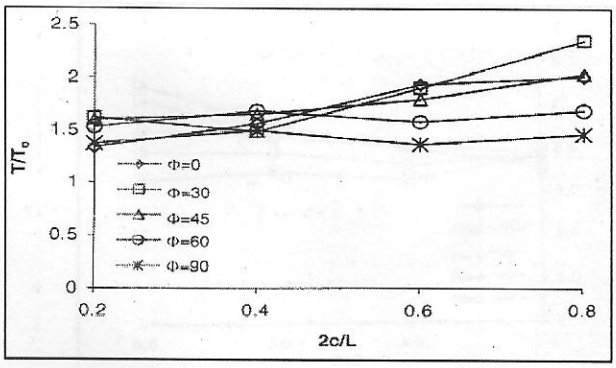

Fig.3.Effect of crack size and position on buckling temperature of antisymmetrically stacked hybrid composites plate.

The buckling behavior of symmetrically stacked hybrid plate is shown in **Fig. 4**.

Fig. 3 shows that, the buckling temperature is depending on crack length and crack inclination angle. But T/To ratio in symmetrically stacked plate is greater than antisymmetrically stacked one for fixed crack length and inclination angle. This result shows that the buckling temperature and consequently the buckling resistance of symmetrically stacked hybrid plate is greater than that of antisymmetrically stacked hybrid plates.

The relationship between crack size and buckling temperature is shown in **Figs. 5** and **6**. Buckling temperature is plotted with respect to crack size for various inclination angels of antisymmetrically stacked E-Glass/epoxy plates in **Fig. 5**. The smallest T/T0 ratios are obtained for crack inclination angle of $\Phi = 90°$. On the other hand, it is concluded that, the effect of cracks upon buckling temperature become clear as the crack length increases. Though this behavior is similar for all crack inclination angles, for small inclination angles, this behavior can be seen clearly.

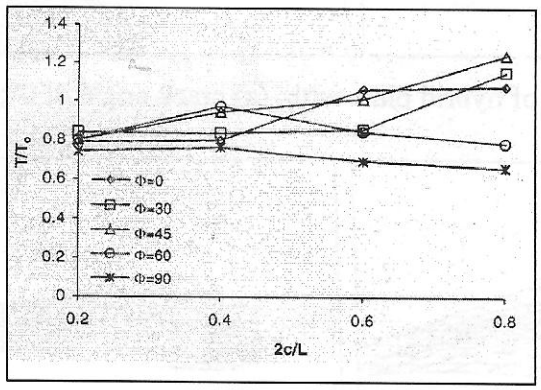

Fig.4. Effect of crack size and position on buckling temperatures of symmetrically stacked hybrid

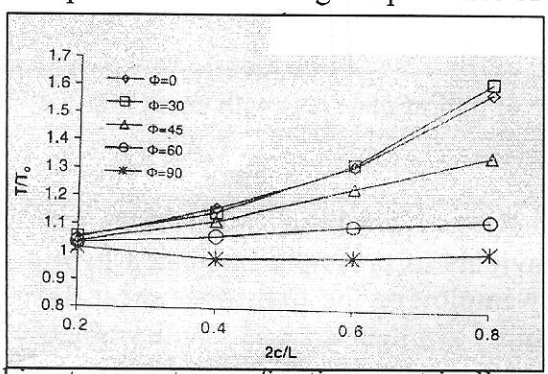

Fig.5.Variation of bucking temperatures of antisymmetrically stacked E-galss/epoxy plate.

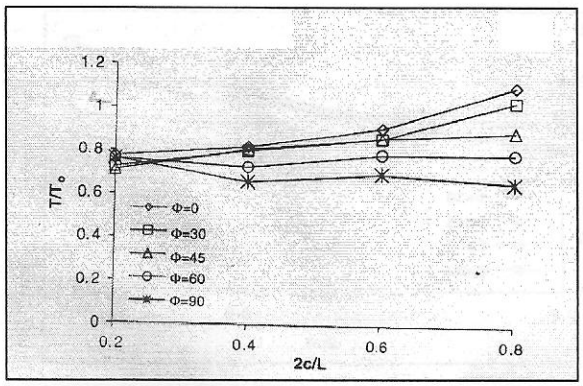

Fig.6.Variation of bucking temperatures of symmetrically stacked E-galss/epoxy plate

The first buckled mode shapes generated glass/epoxy cross-ply laminated plates with inclined crack are shown in **Figs. 7** and **8**. It is found that critical temperature for crack angle of 0°is 26,284 °C. for crack angle of 60° is 20,851 °C. for crack angle of 90° is 17,148 °C and critical temperature for plate without crack is 24,572 °C, respectively. The mode shapes presented in **Figs. 7** and **8** show considerable skewing for the laminated plates

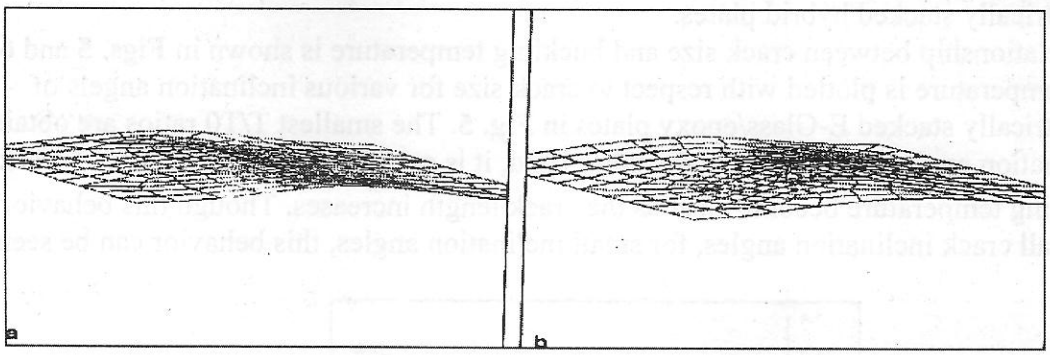

Fig.7.Bukled mode shape of hybrid plate with: (a) crack angle of 0°;(b)crack angle of 60°

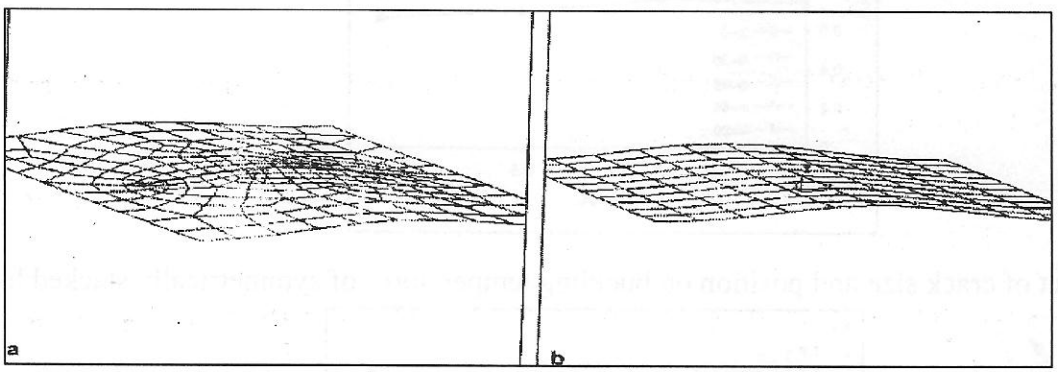

Fig.8.Bukled mode shape of hybrid plate: (a) with crack angle of 90°;(b)without crack

CONCLUSIONS

- Following are the main summarized conclusions drawn from this paper are considered:
- Thermal buckling behaviours of cross-ply laminated hybrid plates with inclined crack have been examined by employing the first-order shear deformation theory and finite lement technique.Both symmetric and antisymmetric lay-up sequence are considered.

- Because of absence of bending-extension coupling, symmetric cross-ply E-glass/epoxy laminates does not yield the highest buckling resistance as expected. Effect of crack upon thermal buckling is minimum while crack inclination angle is 90°.
- As the crack length increases, this effect becomes clear. Effect of cracks upon thermal buckling for hybrid laminated composite plate and E-glass/epoxy laminates are different.
- Effect of crack upon thermal buckling for antisymmetrically stacked hybrid laminates is neative while cracks cause positive effect on symmetrically stacked hybrid plates and effect of cracks upon thermal buckling for antisymmetrically stacked E-glass/epoxy laminates is positive while cracks cause negative effect on symmetrically stacked E-glass/epoxy plates.
- The buckling temperature is affected the larger crack length more than the small crack length as shown in **Figs. 3-6**. For small crack length the high temperature or high thermal stresses can be supported by the imperforated section of the plate. This result can be seen for every perforation angles in **Figs. 3-6**. T / T_0 rates converge the "1" for small perforations at all plates.
- Another result is that buckling temperature of the plate for every perforation angel is to increase while crack length is increasing. This result is expected. Because the higher temperature needs for reaching the same stress level for buckling when the perforation is bigger. If the crack length is great, that means that stressed cross section is fewer so this cross section must be heated much more than when the imperforated section is higher.

REFERENCES

- Abramovich H. Thermal buckling of cross-ply laminates using a first order deformation theory. Comp Struct 1994;28:201-I3.
- Akbulut H. Sayman O. An investigation on buckling of laminated plates with central square hole, ,JRPC 2001:20:1112- 24.
- Avci A. Sahin OS, Uyaner M. Thermal buckling of hybrid laminated composite plates with a hole. J Compos Struct 2005:68:247- 54.
- Bathe K.J. Finite element procedures in engineering analysis. Engle-wood Cliffs (NJ)Prentice-Hall, Inc.; 1982.
- Bednarczyk H. Righter M. Buckling of plated due to self-equilibrated thermal stresses. J Therm Stress 1985:8:139 -52.
- Chandrashickhara MR. Buckling of multilayered composite plates under uniform temperature field. In: Birman V, Hui D. Thermal effects on structures and materials. ASME Pub., vol. 203. AMD, vol. 110; 1990. p. 29 -33.
- Chang JS, Shiao FJ. Thermal buckling analysis of isotropic and composite plates with hole. J Therm Stress 1990:13:315-32.

- Chen L.W, Lin PD. Chen LY. Thermal buckling behavior of thick composite laminated plates under non-uniform temperature distribution. Comp Struct 1991:41:637-45.
- Chen LW, Lin PD. Chen LY. Thermal buckling behavior of thick composite laminated plates under non-uniform temperature distribution. Comp Struct 1991:41:637-45.
- Chen LW. Lin PD. Chen LY. Thermal buckling behavior of thick composite laminated plates under non-uniform temperature distribution. Comp Struct 1991:41:637- 45.
- Chen W. Liu WH. Thermal buckling of antisymmetric angle-ply laminated plates-an analytical levy-type solution. J Therm Stresses 1993:16:401 -19.
- Chockalingam: S. Mathew TC. Singh G. Rao GV. Critical temperatures of hybrid laminates using finite elements. Comp Struct 1992:43(5):995- 8.
- Huang NN. Tauchert TR. Thermal buckling of clamped symmetric laminated plates. GThin-Walled Struct 1992:13:259-73.
- Jones RM. Mechanics of composite materials. Tokyo: McGraw-Hill Kogagusha Ltd.: 1975.
- Liessa AW. A review of laminated composite plate buckling. Appl Mech Rec 1987:40:575-91.
- Lin CH. Kuo CS. Buckling of laminated plates with holes. J Compos Mater 1989:23:536- 53.
- Mathew TC, Singh G, Rao GV. Thermal buckling of cross-ply composite laminates. Comp Struct 1992:42(2):281-7.
- Murphy K D, Ferreira D. Thermal buckling of rectangular plates. Int J Solids Struct 2000:38:3979-94.
- Prabhu MR. Dhanara.j R. Thermal buckling of laminated composite plates. Comp Struct 1994:1193-204.
- Sahin OS. Avci A. Kaya S.Thermal buckling of orthotropic plates with angle crack. J Reinf Plast Compos 2004:23(16): 1707- 16.
- Sun LX. Hsu TR.Thermal buckling of laminated composite plates with transverse shear deformation. Comp Struct 1990:36(5): 883-9.
- Thangaratnam KR, Ramachandran J.Thermal buckling of composite laminated plates. Comp Struct 1989;32:1117-24.
- Thangaratnam KR. Ramaohandran J. Thermal buckling of composite laminated plates. Comp Struct 1989;32:1117 -24.

- Wang X, LU G, Xiao DG. Non-linear thermal buckling for local delimitation near the surface of laminated cylindrical shell. Int J Mech Sci 2002:44:947-65.
- Wang X, Lu G. Local buckling of composite laminar plates with various delaminated shapes. Thin-Walled Struct 2003:41:493-506.

- Whitney JM. Shear correction factors for orthotropic laminates under static load. J ;Appl Mech 1973 (march):302-4.

WOVEN FACTOR FOR THE MECHANCIAL PROPERTIES OF WOVEN COMPOSITE MATERIALS

Dr. Kadhim H. Ghlaim
Dejla University College

ABSTARCT

In the past years, the use of composite materials in the aircraft industry, among others, has grown immensely. Composite systems offer an advantage over traditional aircraft materials (metals) because they tend to exhibit higher strength/weight and stiffness/weight ratios than metals, thus making the aircraft lighter and improving performance. Woven composites are increasingly considered for such applications because they offer ease in manufacturing of complicated geometries, but the mechanical properties for different weave patrons of the material is even less well characterized than that of non-woven (angle-ply) laminates. For this reason and because the woven composite mechanical properties is impotent for the theoretical work of the presented work way. The woven factors were evaluated and measured for the composite with different weave patrons, fiber materials and matrix materials. The woven factors were calculated from the measuring mechanical properties from tensile tests of woven composite and for the cross-unidirectional composite made from the same materials. Three types of fiber were used which are E-Glass, Kevlar, and Carbon, while epoxy and polyester were used as a matrixes. The results showing that the woven factors for the Kevlar is higher than the E-Glass and the Carbon and the composites reinforce epoxy have higher woven factors than the composites reinforced polyester.

معاملات النسج في الخواص الميكانيكي للمواد المركبة النسيجية

الخلاصة

ازداد استعمال المواد المركبة في السنوات الاخير للما تتميز به من خواص نسبية للمقاومة الى الكثافة و الشدة الى الكثافة و التي جعلت الاجزاء الميكانيكية اقل وزنا . وتميزت منها المواد المركبة النسيجية لهولة تشكيلها بتظاريس معقدة الشكل. لهذا السبب اصبح استخراج الخواص الميكانيكية لها ذ اهمية يالغة في التحليلات النظرية. لكن وبسبب تغير طبيعة النسج وسمكة و ترتيبه فان الخواص الميكانيكية لها امتلكت التعقيد من ناحية التعامل و التخمين. في هذا البحث استحدثت معاملات خاصة بالنسج للمواد المركبة النسيجية تمثل نسبة الخواص الميكانيكية للمواد النسيجية الى الخواص الميكانيكية لمثيلاته للمواد المركبة احادية اتجاه الالياف. اشتقت في هذا البحث العلاقات بين الخواص الميكانيكية محتوية على هذه المعاملات ونفذت تجارب للمواد المركبة النسيجية و الاحادية لتخمين هذه المعاملات. المواد المركبة المستخدمة صنعت من الياف مختلفة هي الكفلر و الكاربون و الالياف الزجاجية بينما اختلفت المواد الطامرة من الايبوكي الى البولستر. اظهرت النتائج ان معامل النسج للمواد المركبة بالياف الاكفلر هي اعلى منه للكاربون و الالياف الزجاجية. وانها للمواد المركبة بمادة طمر ايبوكسي اعلى منه للبولستر.

KEYWORDS: woven composite materials, tensile, stress, Young modulus, Poisson's ratio, satin.

INTRODUCTION

Woven fiber reinforced plastics are becoming increasingly important as they have the following advantages over laminates made from individual layers of unidirectional materials(Tsai et.al 1990)

- Improving formability and drape
- Bi-directional reinforcement in a single layer
- Improving impact resistance
- Balanced properties in the fabric plane

There is no mathematical modeling for the mechanical properties of woven fiber reinforced composite, then approximate one was derived here using the approximation that the woven fibers are constructed from two orthotropic unidirectional fiber plays with the effect of bent yearn through the weave.

Consider the 0,90 cross ply composite shown in **Fig. 1**.

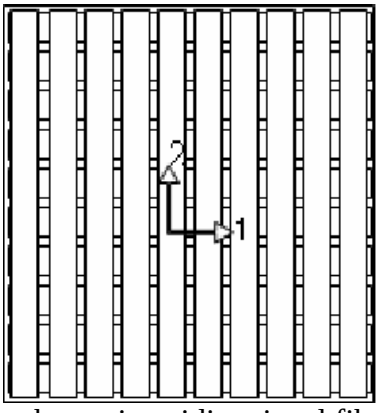

Fig. 1. The composite plate of two orthotropic unidirectional fibers is considered as an infinite-end satin woven fibers composite.

Using the lamina stress-strain relations then for this laminate for presented plate of two orthotropic layers (Rao 1999)

$$A_{ij} = \sum_{k=1}^{N} (Q_{ij})(z_k - z_{k-1})$$

Then

$$[A] = h\begin{bmatrix} \frac{Q_{11}+Q_{22}}{2} & Q_{12} & 0 \\ Q_{12} & \frac{Q_{11}+Q_{22}}{2} & 0 \\ 0 & 0 & Q_{66} \end{bmatrix} \quad \text{and} \quad [a] = [A]^{-1} \tag{1}$$

then

$$a_{11} = a_{22} = \frac{2(Q_{11}+Q_{22})}{h\{(Q_{11}+Q_{22})^2 - 4Q_{12}^2\}} = \frac{2(E_{11}+E_{22})(1-\nu_{12}\nu_{21})}{h\{(E_{11}+E_{22})^2 - 4\nu_{21}^2 E_{11}\}} = \frac{2(1-\nu_{12}\nu_{21})\left(1+\frac{\nu_{12}}{\nu_{21}}\right)}{hE_{11}\left\{\left(1+\frac{\nu_{12}}{\nu_{21}}\right)^2 - 4\nu_{21}^2\right\}}$$

$$a_{12} = a_{21} = \frac{-4Q_{12}}{h\{(Q_{11}+Q_{22})^2 - 4Q_{12}^2\}} = \frac{-4\nu_{21}E_{11}(1-\nu_{12}\nu_{21})}{h\{(E_{11}+E_{22})^2 - 4\nu_{21}^2 E_{11}\}} = \frac{-4(1-\nu_{12}\nu_{21})\nu_{21}}{hE_{11}\left\{\left(1+\frac{\nu_{12}}{\nu_{21}}\right)^2 - 4\nu_{21}^2\right\}} \quad a_{66} = \frac{(Q_{11}+Q_{22})^2 - 4Q_{12}^2}{hQ_{66}\{(Q_{11}+Q_{22})^2 - 4Q_{12}^2\}} = \frac{1}{hG_{12}} \tag{2}$$

Then the an infinite-end satin woven fibers composite properties are

$$
\begin{aligned}
&(E_1)_\infty = (E_2)_\infty = \frac{1}{ha_{11}} = \frac{\left\{\left(1+\frac{\nu_{21}}{\nu_{12}}\right)^2 - 4{\nu_{21}}^2\right\}}{2(1-\nu_{12}\nu_{12})\left(1+\frac{\nu_{21}}{\nu_{12}}\right)} E_{11} \\
&(G_{12})_\infty = \frac{1}{ha_{66}} = G_{12} \\
&(\nu_{12})_\infty = -\frac{a_{12}}{a_{11}} = \frac{2\nu_{21}}{\left(1+\frac{\nu_{21}}{\nu_{12}}\right)} = \frac{2\nu_{12}\nu_{21}}{(\nu_{12}+\nu_{21})}
\end{aligned}
\tag{3}
$$

For a woven fibers of finite-end satin, the properties will be decreased due to fibers bent assume that there a multiplication factors which when multiplied by the infinite-end satin woven fibers composite properties give the properties of the woven fibers of finite-satin then:-

$$
\begin{aligned}
&(\mathrm{E}_{11})_w = (\mathrm{E}_{22})_w = \mathrm{W_E}(E_{11})_\infty = \mathrm{W_E} \frac{\left\{\left(1+\frac{\nu_{21}}{\nu_{12}}\right)^2 - 4{\nu_{21}}^2\right\}}{2(1-\nu_{12}\nu_{12})\left(1+\frac{\nu_{21}}{\nu_{12}}\right)} E_{11} \\
&(\mathrm{G}_{12})_w = \mathrm{W_G}\ \mathrm{G}_{11} = \mathrm{W_G}(G_{12})_\infty \\
&(\nu_{12})_w = (\nu_{21}) = \mathrm{W}_\nu\ (\nu_{12})_\infty = \mathrm{W}_\nu \frac{2\nu_{12}\nu_{21}}{(\nu_{12}+\nu_{21})}
\end{aligned}
\tag{4}
$$

Where W_E, W_G and W_ν are new factors call the woven multiplication factors for E_{11}, G_{12}, and ν_{12} respectively. These factors can be evaluated from the evaluation of these properties experimentally which are done in the tensile tests of the 0, 90 composite plates and the woven fibers composites formed.

Now because of the homogenous orthotropic behavior of the woven fiber lamina the mechanical properties of angle ply woven lamina were stay covered by expressions

For angle ply woven lamina (Sharma 2000).

$$
\begin{aligned}
&\mathrm{E_{xx}} = \mathrm{E_{yy}} = \left[\frac{\mathrm{m}^4+\mathrm{n}^4}{\mathrm{E}_{11}} + \left(\frac{1}{\mathrm{G}_{12}} - \frac{2\nu_{12}}{\mathrm{E}_{11}}\right)\mathrm{m}^2\mathrm{n}^2\right]^{-1} \\
&\mathrm{G_{xy}} = \left[\frac{1}{\mathrm{G}_{12}} + 4\left(\frac{2(1+\nu_{12})}{\mathrm{E}_{11}} - \frac{1}{\mathrm{G}_{12}}\right)\mathrm{m}^2\mathrm{n}^2\right]^{-1} \\
&\nu_{\mathrm{xy}} = \mathrm{E_{xx}}\left[\frac{\nu_{12}}{\mathrm{E}_{11}} - \left(\frac{2(1+\nu_{12})}{\mathrm{E}_{11}} - \frac{1}{\mathrm{G}_{12}}\right)\mathrm{m}^2\mathrm{n}^2\right] \\
&\nu_{\mathrm{yx}} = \frac{\mathrm{E_{yy}}}{\mathrm{E_{xx}}}\nu_{\mathrm{xy}}
\end{aligned}
\tag{5}
$$

FABRICATION OF LAMINATED PLATES TEST SPECIMENS

Fiber Reinforcements and Matrix Resins

As mentioned earlier, the fibrous composite laminates fabricated mainly from two main constituents, which are the fibers reinforcements, and the unsaturated matrix resin. It is important to remember that the inter ply layer, or the adhesive layer between any two successive layer is the resin itself with some adding thickness for distinguishing this interply layer. The followings demonstrate the physical and chemical specification of these two constituents.

(A) The Fiber Reinforcements

The fiber materials used as reinforcements in the presented work are E-Glass, Carbon, and Kevlar aramid fibers. Now the compositions, forming, and properties were listed.

I) E-Glass

The type used in the presented work is E-glass, which is the material most widely used as a reinforced medium for plastic as well as for textile fiberglass product applications. The representative chemical compositions of these four glasses are given in **Table 1** and the inherent properties are given in **Table 2**.

Table 1 Glass composition

	Material, percentage weight (%)							
Glass type	Silica	Alumina	Calcium oxide	Magnesia	Boron oxide	Soda	Calcium fluoride	Minor oxides
E-glass	54	14	20.5	0.5	8	1	1	1
Commercial fiberglass used in the present work								
A-glass	72	1	8	4	-	14	-	1
ECR-glass	61	11	22	3	-	0.6	-	2.4
S-Glass	64	25	-	10	-	0.3	-	0.7

Table 2 Inherent properties of glass fibers

Glass type	Specific gravity	σ_{ult} (MPa)	E_t (GPa)	α (10^{-6}/K)	Dielectric constant(a)	Liquidus temperature ^oC
E-glass	2.58	3450	72.5	5.0	6.3	1065
Commercial fiberglass used in the present work						
A-glass	2.50	6043	69.0	8.6	6.9	996
ECR-glass	2.62	3625	72.5	5.0	6.5	1204
S-Glass	2.48	4590	86.0	5.0	5.1	1454

II) Carbon Fibers

Fiber produced by the pyrolysis of organic precursor fibers, such as rayon, polyacrylonitrile (PAN), and pitch, in an inert environment. Carbon fibers typically carbonized in the region of 1315 oC and assay at 93 to 95% carbon. There are some types of carbon fibers (which their properties are available in (Reinhart et.al 1987)), the commercial type was used in presented work is P-55 carbon-high modulus fiber which its properties are shown in **Table 3.**

Table 3.Mechanical properties of P-55 carbon-high modulus fiber.

Product name	Manufacturing	Precursor type	Density Kg/m^3)	σ_{ult} (GPa)	E_t (GPa)
P-55	Union Carbide	Pitch	2000	1.73	379

III) Kevlar

The predominate organic reinforcing fiber used in advanced composites since the early 1970s has been aramid or aromatic polyamide, known as Kevlar. Kevlar 49 fabric with the mechanical properties shown in **Table 4** was used in the tests.

Table 4.Mechanical properties of Kevlar 49 used in the presented work

Material	Density Kg/m^3	Filament diameter μm)	E_t (GPa)	σ_{ult} (GPa)	ε_{break} (%)	Available yarn count, No. Filaments
Kevlar 49	1440	12	131	3.6	2.8	≈150

(B)The Unsaturated Matrix Resin:

Two types of matrixes were considered in the tests, which are polyester resin and epoxy resin.

I) Polyester resin

It is used a chemical compound of reactive polymers (glycol's or "phthalic" anhydride with the acid "malice" anhydride). The compound is sTable liquid for months or even years, as long as the carbon double – bonds in the poly –molecular structure, is kept conservative. In his patents, sixty years ago, Ellis (Reinhart et.al 1997) discovered that the adding of a reactive monomer (usually referred to "peroxide" catalyst or "styrene") then an exothermic reaction (rejecting heat) or "curing" will be set up involving the conversion of double – bond into single – bond through cross – linkage polymerization process. The added catalyst initiates and shares the polymer network within certain duration time, called the "gel time" of the process. A typical catalyst, frequently used in practice, is the (MEKP, refereed to methyl ethyl ketone proxide). In order to decrease the unprofiTable much gel time, during the lay – up procedure, an "accelerator" agent may be employed for this purpose, like the "cobalt – naphthenate" as being used for a general – purpose polyester resin.

The new product is, hence, the "saturated" polyester resin. Depending on the mole ratio of the phthalic / maleic, and the mass percentage of the catalyst / accelerator agents, the mechanical properties of the resin will be cited. Other glycol compounds and additive agents produce wide variety of resin type for broad range of applications. Recently, the polyester resin, as refereed to "Palatal P50T" (Whitny et.al 1970), is found commercially used and officially approved in German standards under DIN 16946.

(C) Fabric Forms and Materials Used:

The geometrical aspect of the fibers used in the presented work have the detail shown in **Table 5**, the selection of different fiber materials is to study the effect of it on the properties and impact, also the using different fabric forms and weights are to study the fabric effect and to determine the woven facture defined in the theoretical part of work. The matrix types and their density are tabulated also.

Table 5.materials used in the presented tests

(A) Fibers

Fiber material	Weave	Construction tows/cm	Mass/area kg/m^2
E-glass	Plain	2.5*2.5	0.500
	Plain	12.5*12.5	0.260
	5-end satin	5*5	0.280
	Random	-	0.450
Carbon	Plain	7*7	0.170
	3-end satin	5*5	0.210
Kevlar	3-end satin	7*7	0.230

(B) Matrixes

Polyester	ρ= 1268 kg/m^3	Epoxy	ρ= 1430 kg/m^3

Mould Preparation

There are two groups of samples molded, matrix samples, and layered fiber composite plates samples. The matrix samples was made to verifying the mechanical properties of matrix specially because the environment conditions and process of molding are vary important parameters effecting on the properties, because of that there is no offered properties can be use it directly, then the Tensile, Bending, and torsion tests were done. Composite plates samples was made for using different fibers and matrix material to verifying mechanical properties and to use them as target in the high velocity impact test.

I) Matrix Samples:

For product the samples of tests (Tensile, Bending), made one sample for each test from pure epoxy with standard dimensions and then used these samples to make the moulds.
Moulds that used, produced from paste of panes rolled out at pane and then formed the shape of each sample on it as shown in **Fig. 2**.

Fig. 2 matrix sample produced from paste of panes rolled out at pane and then formed the shape of tensile and bending tests.

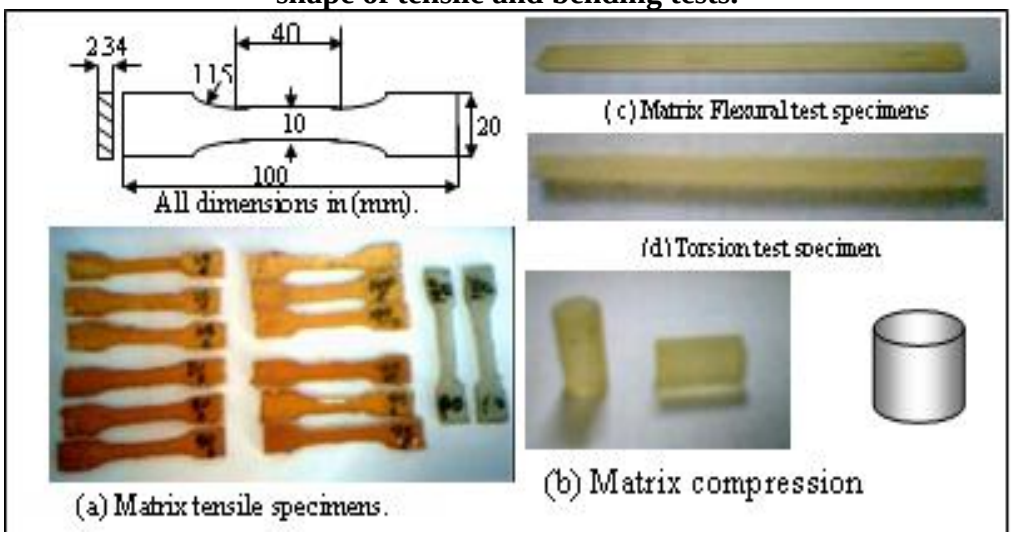

Fig. 3 matrix specimens fabricated and used for tests

The tensile test specimens have been produced according to (D638) as shown in **Fig. 3.a**. The tensile test specimens produced for pure epoxy. The tensile test specimens produced using a mould shown in **Fig. 2**, And after solidification made grinding processes for each specimen to get the standard dimensions.

II) Composite Plate Samples

The plate strip specimens used in the investigation were fabricated from the fiber matrix plies, and symmetrical lay – up were prepared by using a 30*30cm ceramic open mold with x-ray photo sheet painted with wax film to avoid abrasive and inshore flattening as shown in the schematic

arrangement shown in **Fig. 4**, the molder applies a pigments "release" material to the mold, as the First step in making any open mold product. Without such material, the part will permanently bond to the mold surface.

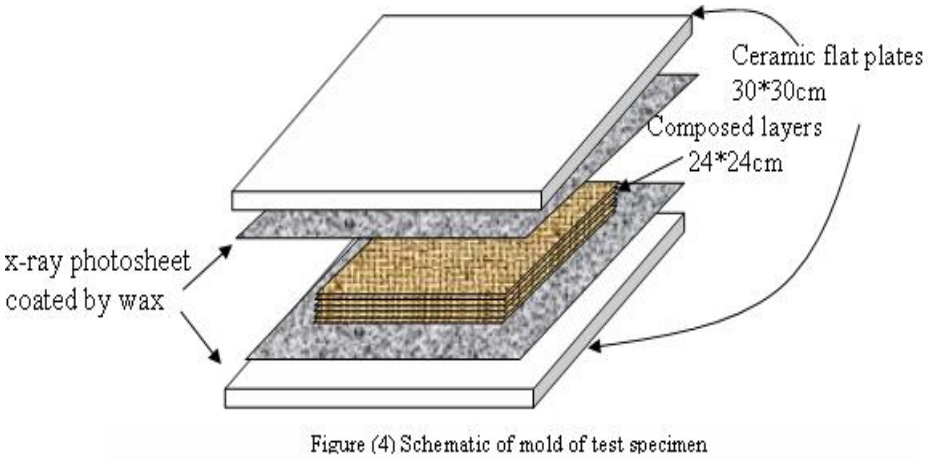

Fig. 4 Schematic of mold of test specimen

Secondly, a pre – measured unsaturated polyester and catalyst (or matrix) are then thoroughly mixed together, and for ensuring complete air removal and wet out, it should cover the base surface completely especially at the end edges.

The Thirdly step is the application of fiber in the resin layer, these woven or chopped fiber layer are put in the resin layer and with using brushes and rollers the fiber layer would saturated by resin, then another fiber sheet would be putted and return the process until end layer, x-ray photo sheet coated with wax will cover the composite and with rolling over all layers to ensuring complete air removal. When using polyester resin, the curing step of the specimens, which are a change of properties of thermosetting resin by chemical reactions, this process forming a strong three-dimensional network thus, the cross- link structure is known as curing.. The curing step related to a curing temperature, and curing time Thus, the specimens were cured according to the manufacture's recommendations, in a dryer oven for the recommend time and temperature are 8hr and 70 0C respectively (Thompson 2004).

The pressure applied through the forming of the specimens was optimized from trail and error to give approximate 60% fiber volume fraction, which was calculated from the mass fraction, the composite volume is equal to the summation of fiber and matrix volumes

$V_c = V_F + V_M$ or $1 = v_F + v_M$

Where V and v represent the volume and volume fraction respectively, and subscripts C, F and M represent the composite, fibers and matrix respectively.

Form $V = m/\rho$ then

$m_c / \rho_c = m_F / \rho_F + m_M / \rho_M$

Where m and ρ are the mass and density respectively. The density of composite plate can be calculated from $\rho_c = m_c / V_c$, the mass of plate was measured using three digital electronic balance, the volume of the plate was measure by hand Verna.

The mass of fiber can be measured by multiplying the area of all layers times the mass per unit area {see **Table5**} and the density of the fiber is from **Tables 2** to **4**, then the volume fraction of fiber will be calculated using

$$v_F = V_F / V_c = (m_F / \rho_F) / (V_c) \quad (6)$$

Manual scissors, rotating grinding, and manual grinding used to cut the plies for the lay-up. For the tensile specimens the patterns are necessary.

II) Test samples:
Three types of composite sample are used which are the tensile test specimens, friction disk specimens, and impact test specimens
Tensile tests were conducted in according to the (ASTM D412) standard(Noble 1996). The test specimens, shown in **Fig. 5** with strain gauge at center and locate normal to the length to measure the lateral stain, any composite where tests for two direction principle, and 30o to evaluate the required material properties.

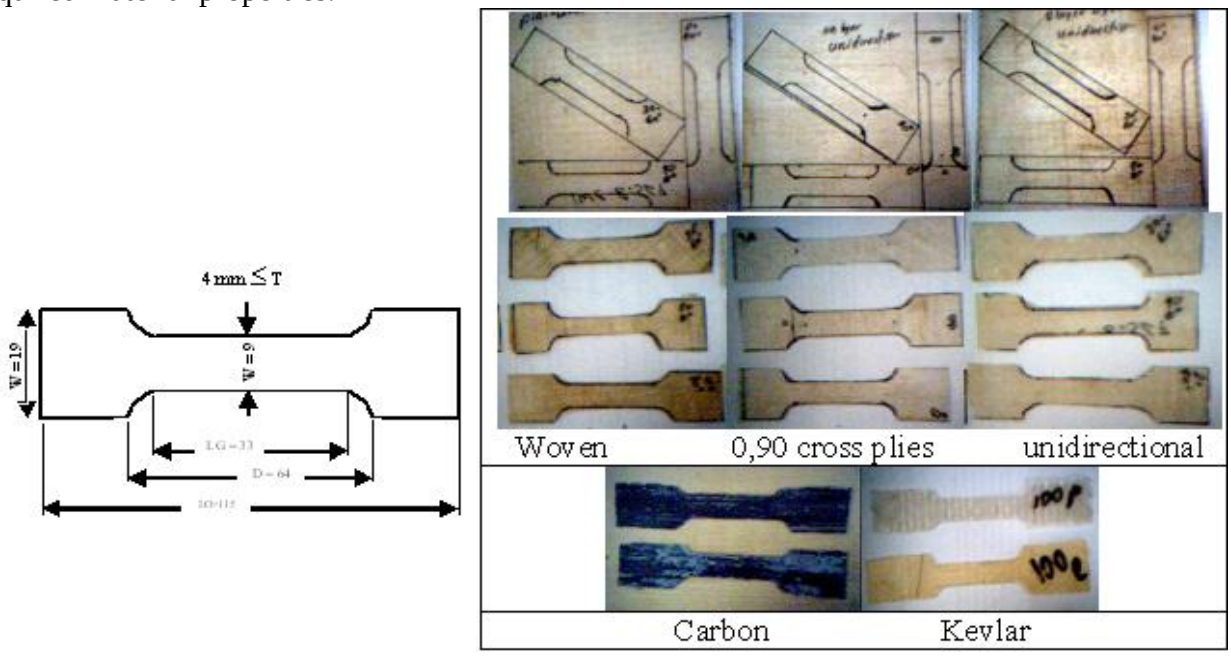

Fig. 5 some specimens use for testing the properties

Tests for Mechanical Properties
The mechanical properties for matrixes were measured using four tests (tensile, compression, bending, and torsion), while the mechanical properties of composites were measured using (tensile and friction).

Tensile and Compression Tests:
Tensile and compression testing device, which used type PHYWE, model D-3300 and has a maximum supported load 30KN that displayed by a digital display of a strain gage and measuring displacement using a dial gage as shown in **Fig. 6.a**. In tensile and compression tests used a digital camera to record the force and displacement values in each moment to get more accuracy.

Fig. 6 (a)Tensile tester (b) Microstrain meter

The tensile test was used for matrix and composite, The stress and strain in normal to the load axis is $\sigma_L = F / A$, and $\varepsilon_L = \delta / LG$, while the lateral srtain is from strain gauge directly, where the strain gauge used is Omega using quarter Bridge (**Fig. 6.b**) and 120Ω strain gauge prop was used. Then the passion's ratio can be determined using $\nu_{12} = -\varepsilon_T / \varepsilon_L$, the modulus of elasticity ($E_{11}=E_{22}$) and the ultimate tensile stress (σ_{ult}) are evaluated from the stress strain curves.
For composite specimens the modulus of rigidity can be measured after knowing E_{11}, E_{22}, and ν_{12} and from E_{xx} evaluated from the tensile test of 30^0 specimens with m= cosθ, and n=sinθ and from elasticity relation for orthotropic lamina

$$E_{xx} = E_{yy} = \left[\frac{m^4 + n^4}{E_{11}} + \left(\frac{1}{G_{12}} - \frac{2\nu_{12}}{E_{11}} \right) m^2 n^2 \right]^{-1} \quad (7)$$

The unique unknown is G_{12}, which can be calculated.
For using results for woven composite and the 0,90 composite the new woven multiplication factures W_E, W_G, and W_ν can be calculated from eq. (4).

RESULTS

Matrixes

The mechanical properties the matrixes (epoxy and polyester) were found using the tensile, compression and torsion tests. The results of these tests are shown in **Fig.s** (**7** to **9**), while there evaluated properties from these tests are listed in **Table 6**.

It was shown that the epoxy resin used is equivalent to the epoxy casting resin, no filler at 25oC(Rao 1999). The polyester resin used is equivalent the cast polyester neat resin (Rao 1999). It was shown that the epoxy resin have amore strength and modulus than the polyester resin, this behavior is known because of the chemical composition bond in the epoxy which were give a longer chains and network for its chemical structure. And that is give the same resin for appearing the instability point in the epoxy resin and not occurs in the polyester resin.

The compression stress strain curves shown in **Fig. 8** show that the epoxy resin has greater compression modulus and smaller ultimate compression strength than the polyester resin and these results were conventional with the earliest tests (Rao 1999).
Because of the assumption that the resins were isotropic then the measuring of the modulus of rigidity is benefit to evaluate the poisons ratio for the resins and the ultimate shear strength, which

is importants with the ultimate tensile strength in the delamination failure criteria used in the theoretical parts of the thesis.

Fig. 9 shows the shear stress shear strain relations for the resins used. In general the ability of resin in the shearing load relative to tensile load is grater than the metallic materials. That is Appear clearly for the epoxy resin and less in the polyester resins.

The summary of the mechanical properties for the epoxy and the polyester are shown in **Table 6**.

Table 6. The measured mechanical properties for matrixes.

Test →	Tensile				Compression		bending	Torsion			
Matrix↓	E_t (MPa)	σ_{Yt} (MPa)	σ_{ult} (MPa)	ε_F (%)	E_c (MPa)	σ_{Yc} (MPa)	E_b (MPa)	G (MPa)	τ_{ult} (MPa)	γ_F (%)	ν
Polyester (p)	933	33.8	58.5	9.4	1276	79.2	1352	324	37.2	13.4	0.44
Epoxy (e)	1714	47.7	57.6	5.2	1875	76	2563	620	80.6	17.9	0.382

Composites

Two types tests were used for measuring the mechanical properties of the composites, which are the tensile tests and the friction tests. the stress-strain curve for the tensile are shown in **Fig.s(10-19)** . The **Fig.s (a)** the tensile test in the direction of the fiber, which have a strain gauge to measure the lateral stain and the Poisson's ratio. While the **Fig.s (b)** represent the tensile tests in the (30^o) inclination angle with the fiber direction to evaluate the modulus of rigidity of the composites.

It is clear that the effect of the mechanical properties of the matrix type on the overall properties for the composite ply. This effect is decreased as increasing the properties of the fiber as in the stress strain curve for Kevlar reinforcement shown in **Fig. 12**.

The summary of the mechanical properties measured and evaluated from **Fig.s (10 to 12**) are listed in **Table 7**

Table 7 the mechanical properties of manufactured 0-90 fiber reinforced composite

0-90 specimens		Mechanical properties					
Fiber	Matrix	σ_{ult}(MPa)	$E_1=E_2$(MPa)	ν_{12}	E_{30}(MPa)	σ_{ult30}(MPa)	G_{12}(MPa)
Carbon	Epoxy	130	8292	0.048	4714	69	1349
Carbon	Polyester	105	5098	0.044	3105	64	925
E.Glass	Epoxy	87	4183	0.103	2138	59	573
E.Glass	Polyester	79	3957	0.095	2077	46.5	564
Kevlar	Epoxy	210	14241	0.075	5756	97	1422
Kevlar	Polyester	194	11492	0.038	5610	89	1498

The evaluations of the weave factors derived in the theory were needed to measure the mechanical properties of the woven composite. The stress strain relations for the tensile tests of the different weave structure of the fibers were shown in **Fig.s (13 to 19)**. The same effects of the matrix types were found as in **Fig. 13**, for this reason and because of the lower cost of the polyester resin the polyester resin were used for the other types of woven fiber composites.

It was shown that the epoxy matrix not only gives larger properties than polyester but also give large woven factors. This is because of its higher properties.

The composite properties were affected directly with the fiber properties. This cause the largest properties for the Kevlar fiber composite shown in **Fig. 19** and less for the carbon fiber composites {**Fig.s (17 and 18)**} and the lowest in the glass fiber composites {**Fig.s (14 and 17)**}.
The study woven style was affecting on the fiber composite properties as shown in **Fig.s (12 to 16)**, the meshing size affect was shown for **Fig. 13** and **Fig. 14**. It was shown that the greatest mesh size {**Fig. 13**} give large Young modulus and tensile strength than the low mesh {**Fig. 14**}. This is due to the largest consolidation through the weave for the largest mesh size. In the addition that the largest mesh size give lower number of the fiber bents.
The different weave styles for the same mesh size was not available through the period of the work, but the results for the available weave give that the increasing the number of end satin cause increasing the ultimate stress and Young modulus and the woven factors because the increasing the number of satin give to reaching to the infinite satin for E-glass and Carbon fibers. This conclusion can be generalized to all types of woven fiber.
The chopped random E-glass has the stress strain relation shown in **Fig. 16**, the random fiber was not need to find its modulus of rigidity using inclination tensile test because of it isotropic behavior

The results were summarized in **Table 8**
From **Table 8** it was shown that the Kevlar composite material has higher woven factors than the carbon and E-Glass composites, that is because the higher modulus for the Kevlar with it flexible yarn give more closely to the unidirectional fibers than that for the other types of fibers. The composite with epoxy matrix has higher woven factors than that for polyester matrix composite, this is because of higher modulus for epoxy. The satin weave composites have higher woven factors because of there geometries that were approaching to the cross unidirectional composite as the satin increase and be the same for an infinite satin woven composite as discussed previously.

Table 8. The measured mechanical properties for the composites manufactured.

Composition		Woven composite ply							0-90 composite ply				Woven factors		
Fiber	Matrix	Style	No. of Layers	h (mm)	σ_{ult} (MPa)	$E_1=E_2$ (MPa)	ν	G_{12} (MPa)	σ_{ult} (MPa)	$E_1=E_2$ (MPa)	ν	G_{12} (MPa)	W_E	W_{ult}	W_G
E-Glass	Epoxy	Plain (2.5*2.5)	3	1.8	53.94	2611	0.096	473	87	4183	0.103	573	0.79	0.62	0.83
E-Glass	Polyester	Plain (2.5*2.5)	3	1.82	46.61	2226	0.112	474	79	3957	0.095	564	0.75	0.59	0.84
E-Glass	Polyester	Plain (12.5*12.5)	6	1.9	43.45	2051	0.093	448	79	3957	0.095	564	0.72	0.55	0.79
E-Glass	Polyester	5-end satin (5*5)	5	1.75	41.08	2138	0.045	455	79	3957	0.095	564	0.74	0.52	0.81
E-Glass	Polyester	Random	4	1.8	32.39	3184	0.231	1293	79	3957	0.095	564	-	-	-
Carbon	Polyester	Plain (7*7)	6	1.72	54.6	3023	0.061	583	105	5098	0.044	925	0.77	0.52	0.63
Carbon	Polyester	5-end satin (5*5)	5	1.7	59.85	3512	0.085	550	105	5098	0.044	925	0.83	0.57	0.59
Kevlar	Polyester	3-end satin (7*7)	6	1.85	166.8	9517	0.043	852	194	11492	0.038	1498	0.91	0.86	0.57

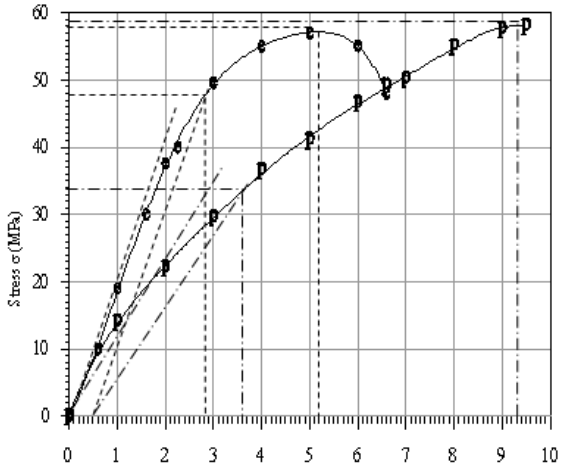

Fig. 7 Experimental tensile Stress-Strain curves for polyester (p) and epoxy (e) tensile test (Tensile speed = 3mm/min).

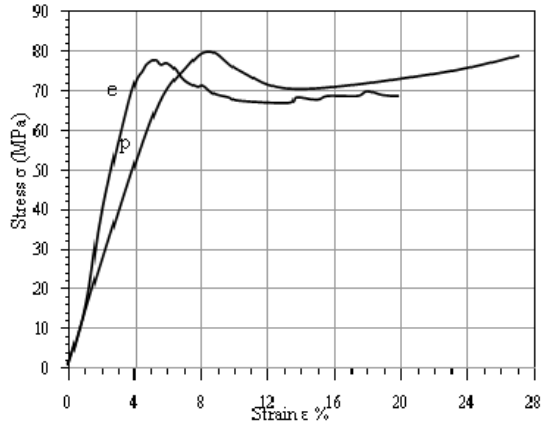

Fig. 8. Experimental compression Stress-Strain curves for polyester (p) and epoxy (e), Compression test (Compression speed = 3mm/min).

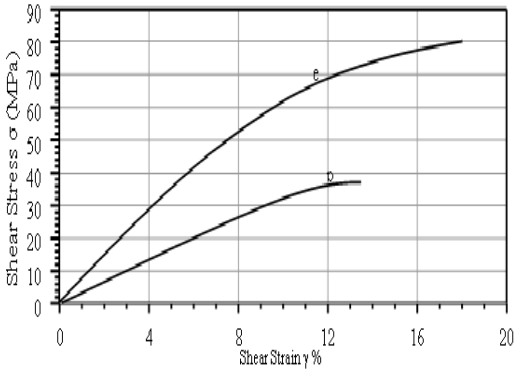

Fig. 9. Experimental Shear Stress- Shear Strain curves for polyester (p) and epoxy (e), Torsion test

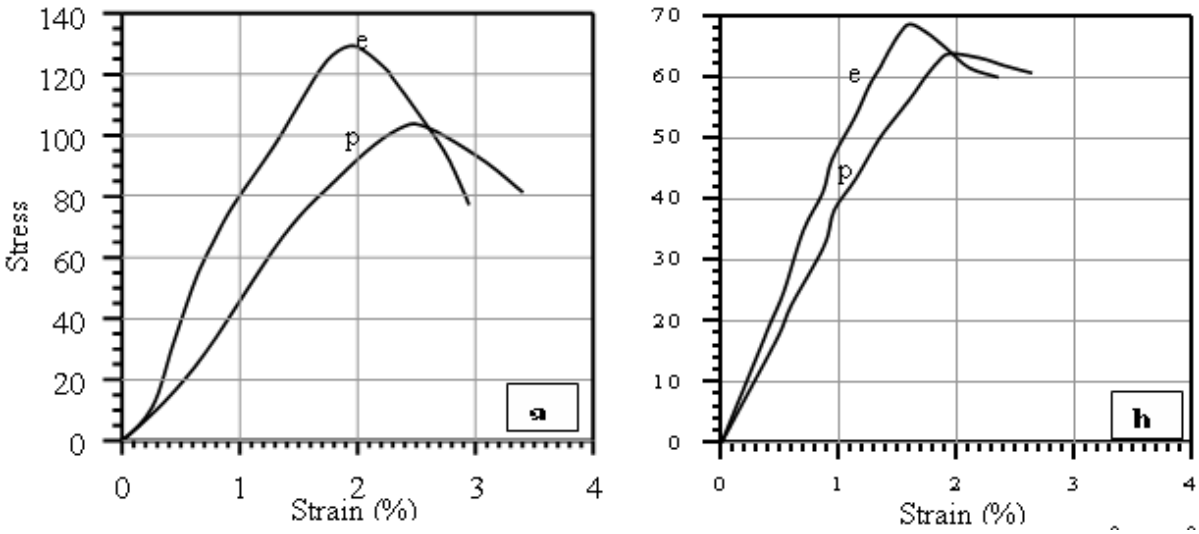

Fig. 10. Tensile stress-strain curves for 0-90 carbon reinforced {polyester (p) and epoxy (e). a) 0^o, b) 30^o

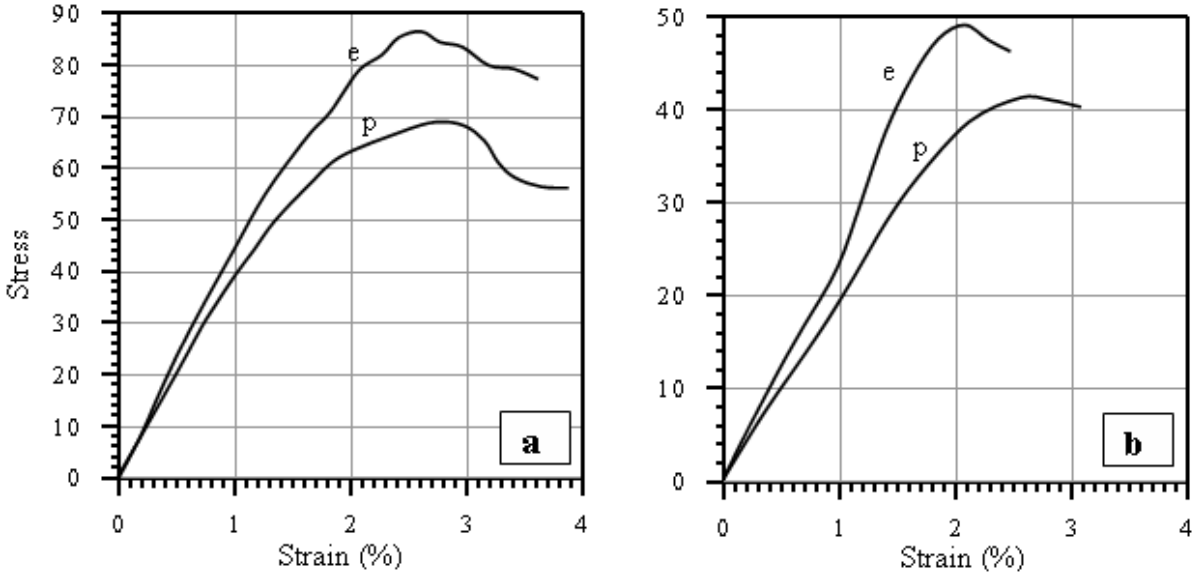

Fig. 11. Tensile stress-strain curves for 0-90 E-glass reinforced {polyester (p) and epoxy (e). a) 0^o, b) 30^o

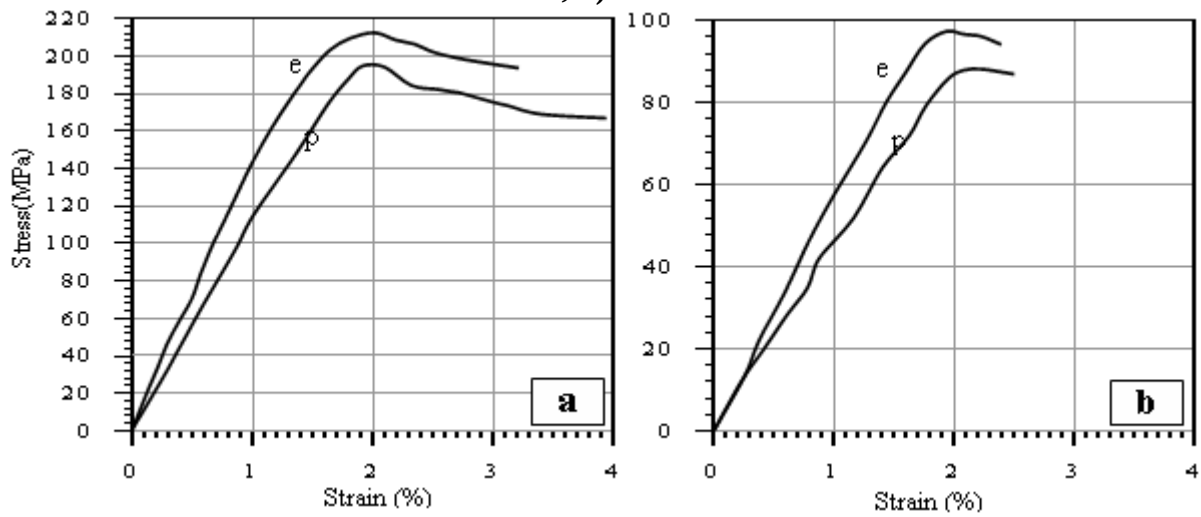

Fig. 12. Tensile stress-strain curves for 0-90 Kevlar reinforced {polyester (p) and epoxy (e). a) 0^o, b) 30^o

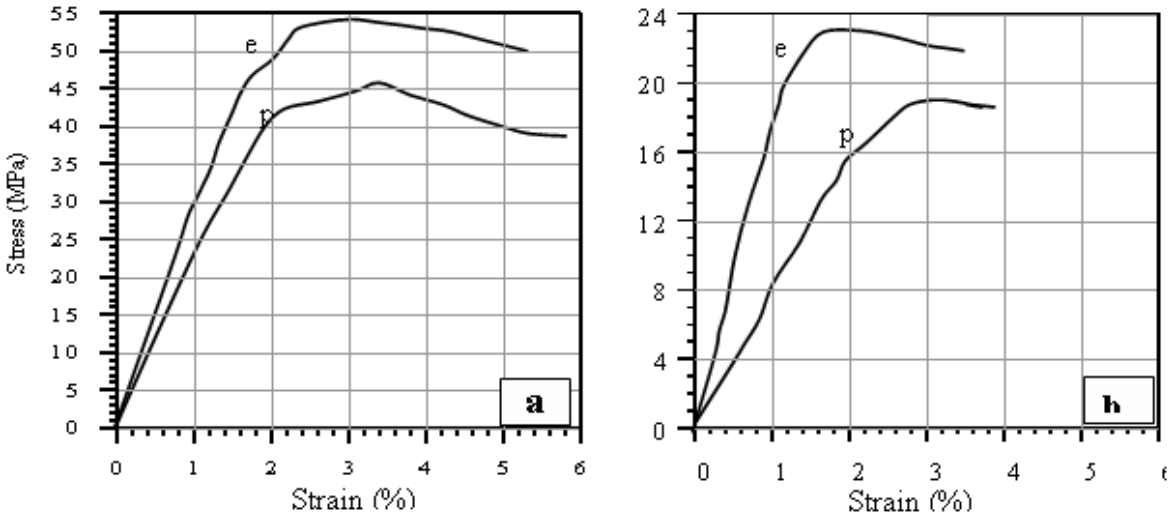

Fig. 13. Tensile stress-strain curves for plain-woven E-glass fiber (2.5*2.5) reinforced {polyester (p) and epoxy (e)}. a) 0^o, b) 30^o

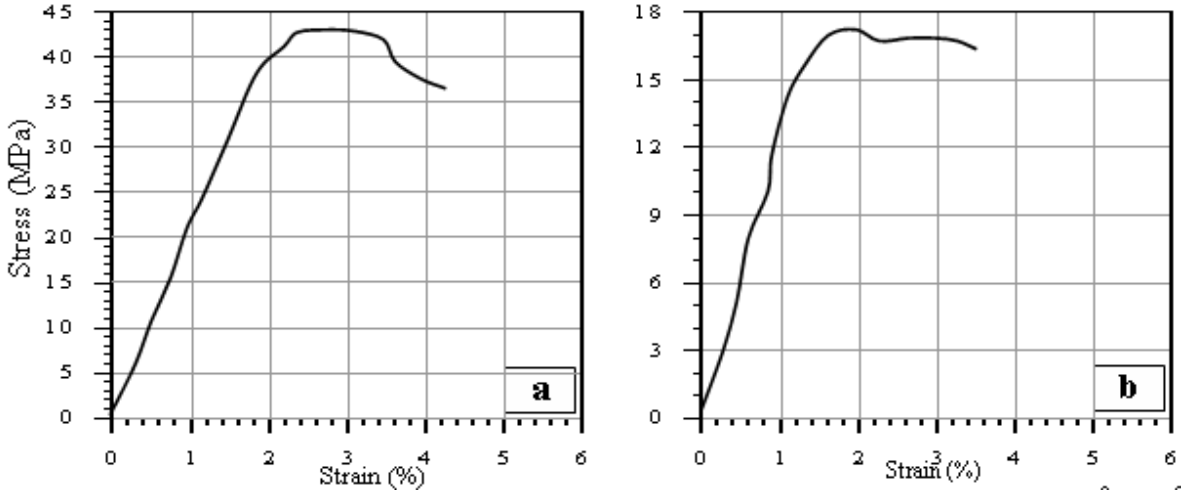

Fig. 14. Tensile stress-strain curves for plain-woven E-glass fiber (12.5*12.5) reinforced polyester. a) 0^o, b) 30

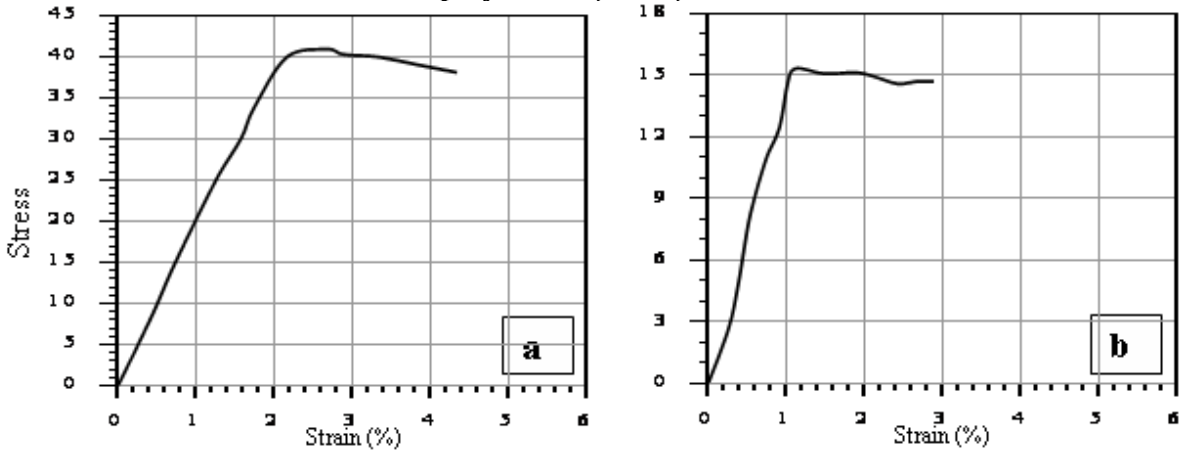

Fig. 15. Tensile stress-strain curves for 5-end satin woven E-glass fiber (5*5)) reinforced polyester. a) 0^o, b)30^o

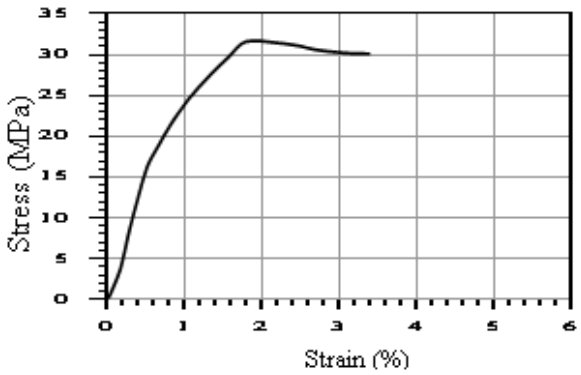

Fig. 16. Tensile stress-strain curves for random chopped E-glass fiber reinforced polyester

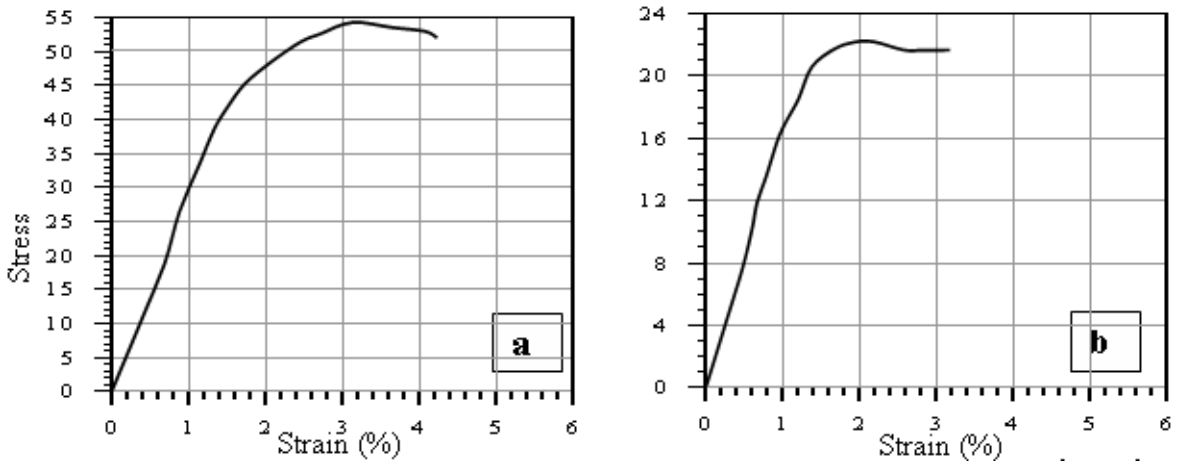

Fig. 17. Tensile stress-strain curves for plain-woven carbon fiber reinforced polyester. a) 0^o b) 30^o

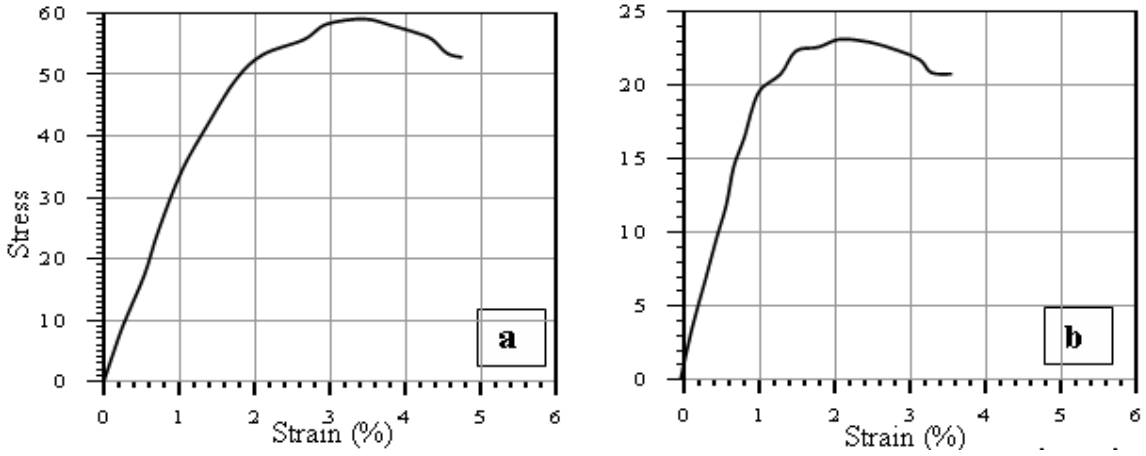

Fig. 18. Tensile stress-strain curves for 5-end satin woven carbon fiber reinforced polyester. a) 0^o, b) 30

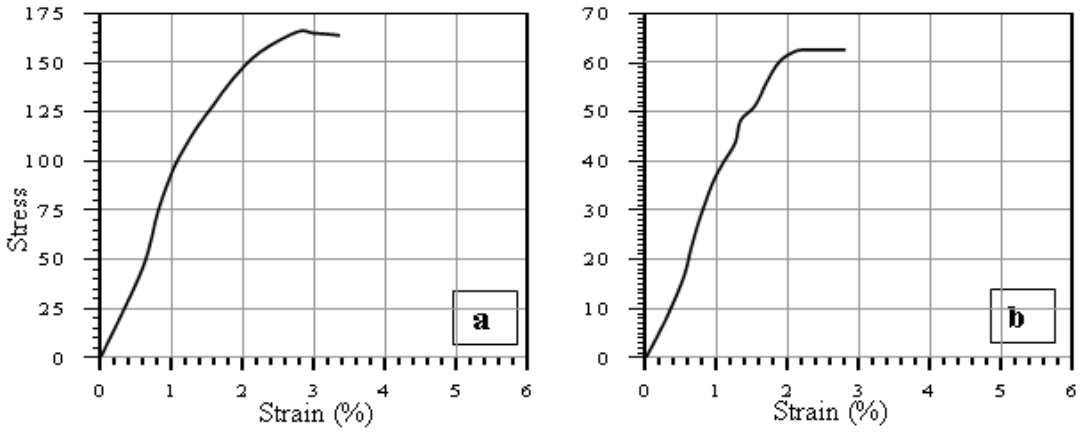

Fig. 19. Tensile stress-strain curves for 3-end satin Kevlar fiber reinforced polyester. a) 0^o, b) 30^o

* CONCLUSIONS

The tensile test for cross play and woven composite were done to evaluate the ratio of mechanical properties for the woven composites to that for cross composite, which were call the woven factors for woven composite materials. It was shown that the woven composites have lower mechanical properties than the cross ply composites. The Kevlar composite material has higher woven factors than the carbon and E-Glass composites. The composite with epoxy matrix has higher woven factors than that for polyester matrix composite. The satin weave composites have higher woven factors for different types of fiber composites.

* REFERENCES

- Tsai and Hahn and Delaware, "Composites Design Encyclopedia" (1990).
- J.S.Rao," Dynamics of Plate", Narosa Publishing House, 1999.
- S.C. Sharma, "Composite Materials", Narosa Publishing House (2000).
- T.J. Reinhart, C.A. Dostal, M.S. Woods, H.J. Frissell, A.W. Ronke, D.M. Jenkins, K.L. O'Keefe, K.L. Pilarczyk, R.L. Stedfeld and K.M. Mills,"Engineering Materials Handbook. Volume 1, Composites" ASM International, (1987).
- Roger L. Ellis and Craig A. Rogers," Ballistic impact resistance of graphite composites with superelastic SMA and Spectra hybrid components", AIAA, pp1-11, (1997).
- J.M.Whitny " Shear deformation in heterogeneous anisotropic plates" J of Appl. Mech.(37), 1970 pp.1031.
- Joseph Earl Thompson, " Compaction and Cure of Resin Film Infusion Prepregs", M.Sc. thesis, the faculty of the Virginia Polytechnic Institute and State University, December 22, (2004)
- Dr. Noble B., " Tensile and Impact Properties of Metals and Polymers", TQ Education and Training Ltd,(1996)

PULSE WIDTH MODULATION FOR HIGH PERFORMANCE HYBRID STEPPER MOTOR

Prof. Dr. Qais S. AL- Sabbagh **M.Sc. Student Ali Sabah Mahdi**

College of Engineering/ University of Baghdad, Iraq- Baghdad

الخلاصة

هذا البحث يقوم بتنفيد طريقة السيطرة الأتجاهية العالية الأداء لسيطرة على تيار وسرعة محرك الخطوة الهجين (HSM) لتحسين الأداء الدينامي لهذا المحرك. هذه الفائدة الأساسية من محركات الخطوة على غرار الأنواع الأخرى من المحركات. طريقة السيطرة ذات الحلقة المفتوحة تبين أداء دينامي سيء. أن محركات الخطوة كثيرة الأستعمال في الحركات الدقيقة التي تتطلب دينامية عالية. على أية حال، طريقة السيطرة ذات الحلقة المفتوحة غير كافية، لذا طريقة السيطرة ذات الحلقة المغلقة تكون مطلوبة. طريقة السيطرة الأتجاهية سوف تحسن الأداء الدينامي للمحركات الخطوة. تم تصميم وتنفيد نموذج محرك الخطوة الهجين HSM بأستخدام برنامج MATLAB/ SIMULINK. أن نموذج HSM مستند على الدوائر المكافئة اللاخطية الذي تمثل عمل المحرك. تم مقارنة نتائج المحاكاة للمحرك الهجيين (HSM) مع نتائج الدائرة العملية (RDK) وتم الحصول على أتفاق قريب في النتائج.

ABSTRACT

This paper presents a high performance vector control approach of the current and speed for Hybrid Stepper Motor (HSM) to improve the dynamic performance of the motor. This is the basic advantage of stepper motors over other types of motors. The open loop controller shows a poor dynamic performance. The stepper motors are widely used in precise motions which is required a high dynamic. However, an open loop control is insufficient, so a closed loop control is required. The field oriented control will improve the dynamic performance of the stepper motor which becomes as

a high- dynamic ac- servo. A design and implementation model of HSM using in MATLAB/ Simulink is given. The model is based on nonlinear equivalent circuits representing the operation of the motor. The simulation results of the HSM are compared with practical results of reference design kit (RDK) stepper motor, and a close agreement is noticed.

INTRODUCTION

The HSM is used in many applications [1], such as robotics system, printers and consumer electrics. The HSM is a double salient machine which incorporates a permanent magnet in the robots as described in [2]. Stepper motors are a class of electromechanical device used to produce discrete or non-continuous motion. Stepper motor fall within a broader class of devices known as incremental motion devices, which include incremental actuators and other digital control devices used in motion control. Stepper motor is a synchronous motor with the magnetic field controlled by using electronic switches to rotate the rotor [3]. The theory of stepper motor is similar to a permanent magnet synchronous motor. The motor rotation not only has a direct relation to the number of the input pulses, but its speed is related to the frequency of the pulses [1]. However, precise position, velocity, or acceleration control is required and when very small steps of control are necessary, electrical stepper motors have many advantages.

In the open loop control, the HSM can produce only 50% of its nominal torque. A large torque reserve is required to overcome any load variation. In this classical control scheme there is no feedback of load position to the controller. The motor must response to each excitation change. If the excitation changes are made too quickly the stepper motor can lose steps and, therefore, it is unable to move the rotor to the new demanded position. So a permanent error can be introduced between load position and position expected by the controller. All these limitations can be overcome with a closed loop controller. In this case, the motor requires a rotor position sensor for providing the proper commutation sequence.

In the classical control scheme the stepper motor is driven by a discrete sequence of current pulses. Regular stepping introduces large overshoot, resonance and **torque** ripple problem which have plagued the stepper motor for a long time. In order to

reduce these problems, a micro-step excitations are applied to inject various ratio currents into phase coils. So the position resolution will be improved [4]. The HSM is a two phase synchronous machine and can be driven as the permanent magnet synchronous motor (PMSM). A better performance of the HSM can be obtained by driving it with field oriented control (FOC), rather than stepping [5]. In this paper, we present experimental results of the field oriented control for a new speed and position estimation strategy of HSM drive. Finally, a simulation of the nonlinear model of the HSM is done. The simulation and experimental results show the validity of the proposed vector control approach.

- MATHMATICAL MODEL OF HSM

The motor considered in this paper is a two phases HSM with the following assumptions:

- Non-salient pole structure (uniform air gap).
- Sinusoidal winding distribution, i.e. (sinusoidal flux distribution).
- Negligible magnetic saturation and iron losses.
- Constant self inductances.

With these assumptions, the equivalent model of the HSM with two- phases winding on the stator and no windings on the rotor is shown in Fig.1.

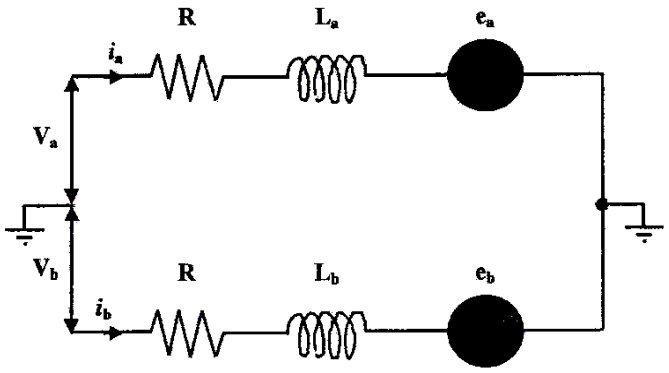

Fig.1. The equivalent circuit of a two phase HSM.

The HSM can be described by a set of voltage differential equations [6].

$$v_a = \mathbf{R}\, i_a + \mathbf{L}\, \mathbf{d}\, i_a/\mathbf{dt} - \mathbf{Km}\, \mathbf{w}_m\, \mathbf{sin(Nr}\, \boldsymbol{\theta}_m\mathbf{)} \quad \textbf{(1)}$$

$$v_b = R\, i_b + L\, d\, i_b /dt + Km\, w_m \sin (Nr\theta_m + 90) \quad (2)$$

Where,

i_a and i_b = Current in phase (a) and phase (b) (A).

v_a and v_b = Voltage in phase (a) and phase (b) (V).

R = Resistance in each phase (ohm).

L = Self inductance in each phase (h).

Nr = Number of stator pole.

Km = Motor torque constant.

w_m = Mechanical angular speed of the rotor (Rad/Sec).

θ_m = Mechanical angle of the rotor (Rad).

The electromagnetic torque in the air gap is given by the following equation:

$$Km (- i_a \sin(Nr\, \theta_m) + i_b \sin(Nr\, \theta_m + 90)) - TL = J dw_m / dt + Bw_m \quad (3)$$

Where,

TL = Load torque (Nm).

J = Moment of inertia ($kg.m^2$)

B = Viscous friction coefficient (Nms/R).

Finally, the equation for angular velocity of the rotor completes the HSM model:

$$w_m = d\theta_m / dt \quad (4)$$

The relationship between electrical and mechanical angle (position) of the rotor is given by:

$$\theta_e = Nr\, \theta_m \quad (5)$$

The mathematical model of HSM in (a-b) reference frame called (stator reference frame) is not suitable for speed control process, because the model has time varying quantities (voltage, current, and mutual inductances) that can lead **to make solution**

of motor equation is very complicated. It is possible to eliminate time varying quantities by using the Park transformation while allows conversion of the stationary reference frame fixed on the stator (i.e. (a-b) components) into reference frame fixed on the rotor (i.e. (d-q) components), where (d) stand for direct axis and (q) for quadrature axis. The (d-q) reference frame can obtained by rotates (a-b) reference frame by an electrical rotor position (Nr θm) as shown in Fig.2.

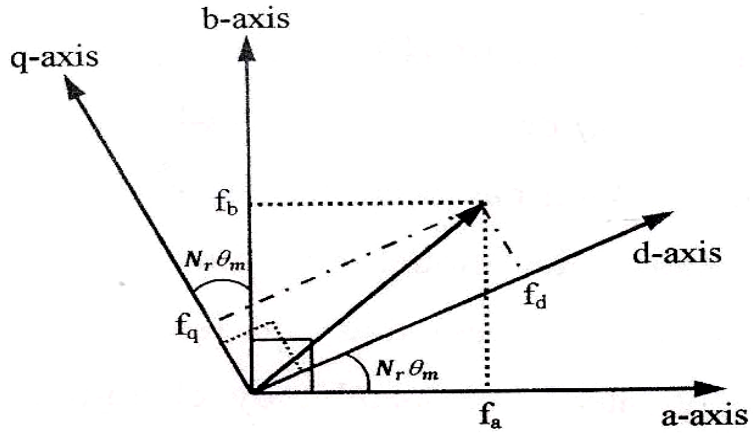

Fig. 2: Transformation of (a-b) to (d-q) reference frame.

The equation of Park transformation can be expressed as [7].

$$\begin{bmatrix} f_d \\ f_q \end{bmatrix} = K_s^e \begin{bmatrix} f_a \\ f_b \end{bmatrix} \tag{6}$$

Where, (k_s^e) is the Park transformation matrix which is given by:

$$K_s^e = \begin{bmatrix} \cos(\mathrm{Nr}\theta_m) & \sin(N_r\theta_m) \\ -\sin(N_r\theta_m) & \cos(N_r\theta_m) \end{bmatrix} \tag{7}$$

Now, multiply equation (1) through (4) by Park transformation and rearrange these equations to obtain new model HSM in (d-q) reference frame as:

$$v_{ds} = \mathrm{R}\ i_{ds} + \mathrm{L}\ \frac{di_{ds}}{dt} - \mathrm{L}\ \mathrm{N}_r\ \omega_m\ i_{qs} \tag{8}$$

$$v_{ds} = \mathrm{R}\ i_{qs} + \mathrm{L}\ \frac{di_{qs}}{dt} + \mathrm{L}\ \mathrm{N}_r\ \omega_m\ i_{ds} + \mathrm{K}_m\ \omega_m$$

(9)

$$\mathrm{K}_m\ i_{qs} - \mathrm{T}_l = \mathrm{J}\ \frac{d\omega_m}{dt} + \mathrm{B}\ \omega_m \qquad \textbf{(10)}$$

$$\frac{d\theta_m}{dt} = \omega_m \qquad \textbf{(11)}$$

- VECTOR CONTROL PRINCIPLE

During the past decade, several authors have presented the principles of vector control of AC motors [3, 8]. However, the vector control principle consists of controlling the angle and amplitude components of the stator field. For ease of motor equation representation, the components of the stator current are represented in a rotating reference frame (d-q) aligned with the rotor axis, i.e., with the magnet flux. The motor torque for a permanent magnet machine as in HSM depends only on the quadrature (q) current (torque) component. In this case, the most convenient control strategy is to set to zero the direct (d) current components to minimize the torque versus the current ratio and then increase the motor (and converter) efficiency. The control of current components requires the knowledge of the instantaneous rotor position. It can be seen that field orientation can be implemented when the winding current are adjusted so as to produce a current space vector that lies exclusively in the quadrature direction by setting direct current component equal to zero (id = 0). Torque will then be proportional to the magnitude of the current space vector. The block diagram of the proposed method of vector controlled HSM is shows in Fig. 3.

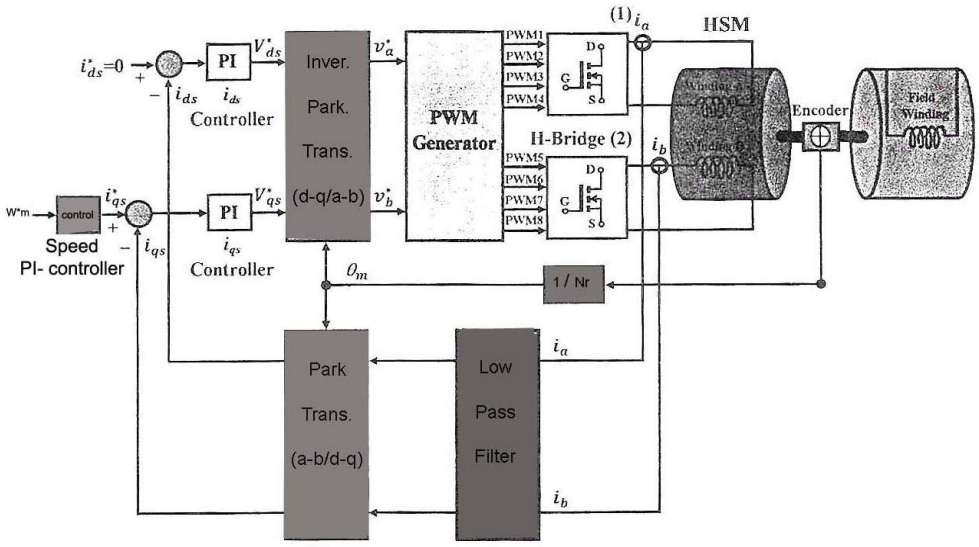

Fig. 3: Block diagram of vector controlled HSM [3].

This vector control scheme consists of a speed PI controller and two current PI controllers in the synchronous reference frame. The rotor speed is measured using encoder and the rotor position is calculated by integrating rotor speed (1/Nr) with respect to time. A low Pass Filter (LPF) has been used to eliminate the effect of unwanted high frequency signals that may be introduced during the measurements processes. However, for the conventional modules of vector control such as Park and Inverse Park transformation, sinusoidal PWM generation module, and a double H-Bridge power inverter are also included as well as the controlled HSM .

- POWER CONVERTER DESIGN

The HSM will be supplied by two identical H- bridge bipolar voltage source inverters as shown in Fig.4 (a, b).

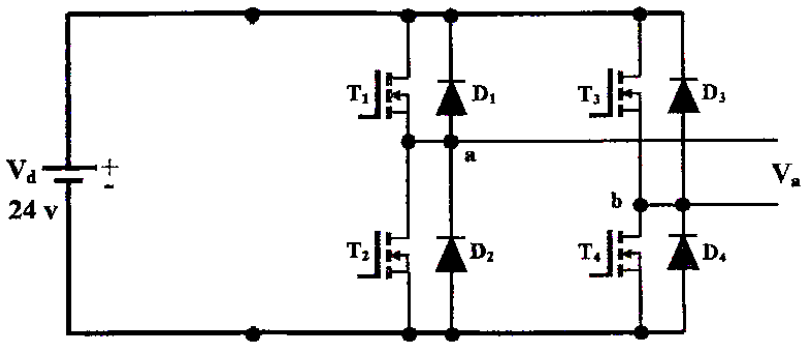

Fig.4.a: H- bridge (1) bipolar voltage source inverter [1].

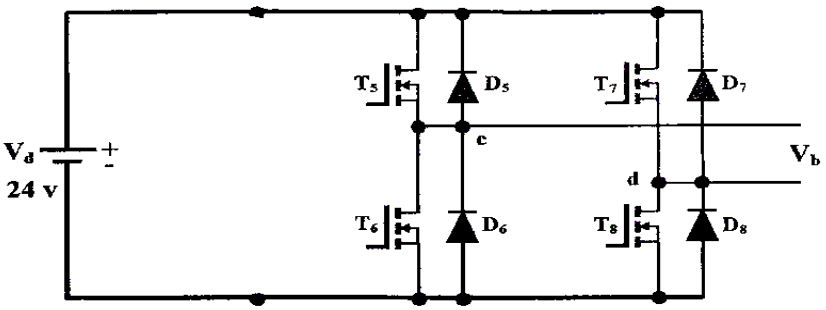

Fig.4.b: H- bridge (2) bipolar voltage source inverter [1].

Transistor (MOSFET) has been used as switching elements in the H- bridge inverter. These elements will control using the well known Sinusoidal Pulse Wave Modulation (SPWM) technique. However, the output voltage and the reference voltage waveforms from H- bridge inverters (1) and (2) are obtained using MATLAB/ Simulink as shown in Fig.5 and Fig.6.

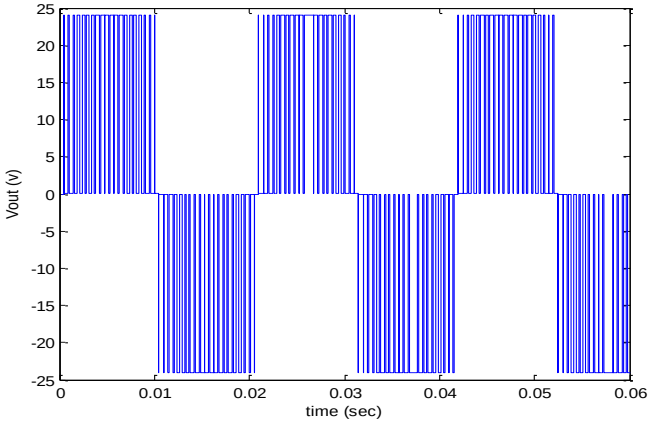

Fig.5: Output voltage from H- bridge (1).

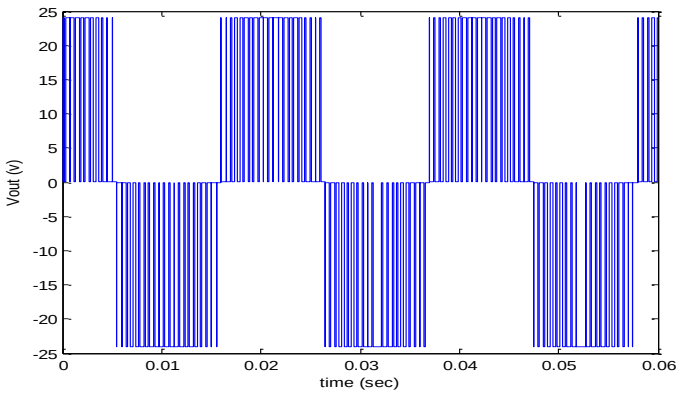

Fig.6: Output voltage from H- bridge (2).

From these results, it should be noted that the output phase voltage is shifted by (90º) due to the fact that the supplied HSM consist of two phase windings.

- SIMULATION OF HYBRID STEPPER MOTOR

The open loop pulse width modulation HSM system consists of the test input in the form of sine and cosine of 50Hz frequency and SPWM has been used to control the magnitude and frequency of AC output voltage of an inverter are shown in Fig.7. The simulated hybrid stepper motor is shown in Fig. 8, HSM can be divided into two subsystems, the electrical system and the mechanical system. In the open-loop control scheme, there is no feedback information of a position to the controller, and therefore it is imperative that the motor must respond correctly to each excitation change. If the excitation changes are made too quickly, the motor is unable to move to the new demanded position and consequently there is a permanent error in the actual position compared to the position expected by the controller. The vector controller is applied for closed-loop system to avoid the problems in open one. The idea of vector control is to study the effect of motor controller (speed and current controllers) on the performance of overall system, and to demonstrates how the value of switching frequency can contribute to change the performance of the proposed vector control of HSM, one technique have been studied through simulation by using MATLAB/ Simulink. High switching frequency is used to avoid the ripple in low frequency. The proposed vector control of HSM will be simulated using MATLAB. The values of PI controllers are used in the simulation. System's simulations were performed using a model of the HSM as shown in Fig. 9. The parameters of the motor are used in the modeling of HSM. These parameters are the same as that for real motor and they are used in the experiments and will be kept constant during simulations.

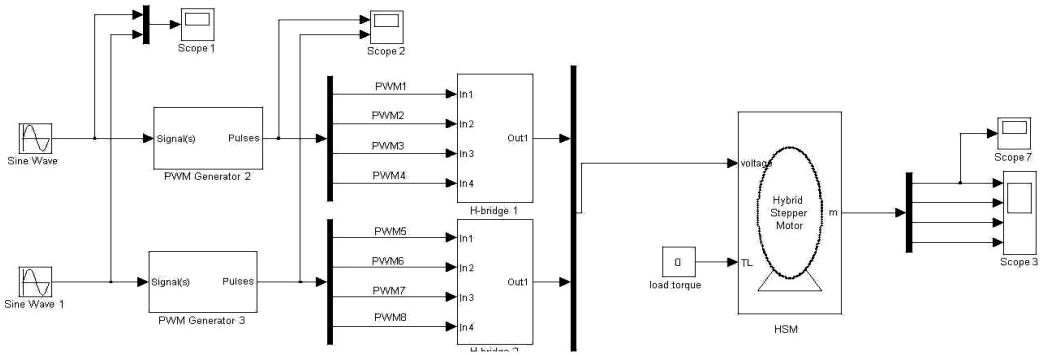

Fig.7: Open loop system.

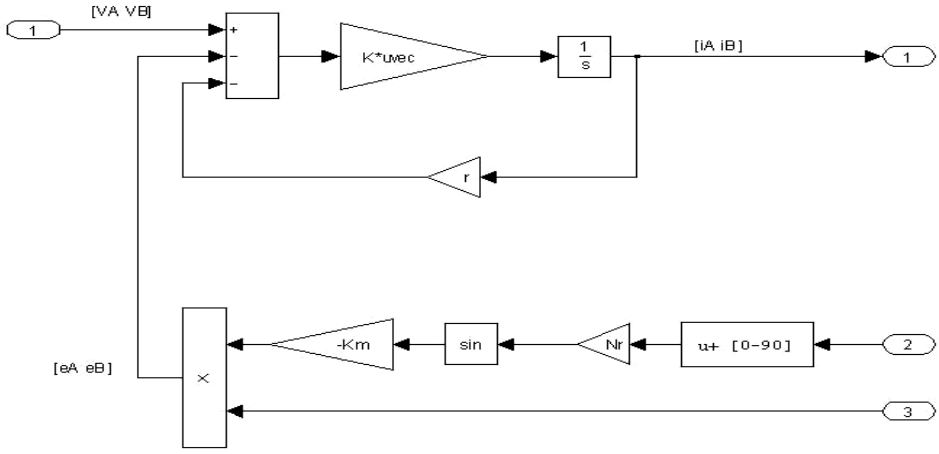

Fig. 8.a: Hybrid Stepper Motor Electrical part.

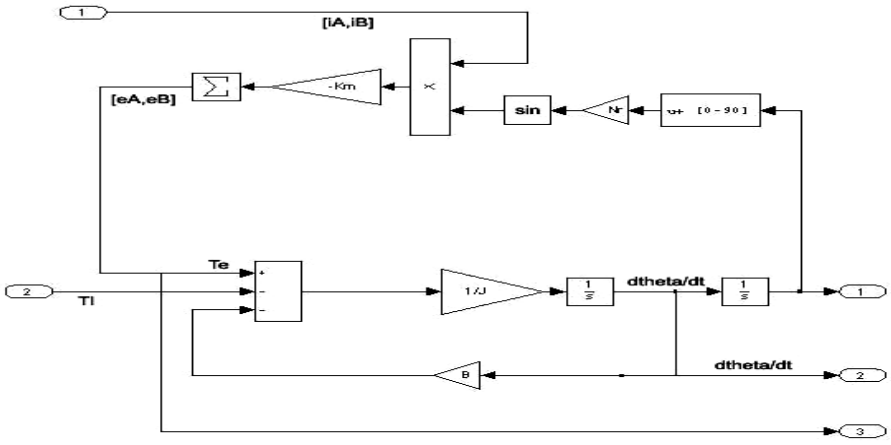

Fig. 8. b: Hybrid Stepper Motor Mechanical part.

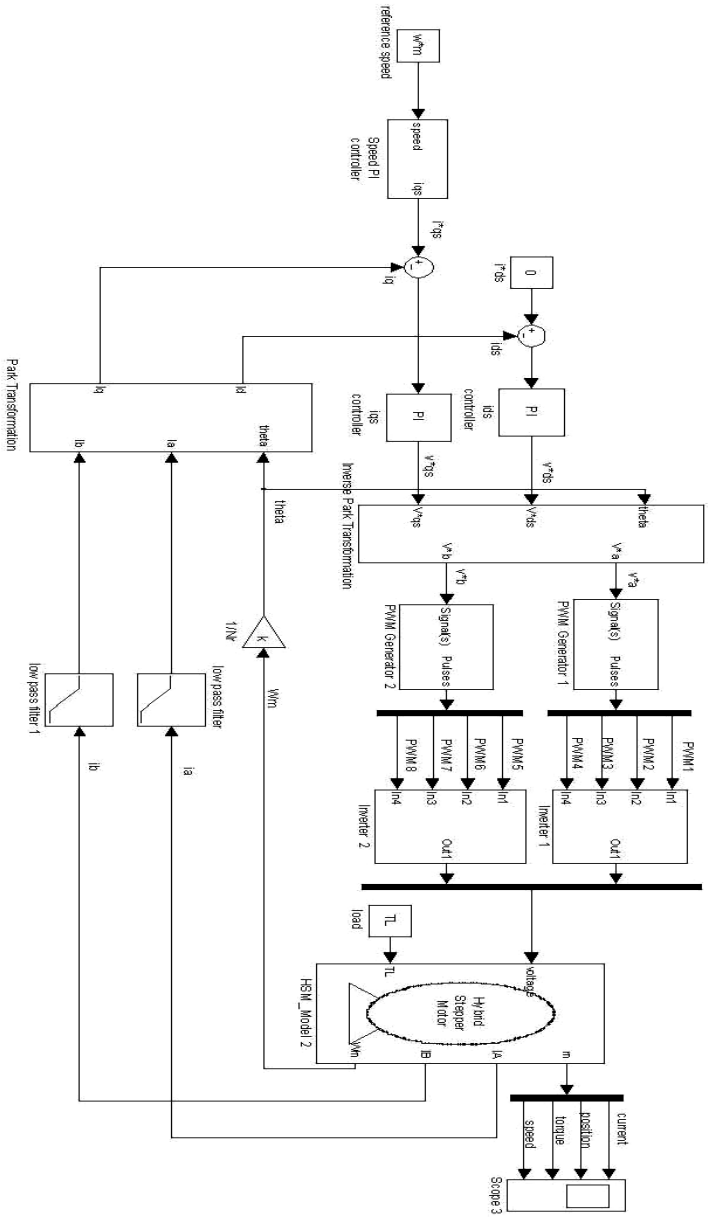

Fig. 9: Closed loop system.

- SIMULATION RESULTS

The simulation system consists of open loop system and closed loop system

OPEN LOOP RESULTS

Fig. 10 shows the currents for phase A and B of the stepper motor when load torque is 0.25 (Nm) and carrier frequency is 20 (KHz) sinusoidal current. The phase current oscillations occur as effect of PWM inverter.

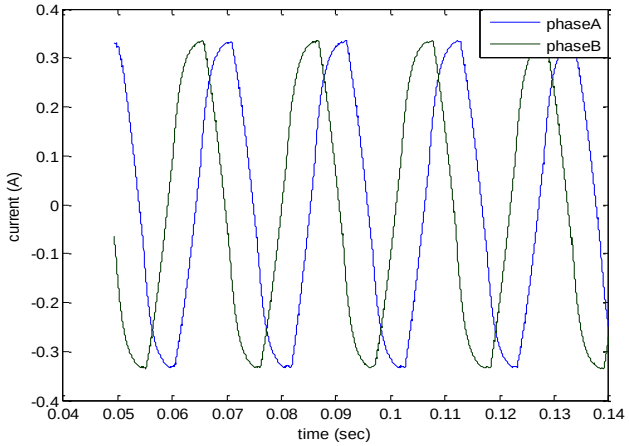

Fig. 10: Simulated windings current for phase (A,B) at 0.25 Nm load torque.

Fig. 11, Fig. 12 and Fig. 13 illustrate the dynamic behaviour of the motor when the load torque is 0.25 (Nm) and carrier frequency is 20 (KHz). The motor torque and speed contain oscillations due to PWM inverter**.**

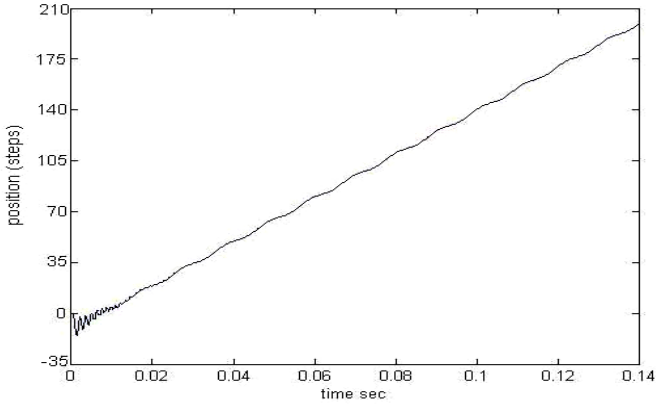

Fig. 11: The position of HSM at 0.25 Nm load torque.

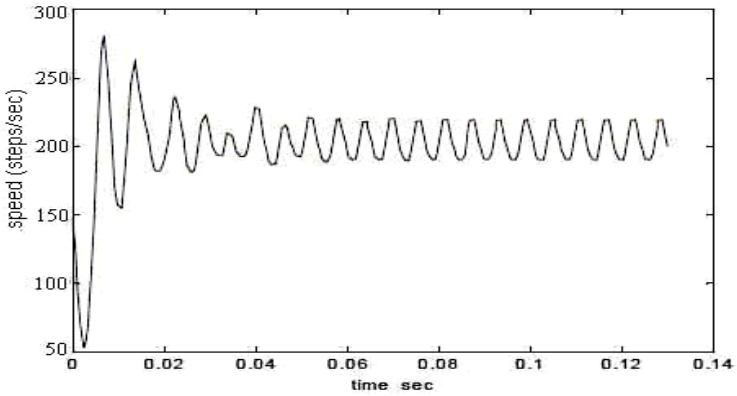

Fig. 12: The speed of HSM at 0.25 Nm load torque.

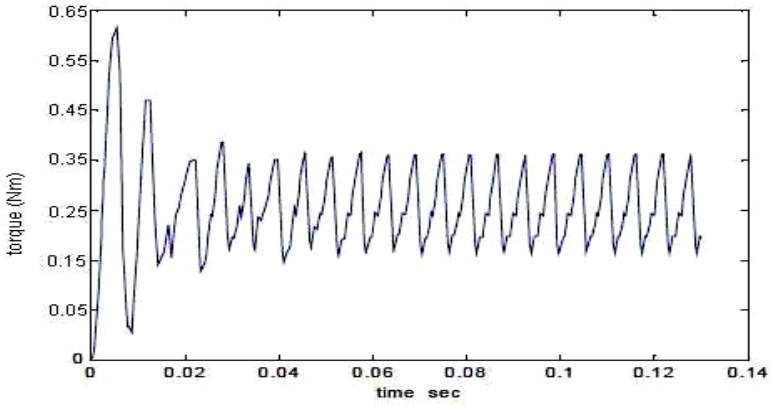

Fig. 13: The torque of HSM at 0.25 Nm load torque.

CLOSED LOOP RESULTS

The switching frequency of the PWM inverter is 20k Hz. According to the vector control principle, the stator currents can be transformed into a frame of reference which is moving with the rotor flux. Therefore, optimal utilization of the machine is achieved if the stator current is only fed in the quadrature axis (id = 0). This condition can be attained by selecting suitable value of speed and current controller parameters through tuning procedures. However, this idea has been confirmed when we obtained the winding current in (d-q) reference frame. Fig.14 shows the winding current in (d-axis), and Fig.15 illustrates the winding current in (q-axis).

From these result, it can be observed that after 0.01 sec the winding currents remain constant and thus the motor is in steady state mode. Also, the current waveforms have few harmonics because the selected value of switching frequency was high enough to eliminate these harmonics. During startup, the speed of the motor will increase until reaching the desired speed at 0.25 sec as shown in Fig.16. In Fig.17, the rotor position is reported in steady state with a desired speed of 100 (rad/sec).

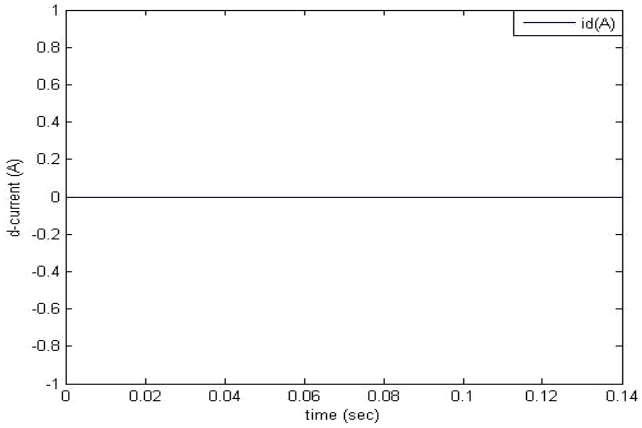

Fig.14: Simulated winding current in (d-axis) with high switching frequency.

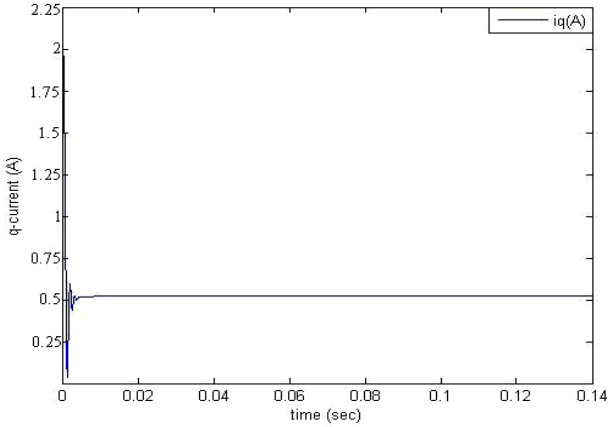

Fig.15: Simulated winding current in (q-axis) with high switching frequency.

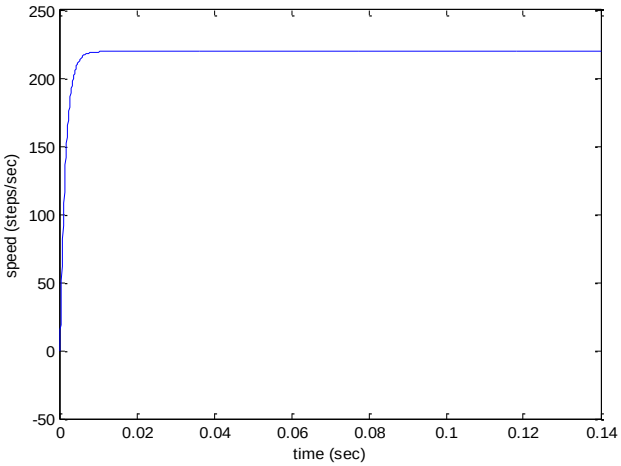

Fig.**16: Motor speed response with high switching frequency.**

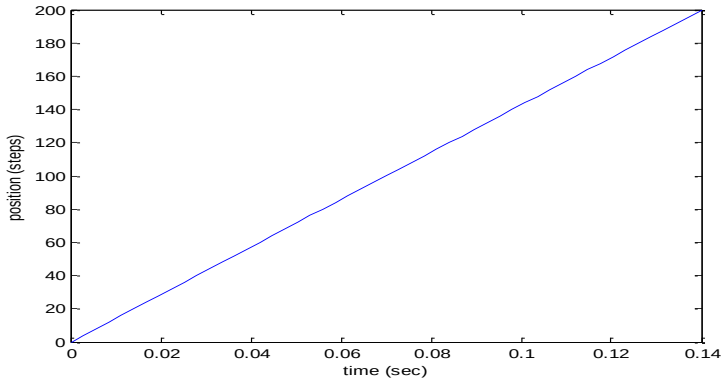

Fig. 17: Motor rotor position with high switching frequency.

- EXPERIMENTAL SETUP

The Stellaris stepper motor control reference design kit (RDK) contains all the necessary hardware and software design, and integrate stepper motor applications. The stepper RDK design kit consists of a board containing a Stellaris® microcontroller, motor drive electronics, a stepper motor, and firmware to run the motor. The stepper RDK microcontroller is shown in Fig. 18. The stepper RDK includes the following product features:

- Advanced PWM control of bipolar HSM.
- Software-based PWM control to operate high-torque steppers at high step rates.
- Fast and slow decay modes.
- Full-step, half-step, micro-step, and wave modes.
- High step rates up to 10000 steps / sec.
- Programmable holding current.

The stepper RDK firmware is designed to show how stepper motor control can be done using a Stellaris microcontroller and motor drive circuits. All of the stepper sequencing is performed in the microcontroller; no external stepping logic is required. The stepper RDK firmware provides maximum flexibility by implementing three different methods for controlling the stepper motor winding current. It also provides a number of user adjustable parameters which allows experimentation to find the best **settings for use in a particular application. The firmware is implemented as several layers, with a well defined stepper Architecture Programming Interface**

(API) to make it easy to integrate with a user's application code. It includes, as the application, a user interface which is used for demonstrating how to use the stepper firmware. The user interface can be used initially for experimenting with the motor and settings, and can later be replaced by the real application software. There are two user interfaces: an on-board interface, and an off-board interface. The on-board interface uses a potentiometer knob, a button, and two LEDs to operate the stepper motor. The off-board interface uses a USB-connected serial port and graphical application which provided extensive control of the firmware. Refer to the stepper RDK user's manual for details of using the on-board and off-board interfaces.

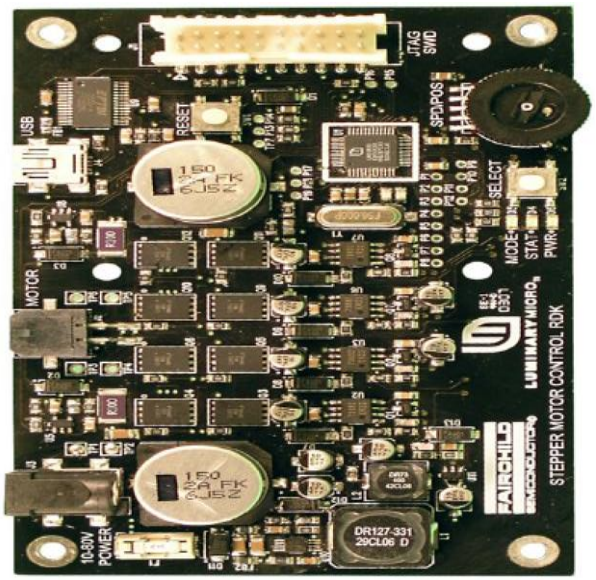

Fig. 18: Stepper Motor Control Board.

- EXPERIMENTAL RESULTS

The experimental results introduced in this section will be used to verify the effectiveness and performance of the proposed vector control of HSM. However, the proper information about rotor speed and position is required and essential for real time implementation of the high performance vector control. In closed loop PWM stepper motor system, Fig. (19, 20, 21) show the current and speed of the steady state of the motor when target speed is 221 (steps/sec), target position is 3475 steps, carrier frequency is 20 (KHz) and constant load torque is 0.25 Nm when the mode of phase excitation is full-step, half-step, micro-step. In full step excitation, two phases HSM has a step size of 1.8 degrees and 50 rotor teeth **corresponding to 200 steps per**

revolution. In half step excitation, two phases HSM has 400 steps per revolution causing the rotor to rotate at half distance so that amplitude of the current will be reduced. Advantage of a step motor operation in half step mode is position resolution increased by a factor of two compares to full step mode. In micro step excitation, the current is change in the windings in fraction of rated current so that increased step position resolution as result of a smaller step angle.

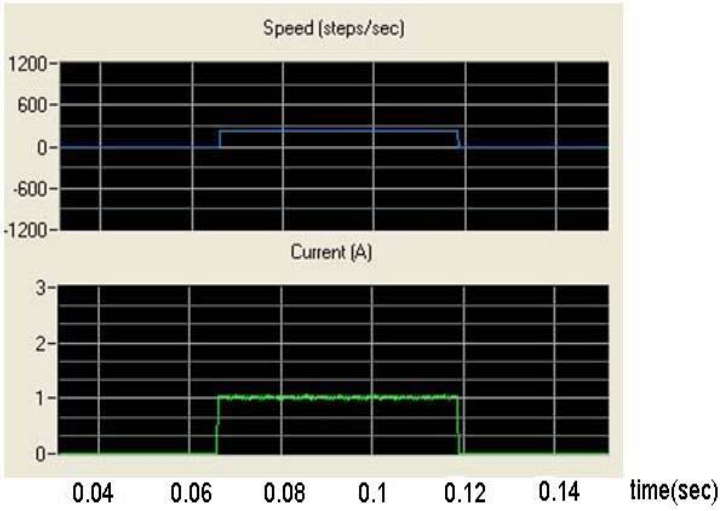

Fig. 19: Current and speed of HSM for full-step and 221(steps/s).

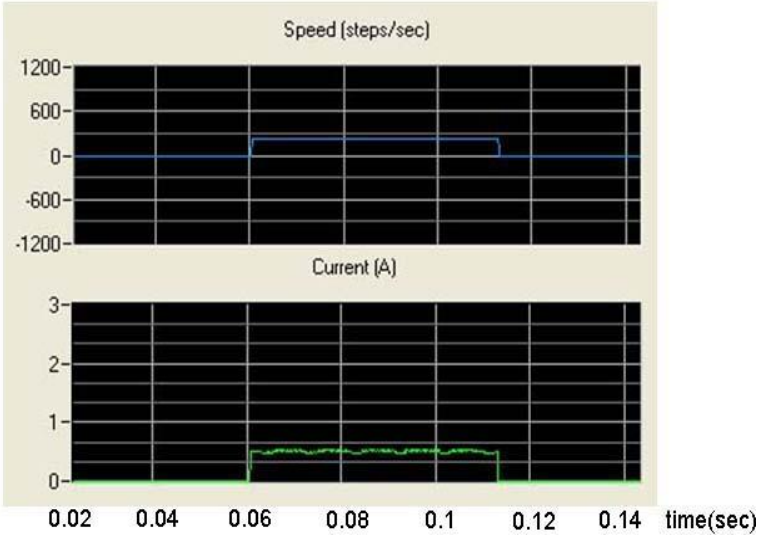

Fig. 20: Current and speed of HSM for half-step and 221 (steps/s).

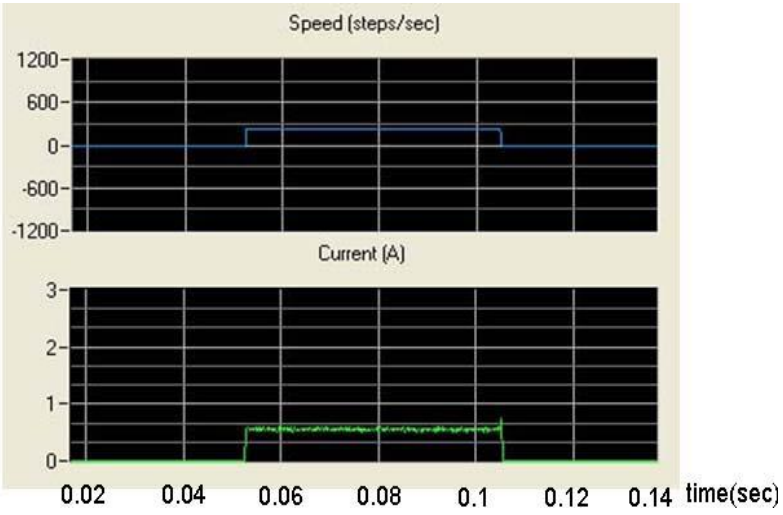

Fig. 21: Current and speed of HSM for micro-step and 221 (steps/s).

CONCLUSIONS

The proposed vector control of HSM using state estimation has been found to be well suited to the speed and rotor position estimation of the HSM. The developed method can be extended for the estimation of any other set of parameters/states in HSM control and may also be used with other control methods which require the accurate knowledge of a high number of parameters. It has been illustrates that the HSM can be transformed into a highly dynamic brushless DC- motor with vector control. This can lead to overcome the usual problems of HSM such as high currents, overheating and acoustic noise. To compare the results for speed and current between simulation and practical circuit, it found that the practical speed results are symmetrical to the simulation speed results but the current in practical results are less oscillation than simulation because simulation circuit used PI controller in closed loop system to control the current and speed of HSM while in practical circuit LM3S617 microcontroller is used to control the speed and current of HSM. PI controller depended on principle of trial and error to adjust the proportional and integral gain while LM3S617 depend on the accuracy of the software and electronic device.

REFERENCES

- P.P. Acarnely, Stepping Motors: A Guide to Modern Theory and Practice, 2nd ed. Stevenage, U.K.: Peregrinus, 1994.

- T. Kenjo, Stepping Motors and Their Microprocessor Control, Oxford, U.K. Clarendon, 1994.

- A. B. Behal, "Field Oriented Control of Step Motors", M.Sc. Thesis, Department of Electrical Engineering, Cleveland State University, Dec., 2004.

- N. M. Matsui, M. W. Nakamura, and R. T. Kosaka, "Instantaneous Torque Analysis of Hybrid Stepping Motor", IEEE Transactions on Industrial Electronic, Vol. 60, No. 6, Jan., 2009.

- A. S. Rubaai, M. F. Sitiriche, M. J. Garuba, and L. D. Burge, "Implementation of Artificial Neural Network Based Tracking Controller for High Performance Stepper Motor Drives", IEEE Transactions on Industrial Electronics, Vol. 54, No. 1, PP. 218-227, Feb., 2007.

- L. O. Hoang, P. H. Brunelle, and G. T. Sybille, "Design and Implementation of a Versatile Stepper Motor Model for Simulink's SimPower Systems", IEEE Transactions on Industrial Electronics, Vol. 20, No. 3, Dec., 2008.

- J. R. Frus and B. C. Kuo, "Closed loop Control of Step Motors Using Waveform Detection", Proceedings of the International Conference on Stepping Motors and System, University of Leeds, U.K., PP. 77-84, 1990.

- W. J. Douglas, " Stellaris® Stepper Motor RDK Software Reference Manual, Publication Number RDK Stepper", Luminary Micro, Inc., 2008.

EFFECT OF INNER BOUNDARIES GEOMETRY ON NATURAL CONVECTION HEAT TRANSFER IN HORIZONTAL ANNULI

Kadhum A. Jehhef
Ass. Lecturer
Institute of Technology

Faris A. Badawy
Ass. Lecturer
Institute of Technology

ABSTRACT

An analytical modeling of natural convection in physically-based analysis is developed for investigate free convective heat transfer in horizontal eccentric annulus between a circular outer cylinder and heated different shape inner envelope with used four models of the shapes of the inner cross section of (circular, triangular, square and hexagon inner boundary). The main objective of this paper was taking a composite model based on asymptotic solutions for three limiting cases: pure conduction, laminar boundary layer convection and transition flow convection. Laminar conditions up to Rayleigh number Ra_{Pi} of 5×10^4 were investigated. By using data from MATLAB simulations for a wide range of two cylinder temperature difference in order to study the effects of annulus diameter ratio, Rayleigh number, and the cross section geometries of inner cylinder on the Nusslte number and the ratio of thermal conductivity. The numerical result illustrated for the circular the increasing the Rayleigh number leading to slightly increasing the non-dimensional Nusslte number with various value of annulus diameter ratio and when used the high annulus perimeter ratio (P_o/P_i) about (4.5,2.6,1.6 and 1.175). There is rapid increasing in the non-dimensional ratio of thermal conductivity with increasing the Rayleigh number at the high values of (P_o/P_i), and the result showed that the non-dimensional ratio of thermal conductivity and the Nusslte number values of the (triangular, square and hexagon) less than in the case of circular inner boundary, but the hexagon model showed the Nusslte number more that than in the (triangular and square). the mathematical results compared with model developed by pervious numerical the model and data are in good agreement, with an average RMS difference of 10.6% for the circular annulus of dimensional Nusselt number (Nu_{Pi}) and less than 4.9 % and 9.8% for the square inner geometry non-dimensional ratio thermal conductivity.

Keywords: laminar boundary layer, transition flow, conduction shape factor.

دراسة تأثير الشكل الهندسي للحدود الداخلية على انتقال الحرارة بالحمل الحر داخل اسطوانتان افقيتان متحدتا المركز

الخلاصة

يتضمن البحث الحالي استخدام النمذجة التحليلية لانتقال الحرارة بالحمل الحر بالتحليل الفيزيائي لهذه العملية وتم تطويره لدراسة الحمل الحر داخل نماذج من الاسطوانات متحدة المركز الافقية بين الاسطوانة الخارجية الدائرية دائما والاسطوانة الداخلية التي تم تغييرها الى ثلاثة اشكال هي (المثلثية , المربعة و السداسية) من حيث المقطع العرضي. الهدف الرئيسي من البحث هو نموذج مركب مستند الى الحل التناضري لثلاث مناطق حرارية هي التوصيل الصرف , الطبقة المتاخمة الحرارية لمناطق الحمل الحر والانتقالي. والدراسة تعرضت فقط للظروف الطباقية لقيم رالي الاكبر من 5×10^4 . وباستخدام محاكاة المعادلات ببرنامج الماتلاب MATLAB لفروق واسعة من درجات الحرارة بين الاسطوانتين تم استقصاء تأثير كلا من نسب محيطات الاسطوانتين ورقم رالي وشكل المقطع العرضي للاسطوانة الداخلية على رقم نسلت اللابعدي وقيم نسبة الموصلية الحرارية اللابعدية. واوضحت النتائج النظرية الزيادة في قيم رالي تؤدي الى زيادة في قيم رقم نسلت اللابعدي لنسب المحيطات

(P_o/P_i) تتراوح بين(4.5,2.6,1.6, 1.175). وهناك زيادة متسارعة لقيم نسبة الموصلية الحرارية اللابعدية عند القيم العالية لنسب المحيطات وان استخدام النماذج (المثلثية , المربعة و السداسية) يعطي رقم نسلت اقل مما موجود في النموذج الدائري ولكن النموذج السداسي يكون اكبرمن النماذج (المثلثية و المربعة) ويكون اقرب لحالة النموذج الدائري من بقية النماذج وقورنت النتائج مع النتائج الرياضية لبحوث تحليلية سابقة ووجد تقارب بقيمة 10.6 % عند المقارنة مع نتائج البحوث السابقة قيم رقم نسلت اللابعدي لنموذج دائري و9.8 % و4.9 % لقيم نسبة الموصلية الحرارية اللابعدية لنموذج مربع.

INTRODUCTION

The process of natural convection heat transfer in annular space was the subject of many theoretical and experimental studies because of their great importance in many engineering applications. This process is of technological importance in the design of heat exchanger device, solar collectors, cooling of electrical and electronic components, underground electric transmission cables using pressurized gas and others. The majority of these studies are related to cylinders, whose cross sections are circular and their walls are maintained at constant temperatures. For natural convection in an annulus. The laminar boundary layer flow limit and the low Rayleigh number transition flow limit (Char and Hsu, 1998). The effect of vertical eccentricity and temperature dependent properties are investigated numerically by (Shahraki 2002) and (Char and Lee, 1998) numerically the effect of maximum density on natural convection of micropolar fluids between horizontal eccentric cylinders. Considerable works was done on investigating natural convection in horizontal annuli with inner cylinder only (Yoo, 1996), (Elsherbiny and Moussa, 2004) and (Alshahrani and Zeitoun, 2005). (Glakpe and Asfaw, 1987) use the numerical prediction of laminar natural convection in two-dimensional enclosures with inner bodies of irregular but basically cylindrical shape is the subject of thier paper. This problem models, for example, the fluid dynamics in a nuclear spent-fuel storage container in which the inner body represents tight water or a fast breeder reactor fuel assembly. The solution method described employs a no orthogonal coordinate system in which the surfaces of the inner and outer boundaries coincide with coordinate surfaces. The coordinate system is generated with simple algebraic expressions. The transformed equations of motion and energy are derived on a control volume basis with central and upwind finite differences. Details of the derivation are provided. The discrediting equations are solved within the framework of the simplest scheme for orthogonal systems. And (Chang et al., 1983) Study the horizontal annulus with different inner and outer boundary shapes are presented in the literature. Those that include average heat transfer as $1.96 \leq (P_o/P_i) \leq 3.93$ and $4\times10^3 \leq Ra_{Pi} \leq 3.2\times10^6$ include the concentric inner square.

(P. Teertstra et al., 2005) presented a analytical model is developed for natural convection in the two-dimensional region formed by an isothermal, heated horizontal cylinder concentrically located in a larger, cooled horizontal cylinder. The model is comprised of a combination of three asymptotic solutions, the diffusive limit, the laminar boundary layer limit, and the transition flow limit, and is applicable to a wide range of aspect ratios and inner and outer boundary shapes. Validation of the model is performed using numerical and experimental data from the literature for the circular annulus and a number of other geometries. The model and data are in good agreement, with an average RMS difference of 6% for the circular annulus and less than 9% for the other geometries.

(H. L. Zhang et al., 2007) presented a numerical computations are performed for the natural convection in circular enclosures with inner polygonal cylinders. The polygon surface and the

outer envelope are at constant but different temperatures. A body-fitted coordinate system is used. The coordinate system is generated via simple algebraic equations. The transformed governing equations are discredited on a control volume basis with power-law finite difference scheme. The SIMPLE-like algorithm is used to deal with the linkage between pressure and velocities. The numerical results are compared with the experimental data available in the literature, and the agreement between the numerical and experimental results are very good.

Alshahrani and Zeitoun, (2006) perform study on natural convection heat transfer between two horizontal concentric cylinders with two fins attached to the inner cylinder was numerically investigated using finite element technique together with SIMPLER algorithm. Laminar conditions up to Rayleigh number of 5×10^4 were investigated as well as effects of annulus diameter ratio, fin length and fin inclination angle on this type of flow.

Through literature survey showed that comparatively little work was focused on natural convection in annuli with change the shape of the inner cylinders on natural convection in horizontal annuli. The main objective of this paper validate model using numerical data full range of Ra_{Pi} from convection applicable to wide range of geometries relative boundary sizes circular annulus annuli with different inner, outer boundary shapes

PHYSICAL MODEL AND FORMULATION

Analytically based models that utilize readily available information, such as physical dimensions, thermo physical properties and average temperature or heat flux values for boundary conditions, provide the engineer with a set of analysis tools perfectly suited for the initial phases of the design. These models can also be easily implemented into design tools using a variety of platforms, including symbolic mathematics software such as MATLAB, or in a spreadsheet environment such as Excel. The geometry dimensions and the ratios of the perimeter of the horizontal annuli used in this search provide in the Table (1).

The problem of interest, as shown in Figure. 1, involves natural convection in an annular region with uniform temperature boundary conditions T_i and T_o on the inner and outer surfaces, respectively. In all previous studies, the geometry of the annulus is expressed in one of two ways. The first uses the aspect ratio, a non-dimensional quantity defined as d_o/d_i, with values for all configurations limited to the range:

$$1 < \frac{d_o}{d_i} < \infty$$

The second method used to express the annulus geometry is the gap spacing δ, defined by:

$$\delta = \frac{d_o - d_i}{2} \quad 0 < \delta < \infty \qquad (1)$$

where δ is defined as the distance between the centers of the inner and outer cylinders. In all cases, the annulus length L is assumed to be large compared to the diameter, such that all heat flow in the axial direction can be neglected. The independent parameters are non-dimensionalized by the Rayleigh number, defined using the overall temperature difference, $\Delta T = T_i - T_o$, and the perimeter of the inner body, P_i, is selected as the characteristic length for the horizontal annulus problem (P. Teertstra et al., 2005):

$$Ra_{pi} = \frac{g\beta\Delta T(P_i)^3}{\alpha\nu} \qquad (2)$$

The Rayleigh number is also widely used, especially for fluids with Pr larger than one, such as water or various oils. Where the thermophysical properties (pr, k, α, ν) are determined the bulk fluid temperature, T_b, which can be approximated by the arithmetic mean was (47.5 ^oC).

$$T_b = \frac{(T_i + T_o)}{2} \qquad (3)$$

The Problem Definition:

- 2D horizontal annulus
- Steady state, natural convection
- Concentric inner and outer cylinders
- Isothermal boundary conditions, $T_i > T_o$
- And the non-dimensional Geometry Relative boundary size:

$$P_o / P_i \Rightarrow d_o / d_i$$

In this paper will be used four inner characteristic lengths for the following boundaries: circular, triangular, square and hexagon ($P_i = \pi\, d_i$, 3b, 4b and 6b) respectively from Table (1). (P. Teertstra et al., 2005), (Michael et al., 2006) and (Culham, et al., 2004) present an analytical method for calculating the total heat transfer rate in regions bounded by an arbitrarily shaped heated inner body and an arbitrarily shaped surrounding cooled enclosure. The general formulation of the model represents a combination of three asymptotic terms, corresponding to the three modes of heat transfer representing the enclosed fluid region. Assume linear superposition of diffusive, convective limits (P. Teertstra et al., 2005):

$$Nu_{pi} = S_{Pi}^{*} + Nu_{conv} \qquad (4)$$

For the model validating, the model for natural convection in the horizontal annulus is validated using experimental and numerical average heat transfer data for four different geometries from the literature, having both similar and different inner and outer boundary shapes, the simplified model for the circular annulus is compared with data from number of previous studies, including (Glakpe and Asfaw 1987), (Chang et al. 1983), (Teertstra et al. 2006) and (Zhang et al. 2007). Substituting the simplified expressions for the diffusive, laminar boundary layer and transition flow limits into the general expression, and simplifying yields.

$$Nu_{conv} = \frac{1}{\left[(1/Nu_{tr})^n + (1/Nu_{bl})^n\right]^{\frac{1}{n}}} \qquad (5)$$

Where Nu_{Pi} non-dimensionalizing Nusselt number, is combined with the remaining convective terms using linear superposition. The convective terms Nu_{bl} laminar boundary layer flow, N_{tr} transition flow at low Rayleigh number and S^{*}_{Pi} represented the conduction shape factor combination parameter n chosen from validation using analytical modeling of natural convection in horizontal annuli modeling of natural convection in horizontal annuli from the (P. Teertstra 2004). Nu_{bl} represents the limiting case of high Rayleigh number heat transfer by laminar natural convection at the inner and outer walls, where the fluid in the core region is quiescent and of uniform temperature. The other convective limit Nu_{tr} corresponds to the limiting case of low

Rayleigh number, where boundary layers at the heated and cooled walls grow quickly. As a result, the temperature profile approaches that of pure conduction, fluid movement is induced in the core region, and convective heat transfer occurs at the top and bottom regions of the enclosure.

Average heat transfer rate in the annulus is non-dimensionalized using one of two methods: the effective conductivity ratio and the Nusselt number. The dimensionless effective conductivity ratio, first proposed by Beckmann (Beckmann, 1931) is based on the formulation for conduction shape factor in a circular annulus (P. Teertstra 2004):

$$S_{Pi}^{*}=\frac{2\pi}{\ln(d_o/d_i)_e} \tag{6}$$

The diameter of the equivalent inner circle is determined by preserving the inner boundary perimeter, such that $d_i = P_i/\pi$, while the outer circle diameter is based on preserving the A area between the boundaries.

$$A=\frac{\pi}{4}\left(d_o^2-d_i^2\right) \tag{7}$$

$$d_o=\sqrt{\frac{4A}{\pi}+\frac{P_i^2}{\pi^2}} \tag{8}$$

Substituting into Eq. (6) gives an approximate model for the dimensionless conduction shape factor for the general annulus as a function of the inner perimeter and cross sectional area including the noncircular inner boundary as (P. Teertstra 2004):

$$S_{Pi}^{*}=\frac{2\pi}{\ln\sqrt{4\pi(A/P_i^2)+1}} \tag{9}$$

Total heat transfer rate non-dimensionalzed by Nusselt number (Michael et al., 2006).

$$Nu_{pi}=\frac{LQ}{kP_i(T_i-T_o)} \tag{10}$$

Where L: arbitrary length, therefore the heat flow rate expressed as Q in this work is the total heat flow rate per unit length in the axial direction with units W/m. This dimensional the quantity of interest in the study, the total heat transfer rate Q between the plate and the enclosed through the fluid region is non-dimensionalized by the Nusselt number defined using the same temperature difference and length scale as Ra_{Pi}.

The laminar boundary layer flow term Nu_{bl} can be finding from (Michael et al., 2006):

$$Nu_{bl}=\frac{(1.028)F(Pr)Ra_{Pi}^{1/4}}{\left[1+\left(d_i/d_o\right)_e^{3/5}\right]^{5/4}} \tag{11}$$

Where the Prandtl number function, F(Pr), as defined by (Churchill, 1975) as:

$$F(Pr)=\frac{0.67}{\left[1+(0.5/pr)^{9/16}\right]^{4/9}} \tag{12}$$

And the N_{tr} transition flow represented by the expression of (P. Teertstra 2004):

$$Nu_{tr}=\frac{1}{720\pi^4}\frac{\left((d_o/d_i)_e-1\right)^3}{\left(1+\left(d_o/d_i\right)_e\right)}Ra_{Pi} \tag{13}$$

Through the use of an effective conductivity, the effects of convection on heat transfer in the annulus are included in this conduction expression (P. Teertstra 2004):

$$Q = S^{*}_{Pi} k_{eff} (T_i - T_O) \quad (14)$$

Solving for k_{eff} and normalizing using the actual thermal conductivity of the medium yields (Culham, et al., 2004):

$$\frac{k_{eff}}{k} = \frac{Q}{k(T_i - T_o)} \frac{\ln(d_o/d_i)_e}{2\pi} \quad (15)$$

For the noncircular inner boundary the data of the inner perimeter (Pi) given by the table (1) and the equivalent diameter of outer circular boundary ((do)e) given by equation (Eq.8).

RESULTS AND DISCUSSION

Figure (2) shows the output data employed in the present investigation of rate non-dimensional Nusselt number (Nu_{Pi}) Eq (4) of the natural convection in horizontal annuli with the Rayleigh number (Ra_{Pi}) of the circular inner boundary of four perimeter ratios (P_o/P_i) are (1.175, 1.2, 2.6 and 4.5) respectively at combination parameter n=1. Another method of representing data of heat transfer within the annulus was to be represented in terms of the effective thermal conductivity ratio (k_{eff}/k) versus Rayleigh number Ra_{Pi}, where (k_{eff}/k) is the equivalent thermal conductivity must above the unity for both of conduction and convection in the annuli this found in the Figure (3) shows values of the rate non-dimensional thermal conductivity ratio (k_{eff}/k) Eq (14) and the Rayleigh number (Ra_{Pi}) of the circular inner boundary for ratios of perimeter are (1.175, 1.2, 2.6 and 4.5) respectively at combination parameter n=1. The numerical result illustrated for the circular the increasing the Rayleigh number leading to slightly increasing the non-dimensional Nusslte number with various value of annulus diameter ratio but there is high non-dimensional Nusslte number values when used the low annulus perimeter ratios (P_o/P_i) about (1.6 and 1.175). and we observe a rapid increasing in the non-dimensional ratio of thermal conductivity with increasing the Rayleigh number at the high values of (P_o/P_i) about (2.6 and 4.5). The results indicate the existence of three heat transfer regimes similar to the case of annulus. The first is the conduction dominated regime where the Nusselt number is approximately flat. The convection dominated regime where Nusselt number is strongly depends on Rayleigh number. in the other hand when the region between the two boundaries increase we show that the values of Nusselt number decrease in he range of Rayleigh number between 1×10^4 to 1×10^7.

Figures (4 to 6) show the effect of the inner boundary geometry on the rate non-dimensional Nusselt number (Nu_{Pi}) Eq (4) of natural convection in horizontal annuli in the present investigation with the Rayleigh number (Ra_{Pi}) of the (triangular, Square and hexagon inner boundary) respectively. For three (P_o/P_i) ratios are (1.96, 2.96 and 3.96) at combination parameter n=1. Increasing the Rayleigh number leading to increasing the non-dimensional Nusslte number and we show that the increasing the (P_o/P_i) ratios leading to decreasing in the values of Nusslte number for example when the Rayleigh number 1×10^3 the values of Nusslte number were (Nu_{Pi} =10.5) at (P_o/P_i=1.96) and decreasing to (Nu_{Pi} =5.9) at perimeter ratio (P_o/P_i=3.96). and the Nusslte number values of the (hexagon inner boundary) more than in the case of (triangular and square), the Nusslte number values of the (triangular, Square and hexagon) less than in the case of circular

inner boundary, for example when the Rayleigh number 1×10^3 the values of Nusslte number were (10.5) at (P_o/P_i=1.96) and decreasing to (5.9) at (P_o/P_i=3.96)

But in the case of Figures (7 to 9) show that the the effect of the inner boundary geometry on the rate non-dimensional thermal conductivity ratio (k_{eff}/k) with the Rayleigh number (Ra_{Pi}) of the (triangular, Square and hexagon inner boundary) respectively. For three (P_o/P_i) ratios is (1.96, 2.96 and 3.96) at n=1. Increasing the Rayleigh number leading to increasing the non-dimensional thermal conductivity ratio (k_{eff}/k) show rapid increasing of value of thermal conductivity ratio (k_{eff}/k). and the result showed that the non-dimensional ratio of thermal conductivity increasing with increase the perimeter ratios (P_o/P_i) for example when the Rayleigh number 1×10^4 the values of Nusslte number were (k_{eff}/k =1.15) at (P_o/P_i=1.96) and increasing to (1.71) at (P_o/P_i=3.96) and the non-dimensional ratio of thermal conductivity of the (triangular, Square and hexagon) less than in the case of circular inner boundary.

Validate model using analytical modeling of natural convection in horizontal annuli modeling of natural convection in horizontal annuli from the Teertstra [9] presents the following analytical model for the Nusselt number based on a combination of laminar boundary layer models on the inner (cooled) and outer (heated) surfaces, From a comparison of the data and model for all test cases examined in his work a value for the combination parameter n in Eq.(5) was selected, n=1, that provides the lowest combined difference. The resulting general form of the model is:

$$Nu_{conv} = \frac{1}{\left(\frac{1}{Nu_{tr}}\right)+\left(\frac{1}{Nu_{bl}}\right)} \qquad (18)$$

Figure (10) shows the effect of inner boundary models (circular, triangular, square and hexagon inner boundary) on the rate non-dimensional Nusselt number convective terms Eq. (11) at (P_o/P_i=1.96) at Combination parameter n=1.the result show the circular given high value of (Nu_{Pi}) and the hexagon inner boundary was the higher value compared with the (triangular and square). Finally, numerical data prediction values presented by all inner boundary model used in this research compared with data of (Yoo, 1996) for circular inside cylinders only, resulting in perimeter ratio values of (P_o/P_i = 2.96), where take two values of dimensional Nusselt number (Nu_{Pi}) Eq (4) at Rayleigh number (Ra_{Pi}) of 1×10^7 for the two works and the difference between the data and the model is 10.6% as shown in the Figure (11) given comparison between the for the relation between dimensional Nusselt number (Nu_{Pi}) with the Rayleigh number (Ra_{Pi}) at Combination parameter n=1. Also the Figure (12) show the effect of inner boundary models geometry on the rate non-dimensional ratio thermal conductivity at (P_o/P_i=1.96) at Combination parameter n=1, all cases examined in this work, and the data of the square model compared with the same in the analytical modeling data of (Chang et. al. 1983) the results with an average RMS difference of approximately 4.9 % and (Teertstra et. al. 2004) the results show a RMS difference of approximately 9.8% for. and show that the used the models of Hexagon inner boundary gives high values of Nusselt number comparison with the anther models except the circular model where it is high values.

CONCLUSION

Natural convection heat transfer between two horizontal concentric cylinders with four models of different geometry inner cross section cylinder of (circular, triangular, square and hexagon inner boundary). It was investigated numerically using asymptotic solutions technique. Laminar conditions up to Rayleigh number Ra_{Pi} of 5×10^7 were investigated. Effects of annulus perimeter ratio (P_o/P_i), Rayleigh number, and inner cylinder geometry on the non-dimensional Nusslte number (Nu_{Pi}). The results show that the non-dimensional Nusslte number (Nu_{Pi}) increasing with increase the Rayleigh number in the all models, and the Nusslte number (Nu_{Pi}) decreased by (44%) with increasing the perimeter ratio (P_o/P_i) from 1.96 to 3.96 and the effective thermal conductivity ratio (k_{eff}/k) increased by (32%) with increased the perimeter ratio (P_o/P_i) from 1.96 to 3.96, also the hexagon inner boundary gives high values of Nusselt number comparison with the other models but less than the circular. the results compared with model developed by pervious numerical the model and data are in good agreement, with an average RMS difference of 10.6% for the circular annulus of Nusselt number (Nu_{Pi}) and less than 4.9 % and 9.8% for the square inner geometry non-dimensional ratio thermal conductivity (k_{eff}/k).

REFERENCES

- Alshahrani, D. and Zeitoun, O., 2005 “Natural Convection in Horizontal Cylindrical Annuli”, submitted for publication in Alexandria Engineering Journal, Alexandria, Egypt.
- Beckmann, W., 1931."Die Warmeubertragung in Zylindrischen Gasschichten bei Naturlicher Konvection", Forsch. Geb. d. Ingenieurwesen, Vol. 2, No. 5, pp 165-178,
- Churchill, S.W. and Usagi, R., 1972. “A General Expression for the Correlation of Rates of Transfer and Other Phenomenon,” A.I.Ch.E. Journal, Vol. 18, pp. 1121 – 1128.
- Churchill, S. W., and Churchill, R. U., 1975, “A Comprehensive Correlating Equation for Heat and Component Heat Transfer by Free Convection,” AIChE J., 21, pp. 604–606.
- Char, M.I. and Y.H. Hsu, 1998. "Comparative Analysis of Linear and Nonlinear Low-Reynolds Number Eddy Viscosity Models to Turbulent Natural Convection in Horizontal Cylindrical Annuli," Numerical Heat Transfer, Part A, 33: 191-206.
- Char, M.I. and G.C. Lee, 1998. "Maximum Density Effects on Natural Convection of Micropolar Fluids between Horizontal Eccentric Cylinders," Int. J. Engng. Sci., 36(2): 157-169.
- Chang, K.S., Won, Y.H. and Cho, C.H., “Patterns of Natural Convection around a Square Cylinder PlacedConcentrically in a Horizontal Circular Cylinder,” Jour-nal of Heat Transfer, Vol. 105, 1983, pp. 273 - 280.
- D. Alshahran, O. Zeitoun 2006. "Natural Convection in Horizontal Annulus With Fins Attached to Inner Cylinder". Graduate student, King Saud University, Riyadh, Saudi Arabia.

- ElSherbiny, S. M. and Moussa, A. R., 2004 "Natural Convection in Air Layers between Horizontal Concentric Isothermal Cylinders", Alexandria Engineering Journal, Vol. 43, pp. 297-311.
- Glakpe, E.K. and Asfaw, A., "Prediction of Two-Dimensional Natural Convection in Enclosures with Inner Bodies of Arbitrary Shapes" Numerical Heat Transfer, Part A: Applications, vol. 20, 1987, pp. 279-296.
- H. L. Zhang[1], W. Q. Tao[1] and Q. J. Wu[1] 2007"Numerical simulation of natural convection in circular enclosures with inner polygonal cylinders, with confirmation by experimental results" Department of Power Machinery Engineering, Xi'an Jiaotong University, 710049 Xi'an, Shanxi, China, pp.249-258.
- P. Teertstra, 2004."Comprehensive Review of Natural Convection in Horizontal Circular Annuli" Microelectronics Heat Transfer Laboratory Department of Mechanical Engineering University of Waterloo, Waterloo, Ontario, CANADA N2L 3G1.
- P. Teertstra , M. M. Yovanovich and J. R. Culham 2005. "Analytical Modeling of Natural Convection in Horizontal Annuli" Microelectronics Heat Transfer Laboratory Microelectronics Department of Mechanical Engineering University of Waterloo, Ontario, Canada Waterloo, 12 January,
- Peter Teertstra, M. Michael Yovanovich, J. Richard Culham. 2006, " Modeling of Natural Convection in Electronic Enclosures" Microelectronics Heat Transfer Laboratory, Department of Mechanical Engineering, University of Waterloo, Waterloo, Ontario, N2L 3G1, Canada Journal of Electronic Packaging JUNE Vol. 128 / 165.
- Shahraki, F., 2002. "Modeling of Buoyancy-Driven Flow and Heat Transfer for Air in a Horizontal Annulus: Effects of Vertical Eccentricity and Temperature Dependent Properties," Numerical Heat Transfer, Part A, 42: 603-621.
- Teertstra, P.M., , 2003, "Models and Experiments for Laminar Natural Convection from Heated Bodies in Enclosures", Ph.D. Thesis, Department of Mechanical Engineering, University of Waterloo, Waterloo, Ontario, Canada.
- Teertstra, P.M., Yovanovich, M.M. and Culham, J.R., 2004. "Analytical Modeling of Natural Convection in Concentric Spherical Enclosures," 42nd Aerospace Sciences Meeting and Exhibit Conference, Reno, NV, Jan. 5 – 7.
- Yoo, J-S, 1996 "Dual Steady Solutions in Natural Convection between Horizontal Concentric Cylinders," International Journal of Heat and Fluid Flow, Vol. 17, pp. 587 - 593.

NOMENCLATURE

A	area, m^2
b	side length of the inner geometry, m
cp	specific heat, J /kg K
F(Pr)	Prandtl number function
g	gravitational acceleration, m/ s^2

k thermal conductivity, W/mK
P perimeter inner and outer Boundary, m
n combination parameters
Nu_{Pi} Nusselt number,
Pr Prandtl number, ν/ α
Q total heat transfer rate, W
R thermal resistance,
Ra_{Pi} Rayleigh number,
S^*_{Pi} Conduction Shape Factor,
T_f film temperature,
T_i inner Boundary temperature, °C
T_o outer Boundary temperature, °C

Greek

α thermal diffusivity, m2/s
β thermal expansion, 1/K
μ dynamic viscosity, Ns/m^2
ν kinematic viscosity, m2/s
ρ mass density, kg/m3
δ thickness between the inner and outer Boundary, m
ΔT temperature difference, $=T_o-T_i$, °C

Subscripts

bl boundary layer flow asymptote
conv convection
eff effective
f fluid
Pi perimeter inner Boundary
Po perimeter outer Boundary
tr transition flow asymptote
i inner
o outer

Table (1) Run conditions

Geometry	Perimeter ratio (Pi/Po)	Number of sides (nb)	Length of side b (m)	Inner Perimeter (P_i)
Circular	**1.175** **1.2** **2.6** **4.6**			**πd_i**
Triangular	**1.96** **2.96** **3.96**	**3**	**0.01**	**3b**
Square	**1.96** **2.96** **3.96**	**4**	**0.01**	**4b**
Hexagon	**1.96** **2.96** **3.96**	**6**	**0.01**	**6b**

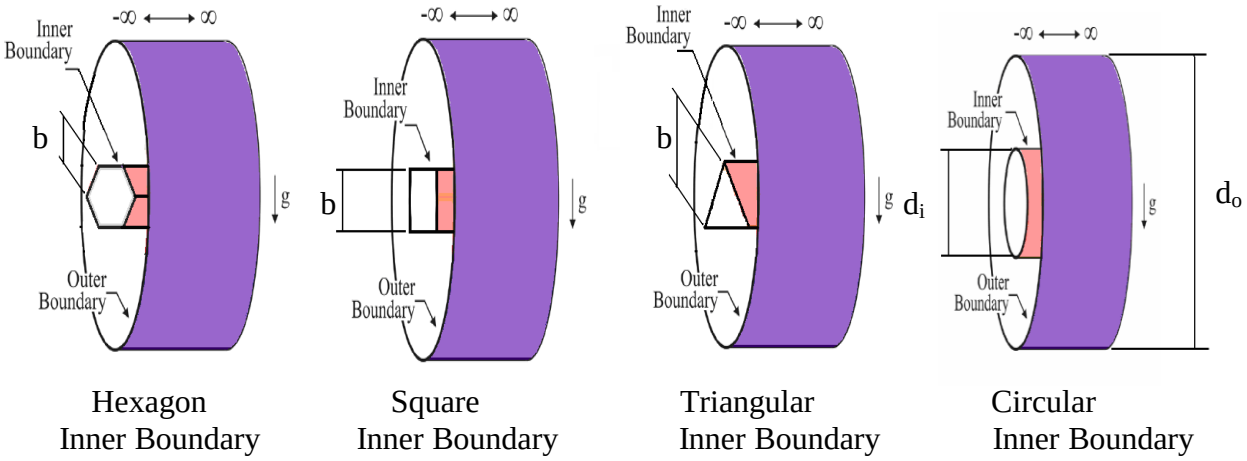

Figure (1) Cross sections of selected geometries of inner boundary cylinder

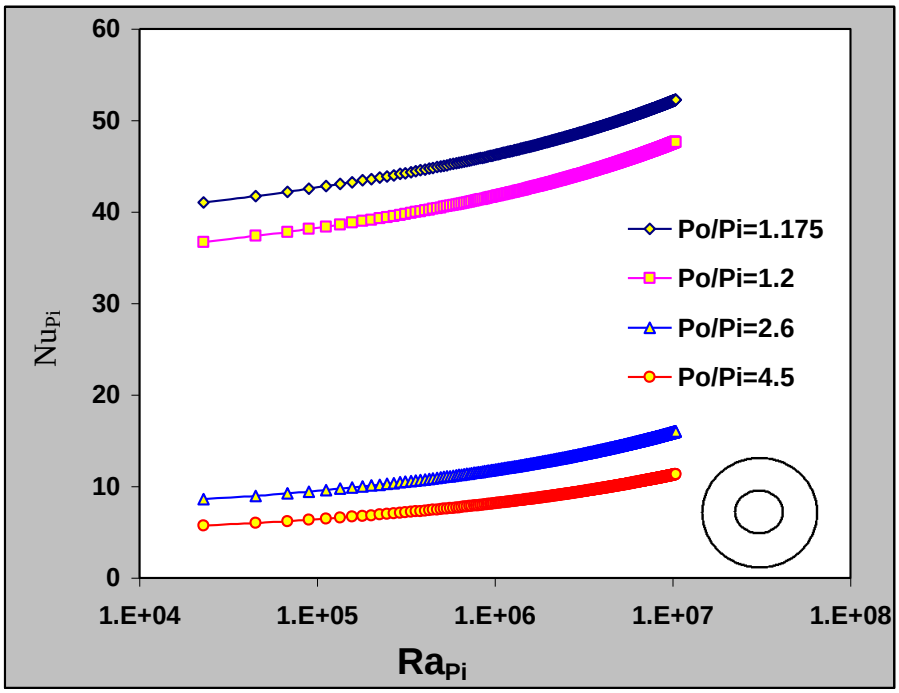

Figure (2) illustrate the effect of the increasing the perimeter ratios (P_o/P_i) on the rate non-dimensional Nusselt number at combination parameter n=1 for circular inner boundary model.

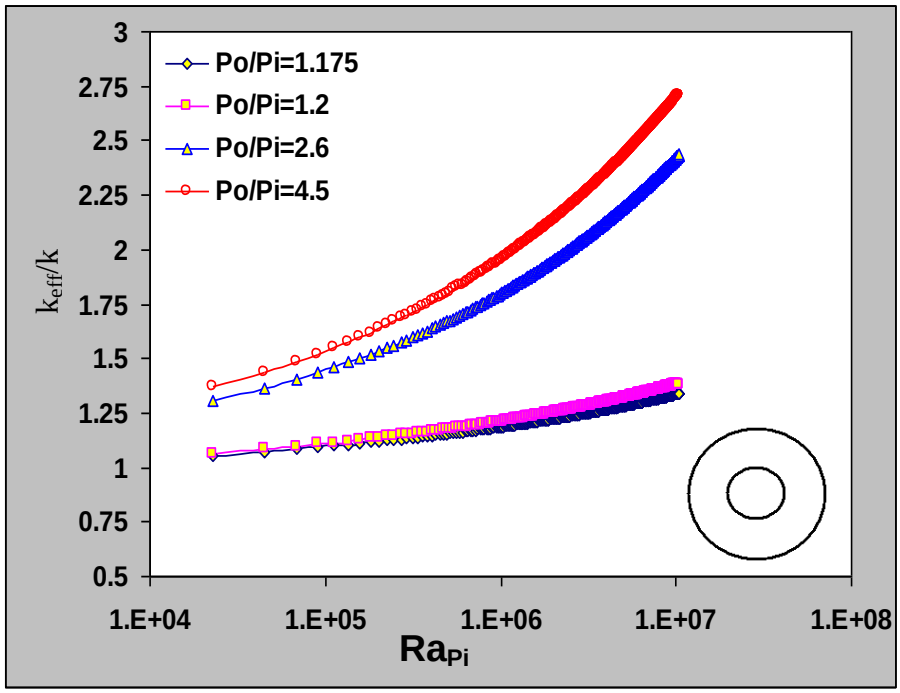

Figure (3) show the effect of the increasing the perimeter ratios (P_o/P_i) on the rate non-dimensional ratio thermal conductivity at combination parameter n=1 for circular inner boundary model.

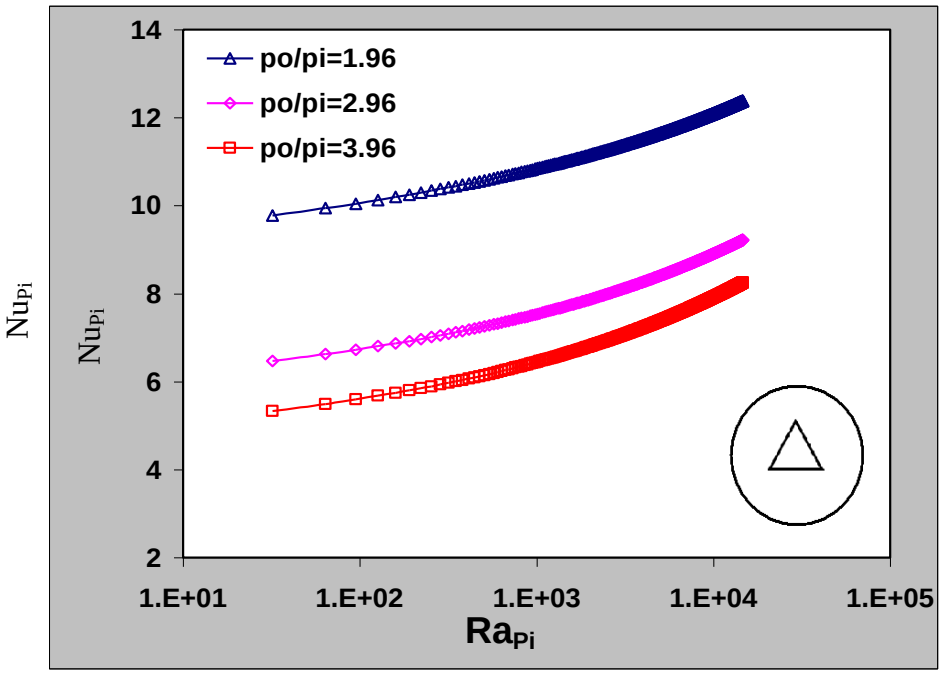

Figure (4) illustrate the effect of the increasing the perimeter ratios (P_o/P_i) on the rate non-dimensional Nusselt number at combination parameter n=1 for triangular inner boundary model.

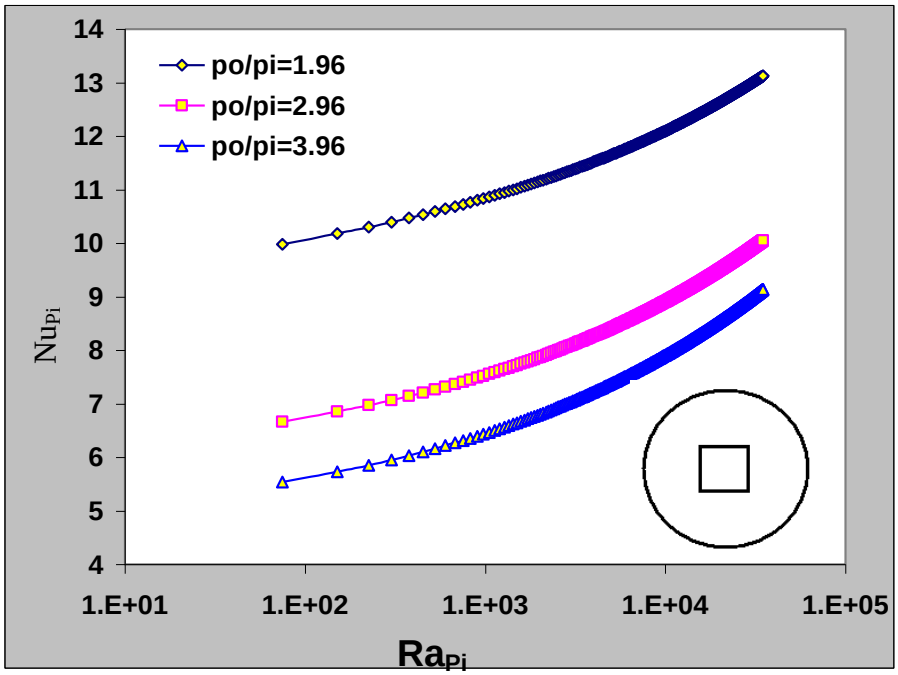

Figure (5) show the effect of the increasing the perimeter ratios (P_o/P_i) on the rate non-dimensional Nusselt number at combination parameter n=1 for square inner boundary model.

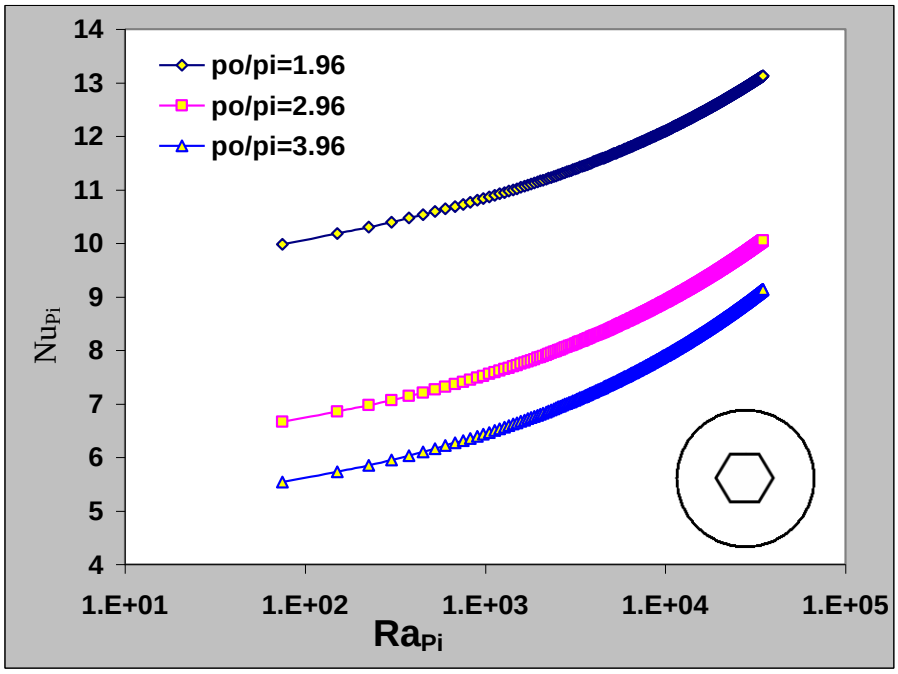

Figure (6) show the effect of the increasing the perimeter ratios (P_o/P_i) on the rate non-dimensional Nusselt number at combination parameter n=1 for hexagon inner boundary model.

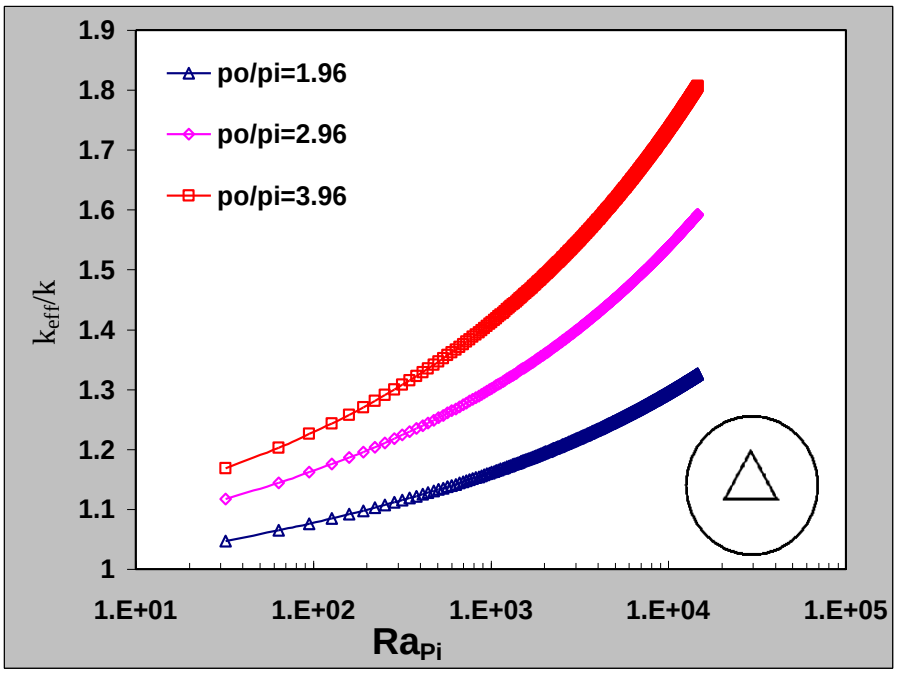

Figure (7) show the effect of the increasing the perimeter ratios (P_o/P_i) on the rate non-dimensional ratio thermal conductivity at combination parameter n=1 for triangular inner boundary model.

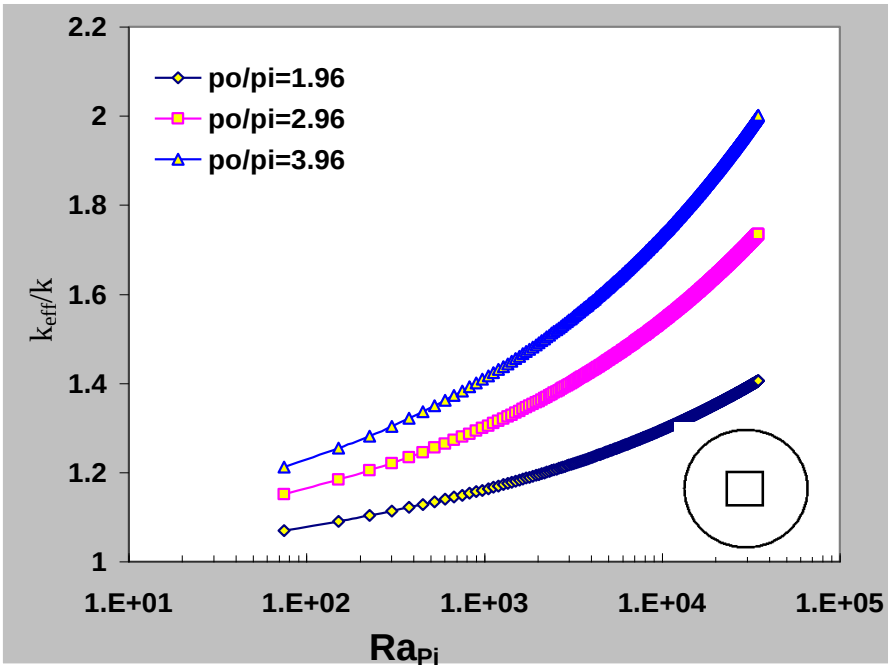

Figure (8) show the effect of the increasing the perimeter ratios (P_o/P_i) on the rate non-dimensional ratio thermal conductivity at combination parameter n=1 for square inner boundary model.

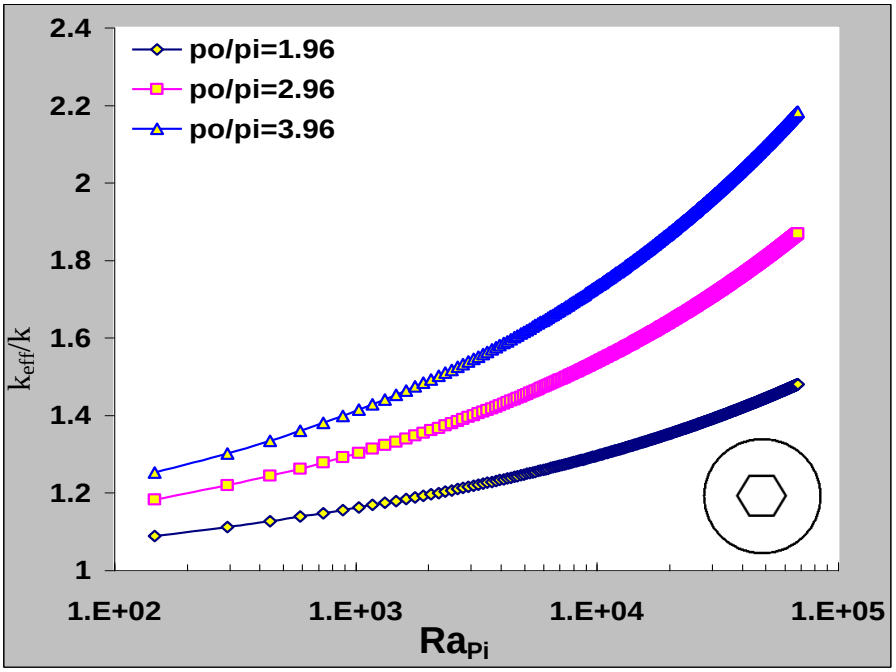

Figure (9) show the effect of the increasing the perimeter ratios (P_o/P_i) on the rate non-dimensional ratio thermal conductivity at combination parameter n=1 for hexagon inner boundary model.

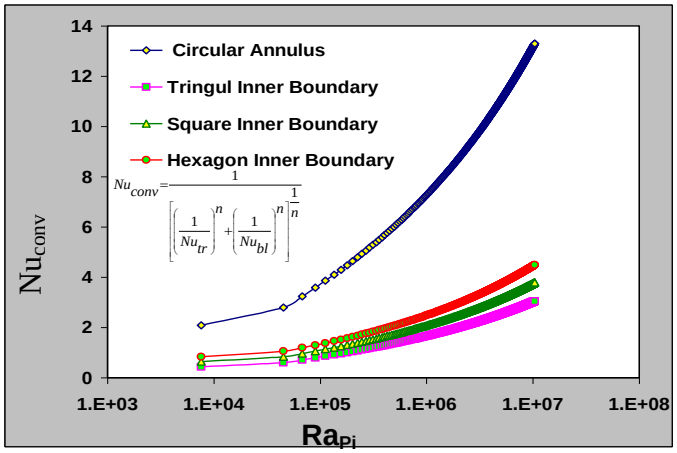

Figure (10) effect of inner boundary models on the rate non-dimensional Nusselt number convective terms at perimeter ratio (P_o/P_i=1.96) at combination parameter n=1.

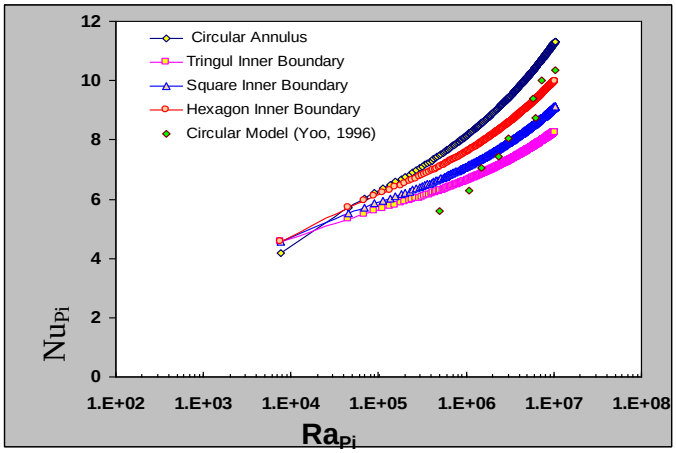

Figure (11) show the effect of the increasing the perimeter ratio (P_o/P_i=2.96) on the rate non-dimensional ratio thermal conductivity at combination parameter n=1 for all inner boundary model.

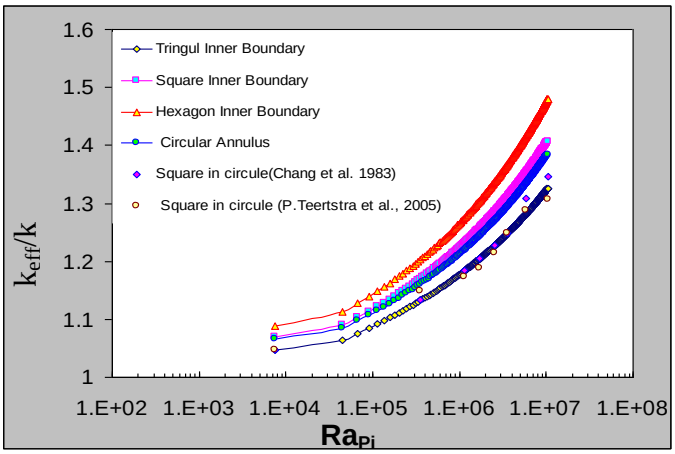

Figure (12) represented the comparison of the results of inner boundary models on the rate non-dimensional ratio thermal conductivity at perimeter ratio (P_o/P_i=1.96) at combination parameter n=1 with the pervious works.

Number 4 Volume 16 December 2010 Journal of Engineering

ESTIMATION OF RADON-222 CONCENTRATIONS IN A RESIDENTIAL AREA IN BAGHDAD CITY

Dr. Salam J. AlMaliky, . Dept. of Environmental Engineering, Eng. College , AlMustansiriya University.
Dr. Baha` ElDin Ma`rof, Ministry of Sciences and Technology.
Ahmed H.Ali, Dept. of Environmental Engineering, Eng. College , AlMustansiriya University.

ABSTRACT

Airborne radioactive particulates (for both indoor and outdoor air), in Al-Jaderiya region (Baghdad), have been collected to measure the concentration of Radon-222 daughter products of gamma ray emission (^{214}Pb, ^{214}Bi and ^{218}Po) and hence calculate the concentration of Radon-222. 24 samples were analyzed (12 indoor and others outdoor), using gamma ray spectrometric system based on a High purity Germanium detector (HpGe) of (40%) efficiency. The average concentrations of Radon-222, were found to be (93.7 Bq/m^3) and (18.9 Bq/m^3), in indoor and outdoor air respectively. The comparison of these concentrations with some internationally typical values has showed that the concentrations of Radon-222 are higher in outdoor air of the area of study compared with many regions in USA and other countries. On the contrary, the concentrations of Radon-222 in indoor air of the area of study are less than those in many European countries.

KEYWORDS

Natural radioactivity, Radon-222, indoor air, outdoor air, Spectrometric System.

خلاصة

تم جمع نماذج الهواء للدقائق المشعة العالقة في ألجو (الداخلي و الخارجي) في منطقة الجادرية (بغداد) لغرض قياس تراكيز نواتج انحلال الرادون−222 الباعثة لأشعة جاما (ألرصاص−214، ألبزموث− 214 و البولونيوم− 218) و من ثم حساب تركيز الرادون− 222. تم تحليل (24) نموذجا، (12 منها للهواء الداخلي و البقية للهواء الخارجي)، باستخدام منظومة تحليل أطياف جاما عالية النقاوة مستندة على عداد جرمانيوم نقي ذي كفاءة(40%). اظهرت النتائج ان معدل تراكيز الرادون−222 في الهواء الداخلي و الخارجي هي (93.7 بكريل/م^3) و (18.9 بكريل/م^3) على التوالي. ان مقارنة تلك النتائج مع مثيلاتها على المستوى العالمي تظهر ان تراكيز الرادون−222 في الهواء الخارجي لمنطقة الدراسة اعلى من قيمها في عدد من مناطق الولايات المتحدة الامريكية و دول اخرى. على العكس من ذلك، فقد كانت تراكيز الرادون−222 في الهواء الداخلي اقل من قيمها في العديد من الدول الاوربية .

كلمات دالة

الاشعاع الطبيعي، غاز الرادون−222، هواء داخلي، هواء خارجي، منظومة تحليل اطياف.

INTRODUCTION

Periodical monitoring of Radon-222 concentration had been emphasized by many international studies. They proved that the inhalation of short-lived decay products of Radon-222 accounts for about one half of the effective dose equivalent from all natural source of radiation and may sometimes lead to a high enough dose to cause cancer for human (Kulwant et.al, 2006).

The recent pooled analysis of key European studies estimated that the risk of lung cancer increases by 16% per 100 $Bq.m^{-3}$ increases in radon concentration. The dose–response relation seems to be linear without evidence of a threshold, meaning that the lung cancer risk increases proportionally with increasing radon exposure. Furthermore, the new results show that if a threshold exists, it should not be higher than 150 $Bq.m^{-3}$.

Recent studies showed that background levels of radon in outdoor air of most American cities are generally quite low, about 0.1 to 15 $Bq.m^{-3}$ (Krewski et.al, 2005), while, as regard to the indoor air, these studies have assessed that the Radon-222 annual mean levels in dwellings of 11 European countries is above 400 $Bq.m^{-3}$ for existing dwellings and above 200 $Bq.m^{-3}$ for future dwellings (Ernesto et. al, 2008). Also, EPA recommends homes be fixed if the radon level is 148 $Bq.m^{-3}$ or more.

GAMMA SPECTROMETRIC ANALYSIS OF ^{214}Pb AND ^{214}Bi

The activity concentrations of ^{214}Pb and ^{214}Bi in the samples of a Gamma spectrometric system may be calculated according to the following equation (Walsh et. al, 1983):

$$A_{Ei} = \frac{N_{Ei}}{\varepsilon \times t \times \gamma_d \times V_s} \quad (1)$$

The parameters E, ε_E and γ_d that are needed for Eq. (1) are listed in **Table 1**. Also, Concentration of ^{218}Po is calculated from the following relationship (UNSCEAR, 1977):

$$C_{Po\text{-}218} \approx 1.55\, C_{Pb\text{-}214} \quad (2)$$

Table 1 Parameters of gamma energy, detection efficiency and percent yield of Radon daughters (Walsh et. al, 1983)

Nuclide	E (keV)	ε_E	γ_d
^{214}Pb	351.9	0.04739	37.1
^{214}Bi	609.3	0.02253	46.1

CALCULATION OF RADON CONCENTRATION IN INDOOR AND OUTDOOR AIR

The concentration of Radon-222 in indoor and outdoor air may be calculated from the following equations (Stephen, 2008):

$$X_{Eq} = 0.106X_1 + 0.514X_2 + 0.380X_3 \quad (3)$$

$$X_{Rn} = \frac{X_{Eq}}{F} \tag{4}$$

The X_{Eq} to determine Radon gas concentration is 0.4 for indoor exposure and 0.8 for outdoor exposure (Ali, 2002).

The measured Radon-222 (in Bq/m^3) can be converted to Working Levels (WL)[1] by the use of the relationship (Stephen, 2008) :

$$WL = \frac{X_{Rn} \times F}{3700} \tag{5}$$

AIR SAMPLING PROGRAM:

Twenty four samples (outdoor and indoor air), were taken in different locations in Al-Jaderiya region (inside the complex of The Ministry of Science and Technology-Baghdad/ Iraq). Twelve samples were collected for indoor air from basement, ground, and the first floor. Other samples were collected for outdoor air from different locations outside the buildings. The duration for each sample was 1-2 hrs.

These samples were analyzed with a gamma spectrometric system as shown in **Fig.**1.

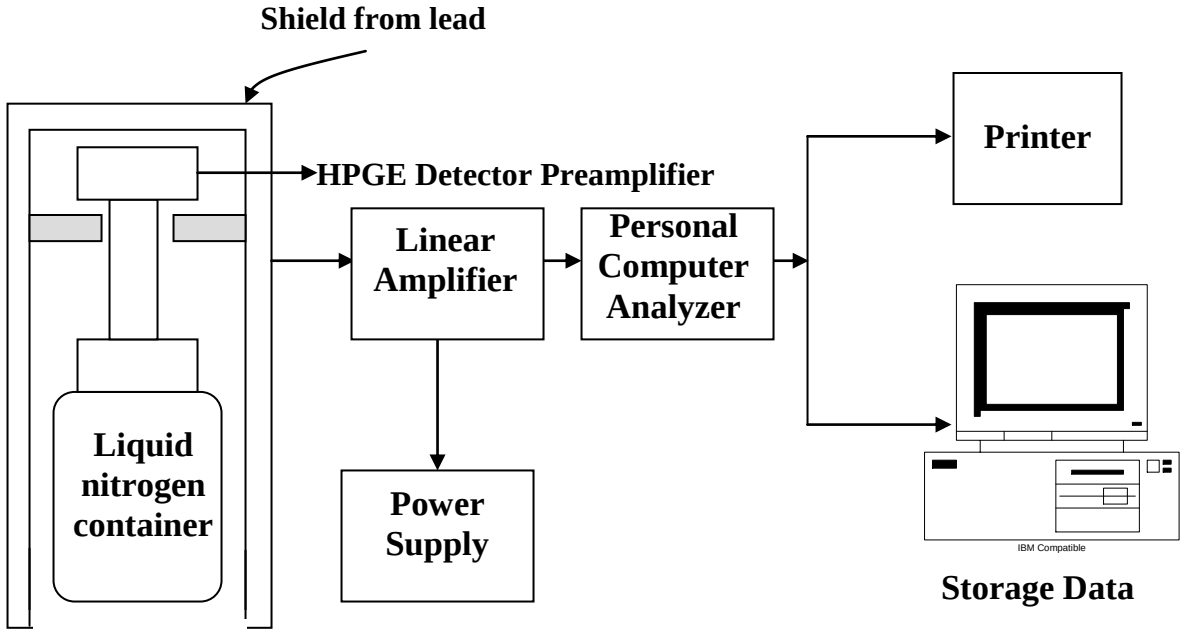

Fig.1 Gamma ray spectrometric system.

[1] WL is a measure of the concentration of potential alpha particles per liter of air

RESULTS AND DISCUSSION

Estimation of Radon-222 Concentrations in Outdoor Air

The activity concentration of ^{214}Pb and ^{214}Bi in outdoor air, measured by gamma spectrometric system are used as an input for eq.(2) to determine ^{218}Po concentration in outdoor air (**Table 2**).

Table 2. Measured concentrations of ^{214}Pb and ^{214}Bi and calculated 218Po concentrations in outdoor air.

Sample No.	Radon Decay Products Concentrations (Bq/m^3)		Calculated ^{218}Po concentrations (Bq/m^3)
	^{214}Pb	^{214}Bi	
1	8.5	20.6	13.2
2	7.8	16.1	12.1
3	10.8	23.8	16.7
4	16.3	16.3	25.3
5	15.6	24.9	24.2
6	10.0	16.7	15.5
7	8.2	15.7	12.7
8	12.7	20.6	19.6
9	12.3	21.9	17.5
10	10.5	16.8	16.3
11	13.4	22.6	20.7
12	9.7	20.0	15.0

Radon-222 concentrations in outdoor air were calculated according to eq. (3) and (4), and listed in **Table 3**. These concentrations were converted to WL using eq. (5).

The concentrations of Radon-222 in outdoor air are ranged from 14.3- 25.1 Bq/m^3 and the average concentration is 18.9 ± 3.3 Bq/m^3.

ESTIMATION OF RADON-222 CONCENTRATIONS IN INDOOR AIR

The activity concentration of ^{214}Pb and ^{214}Bi in indoor air, measured by gamma spectrometric system are used as an input for eq.(2) to determine ^{218}Po concentration in indoor air (**Table 4**).

Table 3. Calculated concentrations of Radon-222 in outdoor air.

Sample No.	Radon-222 Concentration		
	Bq/m^3	pCi/l	WL
1	16.9	0.46	0.004
2	14.3	0.38	0.003
3	20.5	0.55	0.004
4	21.6	0.58	0.006
5	25.1	0.68	0.005
6	16.4	0.44	0.004
7	14.4	0.39	0.003
8	20.5	0.55	0.004
9	20.6	0.56	0.004
10	16.8	0.45	0.004
11	22.1	0.60	0.005
12	17.7	0.48	0.004
Average concentrations	18.9 ± 3.3	0.51 ± 0.009	0.004 ± 0.0008

Table 4. measured concentrations of ^{214}Pb and ^{214}Bi, and calculated ^{218}Po concentrations in indoor air

Sample No.	Location	Radon-222 Decay Products Concentrations (Bq/m^3)		Calculated ^{218}Po concentrations (Bq/m^3)
		^{214}Pb	^{214}Bi	
1	Cellar	45.7	57.8	70.8
2	Cellar	40.3	56.4	62.5
3	Cellar	42.6	61.4	66.6
4	Ground floor	23.3	36.2	36.1
5	Ground floor	36.7	49.2	56.9
6	Ground floor	27.1	41.9	42.6
7	Ground floor	39.1	60.6	60.6
8	Ground floor	35.3	54.8	52.9

9	First floor	20.7	28.4	32.1
10	First floor	18.6	26.2	28.8
11	First floor	19.0	24.0	29.5
12	First floor	20.2	29.7	31.3

The concentrations of Radon-222 in indoor air were calculated according to eq. (3) and (4), and listed in **Table 5**. These concentrations were converted to WL using eq. (5).

The average concentration of Radon-222 in indoor air is 93.7 ± 30.7 Bq/m^3 (2.5 ± 0.8 pCi/l). The maximum concentration was noticed in the cellar (132.4 Bq/m^3). This can be justified because it is closer to the soil than other floors and as soil is the larger source of Radon-222 that comes from decay of Radium in soil. In addition, the ventilation rate in the cellar is less than that in upper floors (Muirhead, 2002); while the minimum concentration was observed in the first floor (55 Bq/m^3).

Table 5. Calculated Radon-222 concentrations in indoor air.

Sample No.	Location	Radon-222 Concentration		
		Bq/m^3	pCi/l	WL
1	Cellar	132.4	3.6	0.014
2	Cellar	121.9	3.3	0.013
3	Cellar	130.6	3.5	0.014
4	Ground floor	73.9	1.9	0.008
5	Ground floor	108.9	2.9	0.012
6	Ground floor	85.9	2.3	0.009
7	Ground floor	123.8	3.3	0.014
8	Ground floor	111.4	3.0	0.012
9	First floor	62.1	1.6	0.007
10	First floor	56.4	1.5	0.006
11	First floor	55.0	1.5	0.006
12	First floor	62.5	1.7	0.007
Average concentration		93.7 ± 30.7	2.5 ± 0.8	0.010 ± 0.003

CONCLUSIONS

- The concentration of Radon-222 in area of study is within the internationally acceptable limits.
- The concentrations of outdoor Radon-222 in study area are higher than those reported for many regions in USA and other countries. This may need more studies so as to point out the causes for such high levels. On the contrary, the concentrations of indoor Radon-222 in study area are less than those reported for many regions in USA and other countries.
- The minimum concentration occurs in the first floor which proofs that Radon-222 concentration decreases with altitude from the ground surface.
- The ratio between indoor and outdoor Radon-222 concentration (average) as calculated in this study is about (5). This proofs that the sources of Radon-222 in indoor air are more than those in outdoor air and that indoor air is in a confined space and that the outdoor

concentration is affected by atmospheric stability, which is a function of incoming solar radiation and of surface wind speed.

REFERENCES

- Ali H. Azeez, "An Estimation of Radiation Doses Resulted from Breathing of Radon-222 Gas in Indoor and Outdoor Buildings", A thesis Submitted to the University of Basrah, College of Science, 2002.
- Ernesto Vocaturo, Eva Kunseler, Gabriela Slovakova, Juri Ruut, Olga Cavoura, Peter Otorepec. 4.6 V1.0 "Radon levels in dwellings", ENHIS, Menu. , Home\ Environment and health issues\ UV and ionizing radiation, 11 January 2008.
- Krewski D, JH Lubin, JM Zeilinski, M Alavanja, VS Catalan, RW Field, et al, AResidential Radon and Risk of Lung Cancer: A Combined Analysis of 7 North American Case-control Studies, Epidemiology, 2005 March.
- Kulwant Singh, Surinder Singh, Rohit Mehra, Manmohan Singh, H.S. Sahota and Z. Papp, "Measurement of radon and thoron progeny outdoors in Malout, India, using grab aerosol sampling and beta counting", J. Radiation measurements v.41 issue 1, pages 108-111, Jan.2006.
- Muirhead R Colin, "Uncertainties in assessing health risks from natural radiation, including radon", International congress series, v.1225, P. 231-237, February 2002.
- Stephen J Wozniak**, "**HANDBOOK OF RADON, health, economic and building aspects", www.seered.co.uk, January 2008.
- UNSCEAR, "Radon-222, Radon 222 and their Short Lived Decay Products Standard Source", 1977.
- Walsh P. J., W. M. Lowder "Assessing the Risk from Exposure to Radon in Dwellings", Oak Ridge National Laboratory, Operated by Union Carbide Corporation of the United States , Department of Energy, July in 1983.

NOTATIONS

γ_d : Percent yield (number of gammas per disintegration for a transition at energy E).

ε_E : The detection efficiency of energy E.

Vs : The volume of sample (m^3).

A_{Ei}: The specific activity (Bq/m^3).

F: the equilibrium factor.

N_{Ei}: The net peak area of a peak at energy E.

t :the counting live time.

X_1, X_2 and X_3: the activity concentration of Po-218, Pb-214 and Bi-214, respectively.

X_{Eq}: the Equilibrium Equivalent Concentration (EEC) of Radon daughter products.

X_{Rn}: Radon-222 gas concentration.

UNSCEAR: United Nation Scientific Committee on the Effects of Atomic Radiation

SURFACE TEMPERATURE EFFECT ON THE THERMOHYDRODYNAMIC PERFORMANCE OF JOURNAL BEARING IN HEAVY DUTY MACHINERY

Dr. Basim A. Abass
Assist. Prof.
Mech. Eng. Dept.
Babylon University

Dr. Ala M. Hosain
Assist. Prof.
Mech. Eng. Dept.
Babylon University

Basim R. Sadiq
Graduate student
Mech. Eng. Dept.
Babylon University

ABSTRACT

Increasing high demands for concept design requires journal bearing to work under several operating condition. The purpose of this work is to study the effect of surface temperature on the performance of journal bearing for heavy duty machines. Steady state thermohydrodynamic model (THD) for journal bearings has been developed. The generalized Reynold's equation, energy equation in the oil film, and the heat transfer equation in the bush and shaft are solved simultaneously. It was found that the shaft temperature has a great effect on the performance of the bearing.

الخلاصة :

أن الاعتماد المتزايد على مبدأ التصميم يحتاج إلى مساند مقعديه تعمل تحت ظروف عمل متعددة. أن الغاية من هذا البحث هو دراسة تأثير درجة حرارة السطح على أداء المسند المقعدي المستخدم في المكائن ذات الأحمال العالية. تم اعتماد النموذج الثرموهيدروديناميكي المستقر لأغراض هذا البحث. تم حل معادلة رينولدز ،التي تأخذ بنظر الاعتبار تغير لزوجة الزيت مع درجة الحرارة، معادلة الطاقة لطبقة الزيت ، ومعادلة انتقال الحرارة خلال جداري البوشة الخارجية ومحور نقل الحركة آنيا للحصول على توزيع الضغط وتوزيع درجات الحرارة خلال طبقة الزيت. لوحظ أن لدرجة حرارة المحور تأثير كبير على أداء المسند المقعدي.

KEY WORDS: Hydrodynamic lubrication, Thermal effect, Partial journal bearing

INTRODUCTION:

Journal bearings are designed for heavy-duty machinery to work under several operating conditions. In the past two decades, a great deal of research had been conducted to investigate the performance of journal bearings under a variety of operating conditions, Oscar Pinkus and Sargit S. (1979)**,** Suganami and Szeri (1979), Cowking(1981), Seireg and Dandage (1982). Many works had been performed to investigate the thermal effect in a finite journal bearing theoretically and experimentally, Ferron et.al.(1983**),** Mitsui et.al. (1983), Lund and Hansen (1984), Boncompain et.al. (1986), Costa et.al. (2000). Khonsari and Esfahanian (1988) extended the thermohydrodynamic theory to include the effect of solid particles carried by the oil in the hydrodynamically lubricated journal bearings. An experimental investigation of thermal effects in circular and elliptical plain bearings has been executed by M.T. Ma and C. M. Taylor (1996). The results obtained through this work shows that thermal effects are significant in both bearings .The effects of various geometric factors and operating conditions on the thermal performance of journal bearing had been studied by Pierre and Fillon (2000), and Nassab and Moayeri(2002). Another works had been carried out investigating the methods of solving the energy equation, Hatakenaka and Tanaka (2002) and Jang and Khonsari (2004). M Fillon and J. Bonyer (2004)

made a thermohydrodynamic analysis to a worn plain journal bearing. They showed that the worn bearing presents not only some disadvantages but also advantages , such as lower temperature. U. Singh et.al. (2008) analyze the steady state thermo-hydrodynamic of cylindrical fluid film journal bearing with an axial groove. From the parametric study it was found that the temperature of the fluid film raises due to frictional heat therby viscosity and load capacity decreases.

A thermohydrodynamic performance of grooved oil journal bearing has been made by L. Roy (2009). It had been shown during this work that feeding of oil from the bottom is very less preferable since the load capacity is lesser and the temperature development is more.

The present work represents an attempt to study the effect of journal surface temperature, as an external heat source, affecting the performance of journal bearing.

MATHEMATICAL MODEL

Hydrodynamic-lubrication sub model

The modified Reynold's equation that considers the variation of oil viscosity with temperature is employed to describe the relation ship between the hydrodynamic pressure and the lubricant film thickness Khonsari and Esfahanian (1988):

$$\frac{\partial}{\partial \bar{x}}\left(\overline{F}\,\bar{h}^{3}\frac{\partial \bar{P}}{\partial \bar{x}}\right)+\left(\frac{R}{L}\right)^{2}\frac{\partial}{\partial \bar{z}}\left(\bar{F}\,\bar{h}^{3}\frac{\partial \bar{P}}{\partial \bar{z}}\right)=\frac{\partial}{\partial x}\left(\bar{G}\,\bar{h}\right) \tag{1}$$

Where:

$$\overline{F}=\frac{\int_0^1\left(\int_0^1\frac{\bar{y}}{\bar{\mu}}d\bar{y}\int_0^{\bar{y}}\frac{1}{\bar{\mu}}d\bar{y}-\int_0^1\frac{\bar{y}}{\bar{\mu}}d\bar{z}\int_0^1\frac{1}{\bar{\mu}}d\bar{y}\right)d\bar{y}}{\int_0^1\frac{1}{\bar{\mu}}d\bar{y}} \tag{2}$$

$$\overline{G}=\frac{\int_0^1\left(\int_0^{\bar{y}}\frac{1}{\bar{\mu}}d\bar{y}\right)d\bar{y}}{\int_0^1\frac{1}{\bar{\mu}}d\bar{y}} \tag{3}$$

The oil film thickness can be evaluated as:

$$\bar{h}=\frac{h}{c}=1+\varepsilon\cos\bar{x} \tag{4}$$

The viscosity in equation (1) follows the empirical viscosity- temperature relationship suggested by Ferron et.al:

$$\bar{\mu}=k_o-k_1\bar{t}+k_2\bar{t}^{\,2} \tag{5}$$

The solution adopted in this work considers the viscosity variation across the film thickness of the lubricant.

Heat transfer sub model

The temperature in the lubricant can be determined from the following steady state energy equation:-

$$\lambda_1 \bar{u}\frac{\partial \bar{t}}{\partial \bar{x}} + \lambda_1\left(\frac{\bar{v}}{\bar{h}} - \bar{u}\frac{\bar{y}}{\bar{h}}\frac{\partial \bar{h}}{\partial \bar{x}}\right)\frac{\partial \bar{t}}{\partial \bar{y}} = \frac{1}{\bar{h}^2}\lambda_2\frac{\partial^2 \bar{t}}{\partial \bar{y}^2} + \frac{\bar{\mu}}{\bar{h}^2}\lambda_3\left[\left(\frac{\partial \bar{u}}{\partial \bar{y}}\right)^2 + \left(\frac{\partial \bar{w}}{\partial \bar{y}}\right)^2\right] \quad (6)$$

Where:

$$\lambda_1 = \frac{\rho U C_o R}{k_{oil}} \quad (7)$$

$$\lambda_2 = (\frac{R}{c})^2 \quad (8)$$

And

$$\lambda_3 = (\frac{R}{c})^2 \frac{\mu_i U^2}{k_{oil} t_{in}} \quad (9)$$

The temperature distribution through the solid boundaries (journal and bearing) can be evaluated by solving the heat conduction equation. The steady state heat conduction equation can be written as:

$$\frac{\partial^2 \bar{t}}{\partial \bar{r}^2} + \frac{1}{\bar{r}}\frac{\partial \bar{t}}{\partial \bar{r}} + \frac{1}{\bar{r}^2}\frac{\partial^2 \bar{t}}{\partial \theta^2} = 0 \quad (10)$$

Bearing parameters:

The fluid film forces are calculated as follows:.

$$\bar{w}_{\bar{r}} = \int_0^1 \int_0^{2\pi} \bar{p}\cos\bar{x}\,d\bar{x}\,d\bar{z} \quad (11)$$

$$\bar{w}_{\bar{t}} = \int_0^1 \int_0^{2\pi} \bar{p}\sin\bar{x}\,d\bar{x}\,d\bar{z} \quad (12)$$

Where $\bar{w}_{\bar{r}}$ and $\bar{w}_{\bar{t}}$ are the components of dimensionless load in the direction of line of centers of the journal and the normal to it.

The attitude angle (ϕ) can be computed as:

$$\phi = \tan^{-1}(-\frac{\bar{w}_{\bar{t}}}{\bar{w}_{\bar{r}}}) \quad (13)$$

BOUNDARY CONDITIONS

In the case of the 120° partial arc journal bearing, as shown in fig.(1), the following boundary conditions are used to solve the Reynolds' equation:

1. At $\bar{x} = 2\pi/3 - \phi$ $\bar{p} = 0.0$ (14)

2. At $\bar{x} = 4\pi/3 - \phi$ $\bar{p} = 0.0$ (15)

3. At the cavitation zone $\frac{\partial \bar{p}}{\partial \bar{x}} = 0.0$ $\bar{p} = 0.0$ (16)

The temperatures distribution through the oil film can be determined by solving the energy equation subjected to the following boundary conditions :

The oil film temperature at the inlet is assumed to be constant:

At $\bar{x} = 2\pi/3 - \phi$ $t_{mix} = t_{in}$ (17)

At the bearing oil film interface:

$$\left.\frac{\partial \bar{t}}{\partial \bar{r}}\right|_{\bar{r}=1} = -\frac{k_{oil}}{k_b}\,\frac{r_{bin}}{c}\,\frac{1}{\bar{h}}\left.\frac{\partial \bar{t}}{\partial \bar{y}}\right|_{\bar{y}=0} \tag{18}$$

For the shaft oil film interface, assuming that the shaft temperature is independent on circumferential direction, then:

$$\left.\frac{\partial \bar{t}}{\partial \bar{r}}\right|_{\bar{r}=1} = -\frac{1}{2\pi}\,\frac{k_o}{k_s}\,\frac{R}{c}\int_0^{2\pi}\frac{1}{\bar{h}}\left.\frac{\partial \bar{t}}{\partial \bar{y}}\right|_{\bar{y}=1} d\bar{x} \tag{19}$$

The temperature distribution at outer surface of the bearing is:

$$\left.\frac{\partial \bar{t}}{\partial \bar{r}}\right|_{\bar{r}=\bar{r}bout} = -\frac{h_{conv}}{k_b}\,r_{bin}\left(\bar{t}_{bo}-\bar{t}_a\right) \tag{20}$$

NUMERICAL SOLUTION

Governing equations of the problem have been discritized and solved simultaneously using iterative scheme with successive under relaxation. Reynold's equation is made discrete at the spaced grid points in the coordinates ($\bar{x}, \bar{y}, \bar{z}$) to make it suitable for the finite difference method in order to gate the pressure distribution ($\bar{P}$) through the oil film. The grid size of (360) in circumferential direction, (6) across the oil film thickness and (20) across the length of the bearing have been adopted.

The energy equation (6) and the heat conduction equation (10) with the equation of state (5) have been solved simultaneously with the Reynold's equation.

Temperature and pressure distribution in the oil film and solid parts at the mid-plan of the 120 arc partial journal bearing are obtained using the following solution procedure:

1. An initial value of the attitude angle (ϕ) is assumed.
2. Temperature of oil film, bearing bush and the shaft grid points are assumed.
3. The dimensionless value of the oil viscosity for all the points are computed by using equation (5)
4. .The oil film thickness ($\bar{h}$) calculated using equation (4).
5. Initial values of oil pressure for all the grid points are assumed to have zero values except at the inlet zone.

Then iterative scheme with successive under relaxation method is employed to solve the Reynold's equation with the boundary conditions (14),(15) and (16) to obtain the dimensionless pressures of the oil film .The negative values of pressure set to zero during the computation of the of the pressure field. These iterations are stopped when the following convergence criterion for the pressure is obtained.

$$\in \bar{p} = \frac{\sum\sum\left|\bar{p}_{i,k}^{\,n} - \bar{p}_{i,k}^{\,n-1}\right|}{\sum\sum\left|\bar{p}_{i,k}^{\,n}\right|} < 10^{-4} \qquad (21)$$

6. Equations (11 and 12) have been solved and used to get a new value of the attitude angle using equation (13), which compared with the old one. The solution procedure is repeated using the new value of the attitude angle until the difference between the angles of the last two steps are reached less than one degree.

7. Dimensionless values of the fluid velocities ($\bar{u}, \bar{v}, \bar{w}$) are then calculated.

8. The energy equation (6) and the heat transfer equation at the solids (10) with the boundary conditions (17),(18), and (19) are solved simultaneously to get the temperature filed for the whole region.

9. The new oil-film temperature was used to compute a new viscosity field which is subsequently used in Reynolds' equation and simultaneous solutions for the equations are obtained iteratively until the convergence criterion of the temperatures for all points on the boundary between the oil film and the bush (inner bush face) for two successive iteration steps is less than (10^{-6}).

$$\in \bar{t} = \frac{\sum\sum\left|\bar{t}_{i,j}^{\,n} - \bar{t}_{i,j}^{\,n-1}\right|}{\sum\sum\left|\bar{t}_{i,j}^{\,n}\right|} < 10^{-6} \qquad (22)$$

RESULTS AND DISCUSSION

A suitable computer program was prepared and written in (FORTRAN – 90) language , to solve the governing equations of the problem.

Numerical results of a steady state performance of a partial journal bearing with hollow shaft, in condition pertinent to that used in supporting the two necks of cement ball mills was studied. The main data related to this bearing are presented in table (1).

The effect of the temperature of the hollow shaft which receives the heat from the ball mill body and the hot fluid passing through on the performance of the journal bearing coupled with the other operating parameters were studied as follows:

The effect of the temperature of the hollow shaft (t_{si}) on the behavior of the bearing can be shown in figures (2,3). For the same applied load and journal rotational speed, when the shaft temperature(t_{si}) increases the maximum oil film pressure increases as a result of increasing the oil film temperature which causes an increase in eccentricity ratio and hence, reduced minimum oil film thickness (hmin) as shown in figure (2). More clear insight onto the effect of the inner temperature of the hollow shaft on the temperature distribution in the bearing bush can be gained by examining figure (3). It can be shown that as the shaft inner temperature was changed from $50^{\circ}C$ to $60^{\circ}C$ the maximum bearing bush temperature was increased by $7.1^{\circ}C$. This is due to the increase of the temperature difference across the bearing bush.

The effect of the inlet oil temperature on the temperature distribution in bearing bush metal can be shown in figures (4,5). It can be shown from fig.(4) that when the inlet oil temperature increased by $10^{\circ}C$ (from 35to $45^{\circ}C$) the maximum bearing bush temperature increased only by $4.9^{\circ}C$ due to reduction in viscous dissipation in oil film with the decrease in the oil viscosity. Fig.(5) shows the combined effect of the inlet oil temperature and the inner temperature of the

hollow shaft on temperature distribution in the bearing bush metal . It can be shown from the figure that the increase of the inlet oil temperature causes a remarked effect on the temperature distribution in the first half of the bearing bush metal. At the inlet zone, the temperature of the bearing bush was effected by the inlet oil temperature. At the second half of the bearing, it is clear that a small difference in the temperature distribution has been noticed. The effect of bearing surrounding temperature on the temperature distribution can be shown in figures (6,7). As shown in fig. (6) when the bearing surrounding temperature increases by $10^{\circ}C$ (from 35 to $45^{\circ}C$) the maximum bearing bush temperature increased by $2.6^{\circ}C$. This can be attributed to the effect of the surrounding temperature on the heat lost from the bush surface. When the inner surface temperature of the hollow shaft reaches $60^{\circ}C$ with the same surrounding temperature the maximum bearing bush temperature at the mid-plane increased by $2.4^{\circ}C$ as shown in fig. (7).
The effect of lubricant type on the behavior of the partial journal bearing at the same applied load and journal rotational speed can be shown in figures (8,9). Two types of lubricant were used in this case (No.1,and No2). Fig.(8) shows the influence of lubricant type on circumferential temperature distribution in bearing bush metal. Maximum bush metal temperature in this case was increased by $2^{\circ}C$. In other case as the effect of inner temperature of the hollow shaft is taken into consideration a small increase in maximum bush temperature is noticed and there is shifting in the temperature distribution curve. The computer program used in this work has been tested by comparing the results obtained for the full journal bearing with that published by Ferron etal.

(1983) and Nassab etal. (2002) as shown in figures (10-13). It is clear that there is a good agreement between the obtaind and the published results

CONCLUSIONS

- The following concluding remark can be drawn:
- Maximum oil film and bearing bush temperatures increases with the increase of the hollow shaft temperature.
- 2.The maximum oil film pressure increases and the minimum oil film thickness decreases with the increase of the hollow shaft temperature.
- 3.Due to the effect of the shaft temperature on the bearing, a small change in the maximum bearing bush temperature remarked with the change of supplied oil temperature, bearing surrounding temperature, and lubricant viscosity.

Table 1: Partial bearing characteristics used in test case.

Parameter	Symbol	Unit	Value
Journal radius	R	m	0.9
External bearing radius	R_{bout}	m	0.972
Bearing length	L	m	0.9
Radial clearance	c	m	0.0016
Lubrication viscosity at 40 ^{o}C (No.2)	μ	Pa . s	0.241
	k_o		3.6714
Viscosity coefficients	k_1		3.5826
	k_2		0.9112
Lubrication density at 40 ^{o}C	ρ	kg/m^3	860
Lubrication specific heat	C_o	J/kg. ^{o}C	2000
Lubrication thermal conductivity	k_{oil}	W/m. ^{o}C	0.13
Bush thermal conductivity	k_b	W/m. ^{o}C	50
Shaft thermal conductivity	k_s	W/m. ^{o}C	50
Convection heat transfer coefficient	h_{conv}	W/m^2. ^{o}C	80
Inlet oil temperature	t_{in}	^{o}C	40
Ambient temperature	ta	^{o}C	40
Inlet lubricant pressure	P_s	Pa	0.0
Bearing arc angle	--	deg	120
Lubrication viscosity at 40 ^{o}C (No.1)	μ	Pa . s	0.12

Fig.(1) Partial journal bearing with hollow shaft journal

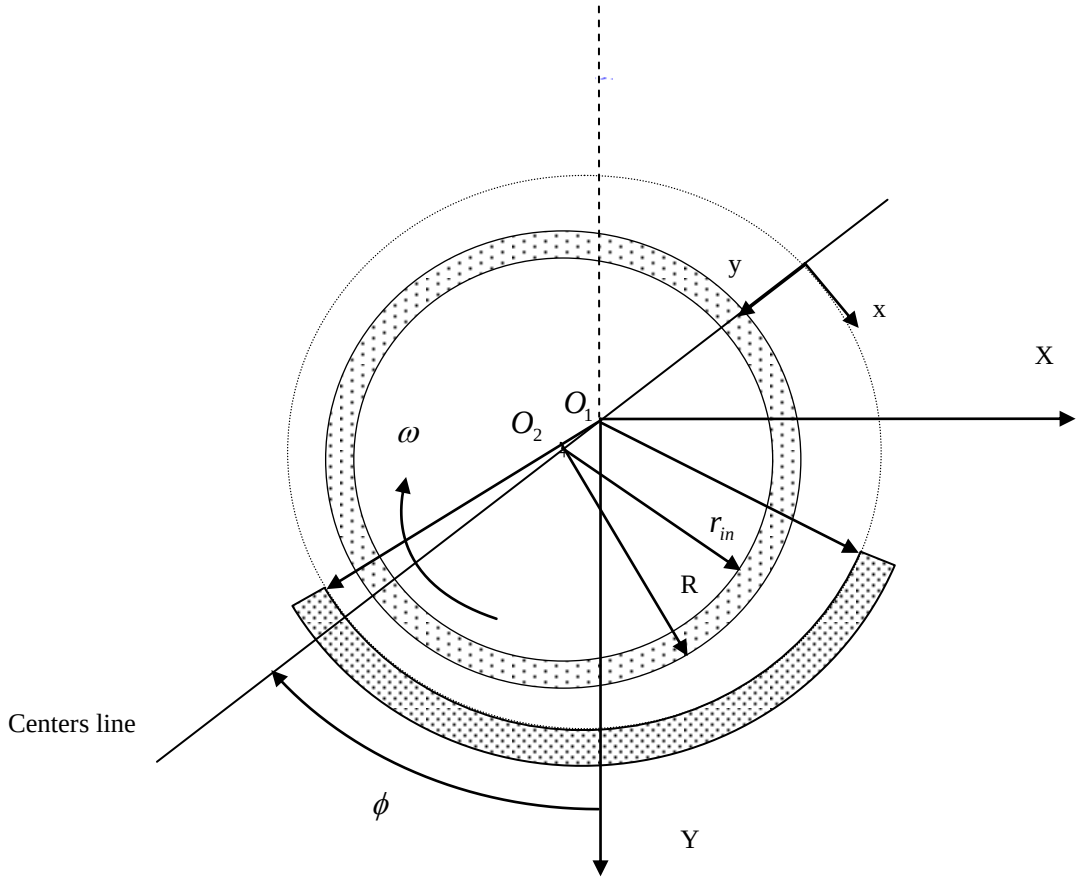

Fig.(1) Partial journal bearing with hollow shaft journal

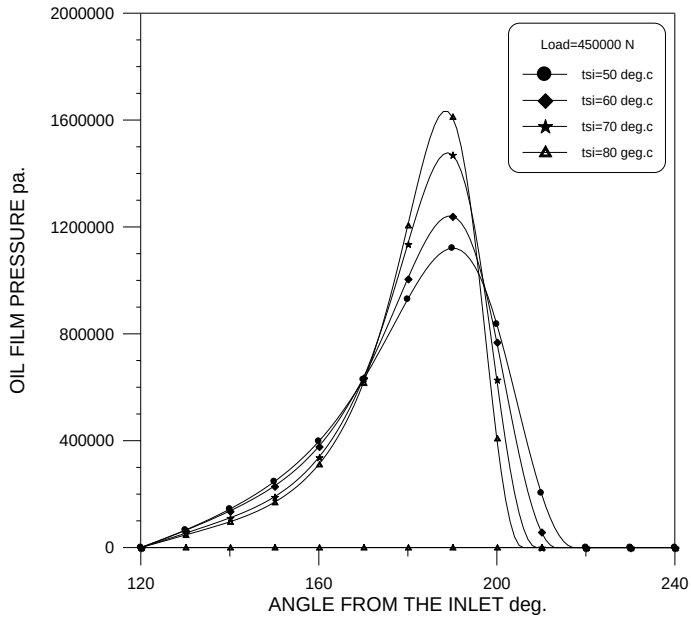

Fig.(2**)** Effect of inner temperature of the hallow shaft on the oil pressure distribution

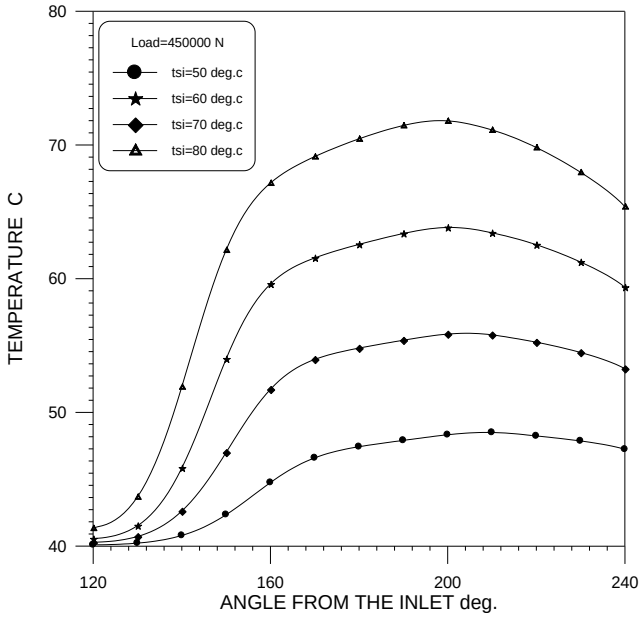

Fig.(3) Effect of inner temperature of the hallow shaft on the temperature distribution of bearing bush

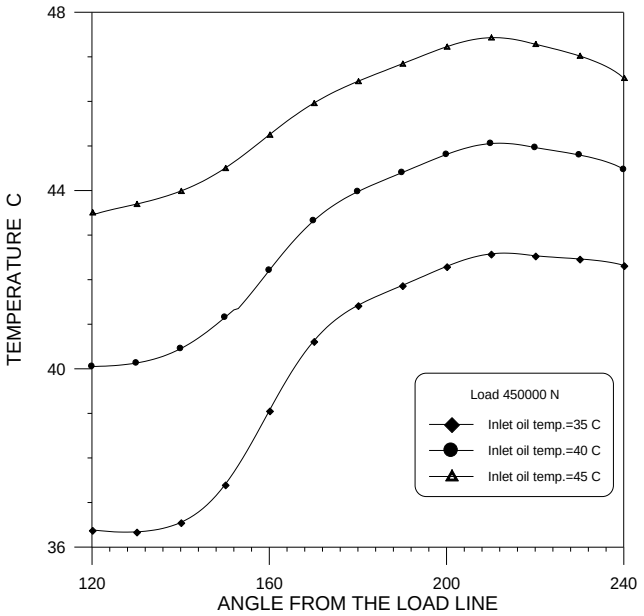

Fig.(4) Effect of inlet oil temperature on the temperature distribution of the bearing bush with out effect of inner temperature of the hallow shaft

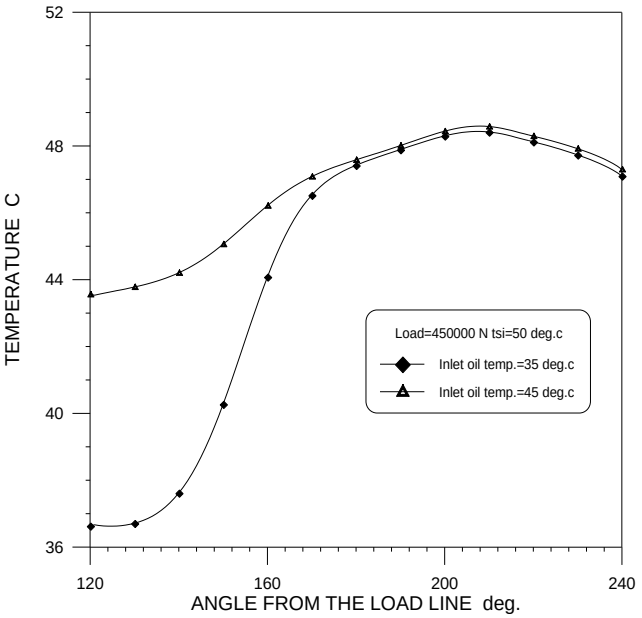

Fig.(5) Effect of inlet oil temperature on the temperature distribution of the bearing bush (tsi=50 ^{o}c)

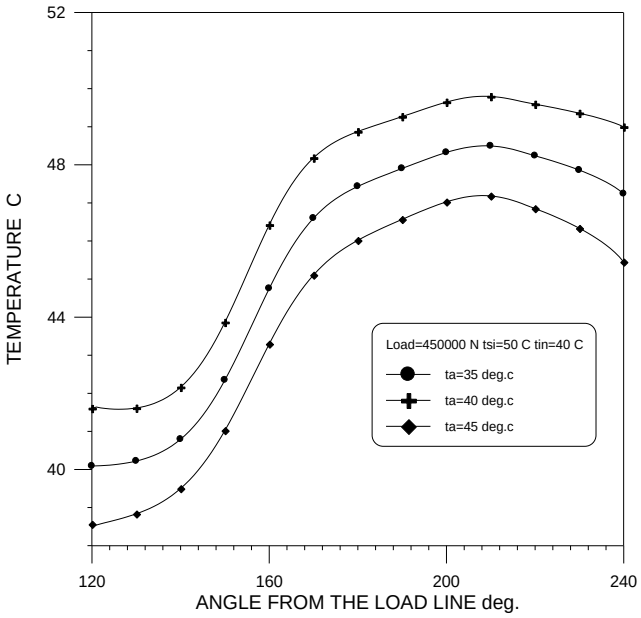

Fig.(6) Effect of ambient temperature on the temperature distribution of partial bearing bush (tsi=$50\,^{o}c$)

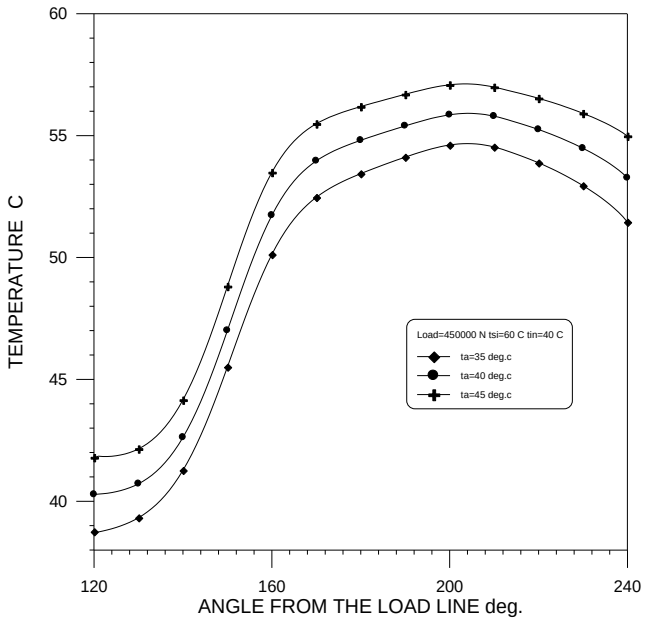

Fig.(7) Effect of ambient temperature on the temperature distribution of partial bearing bush (tsi=$60\,^{o}c$)

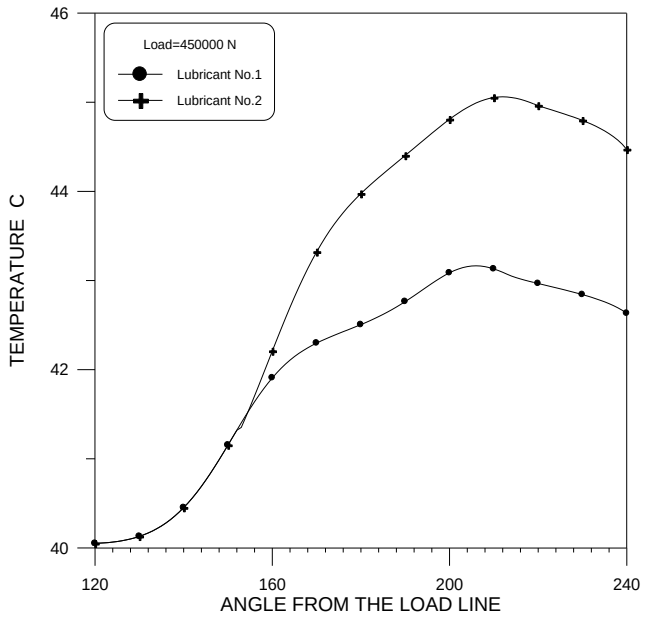

Fig.(8): Effect of lubricant viscosity on the temperature distribution of the bearing bush with out effect of inner temperature of the hallow shaft

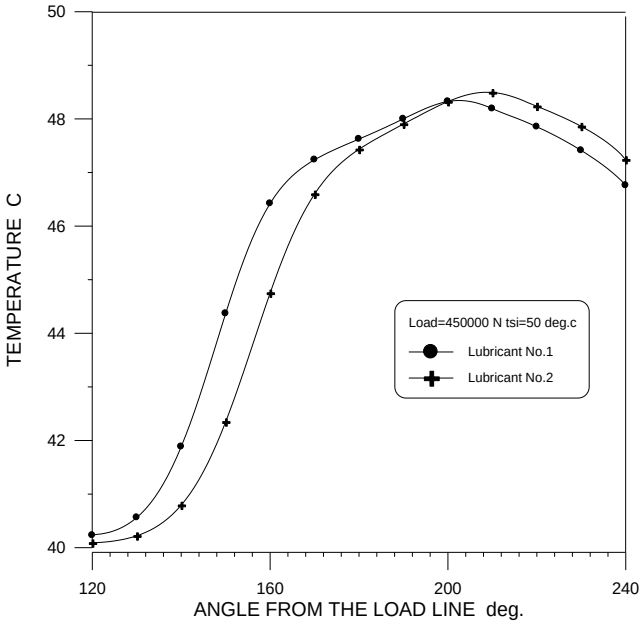

Fig.(9): Effect of lubricant viscosity on the temperature distribution of bearing bush (tsi=$50\,^{o}c$)

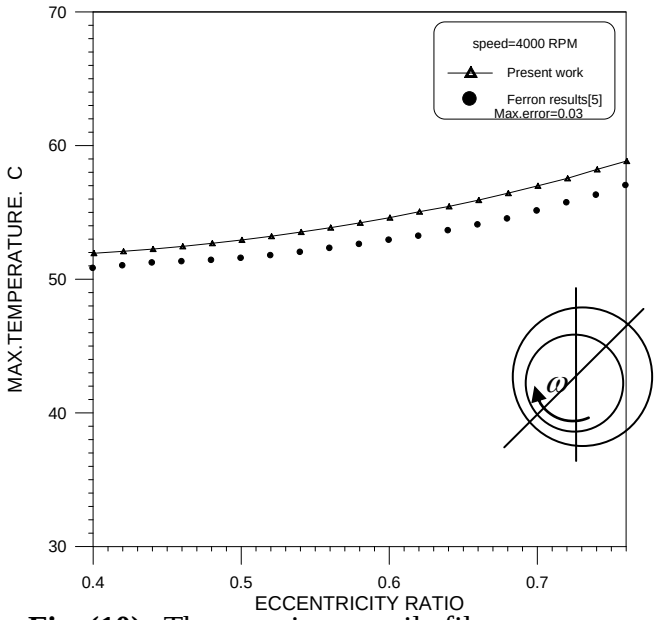

Fig..(10) The maximum oil film temperature versus eccentricity ratio

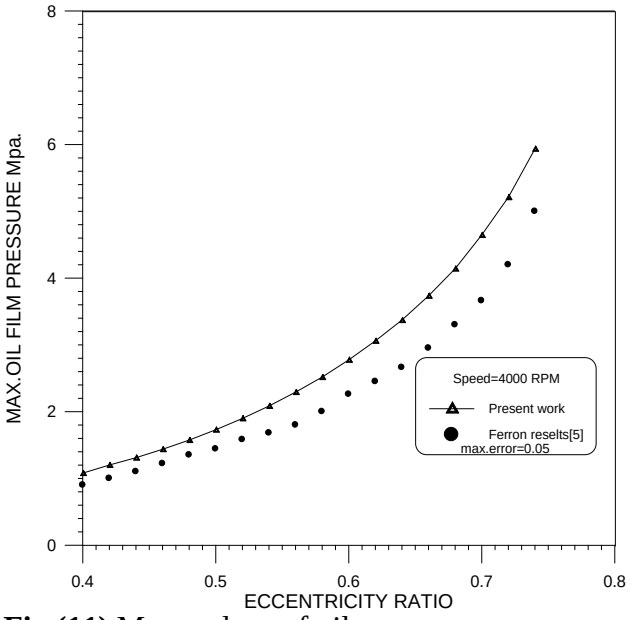

Fig.(11) Max. values of oil pressure versus eccentricity ratio

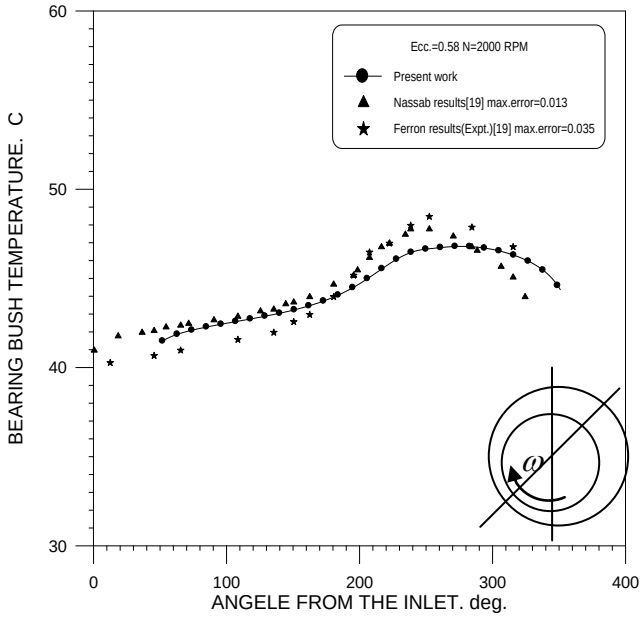

Fig.(12)Temperature distribution for Ferron[5] bearing bush

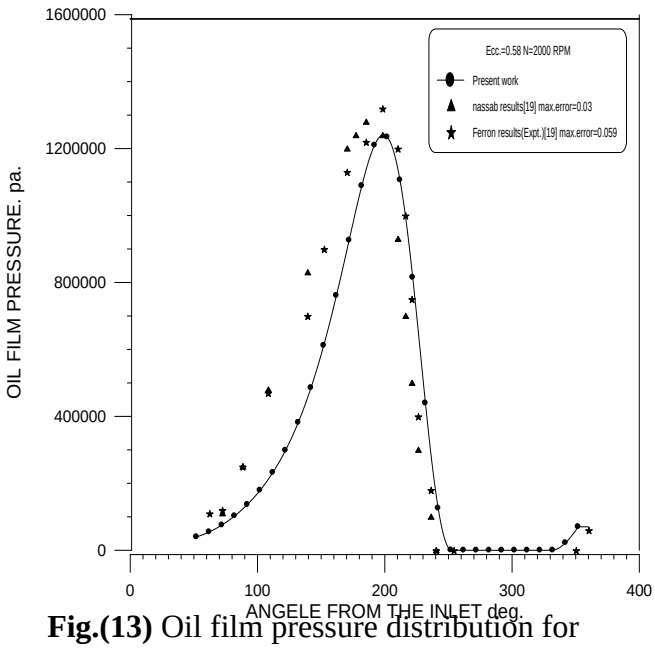

Fig.(13) Oil film pressure distribution for Ferron bearing

REFERENCES

- **E. W. Cowking,** "Themohydrodynamic Analysis of Multi-Arc Journal Bearing", TRIBOLOGY international, pp.217-223, August 1981.
- **H. Heshmat, and O. Pinkus,** "Mixing Inlet Temperatures in Hydrodynamic Bearings", Journal of Tribology, vol. 108, pp.231-248, April 1986.
- **J. Ferron, J. Frene, and R. Boncompain,** "A Study of the Thermohydrodynamic Performance of a Plain Journal Bearing Theory and Experiments", Transaction of the ASME, vol. 105, pp.422-428, July 1983.
- **J. Mitsui, Y. Hori, and M. Tanaka,** "Thermohydrodynamic Analysis of Cooling Effect of Supply Oil in Circular Journal Bearing", Transaction of the ASME, vol. 105, pp.414-421, July 1983.
- **J. Mitsui, Y. Hori, and M. Tanaka,** "An Experimental Investigation on the Temperature Distribution in Circular Journal Bearings", Journal of Tribology, vol.108, pp.621-626, October 1986.
- **J. Mitsui,** "A Study of Thermohydrodynamic Lubrication in A Circular Bearing", TRIBOLOGY international, vol. 20, pp.331-441, December 1987.
- **J. W. Lund, and P. k. Hansen,** "An Approximate Analysis of the Temperature Conditions in a Journal Bearing. Part 1: Theory", Transaction of the ASME, vol. 106, pp.228-106, April 1984.
- **J. Y. Jang, and M. M. Khonsari,** "Design of Bearing on the Basis of Thermohydrodynamic Analysis", Prose Instn. Mech. Eng. Vol. 218 part J: J Engineering Tribology, pp.355-363, 2004.
- **K. Hatakenaka, and M. Tanaka**, "Thermohydrodynamic Performance of Journal Bearings with Partial Reverse Flow and Finger-Type Cavitation", Prose Instn. Mech. Eng. Vol. 216 part J: J Engineering Tribology, pp.315-325, 2002.
- **Khonsari, M. M.Jang, J. Y., and Fillon,** "On the Generalization of Thermodynamic Analyses for Journal Bearings", Journal of tribology, vol. 118, pp.517-519, 1996
- **L. Costa, M. Fillon, A. S. Miranda, and J. C. P. Claro,** "An Experimental Investigation of the Effect of Groove Location and Supply Pressure on the THD Performance of a Steadily Loaded Journal Bearing", Journal of Tribology, vol. 122, pp.227-232, January 2000.
- **L. Roy** "Thermo-hydrodynamic performance of grooved oil journal bearing", Tribology International, vol. 42, pp. 1187-1198, 2009.
- **Ma. M. and Taylor. C. M. ,** "An Experimental Investigation of Thermal Effects in Circular and Elliptical Plan Journal Bearings", Tribology International, Vol.29, pp.19-26, 1996
- **M. M. Khonsari, and V. Esfahanian,** "Thermohydrodynamic Analysis Solid-Liquid Lubricated Journal Bearing", Journal of Tribology, vol. 110, pp.367-374, April 1988.
- **M. M. Khonsari, and H. J. Kim,** "On Thermally Induced Seizure in Journal Bearings", Journal of Tribology, vol. 111, pp.661-666, October 1989
- **M. T. Ma and C.M Taylor,** "An experimental investigation of thermal effects in circular and elliptical plain journal bearings", Tribology International,vol.29, No.1, pp.19-26, 1996.

- **M. Fillon and J. Bouyer,** " Thermohydrodynamic analysis of a worn plain journal bearing", Tribology International, vol.37, pp.129-136, 2004.
- **Oscar P., and Sargit S.,** "Adiabatic Solution for Finite Journal Bearing", Transaction of the ASME, vol. 101, pp.492-496, October 1979.
- **Pierre, and M. Fillon**, "Influence of Geometric Parameters and Operating Conditions on the Thermohydrodynamic Behavior of Plain Journal Bearing", Prose Instn. Mech. Eng. Vol. 214 part J: J Engineering Tribology, pp.445-457, 2000.
- **R. Boncompain, M. Fillon, and J.Frene,** "Analysis of Thermal Effects in Hydrodynamic Bearings", Journal of Tribology, vol. 108, pp.219-224, April 1986.
- **S. A. Nassab, and M. S. Moayeri,** "Three-Dimensional Thermohydrodynamic Analysis of Axially Grooved Journal Bearings", Prose Instn. Mech. Eng. Vol. 216 part J: J Engineering Tribology, pp.35-47, 2002.
- **Serieg, and S. Dandage,** "Empirical Design Procedure for the Thermohydrodynamic Behavior of Journal Bearings", Journal of Lubrication Technology, vol. 104, pp.135-148, April 1982.
- **T. Suganami, and A. Z. Szeri,** "A Parametric Study of Journal Bearing Performance: The 80 Partial Arc Bearing", Transaction of the ASME, vol. 101, pp.486-491, October 1979.
- **U. Singh, L. Roy, M. Sahu** "Steady state thermo-hydrodynamic analysis of cylindrical fluid film journal bearing with an axial groove", Tribology International, vol. 41, pp. 1135-1144, 2008.

NOMENCLATURE

SYMBOL	DESCRIPTION AND UNITS
c	Radial clearance m
C_o	Specific heat of lubricant J/kg.$^{\circ}C$
D	Diameter of journal m
e	Journal eccentricity m
h	Oil film thickness m
h_{conv}	Convective heat transfer coefficient W/m^2.^{o}C
h_{max}	Maximum oil film thickness m
h_{min}	Minimum oil film thickness m
$\bar{h}$	Dimensionless oil film thickness (h/c)
i,j,k	Finite difference mesh indices in circumferential, radial, and axial directions respectively
k_b	Thermal conductivity of the bush W/m^2.^{o}C
k_{oil}	Thermal conductivity of lubricant W/m^2.^{o}C
k_s	Thermal conductivity of the shaft W/m^2.^{o}C
k_o, k_1, k_2	Oil viscosity coefficient
N	Journal speed r.p.m
L	Bearing length m
P	Oil pressure N/m^2

p_{atm}	Atmospheric pressure N/m^2
p_s	Oil supply pressure N/m^2
$\bar{p}$	Dimensionless oil pressure = $(p/\eta_{in})(\frac{R}{U})(\frac{c}{R})^2$
$\bar{p}_s$	Dimensionless oil supply Pressure = $(p_s/\eta_{in})(\frac{R}{U})(\frac{c}{R})^2$
Q_{rec}	Recirculation oil flow rate m^3/s
Q_l	Axial leakage oil flow rate m^3/s
Q_{in}	Supply oil flow rate m^3/s
R	Journal radius m
r_b	Bush radius m
r_{bin}	Bush inner radius m
r_{bout}	Bush outer radius m
t	Oil temperature ^{o}C
ta	Ambient temperature ^{o}C
t_b	Bush temperature ^{o}C
t_{bo}	Bush outer surface temperature ^{o}C
t_{in}	Inlet oil temperature ^{o}C
t_r	Recirculating oil temperature ^{o}C
t_s	Shaft temperature ^{o}C
t_{si}	Inner temperature of the hallow shaft ^{o}C
$\bar{t}$	Dimensionless temperature = t / t_{in}
U	Shaft speed m/s
u	Fluid velocity component in x direction m/s
$\bar{u}$	Dimensionless velocity = u/U
v	Fluid velocity component in y direction m/s
$\bar{v}$	Dimensionless velocity = v/U(R/c)
w	Fluid velocity component in z direction m/s
$\bar{w}$	Dimensionless velocity = w/U
W	Bearing load capacity N
x,y,z	Cartesian coordinate system
r,θ	Cylindrical coordinate
$\bar{x},\bar{y},\bar{z}$	Dimensionless coordinate system

Greek symbols

Symbol	Description and Units	
ε	Eccentricity ratio	-
$\in \bar{p}, \in \bar{t}$	Errors ratios	-
μ	Lubrication viscosity	pa . s
μ_{in}	Inlet lubrication viscosity	pa . s
$\bar{\mu}$	Dimensionless viscosity = $\frac{\mu}{\mu_{in}}$	
ρ	Density of oil	kg/m^3
τ	Shear stress N/m^2	
ϕ	Bearing attitude angle rad	rad
ω	Journal rotational speed rad/s	rad/s

Superscript

$^-$	Dimensionless quantity

EXPERMENTAL INVESTIGATION OF TEMPERATURE FOR STIR FRICTION WELDING DISTRIBUTION

Prof. Dr. Qasim M. Doos. Suhair G. Hussein.
Mechanical Engineering
College of Engineering, Baghdad University.

ABSTRACT

Friction stir welding (FSW) is a solid state joining method for metal and is widely used for Al-Alloys. In the present work ,temperature distributions were investigated for Aluminum alloy (7008), the effect of the main welding parameters such as rotational speed (tool speed) and liner speed (welding speed) on the temperature distribution were investigated .The results show that the rotational speed has a strong effect on the temperature distribution and this effect increases with temperature increase, but the linear speed has an (inverse proportion) with the temperature increase. This effect was less than the rotational speed. Peak temperature was estimated theoretically by using (Bakingham π) theorem to derivate the relationship between the dimensionless heat input and dimensionless peak temperature. In this study a mechanical test (tensile test) for welded specimen was investigated to study the effect of temperature distribution on the mechanical properties of the alloy, results show that Aluminum alloy (7008) was weldable on the (FSW) process and obtain an maximum weld efficiency (81%) with parameters (880 rpm) rotational speed and (1 mm/sec) welding speed. By comparing test results with peak temperature to the Al-Alloy the obtained result was that the welding process is successful when welding temperature be (75-80%) of melting point of the used material.

الخلاصة

اللحام بالاحتكاك والدعج هي إحدى طرق اللحام الحديثة وتعتبر من طرق لحام الحالة الصلبة للمعادن حيث تستخدم بشكل واسع لسبائك الألمنيوم.في هذا البحث تمت دراسة عملية توزيع الحرارة لسبيكة ألمنيوم (7008) ودراسة تأثير متغيرات اللحام مثل (السرعة الدورانية) التي تمثل سرعة أداة اللحام والسرعة الخطية التي تمثل سرعة اللحام على توزيع درجات الحرارة للسبيكة باستخدام ماكنة التفريز الميكانيكي العمودية ومن هذه الدراسة أتضح انه للسرعة الدورانية تأثير كبير على درجات الحرارة ويكون

هذا التأثير ذو علاقة طردية مع ارتفاع درجات الحرارة. اما السرعة الخطية فلها علاقة عكسية مع ارتفاع درجات الحرارة وتاثيرها اقل مما هو عليه في السرعة الدورانية. وتم أيضاً استقراء درجات الحرارة القصوى للسبيكة لقيم مختلفة من السرعة الدورانية والسرعة الخطية عملياً.تمت دراسة نظرية من خلال اشتقاق العلاقة بين كمية الحرارة الداخلة ودرجة الحرارة القصوى للسبيكة ورسمها بيانياً للحصول على معادلة يتم الحصول منها على درجة الحرارة القصوى نظرياً . تم بعد ذلك إجراء فحص ميكانيكي (فحص الشد) للعينات لدراسة تاثير درجات الحرارة على الخواص الميكانيكية للسبيكة بعد لحامها بهذه الطريقة وبناءاً على النتائج التي تم الحصول عليها وجد ان السبيكة قابلة للحام بهذه الطريقة مع الحصول على كفاءة قصوى (81%) باستخدام متغيرات لحام (880 دورة / دقيقة سرعة دورانية مع 1 ملم/ثا سرعة لحام) ومن خلال مقارنة نتائج الفحص مع درجات الحرارة القصوى للسبيكة تم الحصول على نتيجة عملية اللحام نجحت عند وصول درجة حرارة اللحام بما يعادل (75-80%) من درجة انصهار السبيكة.

- **KEYWORD**: Friction stir welding, Temperature Distribution, Peak Temperature.

INTRODUCTION

Welding is a materials joining process in which two or more parts are coalesced at their contacting surfaces by suitable application of heat and/or pressure (Groover, 2002) . The welding processes are devided into three major groups: Fusion welding ,Solid state welding And Adhesive bonding: (Serope, 1997). Friction Stir Welding is a relatively new joining process, invented at the welding institute (Cambridge, UK) in 1991 and developed initially for aluminum alloys, it is a solid-state joining technique. The weld is made in the solid phase, that is no melting. Since its invention, the process has received world-wide attention and today companies in Scandinavia, Japan and the USA are using the technology in production, particularly for joining aluminum alloys. High quality weld can generally be fabricated with absence of solidification cracking, porosity, oxidization and other effects resulting from traditional fusion welding (Hemanth,2006). NASA is using this kind of welding on the space shuttle. This kind of welding can help the shuttle be strong, but light (NASA,2002). FSW has been successfully used to weld similar and dissimilar cast and wrought aluminum alloys, steels as well as titanium, copper and magnesium alloys, dissimilar metal group alloys and metal matrix as well as to weld hollow objects such as tanks and tube/pipe, and parts with 3-dimentional contours (Terry Khaled,2005). Friction Stir Welding method of joining is based on the fact that the metal is subjected to heavy plastic deformation at high temperatures, but lower than the melting point, so the basic concept of FSW is remarkably simple, a rotating tool with pin and shoulder is inserted in the material to be welded, and traversed along the line of interest as shown in Fig.1.

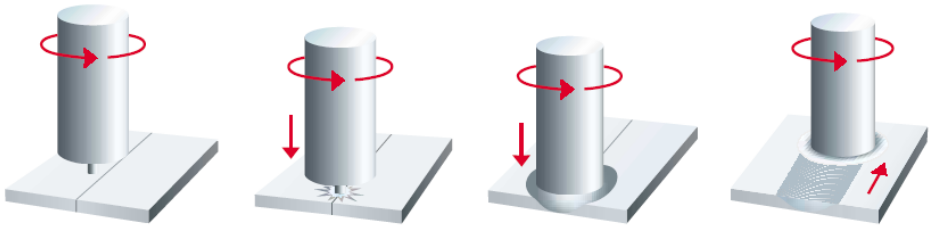

Fig.1: (1 Rotating Tool is Plunged into the Joint Line and Moved Along the Joint. Neither Flux nor Filler Material are Used. (SAPA group, 2003)

Frictional heat, generated mostly under the tool's shoulder, softens the material. During FSW the workpiece is placed on a backup plate and clamped rigidly by an anvil a long the far side to prevent lateral movement. The pin may have a diameter one third of the cylindrical tool and typically has a length slightly less than the thickness of the workpiece. The pin forced into the workpiece until the shoulder contacts the surface of the workpiece while the tool descends further; its shoulder surface touches the top surface of the workpiece and generates heat. The metal is softening and the tool moves along the line of weld. The pin of the rotating tool provides the "stir" action in the material of the workpiece. (Hemanth, 2006).

(Mohanad Okab, 2007) investigate mechanical and microstructural properties of friction stir welding joints for a typical high strength precipitation hardening Aluminum alloys (7020-T6). Effect of welding parameters on mechanical properties of welded joints were investigated using different mechanical tests Based on the stir welding experiment conducted in this study the results show that Aluminum alloy (7020-T6) can be welded using (FSW) process with maximum welding efficiency (87.52%) in terms of ultimate tensile strength using optimum welding parameters (900RPM tool rotational speed, 60 mm/min. welding speed and 0.25mm plunging depth of welding tool). (Hemanth, 2006) in his thesis, developed a three dimensional model to obtain the temperature distribution in the workpiece using ANSYS. A trend line equation which predicts the peak temperature attained during friction stir processing was also developed. The predicted peak temperature is used to obtain the temperature contours through out the workpiece. Friction stir processing was simulated for material Aluminum 5052. Using average values for material properties instead of temperature dependent values affects the final results to a small extent. Using a moving heat source technique is proved to be a reliable method to simulate friction stir processing. (Roy and his group, 2006) developed a dimensionless correlation based on Buckingham's π-theorem to estimate the peak temperature during friction stir welding (FSW)., it can also be used for the selection of welding conditions to prevent melting of the workpiece during FSW. The

correlation includes thermal properties of the material and the tool, the area of the tool shoulder and the rotational and translation speeds of the tool. The peak temperatures reported in the literature during FSW of various materials and welding conditions were found to be in fair agreement with the proposed correlation. (Chao, 2003) formulated the heat transfer of the FSW process into two boundary value problems (BVP)-a steady state BVP for the tool and a transient BVP for the workpiece. To quantify the physical values of the process the temperatures in the workpiece and the tool are measured during FSW. Using the measured transient temperatures. Fields finite element numerical analysis were performed to determine the heat flux generated from the friction to the workpiece and the tool. Detailed temperature distributions in the workpiece and the tool are presented. Discussions relative to the FSW process are then given. In particular, the results show that: The majority of the heat generated from the friction, i.e., about 95%, is transferred into the workpiece and only 5% flows into the tool and the fraction of the rate of plastic work dissipated as heat is about 80%.**(** Richardson, 2003)presented a new heat transfer model for predicting heat transfer in friction stir welding (FSW). In this model, Experimental results indicate that the temperature at the tool shoulder contact surface hardly changes with the weld speed and the tool rotational speed. It can be expected that local melting does occur in FSW. So, both the tool rotational speed and the weld speed do not significantly affect the maximum temperature in the weld. The weld speed affects the distribution of temperature in the workpiece. And a perhaeting time is important in FSW; it makes the weld easier. (Chao and Qi, 1999) in this work, a three-dimensional finite element analysis of the FSW process was used. The modeling effort includes a decoupled heat transfer and a subsequent thermomechanical analysis. The temperature fields during the welding, the residual stress distribution and distortion of the workpiece after the FSW process are studied. The results from the modeling are consistent with the available experimental data and trends. The model is then used to study the fabrication process of the FSW for the effect of plate thickness and welding speed.

THEORETICAL ANALYSIS

The peak temperature of the workpiece and the effective parameter on it was studied by using Buckingham (pi) theorem to develop a dimensionless correlation.

In physical systems, certain quantities, such as mass, length, and time or (force, length, and time), are considered to be fundamental quantities since they cannot be expressed in simpler terms. All other physical quantities may be expressed in terms of these fundamental quantities.

Velocity is a length divided by time, and density is mass per unit volume (length cubed). (Ranaldv, 1992)

Prediction of the dimensionless Correlation Formulla :-(Roy, 2006)

The variables that influence the peak temperature "Tp" are identified as:

- The heat input per unit length to the workpiece ($f\sigma_8 A$).
- The rotational velocity of the tool (w).
- The thermal property of the workpiece. (k/cp)
- The translation velocity of the tool. (V) and
- The initial or preheat temperature of the workpiece. (Tin)

In these variables, σ_8 represents the yield stress of the workpiece at a temperature of 0.8Ts where (Ts) is the solidus temperature, A is the cross sectional area of the tool shoulder defined as. $A = \pi\left(R_o{}^2 - R_i{}^2\right)$ (1)

Where R_o and R_i are the shoulder and Pin radius respectively.

The factor (f) represents the ratio in which heat generated at the tool shoulder / workpiece interface that is transported between the tool and workpiece.

Its value can be calculated based on steady-state one dimensional heat transfer from point heat source located at the interface of dissimilar materials.(Roy, 2006).

$$f = \left[\left(k\rho CP\right)_w\right]^{1/2} \Big/ \left[\left(k\rho CP\right)_T\right]^{1/2} \qquad (2)$$

Where the subscript W and T indicate the workpiece and tool respectively,

k is the thermal conductivity (W/m°C)

Cp is the specific heat , at constant pressure (kJ/kg°C) and ,σ(kg/m^3)

ρ is the density of the material. Thermal conductivity, k and specific heat, Cp are dependent on temperature. The temperature varied from room temperature to high values so the k and Cp changed to form the temperature variation. The values of k and Cp would brought from. (Hemanth, 2006)

The physical quantities are: f ($\sigma_8 A$, Tp, W, V, Tin, k/cp) = 0

The fundamental dimensions in (M, L, T and θ units are):-

$\sigma_8 A = ML/T^2$, Tp = θ , W = 1/T , V = L/T , k/cp = M/LT , Tin = θ

According to Bukingham π-theorem there will be (6) physical quantities and (4) fundamental units.

$\therefore$ 6-4 = 2 $\therefore$ We have two π-terms

$$\therefore \pi_1 = \frac{\theta}{\theta} = \frac{Tp}{Tin}$$

$$\therefore \pi_1 = T^* \qquad (3)$$

$$\therefore \pi_2 = Q^* \qquad (4)$$

The new relationship, written in terms of π_1 and π_2 is:-

$$f_1(\pi_1, \pi_2) = 0$$

$$f_1(T^*, Q^*) = 0 \quad , f_1\left(T^*, \frac{f\sigma_8 \text{A.w cp}}{\text{V}^2\text{k}}\right) = 0$$

$$T^* = f_2\left(\frac{f\sigma_8 \text{A.w cp}}{\text{V}^2\text{k}}\right)$$

$$\therefore T^* = f_2 Q^* \qquad (5)$$

From equation (5) it can be obtained an relationship connect the peak temperature and heat input. From the experimental results we can arrive to the final correlation so (equation 5) leads to final empirical equation that can be seen in result.

EXPERIMENTAL WORK

Due to the lack of specialized stir welding machine, a vertical milling machine was used with variable turning and linear feed. Because the milling machine is not prepared directly to the (FSW), it should be equipped with fixture system. The fixture used was a steel plate with the dimension (350mm x 250mm x 15mm) prepared to be suitable with the table of the Milling Machine. The purpose of this plate was used to fix the plates to be welded on it by using two special steel strips, fig.2 shows the machine with fixture, tool, and plates. The plates were also prevent from sliding during welding by clamping along the long edges of the plates. A low alloy steel welding tool was manufactured to perform the welding of the aluminum plates.

Tool consists of two parts: (part no. 1) adopted to the machine spindle. (part no. 2) consists of two geometries, one of them called the shoulder and the other called the probe. The plates used in this study was AL-alloy (7008H) prepared with the dimensions (200mm x 80mm x 4mm). Each two plates were joining together with the friction stir welding. k-type thermocouples have been used for measuring the temperature distribution.

To read various temperatures with time and save them automatically, a device was manufactured by Integrated Engineering Services (IES) to be compatible with working conditions. This device was used to record the temperatures at the points prepared on aluminum plates. The reader was capable to link with a computer for saving the data that obtained. This device and

thermocouples were calibrated in (C.O.S.A.C). Five points were pointed out on one face of the plates to be welded as shown in Fig. 3.

Fig. 2:All items used during FSW.

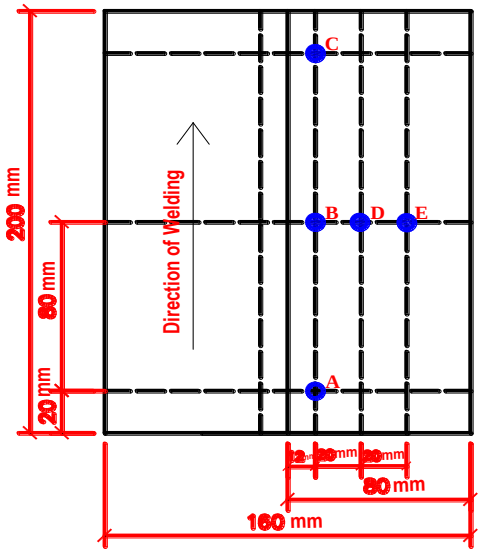

Fig. 3:Locations of tested points

Three points (A, B, and C) were shown along the line of welding (12 mm) far away from this line, which was chosen because of shoulder dimensions. Points (A and C) were (20 mm) from the edge of the plate, while point B was in the center of the plate. Points (E and D) were chosen at right angel to the welding line at point B, with (20 mm) between each of them.Special epoxy mixed with some powder from the same Al-alloy was used to improve heat transfer between the plate and thermocouple**.** Type k thermocouple was fixed on each hole at the points A, B, C, D, and E by using some epoxy.In order to investigate mechanical properties of the welded joints and to evaluate the effect of different welding parameters on these properties, tensile test have been conducted.

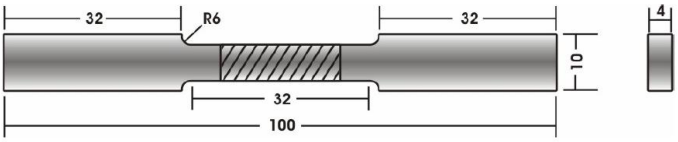

Fig.4: ASTM sub-size sample for tensile test (ASTM, 2003)

The tests had been fulfilled in the laboratories of Specialized Institute for Engineering Industries (SIEI).Fig. 4 shows the sub size sample for tensile test.

RESULTS AND DISCUSSION

Figures from 5 to 10 represent the results of experimental work. In general, the figures represent the relationship between the temperature and time, from Fig.5 it is concluded that the revolution speed and linear velocity had a strong effect on the temperature distribution along the welded plates.

Also, it was noticed that in each curve the peak temperature in(A, B, and C) was affected by the location of welding tool which turning in its limited speed.

The temperature at point (A) began between (30-60)°C then increased highly when the welding tool being at the points of testing, after that the temperatures began to decrease gradually while the welding tool leave the testing point.

From the increase and decrease of temperature at the testing points

This is coincide with point (B) where it's temperature increased as the temperature of point (A) decreased because welding tool passing through point (B) while it leaves point (A).

The highest temperature at point (B) was recorded as the welding tool reaches the point, while it began to reduce when the welding tool leave it. The process of increasing and decreasing the temperature is also true for point (C). The heat building process at point (B) and (C) was very effective factor on the welding process which give more homogenous, smooth and clean welding.

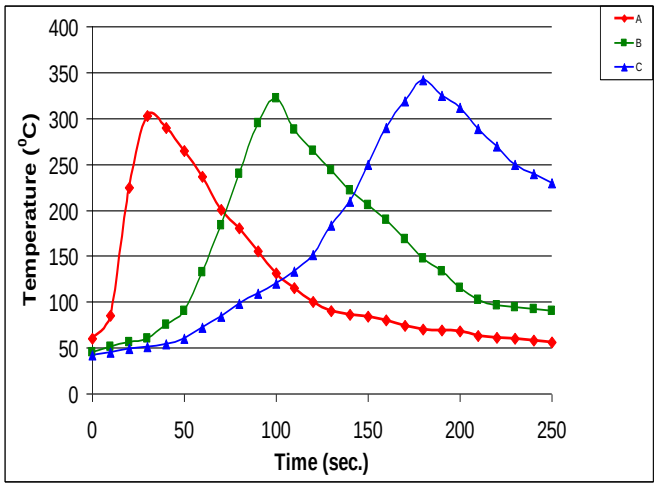

Fig.5:Temperature distribution at points (A, B and C).1430 RPM, 1mm/sec.

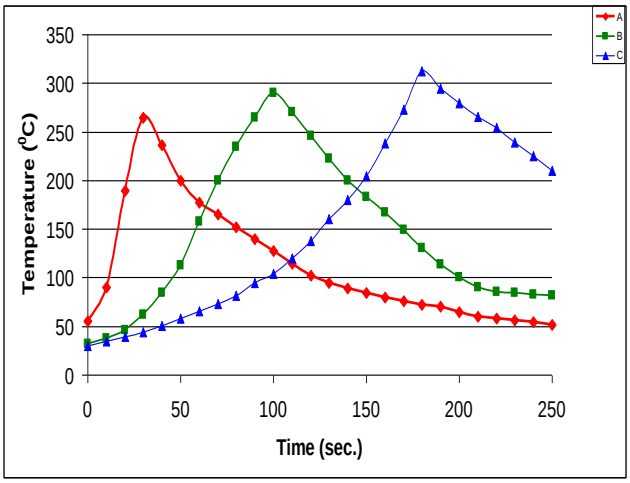

Fig.6: Temperature distribution at points (A, B and C). 1140 RPM, 1mm/sec.

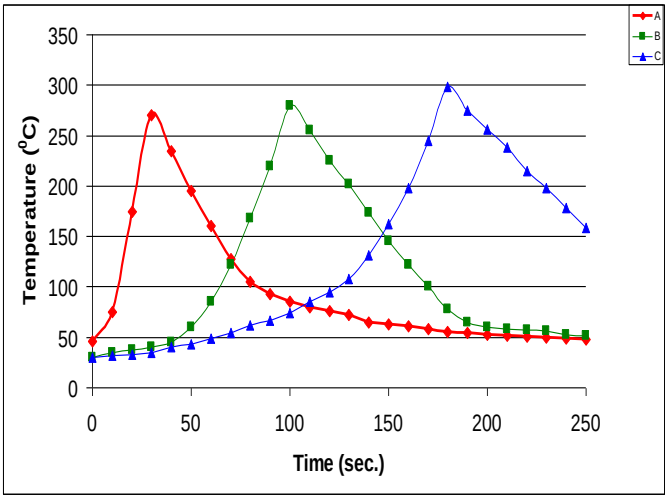

Fig. 7: Temperature distribution at point (A, B and C). 880 RPM, 1mm/sec.

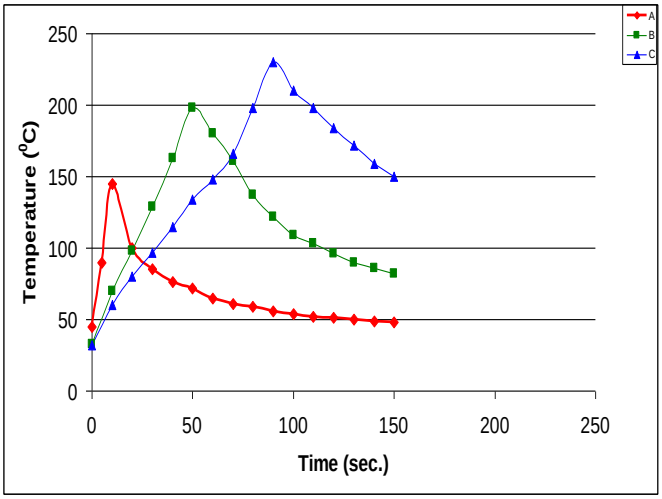

Fig.8: Temperature distribution at point (A, B and C). 1140 RPM, 2mm/sec.

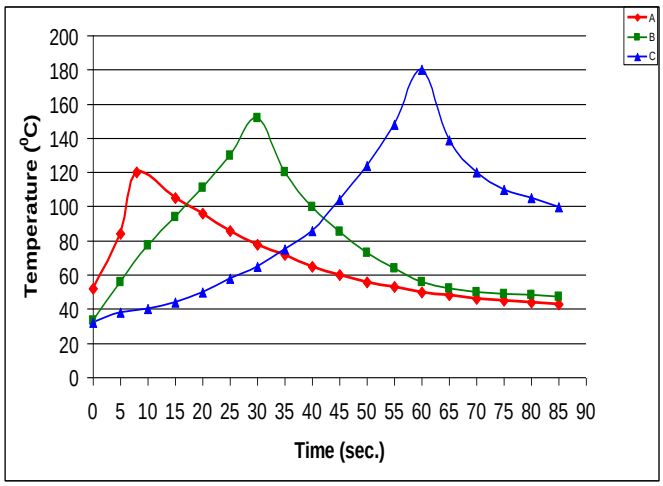

Fig.9: Temperature distribution at point (A, B and C). 1140 RPM, 3mm/sec.

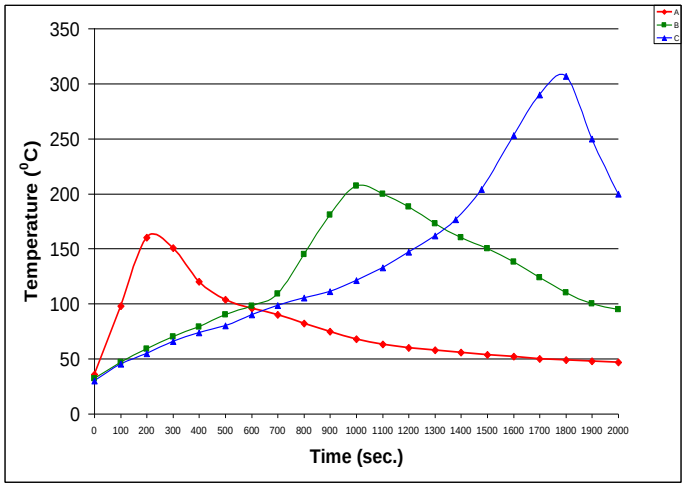

Fig .10: Temperature distribution at point (A, B and C). 700 RPM, 0.1mm/sec.

According to figs. 5,6&7 it was noticed that the increasing of the revolution speed with constant linear velocity, the temperature of testing points increased. This is because of (At high rotational speed, the relative velocity between the tool and workpiece is high and consequently, the heat generation rate and the temperature are also high).

Fig. 11 represent the curves of temperature distribution at point (B) with various revolution speed and constant linear speed.

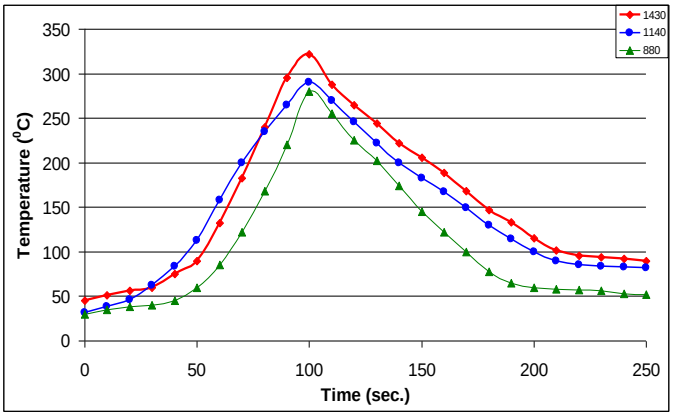

Fig.11: Temperature distribution at point (B) with three variable revolution speeds and constant linear speed (1mm/sec.).

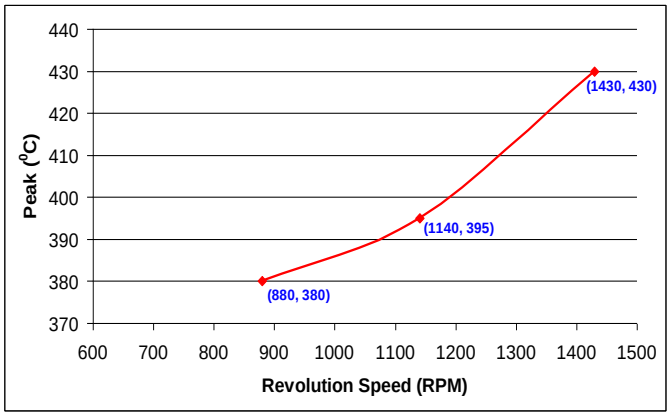

Fig. 12: The effective of rotational speed on the peak temperature.

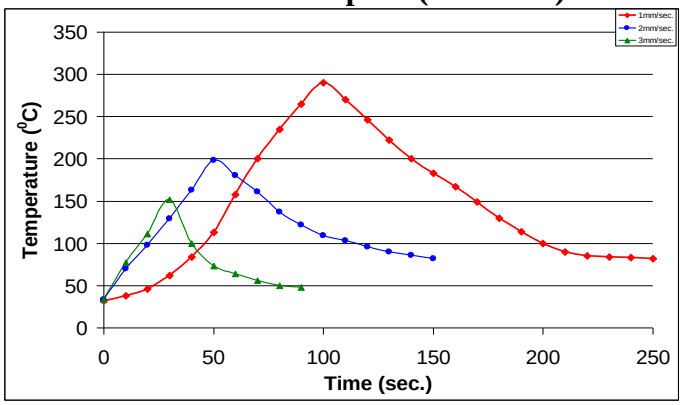

Fig. 13: Temperature distribution at point (B) with variable welding speed and constant revolution speed (1140 rpm).

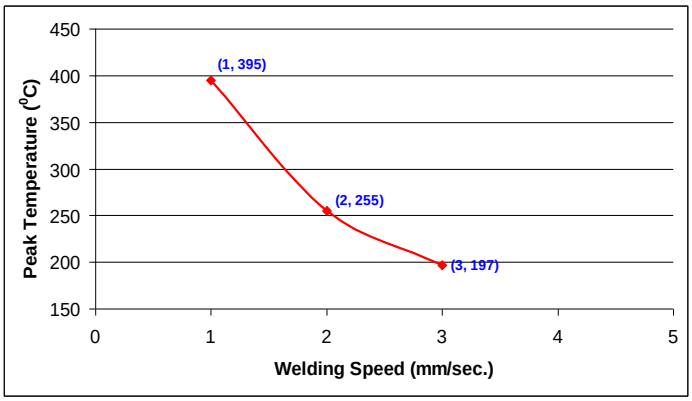

Fig. 14: the effective of linear speed on the peak temperature of welded plate.

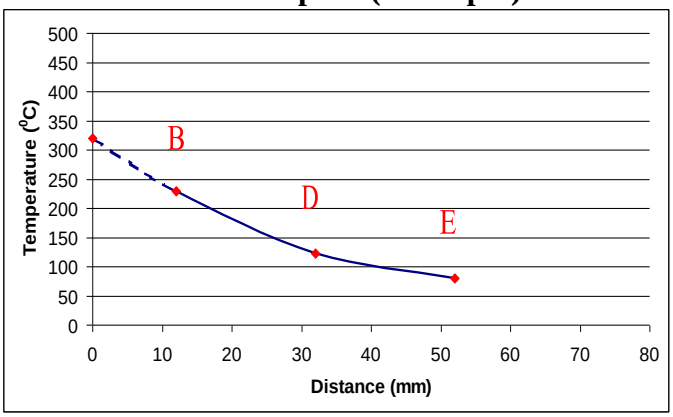

Fig. 15: the Distance from the welding line (700RPM , 0.1 mm/sec.).

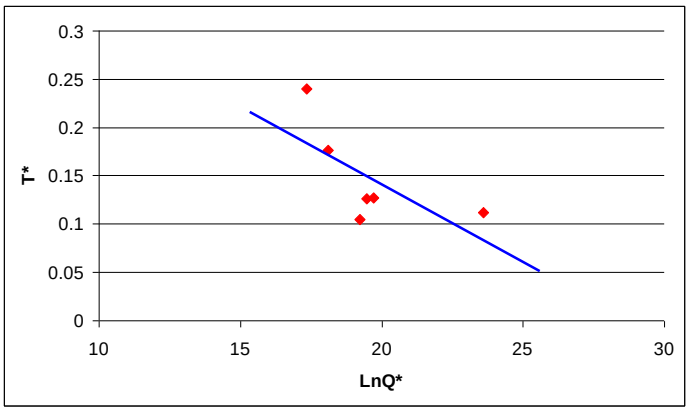

Fig. 16: the relationship between dimensionless peak temperature and dimensionless heat input.

The effect of rotational speed on the peak temperature tested point can be shown in Fig. 12. From figs.7,8&9 it was noticed that the linear speed has a reverse effect on the increasing of temperature, so that with increasing linear speed the temperature become lower and this is because of the fact that at high welding velocity (linear velocity), the heat input per unit length decreased and heat is

dissipated over a large volume of the workpiece. So the points that tested had no enough time to increase the temperature.

Fig.13 represents the variation of temperature at point (B) with variable welding velocity. Fig.14 shows the effect of linear speed on the peak temperature of welded plate.

ESTIMATION OF PEAK TEMPERATURE PRACTICALLY.

The highest temperatures recorded at points E, D, and B which lies on a straight line, were drawn against the distance from interface line of welding. This is shown in fig.15. A nonlinear relationship was noticed in the figure because the governor heat balance was conduction and convection. Extrapolating the line joining the points of testing to get the peak temperature at the interface line of welding. The extrapolating procedure was used because it was not easy to measure the peak temperature of the interface line of welding directly with the instruments available. The peak temperatures are listed below.

Table (1): Peak Temperature (experimentally).

Plate No.	Revolutions Speed (rpm)	Linear Velocity (mm/sec)	Peak Temperature (Exp) (°C)
1	1430	1	430
2	1140	1	395
3	880	1	380
4	1140	1	395
5	1140	2	255
6	1140	3	197
7	700	0.1	320

Results of peak temperature (Tp) calculation during (FSW) :-

According to dimensionless correlations used to calculate the peak temperature of **eq.(5)** with the developed correlation. From the present study we have various parameters, linear velocity and rotational speed, affected on heat input and peak temperature. So, depending on these parameters Fig.16 has been obtained. As can be seen from Fig.16 the data can be fitted by using correlation theory and **eq.(6)** result from the correlation.

$$T^* = 0.468 - 0.0163\ln(Q^*) \qquad (6)$$

By using the equation above the peak temperature has been calculated and listed in table (2).

Table (2):- Peak Temperature theoretically.

Plate No.	Revolutions Speed (rpm)	Linear Velocity (mm/sec)	Peak Temperature (Exp) (°C)
1	1430	1	375
2	1140	1	333
3	880	1	292
4	1140	2	260
5	1140	3	243
6	700	0.1	385

Tensile Test Results:-

To investigate the effect of different welding parameters on tensile strength of welded joint, tensile tests were conducted for each joint using three specimens for each of the welded joints and the results are averaged. The test results compared with the tensile properties of base metal and the welding efficiency for friction stir welding have been calculated for each experiment.

Table (3): Tensile Strength in FSW .

	FSW No.	Revolution Speed (RPM)	Welding Speed (mm/sec)	Tensile Strength (N/mm2)	Joint Efficiency %
1st Set	1	880	1	215.5	81
	2	1140	1	191	72
	3	1430	1	66	26
2nd Set	1	1140	1	191	72
	2	1140	2	119	45
	3	1140	3	fail	fail
3rd Set	1	700	0.1	131	49.6
Base metal	-	-	-	264	-

Note:

- Values of tensile strength are average of (3) specimens.
- Joint Efficiency = test of tensile strength / ultimate tensile strength (Base metal).

According to the results obtained it can be noticed that the mechanical properties affected by temperature distribution for welded plates as is explained below:-

The 1st set of readings in table (3), are the results of tensile test which decreasing with the increasing of revolution speed while the temperature increased with revolution speed increased (see

fig. 12) this means that it's important to select a specified value for revolution speed to get a good joint efficiency.

In the 2nd set of readings in table (3), the result of tensile tests decreasing with increase of welding speed, beak temperature decreased too, (see figure (14)), from studying the behavior of the welding surface it was clear that the welding is non homogenous one, with rough surface and with some cracks in welding zone.

In the third part of table (3), due to longer time of welding when compare it with the above sets, the time affect the configuration of welding, the first zone of the welded plate shows poor welding efficiency joint when compare it with the last zone which shows homogenous and high efficiency joint. This was due to the long time which rise the temperature of plate in the last part of the process, and means that the preheating process in the last part of plate gives the homogenous, smooth, and strong section. This phenomena is agreed with(Richardson, 2003).

From the above discussion it is clear that we must select the optimum values of revolution speed and welding speed to get a good joint because it is not necessary to select high revolution speed or low welding speed to get a good joint as shown in the results of tensile tests.

From these results of mechanical test which shows that the revolution speed (880 RPM) with welding speed (1 mm/s) are the best values of experiment in (FSW) that get (81%) welding joint efficiency. This welding joint efficiency could be considered as a good result compared with fusion welding to the Al-Alloy so the (FSW) for Al-Alloy can be considered a more suitable process.

CONCLUSIONS

According to the results of the present study of FSW process on selected Al-Alloy several conclusions can be written as follows:

- Optimum mechanical properties obtained with peak temperature reach to (75%) of melting point of plate metal.
- The maximum weld strength obtained in this study was (215.5N/mm^2) of 81% weld efficiency.
- We must select optimum welding parameters to obtain good weld and there is no necessary to use high values of revolution speed or linear speed. In the present study the optimum values was 880 RPM with 1mm/sec welding speed.
- A correlation for peak temperature has been obtained. $T^* = 0.468 - 0.0163\ln(Q^*)$

REFERENCES

- [ASTM]" Standard methods of tension testing. Wrought And Cast Aluminum-And Magnesium_Alloy products", 2003.
- G.G.Roy, R. Nandon and T. Debroy" Dimension less correlation for peak temperature in FSW". Science and Technology of Welding and Joining. Vol. 11, No.5, pp.606-608, 2006.
- K. Hemanth Vepakomma, "Three dimensional thermal modeling of Friction stir processing". The Florida State University. Spring semesfer, 2006.
- Mikell P. Groover "Fundamentals of Modern Manufacturing " Johnwilely and Sons InG, Second Edition, 2002.
- Mohanad Okab Yousuf "Invistigation of Mechanical and Microstructural Characteristics of Friction Stir Welded Joints", 2007.
- NASA explores " Creating Astir". October, 2002.
- . R.Nandan, G.G.Roy, and T.Debroy" Numerical Simulation of three-Dimensional heat transfer and plastic flow During Friction Stir welding " Volume 37A. pp. 1247-1259, April, 2006.
- Ranaldv. Giles.(Schaum's outline Series) "Fluid Mechanic and Hudraulics 2/ed". 1992.
- Richardson." A new heat transfer model for friction stir welding ", Transactions of NAMRI / SME. pp. 565-572, volume xxx, 2003.
- Sapa Profiler AB " Friction Stir Welding". SE574 81 veltanda. Sweden, 2003.
- Serope Kalpakjian "Manufacturing processes for Engineering materials". Addition-wesley Publishing Company. Third Edition, 1997.
- Terry Khaled, ph.D."AN out sider Looks At Friction Stir welding ". Technical Advisor, Metallurgy, July, 2005.
- Victor L. Streeter "Fluid Mechanic", printed and bond by Book-martpress, Inc., Eight Edition, 1985

- Yuh J. Chao and Xinhai Qi " Heat transfer and thermo-mechanical Analysis of friction Stir Joining of A A 6061-T6 plates". University of South Carolina, Columbia, SC 29208, pp. 1-10, 1999.

NUMERICAL AND EXPERIMENTAL INVESTIGATION ON THE EFFECT OF RESTRICTION SHAPE ON CHARACTERISTICS OF AIRFLOW IN A SQUARE DUCT

Dr. Khalid A. H. Ismael Dr. Ikhlase M. Fayed Lec. Dr Hanaa Abdul Hadi

الخلاصة:

تم عرض دراسة عملية و نظرية لجريان هوائي ثلاثي الابعاد، كامل التطور ، مضطرب خلال مجرى رباعي المقطع يحتوي على عوائق بأشكال و مواقع مختلفة و لمدى رينولدز يتراوح من $8.2x10^4$ الى $5.6x10^4$.الجانب النظري للمسألة يتضمن حل المعادلات التفاضلية الجزئية الاهليليجية المتمثلة بحفظ الكتلة، الزخم ، الطاقة المضطربة و معدل ضياعها بأستخدام الحجوم المحدد (Finite Volume) . لقد حُلت هذه المعادلات سوية مع الصيغة الجبرية للزوجة المضطربة (Turbulent viscousity)بأستخدام نموذج (k-ε) ، بالاضافة الى أستخدام مفهوم دالة الجدار بالقرب من الجدران لمعالجة تأثرات الاضطراب. في التجارب العملية تم بناء مجرى من مادة (Perspex) علاوة على استخدام مسبار الضغط الخماسي الفتحات لقياس مركبات السرعة الثلاثة في الحيز (مقداراً و اتجاهاً). النتائج بينت ان خسارة الضغط الكلي تعتمد على شكل و موقع العائق، و ان معامل خسارة الضغط الذي يعتمد على شكل و موقع العائق (k_R) يعتمد على عاملين هما نسبة الانسداد في المساحة (A_b) ، و النسبة بين المحيط المبلل بالهواء الى المحيط الحر المتبقي (p_e/P_e)، وان هذا المعامل لا يعتمد على عدد رينولدز(لنفس نسبة مساحة الانسداد اذا ازداد p_e/P_e بنسبة 40% فان نسبة الزيادة في المعامل k_R تكون 7% ، و لنفس p_e/P_e اذا زادت نسبة مساحة الانسداد الى 50% فان نسبة الزيادة في المعامل(k_R) تكون 10%) . و لكن معامل خسارة الضغط نتيجة الاحتكاك (C_f) فأنه دالة لعدد رينولدز.

ABSTRACT :

Experimental and numerical investigation has been under taken to study turbulent flow of air through duct using restriction in different shapes and positions for Reynolds numbers ranges of ($8.2x10^4 \rightarrow 5.6x10^4$).The numerical approach used in this work is the finite volume method for solution of elliptic partial differential equation for the modeling of turbulent (k-ε) model as well as wall function concept near the wall which was used to take the turbulent effects into consideration have been employed.The experimental test rigs were constructed from Perspex, and a five-hole pressure probe was used to measure the three component of air flow velocity vector in space.The results show that the total pressure drop depends on the shape and position of the restriction, and the pressure drop coefficient due to the restriction shape and position (k_R) depends on two parameters; blockage area ratio (A_b) and the ratio between wetted perimeter to the free remainder perimeter (p_e/P_e) and dose not depend on the Reynolds number (for the same blockage area ratio A_b if the p_e/P_e increases 40%, the coefficient k_R increases 7% , and for the same p_e/P_e, if the blockage area ratio increases 50% ,the coefficient k_R increases 10%). But the pressure drop coefficient due to the friction (C_f) is a function of Reynolds.

INTRODUCTION :

Configuration involving arrangements of sequential baffles (ribs, thin obstacles, etc.) attached to a wall are commonly used for supporting and mixing purposes in heat exchangers, nuclear reactor cores , air-cooled turbine blades, wastewater aeration tanks as wall as chemical mixers and other chemical engineering application .

Geometric parameters such as channel aspect ratio, rib to height to passage hydraulic diameter or blockage ratio, rib angle of attack, the manner in which the ribs are positioned relative to one another (in-line, staggered, crisscross, etc.), rib pitch-to-height ratio and rib shape (round versus shape corners, fillet and rib aspect ratio have pronounced effect on flow and heat transfer some of there effects have been studied in experimental and numerical research. Examples of [Han et al. (1978)], [Han (1984)],[lee (1986)],[Taslim and spring (1998)], [son et al. (2002)]. Most of the reported computational efforts [Ooi at al. 2002 & Ooi et.al (2003)] investigated the turbulent flow and heat transfer in duct with ribs using eddy viscosity type turbulence model. However, it is well known that such models are unsuitable for situation that is flow separation in the flow field. [Rasie and Bohasani (2003)] have employed low Re-k-ε turbulence model to investigation flow and heat transfer in passage with attached ribs. In this paper turbulent flow induct with restriction is numerically and experimentally investigated. The main objective of this research is to study the effect of restriction shape and position on the fluid flow characteristics in square duct for fully developed turbulent flow with different Reynolds number.

EXPERIMENTAL FACILITIES:

A centrifugal fan driven by a 550 W, 2200 r.p.m is used to supply the flow of air. The air passes through a duct (150x80 mm cross section and 600 mm length) equipped orifice meter(designed on B.S 1042) to measure flow rates and settling chamber (air box) with honeycomb at the outlet of air box.

The air box rated the air through transparency Perspex square duct (120x120 mm) with sufficient length of (1000mm) for pressure recovery represent the first part of the test section

The second part of test section is also square duct of the same dimensions (120x120x1000 mm) and material (Perspex) of the first part. At the end of the test section, the air was exhausted into the atmosphere. The connection between first and second duct were made in such manner to allow the restriction to be changed. Thirteen restriction of different shape are made from a thin galvanized sheet (1mm) as shown in Fig. (1), five-hole probe is used to measure velocity vector in the flow field down stream of restriction. To determine the magnitude and orientation of the flow vector, the surface pressure is sampled at five locations: on the axis of probe and at four equispaced points on a line encircling this central point. The pressure differentials between selected pairs of these points related to the in flow velocity vector by doing an appropriate calibration to deduce pitch and yaw directions [Hanaa (2006)]

The second duct has (48) static pressure taps on its surface (four section in z-direction of (20, 40, 80,120mm) from the test section with 12^{th} static taps on each section with (3) taps on each surface) as shown in Fig. (2a) all static holes have a diameter of 1 mm. The section duct has four slots in the side surface which are used in the measurement by five hole probe in the four sections (20, 40, 80,120mm), Fig.(2b)

To calculate the average velocity of free stream, the inclined micro manometer is used to measure the different between the total pressure which has been measured

by pitot-tube and static pressure in front of restriction. Correction of the reading of the pitot-tube has been done according to [British standard 1042 (1973)].

The average inlet velocity for all experiments, at entrance region is (7-10 m/s) corresponding to the Reynolds number based on the hydraulic diameter (120mm) of inlet region ($5.6x10^4$-$8.2x10^4$). The static pressure distributions after restriction in each section (20, 40, 80,120mm) are measured from 12^{th} taps, so that the average pressure (P_{av}) in each can be calculated from:

$$P_{avs} = \frac{P_{s1} + P_{s2} + P_{s3} + ... + P_{s12}}{12} \quad (1)$$

to calculate the static pressure coefficient due to the friction(C_f) from:

$$C_f = \frac{P_s - P_{avs}}{1/2 \quad \rho U_{av}^2}$$

where P_s static pressure before restriction.

NUMERICAL WORK:

To analyze the flow field after restriction, governing partial differential equations (conservation of mass and momentum) in three dimensions have been used. To demonstrate the effect of the turbulence on the flow, turbulence model (k-ε) is used.

It is impossible to obtain analytical solution of the partial differential equations, so numerical solution using finite volume will be done for three selection restrictions with different blockage area as shown in Fig.(3), at two Reynolds numbers ($8.2x10^4$and$5.6x10^4$).Assumption about the fluid are Newtonian, Incompressible three dimensional, turbulent flow.

(i) Continuity equation:

$$\frac{\partial U}{\partial x} + \frac{\partial V}{\partial y} + \frac{\partial W}{\partial z} = 0 \quad (2)$$

(ii) Momentum Equations:

$$\frac{\partial U^2}{\partial x} + \frac{\partial UV}{\partial y} + \frac{\partial UW}{\partial z} = -\frac{1}{\rho}\frac{\partial P}{\partial x} + \frac{\partial}{\partial x}\left(\nu_e \frac{\partial U}{\partial x}\right) + \frac{\partial}{\partial y}\left(\nu_e \frac{\partial U}{\partial y}\right) + \frac{\partial}{\partial z}\left(\nu_e \frac{\partial U}{\partial z}\right) + \frac{\partial}{\partial x}\left(\nu_e \frac{\partial U}{\partial x}\right) + \frac{\partial}{\partial y}\left(\nu_e \frac{\partial V}{\partial x}\right) + \frac{\partial}{\partial z}\left(\nu_e \frac{\partial W}{\partial x}\right) \quad (3)$$

$$\frac{\partial UV}{\partial x} + \frac{\partial V^2}{\partial y} + \frac{\partial UW}{\partial z} = -\frac{1}{\rho}\frac{\partial P}{\partial y} + \frac{\partial}{\partial x}\left(\nu_e \frac{\partial V}{\partial x}\right) + \frac{\partial}{\partial y}\left(\nu_e \frac{\partial V}{\partial y}\right) + \frac{\partial}{\partial z}\left(\nu_e \frac{\partial V}{\partial z}\right) + \frac{\partial}{\partial x}\left(\nu_e \frac{\partial U}{\partial y}\right) + \frac{\partial}{\partial y}\left(\nu_e \frac{\partial V}{\partial y}\right) + \frac{\partial}{\partial z}\left(\nu_e \frac{\partial W}{\partial y}\right) \quad (4)$$

$$\frac{\partial UW}{\partial x} + \frac{\partial VW}{\partial y} + \frac{\partial W^2}{\partial z} = -\frac{1}{\rho}\frac{\partial P}{\partial z} + \frac{\partial}{\partial x}\left(\nu_e \frac{\partial W}{\partial x}\right) + \frac{\partial}{\partial y}\left(\nu_e \frac{\partial W}{\partial y}\right) + \frac{\partial}{\partial z}\left(\nu_e \frac{\partial W}{\partial z}\right) + \frac{\partial}{\partial x}\left(\nu_e \frac{\partial U}{\partial z}\right) + \frac{\partial}{\partial y}\left(\nu_e \frac{\partial V}{\partial z}\right) + \frac{\partial}{\partial z}\left(\nu_e \frac{\partial W}{\partial z}\right) \quad (5)$$

Standard k-ε Model [Launder and Spalding]

$$\frac{\partial}{\partial x}(kU) + \frac{\partial}{\partial y}(kV) + \frac{\partial}{\partial z}(kW) = \frac{\partial}{\partial x}\left(\frac{\nu_t}{\sigma_k}\frac{\partial k}{\partial x}\right) + \frac{\partial}{\partial y}\left(\frac{\nu_t}{\sigma_k}\frac{\partial k}{\partial y}\right) + \frac{\partial}{\partial z}\left(\frac{\nu_t}{\sigma_k}\frac{\partial k}{\partial z}\right) + G - \varepsilon \quad (6)$$

$$\frac{\partial}{\partial x}(\varepsilon U) + \frac{\partial}{\partial y}(\varepsilon V) + \frac{\partial}{\partial z}(\varepsilon W) = \frac{\partial}{\partial x}\left(\frac{\nu_t}{\sigma_\varepsilon}\frac{\partial \varepsilon}{\partial x}\right) + \frac{\partial}{\partial y}\left(\frac{\nu_t}{\sigma_\varepsilon}\frac{\partial \varepsilon}{\partial y}\right) + \frac{\partial}{\partial z}\left(\frac{\nu_t}{\sigma_\varepsilon}\frac{\partial \varepsilon}{\partial z}\right) + C_{1\varepsilon}\frac{\varepsilon}{k}G - C_{2\varepsilon}\frac{\varepsilon^2}{k} \quad (7)$$

$$G = \nu_i \left[2\left(\frac{\partial U}{\partial x}\right)^2 + 2\left(\frac{\partial V}{\partial y}\right)^2 + 2\left(\frac{\partial W}{\partial z}\right)^2 + \left(\frac{\partial V}{\partial y}\frac{\partial U}{\partial x}\right) + \left(\frac{\partial V}{\partial z}\frac{\partial W}{\partial x}\right) + \left(\frac{\partial V}{\partial z}\frac{\partial W}{\partial y}\right) \right] \quad (8)$$

where $\nu_t = C\mu \frac{k^2}{\varepsilon}$

ε, is the dissipation term.

The empirical constants appearing in the above equations that are achieved at by comprehensive fitting data for a wide range of turbulent flows are expressed as follows:

Table (1) Empirical constants in the k-ε

C_μ	$C_{1\varepsilon}$	$C_{2\varepsilon}$	σ_k	σ_ε
0.09	*1.44*	*1.92*	*1.00*	*1.30*

BOUNDARY CONDITION:

Boundary Condition at Inlet Duct:

$U(x,y,0)= U_{in}$; $V(x,y,0)= W(x,y,0)=0$

The distribution of the inlet velocity(U_{in})can be interpolated from experimental data(7,10)m/s.

The kinetic and dissipation energy at inlet may be estimated from the following equation [Davidson and Farhanich (1995)] :

$k\,(x,y,0) = k_{in} = C_k\, U_{in}^2$; $\varepsilon\,(x,y,0) = \varepsilon_{in} = C\mu\, k_{in}^{3/2}/\,(0.5 D_h C_\varepsilon)$

where (C_k, C_ε) are constant (C_k=0.003 and C_ε=0.03), while (D_h) represents hydraulic diameter of duct and its value is equal to the section length of the square duct.

Boundary Condition at the Wall:

For no slip ($U=V=W=0$) is the appropriate condition for the velocity component at solid walls [Verstage and Malasekera (1995)]. Due to the viscous influence near wall, the local Reynolds number becomes very small, thus the turbulent modal which is designed for high Reynolds number become inadequate. In this case, the calculation of shear stress near the wall needs a special treatment. In order to adequately avoid these problems, it would be necessary to employ a fine grid near the wall, which would be expensive. An alternative and widely employed approach is to use formula which known as "wall function".

THE GENERAL FORM OF THE GOVERING (PDES):

The general partial differential equations (i.e. sometimes called transport equations) [Patanker (1980)] for continuity, momentum scales k,ε all have the form

$$\frac{\partial}{\partial x}(\rho U\phi) + \frac{\partial}{\partial y}(\rho V\phi) + \frac{\partial}{\partial z}(\rho W\phi) = \frac{\partial}{\partial x}\left(\Gamma_\phi \frac{\partial \phi}{\partial x}\right) + \frac{\partial}{\partial y}\left(\Gamma_\phi \frac{\partial \phi}{\partial y}\right) + \frac{\partial}{\partial z}\left(\Gamma_\phi \frac{\partial \phi}{\partial z}\right) + S_\phi \quad (9)$$

where the three terms on the left side are convection terms and the four terms on the right side are diffusion and source term.

THREE DIMENSIONAL DISCRETIZATION:

The general transport equation may be written as:

$$\frac{\partial}{\partial x_i}(J_i) = S_\phi \quad (10)$$

Where

$$J_i = \rho U_i \phi - \Gamma_\phi \frac{\partial \phi}{\partial x_i} \quad (11)$$

Ji represents all the flux due to both diffusion and convection. The source term may be expressed as a linear expression.

$S_\phi = b\phi_p + c$ (12)

The pressure term is excluded from the source term (in the momentum equation) in the solution procedure, and the linearization is done for all other terms only. Integration using the CV results in:

$J_e - J_w + J_n - J_s + J_f - J_b = (b\phi_p + c)\Delta v$ (13)

where e (east), w (west) ,n (north) and s (south) are the neighboring points of p in the y-direction, f(front), b (back) are the neighboring pointes of p in the z-direction, $\Delta v = \Delta x \Delta y \Delta z$ is the volume of the control volume. Integrating the continuity gives

$F_e - F_w + F_n - F_s + F_f - F_b = 0$ (14)

where the F's are the mass flow rates through the control surface. The general three-dimensional discretization equation is given by,

$$\left(\sum_i a_i - b\right)\phi_p = \sum_i a_i \phi_i + c \quad (15)$$

where $\sum_i a_i = a_p = a_E + a_W + a_N + a_S + a_F + a_B$

$$\sum_i a_i \phi_i = a_E \phi_E + a_W \phi_W + a_N \phi_N + a_S \phi_S + a_F \phi_F + a_B \phi_B$$

$b = S_p \Delta v$, $c = S_u \Delta v$

in which Sp and Su are coefficients in the source terms determined from a suitable finite difference approximation of ($S\phi$) expression for particular dependent variable ϕ.

Solving this using upwind scheme to give values of a_i

$$\left.\begin{aligned} a_E &= D_e + \langle 0, F_e \rangle; a_W = D_w + \langle F_W, 0 \rangle; a_N = D_n + \langle 0, -F_n \rangle \\ a_S &= D_s + \langle F_s . 0 \rangle; a_F = D_f + \langle -F_f . 0 \rangle; a_B = D_b + \langle 0, F_b \rangle \end{aligned}\right\} \quad (16)$$

The convection and diffusion fluxes are given by :

$$\left.\begin{aligned} F_e &= (\rho U)_e \Delta y \Delta z \;\&\; D_e = \Gamma_e \Delta y \Delta z / \delta x_e \;\&\; F_w = (\rho U)_w \Delta y \Delta z \;\&\; D_w = \Gamma_w \Delta y \Delta z / \delta x_w \\ F_n &= (\rho V)_n \Delta x \Delta z \;\&\; D_n = \Gamma_n \Delta x \Delta z / \delta y_n \;\&\; F_s = (\rho V)_s \Delta x \Delta z \;\&\; D_s = \Gamma_s \Delta x \Delta z / \delta y_s \\ F_f &= (\rho W)_f \Delta x \Delta y \;\&\; D_f = \Gamma_f \Delta x \Delta y / \delta z_f \;\&\; F_b = (\rho W)_b \Delta x \Delta y D_b = \Gamma_b \Delta x \Delta y / \delta z_b \end{aligned}\right\} \quad (17)$$

All the coefficients in Eq.(16) and (17) are used for solving of (k and ε), the velocity components are calculated on a staggered grid and their values differ.

Excluded the pressure terms from the coefficient of the source terms Su, the discretized equation for (U_e , V_n , W_f) are

$$\left.\begin{aligned} a_e U_e &= \sum_i a_i U_i + c + (P_P - P_E)\Delta y \Delta z \\ a_n V_n &= \sum_i a_i V_i + c + (P_P - P_N)\Delta x \Delta z \\ a_f W_f &= \sum_i a_i W_i + c + (P_P - P_F)\Delta x \Delta y \end{aligned}\right\} \quad (18)$$

The velocities in Equations (18) will all satisfy continuity if the pressures at the grid points are correct. At the start of the calculation, only guessed values of pressure and velocity are available and continuity will not be satisfied. Therefore, some means of correcting the pressures is needed to achieve a solution. Using SIMPLE procedure [Onbasiogla and Husegin (2003)]. The SIMPLE assume that,

$$P = P^* + P';U = U^* + U';V = V^* + V';W = W^* + W' \Big\} \quad (19)$$

where the asterisk represents a guessed value and the prime is the correction necessary to satisfy continuity.

$$\left.\begin{aligned} a_e U_e^* &= \sum_i a_i U_i^* + c + (P_P^* - P_E^*)\Delta y\Delta z \\ a_n V_n^* &= \sum_i a_i V_i^* + c + (P_P^* - P_N^*)\Delta x\Delta z \\ a_f W_f^* &= \sum_i a_i W_i^* + c + (P_P^* - P_F^*)\Delta x\Delta y \end{aligned}\right\} \quad (20)$$

Subtracting equations (18) from equations (20) we get:

$$\left.\begin{aligned} a_e U_e' &= \sum_i a_i U_i' + (P_P' - P_E')\Delta y\Delta z \\ a_n V_n' &= \sum_i a_i V_i' + (P_P' - P_N')\Delta x\Delta z \\ a_f W_f' &= \sum_i a_i W_i' + (P_P' - P_F')\Delta x\Delta y \end{aligned}\right\} \quad (21)$$

For computational convenience, $\sum_i a_i U_i'$, $\sum_i a_i V_i'$, and $\sum_i a_i W_i'$ are set to zero[Onbasiogla and Husegin (2003)]. Substituting the result of eq.(19) with eq.(21) into continuity equation get:

$$\sum_i a_i P_p' = \sum_i a_i P_i' + c \quad (22)$$

where $\sum_i a_i = a_E + a_W + a_N + a_S + a_F + a_B$

$$\sum_i a_i P_p' = a_E P_E' + a_W P_W' + a_N P_N' + a_S P_S' + a_F P_F' + a_B P_B'$$

$a_E = (\rho_e / a_e)(\Delta y\Delta z)^2$ & $a_W = (\rho_w / a_w)(\Delta y\Delta z)^2$ & $a_N = (\rho_n / a_n)(\Delta x\Delta z)^2$ &

$a_S = (\rho_S / a_S)(\Delta x\Delta z)^2$ & $a_F = (\rho_f / a_f)(\Delta x\Delta y)^2$ & $a_B = (\rho_b / a_b)(\Delta x\Delta y)^2$

$c = F_w^* - F_e^* + F_s^* - F_n^* + F_f^* - F_b^*$

$F_w^* = (\rho U^*)_w \Delta y\Delta z$ & $F_e^* = (\rho U^*)_e \Delta y\Delta z$ & $F_s^* = (\rho V^*)_S \Delta X\Delta z$ &

$F_n^* = (\rho V^*)_n \Delta x\Delta z$ & $F_b^* = (\rho W^*)_b \Delta x\Delta y$ & $F_f^* = (\rho W^*)_f \Delta x\Delta y$

Under relaxation is implemented to a void divergence in the solution variable. The under relaxation factor used in this study is (0.5) for *U,V,W,k* & ε and (0.8) for P .

RESULTS AND DISCUSSION:

Experimental Results:

Pressure Drop Investigation:

The total pressure drop (ΔP_T) through the duct with restriction can be broken down into two components which are pressure drop due to the friction (ΔP_f) and the inertia losses through the restriction (ΔP_R)

$\Delta P_T = \Delta P_f + \Delta P_R$

Pressure Drop Due to the Restriction Geometry ΔP_R:

Fig.(4) shows a typical pressure drop pattern along the duct (with different restriction shapes and different Reynolds numbers). It contains 13 restriction shapes, each restriction has four graphs for different Reynolds numbers.

It is clear that the pressure drop data fall on a straight line in the upstream section, and that near the restriction there is substantial pressure depression. However, the pressure depression is recovered along the downstream data and fall on a straight line again. Without the restriction, the two straight lines would be collinear. Thus the

pressure drop due to the different restriction shape (ΔP_R) is the difference offset by the two lines (between (A) and (B)). The pressure drop component (ΔP_R) can be expressed by

$$\Delta P_R = \frac{1}{2}\rho_{air} U_{av}^2 \ . \ k_R$$

where the k_R: pressure coefficient due to the restriction.

The pressure coefficient (k_R) is due to the inertia losses, so it is independent of Reynolds number [Lee (1986)]. This can be seen in Fig. (5), this figure is plotted between pressure coefficient k_R vs the Reynolds numbers for four shapes and different blockage area ratio of restrictions which are used in this work. It is clear that the values of k_R are roughly constant with the range of Reynolds number which is used for the same restriction [Roberson and Crowe (1977)] .The behaviors of k_R for the other restrictions are in line with the four restrictions which are drawn. The parameters that k_R depends on are: the ratio between the wetted perimeter of the restriction to the free remainder perimeter (p_e/P_e), and the blockage area ratio A_b. Table (2) shows the wetted perimeter and the blockage area ratio for all restrictions which are used in this study.

Table (2) Wetted perimeter and blockage area ratio for all Restriction shapes

Restriction	Blockage area ratio A_b	Wetted perimeter p_e cm	Remainder perimeter P_e cm	p_e/P_e	Average k_R
	0.11	8	40	0.2	0.6
	0.11	12	36	0.53	0.62
	0.11	16	32	0.5	0.65
	0.22	16	32	0.5	0.72
	0.22	12	36	0.33	0.69
	0.22	20	28	0.7	0.74
	0.33	24	24	1	0.75
	0.33	20	28	0.7	0.72
	0.33	24	24	1	0.76
	0.33	12	36	0.33	0.69
	0.44	16	32	0.5	0.79
	0.44	20	28	0.7	0.82
	0.56	24	24	1	0.83

Correlation between k_R , p_e/P_e and A_b :

To create the relation between k_R and the two parameters (p_e/P_e) and A_b assume the general formula between them: $k_R = a.(\frac{p_e}{P_e})^b.A_b^c$

where: a , b and c are correlation constant .

To solve this relation, use statistical program which uses Quais-Newtons method to obtain $$k_R = 0.881(\frac{p_e}{P_e})^{0.064}.A_b^{0.123}$$

and with accuracy of 96% as shown in Fig.(6). It is clear from the correlation equation mentioned above that the effect of the blockage area ratio A_b on k_R is much greater, if the ratio of perimeter is kept constant.

Pressure Drop Due to The Friction ΔP_f :

Fig.(7) is drawn between C_f Vs (z/D_h). In general, as shown in the figure, for all restrictions which are used in the study, the friction factor C_f is a function of Reynolds number. Each restriction uses the relations between C_f and Reynolds number are roughly have same behavior for different Reynolds numbers , but the values of C_f decrease with decreasing of Reynolds number.

The maximum values of C_f in the downstream region after restriction as they appear in the (z/D_h) equal (1/3) or in the distance (4 cm) from restriction in z-direction, except the restrictions number (3,10,11,&12) the maximum C_f appears in the (z/D_h) equal to (2/3) or in the distance (8 cm) from restriction in z-direction.

Total Pressures Coefficients:

The total pressures coefficients after restriction are presented in Fig. (8) for $Re_1=8.2x10^4$ and $Re_4=5.6x10^4$. The Cp_T contours for the same restriction seem to be approximately similar in behavior and have different values with the changing of Reynolds number. When Reynolds number decreases the Cp_T decreases, this explains why the losses decrease when Reynolds number decreases.

It is clear from the figure that the values of Cp_T are positive in the area behind the restriction (positive pressure area), and they are negative in remainder area (suction area), for all restrictions which are used in this study.This distribution depends on the blockage area ratios as shown in Fig. (8). To explain this effect take for example of blockage areas (0.11) and (0.56), the blockage area ratio increases (80%), the value of Cp_T increases around (83%) (i.e. the losses are increased). The main conclusion is that, when the blockage area ratio increases the Cp_T increases also so that the losses increase.

Axial Velocity Distribution:

The axial velocity Distribution for selected three restriction shapes No.(3,9&13) at $Re_1=8.2x10^4$ are presented in Fig.(9). Restriction No.(3,9&13) represent three different blockage area ratios of (0.11,0.33 and 0.56) respectively. This figure is drawn for axial velocity with y-direction in four positions (2, 4, 8 & 12 cm) in z-direction. In each location there are three graphs for different distances in x-direction (3, 6 & 9 cm), these positions represent the points of measurements in z-direction by five-hole probe.

It is clear from the figure mentioned above that for all restrictions the velocity behind the restriction has the lowest value approximately reaching zero, but the values in open area are greater than the main flow velocity.

NUMERICAL RESULTS:

Flow Patterns (Streamlines and Velocity Vectors) :

Streamlines and velocity vectors are plotted in z-x plane at y=6 cm as shown in Fig.(10) (a and b) for three restriction at two Reynolds number.

So far considered flow in which the pressure outside the boundary layer was considered as constant. If, however, the pressure varies in the direction of flow (because of the restriction), the behavior of the fluid may be greatly affected [Massey]. Fig.(10) shows that the streamlines in the upstream region are parallel and the velocity vectors distributions are symmetric in any location, when the flow strikes the restriction (normal to the flow direction), the streamlines approach one another in the open area and large eddies directly form after the restriction, their strength depend on the Reynolds number and the restriction shape and position. The velocity vectors behind the restriction have the lowest values approach to zero and have the highest values in the open area.

Axial Velocity Distribution:

Fig.(11) represents the axial velocity distribution for three selected restriction No.(3,9,13) with different blockage area ratio at $Re_1=8.2x10^4$.

This figure is drawn for axial velocity with y-direction in four positions (2, 4, 8 and 12 cm) in z-direction. In each position there are three graphs for different distances in x-direction (3, 6 & 9 cm), these positions represent the same points of measurement in experimental work.

It is clear from the figure mentioned above that the velocity profiles at x=3 cm and x=9 cm are the same for all z (due to the symmetry of all restrictions used) and the velocity behind the restriction has the lowest values (at x=6 cm), but the values of velocity in the open area are greater than the main flow velocity. The velocity distribution in both cases (theoretically and experimentally) is equintativly the same but there are slightly difference in velocity values for all cases studied.

CONCLUSION:

From Experimental Work

- The pressure drop coefficient due to the restriction shape and position, (k_R) is independent of the Reynolds number in study range but it depends on the blockage area ratio (A_b) and the ratio between the wetted perimeter and free remainder perimeter (p_e/P_e). Correlation equation is created between them.

$$k_R = 0.881\left(\frac{pe}{Pe}\right)^{0.064}.A_b^{0.123}$$

- The total pressure coefficient C_{Pt} decreases when the Reynolds number decreases for same restriction, and it depends on the blockage area ratio, when the blockage area ratio increases around 80% the C_{Pt} increases approximately 83%.
- The axial velocity U has the lowest value behind restriction approach to zero, but the values in open area are greater than those of the main flow velocity. This conclusion is in line with the numerical and Fluent (6.1) results

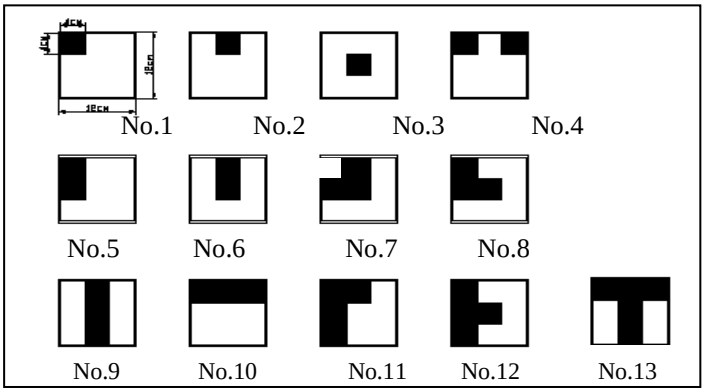

Figure (1) The restrictions shapes.

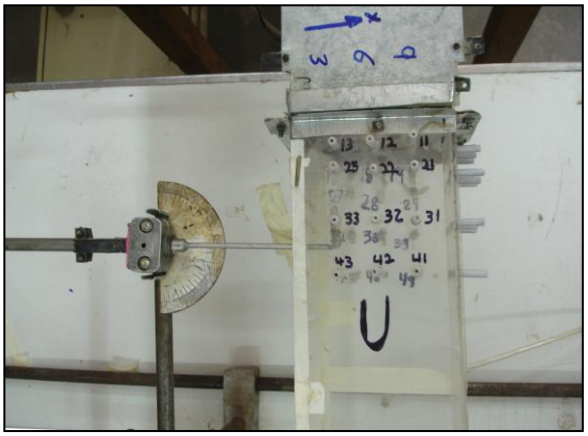

Figure (2a) Photograph shows the static pressure taps.

Figure (2b) Photograph of the air supply and test rig

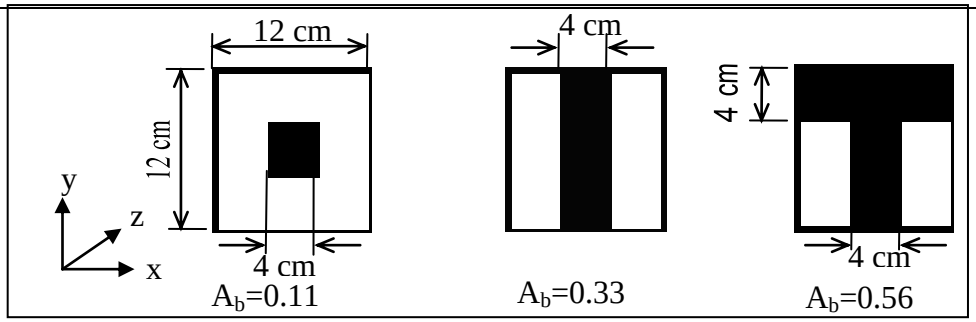

Figure (3) The restriction models

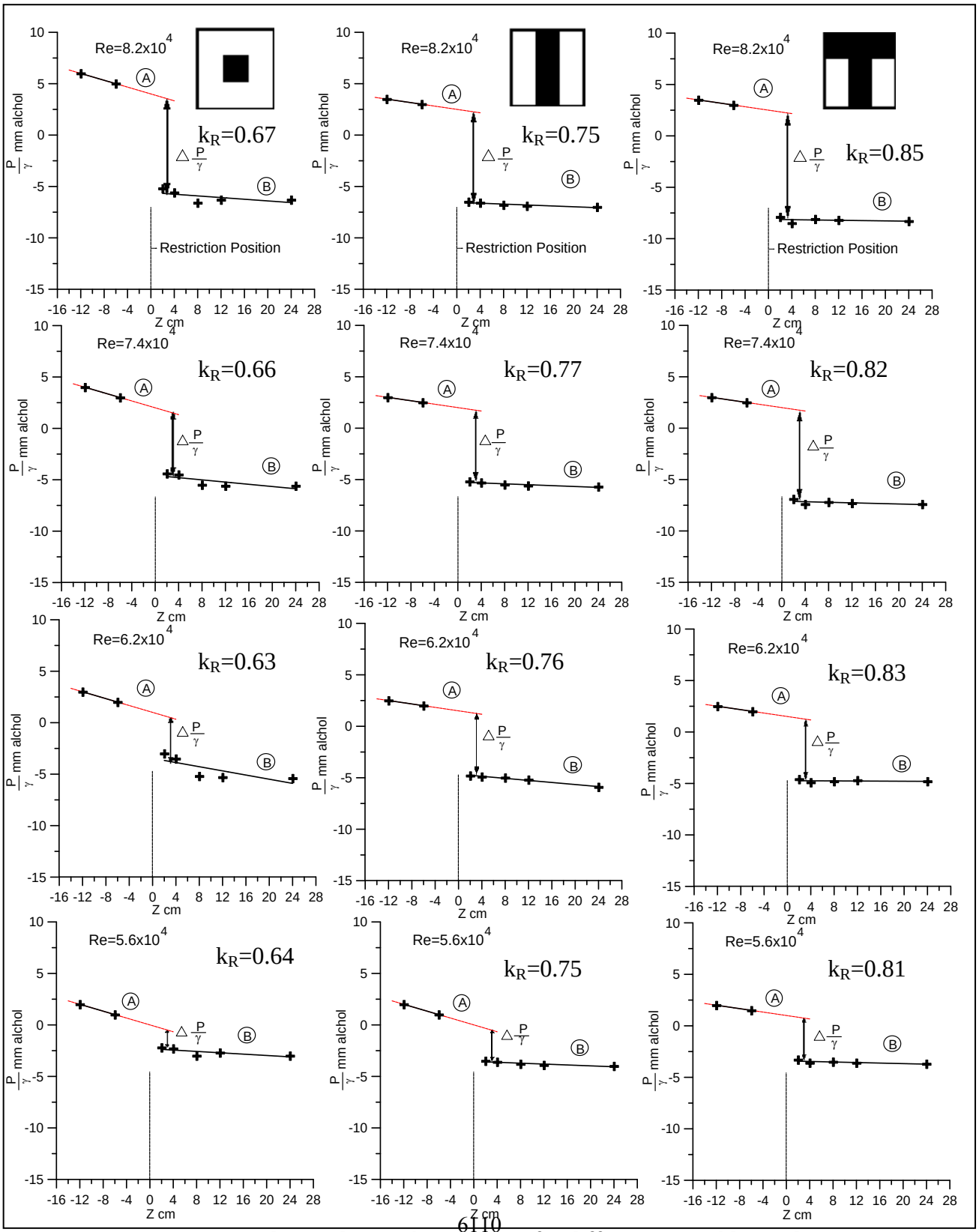

Figure (4) Pressure drop induct with restriction for different Reynolds numbers, Re_1= 8.2x10^4, Re_2=7.4, Re_3=6.2x10^4& Re_4=5.6x10^4.

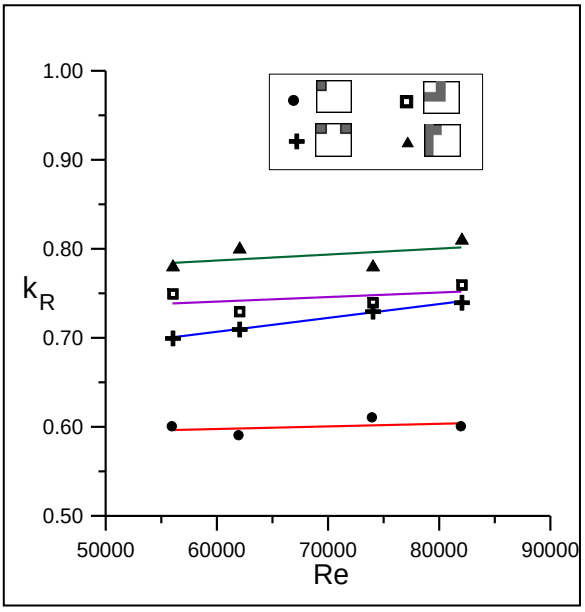

Figure (5) Pressure coefficient Vs Reynolds numbers for different shape.

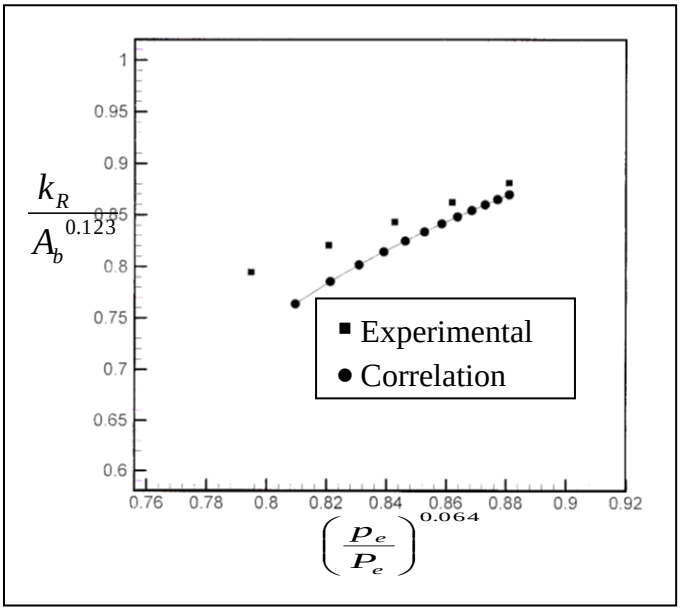

Figure (6) Correlation between pressure coefficient k_R and perimeter ratio p_e/P_e and Blockage area ratio A_b .

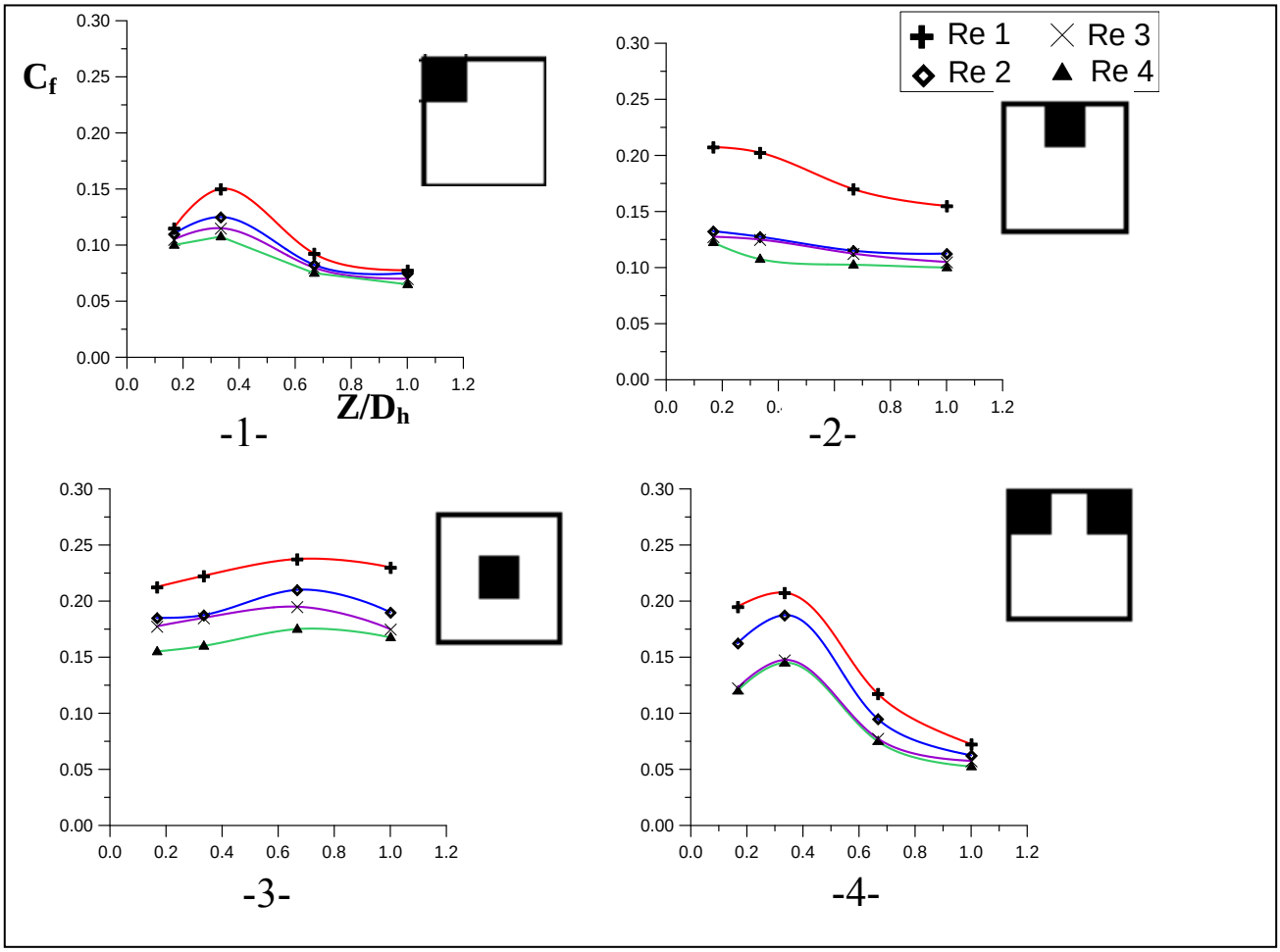

Figure (7) The effect of restriction position on the C_f for different Reynolds numbers, $Re_1= 8.2x10^4$, $Re_2=7.4x10^4$, $Re_3=6.2x10^4$& $Re_4=5.6x10^4$.

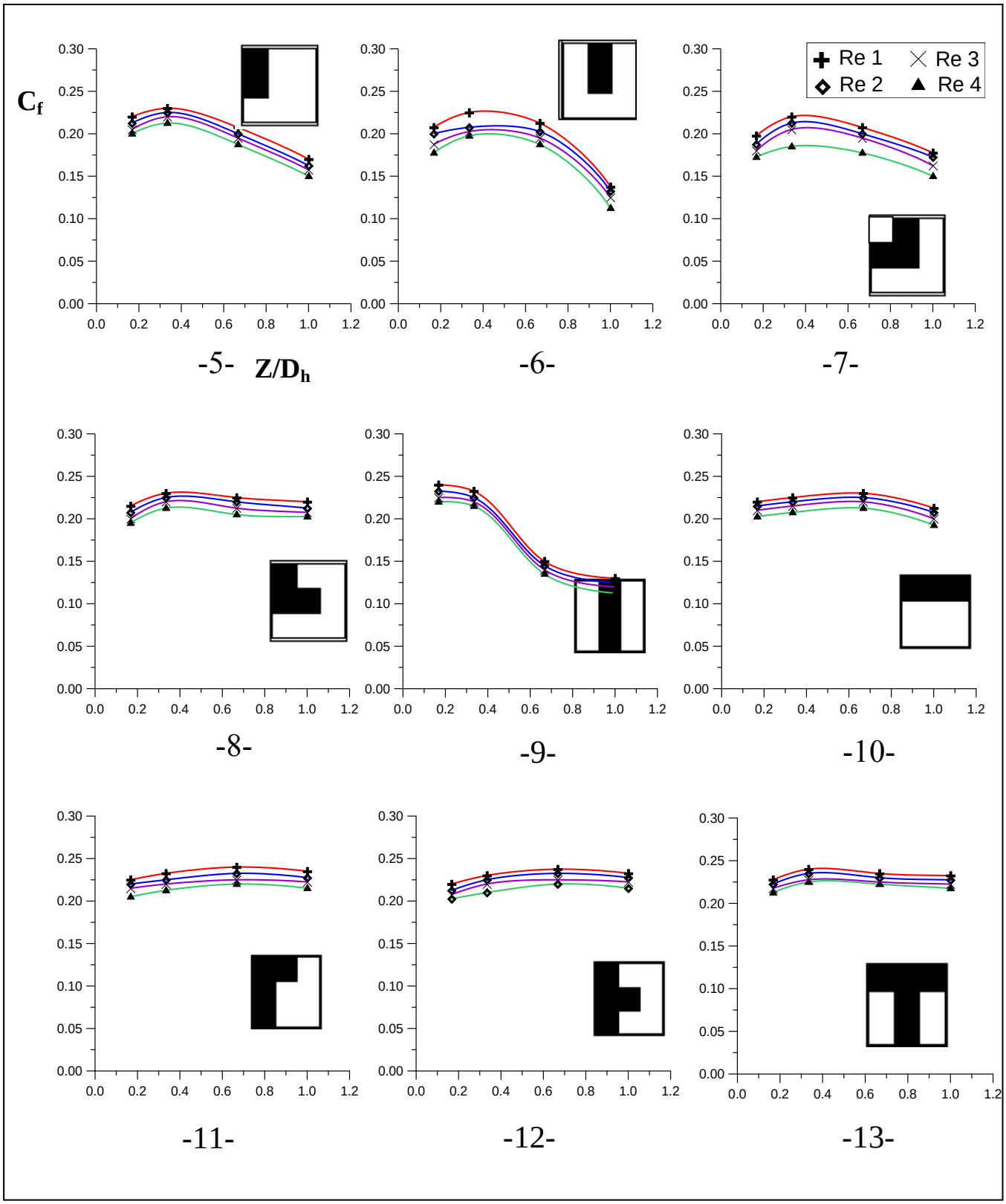

Continued to figure (7)

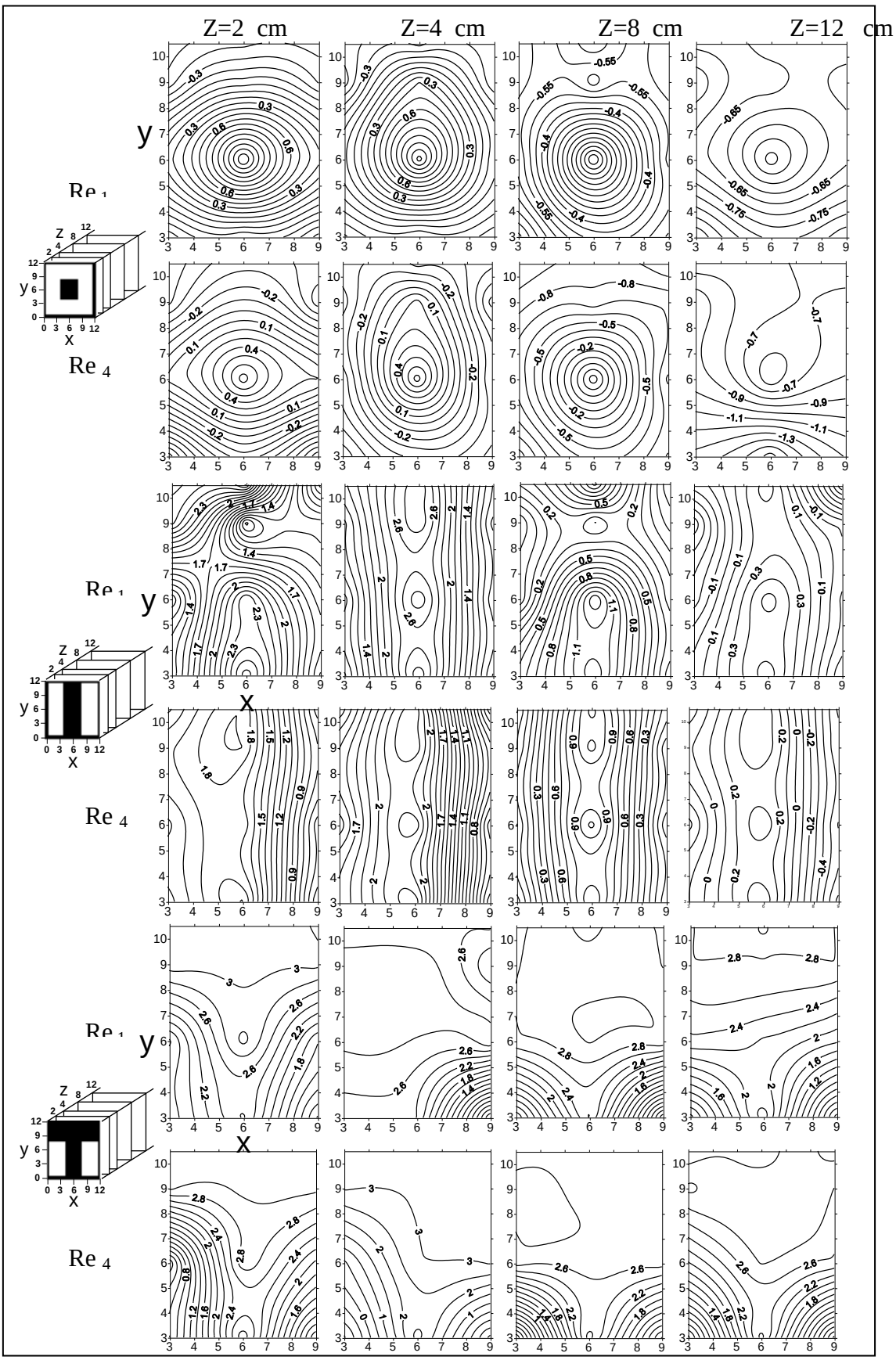

Figure (8) Variation of Total Pressure Coefficient Cp_T for different section at $Re_1=8.2x10^4$ & $Re_4=5.6x10^4$.

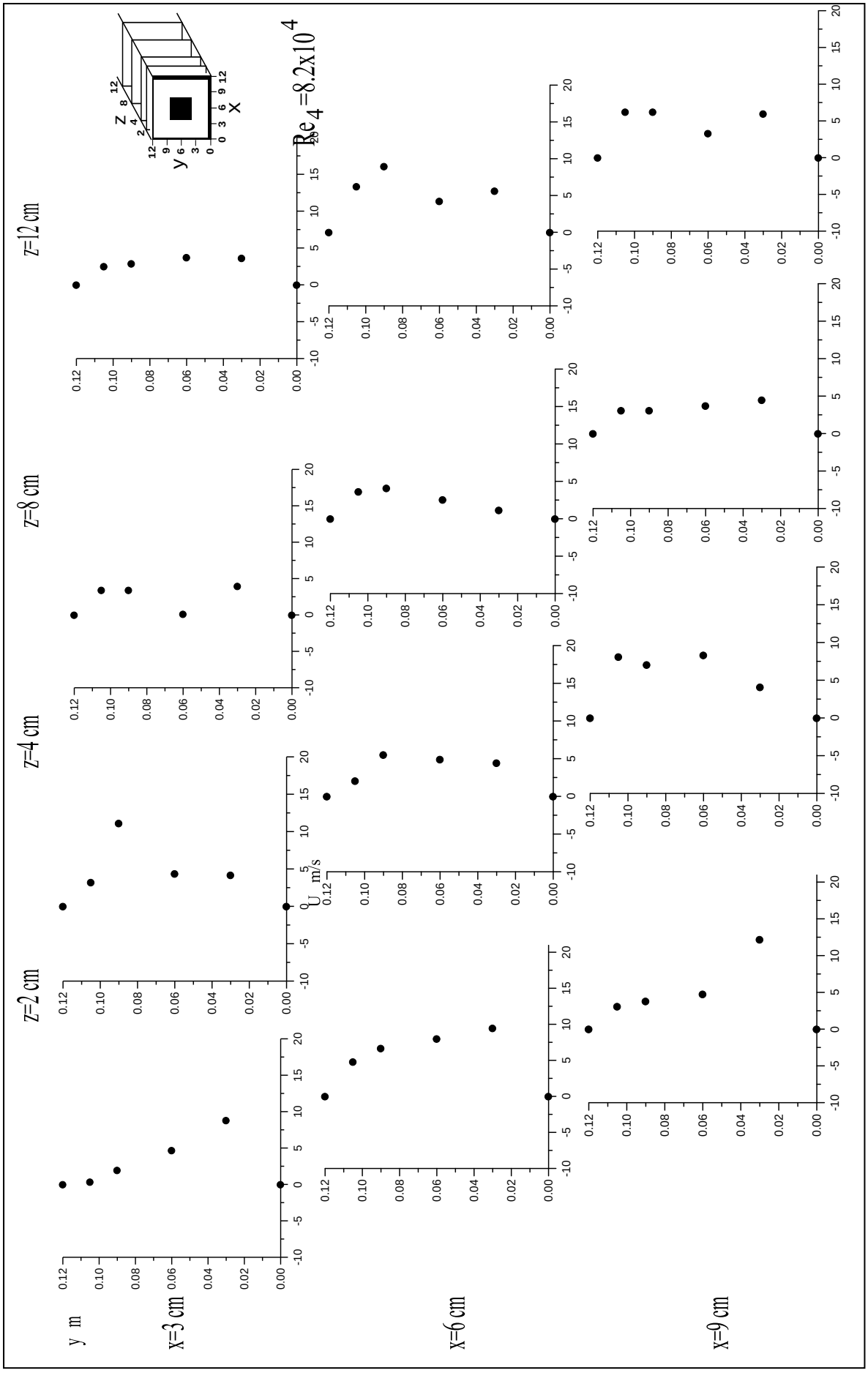

Figure (9) Axial velocity distrbution for different section in expermintal work

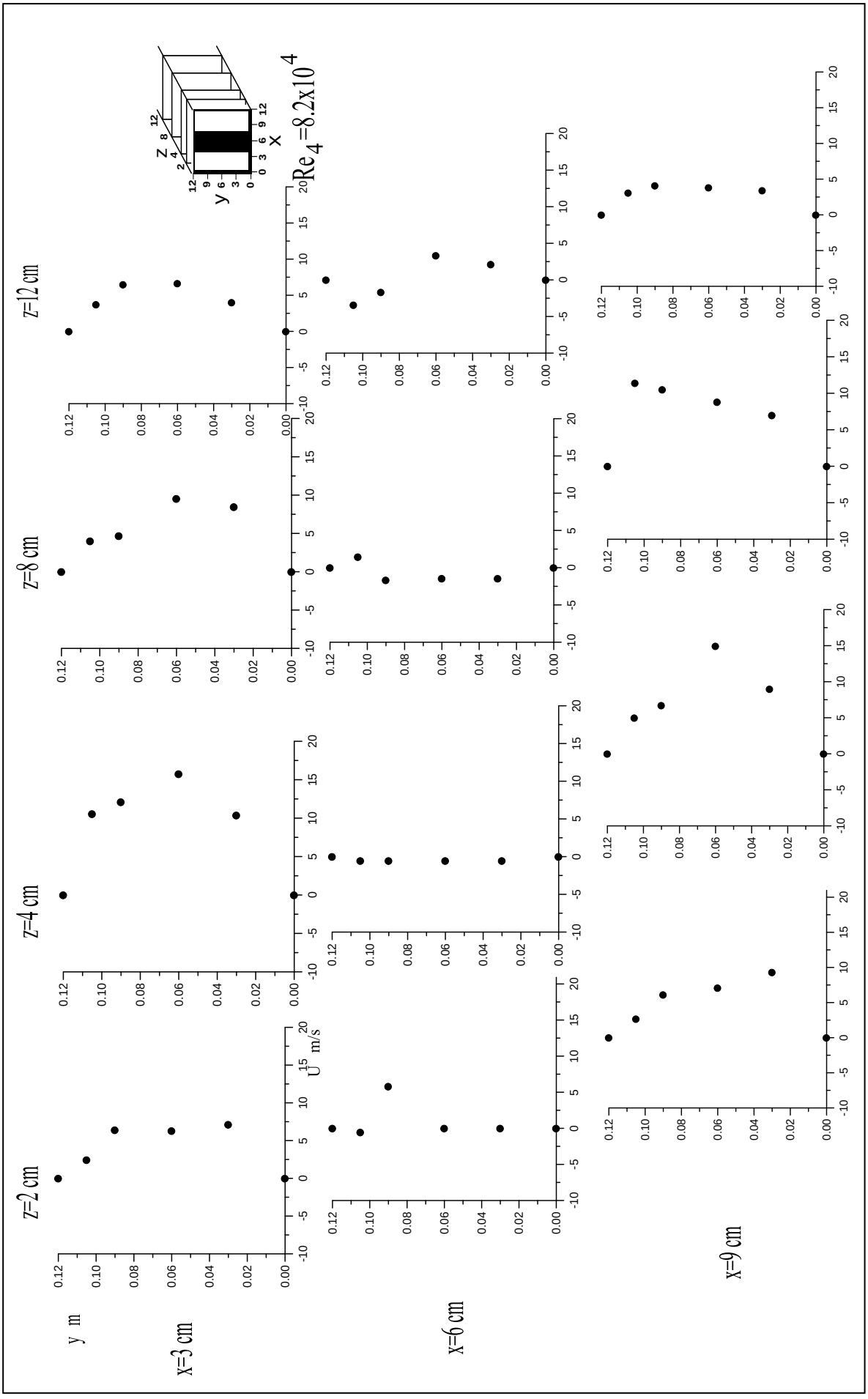

Continued to Figure (9)

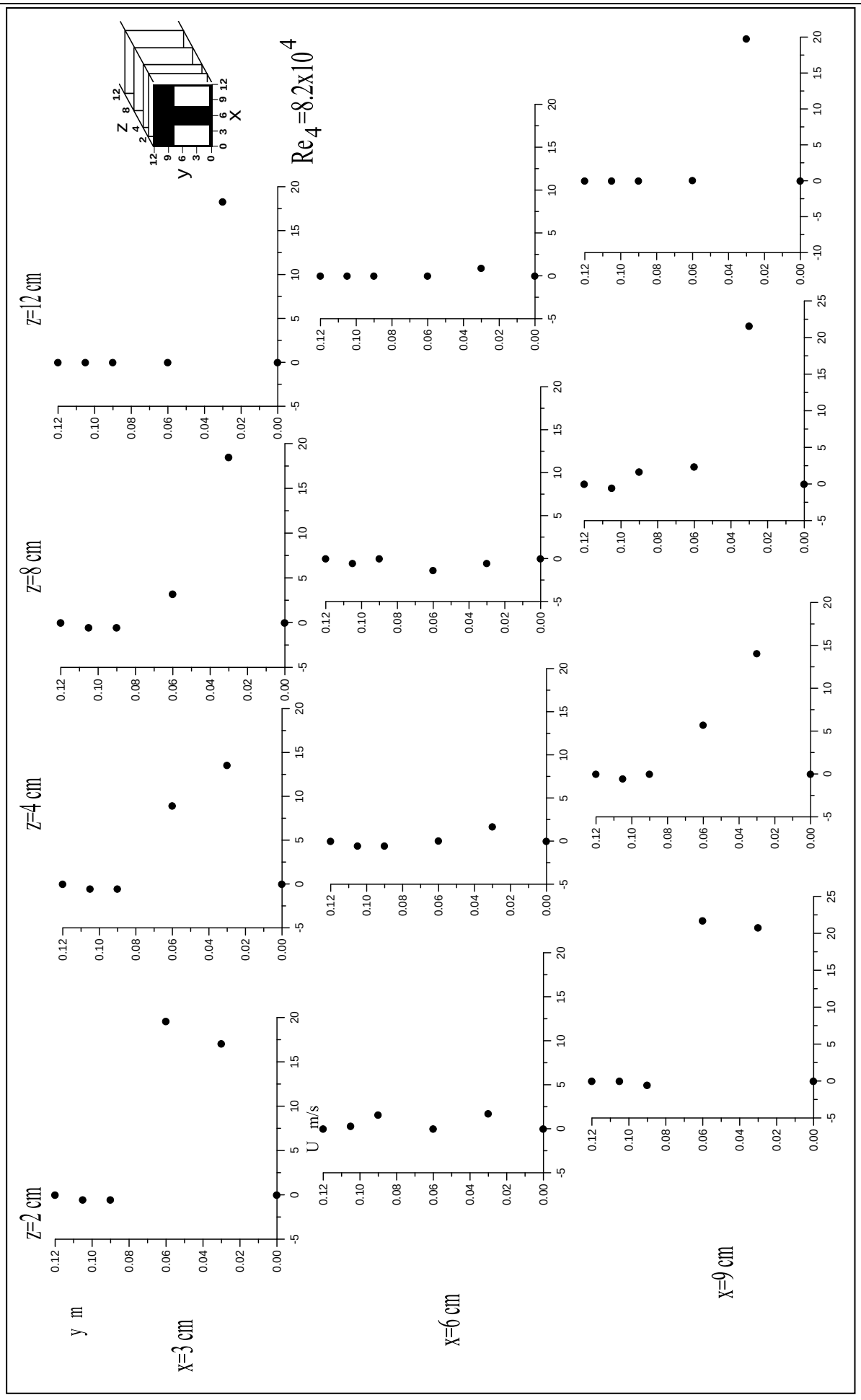

Continued to Figure (9)

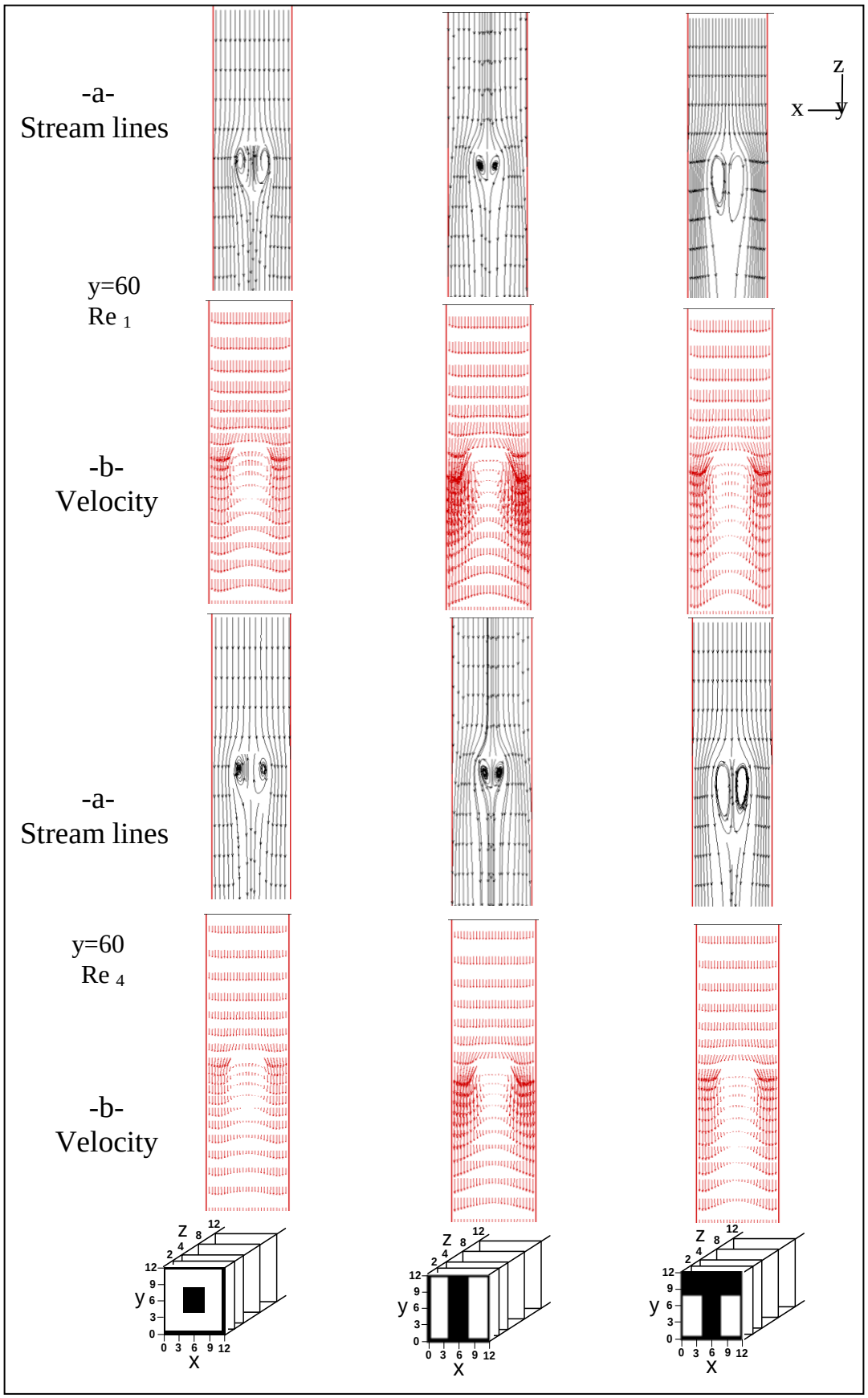

Figure (10) Flow patterns in z-x plane at $Re_1=8.2x10^4$ & $Re_4=5.6x10^4$

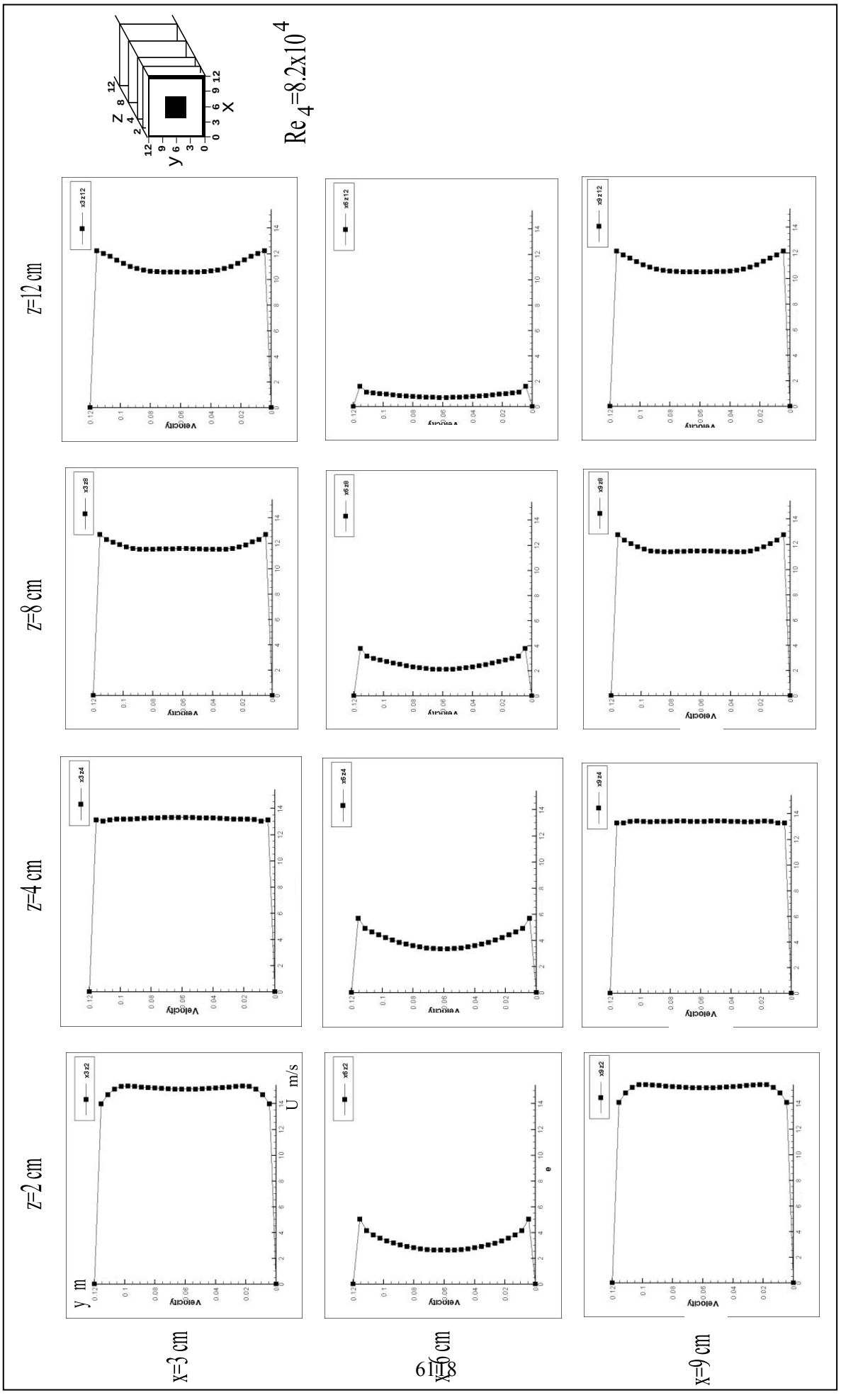

Figure (11) Axial velocity distrubution for different section in numerical work.

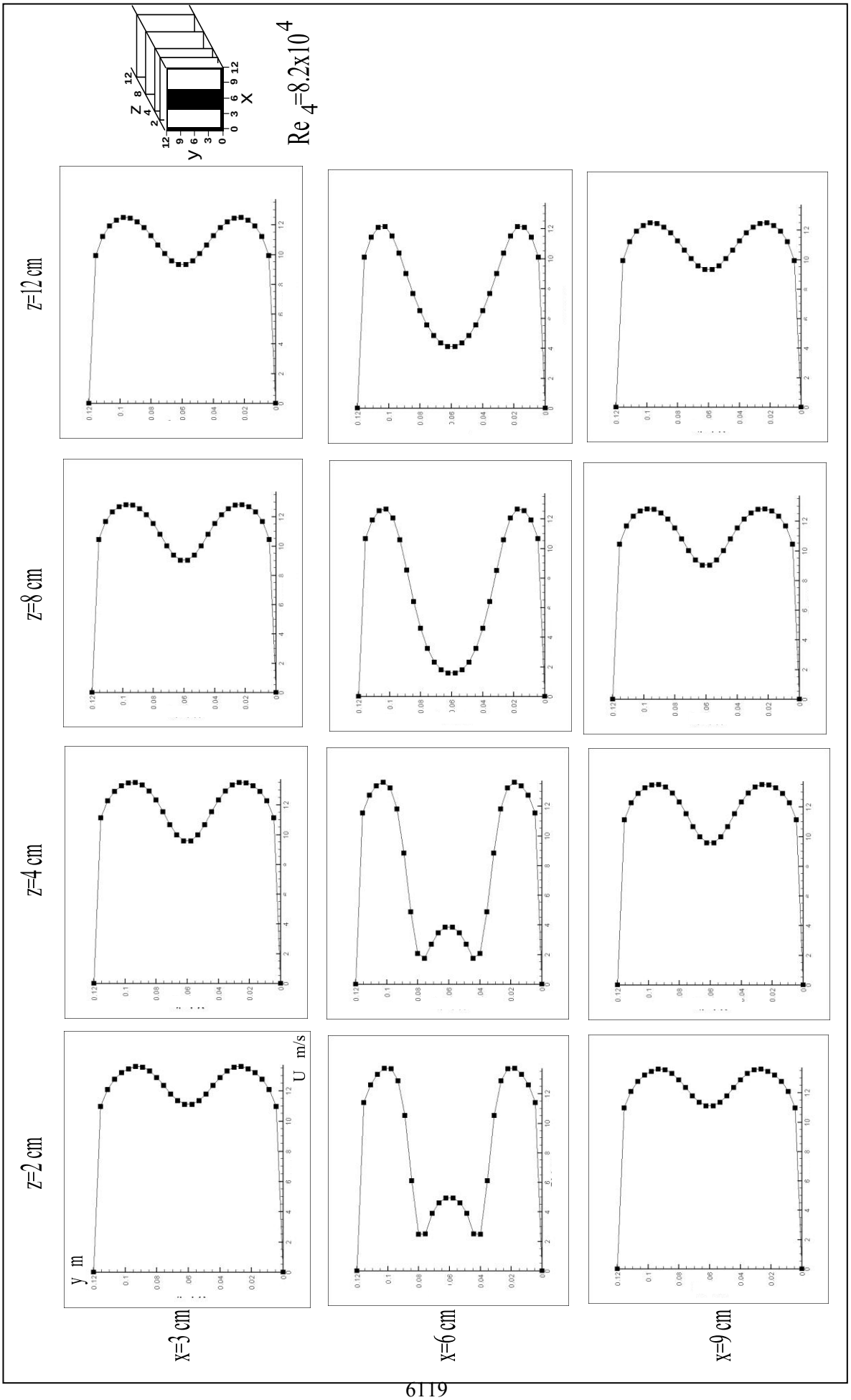

Continued to Figure (11)

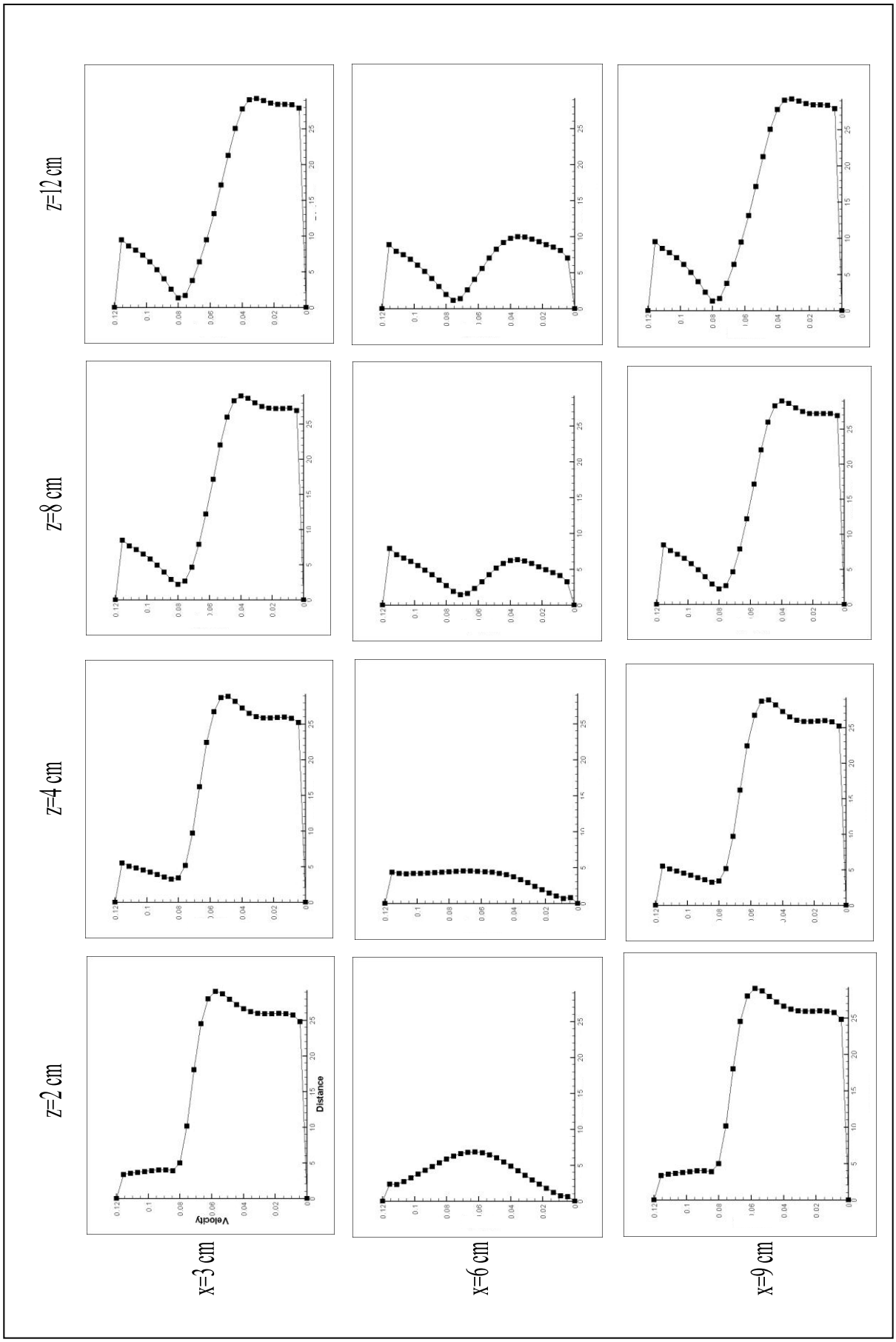

Continued to Figure (11)

REFERENCES

- British-standard 1042, "Method for measurement of fluid flow in pipes", Part 2A, August, 1973.
- Davidson, L., and Farhanieh, B., "A finite volume code employing collocated variable arrangement and Cartesian velocity components for computational geometries.", Dep. Of Thermo and Fluid Dynamics, Chalmers University of Technology, Sweden, November, 1995, Publ. No. 95/11.
- Han, J.C., Glicjsman, L.R., and Rohsenow, W.M.,(1978),"An investigation of heat transfer and friction for rib-roughened surfaces. ", Int. J., Heat and Mass Transfer Vol. 21, pp. 1143-1156.
- Hanaa Abdul hadi" Numerical and Experimental Investigation on the Effect of Restriction Shape on Characteristics of Airflow in a Square Duct." Ph.D thesis of Mechanical Engineering of University of Technology,2006.
- Han,J.C.,(1984),"Heat transfer and friction in channels with two opposite rib-roughened walls. ", Transaction of the ASME, Vol. 106, Nov. 1984.
- Launder, B.T., and Spalding, D.B., "Lecturers in mathematical models of turbulence.' Department of Mechanical Engineering, imperial college of Science and Technology, London, England.
- Lee, Y.N., (1986), "Heat transfer and pressure drop characteristics of an array of plates aligned at angles to the flow in a rectangular duct. ", Int. J., Heat and Mass Transfer Vol. 29, No. 10, pp. 1553-1563, 1986.
- Massey B.S., "Mechanics of Fluids", 4th edition, Van Nostr and Reinhold, 1980.
- Ooi , A. , Iaccarino , G., Durbin , P.A. , and Behnia , M. , (2002). " Reynolds averaged simulation of flow and heat transfer in ribbed ducts. ", International Journal of Heat and Fluid Flow, Vol. 23 , (2002) , pp. 750-757.
- Ooi, A., Iaccarino, G., Durbin, P.A., and Behnia, M., (2003). "Simulation of turbulent flow and heat transfer in complex passage. ", Journal of Heat and Fluid Flow , Vol. 23 , pp. 750-757.
- Onbasioglu, S.U., and Huseyin Oube, H., (2003),"On enhancement of heat transfer with ribs.", Applied Thermal Engineering, Vol. 24, Issue 1, January 2004, pp. 43-57.
- Patanker, S.V., (1980), "Numerical heat transfer and fluid flow ", McGraw.Hill, New York.
- Roberson and Crowe, "Engineering Fluid Mechanics." 6th edition, Copyright 1977, by John Wilely and Sons, Inc.
- Taslim, M.E., Li, T., and Spring, S.D., (1998)," Measurement heat transfer coefficients and friction factor in passage rib-roughened on all walls", Transactions of ASME, Vol. 120, July, 1998.

LIST OF SYMBOLS

Symbol	Title	Units
A_b	Blockage area ratio	m^2
a_E,a_W,a_N,a_S,a_F,a_B	Coefficient in turbulence model	---
C_f	Pressure coefficient due to the friction	---
C_μ, $C_{1\varepsilon}$, $C_{2\varepsilon}$	Constant in turbulence model	---
G_k	Generation rate or turbulence energy	---
i,j,k	Indices which indicate position in (x,y,z)	---
k_R	Pressure coefficient due to the restriction	---
P_{av}	Average pressure	N/m^2
p_e	Wetted perimeter	m
P_e	Remainder perimeter	m
P_s	Static pressure	N/m^2
U, V, W	Mean velocities in x,y,z directions	m/s
U_{av}	Average velocity	m/s
ε	Energy dissipation	m^2/sec^3
μ	Dynamic viscosity	N/sec. m^2
ν	Kinematics viscosity	m^2/sec
ϕ	Dependent variables	---
e, w, n, s, l, r Subscript	Control volume faces	----

VERIFICATION OF LAMINATE COMPOSITE PLATE SIMULATION UNDER COMBINED LOADINGS THERMAL STRESSES

Prof. Dr.Nabeel K. Abid AL-sahib
University of Baghdad
Al-khwarzmi College of Engineering
Mechatronics Department

Asst Prof. Dr.Adnan N. Jameel
University of Baghdad
College of Engineering
Mechanical Department

Dr. Louay S. Yousuf
University of Baghdad
College of Engineering
Mechanical Department

ABSTRACT

This study deals with thermal cyclic loading phenomena of plates which were fabricated from composite materials (woven roving fiber glass + polyester) were exposed to (75 C°) temperature gradient thermal shock for ten times in different stage of conditioning times due to the effect of thermal fatigue using the method of Levy solution and compared these results with both results from experimental published work and (ANSYS Ver. 9) program. A composite laminate plate with fiber volume fraction (υ_f =25.076%) is selected in this study and applying the combined loadings like bending moment (Mo), and in-plane force (Nxx) beside the effect of thermal fatigue. It involves multi theoretical and finite element fields; but the theoretical one contains the derived equation of stresses distribution and evaluating the normal deflection of a middle point for dynamic analysis applying different boundary conditions for heating and cooling. The main present numerical results for a composite plate with (80%) fiber volume fraction claim that the relative reduction in normal deflection and dynamic load factor are (78.593%) and (9.421%) during cooling to (-15 $^{\circ}C$) respectively.

الخلاصة:

هذه الدراسة تتناول ظاهرة التحميل الحراري الدوري للصفائح التي كانت مصنعة من المواد المركبة (ألياف زجاجية + بوليستر) والمعرضة الى انحدار حراري بصدمة حرارية بمقدار (75) درجة سليزية لعشر دورات من مراحل وقت العمل نتيجة لتاثير الكلال الحراري باستخدام طريقة ليفي ومقارنة هذه النتائج مع كلا من نتائج برنامج الانسيز ذات الطبعة التاسعة ونتائج بحث عملي منشور مسبقا. ان الصفيحة الرقائقية المركبة بكسر حجمي (25.076%) تم اختيارها في هذه الدراسة بعد تطبيق الاحمال المركبة مثل عزم الانحناء وقوة الانضغاط الى جانب التحميل الحراري الدوري. ويتضمن هذا العمل عدة جوانب نظرية وعددية ، حيث يشمل الجانب النظري اشتقاق معادلات توزيع الاجهادات وتقييم الانحراف العمودي في نقطة المنتصف للتحليلات الديناميكية مع تطبيق شروط حدية

مختلفة في حالتي التسخين والتبريد. إن أداء النتائج العددية الرئيسية الحالية للمادة المركبة مع كسر حجمي (80%) يؤدي إلى انخفاض نسبي بالانحراف العمودي وعامل الحمل الديناميكي بنسب (78.593%) و (9.421%) نتيجة التبريد إلى (-15 درجة مئوية) على التوالي.

KEY WORD: thermal stress, composite laminate, dynamic analysis, plate simulation, combined loadings.

INTRODUCTION

Many researches before studied the effect of thermal fatigue in woven roving glass fibers with unsaturated polyester composite plate and its application on airspace experimentally. The effect of thermal cycles on tensile properties and coefficient of thermal expansion has been studied on graphite-epoxy 12-ply laminate configuration subjected to 5000 thermal cycles, [Fabmy A.A. and Cunningbam T.G., 1976]; but the method prediction applied on T300 graphite/934 epoxy under hygro-thermo-mechanical fatigue with two step procedure. The initial step consists of determining the composite ply strength associated with each type of cyclic load: mechanical, thermal and hygral. The next step is to determine the effect of combined cyclic loading [Ginty C.A. and Chamis C.C., 1988]. It can be estimate the inter-laminar shear strength (ILSS) of glass/epoxy and glass/polyester composites of woven fabrics by changing the holding time at the holding temperature during the thermal fatigue and hydrothermal shock cycles [Ray B.C., 2005]. In the other hand the inter-laminar shear strength (ILSS) of the thermally conditioned glass fibers of random orientation and epoxy resin laminates followed by ice-cold water quenching from the laminated composite was exposed to (50˚C) temperature and hydrothermal fatigue cycles varied weight fraction constituents of glass fiber reinforced (55,60, 65%), [Ray B.C., 2005], but in the field of cryogenic [Ray B.C., 2005] studied the effect for 55,60, and 65 weight percentages of E-glass fibers reinforced epoxy composites on inter-laminar shear strength during (sub-ambient) at -80˚C temperature in ultra low freezing chamber for 2 hours and subjected to an ambient at 30˚C temperature for 1 hour and investigate the effect of thermal shock on flexural modulus of Kevlar 49/epoxy laminates by thermally conditioned at a (80˚C) for (5, 10, and 20 min) to (-80˚C) for (5 min) or cryogenically conditioned at (-80˚C) for the same time periods to (80˚C) for (5 min). In the present work it can study the effect of combined loadings on the deflection combining with thermal fatigue effect of composite laminate plate.

So that the objectives of this research are:

- In dynamic analysis derive the analytical solution to evaluate the stress-strain field and inter-laminar shear stress (ILSS) distributions for middle point using Levy solution for thermal cyclic under combined loadings.
- It will be compared the results of deflection in z-direction for middle point were obtained from thermal cyclic loading only with that obtained from (cyclic thermal loading + M_o), (cyclic thermal loading +N_{xx}) and (cyclic thermal loading +$M_o + N_{xx}$) as mentioned in Fig. (1) to obtain perfect design of deflection.
- Applying different boundary conditions like (SSSS, CSSS, and CSCS) on composite plate under cyclic thermal loading.

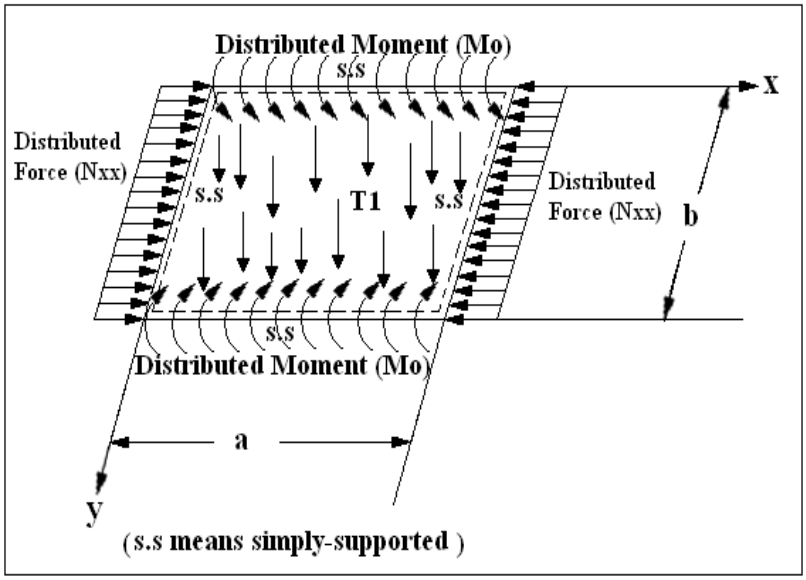

Fig. (1) Plate under thermal and combined loading.

THE CLASSICAL LAMINATED PLATE THEORY (CLPT)

The classical laminate plate theory gives flexibility than the other methods of solution for composite plate depending upon the cyclic thermal loading, in-plane force(N_{xx}), and the bending moment (M_o).

The stress and strain variation through the laminate thickness based on the classical lamination theory (CLPT) includes the following assumptions, [Reddy J.N. 2004]:

- Transverse normal stresses remain straight before and after deformation (strain in z- direction equal to zero).
- Transverse normal stresses rotate and perpendicular to the mid-surface after deformation (strain in xz and yz plane equal to zero).

DISPLACEMENTS KINETIC RELATIONS

If a plate was established of a total thickness (h) composed of (N) orthotropic layers with the principal material coordinates (x_1^k, x_2^k, x_3^k) of the *k*th lamina oriented at an angle θ_k to the laminate coordinate, *x*. The *z*-axis is taken positive downward from the mid plane. The kth layer is located between the points $z = z_k$ and $z = z_{k+1}$ in the thickness direction. The *Kirchhoff hypothesis* theory used instead of *Mendlin* theory by applying the principles of supper position displacements $(u, v, w)$to be such that, [Reddy J.N. 2004] :

$$u(x,y,z,t) = u_o(x,y,t) - z * \frac{\partial w_o}{\partial x}$$

$$v(x,y,z,t) = v_o(x,y,t) - z * \frac{\partial w_o}{\partial y} \quad (1)$$

$$w(x,y,z,t) = w_o(x,y,t)$$

Where:

(u_o, v_o, w_o) : A displacements along the coordinate lines of a materials point on the *x*,*y*-plane. The strain-displacement matrix relations take the form, [Reddy J.N. 2004]:

$$\begin{Bmatrix} \varepsilon_{xx} \\ \varepsilon_{yy} \\ \gamma_{xy} \end{Bmatrix} = \begin{Bmatrix} \varepsilon_{xx}^{(0)} \\ \varepsilon_{yy}^{(0)} \\ \gamma_{xy}^{(0)} \end{Bmatrix} + z * \begin{Bmatrix} \varepsilon_{xx}^{(1)} \\ \varepsilon_{yy}^{(1)} \\ \gamma_{xy}^{(1)} \end{Bmatrix}$$ where:

$$\{\varepsilon^{(0)}\} = \begin{Bmatrix} \varepsilon_{xx}^{(0)} \\ \varepsilon_{yy}^{(0)} \\ \gamma_{xy}^{(0)} \end{Bmatrix} = \begin{Bmatrix} \frac{\partial u_o}{\partial x} \\ \frac{\partial v_o}{\partial y} \\ \frac{\partial u_o}{\partial y} + \frac{\partial v_o}{\partial x} \end{Bmatrix} \quad (2)$$

$$\{\varepsilon^{(1)}\} = \begin{Bmatrix} \varepsilon_{xx}^{(1)} \\ \varepsilon_{yy}^{(1)} \\ \gamma_{xy}^{(1)} \end{Bmatrix} = \begin{Bmatrix} -\frac{\partial^2 w_o}{\partial x^2} \\ -\frac{\partial^2 w_o}{\partial y^2} \\ -2 * \frac{\partial^2 w_o}{\partial x \partial y} \end{Bmatrix}$$

For orthotropic material and layers axes oriented arbitrarily with respect to the laminate coordinates. The Hook's Law relations are [Reddy J.N. 2004]:

$$\{\sigma\}_k = \left[\overline{Q}\right]_k \{\varepsilon\}_k$$

$$\begin{Bmatrix}\sigma_{xx}\\ \sigma_{yy}\\ \sigma_{xy}\end{Bmatrix}^{k}=\begin{bmatrix}\bar{Q}_{11} & \bar{Q}_{12} & \bar{Q}_{16}\\ \bar{Q}_{12} & \bar{Q}_{22} & \bar{Q}_{26}\\ \bar{Q}_{16} & \bar{Q}_{26} & \bar{Q}_{66}\end{bmatrix}*\left(\begin{Bmatrix}\varepsilon_{xx}\\ \varepsilon_{yy}\\ \gamma_{xy}\end{Bmatrix}-\begin{Bmatrix}\alpha_{xx}\\ \alpha_{yy}\\ 2*\alpha_{xy}\end{Bmatrix}*\Delta T\right) \quad (3)$$

And for especially orthotropic (that the material axes coincide with respect to laminates coordinates).

$$\begin{Bmatrix}\sigma_{xx}\\ \sigma_{yy}\\ \sigma_{xy}\end{Bmatrix}^{k}=\begin{bmatrix}Q_{11} & Q_{12} & 0\\ Q_{12} & Q_{22} & 0\\ 0 & 0 & Q_{66}\end{bmatrix}*\left(\begin{Bmatrix}\varepsilon_{xx}\\ \varepsilon_{yy}\\ \gamma_{xy}\end{Bmatrix}-\begin{Bmatrix}\alpha_{1}\\ \alpha_{2}\\ 0\end{Bmatrix}*\Delta T\right) \quad (4)$$

Anyhow in Levy solution (dynamic analysis) the classical laminate plate theory (CLPT) is more suitable than other methods because it is linking the cyclic thermal loading with the combined loadings.

Methodology Discussions of Theoretical and Numerical Experiences

For thermal cyclic analysis the inputs in classical laminate plate theory program can be shown in Table (1):

Table (1) The inputs in classical laminate plate theory program.

a = 0.18 m
b = 0.1 m
x = 0.09 m
y = 0.05 m
z = 0.001667 m
h = 0.004 m
$T_1 = 7500 * \sin(\omega * t)\ \frac{^{\circ}C}{m}$ for heating
$T_1 = -1875 * \sin(\omega * t)\ \frac{^{\circ}C}{m}$ for cooling

It can be taken the algebraic sum of stress field in (x, y, z) directions and deflection in z-direction for heating and cooling. Table (2) shows the verification test for dynamic analysis under

different thermal loading of fiber volume fraction ($\upsilon_f = 0.25076\ \%$) using (Fortran 90 and ANSYS Ver. 9) programs for the plate having aspect ratio (1.8). The four types of combined loading can be used in this section: (Thermal Fatigue), (Thermal Fatigue +Mo), (Thermal Fatigue +Nxx) and (Thermal Fatigue +Mo+Nxx) as mentioned in Figure (1), used (**SHELL 132**) as given in Fig. (2). It has a three-dimensional layered shell element having in-plane and thru-thickness thermal conduction capability. The element has eight nodes with up to 32 temperature degrees of freedom at each node. The conducting shell element is applicable to a three-dimensional, steady-state or transient thermal analysis.

"SHELL 132" was switched element and to be analyzed structurally, the element should replaced by an equivalent structural element such as **" SHELL 91"**. It is used for layered application of a structural shell model up to 100 different layers. The element is defined by eight nodes having six degrees of freedom at each node: translation in the nodal x, y, and z directions and rotation in the nodal x, y, and z directions to evaluate the stress field and deflection in z-direction.

A triangular-shaped element may be formed by defining the same node number. After solving the four types of combined loadings it can be compared the last three type results with first type results to obtain the perfect design of this paper. It can be used both program of finite element analysis to find the deflection and dynamic load factor (D.L.F) which cannot applied this on different fiber volume fractions because absence the knowledge of the number of layers that gives the mass of fiber experimentally. The dynamic load factor in $(T_1 = -15\ ^\circ c)$ is higher than the dynamic load factor in $(T_1 = 60\ ^\circ c)$ because the central static deflection in $(T_1 = -15\ ^\circ c)$ is smaller than the deflection in $(T_1 = 60\ ^\circ c)$ and the percentage error is acceptable on different thermal loadings.

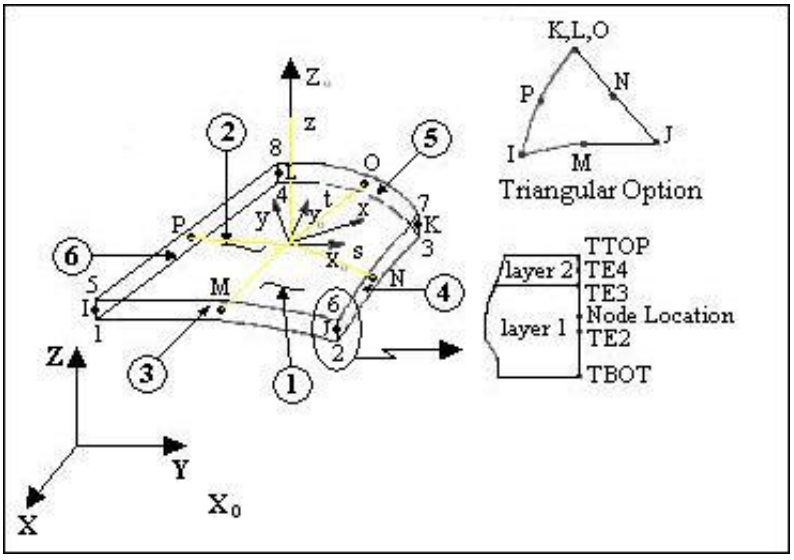

Fig. (2) SHELL 132 3-D thermal shell element.

RESULTS AND DISCUSSIONS

Table (2) estimates the verification test for composite laminate plate under different combined loadings of $(\upsilon_f = 25.076\%)$ for the plate having aspect ratio (1.8). The best case is (thermal cyclic + in-plane force N_{xx}) because the deflection is smaller than the other cases; but the percentage error in (thermal cyclic + in-plane force N_{xx}) and (thermal cyclic+ bending moment M_o + in-plane force N_{xx}) is not accurate because the (ANSYS 9) is the approximate solution. It can be shown the dynamic deflection decrease with the increasing of fiber volume fraction. The dynamic (Fortran 90) program is described in Fig. (3).

Table (2) Verification test for composite laminate plate under different combined loadings of $\upsilon_f = 25.076\%$.

Deflection (m)			
Deflection Field	CLPT	ANSYS Ver.9	Percentage Error (%)
Thermal Cyclic + Bending Moment M_o	-0.1777704 E-3	-0.18819 E-3	5.5367%
Thermal Cyclic + In-Plane Force N_{xx}	-0.7704258 E-6	-0.65088 E-6	15.5168%
Thermal Cyclic + Bending Moment M_o + In-Plane Force N_{xx}	-1.97185 E-5	-1.6735 E-5	15.1304%

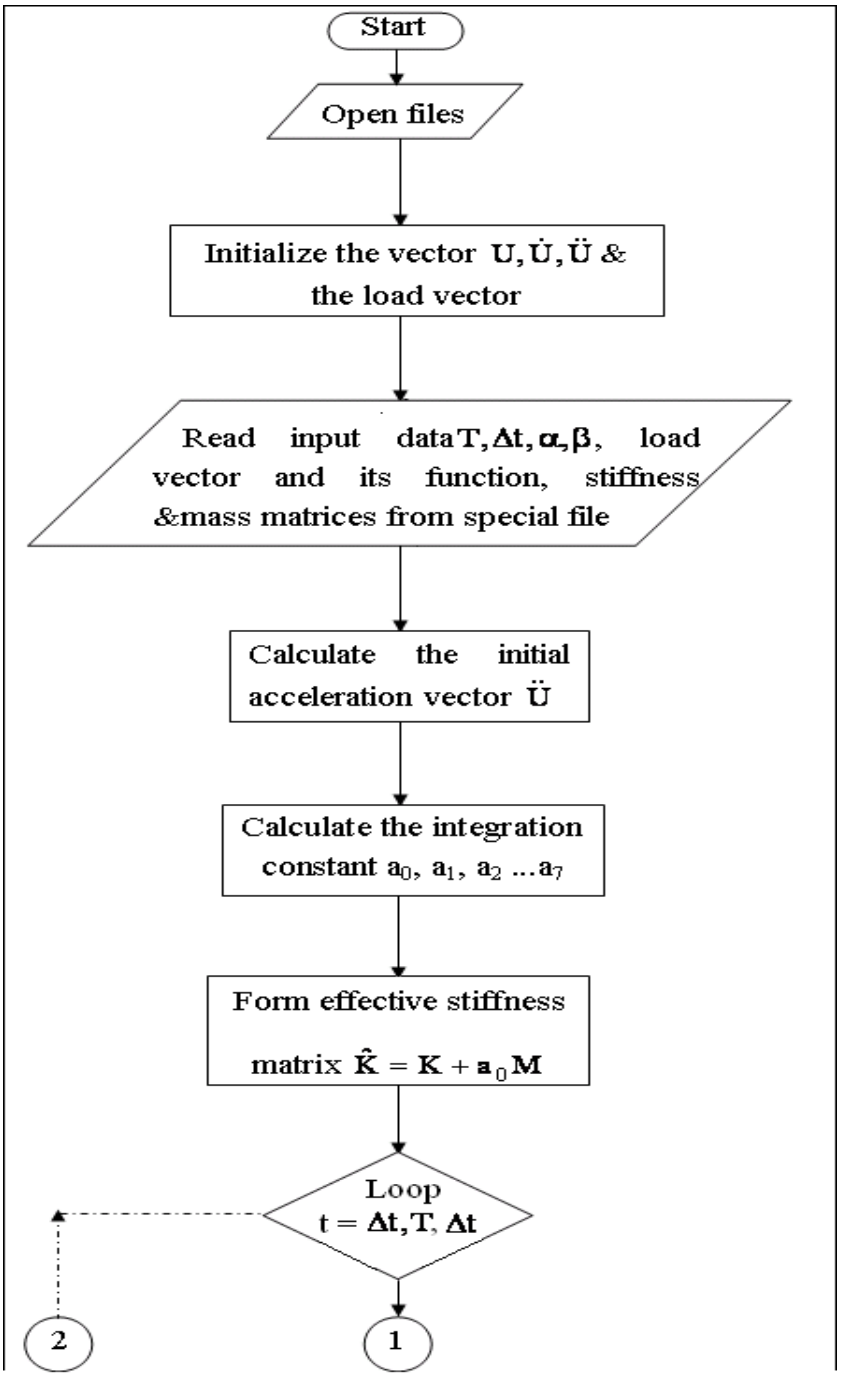
Start
Open files
Initialize the vector U, U̇, Ü & the load vector
Read input data T, Δt, α, β, load vector and its function, stiffness &mass matrices from special file
Calculate the initial acceleration vector Ü
Calculate the integration constant a_0, a_1, a_2 ... a_7
Form effective stiffness matrix $\hat{K} = K + a_0 M$
Loop
t = Δt, T, Δt
2
1

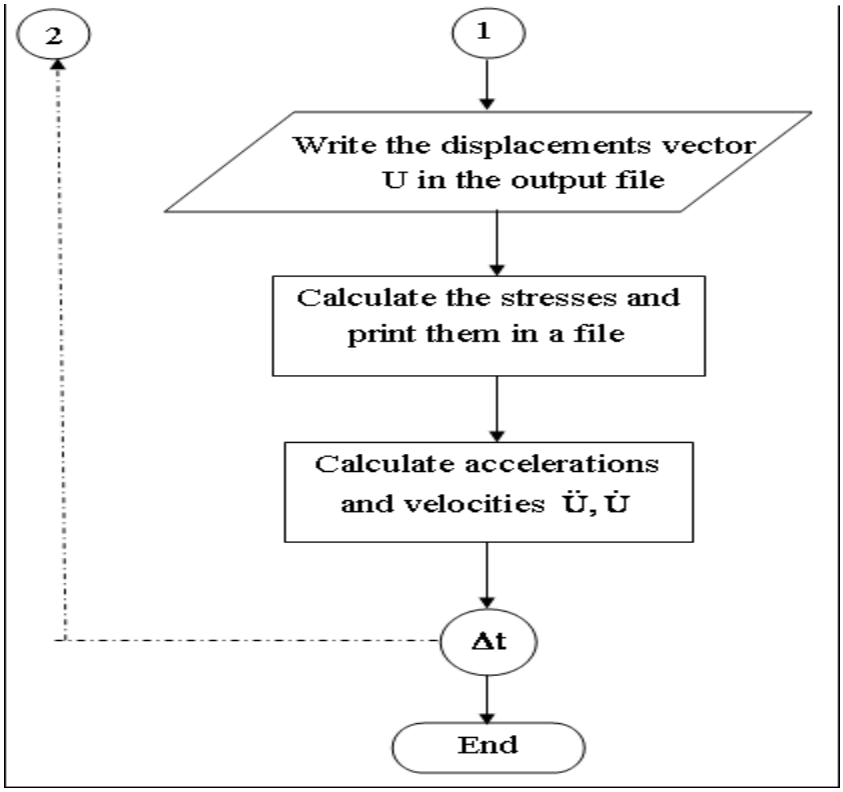

Fig. (3) Flow chart of the dynamic program, [Abdulla F.A. 2001].

Tables (3, 4, 5) show the effect of different fiber volume fractions and different loading percent of combined loading on deflection. In Tables (3, 5) the deflection can be decreased with the increasing of fiber volume fractions for all the increasing of loading percent; but the deflection can be increased with the increasing of loading percent for the same fiber volume fraction. In Table (3) the deflection still constant with the increasing of loading percent of combined loading for the same fiber volume fraction; but the deflection can be decreased with the increasing of fiber volume fractions.

Table (3) Effect of different fiber volume fractions and different load percents of (M_o) on deflection due to thermal cyclic + bending moment(M_o) of aspect ratio (a/b = 1.8).

Deflection (m) * 10^{-3}						
v_f % / Loading Percent of (M_o)	25.076%	40%	50%	60%	70%	80%
20%	-0.0379	-0.02876	-0.02393	-0.01964	-0.01562	-0.01176
40%	-0.07552	-0.05723	-0.04762	-0.03909	-0.03110	-0.02343
60%	-0.11308	-0.08570	-0.07131	-0.05855	-0.04658	-0.03511
80%	-0.15064	-0.11417	-0.09500	-0.07800	-0.06206	-0.04679
100%	-0.18819	-0.14264	-0.1187	-0.09746	-0.07754	-0.05846

Table (4) Effect of different fiber volume fractions and different load percents of (N_{xx}) on deflection due to thermal cyclic + in-plane force(N_{xx}) of aspect ratio (a/b = 1.8).

Deflection (m) * 10^{-6}						
v_f %						
Loading Percent of (N_{xx})	25.076%	40%	50%	60%	70%	80%
20%	-0.65088	-0.48393	-0.39026	-0.3046	-0.22426	-0.14865
40%						
60%						
80%						
100%						

Table (5) Effect of different fiber volume fractions and different load percents of $(M_o \& N_{xx})$ on deflection due to thermal cyclic + bending moment(M_o) + in-plane force (N_{xx}) of aspect ratio (a/b = 1.8).

Deflection (m) * 10^{-4}						
v_f %						
Loading Percent of $(M_o \& N_{xx})$	25.076%	40%	50%	60%	70%	80%
20%	-0.035661	-0.027356	-0.022759	-0.018561	-0.014572	-0.01063
40%	-0.068584	-0.052545	-0.043756	-0.035767	-0.028189	-0.02069
60%	-0.10151	-0.077733	-0.064753	-0.052973	-0.041805	-0.03075
80%	-0.13443	-0.10292	-0.085751	-0.07018	-0.055421	-0.040811
100%	-0.16735	-0.12811	-0.10675	-0.087386	-0.069038	-0.05086

Figs. (4, 5) show the convergence of dynamic central deflection with total degree of freedom. There is a small sudden change increasing in dynamic deflection occurring between numbers of degree-of-freedom (DOF) 81 and 2187 which then reached the steady-state case between numbers of degree-of-freedom (DOF) 2187 and 27783 for different fiber volume fractions for ($T_1 = 60°_C$ and $T_1 = -15\ °_C$).

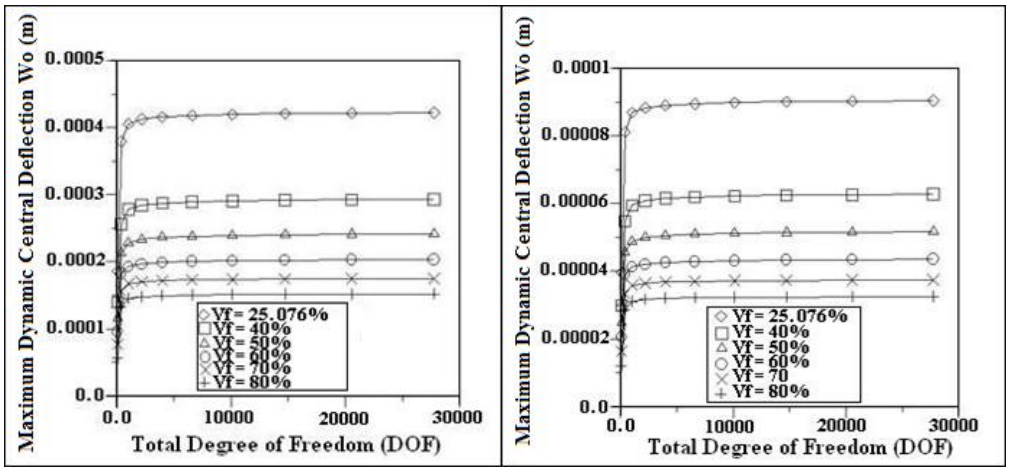

Fig. (4) Convergence of dynamic central deflection with total degree of freedom under $(T_1 = 60\ ^\circ_C)$.

Fig. (5) Convergence of dynamic deflection with total degree of freedom under $(T_1 = -15\ ^\circ_C)$.

Figs. (6, 7) give the convergence of dynamic load factor (D.L.F) with total degree of freedom. There is a large sudden change increasing in dynamic load factor occurring between numbers of degree-of-freedom (DOF) 81 and 14739 which then reached the steady-state case between numbers of degree-of-freedom (DOF) 14739 and 27783 for different fiber volume fractions for ($T_1 = 60^\circ_C$ and $T_1 = -15\ ^\circ_C$). It can be noticed that the dynamic load factor decreased with the increasing of fiber volume fractions, while the fiber volume fractions increased with the increasing of fundamental natural frequency, then the dynamic load factor will be decreased.

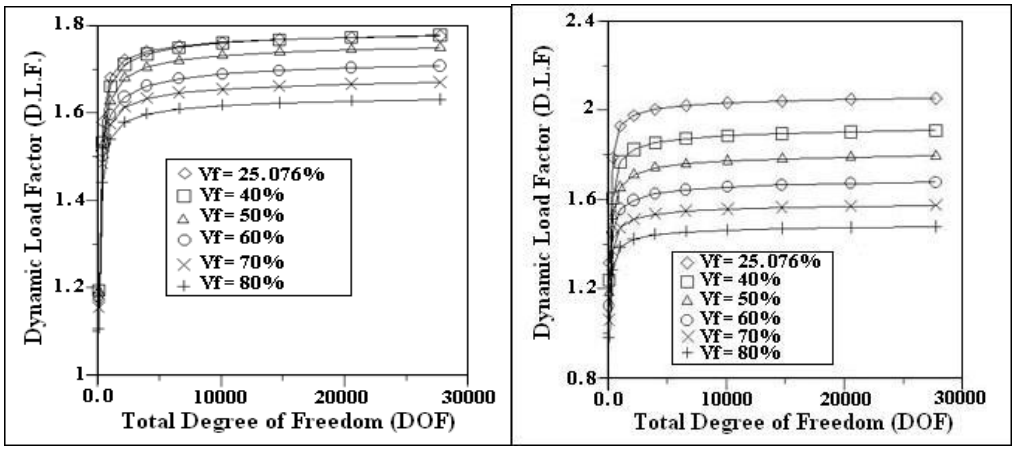

Fig. (6) Convergence of dynamic load factor with total degree of freedom under $(T_1 = 60\ ^\circ_C)$.

Fig. (7) Convergence of dynamic load factor with total degree of freedom under $(T_1 = -15\ ^\circ_C)$.

Figs. (8, 9) illustrate the effect of different fiber volume fractions on dynamic central deflection under thermal loadings ($T_1 = 60^\circ_C$ and $T_1 = -15\ ^\circ_C$) with time. Most of these curves reached to the steady-state case at time = 0.004 (settling time) and the dynamic deflection decreased with the increasing of fiber volume fractions. The best curve is the curve at fiber volume fraction ($\upsilon_f = 0.8$) because it reaches to the rise time first that is mean this curve has low value of rise time, settling time, and overshoot because increasing the fiber volume fractions causing increase in the value of fundamental natural frequency.

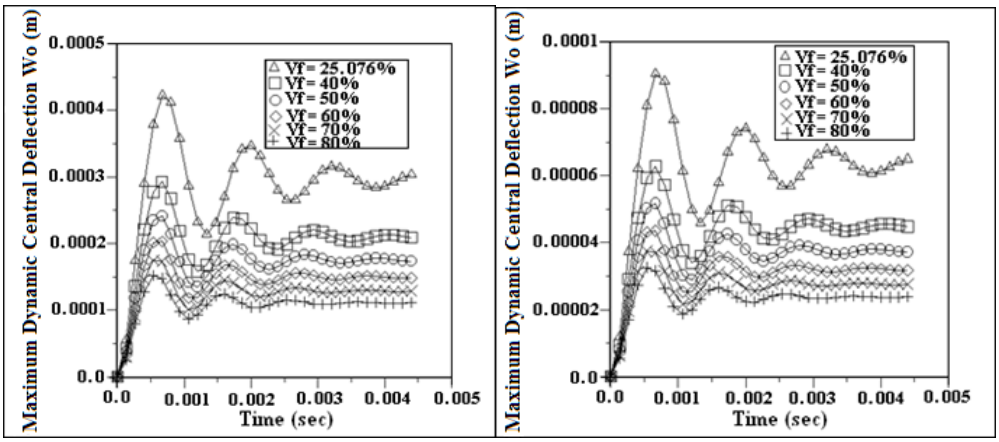

Fig. (8) Dynamic deflection variation with time under different fiber volume fractions of ($T_1 = 60\ ^\circ_C$).

Fig. (9) Dynamic deflection variation with time under different fiber volume fractions ($T_1 = -15\ ^\circ_C$).

Fig. (10) shows convergence of dynamic deflection with total degree of freedom under different combined loadings of $\upsilon_f = 25.076\%$ for simply supported plate with four edges. For the curve concern (thermal cycling + M_o) there is a large sudden change increasing in dynamic deflection occurring between numbers of degree-of-freedom (DOF) 390 and 4998 which then reached the steady-state case between numbers of degree-of-freedom (DOF) 4998 and 7686; but the curve concern (thermal cyclic + $M_o + N_{xx}$) there is a slow increasing of dynamic deflection occurring between numbers of degree-of-freedom (DOF) 390 and 1350 which then reached the steady-state case between numbers of degree-of-freedom (DOF)1350 and 7686. The curve concern (thermal cyclic + N_{xx}) there is no clear change in dynamic deflection with numbers of degree-of-freedom (DOF).

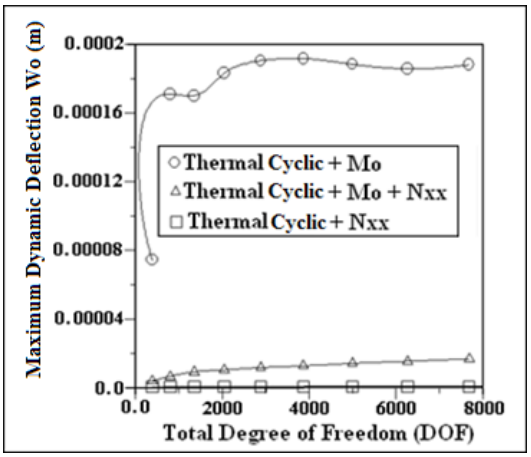

Fig. (10) Convergence of dynamic deflection with total degree of freedom under combined loadings of $(T_1 = -15\ ^{\circ}C)$.

Figs. (11, 12, 13) illustrate the effect of different fiber volume fractions on dynamic deflection with total degree of freedom for (thermal cyclic + M_o), (thermal cyclic + N_{xx}), and (thermal cyclic + $M_o + N_{xx}$) with a plate with aspect ratio (1.8) of simply supported plate with four edges; therefore the best curve is the curve of $v_f = 80\%$ for (thermal cyclic + N_{xx}) because this curve gives a small value of dynamic deflection equal to (0.22426 e-6).

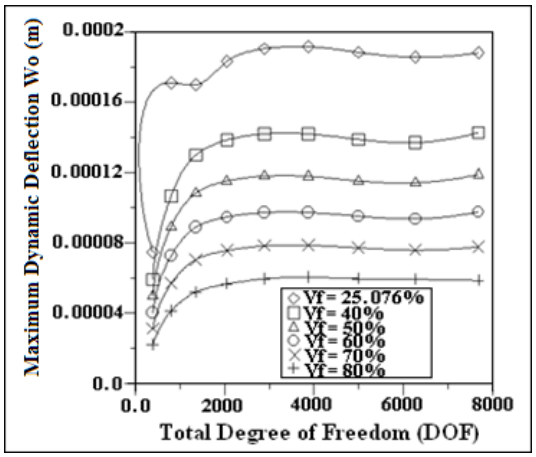

Fig. (11) Convergence of dynamic deflection with total degree of freedom under thermal cyclic + bending moment (M_o) for different fiber volume fractions.

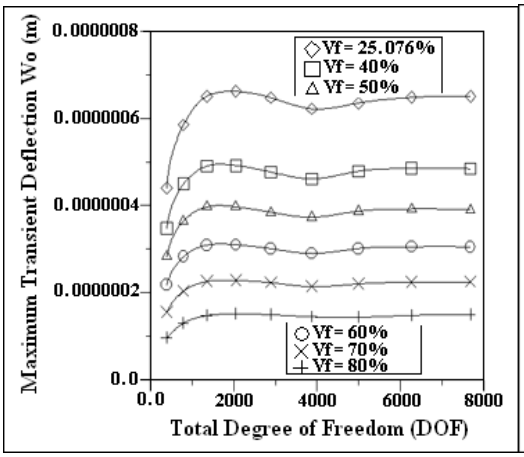

Fig. (12) Convergence of dynamic deflection with total degree of freedom under thermal cyclic + in-plane force (N_{xx}) for different fiber volume fractions.

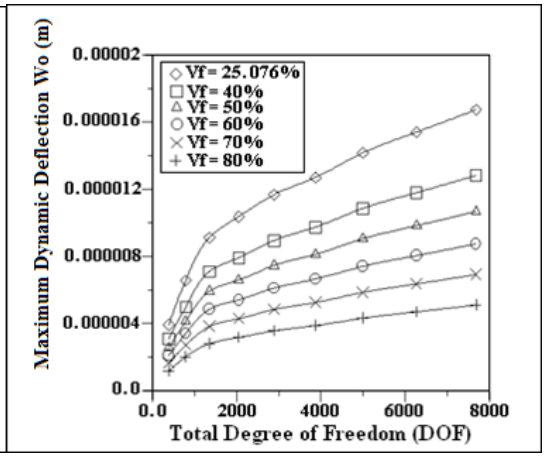

Fig. (13) Convergence of dynamic deflection with total degree of freedom under thermal cyclic + bending moment (M_o) + in-plane force (N_{xx}) for different fiber volume fractions.

Fig. (14) shows comparisons between analytical solution (CLPT) and numerical solution (FEM) with the experimental published work [RayB.C.,2005] of $\upsilon_f = 25.076\%$ under thermal cyclic loading for the plate having aspect ratio (1.8) that concern inter-laminar shear stress varies with time. It can be noticed that the inter-laminar shear stress varies sinusoidal for both experimental and numerical solutions; but for analytical solution the inter-laminar shear stress reduced with time gradually because it applied via Levy solution on analytical part.

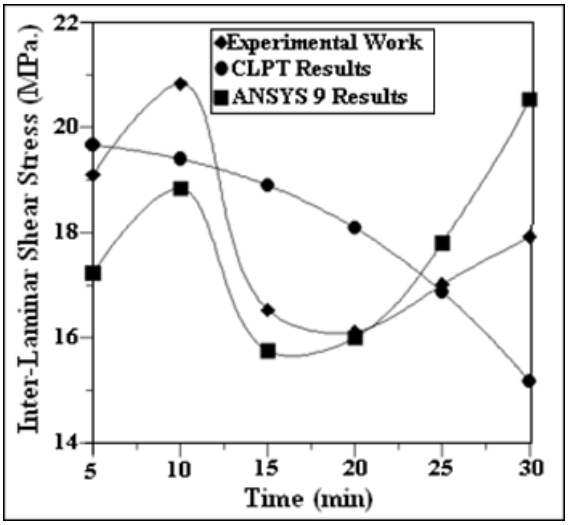

Fig. (14) Comparisons of inter-laminar shear stress varies with time under the effect of thermal cyclic of $\upsilon_f = 25.076\%$.

Fig. (15) gives the effect of different boundary conditions like (SSSS, CSSS, and CSCS) on inter-laminar shear stress varying with time of $\upsilon_f = 25.076\%$ using classical laminate plate theory (CLPT) for the plate having aspect ratio (1.8). The inter-laminar shear stress can be decreased with the increasing of time for all three curves; but the best curve that curve concern (CSCS) boundary condition this curve gives small value of inter-laminar shear stress because to reduce the mismatch between the thermal expansions of the resin and the fiber can be caused the thermal cyclic loading.

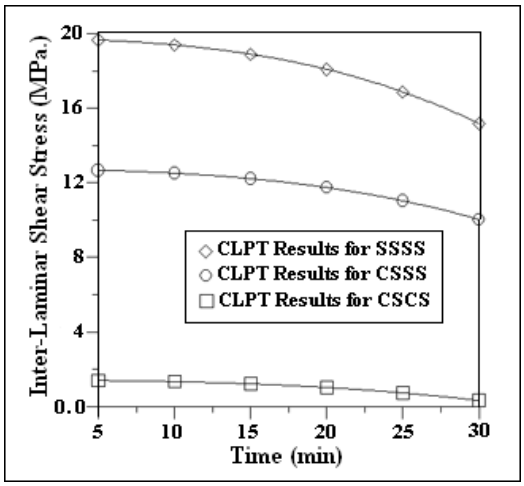

Fig. (15) Effect of different boundary conditions on inter-laminar shear stress varies with time of $\upsilon_f = 25.076\%$ under thermal cyclic loading.

Fig. (16) show the effect of different boundary conditions like (SSSS, CSSS, and CSCS) on central deflection varies with time of $\upsilon_f = 25.076\%$ using classical laminate plate theory (CLPT) for the plate having aspect ratio (1.8). The curve concern the boundary condition (SSSS) decreased with time; but the curve concern the boundary condition (CSSS, CSCS) have its value the minus sign because the particle's compression of composite laminate plate leads to concave upward occur in deflection direction due to this boundary condition. The conclusion of this minus sign the increasing of fixed or clamped edges gives increasing in concave upward instead of downward central deflection under thermal cyclic loading.

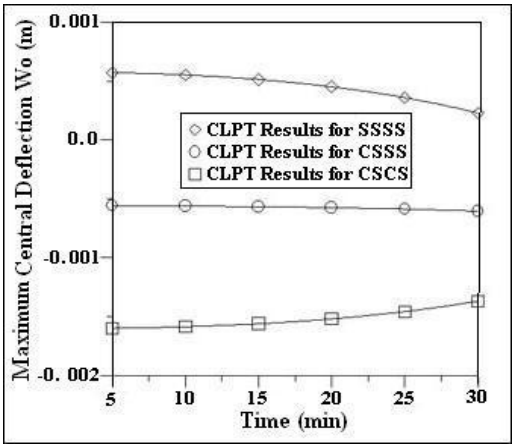

Fig. (16) Effect of different boundary conditions on central deflection varies with time of $\upsilon_f = 25.076\%$ under thermal cyclic loading.

Figs. (17, 18) illustrate the effect of different boundary conditions like (SSSS, CSSS, CSCS) on normal stresses in the (x, y) directions varies with time of $\upsilon_f = 25.076\%$ under thermal cyclic loading using classical laminate plate theory (CLPT) for the plate having aspect ratio (1.8). In the two figures, the curves have (SSSS, CSSS) boundary conditions that the normal stresses decreasing with the increasing of time because the most value of coefficient of thermal expansion decreased with time and that effect on the decreasing of normal stresses; but the positive sign of the value of normal stresses because of the case of the particle of composite laminate plate is tension due to these boundary conditions. The curve (CSCS) boundary condition casing decrease in the value of normal stress with time increasing; but the negative sign because of the particle of composite plate suffer from compression. The conclusion of these curves the increasing in the clamped or fixed edges causing increasing in particle's compression.

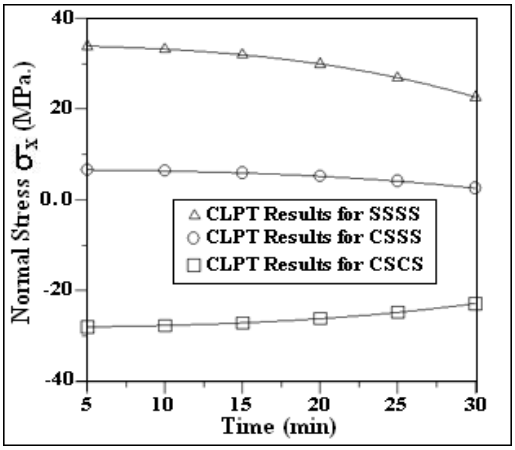

Fig. (17) Effect of different boundary conditions on normal stress (σ_x) varies with time of $\upsilon_f = 25.076\%$ under thermal cyclic loading.

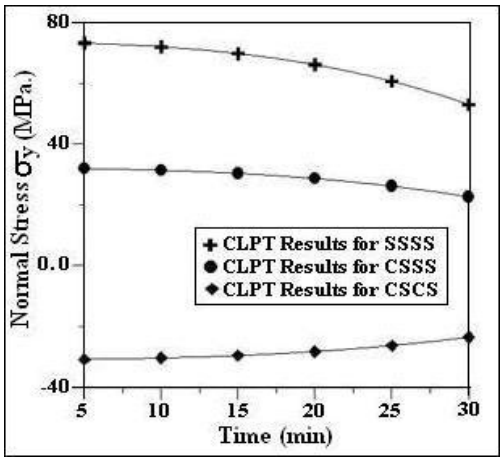

Fig. (18) Effect of different boundary conditions on normal stress (σ_y) varies with time of $\upsilon_f = 25.076\%$ under thermal cyclic loading.

Figs. (19, 20) show the effect of different boundary conditions on normal strain in the (x, y) directions varies with time of $\upsilon_f = 25.076\%$ under thermal cyclic loading using classical laminate plate theory (CLPT) for the plate having aspect ratio (1.8). The comment is the same as in Figs. (17, 18) because the stress is equal the multiplication of strain on material properties matrices and the positive, negative sign because the expansion and contraction on the particles of composite laminate plate.

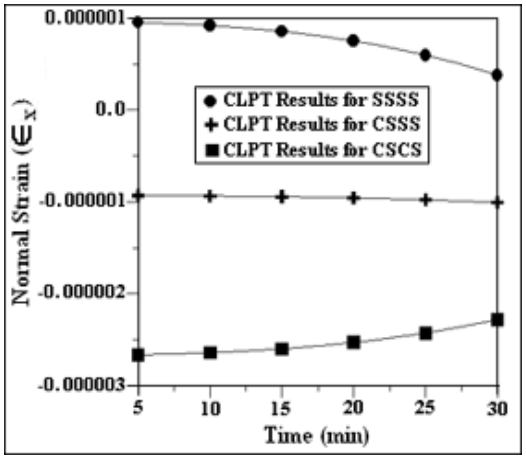

Fig. (19) Effect of different boundary conditions on normal strain (ε_x) varies with time of $\upsilon_f = 25.076\%$ under thermal cyclic loading.

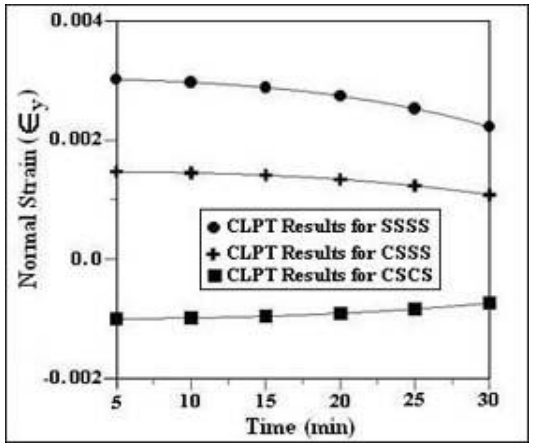

Fig. (20) Effect of different boundary conditions on normal strain (ε_y) varies with time of $\upsilon_f = 25.076\%$ under thermal cyclic loading.

CONCLUSIONS

This research conclude from its obtaining results under dynamic load (free vibration and dynamic response) of fiber-reinforced laminated plates comparing with analytical work, FEM and other investigations using different numerical and theoretical methods as follow :

- the maximum dynamic central deflection is decreased with the increasing of different fiber volume fractions of heating and cooling and that due to due to the increasing of the value of natural frequency (free vibration analysis) for both thermal loadings ($T_1 = 60°_C$ and $T_1 = -15\ °_C$).
- the increasing of fiber volume fractions causing decreasing in overshoot percent, rise time, and settling time; but all the plate with different fiber volume fractions have the same settling time and reached to the steady-state at the same time.
- The test of inter-laminar shear stress that the inter-laminar shear stress varies sinusoidal for both experimental, [3] and numerical solutions; but for analytical solution the inter-laminar shear stress reduced with time gradually.
- The effect of different percent of combined loadings and different fiber volume fractions on deflection. In the case of (thermal cyclic + M_o) and (thermal cyclic + $M_o + N_{xx}$) the deflection can be decreased with the increasing of fiber volume fractions for all the increasing of combined loadings percent; but the deflection can be increased with the increasing of loading percent for the same fiber volume fraction; but the deflection still constant with the increasing of loading percent of combined loading for the same fiber volume fraction for (thermal cyclic + N_{xx}).

REFERENCES

- Abdel A. Fabmy and Tbomas G. Cunningbam," Investigation of Thermal Fatigue in Fiber Composite Materials", National Aeronautics and Space Administration, WASHINGTON, July, 1976.

- B.C.Ray," Thermal Shock and Thermal Fatigue on Delamination of Glass Fiber Reinforced Polymeric Composites", Journal of Reinforced Plastics and Composites, Vol.24, No.1, 2005.

- B.C,RAY," Hydrothermal Shock Cycles on Shear Strength of Glass Fiber-Polyester Composites", Journal of Reinforced Plastics and Composites, Vol. 24, No. 12, 2005.

- B.C,RAY," Effect of thermal shock on interlaminar strength of thermally aged glass fiber reinforced epoxy composites", Journal of Applied Polymer Science, 2005.

- B.C.Ray," Hydrothermal Fatigue on Interface of Glass-Epoxy Laminates", Journal of Reinforced Plastics and Composites, Vol.24, No.10, 2005.

- B.C,RAY, " Loading rate sensitivity of glass fiber-epoxy composite at ambient and sub-ambient temperatures", Journal of Reinforced Plastics and Composites, 2005.

- B.C,RAY, "Effect of thermal shock on flexural modulus of thermally and cryogenically conditioned kevlar/epoxy composites", Journal of Advanced Composites Letters, Vol.14, No.2, 2005.

- Carlo A.Ginty and Christos C.Chamis," Hygrothermomechanical Fiber Composite Fatigue: Computational Simulation", NASA Technical Memorandum 100840, March, 1988.

- Fadhel Abbas Abdulla," Analysis of Composite Plate Subjected to Impact Load", M.Sc. Thesis, AL-Mustansiriyah University, Mechanical Engineering Department, March, 2001.

- J.N. Reddy," Mechanics of Laminated Composite Plates and Shells", Second Edition, 2004.

SYMBOLS

English Letters

a	Large Span of Rectangular Plate (Length)
b	Small Span of Rectangular Plate (Breadth)
CSSS	Plate Subjected To Clamped-Simply-Simply-Simply Supported Boundary Condition

CSCS	Plate Subjected To Clamped-Simply-Clamped-Simply Support Boundary Condition
h	Thickness of Rectangular Plate
ILSS	Inter-Laminar Shear Strength
M_o	Bending Moment Per Unit Length Applied In y-Direction Of The Plate
N_{xx}	In-Plane Direct And Shear Forces
$\overline{Q}_{ij}$	Transformed Reduced Stiffness Elements
SSSS	Plate Subjected To Simply-Simply-Simply-Simply Supported Boundary Condition
T_1	Gradient Uniform Temperature
u_o, v_o	Extensional Displacement Components In The 2-D Coordinate System
u, v, w	Displacement Components In The 3-D Coordinate System
w_o	Mid-Plane Deflection Along z-Direction
x, y, z	The Cartesian Coordinate System
z_k, z_{k+1}	Upper & Lower Lamina Surfaces Coordinates Along z-Direction

Greek Letters

$\alpha_x, \alpha_y, \alpha_{xy}$	Direct And Shear Coefficient Of Thermal Expansion Respectively
ΔT	Temperature Variation Through Laminate Thickness
θ	Orientation Angle From x-Axis
υ_f	Fiber Volume Fraction
$\begin{Bmatrix} \varepsilon_{xx} \\ \varepsilon_{yy} \\ \gamma_{xy} \end{Bmatrix}$	Cartesian Strain Vector
$\begin{Bmatrix} \sigma_{xx} \\ \sigma_{yy} \\ \sigma_{xy} \end{Bmatrix}$	Cartesian Stresses Field Vector

NUMERICAL AND EXPERIMENTAL INVESTIGATION OF STEAM FILM CONDENSATION ON A VERTICAL TUBE

Wail S. Sarsam
Mech. Eng. Dept.
College of Engineering
University of Baghdad
Baghdad-Iraq

Luma F. Ali
Mech. Eng. Dept.
College of Engineering
University of Baghdad
Baghdad-Iraq

ABSTRACT

Film condensation of steam on a vertical tube is investigated numerically and experimentally, in the present work. A mathematical model was set based on the basic conservation laws of mass and energy, Nusselt′s analysis of film condensation, and empirical equations available in the literature. Then, a simulation program in FORTRAN language was developed which simulates the film condensation of steam on a vertical tube. A complete steam tables subprogram was also developed and incorporated with the main program. The experimental work was carried out using a steam condensation test bench. The inlet and outlet cooling water temperatures, steam temperature and pressure, tube surface temperature at center, and cooling water flow rate are recorded during each experimental test run. The inlet cooling water temperature, steam temperature, and cooling water flow rate are used as an input for the numerical program, then the program calculates tube surface temperature distribution, cooling water temperature distribution, local heat transfer rate, local condensation heat transfer coefficient, condensate boundary layer thickness distribution, total heat transfer rate, and average condensation heat transfer coefficient. The effect of various parameters on the condensation heat transfer coefficient, such as steam temperature, steam-surface temperature difference, and the presence of non-condensable gas were investigated and reported graphically. It was found that increasing (steam-surface) temperature difference while keeping the steam temperature constant results in an increase in condensate boundary layer thickness, which in turn causes a decrease in condensation heat transfer coefficient. On the other hand, increasing steam temperature and keeping the (steam-surface) temperature difference constant leads to an increase in condensation heat transfer coefficient. In addition, the presence of non-condensable gas with different concentrations was also investigated and it was shown that it causes a noticeable reduction in the average condensation heat transfer coefficient. An equation for calculating average condensation heat transfer coefficient on a vertical tube was also developed. The experimental data obtained from the test runs were compared with numerical results and showed good agreement. Thus, it can be concluded that the present computational program is suitable for simulating steam condensation on a vertical tube.

الخلاصة

تمت دراسة تكثف بخار الماء الغشائي على انبوب عمودي، عددياً وعملياً، في البحث الحالي. تم وضع النموذج الرياضي بالاستناد الى قوانين الحفظ الأساسية للكتلة والطاقة وباستعمال معادلات تجريبية متوفرة في الأدبيات المنشورة. تم اعداد نموذج رياضي مستند على قوانين الحفظ الأساسية للكتلة والطاقة، تحليل نسلت للتكثف الغشائي، ومعادلات تجريبية متوفرة في الأدبيات المنشورة. ومن ثم اعداد برنامج محاكاة بلغة الفورتران لنمذجة تكثف بخار الماء الغشائي على إنبوب عمودي. كذلك تم بناء برنامج

فرعي لحساب خواص بخار الماء ودمجه مع البرنامج الرئيسي. العمل التجريبي نفذ باستعمال منصة إختبار تكثف بخار الماء. إن درجتي حرارة الدخول والخروج لماء التبريد, درجة حرارة وضغط بخار الماء، درجة حرارة إلانبوب السطحيّة في المركز، و نسبة تدفق ماء التبريد قد سجلت أثناء كل تشغيل إختباري عملي. لقد تم استخدام كل من درجة حرارة الدخول لماء التبريد، درجة حرارة بخار الماء، ونسبة تدفق ماء التبريد كمدخلات للبرنامج العددي، ثم يقوم البرنامج بحساب توزيع درجة حرارة سطح الإنبوب ، توزيع درجة حرارة ماء التبريد، معدل انتقال الحرارة الموضعي، معامل انتقال الحرارة الموضعي بالتكثف, توزيع سمك طبقة السائل المتكثف المتاخمة، معدل انتقال الحرارة الكلي، ومعامل انتقال الحرارة المتوسط بالتكثف. تمت دراسة تأثير العوامل المختلفة على معامل انتقال الحرارة بالتكثف، مثل درجة حرارة البخار، الإختلاف بدرجة الحرارة بين بخار الماء و سطح الانبوب، وكذلك وجود غاز غير قابل للتكثف. لقد وجد ان زيادة الإختلاف بدرجة الحرارة بين بخار الماء و سطح الانبوب مع بقاء درجة حرارة البخار ثابتة يؤدي الى زيادة في سمك طبقة السائل المتكثف المتاخمة، والتي تسبب بدورها نقصان في معامل نقل الحرارة بالتكثف. من الناحية الأخرى، زيادة درجة حرارة بخار الماء وبقاء الإختلاف بدرجة الحرارة بين بخار الماء و سطح الانبوب ثابتاً يؤدي إلى زيادة في معامل انتقال الحرارة بالتكثف. بالإضافة الى ذلك، تاثير وجود غاز غير قابل للتكثف بنسب مختلفة قد درس أيضا ووجد بأنّه يسبب تخفيض ملحوظ في معامل انتقال الحرارة بالتكثف. تم كذلك اعداد معادلة لحساب معامل انتقال الحرارة بالتكثف على انبوب عمودي. البيانات التجريبية التي تم الحصول عليها من التجارب العملية قورنت بنتائج البرنامج العددية وتم الحصول على توافق جيد بينهما. وبهذا، يمكن الاستنتاج بأن البرنامج الحسابي الحالي مناسب لنمذجة تكثف بخار الماء على إنبوب عمودي.

KEYWORDS: Film Condensation, Steam, Two-Phase, Vertical Tube, Non-Condensable.

INTRODUCTION

The problem of heat transfer with phase change received extensive attention in the literature due to its wide range of applications in such diverse fields as heat exchange systems, chemical processing plants, evaporative condensers, distillation facilities, chemical vapor deposition processes, and many other industrial applications, including nuclear power plants. One of these problems is the heat transfer analysis of film condensation which is an important area in the design of heat exchangers. This mode of heat transfer is often used because high heat transfer coefficients can be achieved. However, in practical operations of the condensers, small amounts of non-condensable gas may exist in working vapors due to characteristics of the system. It is well known that the presence of non-condensable gas in a vapor can greatly reduce the performance of the condensers **(Collier, 1972)**.

The heat transfer rates of laminar film condensation on vertical or nearly vertical surfaces were first predicted by **(Nusselt, 1916)**. In Nusselt analysis, the condensate film was assumed to be thin and to have negligible inertial effects. Furthermore, it was assumed that the shear stress at the liquid-vapor interface was zero and that the temperature profile within the condensate film was linear. Following the publication of Nusselt's findings, many researchers attempted to improve the accuracy of the original analysis by implementing more realistic assumptions. **(Rohsenow, 1956)** modified the Nusselt's analysis by including the energy convection in the heat balance equation, but neglecting the inertial effects and suggested the modified latent heat of evaporation to account for the effect of the condensate temperature profile.

The heat transfer characteristics for laminar filmwise condensation along a flat plate with variable surface temperature using Nusselt's theory were studied by **(Hosokawa et al., 1999)**. They calculated the local and averaged heat transfer coefficients on a condensing surface temperature on the heat transfer characteristic and they found that this characteristic on a condensing surface depends on the temperature distribution on the surface. Furthermore, they also investigated the effects depending on whether the cooling water was flowing co- or counter-current to the direction of the condensate flow. Furthermore, **(Moon et al., 1999)** investigated the local heat transfer coefficient experimentally for the reflux condensation in a vertical tube in a countercurrent flow between the steam-air mixture and the condensate. It was concluded that the presence of the air in gas up flow causes a remarkable decrease of the heat transfer coefficients compared to the same flow rate of pure steam.

The effects of non-condensable gas on the direct contact film condensation of vapor mixture under an adiabatic wall condition were investigated by **(Lee et al., 2001)**. They carried out a series of experiments for condensation of the steam/air mixture into the water film on the nearly vertical wall. The air mass fraction, the velocity of the mixture, the water film flow rate, and the subcooling at the inlet were selected as the experimental parameters affecting the direct contact condensation heat transfer coefficients. They found that the average heat transfer coefficients decrease as the air-mass fraction of the mixture increase, due to air concentration resistance near the interface.

The effects of the flowing mixture of steam and air on the condensation heat transfer at atmospheric pressure varying the air concentration was accomplished experimentally by **(Chung et. al., 2004)**. Rates of heat transfer had been measured on a single face of a water-cooled flat plate suspended vertically in a cylindrical test section as steam and mixtures of steam and air flowed over it. The test results for pure steam showed good agreement with the predictions of the Nusselt analysis of natural convection condensation and the steam flow didn't affect the heat transfer. Moreover, it was concluded that the small steam flow over the cooling plate showed negligible effect to the condensation heat transfer but the mixture flow enhanced the heat transfer substantially. Besides the same authors, **(Chung et al., 2004)** presented later experimental results comparing film-wise and drop-wise condensations of steam and mixtures of steam and air at atmospheric pressure. By using the same test rig, both film-wise and drop-wise condensation heat transfer rates were measured, varying the air concentration, on a single face of water-cooled flat plates suspended vertically in a cylindrical test section as steam and mixtures of steam and air flowed over it. In the pure steam cases, the drop-wise condensation showed much higher heat transfer rates than film-wise condensation, which showed good agreement with Nusselt theory of natural convection condensation. However, in the steam and air mixture cases, as expected, both modes of condensation fell in similar range of heat transfer rates and these rates of heat transfer were governed more by the thermal resistance of the air rich layer.

The accurate steady and unsteady numerical solutions of the full two-dimensional governing equations for the Nusselt problem were presented by **(Phan and Narain, 2007)**. The computational approach of the Nusselt problem, which is composed of film condensation of saturated vapor on a vertical wall, produced results in agreement with the Nusselt solution. In that work, it was shown that the waves and wave effects were quite sensitive to the presence or absence of the wall noise. This sensitivity to the frequency and wavelength spectrum of the wall noise was exploited either to suppress or enhance the wave effects. Also, the results for this problem affirmed that heat transfer rates and shear rates were significantly enhanced by the presence of waves. Afterward, (Xu et al., 2008) studied the laminar film condensation of saturated steam on an isothermal vertical plate. They reduced the two ordinary boundary layer equations of momentum and thermal energy to two ordinary differential equations by means of a set of similarity transformations. Their work showed the validity and the great potentially of the proposed technique for the nonlinear problems with multiple solutions.

A comprehensive investigation for the steady-state mixed convection of a condensate film on an isothermal vertical tube in dry saturated vapor with a forced flow was performed by **(Chang, 2008)**. His analysis took into account the inertia and convection effects in the condensate layer and the resistance at the liquid-vapor interface. The numerical results indicated that the effect of the forced-flow parameter increases as the thickness of the liquid condensate layer increases. Another related problem is that of **(Shang and Zhong, 2008)** applied successfully the dimensionless velocity component method to the laminar free film condensation from vapor-gas mixture for similarity analysis and transformation of whole system of the governing partial differential equations. The set of dimensionless variables of the transformed mathematical model greatly facilitates the analysis and calculation of the velocity, temperature and concentration fields, and heat and mass transfer of the film condensation from the vapor-gas mixture. It was confirmed that

the presence of the non-condensable gas is a device factor in decreasing the heat and mass transfer of the film condensation and it was found that an increase of the wall temperature will increase the negative effect of the non-condensable gas on heat and mass transfer of the film condensation from the vapor-gas mixture.

In order to investigate steam film condensation on a vertical tube, a mathematical model based on the basic conservation laws of mass and energy, Nusselt′s analysis on film condensation, and empirical equations available in published literature is developed in the present work. Additionally, a computer program simulating steam film condensation on a vertical tube utilizing the above mathematical model is elaborated. Then, experimental test runs are carried out using a condensation unit test bench. The experimental data obtained are compared with the results of simulation program. The effects of various parameters on the condensation heat transfer coefficient, such as steam temperature, steam-surface temperature difference, and the presence of non-condensable gas are investigated and reported graphically.

MATHEMATICAL MODEL

The elemental volume taken into consideration is shown in **Fig. 1**. From which, it can be seen that cooling water moves upward through the inner diameter of the condenser tube from section ($x+ dx$) to (x), while the condensate film thickness increases in moving from section (x) to ($x+ dx$). The liquid film starts forming at the top of the tube and flows downward under the influence of gravity. The thickness of the film increases in the flow direction (x) because of continued condensation at the liquid–vapor interface. Heat in the amount of (h_{fg}) is released during condensation and is transferred through the film to the tube surface at temperature (T_s), which must be below the saturation temperature (T_{sat}) of the vapor for condensation to occur **(Cengel, 2003)**.

The analytical relation for the heat transfer coefficient in film condensation on a vertical plate was first developed by **(Nusselt, 1916)** under the following simplifying assumptions:

- Both the plate and the vapor are maintained at constant temperatures of (T_{wall}) and (T_{sat}), respectively, and the temperature across the liquid film varies linearly.
- Heat transfer across the liquid film is by pure conduction (no convection currents in the liquid film).
- The velocity of the vapor is low (or zero) so that it exerts no drag on the condensate (no viscous shear on the liquid–vapor interface).
- The flow of the condensate is laminar and the properties of the liquid are constant.
- The acceleration of the condensate layer is negligible.
- The volume element of condensate liquid film on a vertical plate considered in Nusselt's analysis is shown in **Fig. 2**, from which, a relation for calculating condensate liquid film thickness over a flat plate at any location (x) is given as;

$$\delta_x = \left[\frac{4\, K_l\, \mu_l (T_s - T_{wall\ x})\, x}{g\, \rho_l\, (\rho_l - \rho_v)\, h_{fg}} \right]^{1/4} \tag{1}$$

Also, the local value of condensation heat transfer coefficient ($h_{cond\ x}$) over a flat plate is given by;

$$h_{cond\ x} = \frac{K_l}{\delta_x} = \left[\frac{g\, \rho_l\, (\rho_l - \rho_v)\, h_{fg}\, K_l^3}{4\, \mu_l (T_s - T_{wall\ x})\, x} \right]^{1/4} \tag{2}$$

Then, the mean (average) value of condensation heat transfer coefficient over a flat plate and for the whole plate surface ($h_{cond\ av}$) is given by;

$$h_{cond\ av} = \frac{1}{L}\int_0^L h_{cond\ x}\, dx = 0.943\left[\frac{g\,\rho_l\,(\rho_l-\rho_v)\,h_{fg}\,K_l^3}{\mu_l (T_s - T_{wall})\,L}\right]^{1/4} \quad (3)$$

The condensate film in an actual condensation process is cooled further to some average temperature between (T_s) and $(T_{wall\ x})$, releasing more heat in the process. Therefore, the actual heat transfer will be larger. **(Rohsenow, 1956)** showed that the cooling of the liquid below the saturation temperature can be accounted for by replacing (h_{fg}) by the modified latent heat of vaporization (h'_{fg}) defined as;

$$h'_{fg} = h_{fg} + 0.68\,Cp_l\,(T_s - T_{wall\,x}) \quad (4)$$

For the calculation of the condensate film boundary layer thickness, **Eq. (1)** for steam condensation over a vertical plate derived by **(Nusselt, 1916)** was used, because the thickness of the condensate film boundary layer is small when compared with the tube diameter, and using the modified latent heat of vaporization **(Rohsenow, 1956)**, **Eq. (4)**. The buildup of the condensate liquid film starts from top of the tube while moving downward, while the cooling water comes from the bottom of the tube and moves upward. Thus, the numerical program was made to perform the simulation process starting from the top of the tube and moving downward with the condensate film boundary layer. Therefore, initial estimation of the outlet cooling water temperature must be made and an iteration process must be performed until reaching convergence for the inlet cooling water temperature through changing of the outlet cooling water temperature.

In **Eq.(1)**, there exist two unknowns, the condensate film thickness (δ_x) and tube wall temperature $(T_{wall\ x})$, which requires estimation of the wall surface temperature and solving for condensate film thickness, then, heat transfer rate is calculated by two ways, first, by conduction from the liquid film surface at a temperature of (T_s) to an estimated outside tube surface at a temperature of $(T_{wall\ x})_{est}$, and second, by conduction and convection from an estimated outside tube surface at a temperature of $(T_{wall\ x})_{est}$ to the cooling water entering the element with a temperature of $(T_{w\,x})$, when both values of heat transfer rate become equal with a specified tolerance, then the estimated value of tube wall surface temperature is correct, otherwise, iteration process must be made by correcting the estimated tube wall surface temperature.

The heat transfer rate from the liquid film surface, which is assumed to be at steam temperature, through an elemental length (dx), shown in **Fig. 1,** with an outside surface temperature of $(T_{wall\ x})$ is equal to the heat transfer rate from the outside surface of the same element at a temperature of $(T_{wall\ x})$ to the cooling water entering the element with a temperature of $(T_{w\,x})$, this gives, **(Incropera et al., 2007)**;

$$Q_x = \frac{T_s - T_{wall\ x}}{R_f} = \frac{T_{wall\ x} - T_{w\,x}}{R_t + R_{in}} \quad (5)$$

Where,

$$R_f = \frac{\ln\left((r_2+\delta)/r_2\right)}{2\,\pi\,K_l\,dx} \quad (6)$$

$$R_t = \frac{\ln(r_2/r_1)}{2\pi K_t\, dx} \tag{7}$$

$$R_{in} = \frac{1}{h_{in}\, A_{x\ in}} \tag{8}$$

For the range of cooling water flow rates used, the Reynolds number values calculated showed that the flow is laminar. Also, for the length of tube used and range of Reynolds number values, it was found that the flow is neither hydro-dynamically nor thermally fully developed. Therefore, the correlation proposed by **(Sieder and Tate, 1936)** was used for the calculation of the inside convection heat transfer coefficient of the cooling water as;

$$Nu_{in} = \frac{h_{in}\, d_h}{K_l} = 1.86 \times \left[\mathrm{Re\ Pr}\,\frac{d_h}{x}\right]\left[\frac{\mu}{\mu_{\mathrm{wall}}}\right]^{0.14} \tag{9}$$

Where, $\mathrm{Re} = \dfrac{\rho_l\, V_l\, d_h}{\mu_l}$ (10)

Eq. (9) is used with the following conditions; $\begin{bmatrix} \text{Hydrodynamic entry length} = 0.05\ \mathrm{Re}\ \mathrm{d_h} \\ \text{Thermal entry length} = 0.05\ \mathrm{Re\ Pr\ d_h} \\ \mathrm{Re} \le 2300 \end{bmatrix}$

The local condensation heat transfer coefficient ($h_{cond\ x}$) is calculated from the following relation;

$$h_{cond\ x} = \frac{Q_x}{(T_s - T_{wall\ x})(2\pi\, dx\, r_2)} \tag{11}$$

While the average condensation heat transfer coefficient ($h_{cond\ av}$) can be calculated using the following relation;

$$h_{cond\ av} = \frac{Q_{tot}}{(T_s - T_{wall\ center})(2\pi\, L\, r_2)} \tag{12}$$

STEAM TABLE FORMULATION

The steam table was developed as a subroutine for the simulation program. The steam and water properties were calculated using special correlation techniques including some numerical constants. Before calculating the steam and water thermodynamic properties, the following reduced dimensionless quantities were introduced as follows, **(U K Steam Tables, 1970)**;

$$\beta = \frac{P_{sat}}{P_{c1}},\quad \text{the reduced saturation pressure} \tag{13}$$

$$\theta = \frac{T}{T_{c1}},\quad \text{the reduced temperature} \tag{14}$$

$$\chi = \frac{\nu}{\nu_{c1}}, \quad \text{the reduced volume} \tag{15}$$

$$\varepsilon = \frac{h}{P_{c1}\,\nu_{c1}}, \quad \text{the reduced enthalpy} \tag{16}$$

Where, $P_{c1} = 221.2\,bar$ (exactly)

$T_{c1} = 647.3^{\circ}\mathrm{K}$ (exactly)

$\nu_{c1} = 0.00317\,m^3/kg$ (exactly)

$P_{c1}\nu_{c1} = 70.1204\,kJ/kg$ (exactly)

The reduced saturation pressure (β) as a function of the reduced temperature (θ) was calculated using the following equation, **(U K Steam Tables, 1970)**:

$$\beta = \exp\left[\frac{\frac{1}{\theta}\sum_{n=1}^{5} K_n(1-\theta)^n}{1+K_6(1-\theta)+K_7(1-\theta)^2} - \frac{+(1-\theta)}{+K_8(1-\theta)^2+K_9}\right] \tag{17}$$

All values of the numerical constants for the steam table correlations are available in tables listed in appendix (A). The steam table correlations were sub-divided into two groups as follows:

1. Correlations for Saturated Liquid Properties

a. Reduced Volume (χ)

$$\begin{aligned}\chi = {} & A_{11}a_5 Z^{-5/17} + \left[A_{12} + A_{13}\theta + A_{14}\theta^2 + A_{15}(a_6-\theta)^{10} + A_{16}\left(a_7+\theta^{19}\right)^{-1}\right] \\ & - \left[\left(a_8+\theta^{11}\right)^{-1}\left(A_{17}+2A_{18}\beta+3A_{19}\beta^2\right)\right] \\ & - \left[A_{20}\theta^{18}\left(a_9+\theta^2\right)\left\{-3(a_{10}+\beta)^{-4}+a_{11}\right\}\right] \\ & + 3A_{21}(a_{12}-\theta)\beta^2 + 4A_{22}\theta^{-20}\beta^3\end{aligned} \tag{18}$$

b. Reduced Enthalpy (ε)

$$\begin{aligned}\varepsilon = {} & A_0\theta - \sum_{n=1}^{10}(n-2)A_n\theta^{n-2} + A_{11}\left[Z\left\{17\left(\frac{Z}{29}-\frac{Y}{12}\right)+50\frac{Y'}{12}\right\} + a^4\theta - (a^3-1)\theta YY'\right]Z^{-5/17} \\ & + \left\{A_{12} - A_{14}\theta^2 + A_{15}(90+a_6)(a_6-\theta)^9 + A_{16}\left(20\theta^{19}+a_7\right)\left(a_7+\theta^{19}\right)^{-2}\right\}\beta \\ & - (12\theta^{11}+a_8)\left(a_8+\theta^{11}\right)^{-2}\left(A_{17}\beta + A_{18}\beta^2 + A_{19}\beta^3\right) \\ & + A_{20}\theta^{18}(17a_9+19\theta^2)\left\{(a_{10}+\beta)^{-3}+a_{11}\beta\right\} + A_{21}a_{12}\beta^3 + 21A_{22}\theta^{-20}\beta^4\end{aligned} \tag{19}$$

Where,

$$Z = Y + \left(a_3 Y^2 - 2a_4\theta + 2a_5\beta\right)^{1/2} \tag{20}$$

$$Y = 1 - a_1\theta^2 - a_2\theta^{-6} \tag{21}$$

$$Y' = -2a_1\theta + 6a_2\theta^{-7} \tag{22}$$

c. Dynamic Viscosity (μ)

$$\mu = \mu_0 \times \exp\left[VR \times \sum_{i=0}^{5}\sum_{j=0}^{4}\left(BB_{i,j}\left(TR-1\right)^i\left(VR-1\right)^j\right)\right] \tag{23}$$

Where,

$$\mu_0 = \left\{\left[\frac{1}{TR}\right]^{1/2}\left[\sum_{i=0}^{3} AA_i TR^i\right]^{-1}\right\}\times 10^{-6} \tag{24}$$

$$TR = 647.27/T(K) \tag{25}$$

$$VR = 0.003147/v \tag{26}$$

d. Thermal Conductivity (K)

$$\begin{aligned} K\times 10^3 = {} & a_0 + a_1\left[\frac{T}{T_0}\right] + a_2\left[\frac{T}{T_0}\right]^2 + a_3\left[\frac{T}{T_0}\right]^3 + a_4\left[\frac{T}{T_0}\right]^4 \\ & + \left(P - P_{sat}\right)\left\{b_0 + b_1\left[\frac{T}{T_0}\right] + b_2\left[\frac{T}{T_0}\right]^2 + b_3\left[\frac{T}{T_0}\right]^3\right\} \\ & + \left(P - P_{sat}\right)\left\{c_0 + c_1\left[\frac{T}{T_0}\right] + c_2\left[\frac{T}{T_0}\right]^2 + c_3\left[\frac{T}{T_0}\right]^3\right\} \end{aligned} \tag{27}$$

2. Correlations for Saturated Vapor Properties

a. Reduced Volume (χ)

$$\chi = I_1\,\theta/\beta - \sum_{r=1}^{5} r\beta^{r-1}\sum_{s=1}^{n(r)} B_{rs} X^{z(r,s)} + 11\left(\frac{\beta}{\beta_L}\right)^{10}\sum_{s=0}^{6}\beta_{9s}X^s - \sum_{r=6}^{8}\frac{(r-2)\beta^{1-r}\sum_{s=1}^{n(r)} B_{rs}X^{Z(r,s)}}{\left\{\beta^{Z-r} + \sum_{d=1}^{l(r)} b_{rd}X^{x(r,d)}\right\}^2} \tag{28}$$

b. Reduced Enthalpy (ε)

$$\varepsilon = B_0\theta - \sum_{s=0}^{5} B_{0s}(s-2)\theta^{s-1} - \sum_{r=1}^{5}\beta^r \sum_{s=1}^{n(r)} B_{rs}(1+Z(r,s)b\theta)X^{Z(r,s)}$$
$$\sum_{s=1}^{n(r)} B_{rs}X^{Z(r,s)}\left\{(1+Z(r,s)b\theta) - \frac{b\theta\sum_{d=1}^{l(r)} X(r,d)b_{rd}X^{x(r,d)}}{\beta^{2-r}+\sum_{d=1}^{l(r)} b_{rd}X^{x(r,d)}}\right\}$$
$$-\sum_{r=6}^{8}\frac{}{\beta^{2-r}+\sum_{d=1}^{l(r)} b_{rd}X^{x(r,d)}} \qquad (29)$$
$$+\beta\left(\frac{\beta}{\beta_L}\right)^{10}\sum_{s=0}^{6}\left[\left\{1+\left(\frac{10\beta_L'}{\beta_L}+sb\right)\right\}B_{9s}X^s\right]$$

Where,

$$X = \exp\{b(1-\theta)\} \qquad (30)$$

$$\beta_L = L_0 + L_1\theta + L_2\theta^2 \qquad (31)$$

$$\beta_L' = \frac{d\beta_L}{d\theta} = L_1 + 2L_2\theta \qquad (32)$$

COMPUTER PROGRAM FLOW CHART

The mathematical model described previously was solved numerically through a numerical calculation algorithm implemented by a developed computer program written in FORTRAN language. The flow chart of the computer program is shown in **Fig. (3)**. The inlet cooling water temperature, steam temperature, and cooling water flow rate are used as an input for the numerical program, then the program calculates tube surface temperature distribution, cooling water temperature distribution, local heat transfer rate, local condensation heat transfer coefficient, condensate boundary layer thickness distribution, total heat transfer rate, and average condensation heat transfer coefficient.

EXPERIMENTAL TEST RIG

A bench-top condensation unit manufactured by Gunt, which is a German company, is used for performing the experimental work. It consists of the following parts, (see **Fig. 4)**;

(1. Socket for PC interface, **2.** Display and control panel, **3.** Vessel (Glass cylinder), **4.** Electric heater with power adjuster, **5.** Cooling water connections, **6.** Water jet vacuum pump, **7.** Water jet vacuum pump adjustment valve, **8.** Flow rate sensor, **9.** Temperature sensor, **10.** Cooling water adjustment valve, **11.** Condenser tubes, **12.** Pressure switch, **13.** Condensate separator, **14.** Drop collector, and **15.** Level sensor **)**.

The bench-top unit provides clear demonstrations of condensation processes in a glass cylinder. The system has one condensation tube with a polished gold-plated surface for drop-wise condensation, and one condensation tube with a matt surface for film-wise condensation, which is investigated in the present work. The two condenser tubes are fitted in the upper part of the vessel. Cooling water flows upward through the inside of the condenser tubes. The heat given off by the steam at the condensation tubes can be determined from the measurement of the feed (inlet) and return (outlet) temperatures and the mass flow rate of the cooling water. The inlet and outlet water temperatures are measured via a PTC sensor with transmitter. The flow rate of cooling water is adjusted via control valves. The electric heater is in the lower part of the vessel, the output power of

the heater is adjustable. The temperature of the steam is measured using a PTC sensor mounted in the upper part of the vessel. While the tube surface temperature is measured via a type (J) thermocouple fixed on the outside surface of each tube in the middle.

The vessel is equipped with a pressure sensor to measure steam absolute pressure and a pressure switch to switch off the heater in the event of excessive overpressure. The vessel can be evacuated using a water jet vacuum pump. In order to prevent the escape of steam from the vessel, the suction pipe of the vacuum pump is fitted with cooling system and a water separator. The inlet and outlet cooling water temperatures, steam temperature and pressure, tube surface temperature at center, and cooling water flow rate are all recorded during each experimental test run. All parameters are measured electronically and displayed digitally.

RESULTS AND DISCUSSION

The effect of various parameters on the condensation heat transfer coefficient, steam pressure, steam-surface temperature difference and the presence of non-condensable gas, were investigated both experimentally and numerically and then reported graphically. In addition, the numerical results of the simulation program were compared with the data recorded in the experimental work in order to validate the numerical simulation program.

Figs. 5 to **7** show the predicted values of tube surface temperature at center, outlet cooling water temperature and average condensation heat transfer coefficient, respectively, versus corresponding experimental data recorded during test runs for different values of steam temperature and (steam-surface) temperature difference. **Fig. 5** shows good agreement between the numerical and predicted values. While **Fig. 6** shows that the experimental outlet cooling water temperature is always higher than the predicted one, and that the difference between them increases with increasing steam temperature. This behavior may be attributed to the fact that the heat transfer to the cooling water continues even after the water leaves the effective length of condenser tube until it reaches the point where the outlet cooling water thermocouple is fixed. This makes the thermocouple reading always higher than the predicted value with noticeable error. This relatively large error in the outlet cooling water temperature leads to a relatively large difference between the predicted and experimental values of the average condensation heat transfer coefficient shown in **Fig. 7**, which shows a maximum error of about (23 %). From the above three figures, it can be concluded that the numerical program can be used to simulate the condensation of steam on a vertical tube with acceptable accuracy.

The variation of predicted tube surface temperature along the condenser tube for different values of steam temperature and for a (steam-surface) temperature difference of (6.5 ^{o}C) is shown in **Fig. 8**. From which, it is clear that higher steam temperature leads, as expected, to a higher tube surface temperature. Also, it can be noticed that the decrease of surface temperature is approximately linear until reaching a point near the end of tube where the drop in temperature becomes faster, which may explained by the fact that the cooling water enters the condenser tube at the bottom and flows upward, and since the convection heat transfer coefficient at the tube entry is maximum, then the heat transfer rate to the cooling water will be higher and this will cause a faster reduction in tube surface temperature.

The cooling water temperature distribution curves along the condenser tube at different values of steam temperature and for an inlet water temperature of (20.1 ^{o}C) and a water flow rate of (30 l/h) are shown in **Fig. 9**. From which, it is clear that higher steam temperature gives a higher cooling water temperature along the entire tube length, which results from a higher tube surface temperature at high steam temperature shown **in Fig. 8**.

The local heat transfer rate (Q_x) distribution curves along the condenser tube at different values of (steam-surface) temperature difference and for a steam temperature of (95 ^{o}C) are shown in **Fig. 10**. From which, it is obvious that increasing (steam-surface) temperature difference increases the local heat transfer rate along the whole tube. Also, it can be observed that local heat

transfer rate increases relatively slow at the beginning of the tube, then speed up a little towards the tube end, which may explained by the fact the cooling water have a maximum convection heat transfer coefficient at its entry to the condenser tube at the bottom.

The distribution curves of local heat transfer rate (Q_x) along the condenser tube at different values of steam temperature and for a (steam-surface) temperature difference of (6.5 ^oC) are shown in **Fig. 11**. From which, it is apparent that increasing steam temperature increases the local heat transfer rate along the entire tube length. Also, it can be observed that local heat transfer rate increases relatively slow at the beginning of the tube, then speed up a little towards the tube end. This trend may be explained in the same way as that of **Fig. 10**.

Curves representing a plot of condensate film thickness along the condenser tube at different values of (steam-surface) temperature difference and for a steam temperature of (95 ^oC) are shown in **Fig. 12**. From which, it is clear that higher condensate boundary layer thickness is obtained at higher values of (steam-surface) temperature difference, which is understandable from observing that the higher local heat transfer rates (Q_x) occur at higher values of (steam-surface) temperature difference shown in **Fig. 10**.

The local values of condensation heat transfer coefficient distribution curves along the condenser tube at different values of (steam-surface) temperature difference and for a steam temperature of (95 ^oC) are shown in **Fig. 13**. From which, it is obvious that the local condensation heat transfer coefficient increases with decreasing (steam-surface) temperature difference, since decreasing (steam-surface) temperature difference causes a decrease in the condensate boundary layer which is clearly shown in **Fig. 12**. The growth in condensate film thickness represents an increase in conductive resistance of the film and thus reducing local value of condensation heat transfer coefficient. In addition, the local value of condensation heat transfer coefficient decreases while moving towards the tube end because of the increase of condensate boundary layer thickness.

Curves representing the distribution of local values of condensation heat transfer coefficient along the condenser tube at different values of steam temperature and for a (steam-surface) temperature difference of (6.5 ^oC) are shown in **Fig. 14**. From which, it is noticeable that the local condensation heat transfer coefficient increases with increasing steam temperature.

The experimentally calculated values of average condensation heat transfer coefficient are plotted versus their corresponding steam temperatures in **Fig. 15** for two cases, pure steam and with presence of non-condensable gas (air) at different concentrations. From which, it can proved that the presence of non-condensable gas with the pure steam even with small concentration can cause a remarkable reduction in the condensation heat transfer coefficient and heat transfer rate, which is a fact observed by many experimental researches in this field. The non-condensable gas can cause a drop in the condensation heat transfer coefficient even to a value of about (10 %) of that for pure steam.

Points representing the intersection of the experimentally calculated values of average condensation heat transfer coefficient with numerical values of the right hand side of Eq. 3 defined as, $\left[\left(g\,\rho_l\,(\rho_l-\rho_v)h_{fg}\,K_l^3\right)/\left(\mu_l(T_s-T_{wall})L\right)\right]^{1/4}$, are shown in **Fig. 16**. Through these points, a line which best fits them is drawn, and it is found that a factor of (1.087) gives the slope of this line, therefore, it can be concluded that an equation for calculating average condensation heat transfer coefficient on a vertical tube can be written as;

$$h_{cond\ av}=1.087\left[\frac{g\,\rho_l\,(\rho_l-\rho_v)h_{fg}\,K_l^3}{\mu_l(T_s-T_{wall})L}\right]^{1/4} \qquad (33)$$

CONCLUSIONS

It was concluded that the values of tube surface temperature and cooling water temperature increase with increasing steam temperature for the same value of (steam-surface) temperature difference. From the elemental heat transfer rate distribution curves, it can be deduced that the heat transfer rate increases with increasing steam temperature and keeping the (steam-surface) temperature difference constant or with increasing (steam-surface) temperature difference and maintaining the steam temperature constant. It was found that increasing (steam-surface) temperature difference while keeping the steam temperature constant results in an increase in condensate boundary thickness, which in turn causes a decrease in condensation heat transfer coefficient. On the other hand, increasing steam temperature and keeping the (steam-surface) temperature difference constant leads to an increase in condensation heat transfer coefficient. In addition, the presence of non-condensable gas with different concentrations was also investigated and it was shown that it causes a noticeable reduction in the average condensation heat transfer coefficient even to a value of about (10 %) of that with pure steam. An equation for calculating average condensation heat transfer coefficient on a vertical was developed, which is given by Eq. 33.

REFERENCES

- Cengel, Y. A., (2003), "Heat transfer - A Practical Approach", 2nd edition, McGraw-Hill Book Company. (Internet Search)

- Chung B., Kim S., and Kim M. C., (2004), "An Experimental Investigation of Film Condensation of Flowing Mixtures of Steam and Air on a Vertical Flat Plate", Int. Comm. Heat Mass Transfer, Vol. 31, pp. 703-710.

- Chung B., Kim S., and Kim M. C., (2004), "Experimental Comparison of Film-Wise and Drop-Wise Condensations of Steam on a Vertical Flat Plates with the Presence of Air", Int. Comm. Heat Mass Transfer, Vol. 31, pp. 1067-1074.

- Chang T., (2008), "Mixed Convection Film Condensation along Outside Surface of Vertical Tube in Saturated Vapor with Forced Flow", Appl. Therm. Eng., Vol. 28, pp. 547-555.

- Collier J. G., (1972), "Convective Boiling and Condensation", McGraw-Hill Book Company, New York.

- Hosokawa T., Entesari-Tatafi J., Kawashima Y., and Kimura F., (1999), "Heat Transfer Characteristics for Laminar Filmwise Condensation Along a Flat Vertical Plate with Three Distinct Cooling Zones", Second Int. Conf. on CFD in the Minerals and Process Industries CSIRO, Melbourne, Australia, 6-8 Dec.

- Incropera, DeWitt, Bergman, and Lavine, (2007), "Fundamentals of Heat and Mass Transfer", 6th edition, Wiley Book Company. (Internet Search)

- Lee H., Kim M., and Park S., (2001), "The Effect of Non-Condensable Gas on Direct Contact Condensation of Steam/Air Mixture", J. Korean Nuclear Society, Vol. 33, pp. 585-595.

- Moon Y. M., No H. C., and Bang Y. S., (1999), "Local Heat Transfer Coefficients for Reflux Condensation Experiment in a Vertical Tube in the Presence of Non-Condensable Gas", J. Korean Nuclear Society, Vol. 31, pp. 486-497.

- Nusselt W., (1916), "Die oberflachen Kondensation des Wasserdampes", Z. Ver. Deut. Ing., Vol. 60, (2) pp. 541-546. (cited in (Collier, 1972))

- Phan L., and Narain A., (2007), "Nonlinear Stability of the Classical Nusselt Problem of Film Condensation and Wave Effects ", ASME, J. Appl. Mech., Vol. 74.

- Rohsenow W. M., (1956), "Heat Transfer and Temperature Distribution in Laminar-Film Condensation", Trans. ASME, J. Heat Transfer, Vol. 78, pp. 1645-1648. (cited in (Collier, 1972))

- Shang D., and Zhong L., (2008), "Extensive Study on Laminar Free Film Condensation from Vapor-Gas Mixture", Int. J. Heat Mass Transfer, Vol. 51.

- Sieder E. N., and Tate G. E., (1936),"Heat transfer and Pressure Drop of Liquids in Tubes", Ind. Eng. Chem., Vol. 28, pp. 1429-1435.

- Xu H., You X., and Pop I., (2008), "Analytical Approximation for Laminar Film Condensation of Saturated Steam on an Isothermal Vertical Plate", Appl. Math. Modeling, Vol. 32, pp. 738-748.

NOMENCLATURE

Latin Symbols

A = surface area [m^2].
b = width [m].
Cp = specific heat at constant pressure [J/kg ^oC].
d = diameter of tube [m].
d_h = hydraulic diameter [m].
dx = length of element [m].
g = acceleration of gravity [m/s^2].
h = enthalpy [J/kg].
h_{cond} = condensation H.T.C. [$W/m^2.{}^oC$].
h_{in} = forced convection H.T.C. [$W/m^2.{}^oC$].
h_{fg} = latent heat of vaporization [J/kg].
K = thermal conductivity [$W/m.{}^oC$].
L = tube length [m].
$\dot{m}$ = mass flow rate [kg/s].
Nu = Nusselt number, dimensionless.
P = pressure [N/m^2].
Pr = Prandtl number, dimensionless.
Q = heat transfer rate [W].
R = thermal resistance [$^oC/W$].
Re = Reynolds number, dimensionless.
r_1 = inner tube diameter [m].
r_2 = outer tube diameter [m].
u = velocity [m/s].
V = cooling water velocity [m/s].
x = tube axial length (vertical-coordinate) [m].
y = y-axis (horizontal-coordinate) [m].

Greek Symbols

δ = condensate boundary layer thickness [m].
μ = dynamic viscosity [kg/s.m].
ν = specific volume = $1/\rho$ [m^3/kg].
ρ = density [kg/m^3].

Subscripts

av = average.
est = estimated.
f = liquid film.
in = inside, inlet.
l = liquid.
out = outlet
s = steam.
sat = saturation.
t = tube.
tot = total.
v = vapor.
w = water.
wall = tube surface.

T = temperature [^{o}C or K]. x = local value at any (x).

APPENDIX (A)
Numerical Constants for the Steam Table Correlations (U K Steam Tables, 1970).

Table 1 Values of numerical constants for **Eq. (17)**

$K_1 = -7.691234564\times10^{o}$	$k_2 = -2.608023696\times10^{1}$	$k_3 = -1.681706546\times10^{2}$	$k_4 = 6.423285504\times10^{1}$	
$k_5 = -1.189646225\times10^{2}$	$k_6 = 4.167117320\times10^{0}$	$k_7 = 2.097506760\times10^{1}$	$k_8 = 10^{9}$	$k_9 = 6$

Table 2 Values of numerical constants for **Eqs. (18)** to **(22)**

$A_0 = 6.824687741\times10^{3}$	$A_1 = -5.422063673\times10^{2}$	$A_2 = -2.096666205\times10^{4}$	$A_3 = 3.941286787\times10^{4}$
$A_4 = -6.733277739\times10^{4}$	$A_5 = 9.902381028\times10^{4}$	$A_6 = -1.093911774\times10^{5}$	$A_7 = 8.590841667\times10^{4}$
$A_8 = -4.511168742\times10^{4}$	$A_9 = 1.418138926\times10^{4}$	$A_{10} = -2.01727113\times10^{3}$	$A_{11} = 7.982692717\times10$
$A_{12} = -2.616571843\times10^{-2}$	$A_{13} = 1.52241179\times10^{-3}$	$A_{14} = 2.2842279054\times10^{-2}$	$A_{15} = 2.421647003\times10^{2}$
$A_{16} = 1.269716088\times10^{-10}$	$A_{17} = 2.074838328\times10^{-7}$	$A_{18} = 2.17402035\times10^{-8}$	$A_{19} = 1.105710498\times10^{-9}$
$A_{20} = 1.293441934\times10$	$A_{21} = 1.308119072\times10^{-5}$	$A_{22} = 6.047626338\times10^{-14}$	$a_1 = 8.438375405\times10^{-1}$
$a_2 = 5.362162162\times10^{-4}$	$a_3 = 1.72\times10$	$a_4 = 7.342278489\times10^{-2}$	$a_5 = 4.97585887\times10^{-2}$
$a_6 = 6.5371543\times10$	$a_7 = 1.15\times10^{-6}$	$a_8 = 1.5108\times10^{-5}$	$a_9 = 1.4188\times10^{-1}$
$a_{10} = 7.002753165\times10$	$a_{11} = 2.995284926\times10^{-4}$	$a_{12} = 2.04\times10^{-1}$	

Table 3 Values of numerical constants for **Eqs. (23)** and **(24)**

$AA_0 = 0.0181583$, $AA_1 = 0.0177624$, $AA_2 = 0.0105287$, $AA_3 = -0.0036744$					
$BB_{i,j}$					
	$j = 0$	1	2	3	4
$i = 0$	0.501938	0.235622	-0.274637	0.145831	-0.0270448
1	0.162888	0.789393	-0.743539	0.263129	-0.0253093
2	-0.130356	0.673665	-0.959456	0.347247	-0.0267758
3	0.907919	1.207552	-0.687343	0.213486	-0.0822904
4	-0.551119	0.0670665	-0.497089	0.100754	0.0602253
5	0.146543	-0.084337	0.195286	-0.032932	-0.0202595

Table 4 Values of numerical constants for **Eq. (27)**

$a_0 = -922.47$	$a_1 = 2839.5$	$a_2 = -1800.7$	$a_3 = 525.77$	$a_4 = -73.44$
$b_0 = -0.9473$	$b_1 = 2.5186$	$b_2 = -2.0012$	$b_3 = 0.5186$	$c_0 = 1.6563\times10^{-3}$
$c_1 = -3.8929\times10^{-3}$	$c_2 = 2.9323\times10^{-3}$	$c_3 = -7.1693\times10^{-4}$	$T_0 = 273.15^{\circ}K$	

Table 5 Values of numerical constants for **Eqs. (28)** to **(32)**

$I_1 = 4.260321148\times10$	$L_0 = 1.574373327\times10^{1}$	$L_1 = -3.417061978\times10^{1}$	$L_2 = 1.931380707\times10^{1}$
$B_0 = 1.683599274\times10^{1}$	$B_{01} = 2.856067796\times10^{1}$	$B_{02} = -5.438923329\times10^{1}$	$B_{03} = 4.330662834\times10^{-1}$
$B_{04} = -6.547711697\times10^{-1}$	$B_{05} = 8.565182058\times10^{-2}$	$B_{11} = 6.670375918\times10^{-2}$	$B_{12} = 1.388983801\times10$
$B_{21} = 8.390104328\times10^{-2}$	$B_{22} = 2.614670893\times10^{-2}$	$B_{23} = -3.373439453\times10^{-2}$	$B_{31} = 4.520918904\times10^{-1}$
$B_{32} = 1.069036614\times10^{-1}$	$B_{41} = -5.975336707\times10^{-1}$	$B_{42} = -8.847535804\times10^{-2}$	$B_{51} = 5.958051609\times10^{-1}$
$B_{52} = -5.159303373\times10^{-1}$	$B_{53} = 2.075021122\times10^{-1}$	$B_{61} = 1.190610271\times10^{-1}$	$B_{62} = -9.867174132\times10^{-2}$

$B_{71} = 1.683998803\times10^{-1}$	$B_{72} = -5.809438001\times10^{-2}$	$B_{81} = 6.552390126\times10^{-3}$	$B_{82} = 5.710218648\times10^{-4}$
$B_{90} = 1.936587558\times10^{2}$	$B_{91} = -1.388522425\times10^{3}$	$B_{92} = 4.126607219\times10^{3}$	$B_{93} = -6.508211677\times10^{3}$
$B_{94} = 5.745984054\times10^{3}$	$B_{95} = -2.693088365\times10^{3}$	$B_{96} = 5.235718623\times10^{2}$	$b = 7.633333333\times10^{-1}$
$b_{61} = 4.006073948\times10^{-1}$	$b_{71} = 8.636081627\times10^{-2}$	$b_{81} = -8.532322921\times10^{-1}$	$b_{82} = 3.460208861\times10^{-1}$

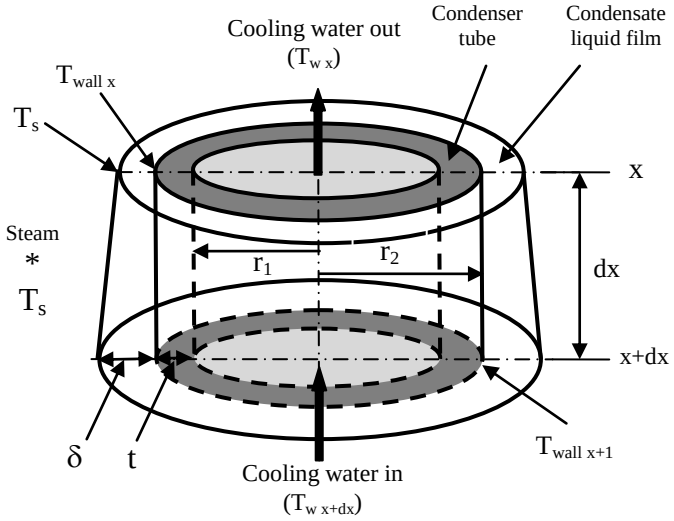

Fig. (1) The elemental volume considered in the present work.

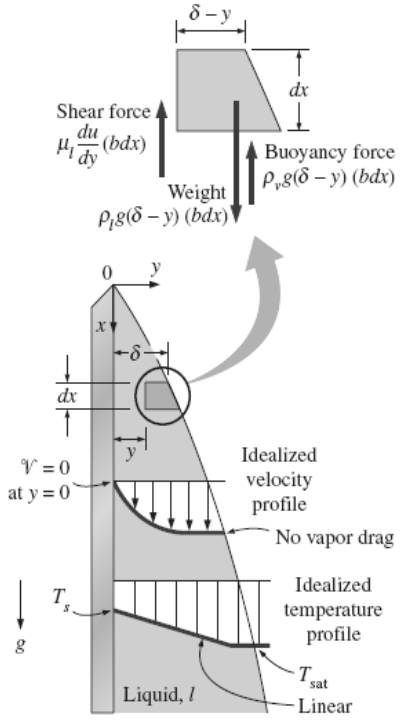

Fig. (2) The volume element of condensate on a vertical plate considered in Nusselt's analysis. **(Cengel, 2003)**

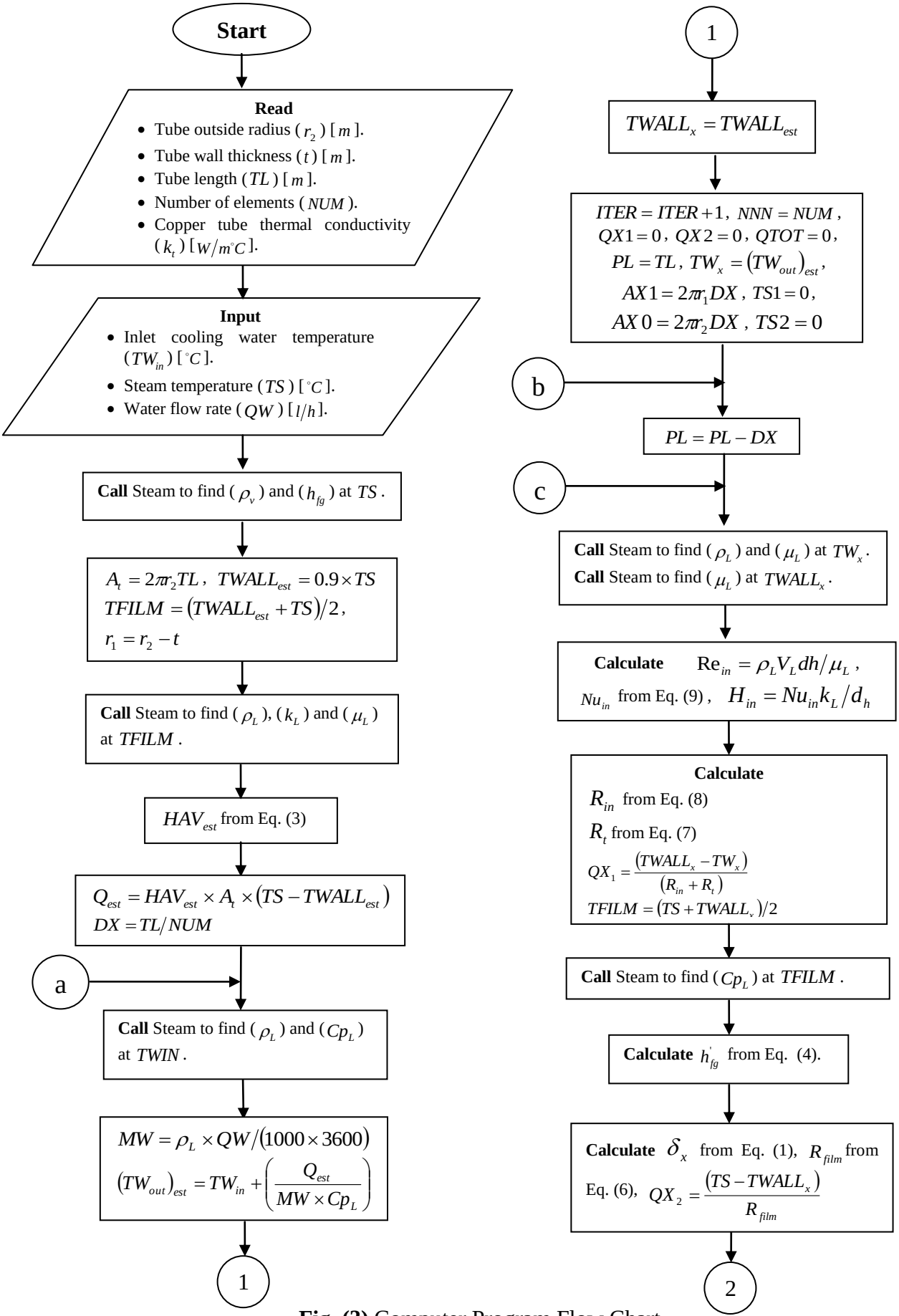

Fig. (3) Computer Program Flow Chart.

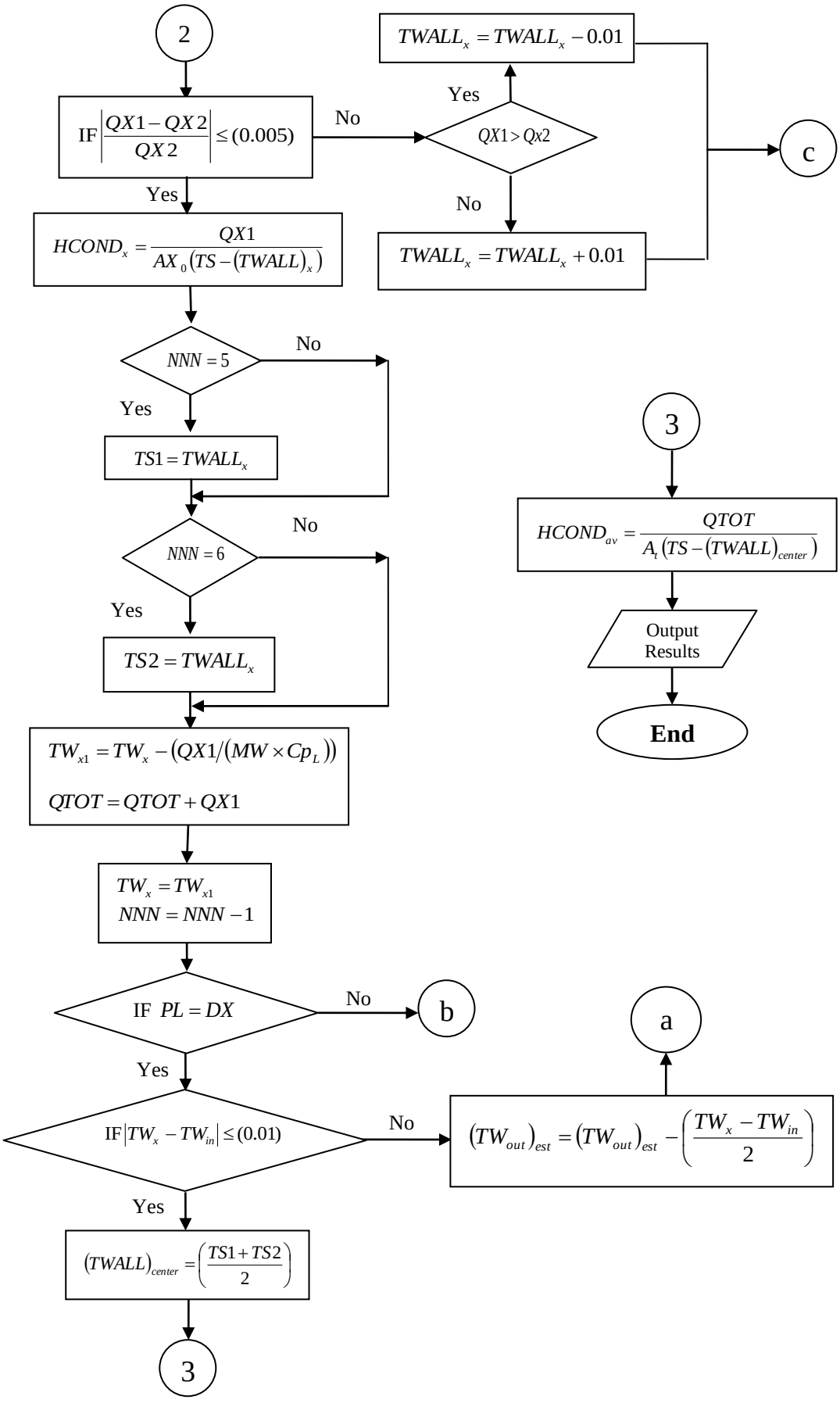

Fig. (3) Continued**.**

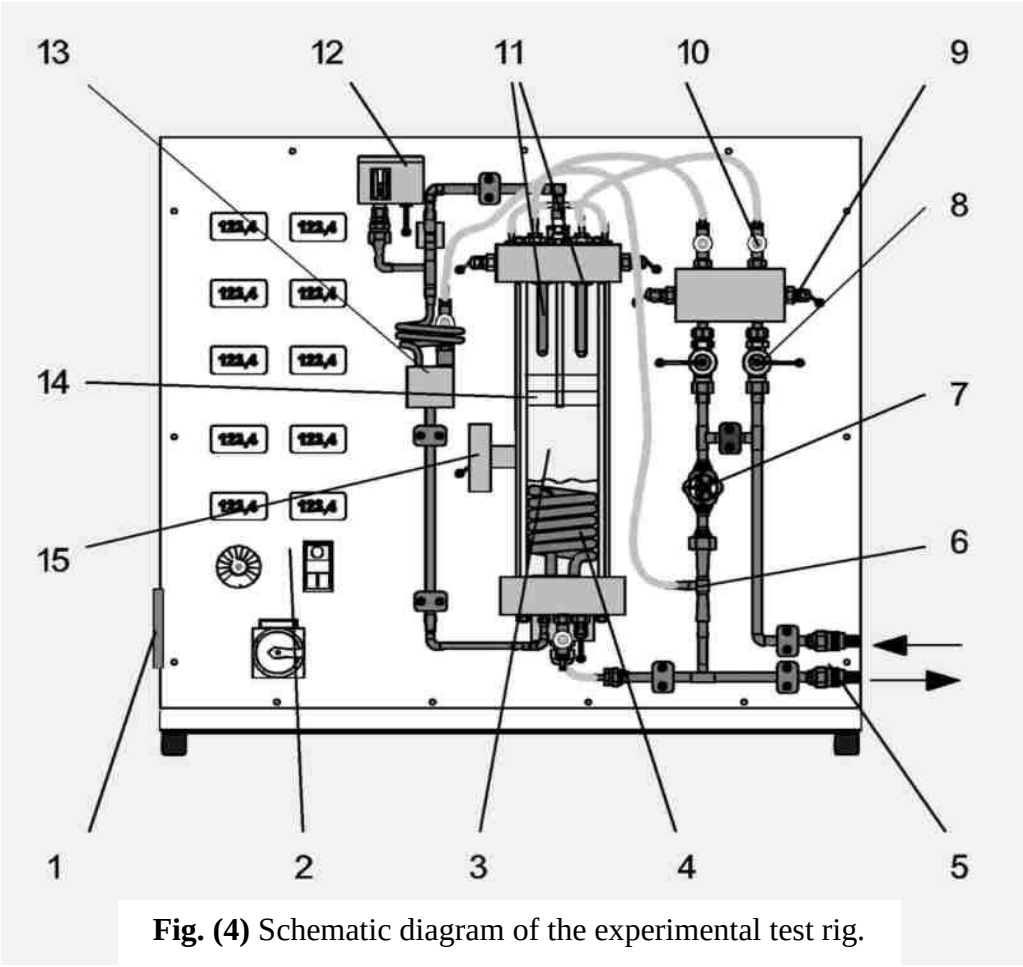

Fig. (4) Schematic diagram of the experimental test rig.

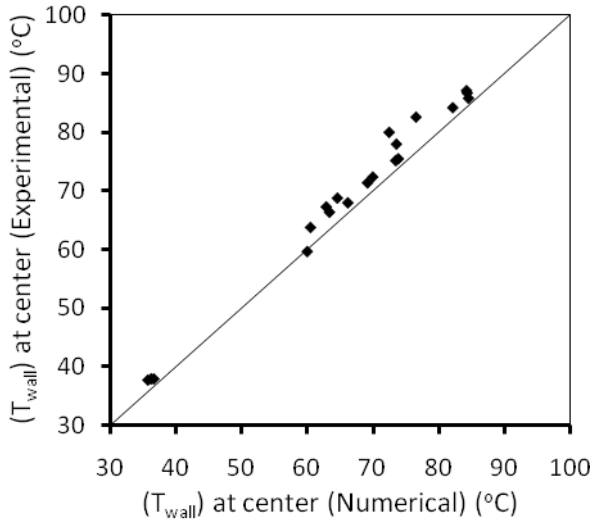

Fig. (5) Predicted tube surface temperature at center versus experimental data.

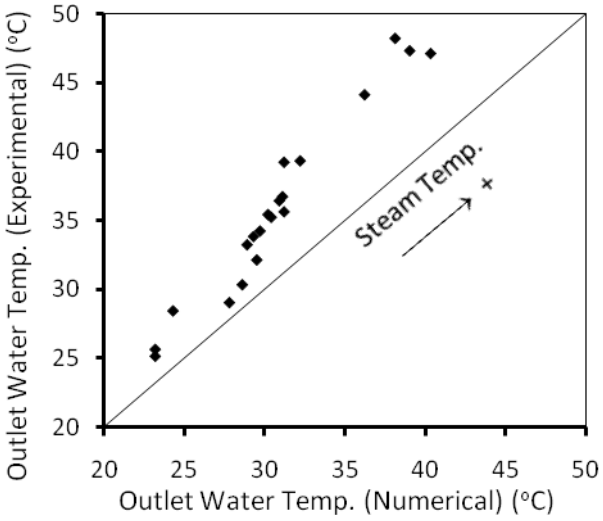

Fig. (6) Predicted cooling water outlet temperature versus experimental data.

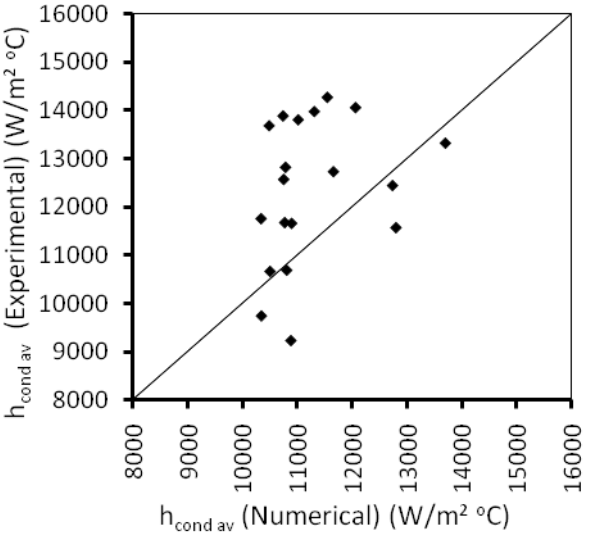

Fig. (7) Predicted condensation heat transfer coefficient versus experimental data.

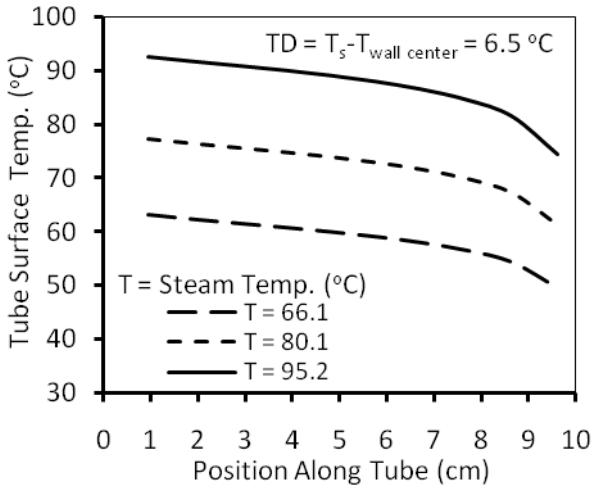

Fig. (8) Variation of tube surface temperature with position along tube for different (steam-surface) Temp. difference.

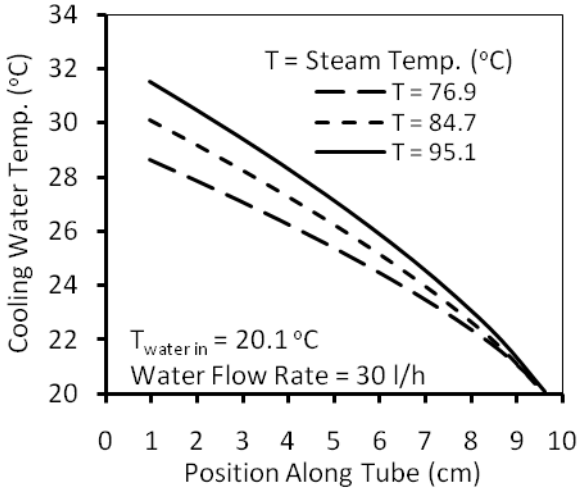

Fig. (9) Distribution of cooling water temperature flowing through the tube for different steam temperatures.

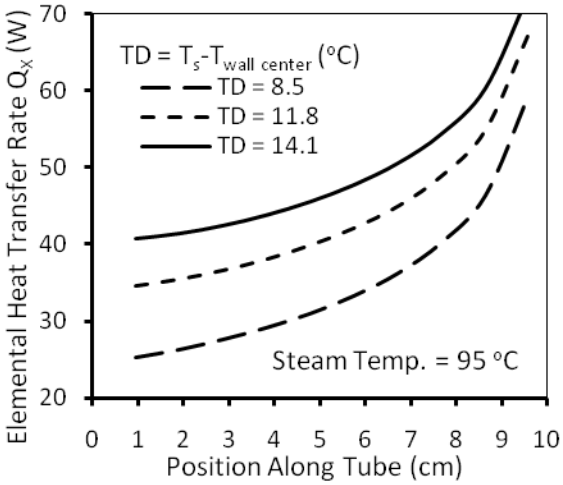

Fig. (10) Variation of local heat transfer rate with position along tube for different (steam-surface) Temp. difference.

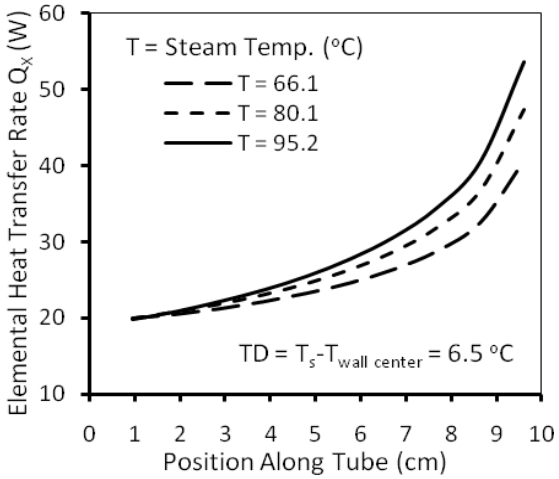

Fig. (11) Variation of local heat transfer rate with position along tube for different steam temperatures.

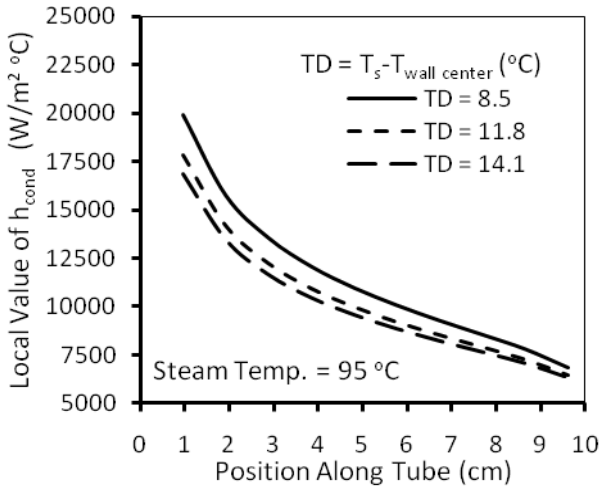

Fig. (13) Variation of local condensation H.T. coefficient with position along tube for different (steam-surface) Temp. difference.

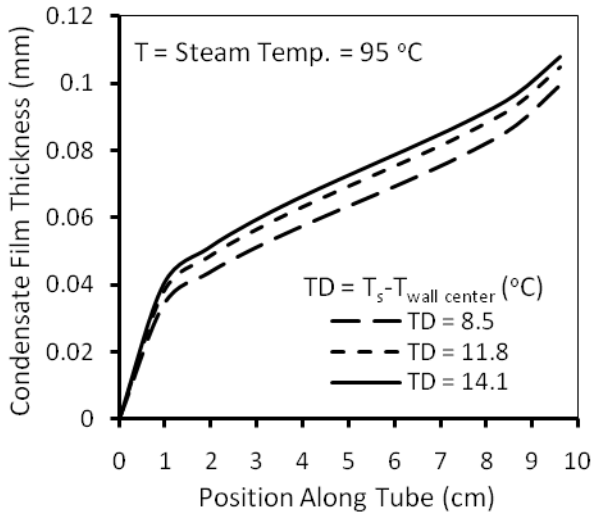

Fig. (12) Distribution of condensate film thickness along tube surface for different

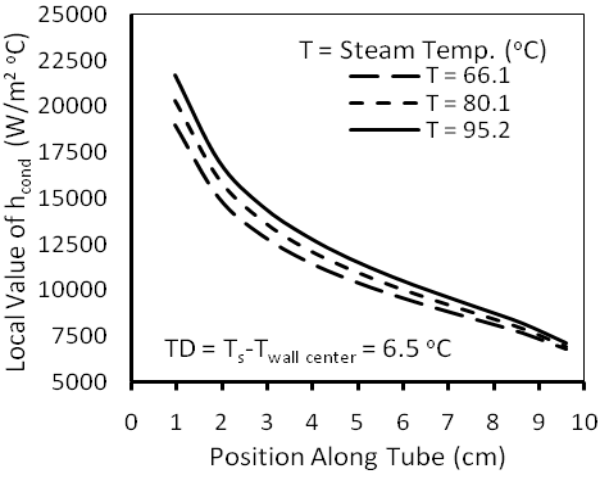

Fig. (14) Variation of local condensation H.T. coefficient with position along tube for different steam temperatures.

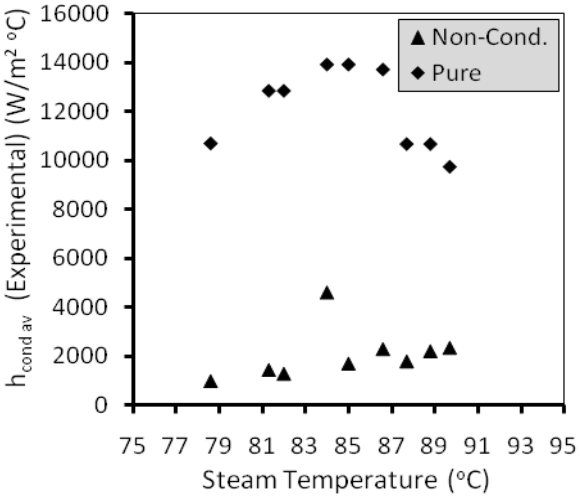

Fig. (15) Comparison of average condensation heat transfer coefficient for pure steam and with the presence of non-condensable gas (air).

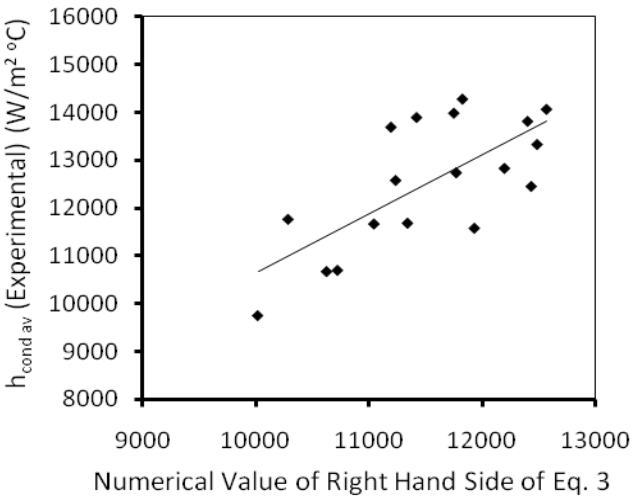

Fig. (16) Plot of experimentally calculated average condensation heat transfer coefficient versus numerical value of right hand side of Eq. 3.

PARAMETRIC STUDY OF SUCTION OR BLOWING EFFECTS ON TURBULENT FLOW OVER A FLAT PLATE

Prof.Dr. Najdat Nashat Abdulla & Miss.Sajida Lafta Ghashim Jassim
University of Baghdad
College of Engineering
Mechanical Engineering Department

ABSTRACT

The two-dimensional, incompressible, and turbulent boundary layer flow over a flat plate with suction or blowing from a spanwise slot is examined numerically. The mathematical modeling involves the derivation of the governing partial differential equations of the problems. These are the continuity, the momentum, the energy and the (K-ε) turbulence model. Besides, the perfect gas law is also used. A numerical solution of the governing equations is approximated by using a finite volume method, with staggered grid and modified SIMPLE algorithm. A computer program in FORTRAN 90 is built to perform the numerical solution.The developed computational algorithm is tested for the flow over a flat plate (4m) long with uniform suction or blowing velocity ratios of (V/U_∞ =± 0.0185, ± 0.0463 and ±0.0925 m/s) are imposed on the slot for Reynolds number of (1.36×10^7), based on the plate length. The position of the slot change in the range of (X/L=1/4, 1/2 and 3/4) from leading edge and also, change width of slot in the value equal (0.12, 0.2 and 0.28m).The plate temperature is (70 °C), with the free stream velocity and temperature are (8.6m/s) and (25 °C) respectively. In addition, the effects of pitch angles on the flow field are investigated in the range of ($30^o \leq \alpha \leq 150^{o)}$.The numerical results show that, for a uniform blowing, location of slot equal (X/L=1/4) from leading edge, a significant reduction of skin friction coefficient, wall shear stress and boundary layer thickness [displacement and momentum] to occur. While, an increase in boundary layer shape factor. Reynolds stress (uv) is more decreased than [(uu) and (vv)], mean velocity profiles in wall coordinates and dimensionless distance (U^+, y^+) decreases. When slot location is moved downstream to locations (X/L=1/2 or 3/4) a similar behavior can be said and most effective slot is obtained as (slot at X/L= 3m) from leading edge. While width of slot equal (0.28m) is better than values equal (0.12m and 0.2m). An opposite observations for the case of suction. The numerical results are compared with available numerical results and experimental data and a satisfactory results are obtained.

الخلاصة

تم بحث جريان الطبقة المتاخمة المضطربة الثنائي البعد واللأنضغاطي والمستقر على صفيحة مستوية مع وجود شق صغير دراسة عددية. يتضمن النموذج الرياضي اشتقاق المعادلات التفاضلية الجزئية للمسالة ، والتي هي معادلات الاستمرارية، الزخم، الطاقة ومعادلة نموذج (K - ε) للاضطراب.بالاضافة الى ذلك,تم استخدام معادلة الغاز المثالي. تم حل المعادلات عدديا باستخدام طريقة الحجوم المحددة (Finite Volume Method) مع الشبكة المزحفة (Staggered Grid) باستخدام خوارزمية (Simple Algorithm) . تم بناء برنامج حاسوبي بلغة (FORTRAN 90) لانجاز الحل العددي. النموذج العددي يتضمن الجريان على صفيحة مستوية طولها (4m) مع فرض نسب سرع دفع أو سحب على الشق مقدارها (±0.0463,± ±0.0185, V/U_∞=0.0925) لعدد رينولد ($1.36x10^7$) وذلك بالاعتماد على طول الصفيحة. دراسة تاثير تغير موقع الشق بمعدل(X/L=1/4, 1/2, 3/4)مع استعمال قيم مختلفة لعرض الشق (0.12,0.2,0.28m). درجة حرارة الصفيحة كانت (70°C) بينما كانت سرعة ودرجة حرارة الجريان الحر (8.6 m/ s),(25°C) على التوالي. بالاضافة الى ذلك، تم التحقق من تاثير زاوية الخطوة على حقل الجريان بحدود($30° \leq \alpha \leq 150°$) . من خلال النتائج العددية نلاحظ انه في حالة الدفع، عند اختيار موقع الشق ببعد(X/L=1/4) عن مقدمة الصفيحة, نلاحظ نقصان معامل الاحتكاك ، الاجهاد القصي مع نقصان سمك الطبقة المتاخمة (الزخم،السمك) ، بينما معامل شكل الطبقة المتاخمة يزداد، اجهادات Reynolds (uv) اكثر نقصان من (uu) و(vv)، الابعاد اللابعدية (U^+,y^+) تقل، وعندما يتم تسليط سرعة الدفع من خلال شق اخر يبعد عن مقدمة الصفيحة مثلا(X/L=1/4, 1/2) نلاحظ انه نفس الشي يحدث وافضل موقع فعال يبعد (X/L=3/4). اما مقدار الشق الذي يساوي(0.28m) افضل من بقية القيم الاخرى التي تساوي (012,0.2m) عكس الشي يمكن ملاحظته في حالة السحب. وتم مقارنة النتائج العددية مع النتائج العددية والعملية المتوفرة وكانت نتائج المقارنة مقاربة مع اختلاف بسيط مع النتائج العددية.

KEY WORD: Local forcing, Turbulent boundary layer, effect of suction and blowing, Drag reduction, Boundary layer control.

INTRODUCTION

A turbulent boundary layer is one of the wall turbulence flows that affected by the presence of solid wall. According to experimental data, a turbulent boundary layer made up of inner and outer regions. The effects of wall suction or blowing have been studied experimentally and numerically, the physics of a blowing or suction boundary layer is in fact mostly a no slip boundary layer that is perturbed slightly by the addition / extraction of a small amount of fluid. Literature survey reveals that several methods have been done to investigate the effect of suction and blowing numerically and numerically by the authors:

Park and Choi [1999] studied the effects of uniform blowing and suction over a flat plate on a turbulent boundary layer flow using the direct numerical simulation technique. The integration method used to solve Navier-Stokes equations. The magnitudes of blowing or suction are less than 10% of the free- stream velocity. The skin friction and near- wall turbulence intensities are significantly changed by blowing and suction. In the case of uniform blowing, the skin friction on the slot rapidly decreases. The streamwise vortices above the wall are lifted up by blowing, and thus the interaction of the vortices with the wall becomes weaker. Accordingly, the lifted vortices become stronger in the downstream due to less viscous diffusion (above the slot) and more tilting and stretching (downstream of the slot), resulting in the increase of the turbulence intensities as well as the skin friction downstream of the slot. The opposite is observed in the case of uniform suction. For both cases of blowing and suction, the streamwise turbulence intensity recovers quickly from blowing or suction, while other components of the turbulence intensities and Reynolds shear stress recover in a longer downstream distance.

Kim and Sung [2003] investigated the effects of time-periodical blowing through a spanwise slot on a turbulent boundary layer. The blowing velocity was varied in a cyclic manner from 0 to $2A^+$ (A^+= 0.25, 0.50, and 1.00) at a fixed blowing frequency of f^+ =0.017. The effect of steady blowing (SB) was also examined, and the SB results were compared with those for periodic blowing (PB). PB reduced the skin friction near the slot, although to a slightly lesser extent than SB. PB was found to generate a spanwise vertical structure in the downstream of the slot. This vortex generates a reverse flow near the wall, there by reducing the wall shear stress. The wall- normal and spanwise turbulence intensities under PB are increased as compared to those under SB, whereas the streamwise turbulent intensity under PB is weaker than that under SB. PB enhances more energy redistribution than SB. The periodic response of the streamwise turbulence intensity to PB is propagated to a lesser extent than that of the other components of the turbulence intensities and the Reynolds shear stress.

Munem [2004] developed a general method for numerical solution of the steady state, two dimensional and incompressible turbulent flow over a flat plate with uniform suction or blowing. Turbulence effect was handled through considering K-ε model.The solution algorithm SIMPLE in cartesion coordinates system with staggered grid technique was used to solve the Navier- Stockes equations with continuity equation. The results show that, for uniform blowing, the skin friction rapidly decreases near the slot and increases in the downstream of the slot, the most effective pitch angle is obtained as (α= 60^o) which gives the maximum reduction of skin friction coefficient. Near the blowing slot, the velocity fluctuations and Reynolds shear stress decrease, because their profiles are shifted away from the wall. An opposite observations are obtained for the case of suction velocities. Results were compared with available numerical and experimental data show a good agreement.

Krogstad and Kourakine [2000] investigated the effects of localized injection through a porous strip on a turbulent boundary layer at zero pressure gradient conditions experimentally. The magnitude of the injection velocity were kept very small (less than 1% of the free-stream velocity) to prevent separation near the injection strip and to keep the perturbations small. It was found that, the injection increases all the Reynolds stresses and, this perturbation dies out very slowly as the affected layer is sandwiched between the outer edge of the incoming boundary layer and a new layer that develops at the wall. A study of the anisotropy tensor indicated no effects of the blowing rate on the flow anisotropy downstream of the injection region.

Park, Park and Sung [2003] performed an experimental study to investigate the effect of periodic blowing and suction on a turbulent boundary layer. Partical Image Velocimetry (PIV) was used to probe the characteristics of the flow. Local forcing was introduced to the boundary layer via a sinusoidally – oscillating jet issuing from a thin spanwise slot. Three forcing frequencies (f^+= 0.044, 0.066, and 0.088) with a fixed forcing amplitude (A^+ = 0.6) were employed at Reθ = 690. The effect of three different forcing angles (α = 60^o, 90^o and 120^o) was investigated under a fixed forcing frequency (f^+ = 0.088). The PIV results showed that, the wall- region velocity decreases on imposition of the local forcing. Inspection of the phase- averaged velocity profiles revealed that, spanwise large- scale vortices are generated downstream of the slot and persist father downstream. The highest reduction in skin friction was achieved at the highest forcing frequency (f^+ = 0.088) and a forcing angle of (α = 120^o). The spatial fraction of the vortices was examined to analyze the skin friction reduction.

The present work deals with the calculation of the steady, two dimensional, incompressible and turbulent boundary layer over a flat plate with uniform suction and blowing,The main objective of the present work will be as follows:

- Investigation of the important parameters of the boundary layer (skin friction coefficient, displacement thickness, momentum and shape factor) in upstream and in the downstream of the slot.
- Using different positions of the slot in the range of (X/L= 1/4, 1/2 and 3/4) from the leading edge with a different slot widths (0.12, 0.2 and 0.28m).
- Using different blowing and suction velocity ratios with a different pitch angles ($30° \le \alpha \le 150°$).
- Studying the profiles of time- mean velocity component at several streamwise locations for different blowing and suction velocity ratios.

PROPLEM DESCRIPTION

In the present study, a direct numerical simulation is performed to study the effect of uniform blowing or suction from a spanwise slot on a turbulent boundary layer over a flat plate see Figure (1). The free stream velocity (U_∞) was (8.6 m/s) over a flat plate of (4m) long with imposed uniform suction or blowing velocity ratios on the slot with range of ($\frac{V}{U_\infty}$ = ±0.0185, ±0.0463 and ±0.0925) for Reynolds number of (1.36×10^7) based on plate length .Also, the effects of pitch angles on the flow field are investigated in the range of ($30° \le \alpha \le 150°$).

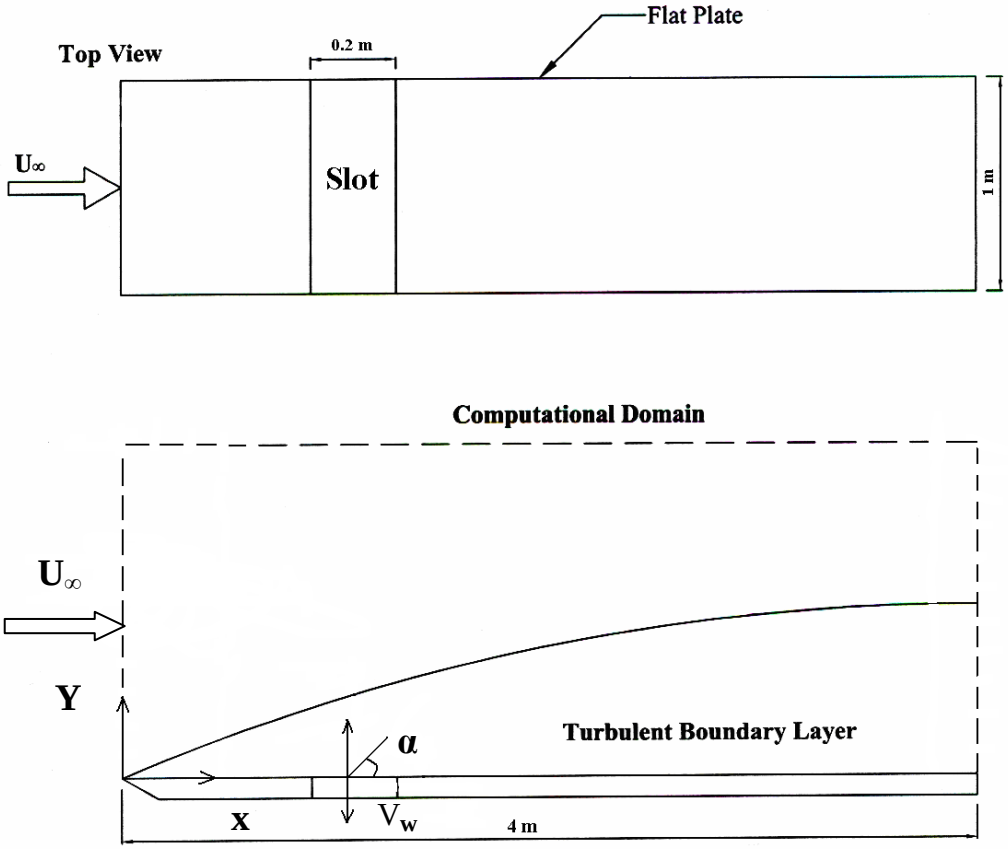

Fig. (1) Schematic diagram of computational domain

-MATHEMATICAL MODEL

The ensemble-mean equations of motion for steady state, two dimensional and incompressible flow over flat pate can be written in cartesian coordinates as follows [Awbi 1991]:

- Continuity Equation

$$\frac{\partial(\rho U)}{\partial x}+\frac{\partial(\rho V)}{\partial y}=0 \tag{1}$$

-Momentum Equations

$$\rho U\frac{\partial U}{\partial x}+\rho V\frac{\partial U}{\partial y}=-\frac{\partial P}{\partial x}+\frac{\partial}{\partial x}\left[\mu_e\frac{\partial U}{\partial x}\right]+\frac{\partial}{\partial y}\left[\mu_e\frac{\partial U}{\partial y}\right]+\frac{\partial}{\partial x}\left[\mu_e\frac{\partial U}{\partial x}\right]+\frac{\partial}{\partial y}\left[\mu_e\frac{\partial V}{\partial x}\right] \tag{2}$$

$$\rho U\frac{\partial V}{\partial x}+\rho V\frac{\partial V}{\partial y}=-\frac{\partial P}{\partial y}+\frac{\partial}{\partial x}\left[\mu_e\frac{\partial V}{\partial x}\right]+\frac{\partial}{\partial y}\left[\mu_e\frac{\partial V}{\partial y}\right]+\frac{\partial}{\partial x}\left[\mu_e\frac{\partial U}{\partial y}\right]+\frac{\partial}{\partial y}\left[\mu_e\frac{\partial V}{\partial y}\right] \tag{3}$$

- Energy Equation

The conservation of thermal energy in the control volume [Awbi 1991]:

$$\frac{\partial}{\partial x}(\rho UT)+\frac{\partial}{\partial y}(\rho VT)=\frac{\partial}{\partial x}(\Gamma_e\frac{\partial T}{\partial x})+\frac{\partial}{\partial y}(\Gamma_e\frac{\partial T}{\partial y}) \tag{4}$$

- Equation of a Perfect Gas

$$P = \rho RT \tag{5}$$

- Standard K-ε Model

$$\rho U\frac{\partial K}{\partial x}+\rho V\frac{\partial K}{\partial y}=\frac{\partial}{\partial x}\left[\frac{\mu_e}{\sigma_K}\frac{\partial K}{\partial x}\right]+\frac{\partial}{\partial y}\left[\frac{\mu_e}{\sigma_K}\frac{\partial K}{\partial y}\right]+\mu_t\left[2\left(\frac{\partial U}{\partial x}\right)^2+2\left(\frac{\partial V}{\partial y}\right)^2+\left(\frac{\partial U}{\partial y}+\frac{\partial V}{\partial x}\right)^2\right]-\rho\varepsilon \tag{6}$$

$$\rho U\frac{\partial \varepsilon}{\partial x}+\rho V\frac{\partial \varepsilon}{\partial y}=\frac{\partial}{\partial x}\left[\frac{\mu_e}{\sigma_\varepsilon}\frac{\partial \varepsilon}{\partial x}\right]+\frac{\partial}{\partial y}\left[\frac{\mu_e}{\sigma_\varepsilon}\frac{\partial \varepsilon}{\partial y}\right]+c_{1\varepsilon}\frac{\varepsilon}{K}\mu_t\left[2\left(\frac{\partial U}{\partial x}\right)^2+2\left(\frac{\partial V}{\partial y}\right)^2+\left(\frac{\partial U}{\partial y}+\frac{\partial V}{\partial x}\right)^2\right]-c_{2\varepsilon}\rho\frac{\varepsilon^2}{K} \tag{7}$$

Table (1) Empirical constants in the (K-ε) [Lai and Makomaski 1989]

C_μ	$C_{1\varepsilon}$	$C_{2\varepsilon}$	σ_K	σ_ε	σ	σ_t
0.09	1.44	1.92	1.00	1.30	0.7	0.9

- BOUNDARY CONDITIONS

1. Upstream Boundary Conditions:

$$U_{up}=U_\infty \qquad V_{up}=0 \qquad \varepsilon_{up}=\frac{K_{up}^{1.5}}{0.005h} \qquad K_{up}=0.03(U_\infty)^2 \tag{8}$$

2. Downstream Boundary Conditions:

Normally the velocities are known only where the fluid enters the calculation domain. At downstream, the velocity distribution is decided by flow field within the domain. For incompressible flow, the gradients normal to the downstream surface of all quantities are assumed **:**

$$\phi_{NI,J}=\phi_{NI-1,J}$$

3. Wall Boundary Conditions:

The wall is the most common boundary encountered in confined fluid flow problems. In this section, a solid wall parallel to the u-direction is considered. The no-slip condition (u=v=*0*) is the appropriate condition for the velocity components at solid walls [Versteeg and Malalasekera 1995].In the case of turbulent flow, the calculation of shear stress near the wall needs a special treatment. This is due to the existence of boundary layers, across which steep variation of flow properties occurs and the standard (K-ε) model becomes inadequate. In order to adequately avoid these problems, it would be necessary to employ a fine grid near the wall, which would be expensive. An alternative and widely employed approach is, to use formula which known as "wall function"

4. Free Stream Boundary Condition:

At y= δ:

$$U=U_\infty,\frac{\partial u}{\partial y}=0,P=P_\infty,T=T_\infty$$

NUMERICAL SOLUTION

For the case of steady state, incompressible and two-dimensional turbulent flow, the general equation [Patanker 1980]:

$$\frac{\partial}{\partial x}(\rho u\Phi)+\frac{\partial}{\partial y}[\rho v\Phi]=\frac{\partial}{\partial x}\left[\Gamma_\Phi\frac{\partial\Phi}{\partial x}\right]+\frac{\partial}{\partial y}\left[\Gamma_\Phi\frac{\partial\Phi}{\partial y}\right]+S_\Phi \quad (9)$$

Where:

$$\frac{\partial}{\partial x}(\rho U\Phi)+\frac{\partial}{\partial y}(\rho V\Phi)=Convection\ term$$

$$\frac{\partial}{\partial x}\left[\Gamma_\Phi\frac{\partial\Phi}{\partial x}\right]+\frac{\partial}{\partial y}\left[\Gamma_\Phi\frac{\partial\Phi}{\partial y}\right]=Diffusion\ term$$

S_Φ= *Source term.*

The source term (S_ϕ) often depends on the dependent variable (ϕ). According to [Patanker 1980] the source term can be expressed as a linear form: $S_\phi = S_u + S_p\phi_p$

A control finite volume method developed by [Versteeg and Malalasekera 1995] is used to discretize the governing equations. These discretization equations are solved by using SIMPLE algorithm with hybrid scheme

- the final discretised algebraic equation:

$$A_P\phi_P = A_E\phi_E + A_W\phi_W + A_N\phi_N + A_S\phi_S + S_u \quad (10)$$

Where:

$$A_p = A_E + A_W + A_N + A_S - S_p$$

Where:

A_E = [[0,D_e-0.5F_e]]+[[-F_e,0]]

A_W = [[0,D_w-0.5F_w]]+[[F_w,0]]

A_N = [[0,D_n-0.5F_n]]+[[-F_n,0]]

A_S = [[0,D_s-0.5F_s]]+[[F_s,0]]

- FURTHER NUMERICAL CALCULATION

The most important parameters for boundary layer flow, skin friction coefficient C_f, displacement thickness δ^*, momentum thickness θ, and shape factor H. these parameters are defined by the following equations [Schlichting 1968]:

$$C_f = \frac{2\tau_W}{\rho U_\infty^2},\ \delta^* = \int_0^\delta\left(1-\frac{u}{U_\infty}\right)dy\ ,\ \theta = \int_0^\delta\frac{u}{U_\infty}\left(1-\frac{u}{U_\infty}\right)dy,\ H=\frac{\delta^*}{\theta}, \quad (11)$$

Where: $\delta = \frac{0.376x}{\mathrm{Re}_x^{0.2}}$

- the displacement thickness (δ^*) is computed :

$$\delta^* = \int_0^{\delta}\left(1-\frac{u}{U_\infty}\right)dy = \int f(x_n)dx$$

a numerical integration methods used which is called Trapezoidel rule (or integration with unequal segments) can be used.

The general form of this method of integration is:

$$I = h_1\frac{f(x_1)+f(x_0)}{2} + h_2\frac{f(x_2)+f(x_1)}{2} + \ldots\ldots + h_n\frac{f(x_n)+f(x_{n-1})}{2} \qquad (12)$$

using the same numerical method to compute the momentum thickness.

- RESULTS AND DISCUSSIONS

Fig. (2) shows that the skin friction coefficient is changed significantly close to the region of local suction and blowing.In the case of no forcing, it is seen that, the skin friction coefficient decreases with the flow direction due to the decrease of the velocity gradient at the wall.

In the case of uniform blowing ,the skin friction on the slot rapidly decreased .The near –wall streamwise vortices were lifted up by blowing, and thus interaction of the vortices with wall become weaker .Accordingly, the lifted vortices became stronger in the downstream due to less viscous diffusion (above the slot) and more tilting and stretching (downstream of the slot), resulting in the increase of the turbulence intensities as well as the skin friction downstream of the slot.

In the case of uniform suction, the skin friction on the slot increased significantly. The near-wall streamwise vortices were drawn toward the wall by suction, and thus viscous diffusion became very effective near the slot, resulting in weaker streamwise vortices in the downstream of the slot. Therefore, the turbulence intensities as well as the skin friction decreased downstream of the slot. A similar trend were observed for blowing and suction for channel flow simulations by [Park and Chio 1999] for turbulent boundary layer flow.

Fig. (3) show that the reduction of skin friction increases with increasing the velocity of blowing. Moreover, the reduction of skin friction may be related to the role of the large scale vortical structure in the vicinity of the wall. Therefore, the largest skin friction reduction is obtained at the higher blowing velocity ratio. While suction shows that, the reduction of the skin friction increases with decreasing the velocity of suction.

Fig. (4) examine the effect of the pitch angle on the reduction of skin friction..The most effective pitch angle is obtained as (α=90°), which gives the maximum reduction of skin friction reduction. While the skin friction reduction is insignificant when (α) is larger than (90^o) in the case of blowing. An opposite effect is observed in the case of suction.

Fig. (5) show the variation of the skin friction coefficient at various position of the slot over a flat plate. For uniform blowing at locations 1m or 2m (X/L=1/4 or 1/2) from leading edge a significantly reduction in skin friction is created, but when the blowing is moved downstream to location at 3m (X/L=3/4) from leading edge, a

maximum reduction in skin friction coefficient is seen. While the uniform suction shows an opposite observations.

Fig. (6) show the variation of the skin friction coefficient at different values for width of slot. For uniform blowing, the maximum reduction of skin friction is observed at width of slot (0.28 m). On the other hand, an opposite behavior is detected for suction case.

Fig. (7-11) show that, the shape factor increases with uniform blowing and decreases with uniform suction, as compared to that of the unperturbed flow. From the variation of the shape factor shown in these figures, it can be said that, uniform blowing shows the characteristics of adverse pressure gradient flow, while uniform suction shows that of favorable pressure gradient flow. The value of shape factor is different from the normal range (1.2 - 2.4) because the distribution of velocity effected by suction or blowing. Near the exit of the computational domain, the shape factors for the cases of suction are nearly the same as that of the unperturbed flow. On the other hand, the shape factors for the cases of blowing are still different from that of the unperturbed flow, meaning that the recovery distance for the shape factor due to blowing is longer than that due to suction. For uniform blowing the shape factor increases with increasing the velocity ratios, pitch angle, width of slot and when the slot moves downstream. An opposite observations are obtained for the case of suction. This is consistent with observation of numerical results of Park and Chio [1999].

Fig. (12-23) show the limiting behavior of turbulence intensities (uu and vv) and the Reynolds shear stress (uv) at the blowing and suction walls. Its clear that, uniform suction decreases the magnitudes of the velocity fluctuations, while uniform blowing increases them near the slot. It is also seen that near the slot for suction the profile of the turbulence intensities shifts toward the wall, and for blowing away from the wall, but at downstream of the slot, the an opposite behavior is observed. This is consistent with the results of Chung and Sung [2001]. The increases or decreases in the maximum values of turbulence intensities and Reynolds shear stress depend on the blowing or suction velocity ratios. Above the slot, in case of blowing, when increased the velocities of blowing, the (uu) and (uv) are more decreased than (vv), while (vv) is more decreased than (uu) and (uv) in the case of suction. The same behavior opposerved at different pitch angles, different slot widths and different positions of the slot for uniform blowing and suction.

Near the wall behavior of the streamwise velocity profiles in term of $\left(U^+ = \frac{U}{u_\tau}\right)$ are shown in Fig. (24). Here, the local friction velocity $\left(u_\tau = \sqrt{\frac{\tau_w}{\rho}}\right)$ is calculated along the streamwise direction over a flat plate. For the case of blowing, the velocity retardation at the wall leads to a reduction in the local skin friction coefficient (Cf) because of the small friction velocity and this reduction is increased with increasing velocity of blowing. The opposite is observed for the case of the suction.

Fig. (25) show the streamwise mean velocity profiles for forcing angle in the range ($30° \le \alpha \le 150°$). For uniform blowing, the forcing angle of ($\alpha \le 90°$) caused more significant reduction on (U^+), while an opposite behavior is observed in the case of the suction.

Fig. (26) for uniform blowing, the slot location at 3m (X/L=3/4) from leading edge gives better results for mean velocity than the locations 1m or 2m (X/L=1/4 or 1/2) from leading edge, but in the same location the flow does not appear significantly affected by the suction .

Fig. (27) show the predicted mean velocity profile in wall coordinates at different values of slot widths. Wider width of slot appears to be the most effective choice to reduce mean velocity profile; a reverse effect is showed for the case of the suction.

COMPARISON OF THE RESULTS

The numerical result of the present work is compared with available numerical result and experimental data. Some of the results show a discrepancy. This difference seems to be due to different magnitudes of blowing and suction velocities applied and also due to different widths of blowing and suction areas.

In Fig. (28), the predicted skin friction coefficient is compared with the numerical data of [Park and Chio 1999]. As displayed in figures, the present simulation shows good agreement with the numerical data for two cases blowing and suction.

Fig. (29) show the comparison of the shape factor with the numerical results of [Park and Chio 1999]. Satisfactory predictions have been obtained with the present results and a good agreement with available numerical data is observed

It can be seen from the Fig. (30), that the present prediction of skin friction coefficient is in a reasonable agreement with the carefully reviewed numerical data of [Munem 2004].

.

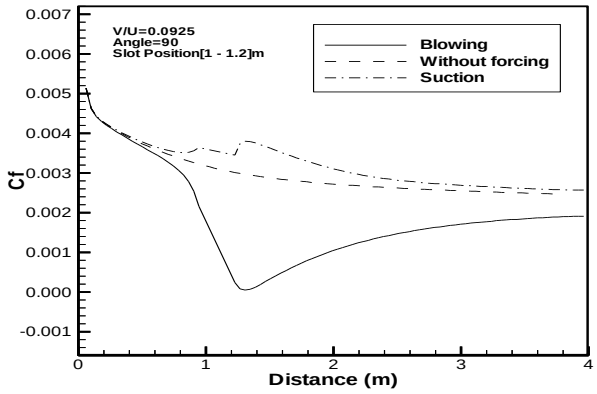

Fig. (2) Streamwise variation of skin friction coefficient for blowing, suction and without forcing.

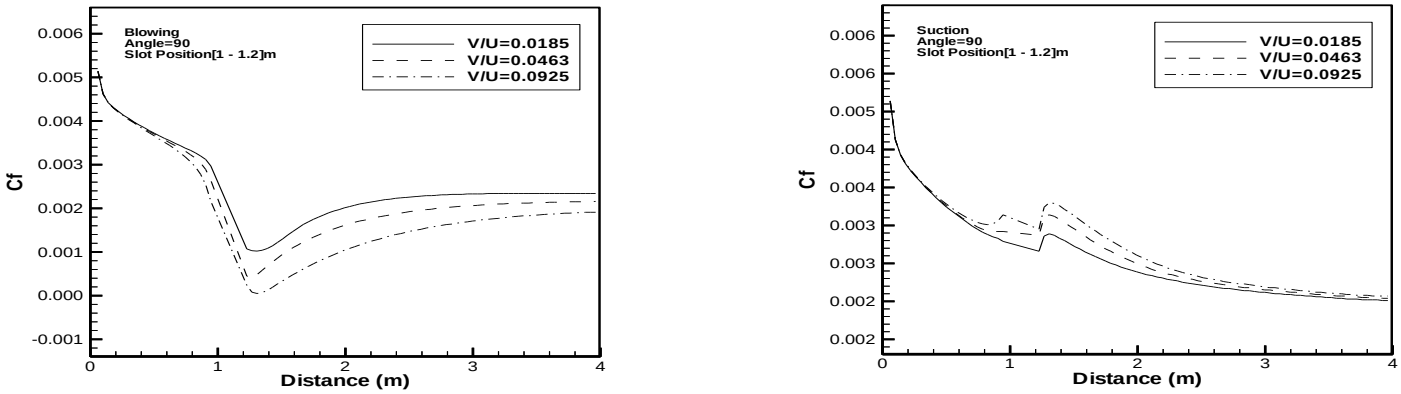

Fig. (3) Variation of skin friction coefficient for various velocity ratios

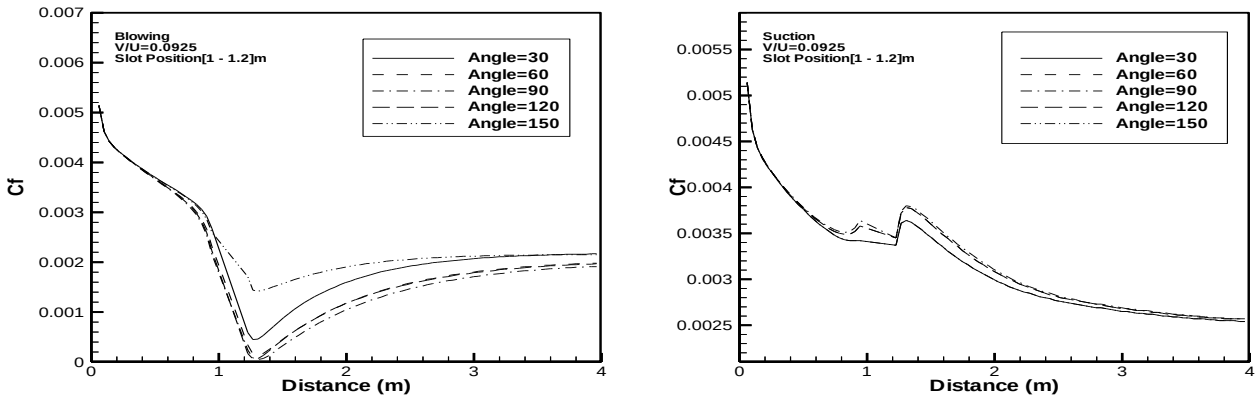

Fig. (4) Variation of skin friction coefficient at various pitch angles.

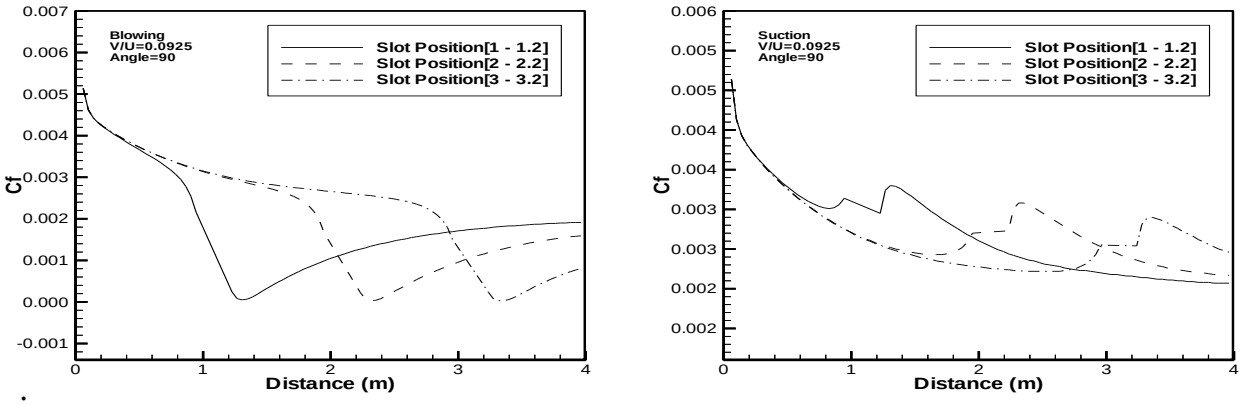

Fig.(5) Variation of skin friction coefficient at various positions of the slot.

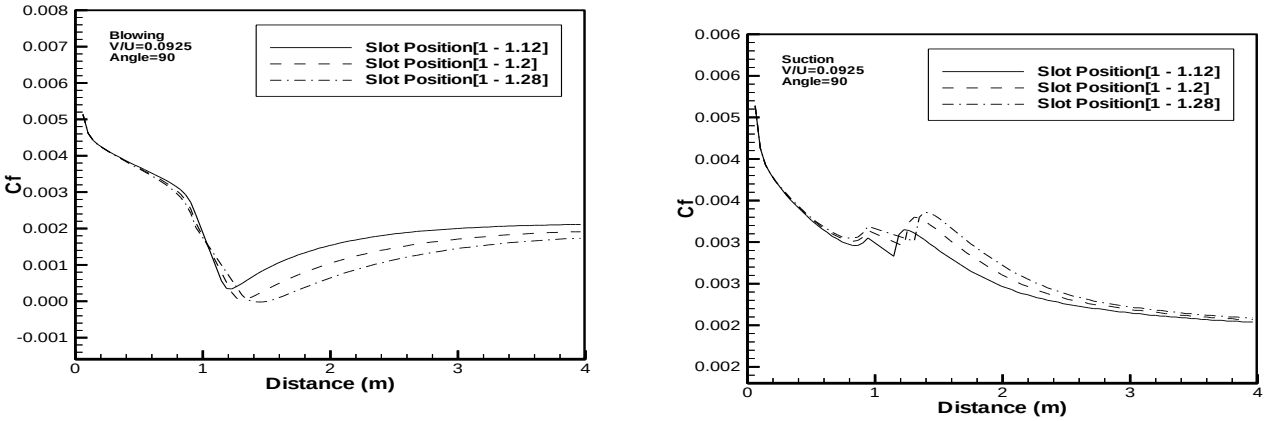

Fig. (6) Variation of skin friction coefficient at different values for width of slot.

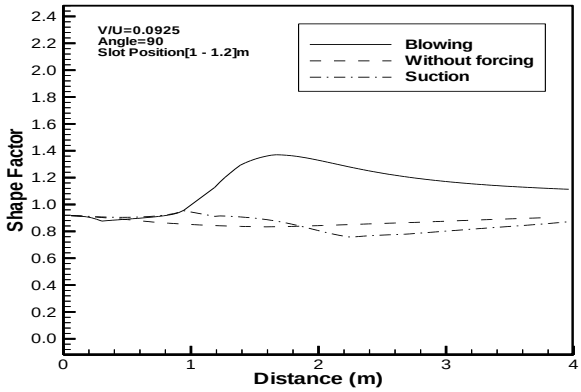

Fig. (7) Streamwise variation of shape factor for blowing, suction and without forcing.

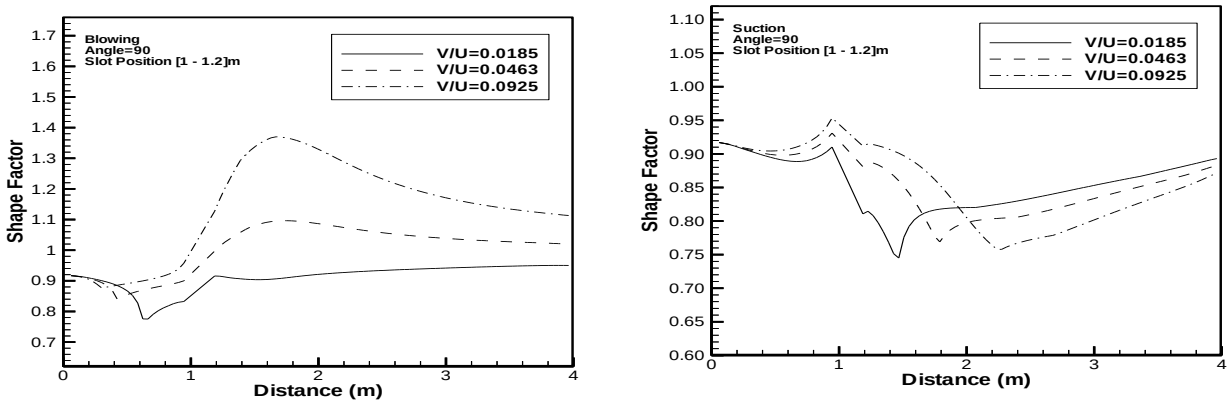

Fig. (8) Variation of shape factor for various velocity ratios.

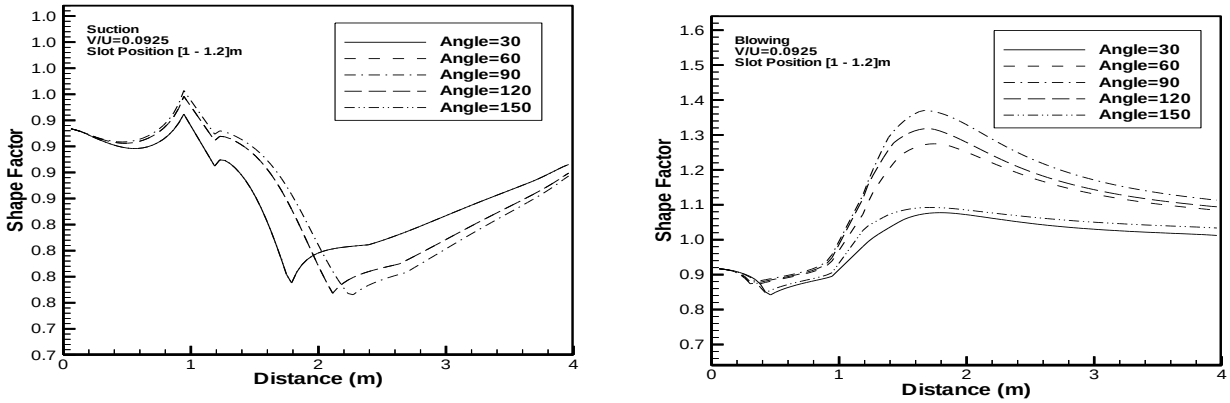

Fig. (9) Variation of shape factor at various pitch angles.

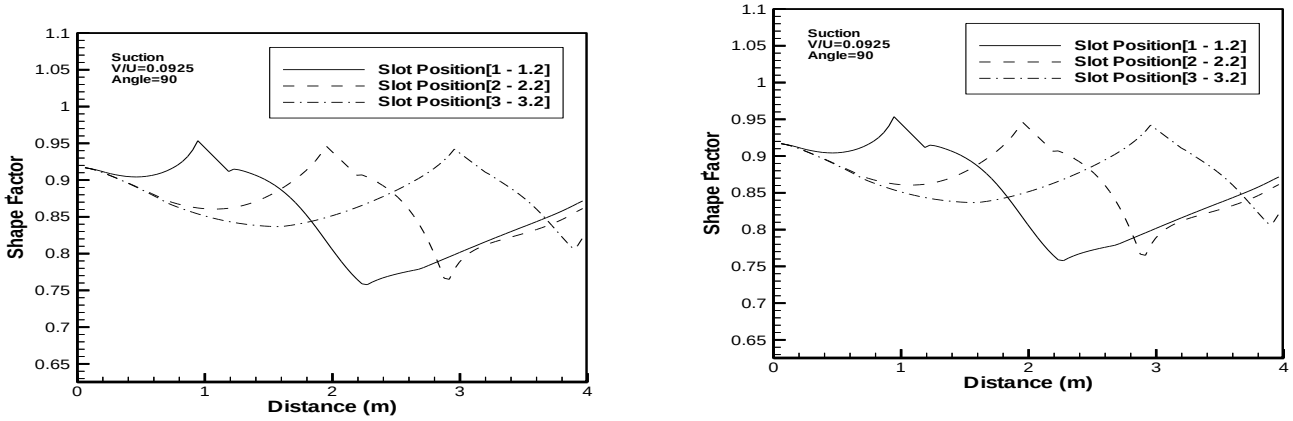

Fig. (10) Variation of shape factor at various positions of the slot.

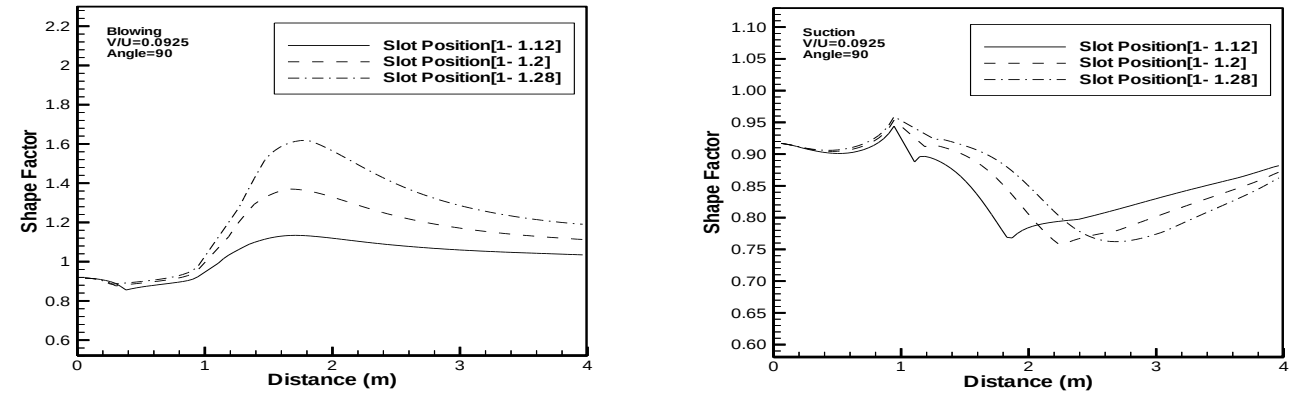

Fig. (11) Variation of shape factor at different values for width of slot.

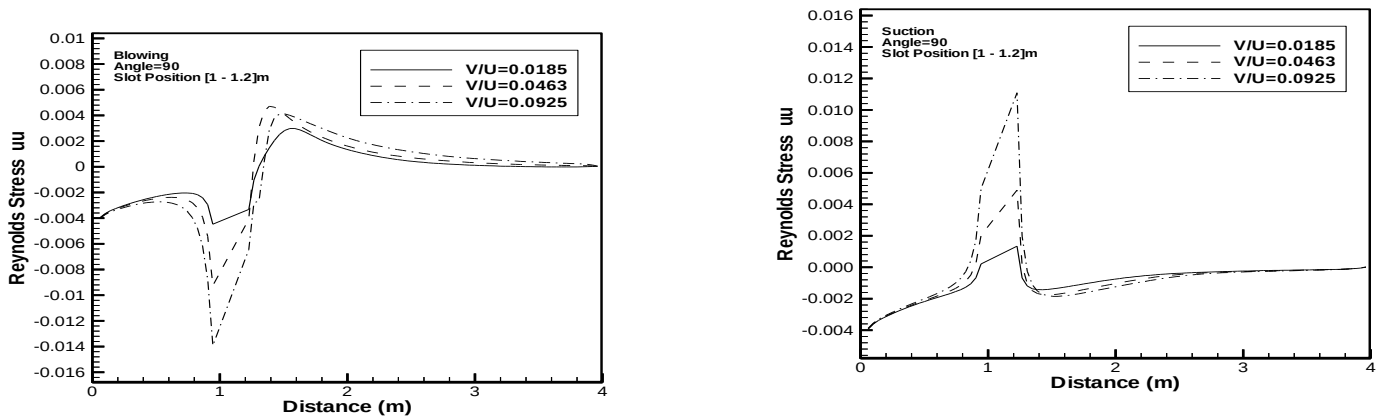

Fig. (12) Variation of the Reynolds stress (uu) for various velocity ratios.

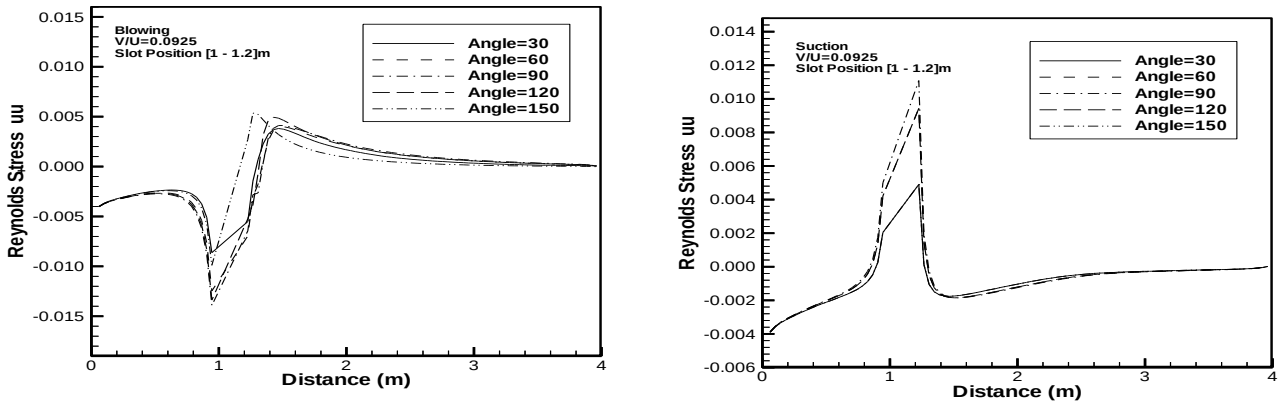

Fig. (13) Variation of the Reynolds stress (uu) at various pitch angles.

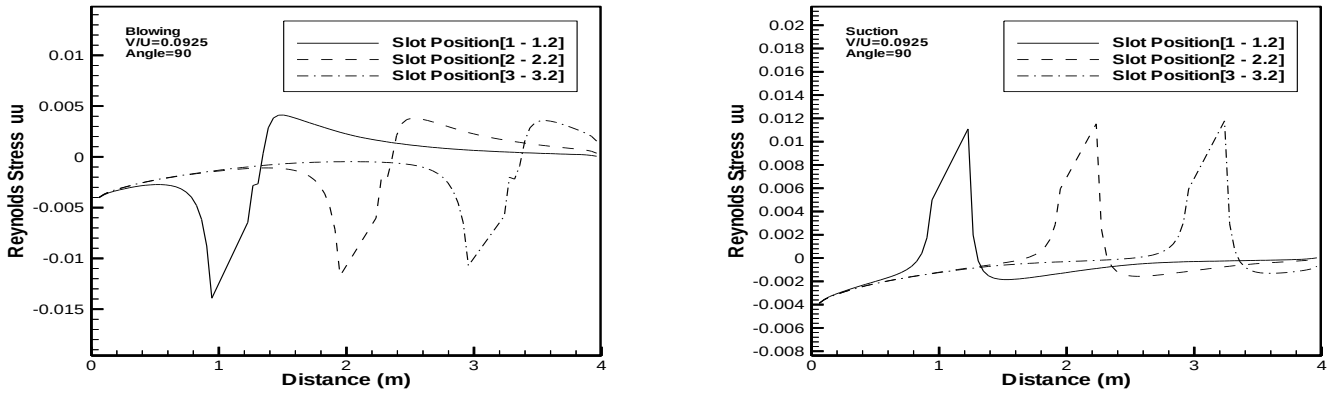

Fig. (14) Variation of the Reynolds stress (uu) at various positions of slots.

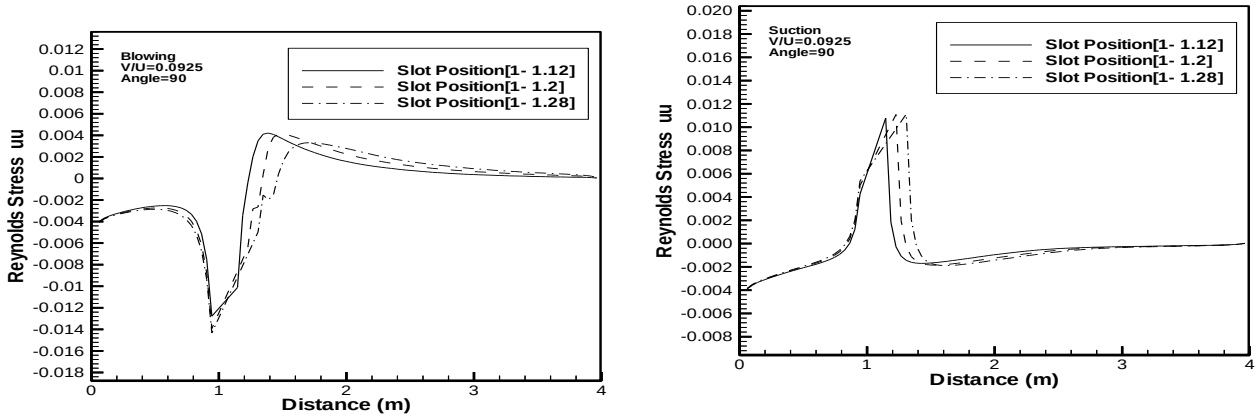

Fig. (15) Variation of the Reynolds stress (uu) at different values for width of slot.

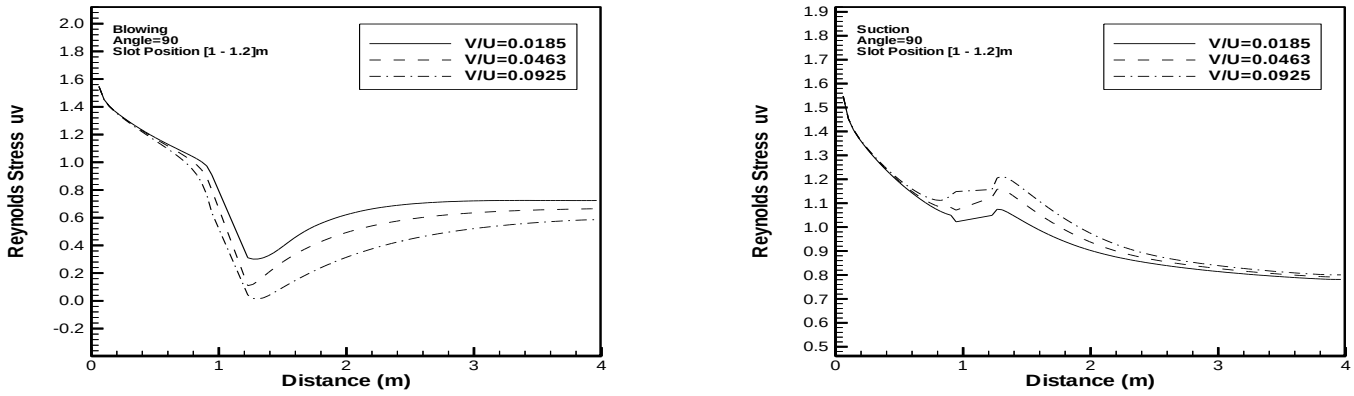

Fig. (16) Variation of the Reynolds stress (uv) for various velocity ratios.

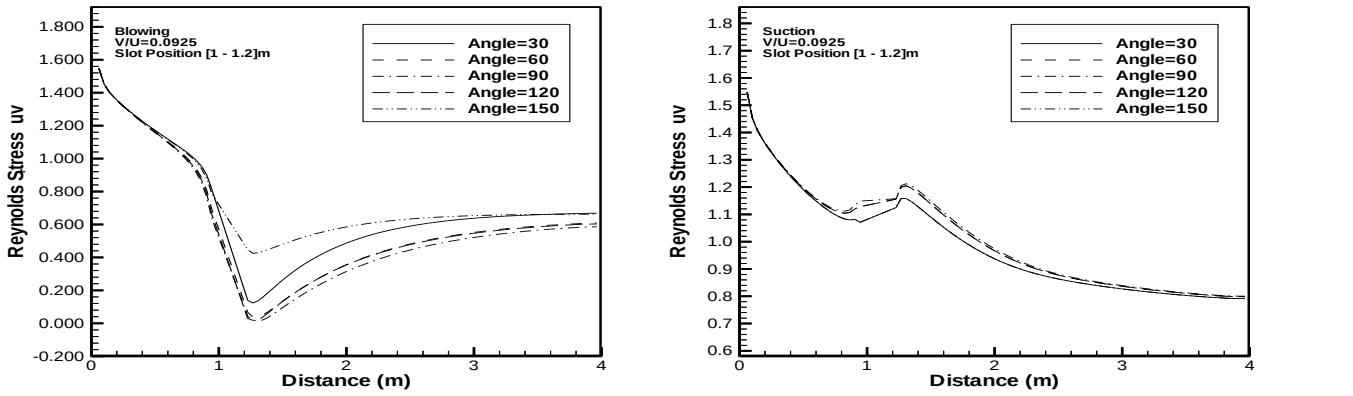

Fig. (17) Variation of the Reynolds stress (uv) at various pitch angles.

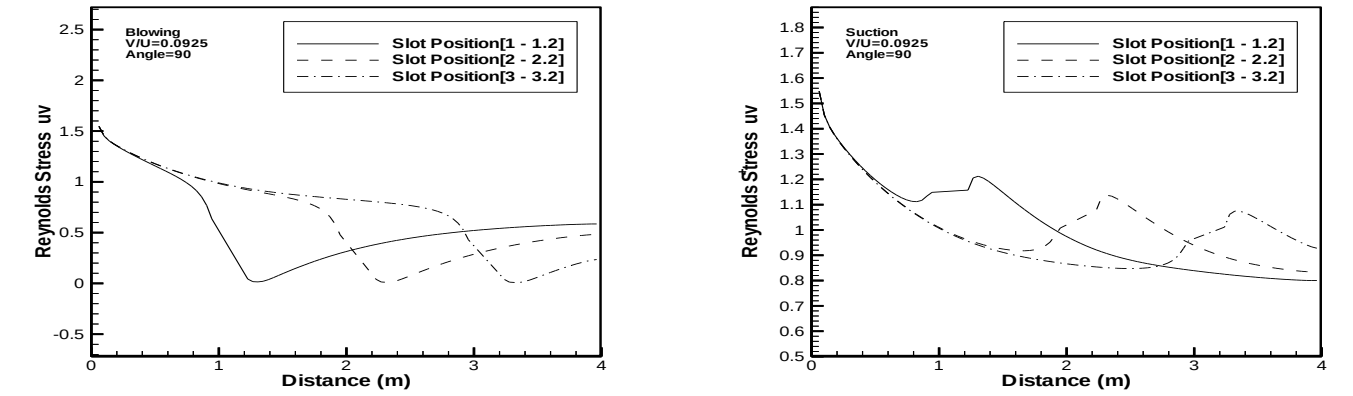

Fig. (18) Variation of the Reynolds stress (uv) at various poisons of the slot.

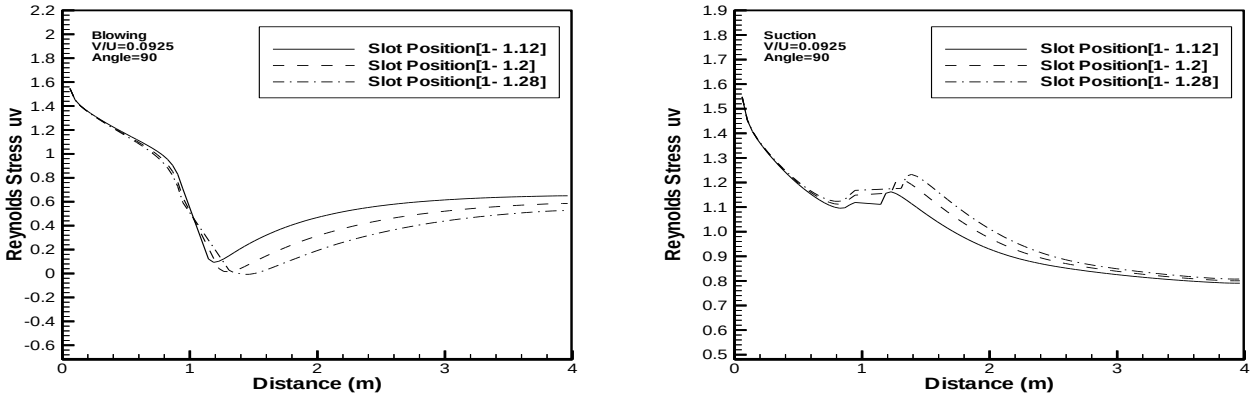

Fig. (19) Variation of the Reynolds stress (uv) at different values for width of slots.

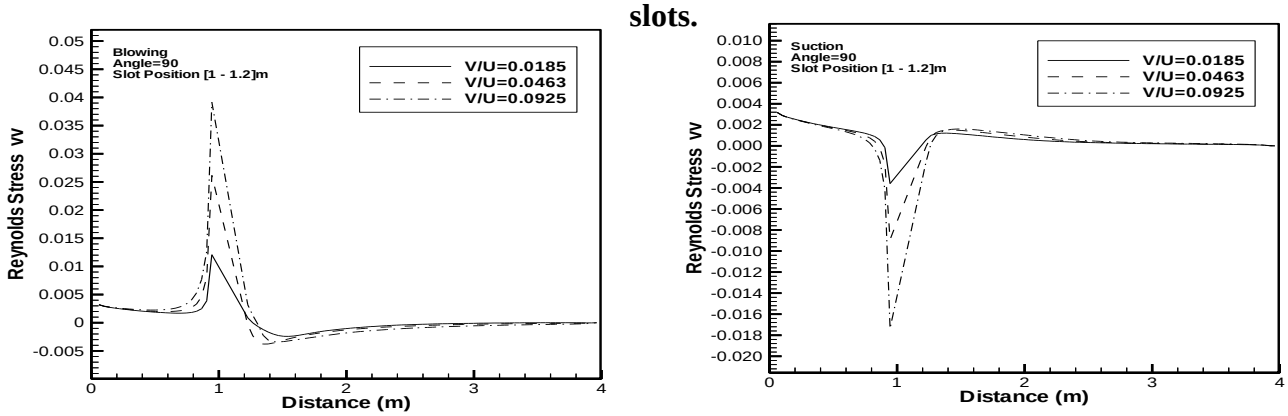

Fig. (20) Variation of the Reynolds stress (vv) at various velocity ratio.

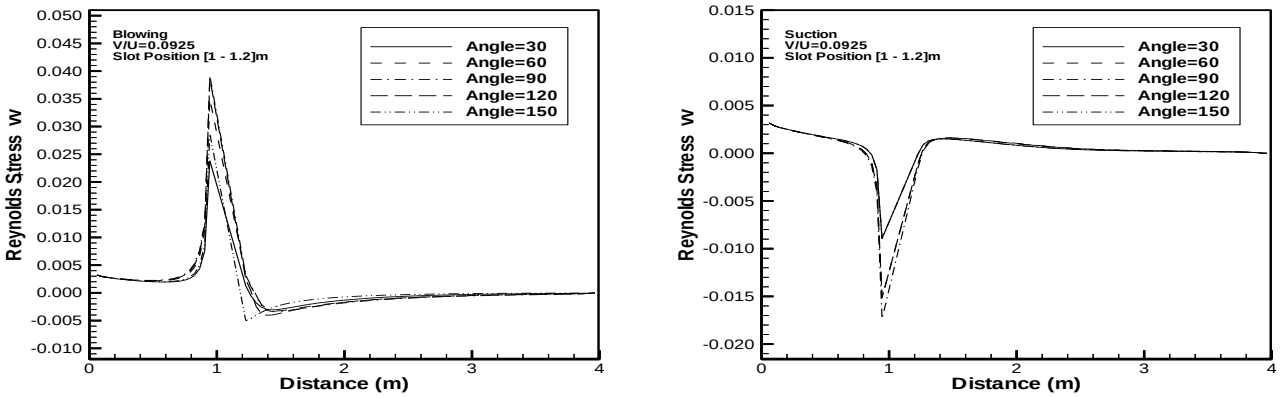

Fig. (21) Variation of the Reynolds stress (vv) for pitch angles.

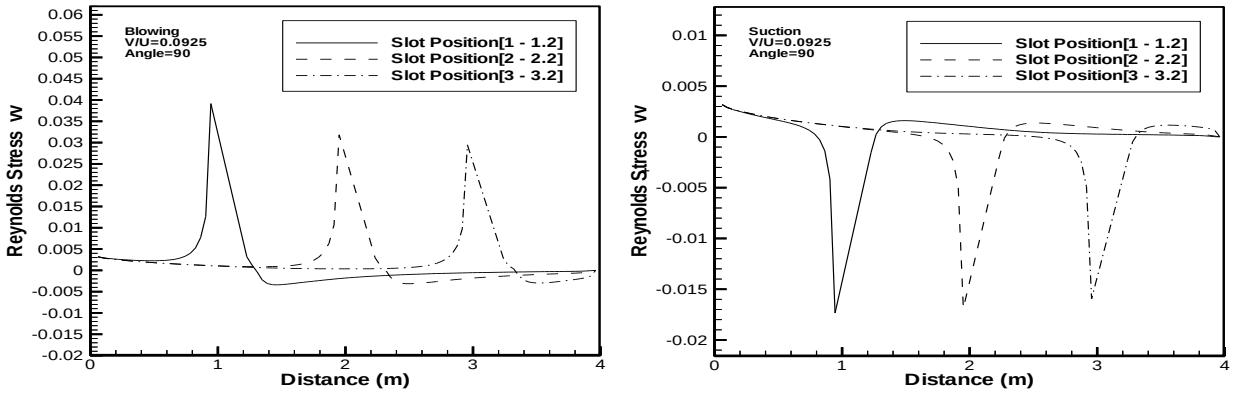

Fig. (22) Variation of the Reynolds stress (vv) at various positions of the slot .

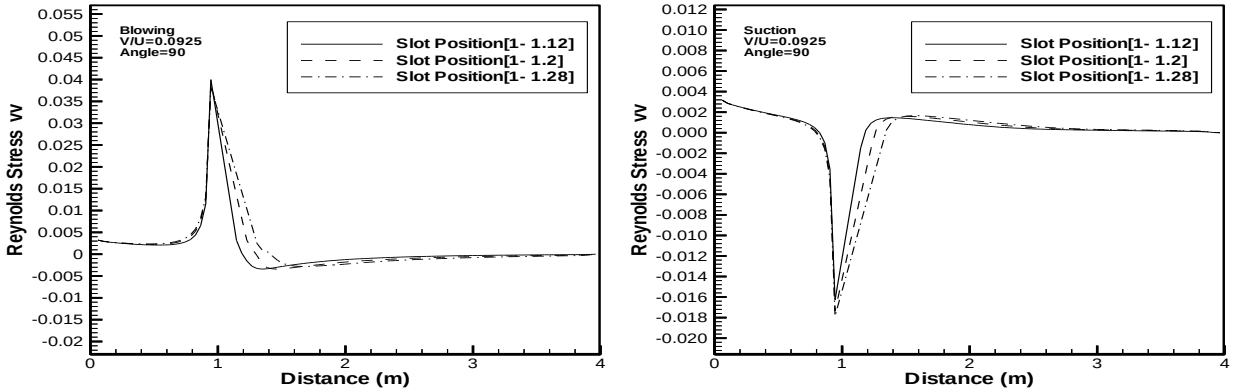

Fig. (23) Variation of the Reynolds stress (vv) at different values for width of slot.

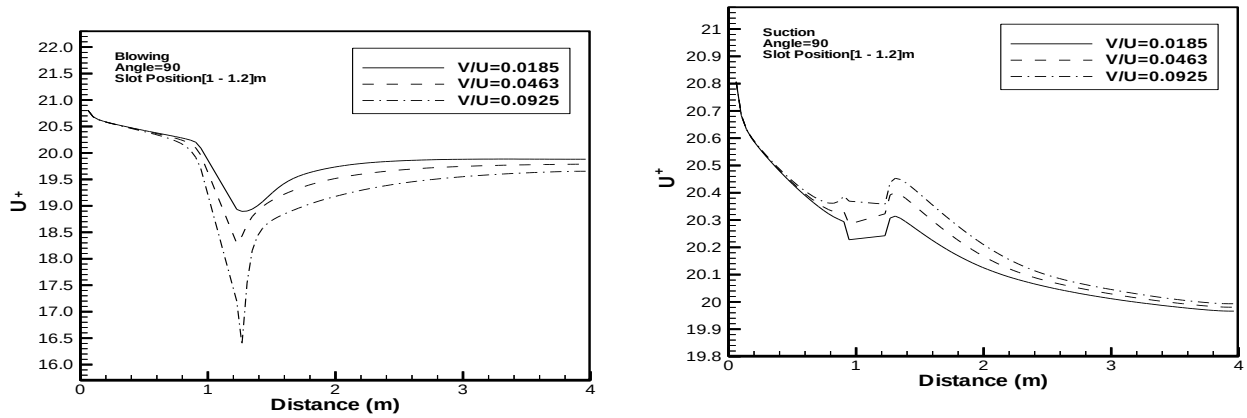

Fig. (24) Variation of mean velocity profiles in wall coordinates at various velocity ratios.

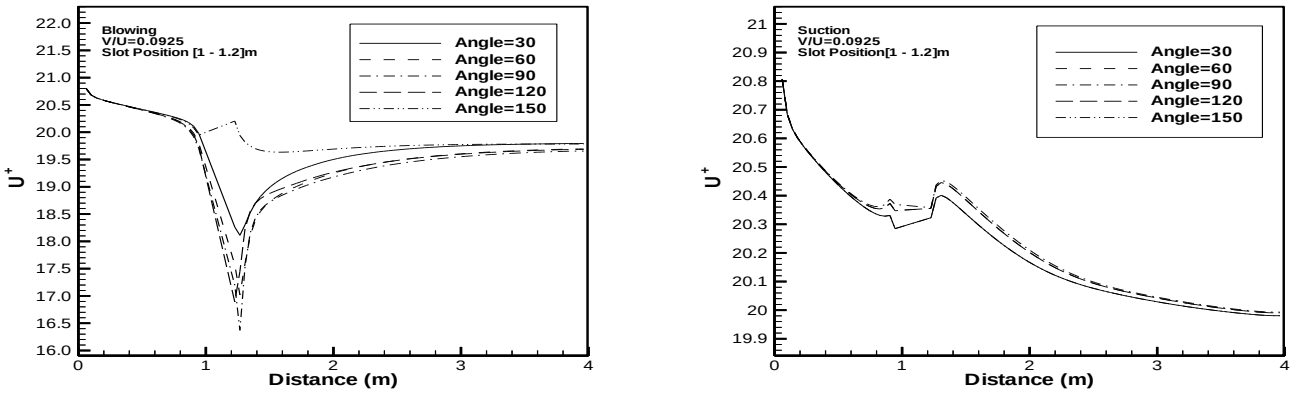

Fig. (25) Variation of mean velocity profiles in wall coordinates at various pitch angles.

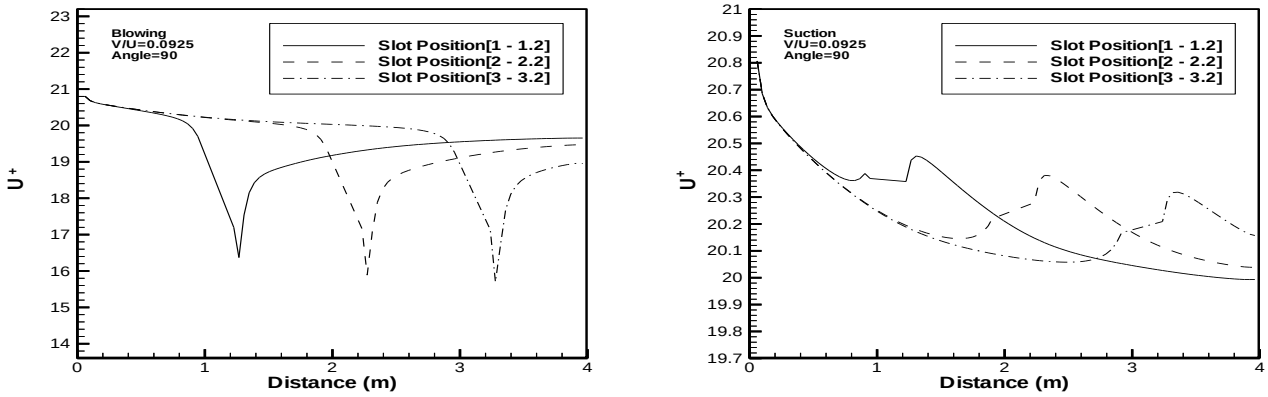

Fig.(26)Variation of mean velocity profiles in wall coordinates at various positions of the slot .

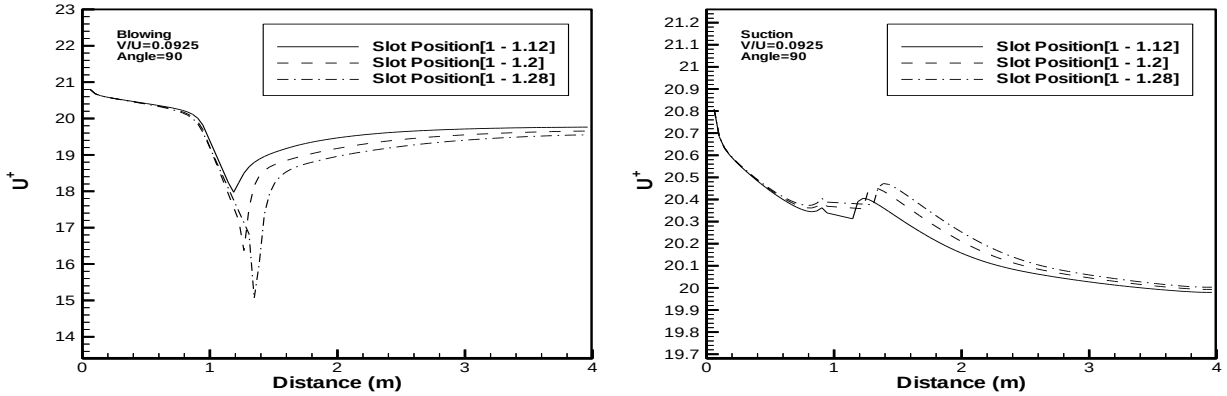

Fig. (27) Variation of mean velocity profiles in wall coordinates at different values for width of slot .

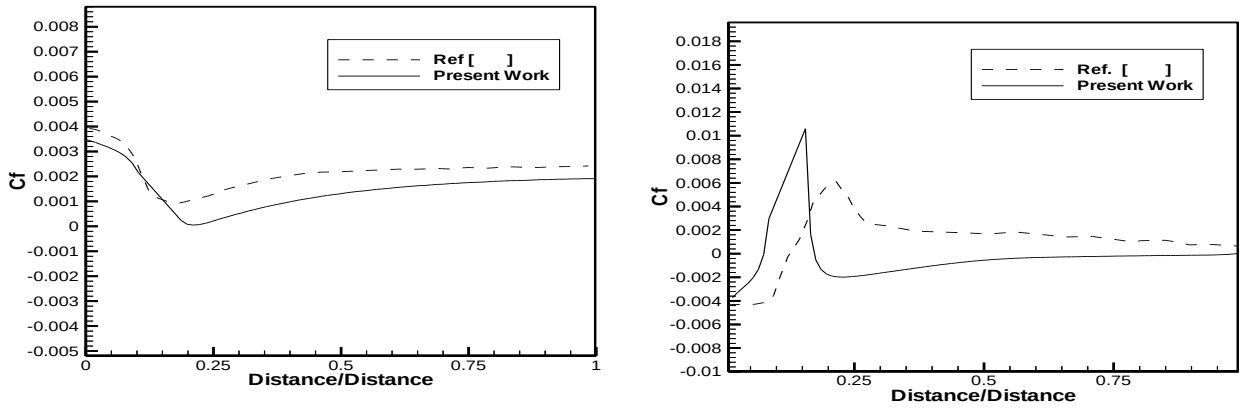

Fig. (28) Comparison of skin friction coefficient with numerical results of [Park and Chio 1999].

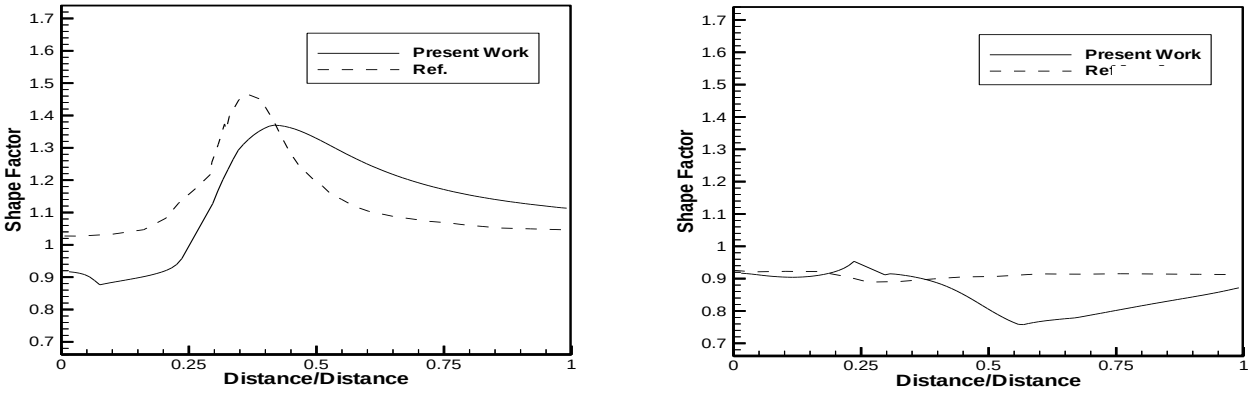

Fig. (29) Comparison of the shape factor with numerical results of [Park and Chio 1999].

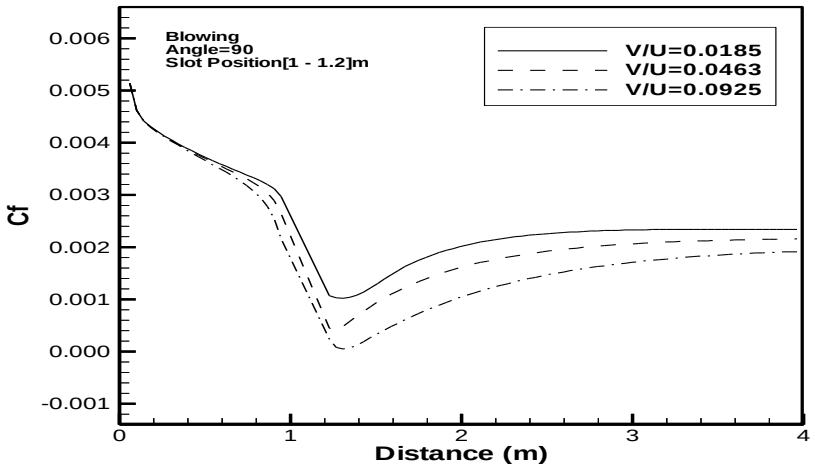

Present work

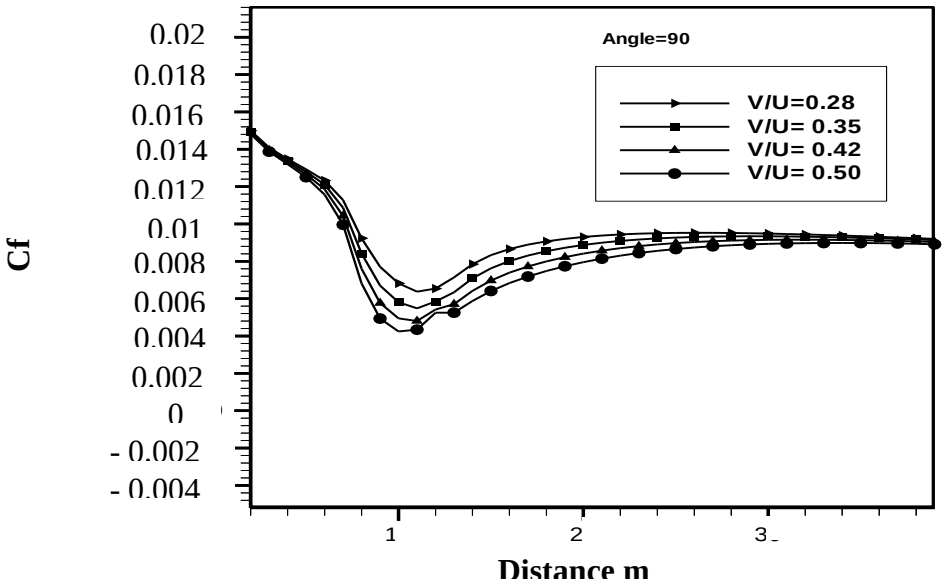

Reference [Munem 2004].

Fig. (30) Comparison of skin friction coefficient with numerical results of [Munem 2004]

CONCLUSION

- In the case of blowing, near the slot, the skin friction coefficient decreases and increases in the downstream of the slot. While a reverse action is observed for the case of suction.
- The largest skin friction reduction is obtained at the higher blowing velocity ratios for uniform blowing.

- The most effective pitch angle is obtained as (α=90°) which gives a maximum reduction in skin friction coefficient.
- For uniform blowing, location of slot at 3m (X/L=3/4) from leading edge is more effective location for reduction of skin friction coefficient, while a reverse action is observed for the case of uniform suction.
- It was found that, a width of slot equal (0.28m) gives the maximum reduction in skin friction coefficient for uniform blowing.
- Blowing causes a decrease in boundary layer thickness and increase in shape factor, while suction causes a reverse effect. The increase or decrease is proportional to the velocity ratios, positions of slot, and widths of slot.
- Above the slot, in case of blowing, when increased the velocities of blowing, the (uu) and (uv) are more decreased than (vv), while (vv) is more decreased than (uu) and (uv) in the case of suction.
- For uniform blowing, [U^+] decrease with increasing velocity ratios, pitch angles, positions of slot and widths of slot. While a reverse action is observed for the case of the suction.

REFERENCES

- Awbi, H. H., "Ventilation of Building", Department of Construction Management and Engineering, Unversity of Reading, London (1991).

- Kim, K. and Sung, J. H., "Effect of Periodic Blowing from Span Wise Slot On A Turbulent Boundary Layer", AIAA. Journal, Vol.41, No.10, PP.196-1924, October (2003).

- Krogsted, P. A. and Kourakine, A., "Some Effects of Localized Injection on the Turbulence Structure in a Boundary Layer", Physics of Fluid, Vol. 12, No. 11, pp.2990-2999, November (2000).

- Lai, K. Y. M., and Makomaski, A. H., "Three Dimensional Flow Pattern Upstream of a Surface Mounted Rectangular Obstruction", Transctions of the ASME, Journal of Fluids Engineering, Vol. 111, pp. 449-456, December (1989).

- Munem, D. S., "Effect of suction and Blowing on the Flow Over A Flat Plate ", MSC. Thesis, Mechanical Engineering Department, University of Baghdad, October (2004).

- Park, j. and Choi, H., "Effects of Uniform Blowing or Suction from a Span Wise Slot on a Turbulent Boundary Layer Flow", Journal Physics of Fluids, Vol.11, No.10, pp. 3095-3105,October (1999).

- Park, Y.S., Park, S.H., and Sung, H. J., " Measurement of Local Forcing on a Turbulent Boundary Layer using PIV",Journal Experiments in Fluids, Vol.34, PP. 697-707, April (2003).

- Patankar, S. V., "Numerical Heat Transfer and Fluid Flow", Hemisphere Publishing Corporation, Taylor & Francis Group, (1980).

- Schlichting, H., "Boundary Layer Theory", Sixth Edition, McGraw- Hill Book Company, New York (1968).

- Versteeg, H.K., and Malalasekera, W., "An Introduction to Computational Fluid Dynamics-The finite volume method", Longman group Ltd., (1995).

FORGEABILITY OF 25%GRPOM (CELCON^{R}) TO PRODUCE SPUR GEAR UNDER HOT CONDITIONS THROUGH SLOW SPEED PRESS.

Talib.H.Rashid
Mech.Eng. dept.
University of Baghdad.

ABSTRACT

This research studied forgeability of preheated billet of 25%GRPOM plastic through closed die forging technique using spur gear design. The type of deformation was discussed as well. This process had done after heating the billet and die assembly at 100^{o}C to achieve complete gear shape taking into consideration testing the product to insure no inside or outside defects with improvement in the mechanical properties. Cycle time to produce a complete shape was two minutes.

الخلاصة:

درس البحث قابلية العينة المسخنة مسبقا لمادة الاسيتل المقواة بنسبة (25%) الياف زجاجية على الكبس خلال عملية القالب المغلق باستخدام قالب ترس عدل . كما ناقشت نمط التشوهات على القطعة المشغولة. اجريت العملية بعد تسخين العينة و مجموعة القالب لدرجة (100 ^{o}م) لغرض انجاز ترس كامل الشكل اخذين بالاعتبار فحص المنتج من الداخل و الخارج لضمان خلوه من العيوب مع تحسن الخصائص الميكانيكية. استغرق وقت العملية لانتاج شكل كامل دقيقتين

KEY WORDS: (Forging , GRPOM, Recovery, Dwell time).

CLAIMS:

- Forgeability of 25%GRPOM (celcon^{R}) through closed die forging technique to produce spur gear at (100^{o} C) conditions
- Behavior of the polymer through forging action taking into consideration that typical forging process usually done at a temperature (5^{o}C) just below melting point (Kulkarni 1995). Melting temperature for it is about (166^{o}C).

INTRODUCTION

Polyoxmethylene always has been referred to as polyacetal resin. This polymer as an engineering material has been fabricated by forging process after being filled with 25%glass to get high stiffness. (GR POM) can be difficult cold forged (Wang & Lin 2007). It is almost fabricated after heating the billet and the tools to a temperature Just below softening point (KULKARNI 1995) to make it non-recoverable and ductile enough to reduce spring back phenomena and to achieve product with high strength and stiffness better than what injection molding process does (CRAWFOR1985).

In general a polymer can be either cold or warm formed. Solid phase forming (spa) indicates any of them (Wang & Lin 2007).

Press forming is to use a slow squeezing action of a press to transfer uniformly a great a mount of compressive force to the bulk of material (work piece) in three directions (COFFMAN1990). This process yields parts that have high strength to weight ratio thus is often used in the design of a particular applications where this property is of great demand (CRAWFOR 1985). Compressive force in such technique actually depends on the billet dimensions and the amount of deformation for the work piece which is forged below softening point. 25%glass reinforced acetal is a thermoplastic, ductile after preheating. Closed die forging technique mostly used when the design beyond injection molding technique capability such as ultra high molecular weight polymer, complex design geometry or higher strength and stiffness are wanted (COFFMAN 1990). The most powerful advantages of plastic gears may be the design opportunities they afford. Gear geometries overlooked by designers used to metal are often easy to mold in plastic, and they can reduce drive size, weight, and cost, in addition to their resistance to solvents and alkalizes and service temperature closed to $100C^{0}$. GRPOM has excellent clarity, dimension stability which prevents shrinkage (COFFMAN 1990).

APPLICATIONS:

Spur plastic gears are usually used after machining for:

- Low speed applications.
- Power transmissions.
- Film winding.

Examples of spur GRPOM gear uses:

- Windup alarm clock.
- Washing machine.
- Electric screw driver.
- Oscillating sprinkler.

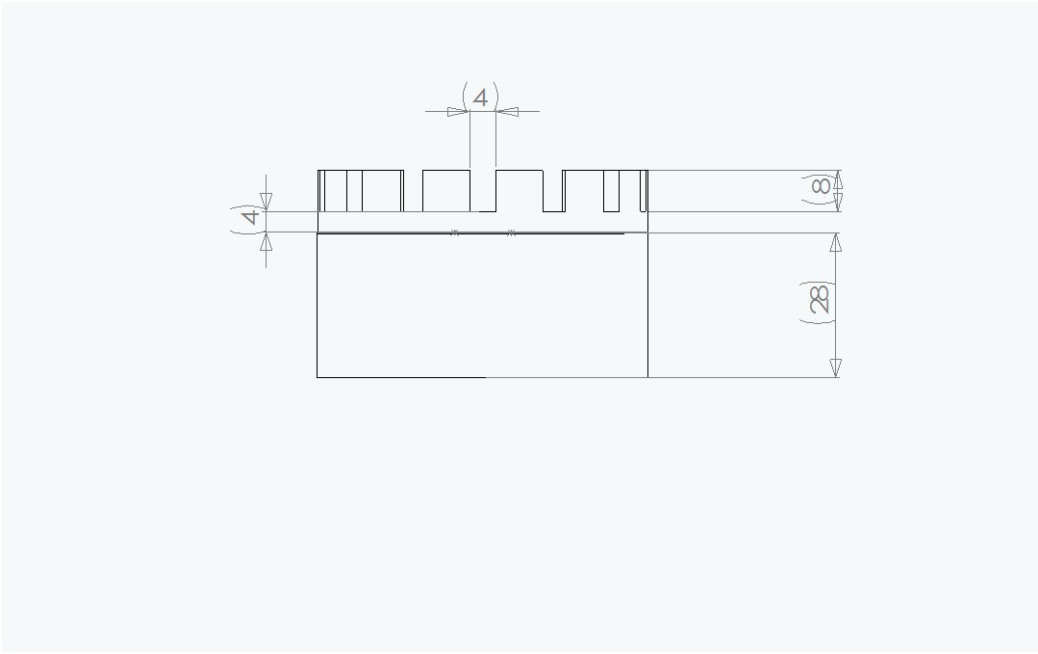

FRONT VIEW

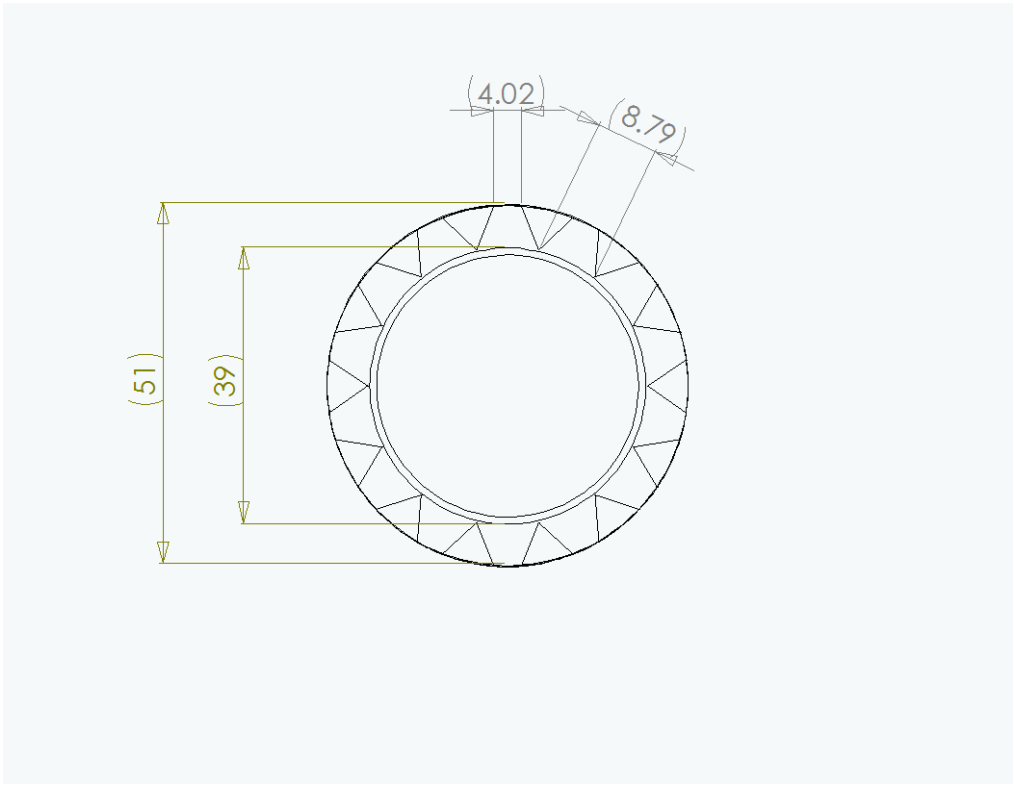

TOP VIEW

Fig.1: DIE DESIGN (in mm)

EXPERIMENTAL PROCEDURES: (Fig.2, Fig.3)

- The process was done using slow speed press.
- The billet was a solid rod of GRPOM with cross section area of (25mm); length was (65mm).
- Number of samples (billets) used =20
- The die of gear had out side diameter equal (51mm) and inside equal (39mm). Tooth number = 14.
- A load cell consisted of strain gauge was used to transmit the compressive load to the strain recorder then to an amplifier. The amplifier then connected to Bryan X-Y plotter to get graphs of load against displacement, then to be converted later to (stress-(strain) curves describing the style of flow done by yielding action.

Billet specifications:
Tensile strength = 65Mpa
Hardness (R.W) = 80(scale M)
Melting point = 166^{o}C
The billet was put into the die and whole assembly was placed in an oven over night. The temperature was adjusted to 100 ^{o}C . The strain gauge was insulated from the hot punch by the use of an asbestos slab to prevent unwanted effect of strain gauge due to heating. After putting the die assembly below the machine punch, switching on, then
The press head was brought down and the forging carried out. When the pen of the plotter started to move vertically, load was again held constant at that particular point. The process took two minutes to achieve complete plastic gear.(see Fig.2).

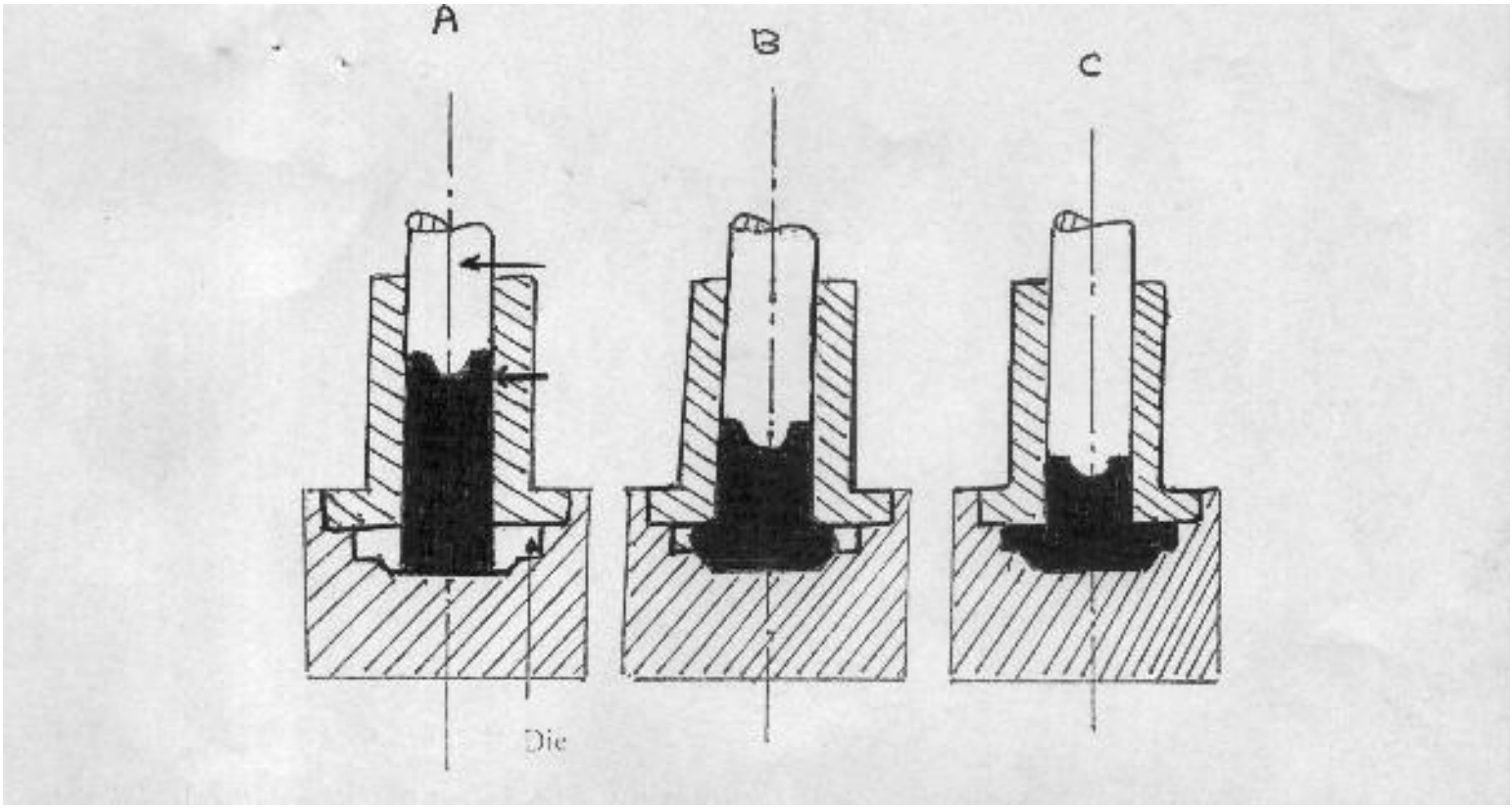

Fig.2- stages of gear formation:

A. The punch is ready to forge the billet.
B. The pressure increased gradually to (80)Mpa to fill the cavity of the die except corners of tooth.

PUNCH

C. The shape of spur gear was completed under 110Mpa.

RESULS & DISCUSSION:

Product test:

The final result was a complete plastic gear produced through closed die forging process in two minutes for each sample(Fig.4), taking into consideration no inside or

outside defects, but a smooth, shinny plastic gear was achieved with improvement in the mechanical properties, but in the direction of loading.
Tensile strength = 140Mpa (in one direction).
Tensile modulus = 4.2Gpa (in one direction).
.Hardness (R.W) = 87 (scale M)
Stress at 1% strain = 10Mpa

Yield stress at 3.5 strain = 56Mpa

Forging pressure: this was the stress required to form the gear shape due to punch action through the forging process indicated by stress-strain curve below.

1st stage = 80Mpa

2nd stage = 110Mpa

Dimensions stability were within 1% in three dimensions achieved after dwell time equal to 50second to reduce recovery action, in addition to eight hours outside the die to insure complete stability of dimensions that should not exceed 1%.

Dimensions of rod specimen in mm prepared for tensile test under designation of DIN 638 (see Fig.3)

Table.1

Nominal Diameter	Length of Radial Section	Standard Length	Length of the Jaws	Groove Length
22.2	51.5	400	89	57

Notes :

- the diameter of the machined portion (a straight section groove) was 60% of the original length.
- the length of the machined portion was 57.0 mm.
- test specimen was machined for preparation.
- five specimens were tested at room temperature, test time for each was three minutes.
- the grips were tightened in proper way to prevent slippage of the specimen.
- the tensile strength was calculated by dividing the maximum load in Newton by the original minimum cross-sectional area of the specimen in square meters expressing the result in Pascal.

- the modulus was calculated by extending the initial linear portion of the load-extension curve and dividing the difference in stress corresponding to any segment of section on this straight line by the corresponding difference in strain.
- the specimens were considered under type Rigid and Simi rigid III rods that speed of test is 5 mm/min .

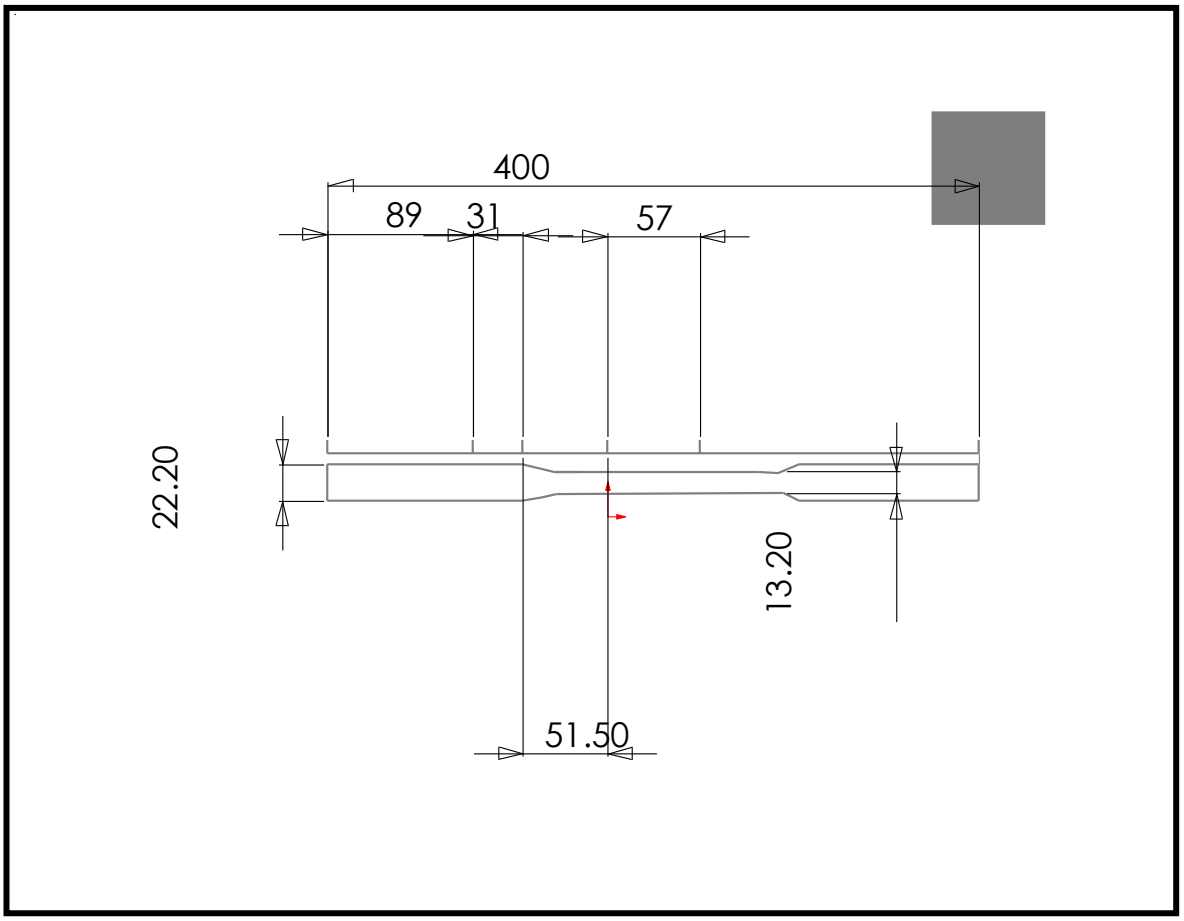

Fig.3 : Tensile test specimen (dimensions are in table.3)

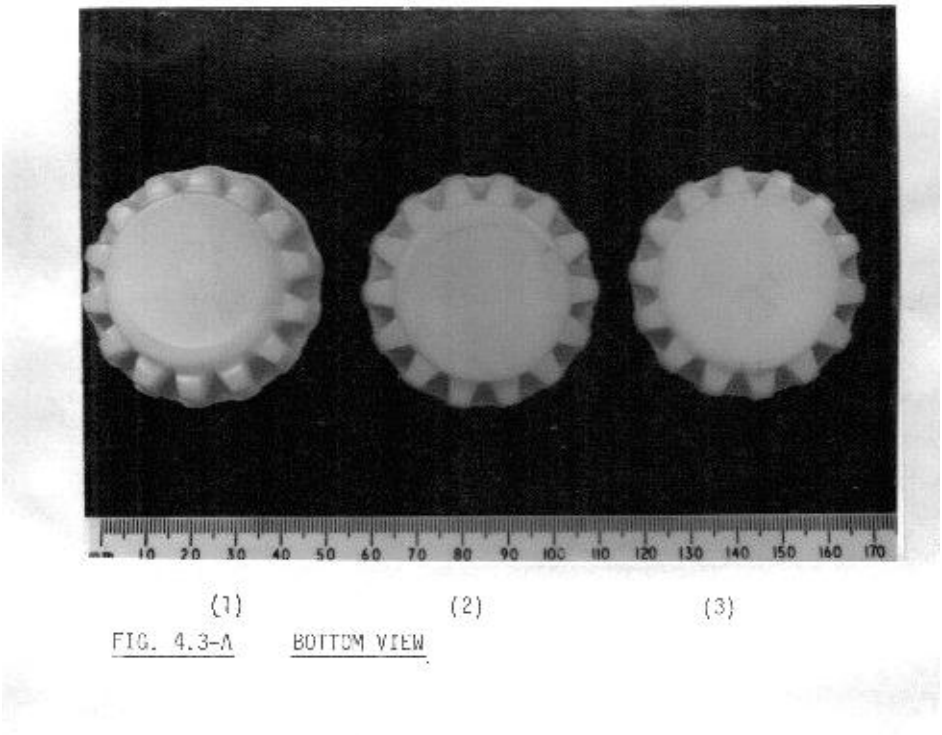

Fig.4: a smooth shinny plastic spur gear product -before machining- using glass reinforced acetal (celcon^{R}) billet heated at 100^{o} C .

Load – Displacement curves behavior:

According to Fig.5, two types of deformation behavior can be recognized

- Elastic range which is represented by (OA), that 22 KN was the load applied to achieve reduction in height equal to 1.25 mm.

- Viscous non-linear plastic deformation range that occurred because this polymer behaved as viscous element and non-linear simultaneously. These behaviors represented by:
- (AB) which is the deformation occurred due to increased load from 22 KN (yield point) to 45 KN that was the load required to achieve displacement equal to 11.75mm at the plastic zoon.
- 2. (BC) which is the deformation occurred due to increased load from 45KN to 80KN to fill the whole cavity of gear die. For this section, a reduction in height equal to 3mm was achieved. Hence a total reduction in height through whole process was 16.5mm.

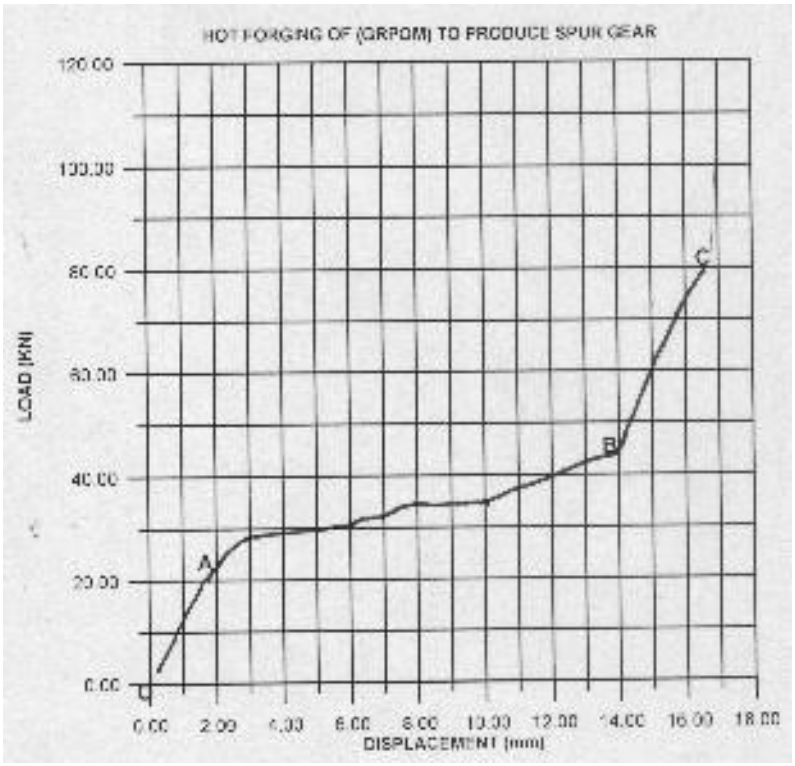

Fig.5: load – displacement curve

Stress-Strain relation:

From Fig.6, the style of deformation indicates the pressure required through each step of gear formation that allowed strain to be represented according to the viscoelastic manner of the plastic material causing the plastic deformation to follow anon-linear strain path supposed to be horizontal straight line, but it is not, because the behavior of the polymer mentioned above (J.C.Choi 1999).

- Yielding action of the polymer was starting at applied pressure of 56Mpa, then increased to 70Mpa to achieve a viscous non-linear part of 12% strain.
- A second part of strain - which is approached 17% achieved due to constant pressure of 80Mpa. At this stage, the polymer filled gear die except tooth.
- The pressure, then increased rapidly approaching 110Mpa until strain held constant and whole gear would be formed after two minutes time.

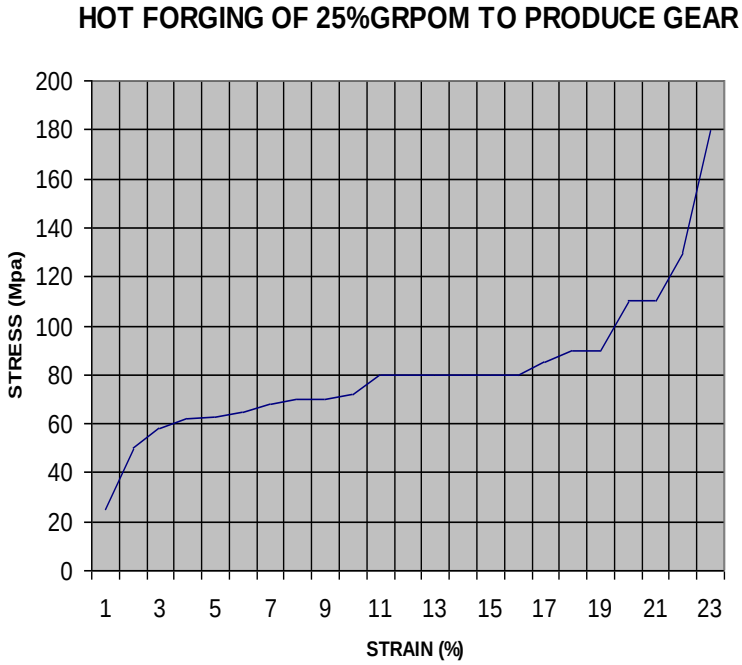

Fig.6: stress – strain curve

CONCLUSIONS:

- The plastic material 25%GRPOM was capable of being used to produce gear through closed die forging technique after heating the billet & tools at (100^{o}C).
- Cycle time for the same work done at typical heating is 50 second (Kulkarni 1995), while it took 120second (including dwell time) to produce a complete gear.
- Excessive pressure were needed to fill the corners of the gear die with polymer to achieve complete tooth filling. That flange shape of the die required a stress of 80Mpa, while the tooth formation required 110Mpa.
- The material showed viscoelastic behavior as it indicated in fig.5.
- Mechanical properties improved more as long as heating far away below softening point, but with too long cycle time to prevent possibility of recovery, So, care should be taken in choosing the right polymer.

REFERENCES:

- **Chengliang. Hu Keshang.Wang & Qnan.Kua. Lin. (2007). Study on new technological scheme for cold forging of spur gear Journal of materials processing technology. Vol.187-188**
- **J.C.Choi & Y.Choi.(1999) - Precision forging of spur gear with inside relief. International journal of machine tools & manufacture. Vol.39-1999.**
- **K.M.KULKARNI(1995) - Review of forging**
- **N.A.Abdul & T.A.Dean(1986) - An analysis of the forging of spur gear form.**
- **International journal of machine tools design & research. Vol. 261-262 (1986). P.M.COFFMAN(1990) - Forging of plastics by metal working technique.**
- **R.J.CRAWFOR(1985)- Plastic engineering.**
- **Yoyng-Seon Lee & Junes-Hwan.Lee(2002)- Experimental & analysis evaluation for elastic deformation behaviors of forging**

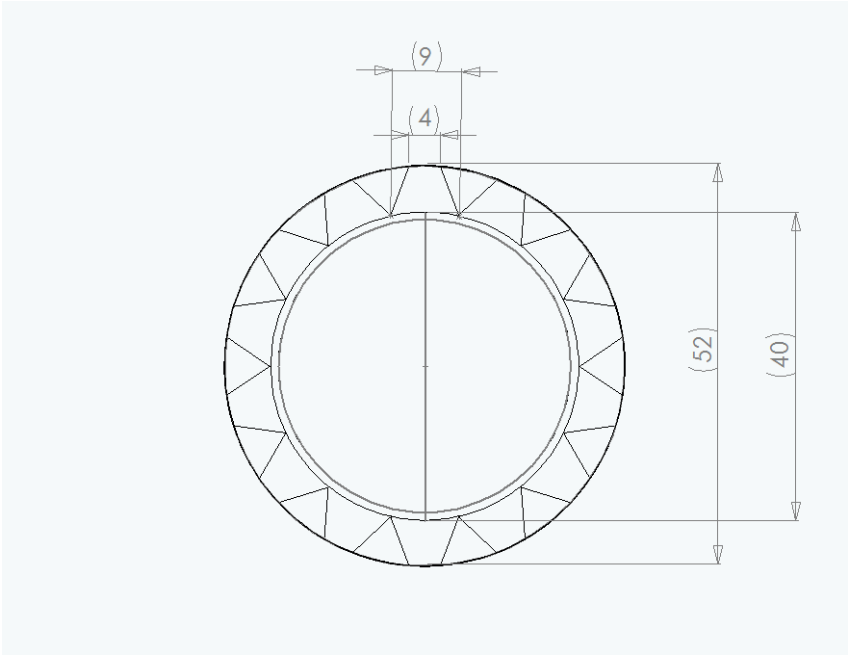
9
4
52
40

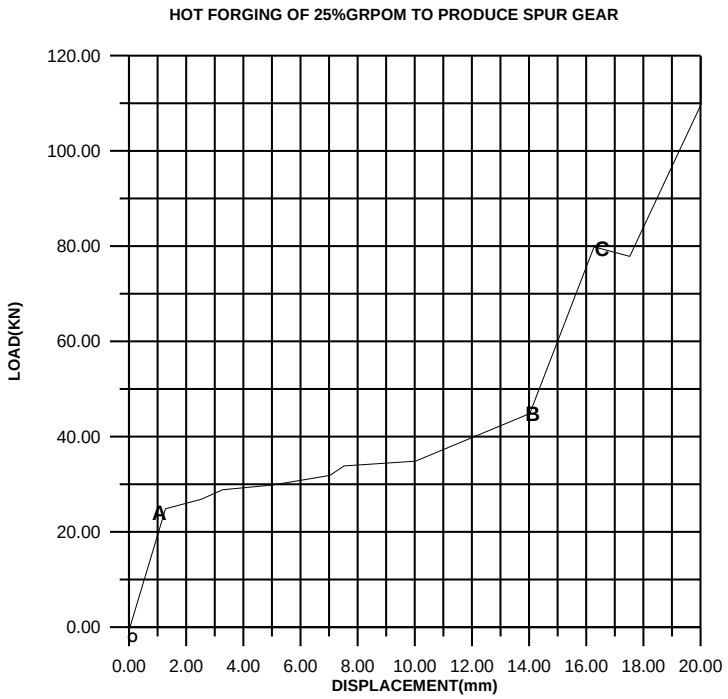
HOT FORGING OF 25%GRPOM TO PRODUCE SPUR GEAR
LOAD(KN)
DISPLACEMENT(mm)
120.00
100.00
80.00
60.00
40.00
20.00
0.00
0.00
2.00
4.00
6.00
8.00
10.00
12.00
14.00
16.00
18.00
20.00
A
B
C
O

REMOVAL OF DIRECT BLUE DYE IN TEXTILE WASTEWATER EFFLUENT BY ELECTROCOAGULATION

Atheer M. Ghalib
Chemical Engineering Department –Collage of Engineering –University of Baghdad

ABSTRACT
Removal of direct blue dye by electrocoagulation method has been investigated using aluminum electrode in a bench-scale electrochemical system. Current density, NaCl concentration, electrocoagulation time, and dye concentration has been studied as effecting parameters in color removal efficiency. Increasing of current density will increase the color removal efficiency and energy consumption as well. While increasing NaCl concentration increase the color removal efficiency but it decrease energy consumption. High dye concentration is needed for extra electrocaogolation time to reach the same efficiency that obtained with low dye concentration .With current applied 0.35 amps. and NaCl concentration of 2 g/l more than 93% efficiency achieved in 14 min. of electrocaogolation time.

KEYWORDS
Dye removal, decolonization, direct blue, electrocoagulation

أزالة صبغة الزرقاء المباشرة من مياه الصناعات النسيجية المطروحه بطريقة التخثيرالكهربائي

الخلاصة

دُرست الازالة اللونية لصبغة الزرقاء المباشرة بطريقة التخثير الكهربائي بأستخدام اقطاب الالمنيوم بنظام كهروكيمياوي مختبري.تم دراسة كثافة التيار, تركيز ملح هدروكسيد الصوديوم, زمن التخثير الكهربائي و تركيز الصبغة كعوامل موثرة في كفائة ازالة اللون.زيادة كثافة التيار تزيد كفاءة ازالة اللون والطاقة المستهلكة,بينما زيادة تركيز الملح يزيد كفاءة ازالة اللون وتقلل الطاقة المستهلكة.تراكيز الصبغة العالية تحتاج الى زمن التخثير الكهربائي أضافي للحصول على نفس الكفاءه التي تم الحصول عليها في تراكيز الصبغة الواطئة. تم الحصول على كفاءه اكثر من 93% بتسليط تيار مقداره 0.35 امبير و2 غم/لتر تركيز ملح هدروكسيد الصوديوم بزمن تخثيركهربائي مقداره 14 دقيقة.

INTRODUCTION

From the early days of textile industries, the wastewaters of those industries were classified as the most polluting effluent, because of the volume of its influent as well as, variability and complexity in pollutant contents involved. In particular, dyeing and finishing processes are responsible for large water pollution.

Dyes are considered to be dangerous organic compounds for the environment. High level of color is not the only reason, but dye may contain chemicals, which are toxic and carcinogenic, they causes variation in pH, high temperature, high biological oxygen demand, high chemical demand and high concentrations of suspended solids. According to articles, nearly 40,000 dyes and pigments are listed which consist of over 7,000 different chemical structures. Most of them are completely resistant to biodegradation processes (Ayhan Demirbas, *2009*).

Dyes used by the textile industry are largely synthetic and are derived from coal tar and petroleum-based intermediates. The primary classification of dyes is based on the fibers to which they can be applied. The chemical nature of each dye determines the fibers for which the dye has affinity and they are mainly divided into acidic dyes, reactive dyes, disperse dyes and, direct dyes (Yang C.-L., McGarrahan, 2005)

Therefore, engineering effort has been focused on handling this problem, in many ways the solution came with several configurations, biological, Physical and chemical methods or combination of two or more of these methods. Biological treatment processes are often ineffective in removing dyes which are highly structured polymers with low biodegradability(O.T. Can, M. Bayramoglu, M. Kobya, 2003) .Therefor, the needing of pre-treatment appear obviously(D. Georgiou, P. Melidis, 2003)

In addition, many other treatment processes adopted to achieve the adequate settlement to eliminate dyes which listed under physico-chemical methods such as : adsorption on activated carbon, polymer and mineral sorbents or biosorbents(T. Robinson.,2002, A. Pala,2002)

Chemical oxidation by ozone and hydrogen peroxide (E.G. Solozhenko,1995) and combining hydrogen peroxide with UV(A. Aleboyeh,2003, E. Kusvuran,2004) photolysis(W. Chu,2002)

Among the above methods, electrochemical treatment appear to achieve strong promotion to dyes removal treatment ether by direct or indirect electrochemical technique, electrocoagulation draw attention in last years ,Aluminum and iron sheets have been used as consumable anodes to generate coagulants that adsorb and remove organic dyes(*M. Kashefialasl*,2006, C. Phalakornkule,2009).

An aluminum coagulant removes colorant by complexation and electrostatic attraction followed by coagulation adsorption. Three main processes occur during electro-coagulation: electrolytic reactions at the surface of electrodes, formation of coagulants in aqueous phase, adsorption of soluble or colloidal pollutants on coagulants, and removal by sedimentation and floatation Electrochemical coagulation for textile effluent decolonization.[Chen-Lu Yang a,2005, A. Wilcock,1992)

Aluminum sheets as consumable electrodes, Al^{3+} ions are produced on the anodes.

$$Al \rightarrow Al^{3+} + 3e^{-} \text{ (at anode)} \quad (1)$$

$$3H_2O + 3e- \rightarrow \frac{3}{2} H_2 + 3OH^{-} \text{ (at cathode)} \quad (2)$$

The destabilized particles then aggregate to form flocs. In the meantime, the tiny hydrogen bubbles produced at the cathode induce the floatation of most flocs, helping to effectively separate particles from wastewater. In addition, the cathode may be chemically attacked by OH− ions generated together with H2 at high pH values.(T. Picard,2000)

$$2Al + 6H_2O + 2OH^{-} \rightarrow 2Al(OH)_4^{-} + 3H_2 \quad (3)$$

$Al(aq)^{3+}$ and OH^{-} ions generated by electrode reactions (1) and (2) react to form various monomeric species which transform finally into $Al(OH)_3$ according to complex precipitation kinetics (A. G¨urses,2002). Several interaction mechanisms are possible between dye molecules and hydrolysis by-products.

EXPERIMENTAL

Bench-scale electrochemical system was used in this study. It consists of power supply model (KW/IC-TRIPLE, SCHWEIZ) with digital multimeter DT-832, cylindrical electrochemical reactor (9.5 cm diameter, 10cm high) made of PVC, provided with 7.5*4.5*1 cm graphite cathode, solid aluminum wire of 77 cm^2 total area represent the anode electrode was coiled around the cathode as show in fig.(1). Approximately 0.5 cm separated between the two electrodes. Before and at the end of each run, electrodes were washed thoroughly with water, dipped in HCl solution.

Synthetic dye wastewater prepared by dissolving 50, 25, 10 ppm direct blue dye directly in a distilled water, using a commercially available Direct Blue , which its chemical structure shows below.1,2 and 4 g of NaCl was added to each liter of solution and different currents of 0.1,0.2 and 0.35 amps. were supplied to the system .The samples had been taken every two minute .All samples were allowed to settle for 20 min and after that they were analysed

a UV-Vis spectrophotometer (Spectro SC, USA) at the wavelength of 570 nm was used to determine the color removal efficiency . Where the color removal efficiency is written as:

Color removal efficiency (%) = [(Ao-A)/ Ao)]*100

where Ao and A are the light absorbance of dye before and after electrocoagulation, respectively.

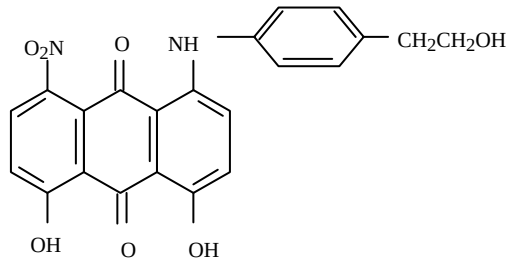

Chemical structure of Direct Blue

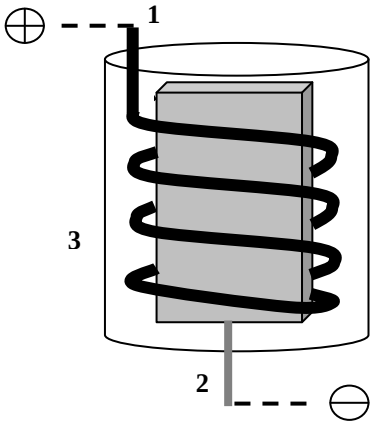

1-aluminum anode 2-graphite cathode 3-PVC cell body

Fig.(1) Schomatric of electrochemical cell reactor

RESULT AND DISCUSSIONS

The efficiency of color removal of direct blue dye was investigated as a function of current density and electrocoagulation time at constant NaCl concentration of 2 g/l and dye concentration of 20 ppm.

Fig.2 shows the color removal efficiency increases with increasing current applied to the reactor cell, when the current is 0.1 amp. The color removal reached 0.76 in 10 min. and over 0.9 in same time on 0.2 amp. As well as the color removal remarkably increased to reach over 0.93 on 0.35 amp. The amount of Al-coagulant in the solution is the factor determent the efficiency of color removal, this amount present sufficiently when the current is rising. Also the coagulation time offset the regression in the color removal efficiency resulted from falling behind of current applied to the solution.

Picking the proper working current density limited by economic motive, knowing the fact that choosing high current rising energy consumption. As shown in fig. 3

Fig.4 shows the effect of NaCl concentration on efficiency of color removal at constant current of 0.35 amp. and 20 ppm dye concentration.

Increasing the concentration of NaCl in solution increases the efficiency of color removal.

However, in solution contain 0.5 g/l of NaCl the color removal is 0.76 in 10 min. of electrocoagulation time and in 1 g/l of NaCl the efficiency is 0.83 at the same time, while its reach 0.87 in 4 g/l of NaCl .

The above resulted from that during the operation chloride (Cl^-) was present in solution and oxidation to produce chlorine gas (Cl_2) on the surface of the anode. Some Cl_2 evolved from the surface as tiny bubbles while the majority of Cl_2 dissolved and equilibrated with hypochlorous acid (HClO), trichloride ions (Cl_3^-), and hypochlorite (ClO^-) in the solution These are strong oxidizing agents and can be used to further oxidize the dye, that is not quite distinct in this study because of 20 ppm of dye isn't adequacy amount to late the oxidizing agents play a significant role in the removal process.

In the other hand, the increasing of NaCl concentration will reduce the voltage of the cell that causes reducing in energy consumption as shown in fig.(5) above obviously appear because of increasing the salt concentration mean increase in solution conductivity that result low cell voltage and low energy consumption.

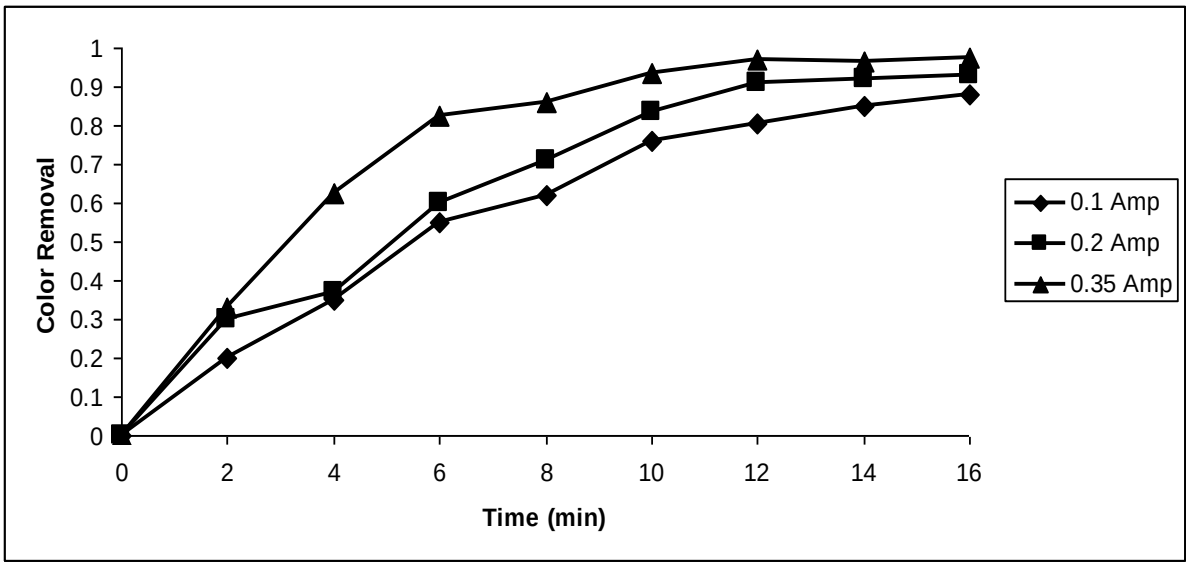

Fig.(2) effect of current density on the color removal efficiency 20 ppm,2g NaCl

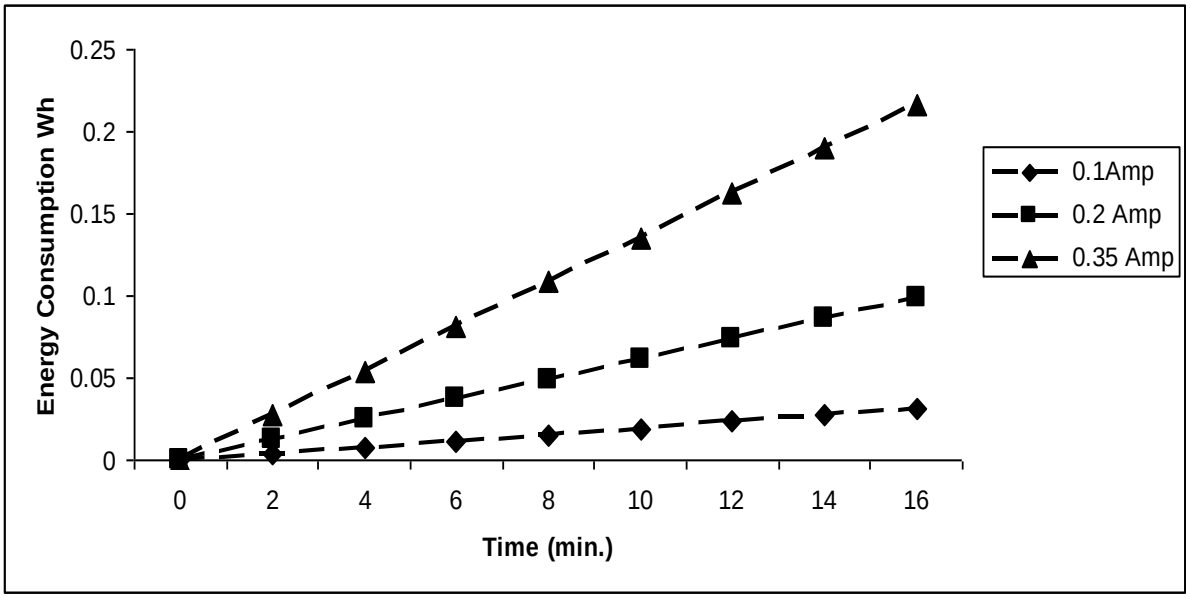

Fig.(3) effect of cuurent density. on the energy consumption in 2g/l NaCl, 20 ppm,

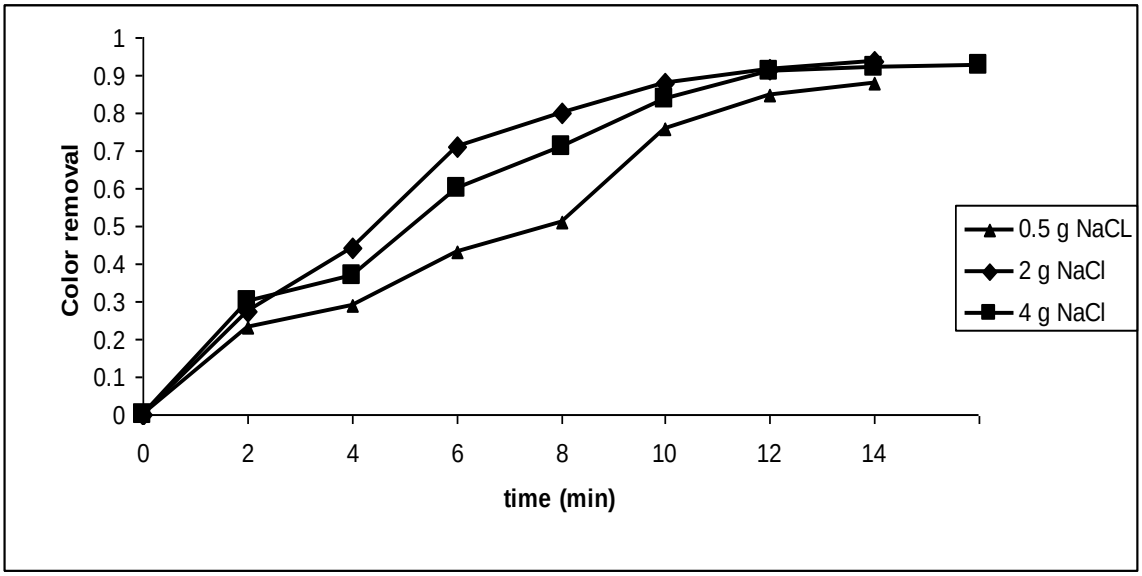

Fig.(4) effect of current density on the color removal efficiency 20 ppm,0.35A

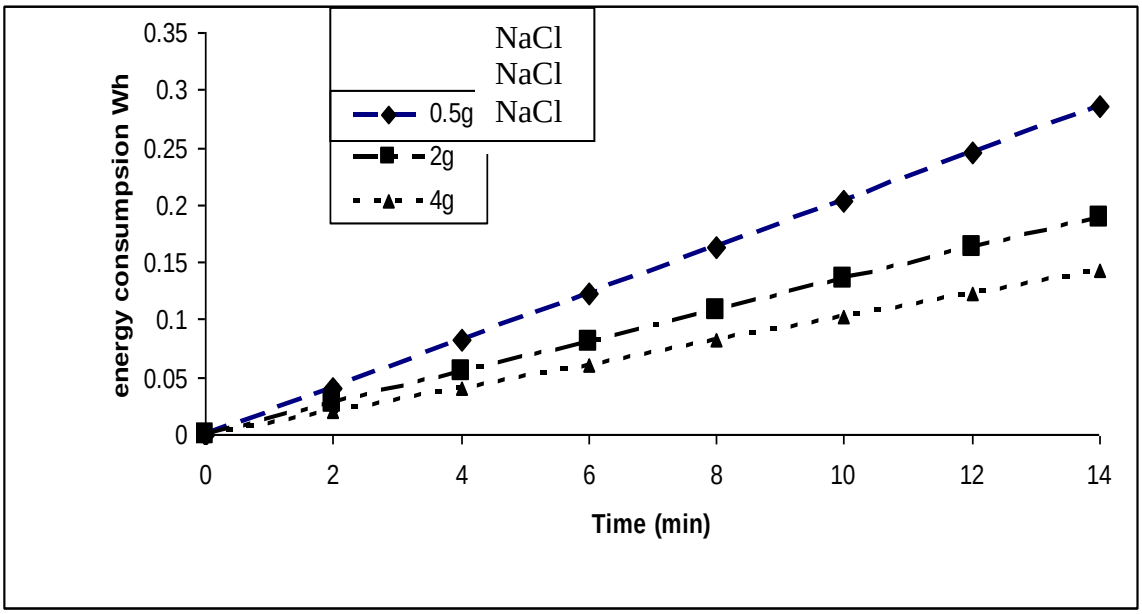

Fig.(5) effect of NaCl conc. on the energy consumption 0.35 A, 20 ppm,

Fig.(6) shows that the effect of dye concentration on color removal efficiency, it observed clearly that the high concentration of dye in solution needs more time to reach the desired removal efficiency that occurred to that of low concentration , however, in 10 ppm dye concentration at 8 min. the color removal efficiency is 0.78 ,in 20 ppm the color removal is 0.71 at 8 min. and its almost 0.55 with 50 ppm at the same time , again the electrocoagulation time offset the regression in color removal efficiency ,it can be reach a maximum value of 94 at 18 min. in 50 ppm dye concentration and 0.93 at 14 min in 20 ppm., also in 10 ppm. More than 90 can be reachs before this time. The reason behind that is high dye concentration needs for Extra time to react with Al-coagulant that generated sequentially in solution.

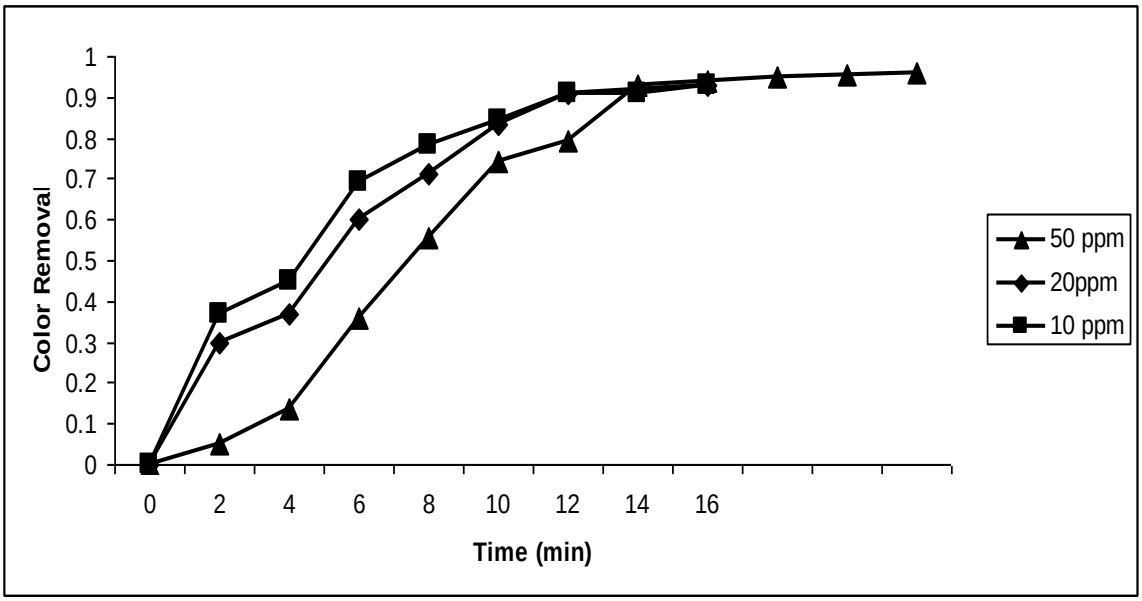

Fig.(6) effect of dye conc. on the efficiency of color removal 0.35 Amp, 2 g/l NaCl

CONCLUSION

Electrocoagulation of direct dye is a sufficient method to treatment textile west. The current density is effective factor in electrocoagulation process also the time of which the dye is in treatment ,NaCl concentration provide additional factor to eliminate dye from solution .picking the working current density and NaCl concentration limited by economic motives. More than 93% color removal efficiency achieve in this research by applying current of 0.35 amps. and NaCl concentration of 2 g/l in 14 min. of electrocaogolation time using aluminum electrode.

NOMENCLATURE

Amp Ampere
ppm part per million

REFERENCES

- Aleboyeh, H. Aleboyeh, Y. Moussa, Decolorization of Acid Blue 74 by ultraviolet/H2O2, Environ. Chem. Lett. 1 (3) (2003) 161–164
- G¨urses, M. Yalc¸in, C. Do˘gan, Electrocoagulation of some reactive dyes: a statistical investigation of some electrochemical variables, Waste Manage. 22 (2002) 491–49
- Pala, E. Tokat, Color removal from cotton textile industry wastewater in an activated sludge system with various additives, Water Res. 36 (2002) 2920–2925
- Wilcock, Spectrophotometric analysis of electrochemically treated, simulated, dispersed dyebath effluent, Text. Chem. Color. 24 (1992) 29–37.
- Ayhan Demirbas , Agricultural based activated carbons for the removal of dyes from aqueous solutions, *Journal of Hazardous Materials, Volume 167, Issues 1-3, 15 August(2009), Pages 1-9*
- Phalakornkule, S. Polgumhang, and W. Tongdaung, Performance of an Electrocoagulation Process in Treating Direct Dye: Batch and Continuous Upflow Processes, World Academy of Science, Engineering and Technology 57,(2009),277-282
- Chen-Lu Yang a, Jared McGarrahan, Electrochemical coagulation for textile effluent decolorization, J. Haz. Mat., Vol. 127, pp40-47, (2005)
- Georgiou, P. Melidis, A. Aivasidis, Use of a microbial sensor: inhibition effect of azo-reactive dyes on activated sludge, Bioprocess Biosyst. Eng. 25 (2002) 79–83.
- E.G. Solozhenko, N.M. Soboleva, V.V. Goncharut, Decolourization of azo dye solutions by Fenton's oxidation, Water Res. 29 (1995) 2206–2210
- Kusvuran, O. Gulnaz, S. Irmak, O.M. Atanur, H.I. Yavuz, O. Erbatur, Comparison of several advanced oxidation processes for the decolorization of Reactive Red 120 azo dye in aqueous solution, J. Hazard. Mater. B109 (2004) 85–93)
- *M. Kashefialasl, M. Khosravi, R. Marandi and K. Seyyedi*, Treatment of dye solution containing colored index acid yellow 36 by electrocoagulation using iron electrodes, M.

Kashefialasl, *et al.* Treatment of dye solution... Int. J. Environ. Sci. Tech., 2006, Vol. 2, No. 4, pp. 365-371

- O.T. Can, M. Bayramoglu, M. Kobya, Decolorization of reactive dye solutions by electrocoagulation using aluminum electrodes, Ind. Eng.Chem. Res. 42 (2003) 3391–3396.)

- T. Picard, G. Cathalifaud-Feuillade, M. Mazet, C. Vandensteendam, Cathodic dissolution in the electrocoagulation process using aluminium electrodes, J. Environ. Monit. 2 (2000) 77–80.

- T. Robinson, B. Chandran, P. Nigam, Removal of dyes from a synthetic textile dye effluent by biosorption on apple pomace and wheat straw, Water Res. (2002) 36.

- Yang C.-L., McGarrahan J. Electrochemical coagulation for textile effluent decolorization. J. Hazard. Mater. 2005; 127: 40-47.

- W. Chu, S.M. Tsui, Modeling of photodecoloration of azo dye in acocktail photolysis system, Water Res. 36 (2002) 3350–3358.

UTILIZATION OF THOMAS MODEL TO PREDICT THE BREAKTHROUGH CURVES FOR ADSORPTION AND ION EXCHANGE

Yasmen A. Mustafa and Shahlaa E. Ebrahim

Environmental Engineering Department-College of Engineering-Baghdad **University**

ABSTRACT

Fixed bed sorption processes such as adsorption and ion exchange do not operate at steady state. The design equations are differential that usually require numerical methods to solve. Thomas gives a general analytical solution for these equations. It is based on second-order reaction kinetics and the assumption of Langmuir isotherm. Computer program for the solution of Thomas model was designed using MATLAB 7.0. Four sets of experimental data are tested to show the capability of Thomas model to predict the breakthrough curves for adsorption and ion exchange processes. These data represent the sorption of o-cresol from water by activated carbon, acetic acid from air by activated carbon, phenol from water by natural zeolite, and trichloroethylene from air by zeolite-5A.The results show that there are a good agreement between the experimental data and the model.

الخلاصة

أن عمليات الامتزاز والتبادل الايوني للطور الثابت تكون متغيرة ، فالمعادلات الخاصة بالتصاميم هي معادلات تفاضلية تحتاج الى حلول بالطرق العددية.

توماس استطاع أن يعطي حل عام تحليلي لهذه المعادلات مستندا على ديناميكية التفاعل من الدرجة الثانية ومعادلة لانكمير عند التوازن. تم اعداد برنامج رياضي لموديل توماس بأستخدام MATLAB 7.0 .

أستخدمت اربعة نماذج من التجارب لغرض أظهار مقدرة موديل توماس للتنبأ بمنحنيات الامتزاز والتبادل الايوني. البيانات مثلت امتزاز الاورثوكريسول من الماء بواسطة الفحم المنشط ، وحامض الخليك من الهواء بواسطة الفحم المنشط، والفينول من الماء بواسطة الزيولايت، وثلاثي كلوروالاثلين من الهواء بواسطة الزيولايت. النتائج بينت ان هناك تطابق جيد بين البيانات العملية والموديل.

KEY WORDS

Fixed bed, adsorption, ion exchange, breakthrough curves, Thomas model.

-INTRODUCTION

Rigorous fixed bed models, usually cast in the form of partial differential equations, allow a realistic mathematical description of the sorption column dynamics. When the equilibrium relationship is linear, an analytical solution for the fixed bed dynamic behavior can always be obtained. For nonlinear systems the governing equations are usually solved numerically. Thomas model gives a general analytical solution for these equations based on second-order reaction kinetics and the assumption of non linear equilibrium relationship of Langmuir isotherm. Thomas neglects the axial dispersion [Chu, 2010].

Thomas model is employed by many researchers to predict the breakthrough curves for adsorption and ion exchange [Chu, 2010, Han, et.al. 2009, Vijayaraghavan and Yun, 2008, Han, et.al, 2007, and Han, et.al, 2007].

Sorption from water or gas on a fixed bed of adsorbent is a process of unsteady state mass transfer between the liquid or gas and solid phase. The concentration of adsorbed substance in both phases is a function of both time and location in bed [Wolborska, 1999].In simple fixed-bed adsorption, the solute undergoing adsorption is removed continually from the carrier liquid or gas and accumulates upon the surface of the solid phase. Such transfer proceeds until the concentration on the solid reaches a value corresponding to equilibrium with the concentration in the feed stream, and the column effluent reaches the feed concentration. Ion exchange is a case of exchange adsorption in which ions chemically bound in the resin phase are displaced in essentially stoichiometric proportions by ions initially in the liquid phase. In either adsorption or ion exchange, the step of accumulation in the solid phase is termed saturation. Sorption is commonly performed in a packed bed where a granular adsorbent such as granular activated carbon or natural zeolite is held stationary in a column and the contaminated water is contacted with the adsorbent by its continuous passage through the bed. In a typical saturation operation, the column effluent is practically free of solute until a state of complete saturation of the entire column is approached. From then on, the effluent concentration increases rapidly toward the original feed concentration. The solute concentration in the effluent may be plotted against the cumulative volume or against the elapsed time; such a plot is termed the concentration history for adsorption or exchange. The point in the concentration history at which solute concentration just reaches a detectable level is known as the breakthrough volume or breakthrough time. The portion of effluent concentration history in which the solute concentration increases from breakthrough to nearly complete saturation has been termed the breakthrough curve, the adsorption wave or the exchange zone. This region is of major practical importance, and the ensuring

derivations will be carried out in order especially to calculate this portion of the entire concentration history [Hiester and Vermeulen, 1952 McCabe, et.al, 2001].

In both operations (adsorption and ion exchange) the concentrations in fluid and solid phase inside the bed depend both on position and time, it is unsteady state rate controlled process, therefore sorption occurs only in a particular region of the bed, known as the mass transfer zone, which moves through the bed with time [Thomas and Crittenden, 1998].

The location of the breakpoint and the shape of the breakthrough curve (degree of concavity) are influenced by many parameters pertaining to the nature of the adsorption equilibrium isotherm and the mass transfer rate [Basheer and Najjar, 1996].

Sorption processes are differential; they usually require numerical methods to solve [Tan, 1984]. The general analytical solution is that of Thomas [Thomas, 1944], it is based on second-order reaction kinetics, but can also apply to diffusion-limited system, as demonstrated by Hiester and Vermeulen [Hiester and Vermeulen, 1952].

The aim of this study is to show the capability of Thomas model to predict the breakthrough curves for both adsorption and ion exchange processes. Four sets of experimental data represent adsorption and ion exchange for liquid and gas are used to test the model.

FIXED BED PROCESS MODEL

Methods of second-order kinetics

The following reactions for ion exchange and for physical adsorption will be considered [Hiester and Vermeulen, 1952, Smith, 1988].

$$A + B.Resin \rightarrow B + A.Resin \qquad (ion\ exchange)$$

$$A + Sorbent \rightarrow A.Sorbent \qquad (adsorption)$$

The rate for ion exchange at the particle surfaces, in the case of ions of the same valence, may be expressed as:

$$\frac{d(A.Resin)}{dt} = K_{kin}\left[(A)(B.Resin) - \left(\frac{1}{\bar{k}}\right)(B)(A.Resin)\right] \qquad (1)$$

Where the parentheses denote concentration, t is the time, K_{kin} is the rate constant for reaction, and $\bar{k}$ is equilibrium constant for the reaction.

Since the resin has a finite capacity, then the sum of the concentrations of $B.Resin$ and $A.Resin$ is equal to a constant [Sherwood, et.al, 1975].

$$(B.Resin) + (A.Resin) = \bar{Q} \qquad (2)$$

Similarly in the solution phase outside the resin, the sum of concentrations of A and B is constant:

$$(A) + (B) = (C_o) \tag{3}$$

The following substitutions may then be made:

$$\left.\begin{aligned} (A) &= (C) \\ (B) &= (C_o - C) \\ (A.Resin) &= (q) \\ (B.Resin) &= (\bar{Q} - q) = (q_\infty - q) \end{aligned}\right] \tag{4}$$

Here q is the amount of A combined per unit weight of dry resin; $\bar{Q}$ is the ultimate capacity of dry adsorbent per unit weight; q_∞ is the capacity of adsorbent that is reached at saturation. For ion exchange, only, $q_\infty = \bar{Q}$ and eq. (1) becomes:

$$\left[\frac{dq}{dt}\right] = K_{kin}\left[C(q_\infty - q) - \frac{1}{k}q(C_o - C)\right] \tag{5}$$

Assuming Langmuir equilibrium under practically isothermal reaction conditions, the rate for adsorption at the solid surfaces may be written [Keinath and Weber, 1968].

$$\frac{d(A.Sorbent)}{dt} = K_{kin}\left[(A)(Sorbent) - \left(\frac{1}{k}\right)(A.Sorbent)\right]$$

Let:

$$\left.\begin{aligned} (A) &= (C) \\ (A.Sorbent) &= (q) \\ (Sorbent) &= (\bar{Q} - q) \end{aligned}\right] \tag{6}$$

$$\left[\frac{dq}{dt}\right] = K_{kin}\left[C(\bar{Q} - q) - \frac{1}{k}q\right] \tag{7}$$

Equations of transport

The material balance on the fluid and solid phase for an infinitesimal thickness of bed at any given cross section (neglecting the axial dispersion) is given by [Sherwood, et.al, 1975]:

$$\varepsilon \frac{\partial C}{\partial t} + \rho_b \frac{\partial q}{\partial t} + U \frac{\partial C}{\partial Z} = 0 \quad (8)$$

Eq. (8) must be coupled with the following equation [Sherwood, et.al, 1975]:

$$\rho_b \frac{\partial q}{\partial t} = KaF(C,q) \quad (9)$$

This equation expresses the rate of addition of solute to the solid phase in terms of the interface mass transfer coefficient Ka and a driving force $F(C,q)$ to be selected [Sherwood, et.al, 1975]. K is the kinetic coefficient based on a unit of exterior particle surface and a is the total surface in a unit volume of packed bed.

The design of a fixed bed device for adsorption or ion exchange requires solution of these two equations.

Thomas solution for sorption breakthrough curves

The most useful treatment of the sorption design problem is that of Thomas [Thomas, 1944]. Thomas assumed that the rate of adsorption on the right hand side of eq. (9) can be represented by an expression suggested by the stoichiometry of the monovalent ion exchange reaction then:

$$\rho_b \frac{\partial q}{\partial t} = Ka \left[C(q_m - q) - \frac{1}{\bar{k}} (C_o - C)q \right] \quad (10)$$

Eq. (10) is expressed in terms of a kinetic coefficient K and the two Langmuir isotherm constants (q_m and $\bar{k}$)

The expression in square brackets is called the "kinetic driving force" and K is the corresponding "kinetic coefficient". It is possible to relate K to individual mass transfer coefficients representing diffusion resistance in fluid and solid phase. Eq. (10) is simplified for further use by redefining the time scale by [Sherwood, et.al, 1975]:

$$\theta = t - \frac{\varepsilon Z}{U}$$

Then equations (8 and 10) become:

$$\rho_b \frac{\partial q}{\partial \theta} + U \frac{\partial C}{\partial Z} = 0 \quad (11)$$

$$\rho_b \frac{\partial q}{\partial \theta} = Ka \left[C(q_m - q) - \frac{1}{\bar{k}} (C_o - C)q \right] \quad (12)$$

Thomas model can be used to reduce equations (11 and 12) to a linear equation by introducing a transformation of the dependent variables. His solution for adsorption

boundary conditions on $C(Z,\theta)$ and $q(Z,\theta)$, such that $C(0,\theta) = C_o = constat$ and $q(Z,0) = 0$, can be expressed by following the nomenclature of Vermeulen et al. [Vermeulen, et.al, 1973]:

$$X = \frac{J(\bar{R}N,\ N\bar{T})}{J(\bar{R}N,\ N\bar{T}) + (1 - J(N,\bar{R}N\bar{T}))\exp((\bar{R}-1)N(\bar{T}-1))} \qquad (13)$$

Where:

$$\left.\begin{aligned} J(u,v) &= 1 - \varphi_1(u,v) \\ \varphi_1(u,v) &= \int_0^u \varphi_o(\lambda,v)\,d\lambda \\ \varphi_o(\lambda,v) &= \exp(-\lambda - v)\, I_o(2\sqrt{\lambda v}) \end{aligned}\right] \qquad (14)$$

I_o is the modified Bessel function of zero order, and the approximate calculation of the J function is:

$$J(u,v) = \frac{1}{2}\left[1 - \mathrm{erf}\left(\sqrt{u} - \sqrt{v}\right) + \frac{exp\left[-(\sqrt{u}-\sqrt{v})^2\right]}{\sqrt{\pi}\left[\sqrt{v} + (u*v)^{1/4}\right]}\right] \qquad (15)$$

Tan [Tan, 1980 and Tan, 1984] modified the work of Hiester and Vermeulen [Hiester and Vermeulen, 1952] by placing the dimensionless eq. (13) of the breakthrough curve, in a new form suitable for microcomputer application:

$$\frac{1}{X} = 1 + \exp(G) \qquad (16)$$

$$G = ln[\varphi_1(N,\bar{R}N\bar{T})] - ln[J(\bar{R}N,N\bar{T})] + (\bar{R}-1)N(\bar{T}-1) \qquad (17)$$

$$\left.\begin{aligned} \varphi_1(N,\bar{R}N\bar{T}) &= J(\bar{R}N\bar{T},N)\left[1 - \frac{\varphi_o(\bar{R}N\bar{T},N)}{J(\bar{R}N\bar{T},N)}\right] \\ \varphi_o(u,v) &= \frac{exp\left[-(\sqrt{u}-\sqrt{v})^2\right]}{2\sqrt{\pi}(u*v)^{1/4}} \end{aligned}\right] \qquad (18)$$

The integral error function erf was approximated as follows [Forbes and Underhill, 1986]:

.

$$\mathrm{erf}\,x = 1 - (a_1 t + a_2 t^2 + a_3 t^3 + a_4 t^4 + a_5 t^5)e^{-x^2} \qquad (19)$$

Where:

$$t = \frac{1}{1+BX} \qquad (20)$$

$$a_1 = 0.254829592,\ a_2 = -0.284496736,\ a_3 = 1.421413741, a_4 = -1.453152027$$

$$a_5 = 1.061405429, \qquad B = 0.3275911$$

The number of transfer unit N, the separation factor $\bar{R}$ and the throughput parameter $\bar{T}$ can be calculated as follows [Tan, 1984, Sherwood et.al, 1975]:

$$N = \frac{KaZ}{U}$$

$$\bar{R} = \frac{1}{\bar{\bar{k}}}$$

$$\bar{T} = \frac{U C_o \theta}{q_m Z \rho_b}$$

$$a = \frac{4}{d_p}(1-\varepsilon) \quad \text{For spherical particles}$$

$$\bar{\bar{k}} = 1 + \bar{k} C_o$$

$$\theta = t - \frac{\varepsilon Z}{U} \qquad (21)$$

K can be estimated for liquid sorption as follows [Treybal, 1985]:

$$\frac{1}{K} = \frac{(\bar{\bar{k}}+1)}{2\bar{\bar{k}}}\left[\frac{C_o/q_m \rho_b}{K_s} + \frac{1}{K_f}\right] \qquad (22)$$

$$K_s = \frac{15 D_s}{(1-\varepsilon) d_p}$$

D_s is the surface diffusivity ,can be estimated experimentally.

K_f Can be estimated from the semi empirical correlation shown below [Sherwood et.al, 1975]:

$$K_f = \frac{D_o}{d_e}\left[2 + 1.45\, R_e^{1/2}\, S_c^{1/3}\right] \qquad (23)$$

Where d_e is the equivalent diameter for non spherical particle of adsorbent.

The equations, that are used to estimate K for sorption of gases, are listed below [Sherwood et.al, 1975]:

$$\frac{1}{K} = \frac{(\bar{\bar{k}} + 1)}{2\bar{\bar{k}}}\left[\frac{1}{K_p} + \frac{1}{K_f}\right]$$

$$K_f = \frac{J_D U}{(Sc)^{2/3}}$$

$$J_D = 1.175(Re)^{2/3}$$

$$K_p = \frac{60 D_p}{S_o(1-\varepsilon)d_p^2}$$

$$S_o = \frac{particle\ surface\ area}{volume\ of\ particle}$$

$$\frac{1}{D_p} = \frac{\tau}{x}\left[\frac{1}{D_k} + \frac{1}{D_f}\right]$$

$$D_k = \frac{19400x}{S_g\rho_p}\sqrt{\frac{T}{M}}$$

$$\bar{\bar{k}} = 1 + \bar{k}p$$

(24)

A computer program was constructed using MATLAB 7.0 software to calculate the outlet concentration at any time, in order to plot the breakthrough curves. Figure (1) shows the flow chart for MATLAB 7.0 program.

Resistance to mass transfer between phases

The precise design of fixed bed units should allow for several sources of mass transfer resistance. The transport and subsequent adsorption of adsorbate onto adsorbent particle consists of three main mechanisms [Scott and Paul, 1987], they are, transport through the fluid boundary layer to the external surface of the adsorbent particle, Interparticle diffusion in the liquid phase (pore diffusion) and/or in the adsorbed state along the pore walls (surface diffusion), and adsorption to the solid surface of the pore.

For eq. (10) to be employed in the design calculations, Thomas kinetics coefficient K must be found from individual phase mass transfer coefficients as mentioned.

In pores of diameter much greater than the mean free path of a molecule diffusion occurs by process of molecular collisions in the gas phase within the pore (Max William or bulk diffusion), but if the molecular mean free path is much greater than the pore diameter diffusion occurs by molecules colliding with the pore walls (Knudsen diffusion) [Smith, 1988].

Both molecular and Knudsen diffusion may occur in the same porous medium when the porous medium contains both macro pores and micro pores. The mean free path in liquids is so small that Knudsen diffusion is not significant.

Surface diffusion coefficient can be obtained by using the procedure described by Foo and Carmen [Foo and Rice, 1979, Carman and Haul, 1954].

RESULTS AND DISCUSSION

Four sets of experimental data [Maghazachi, 1989, Ebrahim, 2010, Mustafa, 1992, and Ibrahim, 1992] are adopted and compared with Thomas model.

The first data applied sorption of acetic acid from air onto activated carbon; the second applied sorption of phenol onto natural zeolite; the third applied sorption of o-cresol from water by activated carbon; and the final data applied the sorption of trichloroethylene from air by zeolite-5A.

Table (1) shows the values of system parameters for the four sets. The breakthrough curves for experimental and theoretical data were plotted in Figures (2 to 5).

Figures (2 and 3) show a comparison between Thomas model and experimental data for the first and second sets, the average absolute errors was 6% and 5% respectively, a good agreement can be observed, and R^2 were 0.930 and 0.963 respectively.

Figure (4) shows a comparison between theoretical and experimental data for the third set. The deviation of Thomas model from the experimental curve is due to that: the number of transfer unit (N) is equal to one for this set of data as shown in Table (1), and R^2 equal to 0.881. High numbers of transfer unit ($N \geq 10$) will give less deviation, [Thomas and Crittenden, 1998].

Figure (5) shows the comparison between theoretical and experimental data for the fourth set. It can be observed that Thomas model is in almost good agreement with the experimental data above 400 second of time, and the deviation widen below this value .This is because that, Thomas model did not account for axial dispersion which is important in this case (low velocity and high concentration) see Table (1). A special consideration may be needed to include the axial dispersion within the resin particle, because axial dispersion for porous particle may be important when flow rates are low and the sorption is fast and strong, this can be seen in gases of low Reynolds number. R^2 was equal to 0.713 [Thomas and Crittenden, 1998].

CONCLUSIONS

The following points can be concluded from the present research:

- Thomas model can be used to some extent predict the breakthrough curve for adsorption and ion exchange for gases and liquids.
- Thomas model gives a general analytical solution that allows for nonlinear equilibrium relationship.
- Less deviation between the experimental data and Thomas model can be obtained for high number of transfer unit (N) and for the case when the axial dispersion have no effect.

Table (1): Values of the systems parameters

Symbol	Units	1st Set [Maghazachi, 1989]	2nd Set [Ebrahim, 2010]	3rd Set [Mustafa, 1992]	4th Set [Ibrahim, 1992]
ρ_b	g/cm^3	0.4	0.58	0.4	0.714
ρ_p	g/cm^3	1.4	2.12	1.4	1.044
d_p	cm	0.068×0.26	0.05	0.068×0.26	0.02
ε	-	0.714	0.3	0.714	0.315
T	K	303	303	313	305
Z	cm	20	10	6	17.5
U	cm/s	157.2	0.142	0.4	2.32
C_o	g/cm^3	43.7×10^{-6}	150×10^{-6}	100×10^{-6}	578×10^{-6}
q_m	g/g	0.488	0.076	0.271	0.045
$\bar{k}$	cm^3/g	236 $x10^3$	70.85 $x10^3$	12.2 $x10^3$	3.45$x10^3$
K	cm/s	4.3	5.2×10^{-4}	4.1×10^{-3}	0.06
N	-	9	3	1	8

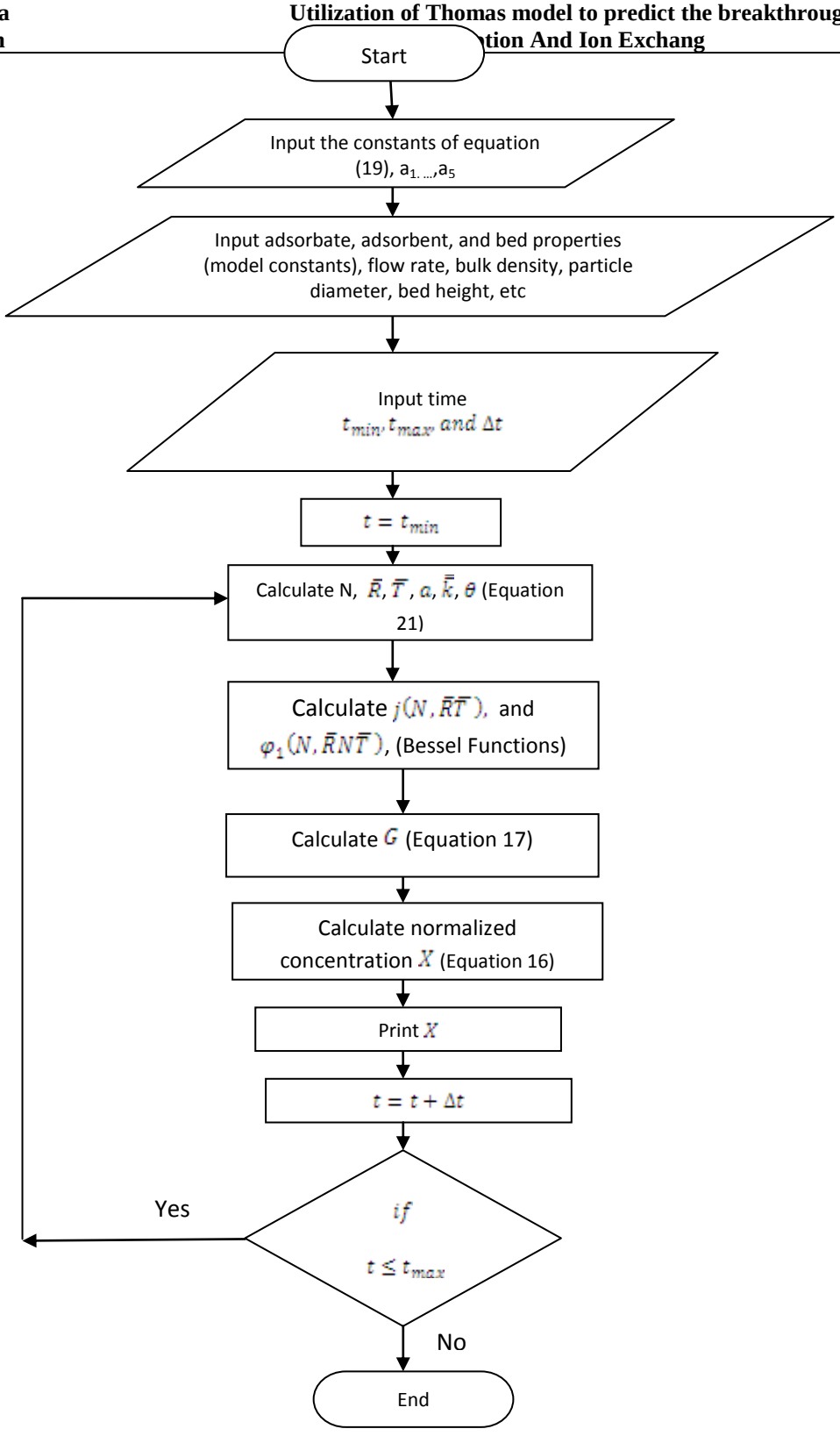

Fig. 1: Flow chart of the program in MATLAB 7.0

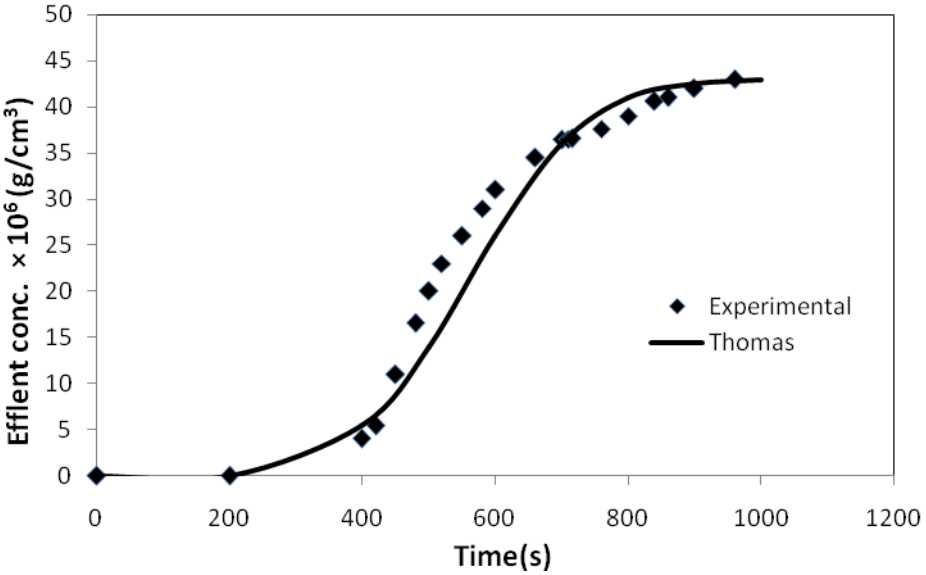

Fig. 2: Experimental and predicted breakthrough curves for sorption of acetic acid from air by activated carbon.

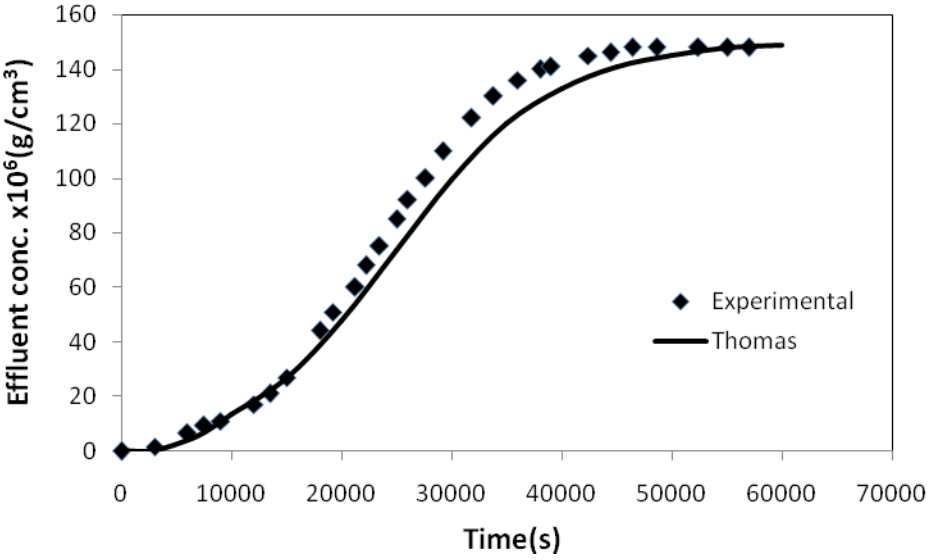

Fig. 3: Experimental and predicted breakthrough curves for sorption of phenol from water by natural zeolite.

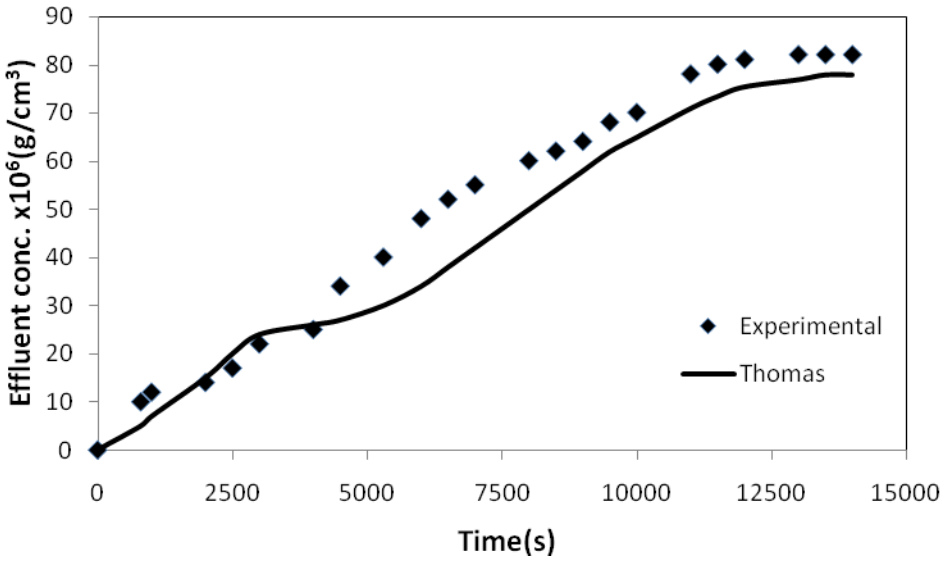

Fig. 4: Experimental and predicted breakthrough curves for sorption of o-cresol from water by activated carbon.

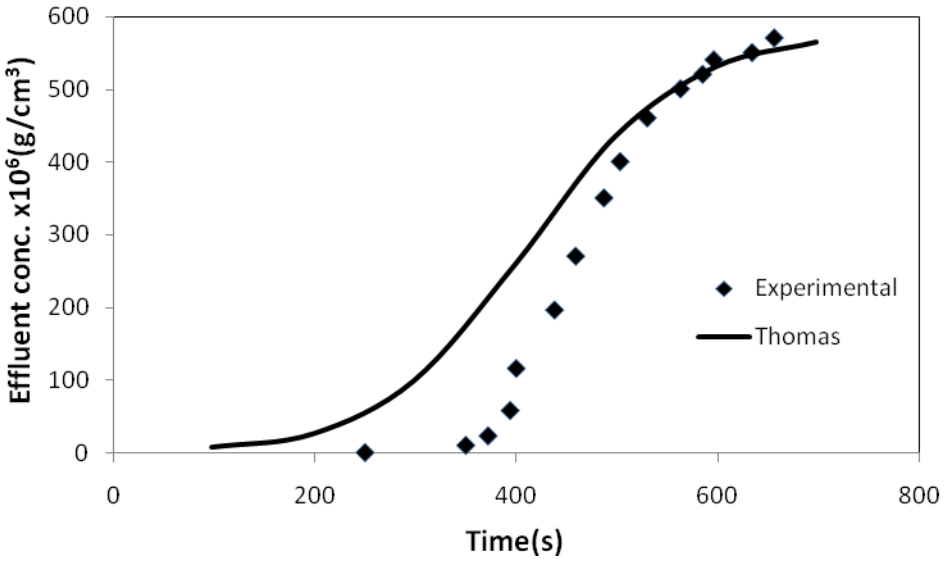

Fig. 5: Experimental and predicted breakthrough curves for sorption of trichloro ethylene from air by zeolite-5A.

REFERENCES

-Basheer, I. A. and Najjar, Y. M., (1996), Predicting Dynamic Response of Adsorption Columns with Neural Nets, Journal of Computing in Civil Engineering, 10, 31-39.

-Carman, P. C., and Haul, R. A. W., (1954), Measurement of Diffusion Coefficients, Proc. Roy. Soc., 222, 109-117.

-Chu,M.A.,(2010), Fixed bed sorption: Setting the record straight on the Bohart-Adams and Thomas models, Journal of Hazardous materials,177,1006-1012.

-Ebrahim, S. E., (2010). Modeling the Removal of Phenol by Natural Zeolite in Batchand Continuous Adsorption Systems, , Journal of Babylon University, (article in press, Vol. 19, No. 4).

-Foo, S. C., and Rice, R. G., (1979), Sorption Equilibria and Rate Studies on Resinous Retardation Beads. 2. Rate Studies, Ind. Eng. Chem. Fundam, 18, 68-75.

- Forbes, S. L., and Underhill, D. W., (1986), Modeling adsorption bed behavior using microcomputer, JAPCA, 36, 61.

-Han,R.,Wang,Y.,Yu,W., Shi,J.,Liu,H.,(2007), Biosorption of methylene blue from aqueous solution by rice husk in a fixed-bed column Journal of Hazardous Materials ,141 , 713–718.

-Han,R., Wang,Y., Zou,W., Wang,Y.,and Shi,J.,(2007), Comparison of linear and nonlinear analysis in estimating the Thomas model parameters for Methylene blue adsorption onto natural zeolite in fixed bed column , Journal of Hazardous Materials, 145, 331–335.

-Han,R., Zou,L., Zhao,Xu,F.,Li,Y.,and Wang,Y.,(2009), Removal of Methylene blue from aqueous solution by chaff in batch mode, Chemical Engineering Journal,149,123-131.

-Hiester, N. K., and Vermeulen, T., (1952), Saturation performance of ion-exchange and adsorption columns, Chemical Engineering Progress, 48, 505- 516.

-Ibrahim, S.K., (1992), Removal of gaseous pollutants from air by adsorption method, M.Sc. Thesis, University of Baghdad.

-Keinath, T. M., and Weber, W. J. Jr.,(1968), A predictive model for the design of fluid-bed adsorber, Journal of Water Pollution Control Federation, 40, 741-765.

- Maghazachi, M. S. K., (1989), Removal of gaseous pollutants from air by adsorption method, M.Sc. Thesis, University of Baghdad.

-McCabe, W. L., Smith, J. C. and Hariott, P., (2001), Unit Operation of Chemical Engineering, 6th edition, McGraw-Hill, USA.

-Mustafa Y. A., (1992), Removal of pollutants from water by adsorption, M.Sc. thesis, University of Baghdad.

-Scott, R. S. and Paul, V. R., (1987), Rate of Humic substance uptake during activated carbon adsorption, J. Environmental Engineering, 113, 1333-1349.

-Sherwood, T. K., Pigford, R. L., and Wilke, C. R., (1975), Mass transfer, McGraw-Hill, USA.

-Smith, J.M., (1988), Chemical engineering kinetics, McGraw-Hill, USA.

-Tan, H. K. S., (1980), Kinetics of fixed-bed sorption processes, Chemical Engineering 24,117-119.

-Tan, H. K. S., (1984), Programs for fixed-bed sorption, Chemical Engineering, 91, 57-61.

-Thomas, H. C., (1944), Heterogeneous Ion Exchange in a Flowing System, Journal of the American Chemical Society, 66, 1664-1666.

-Thomas, W. J., and Crittenden, B., (1998), Adsorption Technology and Design, Reed Education and Professional Publishing Ltd., UK.

-Treybal, R. E., (1985) "Mass transfer operation", McGraw Hill, New York.

-Vermeulen, T., Klein, G., and Hiester, N. K., in , (1973), Chemical Engineering Handbook, ed. R.H. Perry and C.H. Chilton,C.H. 5th ed., section 16.

-Vijayaraghavan, K., and Yun, Y., S., (2008), Bacterial biosorbents and biosorption, Biotechnology Advances, 26, 266–291.

-Wolborska, A., (1999), External film control of the fixed bed adsorption, Chemical Engineering Journal, 73, 85-92.

Nomenclature

A	Solute species
a	Interfacial area of solid phase per volume of bed, m^2/m^3
B	Solute species
C	Concentration of fluid, g/cm^3
Co	Initial concentration, g/cm^3
Ce	Concentration of solute at equilibrium, g/cm^3
Do	Molecular diffusivity, cm^2/s
D_f	Fluid phase diffusivity, cm^2/s
D_p	Particle phase diffusivity, cm^2/s
D_k	Kundsen diffusion coefficient, cm^2/s
D_s	Surface diffusion coefficient, m^2/s
de	Equivalent diameter of the particle, cm
d_p	Particle diameter, cm
K	Kinetic mass transfer coefficient for Thomas model, cm/s
K_f	Mass transfer coefficient for fluid phase, cm/s
K_p	Mass transfer coefficient in pore phase, cm/s
$\bar{k}$	Equilibrium constant or Langmuir constant, cm^3/g
$\bar{\bar{k}}$	$\bar{\bar{k}}=1+\bar{k}c_o$ or $\bar{\bar{k}} = 1 + \bar{k}\,p$
M	Molecular weight, g/gmol
N	Number of transfer units
P	Adsorbate partial pressure, Kpa
P_o	Adsorbate partial pressure in the feed gas mixture, Kpa
$\bar{Q}$	Ultimate capacity of dry adsorbent, g/g
Q	Fluid flow rate, cm^3/s
q	Adsorbate phase concentration (capacity), g/g
q_m	Maximum solid phase concentration value corresponding to complete coverage of surface by a monolayer, g/g
q_∞	Adsorbed phase concentration at saturation, g/g
R	Gas constant, 8.3143 kJ/kmol K
$\bar{R}$	Separation factor
S_o	External surface area per unit volume of particle, 1/cm
T	Temperature, K
T_o	Standard temperature,273K
$\bar{T}$	Throughput parameter
t	Time, s
U	Superficial fluid velocity, cm/s
X	C/Co, Normalized concentration
Z	Bed height, cm
ε	Porosity in packed bed
θ	Contact time, s

ρ_b Bulk density of bed, g/cm^3

ρ_p Particle density, g/cm^3

τ Tortuosity factor

x Fraction void space inside the porous particles

R_e Reynolds number

S_c Schmidt number

FREE VIBRATION RESPONSE ANALYSIS OF BURIED CYLINDRICAL STORAGE TANKS

Dr. Adrian F. Ali (Assistant Professor,
Civil .Dept, College of Engineering,University of Baghdad)
And Hussein Mahmood Ali (M.Sc, Civil Engineering)

ABSTRACT

This study presents a reliable and effective idealization scheme for the free vibration analysis of buried cylindrical storage tanks. The three dimensional problem is transformed into a two dimensional one by using a semi analytical finite element procedure. Conical shell of revolution element is used. to represent the cylindrical wall, top plate, and bottom plate of the tank by an appropriate method. The Combined effect of structure-soil-fluid interaction is of primary importance as concluded in this work. The soil medium is idealized by the elastic half space model, that is, linear springs are assumed to represent the structure-soil interface, added masses and viscous dampers of soil are also included. The liquid region is treated analytically; also analytical integration is used to got the added stillness and mass matrices for hydrostatic and hydrodynamic pressure effects, respectively. The free vibration characteristics of the liquid storage tank are validated against experimen.tal and theoretical results available in literatures.

الخلاصة

تتضمن الدراسة تحليل الاهتزاز الحر للخزانات الاسطوانية المدفونة بأستخدام طرق ملائمة ومبسطة بحيث تم تحويل المسألة ثلاثية البعد الى مجموعة من المسائل ثنائية البعد بأستخدام طريقة شبه تحليلية (Semi Analytical Method) .

لقد تم انتخاب تحليلي للخزان عبارة عن عنصر صدفي بشكل مخروط ناقص . أن من فوائد هذا العنصر هي أمكانية استخدامه لتمثيل كل من جدران الخزان الآسطواني والقاعدتين العليا والسفلى بأستخدام زاويتي تدوير مناسبة للعنصر الصدفي .

تم الاخذ بنظر الاعتبار التاثير المتبادل بين جدران الخزان والسائل الموجود داخله من جهه والتربة المحيطة به من جهه أخرى بحيث تم نمذجة الوسط الترابي أعتمادا على مبدأ نصف الفضاء المرن (Elastic Half Space) يفرض وجود نوابض خطية مرنة (Elastic Springs) مع كتل ومخمدات اضافية للتربة (Added Masses and Dampers) , أما السائل الموجود داخل الخزان فقد تم تحليله رياضيا أخذا بنظر الاعتبار تاثير الضغط الهيدروستاتيكي والهيدروديناميكي للسائل أثناء الاهتزازات حيث تم اشتقاق مصفوفات جساءة وكتلة اضافية (Added Stiffness and Masses) لتمثيل هذا التاثير وتضاف الى مصفوفات الجساءة والكتلة لعناصر جدران الخزان .

خصائص الاهتزاز الحر للخزان تم أثباتها مقارنة مع عدد نتائج عملية ونظرية سابقة . تم أجراء دراسة موسعة تأخذ بنظر الاعتبار اهم العوامل الموثرة على التصرف الديناميكي للخزانات أثناء الاهتزاز الحر ....

INTRODUCTION

Liquid storage tanks are important elements of lifeline and industrial facilities. These structures come in a variety of configurations; they might be elevated, ground-supported, partly or completely buried. In general, cylindrical storage tanks are widely used in practice as compared to other types because they are simple in design, efficient in resisting primary hydrostatic pressure, and can be easily constructed. The free vibration characteristics of liquid storage tanks have been studied by using various methods such as finite element methods, boundary integral techniques and variational methods. As the number and the sizes of these tanks increased, their behavior under free vibration become a matter of concern and led to investigations of their vibrational characteristics. The standard finite element models were shown to be capable, in principle, of dealing with any two or three-dimensional problems. Nevertheless, in cases where the geometry, and elastic, properties of the structure remain independent of the circumferential coordinate, semi-analytical finite element technique can be used to exchange the original Three-dimensional problem into several separate two-dimensional problems by making use of Fourier series expansion in the circumferential direction, The exchange is worthwhile because a single three-dimensional solution is usually mach more expensive than several two-dimensional solutions. In buried tank analysis, there are two aspects of interaction that must be considered:

- Interaction between the tank and the contained liquid.

- Interaction between the tank-liquid system and the surrounding medium.

The contained liquid is treated analytically as a continuum by the boundary solution technique, where the number of unknowns is substantially less than in those analyses where both tank components and liquid are subdivided into finite elements. A complete analysis of the soil-tank system by the finite element method is expensive and complicated; however, an elag.tio half-space model of the soil is employed with a finite clement model of the shell to exhibit the fundamental dynamic characteristics of the overall system

and to assess the significance of the interaction on the free vibration response of tanks.

TANK GEOMETRY AND COORDINATE SYSTEM

A typical shape of tanks under consideration is shown in Fig. (1), it consists of a circular cylindrical, thin-walled liquid containers of radius R, length L_T, and thickness t. The tank is partly filled with liquid to a height, H.A cylindrical coordinate system is used with the center of the base being tile origin. The radial, circumferential, and axial coordinates are denoted r, θ, and z, respectively, mid the corresponding displacement components of a point on the shell middle surface are denoted by $w, v,$ and $u,$ respectively. To describe the location of a point on the free surface during vibration, let ξ measure the superelevation of that point from the quiescent liquid free surface.

TYPES OF VIBRATIONAL MODES

The natural free vibrational modes of a circular cylindrical liquid storage tank can be viewed as a combination of four distinct types of modes [5], and as follows:

- Lateral vibrational modes of the tank wall itself under the action of hydrodynamic pressure, Fig.(2)

- Circumferential vibrational modes involving ($sin(n\theta)$ & $cos(n\theta)$) type modes as shown in Fig. (3).

- Low frequency sloshing modes of the contained liquid, Fig (4)

- Natural modes associated with the motion of a compressible liquid.

The effects of sloshing motion and liquid compressibility are weak [7] therefore, these effects are assumed to be negligible for the purpose of present work.

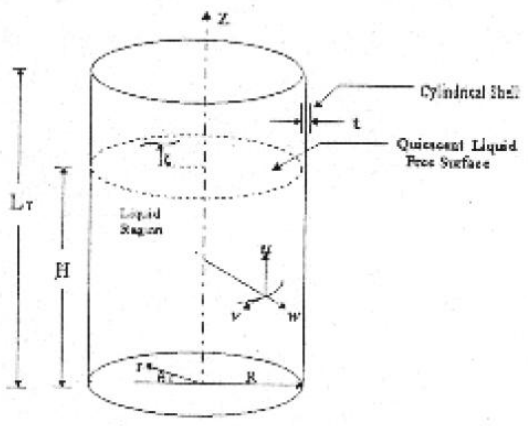

Fig.(1): Cylindrical wall tank and coordinate system

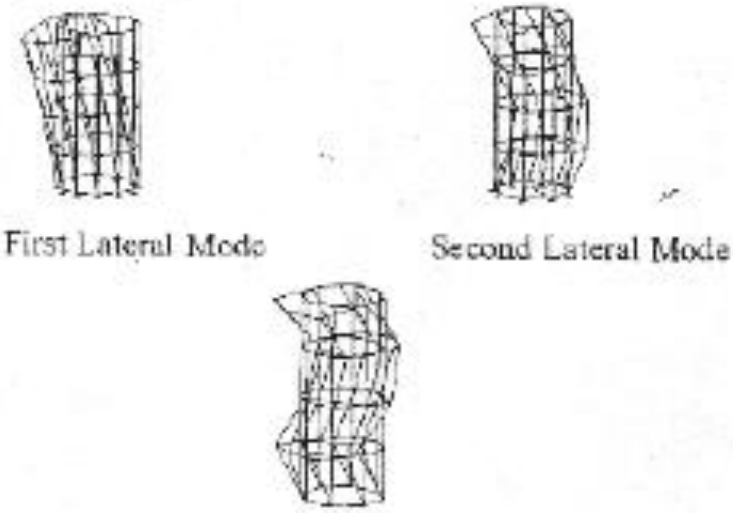

Fig.(2)Lateral Mode Shapes

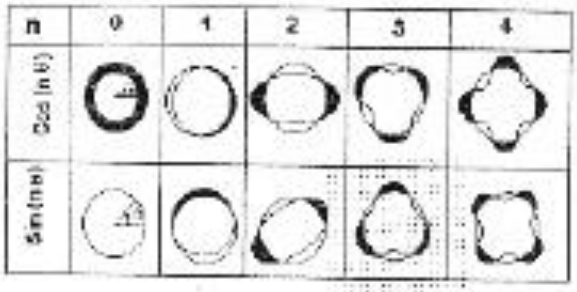

Fig (3) **Mode Shapes of a circular cross Section accordin to Sinusoidal Functions**

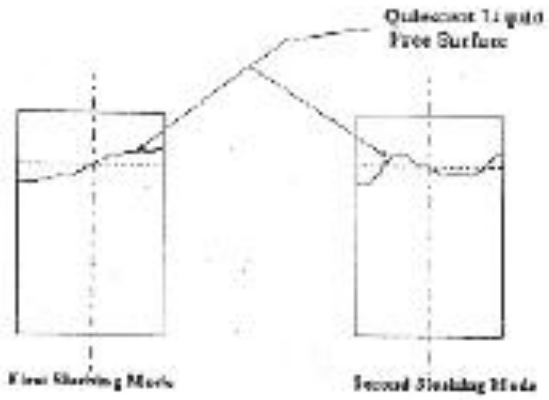

Fig(4) :Sloshing modes

FINITE ELEMENT FORMULATION

Consider the conical shell of Fig. (5). The deformation in the shell can be .expressed in terms of the middle Surface deformations u, v and w, that is, the meridional (axial), tangential and normal displacements, respectively. It is assumed that, the displacement vector $U(r,\theta,z)$ to vary sufficiently smooth along the circumferential (i.e. 0) direction, such that U may he expanded in a finite number of terms of Fourier series along the θ $-$ddirection [4,9], viz.

$$\begin{Bmatrix} u \\ v \\ w \end{Bmatrix} = \sum_{n=0}^{N} \begin{bmatrix} \cos(n\theta) & 0 & 0 & \sin(n\theta) & 0 & 0 \\ 0 & \sin(n\theta) & 0 & 0 & \cos(n\theta) & 0 \\ 0 & 0 & \cos(n\theta) & 0 & 0 & \sin(n\theta) \end{bmatrix} \begin{Bmatrix} u_n^s \\ v_n^s \\ w_n^s \\ u_n^a \\ v_n^a \\ w_n^a \end{Bmatrix} \quad \dots (1)$$

where each term of each series is called a harmonic (or a circumferential wave), n is the order nf each harmonic. and N is the number of Fourier terms. The subscript (s) refers to symmetric components of displacement while (a) applies to antsymmetric components; therefore, the solution becomes capable, of representing the general non-axsymmetric case. The shape functions associated with the axial and tangential displacements (i.e. u and v) are taken to be linear between the nodal points. However, those associated with the radial displacement (i.e., Hermitian polynomials to assure slope continuity at the nodes.

For each harmonic n, the displacement field vector, $\{U_n\}$, in terms of the coordinate z is:

$$\begin{Bmatrix} u_n^s \\ v_n^s \\ w_n^s \\ u_n^a \\ v_n^a \\ w_n^a \end{Bmatrix} = \begin{bmatrix} [f]_{3x8} & [0] \\ [0] & [f] \end{bmatrix}_{6x16} \{a\} \quad \dots (2)$$

$$\text{in which:} \quad [f] = \begin{bmatrix} 1 & \bar{z} & 0 & 0 & 0 & 0 & 0 & 0 \\ 0 & 0 & 1 & \bar{z} & 0 & 0 & 0 & 0 \\ 0 & 0 & 0 & 0 & 1 & \bar{z} & \bar{z}^2 & \bar{z}^3 \end{bmatrix} \quad \dots (3)$$

and the generalized coefficients vector $\{a\}$ is

$$\{a\}^T = \begin{bmatrix} a_1^s & a_2^s & a_3^s & \dots & a_8^s & a_1^a & a_2^a & a_3^a & \dots & a_8^a \end{bmatrix} \quad \dots (4)$$

Introducing the boundary conditions at $z = 0$ and $z = L$ into Eq. (3) gives:

$$\begin{Bmatrix} \{U^s_{no}\} \\ \{U^a_{no}\} \end{Bmatrix} = \begin{bmatrix} [A]_{8x8} & [0] \\ [0] & [A] \end{bmatrix}_{16x16} \{a\} \quad \text{.....(5)}$$

in which

$$\{U^s_{no}\}^T = \left[u^s_{n1} \quad v^s_{n1} \quad w^s_{n1} \quad \frac{\partial w^s_{n1}}{\partial z} \quad u^s_{n2} \quad v^s_{n2} \quad w^s_{n2} \quad \frac{\partial w^s_{n2}}{\partial z} \right] \quad \text{.....(6-a)}$$

$$\{U^a_{no}\}^T = \left[u^a_{n1} \quad v^a_{n1} \quad w^a_{n1} \quad \frac{\partial w^a_{n1}}{\partial z} \quad u^a_{n2} \quad v^a_{n2} \quad w^a_{n2} \quad \frac{\partial w^a_{n2}}{\partial z} \right] \quad \text{.....(6-b)}$$

and the submatrix $[A]$ is of the form:

$$[A] = \begin{bmatrix} 1 & 0 & 0 & 0 & 0 & 0 & 0 & 0 \\ 0 & 0 & 1 & 0 & 0 & 0 & 0 & 0 \\ 0 & 0 & 0 & 0 & 1 & 0 & 0 & 0 \\ 0 & 0 & 0 & 0 & 0 & 1 & 0 & 0 \\ 1 & L & 0 & 0 & 0 & 0 & 0 & 0 \\ 0 & 0 & 1 & L & 0 & 0 & 0 & 0 \\ 0 & 0 & 0 & 0 & 1 & L & L^2 & L^3 \\ 0 & 0 & 0 & 0 & 0 & 1 & 2L & 3L^2 \end{bmatrix}_{8x8} \quad \text{.....(7)}$$

Eq.(5) is now inverted to establish the generalized coefficients vector $\{a\}$ in terms of the generalized nodal displacement vector, $\{U_{8x8}\}$, as follows:

$$\{a\} = [AA]^{-1}\{U_{no}\} \quad \text{.....(8)}$$

$$\text{in which : } [AA]^{-1} = \begin{bmatrix} [A]^{-1}_{8x8} & [0] \\ [0] & [A]^{-1} \end{bmatrix}_{16x16} \quad \text{.....(9)}$$

and the submatrix $[A]^{-1}$ is of the form:

$$[A]^{-1}=\begin{bmatrix} 1 & 0 & 0 & 0 & 0 & 0 & 0 & 0 \\ \frac{-1}{L} & 0 & 0 & 0 & \frac{1}{L} & 0 & 0 & 0 \\ 0 & 1 & 0 & 0 & 0 & 0 & 0 & 0 \\ 0 & \frac{-1}{L} & 0 & 0 & 0 & \frac{1}{L} & 0 & 0 \\ 0 & 0 & 1 & 0 & 0 & 0 & 0 & 0 \\ 0 & 0 & 0 & 1 & 0 & 0 & 0 & 0 \\ 0 & 0 & \frac{-3}{L^2} & \frac{-2}{L} & 0 & 0 & \frac{3}{L^2} & \frac{-1}{L} \\ 0 & 0 & \frac{2}{L^3} & \frac{1}{L^2} & 0 & 0 & \frac{-2}{L^3} & \frac{1}{L^2} \end{bmatrix} \quad \ldots\ldots\ldots\

$$
\left.
\begin{aligned}
S_1 &= 1-\frac{\bar{Z}}{L} \\
S_2 &= \frac{\bar{Z}}{L} \\
N_1 &= 1-\frac{3\bar{Z}^2}{L^2}+\frac{2\bar{Z}^3}{L^3} \\
\hat{N}_1 &= Z-\frac{2\bar{Z}^2}{L}+\frac{\bar{Z}^3}{L^2} \\
N_2 &= \frac{3\bar{Z}^2}{L^2}-\frac{2\bar{Z}^3}{L^3} \\
\hat{N}_2 &= -\frac{\bar{Z}^2}{L}+\frac{\bar{Z}^3}{L^2}
\end{aligned}
\right\} \quad \ldots\ldots\ldots\ldots\ldots\ldots\ldots\ldots\ldots\ldots (14)
$$

Substitute Eq.(11) into Eq.(1) gives:

$$\{U\}=\sum_{n=0}^{N}[\theta_n\ ][N]\{U_{no}\} \quad \ldots\ldots\ldots\ldots\ldots\ldots\ldots\ldots\ldots\ldots\ldots\ldots (15)$$

Strain-Displacement Relations

The strain of the middle surface in terms of the middle surface displacements are given by [4,9]

$$
\begin{bmatrix} \varepsilon_r \\ \varepsilon_\theta \\ \gamma_{r\theta} \\ k_r \\ k_\theta \\ k_{r\theta} \end{bmatrix} =
\begin{bmatrix}
\frac{\partial}{\partial z} & 0 & 0 \\
\frac{1}{r}\sin\phi & \frac{1}{r}\frac{\partial}{\partial\theta} & \frac{1}{r}\cos\phi \\
\frac{1}{r}\frac{\partial}{\partial\theta} & \frac{\partial}{\partial z}-\frac{1}{r}\sin\phi & 0 \\
0 & 0 & -\frac{\partial^2}{\partial z^2} \\
0 & \frac{1}{r^2}\cos\phi\frac{\partial}{\partial\theta} & -\frac{1}{r}\sin\phi\frac{\partial}{\partial z}-\frac{1}{r^2}\frac{\partial^2}{\partial\theta^2} \\
0 & \frac{2}{r}\cos\phi\left(\frac{\partial}{\partial z}-\frac{1}{r}\sin\phi\right) & \frac{2}{r}\left(\sin\phi\frac{\partial}{\partial\theta}-\frac{\partial^2}{\partial z\partial\theta}\right)
\end{bmatrix}
\begin{bmatrix} \mu \\ v \\ w \end{bmatrix} \quad \ldots(16)
$$

where Ø is the angle shown in Fig.(5)

and $\varepsilon, \gamma\ and\ k$ denote normal strain, shear strain and curvature, respectively.

Substituting Eq.(15) into Eq.(16) gives:

$$\{\varepsilon\}=\sum_{n=0}^{N}[p][\theta_n][N]\{U_{no}\} \quad \ldots\ldots\ldots\ldots\ldots\ldots\ldots\ldots\ldots\ldots (17)$$

$$\text{or } \{\varepsilon\} = \sum_{n=0}^{N} [B]\{U_{no}\} = \sum_{n=0}^{N} \{\varepsilon_n\} \quad \ldots\ldots(18)$$

$$\text{in which, } \{\varepsilon\} = [B]\{U_{no}\} \quad \ldots\ldots(19)$$

$$\text{and } [B] = [p][\partial_n][N] = [\,[B_1]\,,\,[B_2]\,]_{6\times 16} \quad \ldots\ldots(20)$$

The submatrix $[B_1]$ refers to the symmetric part of the strain-displacement matrix and $[B_2]$ refers to antisymmetric part.

CONSTITUTIVE RELATIONS

For linearly elastic homogenous and isotropic material, the force and moment resultants can be expressed in terms of the normal and shear strains in the middle surface $\varepsilon_z, \varepsilon_\theta \; and \; \varepsilon_{z\theta}$; in terms of midsurface changes in curvature k_z and k_θ and in terms o fthe midsurface twist, $k_{z\theta}$, as follows [1,9]

$$\{\sigma\} = [D]\{\varepsilon\} \quad \ldots\ldots(21)$$

in which

$$\{\sigma\}^T = [N_z \quad N_\theta \quad N_{z\theta} \quad M_z \quad M_\theta \quad M_{z\theta}] \quad \ldots\ldots(22)$$

where N_z and N_θ are referred to as the effective membrane shear force resultant and the effective twisting moment resultant, respectively,
and the matrix $[D]$ is of the form[4]:

$$[D] = \begin{bmatrix} C & \upsilon C & 0 & & & \\ \upsilon C & C & 0 & & [0] & \\ 0 & 0 & \frac{1-\upsilon}{2}C & & & \\ & & & D & D\upsilon & 0 \\ & [0] & & D\upsilon & D & 0 \\ & & & 0 & 0 & \frac{1-\upsilon}{2}D \end{bmatrix} \quad \ldots\ldots(23)$$

Where $[D]$ is the element constitutive matrix

$$\text{and } C = \frac{Et}{1-\upsilon^2}, \quad D = \frac{Et^3}{12(1-\upsilon^2)}$$

in which E, t, v denote the modulus of elasticity; thickness of the shell element and Poisson's ratio, respectively.
Substituting Eq.(18) into Eq.(21) gives:

$$\{\sigma\} = \sum_{n=0}^{N} [D][B]\{U_{no}\} \quad \ldots\ldots(24)$$

STIFFNESS & MASS MATRIX FORMULATION

The strain energy of any system is given by [1,4,5]

$$U_{1(t)} = \frac{1}{2}\int_0^{L}\int_0^{2\pi} \{\varepsilon\}^T \{\sigma\}\, r\, d\theta\, dz \qquad \text{.....(25)}$$

Substituting Eq.(18) and Eq.(24) into Eq.(25) gives:

$$U_{1(t)} = \frac{1}{2}\int_0^{L}\int_0^{2\pi}\sum_{n=0}^{N}\sum_{n=0}^{N} \{U_{no}\}^T [B]^T [D][B]\{U_{no}\}\, r\, d\theta\, dz \qquad \text{...(26)}$$

For the n^{th} term, Eq.(26) may be expressed conviently in terms of the element stiffness matrix $[K]_e$ as:

$$U_{1(t)} = \frac{1}{2}\sum_{e=1}^{NEL} \{U_{no}\}^T [K]_e \{U_{no}\} \qquad \text{.....(27)}$$

In which, e is the subscript including "element"; NEL is the number of shell element along the shell length.

and $[K]_e$ is of the form

$$[K]_e = \int_0^{L}\int_0^{2\pi} [B]^T [D][B]\, r\, d\theta\, d\bar{z} \qquad \text{.....(28)}$$

The kinetic energy of the shell, neglecting rotary inertia can be expressed as [1,4,5]

$$T(t) = \frac{1}{2}\int_0^{L}\int_0^{2\pi} \rho t \{\dot{U}_n\}^T \{\dot{U}_n\}\, r\, d\theta\, dZ \qquad \text{.....(29)}$$

In which ρ is the mass of the shell per unit volume; $\{U_n\}$ is the displacement vector defined by Eq.(11) and the dots ($\dot{}$) denotes differentiation with respect to the time t.

sub. Eq.(11) into Eq.(29) results in:

$$T(t) = \frac{1}{2}\sum_{e=1}^{NEL} r\rho t \int_0^{L}\int_0^{2\pi} \{\dot{U}_{no}\}^T [N]^T [N]\{\dot{U}_{no}\}\, d\theta\, d\bar{z} \qquad \text{.....(30)}$$

Eq.(30) can be written as:

$$T(t) = \frac{1}{2}\sum_{e=1}^{NEL} \{\dot{U}_{no}\}^T [M]_e \{\dot{U}_{no}\} \qquad \text{.....(31)}$$

In which, $[M]_e$ is the consistent mass matrix of the element which can be defined by:

$$[M]_e = r\rho t \int_0^{L}\int_0^{2\pi} [N]^T [N]\, d\theta\, d\bar{z} \qquad \text{.....(32)}$$

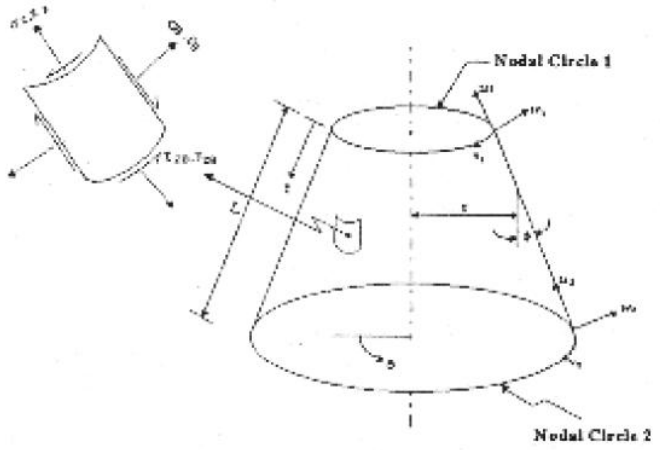

Fig.(5):Conical shell element geometry and internal forces

MATHEMATICAL MODEL

The components of a typical buried cylindrical tank arc explained briefly as below:

- Tank wall: The geometrically axisymmetric shell is discretized as a series of frustums of connected at their modal point circles. In the case of a cylindrical tank, the cone shall be changed to a cylinder since the radius has a constant value. This means that, the angle ϕ indicated in Fig.(5), becomes equal to zero. See Fig(6-a).
- Top and bottom plates: making use of the conical shell element, these plates shall be represented by several elements after putting $\phi = 90$. This concept is shown in Fig.(6-a). A small hole at the center of plate is used to avoid the singularity at the center r=0.
- Contained liquid: the liquid region is treated by an analytical model taking into a count the effect of the hydrodynamic pressure and the initial hoop stresses due to the hydrostatic pressure.

These effect are estimated by considerable details and will be discussed later.

- Surrounding soil. An elastic half space model is used to represent the soil-tank interaction. The interaction system represented by a set of discrete 9lump0 mass springs, and dashpots as shown in Fig.(7). The coefficient m, K and C, for this model are evaluated by the method of continuum mechanics[3].

IDEALIZATION OF LIQUID

Equation Governing Liquid Motion

For the irrotational flow of an incompressible inviscid liquid, the velocity potential function, $\Phi(r,\theta,Z,t)$ satisfying Laplace equation is giving by [5,9]:

$$\nabla^2 \Phi = 0 \qquad \text{..... (33-a)}$$

In the region occupied by the liquid ($0 \le r \le R, 0 \le \theta \le 2\pi, 0 \le Z \le H$)

in which

$$\nabla^2 = \frac{\partial^2}{\partial r^2} + \frac{1}{r}\frac{\partial}{\partial r} + \frac{1}{r^2}\frac{\partial^2}{\partial \theta^2} + \frac{\partial^2}{\partial z^2} \qquad \text{..... (33-b)}$$

In addition to being a harmonic function, Φ must satisfy the proper boundary conditions. The velocity vector of the liquid is the gradient of the velocity potential, and consequently, the liquid-container boundary conditions can be expressed as follows [5]:

- At the tank bottom (assumed rigid), Z=0, the liquid velocity in the vertical direction is zero.

$$\frac{\partial \Phi}{\partial z}(r,\theta,0,t)=0 \quad \ldots\ldots\ldots\

$$P_d(R,0,Z,t) = -\rho_L \frac{\partial \Phi}{\partial t}(R,\theta,Z,t)$$

$$= \frac{-2\rho_L}{H} \sum_{i=1}^{\infty} \frac{\int_0^H \ddot{w}_n(z,t)\cos(\alpha_i z)dz}{\alpha_i I_n'(\alpha_i R)} I_n(\alpha_i R).\cos(\alpha_i R).\cos(n\theta) \quad \ldots(42)$$

HYDRODYNAMIC PRESSURE

Evaluation of the Added Mass Matrix

As a consequence of neglecting the free surface oscillation methods, the motion of the tank wall can be analyzed by introducing an additional matrix in the matrix equation of shell motion, such addition represents the effect of liquid dynamic pressure during vibration. The hydrodynamic pressure exerted on the wall of the tank is given by Eq.(42) and therefore, the work done by such pressure though an arbitrary virtual displacement, $\delta\omega_n \cos(n\theta)$ refers to symmetric component of displacement, can be written as:

$$\delta W = \int_0^H \int_0^{2\pi} \{P_d(R,0,Z,t)\,\delta w_n \cos(n\theta)\} R\, d\theta\, dZ$$

$$= -\sum_{i=1}^{\infty} b_m \left(\int_0^H \delta w_n \cos(\alpha_i z)dz\right)\left(\int_0^H \ddot{w}_n \cos(\alpha_i z)dz\right) \quad \ldots(43)$$

in which, $b_m = \frac{2\pi R \rho_L I_n(\alpha_i R)}{H \alpha_i I_n'(\alpha_i R)}$ .....(44)

The work expression, Eq.(43), gives rise to the definition of the added mass matrix [DM]. In order to compute its elements, one has to express the integral in Eq.(43) in terms of the nodal displacement vector $\{U_{no}\}$. With the aid of the finite element displacement modal, one can write:

$$\int_0^H \ddot{w}_n(z,t)\cos(\alpha_i z)dz = \sum_{e=1}^{NEH} \int_0^L \{Nd(\bar{z})\}^T \{\ddot{U}_{no}(t)\}_e \cos\{\alpha_i[\bar{z} + (e-1)L]\}d\bar{z} \quad \ldots(45)$$

Where NEH is the number of shell elemnt id contact with liquid.

By definition the vector $\{f^{(i)}\}$, as the integrals

$$\{f^{(i)}\} = \int_0^L \{Nd(\bar{z})\}^T \cos\{\alpha_i[\bar{z} + (e-1)L]\}d\bar{z}$$

$$= [0,\ 0,\ f_3^{(i)},\ f_4^{(i)},\ 0,\ 0,\ f_7^{(i)},\ f_8^{(i)}]_e \quad \ldots\ldots\ldots\ldots (46\text{- a})$$

and $\{Nd(\bar{z})\}^T = |0 \quad 0 \quad N_1(\bar{z}) \quad \hat{N}_1(\bar{z}) \quad 0 \quad 0 \quad N_2(\bar{z}) \quad \hat{N}_2(\bar{z})| \ldots.(46\text{-b})$

The vector $\{f^{(i)}\}$ can be defined as:

$$\{F^{(i)}\} = \sum_{e=1}^{NEH} \{f^{(i)}\} \quad \ldots\ldots\ldots\ldots (47)$$

one can rewrite Eq.(45) as follows:

$$\int_0^H \ddot{w}_n \cos(\alpha_i z) dz = \{F^{(i)}\}^T \{\ddot{U}_{no}\} \quad \text{..... (48)}$$

Therefore the expression of the work done, Eq.(43), becomes

$$\delta W = -\sum_{i=1}^{\infty} b_{ni} \{\delta U_{no}\}^T \{F^{(i)}\} \{F^{(i)}\}^T \{\ddot{U}_{no}\}$$

$$= -\{\delta U_{no}\}^T \left(\sum_{i=1}^{\infty} b_{ni} \{F^{(i)}\} \{F^{(i)}\}^T\right) \{\ddot{U}_{no}\} \quad \text{..... (49)}$$

Eq.(49) leads to the definition of the added mass matrix, [DM], as:

$$[DM] = \sum_{i=1}^{\infty} b_{ni} \{F^{(i)}\} \{F^{(i)}\}^T \quad \text{..... (50)}$$

HYDRODYNAMIC PRESSURE

Effect of Initial Hoop Stress

Due to presence of the liquid, tank walls are subjected to hydrostatic pressure which cause hoop tensions. The pressure of such stresses affects the vibrational characteristics of the shell, especially the $\cos(n\theta)$ and $\sin(n\theta)$ mode types, these mode types are shown in Fig.(3).

To incorporate these effects, it is necessary to modify the strain energy expression of the shell and to generalize accordingly the equations of motion. Upon using the finite element modal, the matrix equation can be easily derived, and takes the familiar form with an added stiffness matrix due to the presence of the stress field.

MODIFICATION OF POTENTIAL ENERGY OF SHELL

Consider a circular cylindrical shell acted upon by a static initial stress field which is in equilibrium. The initial stresses in the shell result from the hydrostatic pressure. During vibration, the shell stresses consist of the initial stresses plus additional vibratory stresses. In the subsequent analysis, the bending stresses produced by the initial loading are neglected, i.e., only the initial membrane stresses are considered

Since the initial stress state is in equilibrium, the potential energy of the system in this state may be taken as the reference level. Thus, the internal strain energy of the shell can be written as:

$$\bar{U}(t) = U_1(t) + U_2(t) \quad \text{..... (51)}$$

in which $U_1(t)$ is the strain energy employed in deriving the stiffness matrix [K], of the shell and it is defined by Eq.(25) and $U_2(t)$ is given by

$$U_2(t) = \int_0^H \int_0^{2\pi} (N_\theta \varepsilon_\theta) R \, d\theta \, dZ \quad \text{..... (52)}$$

in which N_o is the initial membrane force resultant in the circumferential direction, and ε_θ is the midsurface strain

Since the initial hoop stress may be large, it is necessary to use the second-order nonlinear strain-displacement equation in the second term of Eq.(51) while using only the linear relationship in the first term [6]

This maintains the proper homogeneity in the order of magnitude of the terms in the integrands. The midsurface strain in Eq.(52), therefore, it can be expressed as

$$\varepsilon_\theta = \frac{1}{R}\left[\frac{\partial v}{\partial \theta} + w\right] + \frac{1}{2}\left\{\left(\frac{1}{R}\frac{\partial u}{\partial \theta}\right)^2 + \left[\frac{1}{R}\left(\frac{\partial v}{\partial \theta} + w\right)\right]^2 + \left[\frac{1}{R}\left(v - \frac{\partial w}{\partial \theta}\right)\right]^2\right\} \quad ..(53)$$

The initial force resultant, N_θ and the liquid hydrostatic pressure, P_s, are in equilibrium, and therefore, it satisfies

$$N_\theta = \rho_1 gR(H - Z); \quad \frac{\partial N_\theta}{\partial \theta} = 0 \quad \ldots\ldots\ldots\ldots\ldots\ldots\ldots\ldots\ldots\ldots(54)$$

EVALUATION OF THE ADDED STIFFNESS MATRIX

Since N_θ is not a function of θ, the strain energy $U_2(t)$ can be written as:

$$U_2(t) = R\int_0^H \left[N_\theta \left(\int_0^{2\pi} \varepsilon_\theta d\theta\right)\right] dz \quad \ldots\ldots\ldots\ldots\ldots\ldots\ldots\ldots (55\text{-a})$$

The strain-displacement relation Eq.(53) is the inserted into the strain energy expression, Eq.(55-a). however, the linear terms of Eq.(53) do not contribute to $U_2(t)$ since

$$\int_0^{2\pi} \cos(n\theta)d\theta = 0 \qquad (n \geq 1) \quad \ldots\ldots\ldots\ldots\ldots\ldots (55\text{-b})$$

Furthermore, the terms can be expressed more conveniently in the following matrix form:

$$\varepsilon_\theta^{nL} = \frac{1}{2}\left([\bar{p}]\{U\}\right)^T\left([\bar{p}]\{U\}\right) \quad \ldots\ldots\ldots\ldots\ldots\ldots\ldots\ldots\ldots\ldots (56)$$

in which {U} is the displacement vector, Eq.(1) [P] is a differential matrix given by:

$$[\bar{P}] = \frac{1}{R}\begin{bmatrix} \frac{\partial}{\partial\theta} & 0 & 0 \\ 0 & \frac{\partial}{\partial\theta} & 1 \\ 0 & 1 & -\frac{\partial}{\partial\theta} \end{bmatrix} \quad \ldots\ldots\ldots\ldots\ldots\ldots\ldots\ldots\ldots\ldots (57)$$

and the superscript nL indicates "nonlinear:. With the aid of Eq.(1) and (57), Eq.(56) can be expressed as:

$$\varepsilon_\theta^{nL} = \frac{1}{2}\left([\bar{p}][\theta_n]\{U_n\}\right)^T\left([\bar{p}][D_n]\{d_n\}\right) = \frac{1}{2}\{U_n\}^T[\bar{p}_n]^T[\bar{p}_n]\{U_n\} \ldots\ldots (58)$$

in which,

$$[\bar{p}_n] = [\bar{p}][\theta_n]$$

$$= \frac{1}{R}\begin{bmatrix} -n\sin(n\theta) & 0 & 0 & n\cos(n\theta) & 0 & 0 \\ 0 & n\cos(n\theta) & \cos(n\theta) & 0 & -n\sin(n\theta) & \sin(n\theta) \\ 0 & \sin(n\theta) & n\sin(n\theta) & 0 & \cos(n\theta) & -n\cos(n\theta) \end{bmatrix} \ldots (59)$$

Inserting Eq.(59) into the strain energy expression (Eq.55), one obtains

$$U_2(t)=\frac{R}{2}\int_0^H\left[N_\theta\{U_n\}^T\left(\int_0^{2\pi}[\bar{p}_n]^T[\bar{p}_n]d\theta\right)\{U_n\}\right]dz$$

$$=\frac{\pi}{2R}\int_0^H(N_\theta\{U_n\}^T[C_n]\{U_n\})\,dZ \qquad \ldots\ldots (60)$$

in which, $$[C_n]=\begin{bmatrix} n^2 & 0 & 0 & 0 & 0 & 0 \\ 0 & n^2+1 & 2n & 0 & 0 & 0 \\ 0 & 2n & n^2-1 & 0 & 0 & 0 \\ 0 & 0 & 0 & n^2 & 0 & 0 \\ 0 & 0 & 0 & 0 & n^2+1 & -2n \\ 0 & 0 & 0 & 0 & -2n & n^2+1 \end{bmatrix} \qquad \ldots\ldots (61)$$

By using the displacement model, Eq.(11), one can write

$$U_2(t)=\frac{1}{2}\sum_{e=1}^{NEH}\{U_{no}\}_e^T[K_H]_e\{U_{no}\} \qquad \ldots\ldots (62)$$

In which $[K_H]_e$ is the element added stiffness matrix which given by:

$$[K_H]_e=\frac{\pi}{R}\int_0^h\left\{N_\theta(\bar{z})\left([N(\bar{z})]^T[C_n][N(\bar{z})]\right)\right\}d\bar{z} \qquad \ldots\ldots (63)$$

IDEALIZATION OF SOIL

The elastic half-space type is used to model the influence of the soil during vibration. The soil in this model is assumed to be homogenous, isotropic, and elastic, and characterized by shear modulus (G_s) and Poisson's ratio (ν_s).

The soil is replaced by a set of an equivalent spring-mass-dashpot system as shown in Fig. (7).There various method used for estimating the spring constant (Ks) viscous damper (Cs) and added mass (mi) of the soil model. The most commonly used approach is to employ formulas from the theory of elasticity, which is used in this study. Formulas tire given in Table (1)

Table(1):Equivalent discrete properties for elastic half-space [3]

Degree of freedom	Spring Constant (K_s)	Viscous Damper (C_s)	Added Mass (m_s)
Vertical	$\frac{4G_s r_0}{(1-\upsilon_s)}$	$1.79\sqrt{K_s \rho_s r_0^3}$	$1.5\rho_s r_0^3$
Horizontal	$\frac{18.2G_s r_0(1-\upsilon_s^2)}{(2-\upsilon_s)^2}$	$1.08\sqrt{K_s \rho_s r_0^3}$	$0.28\rho_s r_0^3$
Rocking	$\frac{2.7G_s r_0^3}{(1-\upsilon_s)}$ (Ref.49)	$0.47\sqrt{K_s \rho_s r_0^5}$	$0.49\rho_s r_0^5$

Where

r_0 = radius of circular plate.

υ_s = Poisson's ratio of the soil

ρ_s = mass density of the soil

G_s = shear modulus of the soil which can be evaluated using following the equation [8]:

$$G_s = \rho_s V_s^2 \quad \text{.....(64)}$$

in which V_s = shear wave velocity

The radius (r_o) in Table (1) is directly used for calculations of the bottom circular plate, with equivalent radius is needed for calculations of the cylintlrical wall for the tank. On basis of equivalent areas, (surface area of the cylindrical wall is equal to the area of circular plate). The equivalent radius may be determined from the following relationship[6]

$r_0 = \sqrt{2RL}$ for horizontal and vertical degrees of freedom

$r_0 = 4\sqrt{\frac{2RL^3}{3}}$ for rocking degree of freedom

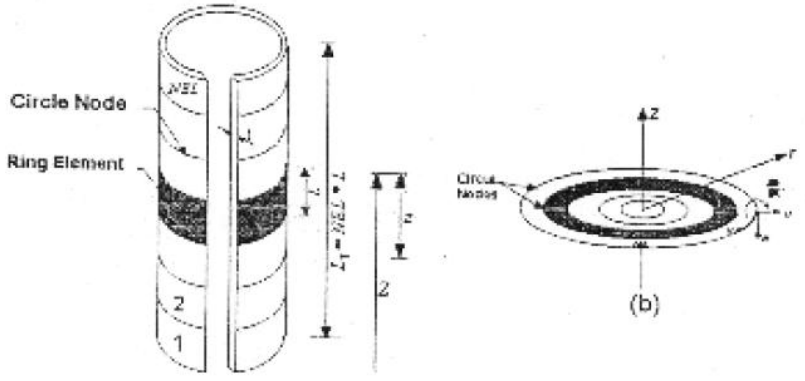

Fig.(6) : Mathematical Model

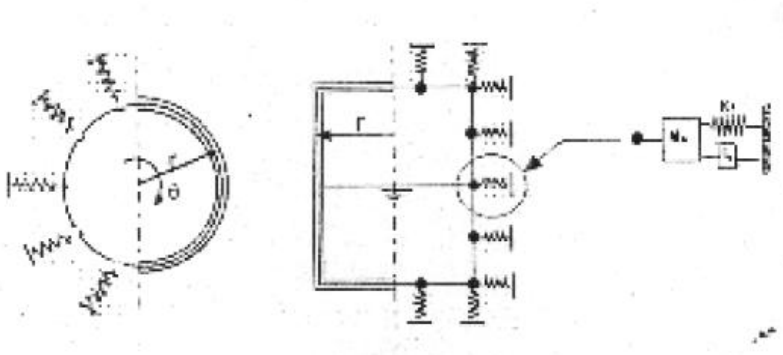

Fig.(7): Elastic half - space modeling for soil-tank interaction

FREE VIBRATION RESPONSE ANALYSIS

A structure is said to be undergoing free vibration when it is disturbed from its static equilibrium position and then allowed external dynamic excitation or support motion.
The undamped free vibration response of any system can be obtained as:

$$[M]\{\ddot{U}\} + [K]\{U\} = \{0\} \quad \text{.....(65)}$$

Where [M] and [K] are the mass and the stiffness matrices of the system, respectively; and $\{U\}$ is the displaecment vector.
Therefore, the natural frequencies (ω) and the mode shape (ϕ) of any systcm governed by Eq.(65) are solution of the eigenvalue problem represented by

$$[[K] - \omega^2[M]]\{\phi\} = \{0\} \text{.....(66)}$$

For non trivial solution of Eq.(66),

$$[K] - \omega^2[M] = 0 \text{.....(67)}$$

Equation (67) is called the frequency equation of the system. Expanding the determinant will give an algebraic equation of m^{th} degree in thequmy parameter ω^2 for a system having. m degrees or freedom. The roots of this equation $(\omega_1^2, \omega_2^2, \omega_3^2, \cdots \omega_m^2)$ represent the frequencies of the in mode of vibration which are possible in the system.

If all m eigenvalue are required and m is relatively small (roughly m < 200), the Jacobi method is a good choice[4] ; therefore, Eq.(66) is solved numerically by the Jacobi method given in Ref(3) for all cases considered in the present study,

CYLINDRICAL STORAGE TANKS

Several cases of liquid storage tanks with widely different properties are presented to demonstrate the applicability of the proposed idealization developed herein and to cover the free vibration characteristics of these tanks. The analysis was applied to various case studies, which were considered by other investigators to serve as a validation procedure for the formulation proposed in the present work: and also to check the convergency of the solution. Examples of both broad and tall tanks are analyzed for each of three cases:

- EMPTY STORAGE TANKS

The properties of the tall and broad tanks are as follows [5,7]:

a- Tall Tank: Radius = 7.32m; length = 21.96m.

b- Broad Tank: Radius. = 18.29m; Length = 12:19m.

Both tanks are assumed to be opened at the top: fixed at the base and have as uniform thickness of 0.0254m (1 in).

The tank's wall is made of steel having the following properties:

$E = 20.67 * 10^7 kN/m^2, v = 0.3, and\ \rho = 78.4\ kN/m^3$

In Table (2), the three lowest natural frequencies of both tanks or the Fourier number (n=0 and n = 1) are presented along with those r tats obtained by Haroun and Housner [5] and by Haroun and Tayel [7]. Inspection of this Table shows excellent agreement between the values of these frequencies.

- Partly Filled Tanks

The small tall and broad tanks described earlier are now assumed to be partly filled with water. Calculations of the natural frequencies for different types of liquid depths are presented in Table (3) along the results obtained by Haroun and Houner [5] for Fourier number (n = 1).

PARAMETRIC STUDIES

To study the effect of tank geometry, liquid depth variation and hydrostatic pressure on natural frequencies, parametric studies for three different cases of soil types were carried out. The three types of soil arc classified as follows:

a) Soil type 1: dense sand and gravel, ρ =17 kN/m^3,Vs=250 m/sec

b) Soil type 2: moist clay, ρ =18 kN/m^3, Vs=150 m/sec

c) Soil type 3: fine - grained sand, ρ =16.5 kN/m^3, Vs=110 m/sec

The properties of material that is used in all cases of the parametric studies are taken as follows:

a) Steel material is used fin both cover and walls of the tank whose properties are:
$E = 20.67 * 10^7 kN/m^2, v = 0.3, and\ \rho = 78.4\ kN/m^3$. Both have a uniform thickness of 0.0508m.

b) Concrete material is used for base plate of the tank whose properties are ;
$E = 20 * 10^6 kN/m^2, v = 0.15, and\ \rho = 78.424\ kN/m^3$. The thickness of the plate is 0.4m.

c) Water is used as a storage liquid o r the tank having density of 10 kN/m^3

EFFECT OF TANK HEIGHT TO DIAMETER RATIO

For this purpose two cases of storage tanks were considered, empty tank and completely full tank. Diameter. D 20m and the tank height , L_T , was varied from 5 to 30m at 5m increments to accommodate the aspect ratio (L_T/D) range of 0.25 to 1.5.

Results of natural frequencies are given in Plots of Figs.(8) and (9).for empty and completely fill tanks , respectively.

From these Plots, it is observed that as the soil medium becomes weaker (having low shear wave velocity) or as tank height increases, the natural frequency of the system, at all modes or vibration for both two cases of the tank., decreases.

It is also noticed by examination of these Tables and Plots, that the natural frequencies of the empty tank are much larger than those of the full tanks regardless of the type or soil. This can be explained by the fact that, the added liquid mass is much larger than that of the shell, and since the natural frequencies are proportional to the square root of

the inverse of the mass, the frequencies of the full tank are reduced appreciably as compared to those of the empty tank.

EFFECT OF LIQUID HEIGHT TO TANK LENGTH RATIO VARIATION.

To demonstrate the effect of liquid depth variation (H/L_T), two types of tanks (tall and broad) were considered for this purpose. Different values of liquid depths for the same three types of the soils were carried out of demonstrate the influence of liquid height on the dynamic characteristics. The resulting natural frequencies are given in Plots of Figs.(10) and (11) for broad and tall tanks, respectively.

It can be observed from these Plots that as the level of fluid increase, the natural frequencies decreases for both types of tanks and for all three types of the surouding soil. This behavior is obvious since the mass of the shell-fluid system increase with the level of fluid, while the structure stiffness properties remain unchanged.

EFFECT OF INITIAL HOOP STRESS DUE TO HYDROSTATIC PRESSURE

To investigate the effect of initial hoop tension due to hydrostatic pressure on the dynamic characteristics the. liquid storage tanks, two filled tanks: (broad and tall) were considered with one type of soil (soil type 1 is chosen for this purpose) with different values of Fourier terms number (n). The resulting natural frequencies for broad and tall tanks are given in Plots of Figs. (12) and (13), respectively.

It can be concluded from these Plots that the initial hoop stress effect has significant influence on the natural frequencies of vibration of tall tank while, the influence is almost insignificant and negligible for most practical purposes in broad tanks. It is of interest to note that the influence of the initial stress becomes more significant as the Fourier term number, n increases.

EFFECT OF WALL THICKNESS VARIATION.

To demonstrate the effect of wall thickness variation, an empty tank of 15m height and 15m diameter is studied for its free vibration characteristics when its wall thickness varies from 1cm to 4cm with one type of the surrounding soil (soil type 1 is also used herein). The resulting natural frequencies are given in Plot of Fig.(14).

It can be seen clearly from these results that the thicker the wall of the tanks is, the higher are the natural frequencies, since the wall's stiffness increases with increasing its thickness.

Table (2): Natural frequencies for empty broad and tall tanks

Tank	Fourier term number	Mode number	Natural frequency (Hz)			
			Present analysis	By Haroun & Housner[5]	By Haroun & Tayle[7]	
					Analytical	Numerical
Broad Tank	0	1	44.41	—	44.40	44.41
		2	44.72	—	44.71	44.72
		3	44.82	—	44.77	44.80
	1	1	34.02	34.01	—	—
		2	43.81	43.86	—	—
		3	44.50	44.54	—	—
Tall tank	0	1	57.79	—	57.72	57.80
		2	109.11	—	108.97	109.14
		3	111.19	—	111.04	111.23
	1	1	19.23	19.26	—	—
		2	56.32	56.42	—	—

Table (3) : Natural frequencies for partly filled broad and tall tanks

Filling ratio (H/L_T)	Mode number	Natural frequency (Hz) , n=1			
		Broad tank		Tall tank	
		Present analysis	By Haroun & Housner (5)	Present analysis	By Haroun &Housner (5)
1	1	6.18	6.18	5.31	5.31
	2	11.3	11.28	15.63	15.64
0.8	1	7.23	7.24	7.04	7.05
	2	12.96	12.96	18.74	18.76
0.6	1	8.79	8.79	9.62	9.64
	2	15.38	15.37	22.2	22.45
0.5	1	9.88	9.88	11.41	11.42
	2	17.09	17.05	24.02	24.03
0.3	1	13.87	13.82	16.45	16.46
	2	24.20	24.00	25.59	25.61
0	1	34.04	34.04	19.24	19.26
	2	43.85	43.86	56.32	56.42

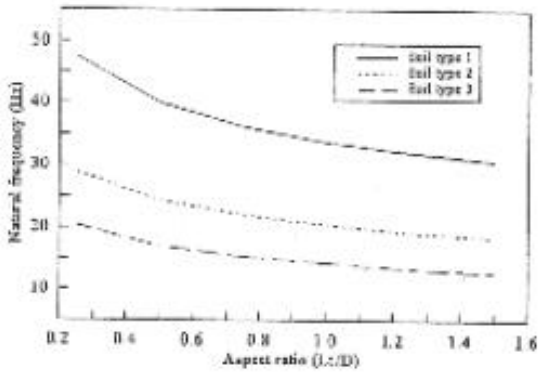

Fig.(8): Fundamental natural frequencies versus aspect ratio (L_T /D) variation of empty tank , n=1

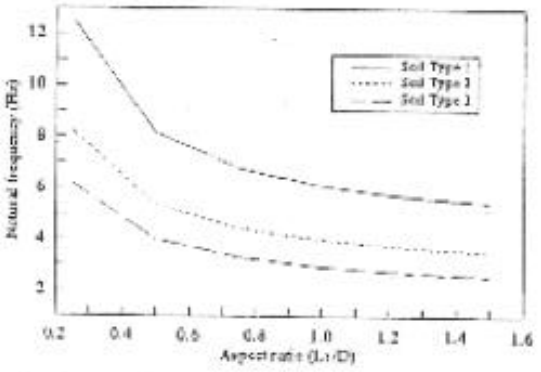

Fig.(9): Fundamental natural frequencies versus aspect ratio(L_T /D) variation of filled tank , n=1

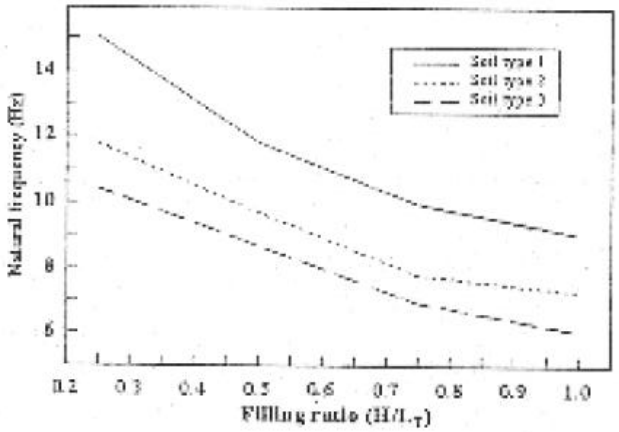

Fig.(10): Fundamental natural frequencies versus filling ratio (H/L_T) variation of broad tank , n=1

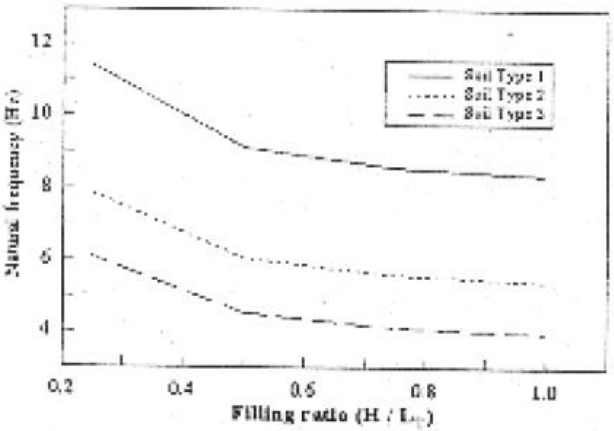

Fig.(11): Fundamental natural frequencies versus filling ratio(H/L_T) variation of tall tank , n=1

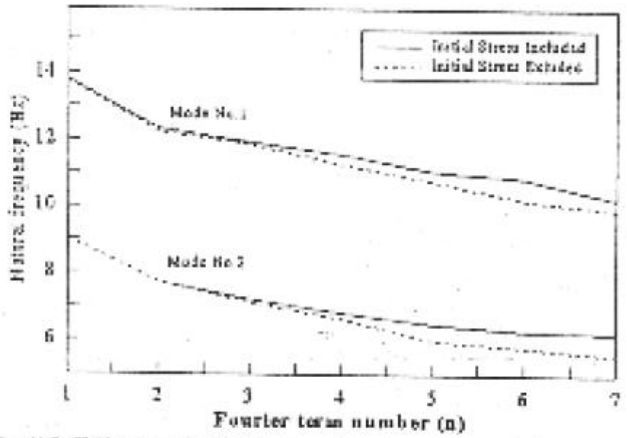

Fig.(12:Effect of initial hoop stress on natural frequencies of broad tank

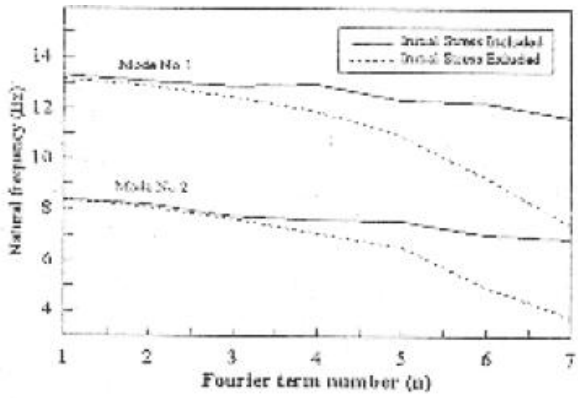

Fig.(13): Effect of Initial hoop stress on naturl frequencies of tall tank

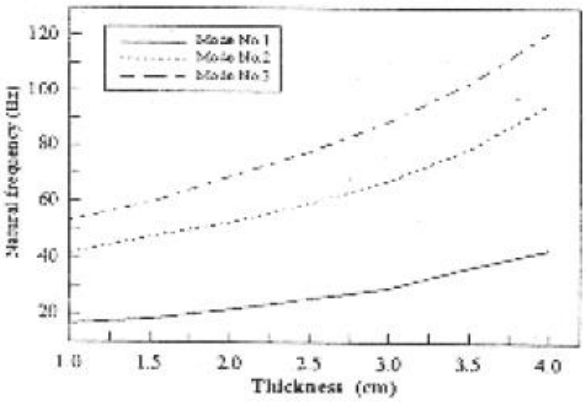

Fig.(14): Effect of thickness variation on natural frequencies of empty tank

CONCLUSIONS

- The main conclusions that can he drawn from the present study are as follows:
- The change of the three-dimensional problem into several separate two dimensional problems using the semi-analytical technique is very useful to reduce the effort required, computer time and memory needed in solving the problem or storage tanks under dynamic loading_
- A conical shell finite element is derived in the present work, which is best suited for the analysis of circular plate, cylindrical arid conical shells. This element becomes more general after including the contribution of symmetric and anti-symmetric turns in the Fourier series expansion.
- The soil-tank interaction was represented by an elastic half-space medium. Variations of the properties of the. Surrounding soil medium are found to have an important influence oil the free and forced vibrational response (earthquake response) of the buried storage tanks.
- It was found that, the .initial hoop stress due to hydrostatic pressure, becomes more significant as the circumference wave number, n, increases, and these stresses have . more influence on the frequencies of vibration of tail tanks than broad tanks.

- It is also found that, the natural frequency is proportional to the wall thickness of the tank. This behavior is related to the fact that the dynamic stiffness of a tank is a function of its wall thickness.

- **REFERENCES**

- Chundruputla, T. R., and Belegmda, A. D. "Introduction to Finite Element in Engineering", 2nd Edition, Prentice-Hill, 1997.
- Chopra A. K. "Dynamics of Structures (Theory and Application to Earthquake Engineering)", Prentice-Hill, 1996.
- Clough, R. W. and Penzien, J. "Dynamics of Structures", McGraw-Hill, 1975.
- Cook, R. D., Mallas, D. S. and Plesha. M. F. "Concepts and Applications of Finite Element Analysis",3rd Edition, John Wiley and Sons, 1989.
- Haroun, M. A. and Housner, G. W. "Dynamics Characteristics of Liquid Storage Tanks" Journal of the Engineering Mechanics Division, ASCE, Vo. 108, No. EM5, October 1982, pp. 783-800.
- Haroun, M. A. and Housner, G. W. "Complications In Free Vibration Analysis of Tanks." Journal of the Engineering Mechanics Division, ASCE, Vo. 108, No. EM5, October 1982, pp. 801-818.
- Haroun, M. A. and Tayel, M. A. "Axisymmetric Vibration of Tanks-Analytical and Numerical" Journal of Engineering Mechanics, ASCE, Vo. 111, No. 3, March, 1985, pp. 329-358.
- Prakash, S., "Soil Dynamics", McGraw-Hill, 1981.
- Zienkiewicz, O. C. "The Finite Element Method", 3rd Edition, McGraw-Hill, 1977

التكنولوجيا والعمارة
تحليل النتاج المعماري من وجهة تكنولوجية

د.نادية عبد المجيد السلام– أستاذ مساعد في قسم الهندسة المعمارية – جامعة بغداد
د.صبا سامي مهدي– مدرس مساعد في قسم الهندسة المعمارية – جامعة النهرين

خلاصة البحث :

يهتم البحث بأقتراح مفردات بحثية تحليلية لرصد النتاج المعماري من وجهة تكنولوجية. ويجري هذا عبر تحديد هيكل شامل لتحليل تكنولوجيا العمارة بالإستناد الى مقترح فيلسوف التكنولوجيا المعاصركارل متشام ، الذي يرى أن الكيان التكنولوجي في أي مكان وزمان يمكن رصده عبر **أربع تجليات: الأشياء والعملية والمعرفة والإرادة.** ويبين البحث أن هذه التجليات يمكن أن تقرأ كواقع سياقي لتكنولوجيا العمارة ، ثم يحدد المكونات التفصيلية لهذه التجليات، التي فيما بينها علاقات تنتظم وتتغير حسب المكان والزمان، لتسبغ على الكيان التكنولوجي خصائصه التي تنعكس على خصائص النتاج المعماري. ومن خلال استكشاف التجليات الاربع، بمكوناتها يشتق البحث المفردات البحثية المؤثرة في صياغة النتاج المعماري، وهذه المفردات هي: **المادة والتعامل بها. – المنشأ وعلاقاته. – بناء التفصيل.– التكتونيةوقيم المادة– التعبير الشكلي.**

Technology and Architecture
Analyzing Architecture from a Technological Standpoint

Dr. Nadia Abdul Majeed Al-salam, Assistant professor / University of Baghdad/ College of Engineering/ Department of Architecture.
Dr. Saba Sami, Assistant lecturer / University of Al-Nahrain/ College of Engineering/ Department of Architecture.

ABSTRACT:

This research is concerned with defining specific analytical terms that could be used in observing the architectural product from a technological view point. This was achieved by founding an inclusive analytical structure for architectural technology based on the view of technology philosopher Carl Mitcham, who states that technology, at a given time and place, could be observed through its four manifestations: Objects, Process, Knowledge and Volition. The research has showed that these manifestations define

architectural technology as the actual context within which relations between components of these manifestations emerge, get organized and change. Five analytical terms have been induced: materials and their processing, structure and its relations, detail building, tectonic values and formal expression. These are introduced as terms affecting the formulation of architectural product, and thus can be used for analyzing it technologically.
Key words: manifestations of technology, materials processing, structural relations, architectural detailing, tectonics, formal expression.

مقدمة:

تحتل التكنولوجيا أهمية متزايدة في العالم المعاصر، إذ تظهر فاعليتها في مختلف النتاج المادي والفكري للحضارة الإنسانية . والعمارة نتاج لفعل تكنولوجي على درجة غير قليلة من التعقيد تتداخل فيه مختلف العوامل والاطراف. لذا أصبح تحليل الفعل المسؤول عن انتاجها وإعطائها كيانها المادي مسألة متسعة المديات. وقد عني الباحثون بهذا الجانب، غير أن ادبياتهم تفصح عن مشكلة بحثية واضحة هي " القصور المعرفي في تحديد المفردات المؤثرة تكنولوجيا في صياغة النتاج المعماري". بذلك وضع البحث هدفا له: تحديد المفردات المؤثرة تكنولوجيا في صياغة النتاج المعماري. وقد إفترض البحث أن: تحديد المفردات المؤثرة تكنولوجيا في صياغة النتاج المعماري يتم عبر قراءة تجليات التكنولوجيا الأربعة: الأشياء والعملية والمعرفة والإرادة.

– تكنولوجيا العمارة في الأدبيات السابقة:

ترد في مجال تكنولوجيا العمارة رؤى متنوعة في النظر الى هيكل تكنولوجيا العمارة وأبعاده . حيث يرى ايميت ، مثلا، أن تكنولوجيا العمارة هي" **فن البناء، وهي نظام يهدف الى جمع المهارات الفنية والعملية والإجرائية بعضها مع بعض**"، فهي دمج لثلاثة عوالم منفصلة،

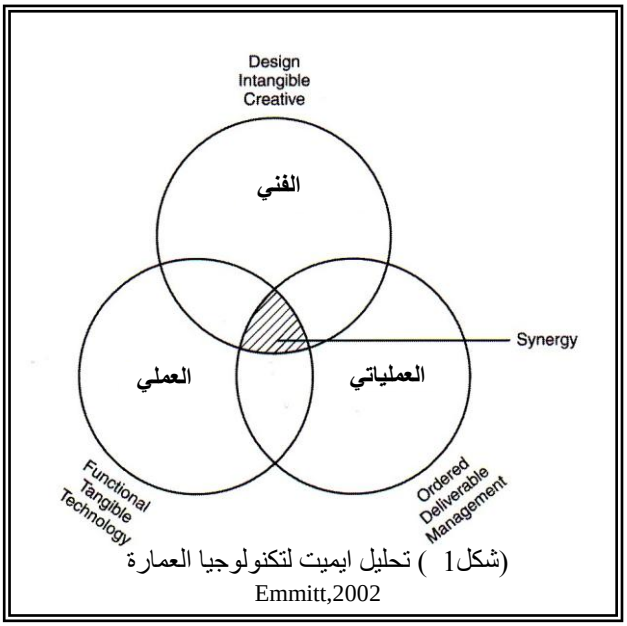

(شكل1) تحليل ايميت لتكنولوجيا العمارة
Emmitt,2002

أولها مكون فني وهو مجال المصمم المبدع، وهو صعب التحديد موضوعيا وذاتي الطبيعة دائما. والثاني هو المكون العملي وهو مجال البنّاء المنفذ، ويجمع المواد الفيزياوية. فهو مجال قابل للتحديد تقنيا و ماديا.أما الثالث فهو المكون الإجرائي، وهو المجال الاداري الذي يجمع المهارات الفنية المصممة مع العملية المنفذة بطريقة منظمة. (Emitt, 2002,p5) **(شكل 1)**

وفي أطروحتها الموسومة (المباني بوصفها سايب – أورغات Buildings As Cyborgs[1]) ترى الباحثة نادية الحسني التكنولوجيا بوصفها "**وسيلة انجاز الانتقال من الفكرة التصميمية إلى الواقع**" (Alhasani ,1990, p3) وتضع مخططا تحليليا للقوى المشّكلة لعملية انتاج العمارة

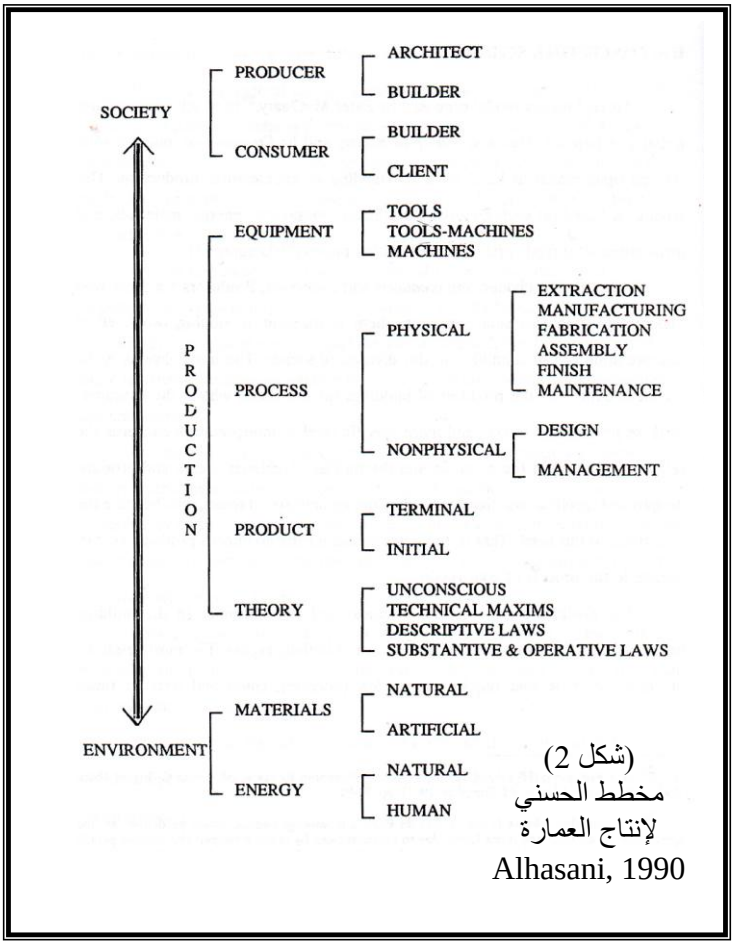

(شكل 2)
مخطط الحسني
لإنتاج العمارة
Alhasani, 1990

(شكل 2)، تظهر فيه تكنولوجيا العمارة وسطاً بين البيئة بمصادرها من مادة وطاقة، والمجتمع بشقيه : منتج ومستهلك. ويظهر انتاج العمارة، أي تكنولوجيا العمارة مكونا من عدة قوى لتشمل: معدات الانتاج وعملياته، ونظريات الانتاج والنتاج نفسه.

وفي دراسات محلية نظرالى تكنولوجيا العمارة بوصفها عملية تحويلية ، وهي تعمل على ثلاثة نظم في العمارة هي نظام الفكر الذي يشمل نظم الإنسان (الزبون والمستخدم) مع حاجاته الأساسية والثانوية ، فضلاً عن نظم الإنسان المصمم وهي فكره وفلسفته وكيفية تعامله مع المشكلة التصميمية.ونظام المادة : الذي يشمل المواد البنائية والمنشأ والإنشاء والخدمات.ونظام الشكل : وتمثله الهيئة الخارجية للنتاج المعماري، أي الشكل وعلاقاته الخارجية والداخلية. وتعمل التكنولوجيا على مادة هذه النظم الثلاثة –حسب الباحث– فتتجلى في العمل التكنولوجي المعماري أبعاد ثلاثة هي على التوالي : بعد الموضوع، وبعد المادة، وبعد الشكل. (رسول، 2003، ص87)

ويرد أيضا في الدراسات المحلية اعتبار التكنولوجيا كيانا ذا أربعة مرتكزات هي : مرتكزمفاهيمي : يتمثل بمجموعة من القيم والمفاهيم الاجتماعية والثقافية والاقتصادية التي تحكم الفعالية التكنولوجية، وآخر معرفي : يتمثل بمجموع المعلومات والمهارات التي يستخدمها الأفراد والمجتمع لفهم الظواهر الطبيعية المحيطة بهم وكذلك مجموعة الأساليب الإدراكية المتبعة للحصول على ذلك المجموع . ومرتكز تقني : وهو مجموع الأفعال والممارسات التصميمية والتنفيذية

[1] السايب- أورغ Cyb-org : نظام يتألف من جزء مكائني وآخر عضوي حيوي عموما بشري.(Alhasani,1990,p11)

والإنتاجية في معاملة المواد والأدوات والعدد، وأخيرا مرتكز مادي : وهو مجموع المنقول من المنتجات والسلع والخدمات التي يملكها المجتمع ويتمكن من استخدامها متحددا بما يمتلك من وسائل ومعارف (حمدالله ،1997،ص19) .

- تجليات التكنولوجيا :

وفي فلسفة التكنولوجيا المعاصرة يقترح كارل متشام[1] بنية تحليلية شمولية ، تستند الى تصنيف وظيفي أو بنيوي[2]، حسب تعبيره، إذ يرى انه يمكن تصنيف التكنولوجيا إلى: أولاً : تلك الحاصلة داخليا في الإنسان وتكون جزءا من فعالياته الجسمانية. وثانياً : تلك التي تصبح على نحو ما جزءا من العالم الطبيعي يتفاعل معه، ولها حياة خاصة بها بعيدا عن الفعل الجسدي الإنساني المباشر. ويرى متشام أن هذا التصنيف يتوافق مع ما يمكن تمييزه من صيغ ظهور التكنولوجيا وهي : **التكنولوجيا كنتاج** product أو ... أشياءobjects. **والتكنولوجيا كعملية process**، ثم **التكنولوجيا كمعرفة knowledge** . كما يبين أن مفهوم الداخل البشري ينحصر بمكون فكري ، تكون الإرادة احد عناصره حيث يمكن تسميته **التكنولوجيا كإرادة volition**.[3] (Mitcham,1978,p232) ، ويظهر مما سبق أن متشام يرى ما هو حاصل داخل الجسم الإنساني باعتباره فعاليات فكرية، **فالجانب الفكري من التكنولوجيا إذن يشمل تجليها كمعرفة وكإرادة. في حين تظهر في الجانب العملي، الذي يحصل خارج جسم الإنسان، كعملية إجرائية ، كما تظهر كأشياء، حيث يمكن أن ينظر لهذه الأشياء كوسائل أداء تقني في الفعل التكنولوجي، كما ينظر لها كنتاج لفعل تكنولوجي أيضا.**

تمتاز رؤية متشام بشموليتها لمجموع الآراء المقدمة أعلاه وإحاطتها بمختلف جوانب الكيان التكنولوجي. ويمكن ملاحظة ذلك في (الجدول1) . وتقدم هذه الرؤية إمكانية قراءة الكيان التكنولوجي في أي مكان وزمان بوصفه خلفية سياقية تنتظم مكوناتها وفق علاقات هي عرضة للتغير أو التحول فتكون مواضيع للرصد والتحليل، بهدف تحقيق الفهم المطلوب لتحولات النتاج المعماري بأثر التكنولوجيا.

---

[1] كارل ميتشام Mitcham Carl : فيلسوف معاصر في التكنولوجيا، ولد في 1941، وهو حاليا أستاذ للفنون الحرة والدراسات العالمية في Colorado School of Mines . حاصل على جائزة الشبكة العالمية للتكنولوجيا،في 2006 عن موضوع الأخلاقيات في التكنولوجيا . اذ يركز اهتمامه على الانعكاسات الأخلاقية للتكنولوجيا.(http://en.wikipedia.org.at:13,sept.,2009)

[2] يرى ميتشام انه يمكن تمييز ثلاثة أسس لتصنيف التكنولوجيا:
1 - تصنيف مادي: مثل بين تكنولوجيا كيميائية و تكنولوجيا كهربائية وغير ذلك.
2 - تصنيف وظيفي او بنيوي.(وهو المقدم في البحث الحالي)
3 - تصنيف تاريخي اجتماعي، وهو الأقل في الأهمية الفلسفية لكن هذا النمط من التصنيف يشكل اختبارا ضروريا للتعميمات الفلسفية. (Mitcham, 1978,p232)

[3] والتفسير المعجمي لكلمة volition هو: عملية استخدام الفرد لإرادته في الاختيار أو في اتخاذ القرار.. الخ. (Oxford advanced learners dictionary, fifth edition,1995) ويستعيض عنها متشام أحيانا في طرحه بكلمة الإرادة :will.

يقترح البحث الحالي اعتماد رؤية متشام في تحليل التكنولوجيا وتطبيقها في مجال تكنولوجيا العمارة . وسيعمد البحث فيما يلي الى عرض أبعاد تجليات التكنولوجيا الأربع ، ثم بيان هذه التجليات في العمارة وإشتقاق مكوناتها التفصيلية وصولا لتقديم هيكل تحليلي شمولي لتكنولوجيا العمارة.

(جدول1) مقارنة مقترح متشام لتحليل التكنولوجيا بالمقترحات في أدبيات تكنولوجيا العمارة

<table dir="rtl">
<tr><td colspan="2" rowspan="3">الدراسات</td><td colspan="6">تحليل التكنولوجيا</td></tr>
<tr><td colspan="2" rowspan="2">الجانب الفكري</td><td colspan="4">الجانب العملي</td></tr>
<tr><td colspan="2">الفعالية</td><td>النتاج</td></tr>
<tr><td colspan="2">متشام</td><td>التكنولوجيا كإرادة</td><td>التكنولوجيا كمعرفة</td><td colspan="2">التكنولوجيا كعملية</td><td>التكنولوجيا كأشياء</td></tr>
<tr><td rowspan="3">دراسات أجنبية في تكنولوجيا العمارة</td><td>ايميت</td><td>المكون الفني
مجال المصمم ومقاصده الذاتية</td><td rowspan="2">----------</td><td colspan="2">المكون العملي
مجال المنفذ
المكون العملياتي
مجال الاداري للفعالية</td><td rowspan="2">----------</td></tr>
<tr><td>الحسني</td><td rowspan="2">----------</td><td colspan="2">تنظير الفعل التكنولوجي
غير واع، مباديء تكنيكية قوانين وصفية، نظريات</td><td colspan="2">النتاج
عمليات الانتاج
معدات الانتاج
فيزياوية، لافيزياوية
عدد، عدد-مكائن، مكائن
ابتدائي،نهائي</td></tr>
<tr><td rowspan="3">دراسات محلية في تكنولوجيا العمارة</td><td>رسول</td><td>بعد الموضوع
سياق (المصمم والمستخدم، والزبون)</td><td rowspan="2">----------</td><td colspan="2">بعد المادة
المنشأ، الانشاء،المادة، الخدمات</td><td>بعد الشكل
التحولات الشكلية
----</td></tr>
<tr><td>حمد الله</td><td>المرتكز المفاهيمي
قيم ومفاهيم تحكم الفعل التكنولوجي</td><td>المرتكز المعرفي
المعارف والمهارات ووسائل نقلها</td><td>المرتكز المادي
المواد الطبيعية والمصنعة</td><td>المرتكز التقني
تقنيات الانشاء</td><td>---------</td></tr>
</table>

التكنولوجيا بوصفها أشياء (Objects):

وضع ممفورد أصنافا من الأشياء التكنولوجية، وقام ميتشام بتوسيع صغير للقائمة شمل تفاصيل وصفية ،كما وسعتها الحسني بإضافة الروبوتات .(Mumford,1947,p410) و(Mitcham,1978,p234) و(Alhasani,1990,p43) وقد تضمنت القائمة **الأدوات البيتية (utensils)** : مثل السلال والقدور والحاويات. كذلك **الأجهزة (apparatus)** : مثل حاويات الصباغة وأفران الطابوق وغيرها. أيضا **المنفعيات (utilities) والمحولات (transformers)** مثل خزانات المياه والطرق والمباني والإنارة وهكذا . **والعدد (tools)** وهي الأدوات التي تستخدم يدويا. وشملت القائمة أيضا **المكائن (machines)** : وهي آلات لا تحتاج استخدام الطاقة البشرية لوجود مصدر طاقة خارجي،لكنها تحتاج الإدارة البشرية. **والمكائن آلية التشغيل (automatons)** وهي المكائن التي تستغني عن عنصر السيطرة البشرية عبر خوارزمية آلية automatic algorithm ومنها الساعات الرقمية .وأخيرا **الروبوتات (robots)** : وهي مكائن آلية التشغيل أيضا ، لكنها تصنع لتقليد العمل البشري اليدوي، او لتقليد كائنات حية عموما.

وينظر لمثل هذه الأشياء التكنولوجية كوسائل تسخر لأداء مهمات الفعل التكنولوجي ، كما يمكن تقييمها كنتاجات، فهي نهايات لفعل تكنولوجي. أي كما عبرت الحسني، الاولى مولدة لعمل (initial) أما الثانية فهي نهاية لعمل (terminal)(مصدر سابق، Alhasani,1990,p2) .

التكنولوجيا بوصفها عملية (Process) :

تتضمن التكنولوجيا كفعالية إنسانية أربعة أنماط أساسية من الفعل الإنساني وهي : الاختراع invention والتصميم design والصنع making والاستخدام using ويرتبط كل من الاختراع والتصميم بالتكنولوجيا كمعرفة وكإرادة. في حين يبقى الصنع والاستخدام مرتبطين بالتكنولوجيا كعملية. (مصدر سابق، Mitcham,1978,p241) فصنع المصنوعات المادية وأستخدامها بكل أشكالها وسماتها هما المظهر العملي للفعالية التكنولوجية.

أ. **التقنية في الصنع والعمل** : تتعامل الممارسة التكنولوجية –كما سبق– مع المصنوعات فقط. في حين يمكن للتقنية ان تتضمن تعاملا مع أشياء طبيعية وبشر وغير ذلك. فهناك تقنية للسباحة وللصفير وللعزف على البيانو ولبناء سيارة وصيانتها. أي هناك تقنية للصنع وللعمل (بتصنيف ارسطو) في حين هناك تكنولوجيا للصنع والاستخدام فقط[1] (المصدرالسابق، p252)

ب. **الصنع والاستخدام** : يعتبر الاستخدام مبدأ أكثر شمولية من الصنع. فكل الصنع يؤدي الى استخدام المصنوعات، لكن ليس كل استخدام ينتج عنه صنع. (المصدر السابق،p253)

ج. **العمل الحرفي والمكننة** : ان الحرفة اليدوية يمكن إن تقود إلى نتائج غير مضمونة، اعتماداً على حكم المنتج واهتمامه. فعنصر المخاطرة كبير والدقة المطلقة غير مضمونة، والناتج هو عمل تقريبي . أما إجراءات الماكنة فهي تحدد الناتج مسبقاً، فالنتائج يفترض بها أن تكون متطابقة مع النوايا وخطورة الحيود عن الأصل ضئيلة جداً. (مصدر سابق:Alhasani,1990,p44) وليس في الحرفة مكان للحس بالاختراع ، فالحرفي يتعلم عن طريق الممارسة طويلة الأمد، وتكتسب الممارسات المطورة المحسنّة عبر تقليد طويل الأمد. اذ يكون الإنسان محكوما بمبدأ انه يجب أن ينحني للتراث التقليدي، وحتى التحويرات والتطويرات التي قد تحصل في الحرفة خلال نقلات مستمرة غير ملحوظة تظهر نفسها كتجديدات غير أساسية، وكاختلافات في المهارة الشخصية (مصدر سابق: Ortega,1961,p148) أما العمل بالمكائن فتعتمد المعرفة فيه على الاكتشاف والاختراع والتجديد(مصدر سابق: Alhasani,1990,p49)

–التكنولوجيا بوصفها معرفة (Knowledge):

[1] يميز ارسطو بين فعاليات الانسان في صنع المصنوعات واستخدامها making and using (techne) وبين فعاليات العمل الانساني doing(praxis) ذات الطبيعة الفكرية وليس اليدوية، التي تشمل مجال السياسة والأخلاق مثلا.(Mitcham, 1978,Types of ,p232 Technology,).

أن التفكير التكنولوجي هو مزيج من التفكير التحليلي والتفكير السياقي. فالتفكير التحليلي، يكون خطيا ومتدرجا وينحو إلى الاستقلال عن القيم الثقافية والشخصية للمفكر بحيث يمكن تكرار النتائج من قبل أي شخص آخر.أما التفكير السياقي فهو غير خطي ، اذ يتحرك من مسار لآخر ومن مستوى لآخر عبر قفزات في المنطق لها ارتباطات معنوية. فهو ذاتي ومرتبط بنظام القيم لدى المفكر (Sandaker,2008,p16) .عليه يمكن تمييز نمطين من المعارف تشغل المساحة الفكرية للصانع ، هما: المعرفة الموضوعية ، والمعرفة غيرالموضوعية(الذاتية).

المعرفة الموضوعية والفكر الواقعي :

وهو نمط المعارف التي يتوجه بها الإنسان الصانع نحو فعله التكنولوجي، بمعزل عن ذاته، بغض النظر عن إدراكه هذا الانفصال أم عدم إدراكه ، وهذا النمط من المعرفة هو المؤهل للتحول إلى علم . ويمكن تسمية النشاط الفكري المنتج لهذه المعرفة **بالفكر الواقعي**.

ان المعرفة العملية الموضوعية هي الأساس في انجاز الفعل التكنولوجي وفق مقاييس الكفاية. وبالتالي فهي وراء تحقيق التقدم التكنولوجي. وتتألف المعرفة العملية من عبارات تعود إلى فعل إنساني Nomo pragmatic statements ، تمثل قواعد لأداء الفعل التكنولوجي (Bunge,1967,in:Mitcham,1983,p68). **ويعتبر الفعل عقلانيا اذا كان مناسبا بأقصى حد للهدف المحدد، وإذا كان كل من الهدف والوسائل المستخدمة للوصول إليه تم اختيارها او العمل بها بتوظيف أفضل معرفة متوفرة.** واعتمادا على مستوى المعرفة المطلوبة في الفعل التكنولوجي، تم التعرف على عدة مستويات من المعرفة العملية التي تحدد **مستوى الفاعلية الفكرية الموضوعية للصانع**. وهي[1] :

- إدراك حسي حركي غير واع لكيفية إنتاج أو استخدام المصنوع artifact . وحيث إن هذه المهارات الحسية الحركية هي غير واعية، فإنها لا تصنف كمعرفة بالمعنى المباشر. وهي تكتسب بالتدرب لدى أستاذ (حاصل عليها مسبقا) وبالتدريب الحدسي عبر المثال المباشر.
- المبادئ التقنية (technical maxims) او قاعدة الإبهام(rule of thumb) في العمل. وتؤلف المحاولة الأولى لتنظيم واضح للعموميات حول المهارات الناجحة في الفعل حيث تحدد الوسائل والطرق التقنية في صنع الأشياء من خلال توفير خطوط توجيهية عامة للعمل.
- القوانين الوصفية (descriptive-laws) أو العبارات براغماتية الطبيعة(nomo-pragmatic). وهذه القوانين هي بصيغ " لأجل (أ) فافعل (ب) " ، مع اعتماد ثابت على الخبرة. فمعرفة الكيف التقنية (know-how) تسندها معرفة العلل التي يعتمدها الصانع بوعي

[1] وردت لدى: (Mitcham,1980,pp234-235)و(Bunge,1983,pp62-76)واستند اليها كل من (Alhasani,1990,p28) و (Angelil,1997,p91) الذي أضاف الى المنظرين (Peter McCleary) في مؤلفه: "History of technology".

في اجراءاته في تحديد وسائل وطرق الانتاج. ويعتبر البعض هذه القوانين التي تخص الفعل "مثل القوانين العلمية لكونها وصفية ظاهريا لكنها مفروضة أو أمرية فقط ضمنيا، لكنها ليست علمية بعد، لكون الإطار النظري الذي يستطيع تفسير القانون ليس ظاهرا بعد."

- النظريات التكنولوجية: هنا توضع مواصفات الوسائل التقنية ضمن اطر عمل فكرية واسعة بقصد توضيح الحالات المادية بالرجوع الى نماذج فكرية شاملة. فالنظريات اما تقوم بربط نظامي لمجموعة من القوانين أو توفر إطارا مبدئيا عريضا لتفسيرها.

ويساعد تراكم الممارسة العملية في التحول من مستوى لآخر باتجاه المعرفة العلمية. حيث "إن المعرفة تحسن فرص تصحيح الفعل، والفعل ربما يقود إلى معرفة أكثر، ليس لأن الفعل هو معرفة بحد ذاته ولكن لأنه في العقول الباحثة الفضولية ربما يقود إلى التساؤل." (مصدر سابق،Bunge,1967,p67) ويمكن للتصنيف السابق أن يمثل أساسا تسلسليا في التطور المعرفي لدى الإنسان باتجاه المعرفة العلمية، وبالتالي فهو يصلح أن يعتمد كأساس فكري لتصنيف تاريخي للتكنولوجيا، يشتق من خلال دراسة النتاج المنجز عبر المراحل التاريخية.

المعرفة غيرالموضوعية والفكر الإرادي :

وهي المعرفة التي تتصل بذات الصانع إذ يعجز فيها عن عزل ذاته عن الموضوع الذي يتوجه نحوه. وهو نمط المعارف التي تخضع لفكر الإنسان في نظرته للكون وأصله ووجوده فيه، وتتدخل في فعله التكنولوجي فيظهر تأثيرها بصيغة قواعد عمل ليس لها تفسير موضوعي بل تكون أسبابها معتقدا عاما أو خاصا أو قناعة شخصية إزاء قضية ما.

ويمكن عموما تسمية أنماط الفكر الذاتي التي تبلورت لدى الانسان على مر الحقب التاريخية "بالفكر الإرادي " لإرتباطه بمظهر الإرادة في التكنولوجيا، الذي يتحدد بدوره تبعا للعقائد الدينية والروحية المختلفة للمجتمعات . فهو متغير في الطبيعة والمساحة التي يحتلها من فكر الصانع تبعا لتغيرات مصدره– أي المعتقد. وقد يلتقي مع الفكر الواقعي ولايعارضه وهو على عدة أنواع . ففي تكنولوجيا المجتمعات القديمة ينتج هذا النمط المعرفي ما سمي بالفكر الميثوبي أي الفكر صانع الأساطير[1]. وللحقبة الاغريقية الكلاسيكية يمكن القول بما يسمى الفكر الميثوفلسفي ، وللحقبة الاسلامية يكون فكر الإسلام هو الفكر الإرادي ، وللعصور الوسيطة في أوروبا يكون الفكر المسيحي. ولكل منها خصوصياته التي تنعكس على تأثيره في المعرفة الواقعية.

التكنولوجيا بوصفها إرادة(Volition) :

يضع ميتشام تفسيره للإرادة كما يلي :

[1] كلمة الميثوبي هي التعريب الذي اعتمده مترجم المصدر(**ما قبل الفلسفة**، فرانكفورت) لمصطلح mythopoeic والتي تعني (صانع الاساطير)(ص19)

"إن التكنولوجيات تبدو متصلة بكل ما يمكن تصوره من إرادة وحافز وحب ورغبة وحاجة ومقصد وإعجاب واختيار...وغيرها. وقد وصفت التكنولوجيا كإرادة على أنها: إرادة البقاء أو إرضاء حاجة بيولوجية أساسية أو إرادة السلطة أو إرادة الحرية أو إرادة مساعدة الآخرين أو إرادة حب الغير أو إرادة الثروة وإرادة اقتصادية أو إرادة الشهرة أو إرادة تحقيق الذات. وكل من هذه الأنواع يتوقع لها إنتاج أنماط مختلفة من التكنولوجيا" (مصدر سابق، Mitcham,1978,p258). ويقرّ ميتشام بصعوبة معالجة التكنولوجيا من هذا المنظار ويعزي ذلك إلى الأسباب التالية (نفس المصدر، pp258-259) :

أ . إن الإرادة هي الأكثر تفردا(individualized) وذاتية(subjective) بين التجليات الأربعة للتكنولوجيا. ولذا يمكن وجود معنى خاص للدافع لكل شخص، وهذا المعنى فريد(unique) إلى حد ما، وبارتباطه بالصنع وبالاستخدام تنشأ عنه تكنولوجيا فريدة. ومثل هذه الفردانية(individuality) لا يكون لها توابع اجتماعية أو عامة ما لم تتحد مع إرادات مشابهة لآخرين لتنتج ما يمكن أن يسمى **فعل إرادة اجتماعي أو جماعي أو ثقافي** .

ب . هناك دائما في الإرادة مشكلة التعامل ما بين المقاصد الذاتية والوسائل المادية. فالسؤال الدائم هو: هل يكون الفعل أو الوسائل المختارة فيه تعبيراً مناسباً عن مقصد معين بحيث يمكن الاستنتاج بصورة سليمة من خصائص احدها إلى خصائص الآخر؟ فلأجل تجنب الوقوع في خطأ إلصاق إرادة ما بفعل تكنولوجي لا بد من توضيح الطبيعة الجوهرية للعمليات والأشياء التكنولوجية وهو ما يمكن اشتقاقه عبر الدراسات التاريخية والاجتماعية والبيئية للتكنولوجيا.

ج . إن فعل الإرادة هو فعل عملي فيه عزم ، ومملوء بقصد معين نابع من قلب الأنا ego ويخترق الأنا، ويفرض عليها سلوكا مستقبليا معينا. فالإرادة تعتمد على فكرة الذات التي تمتلكها الأنا، أي لا يمكن أن يعرف المرء كفاحا معينا إلا إذا كون صورة معينة عن ذاته.

يمكن مما سبق القول ان مفهوم ميتشام عن الإرادة يعبر عن **الدوافع المفاهيمية وراء الفعل التكنولوجي** وهي الدوافع الإنسانية الذاتية، التي تتبلور عند تكوين المرء لصورة معينة عن ذاته، وبالتالي عن وجوده وغايته، أي تحديده لموقف فلسفي في الحياة. ويبدو بحسب طرح ميتشام ، أن انعكاس هذه الإرادة على خصائص الفعل التكنولوجي ونتاجه يبقى صعب التحديد كعلاقة بين سبب ومسبب، ما لم تكن هذه الإرادة مصرح بها من قبل الفرد. لكن عند توحد هذه الإرادة مع إرادات أخرى مشابهة على مستوى المجتمع يظهر نمط تكنولوجي بمواصفات واضحة ذات معنى واضح قابل للتحديد بأقرب ما يكون الى الصواب. فالتكنولوجيا الحديثة، مثلا، التي نشأت في عصر الثورة الصناعية في اوروبا، نسب اليها انها اظهرت اهتماما بقيم معينة كمفهوم الكفاية المادية الذي يهتم بنواحي النفعية والجوانب العملية وإحلال التقييم العقلاني بدل التفسيرات الغامضة التي تعتمد

الحدس والخرافة في المجتمعات البدائية. (مصدر سابق، حمد الله،1997،ص37–ص39) فمثل هذه القيم أمكن تشخيصها كإرادة حاكمة للفعل التكنولوجي بظهورها على مستوى المجتمع ككل.

ويبدو أن طبيعة الصورة التي تكونها الأنا عن الذات تتأثر بالمحيط الاجتماعي وقيمه وخصائصه، أي سياقه ، وتتبلور تبعا لها قيم رمزية، تخص الذات المفردة والمجتمع، تظهرفي النتاج التكنولوجي، مثل العمارة. ويلاحظ أنه : في التكنولوجيا الحديثة التي يكون فيها المصمم منفصلا عن المنفذ. يحمل النتاج التكنولوجي قيما مفاهيمية للاثنين معا ، أو إرادتهما معا، حيث يكون كل منهما واعيا بالفعل التكنولوجي وواعيا لذاته ودورها فيه. أما في التكنولوجيا القديمة، فهناك طرف واحد هو المصمم والمنفذ في آن واحد، فالإرادة هنا واحدة ، وتتطابق غالبا مع إرادة المجتمع، وذلك لضعف الوعي الذاتي للصانع وخضوعه لقيم المجتمع.

– التجليات الأربعة في تكنولوجيا العمارة:

أظهر البحث فيما سبق كيف يمكن للتكنولوجيا أن تتمظهر في أربع تجليات رئيسية تبدو كوسط سياقي يمكن من خلاله تشخيص ملامحها . ولأن العمارة نتاج إنساني ، فإن حضور التكنولوجيا الفاعل في الكيان المعماري يغدو أمراً محتماً ، الأمر الذي يفصح عن إمكانية قراءة وتحليل تجلياتها الأربع في العمارة نفسها ، وسيحاول البحث من خلال عرضه تأشير الجوانب التي يمكن ترجمتها إلى أدوات تعين في استكشاف النتاج المادي للعمارة من موقف تكنولوجي.

<u>الأشياء في تكنولوجيا العمارة :</u>

يتمثل **مظهر الأشياء** في تكنولوجيا العمارة ، **بالنتاج المعماري ذاته بتجليه الفيزياوي بصيغة مبان مؤلفة من المركبات البنائية بمقاييسها ووظائفها المختلفة.** حيث تشكل هذه المركبات مع بعضها البعض علاقات متنوعة تصبح مواضيعا للرصد في الدراسات التي تتناول النتاج المعماري تكنولوجيا. فترد في مثل هذه الدراسات تفصيلات عديدة تتبع توجه الدراسة.

فقد يتم أختيار احدى المركبات نفسها، مثل مركبة الجدار الخارجي، موضوعا لدراسة يتم فيها مثلا رصد تغير تعبيرات حرفة اليد والماكنة في النتاج المعماري.إذ يدرس من جانب المواد المستخدمة، ومعالجتها، واسلوب إنتاجه وتمثيله. (مصدر سابق:Alhasani,1990,p104) بالمقابل، قد يجري تناول ما يتولد عن تجميع مركبات المبنى من فضاءات، وخصائص وعلاقات تنشأ بين هذه الفضاءات ، فتدرس مواضيع مثل العلاقات بين الفضاءات الداخلية، سعتها ودرجة انفتاحها على بعضها ووظيفيتها وتوقيعها، والعلاقات بين الداخل والخارج ، وحتى التكوين الخارجي العام ، وكل ذلك من زاوية نظر تكنولوجية. (مصدر سابق: حمد الله ،1997،ص93- ص97)

بذلك يمكن تحديد مركبات المبنى بوصفها ما يمثل مظهر الأشياء في تكنولوجيا العمارة. حيث يصبح حضور العلاقات المختلفة التي تقرأ على المركبة الواحدة ، أو العلاقات ما بين

المركبات بعضها مع بعض، التي يقوم عليها النتاج المعماري، مواضيع لرصد النتاج المعماري وتحليله من موقف تكنولوجي.

العملية في تكنولوجيا العمارة:

يشتمل هذا المظهر على مجموعة مكونات ترد لدى الباحثين بتصنيفات مختلفة.

فعند إيميت يشتمل المظهرعلى المكونين: العملياتي، وهو مجال البنّاء المنفذ ، وهو بالتالي الجانب المادي الفيزياوي بما يتضمنه من **مواد وعدد وتقنيات**، والمكون الإداري ويتضمن الهيكل الإداري المنسق لعملية التنفيذ. (مصدر سابق:Emmitt,2002,p5) ويحدد ايميت بوضوح أن تكنولوجيا العمارة **تعنى بإنجاز التفاصيل التصميمية التي تجعل المبنى ممكنا للتنفيذ الموقعي**." (المصدر السابق،p29)

وفي يتطابق مكون ايميت العملياتي، مع ما يرد باعتباره عمليات فيزياوية. في مقابل مكونه الإداري الذي يمثل عمليات غير فيزياوية. وبمزيد من التفصيل لهذين المكونين، يظهر أن العملية التنفيذية غيرالفيزياوية تشتمل **التصميم والإدارة**. أما العمليات الفيزياوية البنائية فتفصّل على **أساس مرحلي**، بدءا **باستخراج المادة الأولية** من الطبيعة لغاية تجميع المركبات البنائية. وهو ما يمكن تفصيله الى **عمليات معالجات المواد**، ثم **تقنيات الإنشاء** التي تستخدم هذه المواد، كما ورد في مخطط الحسني لإنتاج العمارة.

ويؤسس مجمل ما سبق، إضافة الى **أهمية التفاصيل**، أهمية الالتفات **إلى المواد ونوعياتها وكيفيات معالجتها**، علاوة على **النظم المنشئية وتقنيات الإنشاء** ، وذلك عند البحث في تكنولوجيا العمارة. وبهذا الصدد يرى فيتشن **أن دراسة عملية إنشاء المباني** يشمل تناولها من ثلاثة اعتبارات **هي : المواد البنائية والنظم المنشئية وتقنيات الإنشاء** (Fitchen , 1999, p16)

ويفصح التعامل مع مواد البناء عن قيم قابلة للرصد مثل استخدام المادة وفقاً لخصائص السطح الخارجي، وإظهار خصائص المادة المنشئية والوحدة البصرية (التميمي، 2006 ، ص 96). أما التقنيات، فتظهر قيمها في إطار التفاصيل التي اشير إليها أعلاه. كذلك النظم المنشئية بوصفها المباديء التي تنتظم تبعا لها تقنيات الإنشاء ، إذ تقدم هذه النظم بأنواعها علاقات وقيما مثل العمق التنظيمي للمنشأ ، وتاثير التصميم المنشئي على التقسيم الفضائي ، وتعددية الأنماط المنشئية، وعلاقة منظومة المنشأ بالقشرة الخارجية ،وهكذا (مصدر سابق: التميمي ، 2006، ص 96). ويمكن للعملية البنائية أن ترد مفصولة الى جانبين (مرتكزين) **–على أساس نوعي– : الأول مادي** ، وهو يشتمل على **المواد البنائية** المختلفة المصنعة وغير المصنعة وما تحققه من **أنواع النظم المنشئية** مصمت أو هيكلي أو نظام السطوح ، كما يشتمل على **أنواع المنظومات الخدمية الساندة،من** إنارة وتكييف وصرف الصحي(مصدر سابق: حمد الله، 1977،ص62–ص74) . أما **الثاني**

فهو تقني ويشمل وسائل الإنتاج(القاعدة الإنتاجية) أي **عدد الإنتاج وتجهيزاته** من مكائن أو عدد حرفية، وكذلك أساليب الإنتاج (القاعدة التنفيذية) أي **تقنياته وإجراءاته** والتي تفصّل أنواعها الى حرفيّ ومرشّد ومصّنع (نفس المصدر،ص52-ص59). بناءعلى ما سبق، يمكن تفصيل مظهر العملية في بنية تحليل تكنولوجيا العمارة الى ثلاثة مكونات:

أ . **المواد البنائية:** حيث يشمل المكون أنواع المواد البنائية الطبيعية والمصنعة،وما يجرى عليها من معالجات لغرض تهيئتها كوحدات بنائية.

ب . **تقنيات الإنشاء** : وهي المكون الذي يضم الأساليب – الكيفيات– المتبعة في التعامل مع الوحدات البنائية لإنتاج المبنى. وهو بذلك يتضمن النظم المنشئية بأنواعها . كما يتضمن العدد والتجهيزات المستخدمة في هذه الإجراءات.

ج .**إدارة العملية البنائية:** وهومكون غير فيزياوي ، يتضمن الهيكل المسؤول عن تنظيم العملية البنائية وقيادتها والتنسيق بين أطرافها.

<u>المعرفة في تكنولوجيا العمارة:</u>

في هذا المظهر يعود البحث الى ما سبق في فقرة التكنولوجيا بوصفها معرفة. إذ تظهر في أفكار بعض الباحثين في تكنولوجيا العمارة نفس توجهات البحث الحالي المؤطرة بمقترح متشام. ففي مجال ما عرفه البحث بالمعرفة الواقعية، ترد مستويات المعرفة الواقعية سالفة الذكر[1]، باعتبارها نظريات للإنتاج[2] تحدد فرقا بين تكنولوجيا قديمة حرفية ، وتكنولوجيا حديثة مكائنية ، ولكل منها خصائصه. وقد بين البحث أن المعرفة التكنولوجية تتزود من منبع فكري آخر هو الفكر الإرادي الذي ينتج معرفة ذاتية، تفرض قواعد عمل لاعلاقة لها بالكفاية التكنولوجية. وهذا النوع من المعرفة مزامن للمعرفة الواقعية يقويه ويتكامل معه، أو يعاكسه ويؤخره، أو لا يضيف له شيئا سلبا أم إيجابا. **فالمعرفة الموضوعية الواقعية والمعرفة الذاتية الإرادية تمثلان المكونين الأساسيين في مظهر تكنولوجيا العمارة المعرفي.**

[1] راجع مبحث: مستويات المعرفة الواقعية الموظفة في الفعل التكنولوجي .
[2] راجع مخطط الحسني لانتاج العمارة.

المعرفة الموضوعية في النتاج المعماري:

إن تغير مستويات المعرفة الواقعية في النتاج المعماري، يمّكن من قراءته تكنولوجياً. فبالإستعانة بتصنيف أورتيغا لأنماط التكنولوجيا (Ortega,1961,p114) يمكن رؤية العمارة بشكل: عمارة تكنولوجيا بدائية ، وعمارة تكنولوجيا الحرفة، ثم عمارة التكنولوجيا المعقلنة.

فأنماط العمارة البدائية تنتج عن تكنولوجيا بدائية بسيطة ليس لقاعدتها المعلوماتية تصنيف ضمن مستويات المعرفة الموضوعية ، فهي كما سماها أورتيغا تكنولوجيا المصادفة. إذ لا ينظر الإنسان البدائي لنفسه كمخترع لاختراعاته بل يبدو الإختراع له كجزء من قدرة الطبيعة في تجهيزه بأدوات جديدة وليس العكس. (المصدر سابق، p144) فموادها الأولية تستعمل كما يجدها الإنسان في الطبيعة دون تغيير يجرى عليها، وإجراءات إنشائها من السهولة والبساطة مما يجعلها سهلة المزاولة من قبل أفراد الجماعة جميعا. كما إن أشكالها، مستوحاة من الطبيعة وغير محكومة بهندسة قوية ، ويربط ذلك بانعدام التصور لدى الإنسان البدائي عن أية تفسيرات كونية(Gelernter,1995,p36) مما يحيل الموضوع الى الفكر الإرادي المنتج للمعرفة الذاتية.

أما تكنولوجيا الحرفة، فمن أمثلتها تكنولوجيا الإغريق وروما ما قبل الإمبراطورية وتكنولوجيا العصور الوسيطة. (مصدر سابق: Ortega,1961,p145) إذ يعتمد انتاج العمارة (المباديء التقريبية) في البداية ، ثم مع زيادة الخزين التكنولوجي، تصاغ قواعد وتنظيمات للعملية الإنتاجية من حيث الوسائل المعتمدة والطرق المتبعة(قوانين وصفية). فقد حقق الإغريق، مثلا، مجموعة من التفاصيل الإنشائية الدقيقة التي تطلب انجازها إدراكا واعيا بتقنيات المادة المتداولة في البناء –وهي الحجر– من ذلك إجراءات نقل هذه الأحجار من مقالعها ورفعها وتوقيعها بدقة في أماكنها في المبنى بما يحافظ على نظافة حافاتها وربطها. ويذكر جلنتر أن كتابات الإغريق في العمارة لغاية القرن الرابع قبل الميلاد تركزت في شرح النسب والخصائص المقبولة لأنساق الطرز المتداولة، وفي مناقشة شؤون تقنيات الإنشاء، وهي قد كتبت برأيه لتثبيت القواعد وللمساعدة في تدريب المعماريين الشباب.(مصدر سابق ، Gelernter,1995,p59)

وفي عمارة التكنولوجيا المعقلنة يبرز اعتماد العلم أساسا لبنيتها، وحدوث الترابط الملزم بين الفكر العلمي الموضوعي والفعل ، فتخضع العملية الإنتاجية بتفاصيلها الإجرائية ونتائجها المأمولة للفحص الفكري والدراسة العلمية قبل الشروع بالتنفيذ، تلافيا للعقبات والأخطاء على مستوى الواقع . (مصدر سابق ، حمد الله، 1997 ،ص18). وقد ظهر تأثير الماكنة في إنتاج العمارة وفق أطر التقييس والتصنيع المسبق الكميّ للعناصر والمركبات البنائية ، سعيا وراء تحقيق كفاية أعلى في العملية البنائية وتكلل ذلك بتبلور الطراز العالمي في العمارة **International Style** في ثلاثينات القرن العشرين. (مصدر سابق: رسول ، 2003، ص172) أما اليوم فيجري التحول نحو تكنولوجيا الآلات

الرقمية التي تعتمد التصنيع بمساعدة الحاسوب (CAM **Computer Aided Manufacturing**) ، والتي تلعب دوراً حاسماً في تحول كامن للنموذج **potential paradigm shift** من الإنتاج الكمي والتقييس الملازم له إلى فكرة إنتاج عناصرمتخالفةً . حيث يتم الاعتماد على الحاسوب في المراحل الإنتاجية الثلاث أي في التصميم وإنتاج العناصر ثم بالتركيب. فبالإمكان برمجة الروبوت ليغير في مواصفات النتاج، وبصورة ذاتية ، ليحقق تخالفا وتنويعا في الإنتاج دون الإخلال بمتطلبات الكفاية من حيث الزمن والطاقة والمادة المصروفة. بذلك فإن طموح المصممين والمصنعين المتناقض ظاهرياً في الجمع بين التخالف **differentiation** والاقتصاد بدأ يشهد حلاً ، خلال ما يسمى **mass customization** أي التصنيع الكمي المنوع حسب الرغبة.(Menges,2006,p71-76)

المعرفة الذاتية في النتاج المعماري:

ينعكس حضور ما سماه البحث الفكر الإرادي في ممارسات مختلفة لقواعد العمل التكنولوجي في مجال البناء كما في المجالات الأخرى.

ويمكن توضيح نشاط هذا الفكر في إنتاج معرفة ذاتية من خلال فكر المجتمعات القديمة (الفكر الميثوبي) الذي سبقت الإشارة اليه ، حيث يقدم من السلوكيات ما يتنافى تماما مع مبدأ الكفاية المفترض في الفعالية البنائية التكنولوجية، وقاعدة العمل فيها تحقق أهدافا ذاتية عاطفية، وليس أهدافا عملية. ففي ضوء سيادة هذا الفكر في مجتمع العراق القديم مثلا، يمكن تفهم تشييد مبنى المعبد البيضوي في خفاجة بأكمله فوق حفرة مملوءة برمل أبيض نقي عمقها ثمانية أمتار، والتي فسرت بأنها تجسد الرغبة في عزل المعبد عما يحيط به من أشياء دنيوية غير طاهرة (مورتغات،1974، ص64) . كما يمكن في ضوء هذا الطرح، استيعاب ممارسة استخدام تماثيل تزرع في اسس المبنى، بشكل أوتاد أو مسامير كبيرة يصنع الجزء الاعلى منها على شكل انسان (شكل 3) وتفسر بكونها تعبر عن فكرة ثبوت البناء في الارض وقد تزوده بدفاع سحري ضد القوى الشريرة (المصدر السابق،ص64)

(شكل 3)مسامير الاسس في مباني العراق القديم (مورتغات،1975)

ولعل الظاهر أن تكنولوجيا العمارة المعقلنة حجبت أية فاعلية للفكرالإرادي

المرتبط بالذات، وأعتمدت كليا على المعرفة الواقعية العلمية. غيرأن ما يمكن قوله بهذا الصدد ان الفكر الإرادي قد إلتقى كليا مع توجه المعرفة الواقعية وهدفها في الكفاية التكنولوجية، مما وحد دوريهما في الإنتاج.

الإرادة في تكنولوجيا العمارة:

يمثل هذا الوجه من التكنولوجيا المظهر الذاتي في الجانب الفكري للتكنولوجيا كما تبين، ويروم البحث هنا الفصل بين الفكرة التصميمية المعمارية التي يضعها المصمم وبين الإرادة، التي تحكم **الدوافع المفاهيمية** التي أفرزت تلك الفكرة. أو بعبارة أخرى **الموقف الفلسفي الذي يشخص وراءها، والذي يكشف ، طبيعة المشروع الحياتي الذي اعتنقه منتجو العمل.** إذ لا ينطبق الإثنان معا. لكن الأول يعين في فهم الثاني وبيان طبيعته. ففي المشاريع المعمارية التي تراعي المؤثرات البيئية، مثلا، تطرح مختلف الأفكار التصميمية التي تنعكس على الشكل المعماري، مثل مشروعي المعمار نورمان فوستر في**(شكل 4)**. إذ يحرص فوستر على استثمار
المؤثرات البيئية في عملية التصميم من خلال توظيفها رقميا. لكن هذه الأفكار بدورها، على تنوعها، تفصح عن طبيعة الإرادة في الفعل التكنولوجي بكونها موجهة بيئيا eco-centered.

وهو نمط من إرادة التكنولوجيا أسفر عن تطوير تكنولوجيات الاستدامة المختلفة.

يبرز بالمقابل من النتاج المعماري مثلا، ما يكشف عن إرادة مختلفة تمام الإختلاف عن الإرادة الموجهة بيئيا ، فبالنظر الى مشاريع مثل مشروع برج خليفة يطفو على السطح نمط من الإرادة هو ذات النمط الذي يطبع معظم المشاريع العمرانية في مدينة دبي ، إن لم يكن كلها ، وهو إرادة الثروة والإقتصاد – بإستعارة تعبير متشام– إذ يمكن استشفاف هذا النمط الإرادي في مظاهر البذخ والإستهلاك لموارد الطاقة والبيئة التي نحت إليها هذه المشاريع .

وبناء على ما سبق ، يتوضح مظهر الإرادة، بكونه ممثلا للدافع المفاهيمي وراء فعل البناء، أو بدرجة أعمق الموقف الفلسفي الذي يقفه المنتجون، والذي تتبلور عنه قصديا فكرة المصمم التصميمية لمشروعه المعماري ، وتقع في خدمته مجمل الاعتبارات التكنولوجية الموظفة في

(شكل 4) تكنولوجيا الإرادة الموجهة بيئيا. مشاريع نورمان فوستر. (Abel,2004)

تحقيق النتاج ، بقيمه الجمالية وتعبيراته الشكلية. وبالعودة الى ماسبق بيانه عن عائدية الإرادة، يمكن تمييز مكونين اساسيين في مظهر تكنولوجيا العمارة بوصفها إرادة:

أ. الإرادة الفردية: وهي سهلة التحديد إذا ما صرح بها من قبل المنتج وترتبط بوعي المنتج لذاته ومشروعه الحياتي الخاص .

ب. الإرادة الجماعية: وتظهر عند سيادة توجه فلسفي معين يمارس سلطته على الإرادات الفردية، فيوحدها ويوحد نمطها التكنولوجي ومثاله ما شرح اعلاه عن عمارة الإستدامة. كما تظهرالإرادة الجماعية في العمارة التاريخية التي تذوب فيها إرادة الفرد مع الإرادة الجماعية، والتي من أمثلتها وصف فرانك لويد رايت للعمارة الغوطية مثلا في كونها " تذيب المادي وصولا الى الروحي" (Weston,2003,p44)

- المفردات البحثية في دراسات تكنولوجيا العمارة:

تقدم التجليات الأربع السابقة: الأشياء والعملية والمعرفة والإرادة، مجموعة من المؤشرات التي يمكن اتخاذها مواضع للاستدلال على طبيعة فاعلية وتحولات العلاقات القائمة بين مكوناتها المختلفة وهي ليست الوحيدة ممكنةالإشتقاق، لكنها حسب البحث الحالي أبرز ما يمكن تناوله لقراءة النتاج المعماري وتحولاته من وجهة تكنولوجية، وفيما يلي بيان هذه المفردات.

المادة ومعالجاتها :

ترصد هذه المفردة قيما تنتج عن تعامل الصانع مع المواد البنائية. فتنفيذ التصميم يعني تحويله إلى شيء فيزياوي. ولتصور التصميم يحتاج كل من البنّاء والمعمار الى مواد طبيعية أو صناعية. وفهم هذه المواد ، له طابع فني وآخر علمي يصبح أساسا للاختيار والتحكم وإعطاء هذه المواد تشكيلها النهائي (Alhasani, 1990, p22) . ويؤثر كل من معالجة المواد وتصنيعها في خصائصها، كما يضبط ويحسن، وأحيانا يلغي خصائصها الطبيعية. فقد أصبحت التكنولوجيا أداة للتلاعب بخصائص المواد وقيمها، وجعلها بشكل ما بلا خصائص محددة أو ذات تشعب مذهل في الخصائص. بذلك أضحت المادة في صراع بين الطبيعة والثقافة، وبين الضرورة والإمكان، والتكنولوجيا هي الوسيط في ذلك." (Sandaker,2008,p29)

ويتضمن التشكيل النهائي للمواد مختلف المقاييس التي يمكن للمادة أن تشكلها : من التفصيل الدقيق ، وحتى الكيان المعماري الكامل . ويجري هذا التعامل بشكل مباشر أثناء العملية التنفيذية. فهي بالتالي مفردة تربط مباشرة الفعالية البنائية بالنتاج ، أي بعبارة أخرى يمكن تأشيرها في **مظهر تكنولوجيا العمارة بوصفها عملية.** لقد أبدى بعض منظري العمارة آراءهم في العمارة من منطلق التعامل بالمادة وانعكاس هذا التعامل على الشكل. فدافع سمبر[1] عن مسألة اللون في العمارة

[1] كوتفريد سمبر Goterfied Semper 1803-1879 :معماري منظر الماني...اكدت مؤلفاته في نظرية العمارة على تأثير المنشأ في الطراز كما سعى الى تشجيع استخدام أكبر للألوان. (AD, vol. 51,1981, p10)

الإغريقية من منطلق عقلانية تعامل هؤلاء مع المادة، إذ بين أن الإغريق بنوا معابدهم الاولى بحجر poros غير الجذاب، الذي كان بحاجة لطلائه بالجص ثم تلوينه. ثم إنهم في النماذج المتأخرة التي انجزت بمرمر pentelic الأبيض الجيد كانوا مجبرين على إتباع ذلك النموذج القاعدة لكن دون الحاجة إلى الجص قبل التلوين. وبين انه تحت أشعة الشمس الساطعة كان المرمر البراق سيبدو غير مريح للعين، وتم تحسين ذلك عبر التلوين. وان القشرة الذهبية التي نراها ونعجب بها اليوم ليست كما افترض سابقا رواسب الزمن بل هي بقايا أصباغ قديمة (مصدر سابق: Weston,2003, p61) .

المنشأ وعلاقاته :

تظهر هذه المفردة عقلانية توظيف الصانع للمنشأ والعناصر المنشئية وتأثير ذلك على خصائص الشكل، حيث يمكن للمنشآت أن تلعب دوراً مهماً كمنظم للفضاءات ، ويمكن أن تؤدي وظائف أخرى تلحق بها ، كأن تكون عوازل بيئية أو مرشحات إضاءة (مصدر سابق: Sandaker , 2008 , p2) ، فالوظيفة الأساسية للمنشأ تتمثل بنقل القوى والأحمال وإيجاد الموازنة المنشئية للمبنى، بحيث يركز الشكل المنشئي على عكس الانتقال الطبيعي للقوى بأقل مسارات ممكنة. (مصدر سابق:التميمي،2006،ص17) وهذه المفردة أيضا **من المفردات المتضمنة في مظهر العملية في تكنولوجيا العمارة** ، إذ يمكن إعتبارها مشتملة ضمن مكون تقنيات الإنشاء ، لكونها تمثل القرار التنظيمي لكيفية صياغة الوحدات البنائية وتجميعها .

نوقشت علاقة المنشأ بالشكل في العمارة من عدة جوانب أهمها مدى عقلانية الانشاء وكفايته. فقد أكد فيوليه لودوك على ما يسمى بالصراحة المنشئية، فالشكل عنده يجب أن يتوحد مع الانشاء توحدا حقيقيا انطولوجيا. بذلك وصف العمارة الغوطية بالكمال من منطلق الترابط العضوي بين عناصرها المنشئية وشكلها المعماري، وآمن أن الحقيقة المتضمنة في الشكل الطرازي، مثل حالة الطراز الغوطي، تقع في المدى الذي جرى فيه اظهار النظام الخفي من العلاقات المسؤولة عن انشاء الشيء المعماري. (مصدر سابق، Angelil,1997,p386)

بناء التفصيل :

ويدور هذا المحور حول التقنية المتبعة في التنفيذ التي تحقق تفاصيل الشكل ، وتظهر تفهم الصانع وتمكنه من مادته وتقنياته، وهي مفردة ترتبط أيضا بتكنولوجيا العمارة بوصفها عملية. فللتفصيل دور في التعبير عن تكنولوجيا تنفيذه، وبالتالي نمط العمليات الفكرية الموظفة في إنتاج المبنى. وفي هذا الاطار يرى ماركو فراسكاري المعماري والمنظر أن :

"التفاصيل هي المكان حيث تنتظم المعرفة في نسق يجد العقل فيه فاعليته التي هي المنطق....وان التكنولوجيا بوجودها ذي الوجهين في ممارسة المنطق (the techne of logos) ومنطق الممارسة(the logos of techne) هي الأساس لفهم دور التفاصيل. أي إن إنشاء العمارة

وتفسيرها موجود كلاهما في التفصيل. ويمكن تعريف التفصيل المعماري بأنه اتحاد بين الإنشاء الذي هو نتاج منطق الممارسة والتأويل الذي هو نتاج ممارسة المنطق. " (Frascari,1995,p500)

وترى الحسني "أن المنطق الإنشائي للتفصيل، يرتبط بشدة بالمنطق البصري، وهو يلقي الضوء على طريقة استخدام المادة وعلى **عملية الإنتاج** .(Alhasani, 1990, p106) **ففحص التفاصيل بصريا يمكن ان يقودنا إلى منطق إنشائها، وبالتالي تقييمها تكنولوجيا.**

ويظهر عبر الدراسات أن موضوع تجميع المركبات البنائية يمكن تناوله عبر **بناء التفصيل الذي يصوغ العلاقة بينها**، إذ درس إيميت، مثلا، عوامل تصميم التفصيل البنائي المعبَرعنها بقضايا متداخلة تتضمن متطلبات الإحتواء والوظيفة، والقابلية البنائية، وقضايا البيئة والجودة، وكل ذلك ضمن وقت وكلفة محددين، واعتمادا على الفعل الإنساني (Emitt,2002, pp5-6).

التكتونية[1] وقيم المادة:

يعرف التكتونيك بأنه : تعبير خاص ينشأ عن المقاومة الساكنة للشكل الإنشائي وبطريقة يكون فيها التعبير الناتج يمكن عزوه إلى المنشأ والإنشاء فقط. (نفس المصدر، pp19-20)

تتصل مفردة القيم التكتونية مباشرة بالمعرفة التكنولوجية، اذ تعبرعن مدى وعي البنّاء بجماليات المنشأ والمادة، وقابليته في اظهارها على الشكل . فالمعرفة التكنولوجية ، بكيفيات اشتغال المادة البنائية ومدى طواعيتها ومرونتها وطبيعتها وما ينتج عنها من معرفة بنظم إنشائها، يولد بدوره مرونة في التعامل معها ترتقي باستخدامها من مجال الحرفة والصنعة والإجادة فيها إلى المستوى الفني والجمالي ، مما يجعل هذه الإجادة ، وما ينسحب عليها من تعبيرات جمالية وفنية(أي قيم تكتونية) مؤشراً للرصد ، ويشير فرامبتون الى رؤية فيتوريو غريغوتي Vittorio Gregotti في أن **الإمكان التكتوني لأي مبنى ينبع عن قابليته في إظهار كل من السمات الشعرية والمعرفية لمادته في آن واحد.**(Frampton,1995,p26) . وقد تتبع كينيث فرامبتون، في مؤلف خاص ، تراث التكتونيك منذ الوعي به في القرن التاسع عشر وامتداده إلى القرن العشرين. ففي الفصل الخاص بتكتونيك العمارة الفرنسية والانكليزية في القرن التاسع عشر، يرى فرامبتون أن فكرة التكتونيك تمحورت حول المثال الإغريقي الغوطي بالنسبة للعمارة الفرنسية،وحول الإحياء الغوطي بشكل مشترك بين الفرنسية والانكليزية. (مصدر سابق،Frampton,1995,p30)

[1] التكتونيك tectonic كلمة إغريقية الأصل مشتقة من الكلمة tekton التي تعني النجار أو البنّاء. وفي القرن الخامس قبل الميلاد تطور للمصطلح بعد آخر فتحول من الدلالة على شيء محدد فيزياوي مثل النجارة الى مفهوم الصنع بصورة أعم وتضمن فكرة ال poesis - الصنع لدى أرسطو- ومن كلمة tekton نفسها تطور مصطلح البنّاء الأستاذ architekton. في 1892، بين ادولف هنريش بوربين، في دراسة فلسفية، المضمون الجمالي للكلمة فكتب:" ان التكتونيك تتوجه نحو الإنشاء أو الصنع لعمل حرفي أو فني ...فهي تعتمد كثيرا على التطبيق الصحيح لقواعد العمل الحرفي أو درجة منفعته التي أمكن تحقيقها". (Frampton,1995,pp3-4)

التعبير الشكلي :

ويتمثل بمجموعة العناصر المعمارية التي تحقق رمزية معينة تظهرعلى **النتاج التكنولوجي،** ويرسخ منبعها مباشرة في **التكنولوجيا كارادة** . يقول ممفورد :

> **"يتميز الإنسان عن الحيوان بقابليته على الترميز. فهو بخلاف الحيوانات لا يستجيب فقط للإشارات البصرية والصوتية، بل يستطيع تجريد وإعادة تمثيل أجزاء من بيئته، وأجزاء من تجربته وأجزاء من ذاته في أشكال رمزية منفصلة ودائمة....وقد طور الإنسان عبر الفنون وسائل خاصة لتخليد واستذكار تجربته الجوهرية في الحياة ومشاركتها مع الآخرين. وبمساعدة الرمز لم يوحد الإنسان فقط الزمن الماضي مع الحاضر، لكنه ربط الحاضر مع الإمكانات المثالية التي يمكن أن تنشأ في المستقبل."**
> (Mumford,1951,pp17,18)

يظهر الإنسان رموزه في أشكال الفنون المختلفة من رسم ونحت وموسيقى وأزياء وفي العمارة كذلك. وفي هذا الإطار تبين الحسني أن:" المجتمع يلصق دلالات معينة بالسمات المختلفة للبيئة المبنية وتتضمن هذه ارتباطات بذكريات الماضي أو الحاضر وبالهوية وبالثقافة وبالمقاصد.(مصدر سابق: Alhasani,1990,p101)

ويمكن لدلالات للتعبير الشكلي أن تقرأ فيما يقدمه مجموع المركبات البنائية من علاقات عامة، مثال ذلك رصد ممفورد لميل تيار العمارة الحديثة نحو التبسيط المفرط – للمركبات البنائية – بداعي الوظيفية والإعتبارات الموضوعية في التصميم مبينا "أن للاقتصاد والبساطة جذورها في الروح الإنسانية، إذ تتمثل في الرغبة في التخلص من الرمزية المفرطة، وفي تجنب التزيين بأي نوع ، وفي اختزال حتى الكلام إلى أبسط صوره وفي التزام الصمت حينما لا يكون هناك ما يقال.فحتى الوظيفة الميكانيكية ذاتها تستند إلى قيم إنسانية: مثل الرغبة في النظام والأمان والسلطة.(مصدرالسابق: Mumford,1951, pp118-119)

استنتاجات البحث:

عني البحث بتقصي امكانات تحليل تكنولوجيا العمارة ، وصولا الى هيكل تحليلي شمولي **(شكل 5)** استند فيه الى الطرح المقدم من قبل فيلسوف التكنولوجيا المعاصر كارل متشام. فقد أظهر البحث إمكان بحث تكنولوجيا العمارة عبر أربع تجليات هي: الأشياء والعملية والمعرفة والإرادة. وقد حدد المكونات الرئيسية لكل من هذه التجليات وكما يلي:

- ظهرت مركبات المبنى بمقاييسها المختلفة ممثلة لمظهر تكنولوجيا العمارة كأشياء.
- تحددت مواد الإنشاء وتقنياته وإدارة العملية البنائية بوصفها المكونات الأساسية لمظهر تكنولوجيا العمارة كعملية.
- توضح اشتمال مظهر المعرفة لتكنولوجيا العمارة على نمطين معرفيين هما المعرفة الذاتية والمعرفة الموضوعية.
- توضح إشتمال مظهر الإرادة في تكنولوجيا العمارة على نمطي الإرادة الجماعية والإرادة الفردية.

وقد لاحظ البحث أن هذه التجليات بمكوناتها المختلفة يمكن أن تقرأ كواقع سياقي لتكنولوجيا العمارة ، إشتق من خلالها مجموعة مؤشرات موضوعية ، لتصبح هذه المؤشرات أدوات ومفردات يستعان بها في قراءة النتاج المعماري من وجهة تكنولوجية. ففي إطار هذه المفردات يمكن رصد العلاقات المختلفة التي تقيمها مختلف مكونات تجليات تكنولوجيا العمارة ، وتقييم تغيراتها وتحولاتها، التي تشكل مواضيع الدراسات والأبحاث في مجال تكنولوجيا العمارة.

وهذه المفردات هي :

– المادة والتعامل بها. – المنشأ وعلاقاته. – بناء التفصيل.– التكتونية وقيم المادة– التعبير الشكلي. حيث وضح البحث ارتباط كل من المفردات الثلاث الأولى بمظهر تكنولوجيا العمارة كعملية، في حين ارتبطت مفردة التكتونية بمظهر المعرفة ، وارتبطت مفردة التعبير الشكلي بمظهر الإرادة في تكنولوجيا العمارة.

ويبين **(الشكل 5)** الهيكل التحليلي المقترح لتكنولوجيا العمارة ، بمفرداته الخمسة ، وقد اسقطت في مجالها نماذج من العلاقات المطروقة في بحوث سابقة في تكنولوجيا العمارة وكما ورد في متن البحث.

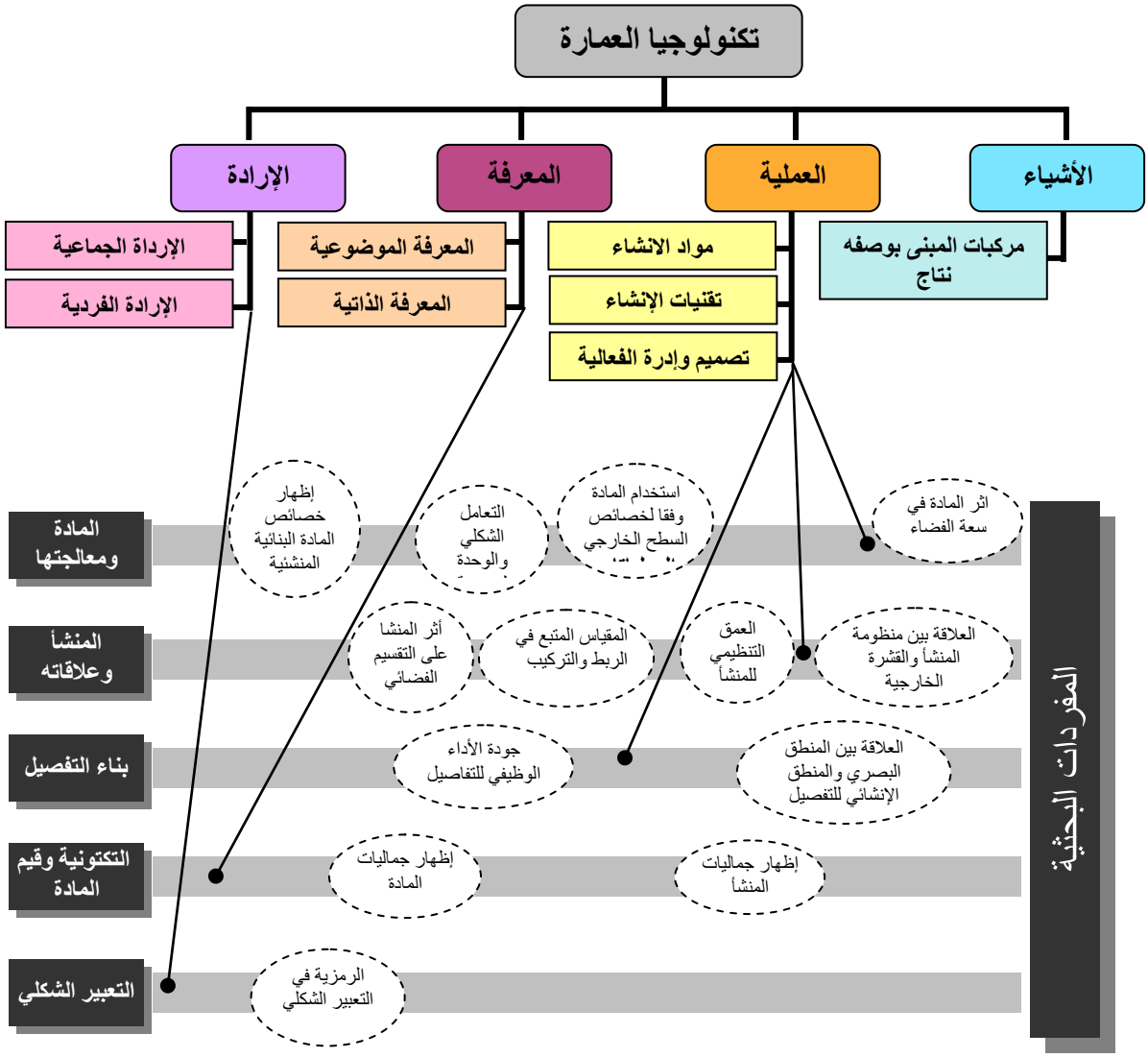

(شكل 5) : هيكل خلاصة البنية التحليلية لتكنولوجيا العمارة
اعداد الباحثة

مصادر البحث:

- التميمي، اسامة عبد المنعم.**أثر تطورات تكنولوجيا المنشأ في التشكيل المعماري**، رسالة ماجستير، جامعة بغداد، كلية الهندسة، 2006.
- حمد الله، رغد نعمة الله. **التكنولوجيا والشكل**، رسالة ماجستير، جامعة بغداد، كلية الهندسة، 1997.
- رسول، هوشيار قادر. **العمارة والتكنولوجيا: دراسة تحليلية للفعل التكنولوجي في العمارة.** اطروحة دكتوراه،جامعة بغداد، كلية الهندسة، 2003.
- فرانكفورت، هنري. و آخرون . **ماقبل الفلسفة : الانسان في مغامرته الفكرية الاولى**، ترجمة جبرا ابراهيم جبرا، منشورات دار مكتبة الحياة – فرع بغداد بالاشتراك مع مؤسسة فرانكلين المساهمة للطباعة و النشر، 1960 .
- مورتغات، أنطون. **الفن في العراق القديم** ،ترجمة: عيسى سلمان وسليم طه التكريتي، وزارة الاعلام،مديرية الثقافة العامة، بغداد،1975.

- Alhasani,Nadia Mehdi. **Buildings as cyborgs: Expression of hand and machine craftsmanship in architecture**, Ph.D.,University of Pennsylvania, 1990.
- Angelil,Marc M. **Technique and Formal Expression In Architecture**, Ph.D., Swiss Federal Institute of Technologym Zurich, 1997.
- Bunge, Mario. **Towards a Philosophy of Technology,** 1967, in Philosophy and Technology, ed. Carl Mitcham, New York 1983.
- Emmitt,Stephen. **Architectural Technology**, Blackwell Science, London,2002.
- Fletcher,Banister. **A History Of Architecture**,18th ed. RIBA,New York,1975.
- Fitchen,Jhon. **Building Construction Before Mechanization,** Mit Press, London,1999.
- Frampton, Kenneth. **Studies in Tectonic Culture** , MIT Press, London,1995.
- Gelernter,Mark. **Sources of Architectural Form**, Manchester University Press, New York,1995.
- Menges,Achim. **Manufacturing Diversity**, in Architectural Design, Wily-Academy, March/April ,2006.
- Mitcham,Carl. **Types of Technology,** in Research and Philosophy, 1978,Vol 1., St Catharine College, U.S.A.
- Mumford, Lewis. **Art and Technics**, Columbia University Press, New York, 1952.
- Mumford,Lewis. **Technics and The Nature of Man**, 1966, in **Philosophy and Technology,** ed. Carl Mitcham, New York 1983.
- Ortega, Jose y Gasset. **Man The Technician ,** in: History as a System, Norton Library Inc. , New York,1961.
- Sandaker,Bjorn Normann. **On Span and Space**, Routleage, New York, 2008.
- Weston,Richard, **Materials, Form, and Architecture**, Laurence King Publishing Ltd, London,2003

على الشبكة العالمية: موقع http://www.wikepedia.org

استخدام كسر الطابوق الطيني المعاد كبديل عن الحصى في انتاج بلوك نمطي اقتصادي

سلام سمعان عبدالاحد

معهد التكنولوجيا– بغداد

الخلاصة : خلال العقود الخمسة الماضية اتضح ان هناك حاجة ماسة الى تعاون وثيق بين المهندس المعماري العراقي والمهندسيين والفنيين العاملين معه لوضع حلول محددة في "مواد ونظم وتكنولوجيا البناء في العراق" . المهندس المعماري يجب ان يكون قائد مجموعة البناء ويترك دور البطل و كمثال على هذا التفاعل قمنا بهذا البحث " استخدام كسر الطابوق الطيني المعاد كبديل عن الحصى في انتاج بلوك نمطي اقتصادي" .البلوك قياساته (25x25x12.5cm) ويعادل في الحجم ثلاثة طابوقات فنية. المقترح يستخدم كسر الطابوق الطيني كمادة تخلط مع الرمل والاسمنت وبدون استخدام الحصى و يمكن انتاجه يدويا او ميكانيكيا . البحث استخدم الطابوق المكسر اوالمهشم. وتم عمل بلوكات نموذجية وتم فحصها و تصويرها.استخدم البحث 40–65% من كسر الطابوق في حجم الخلطة الخرسانية , وقد اتضح زيادة قيمة العزل الحراري بمقدار 70–80%, كما لاحظ الباحث ان كلفة بناء الجدران الحاملة وغير الحاملة عند استخدام البلوك المقترح تقل بحوالي النصف عن كلفة البناء بالطابوق الفني بالاسعار السائدة حاليا.ان هذا البحث المتواضع هو واحد من العديد من البحوث المطلوبة في العراق عند استخدام مواد البناء المعادة في انتاج مواد بناء جديدة .

KEY WORDS: building materials recycling, clay bricks, modular coordination economy lightweight insulated blocks, sustainable environment

كلمات مرشدة : اعادة استخدام مواد البناء, الطابوق الطيني الفني, تنميط القياسات , بلوك اقتصادي خفيف الوزن ذات عزل حراري متميز,البيئة المتوازنة .

ABSTRACT

During the last 5 decades , it is evident that there is a drastic need for close cooperation between the Iraqi architect and other engineers, technicians working with him , towards solving particular problems related to materials , system building technology in Iraq .The architect need to become a leader of the building team instead of becoming"a Hero". The research develop a light weight modular block (25x25x12.5cm), equivalent in volume to 3 bricks (25x12.5x7.5 cm).The proposed modular block use broken or crushed bricks as an aggregate instead of stone. The block can be handled easily, it can be produced mechanically i.e. via compressors or manually. The research cover the use of recycled "broken or crushed" bricks by making samples , record photos and statistics .The samples uses 40-65% of the volume recycled bricks .The insulating factor increased up to 70 -80% while cost decreased by approximately half. The paper is one of many applied research topics needed to be tackled on recycling, sustainability and environment improvement in Iraq.

الحاجة الى البحث في نظرية البيئة المستدامة ودور المهندس المعماري العراقي :

ان تحسين البيئة "sustainable environment" يتطلب اعادة استخدام مخلفات الصناعة وبقايا مواد الانشاء لغرض انتاج مواد بنائية جديدة. ان انقاض البناء في العراق وكما هو الحال في دول العالم الاخرى يتم تجميعها في مناطق عشوائية في اطراف المدن و تأخذ مساحات شاسعة تمتد الى المناطق السكنية والزراعية وتشكل خطرا على البيئة والانسان, وعند النظر بعمق في هذه المسألة في العراق نلاحظ في العقود الاخيرة عدم اكتراث المهندسين والمهتمين بالبيئة في هذا الموضوع, ونخص منهم المعماريين و من ذوي العلاقة بالاختصاصات المتداخلة لغرض تحسين البيئة بصورة عامة , ان البحث في هذا الموضوع ضروري رغم انه يعتبر حالة من "التخلف الفكري والاجتماعي ". لقد تقدمت المعرفة الهندسية في اعادة استخدام موادالبناء "Building materials recycling" في بلاد كثيرة في العالم وأدت الى معالجات واقعية نحو تحسين البيئة ورفاهية الانسان . ان هذه البحوث والمعالجات لم تتحرك في العراق بعد . و من اهم اسباب ذلك هو اجتماعي بالدرجة الرئيسية بينما ثبت في كثير من دول العالم ان استخدام المواد الموجودة في الطبيعة وتغيير شكلها ومحتواها لتلبية حاجات الانسان المتنوعة هي عملية متكاملة تبدأ بالمواد الموجودة في الطبيعة وتستمر بصورة مستديمة لتشمل المواد الاولية والمواد المعادة وتشكل حلقة شبه محكمة من التوازن بين الانسان والطبيعة , (جدول رقم1) .ان التوازن البيئي المطلوب وعلى سبيل المثال اعادة استخدام البلاستيك بأنواعه , بقايا الزجاج , المعادن بأنواعها كذلك الورق والكرتون بأنواعه والمثال في بحثنا هذا هو اعادة استخدام مواد البناء والانقاض المهملة ومنها كسر الطابوق الطيني كل هذه المواد قابلة لأعادة الاستخدام ويمكن اعتبارها ثروة عراقية مهملة حاليا وفي حال عدم استخدامها عقلانيا فهي تشكل خطر على البيئة والمناطق السكنية والزراعية وعلى صحة الانسان العراقي بالدرجة الاساس.[11-12]

البحث يركز على اعادة استخدام كسر الطابوق الطيني وامكانية جمعه من مناطق رمي الانقاض ومن معامل الطابوق كذلك من مواقع البناء عموما واستخدامه في انتاج بلوك عراقي نمطي (25x25x12.5cm) ذات عزل حراري وصوتي متميز وبسعر اقتصادي مناسب جدا.

يجب على المهندس العراقي ان يدخل في مجال المشاركة في بحوث وتطبيقات في تحسين المناخ والمساعدة في التقليل من تأثير ثقب الاوزون الذي اصبح قلقا يهدد سكان العالم بأسره.حيث ان دور المهندسين والفنيين العراقيين يجب ان يتغير الى الافضل نحومعالجة هذه الظاهرة السلبية.

ان موضوع البيئة المستدامة قد تطور كثيرا في العقود الاخيرة عندما كان المهندسون و الفنيون العراقيون غير متواصلين مع العالم والان ونحن في بداية القرن الواحد والعشرين يكون المطلوب من المهندس العراقي التفاعل مع هذا الموضوع وعمل بحوث واستنتاج قوانين بناء تخص العراق تحديدا والتواصل مع المهندسين والعلماء في العالم ومن خلال الانترنت والاطلاع على الابحاث المتميزة والتي اصبحت متوفرة وبدون مقابل وان يؤدي ذلك الى اعادة الثقة في النفس للمهندس العراقي وتقدير المجتمع المحلي و الدولي له.

موجز حول اعادة استخدام المواد" Recycling" بصورة عامة ومواد البناء بصورة خاصة :

خلال العقود الماضية أقر الباحثون في دول عديدة من العالم على وجوب تحسين البيئة والحد من تجميع المواد المعادة كأنقاض البناء والمواد الثانوية الناتجة عن الصناعة . ولغرض الاستفادة من قسم من هذه المواد في اعادة التصنيع وادخالها مع مواد جديدة تفيد الانسان بشكل عام وتساعد خاصة في بناء المساكن الجديدة وبذلك يقل التلوث ومن ثم يتم تحسين البيئة بصورة عامة.ان انقاض البناء التي تجمع في اماكن عشوائية اصبحت تشكل مساحات شاسعة تشاهد في ضواحي مدينة بغداد على سبيل المثال, ان اغلب هذه المناطق غير مرخصة وقد وصل حدود "مناطق الطمي" الى المناطق السكنية والزراعية على حد سواء واصبحت تشكل مصدرا للامراض والتلوث وعند التعمق في هذه المشكلة في العراق نلاحظ ابتعاد الدولة وخاصة المهندسين والمختصين بالبيئة عن معالجة هذا الموضوع. ان المعرفة الهندسية" Know-How" في مجال اعادة استخدام المواد قد وصلت الى مراحل متقدمة عالميا ولكنها لا زالت دون المستوى المطلوب في العراق. ان هذه الخلاصة غير منطقية في العراق بينما نلاحظ في اغلب دول العالم يتم معالجة هذه المواد والاستفادة منها واصبح ذلك جزء لا يتجزء من حياة المجتمع وخاصة من الناحية الاقتصادية ونخص هنا بالذكر بعض المواد المتيسرة بكميات كبيرة جدا تناسب اعادة الاستخدام الاقتصادي ومنها البلاستيك بانواعه – الزجاج– سبائك المعادن – الورق والكرتون[11] وفيما يخص بحثنا الحالي " استخدام كسر الطابوق الطيني المعاد كبديل عن الحصى في انتاج بلوك نمطي اقتصادي".لقد خلص البحث ان مواصفات الطابوق الطيني المهمل والذي يمكن تحويله الى مادة مهشمة بشكل كرات غير منتظمة بقياس (1,2,3cm) بأستخدام الكسارات او الطواحين المستوردة او يتم شطر الطابوق صورة رقم (1) ويعتبرهذا البحث هو الاول في عدة بحوث تستخدم مادة الطابوق الطيني المعاد في بناء الجدران الغير حاملة في المباني ذات الطابع الهيكلي كذلك كجدران حاملة بدلا البناء بالطابوق الفني ذو الكلف العالية كما يمكن تطوير البلوك المقترح من مواد اخرى عديدة منها الرمل والقصب العراقي والنايلون المعاد والبلاستيك المثروم المعاد وقد يحتاج ذلك الى اضافات قليلة من مادة الاسمنت

او مواد اخرى تزيد التصلب وحسب الحاجة. وسنتطرق في بحوث قادمة في استخدام الرمل والحصى والاسمنت والقصب العراقي و"خشب القوغ " والاسفلت والنايلون المعاد كذلك اكياس التسوق ونايلون الزراعة المغطاة بعد استخدامها اضافة الى مواد كثيرة اخرى متوفرة في العراق في الطبيعة مثل الفوسفات والكاولين والاكاسيد المتنوعة[13] .

البحث يؤكد على دور المهندس المعماري العراقي ويحثه على التفاعل في مجال اعادة استخدام المواد بصورة عامة حيث انه مؤهل للابداع في مجالات كثيرة سواء في تصميم المباني او بأعداد تفاصيل البناء كذلك في طريقة صناعة المواد الانشائية دراسة قياساتها واشكالها الهندسية كذلك اقتراح مواد الانهاء عند استخدامها في المباني بصورة عامة وفي هذا السياق تطرق البحث الى استخدام كسرالسيراميك وقطع المرمر الملون حيث يمكن بذلك تحسين المنظر الخارجي او الداخلي للبناء صورة رقم (5–6).

الجدول رقم(1)يمثل بعض حالات اعادة استخدام المواد "recycling" في بعض دول العالم كذلك في العراق حاليا.

المادة المعادة	نسبة الاستخدام في المنتوج الجديد	الحالة عالميا	الحالة في العراق والتوصيات
المباني المهدمة بكافة انواعها –المساكن القديمة –المدارس التي سيعاد بناءها. –المباني العامة التي ستهدم لاعادة البناء او لأقامة شوراع جديدة او متنزهات....الخ.	20–50%	يتم فرز المواد وقد تستعمل كأملاءات للطرق السريعة او السدود او الجسور و حشوات في بعض المباني المتخصصة . "sub – base"	لم تستعمل بعد في العراق حيث تحتاج الى دراسات محلية من قبل المهندسين . ان الطابوق الطيني على سبيل المثال يمكن نزعه باستخدام طرق عديدة منها توجيه نيران بالمحارق الغازية مثلا على الجدران ولغاية نحو 540C° فيسقط الطابوق ثم ينظف ويعاد استخدامه وهذا ما تضمنه بحثنا: "استخدام كسر الطابوق الطيني المعاد كبديل عن الحصى في انتاج بلوك نمطي اقتصادي" لقد وصل البحث الى نتائج مشجعة جدا ويحتاج الى التوسع في انتاج انواع من البلوك ومواد البناء الاخرى والتطبيقات عليها خاصة بعد زيادة اسعار المواد الانشائية بشكل عام كما بدأ المقاولين في البحث عن الطابوق المستخدم ولكن يحتاجون في ذلك الى مساعدة فنية في كيفية نزع الطابوق من الانقاض وقد اطلعنا عبر الانترنت[12] على طريقة تسخين الجدران المهدمة الى درجة حرارة 540c° فينفصل الطابوق ويمكن تنظيفه واعادة استخدامه كذلك قام العديد من المقاولين في نزع حديد التسليح عن الصبات المهدمة وتعديله واعادة استخدامه رغم انه يفقد بعض من قوته عند التعديل ويجب ان يؤخذ ذلك بنظر الاعتبار عند احتساب القوى في الاستخدامات الجديدة.

المطاط بكافة انواعه وخاصة اطارت السيارات	80–90%	متداول عالميا وبشكل واسع	متداول على نطاق ضيق في صناعة احتياجات صناعة الاثاث (الدوشمة) كذلك كمفاصل تحمل لبعض ادوات السيارات.
–الاثاث الخشبية –الاثاث المعدنية كالالمنيوم	60-90% وحسب نوعياتها	متداول عالميا وخاصة الاثاث المعدني	يعاد استخدام الاثاث الخشبية التالفة وبقايا الاعمال النجارية من اجل صناعة حلفة المبردات. كذلك استخدام الالمنيوم المعاد في صناعة بعض احتياجات السيارات على سبيل المثال.
البلاستيك بكافة انواعه PVC-PET Himpic الضانديق البلاستيكية اكياس النايلون نايلون الزراعة المغطاة	60-95%	يستخدم في صناعة البلاستيك بعد ان يثرم على شكل حبيبات ويضاف الى الحبيبات الجديدة	اعادة استخدام البلاستيك حالة واقعية منذ سنوات كثيرة ويستخدم مثروم البلاستيك لوحده او مع اضافة حبيبات جديدة لصناعة الانابيب والتأسيسات الصحية كذلك الاثاث الاقتصادية و لعب الاطفال واحتياجات المطبخ.
بقايا عمل زجاج الشبابيك والابواب وهو في الغالب مستورد وذات نوعية جيدة	70-95%	متداول منذ القديم في العراق(في بابل على سبيل المثال) ولازال.	يستفاد من الزجاج المعاد بكثافة في صناعة قواعد "اللالات" للاضاءة ويتم تلوين الزجاج في المصاهر وبألوان جميلية كالفيروزي والازرق والاحمر. ان المواد الزجاجية المعاد صناعتها سهلة التداول والعمل وان اعادة صناعتها لا يكلف اموالا كثيرة كذلك يرفع المنتوج الذوق العام ويحسن الفنون التشكيلية وخاصة السيراميك والزجاج وهذا يطور مراكز الشباب ويسهل عمل الفنانيين المتفرغين في هذا المجال.

المعادن بصورة عامة وخاصة التي يمكن صهرها بدرجات اقل من 1000 درجة مثال ذلك الالمنيوم وتتوفر بقاياه بكميات كبيرة لدى صناع الشبابيك.	95%	متداول في كثير من دول العالم	يذوب معدن الالمنيوم في حرارة 500-600C° يتم في العراق اذابة المعدن وتحويله الى بلوكات تصدر في الغالب الى الدول المجاورة .يحتاج الموضوع الى تدخل المهندسين ومصممي القوالب واختصاصات متعددة للنهوض بهذا الموضوع.
النحاس ويشمل بقايا الاعمال الكهربائية, التحف المتروكة, التماثيل والنصب التالفة ومواد نحاسية متفرقة اخرى.	95%	متداول في كافة دول العالم	المطلوب تطوير هذا الاستخدام في صناعة التحف والنصب التذكارية ويحتاج ذلك الى تدخل المهندس المعماري والفنانين لغرض تنقية النحاس من خلال زيادة عدد المصاهر في كليات الفنون ومراكز الشباب في الجامعات والمعاهد.
الحديد , شواصي السيارات والمكائن والمعدات المهملة	60–70%	متداول في دول محدودة	بالنظر للحرارة العالية المطلوبة لصهر معدن الحديد ولتوقف العمل في معمل الحديد في العراق ولعقود ماضية.انحصر العمل في هذا المجال.
الدهون بكافة انواعها	20-30%	متداول في بعض دول العالم	نظرا لكلفة المنتجات النفطية العالية يتم جمع الدهون التالفة واستخدامها في طلي القوالب المعدنية واستخدامات متفرقة اخرى .

* بعض المواد المذكورة في هذا الجدول تخص اعادة استخدام مواد البناء المهملة في مواقع البناء وخاصة في مشاريع البناء الكبيرة والمقصود هنا كسر الطابوق الطيني الفني كذلك كسر المرمر بأنواعه والحجر بأنواعه .

*المواد الاخرى المذكورة في الجدول يمكن البحث فيها بشكل موسع من اجل انتاج مواد بنائية متنوعة وخاصة ما يتعلق بالاستفادة من البلاستيك المعاد وبقايا الزجاج وبقايا الاخشاب بأنواعها .

مواد ونظم وتكنولوجيا البناء في العراق ودور المهندس المعماري العراقي :

ان موضوع البناء متعلق في مجمله تقريبا بحركة الاسكان وصناعة مواد البناء. ان هذا الموضوع تراجع كثيرا خلال العقود الخمسة الماضية واختصارا نسجل هنا ماجاء في مقالة الدكتور باسم الانصاري حيث يوجز تاريخ موضوع الاسكان في العراق بالنقاط التالية[5] :

- توقف العمل في تنفيذ مخطط اسكان عام عراق" GHPI" والذي حدد عدد الوحدات السكنية المطلوبة 3380 الف وحدة لغاية عام 2000 [9].ان هذه الدراسة ذات المستوى العالمي قد تمت تحت اشراف الامم المتحدة وشارك فيها مجموعة من الجامعات البولونية والعراقية وامتد العمل بها لست سنوات وتعتبرمتقدمة مهنيا ويمكن الاعتماد عليها لحين قيام دراسات جديدة .
- توقف رصد التخصيصات المالية في المناهج الاستثمارية للمشاريع السكنية .
- الغاء التنظيمات الادارية المتخصصة بقطاع الاسكان مثل المؤسسة العامة للاسكان وتشكيلاتها في عام 1987
- بيع معامل البناء الجاهز ومعامل الطابوق الحديثة ومعامل الثرمستون الى القطاع الخاص.
- بيع الوحدات السكنية العائدة للدولة عن طريق المزايدات العلنية مما اضعف قدرة فئة محدودي الدخل للحصول على مسكن .
- تسرب ملاكات القطاع العام التي تخصصت في مجالات الاسكان والى مهن اخرى لا علاقة لها بالاسكان,والمطلوب الان ونحن متجهين الى العقد الثاني من القرن الواحد والعشرين هو اعادة النشاط الى قطاع الاسكان وخاصة من خلال تنشيط القطاع الخاص والبنوك العقارية المحلية و اصدار القوانين التي تهتم بذلك.

البحوث المطلوب القيام بها في العقد الاول من القرن الواحد والعشرين يفضل ان تأخذ اتجاها جديدا حيث وصلت حالة " مواد ونظم وتكنولوجيا البناء في العراق" الى مستوى لا تحسد عليه بعد ان بيعت المعامل والغيت العديد من الدوائر التي تهتم بالبناء[5] . ان اهم الخطوات التي ادت الى تراجع اداء مواد البناء هو بيع المعامل الى ما يسمى بالقطاع الخاص في التسعينيات من القرن العشرين واهم تلك المعامل هي مصانع الطابوق الفني ومصانع الثرمستون مما ادى الى تراجع مواصفات المواد وطرق انتاجها.وبذلك اصبح الاعتماد الاعظم على المعامل الاهلية التي تعتمد النفط الاسود والتبن كوقود ويكون انتاجها غيرنظامي ومنخفض الجودة. البحث يدور حول العودة الى الاوليات ويستوجب تدخل المهندسين العراقين في معالجة الواقع الجديد وخاصة وضع المواصفات والتفاصيل وعدم الاعتماد على دخول الشركات الاجنبية مستقبلا للبناء واعتبار ان ذلك سيكون له طابع سحري, كذلك يجب ان يراقب اعمال هذه الشركات عند دخولها والنشاطات التي تقوم بها مع العودة الى تنشيط المواصفات القياسية العراقية "ISO-IRAQ" ورفعها الى المستوى العالمي .واصدارها بشكل قوانين ملزمة .

ان ثبات التفاصيل المعمارية البنائية في النصف الثاني من القرن العشرين وبأعداد محدودة اعطى انطباعا خاطئا الى المهندسين والفنيين حيث تصور البعض ان البناء في العراق يتم فقط بالطابوق الفني المصنوع من الطين الزراعي في الغالب وهذا هو الواقع من الناحية العملية وظل هذا الواقع وامتد الى القرن الواحد والعشرين . ان جدار بسمك 36cm هو بناء متميز من حيث التنفيذ ومن حيث العزل الحراري ولكن ذلك يتم على حساب الكلفة العالية للطابوق وبالنتيجة المباني التي تقام منه.

ان كلفة البناء بالطابوق الطيني عند استعمال مونة الاسمنت في سنة 2009 لم يعد في امكانات ذوي الدخل المحدود والمتوسط هذا من ناحية ومن ناحية اخرى عدم توفر انتاج الطابوق الطيني في المناطق الشمالية وان استخدامه في تلك المناطق اي نقله من الجنوب هو عملية غير منطقية وتزيد كلفة البناء بمعدل 50–70%. ان بحوثنا في الفترة الاخيرة في " مواد ونظم وتكنولوجيا البناء في العراق" تتصدى لمثل هذه المشاكل ومن اجل تنويع المواد الانشائية والبحث في البدائل وحسب المناطق والمواد الاولية المتوفرة والبحث الحالي " استخدام كسر الطابوق الطيني المعاد كبديل عن الحصى في انتاج بلوك نمطي اقتصادي"" هو احدى هذه المحاولات وستظل الحاجة ملحة الى بحوث عديدة في مجال البناء الجاهز القليل الوزن للوحدات البنائية للجدران الحاملة وغير الحاملة والسقوف بأنواعها ولكافة مناطق العراق. ان الشخص الاكثر قدرة على استيعاب هذه المشكلة وتحسين الموجود وايجاد البدائل هو المهندس المعماري العراقي ويجب ان يكون له دور ريادي في هذا المجال , ومن ناحية اخرى يجب على المتخصصين ومن ثم المجتمع تقبل المقترحات والبحوث والتغيير ومن اجل تطوير البناء في العراق والحد من استيراد المواد الانشائية وهذا ما نلاحظه في العقد الاول من القرن الواحد والعشرين حيث يستورد الطابوق ومواد بناء كثيرة اخرى مثل بلوك تبليط الشوارع من الدول المجاورة والتي يمكن انتاجه محليا بيسر وبكلف مناسبة ومن خلالها ذلك يمكن معالجة البطالة ايضا.ان الاشكال والتفاصيل المعمارية يجب ان تعتمد على القياسات النمطية وهو علم قد تطور بداية النصف الثاني من القرن العشرين ويعتمد بالاساس على الوحدة القياسية (10cm) بالنظام الفرنسي والتي تساوي تقريبا اربع انجات بالنظام الانكليزي.

ان العراق يحتاج اليوم الى قوانين بناء ISO-IRAQ تخص القياسات النمطية تصدر على شكل علمي كذلك تتعرض الى الاوزان وقوى التحمل وغير ذلك .

ان هذه المفارقات قد جاءت مع بداية صناعة الطابوق في العراق حيث ان القوالب الاجنبية التي استخدمت ولازالت تستخدم تعتمد مضاعفات الانجات (10in,5in,3in) والمساوية الى (25x12.5x7.5cm) ولحين ثبات القياسات العراقية للطابوق الطيني والتي قد تكون(20x15x10cm) والحجم الاخر قد يكون (30x20x15cm) .

ان هذه الملاحظات تنطبق على تطوير كافة مواد البناء القديمة والحديثة, كذلك يجب ان تشمل قياسات الفضاءات في التصاميم الحديثة ومثال ذلك يكون التسلسل النمطي

1,3,6,9,12,18,24,60,90,120,180,240,300,360M……etc. حيث M=10cm . ان هذا الموضوع واسع وسنقوم ببعض البحوث في هذا المجال فيما يخص تطبيقاته في العراق .

الاشكال المعمارية وبعض الاستخدامات البنائية الممكنة "للبلوك النمطي المقترح:

ان البلوك المقترح قد تم تصميمه ليعطي امكانيات معمارية واسعة حيث يمكن التحكم باوجه البلوك المقترح بما يراه المهندس المعماري وعلى سبيل المثال 1- تكون واجهاته صقيلة 2- امكانية الصبغ والمعالجة فيما بعد 3- اكساءه بمواد جمالية بأستخدام السيراميك او بقايا المرمر اوالحجر بأنواعه وحسب تصاميم البناء المطلوبة . ان اضافة مثل هذه المواد الجمالية عند صناعة البلوك يمكن السيطرة عليها بصورة دقيقة خاصة عندما يتم العمل بشكل يدوي ولأغراض محددة معماريا وقد تم تجربة ذلك في البحث صورة رقم(5). ان هذا البحث سيساهم في معالجة البطالة وخاصة في المناطق الريفية واطراف المدن ويكون ذلك ممكننا عندما يتم العمل بشكل يدوي كثيف او عند استخدام الطرق الميكانيكية كما هو الحال الان في معامل البلوك الكونكريتي التي تستخدم المكابس [1].

ان من بين مزايا البلوك المقترح الخارجية والداخلية وفيما يخص المعالجات المعمارية:

- عند استخدام البلوك المقترح كجدران حاملة او غير حاملة ,يتم ذلك بسمك 25cm صورة رقم(4). اما الفجوات الموجودة في البلوك فيمكن تركها كما هي وقد تملأ بالتراب النظيف للحصول على عازل حراري وصوتي ممتاز.[3]
- اما عند استخدام البلوك كقواطع بسمك 12.5cm, يمكن بذلك الحصول على زخارف دائرية او نقوش وتشكيلات كثيرة خاصة عند وضع بعض المواد الجمالية اثناء الانتاج.
- يمكن تغيير الفتحة الدائرية في القوالب والتي هي بقطر 15cm الى فتحة مربعة 15×15cm و قد تستخدم هذه الزخرفة لوحدها او بالتداخل مع زخارف وتصاميم اخرى وهي كثيرة الاحتمالات.
- يمكن الجمع بين ½ بلوكة مع البلوك المتكامل الفتحة صورة رقم(2) وبزخارف عديدة وقد تم في التجربة عمل ½ بلوك و ترك باقي الاحتمالات بتصرف المهندس المعماري ومهندس الانتاج .
- ان هذا البلوك لا يحتاج الى تسليح ,البحث لم يتعمق في فحوص القوى وقد تم فقط فحص بلوك نموذجي 12.5x25x25cm وكانت النتيجة مشجعة (compressive strength62Mpa) للبلوك المعرض للهواء لمدة 28 يوم وحسب المواصفة ASTM C-39
- وفي حال كون سمك الجدار 37.5cm فتكون احتمالات العزل الحراري والصوتي افضل بكثير كما يمكن تصميم زخارف واشكال معمارية كثيرة تنتج عن تداخل البلوكات المختلفة.
- اضافة الى البلوك المذكور انفا يمكن انتاج بلوكات نمطية اخرى مثال ذلك (50x50x12.5 cm)–(60x60x30cm)–(90x60x30cm) –(120x90x30cm).وتكون هذه

البلوكات مجوفة وبأوزان تتراوح بين 50kg-200 حيث يتم نقلها ورفعها الى مواقعها بسيارة الحمل ذات الرافعات .

- ان التطور الاخر المهم ايضا في مجال استخدام البلوك النمطي المقترح هو اعداد دراسات وتصاميم وبحوث حول دمج البلوك النمطي المقترح صورة رقم(3) مع المواد البنائية المتداولة حاليا كالطابوق الطيني الفني والبلوك الكونكريتي الاعتيادي كذلك بلوك الثرمستون بعد ان يعود الى سوق مواد البناء في العراق.

(صورة رقم 1) كسر الطابوق الطيني المستخدم كبديل عن الحصى في انتاج البلوك المقترح (25x25x12.5 cm) .يلاحظ ان هناك حالتين للاستخدام ,الكسر الطولي المعمول بالفاس بارتفاع 7.5 cm والكسر المهشم بالفاس او بكسارات بسيطة او اوتوماتيكية وبقياسات (1,2,3)

(صورة رقم 2) البلوك المقترح (25×25×12.5) ويمكن انتاجه بقياسات اخرى تستخدم لبناء الجدران والسقوف الجاهزة مثال ذلك(25×50×12.5) – (50×50×12.5)– (50×75×12.5) يتم التعرض لذلك بالتفصيل في بحوث قادمة

(صورة رقم3) البحث يقارن 3 مواد انشائية عراقية متداولة
1–الطابوق الطيني (25×25×12.5) , 2– البلوك الكونكريتي الاعتيادي(40×20×16)
3– البلوك المقترح (25×25×12.5)

(صورة رقم 4) احدى حالات الربط للبلوك المقترح (25×25×12.5) لاحظ امكانية
ان يملأ الفراغ الدائري بالتراب اثناء البناء لزيادة العزل الحراري

(صورة رقم5) بعض حالات استخدام مادة قطع السيراميك كذلك كسر المرمر وهي ملائمة لتفاصيل معمارية متنوعة لتجميل المباني من الداخل او من الخارج كذلك لاغراض الديكور

(صورة رقم 6) بعض حالات استخدامات اخرى للبلوك المقترح – حاويات للزراعة الداخلية او الخارجية نافورات متنوعة ..... لغرض تحسين البيئة في الداخل او في الخارج

طريقة انتاج البلوك المقترح:

ان طريقة انتاج البلوك المقترح مماثلة لعمل البلوك الكونكريتي الاعتيادي التي تتم بأستخدام الماكنة الاوتوماتيكية المخصصة لذلك حيث يتم انتاج 16 بلوك في الوقت الواحد بواسطة كبس الخليط والذي قد تم ترطيبه قبل وقت مناسب من عملية الانتاج. المواد الداخلة في العمل هي الاسمنت والرمل والحصى (1:3:6) اما الانواع ذات المواصفات الغير جيدة فتكون نسبة الخلط (1:3:12) .

اما في حالة انتاج البلوك المقترح والتي تم تجربتها في البحث , يتم خلط الاسمنت والرمل وكسر الطابوق الطيني 1- المشطور عموديا بأرتفاع 7.5cm بالفأس او 2- المهشم بالكسارات الاوتوماتيكية او النصف اوتوماتيكية او اليدوية وبقياسات (1,2,3cm) وهذا يناسب كافة احتمالات البناء للدور المنفردة او المجاميع السكنية التي تقوم على مبدأ التعاون الذاتي"self-help" .

ان الاسباب التي دعتنا الى القيام بهذا البحث لأنتاج البلوك النمطي كمادة بنائية في العراق هي التالي:

- ان تكاليف انتاج البلوك النمطي قيد البحث اقل من البلوك الكونكريتي الاعتيادي بمعدل 45% تقريبا وهذا ناتج عن ان كلفة الطابوق المعاد هي قليلة جدا مقارنة بكلفة الحصى الجديد .
- اتضح من بحوث لأساتذة اختصاصيين عراقيين[3] ان العزل الحراري لمادة الطابوق الفني متفوق كثيرا على مادة البلوك المقترح وحيث ان نسبة الكسر هي اكثر من نصف حجم المواد المستخدمة فالمتوقع يكون مقدار العزل الحراري متميزا.
- لقد اتضح من التجربة التي قمنا بها ان كسر الطابوق اكثر التصاقا بخليط الاسمنت والرمل من التصاق الحصى عند الفحص اليدوي.اما امتصاص كسر الطابوق للماء يقل بشكل ملحوظ عند نقع الكسر المهشم لمدة 24 ساعة مع تبديل الماء اثناء العمل ولمرة واحدة وبذلك تقل قابلية امتصاص الماء وكذلك تقل الملوحة بشكل ملحوظ .
- ان المسكن او اي مبنى اخر يحتاج الى لمسات فنية في الواجهات الداخلية والخارجية وهذا متوفر في البلوك النمطي المقترح صورة رقم(5) حيث يمكن اضافة مواد تجميلية وتكون بعدة احتمالات ويحتاج ذلك الى تصاميم ومقترحات من قبل المهندسين المعماريين .
- البلوك المقترح هو منتوج صقيل ولا يحتاج الى انهاء من الداخل او من الخارج .
- عند مراجعة البحث سيلاحظ المهندسين والفنيين لكافة الاختصاصات ان هناك امكانيات كثيرة جدا لتطوير مواد البناء في العراق والمطلوب اخذ المبادرة العلمية من الجميع.
- ان البحث هو ذات طابع معماري/مدني ويعالج التداخل بين هذين الاختصاصين واللذان يجتمعان في تصميم قوالب مواد البناء وطريقة انتاجها وكذلك في اعداد التفاصيل البنائية.
- اما فيما يخص قوة تحمل البلوك المقترح والذي سيستخدم في بناء الجدران الحاملة وغير الحاملة والقواطع ,وقد تم تجربة فحص بلوك واحد قياس 12x25x25cm وبلغت قوة تحملها

(compressive strength55Mpa) ويحتاج الموضوع الى تعمق وفحوص عند تغيير نسب المواد المستخدمة وطريقة الانتاج

العزل الحراري للبلوك المقترح ومقارنته مع الطابوق الطيني والبلوك الكونكريتي الاعتيادي:

يركز البحث على محورين مهمين فقط وهما 1–العزل الحراري والصوتي وزيادة ذلك من خلال استخدام كسر الطابوق المتميز 2– تقليل كلفة انتاج القطعة الواحدة من البلوك المقترح ومن خلال الاستفادة القصوى من كسر الطابوق الذي يتم الحصول عليه بدون مقابل من مواقع البناء ومواقع الطمي .وفيما يخص العزل الحراري, يقع العراق ضمن المنطقة المدارية الحارة والتي يغلب عليها المناخ الصحراوي حيث يستمر فيها فصل الصيف لاكثر من ستة اشهر وتسطع خلاله الشمس لاكثر من اربعة عشرة ساعة يوميا وبذلك تتعرض السطوح الخارجية للجدران والسقوف الى موجات حرارية كبيرة[4].وعليه فأن نوعية واختيار المواد الانشائية للجدران والسقوف من قبل المهندس المعماري يعتبر امر محوري في تحديد العزل الحراري ويؤثر ذلك خاصة في تقليل الحمل الكهربائي المطلوب في فصل الصيف لاغراض التبريد[3].

نلاحظ في الجدول رقم (2) ان اعلى عزل حراري يتوفر عند استعمال الطابوق الطيني ويليه في ذلك البلوك المقترح ومن بعده البلوك الكونكريتي الاعتيادي . كما نلاحظ ان العزل الحراري للبلوك المقترح يوازي تقريبا العزل الحراري للطابوق الطيني الفني(الجمهوري), وعند املاء التجويف الدائري بالتراب النظيف اثناء البناء يزداد العزل الحراري والصوتي.الباحث سيقوم بالتعاون مع مهندسين اختصاص بتقصي هذا الموضوع وكل ذلك يقع ضمن مجال تطوير "مواد ونظم وتكنولوجيا البناء في العراق".

ان زيادة سمك الجدار للبلوك المقترح للجدران الخارجية وجعلها 37.5cm (بلوكة ونصف) يرفع العزل الحراري والصوتي وان ذلك يعتمد على التفاصيل المعمارية التي يعدها المهندس المعماري, كما ان لتوجيه المسكن او المبنى مناخيا يكون له دور مهم في تقليل تسرب الحرارة الى الداخل كذلك وجود الاشجار المناسبة حول المبنى من حيث الانواع والارتفاعات ويكون ذلك مرتبط بحسابات المهندسين الاختصاصين في الكهرباء والتبريد وبالتعاون مع المهندسين الاختصاصيين في تحسين البيئة والتبريد[3,2].

ويبقى الهدف دائما محاولة مستمرة في التجديد في عملية التصميم والاستفادة من التجربة والخطأ واضافة التجارب الكثيرة في مجال التصميم ومثال ذلك الاستفادة من حركة الهواء الافقية والعمودية التي كان لها دور فعال في تحسين البيئة الداخلية والخارجية للبيت البغدادي وكل ذلك يدركه بشكل ابداعي المهندس المعماري المتمرس, اضافة الى عامل المواد الاولية الداخلة في صناعة البلوك المقترح , يجب على المهندسين ان يضعوا في اعتباراتهم وبشكل علمي حركة الشمس خلال ساعات اليوم وخلال الفصول بالنسبة الى تعرض الجدران والسقوف كذلك ان يأخذوا دروسا من البيوت التراثية فيما يخص التهوية عموديا وافقيا , حيث يجب ان لايكون هناك فضاءات غير معرضة الى الخارج وان لايزيد عمق اي

فضاء عن 6 متر على سبيل المثال وهذا ما كان الحال عليه في البيوت التراثية البغدادية حيث كانت كافة الغرف مواجهة الى الفضاء الداخلي . اما في النموذج الغربي المتداول منذ النصف الثاني من القرن العشرين فأن الفضاءات تكون مواجهة الى الخارج , ويتم الاستفادة من قدرات المهندس المعماري في ان يجعل المسكن او الشقة ذات واجهات متكسرة عديدة . ان هذا البحث لم يتوسع في هذا المجال وهناك بحوث واطروحات مناسبة يمكن الاطلاع عليها[10] . البحث يعتبر ان موضوع المناخ حيوي جدا و ذات اهمية كبيرة في مجال "مواد ونظم وتكنولوجيا البناء في العراق" في هذه المرحلة الانتقالية التي تتطلب تطبيقات هندسية جديدة.

جدول رقم(2) : مقارنة بعض مواصفات العزل الحراري للمواد الثلاث الداخلة في البحث

- القراءات سجلت كمعدل ولعدة مرات وتمت في شهر تموز الساعة 12 ظهرا –2009
- اخذت بعض القراءات من بحوث متخصصة.[2,3]

المادة الانشائية ومواصفاتها القياسية	مقطع الجدار	المعامل الكلي لانتقال الحرارة $w/m^3.k$	متوسط درجة حرارة السطح الداخلي C°	متوسط درجة حرارة السطح الخارجي للجدار C°
الطابوق الطيني الابعاد 25x12.5.x7.5cm الحجم : $2343cm^3$ الوزن :2450gr	25cm	2.013	38.80 C°	53.10 C°
البلوك الكونكريتي الاعتيادي الابعاد 40x20x16cm الحجم : $12800cm^3$ الوزن : 16100gr	20cm	3.48	40.7 C°	56.20C°
البلوك المقترح في البحث الابعاد : 25x25x12.5cm الحجم:$7812cm^3$ الوزن:6350 gr	25cm	2.150	37.70C°	51.05C°

مقارنة كلفة المواد والعمل للمتر المكعب الواحد "الهيكل فقط" بين البلوك المقترح مع الطابوق الطيني والبلوك الكونكريتي الاعتيادي:

يركز البحث على محورين مهمين فقط وهما 1–العزل الحراري وزيادة ذلك من خلال استخدام كسر الطابوق المتميز في العزل الحراري 2– تقليل كلفة انتاج القطعة الواحدة من البلوك المقترح ومن خلال الاستفادة القصوى من كسر الطابوق الذي يتم الحصول عليه من مناطق الانقاض والمصادر الاخرى.

جدول رقم (3) يلخص دراسة عامة عن كلفة البناء" الهيكل فقط "عند استخدام البلوك المقترح وقد تم احتساب الاسعار على طريقة الحجوم والتي يعتبرها الباحث اكثر فعالية من احتساب كلفة المتر المربع للجدران . حيث ان البحث عام وتعتمد الحسابات على سمك الجدران الخارجية فقد تكون 25cm او 36cm للطابوق الطيني وتكون 20cm أو 40cm للبلوك الكونكريتي و 25cm أو37.5cm او50cm للبلوك المقترح ويعتمد ذلك على اختيارات المهندس المعماري في اعداد التفاصيل البنائية والتي تعتبر ذات اهمية قصوى في ايجاد موازنة بين تحسين البيئة الداخلية والخارجية وكذلك في تحديد كلفة البناء بصورة عامة .ان البحث يؤكد ومن خلال التجربة التي قمنا بها ان كلفة انتاج البلوك المقترح هي اقل من كلف مادة الطابوق الطيني و كذلك اقل من البلوك الكونكريتي الاعتيادي وذلك بسبب استخدام كسر الطابوق الذي يؤخذ من مناطق تجمع الانقاض ومن معامل صناعة الطابوق او من مواقع البناء وبسعر زهيد جدا .

ان البحث ومن خلال التجربة التي قمنا بها نستنتج ان سعر البلوك المقترح هو اقتصادي في الطريقتين المقترحتين اليدوية والاوتوماتيكية ويتلخص ذلك كالتالي :

- الطريقة اليدوية , يتم خلط المواد السمنت والرمل وكسر الطابوق عند انتاج البلوك النمطي لغرض بناء دار واحدة او عدد محدود من الدور مثال ذلك عشرة دور سكنية والتي تعتمد تعاون الجماعة "self-help" ويكون اغلب العاملين من اصحاب الدور انفسهم ويتم صب البلوك في قوالب بسيطة معدة من الطابوق الفني "المصمط" (25x12.5x7.5cm) يتم ترتيبها على الارض او على مصاطب حديدية بأرتفاع 90cm .
- يقدر الباحث ان الفرد الواحد يستطيع انتاج نحو 50–100 بلوك في يوم عمل يستمر 8 ساعات. وعندما يكون عدد العاملين خمسة على سبيل المثال فأنهم ينتجون نحو 500 بلوك يوميا.
- الطريقة الميكانيكية يستخدم فيها الاسمنت والرمل وكرات الطابوق التي بقطر (1,2,3cm) والتي تعد مسبقا بالكسارات ويتم الانتاج الميكانيكي بطريقة مشابهة لانتاج البلوك الكونكريتي الاعتيادي حيث يرطب الخليط قبل نحو ساعة ويوضع في بودقة الانتاج المرتفعة عن الارض وبعدها يدخل الخليط في القوالب الاوتوماتيكية.ان الانتاج بهذه الطريقة يكون ذات كميات كبيرة و

يحتاج الى عمال مدربين لهذا الغرض.

- ان كل ما يخص عناصر الكلفة وتحديدها للبلوك المقترح يجب ان يخضع الى دراسات ميدانية ويتم تسجيل اسعار المواد الاولية وكلفة العمل وبيان ان كان الانتاج في موقع البناء او في مواقع اخرى . كذلك تحديد ان كان الانتاج سيتم من قبل اصحاب الدار المزمع انشاءه او من خلال معامل بسيطة او متطورة في مواقع اخرى.

ان احتساب الكلف عند ادخال البلوك المقترح وأية مواد انشائية اخرى الى السوق العراقية يجب ان يدخل في مشاريع تجريبية" Pilot Projects"لبناء دار نموذجي او مجموعة دور ومن ثم تعدل النتائج ولحين استقرار المادة الجديدة كمنافس او مكمل للمواد المتداولة في السوق اصلا . ان عدد المواد الانشائية المتداولة حاليا محدود جدا وهذا يثير القلق حيث ان المواد الاولية التي يمكن استخدامها في صناعة المواد الانشائية في العراق كثيرة جدا ويجب على المختصين التوغل في مجال صناعة المواد الانشائية , لقد تأخر العراق عن الدول المتقدمة وحتى النامية في هذا المجال بعشرات السنين.....

جدول رقم (3) : مقارنة كلفة البناء للهيكل فقط (بدون انهاء) , الاسعار احتسبت في شهر تموز 2009 تم تقدير المواد المطلوبة بالحجوم علما بانه لم يحتسب كلف الماء المستخدم واجور النقل .

المادة الانشائية	كلفة الموادالاولية–دينار عراقي		اجور العمل	كلفة القطعة الواحدة
البناء الطابوق الطيني الابعاد 25x12.5.x7.5cm الحجم : $2343cm^3$ الوزن :2450gr	تشمل الكلفة فقط استغلال الاراضي الزراعية بدون مقابل حيث لم يصدر قانون يمنع ذلك .		50%	250–300 دينار
البلوك الكونكريتي الاعتيادي الابعاد 40x20x16cm الحجم : $12800cm^3$ الوزن : 16100gr	الاسمنت	Cm^3 400 دينار		1000 دينار
	الرمل	Cm^3 50 دينار	50%	
	الحصى	Cm^3 50 دينار		
البلوك المقترح في البحث الابعاد : 25x25x12.5cm الحجم:$7812cm^3$ الوزن:6350 gr	الاسمنت	Cm^3 400 دينار		500 دينار
	الرمل	Cm^3 50 دينار	30%	
	كسر الطابوق	Cm^3 10 دينار		

النتائج :

اتضح لنا خلال عمل هذا البحث ان المادة البنائية المقترحة "البلوك النمطي المقترح المحتوي على كسر الطابوق الطيني ذات العزل الحراري " هي احدى المواد الممكن ادخالها الى جانب مواد البناء المتداولة حاليا مثل الطابوق الطيني والبلوك الكونكريتي الاعتيادي ومن بين المؤشرات التي توضحت من البحث التالي:

- "البلوك العراقي النمطي المقترح المحتوي على كسر الطابوق الطيني ذات العزل الحراري والصوتي " هو حالة متقدمة لمشاركة المهندس المعماري العراقي في اقتراح مواد بنائية مساندة للمواد الانشائية المتداولة.
- على المهندسين كافة والمهتمين بالبناء بصورة عامة تقبل ادخال عشرات من مواد البناء الجديدة وخاصة تلك التي يتوفر لانتاجها المواد الاولية المتيسر الحصول عليها ونقلها وتصنيعها وهي قليلة الكلفة في النقل والانتاج وسهلة العمل اثناء المناولة في مواقع البناء.
- العزل الحراري في العراق يعتبر ذات قيمة مهمة في مواصفات المواد الانشائية الجديدة ونلاحظ ان البلوك النمطي المقترح متفوق في هذه المواصفة مقارنة بالبلوك الكونكريتي الاعتيادي .
- سهولة انتاج البلوك المقترح بكميات صغيرة تكفي لمسكن واحد على سبيل المثال وهذا مناسب لعمل العوائل او افراد الجيرة لانجاز العمل بكلف بسيطة .
- ان القوالب المطلوبة بسيطة ووقد تكون عبارة عن طابوق طيني "مصمت" كما يمكن تطوير قوالب معدنية لهذا الغرض كذلك يمكن استخدام طريقة المكابس الاوتوماتيكية المتبعة في صناعة البلوك الكونكريتي الاعتيادي .
- ان قطعة "البلوك العراقي النمطي المقترح المحتوي على كسر الطابوق الطيني ذات العزل الحراري " (25x25x12.5cm) تكلف عند صناعتها يدويا 500دينار عراقي . بينما تكون كلفة البلوك الاعتيادي بأعتماد اسعار المواد الاولية في تموز 2009 واضيف لها كلفة العمل 50%, والمساوي لحجم 3 طابوقات طيني تكلف مع العمل1000 وبذلك يكون الفارق80% لجدار عرضه 25cm . صورة رقم(3)
- العزل الحراري يزيد نحو 50% عند استخدام البلوك المقترح عن العزل الحراري لجدار سمكه 24cm من الطابوق الطيني الفني ويزداد الى 60%عند املاء الفتحات بالتراب النظيف.
- ان دور المهندس المعماري هو محوري في ايجاد بدائل " المواد ونظم وتكنولوجيا البناء " المناسبة للحالة في العراق من حيث المواد الاولية , كفاءة اليد العاملة , وهذا ما يرمي اليه هذا البحث كمثال على العديد من البحوث المطلوبة.
- التفاصيل المعمارية في هذا البحث هي نماذج للتفاصيل الممكنة والكثيرة عند استخدام البلوك النمطي للحالات المتوقعة في البناء والديكور وتصميم الحدائق ايضا صورة رقم(5)

التوصيات:

بعد 2003 وخلال قيامنا بالعديد من البحوث والدراسات فيما يخص " مواد ونظم وتكنولوجيا البناء في العراق" يمكننا تقديم التوصيات التالية :

- اعادة طباعة الدراسات الخاصة بالمشاريع التي خطط لها او تحققت في العراق في فترة السبعينات من القرن العشرين لاهميتها القصوى .
- الاهتمام بشكل خاص بنشر الدراسات التي تمت حول مشروع اسكان عام عراق "General housing program Iraq 2000 – GHPI " . الذي قامت به مؤسسة Pol- service البولونية وبمشاركة مكتب دار العمارة الاستشاري واشرفت عليه الامم المتحدة وقد دام العمل فيه ست سنوات . الباحث شارك في هذا العمل وقامت شركة اجنبية بتنفيذ عدد من العمارات السكنية ذات ثلاث طوابق ملائمة للحالة الاجتماعية العراقية من تصميم الباحث .
- اعادة طباعة الدراسات ومخططات المدن التي تمت اغلبها بمشاركة المكاتب الاجنبية وكانت على مستوى عالمي ولغرض الاستفادة منها في اعداد مخططات لكافة المدن والاقضية في العراق وتوفير هذه المطبوعات للدارسين والمواطنين كثقافة عامة .
- اعداد دراسات جديدة لمواقع السدود والجسور والطرق السريعة القديمة كذلك المتوقع انشاءها في السنوات القادمة لاهميتها .
- ان بعض مشاريع المدراس الحديثة التي نفذت بالبناء الجاهز في السبعينات كانت ناجحة ويمكن الاستفادة منها لوضع اسس للاعداد الكبيرة من المدراس المطلوب بناءها في العراق .
- ان قطاع الصحة بحاجة الى عيادات نموذجية ومستشفيات متكاملة وذلك يحتاج الى دراسات محلية لوضع خطط هندسية في هذا المجال .
- ان قطاع الاسكان يحتاج الى نهوض شامل ولكن من خلال القطاع الخاص وفتح بنوك عقارية محلية كما في دول الخليج على سبيل المثال, ويتحدد دور الدولة في الاشراف على العمل واعطاء القروض المشروطة .
- اعداد مناهج مناسبة لتطوير البناء في العراق من كافة جوانبه مع اعتماد اقتراحات الاستشاريين العراقيين الذين شاركوا في مثل هذه الاعمال منذ السبعينات من القرن العشرين.
- ان تتبنى وزارة العمل والشؤون الاجتماعية تمويل مشاريع البناء الصغيرة والمتوسطة كذلك تدريب الكوادر الشابة في التخطيط و البناء و تنويع طرق التنفيذ المناسبة في العراق .
- تشجيع انتاج مواد العزل الحراري والتي ستكون جزء من مواد البناء الجديدة التي تستعمل ضمن الجدران والسقوف المجوفة " cavity walls " على سبيل المثال.
- الاهتمام بالمواصفات الدولية والتي كان العراق جزءا منها "ISO- IRAQ" والتي بدأت انطلاقتها في السبعينات من القرن العشرين وكادت ان تصبح قوانين عراقية .

ARABIC REFERENCE:

* المهندس انيس جواد سلمان– تركيب المباني – الجدران الحاملة وتفاصيلها المعمارية وزارة التعليم العالي والبحث العلمي – الجامعة التكنولوجية –1987
* الحديثي عبد الاله (حسابات الاشعة الشمسية على سطوح الابنية المختلفة) تقرير من منشورارات مركز بحوث البناء – مجلس البحث العلمي /العراق 1975
*الدوري – مجيد و علي حسين عاطف (الصفات الحرارية لمواد البناء والانهاء المستخدمة في العراق) المؤتمر الاول للطاقة – وزارة النفط– العراق .....
* كامل شعبان عوني الجوادي مقداد (التحليل المناخي المناسب للعراق واثره على العمارة) تقرير من منشورات مركز بحوث البناء / مجلس البحث العلمي / العراق 1973
* السكن اللائق من حقوق الانسان الاساسية جريدة الصباح العدد(674) تشرين الاول 2005 – د.باسم الانصاري.
* دراسة حول نظم البناء المفتوح بأستخدام بلوك الثرمستون والواح الثرمستون المسلحة في العراق. المؤسسة العامة للصناعات الانشائية – سلام سمعان عبدالاحد 1985

ENGLISH REFERENCES :

* The construction of buildings
Volume one foundations , walls , floors , roofs
R.BARRY A.R.I.BA. 1965
*Sustainable buildings in New Zealand
Paper produced by the PENZ presidential task comm.
Author Dr. Carol Boyle - 2002
* GHPI- general housing program Iraq 2000
Pol service – Poland jointly with Dar Al- Imara –Iraq consultants
1976-1982-reports 1,2,3 .
Salaam Samaan Abdul-ahad .”team leader”
GHPI is a comprehensive study . it was an advanced consultancy work. Many consultants engineers , scientists participated .
The out come can be revised and implemented in the present time .
*The impact of geometrical form orientation of habitat units in hot Arid zones – Fadi Hikmat 1992
University of technology – Baghdad – Iraq
Internet reviews:
*Recycling and reuse of building materials
www.umich.edu/~nppcpub/resources/compendial/ARCHpdfs/ARCHr&rintro.pdf.
* Recycled clay brick as an aggregate for concrete
http://hrcak.srce.hr/file/44759
* The use of plastic bags in making of adobe bricks .
http://www.adobeasw.com/abstract09/santosfilho09theuseofplastic.pdf

دراسة تجريبية لمبادل حراري صفائحي كمبرد هواء

مدرس مساعد/احمد أديب عبد الواحد
رئاسة جامعة النهرين / القسم الهندسي

الخلاصة

لكون تبريد الهواء بإضافة الماء يكون محدداً بمدى معين من الرطوبة التي نستطيع إضافتها إليه والتي بدورها تعتمد على المحتوى الرطوبي للهواء لذلك يتم اللجوء إلى طريقة تبريد الهواء بالترطيب غير المباشر لذا يهدف البحث الحالي إلى دراسة موضوع انتقال الحرارة عبر أسطح مبادل حراري صفيحي متعامد الجريان ومعرفة الظروف المثلى المؤثرة على كفاءة الترطيب ومقدار الطاقة الحرارية المنتقلة عبر أسطح المبادل .

تم حساب فعالية الترطيب ومقدار الطاقة الحرارية المنتقلة عبر أسطح المبادل ومدى تأثرهما بكل من تياري الهواء الرئيسي والثانوي حيث تم تثبيت كمية الهواء الثانوي مع تغيير كمية الهواء الرئيسي مرةً وتغيير ظروف الهواء الرئيسي الداخل عند معدل تدفق معين للهواء الرئيسي مرةً أخرى بعدها يتم تثبيت كمية الهواء الرئيسي مع تغيير كمية الهواء الثانوي مرةً وتغيير ظروف الهواء الرئيسي الداخل عند معدل تدفق معين للهواء الرئيسي مرةً أخرى , وللوصول إلى هذا الهدف تم استخدام جهاز مختبري تتوفر فيه إمكانية قياس معدلات تدفق الهواء ودرجات الحرارة للبصلتين الجافة والرطبة عند مقاطع الدخول والخروج لكلا التيارين الرئيسي والثانوي .

وجد إن زيادة كلاً من فعالية الترطيب ومقدار الطاقة الحرارية المنتقلة عبر أسطح المبادل ترتبط بزيادة تدفق الهواء الثانوي ونقصان تدفق الهواء الرئيسي حيث تزداد فعالية الترطيب بنسبة 16% لتصل إلى 51%عند تغيير معدل تدفق الهواء الثانوي من صفر إلى 0.2kg/s وكذلك الحال بالنسبة لمقدار الطاقة الحرارية حيث تزداد بنسبة 35% لتصل إلى 1.15kW , كما إن فعالية الترطيب تقل بنسبة 12% عند زيادة معدل تدفق الهواء الرئيسي بنسبة 12% وكذلك الحال بالنسبة لمقدار الطاقة الحرارية حيث تقل بنسبة 21% لنفس نسبة النقصان في معدل التدفق أعلاه .

Experimental study of plate heat exchanger air cooler

ABSTRACT

As cooling air using water injection was limited by a range of humidity ratio so indirect humidification for air consider , this research take the study of heat transfer through a perpendicular plate heat exchanger to discover the influence optimum conditions on dehumidification efficiency and the amount of heat transfer energy across the plates of heat exchanger so calculating dehumidification efficiency and the amount of heat transfer energy across the plates of heat exchanger depending on the change of primary and secondary air flow rate using an experimental apparatus with an instruments for measuring air flow rate , dry bulb temperature and wet bulb temperature on air entry and exit sections , experimental procedure by fixing primary air mass flow rate with changing secondary air mass flow rate once and the condition of entering primary air

another time , also fixing secondary air mass flow rate with primary air mass flow rate once and the condition of entering primary air another time .

Results show that the increasing of both the dehumidification efficiency and the amount of heat transfer energy across the plates of heat exchanger depend on the increasing of secondary and decreasing of primary air flow rate , percentage of increasing dehumidification efficiency 16 when secondary air mass flow rate increase from 0 to 0.2 kg/s and percentage of increasing heat transfer 35 with above flow rate , percentage of decreasing dehumidification efficiency 12 when primary air mass flow rate increasing percentage 12 and percentage of increasing heat transfer 21 with above flow rate .

KEYWORD : air-cooler , dehumidification , heat exchanger , heat transfer , Two stage .

المقدمة

المبادلات الحرارية هي وسائل لنقل الطاقة الحرارية من احد الموائع إلى مائع آخر بدون حدوث عملية خلط بينهما , وتوجد أنواع عديدة للمبادلات مثل الصدفة والأنابيب shell & tubes والمبادلات الحرارية الصفيحية plate واللولبية spiral وذوات السطوح المكشوطة scraped surface . كما إن المبادلات الحرارية هي جزء مهم لا يمكن الاستغناء عنه في كثير من المجالات الحيوية ، فالمرجل Boiler المستخدم في محطات توليد الطاقة الكهربائية أو المستخدم لتسخين المياه في منظومات التكييف ما هو إلا مبادل حراري والمبخر evaporatorالجزء الفعال في منظومات التكييف والتبريد وبرج التبريد cooling tower المستخدم في منظومات التكييف أو المستخدم في صناعة الحديد والصلب هو عبارة عن مبادل حراري من النوع المفتوح كما إن هناك أجهزة موجودة في كل بيت يعتمد عملها على المبادلات الحرارية مثل الثلاجة المنزلية وكذلك المبردة التبخيرية أو مبردة الماء , وفي السيارة يتم تبريد الماء الحار المستخدم لتبريد المحرك بواسطة المبادلة الحرارية , وهكذا نرى المبادلات الحرارية هي العمود الفقري لكثير من الصناعات والأجهزة .

في المبادلات الحرارية الصفيحية يتم وضع صفيحة رقيقة من المعدن بين مائعين ليتم عبرها نقل الطاقة الحرارية , ومن المعادن الشائعة الاستعمال لصنع هذه الصفائح : الحديد المغلون , التيتانيوم , النيكل , التيتاليوم .

تعتمد طريقة تبريد الهواء تبخيرياً بمرحلتين على تبريد الهواء الخارجي إلى درجة حرارة اقل من الممكن تحقيقه بمرحلة واحدة مع حصيلة اقل للرطوبة المضافة إلى الحيز المكيف .

بدأت محاولات pescod [Heat exchangers , 1988] منذ عام 1968 عندما كانت المبادلات الحرارية غالباً ما تصنع من المعادن إلا أن كلفة الصيانة وأسعار الإنشاء أدى إلى عدم نجاح هذا الأسلوب مما شجعه على تطوير المبادل الحراري لاستخدامه في منظومات التبريد غير المباشر وذلك باستعمال الصفائح لتشكل مسارين متعامدين لتياري الهواء وتستخدم دافعتين للهواء كذلك مضخة تدوير الماء ومنفث Nozzle يرش الماء فوق مسار تيار الهواء الثانوي والداخل من أسفل المبادل الحراري بحيث يقوم بتبريد الهواء الداخل للحيز المراد تكييفه ، بينما يطرح الهواء الثانوي للجو وبهذا الأسلوب بحث pescod ملائمة التبريد ألتبخيري غير المباشر لظروف مناخية مختلفة لقارة استراليا وتبين انه ملائم لمعظم أجواء استراليا ما عدا المناطق التي تزيد فيها درجة الحرارة البصلة الرطبة للهواء على $25\ ^oC$ والجافة $36\ ^oC$.

في سنة 2002 نجحت شركة Canada Composting Inc [An experimental study of a cross-flow type plate heat exchanger for dehumidification/cooling , 2002] بتطوير أداء المبادلات الحرارية الصفيحية ومنها أن تجعل إحدى صفائح المبادل على الأقل الكترودياً لتكوين حقل الكترودي لزيادة معدل انتقال الطاقة الحرارية ما بين مائع التثليج والمائع الناقل للحرارة , أما التصميم الثاني فيعتمد على إضافة جريان حلقي ويتم بتوسيع سطح الزعنفة لزيادة مساحة التبادل الحراري مع عمل فتحات شعاعية لحلقات الجريان لعمل اضطراب إضافي بالجريان وبالتالي زيادة التبادل الحراري .

وفي عام 2003 أثمرت الدراسات والأبحاث التي أجرتها شركة Davis Energy Group [development of an improved two-stage evaporative cooling system , 2004] على تحقيق الأهداف التي تطمح إليها وهي الأداء الأفضل مع تقليل كلفتي الإنشاء والتشغيل إضافةً إلى كمية اقل للرطوبة داخل الحيز المكيف وذلك عن طريق جعل عرض المبادلات حراً مع تغيير موقع المحرك الكهربائي.... الخ .

الفرضيات

يتناول هذا البحث تحليل تصرف مبادل حراري صفائحي يستخدم لتبريد الهواء بمرحلتين وذلك بالاعتماد على معادلتي حفظ الكتلة وحفظ الطاقة وبالاعتماد على الفرضيات التالية :

- يعامل الغاز على انه غاز مثالي .
- الضغط الجوي على أساس مستوى سطح البحر ويساوي 103.5kpa (لنتمكن من استخدام المخطط المصردي psychometric chart) .
- لا يوجد إضافة أو طرح للكتلة والطاقة من وإلى النظام .

الجزء العملي

تم في هذه الدراسة استخدام مبادل حراري صفائحي من صفائح الألمنيوم كما في الأشكال (1) و(2) و(3) وبسمك (1mm) بالأبعاد (66*52cm) لكل صفيحة ويبلغ عددها (30) صفيحة رتبت بحيث تكون المسافة البينية لممرات الهواء الرئيسي (1cm) والمسافة البينية لممرات الهواء الثانوي (3cm) واستخدمت قطع خشبية بسمك (1cm) وعرض (3cm) على طول مسافة المبادل لحفظ المسافة بين الصفائح لممرات مجرى الهواء الرئيسي والثانوي . تثبت الصفائح مع القطع الخشبية باللوالب وباستخدام أربع مساند . تم طلاء القطع الخشبية بمانع الرطوبة لئلا يمتص الخشب الماء ولمنع تسرب الماء أو الهواء من خلالها . استخدمت الحشوة الخشبية (الحلفة) بين صفائح المبادل من جهة مجرى الهواء الثانوي وذلك لزيادة المساحة السطحية لتلامس الهواء مع الماء ولعمل اضطراب في مجرى الهواء كما تعمل الحشوة على توزيع الماء لكي يشمل جميع أسطح الصفيحة مما يزيد من كفاءة التبلل وهذا يؤدي إلى زيادة فعالية التبريد للمبادل .

يجهز الماء إلى مجرى الهواء الثانوي لترطيب الحشوة الخشبية وصفائح الألمنيوم باستخدام أنابيب بلاستك مثقبة توزع الماء على الحشوة بصورة متساوية والتي تجهز من خلال أنبوب تجهيز رئيسي . لتدوير

الماء استخدمت مضخة ذات سعة (20L/min) . وضع المبادل الحراري داخل الجهاز وثبت باستخدام حامل على شكل سكة لسهولة الصيانة . يفصل بين مجرى الهواء الثانوي والرئيسي صفيحتان الأولى أمام المبادل من جهة الدخول للهواء المعامل ترتبط بالحامل وحوض الماء والأخرى من جهة الخروج من المبادل وتمتد إلى قاعدة الحوض حيث يتم من خلالها فصل الحوض إلى جزأين أسفل المبادل . استخدمت مروحة لسحب الهواء الثانوي من خلال فتحة في سقف الجهاز بعد مروره من خلال الحشوة الخشبية المثبتة في مجرى تيار الهواء الثانوي إلى الخارج . يتجمع الماء النازل من الحشوة الخشبية في الحوض أسفل المبادل ويعوض عن الماء المتبخر بتجهيز الحوض بالماء باستخدام طوافة .

استخدمت مزدوجات حرارية (Thermocouples) نوع T مصنوع من مادتي (copper – constantan) ومحرار زئبقي لقياس درجة حرارة البصلة الجافة للهواء ، فقد تم تثبيتها في مجرى الهواء المراد قياس درجة حرارته . وكذلك استخدم نفس النوع من المزدوجات الحرارية لقياس درجة حرارة البصلة الرطبة للهواء حيث لف على نهايتها قطعة من قماش قطني بشكل فتيل (wick) تغمر نهايتها في قارورة مملوءة بالماء المقطر . تتصل أطراف المزدوجات الحرارية بعد توزيعها على مناطق القياس وباستخدام أسلاك معادلة بمفتاح اختيار (selector switch) الذي يتيح قياس الإشارة الكهربائية لعدة مزدوجات ويستخدم جهاز مؤشر درجة الحرارة رقمي (digital temperature indicator) يقوم بتحويل الإشارة الكهربائية التي نحصل عليها من المزدوج الحراري إلى قراءة لدرجة الحرارة بدقة (0.1%) ضمن حدود درجات الحرارة المقاسة (للتأكد من دقة قراءات جهاز قياس درجة الحرارة تم إجراء عملية المعايرة قبل البدء بالقراءات وذلك بوضع متحسس المزدوج الحراري في إناء يحتوي على ماء مقطر مع جريش الثلج وتم قياس درجة الحرارة عن طريق جهاز قياس درجة الحرارة الالكتروني فظهرت النتيجة 4.0^0C- ومن ثم سخن الماء إلى درجة الغليان 100.0^0C وتم قياس درجة الحرارة فظهرت النتيجة 99.9^0C) . لقد وزعت عدة مزدوجات حرارية في مواقع وارتفاعات مختلفة لكل مقطع قياس لكي يتم تجاوز الخطأ الحاصل في القياس بسبب عدم تجانس الهواء لنفس مقطع القياس (حيث يتم وضع مزدوجين حراريين لكل مقطع قياس احدهما في وسط مقطع الاختبار والآخر عند حافته) وتم أخذ متوسط درجة الحرارة لكل مقطع قياس وقد وزعت المزدوجات الحرارية لقياس درجات الحرارة حيث تم قياس درجة حرارة البصلة الجافة والرطبة للهواء المار في مجرى تيار الهواء الرئيسي للمبادل الحراري باستخدام مزدوجات حرارية ثبتت على وجه المبادل باستخدام أنابيب رفيعة عند الدخول والخروج من المبادل وكذلك تم قياس درجة حرارة البصلة الجافة والرطبة لنقاط الدخول والخروج للهواء الثانوي من المبادل الحراري عند الخروج من منظومة التبريد .

خطوات إجراء التجارب

1 – يتم تشغيل مروحتي الهواء لتياري الهواء الرئيسي والثانوي ويتم السيطرة على سرعته بتحريك بوابتي فتحتي الدخول ويتم قياس معدل سرعة الهواء لكل من تياري الهواء الرئيسي والثانوي .

2 – تؤخذ قراءات درجات الحرارة للبصلة الجافة عند مدخل ومخرج المبادل الحراري من جهتي تياري الهواء الرئيسي والثانوي وكذلك تؤخذ قراءة درجات الحرارة للبصلة الرطبة عند الدخول والخروج .

3 – تشغيل مضخة الماء ويتم التأكد من تجانس توزيع الماء على السطح العلوي من المبادل الحراري ومن ثم تتم ملاحظة درجات حرارة الهواء للبصلة الرطبة والجافة .

القراءات

تم إجراء 6 تجارب بمعدل 270 قراءة بالطريقة المبينة أدناه :

أ – تغيير سرعة تيار الهواء الرئيسي مع ثبوت سرعة الهواء الثانوي .

1 . تاريخ إجراء التجربة 8 / 4 / 2007 .

U_p	DBT_{pi}	WBT_{pi}	DBT_{po}	WBT_{po}	DBT_{si}	WBT_{si}	DBT_{so}	WBT_{so}
1.78	19.2	12.7	16.7	13	20.3	14.3	15	14
1.75	19.8	13.5	17	13.3	20.4	14	15.3	14.5
1.73	19.7	13.4	17.2	13.3	20.4	14	15.2	14.5
1.63	19.9	13.8	17.1	13.4	20.6	14.2	15.5	14.8
1.57	19.9	13.8	17.3	13.3	21	14.3	15.5	14.7

2 . تاريخ إجراء التجربة 11 / 4 / 2007 .

U_p	DBT_{pi}	WBT_{pi}	DBT_{po}	WBT_{po}	DBT_{si}	WBT_{si}	DBT_{so}	WBT_{so}
1.78	25	16.3	18.2	14.1	19.2	13.9	15.6	15.1
1.75	25.9	17.3	19.2	15	20	14.5	16.4	15.7
1.73	25.9	17.3	19.1	15.2	20.3	14.8	16.8	16
1.63	25.9	17.4	18.8	15.1	20.3	14.8	16.5	15.9
1.57	26.8	18.4	18.9	15.5	21.2	15.5	16.7	16

3 . تاريخ إجراء التجربة 17 / 4 / 2007 .

U_p	DBT_{pi}	WBT_{pi}	DBT_{po}	WBT_{po}	DBT_{si}	WBT_{si}	DBT_{so}	WBT_{so}
1.78	29.1	18.8	20	15.9	17.2	16.6	20.9	15.2
1.75	29.3	19	20.5	16	17.4	16.6	21.2	15.1
1.73	29.3	18.8	20.4	16	17.3	16.6	21.4	15.2
1.63	30	19.2	20.3	16	17.8	16.9	21.8	15.3
1.57	31.7	20	19.8	15.9	17.5	16.7	21.9	15.2

4 . تاريخ إجراء التجربة 18 / 4 / 2007 .

U_p	DBT_{pi}	WBT_{pi}	DBT_{po}	WBT_{po}	DBT_{si}	WBT_{si}	DBT_{so}	WBT_{so}
1.78	29.3	19.1	21.5	16.5	22.1	16	17.9	17
1.75	31.3	19.7	21.9	17.1	22.8	16.6	18.2	17.5
1.73	31.8	20.1	22	17.1	23	16.6	18.6	17.8
1.63	33.2	21	22.3	17.6	23.3	17.2	19.7	18.6
1.57	34.4	21.7	22	17.6	23.3	17.2	19.4	18.6

5 . تاريخ إجراء التجربة 24 / 4 / 2007 .

U_p	DBT_{pi}	WBT_{pi}	DBT_{po}	WBT_{po}	DBT_{si}	WBT_{si}	DBT_{so}	WBT_{so}
1.78	37.6	22.3	24.4	18.3	23.8	18	19.7	18.9
1.75	39.1	22.4	25	18.8	24.4	18.4	20.1	19.3
1.73	40	23.3	24.8	18.8	24.6	18.6	20.6	19.9
1.63	40.6	23.4	24.5	18.4	24.6	18.3	20.2	19.4
1.57	43	24.4	24.3	18.5	24.8	18.5	20.4	19.5

ب – تغيير سرعة الهواء الثانوي مع ثبوت سرعة تيار الهواء الرئيسي .

تاريخ إجراء التجربة 8 / 4 / 2007

U_s	DBT_{pi}	WBT_{pi}	DBT_{po}	WBT_{po}	DBT_{si}	WBT_{si}	DBT_{so}	WBT_{so}
4	19.2	12.7	16.7.	13	20.3	14.3	15	14
3.95	20.5	14	17.4	13.5	21.4	14.4	16.2	15.1
3.15	20.9	14	18.1	13.7	22.3	14.7	16.7	15.3
2.08	20	15.2	18.3	15.1	20.6	14.8	17.6	16.4
0	20.5	14.9	18.4	16	20.8	15.6	21.2	16.5

الحسابات

بمعرفة درجتي حرارة البصلة الجافة والرطبة عند مقطع خروج الهواء الرئيسي نستطيع استخدام المخطط المصردي لإيجاد كثافة الهواء عند هذا المقطع , أما سرعة الهواء فيتم قياسها مباشرة بواسطة جهاز قياس سرعة الهواء الموضح في الشكل رقم (3) وبمعرفة أبعاد المقطع نستطيع حساب مساحته بعده يتم حساب معدل تدفق الهواء الرئيسي ألكتلي كما يلي :

$$\dot{m_p} = \rho_a * A_p * U_p \qquad (1)$$

كما تم حساب معدل تدفق الهواء الثانوي الكتلي كما في أعلاه لكن عند مقطع خروج الهواء الثانوي باستخدام المعادلة :

$$\dot{m_s} = \rho_a * A_s * U_s \qquad (2)$$

تم اعتماد العلاقة التي استخدمها pescod في تجاربه لحساب فعالية الترطيب (هي عبارة عن هبوط درجة حرارة الهواء الرئيسي الجافة نسبةً إلى الفرق بين درجة حرارة الهواء الرئيسي الجافة ودرجة حرارة الهواء الثانوي الرطبة) وهي :

$$\varepsilon = \frac{DBT_{pi} - DBT_{po}}{DBT_{pi} - WBT_{si}} \qquad (3)$$

ويمكن معرفة كمية الطاقة الحرارية المنتقلة باستخدام المعادلة التالية حيث يبرد الهواء الرئيسي تبريداً محسوساً : sensible cooling

$$Q = m_p^{\cdot} * cp_a * (DBT_{pi} - DBT_{po}) \quad (4)$$

النتائج والمناقشة

يمرر الهواء الرئيسي خلال المبادل الحراري ألصفائحي لتبريده تبريداً محسوساً بطريقة التبريد ألتبخيري غير المباشر وقد تم الحصول على نتائج الاختبارات من خلال تشغيل المنظومة بصورة كاملة , فقد استخدمت الحشوة الخشبية بين صفائح المبادل لمجرى تيار الهواء الثانوي لزيادة المساحة السطحية لتلامس الهواء مع الماء ولعمل اضطراب في مجرى تيار الهواء الثانوي بالإضافة إلى تحسين توزيع الماء لكي يشمل جميع أجزاء سطح الصفيحة ولتقليل سرعة نزوله إلى الحوض بحيث يمر في مسار أطول ويزيد من تلامس الهواء مع الماء حيث تتحول الحرارة المحسوسة في الهواء الثانوي إلى حرارة كامنة لتبخير الماء .

لمعرفة تأثير كل من تدفق الهواء الرئيسي وظروف الهواء الداخل على فعالية الترطيب نقوم بتثبيت كمية الهواء الثانوي عند قيمة 0.2 كغم/ثا (أي جعل فتحة دخوله بأقصى ما يمكن) , نحصل على الشكل (4) الذي يمثل العلاقة بين معدل تدفق الهواء الرئيسي الكتلي وفعالية الترطيب لظروف دخول مختلفة للهواء الرئيسي الذي أتضح منه إن فعالية الترطيب تأخذ بالتناقص كلما زاد معدل تدفق الهواء الرئيسي لمختلف ظروف المدخل بثبوت كمية الهواء الثانوي وهذا يعود إلى إن الكمية المحددة للهواء الثانوي قادرة على استيعاب رطوبة معينة لا تستطيع تجاوزها , كما يتضح إن أقصى فعالية ترطيب تكون عند ظرف هواء رئيسي داخل 33DBT,21WBT بعدها تبدأ بالانخفاض . أقصى فعالية ترطيب عملية في هذه الدراسة كانت 70% عند معدل تدفق كتلي 0.312 كغم/ثا للهواء الرئيسي .

ولمعرفة تأثير كل من تدفق الهواء الرئيسي وظروف الهواء الداخل على مقدار الطاقة الحرارية المنتقلة عبر أسطح المبادل نقوم بتثبيت كمية الهواء الثانوي عند قيمة 0.2 كغم/ثا أيضاً , الشكل (5) يمثل العلاقة بين معدل تدفق الهواء الرئيسي الكتلي والطاقة الحرارية المنتقلة عبر أسطح المبادل لظروف دخول مختلفة للهواء الذي يتضح منه إن الطاقة الحرارية تأخذ بالتناقص كلما زاد معدل تدفق الهواء الرئيسي لمختلف ظروف الهواء الرئيسي الداخل بثبوت كمية الهواء الثانوي إلى أن يصل إلى حد يستقر فيه مقدار الطاقة الحرارية ولا يزداد بزيادة كتلة الهواء الرئيسي المارة وهذا يعود إلى إن الكمية المحددة للهواء الثانوي قادرة على استيعاب طاقة حرارية كامنة معينة تسحب طاقة حرارية محسوسة من الهواء الرئيسي لا تستطيع تجاوزها , كما يتضح إن أقصى طاقة حراري منتقلة تكون عند ظرف هواء رئيسي داخل 33DBT,21WBT . كما إن أقصى طاقة حرارية عملية منتقلة عبر أسطح المبادل في هذه الدراسة كانت 4.5kW عند معدل تدفق كتلي 0.312 كغم/ثا للهواء الرئيسي .

ولدراسة تأثير كل من تدفق الهواء الثانوي وظروف الهواء الداخل على فعالية الترطيب تم تثبيت كمية الهواء الرئيسي عند قيمة 0.35354 كغم/ثا (أي جعل فتحة دخوله عند أقصى ما يمكن) , نحصل على الشكل (6) الذي يمثل العلاقة بين معدل تدفق الهواء الثانوي الكتلي وفعالية الترطيب لظروف دخول مختلفة للهواء الذي يتضح منه إن فعالية الترطيب تزداد كلما زاد معدل تدفق الهواء الثانوي بثبوت كمية الهواء الرئيسي لان زيادة كمية الهواء الثانوي تعني زيادة كمية الماء التي يستطيع حملها لنفس درجة حرارة البصلة الرطبة وبالتالي زيادة فعالية الترطيب , ومن الشكل السابق يتضح لنا أيضاً إن أقصى فعالية ترطيب عملية في هذه الدراسة كانت 51.03% عند معدل تدفق كتلي 0.2 كغم/ثا للهواء الثانوي . تم الحصول على العلاقة أدناه التي تربط معدل تدفق الهواء الثانوي الكتلي بفعالية الترطيب عند ظروف هواء ثانوي داخل 30.3DBT,14.3WBT ولتدفق هواء رئيسي كما ذكر أعلاه :

$$\varepsilon = 4637\ m_s^{\cdot\ 3} - 868.8 m_s^{\cdot\ 2} + 41.97 m_s^{\cdot} + 42.85 \qquad (5)$$

ولمعرفة تأثير كل من تدفق الهواء الثانوي وظروف الهواء الداخل على مقدار الطاقة الحرارية المنتقلة عبر أسطح المبادل تم تثبيت كمية الهواء الرئيسي عند قيمة 0.35354 كغم/ثا أيضاً , الشكل (7) يمثل العلاقة بين معدل تدفق الهواء الثانوي الكتلي والطاقة الحرارية المنتقلة عبر أسطح المبادل لظروف دخول مختلفة للهواء الذي يتضح منه إن الطاقة الحرارية تزداد بزيادة معدل تدفق الهواء الثانوي لمختلف ظروف الهواء الداخل بثبوت كمية الهواء الرئيسي وهذا يعود إلى إن زيادة كمية الهواء الثانوي تسبب زيادة في معامل انتقال الحرارة (h) نتيجة زيادة الاضطراب في الجريان وبالتالي زيادة التبادل الحراري أي تسحب طاقة حرارية محسوسة من الهواء الرئيسي , ومن الشكل أعلاه يتضح إن أقصى طاقة حراري منتقلة تكون عند ظرف هواء ثانوي داخل 30.3DBT,14.3WBT. كما إن أقصى طاقة حرارية عملية منتقلة عبر أسطح المبادل في هذه الدراسة كانت 1.15kW عند معدل تدفق كتلي (0.2 كغم/ثا) للهواء الثانوي . تم الحصول على العلاقة أدناه لحساب كمية الطاقة الحرارية المنتقلة عبر أسطح المبادل بدلالة معدل تدفق الهواء الثانوي لحالة الدراسة هذه :

$$Q = 11.23\ m_s^{\cdot\ 2} - 0.078 m_s^{\cdot} + 0.745 \qquad (6)$$

مما ورد سابقاً نستطيع القول إننا نستطيع الحصول على أقصى فعالية ترطيب وأقصى كمية طاقة حرارية منتقلة للمبادل قيد الدراسة عند معدلات تدفق 0.312 كغم/ثا للهواء الرئيسي و 0.2 كغم/ثا للهواء الثانوي لظروف دخول 33DBT,21WBT و 30.3DBT,14.3WBT كلاً من الهواء الرئيسي والثانوي على التوالي .

الاستنتاجات والتوصيات

بعد مناقشة النتائج تم التوصل إلى ما يلي :

1. زيادة معدل تدفق الهواء الرئيسي تسبب نقصان كلاً من فعالية الترطيب ومقدار الطاقة الحرارية المنتقلة عبر صفائح المبادل أي ان العلاقة التي تربط بينهما عكسية .
2. فعالية الترطيب ومقدار الطاقة الحرارية المنتقلة عبر صفائح المبادل يتناسبان طردياً مع معدل تدفق الهواء الثانوي حيث يزدادان بزيادته .

3. الحصول على العلاقات التالية لحساب كلاً من فعالية الترطيب ومقدار الطاقة الحرارية المنتقلة عبر أسطح المبادل بدلالة معدل تدفق الهواء الكتلي :

$$\varepsilon = 4637\ \dot{m_s}^{\,3} - 868.8\dot{m_s}^{\,2} + 41.97\dot{m_s} + 42.85$$
$$Q = 11.23\ \dot{m_s}^{\,2} - 0.078\dot{m_s} + 0.745$$

يمكن إجراء عدة تغييرات لتطوير الجهاز من جهة والحصول على حالات دراسة أخرى من جهة ثانية , ومن بين هذه التغييرات :

- تغيير مروحتي كل من الهواء الرئيسي الثانوي أو إحداهما لزيادة معدلات التدفق وبالتالي معرفة تأثيرهما على النتائج .
- تغيير المسافات بين صفائح المبادل زيادةً أو نقصان .
- تغيير المعدن المستعمل في صنع المبادل على أن يكون مقاوماً للصدأ .

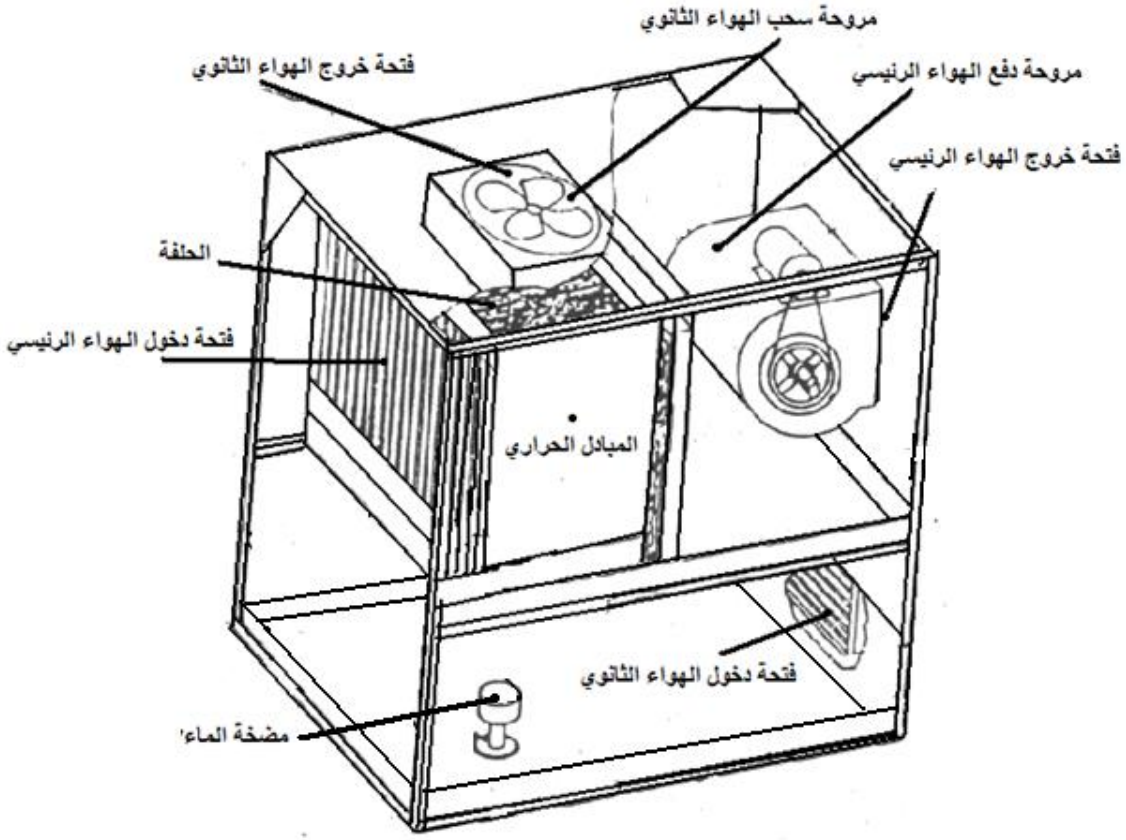

شكل(1) مخطط الجهاز المستخدم

شكل (2) الجهاز المستخدم

شكل (3) الجهاز المستخدم

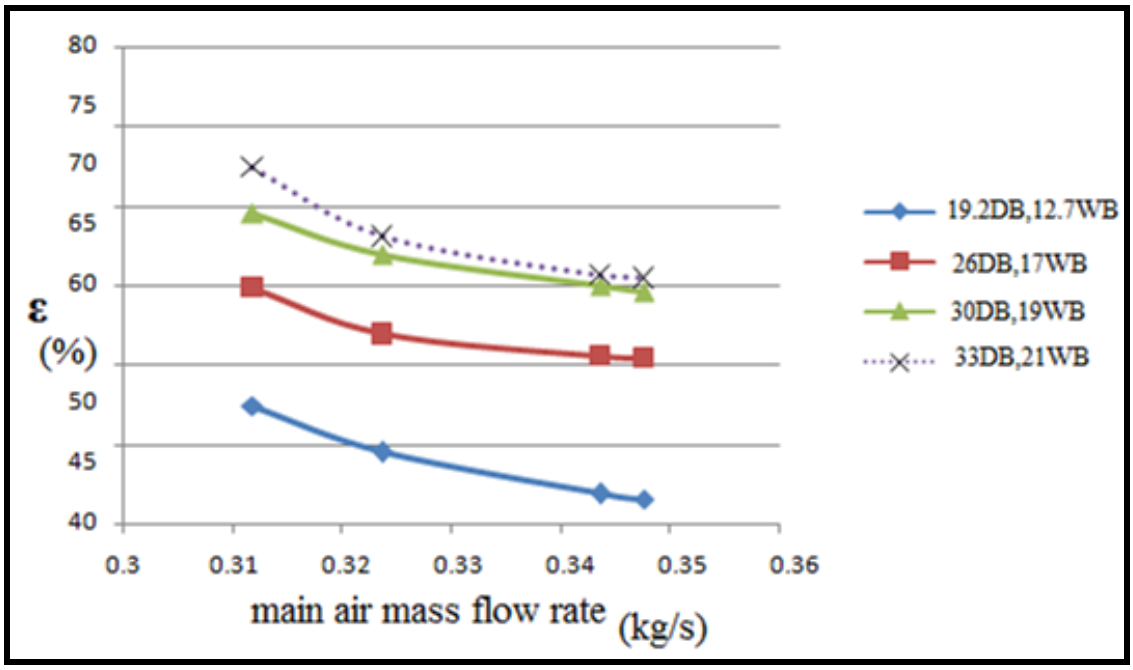

شكل (4) فعالية الترطيب نسبةً إلى معدل تدفق الهواء الرئيسي الكتلي لظروف هواء رئيسي داخل مختلفة

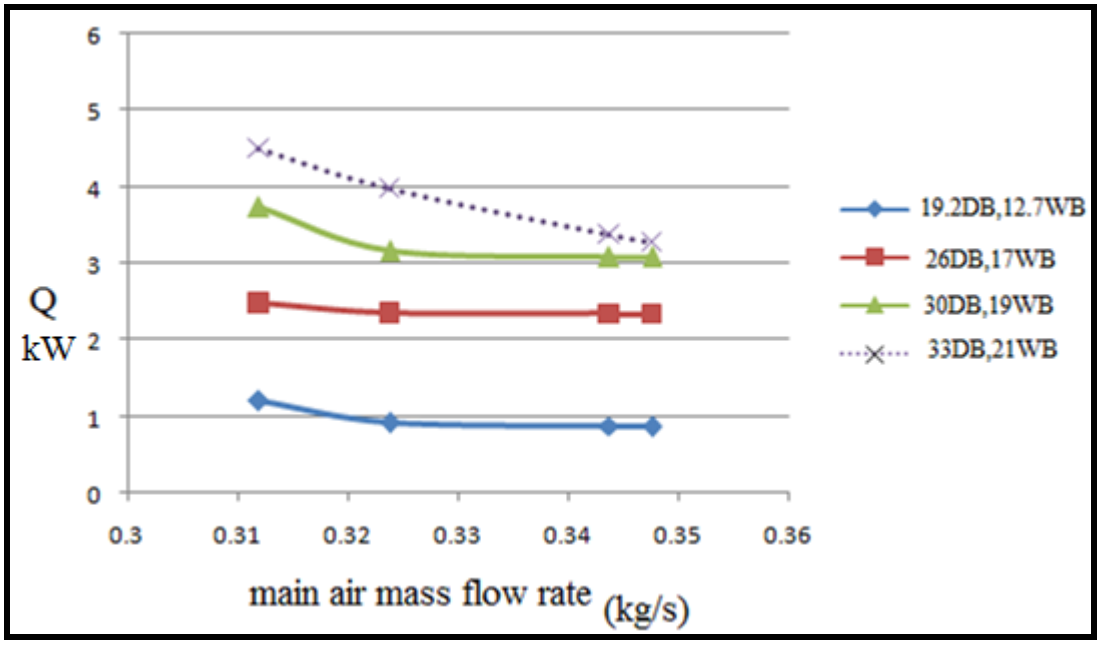

شكل (5) الطاقة الحرارية المنتقلة عبر سطحي المبادل نسبةً إلى معدل تدفق الهواء الرئيسي الكتلي لظروف هواء رئيسي داخل مختلفة

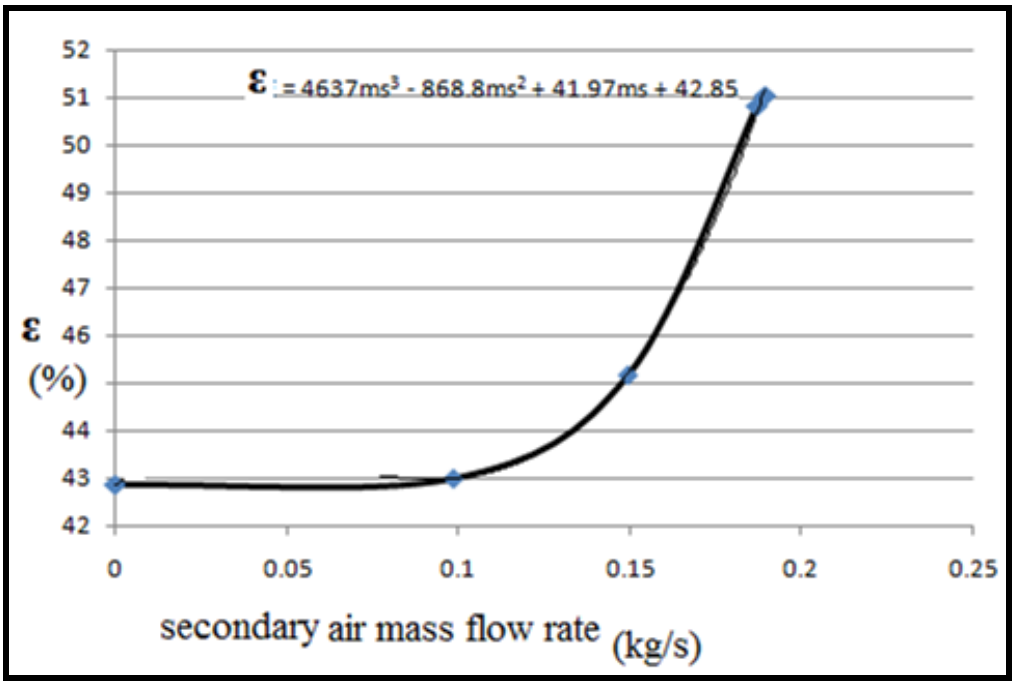

شكل (6) فعالية الترطيب نسبةً إلى معدل تدفق الهواء الثانوي الكتلي

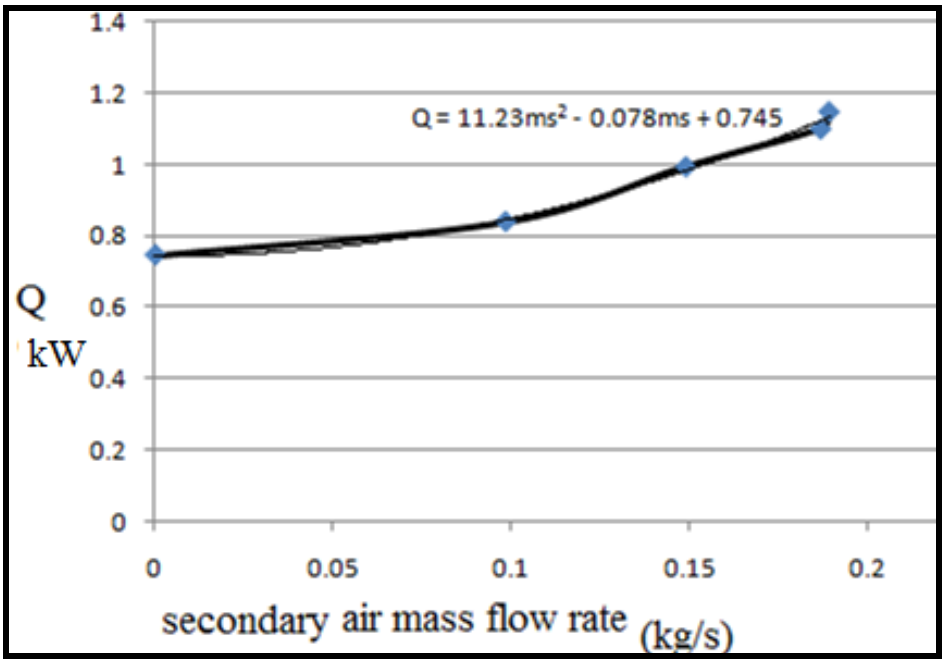

شكل (7) الطاقة الحرارية المنتقلة عبر سطحي المبادل نسبةً إلى معدل تدفق الهواء الثانوي الكتلي

المصادر

- Davis Energy Group for California energy commission , " Indirect-Direct evaporative cooler (IDEC) Development Project Final report ", 1995 , P500.
- Davis Energy Group for ACMA technologies Pte. Ltd , " Evaporative cooling market study " , 2000 , p27 .
- Davis Energy Group for Heschong Mahone Group and the California energy commission , " Advanced evaporative cooling white paper " , 2002 .
- Davis Energy Group for California energy commission , " Development of an improved two-stage evaporative cooling system " , 2004 , p1 .
- Martin , " Heat exchangers " , Hemisphere Publishing Corporation , 1992 .
- Paykoc , " Basic relationships for heat exchanger " , Kluwer Academic Publishers , 1987 , p29 .
- Picon-Nunez , " Surface selection and design of plate-fin heat exchangers " , 1999 , p7 .
- Saman , " An experimental study of a cross-flow type plate heat exchanger for dehumidification/cooling " , Solar Energy , 2002 , p59 .
- Saunders , " Heat exchangers " , John Wiley & Sons , 1988 , p50 .
- Smith , " Thermal design of heat exchangers " , John Wiley & Sons , 1997 .

قائمة الرموز

U_p	معدل سرعة جريان الهواء الرئيس عند مقطع الخروج	m/s
U_s	معدل سرعة جريان الهواء الثانوي عند مقطع الخروج	m/s
Ap	مساحة مقطع الخروج للهواء الرئيسي وتساوي 0.16775	m^2
As	مساحة مقطع الخروج للهواء الثانوي وتساوي 0.04	m^2
DBT_{pi}	درجة حرارة البصلة الجافة للهواء الرئيسي الداخل	^oC
WBT_{pi}	درجة حرارة البصلة الرطبة للهواء الرئيسي الداخل	^oC
DBT_{po}	درجة حرارة البصلة الجافة للهواء الرئيسي الخارج	^oC
WBT_{po}	درجة حرارة البصلة الرطبة للهواء الرئيسي الخارج	^oC
DBT_{si}	درجة حرارة البصلة الجافة للهواء الثانوي الداخل	^oC
WBT_{si}	درجة حرارة البصلة الرطبة للهواء الثانوي الداخل	^oC
DBT_{so}	درجة حرارة البصلة الجافة للهواء الثانوي الخارج	^oC
WBT_{so}	درجة حرارة البصلة الرطبة للهواء الثانوي الخارج	^oC
ε	فعالية الترطيب	%
$\dot{m_p}$	معدل التدفق الكتلي للهواء الرئيسي	kg/s
$\dot{m_s}$	معدل التدفق الكتلي للهواء الثانوي	kg/s
ρ_a	كثافة الهواء = 1.184	kg/m^3
Q	الطاقة الحرارية المنتقلة بين تياري الهواء	kW
Cp_a	الحرارة النوعية بثبوت الضغط للهواء = 1.005	kJ/kg.K

حقول القوة الخفية في المادة المستعملة في المباني

الباحث:

أنفال مؤيد الحجيات

ماجستير هندسة معمارية (مدرس مساعد)

جامعة بغداد – كلية الهندسة

قسم الهندسة المعمارية

The Hidden Fields in Material that used for Building

ABSTRACT

In the Last Recent Years, the Conservation of Natural Environment Resources be a Problem that to and fro to get a line between two elements, First of one is the Natural Environment Resources Balance , and the other is the Reduction of its Consumption and Limitation of Negative Results upon this Environment, Last Years seeks to but Modern Architecture Concept to Conservator Energy Resources and Natural Sources To Reach that Known Sustainable Buildings Which have the Lessees Effect on the Natural Environment and its Environmental Properties.

On the Concern that Materials is the Main Component of Architectural Configuration and appearance that Architect use it in Sustainable Construction to redecate the Environmental effect and to establish a complete constructing experience in Architectural Field ,in the same Time it been the Basic stone effected the nature by reducting its recourses continually , and thrown Tons of Wastes in Trash areas on the Roods Edges, Resulted the abuse of Hectares of Agricultural lands . this Dangerous Trashes accumulated without any treatment in most of Countries , that Generate Negative reaction Power upon this Environment ,because of Chemical Interactions of This materials (Trashes)between each and other.

Therefore , The study directed in its Problem to Illustrate the Identity and Nature of Projected Power that Causes the accumulation Tons of Materials , and Resulting the action of Change in Material and the Natural of Reaction Generated from Material that Causes Pollution .Research aims to put Sustainable Building (in the point of view of Material that constructs it) in front of nature of Forces that causes Material Change and Changes Through the Running Time of Building age and so….to Have a Wide Lines on Effected Forces of the same Materials that used in Buildings

and causes Environmental Pollution , Today used in the Sustainable Buildings but in the Form that Reeducate the Environmental Pollution of it.

The Research based on the study of Power's Nature That effected materials and influenced by , and its effects on the Environment system, to be the case study of this study.

* خلاصة البحث:

باتت في السنوات الأخيرة مشكلة الحفاظ على مصادر البيئة الطبيعية الناضبة مورقاً يروح ويجيء ليضع خطاً فاصلاً بين حدين, يكمن احدهما في موازنة مصادر البيئة الطبيعية والأخر في تقليل استغلالها, إلا أن أخطرهما الحد من الآثار السلبية المتولدة على تلك البيئة. فجالت سنوات الخبرة الطويلة في مجال العمارة لوضع أفكار معمارية حديثة بهدف المحافظة على مصادر الطاقة والموارد الطبيعية واستدامتها, فتمخضت الجهود بما يعرف اليوم بالأبنية المستدامة التي تعد الأبنية ذات التأثير الأقل ضرراً على البيئة الطبيعية مع المحافظة على الخواص البيئية الجيدة داخل الأبنية .

وبما إن المادة هي لمكون الأساس للتشكيل الذي يعتمده المعماري للإنشاء المستدام (Sustainable Construction) والمظهر لقيام تجربة بنائية متكاملة الخواص في مجال العمارة وتقليل الضرر البيئي . لكن المادة كانت سابقاً ولا تزال تعد حجر الأساس الذي أثقل كاهل الطبيعة باستئصال مواردها بصورة مستمرة لتطرح أطناناً من المخلفات الإنشائية في مكبات النفايات وعلى حدود الطرقات واستغلال لهكتارات من الأراضي الزراعية. هذه المواد الإنشائية الخطرة تتراكم دون معالجة في اغلب الدول, مما يولد قوة رد فعل سلبية على تلك البيئة نتيجة التفاعلات المتبادلة لتلك المواد مع بعضها .

لذا توجهت هذه الدراسة بمشكلة مفادها توضيح ماهية وطبيعة القوى المسلطة المسببة لتراكم أطنان المواد , والمحدثة لفعل التغير على المادة وطبيعة رد الفعل الداخلي المتولدة عن المادة والمسبب للتلوث. لتهدف الدراسة إلى وضع المبنى المستدام من جهة المادة الداخلة في إنشاءه أمام القوى الخفية المسببة لتغير وتغيير المادة خلال فترة عمر المبنى التشغيلي وما بعده, ليكون لدينا خطوط عريضة على القوة المؤثرة على المادة نفسها التي كانت تستعمل في الأبنية والمسببة للتلوث البيئي واليوم تستعمل في المباني المستدامة لكن بصفة مقللة للتلوث البيئي الناجم عنها.

وقد اعتمد البحث في هذا على دراسة طبيعة القوى المؤثرة على المادة والمتأثرة بها وتأثيراتها على المنظومة البيئية ليكون أساس الطرح التطبيقي لهذه الدراسة.

*** المقدمة:**

إن عملية تقليل تأثير البيئة المشيدة على البيئة الطبيعية وتحسين فعالية المبنى لضمان حياة ذات جودة عالية للأجيال المستقبلية يعتبر المقصد الأول للاستدامة,فالمبنى المستدام هو الذي يكون له اقل ما يمكن من التأثيرات الضارة على البيئة الطبيعية ككل, فيتميز بكفاءته في حفظ مصادر الطاقة المتجددة مع كفاءته في تقليل التلوث (Pollution) بمادته المستعملة والأساليب التصميمية والتقنية المتكاملة . (بن حسين, الاستدامة في تصميم المباني,ص. 1-4) (Lawson,1989,p.161) (Mol,A.P.J.,2001,p.43) , وبذلك تقوم الاستدامة على محاور مختلفة تشمل الأتي:

- الموقع والأرض العمرانية المشيد عليها المبنى المصمم .
- الابتكار والتصميم المعماري , بضرورة وضع تصاميم متكاملة ذات فائدة في جوانب الإنارة , والتكييف والتصميم الداخلي والإنشائي.فالمبنى ضمن الموقع يمثل منظومة ايكولوجية خلال جعل الملائمة (Accommodation) أساس مخطط المبنى لتدوير الطاقة بكفاءة .
- إدارة الطاقة , بتقليل الأثر السلبي على المبنى المنشأ وعلى البيئة الطبيعية ,أي كفاءة مصادر الطاقة المتجددة (Renewable Resources) مع كفاءة طاقة المصدر(Energy).
- جودة البيئة الداخلية.
- إدارة المواد والمخلفات, والتي تقع تحت طائلة استخدام مواد وموارد طبيعية مع العناية بدورة حياة المادة في الطبيعة بتحسين تلك المادة.

وهنا يتناغم مع قانون حفظ الطاقة الشكل (Form) والتقنيات الغشائية الخارجية للمبنى مع المادة والألوان . فتوظف المادة ذات القابلية على العزل الحراري والانعكاس للإشعاع وإعادة التوجيه والتشتيت, لتقوم بحفظ الداخل عن الخارج وبالشكل المطلوب , وتحت قانون الحفاظ على الطاقة (Lawson,1989,p.152).

إن معرفتنا أن المادة هي المكون الأساس للتشكيل المعماري , وهي المظهر الذي يعتمد المعماري صياغته ليشكل البيئة المعاشة , ومن معرفة محاور الاستدامة وربط التصميم المعماري وطبيعة البيئة الداخلية التي يحويها وسبل تقليل الطاقة بالمادة التي تدخل في المنشأ المعماري, وطريقة استخدامها ومكانها , وطبيعة تأثيرها إذا فقدت خصائصها على الموقع والتصميم إذا لم يراعى مكان وضعها وخصائصها ,يعتبر محوراً مهما يسلط الضوء على ماهية هذه المادة عندما تكون محوراً أساسياً أكدت عليه الاستدامة.

***هدف البحث ومشكلته:**

إن ماهية القطب المادي تتجسد في قابلية البشر في زمان ومكان معين على تنفيذ النتاج

المعماري وفق الأسلوب المتوفر , حيث تتفاعل الإمكانات التكنولوجية والمعرفة العملية والوسائل التقنية وطريقة توزيع العمل وأساليبه لتشكل السبب لتحقيق الأفعال في المادة الخام (السدخان ,1999,ص.51).هذه المادة الخام (هي محل) مع صورة (وهي حالة) لتلك المادة , فالصورة هي العلة التي تعطي للمادة الوجود , حيث تهيمن الصورة على ذات المادة بتأثير قوة تفعل في المادة فعل التشكيل الفيزيائي الظاهر, وبإخفاق المادة شكلياً نتيجة لسيطرة قوة خارجية مؤدية (لفعل التغير الخارجي عليها) فتبقى تلك المادة مرتبطة مع منظومة الحقول المكونة لها مما قد تسبب أثاراً سلبية على الطبيعة المحيطة المنتمية إليها تلك المادة بمرور الزمن(ابن سينا, "مكتبة الكترونية",ص.83) (الحجيات,2005,ص.98). فبناء نظام بيئي مادي يكون مصحوباً بتنوع كبير من المواد الناتجة من أنشطة البناء, فبعد إن كان يعتقد بان إخفاق المادة عن أداء دورها الشكلي يمكن أن تصنف كمواد خامدة (Inert Materials) , أصبحت ألان تصنف على أنها مادة سمية يمكن إن تسبب مخاطر جسيمة على صحة الإنسان والبيئة (السواط,2004,ص.122).

أن المشاريع المعمارية الخدمية والصناعية ستستنزف كميات ضخمة من المواد الطبيعية لتعيدها بعد انتهاء عمرها الزمني كأثر سلبي (نفاية) على البيئة الأم مسببة إلى ترابط قوة المادة مع قوة المنظومة الكونية مما يؤدي إلى نتائج سلبية لا تحمد عقباها (السواط,2004,ص.), وبموجب ذلك تم تحديد مشكلتي البحث وفق الأتي :

مشكلة البحث العامة, والتي قد انطوت تحت وضع خطوط عريضة على حجم المشكلة المهددة للبيئة في المادة المشكلة لها, حيث تلقي الضوء على طبيعة التأثيرات السلبية المتولدة في المحيط, جراء استمرار تراكم المواد المختلفة للمشاريع الخدمية والصناعية المسببة للتلوث البيئي المستمر .أما المشكلة الخاصة , فهي فتح أفق للتعرف على طبيعة القوة الهجينة للحقول المخفية وراء المادة من استخراجها وتشكيلها ككيان فيزيائي إلى الاستغناء عنها مؤثرة ومتأثرة بالبيئة المحيطة والموقع الإقليمي . ليكون هدف البحث : مواجهة خصائص المادة المتغيرة التي تسبب التلوث المستمر على البيئة من جهة, مع المادة نفسها المستعملة لإنشاء المبنى المستدام ,الذي يعد استعمال مواد قليلة الضرر على البيئة محوراً مهما أكدت عليه الاستدامة.

* **القــوة :**

تعرف القوة بكونها نتاج ومحصلة الظواهر الطبيعية , وهي ترتبط بموفولوجيا المادة التي تتناول المفهوم الديناميكي الذي يتعامل مع تفسير مصطلحات القوة, وهي تأثير يدفع أو يجذب المادة فيؤدي إلى توليد حركة. ترتبط القوة ارتباطا وثيقا بكل العمليات الطبيعية وهي تتراوح من حيث حجمها بين القوى الضئيلة في القوى الذرية الصغيرة إلى قوى الجاذبية الضخمة الموجودة

ما بين الكواكب والنجوم. إن القوى كمية موجهة بمعنى إن لها حجما واتجاهاً معيناً , وإذا تغير احد المكونين , فسوف تكون القوة عرضة للتغيير (Thompson,1975,pp.14-270) (آل نهيان,2006,موقع الكتروني) .

وقد قسم ابن سينا القوة إلى ثلاثة أنواع , وهي قوى سارية في الأجسام التي تحفظ كمالها في أشكالها ومواضعها الطبيعية وأفاعيلها وإذا زالت عن موضعها الطبيعي وأشكالها وأحوالها أعادتها إليها وثبتتها عليها مانعة إياها من حالة اللا معرفة إلى التسخير لتسمى القوى الطبيعية . أما النوع الثاني فهي القوى القسرية التي تفعل في الأجسام أفعالها من تحريك أو تسكين وحفظ نوع , بينما النوع الثالث من القوى فستكون تلك التي تفعل فعلها لا بآلة بل بالإرادة المتجهة لتسمى نفساً فلكية (ابن سينا, "مكتبة الكترونية",ص.84) .

*** المادة :**

إن المادة المستخرجة من مصادر الطبيعة لها صورة تحل بها للظهور إلى الرأي فتشكل كل ما علا على سطح الأرض من منشأ, وان هذه المادة لها أبعاد ثلاثة, يتقاطع الامتدادان الأوليان بزاوية قائمة أما الامتداد الثالث فيقاطع الأوليان على زاوية قائمة أيضا, وبالتالي يغلب الوجود الفيزيائي للمادة. إن المادة لا تتعرى عن البعد الذي فيه نفرض الأبعاد الثلاثة ولا يوجد البعد على انه جزء من وجود المادة بل هي خارجة عن ذات المادة وان كانت حالت فيها مقارنة, وان البعد ليس بذات المادة بل هي مستعدة لقبوله وبالتالي فالمادة مستعدة لقبول الحجم فما فوقه وما دونه والانتقال من حجم إلى حجم, فيمكن للمادة الانفصال من ذاتها إلى مادتين ثم معاودة الاتحاد دون مشكلة في ذاتهما ألا من ناحية الأبعاد الحيزية التي تستغلها المادة , فيزداد الحيز نتيجة لتمانع أبعاد المادتين بالطباع فالبعد يوجب المقاومة ويمنع التداخل ويعني زيادة الحجم الأصلي فيصبح اكبر من حجم المادتين المتلاقيتين. ويطلق على صياغة المادة الأساسية شكلاً, فالجانب المحسوس أو البين من الصورة يدعى شكلا , وبذلك فشكل الشيء صورته المحسوسة أو المتوهمة , وتشكل الشيء : تصور شكله: صوره. وبالتالي فالشكل هو نشاط كل مادة كاملة ويمثل مبدأ الفعالية (Action Principle), فيتم انجاز كل فعالية من خلال الشكل والذي يمكن جعله حاضراً بمساعدة الطبيعة الفيزيائية ويعد حلاً لمشكلة معينة يحددها المحيط , وعند التكلم عن عملية التصميم لا يجب مناقشتها كشكل منفصل لوحده بل كشكل مع مادته ومحيطه, يمكن له أن يتغير ويتأثر بالمحيط إذا تغير أي عنصر من عناصره.(ابن سينا, "مكتبة الكترونية",ص. 83 ,101–102) (جودت, 1995,ص.9) (Fischer,1963,pp.116-117) (Alexander,1967,pp.15-16).

- المادة الإنشائية :

تعد المادة الوسيط الذي يحول النمط الفكري المعماري المسبق إلى نموذج فيزيائي إنشائي ملموس يتحقق فيه مبدأ إنشائي معين للتغلب على القوة المؤثرة على المبنى والمنشأ (Structure) وفق تخطيط معين . تتحقق عملية التحويل للمادة إلى شكل مادي باستنزاف قوة من النظام البيئي مع موارد مستمرة من المادة الأولية والماء والغازات, فتتأثر البيئة بذلك الكيان المضاف وتؤثر بدورها البيئة على الكيان الفيزيائي أو الشكل الجديد في كل مراحله, فهو يتأثر بالبيئة من حيث القوة المسلطة ويؤثر بها بنوع أخر من القوة (السدخان,1999,ص.56)(ابن سينا, "مكتبة الكترونية",ص.84)(السواط,2004,ص.118).

لذا فسيتم التعرف على خصائص المادة الإنشائية والقوة المسلطة عليها المادة , ومن ثم ربط تأثير تلك القوة مع النظام البيئي بشكل متبادل .

- خصائص المادة الإنشائية :

تختلف خصائص المواد المستعملة من واحدة إلى أخرى , لكنها تتشابه بإمكاناتها في المقاومة للقوة المؤثرة الخارجية. فالقوة المسلطة على المنظومة الشكلية للمادة تتغير وتختلف بحسب طبيعة الفعل المسلط ألدائمي أو المؤقت لآنية الشكل وإمكانية تقبله للتغير المستمر .فالمادة بتعاملها مع المحيط الخارجي البيئي تتقبل التغيرات كفعل القوة المسلطة من البيئة برد فعل داخلي لفعل التغير الانفصالي أو الاتصالي للقوة المسلطة , أي يحصل مقاومة داخلية طبيعية للمادة تدعى الانحراف (Deformation) الذي يتعرض له شكل العناصر الإنشائية, فيظهر تغير بسيط للترتيب الداخلي للمادة سرعان ما يختفي ليعود الترابط الداخلي للمادة بمجرد زوال القوة المؤثرة لخاصية المرونة بالمادة(Elastically Materials) .كمثال الأجسام التي تمتلك شكلاً ستاتيكيا كالأجسام الصلبة مثل الحجر , الفولاذ, الألمنيوم تملك خاصية عدم الحساسية للتشوهات (Perturbations) أي حالة من الصلابة •,وإذا مرت بتفاعل مع منظومات خارجية فإنها تبقى متماثلة شكليا مع نفسها بالتأثير على استقراريتها التركيبية (Structural Stability) فتجتمع الأجزاء الأولية للمادة غير القابلة للتجزئة (الذرات) بطريقة معينة, ويحصل قوة التغيير نتيجة إعادة الترتيب الذري الداخلي للمادة بطريقة مغايرة لما كانت عليه فيعاد صياغة المنظومة الشكلية كرد فعل لقوة التغير المسلطة على المادة. ولكن يمكن أن تعجز المادة عن حالة الاتزان الطبيعية أي تصل إلى حد المرونة (Elastic Range) بسبب التأثير المتزايد للقوة فتتحول قوة رد الفعل بدل من كونها مقاومة للجسم إلى قوة مفعول بها

• الصلابة :هي درجة التغير في شكل المادة بفعل القوة المسلطة عليها,ترتبط بمعامل المرونة, فكلما كانت قيمة معامل المرونة عالية كانت المادة صلبة. ومثال ذلك الفولاذ والألمنيوم والحجر (السدخان,1999,ص.59).

,فيتغير الشكل الظاهري الفيزيائي مؤثراً على المنظومة الشكلية الأصلية . فتتصرف المادة هنا بلدانة (Plasticity) بدل المرونة , فتبقى المادة مشوهة , ويتناسب التشويه مع مقدار القوة المسلطة بشكل غير ثابت فتزداد بسرعة بعلاقة طردية ويستمر كتشوه حتى بعد زوال القوة المسلطة .فالمادة ببلوغها نقطة الخضوع تتحول من صفة المرونة التي تحسب للمادة تخطيطياً من قبل المصمم في المنشأ إلى صفة اللدانة التي تعد تشوهاً للمادة . كمثال على ذلك زيادة تأثير قوة التشويش المسلط على المادة الإنشائية فيحصل لها لدانة أو ما يعرف بالإخفاق التام الاعتيادي نتيجة عدم استقرارية قوة التغيير• الداخلي للمادة,(شكل –1). (ابن سينا, "مكتبة الكترونية",ص. 84) (جودت,1995,ص.9) (Alexander,1967,pp.15-16) (الحجيات,2005,ص. 98, 63–65) (Thom,1975,pp.19-102) (السدخان,1999,ص. 58–59) .

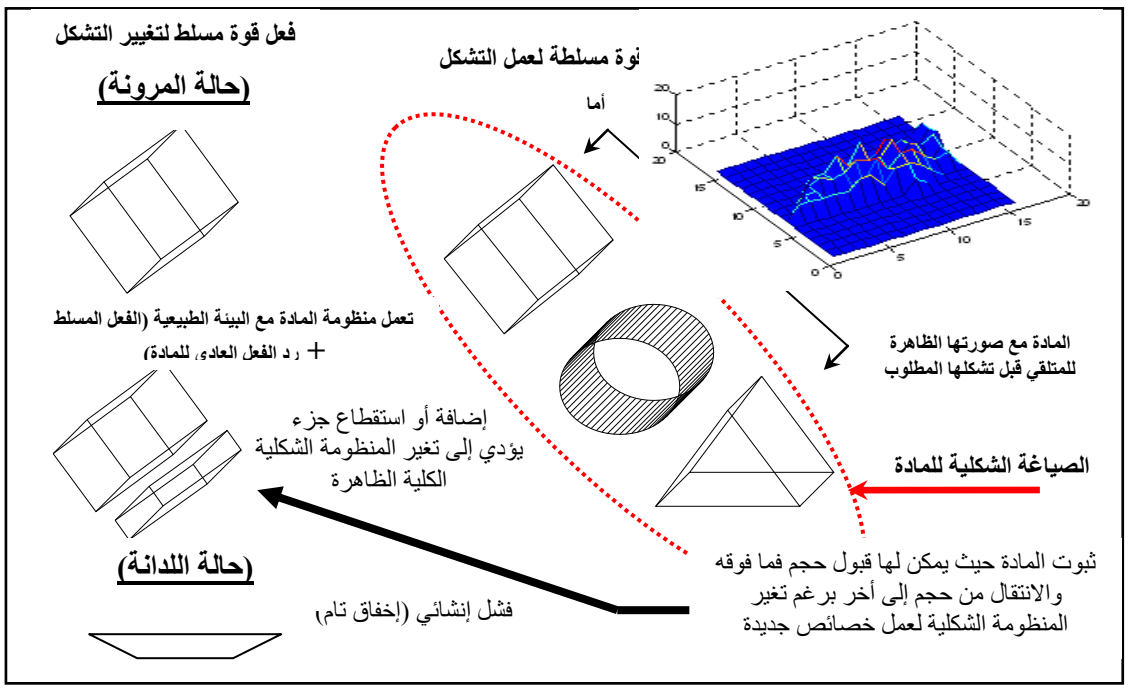

(شكل–1) حالة الثبوت والتغيير الشكلي (الفشل الإنشائي) للمادة (الباحثة)

عن مصدر : (السدخان,1999,ص.58–59) (الحجيات ,2005,ص98 , 63–65)

(ابن سينا,مكتبة الكترونية,ص.84)

إن التفكير المسبق بنوع المادة يوفر قدرة داخلية في المادة لمقاومة أنواع الإجهاد الذي تسببه القوة المؤثرة على بنية الشكل نتيجة لوجوده في البيئة (السدخان ,1999,ص.55).

• إن التغيير صفة مرتبطة بعوامل داخلية خاصة للمادة وهي ضرورية لتقبل الشكل المتطور المتقبل لكل التغيرات الخارجية والملائم لعصره ومواد بناء البلد المنشأ عليه ,أما التغير فهو صفة خارجية مرتبطة بالعوامل الخارجية التي تحاول إحداث التغير والتي تظهر عادة على ما يمكن رؤيته من المبنى المعماري, ترتبط هذه الصفة بكم ونوع المعلومات ومن خلالها يظهر تأثيرها (الحجيات,2005,ص.98).

لذا يلاحظ أن خصائص المادة تتغير عند عدم قدرة المادة على تحمل القوة المسلطة من البيئة عليها لمرونتها القليلة أو لان القوة المسلطة اكبر من معامل المرونة لديها , مما يسبب فشلا شكليا وبالتالي إنشائياً.

- **<u>الأداء الوظيفي للمادة الإنشائية ضمن حدود العمر الزمني :</u>**

إن المادة تبقى تحمل صورتها الظاهرية التي صاغتها أيدي أرباب العمل مؤدية لوظيفتها , حيث تتداخل النظم المادية مقاسمة لغة عامة (رمزية Syntax) ومتفقة في المعاني (Meaning) والمقصود عند الرسائل التي تغيرها داخلياً والتي تعمل كمختارات للسلوك (Manor Selection)وردود الفعل تجاه تغير حالة المناخ الخارجية الطبيعية.لكن يمكن أن تحصل حالة انتهاء العمر الاقتصادي للمبنى ,وبالتالي تتجاوز المادة ببقائها خطاً احمر قد خط لها ألا وهو العمر المادي (Physical age) أو الفعلي للمبنى الذي يمكن أن يكون أطول من العمر الاقتصادي لذلك المبنى . ويعد تحت طائلة إدخال منشأ مادي إلى النظام البيئي متضمن سلسلة التفاعلات المتبادلة المستمرة حتى تتم إزالة ذلك المنشأ من حيز البيئة المعمارية العمرانية ليتراكم كمخلفات في حيز مناطق تجميع المخلفات, مع احتمالية استبقاء عمر لهذه المادة المكونة .وبالتالي تتراكم المادة في مساحات الأراضي الشاسعة وحدود الطرقات, ومما يؤخذ بالاعتبار حجم المادة المتراكمة الفيزيائية كوجود سلبي إضافة إلى الآثار غير الفيزيائية غير المنظورة المؤثرة بصورة مباشرة أو غير مباشرة آنية و مستقبلية ناتجة من تغير خصائص المادة الكيميائية وتولد الانبعاث الضار وحجم التلوث المتسبب, (شكل – 2).(شاهين,ألبدري,2007,ص.144)(الحجيات,2005,ص.98)(Stitt , 1999,p.43) (ألبدري,2006,ص.14–15, 206) (السواط ,2004,ص.

وبالتالي فيلاحظ إن فشل المادة يكون أما نتيجة الإخفاق الشكلي ومن ثم الإنشائي , أو بسبب انتهاء عمر المبنى بأداء وظيفته فيلغى من حيز الوجود . وعليه تبقى بعض المواد كشكل في حيز الوجود دون أدائها لوظيفة معينة.

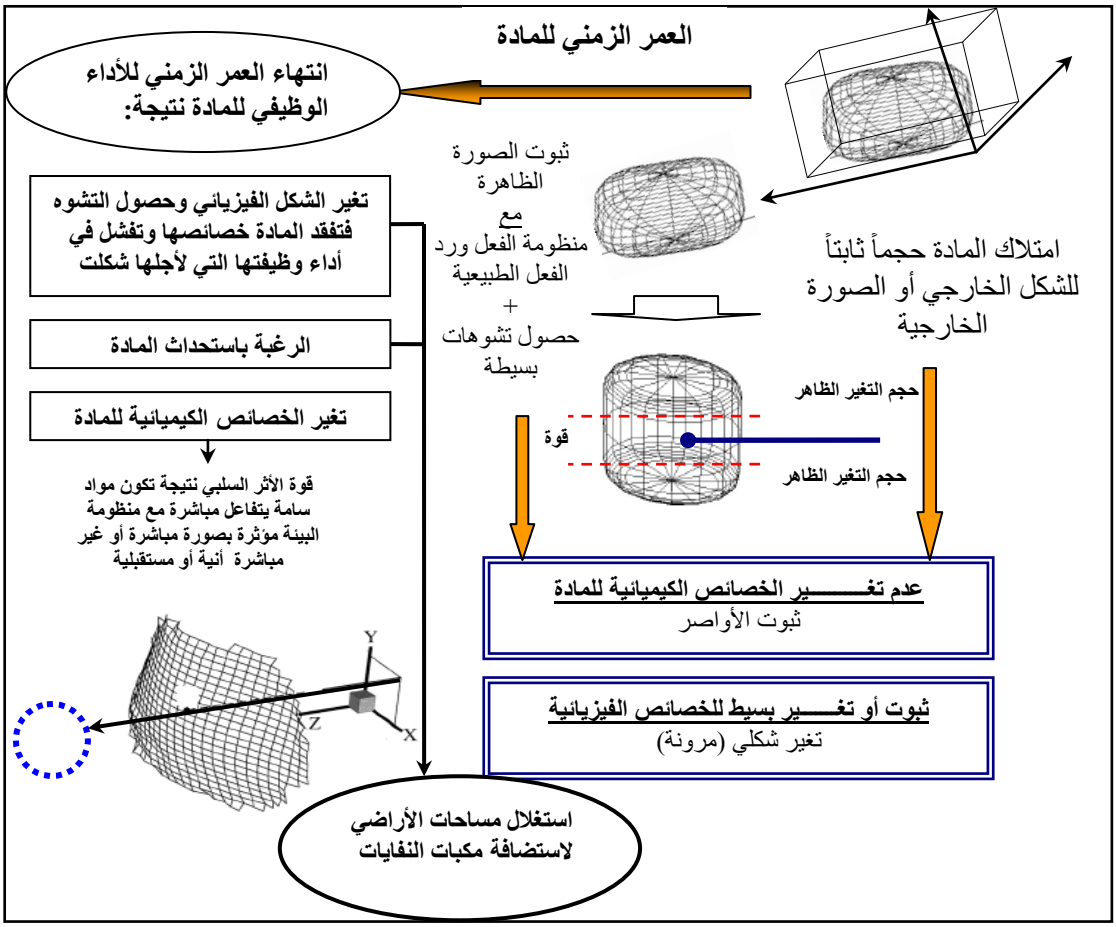

(شكل – 2) ثبوت وتغير الخصائص الفيزيائية والكيمائية للمادة خلال العمر الزمني المقرر

(الباحثة) عن مصدر (ألبدري,2006,ص.14–15 ,206) (لجنة في وزارة التربية العراقية,2006,ص.15–18) (السواط,2004,ص.124–132)

– المادة كنفاية صناعية :

تعد النفايات الصناعية الصلبة مواد معقدة التركيب وغير متجانسة , وتقل قيمتها الاقتصادية عن تكلفة جمعها لإعادة استخدامها, ومن ثم يتم التخلص منها باعتبارها مخلفات للإنتاج.لا تقتصر صعوبة التخلص من المخلفات الصلبة على حجمها الضخم, لكن بعض هذه المخلفات مثل العلب المعدنية ونفايات البلاستك وهياكل السيارات القديمة وكذلك مخلفات البناء تستطيع مقاومة العوامل الطبيعية إلى حد كبير (تغير الخصائص الفيزيائية مع ثبوت أو تغير الخصائص الكيميائية), ولذا لا يمكن التخلص منها بسهولة وتبقى من ملوثات البيئة الثابتة التي لا تتغير لسنوات عديدة والتي تسبب أثارا سلبية ناتجة من زيادة حجم الانتروبيا (الطاقة السلبية)المتولدة كقوة مؤثرة على المنظومة البيئية , حيث لا يمكن للنظام البيئي الطبيعي القيام بالتحامها فيسبب تفكك أواصر المنظومة المادية البيئية (المنظمة العربية للتنمية الصناعية والتعدين,2002, ص.1–2) (عيد,2001, ص.234).

- تفكك الأواصر الطبيعية للمادة :

إن استمرارية المادة بالوجود كنفاية يعني استمرارية خضوع المادة لعوامل الطبيعة وتأثيرات الموقع, وهذا يعني بدأ مرحلة تفكك أواصر المادة (التأثير الكيميائي),إذ بمجرد إن تبدأ القوة باللعب على طبيعة الأواصر المكونة لتلك المادة فإنها ستعمل على تفككها لتبدأ عملية التغيير الداخلية, وهي انتصار فعل القوة على رد فعلها الطبيعي الذي لا يستطيع مقاومة القوة فيبدأ بحصول نوع من التفكك بين الأواصر (حالة التغيير الكيميائي) نتيجة دخول المادة المنتقاة تفاعلاً مع ما موجود في الطبيعة من غازات ومواد متراكمة سواءً أكانت صلبة أم غازية فيحصل لها ترتيب فضائي مؤقت بين ذراتها يدعى المعقد النشط , يكون الأخير غير مستقر بسبب طاقته العالية سرعان ما يتفكك, ليعطي أما المواد المتفاعلة نفسها فلا يحدث تفاعل أو ليعطي النواتج,(شكل – 3).(لجنة في وزارة التربية,2006,ص.15–18).

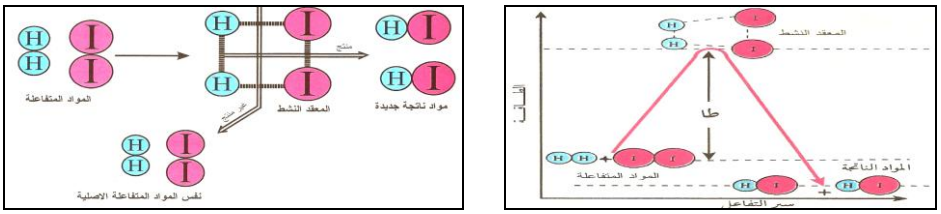

(شكل – 3) مخطط يوضح المواد المتفاعلة والناتجة من التفاعل والمعقد النشط

(لجنة في وزارة التربية,2006,ص.17–18)

وعليه فالمادة النافقة الداخلة حيز التفاعل والتي حصل لها تغير فيزيائي وأخر كيميائي والناتج عن تفكك أواصرها ,قد أصبحت مواد أخرى لا يمكن الاستفادة منها وتراكمت في مناطق تجميع النفايات وبدأت هذه المواد مع ما يسلط عليها من قوى تبث إلى المحيط قوى من نوع أخر هي سلبية في كثير من الأحيان. وكمثال على ذلك جزيئة البنزين (C6H6) تعد من المواد السامة جداً حيث تعرقل تشكل الدم في النخاع العظمي والحد المسموح به منها في المناطق الصناعة (20 ملغم / لتر), يمكن لحلقة البنزين أن تغير ذرة أو أكثر من ذراتها بذرة أخرى ويمكن لها تفكيك أواصرها نتيجة لقدرة ذرات الكاربون على الارتباط مع نفسها أو مع غيرها بطرق عديدة فقد ترتبط بروابط أحادية أو ثنائية أو ثلاثية , فبعملية الاحتراق الناتجة من العمليات الصناعية تنتج نواتج عرضية هي حصيلة التغير الشكلي للبنزين منتجةً الكاربون(C) وأول اوكسيد الكاربون (CO) وثاني اوكسيد الكاربون (CO2) مع إنتاج طاقة عرضية هي حرارة متولدة من عملية الاحتراق ,(شكل – 4).

أما اتحادها فيمكن لحلقتين من البنزين الاتحاد مع ذرتي أوكسجين عند كربون مجاور على كل حلقة من حلقتي البنزين لينتج مركب ثنائي البنزين متعدد الكلور متعدد الديوكسينات

(PCDD)عالي السمومية ويمكن استمرار الاتحاد لينتج (17) متجانس بذرات كلوردين يمكن إن تحل في المواقع (2) (3) (7) (8) (أي المواقع الأحادية) (شكل – 5), لتشكل خطراً على الصحة والبيئة فبزيادة الإحلال من أربع إلى ثماني ذرات كلوردين تسفر عموما عن نقص ملحوظ في القدرة (لجنة في وزارة التربية العراقية ,2006,ص. 166–215) , (برنامج الأمم المتحدة للبيئة" اتفاقية بازل وستكهولم",2004,ص. 6–9).

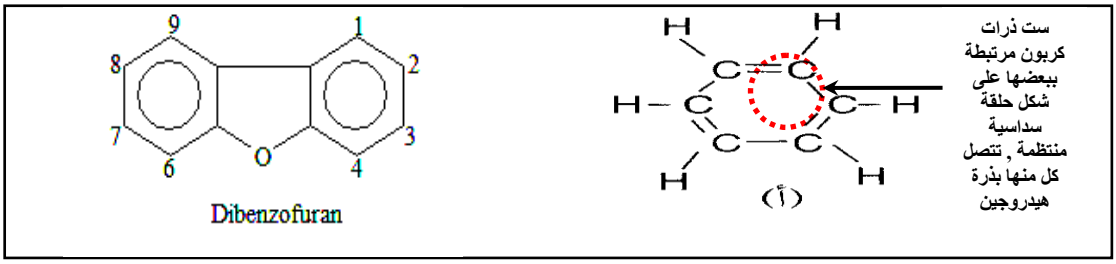

(شكل – 4)جزيئة البنزين (C6H6) **(شكل – 5) مركب ثنائي البنزين متعددة الكلور متعددة الديوكسينات**

(لجنة في وزارة التربية,2006,ص.206)

(برنامج الأمم المتحدة للبيئة,2004,ص. 6)

إذن المادة الداخلة كنفاية إلى البيئة تصبح بعد فترة مادة أخرى نتيجة دخولها حيز التفاعل مع البيئة والغازات والمواد الصلبة والسائلة , فتصبح مواد ذات سمية عالية.

–المادة كأثر سلبي على المنظومة البيئة :

إن القوة المتولدة من المادة والمؤثرة عليها تبقى مرتبطة مع النظام البيئي الطبيعي الأزلي المرتبط بالكون, بحيث أن الأثر السلبي المتولد من الأنبعاثية الضارة ينعكس من منظومة المادة إلى المنظومة الكونية المترابطة معاً, وبهذا فان النسق الجديد لا يمكن الوصول إليه أو الإحاطة به ,إذ أصبح الإنسان غير قادر على معرفة الظواهر بذاتها (التفسير الرياضي) بل يمكنه فقط العلم بأحوال الظاهرة وتفسيراتها المتعددة تبعا لتغيرها.فالنسق الكوني المفروض علينا هو ما يهمنا بهذا النظام المادي ,لنكون مدركين بضرورة التلاعب بالوسائل والغايات للأجزاء المكونة للكليات الأكبر والتي تعمل مع بعضها بطريقة تخدم البيئة المنسقة بين الأنظمة المختلفة. إن فشل المادة شكليا لن يقصي الكتلة أو قوة الطاقة الناتجة,فإحراق وردة حتى تستحيل رماداً لا يمكن أن يحول الطاقة إلى الفناء والدليل أن الكتلة تبقى بعد زوال شكلها الأساسي.كما إن فشل المادة المستعملة في تشكيل الأبنية أو عدم استغلالها لن يلغي الأثر السلبي الذي سيتولد منها بمرور الزمن(ألبدري,2006,ص.5–6, 14) (بريجز,1986,ص.163–179).

– حقول القوة الخفية المؤثرة والمتأثرة بالمادة :

وهي مجموعة معقدة من الحقول الخفية غير الظاهرة (Hidden Fields) التي تدير جميع مراحل التشكل الجيني للكائن الحي وتعطي للأشياء شكلها النهائي. تبدأ من الأجسام الصغيرة المكونة للمادة, فتتكون من ذرات لها حقل خاص بها يختلف عن حقلها عندما تكون الكترونات أو جزيئات , يدار من منظومة مختلفة كلياً عند نهاية وجود المادة بالطبيعة التي تسيطر عليها وترتبط بدورها مع النظام الكوني وصولا إلى المجرات الأكبر. فيسيطر الحقل الأكبر على الحقل الأصغر وهكذا بترتيب تصاعدي متشابك , فتتشابك الحقول غير المادية ذات الإبعاد الميتافيزيقية الخارجة عن إطار ما يمكن قياسه , تدخل الزمن وتتأثر به وتستمر مع استمرار الزمن اللانهائي , وعند هلاك أو تحول المادة فان الحقول المولودة لن تموت حتى لو بادت المادة المكونة لهذه الحقول . توجد في الإشكال الساكنة كالمادة المكونة للهيكل الإنشائي وهذه الحقول تعمل بالارتباط مع قوى المادة وخصائصها, حيث يكتمل للكينونة شكلها النهائي ويبقى حقل الشكل في مكانه ليثبت الشكل النهائي أمام اضطرابات البيئة. (بريجز,1986,ص.163-179) (Handler ,1990,p.25) (ابن سينا ,"مكتبة الكترونية",ص.84).

إن التراكم المستمر للمواد المتخلفة دون معالجة سيؤدي إلى سحب مستمر للطاقة الموجودة في الطبيعة والمتمثلة بالمادة الأولية, والغازات , المياه,....الخ, ومن ثم بعث نوع من القوة لا يمكن الاستفادة منها هي (الانتروبيا) التي ستبقى داخل نظام البيئة فيحصل اختلال بالنظام الكوني نتيجة حجم المخرجات التي لا تستطيع الكائنات الحية التي تقتات على النظم السالبة (الانتروبيا) الإيفاء بحجمها (أي اختلاف حجم المدخلات مما يعني إخلالاً في عملية الموازنة) , مما يجعل رد الفعل الطبيعي لا يوازي الفعل المسلط على المنظومة البيئية فيسبب خللاً في النظام البيئي ومن ثم النظام الكوني عموماً(شاهين,ألبدري,2007,ص.143) (الحجيات,2005,ص.56-58).

من ملاحظة السابق , نرى أن المادة تنتج من البيئة باستنزاف مواردها, ومن ثم تعمل كشكل لأداء وظيفة معينة ,تتعرض لقوة الطبيعة باستمرار فتتفاعل معها بتأثير متبادل بين الفعل ورد الفعل, ويحصل الفشل الإنشائي باستمرار لزيادة قوة الفعل عن قدرة المادة على التحمل, أو لان القوة في النظام البيئي لم يتم حسب حساب لها,أو ربما قد ينتهي العمر الاقتصادي للمبنى . فتدخل المادة كنفاية إلى النظام البيئي كقوى سلبية مؤثرة عليه, لان المادة تتقبل حجم فما فوقه ويمكنها الانتقال من حجم إلى الأخر فتتفاعل مع ما موجود في الجو من غازات وتتحد معها, فتسبب التلوث البيئي . لذا فالتلوث البيئي سببه ليس خصائص المادة في قابليتها على التحمل فقط بل أيضاً قد تكون الخصائص عالية ولكن انتهاء العمر

الاقتصادي للمبنى مع استبقاء عمر مادي يسبب تراكم المادة كشكل فيزيائي دون معالجة وتتفاعل قوة المادة مع قوة البيئة فتتولد غازات سامة تسبب التلوث الذي يتحد بدوره مع النظام البيئي الكلي.

*** قطاع البناء والتفكير المستدام :**

لقد تعالت الأصوات لتعاظم خطر التحديات البيئية التي أصبحت تهدد كوكب الأرض, وفي مقدمتها تناقص الموارد الطبيعية بشكل كبير وارتفاع معدلات المخلفات والملوثات. فجاء مؤتمر مستقبلنا المشترك عن البيئة والتنمية (1987م) مشدداً على أهمية مشاركة قطاعات البناء والتشييد في الحفاظ على البيئة وخفض إنتاج مخلفات البناء وإعادة استخدامها .ولذلك تم وضع قطاع البناء تحت المجهر للموارد الأولية المتزايدة التي يستنزفها ومعدلات المواد المتخلفة الناتجة عنه . فقد أظهرت الدراسات المبكرة التي قام بها المعهد العربي لإنماء المدن في عام (1986م) حجم مخلفات البناء والهدم بنسبة (69.4%) من المجموع الكلي لجميع المخلفات الأخرى بشتى أنواعها في (42) مدينة عربية . وحلاً لذلك ظهرت أفكار حديثة للحفاظ على البيئة والتطوير المستدام, وضعت على عاتقها الإيفاء بالتزامها في الحفاظ على البيئة, وتقليل التلوث.(السواط,2004,ص.117-118) وواجهت عدة مشاكل منها :

1. تنامي الحاجة لبناء أعداد إضافية من المساكن , الأسواق, المصانع, المباني الصحية....الخ.مما يعني تزايد حجم المواد الأولية المطلوبة من البيئة.
2. استمرار عمليات ترميم وصيانة وهدم المباني القديمة القائمة , مما يجعل من مشكلة المواد المتخلفة من البناء بتزايد مستمر.

لقد عدت الاستدامة الحفاظ على البيئة , بتقليل المادة المستنزفة منها , وتقليل تأثير تلك المادة على البيئة في أول بنودها . وبما أن قطاع البناء يعتمد المادة في أنتاج الوحدات الجديدة, وكذلك ما يلقى بعد انتهاء العمر الزمني للمبنى مادة متخلفة عنه , لذا فبدراسة الاستدامة والمادة يمكننا أن نجيب على مدى أمكانية التفكير المستدام في تقليل التلوث البيئي بالمادة .وهل يمكن آن يعد التصميم المستدام فعلاً مقللاً للآثار السلبية على البيئة بطبيعة الترابط بين القوى المشكلة للنظام البيئي .ألإجابة على ذلك خلال الأتي :

- دراسة المادة وفق التفكير المستدام :

إن المواد المستعملة في أنشاء الأبنية المستدامة هي نفسها التي كانت تستعمل في إنشاء مثيلاتها من الأبنية, فتتشابه في خصائصها للمقاومة والمتانة والصلابة (السدخان ,1999,ص.).إلا أن هنالك بنود ظهرت بالتفكير المستدام للبيئة تم التأكيد عليها, وهي :

- إمكانية التلاعب بخصائص المادة :

خلال السنوات القليلة الماضية ومن خلال التقدم التكنولوجي في حقول مواد البناء, حصل تلاعب كبير بخصائص المادة ,فتميزت اليوم باقتصاديتها ,وسهولة وسرعة تثبيتها بالهيكل الإنشائي ,قيم عزل عالية لتحقيق استهلاك بالطاقة, مقاومة للحريق,مع قابلية عالية لمقاومة الرطوبة والتعفن والتلف.لقد تم تحقيق نوعيات عالية من متطلبات الأبنية المستدامة باستخدام أنواع من المواد سواء العازلة أو الناقلة كاستخدام (Fiber Optics) حيث يمكن نقل (1 ميكابايت) في الثانية , ويمكن أن يزيد إلى (ألف ميكابايت) في الثانية باستخدام تقنية الليزر (ألبدري,2006,ص.78,35). إن تطور المواد وتحسين خصائصها لم يتوقف فقط على العزل والمقاومة, لكن تميزت المواد بخفة وزنها وإمكانية تحملها العالية للإثقال كالمعدات المعدة لاستقبال الرافعات السككية (Monorail) والجسرية(Cranes).كما تم توظيف الأبعاد المودیولية (Modular Dimension) للمرونة والتنوع,كالتي استعملت في مشروع معمل (Cambria) لإنتاج رغوة وحبيبات البلاستك في ولاية بنسلفانيا,لتقليل عمليات الإتلاف والفضلات الإنشائية العرضية. كما تم في كثير من المشاريع تقليل استعمال الاصماغ التقليدية الحاوية على نسب مختلفة من المكونات العضوية الطيارة (VOC) في عمليات التسطيح و الاستعاضة عنها بمادة الاولفين البلاستيكي ذا اللحام الحراري (المصدر السابق,ص.218,216).لقد ظهر تطور اكبر لعشرات من المركبات والسبائك المعدنية عن طريق ما يعرف بنظام المواد الذكية, بالاستعانة بأحدث البرامج الحاسوبية,وقد تم استخدام هذه المواد المتطورة في كثير من الصناعات المختلفة مثل صناعة المنظومات الإنشائية المتطورة وهياكل السيارات .وتعد مواد لها القابلية على إصلاح نفسها ذاتيا لدى تعرضها لتأثير القوة الخارجية المدمرة,وبذلك يعود الهيكل الخارجي بعد تعرضه لقوة الفعل الصادمة إلى ما كان عليه. حيث تم التوصل إلى صناعة مادة تحوي ملايين الكبسولات الممتلئة بسائل ترميمي هو من مادة (Dicyclopentadiene), هذه الكبسولات لا يتجاوز قطرها 250 جزءاً من البوصة,ولدى تعرض الهيكل الخارجي إلى قوة خارجية فان تلك الكبسولات تتمزق محررة سائل الترميم والذي هو عبارة عن تلك المادة البوليميرية,عندها تعمل الخاصية الشعرية على سحب السائل إلى مكان الصدع أو الشق,والذي يتصلب في غضون دقائق وينجم عن ذلك عودة الهيكل إلى ما كان عليه بنسبة(90%))(موقع الدي في دي العربي, 2007, موقع الكتروني علمي). يمكن لهذه الآلية استهلاك كافة كبسولات الإصلاح , ومن هنا تواصلت الأبحاث لتطوير مواد أكثر فاعلية,ففي مختبر كالتش لعلوم المواد تم ابتكار ما عرف بالسبيكة الفقاعية(Bubbloy),والتي تتكون من البلاديوم والنيكل والنحاس والفسفور,وتتميز بخفة وزنها ومتانتها العالية وقدرتها على استعادة شكلها الأصلي ذاتياً بعد تعرضها لقوة خارجية تسبب انبعاجها أو تشوهها.إن اعتماد أسلوب

التغذية الاسترجاعية(Feedback) خلال عملية التصميم الأولية وصولاً للتصاميم النهائية النموذجية من خلال اعتماد عملية تحليلية للمادة في منشأ افتراضي لكل ساعة في برامج حاسوبية بدلاً من المعرفة المتأخرة بحجم الضرر , وبهذا سيساعد هذا الأسلوب على تزويد المصممين بالمعلومات الدقيقة مما يقودهم إلى اتخاذ القرار التصميمي الصحيح والناجح في التعامل مع المادة واختيارها(Whole Building Design,2000,pp. 1-4)(Snyder,1979,pp.151-163) (موقع الدي في دي العربي, 2007, موقع الكتروني علمي).

-مفهوم إمكانية التدوير :

ويعني إعادة استخدام المادة الملوثة أو النافقة للحد من تأثيرها على البيئة وزيادة الاستفادة من الخامات المستخدمة , إن عملية تبادل النفايات تستند على افتراض بسيط مفاده بان نفاية صناعة ما يمكنها إن تكون المادة الخام لصناعة أخرى. ليمثل أفضل حل للتعامل مع النفايات من خلال إعادة دورة حياة تلك المواد التالفة , لضمان القياس الصحيح للمدخلات وتخفيض التلوث أثناء النشاط الاقتصادي وبعده (المنظمة العربية للتنمية الصناعية والتعدين,2002,ص.2-3 , 5). إن عملية التحول هذه تؤدي إلى تغير خواص المادة الفيزيائية بمعالجة طبيعية ,حيث إن الكثير من الأبنية العامة والمصنعية تم فيها أكساء الأرضيات الخارجية المغطاة بألواح الفايبر عالي الكثافة المصنوع من مخلفات الورق المعاد, وذلك للحد من الآثار السلبية المتولدة من منظومة المادة المصغرة إلى النظام البيئي الأكبر دائرة فيه,(شكل-6).(المنظمة العربية للتنمية الصناعية والتعدين,2002,ص.6)(ألبدري,2006,ص.218).أن المادة التالفة ترتبط بمقياس يعرف بالانتروبيا (يمثل الطاقة الفائضة غير المستفاد منها في نظام الثرموداينامیكا المغلق) (Closed Thermodynamic System). أن الكائنات الحية تقتات على الانتروبيا السالبة ليديم النظام الحي نفسه بحالة توازن من خلال استيراد مواد غنية بالطاقة ,إذ تعمل ردود أفعالها الداخلية على زيادة الأنتروبيا , مما يعطي حالة التوازن. ولتطبيق ذلك تم توظيف الأنظمة الحيوية في النواحي الإنتاجية , حيث تستخدم البكتريا المهندسة وراثياً في صناعة الإنزيمات للتخلص من بعض النواتج والمخلفات الصناعية, فأكثر من (60%) من الإنزيمات المتواجدة في الأسواق تنتج بواسطة عمليات التخمر الميكروبي.فمثلا بكتريا (Alicaligenes entrophus) التي تم اكتشافها في بلجيكا منذ عشرة سنوات , تناول المعادن الثقيلة وتخزينها داخل خلاياها وامتصاصها داخل أغشية مختصة ليتم فيما بعد ترسيبها داخل أماكن خارجية, وتتم هذه العملية بواسطة الأكسدة المباشرة للايونات الذائبة والممزوجة.(المنظمة العربية للتنمية الصناعية والتعدين,2002,ص.2-3 , 5) (ألبدري,2006,ص.137).

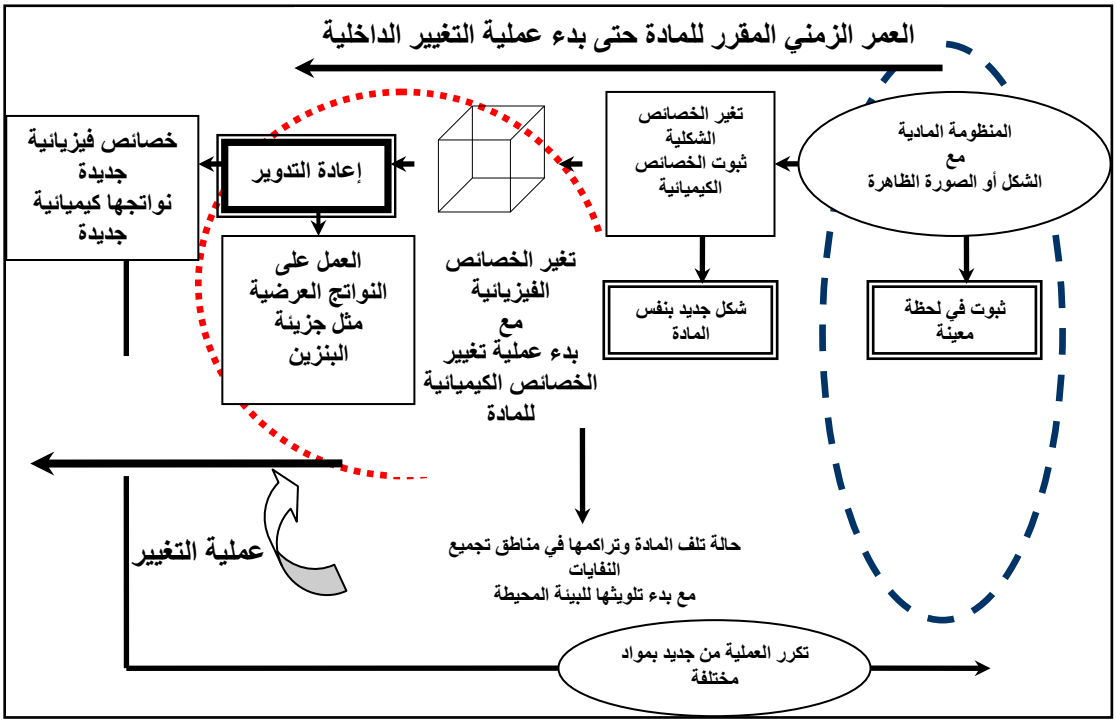

(شكل – 6) عملية التدوير وعلاقتها مع خصائص المادة (الباحثة)

عن مصدر : (Stitt,1999,pp.40-50)

– مفهوم إعادة الاستخدام :

يخضع أي مشروع معماري في دورة حياته لعملية تبديل لبعض أجزاءه وقطعه بصورة مستمرة نتيجة للعطل والتلف مما يؤدي إلى تراكم المواد كنفايات بصورة مستمرة. فجاءت التوجهات الحديثة لتطرح مفهوم جديد هو إزالة البناء (Deconstruction) وهي عملية معاكسة للبناء وتختلف عن الهدم , حيث يتم إزالة جميع الأجزاء الصالحة للاستخدام من المبنى قبل الهدم لتستخدم في المباني الجديدة.حيث تم في معمل (Philip Merrill) لإنتاج حبيبات اللدائن المعادة استعمال مواد إنشائية تالفة كالكونكريت المكسر من المواقع القديمة الموجودة في ولاية ماري لاند الواقع فيها, ليرصف به الطرقات والممرات الجديدة للمعمل, مما يضيف ربح معاكس لعملية تبديل بعض الأجزاء في حالة العطل,(جدول –1). (بن حسين, الاستدامة في تصميم المباني,ص.4) (ألبدري,2006,ص.220–221).

(جدول-1) ابرز المواد الإنشائية والمنشائية التي يتوقع أن تنتج من المشاريع
(Guthrie & Mallett ,1995,p.20)(السواط,2004,ص.128)

أنواع المواد المستخدمة وبالتالي الناتجة	إمكانية إعادة استخدامها	إمكانية تدويرها
المواد الأولية كالرمل والحصى والصخور	أمكانية عالية	غير متاح
الخرسانة كمادة أولية بالبناء	أمكانية عالية	أمكانية عالية
الحوائط الحجرية (Masonry)	أمكانية عالية	أمكانية عالية
الطابوق	أمكانية عالية	أمكانية عالية
البلاط	أمكانية عالية	أمكانية منخفضة
الخشب	أمكانية عالية	أمكانية عالية
الزجاج كالخلايا الشمسية	أمكانية منخفضة	أمكانية عالية
المعادن المستعملة بالأطر	أمكانية منخفضة	أمكانية عالية
البلاستيك كعوازل وزجاج بلاستيكي عازل	أمكانية منخفضة	أمكانية عالية
الكيماويات (الدهانات والمذيبات)	غير ممكن	أمكانية متوسطة

* تقليل الآثار السلبية على المنظومة الكونية:

يمكن تقليل الآثار السلبية المتولدة من تراكم مواد البناء خلال اعتماد منهج المبنى المتكامل , الذي يتميز بتنوع الحلول فتارة يتعامل مع القوة المسببة للفعل بحل وقائي منذ بداية العملية التصميمية , وأخرى يكون بهيئة جرعات علاجية عند المراحل الحرجة من العملية التصميمية أو التنفيذية, وبمعنى أن أنظمة المبنى ككل تتصل وتتعقد وتتكامل بعلاقات مشتركة مترابطة ذات اعتماد متبادل بين الفعل ورد الفعل بتغذية عكسية استرجاعية من خلال التنبؤ المسبق بكل أفعال القوة وتأثيراتها لوضع الحلول وتداركها, حيث تم التأكيد على أن المبنى تتكامل فيه الأنظمة لإدارة المصادر الفيزياوية المادية المرتبطة بالبناء والمصادر غير الفيزياوية وتتمثل بطبيعة القوى المختلفة المسلطة على المنظومة المادية . ووفق ذلك عرف المبنى وفق منظور الفعل ورد الفعل المتبادل بأنه منظومة مادية والتي تؤلف الأجزاء الرئيسة للمبنى (الغلاف الخارجي, الهيكل الإنشائي, الفضاءات الداخلية, المكونات التكميلية والخدمية وغيرها). وهذا يعني أن لكل مجموعة من العناصر ميزة تفاعلية لزمان ومكان معينين والتي تهيكل النظام العام مع البيئة , متضمنة العلاقات الاتصالية والانفصالية مع البيئة المحيطة. إن طبيعة القوة المكونة للمبنى المادي هذا تتميز بصفة التنظيم والعلاقات مع المحيط والتفاعل بين العناصر مما يجعل النظام المادي قادراً على حل المشاكل بنفسه أي إصلاح أنسجته المصابة بنفسه كحال الكائن الحي بعملية التغذية الاسترجاعية (Feed back) .(ألبدري,2006, ص.135-136)

(Handler,1990,p.22) (Croom , 1998,p.24) (موقع الدي في دي العربي, 2007, موقع الكتروني علمي).

إذن الاستدامة لم تغير المادة الموجودة لكنها لعبت بخصائص المادة , ونظرت نظرة شاملة على كل المراحل التي تمر بها المادة,حتى مرحلة نفاق المادة ليتم إعادة استخدامها أو تدويرها ,بالتالي النظرة الشمولية هي التي ميزت التصميم المستدام في تقليل التلوث البيئي.

* التطبيق العملي :

يمكن ملاحظة كيفية تطبيق فكر الاستدامة الرامي إلى اعتماد النظرة الشمولية في الكثير من الأبنية العالمية اليوم,التي اتخذت من تقليل المادة الملوثة للبيئة هدفا لها ,وكالاتي :

- مشروع مركز "RETREAT" للمعماريان Sanjay Prakash ,TERI (1997-2000) :

وصف المشروع : يقع إلى جنوب مدينة دلهي الهندية على مساحة(3000 متر مربع) مؤلف من بنايتين واحدة سكنية والأخرى لإقامة البحوث , يحيط به الحزام الأخضر من كل الجهات.

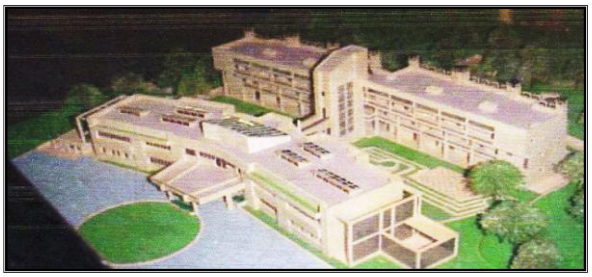

(شكل -7) مبنى مشروع "RETREAT"(Nayak,2005,p.15)

أسباب اختيار المشروع : لقد تم اختيار المشروع لكونه قد صمم ليكون مستقلا بذاته في توليد الطاقة التي يحتاجها المبنى المستدام مع استخدام منظومات التظليل والكاسرات الشمسية , مع توظيف طرق العزل المختلفة , وخزانات الماء , الخلايا الضوئية , وقنوات التبريد المضافة إلى تصميم المبنى لتعد معالجات في استخدام المنظومات المنفعلة (Passive) والطاقات الطبيعية المتجددة. (www.sustainable-buildings.org/case1.pdf).

المعالجات المستخدمة لتحقيق الأداء البيئي الجيد للمبنى ,مع منظومة المادة المستعملة:

- العوازل المختلفة لتقليل الأحمال الحرارية على المبنى كاستعمال الكونكريت الخفيف والمجوف (Vermiculite Concrete), كما يتم استعمال في الجدران (بولستيرن).
- كاسرات شمسية لتظليل الفتحات.
- السخانات الشمسية لتزويد المبنى بالماء الحار ومن مواد معادة التصنيع.

- الخلايا الكهروضوئية لتوليد الطاقة الكهربائية ,مع بطاريات لخزن الطاقة الفائضة.
- القنوات الأرضية للتهوية بإبعاد (70×70سم) تدفن تحت الأرض بأطوال قد تصل إلى (70م) تحافظ على حرارة المبنى وتعمل على تزويده بالتهوية المطلوبة في الأيام المترية .
- المداخن الشمسية ذات الغطاء المعدني لتسخين الهواء المحيط .
- نافخات الهواء (Blower) لتعمل مع منظومة القنوات الأرضية.
- منظومة تبخير (Air washer) ميكانيكية للمحافظة على حرارة المبنى.
- مداخن شمسية لتستغل قابلية مرونة حركة الهواء بواسطة أغطية معدنية فوق المداخن بتسخينها يندفع الهواء الساخن للأعلى ليحل محله هواء القنوات الأرضية البارد.

تحليل المنظومة المادية (Nayak,2005,p.15) :

- خصائص المادة : تم التلاعب الكبير بخصائص المادة كحال اغلب المواد المستعملة حديثاً, حيث تميزت بخفتها مع إمكانية تحمل عالية مثل السطوح المكونة من الكونكريت الخفيف والمجوف...الخ مما يقلل من المادة المستنزفة من البيئة إذا كان المنشأ أكثر ثقلاً, كما انه يزيد من خصائص المادة للتحمل والقدرة على مقاومة القوة المسلطة من البيئة.
- إمكانية التدوير : حصل استعمال مواد معادة (Recycle) ليحفظ كم هائل من المواد المتوقعة لهكذا حجم من البناء , فمثلا القنوات الأرضية قللت من الكثير من المواد التي يمكن أن تستهلك من البيئة, كذلك عمليات الرصف للطرقات الخارجية .إن استهلاك المواد المعادة جنب البيئة إطلاق ألاف الأطنان من غاز (CO_2) وغازات البيت الزجاجي.

لذا فعملية التفكير المسبق بحجم المدخلات التي يحتاجها أي مشروع وما سيتم توفيره من مادة أولية لتشغيله , وحجم المخرجات وأين توضع وكيف تعالج هو من الأساسيات التي يجب أن تدخل ضمن عملية التصميم المعماري لأي مبنى .

*الاستنتاجات:

- إن سبب التلوث البيئي هو تراكم المواد دون معالجة نتيجة لفشل المادة أمام القوة البيئية المسلطة, أو لفقدان الضرورة لتلك المادة فترمى كنفاية .
- يحصل للمادة النافقة تحلل فيزيائي– كيميائي يسبب انبعاث غازات سامة فيتسبب التلوث.
- حقول القوى الخفية هي مجموعة من الحقول المخفية التي تربط النظام الكوني ومن ثم البيئي بنظام المادة , فتربط قوى التلوث الخاصة بالمادة مع باقي المنظومة الكونية بتشابك , فتسهم المادة مع غيرها من المواد بتلويث مستمر لا يمكن التئامه.

- جاء التفكير المستدام , ليؤكد أن المادة الداخلة في منشأته هي نفسها التي استعملت في مثيلاته وتعالت الصيحات عليها لتسببها بالتلوث البيئي, لكن مع تلاعب كبير بخصائص المواد بحيث تستطيع تحمل القوى المسلطة بشكل اكبر مع خفة بالوزن لتقليل استغلال موارد البيئة .
- تم اعتماد النظرة الشمولية بالأبنية , حيث يتم التفكير بالمادة كشكل بأبسط مدخلات مع أحسن خصائص, يضاف إلى ذلك التفكير بالمادة إلى أين تصير بعد انتهاء الحاجة منها.
- جاءت عمليات التدوير وإعادة الاستخدام كحلول لتقليل استنزاف خامات الأرض, مع تقليل التراكم الفيزيائي للمواد وبالتالي عمليات التحلل المادي والمسبب للتلوث .

لقد جاءت التوصيات معتمدة :

- ضرورة وجود دراسات فاعلة وجدية للقوة المسلطة على الأبنية ومحاولة بناء نظام لتوقع طبيعة رد الفعل لتلك القوة , لتدارك المواقف قبل نشوء الأثر السلبي على الطبيعة. ولخدمة ذلك وجب التأكيد على :

– ضرورة استعمال موارد متجددة كالمواد المنتجة من نباتات نامية بدل استعمال موارد لا يمكن استبدالها كخامات النفط والغاز الطبيعي .

– انتخاب مواد كفيلة بتحويل المبنى إلى كائن حي فعال متبادل المنفعة الايجابية مع البيئة الطبيعية.

– العمل على أن تكون المادة مع صورتها تعمل كمجموعات متداخلة ومترابطة من المنظومات المادية التي تنظم لغرض تشكيل المبنى والحفاظ على طاقته من ولادته إلى حالة انتهاء عمره الزمني.

– جعل النظام المادي المصمم كمنظومة متداخلة مع الموقع من خلال جعل الملائمة أساس المخطط الموضوع لإعادة تدوير المادة بكفاءة (Recycled).

– التأكيد على علاقات النظام الرئيس للمبنى المتداخل مع البيئة والأنظمة الثانوية التي تتصل وتتعقد وتتكامل مشتركة بترابط ايجابي متبادل.

– إعادة تصنيع المواد الاستهلاكية من مواد معادة التصنيع أو من مصادر متجددة الطاقة وبدون تلويث للبيئة أو استنزاف للمصادر.

– اعتماد المنظومة الإحيائية الحية كأساس لعمليات التدوير (Recycled).

- ضرورة عمل دراسات تختص بتحليل وتفكيك الأواصر المادية لاستكشاف إمكانية إعادة تصنيعها والحد من أثارها السلبية المتولدة عند إتلافها, مما يعني ضرورة إصدار قرارات وتشريعات للتقليل مما ينجم من مخلفات على الطبيعة .

وبالتالي بات المبنى يعمل كمنظومة حية تتغير خصائصها الفيزيائية ومن ثم الكيميائية ليعاد العمل على عملية (التغيير) هذه لخلق خواص فيزيائية كيميائية جديدة يمكن أن تكون معولاً جديداً لأبنية لها القدرة على خلق نظام عمراني حديث قادر على التفاعل والعيش مع الإنسان والبيئة في مجموع مدخلاته ومخرجاته معاً.

*** المصـادر العربية:**

- ابن سينا,"كتاب النجاة", القسم الثاني" الطبيعيات", ويكي مصدر, المكتبة الحرة, موقع الفلسفة الإسلامية, جمع وترتيب محمد حزين , تحديث للصفحة 15 ديسمبر 2007.
- ألبدري,امجد محمود عبد الله,"التطور والتغير في الفكر الجديد لعمارة الأبنية الصناعية الذكية" , أطروحة دكتوراه- جامعة بغداد ,2006.
- الحجيات,أنفال مؤيد, "الحركة في الشكل المعماري المتطور",دراسة تطبيقية لإمكانية قياس المسار المستقبلي المستمر للشكل المعماري المتطور, رسالة ماجستير- الجامعة التكنولوجية , 2005 .
- السدخان,سهير كريم "المادة والشكل" ,دراسة تحليلية للنماذج المعمارية المعاصرة ,رسالة ماجستير-جامعة بغداد,1999م.
- السواط,علي بن محمد:" أساليب إدارة المخلفات الإنشائية والفرص المتاحة لتدويرها",مديرية إدارة تنسيق المشاريع -أمانة مدينة الدمام, السعودية, 2004م.
- المنظمة العربية للتنمية الصناعية والتعدين ,"المنظور الجديد لإدارة النفايات الصناعية الصلبة في المنطقة العربية" ,الرباط-المملكة المغربية ,2002.
- آل نهيان,محمد بن زايد,"خصائص الحركة الموجية", مكتبة دروس وبحوث الشيخ محمد بن زايد, بحوث ودروس الفيزياء,17-12-2006.
- برنامج الأمم المتحدة للبيئة , مؤتمر الأطراف في اتفاقية استكهولم بشأن الملوثات العضوية الثابتة, مادة(1) 2005+ اتفاقية بازل ," المبادئ التوجيهية التقنية بشان الإدارة السليمة بيئيا للنفايات التي تحتوي مركبات ثنائي البنزين متعددة الكلور متعددة الديوكسينات..... التي تنتج دون قصد أو الملوثة بها ", 2004.
- بريجز، جون:" الكون المرأة" ، ترجمة : نهاد ألعبيدي, الدار العربية- بغداد,1986.
- بن حسين,هند راشد,"الاستدامة في تصميم المباني",
- www.fewa.gov.ae/Image/_dbpics/environment/enviro1_ar.pdf
- جودت,احمد عبد الجبار:"بنية الصورة المعمارية في ضوء نظرية المعرفة الإسلامية", رسالة ماجستير مقدمة لقسم العمارة, كلية الهندسة , جامعة بغداد,1995.

- شاهين, بهجت رشاد– ألبدري,امجد محمود – "منظومة السيطرة على آلية عمل المبنى الصناعي كنظام للمحافظة على الطاقة",مجلة الهندسة–جامعة بغداد,2007.
- عيد,محمد عبد السميع :"التخلص من مخلفات البناء ... مدخل وتطبيق" سجل أبحاث ندوة إدارة المخلفات الصلبة , المعهد العربي لإنماء المدن ,الرباط , المملكة المغربية (نشر بمجلة البناء السعودية, العدد 109), مايو– يونيو,2001.
- لجنة في وزارة التربية ,"الكيمياء" للصف السادس العلمي, المشرف العلمي : كاظم رشيد موسى, الطبعة العشرون ,2006م.
- موقع الكتروني للأخبار العلمية ,"الدي في دي العربي",2007.

DVD4ARAB.COMhttp://hazemsakeek.com/magazine/images/stories/news/get-7-2007-nj9efc5j.jpg

- **المصادر الأجنبية:**

- Alexander ,Christopher :"Notes on the Synthesis of Form" ,Harvard University , Press Cambridge,Massachusetts,1967.
- Croom, T.D.G. Clements "What Do We Mean by Intelligent Building", Paper; Dept. of Construction Management & Engineering; University of Reading; U.K., 1998.
- Fischer, Ernest :"The Necessity of Art ",A Marxit Approach ,Translated by : Anna Bostock ,London ,1963.
- Guthrie & Mallett (1995), Waste Minimization and Recycling in Construction- A Review, A Report Published by Construction Industry Research and Information Association (CIRIA), London, UK.
- Handler ,A ,Benjumin; "System Approach to Architecture ";American Elsevier publishing company inc; New Yorck,1990.
- Lawson, B.R. The act of designing Desugn Methods and Theories, University of Sheffield Department of Architecture. – England, 1989.
- Mol, A.P.J. "Globalization and Environmental Reform:" The Ecological Modernization of the Global Economy, MIT Press, Cambridge, U.S.A. 2001 .
- Nayak,J.K.-Energy Systems Engineering ,Mombai,India-2005.
- Snyder ,J. "Introduction to Architecture Design and the design process", Mc, 'Graw -hill book Co. ,1979.
- Stitt ,F. A, "Ecological Design Handbook: Sustainable Strategies for Architecture, Landscape Architecture, Interior Design and Planning ", Mc Graw –Hill , New York, 1999.
- Thom ,Rene: "Structural Stability and Morphogenesis",W.A.Benjamin,Inc.,Canada,1975.

- Thompson,D Arcy : On Growth and Form, Cambridge University Press,London,1975.
- "Whole building design" ,U.S. Department of Energy ,office of building ,BTS,London ,2000.
- www.sustainable-buildings.org/case1.pdf

المحددات التصميمية لمباني القلاع التاريخية في العراق
(دراسة تطبيقية لقلعة كركوك)

الاستاذ طالب حميد الطالب والباحثة هدى صباح
جامعة بغداد – كلية الهندسة قسم المعماري

الخلاصة:

إن القلاع التاريخية تجهزنا بنقاط اتصال مع العصور السابقة وتعطينا صور مختلفة باختلاف الازمنة والامكنة التي هي بمثابة رسائل ترسلها الأجيال السابقة الى الأجيال اللاحقة مع فكر الحماية المعاصر لتوليد نمط عمراني محمي يستلهم معطيات الماضي ويستثمر إبداعات الحاضر، التي بنيت لتلعب دورا عسكريا وسياسيا واجتماعيا واقتصاديا وتخدم أغراضا متنوعة مما جعلها وحدات معمارية مميزة لذا ركز البحث على القلاع التاريخية في العراق ودراسة معالمها المعمارية وتحليل أهم محدداتها التصميمية، من هنا تبلورت فكرة مشكلة البحث نتيجة قلة الدراسات الأكاديمية المتوفرة عن القلاع وكيفية تطويرها، واستهدف البحث التعرف على القلاع وأنماطها، وأفكارالحماية الامنية عبر التاريخ، واستجلاء خصائص القلاع المحلية بغية التوصل الى أسلوب عملي تطويري للتعامل مع الموجودات الحضرية والعمرانية في قلعة كركوك.

Design Criteria for Historic Fortresses Buildings in Iraq
(Case Study Kirkuk Fortress)

ABSTRACT:

Historic fortresses are providing us with an immediate point of contact with old ages, are giving us different images because of different times and places, they are like materialistic messages from past generations to the present with a contemporary protect thought in order to be a motivation for present creative works, which were built to take military, political, social and economic role, to serve a whole variety of purposes this is what makes fortresses as specific architectural units, so the research concentrated on historic fortresses in Iraq and studied its architectural landmarks and design criteria, therefore the problem is appointed by little studies related to fortresses, and how should be developed, the aims of research are: studying of fortresses, their types besides security defensive concepts, finding out characteristic samples of local experiences in dealing with the fortified fortresses. This fact gave the author motivation to lay ground for a practical method and updated study to give Life to the urban and architectural existences in Kirkuk fortress.

Fortresses are large fortified buildings or group of buildings usually dominating the surrounding country or a stronghold converted to different uses like cultural, social, residential and tourist activities, or a site of ancient earthworks.

There are many classification of fortresses that depend on several factors like: pattern, historical way, time, region, …etc

Most of fortresses have defensive fortified factors like: fortified elements, strategic site, physical shape and construction

More care and attention should be devoted to such monuments like fortresses, whether single buildings or urban agglomerations because of their present state are a source of environmental pollution rather than focal points of interest and attraction.

Iraq is especially wealthy in historic fortresses, a fact that calls for continuous and serious efforts to bring it to its active state, so that it may not remain as neglected and useless.

According to the above facts, the research is oriented to historic fortresses in Iraq especially Kirkuk fortress, as it is very rich in its historic and traditional buildings and urban configurations.

Although several studies were conducted to bring up the dilapidated state of Kirkuk fortress up to the accepted operational active state of construction, but very little was actually done to bring the plans into action.

This reality was one of the main motives to orient this research to this location, especially that the germs of dilapidation are still effecting what remains of its heritage, whether because of war devastation, theft, or neglecting.

Although there are few studies related to the reconstruction of Kirkuk fortress it remains as a superficial and outdated to be a real and effective solution to the present state of the fortress. This fact led the author to verbal proposals and suggestive planning ideas for the physical development in Kirkuk fortress.

The proposal indicated the division of the fortress into three distinctive areas:

Conservation area, Mixed area, and an area of new urban design.

The research ended up with a proposal and recommendation to deal with such locations.

The research focuses on the "Improvement of Kirkuk fortress based on its design criteria" in dealing with its three proposal distinctive areas: Conservation area, Mixed area, and an area of new urban design.

تمهيد:

يقسم البحث الى أربعة محاور: ففي المحور الأول يتم التعرف على مفهوم القلعة وانماطها الرئيسية والمحور الثاني يشمل دراسة الأساليب والعناصر المعمارية المتبعة في تشكيل فكر الحماية لمباني القلاع عبر التاريخ، أما المحور الثالث يعنى باستجلاء نماذج من القلاع المحلية وتحليل أهم محدداتها التصميمية ومعالمها التحصينية والتركيز على قلعة كركوك باعتبارها موضوع الدراسة، والمحور الرابع فيمثل الجانب التطبيقي لتطوير قلعة كركوك من خلال اعداد تصاميم جديدة مقترحة توضح ماسبق.

المحور الأول: القلعة وأنماطها

- تعريف القلعة:

لغوياً:

قلع الشيء (بفتحتين) : نزعه من موضعه، واقلع عن الأمر، تركه وكف عنه واقلع الشيء، انجلى وانكشف، مثل اقلع السحابة، وأقلعت الغمة، وأقلعت السفينة. والقلع (بكسر القاف وسكون اللام): شراع السفينة والقلعة. والقلع (بفتح القاف وسكون اللام): جمع قلوع قلاع أي حصن ممتنع (عاصم-2000).

اصطلاحاً:

في قاموس ويكيبيديا (Wikipedia Encyclopedia) ، تم التركيز على تعريفين رئيسين للقلعة:

- إنها مبنى كبير محصن، أو مجموعة من المباني محاطة بجدران سميكة وغالبا ما تكون مهيمنة على بقية أرجاء البلدة كما انها ملائمة للسكن ويتم استخدامها عن طريق تحويرها.
- إنها مكان للخصوصية، السرية، الأمن أو الملجأ.

وذكرت في (Oxford English Dictionary): هو مكان حصين (A fortified Place) يضم مبنى كبير أو مجموعة من الأبنية أو بقايا وحواجز ترابية أثرية قديمة (EL-Ezabi-1984).

والقلعة طراز من الحصون شاع استخدامها في القرون الوسطى لحماية المدن من العدوان الداخلي والخارجي، وخاصة في العصور التي كثرت فيها الاضطرابات والحروب. ويراعى في اختيار موقعها أن يتميز بالعلو والارتفاع ليشرف على الأرض المحيطة بها (عاصم-2000).

اذن القلعة هي وحدة معمارية قائمة، سواء كانت قصرا، أو مبنى مهم، أو مدينة، وتشترك جميعها بامتلاكها موقع إستراتيجي وعوامل تحصينية دفاعية، ولها قيم معنوية ومادية مميزة، الشكل (1-1).

- انماط القلاع:

- انماط القلاع حسب المسميات:

يمكن تقسيم القلاع حسب مسمياتها إلى ثلاثة أنواع متمايزة:

- القصر (Palace): عبارة عن مبنى فخم، ويستخدم عادة للسكن ويمتاز بصالة رئيسية (Great hall)
- لاستقبال الضيوف وكبار الزوار.
- البلاط الملكي (Royal castle): قصر ذا صفة جليلة يدار من قبل الحاكم والغرض منه التحصين بوجه الهجوم وهذه المملكة تحافظ على السيادة في أوقات السلم أو الحرب، وتلعب دورا رئيسيا في الشؤون السياسية للبلاد ،وتمثل مركزا للقوة والسلطة والقرارات المهمة.
- المدينة المحصنة (Fortified city) : مجموعة من الأبنية شيدت او حصنت لاغراض دفاعية عسكرية (www.mcgilluniversity) وهي أكثر المسميات متوافقة مع موضوع البحث عن قلعة كركوك.

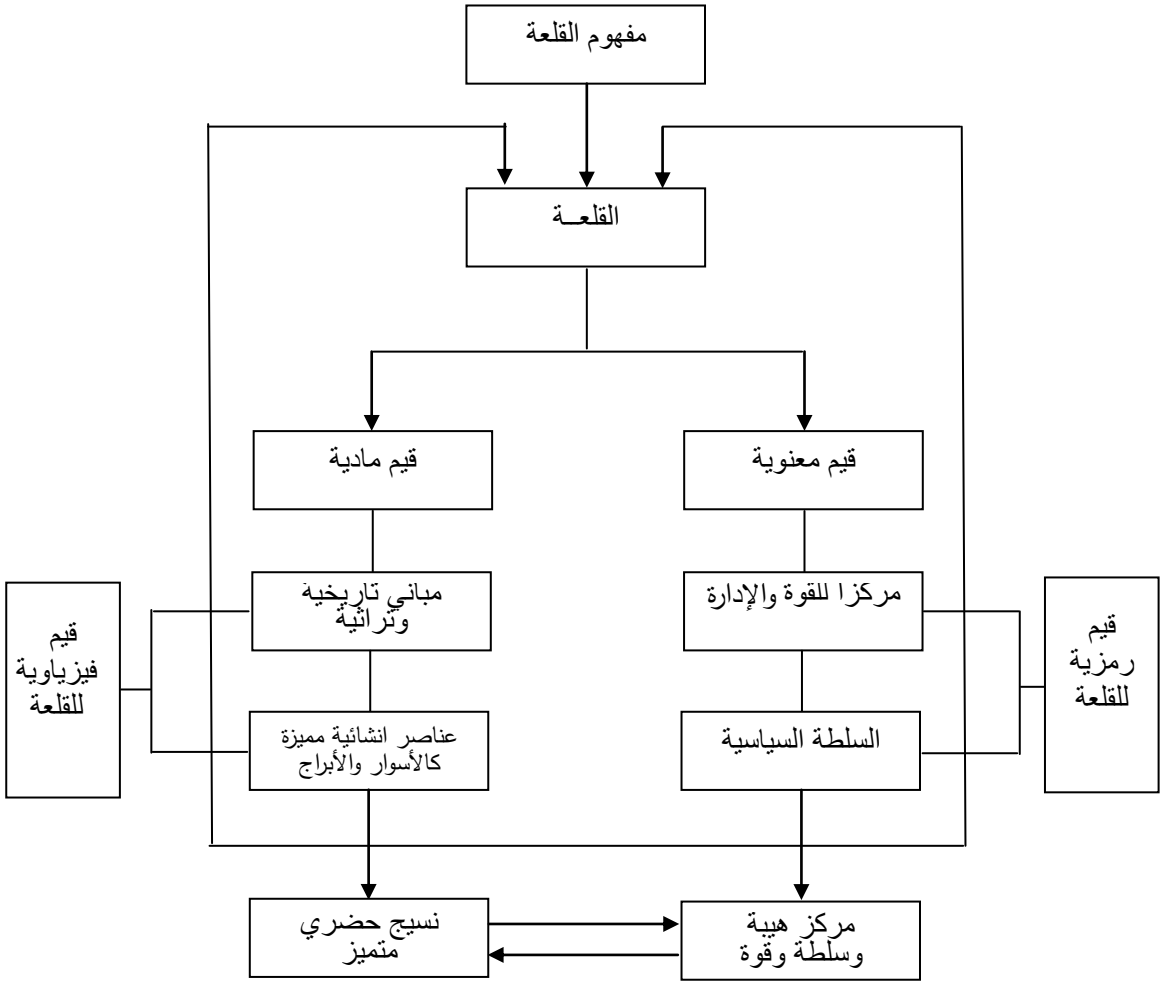

الشكل (1-1) مفهوم القلعة – الباحثة

- انماط القلاع حسب التطور التاريخي لها:

وتصنف حسب التسلسل التاريخي والتغيرات الحاصلة لها:

- الحصن (stronghold): ويدعى أحيانا بالملجأ والذي يجهز المالك عادة بمأوى خلال رحلاته المؤقتة والدائمية أو في أوقات صيده.
- القلاع ذات الفناءات(Courtyard castles): عبارة عن قلاع جديدة مشيدة في أراضي لم تستغل من قبل، مستطيلة الشكل وتمتلك أبراج ركنية ضخمة وتشبه المزارع أكثر من كونها حصون مغلقة.
- المساكن المحمية (Protected homes): ويقصد بها البيوت المحصنة التي اعيد بنائها وحدثت لتكتسب جمالية اضافية، ولقد استبدلت الروافد الخشبية بجدران حجرية صلدة، وأصبحت البوابات اكثر تعقيدا في تصاميمها وتفاصيلها، واحيطت بالخنادق والجسور (www.pounds).

– انماط القلاع حسب الوظيفة:

- حصن وحامية دفاعية وقاعدة للحملات العسكرية المختلفة.

- مركز للقوة السياسية والإدارة الحكومية.
- سكن الملك أو الحاكم سواء بصورة دائمية او مؤقتة.

- انماط القلاع تبعا للهيكل:

- مجموعة من الأبراج الدفاعية.
- أسوار مزودة بفتحات محصنة ومنصات قتالية.
- مبنى كبير محصن أو مجموعة من المباني محاطة بجدران ضخمة (www.morris).

المحور الثاني: الجذور التاريخية لمفهوم الحماية

يتناول فكر الحماية الأمنية في القلاع عبر التاريخ وعوامل نشوؤها كمفهوم للحصانة والدفاع ومقر للحكم والسلطة.

- الجذور الأولى للحماية:

عاش الإنسان في القرون الغابرة في أماكن مرتفعة وبين الصخور التي كونتها الطبيعة أو ساهم في تكويناتها الصخرية هربا من بطش القوى الخارجية سواء من أخطار الطبيعة، أو الحيوانات المفترسة أو من هجمات أجناس بشرية أخرى. كل ذلك جعل الإنسان القديم يبتغي الحماية (Janson–1977) ، الشكل (2–1). ثم أنتقل من الملاجئ الطبيعية وأنشأ بيتاً في العراء وكان بداية تكوين القرية ثم ظهرت المدينة بعد القرية **وتطلب ذلك إيجاد أساليب مختلفة لحماية ممتلكاته من مواد متوفرة في البيئة المحيطة** (Gallion-1963).

- فكرة الارتفاع:

نمت معارف الإنسان في الأعمار والتشييد واقترنت بتقديسه لبعض الظواهر الطبيعية، وبخاصة الظواهر السماوية وبدأ ينحو منحا الهياكل البرجية المرتفعة المتدرجة التي يتربع فوقها المعبد، وان تشييد هذه الأبراج ما هي إلا تعبير عن محاولة الإنسان التقرب الى السماء وزيادة القدسية بالارتفاع، وهرباً من قساوة الكوارث الطبيعية ومخاطرها أيضا (بارو–1979) ، الشكل (2–2) ، (2–3).

أي ان **أكثر الملوك في الحضارات القديمة استخدموا الأماكن المرتفعة والربوات لبناء قصورهم وذلك لتحصين أماكن إقامتهم، ويبدو أنهم اعتقدوا بأن الأماكن المرتفعة لها خصوصية وجمالية وحصانة أكثر من المناطق المنخفضة.**

- الخنادق والأسوار المحصنة:

وقع تغيير جوهري في العمارة السومرية وخاصة في العصر الذهبي تجلى في تقنية البناء، فبعد أن كانت المعابد تشيد فوق ساحة من الأرض المستوية، أصبحت تحفر لها خنادق عميقة لوضع أساسات الجدران

(بارو-1979) ، واحاطة الحرم في المعبد بسور يفصله عن المعالم الأخرى مثلا المعبد البيضوي في تل خفاجي سور بأسوار خارجية بيضوية (شريف يوسف-1982) ، الشكل (2-4).

وفي العمارة البابلية كانت مدينة بابل من احكم مدن الشرق القديم، ووصفها هيرودوت:" تقع على سهل فسيح، يلتف به سور سمكه من الانفساح؛ يتيح لعربة تجرها جياد أربعة أن تندفع فوقه "، ونهر الفرات يقسم مدينة بابل من الشمال الى الجنوب، الذي هو بمثابة خندق طبيعي، وتم إضافة سور مع خندق في فترة نبوخذ نصر لحماية المدينة من الجهة الشرقية (كريشن-1982) ، الشكل (2-5).

نستنتج إن اغلب المدن والمستوطنات القديمة قد سورت بسور للحماية من المخاطر الخارجية فهو بمثابة عازل يعزلها عن العالم الخارجي لا ينفتح به إلا باب أو أكثر، واتخذ أشكالا متعددة، وأضيف الى بعضها سورين أو أكثر بالإضافة الى وسائل تحصينية أخرى مثل الخنادق والأبراج، وتقاس قوة استحكام المدينة بقوة الأسوار ومقاييسها.

- المدن والقصور المحصنة:

يعد قصر مدينة ماري الذي بني على النمط السومري مقرا للحكم والسلطة، وأمتد بناؤه أجيالاً عدة فأضيف إليها أبنية عديدة استلزمتها مهامه الجديدة، وإذا بهذه الأبنية المتلاحقة تتحول الى مدينة كاملة داخل مدينة ماري نفسها ، وأحيطت به جدران سميكة لا ينفتح منها، سوى بوابة واحدة مما جعل القصر قلعة حصينة تصمد للحصار الطويل (بارو-1980) ، الشكل (2-6).

وفي موقع خرسباد (دور شروكين) بلغت الإمبراطورية الآشورية ذروة قوتها المتمثلة بإقامة صرح فني ذي قيمة معمارية وهي القلعة الملكية على شكل حصن مربع تقريباً، يحيط بها سوراً ضخماً يمتلك سبعة أبواب، وضعت على جوانبها الثيران المجنحة ذات الرؤوس البشرية بمثابة حراس للمدينة، وفي الزاوية الجنوبية من المدينة شيد قصر بشكل قلعة ثانية ويمثل الترسانة الملكية التي يستطيع أن يخزن فيها الغنائم التي يحصل عليها في حملاته العسكرية (مورتكات- السنة بلا) ، الشكل (2-7).

أي إن القصور المحصنة كانت في الغالب أماكن لها خصوصيتها السكنية، أو مكانا صيفيا للراحة واستقبال الضيوف وقضاء العطل أيام الصيد، أو معقلا محصنا له، ونوعاً من العزل بين الحياة التي يعيشها الملك والحياة خارج هذه القصور وما التحصينات إلا تعبير واضح عن قوة تحصين المملكة.

- الموقع:

في عصور ما قبل الإسلام نشأت دويلات عربية وكانت تعتمد على التجارة. فالبتراء في وادي موسى شرق الأردن، تمتاز معظم ابنيتها بأنها منحوتة في سفوح الجبال، الشكل (2-8).

ومدينة الحضر التي اشتهرت بموقعها الصحراوي الحصين غرب الموصل بالإضافة الى أسوارها وأبراجها وقصورها ومعابدها واشهرها معبد مرن (شريف يوسف-1982) ، الشكل (2-9).

ويمكننا أن نستنتج إن قيام هذه الدويلات هو تأكيد على نشأة المدن في أماكن مرتفعة أو منيعة كأن تطل على نهر أو وقوعها بين نهرين مما يعطيها عاملاً تحصينيا إضافيا لمنع الأخطار وتفادي الغزوات عنها، وأن اغلب المدن وخصوصاً في وادي الرافدين سلكت نفس الأسلوب من بناء سور خارجي وداخلي وأبراج لتامين مزيدا من الحماية.

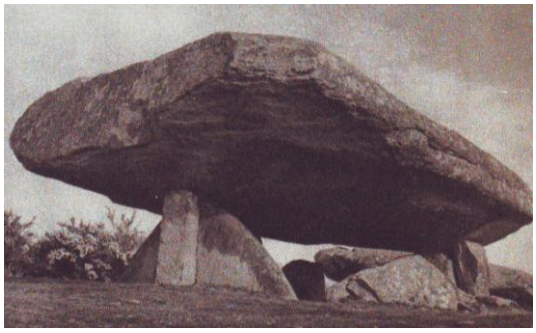

الشكل (2–1) نماذج من التكوينات الصخرية (Huyghe-1962)

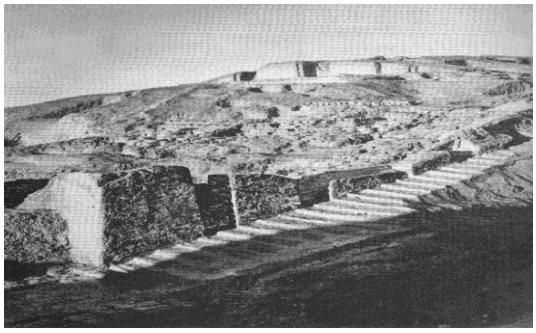

الشكل (2-2) زقورة الوركاء (بارو–1979)

الشكل (2-3) زقورة اورنمو(Janson-1977)

نماذج لتطبيق فكرة الارتفاع واستخدام الربوات

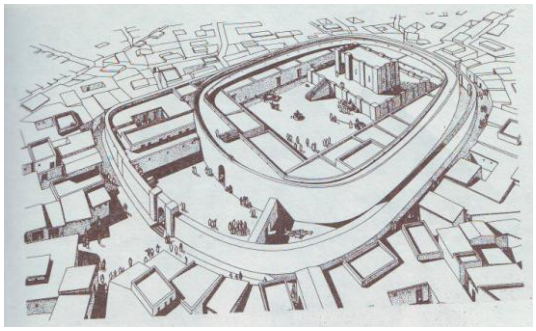

شكل (2–4) المعبد البيضوي (سيتن لويد-1988)

الشكل (2–5) مدينة بابل (دليل وزارة الإعلام - 1972)

نماذج لاستخدام الخنادق والاسوار

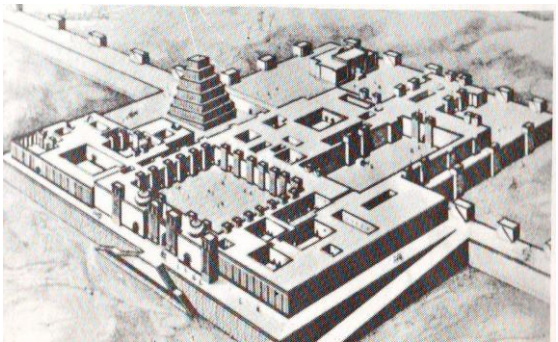

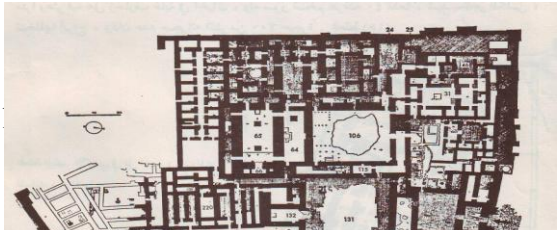

الشكل (2–6) قصر ماري (شريف يوسف- 1982) الشكل (2–7) قلعة خرسباد (شريف يوسف- 1982)

نماذج من القصور والمدن المحصنة

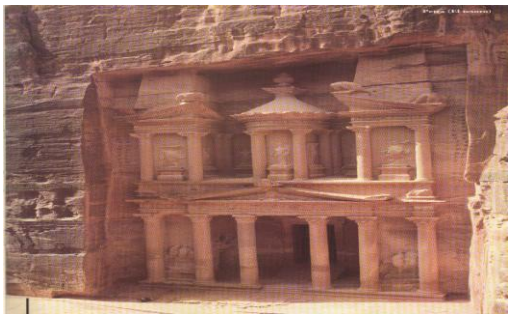

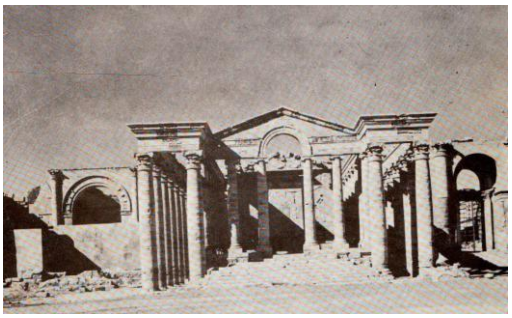

الشكل (2–8) البتراء – الأردن (الدليل السياحي الاردن) الشكل (2–9) معبد مرن – العراق (شريف يوسف- 1982)

نماذج لاستخدام الموقع الحصين

المحور الثالث: القلاع العراقية والمحددات التصميمية المميزة لها

دراسة نماذج من القلاع العراقية مثل (قلعة أربيل، قلعة هيت، وبعض من قلاع الموصل) وتحليلها وفقا للمحددات التصميمية والمعالم الدفاعية التحصينية التي تشتهر بها، والتركيزعلى قلعة كركوك واستجلاء معالمها المعمارية بشكل عام ووسائلها الدفاعية بشكل خاص باعتبارها موضوع البحث.

– قلعة أربيل:

كانت مدينة أربيل في بداية نشوئها عبارة عن قلعة محصنة بأبوابها وأبراجها المحكمة ولحقبة طويلة، ويبلغ ارتفاع مدينة أربيل عن مستوى سطح البحر حوالي 414م حيث تقع مدينة أربيل في الأراضي المتموجة المحاذية للمناطق الجبلية الشرقية من جهة، ومن جهة أخرى تحد السهول الجنوبية والجنوبية الغربية (العزاوي- 2001) ، بينما ترتفع قلعة اربيل حوالي 36م عن سطح المدينة مما يعطيها عاملا دفاعيا وشكلها شبه دائري الشكل (3– 1) ، وليس للقلعة تاريخ محدد، بل يحسب لعدة آلاف من السنين، وتتحدث الآثار والمسلات الحجرية وبعض المنحوتات عن هذه القلعة، وأن المصادر تذهب الى أن هذا التل الأثري (القلعة) يقوم فوق تراكم طبقات أثرية متعاقبة.

– المحددات التصميمية لقلعة اربيل:

* **الموقع الحصين للقلعة** فقد ذكر الرحالة (بكنغهام) : "إن التل الذي تقوم عليه القلعة مربع الشكل ويرتفع على سطح منحدر واسع وهو من صنع البشر ومنظر القلعة يدل على إنها كانت حصنا منيعا مسوراً ليس له باب سوى باب واحد وإذا أوصدت الباب انعزلت القلعة ومن فيها عن الخارج" (الجنابي–السنة بلا).

* **الجدران الصقيلة للأسوار المحيطة بالقلعة** التي كانت السبب الرئيسي في منع المهاجمين من ارتقائها، ولم تخضع مدينة أربيل لفاتح إلا بصعوبة وأقدم إشارة الى ذلك ما نقله (ابن واصل) عن صمودها أمام الاتابكي عماد الدين زنكي– مؤسس اتابكية الموصل– حين حاصرها سنة 526 للهجرة محاولاً ضم هذه المدينة الى إمارته، وبالإضافة الى قول (القزويني) : "إن هذه القلعة كانت من الحصانة بحيث عجز المغول عن افتتاحها مع إنهم ما فاتهم شيء من القلاع والحصون" (نبيل قصاب–2005).

* **آثار لخندق عميق** أحاط في وقت سابق بالقلعة التي تمتلك بوابتان قديمتان وبوابة ثالثة جديدة نسبيا، وتتألف القلعة من ثلاثة إحياء سكنية رئيسية: وهي السراي في الجهة الشرقية، والطوبخانة في الجهة الجنوبية الغربية، والتكية في الجهة الشمالية الغربية (الحيدري– 1985) ، ومن المقترحات التطويرية التي وضعت للقلعة تحسين الشكل الخارجي للقلعة من خلال الاهتمام بالمدرجات والسور ومجموعة المباني المنتشرة على واجهاتها وضرورة تثبيت سفوحها بالنباتات (شيرين احسان–1978) بالاضافة الى دراسة المكتب الاستشاري العراقي الذي تضمن مسح عام للمميزات المعمارية للقلعة وابرازها عند وضع المخططات التطويرية لها (صحيفة الاتحاد–1994) ، الشكل (3–2) (3–3).

– قلعة هيت:

تقع مدينة هيت على الفرات الأعلى، وقال ابن السكيت سميت هيت لأنها في هوة من الأرض والأصل فيها هوت فصارت الواو ياءا). وذكرها هيرودوتس (إنها على مسافة ثمانية أيام من بابل مدينة (ايس) أي (ايث) وهي قائمة على شاطئ نهر صغير يدعى باسمها) (موسوعة المدن العراقية–2005) . وتقع على الطريق البري الذي يربط العراق بالحدود الأردنية من جهة والحدود السورية من جهة أخرى.

وقلعة هيت عبارة عن نصف دائرة بشكل حدوة الفرس ، ومشيدة على تل أثري في مركز المدينة القديمة يحدها من الجهة المستقيمة الشمالية نهر الفرات أما الجهات الثلاثة الأخرى فيحيط بها سور حجري، ويحيط بها شارع حلقي خارجي ذو فعاليات تجارية وصناعية ويخترقها شارع واحد يسمح بمرور السيارات وهو محاذي لنهر الفرات الشكل (3–4).

- المحددات التصميمية لقلعة هيت:

- **الموقع الاستراتيجي للقلعة** الذي يتجلى بوقوعها على تل أثري ذا شكل هرمي، وأعلى نقطة تصل إلى 20م تمثل قلب القلعة أو المنطقة الوسطى لها ثم يبدأ بالنزول تتدرجياً من الجهات الأربعة إلى 18م و16م، ويلاحظ ذلك جليا من جهة النهر فهي تتدرج الى أن تصل الى مستوى السدة التي ترتفع بمقدار 4م عنها، و ان بعض المقترحات التطويرية التي وضعت للقلعة ركزت على التل المتدرج والحفاظ على جمالية الشكل الهرمي من الناحية المعمارية والاستفادة من روحية المنطقة وما تشتهر به من النواعير، الشكل (3-5).

- **السور الطبيعي** حيث أن نهر الفرات يحدها من الجهة الشمالية، اما بقية الجهات فكانت محاطة بسور حجري ضخم يتراوح سمكه بين (1-2) م ويحتوي على دعائم بمسافات غير متساوية ولم يتبق من السور سوى بعض الأجزاء في الجهة الجنوبية والجنوبية الغربية للمدينة.

- **خندق ملحق بقناطر** يحيط بسور القلعة، ويتخذ شكل نصف دائري تتصل نهاياته بنهر الفرات ويسمى الأول بالباب الشرقي والآخر الباب الغربي ويمتد فوقه قنطرتين كبيرتين عند البابين السابقين بالإضافة الى بعض القناطر الصغيرة ولم يبق حاليا أي اثر من آثار هذا الخندق بسبب تبليط ما حول القلعة كشوارع للسيارات (شبكة المعلومات الدولية:مدينة هيت).

- القلاع في الموصل:

تشتهر الموصل بعدة قلاع والتي شيدت في فترات تاريخية متباينة مثل: الحصن الآشوري فوق تل قليعات، والقلعة الاتابكية، وقلعة الحصن الذي أقامها المغول في وسط المدينة، وقلعة باش طابيا وهي بقايا القلعة الاتابكية وتقع في الزاوية الشمالية الشرقية لها، والقلعة الداخلية (ايج قلعة) التي أنشأها الأتراك العثمانيون على نهر دجلة مقابل سوق الميدان الحالي (الديوه جي-1982) ، الشكل (3-6) وسوف يتم التطرق الى أهم القلاع :

- الحصن الآشوري فوق تل قليعات:

يعتبر تل قليعات من أكبر التلال التي تشرف على غرب نهر دجلة ويشرف على السهول الخصبة، وهو يقابل مدينة نينوى، وبنى الآشوريون حصناً فوق هذا التل حيث اتخذوها عاصمة لهم سنة 1080ق.م وتعتبر أول قلعة بنيت بمدينة الموصل، وفي سنة 612ق.م عاد قسم من السكان الى تل توبة المقابل لتل قليعات وأقاموا لها سوراً فسمي بالحصن الشرقي بعد ما اصاب مدينة الموصل الدمار والخراب وبعضهم أعاد تشييد حصن تل قليعات وسمي بالحصن الغربي وأطلق عليهما سوياً الحصنان، الشكل (3-7).

- القلعة الاتابكية:

تقع شمال الميدان وتشرف على نهر دجلة ومنابع عين كبريت، ولا يعرف تاريخ تأسيسها، ولعل العقيليين هم أول من أسسها، وفي سنة (474هـ-1081م) بنى شرف الدولة العقيلي سور الموصل وبعدها احكم جكرمش عمارتها وحفر خندق مع تحصينات إضافية، وصف القلعة الرحالة الأندلسي ابن جبير عندما قال: (في أعلى البلد قلعة عظيمة، قد رص بناؤها رصاً، يتضمن سور عتيق البنية، مشيد البروج وكانت القلعة تتصل بدور

المملكة بممر تحت الأرض يسلكونه عند الحاجة ولم يزل بعض أثار هذا الممر في كنيسة الطاهرة) والتي عثر عليها أثناء عمليات ترميم بعض أقسام الكنيسة، الشكل (3-8).

-قلعة الحصن:

أنشأت عند احتلال المغول لمدينة الموصل سنة (660هـ-1261م) وبعدها جاءت الدولة التركمانية حيث اتخذها الحكام حصنا لهم كونها وسط المدينة وعلى مرتفع يمتد من جامع السراي جامع هيبة خاتون في وقتنا الحاضر الى قرب محلة باب النبي والى باب الجبلين. ومن أهم المعالم المعمارية لقلعة الحصن: السراي، ومسجد السراي، ومقام السيدة نفيسة، وجامع السراي، وشارع زقاق الحصن.

وهناك قلاع أخرى مثل باش طابيا والقلعة الداخلية ايج قلعة (شبكة المعلومات الدولية:قلاع الموصل).

- اهم المحددات التصميمية المشتركة بين قلاع الموصل:

- **الموقع** حيث تشترك اغلبها بامتلاكها مكانا ستراتيجيا إما بوقوعها على تل مرتفع أو إشرافها على نهر فهي تتخذ من التضاريس الجغرافية الطبيعة حصنا منيعا وسورا دفاعيا اضافيا.

2- **أسوار وخنادق وأبراج** وتحصينات أكثر تعقيدا من مثيلاتها من القلاع ظهرت مع توسع الإمبراطوريات الحاكمة آنذاك وتوفير متطلبات عوامل القوة والحماية ومواكبة خط تطور فنون العمارة، ويلاحظ إن المؤسسة العامة للآثار والتراث (المديرية العامة لأثار ومتاحف المنطقة الشمالية) عندما قامت بتوثيق المعالم المعمارية مثل القلاع التاريخية في مدينة الموصل اقترحت عدة مشاريع للمحافظة على بعض الأبنية وإعادة بناء أسوار القلعة والأبواب وبعض الجسور المهمة.

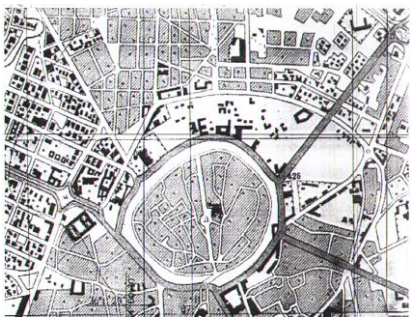

الشكل (3-1) مخطط - شبكة المعلومات الدولية

الشكل (3-2) اربيل- كارت سياحي

الشكل (3-3) بيت تراثي - تصوير

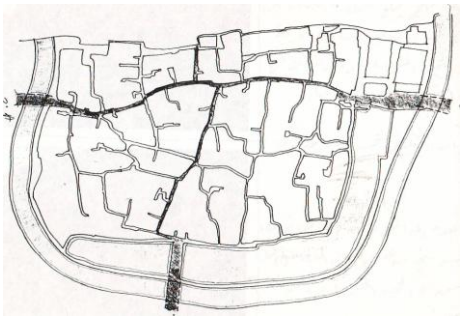

الشكل (3-4) مخطط قلعة هيت - شبكة المعلومات الدولية

الشكل (3-5) نواعير مدينة هيت - تصوير

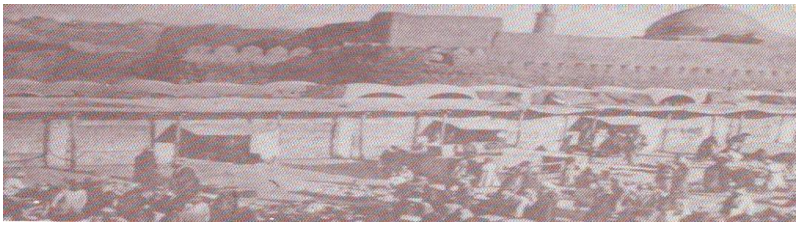

الشكل (3–7) قبة جامع الباشا وبقية السور – الموصل(الديوه جي-1982)

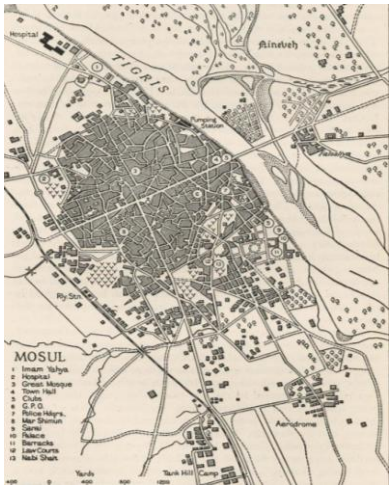

الشكل (3–6) مدينة الموصل– شبكة المعلومات الدولية

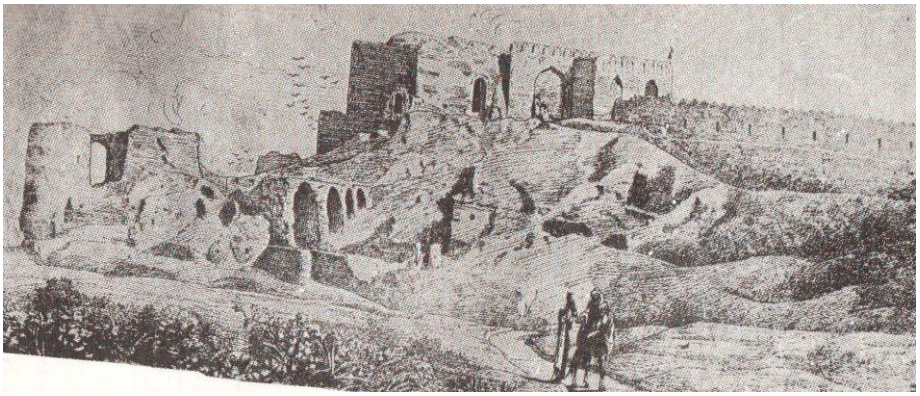

الشكل (3–8) بقايا القلعة الاتابيكية – الموصل(الديوه جي-1982)

– قلعة كركوك:

إن قلعة كركوك كأي مدينة تحتوي على منشات وعلامات دالة مهمة، وميادين معروفة سواءا في ظاهرها أو لربما تراكمات وبقايا أثرية لمدن قديمة سابقة في باطنها، لانها عاشت عصورا مختلفة من حضارات وثقافات التي انقرضت تباعا تاركة شواخص لا تزال تحكي قصة تلك الحقب وقد تستمر بعيدة عن التنقيب وأهالي كركوك يتحدثون منذ أجيال عدة على أن القلعة الحقيقية تقع في جوف القلعة الحالية، وتتكون القلعة من ثلاثة أحياء رئيسية: حمام، وأغالق، وميدان التي تحوي الشواخص المعمارية منها:

– البيوت التراثية:

إن كل محلة تضم عدداً من الأزقة، التي تحتوي بدورها على مجموعة من الدور. وكان عددها يصل الى 797 داراً، أما الآن فتم الإبقاء على 45 داراً، وأهمها دار طيفور، وهو يتكون من ثلاثة دور: الدار الخارجية، والدار الداخلية (المضيف) ، ودار العريس، ويعتبر معلماً أثرياً لكونه يعود إنشاؤه الى أكثر من 200 سنة، الشكل (3–9) ومن الدور الأخرى: (صديق العلاف، وعلي اغا، وسيد فاتح، وميكائيل، وتوما، وعبد الغني) (مقابلة مع مدير دائرة الآثار والتراث). وتشترك البيوت التراثية مع الخصائص التصميمية للدور التقليدية السائدة في العراق كالفناء والإيوان والمدخل المتعرج وهذه الأساليب هي حصيلة فرضتها الظروف المناخية والتأثيرات البيئة

والتطورات الاجتماعية والثقافية، فالبيت التراثي يتميز بالواجهة الخارجية الصماء التي لا تعطي أي مؤشر إلى ما موجود في الداخل.

- القيصرية:

وجدت مؤخرا أثناء التنقيبات التي أجرتها دائرة الآثار والتراث حيث تم الكشف عن 34 محل في الطابق الأرضي (تحت مستوى سطح القلعة) ، يفصل بينها رواق مستطيل الشكل، يعود تاريخ بناؤها الى الحقبة السلجوقية، وكانت تمتاز بأقواسها وعقودها المرمرية ومعروفة لدى العامة باسم (قاتما بازاري) أو (قلينجيلر بازاري) أي سوق صانعي السيوف (الساعتجي-2005) الشكل (3-10).

- الجوامع:

في قلعة كركوك مجموعة من الجوامع أبرزها:

* **الجامع الكبير (اولو جامع) أو (مريمانة):** إن الجامع يقع في الجنوب الغربي للقلعة في محلة حمام ويسمى أيضاً جامع (مريم آنا) ، وكما يظهر من آثاره انه أقيم على أنقاض كنيسة (الساعتجي-2005) وأضيف إليه محراب في بيت الصلاة ومئذنة في الركن الشرقي، الشكل(3-11).

* **جامع النبي دانيال:** أقيم على بقايا كنيسة قديمة وتبلغ مساحته حوالي 400م^2، ويضم مقام ثلاثة أنبياء (دانيال وحنين وعزرا) ، وتعود المئذنة الى أواخر العصر المغولي وبداية العصور التيموري (القرن الثامن الهجري) وهي أعلى شاخص بصري في القلعة ويحيط به مقبرة ذات طابع قديم الشكل (3-12).

* **جامع عريان:** يقع في منتصف القلعة ويعود تاريخ بناؤه الى عام 1142هـ حيث ثبتت في مداخله قطعة من حجر المرمر كتب عليها التاريخ المذكور، ويمتاز بقبته التي تقوم على أربعة أضلاع متساوية ترتكز عليها أضلاع تعلوها ستة عشر ضلعاً تشكل قاعدة القبة التي يصل ارتفاعها الى 15م، ومحرابه محلى بزخارف نباتية وهندسية ملونة وعلى شكل أزهار، تعلو هذه الزخارف (آية قرآنية) ، الشكل(3-13).

- القبة الخضراء:

وردت لها تسميات متعددة معظمها باللغة التركية وهي (يشيل كومبت) ، وتعني القبة الخضراء، و(كوك كومبت) أي القبة الزرقاء، أما الآن فيطلقون عليها القبة الخضراء، لاعتقاد أهالي المنطقة بان القاشاني المستخدم اخضر اللون، ولكن نتيجة الفحص المختبري للقاشاني تبين انه ازرق اللون وتشغل مساحة حوالي 900م^2 وارتفاعها 17م، وشيدت عام 762هـ ، ويعلو مدخل القبة كتابة تاريخية جاء فيها بأنها قبر لفتاة (زوجة احد الأمراء) ، توفيت أثناء سفرها الى مكة المكرمة لأداء فريضة الحج في ذي القعدة من عام 762هـ ودفنت في القلعة، ويحيط بمبنى القبة صحن ذو فضاء مفتوح يحيط به أروقة مسقفة ذات أعمدة مربعة الشكل تنتهي بأقواس مدببة (الرملاوي-1982) الشكل(3-14).

- كاتدرائية ام الاحزان:

تسمى أيضا بكنيسة أم الأحزان بنيت على أنقاض كاتدرائية قديمة كانت للمسيحيين الذين سكنوا في محلة حمام بقلعة كركوك، ويعود تاريخ بنائها الأول إلى سنة 1862م ولم يبق منها إلا جزء من الهيكل وأجزاء من

سقوفها وأعمدتها المرمرية وان أخر تجديد لها كان عام 1903م ولها ملحق عبارة عن مدرسة دينية (مقابلة مع مدير دائرة الآثار والتراث) الشكل (3-15).

اهم المحددات التصميمية في قلعة كركوك:

* **السور والأبراج** : يحتوي السور على البوابة الرئيسية . بوابة الطوب . والبرج ذو فتحات عميقة وضيقة، يعود زمنه الى القرن السابع الهجري أي الحقبة السلجوقية ويلاحظ اختلافاً في الطبقات البنائية المكونة للسور، فالطبقات الأولية السفلى مبنية بالحجر أما الطبقات العليا من الطابوق الشكل(3-16) ، ويؤطر أعلى السور والبرج إفريز من الطابوق الفرشي بهيئة مقرنصات وتم صيانة السور من قبل دائرة الآثار والتراث سنة 1997، ورمم بنفس طرازه القديم ومادته الإنشائية وتحليتها بالطابوق الفرشي، وثبتت مزاغل على السور والبرج وأكمل الدهليز الداخلي (غائب فاضل-السنة بلا) ، وهناك خمسة أبراج في الركن الشمالي الغربي للقلعة مقابل جسر الطبقجلي، وللسور المطل على طريق السليمانية ثلاثة أبراج مبنية باللبن.

***البوابات** : لقلعة كركوك أربع بوابات رئيسية: في الجهة الغربية بوابتان، الأولى بوابة الطوب (طوب قابو) الشكل (3-17) والثانية البوابة الحجرية (داش قابو) وتطلان على نهر الخاصة، بوابتين في الجهة الشرقية هما : بوابة السبع بنات (يدي قزلر) ، وبوابة الحلوجي (حلوة جيلر).

* **الموقع** : بنيت كركوك في الأصل كقلعة على تل دائري غير منتظم مدور ترتفع عن السهول المحيطة حوالي 18م وتشرف على وادي نهر صغير ذي مياه قليلة يفيض عادة في الفصول الممطرة ويعرف بنهر الخاصة (الخاصة صو) (جمال رشيد-2002).

الشكل (3-9) بيت تراثي

الشكل (3-10) القيصرية

الشكل (3-11) الجامع الكبير

الشكل (3-12) جامع النبي دانيال

الشكل (3-13) جامع عريان

الشكل (3-14) القبة الخضراء

الشكل (3–15) كاتدرائية أم الأحزان الشكل (3–16) البرج الرئيسي الشكل (3–17) بوابة الطوب
الأشكال معالم قلعة كركوك – تصوير الباحثة

نستنتج من الدراسات السابقة ان اغلب القلاع تشترك فيما بينها بامتلاكها محددات تصميمية واغلبها تشكل العوامل التحصينية والمميزة لها مثل: عناصر إنشائية فيزياوية، وأساليب إنشائية، وعوامل الموقع الاستراتيجية، والشكل الفيزياوي.

***عوامل تحصينية دفاعية وتشمل:**

أ– عناصر إنشائية فيزياوية: أي امتلاك القلعة لبعض العناصر الإنشائية المميزة كالسور الذي يتباين بين واحد أو اثنين أو حتى ثلاثة، وعدد من ألابراج والبوابات التي تلعب دوراً مهما في رسم ملامح المدينة.

ب– الأساليب الإنشائية: إن اغلب القلاع مبنية باستخدام الحجر والطابوق التي تعتبر مقاومة للظروف الطبيعية والمناخية ولتوفرها كمادة أولية وبشكل عام فإن الأساليب الإنشائية اتجهت نحو التعقيد عبر الزمن حيث تم استخدام وسائل مساعدة لتدعيم العناصر الإنشائية كالجدران الساندة التي تشيد حول القلاع، وفي بعض منها يحفر خندق مائي حول اسوارها ويتم الوصول الى بواباتها عن طريق جسور متحركة التي ألحقت بأوتاد خشبية داعمة تتحكم في قوة استحكام هذه القلاع.

*** عوامل الموقع الإستراتيجية:**

إن معظم القلاع كانت تختار مواقع إستراتيجية دفاعية كأن تطل على نهر أو ساحل بحر أو أن يكون موقعها عالياً سواء فوق تلة طبيعية أو مجموعة تلال أثرية متكونة من توالي الحضارات، أو فوق تلة صناعية من تشييد الإنسان، وإن أكثر المدن القديمة تأسست بفعل وجود الأنهار والبحار التي أحاطتها من عدة جهات فهي بمثابة أسوار طبيعية تحيط بها وتقلل فرص وصول الغرباء إليها بسهولة.

*** الشكل الفيزياوي:**

إن اغلب القلاع أشكالها دائرية لان القانون الرئيسي للشكل الدائري هو إحاطة أكبر مساحة سطحية ممكنة وإذا تم تسقيطها على استخدامات الأرض فيلاحظ إن أغلب المستوطنات القديمة كانت ذات شكل دائري التي نتجت أساساً عن شكل أولي للسياج المستخدم حول ممتلكات الإنسان البدائي كالحقول والماشية فهي تحيط أكبر مساحة ممكنة من الأرض مع اقل استخدام للسياج بالإضافة إلى إعطاء عاملي المرونة والحماية بشكل متساوي من جميع الجهات، الشكل(3–18).

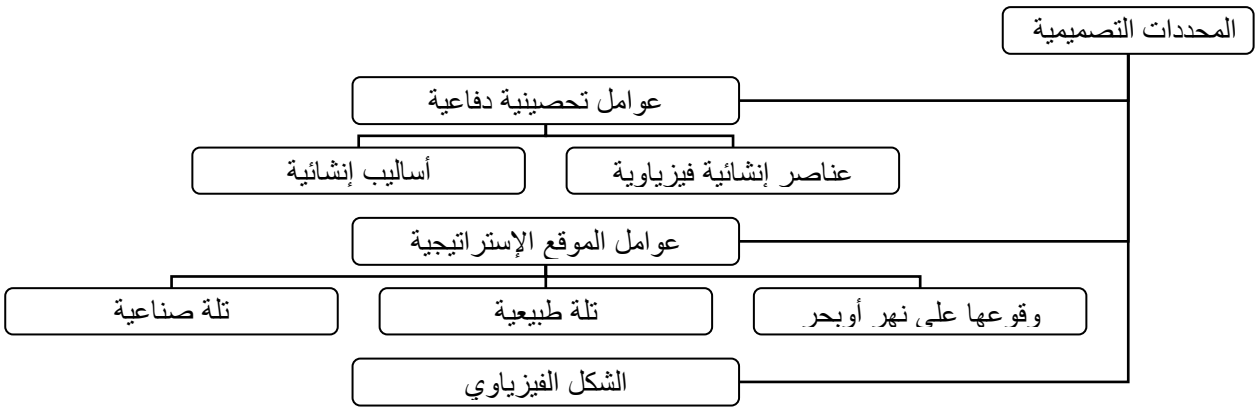

الشكل (3- 18) المحددات التصميمية لمباني القلاع - الباحثة

* المحددات التصميمة فيالسياسات التطويرية لقلعة كركوك:

التعرف على أهم المحددات التصميمية وكيفية الاستفادة من خواصها ومميزاتها في السياسات التطويرية التي وضعتها شركة دوكسيادس بالاضافة الى المشاريع التطويرية المحلية المقترحة للقلعة.

* المقترحات التطويرية لشركة دوكسيادس:

تبنت شركة دوكسيادس عدة تقارير لتطوير قلعة كركوك بالتعاون مع وزارة البلديات العراقية ومجموعة من الخبراء وعند دراسة البرنامج المقترح التطويري والذي قسم الى مرحلتين رئيسيتين اتضح ما يلي:

أ . **المرحلة الأولى :** وتعنى هذه المرحلة بشبكة الطرق الرئيسية والثانوية والاستخدامات المختلفة للأراضي والمناطق المفتوحة الموجودة في القلعة وتحسين مظهر الشوارع من خلال تبليطها ورصفها **أي التركيز على احدى المحددات التصميمية المهمة للقلعة الا وهوالموقع ومعطياته،** وإعادة تفعيل الأنشطة الثقافية والاجتماعية وغيرها في الأراضي المفتوحة ، والعمل على زيادة الوعي للساكنين حول الأهمية التاريخية للقلعة **اي ابراز القيم المعنوية والمادية لها.**

ب . **المرحلة الثانية :** هذه المرحلة اكبر من المرحلة السابقة في مصطلحات التطوير العمرانية بتعريف المحلات الثلاث في القلعة ومنطقة الفعاليات المركزية ، وتوضيح هيكل المؤسسات التعليمية والإدارية و الثقافية والترفيهية والفعاليات التجارية المقترحة **اي التأكيد على الشكل الفيزياوي،** بالاضافة الى مشاريع الإسكان الجديد من خلال إعادة تصميم الأراضي المفتوحة، وعمليات الإصلاح والترميم الضرورية للشواخص المعمارية والتاريخية المهمة (Doxiadis-1976) الشكل (3-19).

***المشاريع التطويرية المحلية لقلعة كركوك:**

وضعت عدة مشاريع تطويرية لقلعة كركوك ابرزها كان مشروع وزارة الثقافة والإعلام – دائرة الآثار والتراث – مفتشية آثار كركوك سنة 1993م وتمثلت بتحويل طابع القلعة من سكني الى سياحي، والمحافظة على الأحياء الثلاث للقلعة وإبراز خصوصية كلا منها ، والمحافظة قدر الإمكان على الأبنية التراثية المتبقية والعمل على إبرازها من خلال تحديدها وعزلها عن المناطق المفتوحة أو المشاريع الجديدة المضافة، والعمل على جعل المنطقة التراثية بشكل حلقي محيط بالقلعة بالإضافة الى الجزء المركزي الوسطي الذي يضم الأبنية التاريخية المهمة، واضافة المشاريع الجديدة بينهما، والربط بين الأجزاء السابقة عن طريق إعادة وترميم شبكة الطرق القديمة والتأكيد على طريق رئيسي شرياني يربط بين بوابتين رئيسيتين في القلعة، وتحسين مظهر مدرجات القلعة الشكل (3–20)، اي **ابراز الموقع الاستراتيجي والمعالم المهمة وهي من المحددات التعريفية الاساسية للقلعة.**

الشكل (3-19) المشروع المقترح لتطوير قلعة كركوك
من قبل دوكسيادس – سنة 1974

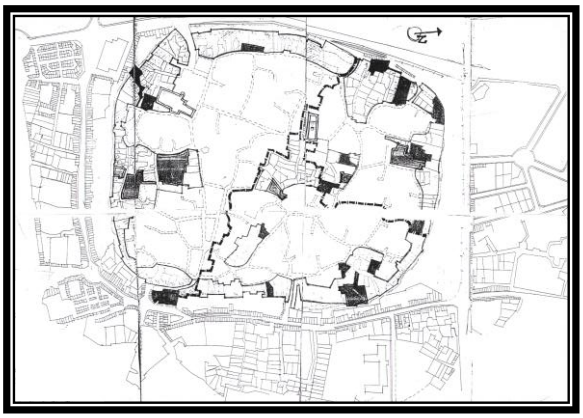

الشكل (3-20) المشروع المقترح من قبل
دائرة الاثار والتراث / مفتشية اثار كركوك -1993

المحور الرابع: تطوير قلعة كركوك وفقا لمحدداتها التصميمية المميزة لها

يمثل الجانب التطبيقي لتطوير قلعة كركوك وكشف آلية العمل بها من خلال التاكيد على المحددات التصميمية لمباني القلاع بصورة عامة وقلعة كركوك بصورة خاصة، وطريقة البحث المقترحة من قبل الباحثة التي تضمنت:

أولا: مرحلة التحري والتقصي

يقصد بها مرحلة دراسة المحددات التصميمية للقلعة كالتعرف على الموقع والمعلومات المتعلقة بواقع الحال والحقائق التاريخية والتحليل الدقيق لها، ودراسة الشواخص المعمارية والمعالم التحصينية المميزة للقلعة وتوثيقها من خلال تصويرها واعداد المخططات اللازمة لها.

ثانيا: مرحلة المعاينة والتحليل

يقصد بها فحص دقيق للنسيج الحضري وأجزائه والتي تشبه المعاينة الدقيقة لنسيج الكائن العضوي الحي المصاب، ومن ثم تشخيص أماكن الوهن والضعف تليها اقتراح الأساليب العلاجية الكفيلة، وتظهر نتائج المعاينة أن هناك مثلا أجزاء تحتاج الى تدخل سريع وطارئ ليتم إنقاذ ما يمكن إنقاذه، وأخرى تحتاج إلى تحسين مظهرها أو أدائها أي ما يشبه في أصولها الجراحة التجميلية، وغيرها تحتاج الى إزالة لان وجودها يسبب ضرراً لا منفعة كاستئصال ألأجزاء المصابة في جسم الكائن العضوي، وعلى أساس هذا تم فرز وتصنيف عمليات التطوير إلى ثلاث مراحل رئيسية:

- مرحلة تتضمن تدخل بسيط أي تحسيني للقلعة مثل المحافظة على شكلها الفيزياوي وابراز موقعها الستراتيجي المهم وتجميل بعض واجهات مبانيها.
- مرحلة تعنى بالتدخل السريع والطارئ لبعض المباني والشواخص التحصينية كالابراج والبوابات والسورالمحيط بالقلعة لإعادة دورها الفعال ضمن المشهد الحضري للمدينة.
- مرحلة الازالة النهائية للمباني المتهرئة وغير الواضحة المعالم والتي تشوه صورة القلعة واستبدالها بمكونات حضرية جديدة تلائم الحاجات المعاصرة للمدينة.

ثالثا: مرحلة اختيار الأسلوب الامثل:

يقصد بها توجيه واختيار الطريقة المناسبة للتطوير فهي تختلف وتتباين من حالة الى أخرى ، وبما هو متوفر من الامكانيات وما تحمله من مزايا تصميمية جديدة في ثناياها. ولسهولة التعامل مع المخططات التطويرية المقترحة تم تقسيم القلعة بصورة عامة الى ثلاث مناطق متمايزة فيما بينها الشكل (4-1):

المناطق الحفاظية للمحددات التصميمية للقلعة: وتشمل الشواخص والمنشات المعمارية الجيدة المتبقية في القلعة والتي تحتاج الى تهذيب وصيانة بسيطة، مثل البوابات، والأبراج، والجوامع، والبيوت التراثية.

المناطق التجميعية: ويقصد بها اعادة تصميم وتجميع لمجموعة المحددات التصميمية للقلعة في مواقع تتوسط المناطق الحفاظية والحضرية الجديدة والتي ستأخذ أجزاءها من المباني المهدمة أو بقايا الهياكل الإنشائية من أعمدة وتيجان وأقواس، واستلهام بعضا من رموزها الشكل (4-2).

المناطق الحضرية الجديدة: إضافة وتصميم منشات وعوامل تحصينية الجديدة في الفضاءات أو الأراضي المفتوحة ، والتي تتلائم مع حاجات القلعة المطورة وحسب التصميم المقترح الشكل (4-3).

الشكل (4–1) المناطق الحفاظية والتجميعية والحضرية الجديدة – تصميم الباحثة

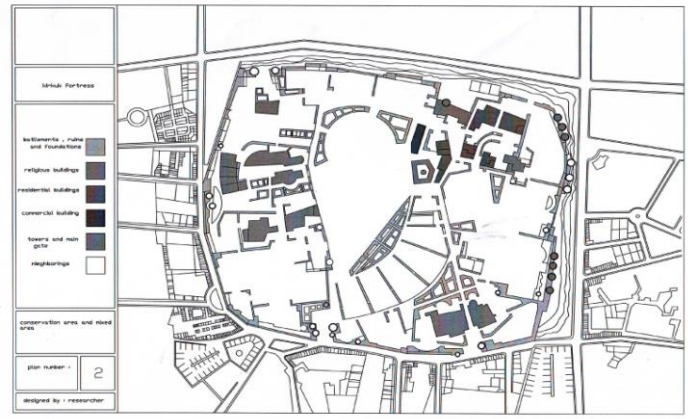

الشكل (4–2) المناطق الحفاظية والتجميعية للمحددات التصميمية للقلعة – تصميم الباحثة

الشكل (4–3) المناطق الحضرية الجديدة – تصميم الباحثة

الاستنتاجات النهائية:

- ان القلعة تعتبر وحدة معمارية قائمة بحد ذاتها وان اختلفت في تسمياتها وانماطها، وتتعزز روحيتها من خلال محدداتها التصميمية والتي غالبا ما تكون بهيئة عوامل تحصينية مميزة لها مثل عناصر انشائية فيزياوية واساليب انشائية وخواص الموقع الاستراتيجية والشكل الفيزياوي التي تعد اركاناً أساسية من بناء صورة المكان ولولاها تفقد القلعة الكثير من حيثياتها الحسية والتكوينية.
- اتخذت القلعة كمفهوم معماري اشكالا متعددة في الماضي السحيق والتي كونت بدورها فكر الحماية الامنية لها بتقادم الزمن من خلال استخدام الاماكن والربوات الحصينة والمرتفعة ومن ثم تدعيمها بالخنادق والاسوار والابراج حيث ان قوة استحكام المدينة أو المبنى كانت تقاس بضخامة العناصر التحصينية وعددها، ولاننسى ان بذرة الاولى في الحماية تتمثل باستخدام الانسان البدائي مواد متوفرة في الطبيعة بهيئة سياج بسيط يحيط بممتلكاته.
- تشترك اغلب القلاع العراقية بامتلاكها محددات تصميمية خاصة بها والتي تعكس بدورها بيئتها وابعادها الثقافية والاجتماعية والمسار التاريخي لها مما يجعلها ذات صفات مميزة وخصوصية واضحة عن مثيلاتها في البلدان المجاورة كتقنيات الانشاء والمواد البنائية والتفاصيل المعمارية والألوان والتي يجب اخذها بنظر الاعتبار عند وضع المخططات التطويرية لها، وعدم التعامل مع القلعة بمعزل عن محيطها فهما ارتبطا بعلاقات فيزياوية وبصرية وحركية عبر الزمن وشكلا سويا مشهدا من مشاهد المدينة.
- الصورة الجديدة لقلعة كركوك تتمثل في ثلاثة مناطق متمايزة فيما بينها ومكملة لمحددات شكلها التصميمي النهائي الا وهي: المناطق الحفاظية، التجميعية،والحضرية الجديدة.

التوصيات:

- ان العمليات التطويرية للقلعة يجب ان تكون على مراحل ومستويات متعددة بعد دراسات واقع الحال، والتعرف على قيمها المعنوية ومكوناتها المعمارية المادية والتي تعمل مجتمعة على افراز مفاتيح تجديدها حضريا وإعادتها الى واجهة الحياة المعاصرة، ويجب متابعة سيرالمخططات المقترحة اثناء عمليات التنفيذ اذ ان التصميم الاساس لا يعتبرانجازا بحد ذاته ما لم يرتبط بمشاكل ومعوقات واقع الحال وتقديم الحلول المناسبة لها.
- يتطلب التعامل مع المواقع التاريخية المهمة خبرة جيدة ودقة متناهية من خلال الابقاء قدر الامكان على معالمها التعريفية وعدم التسرع في التخلص منها وان كانت متهرئة فقد تدلي هذه الادلة مستقبلا بمعلومات جديدة تساعد على فهمها بشكل اكثر عمقا وبالتالي تؤثر على العملية التطويرية ككل.
- يجب إن تعهد المسؤوليات لهكذا نوع من المشاريع الحضرية الكبيرة الى فريق عمل متكامل في اختصاصاته ذوي دراية وخلفية تاريخية وثقافية مناسبة، وان لا تتوزع الى جهات عديدة فبسبب الاحتكاك المستمر بينهم

واختلاف الآراء قد يؤدي الى خلافات وصراعات وينتهي الأمر بنهايات مغلقة وتأخيرات حيوية وتعطيل سير المشروع.

المصادر العربية:

- ـــ، "تطوير قلعة اربيل"، صحيفة الاتحاد، أربع حلقات متتالية،1994.
- ـــ، "هيت"، موسوعة المدن العراقية، ميزوبوتاميا، العدد 5-6، بغداد، مطبعة إيلاف،2005.
- بارو، اندريه، "بلاد اشور"، ترجمة وتعليق عيسى سلمان وسليم طه التكريتي، بغداد، دار الرشيد للنشر، 1980.
- بارو، اندريه، "سومر فنونها وحضارتها"، ترجمة وتعليق عيسى سلمان وسليم طه التكريتي، بغداد، 1979.
- جمال رشيد احمد، " كركوك في العصور القديمة ، كركوك"، بحوث المؤتمر العلمي حول كركوك، اربيل، دار ئاراس للطباعة والنشر،2001.
- الجنابي، هاشم خضر، "مدينة أربيل دراسة في جغرافية الحضر"، الموصل، دار الكتب للطباعة والنشر.
- الحيدري، عبد الباقي عبد الجبار، "التجديد الحضري لقلعة اربيل"، الموصل، مطبعة جامعة الموصل، 1985.
- الدليل السياحي (الأردن) ،2000 .
- الدليل السياحي (بابل)، بغداد ،وزارة الاعلام ،مديرية الاثار العامة ،1972.
- الديوه جي، سعيد، "بحث في تراث الموصل "، بغداد، المؤسسة العامة للاثار والتراث، المديرية العامة للاثار ومتاحف المنطقة الشمالية،1982.
- الرملاوي، جرجيس محمد، مجلة التراث الشعبي، العدد 2، السنة 13، شباط 1982.
- الساعتجي، صبحي، "احياء كركوك ومعالمها"، ترجمة نصرت مردان، موسوعة المدن العراقية، ميزوبوتاميا، العدد 5-6،بغداد ،مطبعة ايلاف، 2005.
- ستين لويد، "فن الشرق الأدنى القديم"، ترجمة محمود درويش، بغداد، دار المأمون للترجمة والنشر، 1988.
- شريف يوسف، "تاريخ فن العمارة العراقية في مختلف العصور"، بغداد، دار الرشيد للنشر،1982.
- شيرين إحسان شيرزاد، "تطوير قلعة اربيل"، ترجمة عرفان سعيد، رسالة ماجستير، 1978.
- عاصم محمد رزق، "معجم مصطلحات العمارة والفنون الإسلامية"، مصر، مكتبة مدبولي،2000.
- العزاوي، عباس، "اربيل في مختلف العصور"، بغداد، شركة الخنساء للطباعة،2001.
- غائب فاضل كريم، "ذاكرة كركوك في شواهد وآثار تاريخية شاخصة"، كركوك.
- كريشن، فريتز، "عجائب الدنيا في عمارة بابل"، تعريب صبحي انور رشيد، بغداد، المؤسسة العامة للاثار والتراث،1982.

- مورتكات، انطوان، "الفن في العراق القديم "، ترجمة وتعليق سلمان وسليم طه التكريتي، بغداد، مطبعة الاديب البغدادية.
- نبيل قصاب، " قلعة اربيل الاثرية "، موسوعة المدن العراقية، ميزوبوتاميا، العدد 5-6، بغداد، مطبعة ايلاف،2005.
- هدى صباح فخرالدين، "الحفاظ وإعادة التاهيل الحضري للقلاع التاريخية في العراق"، رسالة ماجستير، جامعة بغداد، كلية الهندسة، قسم الهندسة المعمارية،2007.

المصادر الأجنبية:

- Doxiadis, "Kirkuk Final Qala Conversation Study" report No.9. prepared for the Ministry of Municipalities of the Government of the Republic of Iraq, National Center for Engineering & Architectural Consultancy, Baghdad, 1976.
- El – Ezabi, "English – Arabic Research's Dictionary", Oxford University Press, England, 1984.
- Gallion, Arthur B., "The Urban Pattern", Van Nostrand Reinhold Company, New York, 1963.
- Huyghi, Rene, "Laroucce Encyclopedia of Prehistoric and Ancient Art", Paul Hamlyn Ltd. , Czechoslovakia , 1962 .
- Janson, H.W., "History Of Art", Harry N. Abrams, New York, 1977.
- Spreiregen, Paul, "The Architecture of Town and Cities", Mc Graw Hill, The American Institute of Architects, United States of America, 1965 .

الانترنيت :

- شبكة المعلومات الدولية: قلعة اربيل.
- شبكة المعلومات الدولية: مدينة هيت.
- شبكة المعلومات الدولية: قلاع الموصل.

http//:www.mcgilluniversity .
http//:www.castledefinitionofcastlebythefreeonlineencyclopediahtm .
http//:www.castles .
http//:www.pounds .
http//:www.morries .

السبل التخطيطية والتصميمية لتحقيق مبادىء الاستدامة التقليدية في عمارة الإسكان المحلية المستقبلية

ميساء ازيارة محمد - مدرس مساعد
قسم الهندسة المعمارية -كلية الهندسة -جامعة بغداد

خلاصة :

ان مفهوم الاستدامة اصبح اليوم من اهم المفاهيم المتداولة في الاوساط العلمية والاكاديمية ,اذ ان التوجهات الحديثة في مجال العمارة والتخطيط تدعو الى التعامل مع البيئة ونظامها الايكولوجي بشكل اكثر وعيا وذلك بالتوافق بين الاداء الاقتصادي والمسؤولية الاجتماعية وسلوكيات الحفاظ على البيئة,وهذا مايطلق عليه ب"العمارة المستدامة ",والذي يتجلى باوضح صوره في العمارة التقليدية للوحدات السكنية التراثية من خلال تفاعل عمارتها مع البيئة المحيطة وهذا ماتناوله البحث بالتحليل والدراسة وتشخيص اهم المبادىء التي اعتمدها تصميم هذا المسكن واهم المعالجات المناخية والاسس التصميمية لاختيار مواد البناء واساليب الانشاء .كما تناول البحث واقع حال عمارة الاسكان المعاصرة .ومن خلال هذا التحليل والمناقشة توصل البحث الى مدى تجاوب الوحدات السكنية التقليدية مع البيئة المحيطة واستغلال الطاقات الطبيعية للوصول الى منطقة الراحة للانسان وبالتالي تاشير اهم السبل التصميمية والتخطيطية لتحقيق الاستدامة في عمارة الاسكان المحلية المستقبلية .

ABSTRACT

Today, the term "sustainability" became one of the most important concepts of interest in scientific and academic debates. The modern approaches in planning and architecture call for respect of the environment and its ecological system through the harmony among three aspects: economical performance ,social responsibility and protection behaviors on environment, which is called "sustainable architecture ".Obviously, this term can be seen in traditional residential dwellings architecture through the interaction with its local environmental conditions .This is what this research deals with by the study and analysis, to determinate the most important principles of traditional house design in terms of climate

treatment , building materials choosing and construction methods .In other aspect, the research referred to the existing manners of recent housing architecture .From this analysis and discussion the research explain the wide response of traditional housing to the local environment and exploitation of the natural potentials to the realization of the comfort zone of occupants. Finally, the research tries to indicate the most important planning and design principles to achieve the sustainability in future local housing architecture.

المقدمة :

- مشكلة البحث:

لقد شهد القرن العشرين وخاصة النصف الثاني منه ولحد اليوم تطورات كبيرة في مختلف مجالات الحياة في الصناعة والنقل والمواصلات والبناء والتي اعتمدت بشكل أساسي على استهلاك الطاقة والموارد الطبيعية التي تمتاز بانها ناضبة ,ومن هذه القطاعات قطاع البناء والتشييد بصورة عامة ومشروعات الإسكان بصورة خاصة ,حيث تشير الدراسات ان 40-50% من الطاقة تستهلك في قطاع البناء والتشييد وان ثلاثة مليارات طن سنويا من الموارد الأولية الطبيعية تستخدم في هذا القطاع .وهذا يهدد بالإخلال في توازن البيئة الطبيعية وعلى مستقبل البشرية خاصة داخل المدن الكبيرة المزدحمة.وان المعالجات التخطيطية والتصميمية التي توضع لمواجهة هذا التهديد على المستوى المحلي غائبة وهذا نلاحظه من خلال مشاريع الاسكان التي تنشا اليوم والتي جاءت غير متلائمة مع الطبيعة المحلية بيئيا بل وحتى اجتماعيا.

- هدف البحث :

بيان أهم السبل لتحقيق الاستدامة في عمارة الإسكان مستفيدا من المعالجات التقليدية في المدينة القديمة لمواجهة الظروف الطبيعية المحيطة بها بأقل استهلاك للطاقة .اي التعامل مع البيئة المحيطة بشكل اكثر توازنا.خاصة من قبل المعماريين والمصممين .للبحث عن بدائل تخطيطية وتصميمية للمدن الحديثة والمجمعات السكنية الجديدة من خلال الاستفادة من مصادر الطاقة الطبيعية الجديدة منها والمتجددة .

منهجية البحث :

اعتمد البحث:المنهج التحليلي للمعالجات المناخية التقليدية والأسس التصميمية لاختيار مواد البناء وأساليب الإنشاء للوحدات السكنية التقليدية اعتمادا على المؤثرات البيئية المحيطة وأثرها على تصميم الوحدات السكنية لاستنباط اسس تخطيطية وتصميمية .

فرضية البحث :

ان اعتبار مبدأ المسكن المتوافق بيئيا أساس لتصميم الوحدات السكنية في المستقبل ضروري لحماية البيئة والحفاظ على مكوناتها الطبيعية وتقليل التلوث والأضرار التي سببتها الوسائل الحديثة في البناء كجزء أساسي من التنمية المستدامة والحفاظ على الموارد الطبيعية للأجيال القادمة على كوكب الأرض .

<u>– مفهوم التنمية المستدامة وأثرها في التخطيط والعمارة :</u>

الاستدامة كلمة قديمة لها جذور في اللغة اللاتينية وهي اشتقاق عن كلمة sustain التي تعني to hold up ;to support from below التي من معانيها :يبقي ,يطيل البقاء ,يدعم او يساند ,من هنا جاء استخدام هذا المصطلح ليعطينا معنى إطالة البقاء ودعم مصادر الطاقة ووسائل المعيشة على كوكب الأرض (Senosiain,2003) .

على مر العصور كان كل مجتمع ,على تنوع بيئته الطبيعية وموروثه الحضاري بل وحتى قيمه الروحية ,يستنهض أبناءه للحفاظ على وجوده وكيانه .ان المجتمعات التقليدية هي المكان الذي تتجسد فيه الاستدامة مفهوما وأسلوبا للمعيشة .

ان مفهوم الاستدامة موجود منذ القدم ,وبالتالي فان الاسلاف لم يستخدموا مصطلح الاستدامة كتعبير عن طريقة معيشتهم وكيفية توفير مصادر العيش والأسلوب الذي يبنون به بل عاشوا المفهوم وطبقوه بشكل عفوي وتلقائي .لقد كان تفاعلهم مع البيئة المحيطة والاستغلال الأمثل للموارد الطبيعية جزءا من ضمان بقائهم على هذه الأرض بالتوافق معها واستغلال ما تجود به من خيرات والتكيف مع الظروف الصعبة كالمناخ القاسي وشح بعض الموارد والكوارث الطبيعية .لقد كان مفهوم الاستدامة متواجدا في نمط حياتهم لان البيئة المحيطة كانت مصدر حياتهم ,وبالتالي حافظوا على مواردها وزادوا من خيراتها وصانوا نعمة الله عليهم ,الاستدامة بالنسبة لهم كانت عفوية وتلقائية ,نابعة من نمط معيشتهم ولم تكن شيئا مقحما او مفروضا او قسريا .مما لاشك فيه ,فان عفوية تعامل الأجداد مع البيئة لم تكن عشوائية او فطرية بل استندت على ارث عميق من التجارب والتعلم عبر مبدأ "التجربة والخطأ " يدعمه فكر مبدع وبصيرة نافذة .

ان من اشمل التعريفات للتنمية المستدامة تعريف المنظمة العالمية للبيئة والتنمية (WCED) باعتبارها تعني تلبية احتياجات المجتمع في الوقت الحاضر بشكل يوفر للأجيال القادمة الإمكانيات لتحقيق احتياجاتها (WCED,1987) .هذا التعريف يشير الى تطوير أساليبنا في الحياة والبناء بشكل أكثر احتراما للبيئة عبر الاستغلال الكفء لمصادر الطاقة الطبيعية التقليدية منها والمتجددة والتقليل من التأثيرات الضارة لاستخدام الطاقة كالتلوث والغازات السامة .والتركيز على التقنيات الصديقة للبيئة خاصة في مشروعات الإسكان

- التصميم والتخطيط المستدام خطوة أساسية لاستدامة مشروعات الإسكان :

سادت العالم اليوم مصطلحات عديدة منها العمارة الخضراء (Green Architecture), التصميم المستدام(Sustainable Design), والتصميم البيئي أو الايكولوجي(Environmental or Ecological Design). وهي مسميات مهما بدت متعددة إلا أنها تسعى في مجموعها لتحقيق التوازن بين احتياجات الإنسان من جهة والحفاظ على الموارد الطبيعية من جهة أخرى للتقليل من نسب التلوث البيئي.لذا سيتم تحديد مفهوم التصميم المستدام كخطوة أساسية لتحقيق الاستدامة التقليدية :

التصميم المستدام هو مفهوم متكامل له بعد فلسفي أكثر من كونه مجرد شكل خارجي للمبنى (Kim & Rigdon ,1998) .أهم ما يميز التصميم المستدام كونه شموليا يسعى لتكامل العمارة والتخطيط مع التخصصات الأخرى سواء أكانت هندسية ,اجتماعية ,اقتصادية او صحية .

ان العمارة المستدامة أصبحت ذات بعد تكاملي مع البيئة وصارت لابد من ان تأخذ العديد من الأولويات بنظر الاعتبار مثل :الحفاظ على البيئة ,تقليل التلوث,ترشيد استهلاك الطاقة ,توفير بيئة صحية مريحة للإنسان ,تطوير أساليب جديدة للبناء والتصميم البيئي المعتمد على الطاقات الطبيعية والمتجددة . (الزبيدي:2001)كل هذا ينبغي ان يكون مقترنا بالأداء الاقتصادي طوال عمر المبنى سواء في التصميم او مواد البناء وحتى إمكانية الاستفادة منه بعد انتهاء الحاجة سواء بإعادة الاستخدام او من مواده الأولية بما يقلل من التأثير السلبي على البيئة .

-مفهوم الاستدامة في التخطيط والعمارة التقليدية :

ان العمارة هي الوسيلة الأساسية التي ابتكرها الإنسان لحمايته من ظروف البيئة الخارجية القاسية وذلك بالاعتماد على الطاقة السلبية او الذاتية (والتي تعني استغلال مصادر الطاقة الطبيعية كالشمس والرياح وإمكانيات التربة).

ان التصميم المستدام المتوافق مع البيئة ليس فكرة جديدة ,بل انها اقرب ما تكون لكونها فكرة ضائعة في الوقت الحاضر(بسبب الابتعاد عن الحلول البسيطة للمعالجات المعمارية والاعتماد على الحلول الميكانيكية). اذ تتكامل عناصر التصميم المستدام مع الفكر التصميمي للعمارة التقليدية ,التي تم

اختبارها وأثبتت نجاح حلولها عبر فترات طويلة من التجربة والخطأ باستخدام مواد البناء المحلية وبتقنيات بسيطة مدروسة لكنها نابعة من بيئتها المحلية .فالإنسان القديم كان يعيش في الكهف مستفيدا من درجات الحرارة الثابتة نسبيا والتهوية الطبيعية دون التأثير على البيئة وظل الإنسان يحاول استغلال وتطوير الموارد الطبيعية والتكيف مع البيئة لتحسين مستوى المأوى الذي يحميه (Kim&Rigdon,1998).اي كان التكيف يحدث ضمن مبادئ الاستدامة لأنها اعتمدت على الموارد المتاحة والتقنيات النابعة من البيئة حيث كانت الحلول فعالة ومتفاعلة مع البيئة والموارد المتوفرة دون الحاجة لتحويلها او السيطرة عليها .

-المدينة العراقية التقليدية والاستدامة :

تعتبر المدينة العراقية التقليدية بنسيجها المتضام التقليدي أفضل مثال على تطبيق مفهوم الاستدامة على مستوى المدينة ككل, فتخطيط المدينة ومعالجات مسارات الحركة من حيث العرض, الشكل, الطول, التوجيه وتغيير الاتجاه يمثل المرحلة الأساسية للتكيف مع البيئة.يؤدي النسيج المتضام الى تلطيف مؤثرات المناخ القاسية والتخفيف من أثرها خاصة درجات الحرارة العالية والإشعاع الشمسي والرياح المترية والحارة وبالتالي التخفيف من العبء الحراري الإجمالي على الأبنية خاصة الوحدات السكنية **(شكل -1-)**.

ان توافق المسكن مع البيئة ,بكل ايجابياتها وسلبياتها ,تم تحقيقه وفق إستراتيجيتين هما :الحماية والتكيف

الحماية:كانت بالحد من تأثير ظروف البيئة الطبيعية القاسية كالمناخ الحار وقلة الرطوبة النسبية في بعض المناطق وارتفاعها في مناطق أخرى.

اما التكيف: فكان باستغلال الإمكانيات الكامنة لهذه الظروف القاسية والتعامل معها بما يحقق الراحة الحرارية للساكنين واستغلال مصادر الطاقة الطبيعية كالشمس والرياح وقدرة التربة على الخزن الحراري .ان مثل هذه المبادئ الأساسية التي استندت عليها عمارة وتخطيط المسكن التقليدي والتي يمكن مع

بعض التعديل والتحوير والتطوير ان تكون مؤشرات دالة للتصميم والبناء في العمارة والتخطيط المعاصرين خاصة في مجال مشروعات الإسكان . (الزبيدي ,2001)

الشكل -1- النسيج الحضري المتضام في المدينة العراقية التقليدية (مدينة النجف القديمة),
تقارير دراسة التصميم الاساسي لمدينة النجف الاشرف–وزارة البلديات والأشغال العامة –دائرة التخطيط العمراني ,2009

<u>–المبادىء الفكرية لتخطيط وتصميم المسكن التقليدي :</u>

استند الفكر التخطيطي والتصميمي للمسكن التقليدي للتكيف مع البيئة القاسية ولتحقيق مبدأ الاستدامة على المبادئ التالية :

* الفناء الوسطي المفتوح في المسكن التقليدي :

هنا جاء استخدام الفناء الوسطي المفتوح كنقطة مركزية لتحقيق مبدأ التوجه نحو الداخل **(الشكل –2–)** ولتحقيق المرونة باستخدام المسكن حسب تنوع الفعالية والمؤثرات البيئية كاستخدام الفناء الوسطي في ساعات الصباح الأولى ,والسرداب في فترة ما بعد الظهر ثم السطح ليلا في الصيف .اما في الشتاء فتستخدم فضاءات الطابق الأول للاستفادة من أشعة الشمس لوجود نوافذ أكثر من الطابق الأرضي ومواد بناء مختلفة ,كذلك استخدام الفناء الوسطي في الفترات التي تصله أشعة شمس كافية نهارا .

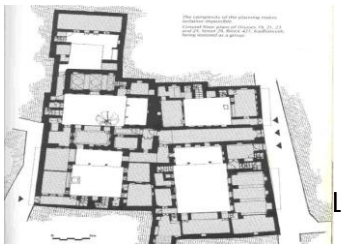

الشكل -2- مسكن تقليدي ذو الفناء الوسطي في مدينة بغداد (وارين,فتحي,),1982,ص120

يكون الأداء الحراري للفناء الوسطي كأحد عناصر التصميم البيئي في المسكن التقليدي معتمدا على كونه يعمل كمنظم حراري Thermal Regulatorمستفيدا من الفرق الكبير في درجات الحرارة ما بين الليل والنهار وتكوين أماكن ضغط متباينة ما بين الشوارع الضيقة المظللة والفناء الوسطي المفتوح (Evans, 1980). (**الشكل –3–**)

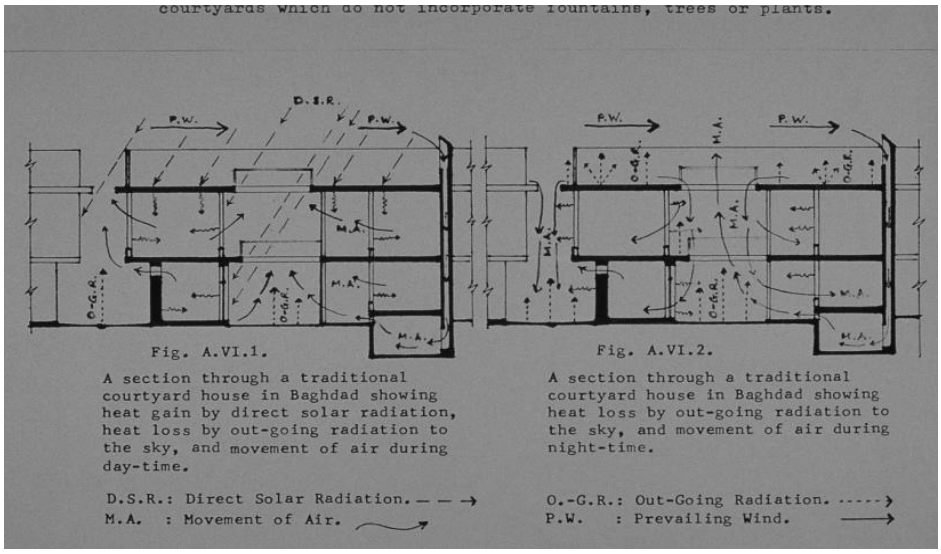

الشكل -3- الاداء الحراري للفناء الوسطي في السكن التقليدي, (العزاوي,2010)

في دراسة لعدد من المساكن التقليدية في مدينة بغداد ,احدهما كان بفناء وسطي مفتوح والآخر كان الفناء الوسطي قد تم تغطيته بمواد خفيفة ,وجد ان الأداء البيئي للفناء الوسطي المفتوح كان أكثر كفاءة من حيث تقارب المدى الحراري اليومي وكونه يكون ضمن حدود الراحة الحرارية للإنسان خاصة في ساعات الصباح الأولى وفترة ما قبل الظهيرة .(**الشكل –4–**).(الزبيدي ,2001)اما الفناء المغلق فقد كاد ان يقترب في أدائه الحراري من درجات حرارة الهواء الخارجي في ساعات الصباح الأولى ,ويقل عنها في فترة ما بعد الظهر اما في المساء وبعد غروب الشمس حيث تبدأ درجات الحرارة الهواء الخارجي بالانخفاض يكون الفناء المغلق أكثر حرارة حتى بعد منتصف الليل لكونه يختزن الحرارة المكتسبة طوال النهار دون ان يتمكن من إعادة إشعاعها الى السماء كما في الفناء المفتوح (الزبيدي

,2001).وهذا يدل على ان الفناء المفتوح هو الحل الأكثر كفاءة لأنه أكثر تفاعلا مع المؤثرات البيئية إضافة لايجابيته الاجتماعية والوظيفية والجمالية .

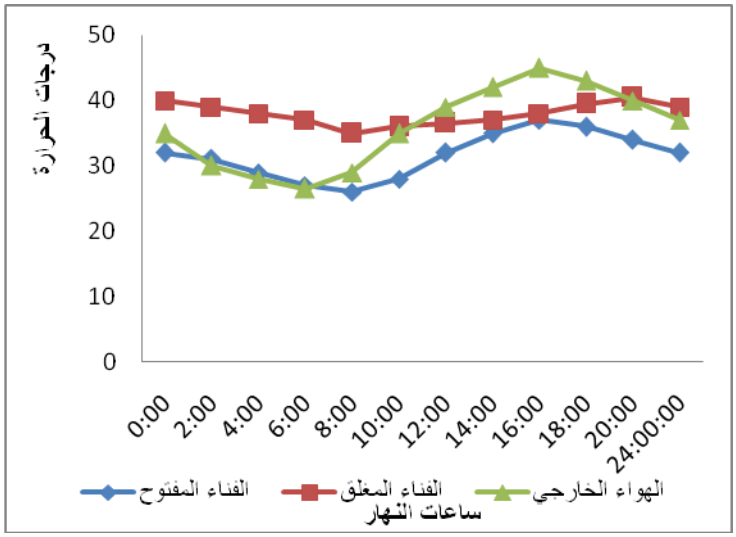

شكل -4- مخطط درجات الحرارة للفناء الوسطي في مسكن تقليدي (الزبيدي,2001),ص25

-الأداء الحراري لقشرة المسكن التقليدي :

يمثل غلاف المبنى Building Envelope للوحدة السكنية التقليدية الحاجز الأساسي بين الداخل والخارج ,حيث يمكن اعتباره الوسط الذي يتم عبره وبواسطته التخفيف من تأثير البيئة الخارجية القاسية لجعل الفضاءات الداخلية مريحة للساكنين .

يعتمد الأداء الحراري لغلاف المبنى (الجدران والسقف) على مبدأ مقاومة انتقال الحرارة وتقليل الكسب الحراري وعكس الأشعة الشمسية قدر الإمكان , لتوفير بيئة داخلية باردة نوعا ما للظروف الخارجية .

لتحقيق هذه الإستراتيجية التكيفية وتوفير بيئة داخلية مريحة ,فان الخصائص الحرارية لمواد البناء المكونة لغلاف المبنى كالسعة الحرارية والمقاومة الحرارية والامتصاصية والانبعاثية لا بد ان تعمل على مقاومة الانتقال الحراري خلالها وتعكس اكبر قدر ممكن من الإشعاع الشمسي (Collier,1995) . عليه فان تحقيق مفهوم الاستدامة تم بالاستفادة من قشرة المبنى ليس كحاجز يفصل بين البيئة الخارجية والفضاءات الداخلية فحسب بل كانت قشرة المبنى جزءا من التصميم للتكيف مع البيئة والتفاعل معها .

- مواد البناء في المسكن التقليدي:

يمتاز المسكن التقليدي باستخدام المواد المتوفرة في البيئة كالطين والحجر والجبس وجذوع وسعف النخيل ,مواد البناء هذه كتلية Massiveكالطابوق للجدران والحجر للأسس وهي مواد ذات سعة حرارية Heat capacity عالية تبعا لسمكها ولها قدرة على خزن الطاقة الحرارية الساقطة عليها لفترات طويلة في الفترة الحارة من اليوم (النهار) ثم إعادة بثها الى الفضاءات الداخلية فترة المساء (بعد الغروب) اي بعد غياب مصدر الطاقة .بذلك يتم تحقيق الموازنة الحرارية Thermal Equilibrium بين الحرارة المكتسبة والمفقودة عبر قشرة المبنى (السطح والجدران)مما يؤدي الى توزيع داخلي منتظم للحرارة داخل المبنى (Evans,1980) .

ان انتقال الطاقة الحرارية من السطوح الخارجية الى السطوح الداخلية يعتمد على السعة الحرارية لمواد البناء وسمكها وتتناسب قدرة المادة على خزن الحرارة وتأخير إعادة بثها الى الداخل ,وهو ما يسمى بالتخلف الزمنيTime lag,تناسب طردي مع سمك المادة .وتمتاز مواد البناء التقليدية بان لها تخلفا زمنيا كبيرا يتراوح بين (12–15) ساعة تبعا لنوع المادة وسمكها (Siani,1980).لذا نجد ان سمك الجدران في المسكن التقليدي يتراوح بين (0.50–0.60–0.75) م حسب موقع الجدار بينما في المساكن الحديثة لا يتجاوز سمك الجدران الخارجية من الطابوق (0.24–0.36)م مما قلل كثيرا من دور قشرة المبنى كوسط للتخفيف من تأثيرات البيئة الخارجية على الفضاءات الداخلية .

في دراسة للأداء الحراري لمسكن تقليدي وآخر حديث ,حيث أخذت قياسات درجات الحرارة لفضاء في الطابق الأرضي في كلا النموذجين بالإضافة الى السطح في المسكن الحديث ,وجدت ان الأداء الحراري للمسكن التقليدي كان أكثر كفاءة من المسكن الحديث (**الشكل–5–**)(الزبيدي,2001). من ذلك نستنتج ان الأداء الحراري للمسكن التقليدي كان اقرب لحدود الراحة الحرارية للإنسان محققا استقرارية حرارية أكثر مما لا يتطلب معه استخدام وسائل التكييف الميكانيكية ,وهذا يعني التقليل من استهلاك الطاقة وتوفير في الكلفة وعدم التسبب في تأثير سلبي على البيئة ذلك بالاستخدام الكفء لمواد البناء المتوافقة مع البيئة المحلية والقابلة لإعادة الاستخدام والتصنيع وهو من أسس الاستدامة .

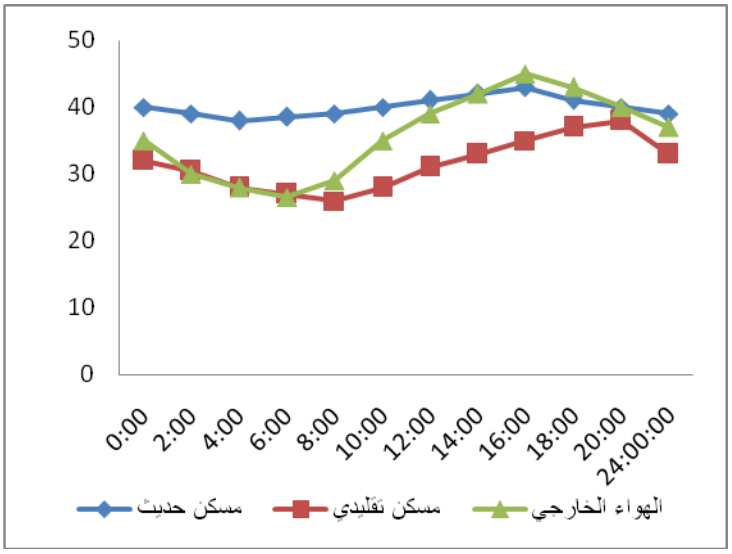

شكل -5- مخطط درجات الحرارة لمسكن تقليدي وحديث (الزبيدي,2001),ص27

- استغلال إمكانات التربة في المسكن التقليدي :

تعتمد فكرة البناء تحت الأرض على تقليل او تحديد تأثير الظروف المناخية الخارجية على الفضاءات الداخلية ,وذلك بالاستفادة من إمكانيات الخزن الحراري لكتلة التربة الذي يسمى التكييف (التبريد والتدفئة بتأثير الكتلة Mass-effect cooling or heating).

يعتمد التبريد والتدفئة بتأثير الكتلة على الخزن الحراري إثناء أكثر الفترات حرارة في السنة وإعادة إطلاقها في الفترة الأكثر برودة وهو المبدأ الذي يعتمد عليه البناء تحت الأرض وذلك بالاستناد على عدة مبادئ أساسية هي (الزبيدي, 2001) :

- الاستفادة من التماس مع التربة لتحقيق الخزن الحراري الفصلي .
- تقليل الذبذبة الحرارية اليومية .
- تأخير وصول الحدود القصوى لدرجات الحرارة اليومية الى الفضاءات الداخلية .
- التهوية او التفريغ الحراري للمبنى إثناء الليل.

ان الاستفادة من خصائص باطن الأرض للوصول الى الراحة الحرارية وتبريد الفضاءات الداخلية اعتمادا على الطاقات الطبيعية يتجسد في السرداب في الأبنية السكنية التقليدية (المعروف الية عمله وتكييفه الطبيعي المبني على التحرك الهوائي عبر البادكير)والذي قد يكون طابق واحد او أكثر تحت

الأرض مع بقاء بقية الفضاءات فوق سطح الأرض حيث يكون البناء تحت الأرض بشكل جزئي .(**الشكل -6-**)

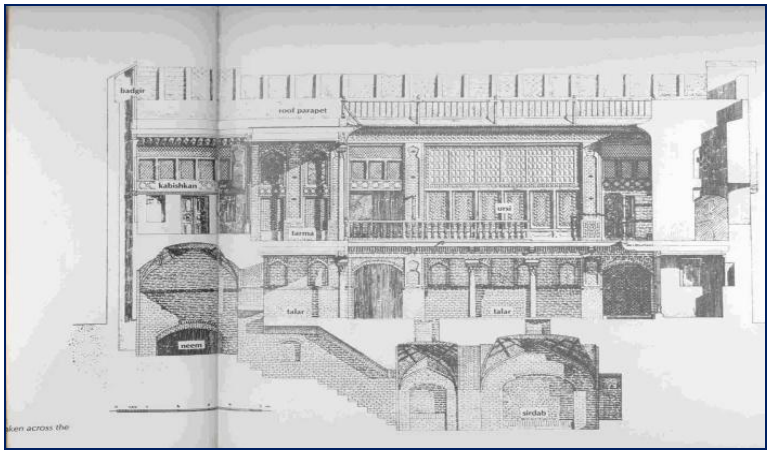

الشكل -6-السرداب احد تطبيقات الاستدامة باستغلال خصائص التربة . وارين,فتحي,1982,ص113

في دراسة عن المسكن التقليدي اتضحت كفاءة الأداء الحراري للسرداب ,خاصة في فترة ما بعد الظهيرة ,حيث تصل درجات حرارة الهواء الخارجي الى حدوده القصوى (**الشكل -7-**).(الزبيدي ,2001)

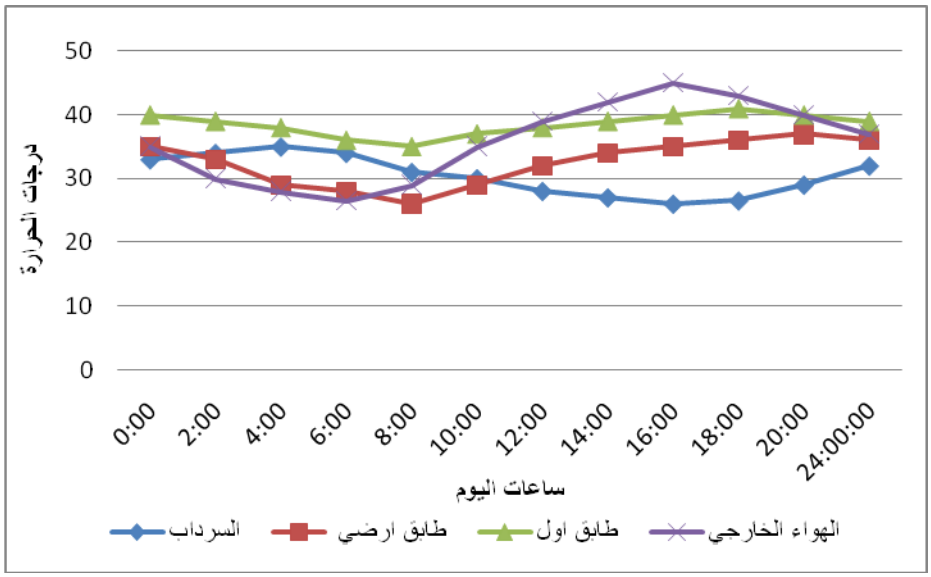

شكل -7- مخطط درجات الحرارة للسرداب في مسكن تقليدي (الزبيدي,2001),ص30

من التحليل السابق للمبادئ التصميمية والتخطيطية للمسكن التقليدي يتجسد مدى التجاوب مع البيئة المحلية واستغلال الموارد المتاحة في البيئة المحيطة لإقامة عمارة توفر الراحة للساكنين وتحافظ على الموارد الطبيعية .وهذا أساس مفهوم التنمية المستدامة المعاصر والذي يجب على العمارة المعاصرة لمدننا العراقية ان تثبت انها قادرة على استيعاب متطلبات هذا المفهوم وذلك لا يمكن إلا من خلال قراءة مبادئ التخطيط والعمارة التقليديين واختيار ما هو ملائم منها للبيئة المحلية والمناخ وتطوير ومزج هذه المبادئ مع التقنيات الحديثة واستخدامها في مشروعات الإسكان المحلية المستقبلية .

– واقع مشروعات الإسكان المحلية المعاصرة:

شهدت مرحلة الخمسينات والستينات تحولات و مفاهيم حديثة في العمارة والتي كان لها الدور الواضح في العراق والعالم العربي ، من خلال تأثر الأكاديميين بهذه التيارات من خلال طروحاتهم وأفكارهم ، ومن خلال الموفدين إلى الخارج والمبعوثين العائدين إلى بلدانهم واتساع نطاق العمل والخبرة الهندسية ، ونشوء الجمعيات الفنية والمعمارية والتخطيطية المشتركة ، اذ اصبح أهم المعماريين يقوموا بتقليد ونقل الأفكار التخطيطية والمعمارية السائدة (مفاهيم العمارة العالمية) وزرعها في مناطق جغرافية متباينة الطبيعة والطبوغرافية والقيم الأخرى .

لم تكتب الاستمرارية لامتداد المدينة التقليدية الحضاري في العمارة المعاصرة ، كذلك إن العمران المعاصر يفتقد إلى كثير من متطلبات واحتياجات المجتمع المسلم ، ولا يعبر بأي صورة عن ملامح شخصيتها الحضارية . وفيما يأتي عرض لبعض المعاني و التطبيقات السلبية من مضامين شخصية وخصائص الإطار العمراني المعاصر لمشروعات الاسكان المحلية:

***الموقع والتخطيط في مشروعات الإسكان المحلية المعاصرة :**

كان الموقع في السكن التقليدي (موقع الوحدة السكنية)على الاغلب قطعة من الارض غير منتظمة الشكل لذا كان الفناء الوسطي منتظم الشكل يسقط اولا في وسط او احد جوانب الموقع وعلى اساسه يتم تصميم بقية فضاءات المسكن .يتم تعديل الموقع بجعل بعض الفضاءات الخدمية غير المنتظمة الشكل او باستخدام الجدران السميكة والتي يستفاد من سمكها في عمل الفتحات والحنايا والخزائن او ملاقف الهواء .كما ان تراتب الوحدات السكنية مع بعضها البعض هو الذي يحدد اشكال الشوارع.فالوحدة

القياسية لتشكيل النسيج العضوي هي الانسان.وبما ان الغالبية العظمى من أشكال القطع السكنية ذات شكل غير منتظم فيصعب تمييز الوحدات السكنية و الفصل بينها على مستوى المخطط (التضام والتكافل).

على العكس من النمط العضوي فأن الشوارع في الاحياء السكنية الحديثة هي التي تحدد مساقط وتوزيع الوحدات السكنية.فالوحدة القياسية لتشكيل النسيج الحضري هي المركبة.وهناك نزعة هندسية لتقسيم الاراضي وفقا للنمط الشبكي فيمكن وبكل سهولة تمييز الوحدات السكنية (التفكك والفردية)على العكس مما كان سائدا في النسيج العضوي. والذي شكل اخفاقا واضحا بالمحدد المناخي الذي تتسم به مدننا العراقية عامة فلا وجود للظل و الضوء وانما مساحات واسعة معرضة للاشعاع الشمسي. (**الشكل –8–**)

الشكل –8– مجمع سكني معاصر في النجف الاشرف ,التفكك والفردية في النمط الشبكي غير المتلائم مع البيئة المحلية, تقارير دراسة التصميم الاساسي لمدينة النجف الاشرف–وزارة البلديات والأشغال العامة –دائرة التخطيط العمراني ,2009

ظل الشكل العضوي طابعا مميزا للمدينة العراقية حتى دخول الانكليز الى العراق فشكل احتلال الانكليز لبغداد,فاصلة تغير الفكر التخطيطي ولكن هناك نقطتان مهمتان شكلت الانفصال العام للبنية العضوية وظهور النمط الشبكي هي:

- اعلان قانون ادارة البلديات سنة1931 و نظام الطرق و الابنية لسنة 1935.والذي بموجبه قسم المدينة والمناطق السكنية الى اصناف حسب الجدول (1).

- تشكيل مجلس الاعمار سنة 1950 خصوصا بعد زيادة الواردات النفطية للعراق.

اذ ظهرت مشاريع اسكانية مبنية على طروحات وافكار غربية من حيث الكثافات وارتفاعات الابنية وعرض الممرات والارتدادت التي لا تتلائم مع متطلبات البيئة المحلية الطبيعية والاجتماعية .(كمونة ,1989,ص86)

الجدول 1 اصناف المناطق السكنية حسب نظام الطرق و الابنية لسنة 1935,الوقائع العراقية

صنف المنطقة السكنية	مساحة القطعةم²	المساحة المشيدة	مسافة الارتداد الامامي	عرض الطريق	عرض المماشي	عرض واجهة القطعة
الاولى	1–100	%100	–	4	3	8
الثانية	101–200	%100	–	8	3	8
الثالثة	201–300	%65	2.5	10	6	15
الرابعة	301–600	%55	4	12	6	20
الخاصة	601–800	%50	5	15	6	25
الممتازة	800–1000	%30	5	15	6	25

*** التظليل والتشجير في مشروعات الإسكان المحلية المعاصرة :**

اعتمدت عمارة المسكن التقليدي على توفير الظل ذاتيا وذلك من خلال تجاور الوحدات السكنية ,تقليل عرض مسارات الحركة خاصة في المحلات السكنية وتظليلها بالبروزات والتطليعات او حتى بناء فضاء او غرفة تمتد فوق الزقاق او مسار الحركة من الطابق الاول .اما الفناء الوسطي فقد كان يوفر ظلالا على اجزاء منه سواء بجدرانه المرتفعة او النباتات والاشجار التي تزرع فيه.

وفيما يخص ابعاد المقطع العمودي لفضاء الشارع السكني ع/عر(الارتفاع الى العرض) ,فان لها علاقة وثيقة بزاوية دخول اشعة الشمس اليه .وكلما زادت هذه النسبة كلما قلت نسبة الاشعة الشمسية النافذة الى فضاء الشارع السكني.ففي النموذج العضوي كانت هذه النسبة تصل الى (3– 4 : 1) فحققت كفاءة مناخية عالية حيث قللت من نفوذ الاشعة الشمسية الى فضاء الشارع السكني. (**الشكل –9–**)

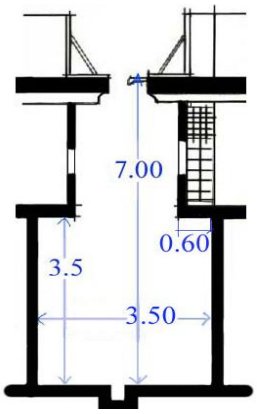

الشكل –9– الكفاءة المناخية من خلال نسبة الارتفاع الى العرض في النموذج التقليدي.**رياض,2007,ص68**

على العكس مما نجده حاليا في المدينة العراقية فتقل نسبة (ع/عر)لتصل الى (1 : 4– 5) .وهذا يعود الى الانظمة و المعايير المحلية للمدينة العراقية (نظام الطرق و الابنية رقم 44 لسنة 1935 وقانون التصميم الاساس لمدينة بغداد رقم 56 لسنة 1973 والتي ساهمت بتقليل هذه النسبة من خلال فرضها للارتدادات الامامية و الخلفية التي تأخذ بنظر الاعتبار المتطلبات الوظيفية فقط دون أية مراعاة لمتطلبات المناخ الحار الجاف للمدينة . (**الشكل –10–**)

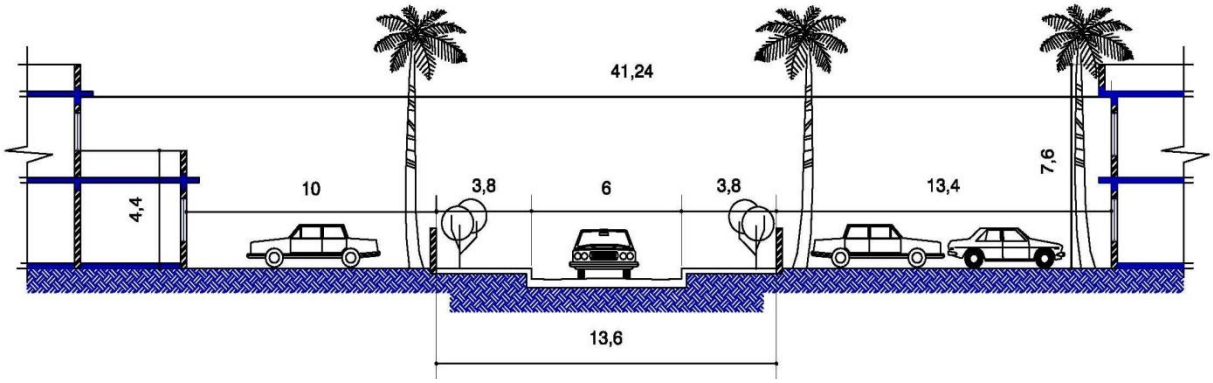

الشكل –10– عدم مراعاة الظروف البيئة المحلية الاجتماعية والمناخية من خلال نسبة الارتفاع الى العرض (ع/عر) في النموذج المعاصر .(**رياض,2007,ص115**)

*** التهوية الطبيعية في مشروعات الإسكان المحلية المعاصرة :**

لقد طورت العمارة التقليدية اساليب مبتكرة للحصول على التهوية الطبيعية.فالفناء الوسطي يعتبر الرئة والمتنفس الرئيسي للمسكن والذي يعمل كمنظم حراري مستفيدا من التذبذب الكبير بين درجات الحرارة ما بين الليل والنهار .كما ان لهندسية الشارع علاقة وثيقة بتحسين المناخ الموقعي ,فالانحناءات في فضاء الشارع وتغير اتجاهه في المناطق الحارة الجافة تساعد على الاستقرار الحراري وركود الهواء البارد اسفل الشارع وكذلك تصفية الهواء من حبيبات الرمل و الاتربة التي تمتاز بها المناطق الحارة الجافة عموما.

على العكس من المحلات السكنية في النموذج الشبكي فتمتاز بشوارعها المستقيمة و الرتيبة التي تتخللها حركة هواء متربة وسريعة وغير مسيطر عليها.**(الشكل-11-)**كذلك في المشروعات الاسكانية المتعددة الطوابق فان التباعد بين الابنية والفضاءات الواسعة المعرضة الى الاشعاع المباشر يسبب خلق دوامات من الغبار والتحرك الهوائي السريع غير المتلائم مع منطقة الراحة للانسان المحلي .**(الشكل -12-)**

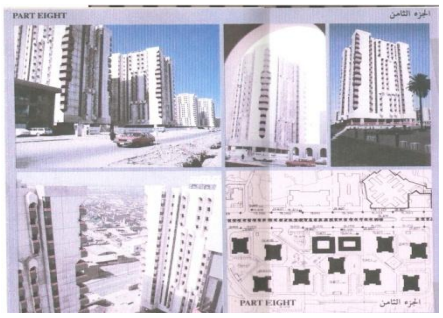

الشكل –11– نمط الشوارع في النموذج المعاصر لا يستطيع خلق جو موقعي خاص وفي المشروعات الاسكانية العمودية نفس المشكلة(شارع حيفا).اعداد الباحث

(الشكل–12–)يوضح متغيرات الراحة الحرارية الملائمة للإنسان العراقي.رياض,2007

	فصل الصيف	فصل الشتاء
درجة الحرارة	26° –28°	20° –22°
الرطوبة النسبية	30% –50%	40% 60%
حركة الهواء	0.5م/ثا–1.5م/ثا	0.07م/ثا–0.5م/ثا

*** مواد البناء في مشروعات الإسكان المحلية المعاصرة :**

مواد البناء المستخدمة في المسكن التقليدي كانت نابعة من البيئة وذات ديمومة عالية كالحجر والطابوق الذي يمكن ان يعمر مئات السنين .كما ان الخواص الحرارية والفيزيائية لمواد البناء التقليدية ساعدت على جعل قشرة المبنى الوسط الذي يخفف من تاثير البيئة الخارجية القاسية كما ذكر سابقا.**الشكل–13–**

الشكل –13–مواد البناء المحلية المتفاعلة مع البيئة الطبيعية. تصوير الباحث

اما مشروعات الاسكان المعاصرة فنلاحظ استخدام المواد ذات المعاملات الحرارية غير المتلائمة مع البيئة المحلية وخاصة في الاسكان العمودي مثل الجدران الكونكريتية المسبقة الصنع وذات السمك الذي لا يتجاوز ال10 سم هذا على مستوى الكتل اما الفضاءات الحضرية فنلاحظ استخدام مادة

الاسفلت في رصف الارصفة والساحات العامة والتي تعمل على تقليل الكفاءة المناخية للفضاء الحضري **.الشكل-14-**

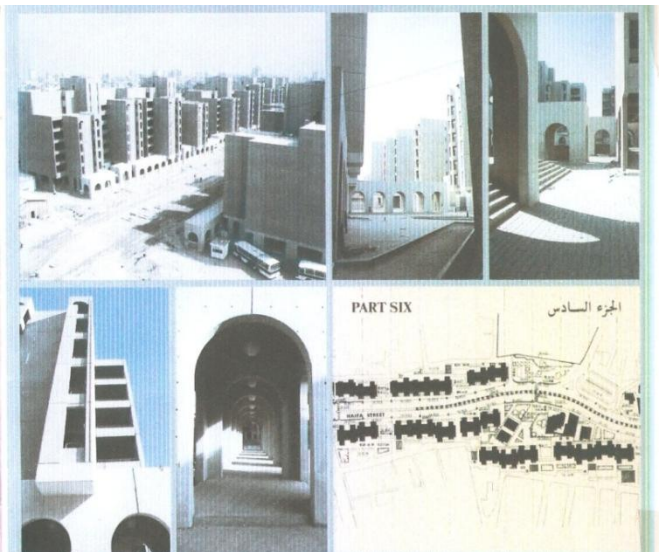

الشكل -14- مواد البناء الكونكريتية المسبقة الصنع مع مساحات التبليط الكونكريتية والاسفلتية الكبيرة تقلل من الاداء الحراري للمبنى وللنسيج الحضري(شارع حيفا),كراس مشروع تطوير شارع حيفا ,1985

<u>- استنباط مبادئ الاستدامة التقليدية في مشروعات الإسكان المحلية المستقبلية :</u>

ان تحقيق الاستدامة في مشروعات الإسكان المستقبلية يأتي عبر تكامل مبادئ التخطيط والعمارة التقليدية للسكن التقليدي مع نظم ووسائل التكنولوجيا الحديثة والذي يحقق :الحفاظ على مصادر مواد البناء والطاقة الطبيعية ,توفير الراحة للساكنين ,التوفير في الطاقة وكلف التشغيل ,تقليل التلوث والمخلفات والتوفير عن طريق إعادة الاستخدام .اي ان يكون متوازنا بيئيا نابعا من بيئته ومتوافقا معها مستفيدا من إمكانياتها ومحافظا على مواردها للأجيال القادمة .

ويمكن ان نستخلص مجموعة من المبادئ التي استند عليها المسكن التقليدي لترشيد استهلاك الطاقة وتوفير الراحة للساكنين دون التأثير على البيئة والتي يمكن ان نطورها كمؤشرات لمشروعات الإسكان المستقبلية :

*** الموقع والتخطيط في مشروعات الإسكان المستقبلية :**

ان تخطيط الموقع يعتبر الخطوة الأساسية التي يمكن على أساسها زيادة كفاءة التخطيط والتصميم للمشروع الإسكاني ,فتسقيط المبنى بشكل مدروس بالنسبة لزوايا سقوط الشمس والرياح السائدة ,التوجيه الصحيح للفضاءات المختلفة تبعا لوظيفة ومتطلبات كل فضاء والاستغلال الأمثل لإمكانيات الموقع الجغرافية والطبوغرافية تمثل مرحلة مهمة في التخطيط وعاملا أساسيا في تلطيف البيئة المحيطة الى درجة تقلل من تأثيرها السلبي على المسكن وتزيد من ايجابيتها لراحة الساكنين .

إن الغاية من تحديد نسبة ارتفاع كتلة الوحدة السكنية إلى عرض فضاء الشارع السكني المقابل لها هو:

- تقليل نفوذ الأشعة الشمسية إلى داخل الفضاء الحضري.
- التحكم باختراق الرياح لفضاء الشارع و خصوصا خلال الفترة الحارة.

وذلك لأنه في مناخ حار جاف مثل مناخ مدينة بغداد تعمل الرياح على الحارة المتربة على رفع درجة حرارة الفضاء فلابد من التحكم بحركتها من خلال عدة إجراءات أولها تحديد حجم الفضاء الحضري بواسطة زيادة نسبة (الارتفاع الى العرض) وذلك عن طريق :

تقليل المسافة الفاصلة بين الكتل السكنية المتقابلة إلى الحد الذي يضمن الملائمة الوظيفية و المناخية في آن واحد وهذا يتطلب تقليل مسافة الحدائق الأمامية الموجودة في القطع السكنية المتقابلة من اجل الوصول إلى النسبة (1: 2– 3) أو الاقتراب منها مما يزيد من تضام الأبنية و لاسيما ذات النمط المتصل أو شبه المتصل. **الشكل –15–**

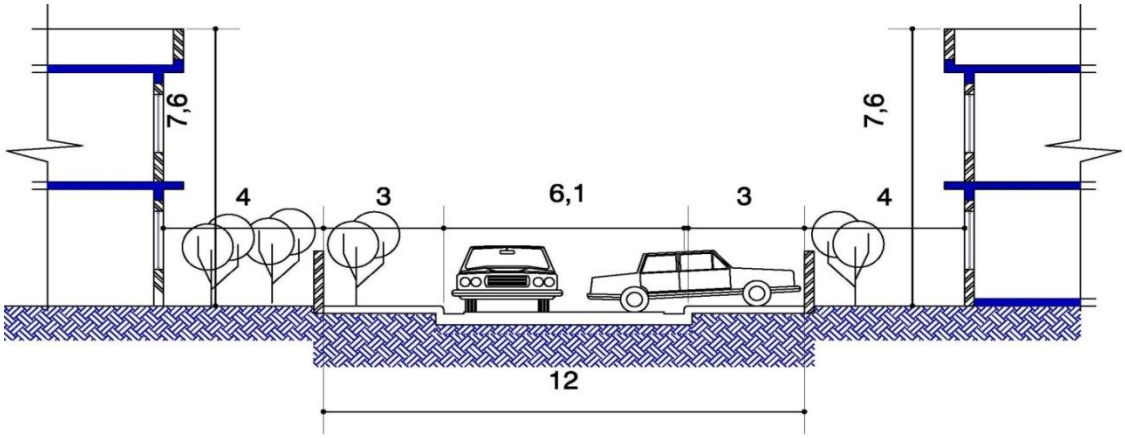

الشكل -15- تقليل المسافة الفاصلة بين الكتل السكنية المتقابلة إلى الحد الذي يضمن الملائمة الوظيفية و المناخية(اعداد الباحثة)

*** التظليل والتشجير في مشروعات الإسكان المحلية المستقبلية:**

لا بد من توفير الظلال في مشروعات الإسكان سواء بالمزروعات والخضرة الطبيعية او وسائل التظليل الأخرى مثل كاسرات الشمس والحجابات Screens والمسقفات مما يقلل من العبء الحراري الإجمالي على المبنى وبالتالي يقلل من الطاقة اللازمة للتكييف .وفرت التقنيات الحديثة وسائل متطورة للتظليل وتقليل نفوذية الحرارة للداخل كالزجاج العاكس والمظلل والمزدوج المزود بعوازل حرارية وكذلك الكاسرات والمظلات التي يمكن التحكم بها يدويا او اليا وحتى بالحاسوب الآلي .

بما إن مناخ المدينة العراقية هو مناخ (حار جاف) ولذلك نحتاج إلى ترطيب الجو و لاسيما خلال فصل الصيف وذلك عن طريق وسائل متعددة منها استخدام النافورات في الساحات الحضرية و استخدام التشجير الكثيف فيها وعل جانبي فضاء الطريق و الذي يؤدي إلى تقليل درجة حرارة الهواء و تكوين مناخ موقعي ألطف نسبيا من المناخ العام بفعل قابلية هذه الأشجار على امتصاص الحرارة و ترطيب الجو بفعل بخار الماء منها بالإضافة إلى التضليل.

وفيما يخص تشجير فضاء الطريق فأن اختيار الأشجار التي تزرع على جانبيه يجب أن تكون من نوع الأشجار الموسمية التي تعطي خواص مناخية جيدة حيث أنها تكون كثيفة التوريق صيفاً لتعطي الظلال أما شتاءاً فتسمح لأشعة الشمس بالنفوذ إلى داخل الفضاء الحضري و لتحقيق ذلك فيجب الاعتناء باختيار التوقيع الصحيح للأشجار و اختيار نوع الشجرة الملائم .

*** التهوية الطبيعية في مشروعات الإسكان المحلية المستقبلية:**

تمثل التهوية الطبيعية أهم إستراتيجيات المسكن التقليدي لتقليل العبء الحراري والتخلص من الحرارة المختزنة في قشرة المبنى لتوفير بيئة مريحة للساكنين.على الرغم من الفتحات الصغيرة الا ان تحقيق التهوية الطبيعية يتم من خلال المعالجات البيئية المعروفة (الفناء الوسطي المفتوح ,البادكير),لذا لابد من دراسة نمط التهوية والإنارة الطبيعية في مشروعات الإسكان المستقبلية سواء عبر الفتحات او ملاقف الهواء للتخلص من الحرارة الزائدة وتوفير هواء نقي حفاظا على صحة الساكنين وتقليل اللجوء الى استخدام وسائل التكييف الميكانيكية .

*** مواد البناء في مشروعات الإسكان المحلية المستقبلية:**

الاختيار المدروس لمواد البناء وكيفية ترابطها مع بعض يمكن ان يكون ذا تأثير ايجابي على صحة وراحة الساكنين ,تقليل الكلف والترشيد في استهلاك الطاقة في مشروعات الإسكان .كما ان مواد البناء الملائمة تقلل من التأثيرات السلبية للمسكن على البيئة دون ان تسبب زيادة في كلفة البناء والصيانة ويمكن وضع بعض الضوابط في اختيار مواد البناء التي يفضل استخدامها في مشروعات الإسكان المستقبلية :

- مواد مأخوذة من الطبيعة وقابلة للتجديد اي يمكن ان تعاد الى الطبيعة دون الإخلال بتوازنها مثل الطابوق الذي استخدمه الاسلاف منذ ألاف السنين وله خواص حرارية وبيئية تتلاءم مع المناخ الحار للعراق .
- مواد يمكن إعادة استخدامها recycling او الاستفادة من المواد المكونة لها مما يقلل من الهدر في المواد الخام او الطاقة اللازمة للتصنيع اي تساعد في الحفاظ على الموارد الطبيعية كالحديد الذي يمكن استخدامه لأكثر من مرة .
- مواد متينة طويلة الأمد وقليلة الصيانة عند الاستخدام مما يوفر من استهلاك المواد الخام لإنتاج مواد بديلة .

- مواد غير سامة ولا تطلق الغازات الضارة لان هذا له تأثير سلبي على صحة الساكنين والذي يمكن ان يمتد الى سنوات طويلة ,كما ان له أثارا سلبية تودي الى تلوث البيئة .
- نقترح التقليل من استخدام التبليط الإسفلتي في أكساء الفضاءات الحضرية وخصوصا الساحات الحضرية لما لها من الأثر الكبير في تقليل الكفاءة المناخية للنسيج الحضري ككل بفعل زيادة الأشعة الشمسية المنعكسة والحرارة المخزونة,وان يقتصر التبليط على الشوارع المخصصة لسير المركبات بينما تستعمل مواد أخرى ذات انعكاسية اقل مثل الحجر أو الطابوق ألفرشي في إنهاء المماشي و الممرات المخصصة لسير السابلة.

*** التصميم البيئي والحفاظ على الطاقة في مشروعات الإسكان المحلية المستقبلية:**

ارتبط مفهوم التصميم البيئي باستغلال الطاقة الذاتية او السلبية passive energy وتقليل الاعتماد على مصادر الطاقة المعروفة لأسباب اقتصادية وبيئية وصحية واللجوء الى مصادر طاقة جديدة ومتجددة وهذا يتم من خلال استغلال مكونات البيئة الطبيعية للحصول على الطاقة اللازمة .

ان مشروعات الإسكان المستقبلية لابد ان تكون متوافقة مع البيئة عبر التصميم المدروس لكل عناصر البناء والموقع وقشرة المبنى والذي سيوفر البيئة الداخلية المريحة للساكنين والترشيد في استهلاك الطاقة مما يعني اقتصادا في كلفة التكييف بالإضافة الى تقليل انبعاث الغازات من التكييف والتهوية والإنارة الميكانيكية والتي تزيد من ظاهرة الاحتباس الحراري على كوكب الأرض .

ان هناك العديد من التقنيات الحديثة والمتطورة التي لابد من أخذها بنظر الاعتبار عند تصميم مشروعات الإسكان مثل :أساليب العزل الحراري ,ترشيد استخدام المياه وإعادة استخدامها ,التخلص من النفايات ,ألواح تسخين المياه الشمسية ,الاعتماد على مصادر طبيعية لتوليد الطاقة الكهربائية خاصة في المواقع التي تبعد عن مناطق توليد الطاقة التقليدية .

- الاستنتاجات والتوصيات :

توصل البحث الى جملة من الاستنتاجات هي:

- استطاع المعمار العربي القديم أن يبتكر حلولا واساليب معمارية و تخطيطية تخفف من قساوة المناخ و خصوصاً فيما يتعلق بتأثيرات الاشعاع الشمسي و حركة الرياح وذلك عن طريق التكوين المتضام للابنية والشوارع المنحنية و الفناءات الداخلية وتدرج الحجم الفضائي للطريق وكانت هذه المعالجات جزء من اسلوب الحياة للمجتمع وفق مبداءي الحماية والتكيف وهي من اساسيات مفهوم الاستدامة .اما التطورات الحديثة في التكنولوجيا ونقل مصادر الطاقة ومواد البناء المتطورة ساعدت على إيجاد حلول بنائية بشكل مغاير, ولكن نجد الكثير من هذه الحلول تستنزف موارد كوكب الأرض على الرغم من التقنيات الحديثة.

- يجب أن يتجاوب المبنى مع البيئة المحيطة وفق مفهوم الاستدامة. عبر التفاعل المتوازن مع الموارد الطبيعية كالشمس, الرياح, طبوغرافية الأرض, ومواد البناء المتوفرة ومواءمتها مع القيم الاجتماعية وعادات وتقاليد المجتمع.

- نلاحظ اهمال المحدد البيئي في تخطيط وتصميم المشروعات السكنية الحديثة ذات النمط الشبكي و الاهتمام بالعامل التقني مما ادى الى تشابه المحلات السكنية الحديثة في نمطها مع أخرى تقع ضمن انطقة مناخية مختلفة مما يؤدي الى مشاكل بيئية ومناخية تتمثل بتعرضها الى التيارات الهوائية الحارة و المتربة و الاشعاع الشمسي.

- أن نظام الطرق و الابنية لسنة 1935 أدى الى ايجاد نمط عمراني غير ملائم مناخيا لمحلاتنا السكنية ولا يستند الى دراسة تخطيطية مسبقة ونتج عنه نسيج عمراني مفكك ذو كثافة سكنية واطئة وغير متلائم مع متطلبات مفهوم الاستدامة .
- التنمية المستدامة هي نتاج جهود المجتمع بأكمله عبر خطوط شمولية طويلة الأمد نحو تحقيق وتطوير مجتمع متوازن وفق سياسات بيئية, اقتصادية, اجتماعية وسياسية مدروسة. أننا إن لم نتخذ من الاستدامة أسلوبا للحياة فلقد عرضنا مستقبل الأجيال القادمة للخطر. وان التحدي الكبير

الذي يواجه المعماريين والمخططين الآن, هو اختيار وتعديل التكنولوجيا المتطورة بما لا يؤثر سلباً على البيئة, وفي نفس الوقت يتم تطوير أدائية ومتطلبات الراحة في المبنى المتوافق بيئياً.

ويوصي البحث :

- الاهتمام بالجانب البيئي في تخطيط وتصميم مشروعات الاسكان التي تعد اساس تكوين المدينة وخصوصا في ظل ماتتمتع به مدننا من مناخ حار جاف مثلا:

- اعتماد الفناء كمكون اساسي لرفع كفاءة التشكيل وتوافقه مع خصائص وسمات البيئة العمرانية الصحراوية من جهة وباعتباره يشكل خطوة اكثر توافقا مع مبادىء العمارة المستدامة .

- تحقيق مفهوم النسيج المتضام في قطاع الاسكان العمودي,مع المرونة في تشكيل الوحدات ا اساسية بما يحد من النمطية مع التنوع والتغير في الطابع.وباعتماد نسبة الارتفاع الى العرض التي تقترب من 1
- اتباع التوجيه الصحيح من ناحية الشمس و الرياح للمحلات السكنية ومكوناتها من فضاءات حضرية و كتل بنائية.
- على مستوى الوحدة السكنية يجب تقليص المساحات الخارجية المكشوفة و المعرضة للاشعة الشمسية الى الحد الذي يتلائم مع الناحية الوظيفية.
- التاكيد على عنصر التشجير لما له من الاهمية البالغة في تحسين المناخ المحلي على مستوى الوحدة السكنية بواسطة ترطيب الجو و لاسيما اذا روعي اختيار انواع ملائمة من الاشجار لطبيعة مناخنا الحار الجاف و هي الاشجار الموسمية وزراعتها بشكل كثيف لتوفير الظلال المطلوبة صيفا.

- على المصمم والمخطط الحضري ان يميز بين عملية تقليد الغرب واتباع انماط حياتهم وبين عملية التحديث Modernization و عدم اهمال المعالجات المتبعة في النمط العضوي لكونه ملائم من الناحية المناخية و انما اخذ الفكرة منها و الاستفادة منها في تصاميمنا و مخططاتنا المعاصرة.

- المصادر:

- الزبيدي,مها صباح,"المسكن المتوافق بيئياً...توجه مستقبلي للعمارة المستدامة والحفاظ على البيئة دراسة مقارنة لكفاءة الأداء البيئي للمسكن التقليدي والحديث",ندوة الإسكان الثانية(المسكن الميسر),الهيئة العليا لتطوير مدينة الرياض,الرياض,2001

- هبه محـــمد رياض, "اثر المناخ على تكوين شكل النسيج الحضري- دراسة مقارنة لمحلات سكنية ضمن مدينة بغداد-",المعهد العالي للتخطيط الحضري والاقليمي, 2007.
- تقارير دراسة التصميم الاساسي لمدينة النجف الاشرف- وزارة البلديات والأشغال العامة -دائرة التخطيط العمراني ,2009.
- العزاوي,صبحي "دراسة تحليلية بيئية لبيوت في الكاظمية",مؤتمر امانة بغداد -مراكز المدن التقليدية - ,امانة بغداد ,2010 .
- كمونة,حيدر عبد الرزاق," التراث المعماري وخصوصية المدينة العربية المعاصرة ",ندوة الخصوصية الوطنية في العمارة العربية المعاصرة ,وزارة الاسكان والتعمير ,بغداد 1989.
- قانون الطرق والابنية رقم 44 لسنة 1935, الباب الاول ,الوقائع العراقية,1935.
- كراس مشروع تطوير شارع حيفا , وزارة الاسكان والتعمير,1985 .
- Collier, Tony, "Design Technology &the Development Process in the Built Environment "1st edition, e&fn spon, UK, 1995.
- Evans, Martin,"Housing, Climate and Comfort "1st edition, the Architectural Press, London, UK, 1980.
- Kim, Jung-Jin&Rigdon, Brenda,"Sustainable Architecture Module: Introduction to Sustainable Design "National Pollution Prevention Center for Higher Education, Michigan, USA, 1998.
- Senosiain, Javier,"Bio-Architecture "the Architectural Press, UK,2003.
- Siani,S,B,"Building in Hot Dry Climate "John Wiley &Sons,UK,1980.
- (WCED) The World Commission on Environment and Development,"Our Common Future", Oxford University Press, Newyork, USA,1987.
- Warren, J. and Ihsan Fethi,, *"Traditional Houses in Baghdad"*, Fexiprint LTD. England,1982.